surfactant science series
volume 99

PHYSICAL CHEMISTRY OF POLYELECTROLYTES

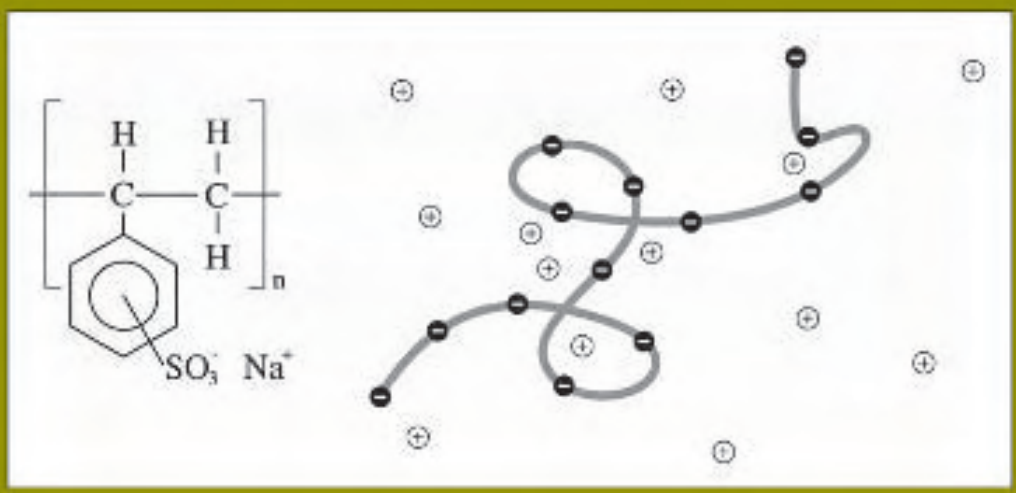

edited by
Tsetska Radeva

This Page Intentionally Left Blank

ISBN: 0-8247-0463-0

This book is printed on acid-free paper.

Headquarters
Marcel Dekker, Inc.
270 Madison Avenue, New York, NY 10016
tel: 212-696-9000; fax: 212-685-4540

Eastern Hemisphere Distribution
Marcel Dekker AG
Hutgasse 4, Postfach 812, CH-4001 Basel, Switzerland
tel: 41-61-261-8482; fax: 41-61-261-8896

World Wide Web
http://www.dekker.com

The publisher offers discounts on this book when ordered in bulk quantities. For more information, write to Special Sales/Professional Marketing at the headquarters address above.

Current printing (last digit):
10 9 8 7 6 5 4 3 2 1

PRINTED IN THE UNITED STATES OF AMERICA

Preface

Polyelectrolytes are polymers bearing dissociated ionic groups. Their unique properties, dominated by strong long-range electrostatic interactions, have been studied over the past few decades. Substantial theoretical and experimental efforts have been made, for example, to understand the origin of ''slow'' domains or ''loose'' clusters in semidilute solutions of highly charged polyelectrolytes. This kind of attractive interaction between macroions is not consistent with the standard theory based on the overlap of the electrical double layers between charged flat surfaces. Charge-fluctuation forces between several polyions due to sharing of their counterions or attraction by expansion of the condensed layers between charged rods have been suggested to explain the appearance of these formations. Particular focus has also been placed on polyion interactions with counterions, since their condensation on the polyion surface is one of the most characteristic properties of the polyelectrolytes. The interaction of polyions with other charged or neutral species and, in particular, the adsorption of ionizable polymers at interfaces, is the second aspect of the physical chemistry of polyelectrolytes that has been extensively studied due both to the fundamental importance of this phenomenon and to its central role in numerous industrial processes.

The interest in polyelectrolyte investigations has increased in the last few years as evidenced by the first two International Symposiums on Polyelectrolytes, held in 1995 and 1998. The number of papers dealing with polyelectrolytes has also increased substantially. This is not surprising considering the wide application of natural and synthetic polymers in medicine,

paper making, mineral separation, paint and food industries, cosmetics and pharmacy, water treatment processes, and soil remediation. The fabrication of layer-by-layer assembled multicomposite films, which fall in a category of novel nanomaterials, presently hold a central place in this area.

The purpose of this volume is to collect results that show the current understanding of the fundamental nature of polyelectrolytes. I hope that its appearance will stimulate the research efforts toward solving many problems in this interdisciplinary field. Practical utilization of these results is beyond doubt. The book is addressed to scientists working in the fields of biochemistry, molecular biology, physical chemistry of colloids and ionizable polymers, and their applications in related technical processes.

The volume consists of three parts. The first deals with static and dynamic properties of salt-free polyelectrolyte solutions and of solutions with added salts. An extension is presented of the counterion condensation theory to the calculation of counterion–polyion, coion–polyion, and polyion–polyion pair potentials and the appearance is predicted of inverted forces leading to the formation of ''loose'' clusters in solutions of polyelectrolytes. The origin of counterion-mediated attraction between like-charged chains is also discussed within a charge fluctuation approach that reconciles the thermal fluctuation approach with the ionic crystal one. A new criterion for counterion condensation is introduced through molecular dynamics simulations of a cell-like model for stiff polyelectrolytes; the effects considered include polyions overcharging, charge oscillations, and attractive interactions. Metropolis Monte Carlo simulation is also applied to calculate counterion distributions, electric potentials, and fluctuation of counterion polarization for model DNA fragments. Theoretical approaches developed for the description of coil–globule transition of polyelectrolyte molecules are treated in two limiting situations—for a single macromolecule at infinite dilution and for a polyelectrolyte gel. Although emphasis is placed on the recent developments in the theory of polyelectrolytes, this first part provides a partial review of the new experimental results that try to explain different aspects of the physical chemistry of polyelectrolytes.

The second part is devoted to adsorption of polyelectrolytes at interfaces and to flocculation and stabilization of particles in adsorbing polymer solutions. A recent theory of the electrostatic adsorption barrier, some typical experimental results, and new approaches for studying the kinetics of polyelectrolyte adsorption are presented in the first chapter of this part. In the following chapters, results are collected on the electrical and hydrodynamic properties of colloid–polyelectrolyte surface layers, giving information on the structure of adsorbed layers and their influence on the interactions between colloidal particles; examples and mechanisms are analyzed of polyelectrolyte-induced stabilization and fragmentation of colloidal aggregates;

self-assembled monolayers from synthetic polyelectrolytes on water or solid surfaces and the role of amphiphilic polyelectrolytes for the emulsion stability are considered. Special attention is given to surface force measurements that show how association between polyelectrolytes and surfactants at solid–liquid interfaces influences surface interactions and structure of adsorbed layers.

The third part discusses polyelectrolyte complex formation and complexation of polyelectrolytes with surfactants and proteins. Mobility of short chains and dynamic properties of polyelectrolyte gels are also considered. Phase transitions in ionic gels are explained with simple models in which polymer–polymer interactions are taken into account at a molecular level. In the second chapter of this part, recent experimental and theoretical advances are summarized for gel electrophoresis, which is invaluable in predicting conformation and structural changes of biologically significant macromolecules. In the following chapters, results are grouped for the stoichiometry, structure, and stability of highly aggregated polyelectrolyte complexes; for the role of hydrophobicity and electric charge of the partners in the protein binding to amphiphilic polyelectrolytes; and for the micellar-like aggregation of surfactants bound to oppositely charged polyelectrolytes.

I wish to thank first Professor Arthur Hubbard, who invited me to edit a volume on this rapidly expanding field. Acknowledgments are due to all authors for their valuable contributions and willing cooperation. I acknowledge with gratitude the assistance of Ani Pesheva in the correspondence, as well as the efforts of our production editor, Paige Force, and of all my friends who contributed to the production of this volume.

Tsetska Radeva

This Page Intentionally Left Blank

Contents

This Page Intentionally Left Blank

Contributors

Bernadette Charleux, Ph.D. Laboratoire de Chimie Macromoléculaire, Université Pierre et Marie Curie, Paris, France

Per M. Claesson, Ph.D. Department of Chemistry, Royal Institute of Technology, and Institute for Surface Chemistry, Stockholm, Sweden

Martien A. Cohen Stuart, Ph.D. Laboratory of Physical Chemistry and Colloid Science, Wageningen University, Wageningen, The Netherlands

Herbert Dautzenberg, Dr.habil.nat Department of Colloid Chemistry, Max Planck Institute of Colloids and Interfaces, Golm, Germany

Andra Dedinaite, Ph.D. Department of Chemistry, Royal Institute of Technology, and Institute for Surface Chemistry, Stockholm, Sweden

Michel Delsanti, Ph.D. Service de Chimie Moleculaire, Commissariat á l'Énergie Atomique Saclay, Gif sur Yvette, France

Markus Deserno, Ph.D. Max-Planck-Institute for Polymer Research, Mainz, Germany

Maurice Drifford, Ph.D. Service de Chimie Moleculaire, Commissariat á l'Énergie Atomique Saclay, Gif sur Yvette, France

Bae-Yeun Ha, Ph.D.* Department of Chemistry and Biochemistry, University of California, Los Angeles, California

**Current affiliation*: Department of Physics, Simon Fraser University, Burnaby, British Columbia, Canada

Masanori Hara, Ph.D. Department of Chemical and Biochemical Engineering, Rutgers University, Piscataway, New Jersey

Nobuyuki Higashi, Ph.D. Department of Molecular Science and Technology, Doshisha University, Kyoto, Japan

Christian Holm, Ph.D. Max-Planck-Institute for Polymer Research, Mainz, Germany

Kazuo Kikuchi, Sc.D. Associate Professor, Department of Life Sciences (Chemistry), Graduate School of Arts and Sciences, University of Tokyo, Tokyo, Japan

J. Mieke Kleijn, Ph.D. Laboratory of Physical Chemistry and Colloid Science, Wageningen University, Wageningen, The Netherlands

Ksenija Kogej, Ph.D. Department of Physical Chemistry, Faculty of Chemistry and Chemical Technology, University of Ljubljana, Ljubljana, Slovenia

Etsuo Kokufuta, Ph.D. Institute of Applied Biochemistry, University of Tsukuba, Tsukuba, Ibaraki, Japan

Sabine Kosmella, Ph.D. Institute of Physical and Theoretical Chemistry, University of Potsdam, Potsdam, Germany

Joachim Kötz, Ph.D., Dr.rer.nat.habil Department of Colloid Chemistry, Institute of Physical and Theoretical Chemistry, University of Potsdam, Potsdam, Germany

Kurt Kremer Professor, Max-Planck-Institute for Polymer Research, Mainz, Germany

Andrea J. Liu, Ph.D. Department of Chemistry and Biochemistry, University of California, Los Angeles, California

Gerald S. Manning, B.A., Ph.D. Department of Chemistry, Rutgers University, Piscataway, New Jersey

Larry W. McLaughlin, Ph.D. Department of Chemistry, Boston College, Chestnut Hill, Massachusetts

Frédéric Millet, Ph.D. Service de Physique L'État Condensé, Commissariat à L'Énergie Atomique (Saclay), Gif-sur-Yvette, France

Tohru Miyajima, Ph.D. Department of Chemistry, Faculty of Science and Engineering, Saga University, Saga, Japan

Udayan Mohanty, Ph.D. Department of Chemistry, Boston College, Chestnut Hill, Massachusetts

Masazo Niwa, Ph.D. Department of Molecular Science and Technology, Doshisha University, Kyoto, Japan

Emile Pefferkorn, Ph.D. Department of Physics of Dispersed Media and Interfaces, Institut Charles Sadron, Strasbourg, France

Patrick Perrin, Ph.D. Laboratoire de Physico-chimie Macromoleculaire, Ecole Supérieure de Physique et de Chimie Industrielles, Paris, France

Evgeni Poptoshev, M.Sc. Institute for Surface Chemistry, Stockholm, Sweden

Tsetska Radeva, Ph.D. Institute of Physical Chemistry, Bulgarian Academy of Sciences, Sofia, Bulgaria

Jolly Ray Department of Chemistry, Rutgers University, Piscataway, New Jersey

Marián Sedlák, D.Sc. Institute of Experimental Physics of the Slovak Academy of Sciences, Košice, Slovak Republic

Jože Škerjanc, Ph.D. Department of Physical Chemistry, Faculty of Chemistry and Chemical Technology, University of Ljubljana, Ljubljana, Slovenia

Christophe Tribet, Ph.D. Laboratory of Physical Chemistry of Macromolecules, Ecole Superieure de Physique et de Chimie Industrielles, and Centre National de la Recherche Scientifique, and University of Paris 6, Paris, France

Valentina V. Vasilevskaya, Ph.D. Nesmeyanov Institute of Organoelement Compounds, Russian Academy of Sciences, Moscow, Russia

Hans Vink, Ph.D. Department of Physical Chemistry, University of Uppsala, Uppsala, Sweden

1

Structure and Dynamics of Polyelectrolyte Solutions by Light Scattering

MARIÁN SEDLÁK Institute of Experimental Physics of the Slovak Academy of Sciences, Košice, Slovak Republic

Static light scattering and dynamic light scattering are useful experimental tools for the investigation of the structure and dynamics of polyelectrolyte solutions as well as for the characterization of polymer systems in general. The structure can be probed by static light scattering (SLS) on a certain length scale (typically from 20 nm to several microns) limited mainly by the light wavelength. Therefore the accessible structural information is usually on the level of a whole polymer chain, interchain correlations, and the solution structure on a large length scale exceeding single chain dimensions and interchain separation distances. Light scattering does not yield direct information on the local structure inside the chain, referred to also as the primary and secondary structure. However, smaller length scales can be probed by very similar techniques in which x-rays or neutrons are used instead of visible light (small-angle x-rays and small-angle neutron scattering). The dynamics probed by dynamic light scattering (DLS) is limited by the technical possibilities of currently available instrumentation (from ca 0.5 μs to seconds). Naturally, the dynamics is related also to the structure. Therefore some structural information can be calculated from the dynamic data, too. In this case, the length scale probed is not limited by light wavelength and extends below 1 nm. Charge interactions in polyelectrolyte solutions dominantly influence the structure and dynamics on the above-mentioned length and time scales, and therefore light scattering is a source of information on the character of these interactions. Absolute values of scattering intensities are thermodynamic quantities that enable us under certain circumstances to calculate such important parameters as polymer molecular weight or the second virial coefficient in the virial expansion of osmotic

pressure. As will be shown throughout this chapter, light scattering from polyelectrolyte solutions is a rather complex and variable subject, and the interpretation of light scattering data is often a nontrivial task. The aim of this chapter is to present the issue of the structure and dynamics of polyelectrolyte solutions by light scattering in a compact form. It is based on the author's own work, which is complemented by selected literature results. It is not intended to be a complete review, and therefore the selection of cited literature is to some extent personal. We acknowledge at this point many valuable works in the field that are not included. Our presentation is focused mainly on linear flexible polyelectrolytes, but many properties are universal and apply also to other polyelectrolyte classes unless explicitly specified in another way. Excluded is the case of polyelectrolyte solutions with multivalent counterions, which will be discussed in a different chapter, and some other special cases specified in the text.

I. BRIEF THEORETICAL BACKGROUND

In general, the source of light scattering from a polymer (or polyelectrolyte) solution is the existence of spatial and temporal fluctuations in refractive index in this scattering medium. The overall scattering intensity measured in an SLS experiment is proportional to the average of the square of refractive index fluctuations in the scattering volume,

$$I(\vec{q}) \cong \langle |\delta n_{\mathrm{if}}(\vec{q})|^2 \rangle \tag{1}$$

where the tensor $\delta\overleftrightarrow{n}(\vec{q})$ is a Fourier transform of the refractive index fluctuation $\delta\overleftrightarrow{n}(\vec{r})$ at a place $\vec{r}$ of the scattering volume, and $\vec{q}$ is the scattering vector, with an absolute value of

$$q = |\vec{q}| = |\vec{k}_{\mathrm{f}} - \vec{k}_{\mathrm{i}}| = \frac{4\pi n}{\lambda_0} \sin\frac{\theta}{2} \tag{2}$$

with n the refractive index of the medium, λ_0 the light wavelength in vacuum, θ the scattering angle, and $\vec{k}_{\mathrm{i}}$ and $\vec{k}_{\mathrm{f}}$ the wavevectors of the initial and final (scattered) beam, respectively. q^{-1} defines the length scale at which the structure is probed. The scattered electric field time autocorrelation function measured in a DLS experiment is proportional to the time autocorrelation function of the fluctuations in refractive index

$$g^{(1)}(t) \cong \langle \delta n_{\mathrm{if}}(\vec{q}, 0)\, \delta n_{\mathrm{if}}(\vec{q}, t) \rangle \tag{3}$$

where the tensor $\delta\overleftrightarrow{n}(\vec{q}, t)$ is a Fourier transform of the refractive index fluctuation $\delta\overleftrightarrow{n}(\vec{r}, t)$ at a place $\vec{r}$ at a time t. The correlation function as given by Eq. 3 reflects temporal correlations of refractive index fluctuations and

can be expressed as a Laplace transform of the spectrum of relaxation times $A(\tau)$

$$g^{(1)}(t) = \int_0^\infty A(\tau) e^{-t/\tau}\, d\tau \tag{4}$$

The spectrum of relaxation times obtained from the correlation function by inverse Laplace transform is frequently a multimodal distribution where separate peaks can be ascribed to different modes. Each mode represents a certain type of motion giving rise to a fluctuation with given frequency (relaxation time) and strength. The position of the peak on the time axis corresponds to the relaxation time τ_i of the particular mode. If the mode is diffusive, a diffusion coefficient $D_i = (1/\tau_i)q^{-2}$ can be ascribed to this relaxation time. The peak area corresponds to the strength of the particular fluctuation (the portion of scattering intensity due to this mode). The total scattering intensity as measured in an SLS (often referred to as integral light scattering) experiment is given as

$$I \cong \int_0^\infty A(\tau)\, d\tau \tag{5}$$

Fluctuations in refractive index in two-component systems (particles and solvent) arise due to density and concentration fluctuations. Density fluctuations are determined by the isothermal compressibility of the scattering medium $RT(\partial\rho/\partial p)$, where R is the gas constant, T is absolute temperature, ρ is density, and p is pressure. For moderate concentrations (up to 20%), the density fluctuations in solution can be assumed to be equal to density fluctuations in the pure solvent. These are relatively fast compared to the time window probed by DLS and therefore not covered in the spectrum of relaxation times. Hence if the solvent scattering is subtracted, only concentration fluctuations are taken into account. The excess light scattering by particles at a zero scattering angle $I(0) = I_{total}(0) - I_{solvent}(0)$ is given by concentration fluctuations and can be related to osmotic compressibility $RT(\partial c/\partial \pi)$, where

$$\frac{Kc}{I(0)} = \frac{1}{RT}\frac{\partial \pi}{\partial c} \tag{6}$$

where π is the osmotic pressure against the solvent, c is the solute concentration in g/L, and the constant K is defined for vertically polarized incident light as

$$K = \frac{4\pi^2 n^2 (dn/dc)^2}{\lambda_0^4 N_A} \tag{7}$$

where N_A is Avogardro's number, n is the solution refractive index, and dn/dc is referred to as the refractive index increment, which represents the scattering contrast of particles in a particular solvent.

The intensity $I(\theta)$ scattered at a nonzero angle θ can be expressed via osmotic compressibility when the size of particles and the range of interparticle forces is reasonably small compared to $2\pi/q$:

$$\frac{Kc}{I(\theta)} = \frac{1}{RT}\frac{1}{p(\theta)}\frac{\partial \pi}{\partial c} \tag{8}$$

where $p(\theta)$ governs both intra- and interparticle interference. The former is due to the interference of light rays scattered from different segments of the same particle, the latter to the interference of light rays scattered from segments belonging to different particles. In the case of homogeneous spheres, $p(\theta)$ can be factored as $p(\theta) = P(\theta)s(\theta)$, where $P(\theta)$ is the so-called single particle form factor, reflecting only the intraparticle interference, and $s(\theta)$ is referred to as the solution structure factor, reflecting only the interparticle interference. This factorization does not hold in general for other particle architectures and is certainly not valid for rigid rods [1]. Nevertheless, it can be considered as a good approximation in most cases. Usually the normalization is such that $P(0) = s(0) = 1$.

Scattering from a collection of identical particles can be also expressed in terms of the so-called particle approach to light scattering as

$$I(\theta) = kNm^2 P(\theta) S(\theta) \tag{9}$$

where k is experimental constant covering the square of the scattering contrast, N is the number of particles in the scattering volume, and m is the particle mass. In this notation, $S(\theta) = 1$ in the absence of interparticle correlations. $S(\theta) \neq 1$ covers interparticle interactions, which are implicitly included in $\partial c/\partial \pi$ in Eq. 8. Thus $S(0)$ does not have to be equal to 1 as distinct from $s(0)$. $S(\theta)$ can be calculated as [2]

$$S(\theta) = S(q) = 1 + 4\pi\rho_n \int_0^\infty [g(r) - 1] \left[\frac{\sin(qr)}{qr}\right] r^2 \, dr \tag{10}$$

where ρ_n is the number density of particles and $g(r)$ is the radial distribution function of particles reflecting the probability of finding a particle at distance r from another particle. $g(r) = 1$ evidently implies $S(\theta) = 1$.

From the point of view of the dynamics, the total excess scattering intensity in the simplest case of a dilute two-component system (solvent and weakly interacting particles with dimensions small compared to q^{-1}) corre-

sponds to the scattering contribution from one mode—translational diffusion of particles. This does not hold in general, where more modes can be observed in the spectrum of relaxation times. This is the case for (1) multicomponent systems, (2) systems with large particles where internal dynamics (dynamics of segments inside the particle) can be seen or rotational diffusion can be seen when particles are asymmetric, (3) concentrated solutions of particles where short-time and long-time diffusion can be seen, etc. In fact, polyelectrolyte solutions are systems where multimodal spectra of relaxation times are obtained.

II. LIGHT SCATTERING APPARATUS

A schematic diagram of the apparatus for static and dynamic light scattering is shown in Figure 1 (top view). The initial laser beam passes horizontally through the sample and defines the wavevector $\vec{k}_i$. Scattered light is detected by a detection unit, which rotates in a horizontal plane. The position of the

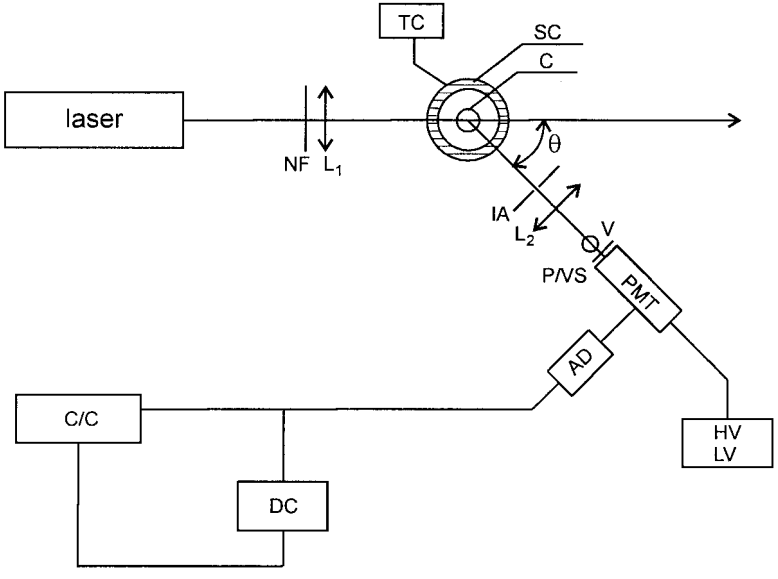

FIG. 1 Schematic diagram of the apparatus for static and dynamic light scattering. NF, neutral optical filters; L_1, focusing lens; SC, scattering chamber; C, sample cell; TC, temperature controller; θ, scattering angle; IA, iris aperture; L_2, objective; V, viewer; P/VS, pinhole/vertical slit; PMT, photomultiplier tube; HV, LV, high voltage, low voltage power supply; AD, amplifier and discriminator; DC, digital counter; C/C, correlator/computer.

detection unit (scattering angle θ) defines the wavevector of the scattered beam $\vec{k}_f$ and hence the scattering vector $\vec{q}$ (Eq. 2). The scattering angle θ can be varied in typical setups from 15° to 150°, which corresponds to values of $q = 0.0042-0.031$ nm^{-1} (for water solutions and the laser wavelength $\lambda_0 = 514.5$ nm). The scattered light is detected by photon counting. Integrated intensities (number of photons per defined, sufficiently long time interval) are measured in an SLS experiment. Fluctuations of the scattering intensities are analyzed by photon correlation in a DLS experiment. The measured quantity is in this case a homodyne autocorrelation function of the scattering intensity, which can be converted into the scattered electric field autocorrelation function $g^{(1)}(t)$ (see Eq. 3). More technical details on the light scattering experiment can be found elsewhere [3].

III. LIGHT SCATTERING FROM POLYELECTROLYTE SOLUTIONS—MULTIMODAL SPECTRA OF RELAXATION TIMES

Multimodal spectra of relaxation times arise as a consequence of the multicomponent nature of polyelectrolyte solutions consisting of solvent (usually water), polyions, counterions originating from the dissociation of ionizable groups on polyions, and low-molecular-weight salt composed of small molecular or atomic ions. Small ions of the salt, which are likely charged, compared to polyions, are referred to as coions. We will also include in our discussion the case of polyelectrolyte mixtures (polyions of the same chemical composition but different molecular weights). Polyelectrolyte solutions in practice have a nonzero width of the polyion molecular weight distribution and can be in principle considered as mixtures, too. Polyions are not always distributed homogeneously in solutions and mixtures, but instead form larger structures referred to as domains or clusters. These structures also contribute to the overall scattering intensity and can be therefore considered as an additional component of the system.

In order to discuss scattering contributions from particular components, we can estimate several parameters coming into play: size, scattering contrast, number concentration, and interparticle interference effects (see Eq. 9). Upon assumption of negligible interparticle interactions [$S(\theta) = 1$], the scattering at zero angle [where $P(0) \equiv 1$] can be written as $I(0) = kNm^2 \cong kN\rho_p^2 V_p^2 \cong N\rho_s^2 R_p^6$, where ρ_p is the particle density, V_p is the particle volume, ρ_s is the overall scattering contrast including density, and R_p is the particle radius assuming its spherical shape. With regard to sizes of particular components in polyelectrolyte solutions, these are largely differing. Radii of small ions are on the order of angstroms (1–2 Å in the case of atomic ions

as Na^+ or Cl^-), the apparent radius of water molecules is approximately 1 Å, radii of gyration of polyions range typically from 5 to 80 nm depending mainly on molecular weight, and radii of polyelectrolyte domains range approximately from 30 to 300 nm. If we realize that the scattering is in our rough approximation proportional to the sixth power of the particle radius, we see that the contributions may largely differ due to particle sizes. Also number concentrations (number of particles per unit volume) can differ largely upon going from the so-called salt-free case (molar concentration of low-molecular-weight salt $c_s \sim 5 \times 10^{-6}$ M) to the high-salt case ($c_s \sim 1$ M) or by varying the polyion molar concentration in a range appropriate for light scattering measurement ($c_p \sim 10^{-10}$ to 10^{-1} M). The scattering contrast of polyions given by the refractive index increment dn/dc is usually higher than for typical pairs of neutral polymers and their solvents (for instance, the value for sodium polystyrene sulfonate (NaPSS) in water is $dn/dc = 0.23$ mL/g). The contrast of small ions in water is comparable with typical values for neutral polymers in their solvents ($dn/dc \cong 0.15$ mL/g). The contrast of polyion domains and their number concentration are quantitatively not known.

It can be deduced from the parameters outlined that the scattering contributions of particular components (giving rise to particular dynamic modes) can be very variable upon changing experimental conditions. In addition, there are also strong interparticle interference effects due to strong interparticle interactions, which dramatically influence scattering intensities and increase the variability. The practical consequence of this discussion is a conclusion that for correct understanding and interpretation of light scattering data, it is useful (if not necessary) to evaluate scattering contributions from particular modes in absolute units and then to discuss them separately. This evaluation is based on the combination of data from static and dynamic light scattering. The total scattering intensity measured in an SLS experiment can be normalized to the scattering from a standard (e.g., benzene). This normalized intensity $I(\theta)/I_B(\theta)$ can be then written as a sum of contributions from particular modes $I(\theta)/I_B(\theta) = A_1(\theta) + A_2(\theta) + A_3(\theta) \cdots$. Since relative amplitudes of the modes $A_i(\theta)/A_j(\theta)$ are known from DLS data, absolute values of amplitudes (in units of benzene scattering), can be calculated, too. For bimodal spectra, where $I(\theta)/I_B(\theta) = A_1(\theta) + A_2(\theta)$:

$$A_2(\theta) = \frac{I(\theta)/I_B(\theta)}{1 + A_1(\theta)/A_2(\theta)} \qquad A_1(\theta) = \frac{I(\theta)/I_B(\theta)}{1 + A_2(\theta)/A_1(\theta)} \tag{11}$$

In order to be able to evaluate contributions from particular modes, there are two requirements: corresponding peaks in the spectrum of relaxation times should not overlap completely, and the amplitudes should not decrease

below approximately 2% of the total scattering intensity. Figure 2 shows relaxation times of dynamic modes observed in polyelectrolyte solutions and mixtures in a whole range of accessible experimental conditions. The data are based mostly on work on model polyelectrolyte systems [well-defined molecular weight standards of NaPSS and weak polyelectrolytes with variable charges—poly(methacrylic) acid and poly(acrylic acid)] but also hold for solutions of linear flexible polyelectrolytes in general. Most features are common also for solutions of globular, rigid, or semirigid (wormlike) polyelectrolytes. Excluded from the general scheme in Figure 2 are extreme cases, such as extra large polyions, where in principle internal modes can be observed, or large highly asymmetrical rigid polyions, where rotational diffusion and bending modes can be observed [4]. The modes shown in Figure 2 (from left to right on the time axis) correspond to (1) diffusion of low-molecular-weight salt, (2) diffusion of polyions or polyion segments in semidilute solutions, (3) ''interaction mode'' in polyelectrolyte mixtures, and (4) diffusion of polyelectrolyte domains. It can be seen from Figure 2 that the four dynamic modes are well separated. There is only a more or less apparent overlap of the polyion diffusion and interaction mode in this schematic diagram (apparent means that at low ionic strengths, where both modes are present, there is no actual overlap). The outline of the rest of the chapter is such that we discuss first aspects of the dynamics (particular dynamic modes) and afterwards aspects of static light scattering, keeping in mind the composite multimodal nature of the integral intensity. The problem of polyelectrolyte domains (clusters), which is equally reflected in both SLS and DLS, will be discussed at the end.

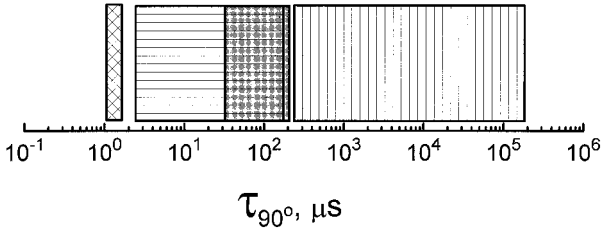

FIG. 2 Relaxation times of dynamic modes observed in polyelectrolyte solutions and mixtures over a broad range of experimental conditions: ⊠ diffusion of low molecular weight salt; □ diffusion of polyions or polyion segments in semidilute solutions; ▦ ''interaction mode'' in polyelectrolyte mixtures; and □ diffusion of polyelectrolyte domains (clusters). The data are based mostly on the work on linear flexible polyelectrolytes. Relaxation times correspond to scattering at 90°. See text for more details.

IV. DIFFUSION OF LOW-MOLECULAR-WEIGHT SALT

Salt ions in polyelectrolyte solutions are atomic ions or low-molecular-weight molecular ions. These are referred commonly to as small ions. Compared to macromolecules or supramolecular structures, the dynamics of small ions is fast and the scattering contribution is very low. Both effects are due to their small dimensions. The measurement of the small-ion dynamics by dynamic light scattering is therefore difficult. Only recently, we succeeded in measuring the diffusion of small ions in our laboratory. We present here the first brief results. Technically, the small-ion diffusion rate is relatively well within the possibilities of current dynamic light scattering instrumentation. For instance, the diffusion coefficient for NaCl in water corresponds approximately to the relaxation time of 4 μs at scattering angle $\theta = 45°$. The more important problem is the extremely weak scattering signal. While the scattering contrast of most small ions in water is comparable with the scattering contrast of neutral polymers in their solvents ($dn/dc \cong 0.15$ mL/g), the small size of such ions compared to polymers or colloids is the main factor. For illustration, the excess scattering from 3M NaCl solution in water is equal to 0.034 in units of benzene scattering. Scattering from water is equal to 0.11 in the same units.

Figure 3 shows the correlation function and the corresponding spectrum of relaxation times for a solution of sodium poly(styrenesulfonate) (NaPSS) in 3.7 M NaCl. Two modes can be clearly recognized. The slower mode corresponds to the diffusion of polyions, which will be discussed in the next section. The faster mode corresponds to the diffusion of salt (NaCl). As expected for a diffusive process, the inverse relaxation time of this mode Γ_{vf} (the subscript ''vf'' refers to ''very fast'') is q^2 dependent (Figure 4). The diffusion coefficient of the salt small ions was calculated from the slope of the dependence $\Gamma_{vf} = D_{vf}q^2$ in Figure 4 as $D_{vf} = (1.7 \pm 0.1) \times 10^{-5}$ cm^{2}s^{-1}. The scattering amplitude of the very fast mode varies proportionally with the salt concentration and is q independent as expected. Figure 5 shows the correlation function and the corresponding spectrum of relaxation times for a pure solution of NaCl in water (no polymer added). Only one diffusive mode is present with the diffusion coefficient matching relatively closely the value of D_{vf} obtained in polyelectrolyte solution.

In the following we apply a rigorous theoretical treatment of the dynamic scattering from a system of oppositely charged point Brownian particles [5] to the case of the NaCl salt. It is assumed that particles ''a'' and ''b'' can be characterized by diffusion coefficients D_a, D_b, charges Z_a, Z_b, and number densities N_a, N_b. The total charge neutrality implies that $N_aZ_a + N_bZ_b = 0$. In a general case ($D_a \neq D_b$), in the small-q limit, the calculated dynamic structure factor $S(q, t) = S(q)g^{(1)}(t)$ is a double exponential $S(q, t) = A_1 \exp(-\Gamma_1(q)t) + A_2 \exp(-\Gamma_2(q)t)$. It holds for $\Gamma_1(q)$ and $\Gamma_2(q)$:

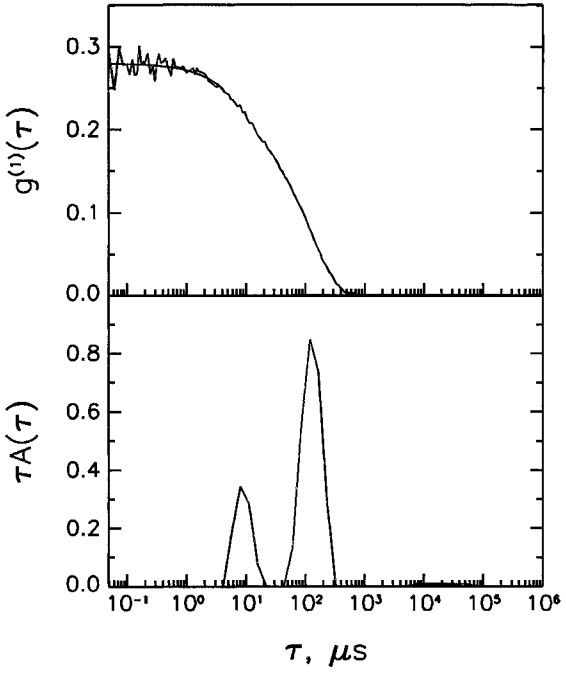

FIG. 3 Correlation function and corresponding spectrum of relaxation times for sodium poly(styrenesulfonate) (NaPSS), M_w = 5,400, in 3.7 M NaCl. Polymer concentration c = 1.9 g/L. Scattering angle $\theta = 30°$.

$$\Gamma_1(q) = D_a\kappa_a^2 + D_b\kappa_b^2 - \frac{k_BT}{6\pi\eta}\,\kappa^3 \tag{12}$$

$$\Gamma_2(q) = q^2\,\frac{\kappa^2 D_a D_b - \kappa(D_a\kappa_b^2 + D_b\kappa_a^2)(k_BT/6\pi\eta)}{D_a\kappa_a^2 + D_b\kappa_b^2 - \kappa^3(k_BT/6\pi\eta)} \tag{13}$$

where η is the viscosity of the scattering medium, k_B is Boltzmann's constant, and T is temperature. κ^{-1} is the total Debye–Hückel screening length due to particles of both types in volume V:

$$\kappa^2 = \kappa_a^2 + \kappa_b^2 = \frac{4\pi}{\varepsilon_0 k_BT}\left(\frac{N_a}{V}\,Z_a^2 + \frac{N_b}{V}\,Z_b^2\right) \tag{14}$$

The first mode has a q-independent frequency $\Gamma_1(q)$ and is referred to as the plasmon mode by analogy with plasmas, in which the plasma frequency is

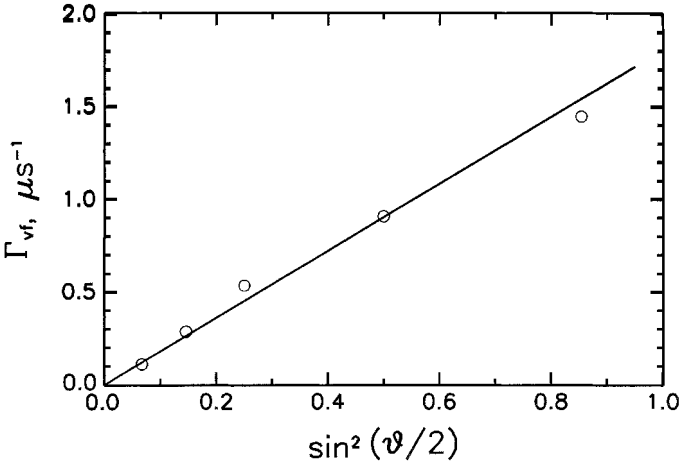

FIG. 4 Angular dependence of the inverse relaxation time $\Gamma_{vf} = 1/\tau_{vf}$ of the very fast mode corresponding to the diffusion of salt (NaCl) in solution of sodium poly(styrenesulfonate) (NaPSS), M_w = 5,400, in 3.7 M NaCl. Polymer concentration c = 1.9 g/L.

also constant. However, with $q \to 0$, the amplitude $A_1(q)$ vanishes. Therefore this mode is difficult to observe, and the dynamic structure factor reduces to a single exponential with a q^2 dependent frequency $\Gamma_2(q)$. Upon neglect of hydrodynamic interactions, which are included in Eq. 13, the formula for the frequency $\Gamma_2(q)$ simplifies, and hence the corresponding diffusion coefficient can be expressed as

$$D = \frac{\Gamma_2(q)}{q^2} = \frac{(1 + |Z_b/Z_a|)D_a D_b}{D_a + |Z_b/Z_a|D_b} \tag{15}$$

This result, obtained upon several approximations, is identical to the classical phenomenological Nernst–Hartley formula for the coupled diffusion of oppositely charged ions [6]. In order to apply this formula to the case of an NaCl solution, we use for the uncoupled diffusion coefficients $D_a = D_{Na^+}$ and $D_b = D_{Cl^-}$, where D_{Na^+} and D_{Cl^-} are values of diffusion coefficient of particular ions obtained from conductivity data extrapolated to infinite dilution ($D_{Na^+} = 1.33 \times 10^{-5}$ cm^{2}s^{-1} and $D_{Cl^-} = 2.03 \times 10^{-5}$ cm^{2}s^{-1}) [7]. Upon substitution into Eq. 15, we obtain $D = 2D_{Na^+}D_{Cl^-}/(D_{Na^+} + D_{Cl^-}) = 1.61 \times 10^{-5}$ cm^{2}s^{-1}. The agreement with the value of the experimentally obtained diffusion coefficient is satisfactory.

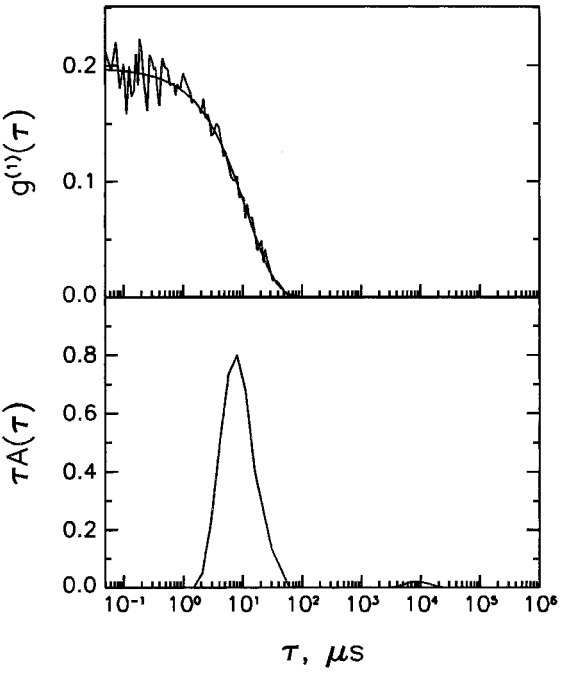

FIG. 5 Correlation function and corresponding spectrum of relaxation times for 3.4 M NaCl in water. Scattering angle $\theta = 30°$.

V. POLYION DIFFUSION

Diffusion of polyions in polyelectrolyte solutions is in the majority of cases influenced by mutual long-range electrostatic interactions. Consequently diffusion coefficients measured by dynamic light scattering are mostly collective (mutual) diffusion coefficients. The translational diffusion coefficient of a single polyion is measurable only in dilute solutions. The necessary dilution is inversely proportional to the concentration of added salt, which screens interactions. Most of the light scattering data on polyion diffusion are available at conditions where the size of polyions and the mean interpolyion distances are smaller than q^{-1} (q is the scattering vector length). The discussion in this section will be based on this assumption, although some exemptions will also be discussed.

The diffusion of polyions is strongly influenced by several factors: the effective charge of the polyion, the concentration of added low-molecular-weight salt (ionic strength), and the polyion concentration (mean interpolyion distance). Because there are usually more diffusive modes observed

in polyelectrolyte solutions, the diffusion of polyions is frequently referred to as "fast diffusion," and the corresponding diffusion coefficient as the fast diffusion coefficient D_f. Figure 6 shows the dependence of D_f on polyion charge. The system investigated is partially ionized solutions of poly(methacrylic acid) (PMA) [8]. PMA is a weak polyacid dissociating in water only slightly (ca. 2%). A stronger dissociation (and hence also charge) is reached by neutralization with sodium hydroxide. The degree of neutralization α is defined as the ratio of the molar concentration of added NaOH to the monomer molar concentration of the polyacid (i.e., the number of NaOH molecules per monomer). The diffusion coefficient increases upon increasing α and levels off at higher values of α. This transition correlates with the results of the Oosawa–Manning theory [9,10], according to which the onset of counterion condensation corresponds to the situation where the mean intercharge spacing along the chain A_c equals the Bjerrum length l_B defined as $l_B = e^2/\varepsilon k_B T$ (e is the electron charge, ε is the dielectric permittivity, k_B is Boltzmann's constant, and T is temperature). For the PMA sample investigated, the condition $l_B = A_c$ corresponds to $\alpha_c = 0.36$. For $\alpha > \alpha_c$, the charge density on polyions is stabilized by counterion condensation and so is the diffusion coefficient. In conclusion, the diffusion coefficient increases with the polyion charge. The small natural ionization at $\alpha = 0$ can be suppressed by decreasing pH (e.g., by addition of HCl). This decrease of

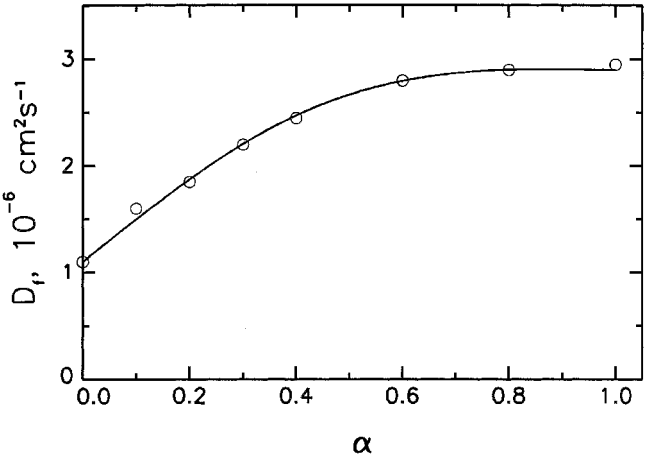

FIG. 6 Dependence of polyion fast diffusion coefficient D_f on degree of neutralization α for poly(methacrylic acid) salt-free aqueous solutions. M_w = 30,000, polymer concentration c = 36.6 g/L. Polymer chains were ionized by neutralization with sodium hydroxide. (Adapted from Ref. 8.)

charge is also reflected in lowering the value of the diffusion coefficient (not shown here). The value of α_c can be changed by changing the solvent dielectric permittivity (and hence the Bjerrum length). The onset of condensation thus shifts to lower charge densities in organic solvents with lower dielectric permittivity [11].

Figure 7 shows the dependence of the polyion diffusion coefficient on added salt concentration [12]. Results for three different molecular weight standards of sodium poly(styrenesulfonate) (NaPSS) with the addition of NaCl are presented. NaPSS is a strong polyelectrolyte, i.e., strongly dissociating in aqueous solutions. The charge is therefore controlled only by counterion condensation (corresponds to the case $\alpha = 1$ for PMA). The general feature of the results in Figure 7 is that the polyion diffusion accelerates upon decreasing the added salt concentration c_s. The symbol c_s refers to molar salt concentration. At high concentrations of added salt c_s, charge effects are screened, and values of diffusion coefficients resemble those of equivalent neutral polymers. At low c_s, very high values of diffusion coefficients are measured, which are not typical for neutral polymers at all. Polyions diffuse much faster than comparable neutral macromolecules at conditions of high charge density and weak screening. The polyion diffusion coefficient increases continuously upon decrease of c_s. The leveling off at very low c_s is due to the fact that the added salt concentration becomes in this case low compared to the concentration of uncondensed counterions.

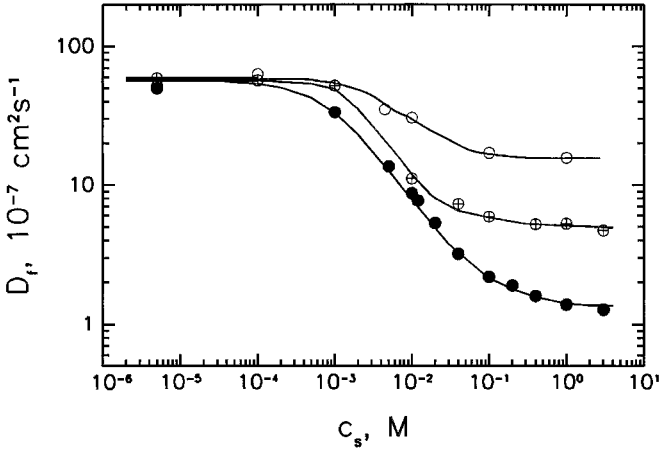

FIG. 7 Dependence of polyion fast diffusion coefficient D_f on molar concentration of added salt (NaCl). Aqueous solutions of sodium poly(styrenesulfonate) (NaPSS), c = 5 g/L, M_w = 5,000 (○), 47,000 (⊕), and 1,200,000 (●). (Adapted from Ref. 12.)

The diffusion coefficient at high c_s decreases with increasing molecular weight. This is similar to neutral polymers where the diffusion coefficient is inversely dependent on the friction factor, which is proportional by the power law to polymer molecular weight, i.e., $D \cong f^{-1} \cong M_w^{-\nu}$. The diffusion coefficient at low c_s is, on the other hand, independent of polymer molecular weight. This can be also documented by a more detailed data set on molecular weight standards of NaPSS [13] (Figure 8).

Figure 9 shows the dependence of the polyion diffusion coefficient on polyion concentration c. This data was obtained on NaPSS standard with M_w = 100,000, but similar dependencies were obtained also on standards with different M_w [14]. The diffusion coefficient is within experimental error independent of c at $c > 0.5$ g/L and sharply decreases upon decreasing c below 0.5 g/L.

Without doing detailed quantitative analysis of the data, it can be stated that the polyion diffusion can be qualitatively described by two theoretical concepts. The first concept capable of qualitative explanation of the polyion diffusion is the concept based on considering polyions as interacting Brownian particles with direct interactions between polyions and hydrodynamic interactions. The short-time collective diffusion coefficient for a system of interacting Brownian particles treated by statistical mechanics is calculated from the first cumulant Γ_1 of the dynamic structure factor $S(q, t)$ as [15–17]

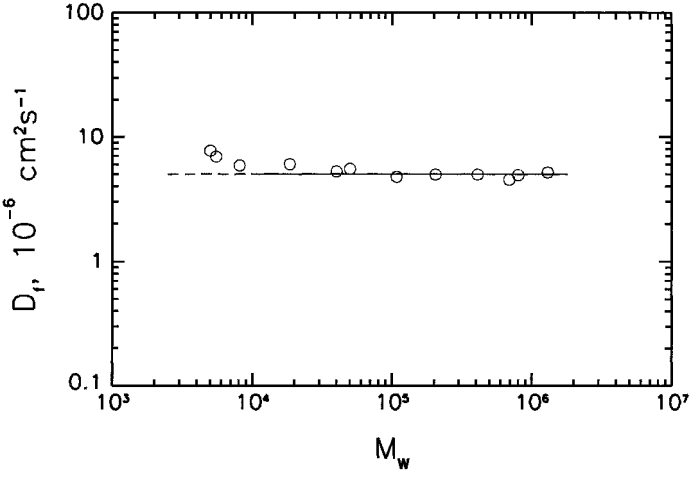

FIG. 8 Dependence of polyion fast diffusion coefficient D_f on polyion molecular weight. Salt-free aqueous solutions of sodium poly(styrenesulfonate) (NaPSS), c = 45.6 g/L. (Adapted from Ref. 13.)

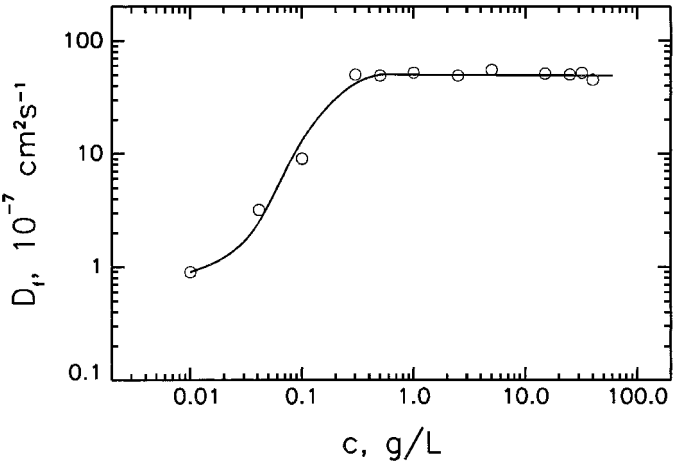

FIG. 9 Dependence of polyion fast diffusion coefficient D_f on polyion concentration. Salt-free aqueous solutions of sodium poly(styrenesulfonate) (NaPSS), M_w = 100,000. (Adapted from Ref. 14.)

$$D = \frac{\Gamma_1}{q^2} = -\frac{1}{q^2}\frac{\partial}{\partial t}\ln S(q, t)\big|_{t=0} = -\frac{1}{q^2}\frac{1}{S(q)}\left.\frac{\partial S(q, t)}{\partial t}\right|_{t=0} = D_0\frac{H(q)}{S(q)} \tag{16a}$$

where $S(q, t) = S(q)g^{(1)}(t)$, D_0 stands for free particle diffusion coefficient (infinite dilution, no interactions), $S(q)$ is the static structure factor reflecting direct interparticle interactions involved, and the term $H(q)$ is known as the hydrodynamic function reflecting hydrodynamic interactions. Equation 16a holds exactly for spherical particles. In the case of coils or rods, the form factor $P(q)$ comes into play such that

$$D = D_0\frac{H(q)}{P(q)S(q)} \tag{16b}$$

The influence of $P(q)$ may be physically viewed as the effect of internal dynamics [4]. The resulting diffusion coefficient D can be either lower or higher than D_0, according to the interplay between the influence of the above-mentioned effects. The dominating factor in the case of polyions in polyelectrolyte solutions is usually the static structure factor $S(q)$. Low values of $S(q)$ yield high values of D. Low $S(q)$ is found at low q, ($q \ll q_m$, where q_m is the wavevector at the peak in $S(q)$, see Section X). For polyion concentrations where extremely high values of D are obtained, the q vectors accessible by light scattering are really small compared to q_m, which corresponds to the q range accessible by SAXS or SANS. Low values of $S(q)$

are due to low osmotic compressibility (see Eqs. 8 and 9). The dependence of osmotic compressibility or $S(q)$ on fundamental parameters as polyion concentration, added salt concentration, polyion charge and molecular weight is therefore reflected in the diffusive behavior via the diffusion coefficient D. In accord with the above-outlined treatment of diffusion, the thermodynamic definition of the collective diffusion coefficient is $D = (1/f_{\text{coll}})(\partial\pi/\partial c)_{\mu,T}$, where f_{coll} is collective friction and μ is chemical potential.

The second concept explaining high diffusion rates of polyions in low salt solutions is referred to as the coupled mode theory [4,6,18,19]. The fast polyion diffusion is explained as a consequence of the coupling of the polyion motion with the dynamics of small and much faster counterions and coions. Both polyions and small ions are charged species creating a common electrostatic field, which fluctuates due to their motion and reversally influences their dynamics. The polyion diffusion coefficient is calculated by solving a three-component diffusion equation in a matrix formalism (three partial diffusion equations for polyions, counterions, and coions, which are coupled through the Poisson–Boltzmann equation for the common electrical potential). Solution of the matrix equation yields three frequency eigenvalues for three eigenmodes, which are (1) the plasmon mode with a q-independent frequency, named by analogy with plasmas, in which the plasma frequency is also constant, (2) the polyion diffusion, and (3) the small-ion diffusion. The analytical solution for the polyion diffusion is given by a complex formula that is not reproduced here. A simpler expression for the zero angle limit of the polyion diffusion coefficient is given upon several assumptions: the added salt is a symmetric 1–1 electrolyte, it has a common counterion with the polyion, and there is the same charge and the same diffusion coefficient of the counterion and coion, respectively

$$D(q = 0) = \frac{1}{2}\,[D_p(1 - \Omega) + D_s(1 + \Omega)] \tag{17}$$

with

$$\Omega = \frac{D_p Z_p - D_s[1 + (2c_s/Z_p c_p)]}{D_p Z_p + D_s[1 + (2c_s/Z_p c_p)]} \tag{18}$$

where D is the diffusion coefficient, Z is the charge, and the indexes p, s refer to polyion (p) and salt (s), respectively. The total molar concentration of the 1–1 electrolyte ions is $2c_s = 2c_s^{\text{add}} + Z_p c_p$, where c_s^{add} is the molar concentration of the added 1–1 electrolyte, c_p is the polyion molar concentration, and $Z_p c_p$ is the molar concentration of counterions that dissociate from polyions. The diffusion coefficients D_p and D_s are infinite dilution values for particular components in the absence of charges (if they were

neutral particles). The asymptotic cases are the excess added salt case and the no added salt case, respectively:

$$D(q = 0) = D_p \qquad \frac{2c_s}{c_p} \to \infty \tag{19}$$

$$D(q = 0) = \frac{D_p D_s(2 + Z_p)}{D_p Z_p + 2D_s} \qquad \frac{2c_s}{c_p} \to Z_p \tag{20}$$

Dependencies of polyion diffusion coefficient on added salt concentration (Fig. 7) can be fitted by using Eq. 17 with Z_p as an adjustable parameter. Values of Z_p giving optimum fits are, however, much smaller than stoichiometric values. The same conclusion can be made upon fitting data on various polyelectrolytes [20].

Most of the data shown in Figures 6–9 are obtained at moderate polyion concentrations, where the structure factor $S(q)$ does not show maxima in the q range accessible by light scattering. The mean interpolyion spacing is small compared to q^{-1}. In this case, the polyion diffusion coefficient is q independent. At relatively low polymer concentrations (~0.01 g/L) and low added salt concentrations, the polyion diffusion coefficient $D(q)$ exhibits angular minima corresponding to angular maxima in $S(q)$ in accord with Eq. 16 [21,22]. The diffusion coefficient at the minimum $D(q_m)$ describes the structural relaxation of the dominant structure giving angular extremes rather than collective diffusion observed at $q \ll q_m$.

On the other hand, a semidilute regime where polyions overlap is eventually reached at high concentrations. In a salt-free case, the fast diffusion coefficient corresponding to polyion diffusion in the dilute regime does not reflect a transition from dilute to semidilute regime. This was demonstrated by measurements on a set of NaPSS standards with a broad range of molecular weights and concentrations, where the dilute–semidilute transition is definitely reached irrespective of the assumed conformations of chains [13,14]. The fast diffusion coefficient is independent of molecular weight and polymer concentration for $c > 0.5$ g/L (see also Figures 8 and 9). This indicates that the collective diffusion of chain segments in semidilute solution is roughly the same as the diffusion of whole chains. The concentration and molecular weight independence of the fast diffusion coefficient in the semidilute regime $D \sim c^0 M_w^0$ was theoretically derived by explicitly considering triple screening for coupled dynamics of ionic species associated with electrostatic, excluded volume, and hydrodynamic interactions [23]. On the other hand, a dilute–semidilute transition can be clearly recognized in scattering data obtained at high c_s [24]. The overall picture is similar to neutral polymers. In the dilute regime, the diffusion coefficient is weakly dependent on concentration and strongly dependent on molecular weight. At the tran-

sition, a much stronger concentration dependence develops, and the diffusion coefficient becomes molecular weight independent. Diffusion in the semidilute regime corresponds to blob diffusion, i.e., $D \sim \xi^{-1}$, where ξ is the blob size or the correlation length of the network. At high c_s, ξ scales as $\xi \sim c^{-3/4}$ [25,26], which agrees with experimental data [24].

Because of strong interactions in polyelectrolyte solutions without added salt, the use of the well-known Stokes–Einstein relation for free particle diffusion $D = k_B T/6\pi\eta R_h$, where η is viscosity and R_h is hydrodynamic radius, is rather limited. Even at very low concentrations, where intermolecular interactions can be neglected due to large intermolecular separations, the friction factor contains in addition to the Stokes–Einstein contribution $f_{SE} = 6\pi\eta R_h$ also a contribution from electrolyte dissipation, so that the total friction factor $f = f_{SE} + f_{eldis}$, where the electrolyte dissipation term reflects the retardation of the polyion motion due to the instantaneous distortion of the surrounding ion atmosphere as the polyion moves through the solvent [27,28].

The Stokes–Einstein relation for free particle diffusion can be applied at infinite dilution upon partial screening of electrostatic effects by added salt. At higher added salt concentrations c_s the polyion diffusion obeys the relation

$$D = D_0(1 + k_D c) \tag{21}$$

where k_D is referred to as the diffusion second virial coefficient. k_D was found proportional to $1/c_s$ (e.g., for NaPSS solutions between c_s = 10 and 500 mM [29]) and proportional to polyion molecular weight M_w at these salt concentrations [29]. D_0 increases with c_s in this interval, which means that the hydrodynamic radius decreases with increasing c_s. In this regime, it is possible to compare data on hydrodynamic radii and radii of gyration from static light scattering. The ratio R_g/R_h reflects macromolecular shape and internal structure. Different values of this ratio correspond to spheres, rods, coils in theta or good solvent, etc. The hydrodynamic radius is related to the ability of solvent to penetrate and flow through the macromolecule. Macromolecules with more open structures are drained deeply, whereas those with more closed structures are drained only at the periphery. This leads to higher values of R_g/R_h in the former case and smaller in the latter. Limiting cases are referred to as the free-draining and nondraining case, respectively. In the free-draining case, the hydrodynamic radius should scale as $R_h \sim M_w$, because each segment of the polyion (each increment of mass) contributes independently to the friction factor f. In the nondraining case, $R_h \sim R_g \sim M_w^{\upsilon}$, where $\upsilon < 1$. The NaPSS behavior was found more close to nondraining behavior (least-draining). It was reported for NaPSS that $1/D_0 \sim M_w^{0.5}$ for c_s = 5 mM to 4 M [30] and $1/D_0 \sim M_w^{0.6}$ in 100 mM NaCl [29]. The R_g/R_h

ratio for NaPSS decreases from 3.0 to 1.8 by increasing c_s from 2 mM to 4 M NaCl [30,31]. For some other polyelectrolytes, D_0 was found independent of c_s in spite of some c_s dependence of R_g, which can be ascribed to less bulky sidegroups on main chains in these polyelectrolytes leading to more free-draining behavior, unless the direct relation between D_0 and R_h was violated (problems due to viscosity, dissipation, etc.) [30].

Finally, we make a comment concerning the long-time self-diffusion in solutions with moderate and high polyion concentrations, i.e., diffusion of a single polyion in a collection of other polyions on time scale $t \gg \tau_I$, where τ_I is the relaxation time of the polyions configuration (τ_I is equal to the time needed for the polyion to diffuse a distance equal to its radius). This diffusion is not measurable by dynamic light scattering. It is necessary to label polyions and consequently measure their diffusion over large distances (long times) by other techniques. This is done either by chemical labeling (FRAP, fluorescence recovery after photobleaching; FRS, forced Rayleigh scattering) or by spin labeling (PFG NMR, pulsed field gradient nuclear magnetic resonance spectroscopy). The long-time self-diffusion of polyions is appreciably slower than the collective diffusion as measured by light scattering. Data on self-diffusion of NaPSS solutions can be found in Refs. 32 and 33.

VI. DYNAMICS IN POLYELECTROLYTE MIXTURES

Polyelectrolyte binary mixtures (two polyions of the same chemical composition but different molecular weights) exhibit at low ionic strength quite specific dynamic behavior [34,35]. Figures 10 and 11 summarize DLS results obtained on binary mixtures of NaPSS without added salt. Figure 10 shows spectra of relaxation times obtained on binary mixtures of NaPSS with M_w = 5,000 and M_w = 1,200,000. The total polymer concentration was maintained at $c = c(P1) + c(P2) = 25$ g/L while the mixture composition $x = c(P2)/[c(P1) + c(P2)]$ was varied. $c(P1)$ and $c(P2)$ are concentrations of component 1 (NaPSS, M_w = 5,000) and component 2 (NaPSS, M_w = 1,200,000), respectively. There are two modes in the spectrum that can be identified with the modes occurring in binary solutions, referred to as the fast and slow mode (although the amplitude of the fast mode is relatively weak). Corresponding diffusion coefficients are marked as D_f and D_s and are discussed in detail in separate sections. In addition, a third mode clearly develops upon mixing of two polyelectrolyte samples. The relative amplitude of this mode reaches a maximum around $x = 0.5$ and decreases to zero in the limits $x \to 0$ and $x \to 1$. This mode is diffusive in nature (relaxation time scales with q^{-2}). With respect to the classification of modes as fast and slow, the new mode appearing in the mixture can be classified as the ''medium mode'' and therefore is marked as D_m in Figure 10. Relative amplitude

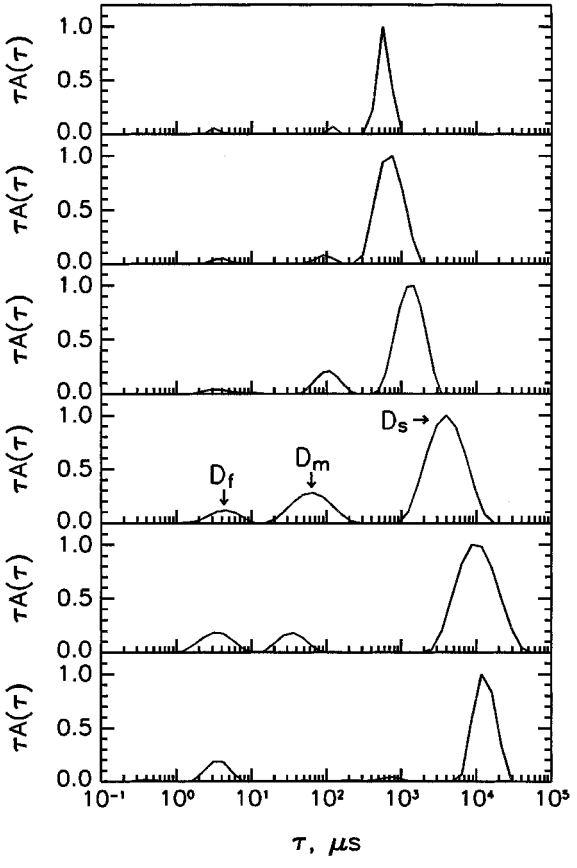

FIG. 10 Spectra of relaxation times for binary mixtures of two polyelectrolyte samples (P1, P2) in water: P1 = NaPSS, M_w = 5,000, P2 = NaPSS, M_w = 1,200,000. The total polymer concentration was c = 25 g/L. The mixture composition $x = c(\text{P2})/(c(\text{P1}) + c(\text{P2}))$ was from top to bottom x = 0, 0.046, 0.188, 0.488, 0.824, and 1.0. All measurements were performed at scattering angle $\theta = 90°$. Three diffusive modes observed for $0 < x < 1$ are marked as D_f, D_m, and D_s, respectively. (Adapted from Ref. 34.)

of the medium mode increases upon decreasing the total polymer concentration (Figure 11). At lower polymer concentrations, it dominates the spectrum of relaxation times. The amplitude of the medium mode is not angularly dependent, indicating that it is not directly related to the formation of any type of larger structures in solution.

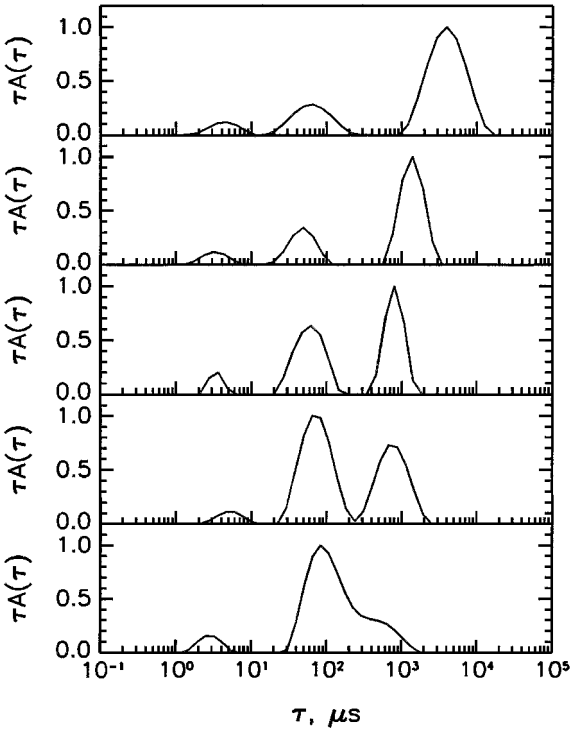

FIG. 11 Spectra of relaxation times for binary mixtures of two polyelectrolyte samples (P1, P2) in water: P1 = NaPSS, M_w = 5,000, P2 = NaPSS, M_w = 1,200,000. The mixture composition was $x = c(\text{P2})/(c(\text{P1}) + c(\text{P2})) = 0.49$. The total polymer concentration was from top to bottom c = 25.0, 15.0, 3.8, 1.7, and 0.58 g/L. All measurements were performed at scattering angle $\theta = 90°$. (Adapted from Ref. 34.)

Analogical mixtures of neutral polymers (analogical means here the same polymer chain lengths, same mixture composition, same total monomer concentration, and very similar solvent quality) do not show this behavior. Figure 12 summarizes results on binary mixtures of polystyrene samples with M_w = 4,000 and M_w = 670,000 in benzene. The total monomer concentration was c = 25 g/L, and the mixture composition was varied from $x = 0$ to $x = 1$. The faster mode in Figure 12 is associated with the diffusion of the low-molecular-weight component (M_w = 4,000) and the slower mode with the diffusion of the high-molecular-weight component (M_w = 670,000). When x increases, the fraction of the low-molecular-weight component in the mixture decreases and consequently the amplitude of the faster mode decreases. On the other hand, the slower mode amplitude increases as the fraction of the

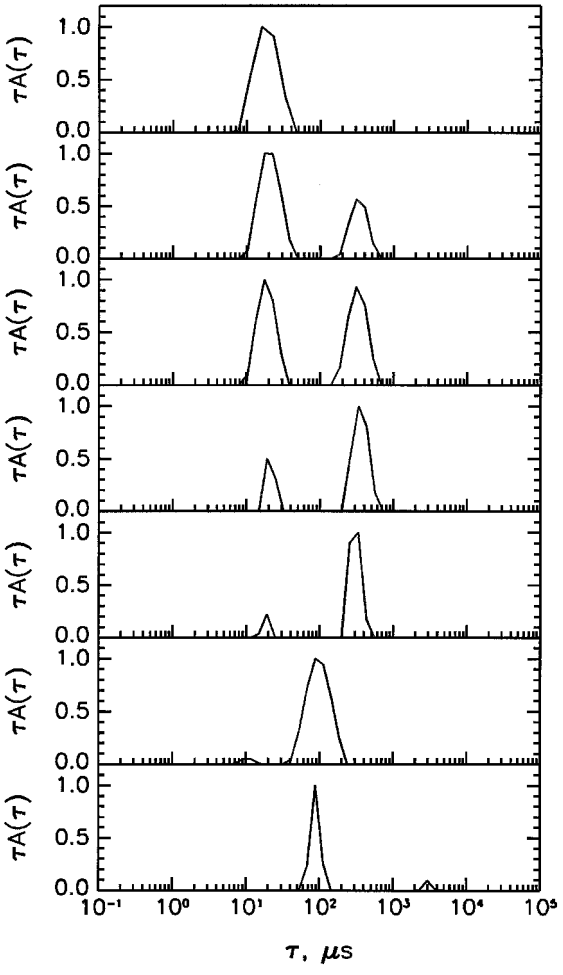

FIG. 12 Spectra of relaxation times for binary mixtures of two polystyrene samples (P1, P2) in benzene: P1 = PS, M_w = 4,000, P2 = PS, M_w = 670,000. The total polymer concentration was c = 25 g/L. The mixture composition $x = c(\text{P2})/(c(\text{P1}) + c(\text{P2}))$ was from top to bottom x = 0, 0.0036, 0.0069, 0.022, 0.057, 0.63, and 1.0. All measurements were performed at scattering angle $\theta = 90°$. (Adapted from Ref. 35.)

high-molecular-weight component in the mixture increases. The comparison of the dynamic behavior of mixtures of neutral and charged polymers shows that the medium mode in polyelectrolyte mixtures is clearly due to electrostatic interactions and therefore we also refer to it as the ''interaction mode.''

The number of eigenmodes (uncoupled modes that are detected if their amplitudes are sufficiently large) in multicomponent mixtures equals the number of components in the mixture [5]. Therefore the appearance of an additional mode in the mixture is expected. Regarding the interpretation of this mode, it should be noted that there is currently no exact theory of polyelectrolyte mixtures that could be directly confronted with our experiments carried out on given conditions. Anyway, eigenmodes in general can be identified with simple types of motions (that can be easily visualized) only in very special cases. Therefore even in the presence of an exact theory, it could be that the motion giving rise to the ''interaction mode'' in the polyelectrolyte mixture cannot be easily visualized. What can be clearly stated is that the appearance of the interactive mode in dynamic light scattering spectrum means that there is a fluctuation in refractive index with given relaxation time.

Theoretical treatment of the dynamics of multicomponent mixtures in general [5,36–38] predicts the existence of two modes in binary mixtures: the cooperative diffusion [fluctuations in the total concentration $c = c(\mathrm{P2}) + c(\mathrm{P1})$] and the so called interdiffusion [fluctuations in the local relative concentration of the two components $c(\mathrm{P2})/c(\mathrm{P1})$]. The latter mode is also referred to as the composition fluctuation mode or heterogeneity mode. The amplitude of the interdiffusion mode exhibits a maximum as a function of the mixture composition. Rigorously speaking, the exact identification of eigenmodes as cooperative diffusion and interdiffusion can be done only in one special case: mixtures of components that differ in optical labeling but are otherwise identical. In other cases, these two modes are only linear combinations of eigenmodes and vice versa. With respect to these theoretical considerations and to experimentally observed characteristics, it can be concluded that composition fluctuations may significantly contribute to the fluctuations we detect as the interactive mode in a polyelectrolyte mixture. However, a major role for other possible mechanisms cannot be excluded. In every case, the dynamics of the polymeric components in a polyelectrolyte mixture at low ionic strength is not uncoupled as in analogical mixtures of neutral polymers. Polyion species in polyelectrolyte mixtures with low ionic strength do not diffuse independently. The interpretation of the fast diffusive mode in a polyelectrolyte mixture as the cooperative diffusion (fluctuations in the total concentration) and its independence of the mixture composition and the total concentration is supported by the molecular weight and con-

TABLE 1 Values of Medium Diffusion Coefficient D_m and Ratio of the Medium Mode Scattering Amplitude vs. the Fast Mode Scattering Amplitude A_m/A_f for Binary Mixtures of Six Different NaPSS Samples in Water. The mixture Composition Was $x = 0.5$ and the Total Polymer Concentration Was $c = 5$ g/L

M_w of mixture components	D_m 10^{-9} cm^2/s	A_m/A_f
100 000 + 1 200 000	90	0.62
47 000 + 1 200 000	138	0.51
5 000 + 1 200 000	237	7.95
5 000 + 100 000	395	4.84
5 000 + 47 000	634	5.22

centration independence of the cooperative polyion diffusion in comparable binary solutions.

Polyelectrolyte solutions with broad polyion molecular weight distributions may be considered also as multicomponent mixtures, and similar effects can, in principle, be expected. Therefore NaPSS mixtures with various components (which can be considered as solutions with various bimodal molecular weight distributions) were investigated [34,35]. The results are presented in Table 1. It can be seen that the amplitude of the interaction mode (normalized with respect to the amplitude of the fast mode) is much larger in the case of smaller molecular weights of the components. The lower the molecular weights of the components, the faster the interaction mode. In all cases, however, the interaction mode is still well separated from the molecular-weight-independent fast diffusive mode. While a more detailed discussion of these results is beyond the current understanding of the mechanism of dynamic processes in polyelectrolyte mixtures, the practical consequence is that the possibility of the occurrence of this mode in dynamic light scattering from solutions of polyelectrolyte samples with broad or bimodal molecular weight distributions should be kept in mind in order correctly to interpret experimental data.

VII. POLYION MOLECULAR WEIGHT

The ability of light scattering to yield polymer molecular weight and other important parameters such as the second virial coefficient in the expansion of osmotic pressure or the single chain structure is one of the most practical applications of this technique. However, because of the complex nature of light scattering from charged polymers leading to multimodal spectra of relaxation times, some caution has to be used. Experimental conditions

should be optimally set so that the total scattering is due to one dynamic mode—diffusion of weakly interacting polyions. In the worse case, the scattering contribution of this mode must be calculated from the total scattering by a combination of static and dynamic light scattering (see Sec. III). In practice, the optimum condition is fulfilled at low polyion concentration and high added salt concentration. In this case the excess scattering (after subtraction of solvent scattering) obeys a formula [39] similar to the general light scattering equation for a two-component system based on fluctuation theory (Eq. 6):

$$\frac{K^*c}{I(0)} = \frac{1}{RT}\left(\frac{\partial \pi}{\partial c}\right)_{\mu_s} \tag{22}$$

The ''solvent'' in this case is a salt solution (solvent with small ions) which is in Donnan equilibrium with the polyelectrolyte solution, the index μ_s means that the chemical potentials of all the solutes except that used in differentiation are constant, and K^* is given as [39]

$$K^* = \frac{4\pi^2 n^2 (dn/dc)^2_{\mu_s}}{\lambda_0^4 N_A} \tag{23}$$

which is again formally equivalent to the formula for neutral two-component systems (Eq. 7). The only difference is that the refractive index increment is at constant chemical potential of salt rather than at the constant concentration of salt. Constant chemical potential of salt is a consequence of the Donnan equilibrium.

The Donnan osmotic pressure in Eq. 22 can be expanded to the virial form

$$\pi = RT\left(\frac{c}{M_w} + (A_2)_{\mu_s}c^2 + (A_3)_{\mu_s}c^3 + \cdots\right) \tag{24}$$

where M_w is the polyelectrolyte molecular weight and $(A_i)_{\mu_s}$ are virial coefficients at the Donnan pressure. Equation 22 can be then written in the form

$$\frac{K^*c}{I(0)} = \frac{1}{M_w} + 2(A_2)_{\mu_s}c + \cdots \tag{25}$$

which is again formally equivalent to the classical Zimm formula commonly used for neutral two-component systems except that experiments must be done at a constant chemical potential of salt (Donnan equilibrium pressure). The polyion molecular weight is obtained via Eq. 25 by double extrapolation

of scattering intensity to zero scattering angle and zero concentration. In practice, a complete angular dependence is measured for several concentrations to perform the double extrapolation. In order to meet fully the condition of constant chemical potential of salt, the experimental procedure should be such that each polyelectrolyte solution is first dialyzed against a given solvent. Then the dialyzed solute and solvent, which are at the Donnan equilibrium after dialysis, should be used for light scattering measurement (excess solution scattering over solvent scattering) and refractive index measurement (difference in refractive index between solution and solvent). The difference between the excess scattering with and without previous dialysis can in most cases be neglected. What cannot be neglected are differences between refractive index increments measured at constant salt concentration and constant chemical potential of the salt (differences between the constants K and K^*). If samples are not dialyzed and refractive index increments are measured only at constant salt concentration, then apparent rather than true molecular weights are measured. According to Eqs. 7, 23, and 25, the apparent molecular weight M'_w is related to the true molecular weight M_w as

$$M'_w = M_w \frac{K}{K^*} = M_w \left[1 + \frac{(\partial n/\partial C_s)_c}{(\partial n/\partial c)_{C_s}} (\partial C_s/\partial c)_{\mu_s} \right]^2 \tag{26}$$

where C_s is the salt concentration in g/L. The term $(\partial C_s/\partial c)_{\mu_s}$ corresponds to the adsorption of salt on the polyion, and the most obvious contribution is from the formation of the electrical double layer (excess of counterions and deficit of coions in the vicinity of the polyion). $(\partial C_s/\partial c)_{\mu_s}$ can be estimated from the theory of Donnan membrane equilibrium or from solving the Poisson–Boltzmann equation to calculate the concentration of counterions and coions in the vicinity of the polyion. It can be expressed as [39]

$$\left(\frac{\partial C_s}{\partial c}\right)_{\mu_s} = -\frac{M_s}{M_w} \left(\frac{\partial c_s}{\partial c_p}\right)_{\mu_s} = -\frac{M_s}{M_w} Z_p a \tag{27}$$

where c_s and c_p are molar concentrations, M_s and M_w are molecular weights of the low-molecular-weight salt and the polyion, respectively, Z_p is the polyion valence, and the factor $a = 0.5$ for low Z_p and $a < 0.5$ for high Z_p. The quantity $(\partial c_s/\partial c_p)_{\mu_s}$ is the adsorption of salt on the polyion in molar concentrations, i.e., the number of salt molecules adsorbed at one polyion. It is to be emphasized that it is a negative adsorption because the salt is expelled from the polyion surrounding. Therefore there is a minus sign in Eq. 27. After entering Eq. 27 into Eq. 26, the following relation between M'_w and M_w is obtained:

$$\sqrt{M'_w} = \sqrt{M_w}\left[1 - \frac{(\partial n/\partial C_s)_c}{(\partial n/\partial c)_{C_s}}\frac{M_s}{M_w}Z_p a\right]$$
$$= \sqrt{M_w}\left[1 - \text{const } M_s\left(\frac{\partial n}{\partial C_s}\right)_c\right] \quad (28)$$

The apparent molecular weight is smaller than the true molecular weight. The difference is greater the heavier the salt is. The validity of Eq. 28 was verified experimentally by its authors [39] (Figure 13).

In typical experiments, the solution and the solvent are brought into equilibrium by dialysis against each other using semipermeable membranes enabling the salt ions to migrate across but preventing polyions from the migration. The Donnan equilibrium is established by a redistribution of salt ions in this way. In cases where polyelectrolyte is soluble in nonionizing (or weakly ionizing) organic solvent, it is possible to perform molecular weight determination without needing to perform equilibrium dialysis. As an example we can mention poly(methacrylic acid) in ethyleneglycolmonoethylether [40]. This does not apply, however, when a mixed solvent is used to enable solubilization by adjusting the solvent dielectric permittivity (e.g., organic solvent plus water). Because many polyelectrolyte samples are strongly hygroscopic (up to 30% water content), it is necessary for the purpose of accurate molecular weight measurement to determine true concentrations. The same care must be taken regarding potential changes in con-

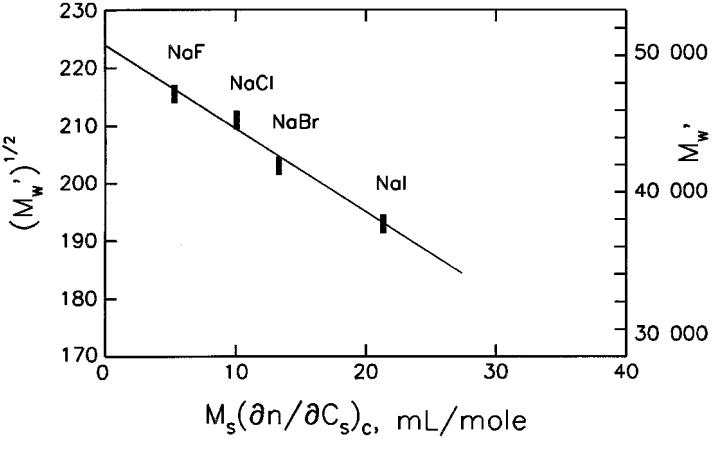

FIG. 13 Dependence of apparent molecular weight M'_w on molar refractive index increment of salt. Poly(methacrylic acid), half neutralized by NaOH, in solutions of various salts. (Adapted from Ref. 39.)

centration during dialysis. We note that the molecular weight measured by light scattering in polydisperse samples is a weight average. By combination with the number average (obtained for instance by osmometry), the sample polydispersity M_w/M_n can be estimated. The last comment concerns the fact that the measured value of M_w includes polyion plus a proportional amount of counterions, i.e., one counterion per each monomer unit. $M_w = c/c_p$, where c is the concentration of the polymer material in g/L (polyions plus counterions) and c_p is the molar concentration of polyions.

VIII. SECOND VIRIAL COEFFICIENT

Under conditions of partly screened interactions in dilute solutions (high added salt concentration c_s and low polymer concentration c), the solution osmotic pressure can be expressed via a virial expansion (Eq. 24). Then light scattering becomes a useful tool to obtain values of second virial coefficients characterizing interactions in solution. The second virial coefficient can be calculated from the slope of the dependence given by Eq. 25. The relation between the true and the apparent second virial coefficient is similar to the relation between the true and the apparent molecular weight (see the previous section for more details and the meaning of the symbols):

$$A_2' = A_2 \frac{K^*}{K} = A_2 \left[1 + \frac{(\partial n/\partial C_s)_c}{(\partial n/\partial c)_{c_s}} (\partial C_s/\partial c)_{\mu_s} \right]^{-2} \tag{29}$$

The dependence of the second virial coefficient on basic quantities such as the solution ionic strength or the polymer molecular weight is usually of greater scientific interest than the knowledge of true vs. apparent values. Therefore the time-consuming dialysis step leading to true rather than apparent values is usually omitted. Hence measured second virial coefficients are usually only apparent values.

As expected, the second virial coefficient decreases upon increase of c_s. The exact form of this dependence is shown in Figure 14 as a log–log plot of the data on sodium poly(styrenesulfonate) in aqueous NaCl solutions obtained by different authors [30,41]. Values obtained by osmometry are also shown for comparison [41]. The general trend is that the dependence is stronger at lower c_s and weaker at higher c_s. It was proposed that $A_2 \sim c_s^{-1}$ in the former case and $A_2 \sim c_s^{-1/2}$ in the latter [41]. The dashed line in Figure 14 represents calculated values of A_2 according to Yamakawa's theory [30,42]. Qualitatively similar dependencies of A_2 on c_s were found also in solutions of poly(methacrylic acid) [43] and some biological polyelectrolytes [22,44]. At very high c_s, a deviation from such dependence leading to theta conditions ($A_2 = 0$) and even to macrophase separation (''salting-out effect,'' $A_2 < 0$) may be eventually reached in some systems. Temperature becomes

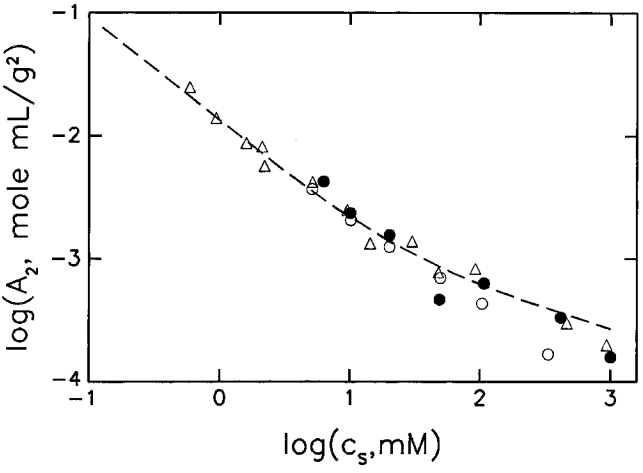

FIG. 14 Dependence of the second virial coefficient on added-salt concentration. NaPSS in NaCl solutions. Results by light scattering from Ref. 41 (●), Ref. 30 (△); and by osmometry from Ref. 41 (○). The dashed line shows calculation of the second virial coefficient by incorporating electrostatic excluded volume effects after Ref. 30.

an important factor in this situation [45]. The molecular weight dependence of A_2 is much weaker than in solutions of neutral polymers. A_2 is almost independent of M_w at lower c_s and only weakly dependent on M_w at higher c_s [46].

The second virial coefficient of polyelectrolytes is treated theoretically either by applying the theory for charged spherical colloids with a correction for the chain character of the polyion or as an extension of the theory of the second virial coefficient for nonionic linear polymers. An example of an extension of the theory of the second virial coefficient for nonionic linear polymers to polyelectrolytes is the above-mentioned Yamakawa approach of using perturbation theory of excluded volume to calculate A_2 [42].

IX. SINGLE CHAIN STRUCTURE

In order to extract information on the single chain structure from SLS data, it is necessary to fulfill the condition of a single mode scattering, similarly to the extraction of molecular weight and second virial coefficient from SLS data (see Sec. VII). A further condition is that the scattering from polyions should not be influenced by intermolecular interference due to intermolecular interactions, i.e., the solution structure factor $S(\theta) = 1$. In this case the total

static scattering intensity is proportional to the single particle form factor $P(\theta)$ (in our case the polyion form factor) (see Eq. 9). The $P(\theta)$ (or $P(q)$) function contains information about the structure of the polymer chain. In principle, three regions can be distinguished in the form factor of a polymer chain assuming a Gaussian coil conformation: (i) $P(q) \cong \exp(-q^2 R_g^2/3)$ for $q^{-1} \gg R_g$, (ii) $P(q) \cong q^{-2}$ for $L_p < q^{-1} < R_g$, and (iii) $P(q) \cong q^{-1}$ for $q^{-1} < L_p$, where R_g is the radius of gyration of the chain and L_p is the so called persistence length (distance along the chain over which the polymer maintains a stiff rodlike structure). The first region is referred to as the Guinier regime and reflects the overall size of the coil, the second region reflects the Gaussian distribution of segments inside the coil, and the third region corresponds to scattering from rigid rods (rodlike segments). This behavior of $P(q)$ is schematically demonstrated in Figure 15, where $q^2P(q)$ is plotted vs. q (the so-called Kratky plot [47]). Naturally, $P(q)$ has different shape when chain conformation deviates from a Gaussian coil. In general, $P(q)$ in region (ii) scales as $P(q) \sim q^{-2/\nu}$, assuming that the radius of gyration scales as $R_g^2 \sim M^{\nu}$. The form of $P(q)$ in the Guinier regime is independent of the chain conformation and always yields the radius of gyration irrespective of the chain internal structure. Because of the limited q range available by light scattering ($q = 0.0042 - 0.031$ nm^{-1} for typical setups), only the Guinier regime and partly regime (ii) can be covered assuming typical sizes of polyions. A much larger range of q values can be obtained by small-angle x-ray scattering (SAXS) and small-angle neutron scattering (SANS). The radius

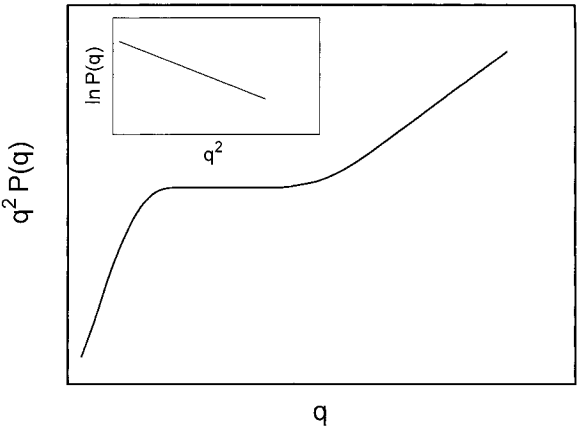

FIG. 15 Schematic representation of a Kratky plot $q^2P(q)$ vs. q for a Gaussian chain. $P(q)$ is the chain form factor, q is the scattering vector. The inset shows a Guinier plot ln $P(q)$ vs. q^2 (see text for details).

of gyration can be calculated from the initial slope ($q \to 0$) of the dependence $\ln P(q) \cong -(1/3)R_g^2 q^2$. The plot of $\ln P(q)$ vs. q^2 is referred to as the Guinier plot [48] (see inset in Figure 15).

An alternative method commonly used to determine the polymer radius of gyration is the Zimm's method [49]. It follows from Eq. 8 upon assumption of weak interparticle correlations [$p(\theta) = P(\theta) \equiv P(q)$] and on the assumption that particles (polymers) interact with each other through only one segment of each particle at a time, which is the better fulfilled the lower the concentration. It holds then that

$$\frac{Kc}{I(q)} = \frac{1}{M_w P(q)} + 2A_2 c \tag{30}$$

where $P(q)$ can be further expressed by a series expansion $1/P(q) = 1 + (1/3)R_g^2 q^2 + \cdots$ and thus

$$\frac{Kc}{I(q)} = \frac{1}{M_w} + 2A_2 c + \frac{1}{3}\frac{R_g^2}{M_w} q^2 + \cdots \tag{31}$$

The radius of gyration can be obtained from Eq. 31 by the Zimm method: angular dependencies are measured for several concentrations, then a double extrapolation to $c = 0$ and $q = 0$ is performed, and R_g is calculated from the slope of the $c = 0$ angular dependence. A more rigorous Guinier analysis is preferred especially for larger polymers ($\gtrsim$100 nm). We would like to note here that while the molecular weight obtained from light scattering is the weight average, the radius of gyration is the z-average, i.e., $R_g^2 = \langle R_g^2 \rangle_z$, and that values of the radius of gyration are not affected by the equilibrium dialysis in contrast to values of molecular weight and second virial coefficient.

Measurement of the polyion form factor in salt-free solutions by light scattering is extremely difficult due to strong intermolecular correlations, which can be avoided only at extremely low polyion concentrations. The scattering signal at these concentrations is, however, very weak. Consequently light scattering data in this concentration range are sparse. Krause et al. [50] reported SLS measurements on salt-free solutions of poly(styrenesulfonic acid) (HPSS) (M_w = 354,000 and 1,060,000) at concentrations as low as $c = 2.7 \times 10^{-4}$ g/L (Figure 16). The work was focused on larger q. Measured angular dependencies were well fitted by a single-chain form factor assuming a coillike chain conformation. The data were also compared to the calculated rod form factor, but very poor agreement was obtained. It was concluded that the chains are quite far from the fully extended conformation. These results disagree with the old view that strongly charged flexible chains in salt-free solution reach fully extended conforma-

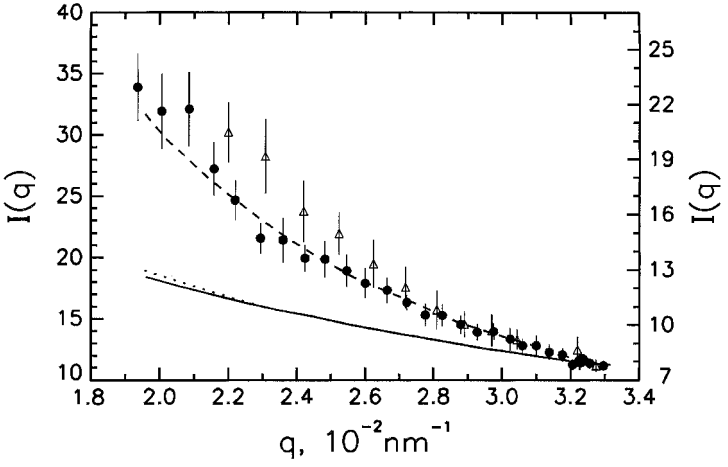

FIG. 16 Angular dependencies of excess scattering intensity for highly diluted salt-free aqueous solutions of poly(styrenesulfonic acid) (HPSS). (●) M_{w1} = 354,000, c = 2.7 × 10^{-4} g/L; (△) M_{w2} = 1,060,000, c = 3.46 × 10^{-4} g/L. The left ordinate corresponds to M_{w1}, the right ordinate to M_{w2}. Intensities are expressed in arbitrary units. The data are compared to the calculated rod form factor of both contour lengths (———, ·····) and a coillike form factor (– – – – –), respectively. (Adapted from Ref. 50.)

tions due to a strong repulsion between charges on the chain, but are in qualitative agreement with current understanding of polyion conformations based on analytical theory [51] or molecular dynamics simulations [52]. They predict that while the chains in dilute salt-free solutions are stretched beyond the good solvent structure, they do not attain a rigid rod structure. Chains do not change appreciably its conformation at low c but shrink appreciably at higher c before overlap or eventually even entanglement occurs. The shrinking is not uniform; chains become more coiled at longer length scales while at shorter length scales (several bond lengths) the structure is not altered [51,52]. This prediction is difficult to prove by light scattering due to the experimental requirement of low c. Relatively more powerful in this respect is SANS, which can utilize the contrast variation method to obtain form factors at conditions of strong interpolyion correlations. On the other hand, SANS is limited to high concentrations due to weak scattering signal [53–56].

Light scattering becomes more powerful at conditions of higher salt concentrations (typically $c_s > 10^{-3}$ M) where interpolyion interactions are partly screened. In this case higher polymer concentrations yielding higher and

more reliable intensities can be used. Results can be extrapolated from these polymer concentrations to infinite dilution, to assure that a pure form factor is obtained. In some cases, however, R_g for $c_s > 10^{-3}$ M was found independent of concentration in the range c = 0.02 to 0.2 g/L [31]. The most frequently treated problem regarding the polyion conformation is the dependence of R_g on c_s. Figure 17 shows data on NaPSS collected from several works [30,31,57]. The general feature is that R_g decreases with c_s approximately by a power law $R_g \sim c_s^{-\beta}$ with exponent $\beta \cong 0.15$. Results on other polyelectrolytes such as quaternized poly(vinylpyridine) [31], ionized poly(acrylic acid) [58], and bacterial hyaluronate [44] show similar behavior with β ranging from 0.15 to 0.25. The chains are appreciably coiled at higher c_s. For comparison with results in Figure 17, we can calculate R_g of chains upon assumption of a fully extended rodlike conformation. For the samples with the smallest and highest M_w, $R_g = \sqrt{L_c^2/12}$ = 142 and 534 nm, respectively (L_c is the contour length).

The chain conformation is determined by the interaction between neighboring segments and the interaction between distant segments along a polymer which, via chain flexibility, are located in each other's vicinity. The former effect determines the local chain stiffness. The latter is referred to as the excluded volume effect and influences the overall conformation. Both types of interaction can be of electrostatic and nonelectrostatic origin. In the absence of excluded volume effects (flexible polyions in a theta state or

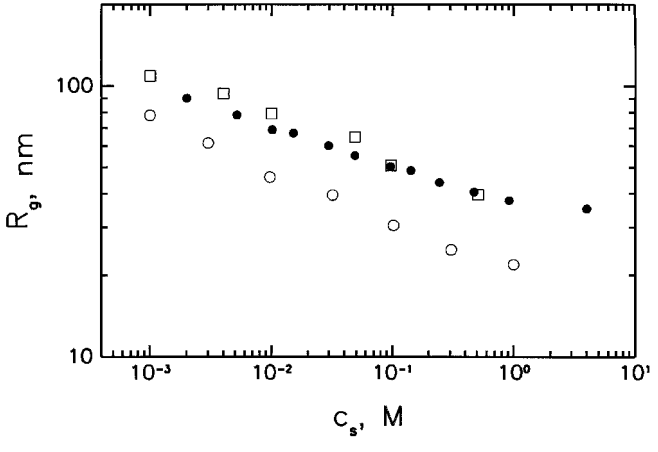

FIG. 17 Dependence of the radius of gyration of NaPSS chains in dilute solution on added salt concentration. Results by static light scattering for samples: (□) M_w = 1,000,000 from Ref. 57; (●) M_w = 780,000 from Ref. 30; and (○) M_w = 400,000 from Ref. 31.

semirigid polyions), the radius of gyration is referred to as ''unperturbed'' (R_{g0}). The local stiffening of the chain can be expressed in terms of a persistence length (distance along the chain over which the polymer maintains a stiff rodlike structure). The total persistence length L_p consists of an intrinsic and an electrostatic part, $L_p = L_0 + L_e$. The intrinsic part L_0 is due to the flexibility of the backbone without charges and is given by fixed bond angles, rotameric states, helical structures, etc. The electrostatic part L_e is given by the contribution of charge interactions to increased stiffness of the chain. The issue of L_e was a subject of intense theoretical work [59–63]. R_{g0} can be expressed in three different ways: (1) $R_{g0}^2 = L_c^2/12$ in the rod limit, where $L_p \gg L_c$; (2) $R_{g0}^2 = L_c L_p/3$ in the random coil limit, where $L_p \ll L_c$; and (3) in the wormlike chain limit, which represents a transition between cases (1) and (2):

$$R_{g0}^2 = L_p^2 \left[\frac{b}{3} - 1 + \frac{2}{b^2} (b - 1 + e^{-b}) \right] \tag{32}$$

where $b = L_c/L_p$. In the presence of excluded volume effects the ''perturbed'' radius of gyration R_g is usually expressed as $R_g^2 = \alpha_r^2 R_{g0}^2$, where α_r is referred to as the expansion factor. Light scattering measures the perturbed radius of gyration, and it is practically impossible to distinguish clearly between particular contributions of the local stiffness and the excluded volume effect to the polyion size solely on an experimental basis.

Several approaches were used to interpret SLS results on the polyion radius of gyration. Upon neglect of the excluded volume effect (assuming $R_g = R_{g0}$), L_p was calculated from the experimental R_g (data for M_w = 780,000, Fig. 17) via Eq. 32 [30]. Then L_e was obtained by fitting $L_p = L_0 + L_e = L_0 + \text{const } c_s^{\sigma}$, with the best fit found around $\sigma = -0.5$. The persistence length obtained in this way is only ''apparent''; nevertheless the power dependence on c_s is consistent with results of other experimental techniques [64] suggesting that $L_e \sim c_s^{-1/2}$ rather than the originally predicted dependence $L_e \sim c_s^{-1}$ by Odijk [61] and Skolnick and Fixman [60]. A different approach to the interpretation of experimental data was based on the combination of both excluded volume and persistence length effects [44,58]. First L_e was calculated on the basis of the OSF theory [60,61], then R_{g0} was calculated via Eq. 32, and finally R_g was calculated using the Gupta–Forsman empirical Monte Carlo expression for the expansion factor α_r [65]. A good agreement between calculation and experiment was achieved for several systems [44,58]. On the basis of substantially lower R_{g0} calculated values compared to experimentally obtained R_g, it was concluded that the electrostatic excluded volume effect dominates over the electrostatic persistence length effect at higher ionic strengths ($c_s \sim 10^{-3}$ M to 1 M). It was pointed out, however, that such treatment requires always $L_e < L_p$ [31].

Another approach to the interpretation of experimental data was based on the assumption of a uniform expansion of the chain, where the interaction energy between the segments was given by two terms: the usual short-range excluded volume and the electrostatic interaction via Debye–Hückel potential [31]. The resulting formula for the expansion factor α_r was used to fit experimental dependencies of R_g with two fitting parameters: the degree of ionization and the intrinsic excluded volume pseudopotential proportional to the Flory–Huggins interaction parameter. This method was applied to a large set of experimental data on R_g of quaternized poly(vinylpyridine) as a function of added salt concentration, backbone hydrophobicity, solvent dielectric permittivity, and the chemical nature of coions and counterions [31]. Although the physical significance of the obtained effective degree of ionization α_f and the intrinsic excluded volume w_0 as fit parameters was critically discussed [31], reasonable conclusions were drawn from such analysis of the data. The main results can be summarized as follows: R_g decreases with the chain hydrophobicity and increases with the solvent dielectric permittivity, and the exponent β in the relation $R_g \sim c_s^{-\beta}$ varies from 0.15 to 0.25 and does not significantly depend on the hydrophobicity below $c_s \sim 10^{-2}$ M. Above $c_s \sim 10^{-1}$ M, a downward curvature in the dependence of R_g vs. c_s (departure from $R_g \sim c_s^{-\beta}$) occurs and significantly depends on hydrophobicity. This curvature determines the solubility limit (''salting out effect'') at high c_s. In terms of the fitting parameters α_f and w_0, α_f dominates at low c_s, while w_0 controls ''the curvature'' and the precipitation at high c_s. A substantial effect on α_f and w_0 was found upon changing the chemical nature of the counterions, especially at high c_s ($c_s > 10^{-2}$ M). Recent molecular dynamics simulations on the effect of added salt on polyion conformation represent a new challenge. They are currently restricted to shorter chains, but they enable us to use full Coulomb interactions without approximations [66].

In the case of intrinsically rigid polyelectrolytes, such as DNA, experimental results [67] show that electrostatic persistence length calculated from the data shows no unique power law dependence on c_s. Compared to the OSF theory [60,61], a much better agreement with these data was achieved later by the calculation of L_e via numerical solution of the Poisson–Boltzmann equation for a toroidal polyion geometry [59,62]. These calculations showed that the exponent β in the scaling $R_g \sim c_s^{-\beta}$ varies from -1 to $-1/4$ upon increase of c_s. A breakdown of the OSF theory for flexible chains (unless $L_e \gg L_p$) was indicated by taking into account fluctuations in the chain configuration [63].

The last comment concerns polyions which are intrinsically rigid (not flexible or semiflexible). In this case, light scattering can provide information on the size and partly also on the shape of the polyions by comparing

experimental form factors with those calculated for different shapes (spheres, ellipsoids, rods). The estimation of shapes requires monodisperse samples [68]. This requirement is met usually for biological polymers.

X. INTERPOLYION CORRELATIONS

A common feature of scattering from polyelectrolyte solutions is the existence of peak(s) in angular dependencies of scattering intensity. Figure 18 shows an example of such a result obtained by static light scattering [50]. The sample is the same as the one as in Fig. 16 (HPSS, M_w = 354,000); the concentration is higher: $c = 5.5 \times 10^{-3}$ g/L to 2.8×10^{-2} g/L. The position of the peak maximum q_m changes as $q_m \sim c^{0.36}$. The same concentration scaling was measured for another sample in this work (M_w = 1,060,000) [50]. Similar angular maxima were reported by SLS for NaPSS by different authors [21], and also for a variety of other polyelectrolytes with different conformations (architectures), e.g., semiflexible proteoglycan monomers ($q_m \sim c^{1/3}$) [69], semirigid succinoglycan polysaccharide ($q_m \sim c^{0.45}$) [22], and rigid TMV particles ($q_m \sim c^{1/3}$) [70]. In accord with the fact that q_m increases with c, angular maxima were also obtained at high q by small-angle x-ray scattering (SAXS) and small-angle neutron scattering (SANS) at correspondingly high concentrations (~10 to 100 g/L) on a large variety of polyelectrolytes [53,54,71–74]. Apparently, qualitatively the same phenomenon is seen by various scattering techniques at different length scales according to the polyelectrolyte concentration. The existence of the peak is clearly due to electrostatic interactions. The addition of salt decreases the height of the peak and eventually, at high c_s, a complete disappearance occurs. The position of the peak either stays constant within experimental accuracy or a slight decrease of q_m is observed upon increasing c_s [70,72]. In the case of weak polyelectrolytes with variable charge densities, the peak gradually develops upon increase of charge density, and q_m moves towards higher q [74]. No change is observed upon stabilization of charge above the Manning–Oosawa counterion condensation limit. A shift of q_m towards higher q upon increasing charge density on variably sulfonated NaPSS was observed, too [75].

The presence of peaks in angular dependencies of scattering intensity can have, in general, several physical origins. Multiple sharp peaks appear in scattering from highly ordered crystalline lattices. Peaks appear also in scattering from simple liquids; the first and largest peak is followed by several others with gradually decreasing peak height. In all cases peaks arise due to interparticle correlations. These correlations are reflected in the solution structure factor $S(q)$, which was defined by Eq. 10, where the radial distribution function of particles $g(r)$ was introduced. We remind the reader that

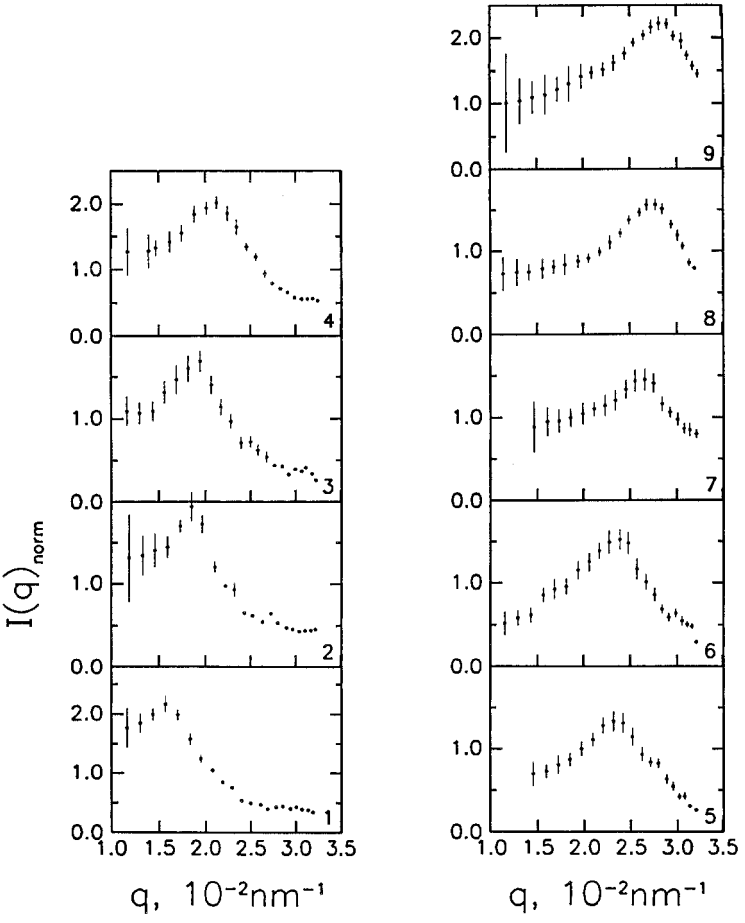

FIG. 18 Normalized excess scattering from salt-free aqueous solutions of poly(styrenesulfonic acid) (HPSS), M_w = 354,000, at concentrations (g/L): (1) 0.00553, (2) 0.00829, (3) 0.01106, (4) 0.01383, (5) 0.01660, (6) 0.01936, (7) 0.02213, (8) 0.02490, (9) 0.02766. (Adapted from Ref. 50.)

$g(r)$ reflects the probability of finding a particle at a distance r from another particle. Thus for the simplest case of hard sphere particles $g(r) = 0$ for $r < R_p$, where R_p is the particle radius. For $r > R_p$, the shape of $g(r)$ depends on the volume fraction ϕ. At low ϕ, $g(r) = 1$ for $r > R_p$ (step function). At high ϕ (ϕ exceeding 0.1–0.3), $g(r)$ exhibits a specific shape reflecting the so-called liquidlike structure (Figure 19). At r equal to the mean interparticle distance, $g(r)$ exhibits a peak [$g(r) > 1$] reflecting the nearest neighbor cor-

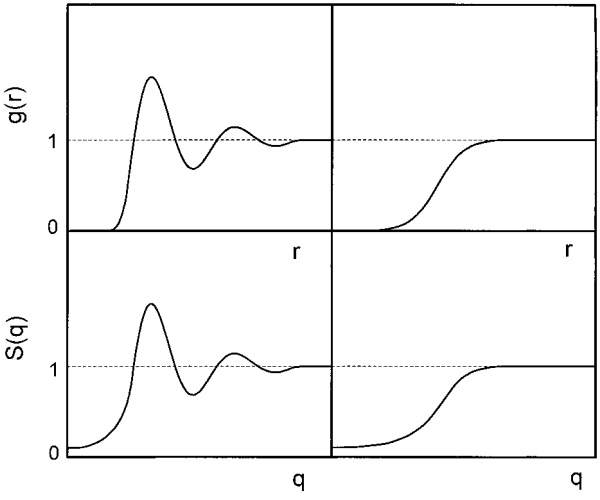

FIG. 19 Schematic representation of the radial pair distribution function $g(r)$ and corresponding solution structure factor $S(q)$ for two cases discussed in the text: liquidlike structure (left) and correlation hole effect (right). See text for more details.

relation. The first peak is followed by several smaller peaks reflecting the positional correlation between the central particle and the outer shells of more and more distant neighbors. These are gradually less and less correlated leading to gradually smaller peaks with $g(r) \rightarrow 1$ for $r \rightarrow \infty$. The corresponding $S(q)$ function is shown in Figure 19, too. Figure 19 shows also $g(r)$ corresponding to the so-called correlation hole effect. It is assumed that there is a shell (''hole'') around each particle, from which other particles are excluded. This assumption leads to a step function $g(r)$ with the discontinuity at r equal the ''effective particle size'' or, more realistically, to $g(r)$ of a sigmoidal shape with inflection point at r given by the ''effective particle size.'' This shape of $g(r)$ does not lead to the presence of peaks in $S(q)$. $S(q)$ is a continuously increasing function of q approaching $S(q) = 1$ at $q \rightarrow \infty$. For completeness, we note that $g(r)$ has multiple delta peaks in the case of ideal crystal lattices leading to sharp multiple peaks in $S(q)$, that for less perfect crystals (lattice defects, paracrystals) a broadening of peaks occurs, especially for higher order peaks, which decrease in height, and that for liquidlike order of polydisperse spheres, the resulting $S(q)$ is strongly modified (the main peak shifts to lower q and decreases in height while the oscillations after the main peak are washed out) [76].

In the correlation hole concept, the $S(q)$ function does not exhibit a maximum. However, upon combination with a monotonically decreasing $P(q)$

function, it leads to a maximum in the scattering intensity $I(q) \cong P(q)S(q)$. The idea of an effective volume of polyions, very similar to the correlation hole concept, was originally created by Doty and Steiner in early studies on proteins [77]. De Gennes et al. [78] defined the scattering peak in a semidilute polyelectrolyte solution as a demonstration of the short range order arising from the hard-sphere-like repulsion between correlation blobs. The chain is considered to be a random walk of correlation blobs of size ξ, where on length scales smaller than ξ the dilute solution scaling applies and on length scales larger than ξ all interactions are screened. The correlation blobs (correlation volumes) are space filling. The correlation volume can be considered as a space around each segment, from which other segments are excluded. The maximum in $I(q)$ is expected for $q_m \sim 2\pi/\xi \sim \kappa \sim c^{1/2}$ (κ^{-1} is the screening length). It was shown based on scaling arguments that $I(q) \ll I(q_m)$ for $q \to 0$ and $I(q)$ decreases as the form factor $P(q)$ for $q \gg q_m$ [78]. The correlation hole concept was used to calculate q dependencies of scattering intensities for spheres and rods [79] and for coils [80]. In the latter case the calculation is focused on semidilute solutions and therefore involves the radial distribution function of the coil segments instead of that of the centers of gravity of the coils.

In order to interpret experimental data, the knowledge of $S(q)$ is required. A direct evaluation of $S(q)$ from the scattering intensity as $S(q) \cong I(q)/P(q)$ is, however, not always accurate. While no problems occur in the case of spheres, the spatial distribution and mutual orientation may be correlated for rods. In solutions of linear flexible polyelectrolytes, the chain conformation reflected in $P(q)$ may depend on the spatial distribution reflected in $S(q)$. These facts must be taken into account in the interpretation of scattering peaks. Several approaches were made to separate $S(q)$ from experimental data. Light scattering results on NaPSS shown in Figure 18 were treated upon assumption of marginal cases for $P(q)$ as rods or Gaussian coils. In both cases $S(q)$ itself displays a peak [50]. In the case of light scattering data on TMV rodlike particles [70], the separation of $S(q)$ from $I(q)$ was justified by the absence of birefringence, which assures that the orientation distribution of rods is isotropic on a macroscopic scale. Again, $S(q)$ itself displays a peak. The SANS technique enabled experimental separation of $S(q)$ by two special methods. The first is based on isotopic labeling, where by deuteration of a fraction of polymer chains, some chains are made invisible for scattering in a properly mixed H_2O/D_2O solvent. When the fraction of visible chains approaches zero, $I(q) = P(q)$. $S(q)$ is obtained from the extrapolation of data acquired upon increasing the fraction of visible chains from zero to one [54]. $S(q)$ obtained in this way contains a clear maximum. The second method is the so called zero-average contrast method, which enables us to obtain partial structure factors (monomer–monomer,

monomer–counterion, and counterion–counterion). The monomer–monomer partial structure factor clearly exhibits a peak [53]. Another indication that $S(q)$ itself contains a peak comes from DLS data, where a minimum in diffusion coefficient appears concurrently with the presence of a maximum in scattering intensity. We remind the reader that $D_{app}(q) \cong 1/S(q)$ and refer the reader to Sec. V for more details. All these experimental observations contradict the correlation hole concept. The liquidlike correlations between polyions or polyion segments appear to be the plausible explanation of the presence of peaks in $S(q)$. The mean separation distance d_{exp} calculated from the position of the maximum in $S(q)$ upon applying Bragg's law $d_{exp} = 2\pi/q_m$ scales ad $d_{exp} \sim c^{-1/3}$ in the dilute regime in accord with simple geometrical considerations. At higher concentrations usually $d_{exp} \sim c^{-1/2}$, which agrees with the mean interchain spacing scaling for anisotropically aligned rods at $c > c^*$ in the Katchalsky cell model [81], but also for the isotropic model [78] (c^* is the crossover concentration from the dilute to the semidilute regime, at which polymers start to overlap). A crossover of the interpolymer structure factor peak scaling from $q_m \sim c^{-1/3}$ to $q_m \sim c^{-1/2}$ was obtained by simulations on linear flexible polyelectrolytes [82]. An experimental report on this transition [73] is based on SANS measurements on a large set of molecular weight standards of NaPSS. However, the question of the exact determination of the dilute–semidilute transition in linear flexible polyelectrolytes is still an open question in contrast to neutral polymers.

Similarly an open question is also what is the range of correlations and whether the presence of only one broad peak (sometimes a feeble secondary maximum) means just the nearest neighbor correlations or whether some kind of longer range order may be present, too. It is known that concentrated solutions of highly charged colloids (latex or silica particles) form colloidal crystals with long-range order. It was shown in a long series of experimental work [71,83] that a two-state structure forms in solutions of highly charged colloids at low concentrations, where ordered domains of particles coexist with less ordered or disordered regions and eventually voids (particle-free regions) may appear and grow. This requires the presence of long-range attractive interactions between like-charged particles [71,83]. Because of the large size of these particles, they can be photographed by ultramicroscopy and their trajectories monitored by video. Experimental mean separation distances of particles d_{exp} calculated from the position of scattering peaks are systematically lower than the theoretical mean separation distances d_0 calculated upon assumption of homogeneously dispersed particles. The relation $d_{exp} < d_0$ was reported also for some linear polyelectrolytes [72,84] and charged microgels of size $R = 20–50$ nm [85]. More work on polyelectrolytes in this area is clearly needed.

A different origin of a peak in the structure factor was proposed for weakly charged polyelectrolytes (~a few %) in a poor solvent (poor with respect to uncharged monomeric units between charges). It was shown that formation of mesophases (microscopic dense regions) originating as a result of the aggregation of poorly solvated parts of chains between charges, is possible. The periodicity of these microdomain structures λ^* may lead to a peak at $q_m \sim 2\pi/\lambda^*$ [86–88].

XI. INHOMOGENEOUS STRUCTURE ON LARGE LENGTH SCALES—POLYION DOMAINS (CLUSTERS)

The structure of polyelectrolyte solutions on large length scales is frequently not homogeneous. Polyion domains (clusters) with dimensions appreciably exceeding the size of single chains are present. They were found in a wide variety of synthetic and biological polyelectrolytes, e.g., poly(L-lysine) [18], *t*-RNA [89], DNA [90], BSA, latex particles, polynucleosomes [91], poly(methacrylic acid) [8,92,93], poly(acrylic acid) [40], NaPSS [13,14,94], quaternized poly(vinylpyridine) [95,96], poly(ethyleneimine) [97], and ionomers with very low charge densities [98], etc. They have no relation to specific chemical structure(s), which would lead to chemically specific type of aggregation. It appears that it is a universal property typical for charged systems as a group of macromolecular compounds. The origin of these structures, the mechanism by which macromolecules of like charge associate into larger structures, and detailed knowledge of their properties are still puzzling. We present in this section the current status of our understanding of this phenomenon while further investigation is in progress.

The presence of multichain domains is reflected in both static and dynamic light scattering results. A slow diffusive mode is observed in spectra of relaxation times and is clearly separated from other modes over a wide range of experimental conditions (see Figure 2). The diffusion coefficient ascribed to this mode is referred to as the slow diffusion coefficient D_s. The associated scattering amplitude is marked as A_s. A_s is calculated from the total scattering intensity by combination of SLS and DLS data (see Eq. 11 in Sec. III). Both A_s and D_s are angularly dependent (Figure 20). A_s is plotted in a Guinier representation, where the slope in the limit $\theta \to 0$ is given by $\ln A_s(\theta) \cong -(1/3)R_{g,app}^2(16\pi^2n^2/\lambda_0^2)\sin^2(\theta/2)$, where $R_{g,app}$ is the apparent radius of gyration. The characterization of R_g as ''apparent'' means that it is not sure whether the scatterers giving rise to the angular dependence of A_s are independent scatterers and that the Guinier approximation is fully applicable. Values of $R_{g,app}$ estimated from $A_s(\theta \to 0)$ evidently exceed dimensions of individual chains and range from 30 to 300 nm, according to ex-

perimental conditions. The plot in Figure 20 also shows that domains are polydisperse in size, giving a curvature in the Guinier plot. Thus the $R_{g,app}$ from the $\theta \rightarrow 0$ extrapolation is rather an upper estimate of the size. Assuming a specific shape of the scatterer, a more detailed analysis regarding polydispersity in sizes can be performed. Relatively broad distribution of sizes are obtained from $A_s(\theta)$ if the scatterers have simple spherical (or close-to-spherical) shape [99]. The distribution function of sizes $D(R_p)$ may range in extreme cases (more polydisperse than the example shown in Figure

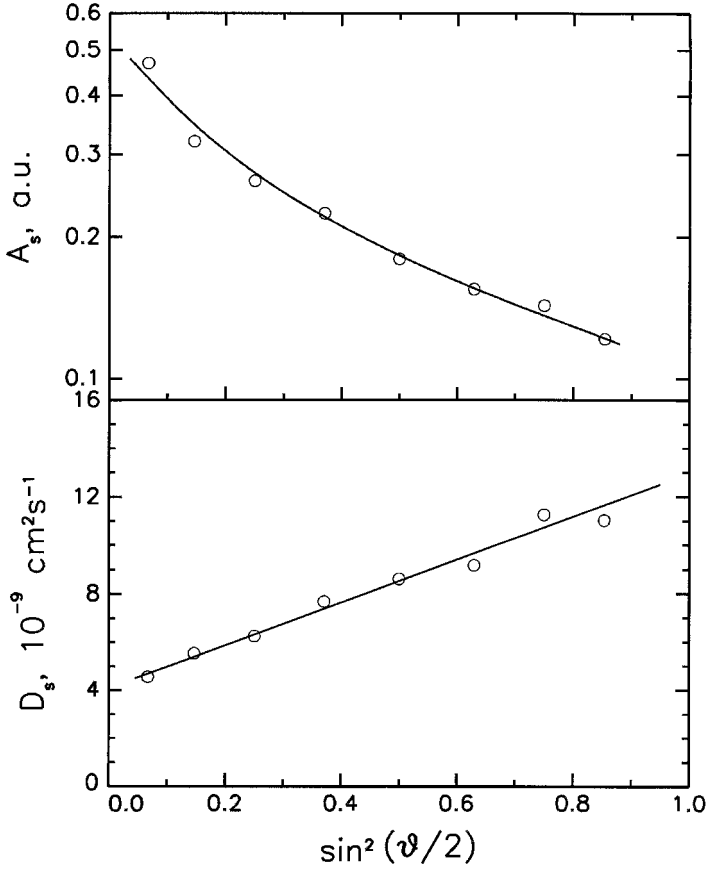

FIG. 20 Angular dependence of the scattering amplitude of the slow diffusive mode A_s (above) and slow diffusion coefficient D_s (below). Sodium poly(styrene sulfonate) (NaPSS) in water, no added salt, M_w = 710,000, polyion concentration c = 10 g/L. A_s is expressed in arbitrary units.

20) from ca. 30 to 300 nm. Very large domains are usually accompanied by a whole spectrum of more numerous smaller ones. The angular dependence of D_s can be explained by two effects: (1) as a consequence of the size polydispersity due to $D_s \cong R_p^{-1}$ and (2) due to the possibility of internal dynamics. In the presence of internal dynamics of scatterers, Eq. 16b yields upon expansion of $H(q)$ and $P(q)$ at low q

$$D(q) = D(0)(1 + CR_g^2q^2 - \cdots) \tag{33}$$

where C is a constant dependent on the internal architecture of the scattering particle and $D(0)$ covers interparticle interactions, i.e., $D(0) \neq D_0$ [100]. The C parameter is determined by the slowest internal mode of motion in the object and is in the range from 0 to 0.2. Thus for R_g comparable to or larger than q^{-1}, a measurable q dependence of D can be obtained. Although the applicability of Eq. 33 to the case of domains is questionable, a quantitative comparison of $R_{g,app}$ values obtained from static data and dynamic data via Eq. 33 was done [13]. Both methods yield rather consistent values except for some systematic shift on the order of 10–20%. The usage of the Stokes–Einstein formula $D_s = k_BT/6\pi\eta R_{h,app}$ to obtain at least apparent hydrodynamic radii is also questionable. A semiquantitative agreement between $R_{g,app}$ and $R_{h,app}$ is obtained upon using solution (not solvent) viscosity for η. The presence of polyelectrolyte domains is reflected also in small-angle x-ray and small-angle neutron scattering data as an upturn at low q. Intensity decreases upon decrease of q for $q < q_m$, but at low q increases again (q_m corresponds to maximum in intensity as described in Sec. X). This behavior was observed qualitatively in many cases, but only a more sophisticated instrumentation capable of working at q almost as low as the light scattering q range made a reliable investigation of the low g upturn possible [101,102]. The size of domains was found independent of polyion molecular weight in the very broad range investigated (NaPSS molecular weight standards with M_w = 5000 to 1 200 000) [13]. This means that the number of polyions per domain may vary from a few chains in the case of high-molecular-weight polyions ($M_w \sim 10^6$) to thousands of chains in the case of low-molecular-weight polyions ($M_w \sim 10^3$). There is currently available no detailed information on the domain internal structure. These objects, in order to be visible by light scattering, have to have scattering contrast, i.e., higher (or lower) refractive index with respect to the rest of the solution. Inhomogeneities in refractive index may arise due to a different arrangement or, more probably, simply due to a different concentration of polyions inside the domain compared to the rest of the solution. Taking into account large sizes of domains and the fact that the scattering contribution from domains A_s is in some cases comparable to the contribution from polyions A_f, it can be concluded

that the number density of domains and/or the scattering contrast of domains is low (see Eq. 9 and the discussion in Sec. III).

The slow diffusive mode associated with the existence of domains is clearly separable from the fast diffusive mode over a wide range of molecular weights and polymer concentrations. Figure 21 summarizes the results obtained on a set of NaPSS molecular weight standards at salt-free conditions [13,14]. It can be seen that D_s decreases with increasing polymer concentration and that this decrease is more pronounced the higher the molecular weight is. An empirical relation $D_s \sim c^{-\gamma M_w^{\delta}}$ with $\gamma = 0.0061$ and $\delta = 0.35$ describes satisfactorily the data at higher concentrations. At very low concentrations the fast and slow diffusion coefficients merge and the domain

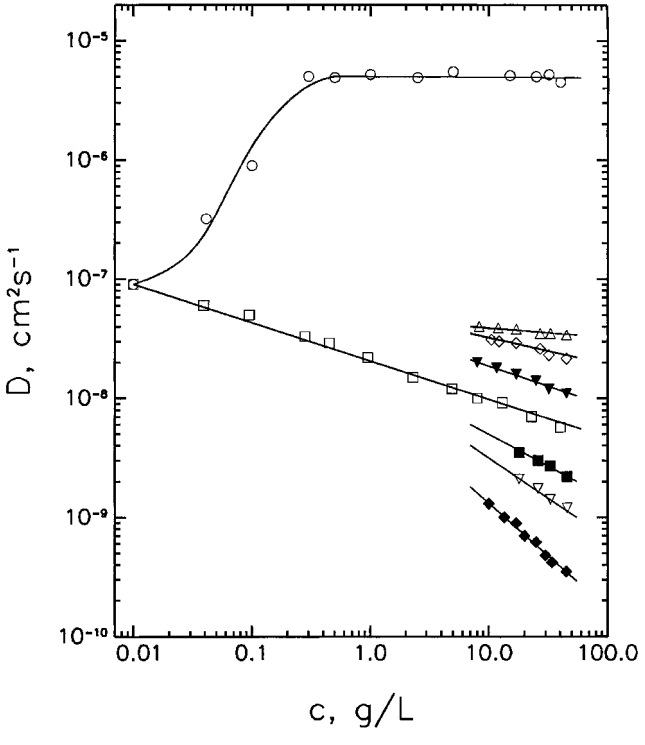

FIG. 21 Concentration dependence of the slow diffusion coefficient D_s. Sodium poly(styrene sulfonate) (NaPSS) in water, no added salt. M_w = (△) 5,000, (◇) 17,400, (▼) 47,300, (□) 100,000, (■) 200,000, (▽) 400,000, and (♦) 1,200,000. Data on the fast diffusion coefficient D_f for sample with M_w = 100,000 is shown for comparison (○). All diffusion coefficients were calculated from scattering data obtained at 90°. (Adapted from Refs. 13 and 14.)

effect seems to weaken. Due to a broad interval of concentrations and molecular weights used, it can be concluded that both dilute and semidilute regimes were covered by these experiments [13,14]. No signature of a dilute–semidilute transition was found in the data concerning the slow diffusive mode, similarly to the data on the fast diffusive mode (see Sec. V). The behavior of the domains does not significantly differ in the dilute and semidilute regimes, respectively. Domains were found also in binary polyelectrolyte mixtures of NaPSS with different molecular weights [34]. As can be seen from Figure 21, binary solutions at higher polymer concentrations yield appreciably different values of D_s (peaks at appreciably different time scales) according to the polymer molecular weight. Only one narrow peak corresponding to the slow diffusion appears in the spectrum upon mixing of binary solutions. This is consistent with the concept of the domain effect and rules out very early speculations that the slow mode could be ascribed to some kind of single-chain slow diffusive motions. In this case, two modes would be present upon mixing. Detailed data on polyion self-diffusion by the pulsed field gradient NMR technique [33] or forced Rayleigh scattering [93] show that polyion self-diffusion coefficients are substantially smaller than D_f but evidently larger than D_s.

The origin of domains (the mechanism by which like-charged polyions associate) is not clear yet, although it has been the subject of numerous experimental investigations. It was concluded that these structures are due to electrostatic interactions, not only because of the presence of charges as a necessary requirement for their occurrence but also because the slow mode appeared to be sensitive to charge interaction parameters like ionic strength and polyion charge. On the other hand, it was shown that the formation of domains is not due to the poor solvation of hydrophobic chain backbones in polar solvents (hydrophobic-type interactions). The possible role of the backbone solvation in the mechanism of the domain formation was investigated by two approaches: (1) Polymer–solvent pairs with different solvent quality for the uncharged chain were investigated. This was the case of poly(acrylic acid) and poly(methacrylic acid), which can be investigated in both the uncharged and the charged state [103]. (2) The solvent quality was worsened by approaching the lower critical temperature in the case of NaPSS, which is known for its strongly hydrophobic backbone [103]. In both cases no correlation between the strength of the domain effect and the backbone solvation was found. In addition, the slow mode was found also in many systems with weakly hydrophobic backbones. It was also reported in quaternized poly(2-vinylpyridine) in ethyleneglycol, which is a good solvent for both neutral and quaternized (''charged'') P2VP [95]. It should be noted at this point that the polyelectrolyte domain effect was found in a

variety of organic solvents, indicating that it is not related to some unique water property.

The response of the slow mode to charge interaction parameters like ionic strength and polyion charge appears to be essential for the understanding of the domain effect. As already discussed in Sec. III, it is necessary to decompose the total scattering intensity into contributions from particular modes and then to analyze them separately. Such analysis [12] shows that both fast and slow mode respond to charge interaction parameters, each in a different way. In general, the fast mode is much more sensitive to charge interaction parameters than the slow mode. The fast mode amplitude A_f increases dramatically upon increase of added salt or ionic strength. This increase is caused mainly by the increase of osmotic compressibility because the intrinsic scattering power of polyions (scattering contrast) is not changing dramatically. For instance no change in the refractive index increment of NaPSS was measured over an interval of added salt concentrations $c_s = 5 \times 10^{-6}$ M to 3 M NaCl (M. Sedlak, unpublished results). The increase of A_f over the range of available c_s is proportional to the polyion molecular weight M_w. This follows from the fact that A_f is independent of M_w at salt-free conditions, while at high c_s close to theta conditions A_f is directly proportional to M_w. Therefore the higher the polyion molecular weight, the larger the change of A_f over a given interval of c_s [12]. The slow mode is also responsive to ionic strength, though in the opposite way. The slow mode amplitude A_s becomes weaker upon an increase of c_s. Figure 22 shows the dependence of both scattering amplitudes A_f and A_s on ionic strength. The presence of counterions is taken into the calculation of the ionic strength as $i = c_s + 0.36c_pN_p/2$, where c_p is the polyion molar concentration, N_p is the degree of polymerization, the factor 0.36 accounts for the fraction of free counterions, and the factor 1/2 originates from the definition of the ionic strength $i = 1/2 \sum_{j=1}^{m} c_j Z_j^2$ where c_j and Z_j are the molar concentration and the charge of the jth ionic species, respectively. As can be seen from Figure 22, A_s smoothly decreases over all accessible ionic strengths, and no sharp transition at specific ionic strength occurs. It can be concluded that the presence of domains (slow mode) is rather a universal phenomenon that can be found in a very broad range of ionic strengths. Only the amplitude (strength of the effect) is varying upon changing ionic strength. The appearance of the slow mode is not connected with any kind of sharp transition similar to phase transitions with a discontinuity in some physical property at strictly defined conditions. The slow mode cannot be characterized as a sign of the existence of the system in some strictly defined ''special regime.'' The apparent sharp transition classified in literature as the ''ordinary–extraordinary'' transition is given mostly by a rapid decrease of the fast mode scattering amplitude upon lowering c_s, which results in a sharp increase of the

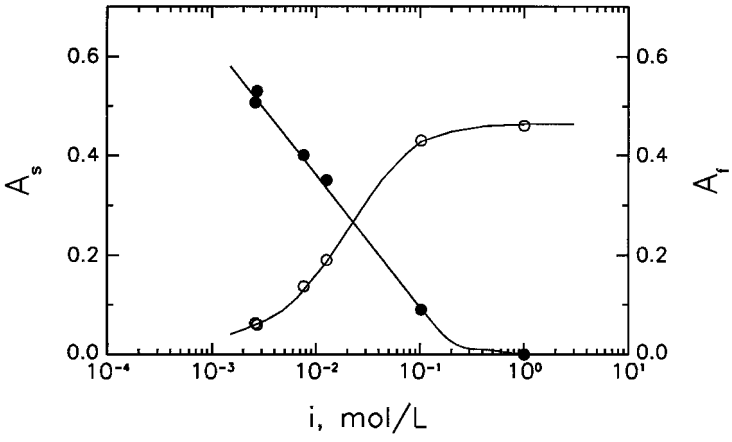

FIG. 22 Dependence of scattering amplitudes of the fast (○) and slow (●) mode on solution ionic strength. Both added salt (NaCl) and free counterions are included in the calculation of ionic strength. Amplitudes represent excess scattering and are expressed in units of the scattering intensity of a benzene standard. Sodium poly(styrene sulfonate) (NaPSS), M_w = 5,000, polyion concentration c = 5 g/L, scattering angle $\theta = 90°$. (Adapted from Ref. 12.)

A_s/A_f ratio and the apparently sudden appearance of the slow mode (or splitting of the diffusion coefficient). The higher the polyion molecular weight, the more misleading is the drop in the A_s/A_f ratio. Very clear is the situation in the case of low-molecular-weight samples such as those in Figure 22, where A_f does not exceed A_s over all c_s investigated and so A_s can be very precisely measured until very high c_s. There is no splitting of the diffusion coefficient at specific c_s in the sense that diffusion coefficients D_f and D_s are well separated over all c_s [12]. At fixed c_s, the amplitude of the slow mode increases with polyion concentration. This change is also rather smooth. The size of the domains as calculated from angular dependencies of A_s gradually decreases with ionic strength [12].

Another important result of the latest investigation on the nature of the domain effect is a conclusion that domains are metastable structures with very long lifetimes. In the following we discuss briefly the main qualitative aspects of the work, which is still in progress. It was found that domains are mechanically disrupted when solution passes through membrane filters with pores smaller than the natural dimensions of the domains. Such filtration is routinely used in light scattering to avoid dust particles in the scat-

tering medium. Domains become smaller and scatter less light after filtration. Importantly, the system does not spontaneously return back after filtration as expected for a system in a true equilibrium. Instead it stays in another metastable state (smaller domains, eventually also less dense, although the change in density is difficult to measure). An opposite process, i.e., coalescence of smaller domains into larger ones, was observed in certain cases only by force. The resistance against mechanical disruption is strongly dependent on the ionic strength. The smaller the ionic strength, the stronger the domains and vice versa. The ionic strength dependence of the slow mode amplitude as shown in Figure 22 can be therefore viewed also as an ionic strength dependence of the stability (strength) of domains.

After a detailed study on the mechanical resistivity where metastable states were influenced by force, a question arose whether these nonequilibrium structures can deviate spontaneously from a metastable state. Therefore systematic experiments were carried out when samples were investigated over long periods of time (up to 30 months). Indeed, a long-term time dependence was observed in some cases. The scattering amplitude of the slow mode gradually decreased from an initial value after the sample preparation to another value. The latter value was in some cases slightly smaller than the initial one; in other cases it was substantially smaller. In many cases no long-term drift (decrease) in the amplitude of the slow mode is measurable even over the above-mentioned long interval of investigation, indicating virtually infinite lifetime of the domains without changes. The metastability can be therefore understood mainly as the ability of the system to exist in different states at given physical and chemical conditions. The metastability explains also the observation [97,99] that the slow mode amplitude depends on the sample history (whether the sample is prepared directly at given c_s or indirectly by dissolving the polymer at different c_s and subsequently changing c_s).

In connection with above-mentioned results, the question arises whether the presence of domains is a result of the inability of the polyelectrolyte bulk material to disperse homogeneously in solution or whether there is also a mechanism by which the heterogeneous domain structure can be generated once the material is dispersed homogeneously in solution. In order to answer this question, careful experiments were performed. An example is shown in Figure 23. NaPSS with M_w = 50,000 was dissolved in 3 M NaCl and filtered with a very fine filter with a pore diameter 0.05 μm. Under such conditions the polymer material is dispersed completely homogeneously and there is no sign of any inhomogeneities at large length scales and no modes present at long times (Figure 23 above). There is one main mode corresponding to polyion diffusion, and another weak mode corresponding to salt diffusion as described in Sec. IV. Then the solution was dialyzed to decrease the salt

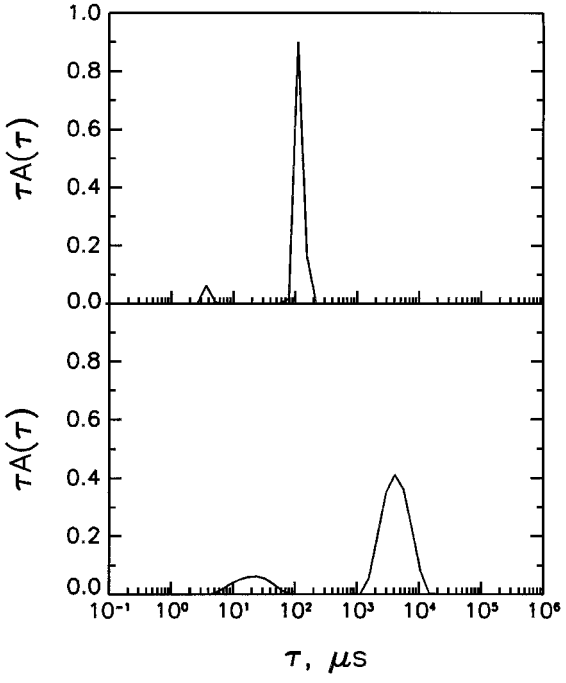

FIG. 23 Spectra of relaxation times for NaPSS, M_w = 50,000, c = 5 g/L, scattering angle θ = 45°. The polymer was first dissolved in 3 M NaCl (above). Afterwards this solution was dialyzed to lower the salt concentration to $c_s = 4 \times 10^{-3}$ M NaCl and measurement was repeated (below). Spectra are normalized so that peak areas correspond to scattering amplitudes of particular modes normalized to benzene scattering.

concentration to 4×10^{-3} M NaCl, and the measurement was repeated (Figure 23). The response of the polyion diffusion is that it becomes faster and the amplitude A_f is smaller. This is consistent with the expectation based on results already presented in Secs. V and XI. A pronounced slow mode with angularly dependent amplitude A_s appears after dialysis. Both spectra in Figure 23 are normalized so that peak areas correspond to scattering amplitudes of particular modes normalized to benzene scattering as described in Sec. III. It is clear from Figure 23 that the scattering contribution of the slow mode after dialysis is so large that it could not be hidden (''overscattered'' by the fast mode) in the sample before dialysis. This is important

since such objections were raised against similar previous dialysis experiments [104]. In order to be very careful and to rule out the possibility that domains in the dialyzed sample may form just during the filtration prior to measurement when polyions are pushed under pressure into micropores of the filter membranes, an alternative method of sample purification by centrifugation was used, too. In conclusion, it can be stated that polyions spontaneously form domains upon lowering ionic strength by dialysis.

The experimental results presented indicate that conditions can be met in polyelectrolyte solutions upon which attractive interactions between polyions become operative. The idea of attractive electrostatic interactions between objects of like charge is relatively old, but historically it was mostly related to charged colloids, which are bigger and thus enable more powerful experimental approaches to be used, such as direct observation by microscopy and videomicroscopy [71,83,105] or even a direct measurement of force between charged particles [105]. A very intense discussion on the attraction was initiated mainly by a long series of experimental work [71,83], where ordered domains of charged particles coexisting with less ordered or disordered regions and voids (particle-free regions) were observed. The experimental knowledge on the domain effect for polymeric macroions is currently much more limited and in our opinion still in a state of collecting fundamental experimental information, which is in many cases rather surprising and puzzling. Therefore we would not like at this stage to proceed into a deep discussion of how current concepts of charge attraction fit the picture in the case of polymeric macroions. This would also go beyond the scope of this chapter. Regarding the concepts developed for charged colloids [20,71,83], the question is whether similar behavior can occur on significantly smaller length scales (polymeric macroions and intermacroion distances are much smaller compared to colloids). Nevertheless several concepts of attraction between polymeric macroions were created. This includes a qualitative concept of charge fluctuation forces given by the dynamics of counterions shared by several polyions [91], analytical calculation [106] and Brownian dynamics simulations [107,108] of the attraction between charged rods given by charge fluctuations along rods due to the condensed multivalent counterions, attraction by expansion of the condensed layer between charged rods or rodlike segments with a decrease of free energy of the condensed layer with approach of polyions [109,110], and attraction due to excluded volume screening by topologically correlated objects [111]. An important aspect is also the violation of the summability of pairwise interactions in certain cases, which means that the overall interaction may be attractive even when the pairwise interaction is repulsive [112–114].

ACKNOWLEDGMENT

The author acknowledges support from the US-Slovak Science and Technology program and from the Slovak grant agency VEGA (grant No. 2/6100/99).

REFERENCES

1. Schneider J, Hess W, Klein R. A dumbbell model for the structure of charged rodlike macromolecules in dilute solution. Macromolecules 1986; 19:1729–1732.
2. Zernike F, Prins JA. Die beugung von röntgenstrahlen in flüssigkeiten als effekt der molekülarordnung. Z Physik 1927; 41:184–194.
3. Chu B. Laser Light Scattering. 2d ed. San Diego: Academic Press, 1991.
4. Schmitz KS. An Introduction to Dynamic Light Scattering by Macromolecules. San Diego: Academic Press, 1990.
5. Akcasu AZ. Dynamic scattering from multicomponent polymer mixtures in solution and in bulk. In: Brown W, ed. Dynamic Light Scattering: The Method and Some Applications. Oxford: Clarendon, 1993:1–75.
6. Berne BJ, Pecora R. Dynamic Light Scattering. New York: Wiley, 1976.
7. Lide DR, ed. CRC Handbook of Chemistry and Physics. 78th ed. Boca Raton: CRC Press, 1997.
8. Sedlák M, Koňák Č, Štěpánek P, Jakeš J. Semidilute solutions of poly(methacrylic acid) in the absence of salt: dynamic light scattering study. Polymer 1987; 28:873–880.
9. Oosawa F. Polyelectrolytes. New York: Marcel Dekker, 1997.
10. Manning GS: Limiting laws and counterion condensation in polyelectrolyte solutions I. Colligative properties. J Chem Phys 1969; 51:924–930.
11. Sedlák M, Koňák Č, Labský J. Dynamic behaviour of poly(methacrylic acid) in methanol solutions. Polymer 1991; 32:1688–1691.
12. Sedlák M. The ionic strength dependence of the structure and dynamics of polyelectrolyte solutions as seen by light scattering: the slow mode dilemma. J Chem Phys 1996; 105:10123–10133.
13. Sedlák M, Amis EJ. Dynamics of moderately concentrated salt-free polyelectrolyte solutions: molecular weight dependence. J Chem Phys 1992; 96:817–825.
14. Sedlák M, Amis EJ. Concentration and molecular weight regime diagram of salt-free polyelectrolyte solutions as studied by light scattering. J Chem Phys 1992; 96:826–834.
15. Pusey PN. The dynamics of interacting Brownian particles. J Phys A: Math Gen 1975; 8:1433–1440.
16. Ackerson BJ. Correlations for interacting Brownian particles. J Chem Phys 1976; 64:242–246.
17. Klein R. Interacting Brownian particles: the dynamics of colloidal suspensions. In: Mallamace F, Stanley HE, eds. The Physics of Complete Systems. Amsterdam: IOS Press, 1997:301–345.

18. Lin SC, Lee WI, Schurr JM. Brownian motion of highly charged poly(L-lysine). Effects of salt and polyion concentration. Biopolymers 1978; 17: 1041–1064.
19. Tivant P, Turq P, Drifford M, Magdelenant H, Menez R. Effect of ionic strength on the diffusion coefficient of chondroitin sulfate and heparin measured by quasielastic light scattering. Biopolymers 1983; 22:643–662.
20. Schmitz KS. Macroions in Solution and Colloidal Suspension. New York: VCH, 1993.
21. Drifford M, Dalbiez JP. Light scattering by dilute solutions of salt-free polyelectrolytes. J Phys Chem 1984; 88:5368–5375.
22. Morfin I, Reed WF, Rinaudo M, Borsali R. Further evidence of liquid-like correlations in polyelectrolyte solutions. J Phys II. 1994; 4:1001–1019.
23. Muthukumar M. Dynamics of polyelectrolyte solutions. J Chem Phys 1997; 107:2619–2635.
24. Koene RS, Mandel M. Scaling relations for aqueous polyelectrolyte-salt solutions. Macromolecules 1983; 16:220–236.
25. Odijk T. Possible relations for semidilute polyelectrolyte solutions. Macromolecules 1979; 12:688–693.
26. Dobrynin AV, Colby RH, Rubinstein M. Scaling theory of polyelectrolyte solutions. Macromolecules 1995; 28:1859–1871.
27. Rendon AV, Estrada HR, Noyola MM, Klein R. Electrolyte friction on charged spherical macroparticles: beyond the Debye–Hückel limit. J Chem Phys 1987; 86(5):2976–2985.
28. Schurr JM. A theory of electrolyte friction on translating polyelectrolytes. Chem Physics 1980; 45:119–132.
29. Tanahatoe JJ, Kuil ME. Dynamic light scattering of a flexible highly charged polyelectrolyte in the dilute concentration regime. Macromolecules 1997; 30: 6102–6106.
30. Peitzsch RM, Burt MJ, Reed WF. Evidence of partial draining for linear polyelectrolytes: heparin, chondroitin 6-sulfate, and poly(styrenesulfonate). Macromolecules 1992; 25:806–815.
31. Beer M, Schmidt M, Muthukumar M. The electrostatic expansion of linear polyelectrolytes: effects of gegenions, co-ions, and hydrophobicity. Macromolecules 1997; 30:8375–8385.
32. Zero K, Ware BR. Mobilities of poly-L-lysine molecules in low-salt solutions. J Chem Phys 1984; 80:1610–1616.
33. Oostwal MG, Blees MH, de Bleijser J, Leyte JC. Chain selfdiffusion in aqueous salt free solutions of sodium poly(styrenesulfonate). Macromolecules 1993; 26:7300–7308.
34. Sedlák M. Dynamic light scattering from binary mixtures of polyelectrolytes. 1. Influence of mixing on the fast and slow mode behavior. J Chem Phys 1997; 107:10799–10804.
35. Sedlák M. Dynamic light scattering from binary mixtures of polyelectrolytes. 2. Appearance of the medium mode upon mixing and comparison with experiments on binary mixtures of neutral polymers. J Chem Phys 1997; 107: 10805–10822.

36. Hammouda B. Dynamics of ternary polymer solutions. Macromolecules 1993; 26:4800–4804.
37. Pusey PN, Fijnaut HM, Vrij A. Mode amplitudes in dynamic light scattering by concentrated liquid suspensions of polydisperse hard spheres. J Chem Phys 1982; 77:4270–4281.
38. Akcasu AZ, Nägele G, Klein R. Identification of modes in dynamic scattering from ternary polymer mixtures and interdiffusion. Macromolecules 1991; 24: 4408–4422.
39. Vrij A, Overbeek JTG. Scattering of light by charged colloidal particles in salt solutions. J Colloid Sci 1962; 17:570–588.
40. Sedlak M. Static and Dynamic Properties of Polyelectrolyte Solutions. Ph.D. dissertation, Institute of Macromolecular Chemistry, Prague, 1989.
41. Takahashi A, Kato T, Nagasawa M. The osmotic pressure of polyelectrolyte in neutral salt solutions. J Phys Chem 1970; 74:944–946.
42. Yamakawa H. Modern Theory of Polymer Solutions. New York: Harper & Row, 1972.
43. Hara M, Nakajima A. Characteristic behavior of light scattering from polyelectrolyte in dilute solution region. Polymer Journal 1980; 12:701–709.
44. Ghosh S, Li X, Reed CE, Reed WF. Apparent persistence lengths and diffusion behavior of high molecular weight hyaluronate. Biopolymers 1990; 30: 1101–1112.
45. Eisenberg, H. Multicomponent polyelectrolyte solutions. Part IV. Second virial coefficient in mixed polyvinylsulfonate KCl systems near the θ temperature. J Phys Chem 1966; 44:137–153.
46. Takahashi A, Kato T, Nagasawa M. The second virial coefficient of polyelectrolytes. J Phys Chem 1967; 71:2001–2010. [Errata: Ibid. 72, 1968].
47. Glatter O, Kratky O. Small Angle X-ray Scattering. London: Academic Press, 1982.
48. Guinier A, Fournet G. Small Angle Scattering of X-Rays. New York: Wiley, 1955.
49. Zimm BH. The scattering of light and the radial distribution function of high polymer solutions. J Chem Phys 1948; 16:1093–1100.
50. Krause R, Maier EE, Deggelmann M, Hagenbuchle M, Schultz SF, Weber R. Static light scattering by solutions of salt-free polyelectrolytes. Physica A 1989; 160:135–147.
51. Donley JP, Rudnick J, Liu AJ. Chain structure in polyelectrolyte solutions at nonzero concentrations. Macromolecules 1997; 30:1188–1193.
52. Stevens MJ, Kremer K. Form factor of salt-free linear polyelectrolytes. Macromolecules 1993; 26:4717–4721.
53. Kassapidou K, Jesse W, Kuil ME, Lapp A, Egelhaaf S, van der Maarel JRC. Structure and charge distribution in DNA and poly(styrenesulfonate) aqueous solutions. Macromolecules 1997; 30:2671–2684.
54. Nierlich M, Boue F, Lapp A, Oberthur R. Characteristic lengths and the structure of salt free polyelectrolyte solutions. A small angle neutron scattering study. Colloid Polymer Sci 1985; 63:955–964.

55. Takahashi Y, Matsumoto N, Iio S, Kondo H, Noda I. Concentration dependence of radius of gyration of sodium poly(styrenesulfonate) over a wide range of concentration studied by small-angle neutron scattering. Langmuir 1999; 15:4120–4122.
56. Pleštil J, Ostanevich YM, Bezzabotonov VY, Hlavatá D, Labský J. Small-angle scattering from polyelectrolyte solutions: dimensions of poly-(methacrylic acid) chains in salt-free solutions. Polymer 1986; 27:839–842.
57. Borochov N, Eisenberg H. Stiff (DNA) and flexible (NaPSS) polyelectrolyte chain expansion at very low salt concentration. Macromolecules 1994; 27: 1440–1445.
58. Reed WF, Ghosh S, Medjahdi G, Francois J. Dependence of polyelectrolyte apparent persistence lengths, viscosity, and diffusion on ionic strength and linear charge density. Macromolecules 1991; 24:6189–5198.
59. Fixman M. The flexibility of polyelectrolyte molecules. J Chem Phys 1982; 76:6346–6353.
60. Skolnick J, Fixman M. Electrostatic persistence length of a wormlike polyelectrolyte. Macromolecules 1977; 10:944–948.
61. Odijk T. Polyelectrolytes near the rod limit. J Polymer Sci 1977; 15:477–483.
62. Bret ML. Electrostatic contribution to the persistence length of a polyelectrolyte. J Chem Phys 1982; 76:6243–6255.
63. Barrat JL, Joanny JF. Persistence length of polyelectrolyte chains. Europhys Lett 1993; 24:333–338.
64. Tricot M. Comparison of experimental and theoretical persistence length of some polyelectrolytes at various ionic strengths. Macromolecules 1984; 17: 1704–1708.
65. Gupta SK, Forsman WC. A general treatment of random-flight statistics with and without excluded volume. Macromolecules 1972; 5:779.
66. Stevens MJ, Plimpton SJ. The effect of added salt on polyelectrolyte structure. European Physical Journal B 1998; 2:341–345.
67. Hagerman PJ. Polyelectrolyte contribution to the persistence length of DNA. Biopolymers 1981; 20:251–268.
68. Kratochvíl P. Classical Light Scattering from Polymer Solutions. Amsterdam: Elsevier, 1987.
69. Li X, Reed WF. Polyelectrolyte properties of proteoglycan monomers. J Chem Phys 1991; 94:4568–4580.
70. Maier EE, Krause R, Deggelmann M, Hagenbüchle M, Weber R, Fraden S. Liquidlike order of charged rodlike particle solutions. Macromolecules 1992; 25:1125–1133.
71. Ise N. Ordering of ionic solutes in dilute solutions through attraction of similarly charged solutes—a change of paradigm in colloid and polymer chemistry. Angew Chem Int Ed Engl 1986; 25:323–334.
72. Ise N, Okubo T, Kunugi S, Matsuoka H, Yamamoto K, Ishii Y. ''Ordered'' structure in dilute solutions of sodium polystyrenesulfonates as studied by small-angle x-ray scattering. J Chem Phys 1984; 81:3294–3306.
73. Kaji K, Urakawa H, Kanaya T, Kitamaru R. Phase diagram of polyelectrolyte solutions. J Phys France 1988; 49:993–1000.

74. Pleštil J, Mikeš J, Dušek K. Investigation of local chain ordering in polyelectrolyte solutions by small-angle X-ray scattering. Acta Polymerica 1979; 30:29–32.
75. Essafi W, Lafuma F, Williams CE. Structure of polyelectrolyte solutions at intermediate charge densities. In: Schmitz KS, ed. Macro-ion Characterization. From Dilute Solutions to Complex Fluids. Washington DC: ACS Symposium Series, 1994:278–286.
76. Klein R. Static scattering properties of colloidal suspensions. In: Brown W, ed. Light Scattering: Principles and Development. Oxford: Clarendon, 1996: 30–102.
77. Doty P, Steiner RF. Macro-Ions. I. Light scattering theory and experiments with bovine serum albumin. J Chem Phys 1952; 20:85–94.
78. de Gennes PG, Pincus P, Velasco RM, Brochard F. Remarks on polyelectrolyte conformation. J Phys 1976; 37:1461–1473.
79. Benmouna M, Weill G, Benoit H, Akcasu Z. Scattering from charged macromolecules. I. Static structure factor. J Physique 1982; 43:1679–1685.
80. Koyama R. Small-angle neutron scattering of polymer solutions. Physica 1983; 120B:418–421.
81. Katchalsky A, Lifson S. The electrostatic free energy of polyelectrolyte solutions. I. Randomly kinked macromolecules. J Polymer Sci 1953; 11:409–423.
82. Stevens MJ, Kremer K. Molecular dynamics simulations of charged polymer chains from dilute to semidilute concentrations. In: Schmitz KS, ed. Macro-ion Characterization: From Dilute Solutions to Complex Fluids. Washington DC: ACS Symposium Series, 1994:57–66.
83. Ise N, Konishi T, Tata BVR. How homogeneous are ''homogeneous dispersions''? Counterion-mediated attraction between like-charged species. Langmuir 1999; 15:4176–4184.
84. Ise N, Okubo T, Yamamoto K, Matsuoka H, Kwai H, Hashimoto T, Fujimura M. Ordered structure in dilute solutions of poly-L-lysine as studied by small-angle x-ray scattering. J Chem Phys 1983; 78(1):541–545.
85. Antonietti M. Structure and viscosity of spherical polyelectrolyte microgels: a model for the polyelectrolyte effect? Polymer and Colloid NATO ASI, Les Houches, Sept 14–24, 1999.
86. Borue V, Erukhimovich I. A statistical theory of weakly charged polyelectrolytes: fluctuations, equation of state, and microphase separation. Macromolecules 1988; 21:3240–3249.
87. Joanny JF, Leibler L. Weakly charged polyelectrolytes in poor solvent. J Phys France 1990; 51:545–557.
88. Moussaid A, Schosseler F, Munch JP, Candau SJ. Weakly ionized polymers in a poor solvent. In: Schmitz KS, ed. Macro-ion Characterization. From Dilute Solutions to Complex Fluids. Washington DC: ACS Symposium Series, 1994:287–296.
89. Patkowski A, Gulari E, Chu B. Long range tRNA–tRNA electrostatic interactions in salt-free and low-salt tRNA solutions. J Chem Phys 1980; 73(9): 4178–4184.

90. Fulmer AW, Benbasat JA, Bloomfield VA. Ionic strength effects on macroion diffusion and excess light-scattering intensities of short DNA rods. Biopolymers 1981; 20:1147–1159.
91. Schmitz KS, Lu M, Gauntt J. Influence of ionic strength on the diffusion of polystyrene latex spheres, bovine serum albumin, and polynucleosomes. J Chem Phys 1983; 78:5059–5066.
92. Sedlák M, Koňák Č, Štěpánek P, Jakeš J. Influence of temperature on the polyelectrolyte dynamics. Partially neutralized solutions of poly(methacrylic acid). Polymer 1990; 31:253–257.
93. Austin ME. Conformational dynamics of a polyelectrolyte system: poly-(methacrylic acid) in aqueous media. Ph.D. dissertation, University of Wisconsin, Madison, 1989.
94. Drifford M, Dalbiez JP. Effect of salt on sodium polystyrene sulfonate measured by light scattering. Biopolymers 1985; 24:1501–1514.
95. Ermi BD, Amis EJ. Model solutions for studies of salt-free polyelectrolytes. Polymer preprints 1995; 36:371–372.
96. Förster S, Schmidt M, Antonietti M. Static and dynamic light scattering by aqueous polyelectrolyte solutions: effect of molecular weight, charge density and added salt. Polymer 1990; 31:781–792.
97. Smits RG, Kuil ME, Mandel M. Quasi elastic light scattering study on solutions of linear flexible polyelectrolytes at low ionic strengths. Macromolecules 1994; 27:5599–5608.
98. Bodycomb J, Hara M. Light scattering study of ionomers in solutions. 5. CONTIN analysis of dynamic scattering data from sulfonated polystyrene ionomer in a polar solvent (dimethylformamide). Macromolecules 1995; 28: 8190–8196.
99. Sedlak M. in preparation.
100. Burchard W, Schmidt M, Stockmayer WH. Influence of hydrodynamic preaveraging on quasi-elastic scattering from flexible linear and star-branched macromolecules. Macromolecules 1980; 13:580–587.
101. Matsuoka H, Schwahn D, Ise N. Observation of cluster formation in polyelectrolyte solutions by small-angle neutron scattering. 1. A steep upturn of the scattering curves from solutions of sodium poly(styrenesulfonate) at scattering vectors below 0.01 Å. Macromolecules 1991; 24:4227–4228.
102. Ermi BD, Amis EJ. Domain structures in low ionic strength polyelectrolyte solutions. Macromolecules 1998; 31:7378–7384.
103. Sedlák M. On the possible role of nonelectrostatic interactions in the mechanism of the slow polyelectrolyte mode observed by dynamic light scattering. J Chem Phys 1994; 101:10140–10144.
104. Ghosh S, Peitzsch RM, Reed WF. Aggregates and other particles as the origin of the ''extraordinary'' diffusional phase polyelectrolyte solutions. Biopolymers 1992; 32:1105–1122.
105. Crocker JC, Grier DG. Interactions and dynamics in charge-stabilized colloids. Materials Research Society Bulletin 1998; 23:24–31.
106. Ha BY, Liu AJ. Counterion-mediated attraction between two like-charged rods. Phys Rev Letters 1997; 79:1289–1292.

107. Jensen NG, Mashl RJ, Bruinsma RF, Gelbert WM. Counterion-induced attraction between rigid polyelectrolytes. Physical Review Letters 1997; 78: 2477–2480.
108. Stevens MJ. Bundle binding in polyelectrolyte solutions. Phys Rev Letters 1999; 82:101–104.
109. Ray J, Manning GS. An attractive force between two rodlike polyions mediated by the sharing of condensed counterions. Langmuir 1994; 10:2450–2461.
110. Ray J, Manning GS. Effect of counterion valence and polymer charge density on the pair potential of two polyions. Macromolecules 1997; 30:5739–5744.
111. Muthukumar M. Double screening in polyelectrolyte solutions: limiting laws and crossover formulas. J Chem Phys 1996; 105:5183–5199.
112. Schmitz KS. A many-bodied interpretation of the attraction between macroions of like charge: juxtaposition of potential fields. Langmuir 1997; 13: 5849–5863.
113. Podgornik R, Parsegian V. Charge-fluctuation forces between rodlike polyelectrolytes: pairwise summability reexamined. Phys Rev Letters 1998; 80: 1560–1563.
114. Weiss JA, Larsen AE, Grier DG. Interactions, dynamics, and elasticity in charge-stabilized colloidal crystals. J Chem Phys 1998; 109:8659–8666.

2

Molecular Dynamics Simulations of the Cylindrical Cell Model

MARKUS DESERNO, CHRISTIAN HOLM, and KURT KREMER Max-Planck-Institute for Polymer Research, Mainz, Germany

I. INTRODUCTION

''Polyelectrolytes are polymers bearing ionizable groups, which, in polar solvents, can dissociate into charged polymer chains (macroions) and small counterions'' [1]; see Figure 1. The combination of macromolecular properties and long-range electrostatic interactions results in an impressive variety of phenomena. It makes these systems interesting from a fundamental as well as a technological point of view.

Some of the relevant questions primarily motivated by scientific interest are the following. How is the size of a polyelectrolyte affected by molecular weight, intrinsic stiffness, solvent quality, or ionic strength? Which observables are well characterized by coarse-grained quantities such as a linear charge density, and which depend on chemical details? How are dynamic quantities like viscosity or electrophoretic mobility related to static properties of polyelectrolytes?

A thorough understanding of polyelectrolytes has become increasingly important in biochemistry and molecular biology. The reason is that virtually all proteins, as well as DNA, are polyelectrolytes. Their interactions with each other and with the charged cell membrane are still shrouded in mystery to a high degree. For instance, a puzzling question is why two equally charged objects should attract each other in the first place.

Unfortunately, theoretical understanding of polyelectrolytes is less developed than the understanding of the properties of neutral polymers. Some reasons are that the presence of long-range interactions renders the application of renormalization group techniques and scaling ideas much more difficult than in the neutral case. The reason is that many new length scales

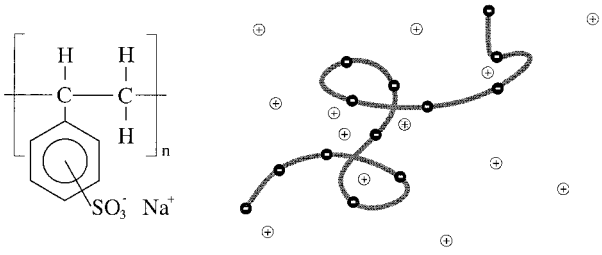

FIG. 1 Example of a flexible polyelectrolyte. Constitution formula for sulfonated polystyrene with sodium counterions (left) and a physicist's picture (right).

appear that are not well separated and therefore can influence each other in a complicated manner. The degrees of freedom related to the counterions contribute largely to the entropy. In contrast, the macroion itself is usually poor in entropy. Hence, there are effects which, despite the strong electrostatic interactions, are in fact entropy driven. For a given chain geometry, the competition between energy minimization and entropy maximization results in a particular equilibrium counterion distribution around the polyelectrolyte. However, this distribution is strongly coupled to the conformation of the macroion itself. In the spirit of John A. Wheeler's famous quote on the relation between space and matter in general relativity, one could say: the chain tells the ions where to move; the ions tell the chain how to curve.

Several approaches are conceivable in order to disentangle the intricate coupling between ion distribution and chain conformation. One possibility is to completely integrate out the counterionic degrees of freedom, yielding a density based Poisson–Boltzmann (PB) theory. On a linearized mean-field level this yields a Debye–Hückel-like theory characterized by a screened Coulomb potential between charged monomers. This approach is frequently used in theoretical descriptions, but it suffers from some consistency problems related to the validity of linearization. However, in the complete nonlinear PB equation the superposition principle no longer holds. This excludes the possibility of simply improving the screened pair-potentials.

A complementary approach is to fix the conformation of the chain and to focus on a detailed description of the counterion distribution. Usually polyelectrolytes stretch due to the electrostatic repulsion of their charged groups. Moreover, many important polyelectrolytes have a large intrinsic stiffness (e.g., DNA, actin filaments, or microtubules). Therefore a rodlike conformation is an obvious first choice; see Figure 2. The remaining problem of charged rods immersed into solution is much easier but is still far from being exactly solvable.

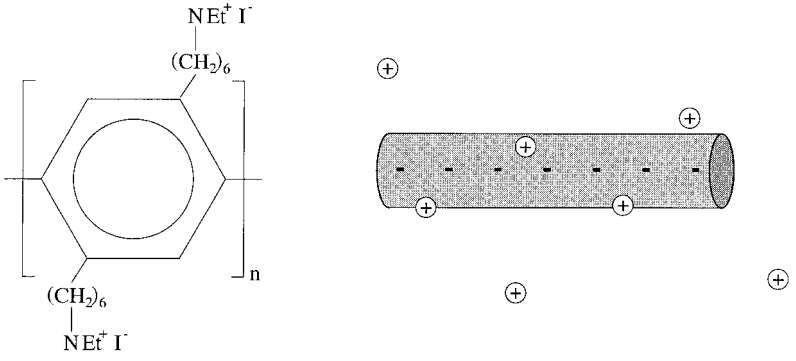

FIG. 2 Example of a stiff polyelectrolyte. Constitution formula for poly(*para*-phenylene) with iodine counterions (left) and a physicist's picture (right).

A common further approximation assumes that the investigation of a small subvolume containing only one rod and its counterions will suffice to unveil much of the interesting physics. The main justification for this approach is that the subvolume has zero net charge. Moreover, the counterions will also efficiently screen higher order multipoles. Hence the interactions between two such subvolumes, which are neglected when focusing on just one rod, will be fairly weak. This approximation is called the cylindrical cell model, and it provides the framework for this study.

The cell model might seem oversimplified—a reproach that cannot be entirely refuted. Nevertheless, it has several important advantages. Its high symmetry permits the definition of conclusive observables. In addition, the nonlinear PB equation can be solved *exactly* in this geometry. It also displays in a clear fashion the key electrostatic feature of a charged rod, viz., the logarithmic potential. Since the volume dependency of the entropy is logarithmic as well, this gives rise to the fascinating effect of partial counterion condensation [2,3]. While a charged sphere loses all its counterions upon dilution, a charged plane keeps all of them. For a charged cylinder the fraction of ions, which upon dilution remain in the vicinity of the macroion, can be anywhere between 0 and 100%.

In essence, strongly charged linear polyelectrolytes use their counterions to reduce their line charge density. Although this concept was introduced a long time ago, varying viewpoints persist. Already going beyond the mean-field description many questions arise: How closely condensed and tightly bound is the ''condensed layer''? What distinguishes condensed from uncondensed counterions? When is the mean-field PB theory a good approximation for real systems? And how does the presence of salt affect the

condensation phenomenon? The theoretical aspects of these investigations can be found in Ref. 4.

Here we present results of molecular dynamics simulations of a cell-like model for stiff polyelectrolytes [5]. We aim to (1) demonstrate the applicability of an alternative condensation criterion [4], (2) validate some proposed correlation corrections for the expected deviations from PB theory [6], and (3) study effects that qualitatively go beyond the mean-field level. The latter include overcharging, charge oscillations, a nonmonotonic zeta potential, and attractive interactions. At the end we try to shed light on specific ionic correlations in the systems investigated. Two-dimensional correlations on the surface of the rods are found to be present, but weakly developed. No hexatic order is observed. The three-dimensional pair correlation function is shown to exhibit a fairly long-range structure. However, this is proven to be imposed by the presence of the rods. This calls into question alternative explanations which assume a three-dimensional Wigner crystal to form on the background of the charged rods. Some simulations of other polyelectrolyte systems with explicit counterions can be found in Refs. 7–11.

II. THE LANGEVIN THERMOSTAT

An important application of molecular dynamics (MD) simulations is to create a sufficiently long trajectory of a model system through its phase space and—by appealing to ergodicity—to identify a time average over this trajectory with a suitable statistical ensemble average. The purpose of the present work is to study the thermodynamic properties of specific polyelectrolyte systems within the canonical ensemble. However, integrating Newton's equations of motion can by construction only yield a microcanonical average. This means that obtaining canonical averages requires going beyond standard Hamiltonian dynamics.

Today a large variety of methods exist that drive the system into the canonic state, e.g., by introduction of artificial degrees of freedom or by coupling the system to a heat bath via stochastic methods. The reader will find more details in Refs. 12 and 13. The choice for the present work is a Langevin thermostat [14]. This means that instead of integrating Newton's equations of motion, one solves a set of Langevin equations,

$$m_i \ddot{\boldsymbol{r}}_i = -\nabla U(\{\boldsymbol{r}_i\}) - \Gamma \dot{\boldsymbol{r}}_i + \boldsymbol{\xi}_i(t) \tag{1}$$

where $\boldsymbol{\xi}_i(t)$ is a δ-correlated Gaussian noise source with its first and second moments given by

$$\langle \boldsymbol{\xi}_i(t) \rangle = 0 \qquad \text{and} \qquad \langle \boldsymbol{\xi}_i(t) \cdot \xi_j(t') \rangle = 6 k_{\mathrm{B}} T \Gamma \delta_{ij} \delta(t - t') \tag{2}$$

where k_{B} is the Boltzmann constant and T denotes temperature. The friction

term $-\Gamma\dot{\boldsymbol{r}}_i$ and the noise $\boldsymbol{\xi}_i(t)$ can be thought of as imitating the presence of a surrounding viscous medium responsible for a drag force and random collisions, respectively. The second moment of $\boldsymbol{\xi}_i(t)$ is adjusted via an Einstein relation such as to reach the canonical state in the limit $t \to \infty$. The dynamics generated by the Langevin equation can alternatively be written as a general Fokker–Planck process. This permits a transparent proof of two important facts: (1) the stationary state of the process is the Boltzmann distribution and (2) it actually converges to it [15,16]. Since for small times the stochastic part is more important than the deterministic one, roughly because $\sqrt{t} \gg t$ for small t, it is actually not necessary to use Gaussian random variables in the simulation [17]. It suffices to use equidistributed random variables with first and second moment being identical to the Gaussian deviate and once more appeal to the central limit theorem.

The Langevin thermostat destroys momentum conservation. However, in reality a ''piece'' of momentum cannot just vanish but has to be transported away. This gives rise to long-range hydrodynamic interactions which are screened by the Langevin thermostat. Hereby, the screening length is inversely proportional to the square root of the friction coefficient [16]. Hence if one is interested in dynamic quantities and hydrodynamic interactions are potentially important, e.g., in a solution, one has to use a different thermostat. One possible choice is ''dissipative particle dynamics,'' which conserves momentum by adding the noise in a pair-wise fashion [18]. Incidentally, if the inertial term $m_i\ddot{\boldsymbol{r}}_i$ is negligible to the other ones, the dynamics becomes overdamped. However, since thermostatics cannot depend on the masses of the particles, the equilibrium properties must be the same in the limit $m_i \to 0$. This method is referred to as ''Brownian dynamics'' [12]. In the present study a Verlet integrator was used to integrate the systems of Langevin equations (1). The time step δt and the friction coefficient Γ were set to 0.01 and 1.0 in Lennard–Jones units (see below).

III. DESCRIPTION OF THE MODEL SYSTEM

The hexagonal prism is the space-filling object closest to a cylinder and thus a natural choice for an approximate implementation of the cell model. Still, it can be implemented in simple cubic periodic boundary conditions.

A. Generating a Cell Geometry

Compared to the spherical cell model, the cylindrical one presents one additional but crucial complication: the charged rod is infinitely long. Several methods have been proposed in the literature to handle this problem [19–22]. They essentially all use as a unit cell a hexagonal prism with a certain

height. This approximates the cylindrical cell by a space-filling object. They differ in the way of obtaining an infinite system via periodic replications and use various kinds of Ewald summations adapted to the respective symmetry. The present work takes a different approach, exploiting the fact that a hexagonal cell can also be obtained within a cubic symmetry.

The basic idea is the following: Take a cube and place a rod along the main diagonal. Upon periodically replicating this system two things happen:

1. The diagonal rod becomes infinitely long.
2. An infinite triangular array of such replicated rods emerges.

The resulting Wigner-Seitz cell of this lattice is a regular hexagon, which can alternatively be viewed as the unit cell. This is illustrated in Figure 3. Observe that the symmetry of the replicated system is still cubic.

Knowledge of the length L_b of the cubic box from Figure 3 is enough to specify the corresponding hexagonal cell model. All other lengths can then be expressed as functions of L_b; compare Figure 4. The separation between two neighboring rods is $d_{rod} = L_b\sqrt{2/3}$. From that follows the side length of the regular hexagon, which is also the maximum separation from the rod, as $s = L_b\sqrt{2}/3$ and its area as $A = L_b^2/\sqrt{3}$. Since the length of the rod segment within the cube is just $L_{rod} = L_b\sqrt{3}$, this immediately shows the

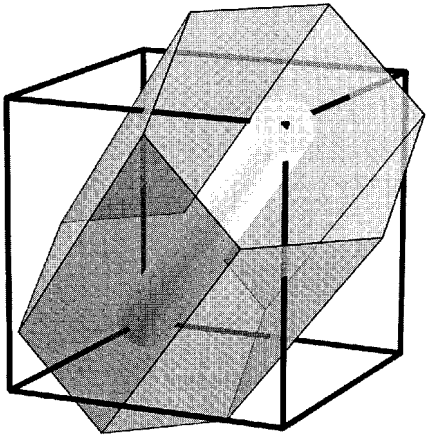

FIG. 3 Realization of the cell model. A rod placed along the main diagonal of a cube yields an infinite triangular array of infinitely long rods upon periodic replication of the original cube. The Wigner-Seitz cell of this lattice is a regular hexagon enclosing the rod. This therefore provides a way of obtaining a hexagonal cell without abandoning a cubic geometry.

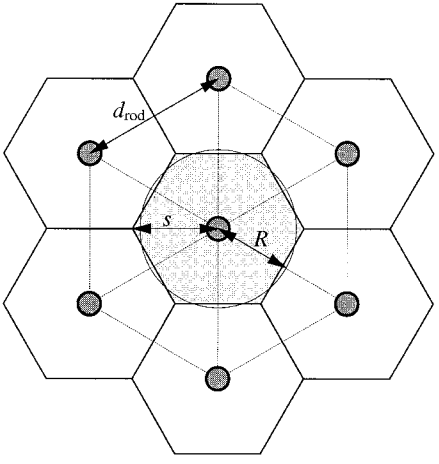

FIG. 4 Some geometric relations in the hexagonal cell model; compare text.

hexagonal cell to have the same volume as the cube. The radius R of a circle with the same area A is then given by $R = L_b/\sqrt{\pi\sqrt{3}}$. This value is most appropriately used for comparing results between the hexagonal and the cylindrical cell model.

If the line charge density of the rod is λ, electroneutrality requires the number of v-valent counterions to be $N = \sqrt{3}L_b\lambda/ve_0$. Hence the average counterion density is given by $n = N/L^3 = \sqrt{3}\lambda/ve_0L^2$ and is thus inversely proportional to L^2 instead of L^3. The number of counterions can therefore be written as $N = (\sqrt{3}\lambda/ve_0)^{3/2}n^{-1/2}$. This has the quite unusual implication of a smaller density requiring more particles. This is ultimately a consequence of the fact that the number of counterions cannot be chosen independently of the cell volume. While this makes the simulation of low densities rather expensive, it gives at the same time rather small dense systems. The latter problem can be circumvented by combining blocks of $2 \times 2 \times 2$, $3 \times 3 \times 3$ or even more elementary cubes to a big cube and using the latter as the unit box for the periodic boundary conditions.

Notice that the ratio between Debye length ℓ_D and rod separation d_{rod} can be written as

$$\frac{\ell_D}{d_{rod}} = \frac{[4\pi\ell_B v^2(\sqrt{3}\lambda/ve_0L_b^2)]^{-1/2}}{L_b\sqrt{2/3}} = \left(\frac{8\pi\xi v}{\sqrt{3}}\right)^{-1/2} \approx \frac{0.2625}{\sqrt{\xi v}} \tag{3}$$

For the important strongly charged case, in which the product of the Manning parameter ξ and the valence v is larger than 1, the Debye length is

smaller than the separation of the two rods. Even for $\xi v = 1$ it is only half as large as the distance between the rod axis and the Wigner-Seitz boundary. Note that this statement is independent of density.

The main advantage of this approach is that such a system can be treated with the plain cubic Ewald sum or one of its mesh-upgrades [13,23,24]. This permits a very efficient way for computing the long-range electrostatic interactions. Its main disadvantage is the coupling of counterion number and cell volume.

B. Interaction Potentials

A specification of two interaction potentials is necessary to describe the model system: (1) an excluded volume interaction preventing two particles from occupying the same position in space and (2) the long-range Coulomb potential.

One of the most widely used choices in molecular dynamics simulations for implementing a hard core is the purely repulsive Lennard-Jones (LJ) potential:

$$V_{\mathrm{LJ}}(r) = \begin{cases} 4\epsilon \left[\left(\dfrac{\sigma}{r}\right)^{12} - \left(\dfrac{\sigma}{r}\right)^{6} + \dfrac{1}{4} \right] & 0 < r \le r_{\mathrm{cut}} \equiv 2^{1/6}\sigma \\ 0 & r_{\mathrm{cut}} \le r \end{cases} \tag{4}$$

The plain Lennard-Jones potential is shifted up, so that its minimum located at $2^{1/6}\sigma$ has value 0, and set to zero beyond that point. The advantage of including the $-r^{-6}$ contribution instead of merely using the purely repulsive r^{-12} is that Eq. 4 is exactly zero beyond r_{cut} and merges smoothly to this value at r_{cut}. The use of a smooth hard core in molecular dynamics simulations is advantageous since the force is the derivative of the potential; therefore the latter should be differentiable. In fact, the derivative must also be bounded to ensure numerical stability of the discrete integrator.

The Coulomb potential of a charge Q is written as

$$\phi(r) = \frac{Q}{4\pi\varepsilon_0\varepsilon_{\mathrm{r}} r} \tag{5}$$

where $\varepsilon_0 = 8.85418 \times 10^{-12}\ \mathrm{C^2\ m^{-2}\ N^{-1}}$ is the dielectric constant of the vacuum and ε_{r} is the dielectric coefficient of the medium. For instance, water at room temperature has $\varepsilon_{\mathrm{r}} \approx 78.5$. The product $\varepsilon_0\varepsilon_{\mathrm{r}}$ will be abbreviated by ε. In the context of thermodynamics it is more convenient to measure electrostatic interaction strength using the so-called Bjerrum length $\ell_{\mathrm{B}} = \beta e_0^2/4\pi\varepsilon$, where $\beta := 1/k_{\mathrm{B}}T$. Recall that the Bjerrum length is the distance at which two unit charges have an interaction energy equal to $k_{\mathrm{B}}T$. For water

at room temperature $\ell_B \approx 7.14$ Å. From this relation one can map the simulation units to real units, if desired. The definition of ℓ_B permits the Coulomb potential of a charge Q to be written as

$$\phi(r) = \ell_B k_B T \frac{Q/e_0^2}{r} \tag{6}$$

Within the periodic boundary conditions employed during the simulations, the presence of such long-range interactions poses both mathematical and technical difficulties. We use the most efficient FFT accelerated Ewald sum, the P3M code, which scales almost linearly with the number of charges [23,24].

For a mechanical system three independent units suffice to define a complete unit system. Dealing with Lennard-Jones particles, it is convenient to choose mass, energy, and length. In that case the latter two are identified with the parameters ϵ and σ from Eq. 4, and m is viewed as the mass of the particle and set equal to one. Time is consequently measured in units of $\tau_{LJ} = \sigma\sqrt{m/\epsilon}$ and temperature in units of ϵ/k_B. Additionally treating electrostatic interactions requires a fourth unit, which here is chosen to be the positive elementary charge $e_0 \equiv 1.60219 \times 10^{-19}$ C.

In this work σ is always used as the unit length and ϵ is always set to the thermal energy $k_B T$. Temperature is implemented via the Bjerrum length. Mass is irrelevant—it would only be needed to translate the Lennard-Jones time τ_{LJ} into "real" time.

IV. POISSON–BOLTZMANN ESSENTIALS

A. The Poisson–Boltzmann Solution

At this stage we want to recall briefly the necessary knowledge about the PB solution of the cell model [25–29,4]. Consider an infinitely long cylinder of radius r_0 and line charge density $\lambda > 0$, coaxially enclosed in a cylindrical cell of radius R. Global charge neutrality of the system is ensured by adding an appropriate amount of oppositely charged (monovalent) counterions. In the following only the case of no extra salt will be discussed.

Within PB theory the individual counterions are replaced by a cylindrical counterion density $n(r)$, where r denotes the radial distance from the cylinder axis. This gives rise to an electrostatic potential $\psi(r)$ satisfying the Poisson equation

$$\left(\frac{d^2}{dr^2} + \frac{1}{r}\frac{d}{dr}\right)\psi(r) = \frac{e_0}{\epsilon}\, n(r) \tag{7}$$

where ϵ is the dielectric constant outside the cylinder and e_0 the positive

unit charge. Conversely, the potential is assumed to influence the counterion density via the Boltzmann factor

$$n(r) = n(R)\exp\{\beta e_0 \psi(r)\} \tag{8}$$

This implies the normalization of the potential to be $\psi(R) = 0$. the dimensionless *Manning parameter* is defined as

$$\xi := \frac{\lambda \ell_B}{e_0} \tag{9}$$

It counts the number of unit charges on the rod per Bjerrum length. In the following the main focus will be on the strongly charged case characterized by $\xi > 1$. A reduced electrostatic potential y and a screening constant $\kappa > 0$ are defined as

$$y(r) := \beta e_0 \psi(r) \tag{10}$$

$$\kappa^2 := 4\pi \ell_B n(R) \tag{11}$$

Combining the Poisson equation (7) with the Boltzmann factor from Eq. 8 gives the PB equation. Using Eqs. 10 and 11 it can be written as

$$y'' + \frac{y'}{r} = \kappa^2 e^y \tag{12}$$

This nonlinear differential equation has to be solved subject to the following boundary conditions for the electric field:

$$y'(r_0) = \frac{-2\xi}{r_0} \qquad \text{and} \qquad y'(R) = 0 \tag{13}$$

The correctly normalized solution to Eq. 12 and 13 can be written as [26,25,29,4]

$$y(r) = -2 \ln \left\{ \frac{r}{R} \sqrt{1 + \gamma^{-2}} \cos\left(\gamma \ln \frac{r}{R_M} \right) \right\} \tag{14}$$

Insertion of the general solution from Eq. 14 into the boundary conditions from Eq. 13 yields two coupled transcendental equations for the two integration constants γ and R_M:

$$\gamma \ln \frac{r_0}{R_M} = \arctan \frac{1 - \xi}{\gamma} \qquad \text{and} \qquad \gamma \ln \frac{R}{R_M} = \arctan \frac{1}{\gamma} \tag{15}$$

Subtracting Eq. 15*i* from Eq. 15*ii* eliminates R_M and provides a single equation.

$$\gamma \ln \frac{R}{r_0} = \arctan \frac{1}{\gamma} + \arctan \frac{\xi - 1}{\gamma} \tag{16}$$

from which γ can be obtained numerically. The second integration constant R_M, which will be referred to as the Manning radius, can be obtained from either of the Eqs. 15*i*/*ii* as soon as γ is known. Note finally that κ and γ are connected via

$$\kappa^2 R^2 = 2(1 + \gamma^2) \tag{17}$$

thereby ensuring the chosen zero of the potential.

Unfortunately, Eq. 16 has to be solved numerically. However, several rigorous statements can still be made:

1. The central approximation in Eq. 8 for the counterion density is that the exponential on the right hand side contains the potential instead of the potential of mean force.* Hence PB theory is by construction a low-density theory.
2. Eqs. 14–16 are invariant under the transformation $\gamma \to -\gamma$. Thus without loss of generality γ can be assumed to be nonnegative.
3. The right hand side of Eq. 16 is monotonically increasing with Manning parameter ξ. Hence γ increases with ξ and decreases with cell radius R. Also, from Eq. 15*ii* it is seen that R_M increases with γ.
4. A general valence v appears as a prefactor on the right-hand side of the Poisson equation (7) and in the exponent of the Boltzmann factor in Eq. 8, which requires the definitions of the potential y and the screening constant κ to incorporate an additional factor of v. This implies a replacement $\xi \to \xi v$ in Eqs. 13*i*, 15*i*, and 16. The remarkable consequence is that within PB theory changing valence or electrostatic interaction strength affects the integration constants γ and R_M in the same way. In particular, at given cell geometry $\{r_0, R\}$ the Manning radius R_M is a unique function of the product of the Manning parameter and the counterion valence, ξv.
5. Only for $\xi > \xi_{min} := \ln(R/r_0)/(1 + \ln(R/r_0))$ does Eq. 16 have a real and nonzero solution for γ, as can easily be seen by determining the slope of the right hand side at $\gamma = 0$. This can be understood in terms of the Manning radius. For $\xi = 1$ Eq. 15*i* gives $R_M = r_0$, i.e., R_M touches the surface of the cylinder. For $\xi > 1$ the Manning radius is outside the cylinder while for $\xi < 1$ it is inside and finally becomes 0 at $\xi = \xi_{min}$.

---

*The potential of mean force between two particles is the effective potential that emerges when integrating out all *other* particles. Apart from the limit of zero density it differs from the plain intermolecular potential. ''In a sense, one enters the realm of rigorous statistical mechanics when this distinction is clearly appreciated'' [30].

6. For values $\xi < \xi_{\min}$ the PB solution can be extended by analytic continuation over the complex numbers. This will not be pursued further, though. Note that the frequent statement of the PB solution changing its nature at $\xi = 1$ is only true in the limit $R \to \infty$ or $r_0 \downarrow 0$, in which indeed $\xi_{\min} = 1$.
7. The value of κ [or, equivalently, the boundary density $n(R)$] enters the theory only via Eq. 17, i.e., only in the combination κR.
8. Equation 16 implies the sequence of inequalities

$$\frac{\pi}{\ln(R/r_0)} \geq \gamma \geq \frac{\pi}{\ln(R/r_0) + \xi/(\xi - 1)}$$

The resulting asymptotic for γ in the dilute limit $R \to \infty$ gives rise to what is often called the ''Manning limiting laws.''

Using the formulae from the last section, the total charge per length $Q(r)$ within a cylinder of radius $r \in [r_0;\ \mathrm{R}]$ can be determined analytically by integrating the counterion density in Eq. 8:

$$\frac{Q(r)}{\lambda} = 1 - \frac{1}{\lambda}\int_{r_0}^{r} dr' 2\pi r' e_0 n(r') = 1 - \left(1 - \frac{1}{\xi}\right) - \frac{\gamma}{\xi}\tan\left(\gamma \ln \frac{r}{R_{\mathrm{M}}}\right) \tag{18}$$

Since $n(r) > 0$, $Q(r)$ decreases monotonically from $Q(r_0) = \lambda$ to $Q(R) = 0$. The latter follows from Eq. 15*ii* and is in agreement with the requirement of global charge neutrality. It is instructive to use the quantity

$$P(r) := 1 - \frac{Q(r)}{\lambda} \tag{19}$$

which is the integrated probability distribution of finding a mobile ion at distance r. In other words, it is the fraction of counterions found within a cylinder of radius r. For simplicity, $Q(r)$ and $P(r)$ will both be referred to as counterion distribution functions. At $r = R_{\mathrm{M}}$ the last term in Q vanishes, giving the Manning fraction $f_\xi := 1 - 1/\xi$ of ions within R_{M}. These are the ions that cannot be diluted away, if the cylinder radius is sent to infinity. The phenomenon itself is generally referred to as *Manning condensation* [2,3]. For ions with valence v, ξ has to be replaced by ξv in Eq. 18.

B. A New Approach to Quantifying Counterion Condensation

If the counterion distribution function P is known, the condensed counterion fraction can be characterized in the following ''geometric'' way: Eqs. 18 and 19 show that P viewed as a function of $\ln(r)$ is merely a shifted tangent function with its center of symmetry at $(\ln(R_{\mathrm{M}}); f_\xi)$. Since, however, $\tan''(0)$

= 0, Manning radius and Manning fraction can be found by plotting P as a function of $\ln(r)$ and localizing the point of inflection.

This property of P, derived within the framework of PB theory, can in turn be used to *define* the condensed fraction [4]. It provides a suitable way to quantify counterion condensation beyond the scope of PB theory, and it is exact in the salt-free PB limit. From here on this method will be referred to as the *inflection point criterion*. This criterion has the advantages of (1) not fixing by definition the amount of condensed counterions (f_ξ and R_M can be determined independently of each other), (2) reproducing the salt-free PB limit, namely $P(R_M) = 1 - 1/\xi$, and (3) quantifying the breakdown of the coexistence of condensed and uncondensed counterions in the high salt limit.

Notice finally that the appearance of the logarithm in the inflection point criterion is related to $\ln(r)$ being the two-dimensional Coulomb potential, i.e., the Green function of the cylindrically symmetric Laplacian. In the corresponding three-dimensional (spherical) problem of charged colloids the Green function $1/r$ would be the appropriate choice for plotting the radial coordinate [31,32]. More details can be found in Ref. 4.

V. GENERIC ION DISTRIBUTION FUNCTIONS

Poisson–Boltzmann theory systematically underestimates counterion condensation. Particularly its difficulties with high density, rod charge, Bjerrum length, and valence indicate the importance of neglected correlations.

On the plain PB level the radius r_0 of the rod is not a completely independent variable, since it enters only in the combination R/r_0; see Eq. 16. This suggests a further simplification of the model system: Instead of explicitly describing the rod as a separate object, one builds it from a sequence of small Lennard-Jones particles lined up along the main diagonal of the simulation cell. This is shown in Figure 5. No bonding potential is needed to maintain this configuration. Instead, the coordinates of the rod-particles are simply not propagated in time by the integrator. It would be quite natural to identify the distance of closest approach of two Lennard-Jones particles with the radius r_0 of the rod. However, a smooth potential like in Eq. 4 has no clear-cut closest distance. Satisfactory results are nevertheless obtained by alternatively using a ''thermal'' distance, at which the interaction energy is equal to $k_B T$. With $\epsilon = k_B T$, the choice in the present study, this yields a thermal distance and thus an effective rod radius of σ.

Upon leaving the PB level, the ratio between counterion diameter σ and rod radius r_0 becomes relevant. This is investigated in Ref. 33. Whereas systematic investigations of resulting effects have not been performed in the

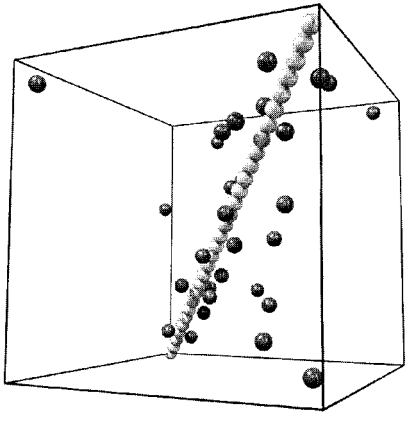

FIG. 5 Generic version of the cell model. Using the same geometry as illustrated in Figure 3, the rod is realized by a chain of ions lined up along the main diagonal. Concerning excluded volume interactions the particles forming the chain and the particles in solution are identical. Electrostatically, however, they differ by the sign of their charge.

For this particular system the Manning parameter is $\xi = 2.88 > 1$, and the implied condensation of counterions is clearly visible. Note that most of the systems studied here contain many more particles, but for the purpose of illustration a small system is more informative.

present work, Sec. VII presents results for systems mapped to physically relevant parameters, DNA and two kinds of poly(*p*-phenylenes), in which the rod has a considerably larger diameter than the counterions.

A. Density Dependence Within Monovalent Systems

At fixed rod radius of r_0 the relevant variable R/r_0 is changed by varying the cell size R and therefore the density. Here we present results for such a density scan for systems with $\ell_B/\sigma \in \{2, 3\}$. The monovalent and positively charged particles forming the rod were placed along the main diagonal with a center–center distance of 1.04245 σ, giving a line charge density of $\lambda = 0.959279\ e_0/\sigma$. In connection with the two presented values for the Bjerrum length this yields Manning parameters of $\xi \in \{1.919, 2.878\}$ and corresponding Manning fractions of $f_\xi = 1 - 1/\xi \in \{0.4788, 0.6525\}$. The cell radius R has been varied between 2.06σ and 124σ, which for monovalent counterions corresponds to ion densities of $7.2 \times 10^{-2}\sigma^{-3}$ and $2.0 \times 10^{-5}\sigma^{-3}$, respectively. The inflection point criterion from Sec. IV.B has been used to determine the radial extension of the condensed layer, $R_M^\star$, and the

fraction of ions within it, $f_\xi^\star = P(R_M^\star)$, where the star denotes the measured quantities. Recall that P is the integrated counterion distribution function from Eq. 19. Technically, the inflection points were determined by fitting a (2:2) rational polynomial in $\ln(r)$ to $r^2 n(r)$ in the vicinity of its minimum. A graphical illustration of the distribution functions is given in Figure 6.

The important things to observe are the following. The measured condensed fraction $f_\xi^\star$ is always larger than the fraction predicted by the PB theory. However, the fraction from the simulation decreases monotonically with decreasing density towards the Manning limit f_ξ. Such a deviation is to be expected, since PB is essentially a low-density theory neglecting local ion–ion correlations. Furthermore, this finding is in accord with two important features of correlations, namely they are more pronounced in dense systems, i.e., the free energy correction describing them goes to zero in the limit of zero density, and they lead to an enhanced counterion condensation [5].

In contrast to the clear tendency of the measured condensed fraction to decrease upon dilution, the behavior of the condensation radius $R_M^\star$ appears to be more complicated. There does not seem to exist a simple monotonic convergence of $R_M^\star$ towards R_M. Rather, for high densities the measured condensation distance is larger than the Manning radius, while for the investigated low densities it is smaller. Unfortunately, a clear-cut statement is difficult, since the localization of the point of inflection in P as a function of $\ln(r)$ is only possible with an error estimated to be of the order of 1%.

For Bjerrum length $\ell_B = 1\sigma$, corresponding to $\xi = 0.9593 < 1$, the radial distribution functions are compared to the PB predictions in Figure 7. It can be seen that the measured and PB predicted distributions almost coincide for all cell sizes under investigation. While this is to be expected for low densities, the remarkable agreement at high densities is somewhat surprising. Apparently, PB theory is a fairly good description of weakly charged systems, i.e., ones that are below the Manning threshold. A possible explanation is that upon increasing density two effects neglected within the PB theory start to compete. On the one hand, correlations increase and tend to enhance condensation. On the other hand, excluded volume interactions become more relevant and lower the counterion density at rod contact.

B. Fitting to a Generalized Poisson–Boltzmann Distribution

If the measured Manning radius $R_M^\star$ can be smaller than the PB prediction, this has the following consequence. Within PB theory f_ξ is monotonically increasing with R_M. Therefore $f_\xi^\star > f_\xi$, and $R_M^\star < R_M$ is incompatible with PB theory. It is impossible to describe such a $P(r)$ with a PB distribution

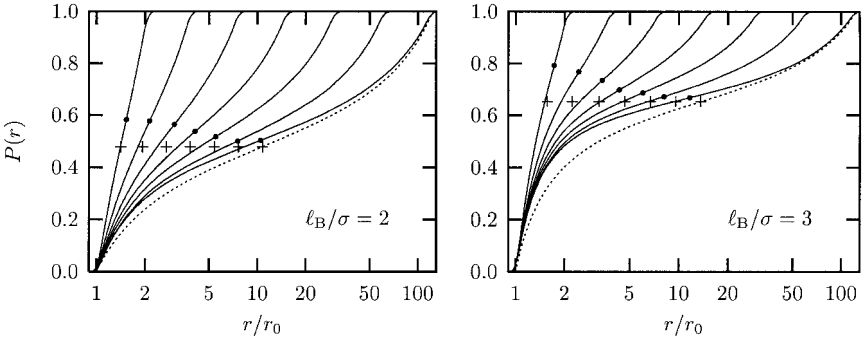

FIG. 6 Counterion distribution functions $P(r)$, as defined in Eq. 19, for various simulated densities. Note that an increasing cell radius corresponds to functions extending towards larger values of r. The heavy dots mark the points of inflection in P as a function of $\ln(r)$, while the crosses mark the positions at which those points would be located on the corresponding PB distribution functions. For the sake of clarity such a PB distribution is only plotted for the system with lowest density, i.e, $R = 123.85\sigma$ (dotted line).

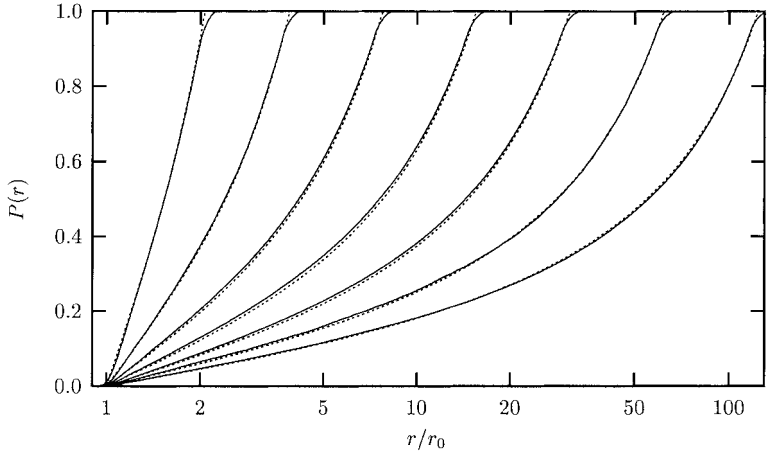

FIG. 7 Counterion distribution functions $P(r)$ (solid lines) for seven systems with the same dimensions as the ones in Figure 6, but with a Bjerrum length $\ell_B/\sigma = 1$. Since the resulting Manning parameter $\xi = 0.959 < 1$, counterion condensation is not expected to occur. This is borne out by the observation that the functions are convex up already at $r = r_0$. In these weakly charged systems the predictions of PB theory (dotted lines) are excellent and can hardly be distinguished from the simulation results.

function in which a somewhat enlarged effective Manning parameter $\xi^\star$ is used. Nevertheless, it would be desirable to use at least some of the knowledge about the ion distribution function from PB theory for evaluating relevant observables in a simulation or in a real experiment. To the lowest order, e.g., within a two-state model, the increase of counterion condensation can be ascribed to such an effective $\xi^\star = 1/(1 - f_\xi^\star)$. To break the monotonic connection between f_ξ and R_M one assumes that the functional form of P is given by the PB form in Eq. 18 and neglects the relation in Eq. 16. Using Eq. 15*i*, this suggests fitting the measured distribution in a region around the inflection point to the form

$$P_{\text{fit}}(r) = 1 - \frac{1}{\xi^\star} + \frac{\gamma^\star}{\xi^\star} \tan\left(\gamma^\star \ln \frac{r}{r_0^\star} + \arctan \frac{1 - \xi^\star}{\gamma^\star}\right) \tag{20}$$

with the three fit parameters $\xi^\star$, $\gamma^\star$ and $r_0^\star$.[†] The condensed fraction is then given by $f_\xi^\star = 1 - 1/\xi^\star$ and the condensed radius by $R_M^\star = r_0^\star \exp\{\arctan[(\xi^\star - 1)/\gamma^\star]/\gamma^\star\}$. Figure 8 illustrates this procedure for one system. While this approach might seem to be very powerful, it suffers from the drawback that the actual numbers depend on the chosen fitting region. Nevertheless, it provides an independent way of quantifying condensation and can even be applied to very noisy data, for which the localization of an inflection point in P as a function of $\ln(r)$ is otherwise virtually impossible.

C. Multivalent Ions

Up to now only monovalent ions have been investigated. For multivalent ions the prediction of the PB theory is that for the distribution function $P(r)$ only the product of the Manning parameter ξ and the counterion valence v matters. Therefore a system of monovalent ions at $\ell_B = 3\sigma$ is claimed to have the same distribution function as a system of trivalent ions at $\ell_B = 1\sigma$. It will now be shown that this statement is an artifact of the PB approximation. Figure 9 shows examples of systems that are ''complementary'' in the described sense. Not only is the condensation enhanced as compared to PB theory, but the enhancement is stronger for the case involving multivalent ions. Two different reasons may be suggested to explain this effect:

[†] It might seem strange to regard the rod radius as a free parameter, but there are two reasons for this. First, this does not force the fit to coincide with the PB form outside the chosen fitting region. Second, not even in a real experiment is the radius of a macroion always known in advance. Rather, it is often necessary to obtain this information within the same measurement [34].

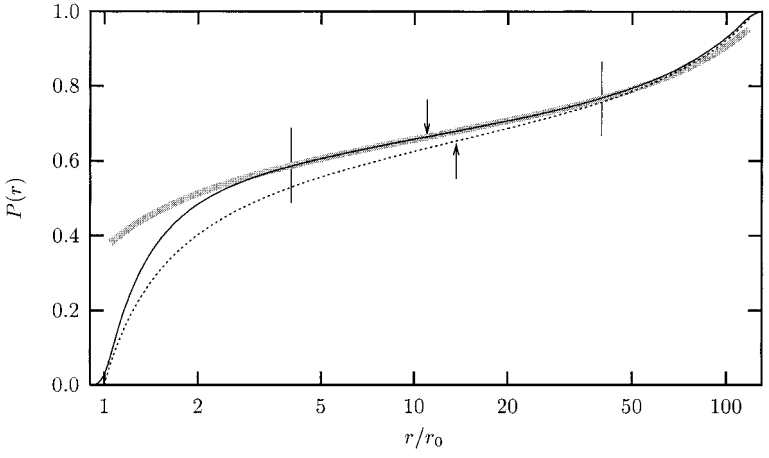

FIG. 8 The functional form in Eq. (20) has been fitted to the measured distribution function (solid line) of the system with $R = 123.85\sigma$ and $\ell_B = 3\sigma$ within the range $[4r_0; 40r_0]$ between the two vertical bars. The $\uparrow$ arrow indicates the inflection point of the PB distribution (dotted line), while the $\downarrow$ arrow indicates the corresponding point $(R_M^\star; f_\xi^\star) = (10.989\sigma; 0.664)$ of the fit (gray stripe). Note that $R_M^\star < R_M$ although $f_\xi^\star > f_\xi$. The result of the fit is $\xi^\star = 2.97414$, $\gamma^\star = 0.456611$, and $r_0^\star = 0.579034\sigma$.

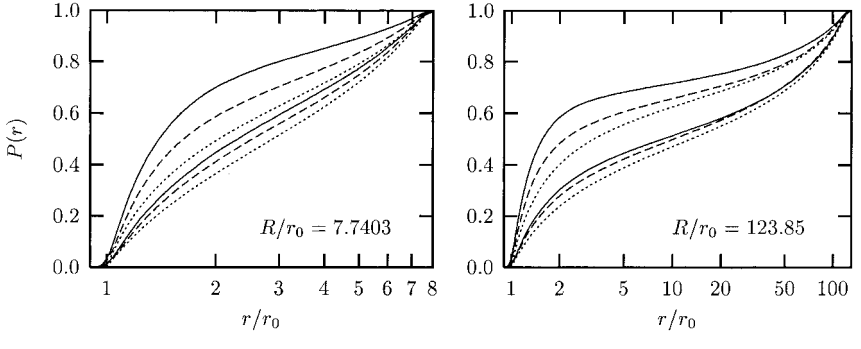

FIG. 9 Counterion distribution functions $P(r)$ versus r/r_0. The high (low) density situation is shown in the left (right) frame. The lower three curves are for $v\ell_B/\sigma = 2$, while the upper three correspond to $v\ell_B/\sigma = 3$. The systems with multivalent counterions (solid lines) always show a stronger condensation than the complementary systems with monovalent ions (dashed lines), which themselves show a stronger condensation than PB theory (dotted lines).

1. At a given charge density, multivalent systems have a lower number density and thus fewer particles. This lowers any kind of excluded volume interactions.
2. The relevant variable for describing the strength of correlation effects is $\ell = \ell_B v^2$ [6]. Hence, an increase in valence is more important than an increase in Bjerrum length.

However, the first point must be taken with great care for the following reason: Within PB theory the limiting expression for the contact density $n(r_0)$ is

$$\lim_{r\to\infty} n(r_0) = \frac{\lambda}{\pi r_0^2 e_0} \cdot \frac{(\xi v - 1)^2}{2\xi v^2} \tag{21}$$

For high rod charge, i.e., large ξ, this expression becomes independent of valence. Hence, replacing monovalent counterions by multivalent ones reduces their total number in the cell, but for a highly charged rod not their density at the rod surface. This statement is in fact an *exact* result for the cell model, and not a consequence of the PB approximation [27].

Taking this into account, the increased condensation must essentially be attributed to correlation effects. From an intuitive point of view one may argue like this: The continuous charge density from the PB theory is actually represented by individual charge carriers, and this discretization is clearly more pronounced for high valent ions. Increasing valence is a route away from density functional theory towards a situation in which strongly interacting individual particles correlate with each other. Particularly at high densities these correlations become very important. For instance, in the dense trivalent system the condensation is enhanced by 30% with respect to the PB prediction.

D. Addition of Salt

The influence of salt on the distribution functions has been discussed within the PB theory in detail in Ref. 4. The general finding was that a low salt content leaves the picture of Manning condensation qualitatively unchanged, while at increasing salt concentration a crossover between Manning condensation and simple salt screening occurs.

If one starts adding N salt molecules to the salt-free solution, one finds that the inflection point gets shifted to smaller values of r, hence the layer of condensed counterions contracts. The second finding is that the *amount* of condensation is only marginally increased. From a certain N on, two more inflection points appear in the region of high r/r_0. This happens typically for a corresponding Debye length being of the order of the cell size itself, indicating the appearance of a characteristic salt-induced change in the con-

vexity of P (as a function of ln r). Upon a further increase in N, one of the two new inflection points shifts towards smaller values of r/r_0, finally fusing with the Manning inflection point and "annihilating" it. Roughly speaking, the inflection points vanish if the Debye length characterizing the salt content becomes smaller than the radius of the condensed layer. In this case it is no longer meaningful to distinguish between condensed and uncondensed counterions. Indeed, for a very high salt content, where the Debye length is much smaller than the radius of the rod, the solution of the PB equation would be the one of a charged plane, and one may consider all excess counterions being condensed—no matter what the charge density of the rod is.

For three systems with numbers of salt molecules $N \in \{0, 104, 3070\}$ a simulation has been performed and compared to the PB prediction in Figure 10. As in the salt-free case the computer simulations show a more pronounced condensation effect towards the rod. Nevertheless, the shape of the distribution functions remains qualitatively the same. Note in particular that the appearance and disappearance of two points of inflection at $N = 104$ and $N = 3070$ respectively, which leads to extremely small curvatures in the PB distribution functions, also leads to very straight regions in the measured distribution functions. The crossover from Manning condensation to screen-

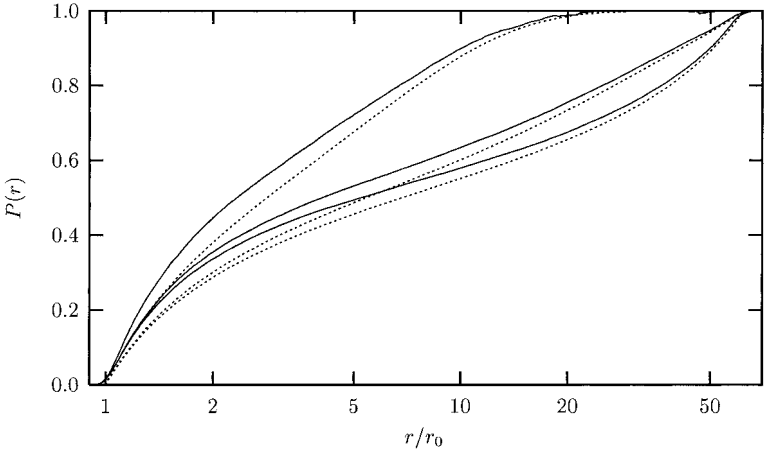

FIG. 10 Distribution functions $P(r)$ for a system that has $R/\sigma = 61.923$, $\ell_B/\sigma = 2.189$, $\xi = 2.1$, and monovalent ions. From bottom to top the number of salt molecules added to the simulation box of length $L_b = 144.446\sigma$ is 0, 104, and 3070, which corresponds to a salt Debye length of ∞, 22.9σ, and 4.2σ, respectively. The solid lines are the result of a simulation, while the dotted lines are the predictions of PB theory.

ing, as described within the PB theory, can be expected to be essentially correct.

It should not be overlooked, however, that the addition of salt ions will affect the distribution function much more dramatically if their valence is larger than the valence of the counterions. In this case, the salt counterions will accumulate in the vicinity of the rod at the expense of the lower valent ''real'' counterions as has previously been demonstrated in a system with a valence mixture of counterions [35].

The PB approach fails to describe the physical situation if one or more of the following conditions apply: (1) the electrostatic interactions are strong, (2) the counterions are multivalent or (3) the density is high. Results of a simulation under such conditions can be seen in Figure 11. Here, a system with box length $L_b/\sigma = 36.112$, i.e., 60 monovalent counterions and a cell size of $R/\sigma = 15.481$, and $\ell_B/\sigma = 4.1698$, i.e., $\xi = 4$, has been investigated after adding 1000 molecules of a 2:2 salt. Since this gives almost 17 times as much salt as counterions and a salt Debye length of $\ell_D/\sigma = 0.33 \ll R/\sigma$, this can essentially be viewed as a charged rod in a bulk 2:2 electrolyte. The most characteristic feature of the charge distribution function is that it overshoots unity, showing a charge reversal of the rod at distances around

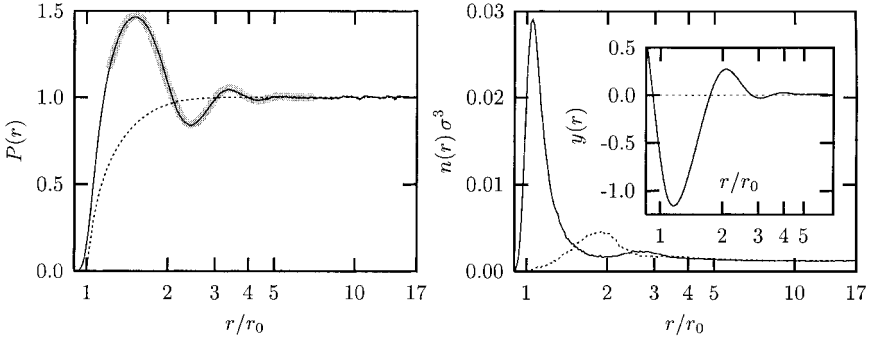

FIG. 11 Charge distribution for a system characterized by $L_b/\sigma = 36.112$, i.e., 60 monovalent counterions and a cell size of $R/\sigma = 15.481$, $\ell_B/\sigma = 4.1698$, i.e., $\xi = 4$, and 1000 molecules of a 2:2 salt within the box volume. The simulation shows a pronounced overcharging effect in $P(r)$ (solid curve, left frame), in contrast to PB theory (dotted curve). The charge oscillations can be described quite accurately by an exponentially damped sine function with period 1.89σ and decay length 0.85σ (gray stripe). The densities $n_{-2}(r)$ (solid line, right frame) and $n_{+2}(r)$ (dotted line) of negative and positive salt ions, respectively, demonstrate the effect of charge layering and local charge reversal, and the inlay shows the dimensionless electrostatic potential $y(r) = \beta e_0 \psi(r)$, which is also oscillating.

$r \approx 1.5\sigma$, while the simple PB prediction is clearly qualitatively off. This phenomenon is usually referred to as overcharging and has been predicted for the primitive cell model first from hypernetted chain calculations [36] and later by a modified PB approach [37,38]. Since $P(R) = 1$ for the reason of global electroneutrality, the overshooting above 1 at small distances implies the existence of a range of r values at which the mobile ion system is locally positively charged, i.e., with the same charge as the rod, such that $P(r)$ can eventually decay to 1. This is seen in the right frame of Figure 11, which shows that $n_{+2}(r) > n_{-2}(r)$ at $r \approx 2\sigma$. Since $P(1.5\sigma) \approx 1.45$, the rod and its innermost layer of condensed ions could be viewed as an effective rod of radius 1.5σ that is negatively charged with Manning parameter $\xi = 1.8$. Since this value is again larger than 1, it entails ion condensation, but this time of positive ions. In fact, it even leads to a second overcharging, as can clearly be seen in Figure 11, where $P(r)$—in decaying from 1.45—overshoots the value of 1 again. Overcharging can thus give rise to layering. In the presented example no less than three layers can clearly be made out. These local charge oscillations also reflect themselves in oscillations of the electrostatic potential, as demonstrated in the inset in the right frame of Figure 11. Notice that these oscillating potentials will also have pronounced effects on the interaction between such right polyelectrolytes.

VI. PRESSURE

Within the anisotropic cylindrical cell model the pressure is related to volume changes leaving the direction along the rod invariant. Simulations constantly yield a smaller osmotic coefficient than predicted by Poisson–Boltzmann theory. For multivalent systems it can even become negative.

A. Defining and Computing the Pressure

In a simulation, the pressure for the primitive cell model is a nontrivial variable to compute for two reasons: First, the long-range electrostatics has to be properly taken into account, and second, the system is inherently anisotropic, hence the relevant observable is the stress tensor.

Neglecting for a moment the second problem, the thermodynamic definition of the isotropic pressure within the canonical ensemble is

$$p = \left(\frac{\partial F}{\partial V}\right)_{N,T} \tag{22}$$

Together with the statistical definition of the free energy,

$$F = -\frac{1}{\beta} \ln \mathrm{Tr}\, \mathrm{e}^{-\beta H} \tag{23}$$

belonging to a system with standard Hamiltonian

$$H = \sum_{i=1}^{N} \frac{\boldsymbol{p}_i^2}{2m_i} + U(\boldsymbol{r}_1, \ldots, \boldsymbol{r}_N) \tag{24}$$

with potential energy U gives the pressure equation

$$pV = Nk_\mathrm{B}T - V \left\langle \frac{\partial U}{\partial V} \right\rangle \tag{25}$$

The angular brackets $\langle \cdots \rangle$ denote a canonical average. For the case of short-range interactions the contribution from U can be further simplified by using

$$\frac{\partial U}{\partial V} = \sum_i \frac{\partial U}{\partial \boldsymbol{r}_i} \cdot \frac{\partial \boldsymbol{r}_i}{\partial V} = \sum_i (-\boldsymbol{F}_i) \cdot \frac{\boldsymbol{r}_i}{3V} \tag{26}$$

Substituting this into the pressure equation (25) gives

$$pV = Nk_\mathrm{B}T + \frac{1}{3} \sum_i \langle \boldsymbol{r}_i \cdot \boldsymbol{F}_i \rangle \tag{27}$$

The second contribution is the average over the classical virial. Assuming only pair forces to be present, this part can be rewritten in terms of them. Let $\boldsymbol{F}_{ij}$ be the force which particle j acts onto particle i and let $\boldsymbol{r}_{ij} = \boldsymbol{r}_j - \boldsymbol{r}_i$ be the vector pointing from particle i to particle j. Then

$$\begin{aligned} \sum_i \boldsymbol{r}_i \cdot \boldsymbol{F}_i &= \sum_i \boldsymbol{r}_i \cdot \sum_j \boldsymbol{F}_{ij} = \frac{1}{2} \times \left[\sum_i \boldsymbol{r}_i \cdot \sum_j \boldsymbol{F}_{ij} + \sum_j \boldsymbol{r}_j \cdot \sum_i \underbrace{\boldsymbol{F}_{ji}}_{=-\boldsymbol{F}_{ij}} \right] \\ &= \frac{1}{2} \sum_{i,j} (\boldsymbol{r}_i - \boldsymbol{r}_j) \cdot \boldsymbol{F}_{ij} = -\sum_{i<j} \boldsymbol{r}_{ij} \cdot \boldsymbol{F}_{ij} \end{aligned} \tag{28}$$

It is of fundamental importance that these two expressions for the virial do *not* coincide under periodic boundary conditions. The reason is that the expression $\boldsymbol{r}_{ij} = \boldsymbol{r}_j - \boldsymbol{r}_i$ for the distance is no longer valid. In general, it has to be corrected by a suitable lattice shift to obtain the actual minimum image expression. The correct expression to use is the double sum, since it is manifestly translationally invariant, like the pressure. A thorough discussion is given in Appendix B of Ref. 39.

Concerning the electrostatic contribution to the pressure, there is the temptation to use the expression $\boldsymbol{r}_i \cdot \boldsymbol{F}_i$ from the virial also for the Coulomb pressure. The technical reason for this is that the Fourier space part of the Ewald sum does not easily give access to the pair forces. This is, however,

not a good idea due to (1) the difference between the two virials under periodic boundary conditions and (2) since the electrostatic energy explicitly depends on the box size. The latter is a consequence of the Coulomb potential not being short-ranged. Luckily, there is a very convenient way of computing the electrostatic contribution to the pressure. It can be derived by realizing that the electrostatic energy U^{C} is a homogeneous function of volume with degree $-1/3$, i.e.,

$$U^{\mathrm{C}}(\boldsymbol{r}_i, \ldots, \boldsymbol{r}_N; V) = V^{-1/3} U^{\mathrm{C}}(\boldsymbol{r}_i V^{-1/3}, \ldots, \boldsymbol{r}_N V^{-1/3}; 1) = V^{-1/3} U^* \tag{29}$$

where U^* is independent of isotropic volume changes. The derivative of the Coulomb energy with respect to the volume is thus given by

$$\frac{\partial U^{\mathrm{C}}}{\partial V} = \frac{\partial (V^{-1/3} U^*)}{\partial V} = -\frac{1}{3} V^{-4/3} U^* = -\frac{U^{\mathrm{C}}}{3V} \tag{30}$$

Combining Eqs. 27, 28, and 30 finally gives the desired pressure equation

$$pV = N k_{\mathrm{B}} T - \frac{1}{3} \sum_{i<j} \langle \boldsymbol{r}_{ij} \cdot \boldsymbol{F}_{ij}^{\mathrm{sr}} \rangle + \frac{1}{3} \langle U^{\mathrm{C}} \rangle \tag{31}$$

where $\boldsymbol{F}_{ij}^{\mathrm{sr}}$ are the short-range pair forces. In Ref. [40] the virial expression $\boldsymbol{r}_i \cdot \boldsymbol{F}_i$ for the pressure is compared with Eq. 31 and it is found that both expressions differ for finite systems. The latter is found to be much closer to the thermodynamic limit. Note also that for a repulsive hard core the virial contribution is positive, while the electrostatic contribution is one third of the energy density, which for neutral systems is usually negative.

For anisotropic systems the stress tensor is the relevant observable to compute. Whereas the ideal gas contribution to the pressure still remains isotropic, the virial must be replaced by

$$\mathsf{p}^{\mathrm{vir}} V = -\frac{1}{3} \sum_{i<j} \langle \boldsymbol{r}_{ij} \otimes \boldsymbol{F}_{ij}^{\mathrm{sr}} \rangle \tag{32}$$

where $\otimes$ denotes the tensor product. For the case of electrostatic interactions the derivation is more complicated and will not be presented here. The reader is referred to Ref. 41. The result is that within the framework of Ewald techniques the electrostatic contribution to the stress tensor, p^{C}, can be decomposed additively into a real space contribution $\mathsf{p}^{(r)}$ and a Fourier space contribution $\mathsf{p}^{(k)}$. They are given by

$$\mathsf{p}^{(r)} V = \frac{1}{2} \sum_{i,j} q_i q_j \sum_{m \in \mathbb{Z}^3}{}' \left[\frac{2\alpha}{\sqrt{\pi}} \mathrm{e}^{-\alpha^2 \boldsymbol{r}_{ijm}^2} + \frac{\operatorname{erfc}(\alpha |\boldsymbol{r}_{ijm}|)}{|\boldsymbol{r}_{ijm}|} \right] \frac{\boldsymbol{r}_{ijm} \otimes \boldsymbol{r}_{ijm}}{|\boldsymbol{r}_{ijm}|^2} \tag{33}$$

$$\mathsf{p}^{(k)} V = \frac{1}{2V} \sum_{k \neq 0} \frac{4\pi}{k^2} \mathrm{e}^{-k^2/4\alpha^2} |\tilde{\rho}(\boldsymbol{k})|^2 \left[\mathbb{I} - 2 \left(1 + \frac{k^2}{4\alpha^2} \right) \frac{\boldsymbol{k} \otimes \boldsymbol{k}}{k^2} \right] \tag{34}$$

Here, $\boldsymbol{r}_{ijm} = \boldsymbol{r}_i - \boldsymbol{r}_j + m L_{\mathrm{b}}$, and the canonical average has not been denoted

explicitly. For details of the notation and the Ewald techniques in general, the reader is referred to the literature [23,24]. Note that the connection to the isotropic case requires the trace of the pressure tensor to be equal to the mean electrostatic energy density, i.e.,

$$\mathrm{Tr}\ \mathsf{p}^{\mathrm{C}} = \frac{U^{\mathrm{C}}}{V} \tag{35}$$

After computing the electrostatic stress tensor, it can be rotated so that the rod points along the *z*-axis. The *xx* and *yy* components of the new tensor then give the pressure perpendicular to the rod, while the *zz* component is the contribution parallel to the rod. A more formal but still numerically convenient approach is the following. Let $\mathsf{d}^{\perp}$ be the projection operator into the plane perpendicular to the diagonal rod, i.e.,

$$\mathsf{d}^{\perp} = \mathbb{I} - \frac{1}{3}\begin{pmatrix}1\\1\\1\end{pmatrix} \otimes \begin{pmatrix}1\\1\\1\end{pmatrix} = \frac{1}{3}\begin{pmatrix}2 & -1 & -1\\ -1 & 2 & -1\\ -1 & -1 & 2\end{pmatrix} \tag{36}$$

Then, the pressure perpendicular to the rod is given by

$$p = \frac{\mathrm{Tr}(\mathsf{d}^{\perp}\cdot\mathsf{p})}{\mathrm{Tr}\ \mathsf{d}^{\perp}} = \frac{1}{2}\,\mathrm{Tr}(\mathsf{d}^{\perp}\cdot\mathsf{p}) \tag{37}$$

In fact, the whole purpose of using the stress tensor is to eliminate the pressure component along the stiff rod. After projecting it out, the left-hand side in Eq. 37 will then simply be referred to as the ''pressure'' of the rod system.

Observe finally that the stress tensor of the generic system constructed from a cubic symmetry is nevertheless *cylindrically* symmetric about the rod. The reason for this nice bonus is that the replicated cubic system still has a three-fold rotation symmetry about its main diagonal. In fact, looking at the new Wigner-Seitz cell only would suggest a sixfold symmetry. However, a symmetric second rank tensor cannot have a discrete rotation symmetry larger than twofold without having complete SO(2) symmetry at the same time. This becomes evident by recalling the possible symmetries of quadratic forms described by a symmetric 2×2 matrix.

B. Pressure Measurements Within the Generic Model

By using Eqs. 36 and 37 we present pressure measurements of the generic systems. However, instead of looking at the actual pressure, it is more convenient to look at the dimensionless osmotic coefficient $\hat{p}$, which is simply the pressure normalized by its ideal gas contribution

$$\hat{p} = \frac{p}{p^{\text{ig}}} = \frac{p}{nk_{\text{B}}T} \tag{38}$$

For an *isolated* cell the pressure is given by the particle density at the outer cell boundary. As a corollary, it must then also be positive. This is a rigorous statement, true for the spherical, cylindrical, and planar cell model [27]. It is a merit of the PB equation that it retains the validity of this exact relation. For the extended density functional theories this no longer holds, and additional terms appear [5].

The osmotic coefficient can be determined from the boundary density generalized to arbitrary valence,

$$\hat{p} = \frac{1 + \gamma^2}{2\xi\upsilon} \overset{R\to\infty}{=} \frac{1}{2\xi\upsilon} \tag{39}$$

where γ is the density dependent integration constant from Eq. 16, in which ξ is replaced by $\xi\upsilon$.

Figure 12 illustrates these measurements for monovalent counterions and three values of ℓ_{B}/σ = 1, 2, 3. Several things may be noted: The osmotic coefficient from the simulations is always smaller than the PB prediction. In the limit of low density both values converge. This also illustrates that the Manning limiting law from the r.h.s of Eq. 39 becomes asymptotically

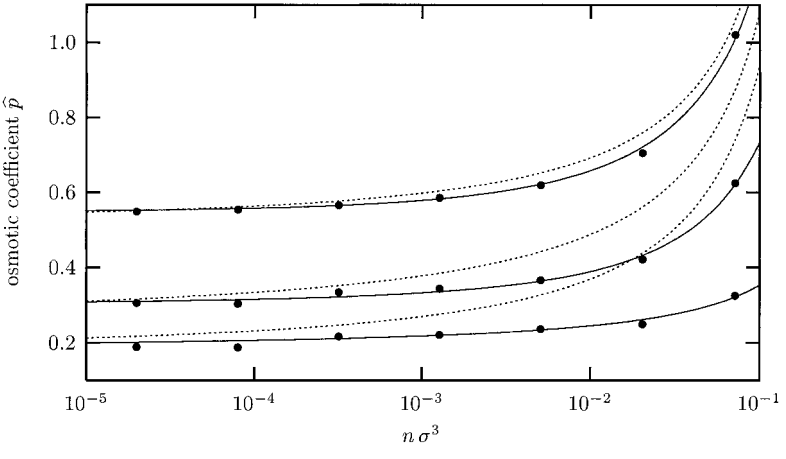

FIG. 12 Osmotic coefficient $\hat{p}$ versus $n\sigma^3$ for monovalent counterions. Heavy dots mark the measurements, while the solid lines are fits that merely serve to guide the eye. The dotted lines are the prediction of PB theory. From top to bottom the Bjerrum length ℓ_{B}/σ varies as 1, 2, 3. The error in the measurement is roughly as big as the dots themselves.

correct for dilute systems. Upon increasing the density, the osmotic coefficient rises less strongly than the PB prediction. This is more pronounced for systems with higher Bjerrum length, and consequently higher Manning parameter. Notice that this has a very remarkable side effect. Over a considerable range of densities the measured osmotic coefficient is much closer to the limiting law than to the actual PB prediction. This makes the Manning limit look much more accurate than it really ought to be. However, the surprising effect should not be over-interpreted, since the underlying reason is nothing but a fortunate cancellation of two errors of approximately the same size.

Those findings can be related to the measurements of the distribution functions presented in Sec. V, since the osmotic coefficient is a measure of the free counterions contributing to the osmotic pressure. The investigation of the distribution functions showed that the amount of condensed ions is always larger than the prediction from the PB theory. This entails a smaller osmotic coefficient. In addition, the stronger deviation at higher density, as well as the asymptotic correctness in the dilute limit, is in accord with the corresponding behavior of $\hat{p}$.

Also for the pressure it is interesting to investigate complementary systems in which the values of Bjerrum length ℓ_B/σ and valence v have been interchanged to keep the product ξv fixed. However, the dependence on only the product ξv is no longer universally valid, but restricted to the dilute limit. In this respect Eq. 39 for the osmotic coefficient is slightly deceiving. From its definition in Eq. 16 γ appears to depend only on ξv. This is true only if two systems with the same cell radius are being investigated. Since the average number density $n = \lambda/\pi R^2 e_0 v$ depends on v, two systems of different valence but the same average density differ in cell radius and universality breaks down. In fact, in the high density limit, in which $R = r_0 + \delta r$, the transcendental equation (16) defining γ can be solved analytically and yields $\gamma^2 = \xi v r_0/\delta r$. Substituting this into Eq. 39 for the osmotic coefficient gives

$$\lim_{R \downarrow r_0} \hat{p} = \frac{1}{2}\left(\sqrt{\frac{\lambda}{\pi r_0^2 e_0 v n}} - 1\right)^{-1} \tag{40}$$

In this limit $\hat{p}$ does no longer depend on Bjerrum length, but it increases with increasing valence. Since in the dilute limit $\hat{p}$ decreases with increasing valence, this implies the functions $\hat{p}(n)$ for different valences to intersect at some point.

Figure 13 summarizes the results of measurements on the multivalent systems with $v = 1, 2, 3$, which yield the same values of ξv as the monovalent ones investigated before. The most striking feature is the appearance

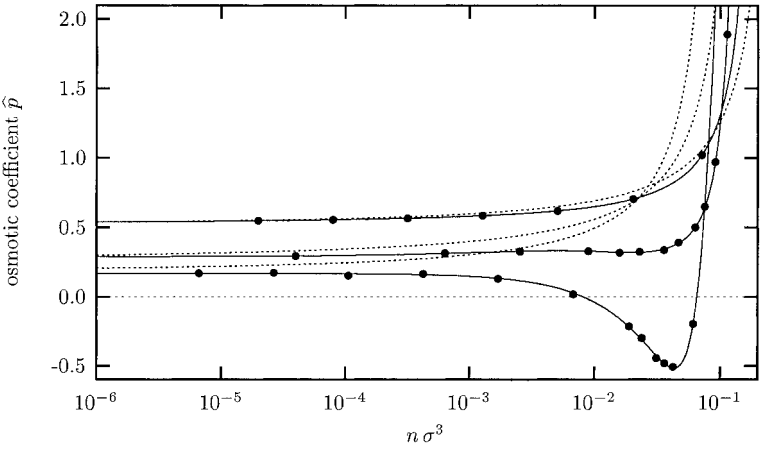

FIG. 13 Osmotic coefficient $\hat{p}$ as a function of density n for different valences. Heavy dots mark the measurements, while the solid lines are fits that merely serve to guide the eye. The dotted lines are the prediction of PB theory. From top to bottom the counterion valence v varies as 1, 2, 3, which gives the same value of ξv as the curves in Figure 12. The error in the measurement is roughly as big as the dots themselves.

of a negative osmotic coefficient in a certain density region of the trivalent case. This implies attractive interactions between the charged rods to be present. If the constraint of a fixed volume in the canonical *NVT* ensemble suddenly were to be replaced by a constant nonnegative pressure, the system would immediately contract, thereby reducing the separation of the rods. Similar observations have been reported in Refs. 20, 33, and 22. In order to trace back the origin of those attractive interactions, Figure 14 displays the osmotic coefficient in the divalent and trivalent cases, split into two contributions: (1) the nonelectrostatic part, comprising ideal gas contribution and the short-range virial, and (2) the electrostatic part, which for visual convenience is plotted with a reversed sign. Hence the difference between those two curves gives the curves in Fig. 13. Several things should be noted:

1. The electrostatic part leads to a monotonically increasing attraction with increasing density. It is almost twice as strong in the trivalent case.
2. The very strong increase of the osmotic coefficient at large densities is due to the virial, i.e., due to repulsive ion–rod and ion–ion interactions.
3. The negative pressure in the trivalent case is the result of a ''sudden'' drop in the virial contribution. Nothing particular can be observed in the electrostatic part.

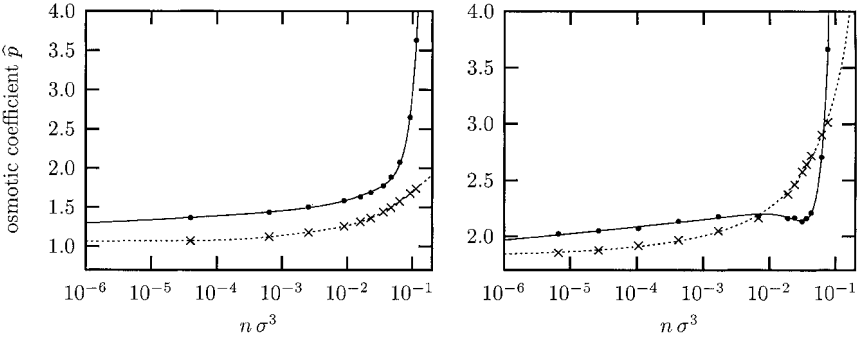

FIG. 14 Osmotic coefficient $\hat{p}$ for the divalent (left) and trivalent (right) systems from Figure 13, separated into the nonelectrostatic contribution coming from virial and ideal gas (heavy dots on solid lines) and negative electrostatic contribution (crosses on dotted lines). Again, the lines are fits that merely serve to guide the eye.

4. The decrease in the virial contribution at high density may be due to the following effect. An important part of the virial results from the force a condensed ion acts onto the rod it is touching. However, this force will be reduced at sufficiently high density when a neighboring rod pulls onto the ion. An alternative explanation suggests that ions condensed on two neighboring rods form a mutually interlocked pattern, which leads to attractions [42,33]. However, various investigations of the simulated data have not revealed such a pattern to exist here.
5. Even at low density the nonelectrostatic contribution to the osmotic coefficient is larger than 1, particularly for the trivalent system. This must originate from the strong repulsive hard-core interactions between condensed ions and the rod, since at those densities interionic repulsions can no longer play a role. This strong repulsion is compensated by the electrostatic attraction of the condensed ions. However, since the latter also acts upon the ions that do not touch the rod, the total pressure drops below the ideal gas contribution.

Contrary to the simulations, the osmotic coefficient from the PB theory is always positive. This has led to the general question whether there could be an attraction between like-charged objects within PB theory. Very recently it has been proved that such attractive interactions are absent on the PB level [43]. An extension of this statement to ions of finite size and to a wider class of boundary conditions can be found in Ref. 44. A fairly general statement in this context is the following: In any local density functional theory, in which the charge density ρ and the electrostatic potential ψ satisfy the inequality $\partial\rho/\partial\psi \leq 0$, the pair interactions are repulsive.

Apart from the phenomenon of a negative osmotic coefficient the remarks which have been made on monovalent measurements also apply here. The actual $\hat{p}$ is smaller than the PB prediction, only this effect is much more pronounced in the multivalent systems. This overestimation of $\hat{p}$ is again accompanied by an underestimation of counterion condensation; see for instance Figure 9. The osmotic coefficient converges to the PB result upon dilution, but already at intermediate densities it is surprisingly well described by the Manning limit $1/2\xi v$. Notice finally that contrary to Figure 12 the curves for different valences intersect. The reason for this is the way in which Eq. 40 depends on valence.

Finally it should be noted that the above measurements cannot be used to infer that attractive forces between charged rods require the counterions to be at least trivalent. The reason is twofold: First, at given valence one can vary Bjerrum length and line charge density. Increasing the Manning parameter will lead to negative pressure in the divalent system. Second, keeping all interaction potentials fixed, the radius r_0 of the charged rod is a relevant observable, as has been demonstrated in Ref. 33. Hence, a general statement about presence or absence of attractive interactions is difficult, since a five-dimensional parameter space is involved: $\{\lambda, \ell_B, v, r_0, n\}$.

VII. REALISTIC EXAMPLES: DNA AND POLY(*p*-PHENYLENE)

Qualitative deviations from Poisson–Boltzmann theory are sometimes very important for real systems. For instance, the zeta potential turns out to be a non-monotonic function of the Manning parameter. This has pronounced influence on the interpretation of electrophoresis experiments.

This section discusses simulations in which the parameters are explicitly mapped to experimental systems. In particular, this mapping affects ion diameter σ, rod radius r_0, Bjerrum length ℓ_B, and line charge density λ. In order to have a rod radius different from σ this requires the introduction of a new potential for ion–rod interactions, for which a modified truncated and shifted Lennard-Jones potential has been used:

$$V_{\text{ion-rod}}(r) = \begin{cases} 4\epsilon \left[\left(\dfrac{\sigma}{r - r_s} \right)^{12} - \left(\dfrac{\sigma}{r - r_s} \right)^{6} + \dfrac{1}{4} \right] & r_s < r \leq r_{\text{cut}} \\ 0 & r_{\text{cut}} < r \end{cases} \tag{41}$$

Here, r is the radial distance from the rod axis to the center of the ion, r_s is a parameter that shifts the Lennard-Jones potential towards larger r, and $r_{\text{cut}} = r_s + 2^{1/6}\sigma$. In Figure 15 the relation between r_s and the rod radius is

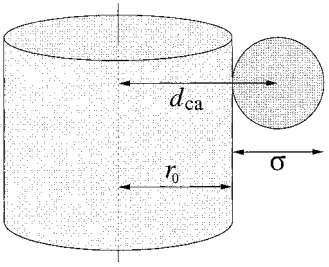

FIG. 15 Connection between several important length scales. The distance of closest approach, d_{ca}, is the sum of the rod radius r_0 and the ion radius $\sigma/2$. From Eq. 41 the distance of closest approach, in the sense of the thermal distance already employed for the Lennard-Jones potential, is found to be $d_{ca} = r_s + \sigma$. Hence the connection between the translation parameter r_s and the rod radius is given by $r_0 = r_s + \sigma/2$.

explained. Since these systems have been investigated either in the presence of salt or at rather high Manning parameter, the phenomena happening in the vicinity of the rod are always well decoupled from the cell boundary. Therefore an even simpler geometry has been chosen for the cell model. The rod has been placed parallel to one of the edges of the cubic simulation cell. This has the advantage that the ion–rod interactions resulting from Eq. 41 can be computed more conveniently.

A. Overcharging for DNA-Like Rods in the Presence of Salt

The essential parameters used for the DNA-like cell models are summarized in Table 1. Figure 16 shows the distribution functions $P(r)$ and the mean electrostatic potential $\psi(r)$ for six DNA-like cell models in the presence of 0.5 mol/L 2:2 salt, for which the line charge density, and thereby the Manning parameter, has been successively increased. Two systems have a smaller Manning parameter than DNA and three a larger. Using the classification of Ref. 4, all systems are beyond the point up to which the concept of Manning condensation is meaningful. That is, the rod charge is compensated by simple salt screening, and no inflection points are present. Within PB theory, no new remarkable features deep in the salt regime should be expected. Contrary to that, however, five of the six presented measurements in Figure 16 show the effect of overcharging, i.e., the rod charge is overcompensated at a certain distance from the rod. Recall the discussion of this phenomenon in the context of generic distribution functions in Sec. V.D. In particular,

TABLE 1 System Parameters for the DNA Simulations

Parameter	Symbol	Value	Value in LJ units
Ion diameter	σ	4.25 Å	σ
Ion valence	v	2	2
Rod radius	r_0	7.86 Å	1.85σ
Line charge density (DNA)	λ	$e_0/1.7$ Å	$2.5\ e_0/\sigma$
Bjerrum length (water)	ℓ_B	7.14 Å	1.68σ
Manning parameter	ξ	4.2	4.2
Box size	L_b	122.4 Å	28.8σ
Corresponding cell radius	R	69.1 Å	16.2σ
Temperature	T	298 K	ϵ/k_B

Figure 11 demonstrates that even in the situation of multiple overcharging the PB theory is unable to account for charge layering.

Integral equation theories give usually much more reliable results at high densities. This is because they appreciate the difference between the potential and the potential of mean force, which is exactly what the PB theory ignores. Figure 17 replots two of the distribution functions from Figure 16 together with predictions from hypernetted chain theory in the HNC/MSA approximation, as it has been presented in Ref. 36. It can be seen that hypernetted chain theory indeed predicts the occurrence of overcharging, while it slightly overestimates its amount.

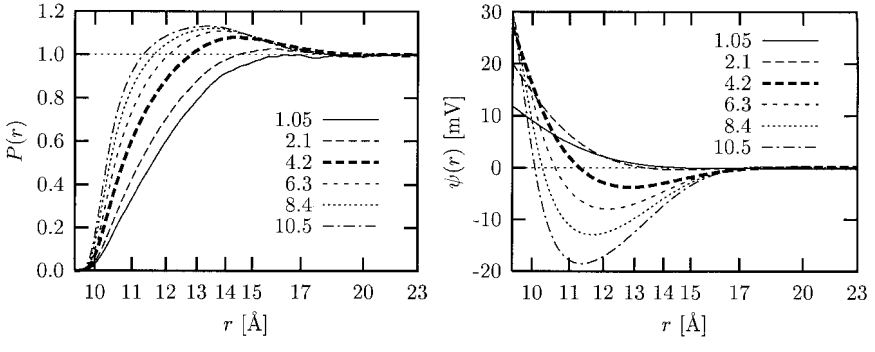

FIG. 16 Ion distribution function $P(r)$ (left) and mean electrostatic potential $\psi(r)$ (right) for DNA-like systems (see Table 1) with 0.5 mol/L added 2:2 salt. The six curves differ in the line charge density of the rod, producing Manning parameters between 1.05 and 10.5 as indicated in the key. The value 4.2 corresponds to DNA. Notice that the radial distance is only plotted up to one third of the cell radius.

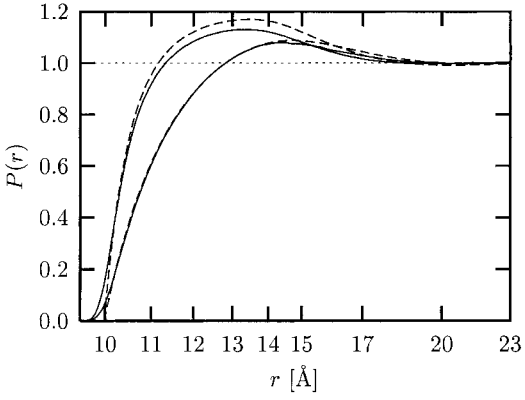

FIG. 17 Distribution functions $P(r)$ for the systems with Manning parameter 4.2 and 10.5 from Figure 16. The solid lines are the results from the molecular dynamics simulations while the dashed lines are the predictions from hypernetted chain theory. (See Ref. 36.)

Another important phenomenon is indicated by the behavior of the mean electrostatic potential in the right frame of Figure 16. It concerns the value of this potential at the distance of closest approach between ions,

$$\zeta = \psi\left(r_0 + \frac{\sigma}{2}\right) \tag{42}$$

which can be identified with the zeta-potential of electrophoresis. This quantity is of importance in the computation of electrophoretic mobilities [45]. Within linearized PB theory of a charged rod within bulk salt ζ depends linearly on ξ. Using the full PB theory leads to the statement that the increase is rather sublinear but still monotonic. However, Figure 16 suggests the following phenomenon. The presence of overcharging effects shows that the mean electrostatic potential can also decrease upon approaching the rod. This calls the monotonic relation between ζ and ξ into question. Figure 18 graphically summarizes various predictions for the ζ-potential as a function of Manning parameter together with results from the molecular dynamics simulations.

Indeed, ζ is found first to increase with ξ, but from a certain value on it decreases and would finally even become negative. Note that this would reverse the drift direction in electrophoresis measurements. While nonlinear and linearized PB theory coincide with the data and with each other for small Manning parameter, they completely fail to predict the back-bending, which already sets in at comparatively small values of ξ. Hypernetted chain

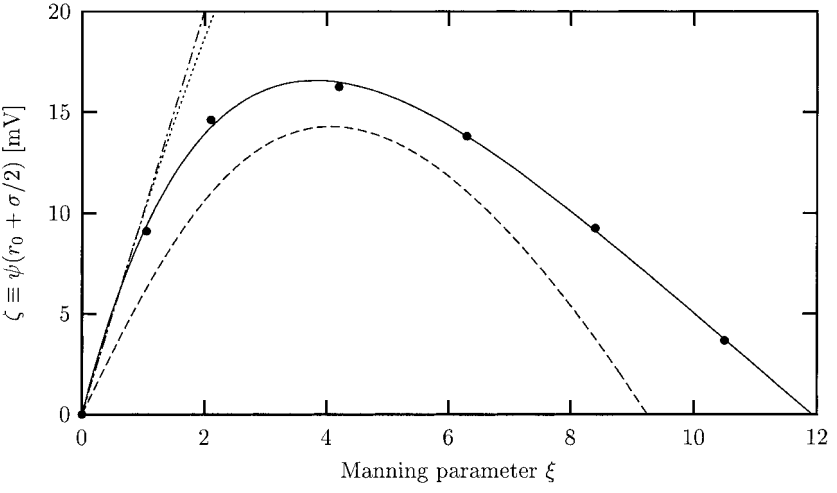

FIG. 18 Zeta potential $\zeta \equiv \psi(r_0 + \sigma/2)$ as a function of Manning parameter for the DNA-like models with 0.5 mol/L added 2:2 salt. The dotted line is the prediction of PB theory, the dash-dotted line is from bulk Debye–Hückel theory, and the dashed line is the result from a hypernetted chain calculation [36]. The solid line is a fit that merely serves to guide the eye.

theory captures this effect, but it underestimates the value of the potential. This is how an overestimated condensation appears on the level of the potential; see Fig. 17. In any case, the success of hypernetted chain theory indicates that local ionic correlations are responsible for both phenomena.

Finally, one might ask how the effect of overcharging depends on salt concentration. Obviously there cannot be any overcharging in the absence of salt, since then even a complete condensation of all ions would merely neutralize the rod. However, it is not clear from the beginning whether an addition of just *some* salt will immediately lead to overcharging. Figure 19 shows simulated distribution functions $P(r)$ and mean electrostatic potentials $\psi(r)$ for a cell model with a DNA-sized and DNA-charged rod ($r_0 = 7.86$ Å, $\lambda = e_0/1.7$ Å), divalent counterions, and varying amount of additional 2:2 salt. The phenomenon of overcharging is indeed observed, but only at sufficiently high salt concentration. This may be illustrated by defining r_1 to be the radius at which overcharging sets in, i.e.,

$$r_1 = \min\{r\colon P(r) = 1\} \tag{43}$$

Figure 20 illustrates the measured r_1 together with a hypernetted chain prediction as a function of salt concentration n. Clearly, r_1 must increase with

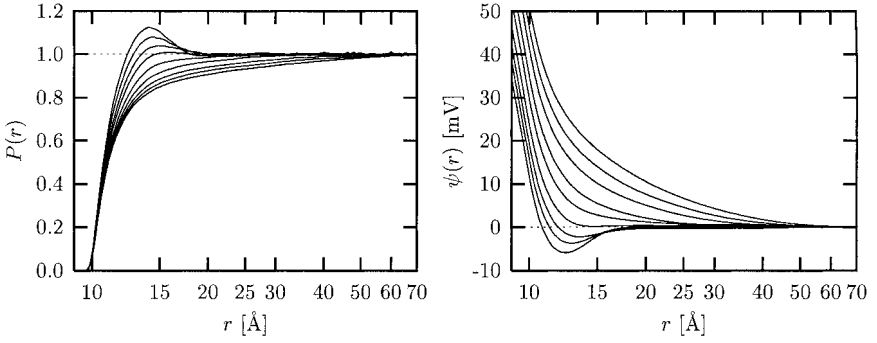

FIG. 19 Ion distribution function $P(r)$ (left) and mean electrostatic potential $\psi(r)$ (right) for systems with Manning parameter $\xi = 4.2$. The nine curves correspond to different numbers N_s of 2:2 salt molecules added to the box: $N_s \in \{8, 17, 34, 68, 135, 270, 380, 540, 760\}$. In the distribution function the salt content increases from bottom to top; in the mean electrostatic potential it increases from top to bottom.

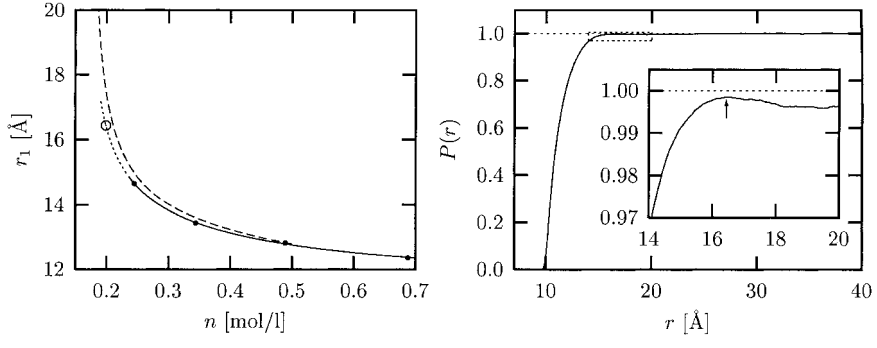

FIG. 20 Left part: Radius r_1 from Eq. 43 at which overcharging sets in for a DNA-sized and charged rod as a function of salt concentration n. The dots are results of molecular dynamics simulations, while the dashed line is the prediction of hypernetted chain theory (Felipe Jimenez Angeles, personal communication). The open circle results from a very long run (90,000 τ_{LJ}) of a system at 0.2 mol/L, and its $P(r)$ together with a magnification of the relevant part is shown in the right frame. The point where it almost touches the line $P = 1$ is taken as r_1. The solid line and its dotted continuation in the left frame is a fit that merely serves to guide the eye. Given the surprising back-bending $P(r)$ in the right frame *before* it crosses the electroneutrality line, the dotted part should actually be replaced by a curve, which ceases roughly at 0.2 mol/L.

decreasing n, since overcharging is reduced and consequently the size of the charge-compensating layer must increase. In fact, hypernetted chain theory predicts that $r_1(n)$ diverges at some *finite* density $n^* \approx 0.18$ mol/L corresponding to a salt Debye length of 3.59 Å, or roughly 200 salt molecules within the simulation box. The simulated values lie below the hypernetted chain prediction, but this is not a feature generally to be expected. In Figure 17 it can be seen that the stronger condensation in hypernetted chain theory should normally lead to a value of r_1 being smaller than in the simulation. To explain this seeming contradiction, it must be noted that with decreasing density the finite radius of the simulation cell becomes relevant. Indeed, the low-salt distribution functions in Figure 19 reach the value 1 essentially at the cell boundary. A reduction of the amount of added salt at fixed cell radius must necessarily lead to values of r_1 being smaller than the hypernetted chain prediction for the bulk, since within a finite cell r_1 cannot diverge. The source of this problem is that a sound comparison with a bulk prediction requires the number of counterions to be much smaller than the number of salt molecules.

An intriguing phenomenon can be observed in the simulation at the density 0.2 mol/L. This corresponds to 220 salt molecules within the box, which is only 10% larger than the estimation for n^* from hypernetted chain theory. The distribution function $P(r)$ of this system shows a back-bending clearly before it crosses the line $P = 1$; see the right frame in Figure 20. Although Figure 11 suggests that overcharging goes along with damped charge oscillations converging symmetrically towards 1, it may also be that there are asymmetric oscillations, i.e., there is a maximum in $P(r)$ but it remains below 1. If this is true, an alternative scenario for the fate of overcharging upon dilution opens up. There still exists a critical density n^*, but instead of diverging, r_1 remains finite but with an infinite slope at n^*. However, independent of the scenario, the determination of n^* by simulation is rather involved, since close to n^* the distribution function $P(r)$ will intersect the neutrality line $P = 1$ at a very acute angle, leaving the determination of r_1 prone to a fairly large error. In any case, the presented simulations have not been able unambiguously to detect overcharging at densities equal to or lower than 0.2 mol/L.

Observe finally that the very existence of such an n^* predicted by hypernetted chain theory should be taken with a grain of salt. This is a statement concerning a low density region, for which integral equation theories are not constructed and hence not as trustworthy as for high densities. On the other hand, any potential overcharging remaining at low densities would be of such a tiny degree that for all practical purposes its presence would be irrelevant. Whether there is a distance far away from the rod, at which

the rod charge is completely neutralized, is first and foremost an academic problem.

B. Distribution Functions and Osmotic Coefficient for Salt-Free Poly(*p*-Phenylene) Solutions

The Manning limiting laws are claimed to apply in the limit of low density. However, an experimental verification of this effect using DNA as rodlike polyelectrolytes is difficult. This is not just a consequence of the usual contrast problems in scattering experiments or the difficulties of keeping a dilute solution salt free. Rather, at low ionic strength the double helix starts to unwind. It would therefore be desirable to have a stiff model polyelectrolyte that does not suffer from this problem. One such system belonging to the class of poly(para-phenylenes) (ppp) has recently been investigated in Refs. 34 and 46. A constitution formula is given in Figure 21, and Table 2 lists four systems that have been simulated based on a mapping to ppp.

In a first step, the simulated ion distribution functions shall be compared with the PB prediction as well as with an extended PB theory using the Debye–Hückel hole–cavity correction function from Ref. 6. Figure 22 shows the corresponding distribution functions for the systems from Table 2. Qualitatively the PB prediction is already a good description of those systems, if one graciously disregards the inevitable problems at the cell

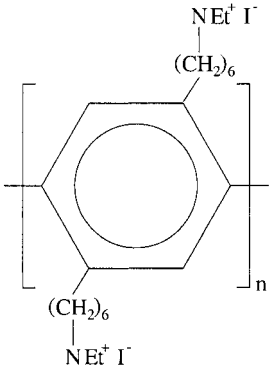

FIG. 21 Constitution formula for poly(*p*-phenylene). The fully aromatic backbone exhibits an excellent chemical stability and has a persistence length of approximately 20 nm. The degree of polymerization used in the studies in Refs. 34, 46 was located between 20 and 40, so that the contour length equals approximately one persistence length at most. The dominant contribution to the signal in small-angle x-ray scattering experiments stems from the iodine ions, since the excess electron density of the backbone is very low.

TABLE 2 Mapping for Four Poly(p-Phenylene) Systems[a]

System	c [g/l]	T [°C]	ξ	σ [Å]	d_{ca} [Å]	R [Å]
1	1.5	40	3.4	7.9	4.4	239.3
2	1.5	40	6.8	8.1	4.4	292.0
3	19.95	25	3.32	7.9	4.4	65.6
4	17.99	25	6.64	8.1	4.4	84.3

[a]Tabulated are polyelectrolyte concentration c, temperature T, Manning parameter ξ, ion diameter σ, distance of closest approach d_{ca} between ions and the rod, and cell radius R corresponding to the given concentration. The experiments have been performed under salt-free aqueous conditions with monovalent counterions. *Source*: Ref. 34.

boundary. However, the presence of correlations shifts the distribution functions up in all four cases. Since this shift is rather small, i.e., the correlations are weak, the Debye–Hückel hole–cavity theory is in fact an excellent description of those systems. Observe, for instance, that in the weakly charged dilute case its prediction can no longer be distinguished from the simulated curve on the chosen scale.

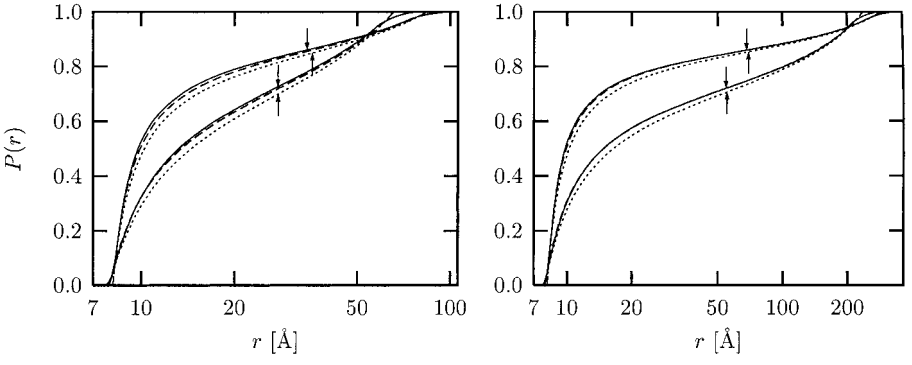

FIG. 22 Distribution functions for the four poly(p-phenylene) systems from Table 2. Left/right frames correspond to high/low density systems (3, 4)/(1, 2), while the upper/lower sets of functions correspond to the strongly/weakly charged systems (2, 4)/(1, 3), respectively. Solid lines are the results of simulation, dotted lines are the PB prediction, and dashed lines are from an extended PB theory using the Debye–Hückel hole-cavity correction [6]. The ↑ arrows indicate the inflection points in the PB distributions, while the ↓ arrows mark those points in the simulated distributions. The deviations of the latter from the PB curves at large r originate from the simulation cell having a quadratic instead of a circular cross-section.

With the help of the condensation criterion from Sec. IV.B, the extent of the correlation-enhanced condensation can be further quantified. The Manning fraction from the molecular dynamics simulation increases only by a fairly small amount. It is at most 4% larger than the PB value. This translates to an effective Manning parameter $\xi_{\text{eff}} = 1/(1 - f_\xi)$ being 5–10% larger than the bare one. This increase is very accurately captured by the Debye–Hückel hole–cavity theory. Its prediction for f_ξ is at most 1% smaller than the value obtained in the simulation. Interestingly, it is even independent of density. This, however, is not a feature to be generally expected and should therefore not be overinterpreted.

In a second step, the osmotic coefficients of the four model systems have been computed. Two distinct approaches have been used for analyzing the simulation results: The first one follows Sec. VI.A and computes the pressure from the stress tensor. The second approach exploits the connection from Eq. 39 between the osmotic coefficient, the Manning parameter, and the integration constant γ of the PB equation. The idea is to use the fitting procedure described in Sec. V.B and from that obtain values $\xi^\star$ and $\gamma^\star$, leading to the osmotic coefficient $(1 + \gamma^{\star 2})/2\xi^\star$. The most straightforward approach of measuring the boundary density is less recommendable, since in the simulation the boundary has a quadratic and not a circular cross-section, i.e., the merely approximate representation of the cell model becomes most visible and questionable here. In contrast to that, the two other approaches ''look'' at regions of the cell, which are away from the boundary. For comparison, also the predictions from the Manning limiting law and the full PB expression are calculated. For the two dilute systems there also exist measurements in Ref. 46 of $\hat{p}$ via osmometry, while for the dense systems this was unfortunately impossible due to counter diffusion problems. Table 3 collects the coefficients for comparison.

TABLE 3 Osmotic Coefficient of the Four Poly(*p*-Phenylene) Systems from Table 2[a]

System	$\hat{p}_{\text{M}}$	$\hat{p}_{\text{PB}}$	$\hat{p}_{\text{MD,1}}$	$\hat{p}_{\text{MD,2}}$	$\hat{p}_{\text{exp}}$
1	0.1471	0.2128	0.2005 (57)	0.201	0.185 (15)
2	0.0735	0.1073	0.1003 (60)	0.102	0.073 (15)
3	0.1506	0.2848	0.2424 (57)	0.260	—
4	0.0753	0.1428	0.1215 (56)	0.129	—

[a]Shown are the Manning limiting law (M), the PB prediction, the simulation result using the stress tensor (MD,1), the simulation result using a PB fit as described in Sec. V.B (MD,2), and results from measurements on this system using osmometry (exp, J. Blaul, personal communication).

The first thing that should be noted is that PB theory gives again a surprisingly good description of the measured coefficients, including the experimentally determined one. A closer look reveals that—as expected—it overestimates $\hat{p}$, and the deviations are larger for the dense systems. Still, PB theory is off by only 7% or 18% for the dilute or dense systems, respectively, thereby confirming the observation already made when looking at the distribution functions. A further indication of this point is that the Manning limit $1/2\xi$ appears to be a lower boundary, which is also in accord with the pressure measurements on the generic systems with monovalent ions from Sec. VI.B. Since there it has also been found that the Manning limit need no longer act as a boundary in the multivalent case (see Fig. 13), it would be very interesting to perform experiments on those systems with, e.g., divalent ions. Observe that the experimental value of $\hat{p}$ for the highly charged dilute system 2 is already at the Manning limit.

Since the experimentally determined osmotic coefficient appears to be smaller even than the molecular dynamics results, this indicates effects to be relevant that go beyond the model used for simulation. Most obvious candidates for this are the neglect of additional chemical interactions between the ions and the polyelectrolyte as well as solvation effects, i.e., interactions between the ions or the polyelectrolyte with the water molecules from the solution. It is for instance demonstrated in Ref. 46 that the osmotic coefficient also depends on whether one uses chlorine or iodine counterions. While one could certainly account for the different radii of these ions when computing the distance of closest approach entering the PB equation, the implications of the different hydration energies is much less obvious to incorporate and in principle requires very expensive all-atom simulations.

Finally it should be noted that the two different methods of analyzing the molecular dynamics data lead to very similar results. While this fact is not particularly useful in a simulation, its consequences for the analysis of experimental data seem promising. In Ref. 34, poly(*p*-phenylene) solutions are investigated by means of small-angle x-ray scattering, which due to the rodlike geometry turns out to be sensitive to the radial ion distribution function. Therefore the measured structure factors can be related to PB distribution functions with effective values of ξ, γ, etc. Fitting the scattering intensity and thereby determining those values permits in principle a measurement of the osmotic coefficient long the lines already described above. What makes this approach so attractive is that it could ideally complement osmometry. If the density becomes too large, the latter suffers from severe problems with counter diffusion, but is is exactly this high density that meets the requirements of good contrast necessary for scattering.

A similar fitting procedure has been applied to the measured data from small-angle x-ray scattering experiments on systems 3 and 4; see also Ref.

TABLE 4 Fit Evaluation of Small-Angle X-Ray Scattering Experiments on Systems 3 and 4

System	ξ	R [Å]	$r_0^\star$ [Å]	R_M^* [Å]	γ^*	$\hat{p}^*$
3	3.32	65.6	8.2	28.19	0.957	0.289
4	6.64	84.3	9.9	39.14	1.014	0.153

[a] ξ is the Manning parameter, R the cell radius implied by the polyelectrolyte concentration, and $r_0^\star$ the rod radius, which had been the only fitting parameter. From this, the integration constant γ^* and the Manning radius R_M^* is determined from the solution of the PB equation. $\hat{p}^* = (1 + \gamma^{*2})/2\xi$ is the attempt to predict the osmotic coefficient of the solution with the help of the PB formula (B. Guilleaume, personal communication).

34. From a fit to the structure factor the radius $r_0^\star$ of the rod has been determined. The integration constant γ^* and the Manning parameter R_M^* the follow from the PB theory. The obtained values are listed in Table 4.

The resulting Manning radius is surprisingly close to the one determined by simulation, particularly for the system with $\xi = 3.32$. The osmotic coefficients constructed from the PB formula are less accurate, 10–20% too large. It would be interesting to observe the effects of introducing more free parameters, similar to the procedure described above, in order to reduce the "Poisson–Boltzmann bias."

VIII. THE QUEST FOR CORRELATIONS

With complete knowledge of the microstate within a molecular dynamics simulation one can in principle determine arbitrary correlation functions. This permits an identification of the deeper reasons underlying the failure of Poisson–Boltzmann theory.

Up to now the following observation repeatedly turned up from the simulations. The nonlinear PB equation provides a fairly good description of the cell model, but it suffers from systematic deviations in strongly coupled or dense systems. It underestimates the extent of counterion condensation and at the same time overestimates the osmotic coefficient. As the common reason for both problems, the neglect of correlations has been proposed, basically for two reasons:

1. The circumstances of the failure—strong coupling and high density—are the situations in which correlations are expected to be important. Furthermore, the effects are just what one would intuitively be inclined to ascribe to correlations.

2. More elaborate theories [36,37,6] that try to incorporate correlations reproduce the trends of the simulations, because they favor an increase in density. At the presence of a charged macroion this will preferably take place close to its surface, thereby leading to a stronger condensation and a concomitant drop in the boundary density and thus pressure.

However, the present situation is at a halfway stage. On the one hand there is general agreement about the presence of correlations being liable for the failure of PB theory. On the other hand, this insight does not shed any light onto the question of which kinds of correlations are important. All one knows from PB theory is that it incorporates *none* of them, since it makes no distinction between the potential and the potential of mean force. The purpose of integral equation theories is to derive analytic expressions for higher order correlation functions. However, there is no prior prescription for the ''correct'' closure equation to be used for decoupling the hierarchy of n-point correlation functions; see, e.g., Chapter 13 in Ref. 30. Therefore the underlying physics is often shrouded in mystery. The correlation correction from Ref. 6 uses a one-component plasma model and its Debye–Hückel approximation as an additional contribution to the free energy resulting from individual ion–ion interactions. Yet in the present version it is unable, even after the inclusion of a hard core, to predict ionic layering in situations in which the simulation proves them to be present. Above that, it gives no access to ionic correlation functions.

In such a situation computer simulations can be enormously helpful. One of their main advantages is that they do not just produce statistical averages of tremendously coarse-grained thermodynamic observables, e.g., energy or pressure. Rather, a simulation often has *complete* knowledge of the microstate of a system, sometimes even as a function of time. If one knows where all ions are and if one has ways to average, one has access to basically all kinds of correlation functions. This section discusses two of them.

A. The Condensed Layer as a Strongly Coupled Liquid

If the surface charge density of the rod is high, a fairly large number of counterions will stay within a condensed layer of small radial extent. Addition of salt will further increase the ionic density in this layer. It is clear that beyond a certain point (high λ, high ℓ_B or enough salt) the ions will no longer distribute independently of each other but get locally correlated. This effect will now be measured for the DNA-sized models from Sec. VII.A, for which 0.5 mol/L of a 2:2 salt has been added in excess to the divalent counterions.

The first issue is to define the innermost layer. For this, a distance from the rod is chosen which contains many counterions but virtually no coions. A distance of roughly 11.5 Å from the rod axis turned out to be quite suitable. This is about a third ion diameter farther out than the distance of closest approach. To avoid difficulties with remaining coions, only the counterions within this distance are taken into account in what follows. In a second step, the coordinates of those ions are radially projected onto the surface of the cylinder of closest approach, and this surface is then rolled out to a flat plane; see Figure 23 for an illustration of this procedure. Finally, the two-dimensional pair correlation function $g(r)$ of these projected points is computed.

One might object that the unrolled flat plane leads one to believe that the pair correlation function depends only on distance, while in reality such a rotational symmetry cannot be expected, due to the rod curvature. However, an investigation of $g(r)$ revealed that the pair correlation function is in fact rotationally symmetric up to essentially a distance that corresponds to half the circumference of the cylinder of closest approach, which is roughly 30 Å. Larger distances can of course only be realized along the rod instead of around it. A possible reason for this surprising symmetry is that at short distances the curvature is not yet perceptible, while at large distances the particles are already uncorrelated.

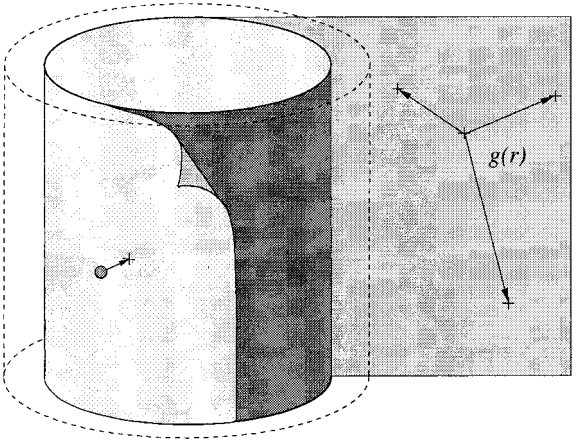

FIG. 23 Illustration of the computation of surface correlations. Counterions within a certain small distance from the rod constitute the innermost condensed layer. Their coordinates are radially projected onto the surface, which after that is unrolled to a flat plane. The two-dimensional pair correlation function $g(r)$ is then determined from the projected points.

Figure 24 shows the measured $g(r)$ for the four most strongly charged systems from Figure 16. The most important thing to observe is that for the strongly charged systems $g(r)$ shows definite signs of correlations. Apart from the trivial correlation hole at small r there is a distance $r_{\max}$ at which ions are more likely to be found than under the assumption of independent distribution. Notice that the maximum in $g(r)$ is not located at $r \approx \sigma$ but much farther out. Hence, its existence is not merely an artifact of close packing of repulsive Lennard-Jones spheres. However, if the condensed ions are assumed to form a triangular lattice on the surface in order to maximize their mutual repulsion, the resulting distance $d_\triangle$ is 25–35% larger than $r_{\max}$. Together with the only weakly pronounced oscillations in $g(r)$ this proves the correlation induced interactions to be rather short range, yet less local than a pure hard core. In any case, the range is several times larger than the average Debye length $\ell_D \approx 0.5\sigma$.

Such two-dimensional pair correlation functions for mobile ions adsorbed on charged planes have recently been investigated theoretically in Ref. 42. The mean separation $d_s = (\nu e_0/\varsigma)^{1/2}$ of ν-valent ions on the completely neutralized plane of surface charge density ς is identified as the important scaling length. The main predictions for the strongly coupled regime $\Gamma_2 := \ell_B$

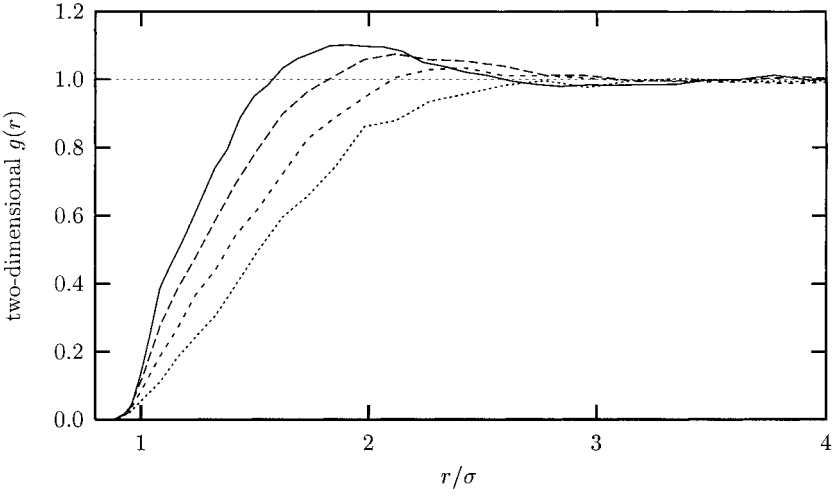

FIG. 24 Two-dimensional pair correlation function $g(r)$ for the projection of counterions within a close condensed layer onto the cylinder of closest approach; see text and Figure 23. The four functions belong to the most strongly charged systems in Figure 16. From solid to dotted the Manning parameter decreases as 10.5, 8.4, 6.3, and 4.2. The last value corresponds to DNA.

$v^2/d_\varsigma > 1$ are (1) $g(r)$ should have a single first peak at a distance about the size d_ς of the correlation hole; (2) the breadth of this peak should decrease with Γ_2 while its maximum should increase. This trend is indeed seen to be true for the functions in Figure 24, only d_ς is roughly 10–20% larger than the actual peak position. One might want to argue that the presence of much salt entails a further increase of the layer density on top of the usual Gouy–Chapman prediction, but the results obtained in Ref. 42 are claimed to be independent of the bulk ionic strength, if the latter is smaller than the layer density. This is here the case, even though not always by an order of magnitude. An alternative explanation may be based on the presence of coions: Although very few of them reside within the innermost condensed layer, there will be an appreciable amount beyond and possibly very close to r_1. Those ions can act as ''bridges''; they attract counterions and thereby reduce the average closest distance between them.

Although $r_{\max} < d_\triangle$, this does not exclude a local hexatic ordering of the counterions. But since $g(\boldsymbol{r})$ is on average rotationally symmetric, establishing signs for this requires the investigation of a suitable 3-point correlation function. The trick is to break the rotational symmetry, which suggests the following procedure: $g(r)$ is proportional to the probability of finding a particle at a distance r, given that there is also a particle at the origin. Now define $g_\rightarrow(\boldsymbol{r})$ to be proportional to the probability of finding a particle at position $\boldsymbol{r}$, given that there is also a particle at the origin *and* given that the particle that is closest to the origin is situated to the right side. This definition is further restricted to be sensitive only for next nearest neighbors and not arbitrary other particles. Thence it answers the question: ''If the nearest neighbor is on the right side, where is the next nearest neighbor?'' A density plot of this observable is shown in the left part of Figure 25. For this, the most highly charged DNA-sized system with Manning parameter $\xi = 10.5$ has been used. Clearly visible are the two correlation holes around the origin and the nearest neighbor as well as a tendency of the next nearest neighbor to be on the side opposing the nearest neighbor. All those effects are trivially explained. However, on top of that no preferential ion accumulations in the ''hexatic directions'' indicated as dotted lines is perceptible. The right part of Figure 25 shows the probability distribution of finding the next nearest neighbor at an angle ϕ with respect to the line joining nearest neighbor and origin. The correlation hole generated by the nearest neighbor is visible, but no increase in $p(\phi)$ at 60°, 120°, or 180°. Rather, the measured data are compatible with a fairly structureless distribution, as indicated by the solid line.

Since the most strongly charged system does not show hexatic order, it will certainly be absent in the other ones. However, the coupling constant Γ_2 introduced above has a value of only about 3 in the system with Manning

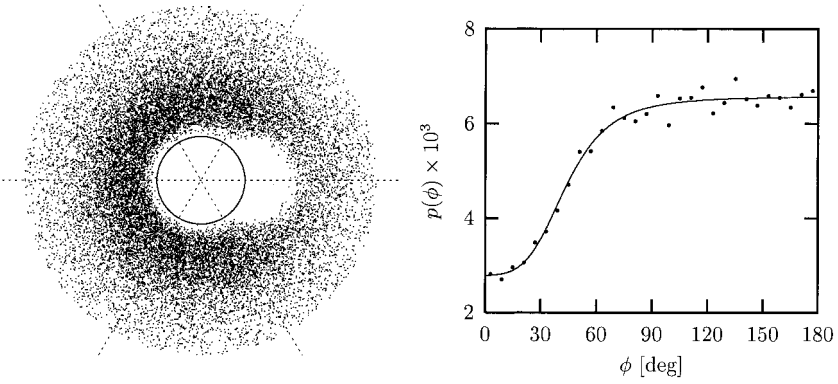

FIG. 25 Left part: Density plot of the three-point correlation function $g_{\rightarrow}(\boldsymbol{r})$ for the highest charged system from Figure 24 with Manning parameter $\xi = 10.5$. If an ion is located at the origin and its *nearest* neighbor is on the right side and not further away than 1.3σ, its *next nearest* neighbor is shown as a dot. The circle around the origin has radius σ and corresponds to the distance of closest approach imposed by the Lennard-Jones potential. The right frame plots the probability distribution of finding the next nearest neighbor at an angle ϕ with respect to a line joining nearest neighbor and origin. The solid line is a guide to the eye.

parameter $\xi = 10.5$. For larger values of Γ_2 one would not only expect much stronger correlations and hexatic ordering but even crystallization of the adsorbed counterions into a two-dimensional Wigner crystal [42,47].

B. The Three-Dimensional $g(r)$

If the radius r_0 of the charged rod is small, its surface is bent very much and renders the formation of a two-dimensional correlated layer rather doubtful. In fact, Ref. 47 suggests that in the case $r_0\lambda \ll ve_0$, or alternatively $r_0/\ell_B \ll v/\xi$, ions will more likely form a three-dimensional correlated structure on the background of the rods, which for high enough coupling can be described as a Wigner crystal. For the generic models investigated in Sec. V this will be tested here by computing the usual three-dimensional pair correlation function $g(r)$. Before that, a few general remarks are appropriate.

If the ions form a three-dimensional crystal structure, there will be a typical minimum distance between ions depending on density. Assuming hexagonal closed packing,* the volume per ion is given by $d_{\mathrm{hcp}}^3/\sqrt{2}$, where

*For the generic models this would be compatible with the hexagonal symmetry along one direction imposed by the rods, with which the Wigner crystal has to arrange.

d_{hcp} is the minimum ion distance. As a function of density it is therefore given by

$$d_{\mathrm{hcp}} = \left(\frac{\sqrt{2}}{n}\right)^{1/3} \tag{44}$$

and varies with the cube root of density. There is, however, another important length scale in the system, which is the separation of the rods. Assuming a system like that in Figure 5 with one rod of line charge density λ placed along the main diagonal of a cubic box of length L_{b}, the separation of rods is $d_{\mathrm{rod}} = L_{\mathrm{b}}\sqrt{2/3}$. Furthermore, the toal number of ions is $\sqrt{3}L\lambda/ve_0$, giving a density $\sqrt{3}\lambda/L^2ve_0$ which varies inversely to L^2 instead of L^3. As a consequence, the separation of the rods as a function of ionic density is given by

$$d_{\mathrm{rod}} = \left(\frac{2\lambda}{\sqrt{3}ve_0 n}\right)^{1/2} \tag{45}$$

which varies with the square root of density. Hence, whatever the details of the actual structure are, if one measures a new characteristic length varying as $n^{1/3}$, it can be viewed as a bulk crystal property, while a length varying with $n^{1/2}$ is rod imposed.

Since the correlations are expected for dense systems, only those have been investigated. Moreover, in the dilute case the three-dimensional $g(r)$ would be too much dominated by the one-dimensional contribution resulting from the strong condensation along the rod, which first would have to be corrected. Hence, in the following only the divalent and trivalent systems from Figure 13 with a density larger than $0.03\sigma^{-3}$ (divalent) or $0.02\sigma^{-3}$ (trivalent) have been investigated. As an example, Figure 26 shows the $g(r)$ for the trivalent system with the lowest, i.e., most negative, osmotic coefficient, which has a density of $0.04247\sigma^{-3}$. The visible structure is quantified by the position $r_{\max}$ of the first maximum, and the important question to be answered is its origin. Figure 27 gives a graphical representation of $r_{\max}$ versus density on a log–log scale. The interesting thing to note is that the density dependence is compatible with a slope $-1/2$. In Eq. 45 this has been seen to be the exponent expected for a rod-imposed structure.

At first sight this finding might appear inevitable. Nevertheless, since $r_0\lambda < ve_0$ for the investigated cases, the inequality from the beginning of this section does in fact hold, albeit not in the strong "$\ll$" version. For this specific situation ve_0/λ is 1.9 for the divalent systems and 2.9 for the trivalent ones. Observe that the inequality does not specify the density of counterions or rods, at which the three-dimensional Wigner crystal is to appear. Rather, Ref. 47 assumes only that a bundle of rods has formed and

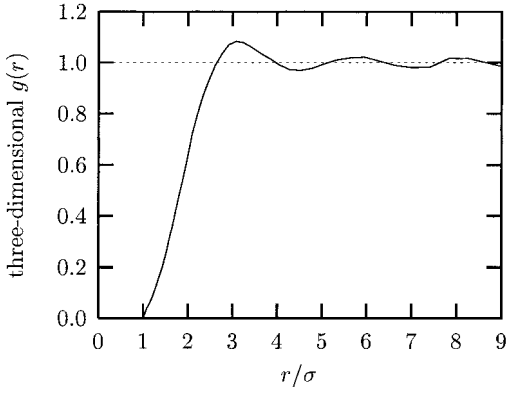

FIG. 26 Three-dimensional $g(r)$ for the generic system with trivalent counterions at a density of $0.04247\sigma^{-3}$. Clearly visible is a structure pointing to local arrangements of the ions, for which the position of the first maximum is taken as a characteristic length.

that the inequality holds. Because the simulations suggest rod-imposed correlations instead of a self-organized Wigner crystal on the background of a homogeneously smeared rod charge, one might want to save the idea by restricting it to higher densities than the ones investigated in the simulation. The reasoning behind this is that the strong localization of ions in the vicinity

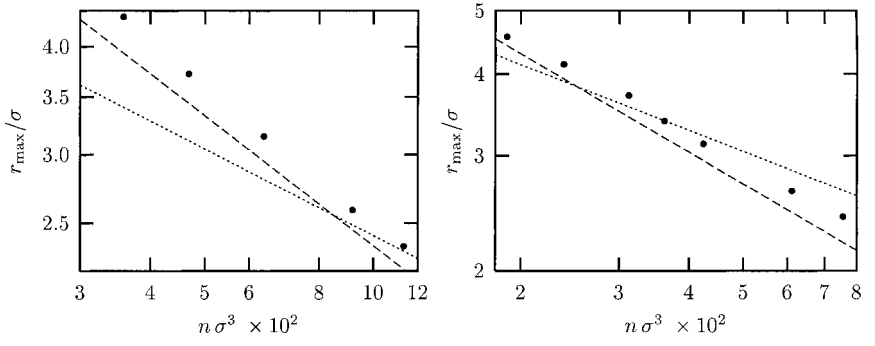

FIG. 27 Double-logarithmic plot of the position $r_{\max}$ of the first maximum in the three-dimensional pair correlation function for the dense divalent (left) and trivalent (right) generic systems from Figure 13 as a function of density. The dashed line is the separation of the rods in those systems, and the dotted line is the minimum ion distance in an hcp crystal.

of the rods gets reduced and the system will appear more homogeneous. However, for the densest systems under investigation the separation of the rods is roughly 2.2σ. Hence the ions can just about pass between the rods. For even higher densities the ions become trapped in the one-dimensional channels between the rods and the system ceases to be ergodic. Anyway, Figure 13 shows that the osmotic coefficient for those high-density systems would be very large, while the interesting phenomenon of negative pressure in the trivalent system is observed exactly for the densities, at which an ion–rod coupling for $g(r)$ has been found. In other words: Whatever kind of correlations are responsible for the attractive interactions, the dominant contribution is not the formation of a three-dimensional Wigner crystal.

IX. CONCLUSION

Theoretical and numerical studies of stiff linear polyelectrolytes within the framework of a cell model have been presented. A criterion for quantifying the phenomenon of counterion condensation was introduced, which turned out to provide a fruitful base for understanding many interesting effects. For instance, it was used to illuminate the transition from counterion condensation to screening, when salt is gradually added to the system. The enhanced counterion condensation caused by ionic correlations and its dependence on parameters such as density, Bjerrum length, valence, and ionic strength was measured. These examples prove the condensation criterion to be a suitable tool for analyzing linear polyelectrolytes. Its application to further problems, such as hydrophobic or structured counterions and its extension to flexible polyelectrolytes appears promising.

The important issue of understanding ion–ion correlations remains a fascinating but difficult problem. For weakly coupled systems, correction terms to the PB free energy density together with a local density approximation have been shown to be very successful in this work. However, they are incapable of describing many effects which qualitatively go beyond mean-field theory, e.g., charge reversal, a nonmonotonic zeta-potential, and attractive interactions between like-charged macroions. Recently attempts have been made to relate such phenomena to the formation of various kinds of Wigner crystals. To assess these theoretical ideas, computer simulations will certainly be indispensable, since they are presently the only practicable way of obtaining sufficiently detailed information on ionic distributions and correlation functions. The numerical investigations presented in this work and the correlation analysis of the obtained data are a further step in this direction. Finally we should remark that this chapter is part of the thesis work of one of the authors (M.D.) [5].

ACKNOWLEDGMENTS

We wish to thank M. Ballauff, M. Barbosa, J. Blaul, B. Guilleaume, F. Jimenez Angeles, M. Lozada-Cassou, and S. May for various contributions to this work. In addition we acknowledge a large computer time grant hkf06 from NIC Jülich and financial support by the German Science foundation.

REFERENCES

1. Barat JL, Joanny JF. Theory of polyelectrolyte solutions. In: Prigogine I, Rice SA, eds. Advances in Chemical Physics. Vol. 94. New York: John Wiley, 1996: 1–66.
2. Manning GS. Limiting laws and counterion condensation in polyelectrolyte solutions I. Colligative properties. J. Chem. Phys. 1969; 51:924–933.
3. Oosawa F. Polyelectrolytes. New York: Marcel Dekker, 1970.
4. Deserno M, Holm C, May S. The fraction of condensed counterions around a charged rod: comparison of Poisson–Boltzmann theory and computer simulations. Macromolecules 2000; 33:199.
5. Deserno M. Counterion Condensation for Rigid Linear Polyelectrolytes. Ph.D. dissertation, Universität Mainz, 1999.
6. Barbosa MC, Deserno M, Holm C. Europhys. Lett. 2000.
7. Woodward CE, Jönsson B. Monte-Carlo and mean field studies of a polyelectrolyte in salt solution. Chem. Phys. 1991; 155:207–219.
8. Stevens MJ, Kremer K. The nature of flexible linear polyelectrolytes in salt free solution: a molecular dynamics study. J. Chem. Phys. 1995; 103:1669.
9. Micka U, Holm C, Kremer K. Strongly charged, flexible polyelectrolytes in poor solvents—a molecular dynamics study. Langmuir 1999; 15:4033.
10. Micka U, Kremer K. From microgel to necklace chains—strongly charged polyelectrolytes in poor solvents. Europhys. Lett., 2000; 49:189.
11. Messina R, Holm C, Kremer K. Strong attraction between charged spheres due to metastable ionized states. Phys. Rev. Lett. 2000; 85:872.
12. Allen MP, Tildesley DJ. Computer Simulation of Liquids. Oxford: Oxford Science Publications, 1997.
13. Frenkel D, Smit B. Understanding Molecular Simulation. San Diego: Academic Press, 1996.
14. Grest GS, Kremer K. Molecular dynamics simulation for polymers in the presence of a heat bath. Phys. Rev. A 1986; 33:3628.
15. Risken H. The Fokker–Planck Equation. 2d ed. Berlin: Springer-Verlag, 1989.
16. Dünweg B. Molecular dynamics algorithms and hydrodynamic screening. J. Chem. Phys. 1993; 99:6977.
17. Dünweg B, Paul W. Brownian dynamics simulations without Gaussian random numbers. Int. J. Mod. Phys. C 1991; 2:817.
18. Español P, Warren P. Statistical mechanics of dissipative particle dynamics. Europhys. Lett. 1995; 30:191.

19. Guldbrand L. The distribution and dynamics of small ions in simulations of ordered polyelectrolyte solutions. Mol. Phys. 1989; 67:217.
20. Nilsson LG, Guldbrand L, Nordenskiöld L. Evaluation of the electrostatic osmotic pressure in an infinite system of hexagonally oriented DNA molecules. A Monte Carlo simulation study. Mol. Phys. 1991; 72:177.
21. Lyubartsev AP, Nordenskiöld L. Monte Carlo simulation study of DNA polyelectrolyte properties in the presence of multivalent polyamine ions. J. Phys. Chem. 1997; 101:4335.
22. Lyubartsev AP, Tang JX, Janmey PA, Nordenskiöld L. Electrostatically induced polyelectrolyte association of rodlike virus particles. Phys. Rev. Lett. 1998; 81: 5465.
23. Deserno M, Holm C. How to mesh up Ewald sums. I. A theoretical and numerical comparison of various particle mesh routines. J. Chem. Phys. 1998; 109:7678.
24. Deserno M, Holm C. How to mesh up Ewald sums. II. An accurate error estimate for the P3M algorithm. J. Chem. Phys. 1998; 109:7694.
25. Alfrey T, Berg P, Morawetz HJ. J. Polym. Sci. 1951; 7:543.
26. Fuoss RM, Katchalsky A, Lifson S. The potential of an infinite rod-like molecule and the distribution of the counter ions. Proc. Natl. Acad. Sci. USA 1951; 37:579.
27. Wennerström H, Jönsson B, Linse P. The cell model for polyelectrolyte systems. Exact statistical mechanical relations, Monte Carlo simulations, and the Poisson–Boltzmann approximation. J. Chem. Phys. 1982; 76:4665.
28. Le Bret M, Zimm BH. Monte Carlo determination of the distribution of ions about a cylindrical polyelectrolyte. Biopolymers 1984; 23:271.
29. Le Bret M, Zimm BH. Distribution of counterions around a cylindrical polyelectrolyte and Manning's condensation theory. Biopolymers 1984; 23:287.
30. McQuarrie DA. Statistical Mechanics. New York: HarperCollins, 1976.
31. Belloni L, Drifford M, Turq P. Counterion diffusion in polyelectrolyte solutions. Chem. Phys. 1984; 83:147.
32. Belloni L. Ionic Condensation and Charge Renormalization in Colloidal Suspensions. Colloids and Surfaces 1998; A140:227.
33. Grønbech-Jensen N, Mashl RJ, Bruinsma RF, Gelbart WM. Counterion-induced attraction between rigid polyelectrolytes. Phys. Rev. Lett. 1997; 78:2477.
34. Guilleaume B, Blaul J, Wittemann M, Rehahn M, Ballauff M. Investigations of rodlike polyelectrolytes in solution by small-angle x-ray scattering. J. Phys. Cond. Matt., 2000; A245:12.
35. Deserno M. A Monte-Carlo approach to Poisson–Boltzmann like free energy functionals. Physica A, 2000; 278:405.
36. Gonzales-Tovar E, Lozada-Cassou M, Henderson D. Hypernetted chain approximation for the distribution of ions around a cylindrical electrode. II. Numerical solution for a model cylindrical polyelectrolyte. J. Chem. Phys. 1985; 83:361.
37. Das T, Bratko D, Bhuiyan LB, Outhwaite CW. Modified Poisson–Boltzmann theory applied to linear polyelectrolyte solutions. J. Phys. Chem. 1995; 99:410.

38. Das T, Bratko D, Bhuiyan LB, Outhwaite CW. Polyelectrolyte solutions containing mixed valency ions in the cell model: a simulation and modified Poisson–Boltzmann study. J. Chem. Phys. 1997; 107:9197.
39. Haile JM. Molecular Dynamics Simulation: Elementary Methods. New York: John Wiley, 1992.
40. Hummer G, Grønbech-Jensen N, Neumann M. Pressure calculation in polar and charged systems using Ewald summation: results for the extended simple point charge model of water. J. Chem. Phys. 1998; 109:2791.
41. Essmann U, Perera L, Berkowitz ML, Darden T, Lee H, Pedersen LG. A smooth particle mesh Ewald method. J. Chem. Phys. 1995; 103:8577.
42. Rouzina I, Bloomfield VA. Macroion attraction due to electrostatic correlation between screening counterions. 1. Mobile surface-adsorbed ions and diffuse ion cloud. J. Phys. Chem. 1996; 100:9977.
43. Neu JC. Wall-mediated forces between like-charged bodies in an electrolyte. Phys. Rev. Lett. 1999; 82:1072–1074.
44. Trizac E, Raimbault JL. Long-range electrostatic interactions between like-charged colloids: steric and confinement effects. Phys. Rev. E 1999; 60:6530.
45. Hunter RJ. Foundations of Colloid Science. Vol. 1. Oxford: Oxford Science Publications, 1987.
46. Blaul J, Wittemann M, Ballauff M, Rehahn M. The osmotic coefficient of a synthetic rodlike polyelectrolyte in salt-free solution as a test of the Poisson–Boltzmann cell model. J. Phys. Chem. B, 2000; 104:7077.
47. Shklovskii BI. Wigner crystal model of counterion induced bundle formation of rodlike polyelectrolytes. Phys. Rev. Lett. 1999; 82:3268–3271.

3

Inverted Forces in Counterion Condensation Theory

JOLLY RAY and GERALD S. MANNING Rutgers University, Piscataway, New Jersey

I. INTRODUCTION

Counterion condensation theory has evolved through several stages. At first, the goal was to formulate a Debye–Hückel theory for the thermodynamic properties of polyelectrolyte solutions, like activities, osmotic pressure, and heats of dilution [1–12], and an Onsager theory for dynamic quantities, like conductivity and mobilities [11,13–26]. It was clear that the Debye–Hückel–Onsager limiting laws, which are leading-order terms in salt concentration expansions, could not simply be adapted to polymer geometries, since polyionic chains usually link many charged groups in a high-density configuration. Unalloyed Debye–Hückel theory would be applicable only to sufficiently weakly charged chains. It was known, however, that a system of continuously charged zero-radius lines and independently mobile oppositely charged point ions is unstable if the charge density of the lines exceeds a precisely determined critical value (L. Onsager, personal communication, 1968). The system becomes stable only if sufficiently many point ions merge their charge with the lines to lower the net ''renormalized'' line charge density to the critical value. The new system of renormalized lines and depleted supply of oppositely charged point ions is stable, and should follow the rules of Debye–Hückel theory to leading order in concentration. If the original lines have charge densities below the critical value, then Debye–Hückel theory should be applicable with no charge renormalization required (to leading order in a concentration expansion). With the assumption that on the relevant scale of a Debye length, a polyionic chain can be modeled as a continuously charged line, there then appears a transparent path to a theory of polyelectrolyte solutions (at low polymer concentrations, so that deviations from ideality are caused predominantly by the electrostatic interactions

between a single chain and the small ions that surround it). The number of counterions that condense on the polymer to renormalize its charge is known; as part of the chain, these ions are not independently active, either thermodynamically or kinetically (the latter depending on the degree of molecular involvement with the chain); and all that is then needed is application of Debye–Hückel–Onsager theory to the interactions between the free counterions (and coions) and the electric field set up by the net charge of polymer and condensed counterions [1,13].

Although a wide assortment of polyelectrolyte properties becomes accessible inside a restricted theoretical frame where the condensed layer of counterions is a featureless continuum, other important problems are blocked unless some model for the structure of the condensed layer is adopted. An obvious example would be the polarizability of the polyion, which must involve a positional shift of the structural charges on the polymer relative to the condensed counterions [27–31]. Another is competitive counterion binding [32–46], when counterions of one species enter the condensed layer, while counterions of a different species exit—a class of problems ranging in complexity from the titration of a polymeric weak acid or base [47] to the binding of drugs and proteins to DNA [48,49]. Response of the condensed layer to deformation of the underlying polyionic structure affects the energetics of the deformation, and a description of what happens to the condensed counterions when DNA, for example, is bent, twisted, or stretched [32,50–52], or when a charged polymer undergoes, say, a helix-to-coil transition [32,53], is an essential element in our understanding of the structural change.

To handle aspects of polyelectrolyte behavior that depend on the particulate structure of the polymer and its condensed layer of counterions, two modifications of the original theory were introduced [32,54]. In recognition of the polyion as a linear linkage of ionized molecular groups, the continuously charged line was replaced with a linear array of discrete charges with uniform spacing; and the condensed counterions were represented by an internal partition function. A surprise was that the condensed layer partition function could be uniquely evaluated as part of the free energy minimization procedure, and the formula for it, and hence for the total free energy of the system, depends only on the linear charge spacing of the polyion. Thus the total free energy of this model, like a Debye–Hückel limiting law, is determined by the linear charge density of the polyion and the valences of the small ions. Numerical values of the condensed layer partition function, first interpreted [32] as a free volume for unimpeded movement of the condensed counterions, are physically reasonable. For DNA, it corresponds to a shell surrounding the phosphate groups of about 7 Å thickness, only slightly larger than the hydrodynamic diameter of a Na^+ ion or the length of two hydrogen-

bonded water molecules. The model contains within itself, therefore, the realistic information that the condensed counterions are part of the structure of the polyion, in the same sense as its electrostricted, low-dielectric constant hydration layer [55,56].

As powerful as this approach proved to be, it failed to unlock yet another class of problems, most conspicuous among them the spatial distribution of small ions surrounding a charged polymer. For the model of a continuously and uniformly charged line, the radial distribution function implicitly has two peaks, a delta function centered on the line to represent the condensed counterions, and a Debye–Hückel peak for the uncondensed counterions, but the delta function is obviously an idealization of the real structure. For the model of the line of uniformly spaced discrete charges, a step function for the condensed counterions, as described above, is only meant as a rough guide to the thickness of the condensed layer. The theory goes through without this picture of the condensed counterions, which arises only after the interpretation of the condensed layer partition function as a free volume [54]. If the condensed counterions are an integral part of the polyion chain in the same sense as its solvation shell, then indeed it can be argued that nothing short of all-atom simulation with explicit solvent molecules, counterions, and coions will suffice for a realistic glimpse of the structure of the condensed layer [55].

A recent attempt to extend the scope of counterion condensation theory to the calculation of counterion–polyion, coion–polyion, and polyion–polyion pair potentials retains structural idealization but may nonetheless be capable of generating useful new information about the real molecular structure of polyelectrolyte solutions [57–59]. The validity of the first and second stages of the theory, as discussed above, has been heavily documented, including the physical reality of the condensed layer and the onset of condensation at a critical charge density [55,56,60,61]. In contrast, the inverted forces predicted by our extended theory have yet to be confirmed by experiment or simulation. We will argue, however, that their presence is at least suggested by current experimental knowledge.

If the electrostatic interaction between two like-charged particles is attractive, we call the interaction inverted; and if the interaction between oppositely charged particles is repulsive, we also call it inverted. Ionic force inversion is not a denial of Coulomb's law. If it exists, it must be a manifestation of many-body interactions. For example, if two like-charged polymers electrostatically attract each other, it can only be through the mediation of counterions and/or polarizable solvent molecules. Force inversion is a topic currently of widespread interest in polyelectrolyte physics (this volume, Chapter 5). We currently believe that inverted forces can arise through several distinct types of interactions, and it may not always be easy to pick

out which one predominately underlies any particular experimental observable. In this chapter we review our own theory of inverted forces and relate it, albeit qualitatively, to specific laboratory phenomena.

The organization of the chapter is straightforward. Section II reviews counterion condensation theory for an isolated polyion in the framework of the ''second stage'' as indicated above. Then in Sec. III the radial distribution function for the counterions and coions is discussed with emphasis on an inverted region at intermediate distances from the polyion. The pair potential for two identical polyions is also discussed in this section, and an inverted attraction is highlighted (an inverted repulsion is found for two polyions identical but for opposite charge). Finally, we review our work on polyion clustering in Sec. IV.

II. CONDENSED COUNTERIONS AND THEIR PARTITION FUNCTION

In this section we consider a single polyion in a thermally averaged environment of small ions. To motivate the model used and the method of analysis, consider first the limiting Debye–Hückel theory of a dilute solution of 1:1 electrolyte, which as the leading term in a concentration expansion is an exact result and may be derived with no reference to interactions at small distances, ion size, or the molecular structure of the solvent. To obtain it, one need only solve the linearized Poisson–Boltzmann equation *far* from an ion with charge q to get a potential of the form $A \exp(-\kappa r)/r$, or $(A/r) - A\kappa$, if the distance r, although large, is still much less than the Debye screening length $1/\kappa$. From the first term, the constant A is identified as q/D, where D is the bulk dielectric constant (since r is large), and then the distance-independent second term is seen to contain the effect of the other ions and leads to rigorous limiting laws.

A polymeric ion is a long string of ionic sites, so it is natural to ask what would happen to the Debye–Hückel theory of a dilute NaCl solution if a subset of the Cl^- ions were linked in a linear array. Consider, then, a long linear lattice of ''chloride ions'' with spacing b with no reference to the size of the charges fixed on the lattice. Recalling that pairwise summation (superposition) is rigorously correct on the Debye–Hückel level, we write the limiting Debye–Hückel work required to assemble the lattice from a subset of chloride ions in NaCl solution as a pairwise sum of terms of the form $(q^2/Dnb)\exp(-\kappa nb)$. Execution of the sum to leading order in electrolyte concentration produces the result $-(q^2/Db)P \ln(\kappa b)$ for the work of assembling the linear array, where P is the number of charged sites in the array. Typically, the nearest neighbor spacing b is small, but the logarithmic dependence indicates that only distant pairs (pairs separated by distances on

the order of a Debye length) contribute significantly to the sum, so the use of the limiting Debye–Hückel pair potential is rigorous. Caution is elicited, however, by a qualitative difference between the logarithmic work in the case of the polyion and the exponentially screened work in spherical geometry: the latter is well-behaved in the limit of infinite Debye length, while divergence of the former suggests that an accumulation of counterions near the polyion cannot be diluted away.

To check for the possibility of a nondilutable counterion layer, we replace the charges q on the linear lattice by renormalized charges $(1 - \theta)q$, $0 \leq \theta \leq 1$, where θ represents the number of nondilutable, or condensed, counterions per charged site on the lattice. Note that we do not assume the existence of a condensed layer, since θ is determined by free energy minimization, and one of the tested values of θ is zero. The limiting Debye–Hückel work w_p required to assemble a large number P of renormalized charges on a linear lattice with spacing b, in units of $k_B T$, is given by

$$w_p = -(1 - \theta)^2 \xi P \ln(\kappa b) \tag{1}$$

where $\xi = q^2/Dk_B Tb$ is the ratio of the Bjerrum length $q^2/Dk_B T$ to the charge spacing b, a convenient dimensionless measure of the linear charge density of the polyion. If there are condensed counterions, there must be a free energy contribution w_{trans} from the transfer process θP Na^+(free) $\rightarrow$ θP Na^+(condensed),

$$w_{trans} = \theta P \ln\left(\frac{\theta}{c_s Q}\right) \tag{2}$$

where c_s is the solution concentration of 1:1 electrolyte, and Q is an internal partition function for the condensed counterions.

The total work w required to assemble the polyion charges is the sum $w_p + w_{trans}$, and for its derivative with respect to θ we obtain

$$\frac{P^{-1}\partial w}{\partial \theta} = -\xi[\theta - (1 - \xi^{-1})]\ln c_s + f(\theta) \tag{3}$$

where $f(\theta)$ is an expression independent of electrolyte concentration c_s that may easily be set down explicitly. In writing Eq. 3, we have combined two $\ln c_s$ terms, one appearing transparently in the formula for w_{trans}, the other implicitly in w_p, since $\kappa^2 = \text{const} \times c_s$. Equation 3 may be regarded as an expansion in electrolyte concentration with a leading $\ln c_s$ term that dominates for sufficiently dilute solutions, and we consider this term first.

There are two cases. When $\xi \leq 1$, $\partial w/\partial \theta > 0$ if $\theta > 0$. The equilibrium state of minimum free energy is therefore at $\theta = 0$, and there are no condensed counterions and no requirement for renormalization of polyion charge, and limiting Debye–Hückel theory goes through unmodified. How-

ever, when $\xi > 1$, the derivative of free energy is negative when the variable θ is less than the value $1 - \xi^{-1}$ but positive when θ exceeds this value. The meaning is that to leading order in c_s there is a stable equilibrium state at $\theta = 1 - \xi^{-1}$. For Debye–Hückel theory to work, the polymer charge must be renormalized by the factor $1 - \theta$, or ξ^{-1}. The charge renormalization is accomplished physically by the condensation of $(1 - \xi^{-1})P$ counterions onto the polyion chain.

The equilibrium value $\theta = 1 - \xi^{-1}$ makes the ln c_s term in Eq. 3 for the free energy derivative vanish. The stability of the condensed layer persists into the next order of approximations if $f(\theta)$ is set to zero at $\theta = 1 - \xi^{-1}$. This condition, $f(\theta)|_{\theta=1-\xi^{-1}} = 0$, written out explicitly, becomes an ordinary equation for the condensed layer partition function Q. Solving it, we find a simple expression for Q

$$Q = 8\pi e(\xi - 1)b^3 \tag{4}$$

where e is the base of natural logarithms. The units are volume per charged polyion site. In the simplest possible model, Q is a free volume for the counterions, pictured as mobile and unhindered with uniform local concentration $(1 - \xi^{-1})/Q$. For DNA, $b = 0.17$ nm, $\xi = 4.2$, and $Q = 1.07$ nm^3. With the free volume interpretation, the condensed counterions are enclosed within a shell around the DNA rod with outer radius 1.7 nm and inner radius 1 nm (a reasonable value for a hard rod cutoff for DNA). The local concentration is then equal to 0.71 ions/nm^3, or 1.2 M (independent of the external 1:1 electrolyte concentration).

Simple as it is, there is much to discuss about the condensed layer partition function Q. An approximation has been made in its derivation. We have assumed that Q does not depend on θ, the number of condensed counterions (in the derivative of the free energy with respect to θ, we have taken $\partial \ln Q/\partial\theta$ as negligible). The physical meaning is that short-range correlations among the condensed counterions are not considered. Within this approximation, Eq. 4 indicates that the sole structural determinant of Q is the linear charge density of the polyion. Note that the result $\theta = 1 - \xi^{-1}$ for the equilibrium *number* of condensed counterions was derived more generally and is not affected by any such approximation.

Insight into the partition function Q may be gained by continuing for the moment to interpret it as a local free volume. Suppose that an aqueous environment is replaced by a solvent of lower dielectric constant. Long-range electrostatic interactions are then enhanced. According to Eq. 4, the condensed layer responds by expanding (ξ is inversely proportional to the dielectric constant). A straightforward interpretation of this behavior follows from the presence of the factor $\xi - 1$ in Eq. 4. This quantity is the reduced linear charge density of the condensed layer. A decrease of bulk dielectric

constant results in a greater number of condensed counterions (according to the equation $\theta = 1 - \xi^{-1}$) and hence an increased linear charge density of the condensed layer. The condensed layer then compensates for the increased electrostatic repulsion by expanding.

A similarly transparent explanation is available for the effect of temperature. If T is increased (at fixed dielectric constant), the value of ξ decreases, and hence the number θ of condensed counterions also decreases. A smaller number of condensed counterions means that the charge density of the condensed layer is less. The free volume, which scales like the charge density of the condensed layer, compensates by contracting. A negative thermal expansion coefficient of the condensed layer (again, at fixed dielectric constant) may be interesting, but it is also easily understood.

The picture of a condensed phase of fully solvated counterions is convenient but not inherent to the theory. If the condensed counterions are instead conceived as partly desolvated, or, equivalently, if the effective local dielectric constant for the condensed layer is less than the bulk value, then the partition function Q becomes a product of the volume of the condensed layer times a Boltzmann factor accounting for the higher local standard-state chemical potential of a condensed counterion relative to a counterion in bulk solution. Since this product is equal to the invariant right-hand side of Eq. 4, we conclude that the volume of the condensed layer is larger than for the case of fully solvated condensed counterions. The condensed layer compensates for a higher ground-state energy by increasing the volume available for translational entropy. Conversely, if the polyion provides a bit of short-range binding energy to the condensed counterions, which is one way of thinking about site-binding or adsorption of the condensed counterions as a monolayer, then the condensation volume contracts, leaving Q invariant in accordance with Eq. 4.

III. PAIR POTENTIALS AND DISTRIBUTION FUNCTIONS

In this section, we discuss the interaction of a counterion and a rodlike segment of a polyion as a function of separation distance r between the two [59]. We consider as well the coion–polyion [59] and polyion–polyion pair potentials [57,58]. In the latter case, the two polyions may be identically charged or oppositely charged. For each type of pair, there is a polyion self-energy of the form of Eq. 1 (for the polyion–polyion pairs the factor P is replaced by $2P$). The essential difference from Eq. 1 is that the number of condensed counterions θ is now a function of the pair separation distance, $\theta = \theta(r)$. Similarly, in the transfer free energy Eq. 2, both θ and the condensed layer partition function Q depend on r. In addition to the self-assem-

bly and transfer work, there is also a Debye–Hückel interaction between the members of the pair, given for the counterion–polyion pair as

$$w_{cp}(r) = -2\xi[1 - \theta(r)]K_0(\kappa r) \tag{5}$$

Similar expressions apply to the other types of pairs, and all of them contain the zeroth-order modified Bessel function of the second kind $K_0(\kappa r)$, or, simply, the Bessel K_0 function. In Figure 1 we show a graph of the smoothly decreasing nonoscillatory Bessel K_0 function, which can subsequently be contrasted with the pair potentials $w(r)$ that emerge only after the three free energy terms (polyion self-energy, counterion transfer, and direct pair interaction) are added and minimized, a procedure that involves determination of the functions $\theta(r)$ and $Q(r)$.

The K_0 function decreases exponentially at large values of κr, that is, when the distance r is larger than the Debye length $1/\kappa$. When r is smaller than the Debye length, an asymptotic expansion becomes valid,

$$K_0(\kappa r) \sim -\ln\left(\frac{1}{2}\,\kappa r\right) - 0.5772\ldots \tag{6}$$

where the numerical term is the Euler γ constant. The logarithmic term is

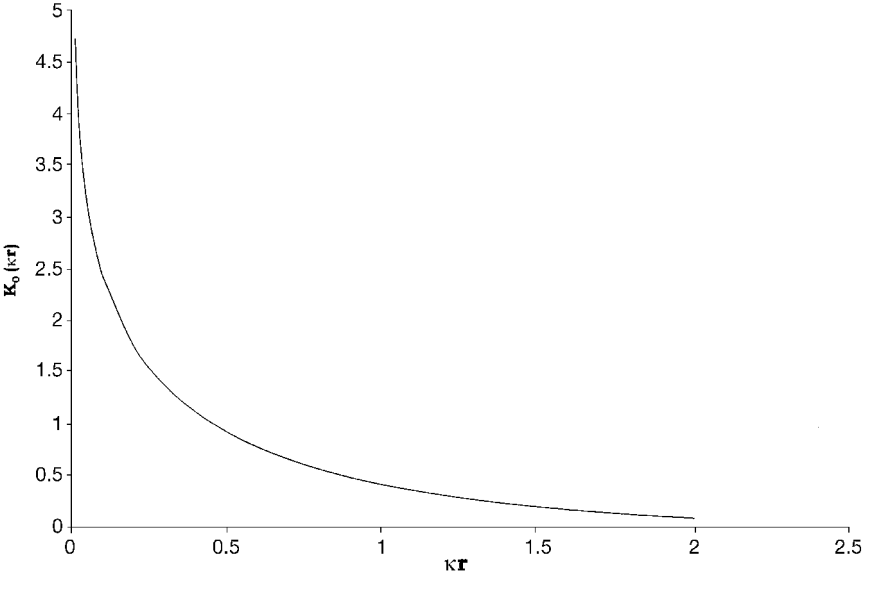

FIG. 1 The zeroth-order modified Bessel function of the second kind, $K_0(\kappa r)$.

crucial, because it contributes on an equal basis with the logarithmic dependence of the self-assembly and transfer terms toward determination of the number of condensed counterions and their properties (partition function). We expect and indeed find that the presence of a counterion, coion, or another polyion fixed at distance r from a given polyion has a profound effect on the condensed counterions and overall free energy. This situation is different from mean-field (Poisson–Boltzmann) theory, wherein a counterion or coion at r has no effect on the average distribution of small ions around the polyion. In fact, if we were doing a mean-field theory, our counterion–polyion pair potential would merely be given by Eq. 5 with $1 - \theta$ equal to its value ξ^{-1} in the absence of the counterion at r.

To proceed, we need a precise criterion for the range of distances in which we may use the logarithmic expansion of $K_0(\kappa r)$. We have divided space (i.e., separation distances r between members of the pair) into many regions. *Far* distances are those on the order of a Debye screening length $1/\kappa$. *Near* distances are much smaller than a screening length; more precisely, these distances remain asymptotically constant as $1/\kappa$ tends to infinity. These two regions of space are present in a Poisson–Boltzmann analysis also [62]. For the counterion–polyion pair, the region of near distances corresponds to the space occupied by the condensed layer, both in counterion condensation and in Poisson–Boltzmann theory. In Poisson–Boltzmann theory, the near and far regions are separated by a single distance that with dilution recedes to infinity like the square root of $1/\kappa$ [63]. This boundary separates the condensed layer from the more diffuse Debye–Hückel-like ion cloud. In Poisson–Boltzmann theory, the two populations of counterions—condensed and diffuse—touch, and until a sharp criterion was introduced [61,64], they could not be distinguished by numerical methods. In counterion condensation theory, the two counterion populations do not touch. They are separated, not by a single distance, but by an *intermediate* region of distances. In turn, the intermediate region consists of a continuum of asymptotic distances. Each distance in the intermediate region recedes to infinity with dilution like a fractional power of $1/\kappa$. The square root corresponds to only one intermediate distance. Intermediate distances close to (but larger than) near distances are those with fractional powers close to zero. Intermediate distances close to (but smaller than) far distances are those with fractional powers close to unity. Since near and intermediate distances are asymptotically much smaller than $1/\kappa$, we use Eq. 6 in these regions. Inverted forces occur in the intermediate region.

We have also introduced a boundary between the near and intermediate regions into the theory. The boundary recedes to infinity logarithmically with $1/\kappa$. Therefore it is a larger distance than any near distance but a smaller distance than any intermediate distance. For given values of $1/\kappa$ necessary

for numerical calculations, we have determined the boundary between near and intermediate regions as $r = 1/e\kappa$, e the base of natural logarithms. The boundary between intermediate and far regions is $r = 1/\kappa$. Inverted forces occur in the intermediate range $1/e\kappa \leq r \leq 1/\kappa$, in other words, inside a Debye length but outside the condensed counterion layer.

The theoretical analysis is similar to the case of an isolated polyion as outlined in the previous section. Here the three work components are added, and the derivative of the sum with respect to $\theta(r)$ at fixed r is set to zero. The ln c_s and constant terms are isolated and independently set to zero, producing formulas for both $\theta(r)$ and $Q(r)$. Substituted back into the expression for the overall work (with reference state at infinity), these optimized functions generate the pair potential of mean force $w(r)$. The radial distribution function $g(r)$ is given by $\exp[-w(r)]$ (the pair potential is in units of k_BT).

We discuss some of the results, beginning with the number of condensed counterions in the case of the counterion–polyion pair. When a counterion is brought from infinity to a distance r in the far Debye–Hückel-like region, the number of counterions condensed on the polyion remains at the same constant value as on the isolated polyion, $\theta(r) = 1 - \xi^{-1}$. When the counterion continues its approach and enters the near region, however, the number of condensed counterions per polyion charge is changed to a different constant value, $\theta(r) = 1 - \xi^{-1} - (1/P)$. Since $P\theta$ is the total number of counterions condensed on the polyion with P charges, this formula signifies that when a counterion is brought from infinity into the near region, a condensed counterion is freed, so that the remaining number of condensed counterions plus one for the counterion at near r is invariant. If the counterion brought into the near region from infinity is Z-valent in a sea of 1:1 electrolyte, then $|Z|$ univalent counterions leave the near region; in this more general case, the linear charge density of the condensed layer, including the Z-valent counterion, is invariant. This property allows us to identify the near region as the space occupied by the condensed layer, in agreement with Poisson–Boltzmann theory. In our model, the condensed layer extends from the polyion out to distance $r = 1/e\kappa$. We will see, however, that the tail of the condensed layer is highly rarified, and for practical purposes a picture of condensed counterions as a monolayer in close association with the polyionic chain is probably reasonably accurate.

When a univalent counterion is brought from infinity into the intermediate region between $1/e\kappa$ and $1/\kappa$, the number of condensed counterions changes progressively with penetration from its constant value when the counterion is at far r to its decreased constant value when the counterion is inside the condensed layer, namely, in the intermediate region,

$$\theta(r) = 1 - \xi^{-1} + P^{-1} \ln \kappa r \tag{7}$$

In Figure 2 we show graphs of $P\theta(r) - P\theta_\infty = \ln \kappa r$ for two ionic strengths. The negative values indicate the *counterion release* effect, which provides an important entropic driving force for the binding of oppositely charged ligand–polyion pairs.

In the case of two identical rodlike polyions each of charge density ξ, approaching in parallel from infinity to distance r, $\theta(r)$ increases from its constant value $1 - \xi^{-1}$ for far r to a higher constant value $1 - (2\xi)^{-1}$ for r in the near region. The physical meaning is that when two polyions are close to each other, counterions condense on the pair as though it were a single polyion of twice the charge density.

Although the number of counterions condensed on a polyion is not changed when a counterion or another polyion is brought from infinity to a far distance r, the structure of the condensed layer is perturbed by the in-

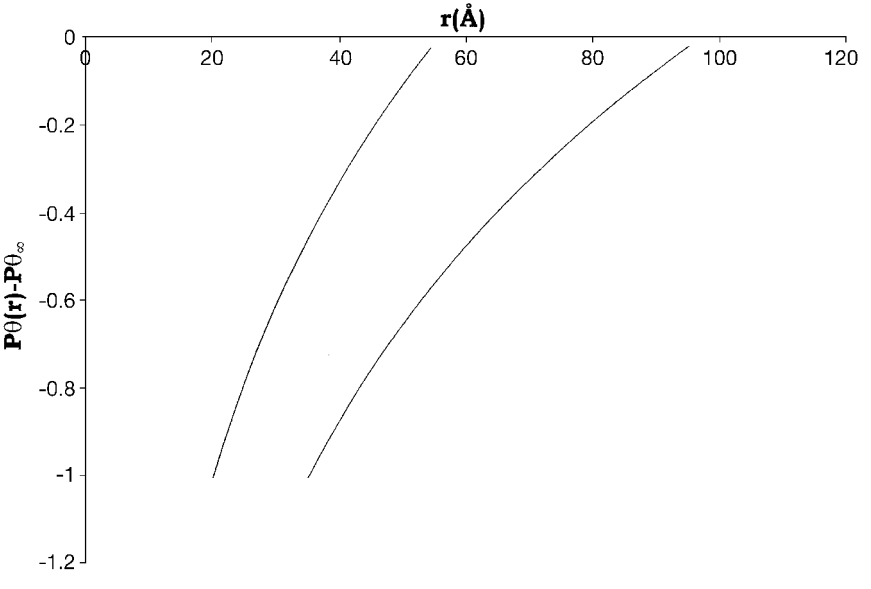

FIG. 2 The number of counterions released from the condensed counterion layer when another counterion is brought from infinity to fixed intermediate distance r from the polyion. Curve on right, Debye length 96 Å (0.001 M NaCl); curve on left, Debye length 55 Å (0.003 M NaCl). The fractional values are understood in the sense of an ensemble or time average. Both curves attain the limiting value of one released counterion when the intruding ion reaches the edge of the condensed layer at $r = (e\kappa)^{-1}$.

trusion (even at far distances). For example, when a counterion is at far r, the partition function of the condensed layer $Q(r)$ is increased from its isolated value Q_∞, given by Eq. 4,

$$Q(r) = Q_\infty \exp\left[\frac{2\xi}{P} K_0(\kappa r)\right] \tag{8}$$

An explanation of the increased partition function follows from the simplified but intuitive interpretation of the partition function as a free volume for the condensed counterions. The counterion at far r is engaged in repulsive electrostatic interaction with the condensed counterions (represented by the Bessel function in Eq. 8), so, in this sense, the condensed layer together with the counterion at r may be conceptualized as a generalized condensed layer. The generalized layer has a higher self-repulsive charge density than the isolated physical layer (which is exclusive of the counterion at r). The counterion at r is *fixed* there and cannot contribute to structural rearrangement of the generalized layer in response to the increased charge density. So, in response to the augmented charge density, the volume of the physical

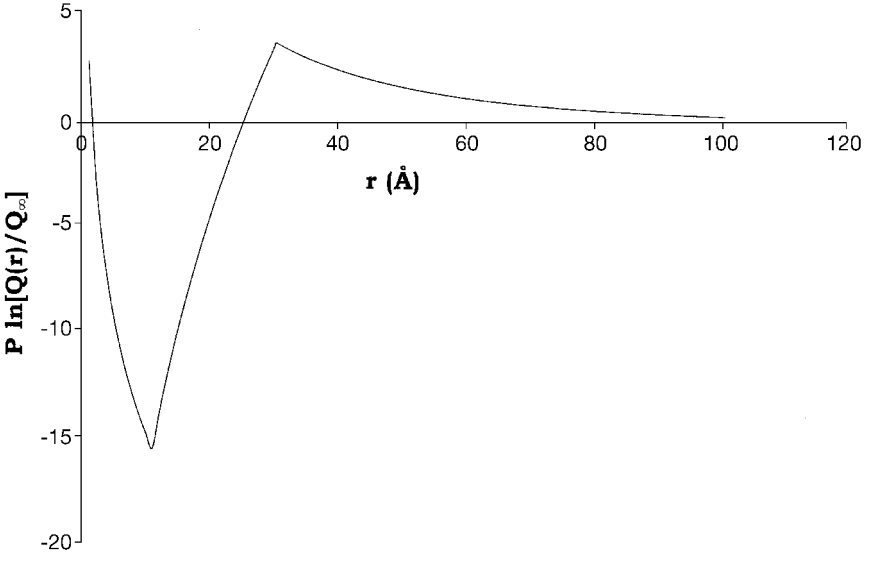

FIG. 3 The partition function of the condensed counterion layer as a function of the distance r from the polyion of another counterion that has been brought from infinity to r. Debye screening length 30 Å (0.01 M NaCl); polyion charge spacing 1.7 Å.

condensed layer expands, thus explaining the trend in Eq. 8. We do not exhibit formulas for $Q(r)$ in the intermediate and near ranges here, but in Figure 3 we show a graph of $P \ln[Q(r)/Q_\infty]$ for the counterion–polyion pair across all three regions. Notice the free-energetically unfavorable contraction of the partition function when the counterion penetrates into the intermediate region.

Figure 4 presents a graph of $Q(r)$ for a pair of identical rodlike polyion segments in parallel with separation distance r. Note the large increase as the two polyions approach through the intermediate range of distances. In a free volume interpretation, the condensed layers expand, providing an increased entropy that would tend to drive an attractive interaction between the polyions.

Plots of the pair potentials $w(r)$ exhibiting inverted forces may be seen in our other publications. The counterion–polyion potential is attractive in the near and far regions but inverted (repulsive) in the intermediate region. For like-charged polyions, the polyion–polyion potential is repulsive in the near and far regions but attractive for intermediate distances. Here we show graphs of the radial distribution functions $g(r) = \exp[-w(r)]$. In Figure 5

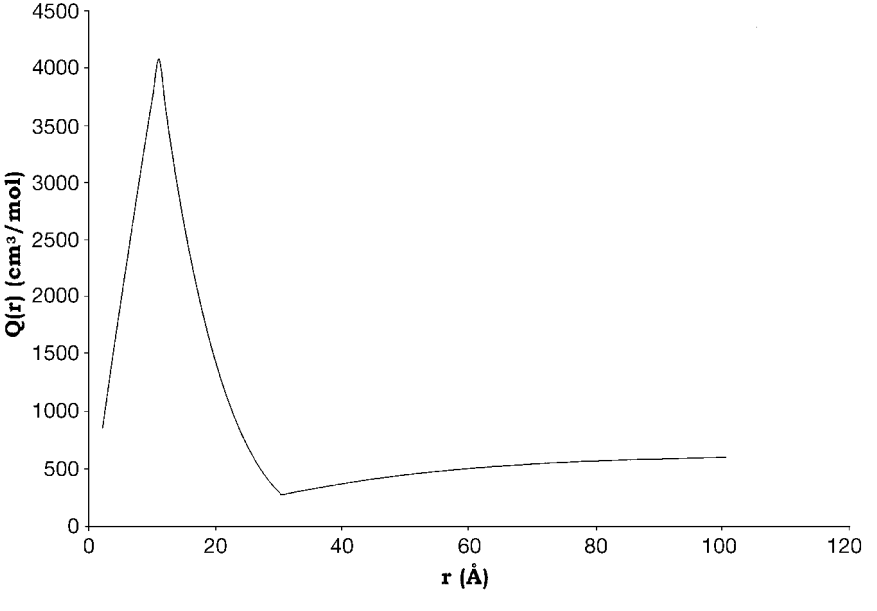

FIG. 4 The partition function of the counterion layer condensed on a pair of identical rodlike polyions in parallel orientation with separation distance r. Debye screening length 30 Å (0.01 M NaCl); polyion charge spacing 1.7 Å.

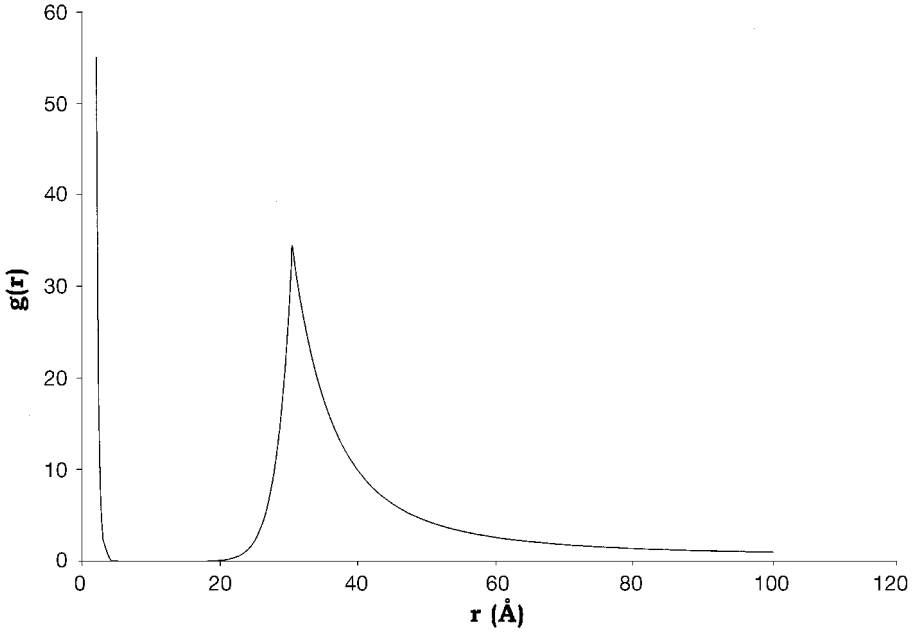

FIG. 5 The counterion radial distribution function shows two peaks, an inner condensed layer peak and an outer peak corresponding to the Debye–Hückel cloud. Debye screening length 30 Å (0.01 M NaCl); polyion charge spacing 1.7 Å.

the radial distribution function for counterions surrounding a polyion has two peaks. The inner peak corresponds to the condensed layer; the outer peak, to the uncondensed Debye–Hückel cloud. The inverted repulsive force produces a spatial gap between the two counterion populations that is nearly devoid of counterions. A counterion finding itself in the outer part of this gap is repelled back into the diffuse cloud. If a counterion is transiently in the inner part of the gap, it is strongly attracted into the condensed layer. Figure 6 shows the coion–polyion distribution function. There is a single coion peak located between the two counterion peaks. This kind of layering might be the expected outcome of short-range packing of spheres, like an ionic crystal, but only long-range electrostatics have been included in our model—note the low electrolyte concentration involved and the associated scale of distances. The coion peak reflects an inverted intermediate-range attractive force; a coion transiently located just within distance $r = 1/\kappa$ is directed toward the polyion.

The inverted attractive force between two identical parallel polyion segments creates a single polyion–polyion peak at intermediate distances in the

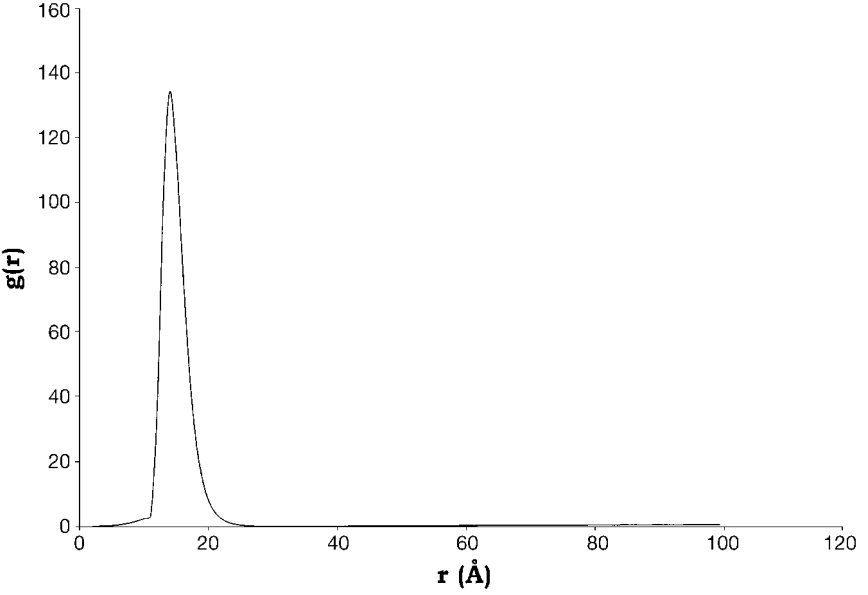

FIG. 6 The coion radial distribution function shows a single peak, located between the two counterion peaks in Figure 5. Debye screening length 30 Å (0.01 M NaCl); polyion charge spacing 1.7 Å.

polyion–polyion radial distribution function shown in Figure 7. The potential of mean force in this case was calculated for a polyion pair at infinite polyion dilution. In other words, the interaction of the two polyions at any distance is not influenced by the presence of other polyions. The distribution function in this illustration is analogous to the radial distribution function for a low-density gas of attracting molecules (like water vapor or CO_2). But the calculation does leave open the possibility of the formation of clusters based on attractive forces at higher polyion concentrations, as discussed in the following section.

The cause of the inverted attraction in the polyion–polyion case is the strong distance dependence of the condensed layer partition function $Q(r)$ revealed in Figure 4. The entropic tendency toward attraction mentioned above in connection with Figure 4 turns out to dominate the balance of forces. Staying with a free volume interpretation of $Q(r)$, we can observe that when two polyions approach, their electric fields merge, and the common field is relatively flat in the space between the polyions. The barrier to entropic expansion of the condensed layers having been removed, the condensed counterions flood into the large volume of space between the poly-

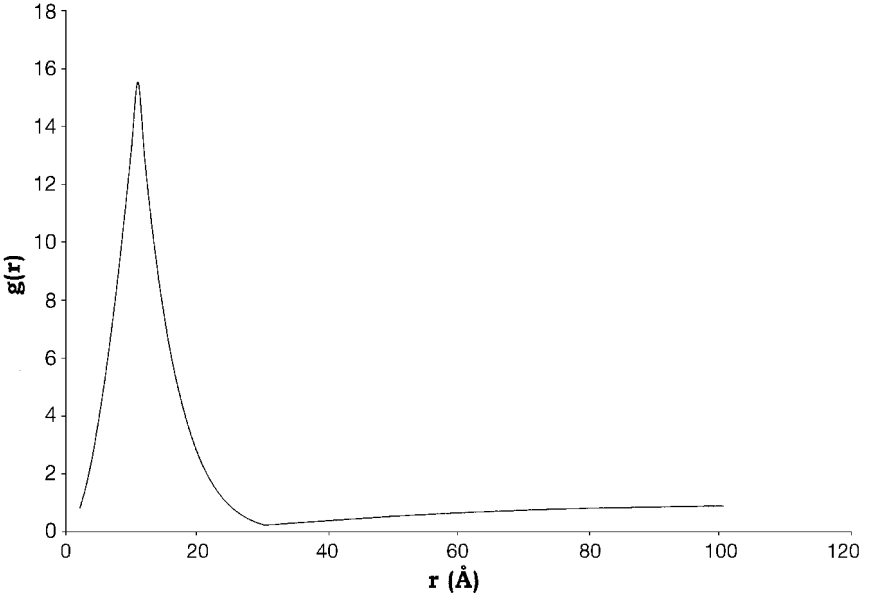

FIG. 7 The polyion–polyion radial distribution function at infinite polymer dilution. An attractive interaction in the intermediate region generates a peak position there. Debye screening length 30 Å (0.01 M NaCl); polyion charge spacing 1.7 Å.

ions, and their increased entropy is the ''glue'' that prevents separation of the polyions.

Figure 8 shows the distribution of condensed counterions in an attractive configuration within the free volume model. As described in detail elsewhere [57], the distribution is obtained by an elliptic integral analysis of the boundary curves of the free volume. The boundaries have different shapes for different distances between the two polyions, but they all belong to the family of Cassinian ovals, or fourth-order ellipses. At far distances, the boundary curves consist of two disjoint closed branches, each enclosing a single polyion. But the boundary merges into a single closed curve surrounding both polyions when the polyions approach into the attractive region, producing a shape typified in Figure 8.

Finally, in Figure 9 we show the distribution function for parallel approach of two polyion segments identical but for opposite charge. There is an inverted repulsion, reflected in the strong depression of $g(r)$ below the value unity.

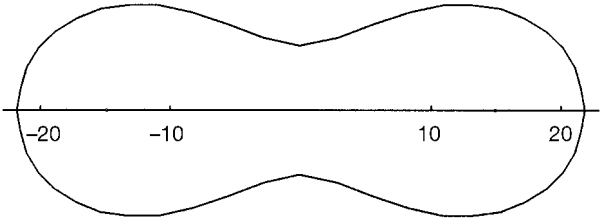

FIG. 8 A calculated cross-section of the cylindrically symmetric distribution of condensed counterions held in common by a pair of identical parallel rodlike polyions when the partition function for the condensed layer is interpreted as a free volume. The numerical scale is in Å, and the polyions pierce the page at ± 15 Å. The Debye length equals 30 Å, so the theoretically calculated condensed layer lies inside the Debye atmosphere, as required on physical grounds. Polymer charge spacing 1.7 Å.

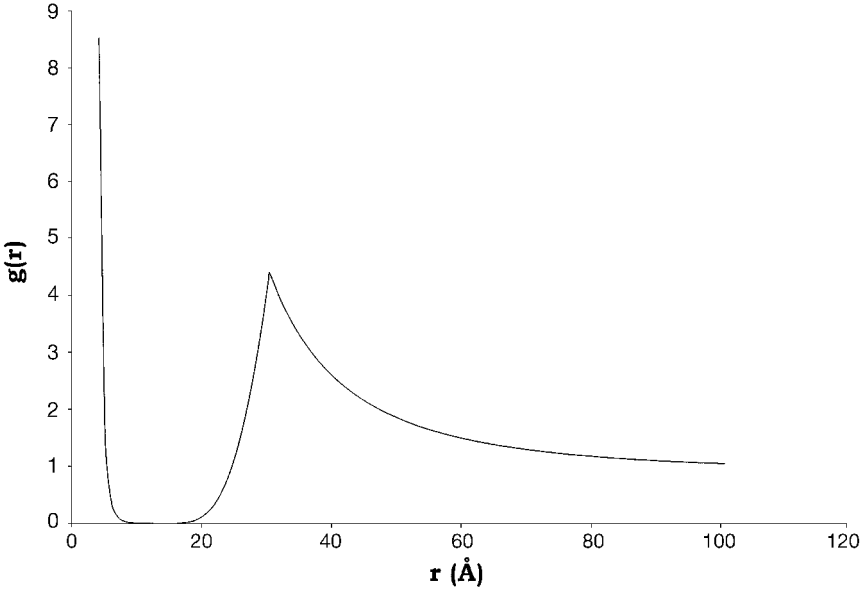

FIG. 9 The radial distribution function for an oppositely charged polyion pair at infinite polymer dilution. The polyions are identical but for opposite charge with charge spacing 1.7 Å.

IV. POLYION CLUSTERS

There is ample experimental evidence that identically charged polymers in the presence of ordinary univalent counterions have a tendency to form loose clusters in solution [65–70], and we have asked whether the attractive polyion–polyion potential discussed in Sec. III can stabilize a finite-sized cluster of parallel rodlike polyions without leading to precipitation [71,72]. The theoretical problem is complicated by a failure of pairwise additivity; the work of assembling N polyions is not equal to the work of assembling the $N(N - 1)/2$ polyion pairs, each in isolation from the other $N - 2$ polyions. To be sure, the Debye–Hückel interaction term for a cluster (the generalization of Eq. 5 above) takes the form of a pairwise sum over polyions,

$$w_{pp}(\{r_{ij}\}) = 2\xi[1 - Z\theta(\{r_{ij}\})]^2 \sum_{i<j} K_0(r_{ij}) \tag{9}$$

where $\{r_{ij}\}$ is the entire set of pairwise rod–rod distance variables. But the overall work of assembling the cluster is not merely the pairwise superim-

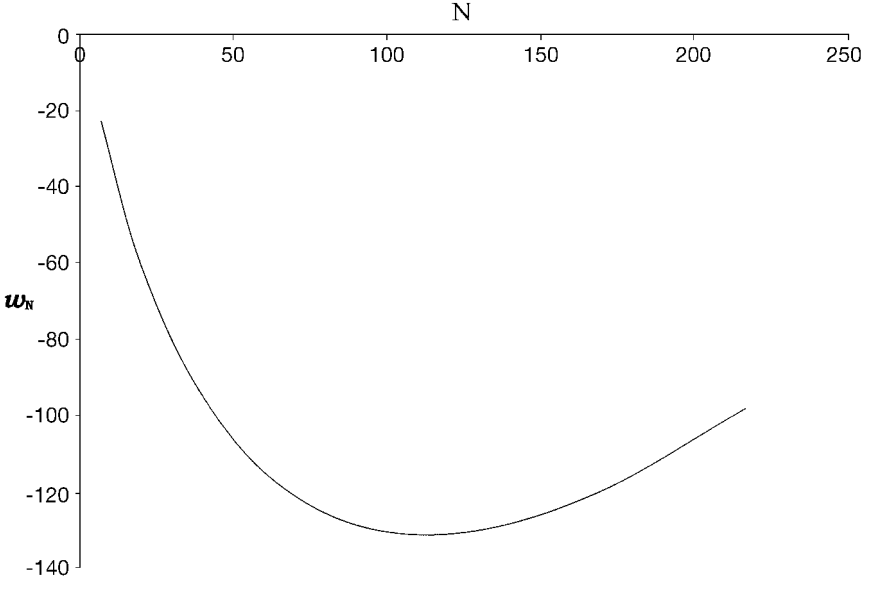

FIG. 10 The free energy required to assemble N parallel polyions in hexagonal array as a function of N. The reported values of reduced free energy w_N are total free energy in units of k_BT divided by the fixed number of charged sites on each polymer.

posable Debye–Hückel work. There are also the intrapolymer and counterion transfer components given by Eqs. 1 and 2, respectively. The final minimized total work is not given by Eq. 9 and is not pairwise additive. In the minimization, each term of the sum in Eq. 9 must be considered separately, and its treatment depends on whether the specific pair separation distance r_{ij} is in the near, intermediate, or far range of distances, as discussed above.

We have calculated the free energy of assembly of N parallel polyions in a hexagonal array up to seven shells, and the results are plotted in Figure 10. The free energy first decreases with an increasing number of polyions, then hits a minimum and increases with further growth of the cluster. The minimum signifies stability of a finite-sized cluster.

ACKNOWLEDGMENT

Our research is supported in part by a United States Public Health Service grant (GM36284).

REFERENCES

1. Manning GS. Limiting laws and counterion condensation in polyelectrolyte solutions. I. Colligative properties. J Chem Phys 1969; 51:924–933.
2. Boyd GE, Wilson DP. Enthalpies of dilution of strong polyelectrolyte solutions. Comparisons with the cell and line charge theories. J Phys Chem 1976; 80: 805–808.
3. Boyd GE, Wilson DP, Manning GS. Enthalpies of mixing of polyelectrolytes with simple aqueous electrolyte solutions. J Phys Chem 1976; 80:808–810.
4. Rinaudo M, Milas M. Ionic selectivity of polyelectrolytes in salt-free solutions. In: Rembaum A, Sélégny E, eds. Polyelectrolytes and Their Applications. Dordrecht-Holland: D Reidel, 1975:31–49.
5. Kwak JCT, Nelson RWP. Mean activity coefficients for the simple electrolyte in aqueous mixtures of polyelectrolyte and simple electrolyte. 4. The systems nickel chloride–nickel poly(styrenesulfonate), zinc chloride–zinc poly-(styrenesulfonate), and cadmium chloride–cadmium poly(styrenesulfonate). J Phys Chem 1978; 82:2388–2391.
6. Paoletti S, Delben F, Crescenzi V. Enthalpies of dilution of partially neutralized maleic acid copolymers in water. Correlation of experiments with theories. J Phys Chem 1981; 85:1413–1418.
7. Hales PW, Pass G. Effect of cation size on the enthalpy of dilution of alkali-metal salts of carboxymethylcellulose. J Chem Soc Faraday Trans 1 1981; 77: 2009–2013.
8. Skerjanc J, Regent A, Bozovic Kocijan L. Heats of mixing of polyelectrolytes and simple electrolyte solutions. J Phys Chem 1980; 84:2584–2587.
9. Kakehashi R, Maeda H. Donnan equilibria of simple electrolytes in polyelectrolyte solutions. J Chem Soc Faraday Trans 1996; 92:3117–3121.

10. Oppermann W, Wagner M. Determination of thermodynamic properties of polyelectrolyte solutions via analysis of the sedimentation equilibrium. Langmuir 1999; 15:4089–4092.
11. Nagaya J, Minakata A, Tanioka A. Conductance and counterion activity of ionene solutions. Langmuir 1999; 15:4129–4134.
12. Essafi W. Structure des polyélectrolytes fortement chargés. Ph.D. dissertation, Université de Paris VI, Paris, France, 1996.
13. Manning GS. Limiting laws and counterion condensation in polyelectrolyte solutions. II. Self-diffusion of the small ions. J Chem Phys 1969; 51:934–938.
14. Manning GS. Limiting laws and counterion condensation in polyelectrolyte solutions. 7. Electrophoretic mobility and conductance. J Phys Chem 1981; 85: 1506–1515.
15. Manning GS. Linear analysis of the polarization of macroions. J Chem Phys 1989; 90:5704–5710.
16. Ander P, Kardan M. Interactions of sodium ions with polyelectrolytes of varying charge density. Macromolecules 1984; 17:2431–2436.
17. Henningson CT, Karluk D, Ander P. Comparison of sodium ion interactions with sodium salts of (carboxymethyl)cellulose and vinylic polyelectrolytes of varying charge density by diffusion. Macromolecules 1987; 20:1286–1291.
18. Shaaban AH, Ander P. Electric transport of aqueous salt-free polyelectrolyte solutions. Polymer Preprints 1993; 34(1):970–971.
19. Ware BR, Klein JW, Zero K. Interaction of a fluorescent spermine derivative with a nucleic acid polyion. Langmuir 1988; 4:458–463.
20. Wandrey C. Concentration regimes in polyelectrolyte solutions. Langmuir 1999; 15:4069–4075.
21. Hoagland DA, Smisek DL, Chen DY. Gel and free electrophoresis of variably charged polymers. Electrophoresis 1996; 17:1151–1160.
22. Gao JY, Dubin PL, Sato T, Morishima Y. Separation of polyelectrolytes of variable compositions by free-zone capillary electrophoresis. J Chromatography A 1997; 766:233–236.
23. Ciszkowska M, Osteryoung JG. Counterion diffusion reveals coil-to-helix transition in polyelectrolytes. J Am Chem Soc 1999; 121:1617–1618.
24. Mohanty U, Searls T, McLaughlin LW. Anomalous migration of short sequences of nucleic acids in polyacrylamide gels: prediction and experiment. J Am Chem Soc 1998; 120:8275–8276.
25. Mohanty U, Stellwagen NC. Free solution mobility of oligomeric DNA. Biopolymers 1999; 49:209–214.
26. Liu H, Skibinska L, Gapinski J, Patkowski A, Fischer EW, Pecora R. Effect of electrostatic interactions on the structure and dynamics of a model polyelectrolyte. I. Diffusion. J Chem Phys 1998; 109:7556–7566.
27. Manning GS. Limiting laws and counterion condensation in polyelectrolyte solutions. V. Further development of the chemical model. Biophys Chem 1978; 9:65–70.
28. Manning GS. A condensed counterion theory for polarization of polyelectrolyte solutions in high fields. J Chem Phys 1993; 99:477–486.

29. Manning GS, Ray J. Fluctuations of counterions condensed on charged polymers. Langmuir 1994; 10:962–966.
30. Mohanty U, Zhao Y. Polarization of counterions in polyelectrolytes. Biopolymers 1995; 38:377–388.
31. Penafiel LM, Litovitz TA. High frequency dielectric dispersion of polyelectrolyte solutions and its relation to counterion condensation. J Chem Phys 1992; 97:559–567.
32. Manning GS. The molecular theory of polyelectrolyte solutions with applications to the electrostatic properties of polynucleotides. Quart Rev Biophys 1978; 11:179–246.
33. Ray J, Manning GS. Theory of delocalized ionic binding to polynucleotides: structural and excluded-volume effects. Biopolymers 1992; 32:541–549.
34. Mattai J, Kwak JCT. Mg and Ca binding to heparin in the presence of added univalent salt. Biochim Biophys Acta 1981; 677:303–312.
35. Mattai J, Kwak JCT. Influence of univalent counterions on the binding of divalent metal ions by the biopolyelectrolyte dextran sulfate. J Phys Chem 1982; 86:1026–1030.
36. Mattai J, Kwak JCT. Binding of La^{3+} ions by dextran sulfate polyanions in aqueous solutions containing excess sodium chloride. J Phys Chem 1984; 88: 2625–2629.
37. Granot J, Kearns DR. Interactions of DNA with divalent metal ions. III. Extent of metal binding: experiment and theory. Biopolymers 1982; 21:219–232.
38. Dais P, Peng QJ, Perlin AS. Binding of magnesium and lanthanum ions to heparin in the presence of sodium ions. A relationship between ^{13}C chemical shift displacements and counterion condensation theory. Can J Chem 1987; 65: 1739–1745.
39. Dais P, Peng QJ, Perlin AS. A relationship between ^{13}C chemical shift displacements and counterion condensation theory in the binding of calcium ion by heparin. Carbohydrate Res 1987; 168:163–179.
40. Rabenstein DL, Robert JM, Peng J. Multinuclear magnetic resonance studies of the interaction of inorganic cations with heparin. Carbohydrate Res 1995; 278:239–256.
41. Rivas BL, Moreno-Villoslada I. Binding of Cd^{2+} and Na^{+} ions by poly(sodium 4-styrenesulfonate) analyzed by ultrafiltration and its relation with the counterion condensation theory. J Phys Chem B 1998; 102:6994–6999.
42. Rivas BL, Moreno-Villoslada I. Evaluation of the counterion condensation theory from the metal ion distributions obtained by ultrafiltration of the system poly(sodium 4-styrenesulfonate)/Cd^{2+}/Na^{+}. J Phys Chem B 1998; 102:11024–11028.
43. Flock S, Labarbe R, Houssier C. Dielectric constant and ionic strength effects on DNA precipitation. Biophys J 1996; 70:1456–1465.
44. Li AZ, Huang H, Re X, Qi LJ, Marx KA. A gel electrophoresis study of the competitive effects of monovalent counterion on the extent of divalent counterion binding to DNA. Biophys J 1998; 74:964–973.
45. Li AZ, Marx KA. The iso-competition point for counterion competition binding

to DNA: calculated multivalent versus monovalent cation binding equivalence. Biophys J 1999; 77:114–122.
46. Raspaud E, Olvera de la Cruz M, Sikorav JL, Livolant F. Precipitation of DNA by polyamines: a polyelectrolyte behavior. Biophys J 1998; 74:381–393.
47. Manning GS. Limiting laws and counterion condensation in polyelectrolyte solutions. 6. Theory of the titration curve. J Phys Chem 1981; 85:870–877.
48. Friedman RAG, Shahin MA, Zuckerbraun S. Polyelectrolyte effects on 9-aminoacridine-DNA binding. J Biomol Struct Dynam 1991; 8:977–988.
49. Jayaram J, McConnell KJH, Dixit SB, Beveridge DL. Free energy analysis of protein-DNA binding: the EcoRI endonuclease-DNA complex. J Comput Phys 1999; 151:333–357.
50. Manning GS. Three persistence lengths for DNA. Biopolymers 1988; 27:1529–1542.
51. Manning GS, Ebralidse KK, Mirzabekov AD, Rich A. An estimate of the extent of folding of nucleosomal DNA by laterally asymmetric neutralization of phosphate groups. J Biomol Struc Dynam 1989; 6:877–889.
52. Williams LD, Maher LJ. Electrostatic mechanisms of DNA deformation. Ann Rev Biophys Biomol Struct 2000; 29:497–521.
53. Benegas JC, Pantano S, Vetere A, Paoletti S. Polyelectrolytic aspects of the thermodynamics of conformational transitions: κ carrageenan in formamide. Biopolymers 1999; 49:127–130.
54. Manning GS. Counterion condensation theory constructed from different models. Physica A 1996; 231:236–253.
55. Young MA, Jayaram B, Beveridge DL. Intrusion of counterions into the spine of hydration in the minor groove of B-DNA: fractional occupancy of electronegative pockets. J Am Chem Soc 1997; 119:59–69.
56. Essafi W, Lafuma F, Williams CE. Structural evidence of charge renormalization in semi-dilute solutions of highly charged polyelectrolytes. Eur Phys J B 1999; 9:261–266.
57. Ray J, Manning GS. An attractive force between two rodlike polyions mediated by the sharing of condensed counterions. Langmuir 1994; 10:2450–2461.
58. Ray J, Manning GS. Effect of counterion valence and polymer charge density on the pair potential of two polyions. Macromolecules 1997; 30:5739–5744.
59. Ray J, Manning GS. Counterion and coion distribution functions in the counterion condensation theory of polyelectrolytes. Macromolecules 1999; 32: 4588–4595.
60. Manning GS. The critical onset of counterion condensation: a survey of its experimental and theoretical basis. Ber Bunsenges Phys Chem 1996; 100:909–922.
61. Deserno M, Holm C, May S. The fraction of condensed counterions around a charged rod: comparison of Poisson–Boltzmann theory and computer simulations. Macromolecules, in press; cond-mat/9906277.
62. Ramanathan GV, Woodbury CP. Statistical mechanics of electrolytes and polyelectrolytes. II. Counterion condensation on a line charge. J Chem Phys 1982; 77:4133–4140.

63. Le Bret M, Zimm BH. Distribution of counterions around a cylindrical polyelectrolyte and Manning's condensation theory. Biopolymers 1984; 23:287–312.
64. Belloni L. Ionic condensation and charge renormalization in colloidal suspensions. Colloids and Surfaces A 1998; 140:227–243.
65. Bruno KR, Mattice WL. Long-range intermolecular interactions in dilute aqueous solutions of ionized poly(L-lysine) at low ionic strength. Macromolecules 1992; 25:327–330.
66. Wissenburg P, Odijk T, Cirkel P, Mandel M. Multimolecular aggregation of mononucleosomal DNA in concentrated isotropic solutions. Macromolecules 1995; 28:2315–2328.
67. Sedlak M. The ionic strength dependence of the structure and dynamics of polyelectrolyte solutions as seen by light scattering: the slow mode dilemma. J Chem Phys 1996; 105:10123–10133.
68. Nierling W, Nordmeier E. Studies on polyelectrolyte solutions. VII. Fast, heterogeneous, and slow diffusion modes of poly(diallyl-*N*,*N*-dimethylammonium chloride) in aqueous alcoholic salt solvents. Polym J 1997: 29:795–806.
69. Ermi BD, Amis EJ. Domain structures in low ionic strength polyelectrolyte solutions. Macromolecules 1998; 31:7378–7384.
70. Skibinska L, Gapinski J, Liu H, Patkowski A, Fischer EW, Pecora R. Effect of electrostatic interactions on the structure and dynamics of a model polyelectrolyte. II. Intermolecular correlations. J Chem Phys 1999; 110:1794–1800.
71. Manning GS, Ray J. Theory of open polyelectrolyte clusters. In: Noda I, Kokufuta E, eds. Yamada Conference L: Polyelectrolytes. Osaka, Japan: Yamada Science Foundation, 1999:21–26.
72. Ray J, Manning GS. The formation of loose clusters in polyelectrolyte solutions, submitted.

This Page Intentionally Left Blank

4

Polyelectrolyte Solutions with Multivalent Added Salts: Stability, Structure, and Dynamics

MAURICE DRIFFORD and MICHEL DELSANTI Commissariat á l'Énergie Atomique Saclay, Gif sur Yvette, France

I. INTRODUCTION

Despite continued theoretical and experimental effort, the behavior of polyelectrolyte solutions is less well understood than that of neutral polymer solutions [1,2]. Solutions of polyelectrolyte chains have complex phase diagrams. Regardless of the a priori repulsive electrostatic interactions between the charged monomers of the chains, precipitation is observed in the presence of multivalent ions. With highly charged polyelectrolyte chains, the spatial distribution of charge is strongly inhomogeneous. The high charge density along the polymer chain produces a high electrostatic potential around it, and a fraction of the ions of opposite charge are in close proximity of the chain. A fraction of counterions is consequently located in the immediate vicinity of the polymer chain; this phenomenon is called counterion condensation [3–9]. Precipitation of polyelectrolytes by multivalent salt has been studied for a long time [10–30] but remains poorly understood.

In the first part of this chapter, we will present the phase diagrams of several polyelectrolytes having different backbones (hydrophobic, hydrophilic, rigid, flexible) and different charged groups (carboxylate, sulfonate, sulfate, phosphate) in the presence of multivalent inorganic or organic counterions. One of the principal objectives is to try to find the parameters that control the solubility of highly charged polyelectrolytes in the presence of multivalent counterions. It appears that essentially two types of mechanisms induce the precipitation of polyelectrolyte. When the chemical affinity between charged groups of polyelectrolyte and counterions is weak, the precipitation is due to electrostatic attractions, and we observe a resolubilization in excess of multivalent salt. If the chemical affinity is strong, the origin of

the precipitation of polyelectrolyte is the formation of stable complexes between charged groups of polyelectrolyte and counterions.

The dynamic behavior of linear charged polyelectrolytes in aqueous solution is not yet understood. The interpretation of dynamic light scattering (DLS) of aqueous solutions of sodium poly(styrene sulfonate) (NaPSS) is particularly complicated. The intensity correlation function shows a bimodal shape with two characteristic decay rates, differing sometimes by two or three orders of magnitude, termed fast and slow modes. The first observations in low salt concentration or salt free solution were reported by Lin et al. [31] for aqueous solutions of poly(L-lysine). Their results are described in terms of an extraordinary–ordinary phase transition. An identical behavior was first observed by M. Drifford et al. in NaPSS [32]. Extensive studies on this bimodal decay on NaPSS in salt-free solution, or solutions where the salt concentration is increased slowly, have been reported [33–36]. The fast mode has been attributed to different origins such as the coupled diffusion of polyions and counterions [34,37,38] or to cooperative fluctuations of polyelectrolyte network [33,39] in the semidilute solutions.

The origin of the slow mode, whose decay rate is molecular weight dependent, has been attributed to a reptation-like mechanism [39,40] or to long-range electrostatic interactions [41] or to some clusters or to temporal domains resulting from chain entanglements [42,43].

Some studies [35,44] indicate that the slow mode was due to large stable clusters that can be completely eliminated by filtration through a small-pore-size (0.05 μm) filter. These data were different from those of Sedlak [45] who reported only a partial suppression of the slow mode after filtration.

We investigate here the dynamic behavior of fully charged NaPSS solutions with multivalent salt ($LaCl_3$) measured by quasi-elastic light scattering. The bimodal decay of the correlation function of polyelectrolyte concentration (C) at constant salt concentration (C_S) is studied first. The ratio C_S/C varies from 0.2 to 10^{-2}. Then the dynamics of the solution at constant C as a function of C_S from C_S/C approximately 10^{-2} to 0.2 are investigated.

II. SOLUBILITY AND STRUCTURE OF HIGHLY CHARGED ANIONIC POLYELECTROLYTES IN THE PRESENCE OF MULTIVALENT CATIONS

A. Strong Polyelectrolytes in the Presence of Multivalent Inorganic Counterions

1. Phase Diagrams of Poly(Styrene Sulfonate)

NaPSS/Multivalent Salts. At a given monomer concentration of NaPSS, for salts with divalent inorganic cations (Ca, Mg, Co, Cu, Ni, Mn, Cd), the

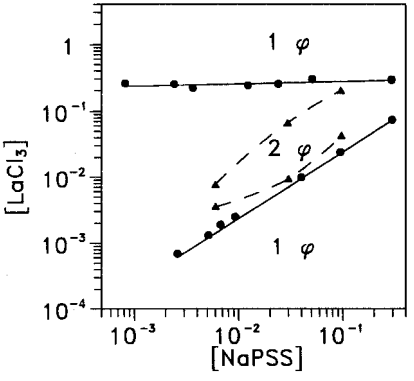

FIG. 1 Experimental phase diagram of NaPSS/$LaCl_3$ (pH 3) for weight average degrees of polymerization: $N = 3.8 \times 10^3$ (circles) and $N = 19$ (triangles). The lines joining the experimental points are guides for the eyes and separate the two-phase region "2 φ" (located inside the lines) from the one-phase regions "1 φ."

mixtures remain homogeneous. In the case of salts with trivalent and tetravalent cations, there exists a salt concentration region where solutions phase separate [17–19]. The visual aspect of a two-phase system is characterized by the presence of a viscous phase of concentrated poly(styrene sulfonate).

In Figures 1 and 2 are reported the phase diagrams for NaPSS/$LaCl_3$ and NaPSS/$Th(NO_3)_4$ systems for a polymer with a high degree of polymeriza-

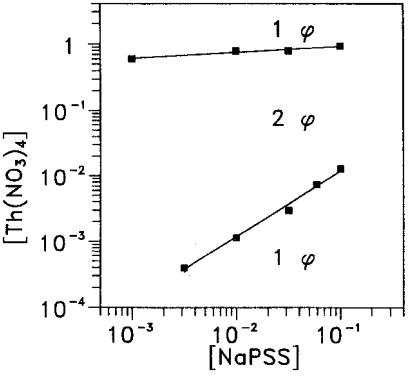

FIG. 2 Experimental phase diagram of NaPSS/$Th(NO_3)_4$ ($N = 3.8 \times 10^3$, pH 3) system. The lines joining the experimental points are guides for the eyes and separate the two-phase region "2 φ" (located inside the lines) from the one-phase regions "1 φ."

tion ($N = 3.8 \times 10^3$). In both systems, the lower salt concentration limit of the two-phase region C_S^* increases when monomer concentration increases and, within the experimental accuracy, is proportional to the monomer concentration. The upper salt concentration limit of the two-phase region C_S^{**} is nearly independent of the monomer concentration. The extension of the two-phase region increases with the valency of the counterion.

Molecular weight dependence of the lower and upper limits in salt concentration, C_S^* and C_S^{**}, at two given monomer concentrations (of the order of 0.1 and 0.01 M), was established for the NaPSS/$LaCl_3$ system [17–19]. The lower limit C_S^* is nearly independent of the degree of polymerization ($19 \leq N \leq 7.8 \times 10^3$). In the opposite, the upper limit salt concentration C_S^{**} decreases as degree of polymerization decreases. This effect is more pronounced at low monomer concentration. The two-phase region shrinks as the size of the polymer decreases. An illustration of this effect is given in Figure 1, where is also reported the phase diagram for the NaPSS with a low degree of polymerization ($N = 19$).

$Ca(PSS)_2$ or $La(PSS)_3$/Multivalent Salts. At monomer concentrations smaller than 10^{-1} M and larger than 10^{-3} M, salt-free $Ca(PSS)_2$ solutions remain homogeneous, whereas salt-free $La(PSS)_3$ solutions demix in two phases and become clear when 0.3 M of $LaCl_3$ is added [18,19]. The experimental phase diagram for the $La(PSS)_3/LaCl_3$ system is presented in Figure 3. The concentration of $LaCl_3$ needed to transit from the two-phase region to the one-phase region is of the same order of magnitude as the concentration C_S^{**} in the $La(PSS)_3/LaCl_3$ system (see Figures 1 and 3).

2. Theoretical Considerations: Electrostatic Model

To describe the solubility of sodium poly(styrene sulfonate) in the presence of z-valent counterions, the electrostatic model [18,19] was introduced. This model takes into account a short-range electrostatic attraction between negatively charged monomers (-1) and those carrying condensed multivalent counterions that are positively charged ($z - 1$). Phase diagrams have been calculated using two techniques: the polymer reference interaction site model (PRISM) [18] and the random phase approximation (RPA) [19]. Both techniques lead to the spinodal equation

$$\frac{1}{NC} + \frac{\sigma^3}{1 - \varphi} + \frac{z_{\text{eff}}^2}{2I} - 2f(1 - f - f')|V_{1Z}| = 0 \tag{1}$$

C is the number of monomers per unit volume, σ^3 represents the volume of the monomer, and $\varphi = C\sigma^3$ is the volume fraction occupied by the polymer. The first term comes from the entropy of polymer and the second one represents the steric excluded volume; water is assumed to be a very good solvent for charged monomers ($\chi = 0$). The third term corresponds to the

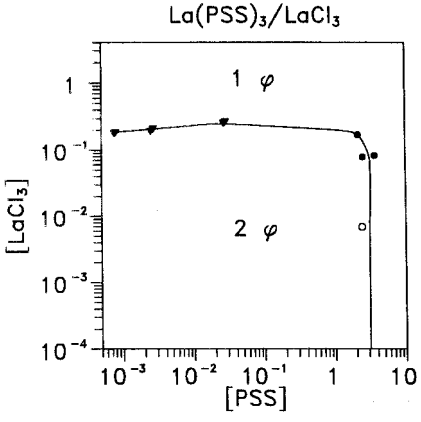

FIG. 3 Experimental phase diagram of $La(PSS)_3/LaCl_3$ ($N = 3.4 \times 10^2$) system. The concentrations are expressed in M. On the x-axis is reported the monomer concentration. The triangles represent the determination of the two-phase region by visual inspection and the circles correspond to titration measurements. Titration at zero salt concentration is arbitrarily reported at $[LaCl_3] = 7 \times 10^{-3}$ (open circle). The line joining the experimental points is a guide for the eyes and separates the two-phase region "2 φ" from the one-phase region "1 φ."

electrostatic repulsion between monomers carrying an effective charge $z_{eff} = zf + f' - 1$, where f and f' are the fraction of monomer with a z-valent and monovalent condensed counterions, respectively. I represents the ionic strength of free ions. The last term arises from an attraction between the negatively charged monomers (-1) and those possessing an effective positive charge of valency $(z - 1)$, due to the electrostatic condensation. The short-range attraction V_{1Z}, computed as corrections to the linearized treatment of the electrostatic interactions, increases with the valency of the counterion and has the form [18,19]

$$V_{1Z} \approx -\pi(-1)^2(z-1)^2 l_B^2 \lambda_D \tag{2}$$

l_B is the Bjerrum length ($=e^2/4\pi\varepsilon\varepsilon_0 kT \approx 7$ Å in water) and λ_D is the Debye screening length equal to $(8\pi l_B I)^{-1/2}$. When the ionic strength I is high enough, the electrostatic attractions are screened.

For a given monomer concentration, the spinodal equation gives two solutions corresponding to the precipitation and the resolubilization limits as the salt concentration increases. The salt concentration at the resolubilization limit increases with the valency z of counterion [18,19]. As we can see in Figures 4–6, the electrostatic model allows the experimental phase diagrams to be explained.

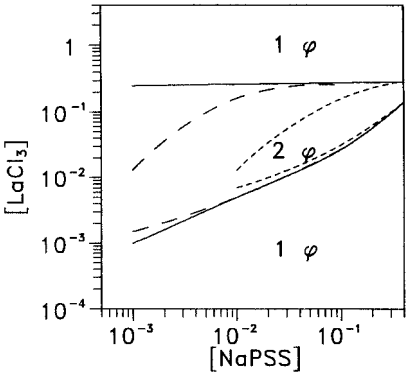

FIG. 4 Theoretical NaPSS/$LaCl_3$ phase diagram. The lines represent the spinodal lines for a degree of polymerization N of 10^6 (solid), 5×10^3 (long dash) and 5×10^2 (short dash).

3. Phase Diagrams of Strong Polyelectrolytes in the Presence of Multivalent Counterions: A General Behavior

Stability of different strong polyelectrolyte/counterion mixtures is reported in this section: sodium poly(vinyl sulfonate), potassium poly(vinyl sulfate), and sodium dextran sulfate. These polyelectrolytes have practically the same charge density. Poly(vinyl sulfonate) (NaPVS) and NaPSS possess the same charged groups (SO_3^-) but they differ by their backbones NaPVS is more

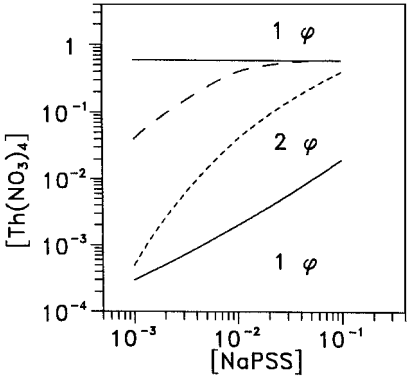

FIG. 5 Theoretical NaPSS/$Th(NO_3)_4$ phase diagram. The lines have the same meaning as in Figure 4.

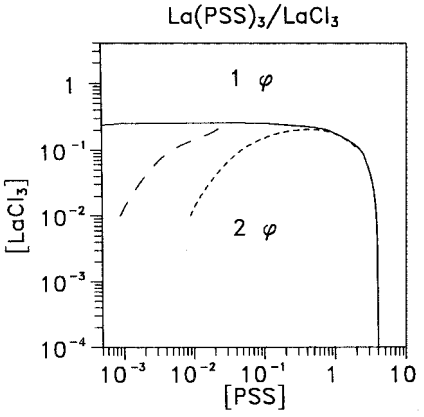

FIG. 6 Theoretical $La(PSS)_3/LaCl_3$ phase diagram. The lines have the same meaning as in Figure 4.

hydrophilic. Potassium poly(vinyl sulfate) (KPVS) and NaPVS have the same backbone but the charged groups are different: sulfate groups (OSO_3^-) instead of sulfonate groups (SO_3^-). Sodium dextran sulfate (NaDS) has a more hydrophilic and less flexible backbone than the previous polyelectrolytes.

As NaPSS, all these polyelectrolytes remain soluble [12–15,22,30] in the presence of divalent inorganic counterions (Ca, Mg, Co, Cu, Ni, Mn, Cd). In the presence of $LaCl_3$, their phase diagrams remain very similar [22,30] (see Figure 7).

The nature of the charged groups (sulfate or sulfonate) and the nature of the backbone of the polyelectrolyte have little effect on the phase diagram of polyelectrolyte/counterion mixtures. Therefore the electrostatic attractions can be considered as the principal driving force for phase separation of highly charged strong polyelectrolytes in the presence of multivalent counterions. A universal behavior is observed whatever the nature of polyelectrolyte or counterions.

B. Highly Charged Weak Polyelectrolytes in Presence of Inorganic Multivalent Counterions

1. Phase Diagrams of Sodium Poly(acrylate)

The main difference between sodium polyacrylate (NaPA) and all strong polyelectrolytes, bearing sulfonate or sulfate groups, appears with inorganic divalent counterions. A phase separation without resolubilization was observed recently by Sabbagh and Delsanti [22,30] with all the divalent coun-

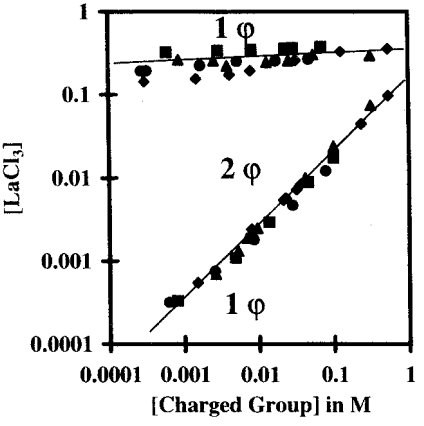

FIG. 7 Experimental phase diagrams of different anionic polyelectrolyte/$LaCl_3$ systems: NaPSS ($N = 3.8 \times 10^3$, full triangles), NaPVS ($N = 39$, full lozenges), KPVS ($N = 2.53 \times 10^3$, full circles), NaDS ($N = 4.6 \times 10^3$, full squares). The finite two-phase region "2 φ" is surrounded by a one-phase region "1 φ" at high and low salt concentration. The full lines are only guides for the eyes.

terions (Ba^{2+}, Ca^{2+}, Cd^{2+}, Co^{2+}, Cu^{2+}, Mg^{2+}, Mn^{2+}, Ni^{2+}). For instance the phase diagram of NaPA ($N = 8.3 \times 10^3$) in the presence of $CaCl_2$ is given in Figure 8. For salt concentrations above the concentration C_S^* the solutions separate into a supernatant with a very low monomer concentration and a precipitate with a high monomer concentration. When the carboxylate concentration is higher than 0.003 M, the salt concentration C_S^* is an increasing function of monomer concentration. The composition of the precipitate is nearly independent of the initial polyacrylate concentration. In the precipitate, the concentration of polymer and calcium are close to the stoichiometric composition ($C/C_S = 2.1$). Similar phase diagrams were observed in alginate and acrylamide/acrylate copolymers [16] in the presence of divalent ions. In contrast to strong polyelectrolytes, no stable suspension appears at high salt concentration.

The phase separation boundary depends on the degree of polymerization of NaPA at lowest monomer concentration (see Figure 9); precipitation appears first for the largest chains of polyelectrolyte. At high monomer concentration, the C_S^* limits become nearly independent of the degree of polymerization. In this monomer concentration domain, a study on NaPA with different divalent counterions (Ba^{2+}, Ca^{2+}, Cd^{2+}, Co^{2+}, Cu^{2+}, Mg^{2+}, Mn^{2+}, Ni^{2+}) shows that their efficiencies to precipitate the sodium polyacrylate are practically the same; C_S^* is a constant [22,30].

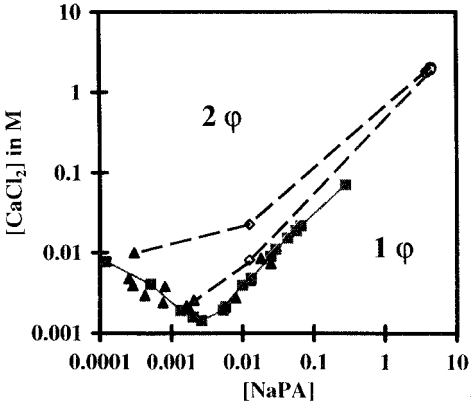

FIG. 8 Experimental NaPA ($N = 8.3 \times 10^3$)/$CaCl_2$ phase diagram: cloud points (full squares), composition of supernatant (full triangles) and of precipitate (open circles). Only a few initial compositions of solutions before the demixion (open lozenges) with the corresponding tie-lines (dash lines) are reported. The full line is only a guide for eyes to indicate the boundary of the two-phase region "2 φ." No resolubilization was observed in excess of calcium chloride.

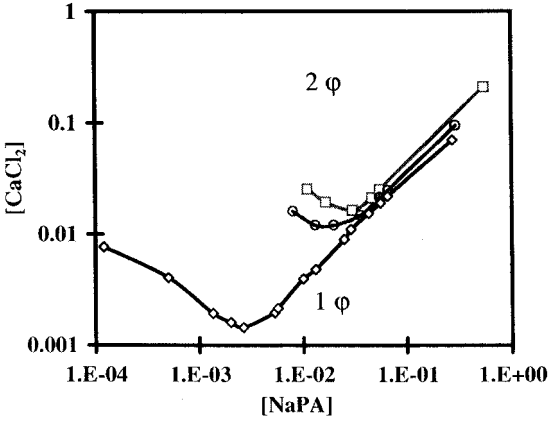

FIG. 9 Experimental NaPA/$CaCl_2$ phase diagrams: $N = 40$ (squares), $N = 70$ (circles), and $N = 8.3 \times 10^3$ (lozenges). The lines joining cloud points are only guides for the eyes.

With trivalent ions NaPA precipitates as NaPSS. The phase diagram of the NaPA/$LaCl_3$ system presents a lower phase separation line C_S^*, which increases with the monomer concentration at highest concentration. The major change is the absence of resolubilization at high salt concentration [22,30].

2. Complexation Between Weak Polyelectrolyte and Divalent Counterions

UV/VIS spectroscopy allows the quantity and the type of complexes formed between cobalt ion and COO^- groups before phase separation to be determined [22,30]. For instance, for 0.0125 M of cobalt in the presence of 0.04 M of NaPA ($N = 40$) all the cobalt ions are chemically bound to carboxylate groups and mostly form dicomplexes: $x_d = [Co^{2+}]_{dicomplex}/[Co^{2+}]_{added} \approx 85\%$ and $x_m = [Co^{2+}]_{monocomplex}/[Co^{2+}]_{added} \approx 15\%$. When the ratio $[COO^-]/[Co^{2+}]$ is kept constant (=4), as the NaPA concentration increases the fractions of cobalt ions in dicomplex and monocomplex forms remain constant: $x_d \approx 80\%$ and $x_m \approx 20\%$. Even if the complexation constants are large, this result cannot be explained with a classical mass action law using macroscopic concentrations (calculated using the total volume of the solution). In fact, the high charge density along the polymer chain produces a high electrostatic potential around it, and counterions are located in the immediate vicinity of the polymer chain. The relevant concentrations are the local concentrations in the close proximity of the polyelectrolyte chain. Assuming that the added divalent counterions are confined in a tube of effective radius R around the polyelectrolyte, the local charged monomer, $[COO^-]_L$, and divalent counterion, $[Co^{2+}]_L$, concentrations (in moles per unit volume) are

$$[COO^-]_L = \frac{1}{6 \times 10^{23} \times \pi b R^2} \quad \text{and} \quad [Co^{2+}]_L = [Co^{2+}] \times \frac{[COO^-]_L}{[COO^-]} \tag{3}$$

where $[Co^{2+}]$ and $[COO^-]$ are the macroscopic concentration, and b ($\approx$2.5 Å) is the distance between charged monomers COO^-. At constant ratio $[COO^-]/[Co^{2+}]$ the local concentrations remain constant. Using the complexation constants, K_1 and K_2, of the cobalt with carboxylate groups [46,47] (see Table 1), the parameter R must be of the order of 7 Å to fit the fractions of cobalt in complex states deduced from UV/VIS spectroscopy measurements.

The ratio $\log K_1/\log K_1K_2$ is approximately a constant ($\approx$0.6 for acrylate groups, see Table 1). Thus fractions of counterions in monocomplex and dicomplex states as functions of K_1 can be computed using the ''tube model.'' When $K_1 > 1$, near the demixion curve ($C_S/C \approx 0.36$) it is 65% of counterions or that which form dicomplexes. This condition is fulfilled for all divalent inorganic counterions with carboxylate groups.

TABLE 1 Association Constants with COO^- Groups

Ions	Ba^{2+}	Mg^{2+}	Ca^{2+}	Mn^{2+}	Co^{2+}	Ni^{2+}	Cd^{2+}	Cu^{2+}
log K_1	0.45	0.55	0.57	0.70	0.70	0.84	1.35	1.85
log K_2	—	—	≈0.30*	—	0.50	0.60	0.85	1.20

K_1 and K_2 are the formation constants of monocomplexes and dicomplexes, respectively. For divalent ions M^{2+} the constants are defined as follows: $[M^{2+}COO^-] = K_1[M^{2+}][COO^-]$; $[M(COO)_2] = K_2[M^{2+}COO^-][COO^-]$. These constants are estimated from a compilation of the stability constants of carboxylic acids with inorganic cations given in the literature [46,47] at ionic strength of 0.1 M (or larger).
*Constant determined from conductivity measurements [22].

UV/VIS spectroscopy measurements are consistent with small-angle x-ray scattering experiments on NaPA/cobalt and NaPA/calcium mixtures [22,29,30], which show that the effective scattering entity is the monomer dressed by the cobalt (or calcium) ions, which are located in the close vicinity of polyacrylate chain. The change of the energy of the x-ray incident beam (or of the counterions) leads to a variation of the apparent contrast of dressed monomers, which can only be explained by assuming that the partial volume of the dressed monomer is larger than the sum of the partial volumes of the charged monomer ($C_2H_3COO^-$) and of the divalent counterions in the isolated and hydrated state. This is a consequence of the chemical association between COO^- groups and divalent counterions, which partially dehydrates both the COO^- group and the divalent counterion. This point is in agreement with refractive index and density measurements, which show also that the chemical association induces a dehydration of monomer and cation [48–52]. However, the hydrophobicity of the monomers complexed by calcium is not strong enough to induce a collapse of the polymer chain at small spatial scale before the demixion. Indeed, the scattered intensity (Figures 10 and 11), x-ray and neutron scattering, decreases with the scattering vector q as q^{-x} with $x \approx 2$ for $q > 0.1$ nm^{-1}. The same q-dependence (at high q-range) was observed by x-ray scattering measurements on highly charged polymethacrylate in presence of Cu^{2+} and Ni^{2+} counterions [27]. This exponent, smaller than 3, indicates that the local conformation of the chain (spatial scale $1/q < 10$ nm) is not collapsed but rather Gaussian. Near demixion, when the chain collapses, a blob structure still exists, as is the case for neutral polymers before demixion [53,54]. In fact, when the concentration of added divalent counterions increases, the repulsive interactions decrease and the conformation of the polymer is collapsed at large spatial scale as shown by viscosity measurements [22,30]. The viscosity decreases as the cobalt (or calcium) ion concentration increases. We think that dicomplexa-

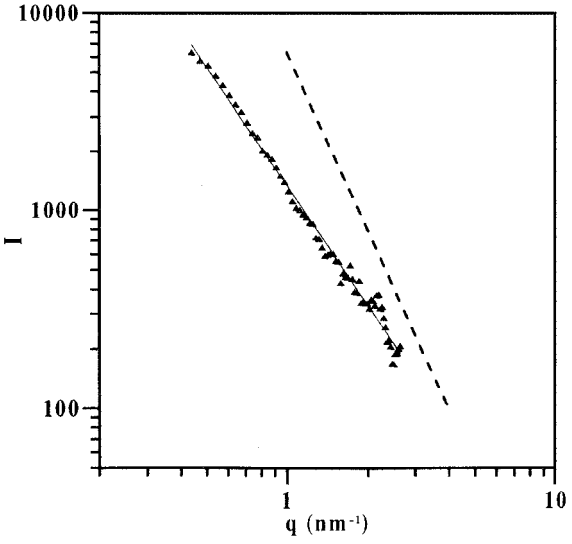

FIG. 10 Variation of x-ray scattering intensity as a function of the scattering vector q for a NaPA sample ($N = 8.3 \times 10^3$, $C = 0.475$ wt%) in presence of calcium chloride ($C_S = 2.4 \times 10^{-2}$ M) near the demixion limit. The dashed line represents a slope -3.

tion essentially occurs between two neighboring monomers of the flexible chain (in the case of NaPA in the presence of calcium or cobalt ions). A few bridges may be formed, but not enough to make a gel. If ion bridges were dominant, the viscosity should strongly increase as divalent salt concentration increases.

The above observations are in agreement with studies on chain contraction of sodium polymethacrylate (NaPMA) in the presence of Ca^{2+} and Cu^{2+} counterions [25]. Static and quasi-elastic light scattering measurements indicate that a PMA chain contracts but does not have a compact spherical structure close to the precipitation threshold.

3. Theoretical Considerations: Electrostatic plus Chemical Association Model

As spinodal equations in the context of RPA can be obtained using a Flory mean field approach [24], this approach was used to describe the stability of the NaPA/$CaCl_2$ system when chemical associations between charged monomers and Ca^{2+} are taken into account. The spinodal line was found to be [22,30]

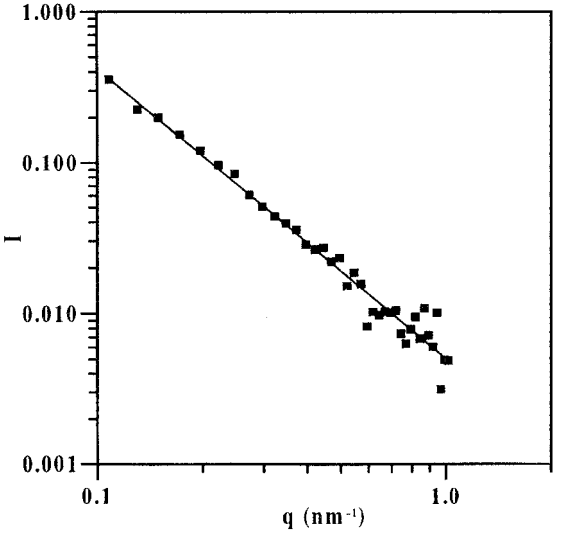

FIG. 11 Variation of neutron scattering intensity measured in a NaPA/$CaCl_2$ solution just at the cloud point ($N = 8.3 \times 10^3$, $C = 2.0$ wt%, $C_S = 9.3 \times 10^{-2}$ M) as a function of the scattering vector q. The squares are the experimental points and the solid line is the best fit, which decreases as $q^{-1.9}$.

$$\frac{1}{NC} + \frac{\sigma^3}{1-\varphi} + \frac{z_{\text{eff}}^2}{2I} - 2(f + f_m)(1 - f - f' - f_m - f_d)|V_{12}| - 2\sigma^3\chi_d f_d = 0 \tag{4}$$

where $z_{\text{eff}} = (f' + 2f + 2f_m + f_d - 1)$. The parameter f_m represents the monomer fraction chemically associated with one divalent counterion (monocomplexation COO^-Ca^{2+}), and f_d is the monomer fraction with a dicomplex ($COOCa_{1/2}$). f and f' are the monomer fractions carrying electrostatically condensed counterions Ca^{2+} and Na^+, respectively. The spinodal expression of the electrostatic model (Eq. 1) is recovered with a supplementary term due to the dicomplexation. The parameter χ_d is related to the interactions between the dicomplexes ($COOCa_{1/2}$) and water molecules. Water is assumed to be a very good solvent for monomers and monocomplexes ($\chi = 0$). The parameter χ_d must be taken to be of the order of 20 to describe the experimental demixion limit measured in the system NaPA ($N = 8.3 \times 10^3$)/$CaCl_2$ in the monomer concentration range 0.005–0.06 M (if σ is chosen to be equal to 5 Å). This large value of χ_d corresponds to a high attraction between monomers that carry calcium in dicomplex state. In other words, the chemical association with a partial dehydration of Ca^{2+} ion and

of charged monomer makes the dicomplexes hydrophobic. The value of χ_d strongly depends on the value of σ, and to give an idea bout the relative importance of the different interactions controlling the precipitation, the different interaction terms of the spinodal equation, calculated for $C = 10^{-2}$ M, are reported in Figure 12. By increasing the salt concentration, the hydrophobic term ($2\sigma^3\chi_d f_d$), due to the dicomplexation, increases and becomes nearly a constant above $C_S/C \approx 0.3$, whereas the repulsive electrostatic term, which stabilizes the polyelectrolyte, decreases sharply. In a first approximation, precipitation occurs when the hydrophobic term is equal to the repulsive term in absolute value, which corresponds to the crossing point of the two upper curves in Figure 12. The crossing point is weakly dependent on the variation of $\chi_d\sigma^3$. Therefore, for two different divalent counterions which are completely associated with carboxylate groups, similar demixion curves will be observed if their χ_d values are of the same order of magnitude. When complexation is absent, the electrostatic attractions with divalent counterions are not strong enough to induce phase separation.

Spinodal curves calculated for different degrees of polymerization N [22,30] show that the demixion limit at low monomer concentrations increases when N decreases; this is due to the entropic term, which becomes dominant in this regime. The position of the minimum of the demixion line depends on the degree of polymerization and on the χ_d value. The theoretical phase diagrams describe semiquantitatively the experimental results.

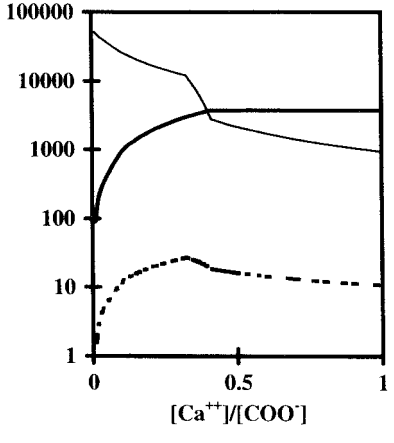

FIG. 12 Variation of interaction terms of the spinodal equation as a function of the added calcium (the monomer concentration is fixed to 0.01 M): (thin full line) repulsive electrostatic term, (thick full line) attractive term due to the dicomplexation in absolute value, (dashed line) attractive electrostatic term in absolute value.

It is important to notice that the association constants decrease with salt concentration at low ionic strength in the Debye–Hückel approximation [55], but at high ionic strength they tend to a constant [46]. At the same time, the complex fraction always increases with salt concentration. The absence of resolubilization is the signature of a dominant dicomplexation. In contrast, if the monocomplexation is dominant, precipitation is expected to be followed by a resolubilization due to charge inversion [20].

C. Phase Diagrams of Weak and Strong Polyelectrolytes in the Presence of Barium and Organic Multivalent Ions

Barium is the only divalent counterion able to precipitate all highly charged polyelectrolytes carrying carboxylate, sulfate, or sulfonate groups [13,15,22,30]. The phase diagram of the NaPVS/$BaCl_2$ [22,30] is similar to that of NaPA/$CaCl_2$, without resolubilization at high barium concentration. The precipitation of poly(vinyl sulfonate) is probably due to a strong chemical association between barium ions and sulfonate groups. It is well known that the barium–vinyl sulfonate monomer [$(C_2H_3\text{-}SO_3)_2Ba$] is poorly water soluble (solubility product close to 5×10^{-4} M^2), which means that the chemical binding of barium with vinyl sulfonate monomers is very strong. All divalent cations other than barium ($M^{2+} \neq Ba^{2+}$) do not precipitate poly(vinyl sulfonate), which is probably due to the high solubility of their sulfonate monomers $(R\text{-}SO_3)_2M$.

Spermidine ($^+H_3N(CH_2)_4NH_2^+(CH_2)_3NH_3^+$) is a cation very different from lanthanum; it is a linear and organic molecule. However, the phase diagrams of strong polyelectrolyte/spermidine and strong polyelectrolyte/$LaCl_3$ systems are similar with a resolubilization at high trivalent counterion concentration (see Figures 13 and 7). Moreover a similar phase diagram is observed with weak polyelectrolytes as NaPA (Figure 13). Indeed, conductivity measurements on mixtures of acetate/methylamine and of vinylsulfonate/methylamine show that there is no chemical association between the primary ammonium (NH_3^+) and the carboxylate (or sulfonate) groups [22,30]. It is interesting to note that similar phase diagrams to the ones presented in Figures 13, 7, 1, and 2 were observed for DNA/spermidine (Sp^{+3}) and DNA/spermine (Sp^{+4}) mixtures [21,26,28]. In these systems the precipitation is also induced by the electrostatic attractions between phosphate charges via polyamine counterions.

These results show that the solubility of polyelectrolytes in the presence of multivalent salt, especially at high salt concentration, depends on the relative affinity between charged groups of the polyelectrolyte and counterions. With organic multivalent cations, as spermidine and spermine, where

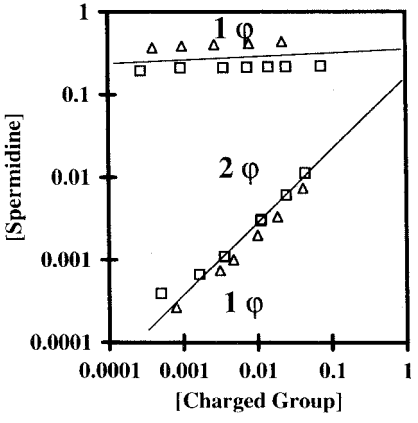

FIG. 13 Experimental phase diagrams of different anionic polyelectrolyte/spermidine systems: NaPA ($N = 8.3 \times 10^3$, open squares); KPVS ($N = 2.53 \times 10^3$, open triangles). The finite two phase region "2 φ" is surrounded by a one-phase region "1 φ" at high and low salt concentration. The full lines are only guides for the eyes.

no chemical association occurs with the charged side groups of polyelectrolyte, the same phase diagrams are observed whatever the polyelectrolyte.

III. DYNAMIC PROPERTIES OF NaPSS/$LaCl_3$ SYSTEM

A. Experimental Method

Since observations and interpretations of quasi-elastic light scattering results are not yet well understood and are controversial, to contribute positively to the debate, we report details on the preparation of the samples and on the treatment of the quasi-elastic data.

The NaPSS sample mostly used in the present study (supplied by Pressure Chemical Co.) has a molecular weight $M_w = 7.8 \times 10^5$ ($N = 3.8 \times 10^3$) and a polydispersity index $M_w/M_n = 1.1$. To purify and eliminate extra free ions, the NaPSS sample is dialyzed against deionized water. The polymer is dissolved in deionized water upon passing it through a MilliQ Millipore system (18 M ohm-cm). The pH is adjusted to a value of 3; in this way lanthanum cations are not hydrolyzed. The added salt used, $LaCl_3$, is of analytical grade. In order to eliminate dust particles in the scattering volume, all manipulations are done in an air-cleaned hood (ADS Laminare MV 29) and water is introduced into the scattering cell through a Millipore or Anotop filter of pore size 0.22 μm. Solutions are centrifuged before quasi-elastic

measurements. In all the measurements the temperature is kept at 25 ± 0.1°C.

A 500 mW beam of an argon ion laser (Spectra Physics 2016, $\lambda = 514.5$ nm) is focused into the center of a 8 mm diameter cylindrical sample cell. The time correlation function of the scattered electric field $g(t)$ is measured in the self-beating mode with a BI2030 Brookhaven correlator (136 channels). The measured autocorrelation function of intensity fluctuations, $G(t) = (\langle I(t)I(0)\rangle - \langle I\rangle^2)/\langle I\rangle^2$ is related to $g(t)$ by $G(t) = A\,g^2(t)$, where the numerical factor A depends on the geometry of the experiment and is of the order of 0.6 to 0.7. At low concentration the correlation function of the scattered field is approximately described by the sum of two exponential functions. The two decay rates are in the ratio of the order of 100 or 1000. A typical example is given in Figure 14. The experimental function $G(t)$ is obtained by superimposing the data collected at different sampling times Δt. In order to determine the behaviors at short times and long times, analysis at sampling times Δt differing by a large factor are performed. Effective decay rates are roughly determined with the cumulant program from Brookhaven using for the base line the measured base line given by the retarded channels ($1163\,\Delta t$). In the case of analysis at short times, this operational method is only a crude first-order correction to eliminate the contribution of the slow component. The sampling time is chosen such that $\Gamma_{\text{feff}}\,136\Delta \approx 7$, where Γ_{feff} is the effective decay rate of the fast mode. The corresponding effective fast diffusion coefficient is $D_{\text{feff}} \approx 10^{-6}$–$10^{-7}$ cm^2/s. In the case of analysis at long times, the Γ_{eff} values, obtained in the range $\Gamma_{\text{eff}}\,136\Delta t \approx 3$–4, lead to a slow effective diffusion: $D_{\text{seff}} = 10^{-8}$–$10^{-9}$ cm^2/s at scattering vector $q = 2.3 \times 10^{-3}$ Å^{-1} (90° scattering angle). In this long times analysis, deviation from single exponential behavior is large, and the polydispersity factor has a value of 0.3–0.4.

In order to detect the influence of the preparation method, some studies are performed on a NaPSS sample purchased from Aldrich, $M_w = 7.0 \times 10^4$ ($N = 3.4 \times 10^2$) and $M_w/M_n = 2.5$ and autocorrelation functions of the intensity fluctuations are measured with a BI9000 correlator. We must also notice that to measure the evolution of the correlation function with time, the function $G(t)$ is fitted according to: $G^{1/2}(t) = A_f \exp(-\Gamma_f t) + A_s \exp(-\Gamma_s t)$. In this study, to eliminate contamination by small ions coming eventually from the walls of the glass cell, the sample ($M_w = 7.8 \times 10^5$) is dissolved into a quartz cell.

B. Results and Discussion

We have first measured the dynamic light scattering of the system NaPSS/$LaCl_3$ in the lower one-phase region to determine the evolution of the ef-

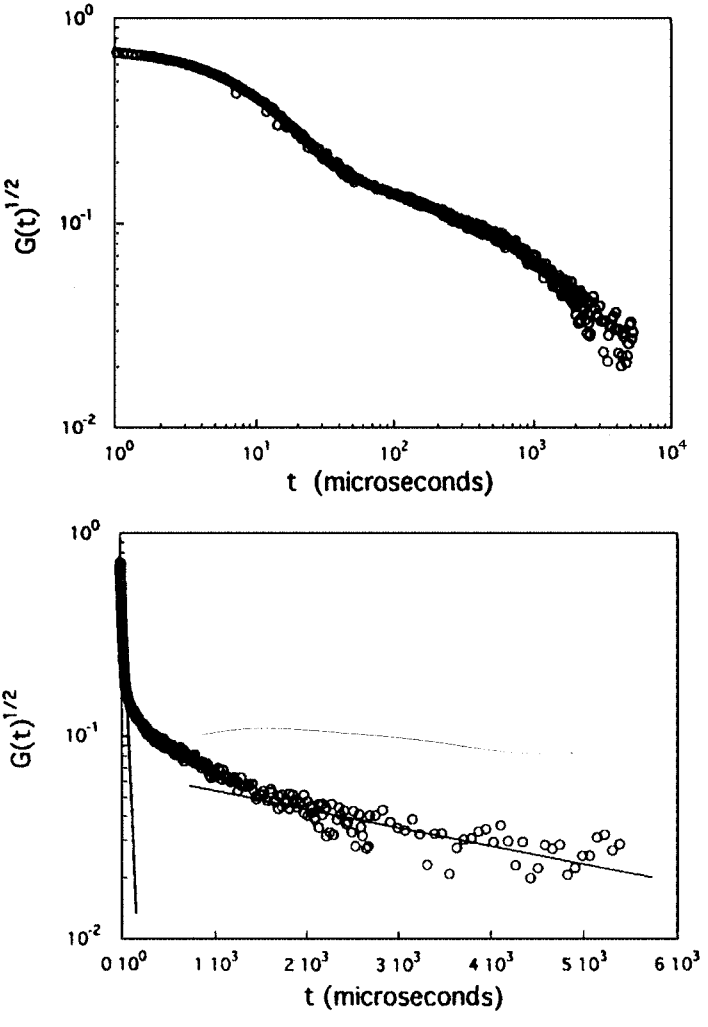

FIG. 14 Example of the bimodal decay of the intensity correlation function of NaPSS/$LaCl_3$ system: NaPSS concentration $C = 0.1$ M and $LaCl_3$ concentration $C_S = 10^{-3}$ M (B-point on Figure 15). The scattering wave vector is $q \cong 2.3 \times 10^{-3}$ Å^{-1}.

fective diffusion coefficients; see Figure 15. We have investigated first the a-line at constant $LaCl_3$ concentration (10^{-3} M), and the b-line at constant NaPSS concentration (10^{-1} M). In this case the ratio C_S/C varies from 0.2 to 10^{-2} on the a-line and from 10^{-2} to 0.2 on the b-line. Some data are obtained in the upper one-phase region at $C = 10^{-1}$ M and $C_S \approx 0.5$ M (D-point).

The evolution of the effective diffusion coefficients following the a-line is shown in Figure 16. A bimodal decay of the intensity correlation function is observed on this line. Two modes (slow and fast) are present, and the amplitude of the slow mode is increasing from A ($C_S/C \approx 0.2$) to B ($C_S/C \approx 10^{-2}$).

The decay rate of the fast mode Γ_{feff} is proportional to q^2 and hence an effective fast diffusion coefficient $D_{feff} = \Gamma_{feff} q^{-2}$ may be defined. The decay rate of the slow process exhibits deviation from q^2-dependence, and the experimental data shows approximately a q^3-dependence characteristic either of internal relaxation modes or of the diffusion of labile tenuous clusters.

The fast effective diffusion coefficient D_{feff} is plotted as a function of polyelectrolyte concentration and it increases as C increases. From the logarithm plot a power law is deduced: D_{feff} varies as $C^{0.45\pm0.05}$.

In the semidilute regime, at very low salt concentration, the chains are entangled and can form an isotropic transient network. In the scaling picture [56,57,58] the solution is described by an assembly of blobs of size ξ, with

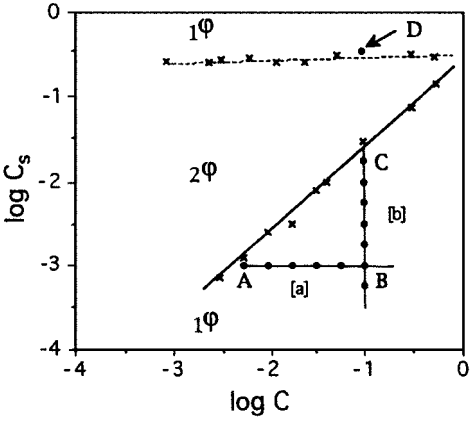

FIG. 15 Experimental study of dynamic light scattering in NaPSS/$LaCl_3$ solution. a-line from A to B at constant C_S concentration; b-line from B to C at constant C concentration. The D-point corresponds to upper one-phase ($C = 0.1$ M, $C_S \approx 0.5$ M).

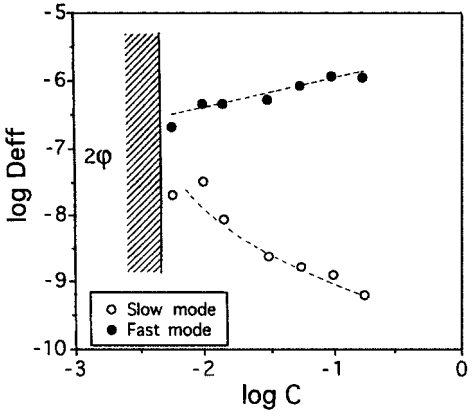

FIG. 16 Dependence of the fast and slow effective diffusion coefficients following the a-line (see Figure 15) as a function of NaPSS concentration (C): fast mode (full circle); slow mode (open circle).

$\xi \approx C^{-1/2}$. The diffusion coefficient scales as $D_{\text{feff}} \approx \xi^{-1}$. Our experimental observation is in agreement with the scaling predictions and with the data obtained by Grüner et al. [33] in salt-free solution of NaPSS.

The slow effective diffusion coefficient (D_{seff}) is decreasing as a function of C in agreement with the data obtained by Sedlak and Amis [34,45,59] in free salt solution of NaPSS. This slow mode behavior is observed with a lot of polyelectrolyte systems [42–45]. In our case D_{seff} varies approximately as C^{-1}. The existence of this slow mode is not yet understood, and it has led various authors to propose different models to explain its origin. It is tempting to relate the slow mode as the diffusion of multichain domains or clusters. The size of the domains may be very large with respect of q^{-1}; as a result, the slow diffusion coefficient is q-dependent. The hydrophobic character of the backbone of NaPSS can introduce some complex behavior. The existence of localized hydrophobic regions has been shown for this highly charged polyelectrolyte [60]. But another study on NaPSS in different solvents [61] seems to show that the existence of the slow mode is not directly correlated to the hydrophobic character of PSS chains.

Figure 17 shows the variation of the effective diffusion coefficients at constant C as a function of salt ($LaCl_3$) concentration. (See the b-line in Figure 15 from B to C).

The fast mode slowly decreases when the salt concentration increases. Since the added salt screens the electrostatic interaction, D_{feff} tends in excess of salt to the hydrodynamic diffusion coefficient (D-point in Figure 15).

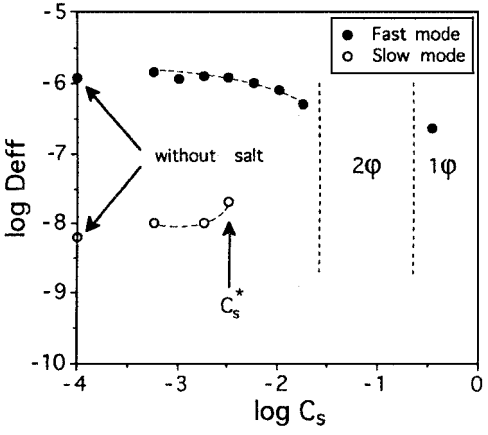

FIG. 17 Dependence of the fast and slow effective diffusion coefficients following the b-line (see Figure 15) as a function of $LaCl_3$ concentration (C_S): fast mode (full circle); slow mode (open circle).

The values of the slow diffusion coefficient are increasing as a function of salt concentration. The amplitude of $D_{s\,\mathrm{eff}}$ is a maximum at the B-point (see Figure 15) and strongly decreases and disappears or becomes too low to be detected. This behavior is identical to that observed in NaCl and $CaCl_2$ [32] where the splitting in the relaxation times depends on the ratio C/C_S.

It is tempting to plot the effective diffusion coefficients as a function of the ratio C/C_S (Figure 18), which varies from 5 to 100 following the a-line and from 100 to 5 following the b-line. The values of the fast diffusion coefficient obtained in the a-line and the b-line are the same, and we observe an identical evolution with C/C_S. The values of the slow mode obtained from the a-line and the b-line are little different, but their evolutions are practically identical. Only on the b-line, the amplitude of the slow mode strongly decreases and becomes undetectable after a critical value of the salt concentration.

The metastability of the slow mode as revealed by its disappearance adding salt or sometimes after filtration [37,44] and/or with time scale [36] is not well understood, and some data obtained in our system NaPSS/$LaCl_3$ may be held to discriminate between different assumptions [42].

Influence of Time Scale on the Slow Mode. We have measured the intensity autocorrelation function of two samples whose composition corresponds to the B-point in Figure 15: one fresh solution and another that was prepared one year ago in the same conditions in a quartz cell without contact with

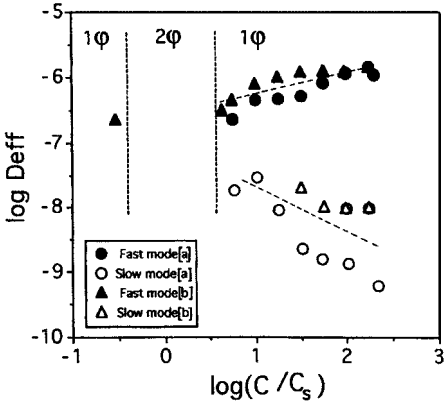

FIG. 18 Dependence of the fast and slow effective diffusion coefficients as a function of C/C_S. The data are obtained both in a-line and in b-line: fast mode (full circle) a-line; slow mode (open circle) a-line; fast mode (full triangle) b-line; slow mode (open triangle) b-line.

air. Figure 19 shows the correlation function at a scattering angle of 90° for the two samples.

A bimodal decay is observed with the fresh solution and only a pseudo-monomodal correlation function is obtained with the old solution, which corresponds to the fast mode. Thus the time dependence of the contribution of the slow mode is an important phenomenon. Our results indicate that whatever these structures are, they must originate in the polyelectrolyte solution. The evolution of the slow mode with time seems to indicate that the fresh solution is not macroscopically in thermodynamic equilibrium with the presence of large clusters which disaggregate with time, indicating that a polyelectrolyte solution with a low external salt concentration ($C_S/C \approx 10^{-2}$) slowly tends to equilibrium in agreement with other observations [36,62,63]. To quantify the evolution of the slow mode with the elapsed time from a fresh solution, we have measured the ratio of the amplitude of the autocorrelation function of the slow mode over the amplitude of the fast one: A_s/A_f. We observe a very slow decrease of this ratio as a function of time. Since the amplitude of the fast mode is time independent, the amplitude of the slow mode decreases to a value that is too small to be observed any longer.

The results on the time evolution suggest that the disappearance of the slow mode is due to the reorganization or melting of large domains of chains. Their disappearance under thermal random motion is, of course, a very slow process.

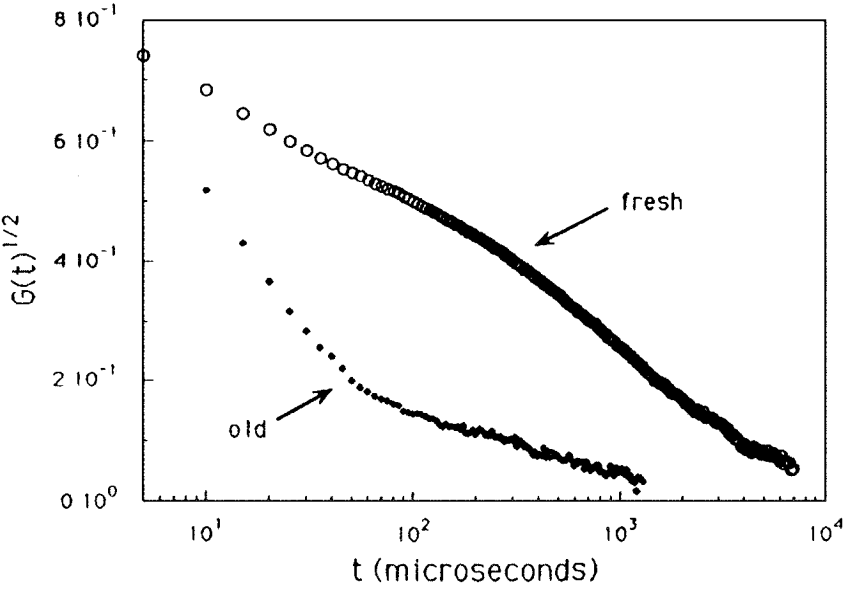

FIG. 19 Disappearance of the slow mode in the normalized intensity correlation function obtained at $C = 10^{-1}$ M and $C_S = 10^{-3}$ M (B-point) as a function of time scale: fresh solution (open circle); solution one year old (full square).

Influence of Filtration Process on the Slow Mode. The filtration with 0.1 μm and 0.05 μm on fresh solution strongly reduces the scattered intensity of the slow and fast modes in agreement with the observations of S. Ghosh et al. [35]. Only a partial removal of the slow mode is obtained. After several weeks however, the amplitude of the slow mode does not increase or grow back after filtration.

Influence of Added Salt on the Slow Mode. As with NaCl and $CaCl_2$, the system NaPSS/$LaCl_3$ presents a "pseudo" splitting phenomenon between the two modes at a critical salt concentration [32]. The amplitude of the slow mode becomes very low and undetectable. Only the fast component of the autocorrelation function is present. These results are analogous to many observations made on a lot of polyelectrolyte solutions and recall the "pseudo-transition" from "extraordinary" phase to "ordinary" phase [31,32,34,37,64]. At last, in the upper one-phase at $C_S \approx 0.5$ M (D-point on Figure 15), a large scattered intensity is observed with only one relaxation time. The value of the effective coefficient diffusion is about 10^{-7} cm^2/s.

A cyclic observation has been made as a function of C/C_S. Following the a-line using a fresh solution, two modes are measured and the amplitudes

of both fast and slow decay are increasing as a function of C/C_S from 5 to 100. On the b-line, the disappearance of the slow mode is observed and only the fast one is observable to the C-point.

At the C-point ($C/C_S \approx 5$), we can dilute the solution to come back on the a-line to the A-point with a constant C/C_S. In this case only one fast mode is observed along the constant C/C_S line (see Figure 18). The simplest interpretation is that at the beginning of the cycle a-line the fresh solution with a low salt concentration is not macroscopically in thermodynamic equilibrium. The presence of large clusters or electrostatic domains is at the origin of the slow relaxation time, and whatever the polyelectrolyte concentration, these domains have a very slow evolution as a function of time. On the b-line, the added salt destroys progressively the electrostatic domains and they melt definitively at a critical salt concentration. In this state, the solution became thermodynamically stable and the nonappearance of the slow mode when we cycle at constant C/C_S between high (C-point) and low (A-point) salt concentration shows that the origin of the slow mode is due to an unstable polyelectrolyte solution. We do not observe the reappearance of the slow mode after cycling during some days [63].

IV. CONCLUSION

The solubility of flexible highly charged polyelectrolytes in the presence of multivalent counterions depends on the affinity between counterions and charged groups of the polyelectrolyte. Two extreme cases can be encountered: in the first one the precipitation is induced by the complexation of the polyelectrolyte with the multivalent ions, whereas in the second one the electrostatic attraction is the principal driving force for phase separation.

For weak polyelectrolytes, like polycarboxylates, complexes are formed with inorganic counterions. The polyacrylate chemically reacts with all inorganic multivalent counterions and precipitation takes place. Before phase separation, the high electrostatic polyelectrolyte potential leads nearly all counterions to form complexes with charged monomers. The demixion limit is related to the fraction of monomer in the dicomplex state, which depends on the polyelectrolyte charge density. The complexation increases as the counterion concentration increases and therefore inhibits polymer resolubilization. For highly charged weak polyelectrolytes in the presence of divalent counterions, the majority of counterions form dicomplexes between two neighboring monomers on the same chain. Dicomplexation partially dehydrates counterions and charged groups of the polymers; therefore the complexes formed are hydrophobic.

In the case of strong polyelectrolytes (sulfonates, sulfates, phosphates) generally no chemical associations occur, and their solubility only depends

on electrostatic interactions. Other factors such as the nature of the polymer backbone (hydrophobicity, rigidity), the nature of the charged groups, and the nature of the counterions have little effect. The important parameter is the counterion valency. A finite two-phase zone exists only for counterions with a valency higher than or equal to 3. Whatever the nature and the shape of the counterions, lanthanium or spermidine (Sp^{3+}) and thorium or spermine (Sp^{4+}), similar phase diagrams are obtained for very different polyelectrolytes. Boundaries are only dependent on the valency of the counterions. A universal behavior that characterizes the strong contribution of electrostatic attraction could be proposed.

The NaPSS/$LaCl_3$ dynamics is characterized by a bimodal decay of the concentration correlation function at very low salt concentration. Two dynamic modes (fast and slow) are present. The fast process is interpreted as a diffusion of blobs of a transient network in the semidilute regime. The origin of the slow mode is not always understood. It can be interpreted as the diffusion of multichain domains (clusters). Due to the large dimensions of the domains, the slow mode does not correspond to a pure diffusive motion.

Both the disappearance of the slow relaxation time on a very long timescale after preparation of solutions (from a few months to one year) and the nonreappearance of this mode when cycling between high and low salt concentrations indicate that the solution, at very low salt concentration, slowly tends to equilibrium. The thermodynamic equilibrium of salt-free polyelectrolyte solution is very difficult to obtain. Strong electrostatic repulsion dominates the solution, and some electrostatic domains or clusters stay present for a long time in the fresh solution. Only with an excess of external salt or with a very long time scale can the solution be in thermodynamic equilibrium.

The set of results presented here allows us to understand better the properties of polyelectrolytes in the presence of multivalent counterions. However, these systems are very complex, and we hope that future experimental and theoretical work will permit us to progress significantly. We must keep in mind that while polyelectrolytes and multivalent counterion systems are interesting from a fundamental point of view, they are also of practical interest, as for instance in the biological field and in depollution process. An extension to polyelectrolyte/charged colloid systems that present some complex phase diagrams is in progress.

ACKNOWLEDGMENTS

We thank all the coworkers, Luc Belloni, Monica Olvera de la Cruz, Jean Pierre Dalbiez, Olivier Spalla, which have contributed to this work. Worth

mentioning is the invaluable contributions of Imad Sabbagh: several paragraphs of this paper summarize his Ph.D. dissertation [22] and Refs. 29 and 30.

REFERENCES

1. Barrat JL, Joanny JF. Theory of Polyelectrolyte Solutions. Advances in Chemical Physics 1996; 94:1–66.
2. Föster S, Schmidt M. Polyelectrolytes in solution. Advances in Polymer Science 1995; 120:51–133.
3. Oosawa F, Imai N. J. Chem. Phys. 1954; 22:2084–2085.
4. Manning GS. J. Chem. Phys. 1969; 51:924–938.
5. Oosawa F. Polyelectrolytes. New York: Marcel Dekker, 1971.
6. Katchalsky A, Alexandrowicz Z, Keden O. In: Conway BE, Barradas RG, eds. Chemical Physics of Ionic Solutions. New York: Wiley, 1966:295–346.
7. Mac Gillivray AD, Winkleman JJ. J. Chem. Phys. 1966; 45:2184–2188.
8. Belloni L, Drifford M, Turq P. Chem. Phys. 1984; 83:147–154.
9. Belloni L. Colloids Surfaces A: Physico Chem. Eng. Aspects 1998; 140:227–243.
10. Michaeli I. J. Polym. Sci. 1960; 48:291–299.
11. Ikegami A, Imai N. J. Polym. Sci. 1962; 56:133–152.
12. Kimizuka H, Yamauchi A, Mori T. Bull. Chem. Soc. Japan 1967; 40:1281–1282.
13. Dubin PL. In: Structure-Solubility Relationships in Polymers. New York: Academic Press, 1977:135.
14. Miyamoto S. Biophys. Chem. 1981; 14:341–346.
15. Narh KA, Keller A. J. Polym. Sci. Part B 1993; 31:231–234.
16. Axelos M, Mestdagh M, François J. Macromolecules 1994; 27:6594–6602.
17. Delsanti M, Dalbiez JP, Spalla O, Belloni L, Drifford M. ACS. Symp. Ser. 1994; 548:381–392.
18. Belloni L, Olvera de la Cruz M, Delsanti M, Dalbiez JP, Spalla O, Drifford M. Nuovo Cimento 1994; 16:727–736.
19. Olvera de la Cruz M, Belloni L, Delsanti M, Dalbiez JP, Spalla O, Drifford M. J. Chem. Phys. 1995; 103:5781–5791.
20. Wittmer J, Johner A, Joanny JF. J. Phys. Paris II 1995; 5:635–654.
21. Pelta J, Livolant F, Sikorav JL. J. Biol. Chem. 1996; 271:5656–5662.
22. Sabbagh I. Ph.D. dissertation, Université de Paris VII France, 1997.
23. François J, Heitz C, Mestdagh MM. Polymer 1997; 38:5321–5332.
24. Warren PB. J. Phys. II France 1997; 7:343–361.
25. Ikeda Y, Beer M, Schmidt M, Huber K. Macromolecules 1998; 31:728–733.
26. Raspaud E, Olvera de la Cruz M, Sikorav JL, Livolant F. Biol. J. 1998; 74: 381–393.
27. Heitz C, François J. Polymer 1999; 40:3331–3344.
28. Raspaud E, Chaperon I, Leforestier A, Livolant F. Biophys. J. 1999; 77:1547–1555.
29. Sabbagh I, Delsanti M, Lesieur P. Eur. Phys. J. B 1999; 12:253–260.
30. Sabbagh I, Delsanti M. Eur. Phys. J. E. 2000; 1:75–86.

31. Lin SC, Lee W, Schurr JM. Biopolymers 1978; 17:1041–1066.
32. Drifford M, Dalbiez JP. Biopolymers 1985; 24:1501–1514.
33. Grüner H, Lehmann W, Falbusch H, Weber R. J. Phys. A. Math. Gen. 1981; 14:L307–L313.
34. Sedlak M, Amis EJ. J. Chem. Phys. 1992; 96:817–826. Sedlak M, Amis EJ. J. Chem. Phys. 1992; 96:826–834.
35. Ghosh G, Peitzsch RM, Reed WF. Biopolymers 1992; 32:1105–1122.
36. Smits RG, Kuil ME, Mandel M. Macromolecules 1994; 27:5599–5608.
37. Schmitz KS, Lu M, Gauntt J. J. Chem. Phys. 1983; 78:5059–5066. Schmitz KS, Lu M, Singh M, Ramsay D. Biopolymers 1984; 23:1637–1646.
38. Drifford M, Dalbiez JP. J. Phys. Chem. 1984; 88:5368–5375.
39. Koene RS, Mandel M. Macromolecules 1983; 16:220–235.
40. Drifford M, Dalbiez JP. J. Phys. Lett. 1985; 46:L311–319.
41. Drifford M, Belloni L, Dalbiez JP, Chattopadhya AK. J. Coll. Interfac. Sci. 1985; 105:587–604.
42. Schmitz KS. Biopolymers 1993; 33:953–969.
43. Forster S, Schmidt M, Antonietti M. Polymer 1990; 31:781–792.
44. Peitzsch RM, Burt MJ, Reed WF. Macromolecules 1992; 25:806–815.
45. Sedlak M. Macromolecules 1993; 26:1158–1162.
46. Martell AE, Smith RM. Critical Stability Constants. New York: Plenum Press, 1974, Vols. 1–6.
47. Yatsimirskii KB, Vasil'ev VP. Instability Constants of Complex Compounds. Oxford: Pergamon Press, 1960:149.
48. Tondre C, Zana R. J. Phys. Chem. 1972; 76:3451–3459.
49. Ikegami A. J. Polym. Sci. A. 1964; 2:907–921.
50. Strauss UP, Leung YP. J. Am. Chem. Soc. 1965; 87:1476–1480.
51. Spegt P, Tondre C, Weill G, Zana R. Biophysical Chemistry 1973; 1:55–61.
52. Zana R. Journal of Polymer Science 1980; 18:121–126.
53. Bauer DR, Ullman R. Macromolecules 1980; 13:392–396.
54. Perzynski R, Delsanti M, Adam M. J. Physique 1984; 45:1765–1772.
55. Tanford C. Physical Chemistry of Macromolecules. New York: Wiley, 1966.
56. de Gennes PG, Pincus P, Velasco RM, Brochard F. J. Phys. Orsay Fr. 1976; 37:1461–1473.
57. Odijk T. Macromolecules 1979; 12:688–693.
58. Dobrynin AV, Colby RH, Rubeinstein M. Macromolecules 1995; 28:1859–1871.
59. Sedlak M. J. Chem. Phys. 1997; 107:10799–10804.
60. Essafi W, Lafuma F, Williams CE. J. Phys. II Fr. 1995; 5:1269–1275.
61. Sedlak M. J. Chem. Phys. 1994; 11:10140–10152.
62. Mandel M. In: Brown W, ed. Dynamic Light Scattering: The Method and Applications. Oxford: Oxford University Press, 1993:319–371.
63. Drifford M, Dalbiez JP, Delsanti M, Belloni L. Ber Buns. Phys. Chem. 1996; 100:829–835.
64. Fulmer A, Julyet A, Benbasat A, Bloomfield VA. Biopolymers 1981; 20:1147–1159.

This Page Intentionally Left Blank

5

Physical Questions Posed by DNA Condensation

BAE-YEUN HA and ANDREA J. LIU Department of Chemistry and Biochemistry, University of California, Los Angeles, California

I. INTRODUCTION

DNA in aqueous solution carries a very high negative charge, with two electronic charges per base pair (or equivalently, per 3.4 Å) along the length of the double helix. In its unpackaged form, DNA is well described as a wormlike chain with a persistence length of approximately 500 Å [1]. However, when DNA is packaged in viruses and cells, it is highly concentrated into configurations where helices are approximately parallel to each other with a surface-to-surface separation of roughly 5 Å. For example, the DNA of the T7 bacteriophage is approximately 10^{-4} times smaller in the phage head than in its unpackaged form [2]. To concentrate DNA to this level by brute force would require a pressure of over 100 atm [3].

It has been suggested that many bacteriophages [4–7] use multivalent cations to package their DNA. When multivalent cationic species (polyamines) known to exist in host bacteria are added to DNA in dilute solution, the chains spontaneously form highly concentrated toroids, of the same shape and size as the in vivo packaged DNA. This phenomenon is known as DNA condensation [8,9]. In addition to polyamines typically found in cells, a wide variety of cations can condense DNA in vitro, generally requiring only that the valency of the cation is three or higher [8,9]. Moreover, it turns out that DNA is not the only polyelectrolyte able to condense in this way. Experiments on other stiff, highly charged polyelectrolytes such as F-actin [10], tobacco mosaic virus, and fd virus [11] also condense into dense bundles. The fact that the attractions are observed for a wide range of stiff polyelectrolytes and a variety of multivalent counterions indicates that specific interactions are not responsible, and that the mechanism may be susceptible to a general electrostatic analysis.

Another striking experimental feature is that the attractions do not appear to lead to macroscopic phase separation. In this sense, the counterion-mediated attraction between the chains appears to have a different character from ordinary attractions that lead simply to phase separation at sufficiently high concentrations. Instead, the chains tend to form dense bundles of a fairly well-defined thickness [8,11]. The precise morphology of the bundles appears to depend sensitively on the persistence length of the polyelectrolyte, the chain length, and the concentration. In the case of dilute DNA, the bundles tend to be toroidal or rod-shaped. Other stiff polyelectrolytes tend to form rodlike bundles or networks of bundles. In each case, however, there is a well-defined cross-sectional thickness for the bundles. We will concentrate on the question of why there is a characteristic cross-sectional bundle diameter, rather than on the specific morphology of the bundles.

II. ORIGIN OF COUNTERION-MEDIATED ATTRACTION BETWEEN LIKE-CHARGED RODS

The question of how counterions mediate attractions between like-charged chains has garnered much attention in the physics community because mean-field Poisson–Boltzmann theory predicts that like-charged rods should repel, regardless of the valency of the counterion [12]. This implies that fluctuation and correlation effects that are neglected in Poisson–Boltzmann theory must be responsible for the attraction.

A. Counterion-Mediated Attraction Between Like-Charged Plates

The mechanism for attraction has also been addressed for a different geometry, namely two like-charged parallel plates in solution. There, integral equation methods [13,14] show that fluctuations within the hypernetted chain approximation (but neglected within mean-field theory) could lead to attractions. Density functional arguments also predict that like-charged plates can attract [15]. Complementary to these two liquid-state approaches is a low-temperature picture, where the counterions crystallize in the plane parallel to the plates [16]. It is obvious that the plates should attract in this ionic crystal phase. The precise form of the attraction depends on fluctuations of the ions around their lattice positions (phonon modes) [17], but clearly the attraction should be strongest at zero temperature. Finally, field theoretical approaches based on one-loop corrections to either Debye–Hückel [18] or Poisson–Boltzmann [19] theory also show that two plates can attract. These theories are appropriate to the high-temperature noncrystalline phase, where thermal fluctuations in the charge density along the plane become correlated

and give rise to an attraction similar to the van der Waals attraction. This attraction vanishes at zero temperature.

B. Counterion-Mediated Attraction Between Like-Charged Rods

There is an important distinction between the plate geometry (the interaction between two like-charged planes) and the rod geometry (the interaction between the like-charged rods), in that the origin of the repulsion is completely different in the two cases. In the plane geometry, all the counterions are condensed. As a result, there is no net effective charge on the plates. On the other hand, the confinement of counterions between the plates leads to an entropic repulsion; this double-layer repulsion is generally much larger than the electrostatic contribution.

For the rod geometry, on the other hand, only a fraction of the backbone charges are neutralized by condensed counterions. This means that each rod still carries a net charge, so two rods will repel each other electrostatically. On the other hand, the entropic repulsion due to confinement of counterions is much weaker.

The fact that the origin of the repulsion is different for plates and for rods means that the overall phase behavior can be different, because the interaction depends sensitively on the competition between the correlation-attraction and the repulsion. However, the mechanisms of attraction that have been proposed for rods are the same as for plates. Thus the ionic crystal picture for plates has been applied to rods [20–23], as has the thermal fluctuation picture (which was developed for rods more than 30 years ago by Oosawa [24–26]). In the case of rods, there are several versions of the ionic crystal model, which differ in microscopic details [21–23,27]. In the thermal fluctuation picture, fluctuations in the condensed counterion density along the rods lead to nonuniformities in the charge distribution, which can become correlated from one rod to another [26,28], leading to an attraction similar to the van der Waals interaction. We have introduced a third approach, called the charge fluctuation approach [29,30], which is an extension of the thermal fluctuation approach to ions of nonzero size, and which captures aspects of both the thermal fluctuation picture and the ionic crystal pictures.

C. Low-Temperature Ionic Crystal Picture vs. High-Temperature Thermal Fluctuation Picture

The discrepancy between the ionic crystal approach and the thermal fluctuation approach described above has led to considerable controversy in the rod case [31,32]. We emphasize that there is no way to reconcile the

two approaches completely, because the thermal fluctuation approach is a high-temperature approximation, while the ionic crystal approach is a low-temperature approximation, and the two are separated by a phase transition, namely crystallization. The same controversy has arisen in other contexts, such as one-component and two-component plasmas [33–35]. The thermal fluctuation approach neglects correlations that are important at lower temperatures because it neglects a length scale that is important at low temperatures or high densities, namely the ionic size. This size prevents the attractive interaction from diverging and is clearly important to ionic crystallization because if all the ions were point charges, the system would collapse onto a point at zero temperature. Most field-theoretical calculations have neglected this size by assuming point ions. However, we have shown that it is straightforward to include this length scale by assuming that charge is correlated over the size of the ion [30]. We call this approach the charge fluctuation approach to distinguish it from the thermal fluctuation approach, which assumes point ions. When the nonzero ionic size is incorporated in this way, we find oscillatory charge correlations that grow in range as the temperature is lowered and eventually diverge at the spinodal for the ionic crystal [29]. Note that it has previously been shown for electrolyte solutions that full Debye–Hückel theory, which includes the nonzero ionic size (as opposed to the Debye–Hückel limiting law, which assumes point ions), also produces oscillatory charge correlations indicative of an incipient ionic crystal [36]. Thus the one-loop field-theoretical approach leads to reasonable qualitative behavior at low temperatures, even though it is unlikely to be quantitatively accurate there. More recently, it has been shown for the case of two plates [37] that at high temperatures, long wavelength fluctuations in the charge density along the plates dominate the interaction, while at low temperatures, short wavelength fluctuations dominate. The long wavelength fluctuations lead to an attraction that diminishes as temperature is lowered, while the short wavelength fluctuations lead to an attraction that increases as temperature is lowered. It is known from simulations that the attraction strengthens as the temperature decreases [20]; this implies that the short wavelength fluctuations are more important. The short wavelength fluctuations in the charge fluctuation model represent liquidlike correlations that are the analogue of the ionic crystal correlations below the freezing transition. Thus we argue that at higher temperatures where the charge correlations are liquidlike, a charge fluctuation picture might more accurately describe the origin of the attraction, but at lower temperatures where the charge correlations are solidlike, the ionic crystal is a better description. Certainly, our approach is a poor one in the ionic crystal phase, just as the ionic crystal approach is a poor approximation above the melting transition. Simulations show that the interactions between chains can be strongly attractive even

when there is significant counterion diffusion along the rods, and only liquid-like ordering of the condensed counterions [20,38]. This is the regime in which the charge fluctuation picture is appropriate.

D. Charge Fluctuation Model

Our calculations have been discussed extensively elsewhere [30], but it is worthwhile to describe the assumptions underlying the model and approach. We start with rods with a uniform negative charge. The actual charge distribution for DNA is helical; this nonuniform distribution can also lead to attractions at very short distances and low temperatures [39], but we have not adopted this more realistic description. The charge on the rods is balanced by counterions, and we also allow for salt. In reality, the counterions are distributed with some spatial density profile around the rods, which can be approximated by the solution to the nonlinear Poisson–Boltzmann equation. We adopt the two-state approximation to describe this density distribution; that is, we divide the counterions into two classes, condensed and free [24,40]. A condensed counterion is approximated to lie on the nearest monomer, and to add a charge Z to the net charge of that monomer, while a free counterion contributes to Debye screening of the electrostatic interactions in the solution. Because condensed counterions can move along the rods or exchange with free counterions, the effective charge of a monomer can fluctuate. If we assume that a large number of condensed counterions can be assigned to a given monomer, then we can apply the central limit theorem to the charge distribution and treat the charge per monomer as a Gaussian variable. Thus we characterize the charge distribution by two quantities: the net charge per monomer, $q = -f_0 + Zf_c$, and the variance in the charge of a monomer on the rod, $\Delta = Z^2 f_c$. Here, $-f_0$ is the bare charge per monomer in units of the electronic charge, and f_c is the fraction of condensed counterions per monomer.

Given the model with random charges on each monomer, we start with the Hamiltonian given by Coulomb interactions between all pairs of charges in the system. We assign charges on the rods a nonzero size, given by the counterion diameter. Charges on free ions in solution, however, are treated as point ions. (The point-ion approximation is a good one as long as the charge density is low. Under the conditions of interest for DNA condensation, the charge density along the rods is high due to counterion condensation, but the charge density in solution is low.) We integrate over free ions at the Gaussian level; that is, we assume that fluctuations in the density of mobile ions are small. In fact, it is possible to integrate over free ions exactly if they are point charges. We make this approximation in order to treat the mobile charges and the fixed charges on the rods in a consistent way. Tracing

over the free ion positions at Gaussian order is equivalent to Debye–Hückel theory [26], while the exact point-ion integration is equivalent to Poisson–Boltzmann theory [41].

Finally, we integrate over the random charges on the rods at Gaussian order. This leads to a one-dimensional Debye–Hückel theory for the monomeric charges. However, it differs from a standard one-dimensional theory in two important respects. First, the charges on the rods have a nonzero size. In our Gaussian approach, the size enters via a form factor for the charged particle. Second, the charges interact with each other, and with the charges on other rods, via three-dimensional screened interactions. In other words, our approximation is equivalent to treating each rod as a one-dimensional Debye–Hückel system that interacts with itself and with all the other rods via a three-dimensional Debye–Hückel system of mobile ions.

How good are our approximations? We have made three main approximations. The first is to include counterion condensation within a two-state model. The second is to introduce the nonzero size within a form factor for the charged particle. The third approximation is to treat the fluctuations along the rods within a quasi-one-dimensional Debye–Hückel theory. Recent calculations by Kardar and Golestanian [19] avoid the two-state assumption by expanding around the Poisson–Boltzmann result. Their calculation provides some justification for the two-state model: when the counterion distribution is approximated with a step function, our expressions $q = -f_0 + Zf_c$ and $\Delta = Z^2 f_c$ are recovered [42]. Expanding around the Poisson–Boltzmann solution with its spatial distribution of counterions (without assuming a step function) is a definite improvement over our theory, but this approach is quite complicated to apply to our bundle system, especially if the ions are assigned a nonzero size.

The second approximation involving the ionic size can be improved upon even within the Gaussian approximation by including the structure of the ion in a self-consistent way [43]. It would be worthwhile to extend our calculations to include this approach.

The third approximation that we have adopted (describing the rods with associated condensed counterions as one-dimensional Debye–Hückel systems coupled to each other through a three-dimensional Debye–Hückel ionic solution) relies on the first term in a perturbation (loop) expansion that is best at higher temperatures and probably diverges in the regime of interest. However, it is important to recognize that good approximations can be useful beyond their range of validity. The important question is, What physics is left out by our description? In the case of *simple* Debye–Hückel theory, two important qualitative effects are left out: ionic associations (counterion condensation) and the possibility of oscillatory charge correlations. We have gone beyond the simple theory by including counterion condensation within

a two-state model. We have also extended the simple theory to include oscillatory charge correlations by allowing for a nonzero ionic size (this is described in greater detail in Sec. II.D). Thus, although our approximations will not lead to *quantitatively* accurate behavior at low temperatures, they predict the correct *qualitative* behavior.

Our approach is similar in spirit (although different in form) to one adopted by Fisher and coworkers to describe criticality in electrolyte solutions. They also adopted a ''two-state'' model to include Bjerrum pairs in chemical equilibrium with free ions, and they note that it is essential to include the nonzero ionic size in order to capture criticality [35].

Finally, we note that the model itself is not accurate in the ionic crystal phase. The condensed counterions sit *on* the rods in our model, whereas they really should sit in between the rods. In other words, the structure of the ionic crystal is not captured correctly by the model. Recent calculations argue that multiple moments perpendicular to the rod axis that arise when counterions lie *between* rods are important to the low-temperature behavior [23]. This is probably a source of greater quantitative error at low temperatures than is the Gaussian approximation.

III. ORIGIN OF CHARACTERISTIC CROSS-SECTIONAL DIAMETER OF BUNDLES

Regardless of whether the ionic crystal or charge fluctuation picture is adopted, the same picture emerges for the interaction between two parallel rods. In both pictures, the range of the attraction is set by the characteristic length scale of charge fluctuations along the length of the rods. Most of the backbone charges are neutralized by condensed counterions in the regime of interest to DNA condensation, so the characteristic length scale is roughly the distance between condensed counterions along the backbone, namely half a base pair. This length scale is extremely short, so the range of the attraction is also short. There is also a repulsion due to the net charge on each rod, whose range is set by the screening length. Under conditions where DNA condenses, the repulsion is longer in range than the attraction. Many other systems have short-range attractions and longer range repulsions [44]. In all those cases, the competition between the two interactions leads to a finite domain size. One would therefore expect the counterion-mediated attraction to lead to stable finite-size bundles, where the size of the bundle is limited by the range of the repulsion, namely the screening length. In fact, this argument is completely wrong. This can be seen from the experimental observation that the bundle size is much larger than the screening length. Below, we argue that the expectation of a stable finite bundle size is fundamentally flawed because it relies on the incorrect assumption that the

counterion-mediated interactions are pairwise additive. Instead, the bundle should be viewed as a domain of a new concentrated phase, and the surface of the bundle is the interface between this concentrated phase and a dilute phase [45].

A. Non-Pairwise-Additivity of Counterion-Mediated Interaction

Neither the short-ranged attraction nor the long-ranged repulsion are pairwise-additive in the regime of interest [46]. First consider the attractive interactions. These arise from correlations between the charge density distributions on different rods. Suppose there are two rods with correlated charge distributions. If a third rod is introduced, its charge distribution will affect those on the other two rods, leading to a three-body contribution to the attraction. Thus the interaction among the three rods must be computed explicitly, without assuming pairwise additivity.

Now consider the repulsive interactions. These originate from the net charge on each rod. That is, not all the backbone charges are neutralized by condensed counterions because the temperature is not zero, so each rod still carries a net negative charge. The net charge of the bundle (i.e., the sum of the net charges of the rods in the bundle) is therefore nonzero for all bundle sizes. However, the total charge enclosed in the bundle is not the same as the net charge of the bundle. The remaining counterions (the free counterions) partition themselves between the volume occupied by the bundle and the rest of the solution. As the bundle grows and occupies a larger fraction of the available volume, a larger fraction of the free counterions will be found in the bundle. In the limit of a very large bundle, the total charge enclosed in the volume of a bundle should be proportional to the surface area of the bundle.

In reality, we expect an even simpler picture. The dielectric constant of the chains is much lower than that of water. Inside a bundle, the effective dielectric constant is therefore quite low, because the chain concentration is extremely high. As a result, there should be nearly complete counterion condensation inside the bundle, so again the total charge of the bundle should be proportional to the surface area of the bundle.

We have calculated the energy of an N-rod bundle explicitly, using the one-loop approximation (the same approximation that we used for two rods) [30,46]. Because the repulsion weakens as the bundle size grows, we find that the repulsion does not limit the bundle size. Instead, the free energy decreases linearly with N, the number of rods in the bundle. Thus the counterion-mediated attraction is no different from more pedestrian attractions such as the dispersion attraction. This calculation does not include the translational

entropy of the rods. Once the entropy is included, the equilibrium phase behavior of the solution will be just like any other solution of particles interacting via attractive interactions. At low concentrations the chains will remain in solution and at higher concentrations they will precipitate out to form a chain-rich phase in equilibrium with a chain-poor phase.

B. Kinetics of Bundle Formation

The analysis above appears to contradict the experimental finding of a well-defined finite bundle size. We argue that the experimental observation is not an equilibrium effect, and that the kinetics of bundle formation lead to a well-defined size. In fact, we believe that the competition of the short-range attraction and longer range repulsion leads to unique kinetics of bundle growth [47].

In order to understand the kinetics of bundle growth, we must first consider the interaction between two rods as a function of the angle between them. The interactions between anisotropic particles such as rods depend sensitively on relative orientation. For most types of interactions, such as excluded volume or dispersion interactions, the interactions are anisotropic only in magnitude. The polyvalent-counterion-mediated interaction between like-charged rods is unusual because not only its magnitude but also its *sign* depends sensitively on the angle between the rods. This can be seen from the following argument. At large separations, two chains repel each other at all angles because the repulsion is longer in range than the attraction. At short separations, however, the two chains can attract each other if they are sufficiently parallel that their charge distributions can become correlated. If the chains are tilted away from parallel, less correlation arises, so the attraction decreases and the free energy increases. On the other hand, if the chains are perpendicular to each other, there is no correlation and the interaction is repulsive. As they are tilted away from a perpendicular configuration, the free energy increases because the repulsion increases; accordingly, there is a barrier in the free energy as a function of angle. This barrier has been calculated by us for two rods within the charge fluctuation model [47], as shown in Figure 1.

Note from Figure 1 that the barrier height is much smaller than the thermal energy for two rods. This is an artifact of our model, where we have modeled the rods as line charges with zero diameter. For more realistic charge distributions, e.g., spread out on the surface of a finite-diameter rod, we calculate the height to be tens of times larger [48]. The reason why the barrier height increases with rod diameter can be seen from a simple geometrical argument. Consider the circular cross-sections of two rods separated by some distance. Since the attraction is short-ranged, only the charge dis-

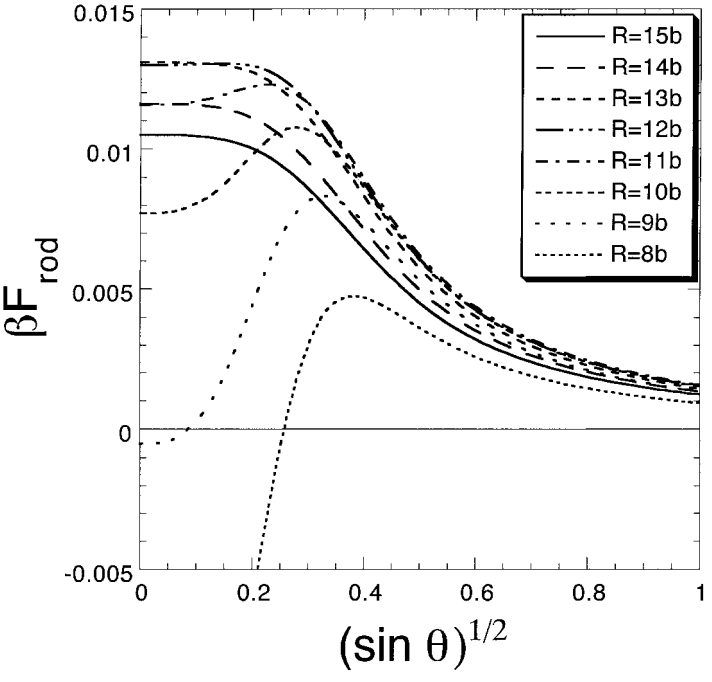

FIG. 1 Plot of free energy of polyvalent counterion–mediated interaction between two rods as a function of the angle between the rods for different rod separations, R (in units of the monomer size b). The two rods are parallel at $\theta = 0$. We then tilt one rod with respect to the other around the axis of separation between the two rods to a nonzero angle θ. The minimum at $\theta = 0$ that appears for short separations arises from the polyvalent counterion–mediated attraction. The minimum at $\theta = 90°$ (which is stable at large separations and metastable at small separations) arises from the repulsion due to the net charge on the rods. For this calculation, $T = 300$ K, $\varepsilon = 80$, and $Z = 2$. In addition, the length of the rods was taken to be 500 Å (the persistence length of DNA). (From Ref. 47.)

tributions along the facing arcs of the two circles can attract. On the other hand, the repulsion is of longer range, so charges at all points along the circular cross-sections can repel. As a result, the repulsion increases relative to the attraction with increasing rod diameter, leading to a higher repulsive barrier. For rods of the thickness of DNA, we find that the barrier is therefore significant, even for just two rods. Of course, since the attraction is short ranged, it is very sensitive to microscopic details and our estimates should not be taken too seriously. However, the predicted *trends* are reliable and have interesting consequences for the kinetics of bundle growth.

To see how the barrier shown in Figure 1 affects bundle growth, consider the interaction free energy between a chain and a bundle of already condensed chains. This free energy contains a barrier as a function of the angle between the chain and the bundle. For sufficiently small bundles, a chain can overcome this barrier and join the bundle; however, the barrier height increases linearly with the bundle diameter because a skewed chain is repelled by the rods in the facing surface of the bundle. For a sufficiently large bundle, the barrier can exceed the thermal energy, but if a chain is very close and nearly aligned with a thick bundle it can rotate into a parallel orientation and join the bundle because the interaction is attractive. On the other hand, if a chain encounters the bundle at too large an angle, it will rotate into a perpendicular orientation to lower the free energy and thereby move away, because the interaction is repulsive. As the bundle grows larger, it is less and less likely that a chain will be able to approach the bundle at a small enough angle for it to fall into the attractive minimum.

Now consider what happens when a bundle of N chains encounters a bundle of M chains. Again, the charges on the facing surfaces of the two bundles will repel each other, leading to a barrier that increases with the product of their diameters. Thus bundle–bundle aggregation is also discouraged as the bundles increase in size.

This kinetic mechanism is, to our knowledge, unique. In equilibrium, the system would phase separate into a dilute phase of randomly oriented chains and a concentrated phase of parallel, hexagonally ordered chains [49]. In most systems that phase separate, there is a nucleation barrier but no barrier to subsequent growth. In our case, the nucleation barrier is negligible [45]. (Note, however, that in the specific case of toroid formation there is a different nucleation barrier to forming a loop of the toroid [50].) Regardless of the nucleation process, there is a barrier to domain growth that increases in height as the domains grow. This inevitably prevents the system from reaching equilibrium.

IV. DISCUSSION

The mechanisms of attraction and domain growth that we have proposed are consistent with known experimental trends for DNA condensation. We summarize these trends below.

A. Minimum Counterion Valence Required for Condensation

DNA generally condenses when trivalent or higher valence cations are added [8]. The charge fluctuation model predicts that the attraction between rods

depends on the cation valence, Z, through the variance in the monomer charge, $\Delta \propto Z$, while the repulsion depends on the net charge, q, which decreases as $1/Z$. Thus the net attraction increases rapidly with counterion valence, giving rise to DNA condensation above some threshold Z_{min}. We find that Z_{min} depends sensitively on the radius of the chains. This is because the repulsion strengthens relative to the attraction as the radius increases, as discussed above. Thus for larger rod radii, a higher valence is required in order for the attraction to dominate at short distances. As we mentioned earlier, precise microscopic details are important at length scales as short as 6 Å, so we do not expect our results to be quantitatively accurate. However, we do find that the attraction disappears near $D = 20$ Å, characteristic of DNA. Thus, a minimum valence of $Z_{min} = 3$ is required to condense DNA within our model [48].

B. Effect of Monovalent Ions

When monovalent salt is added at sufficiently high concentrations, it can reverse condensation, leading to isolated chains in solution [11,51]. This result can also be understood in the context of the charge fluctuation model. In the model, monovalent salt affects the attraction more strongly than the repulsion because the attraction requires a *correlation* of the charge distributions on different rods. Thus the first rod must induce a correlated charge distribution on the second rod, and then the two charge distributions must interact. Both steps in this process are screened. The repulsion, on the other hand, merely requires an interaction between the net charges on each rod. As a result, the attraction is screened more heavily than the repulsion. Moreover, at high monovalent salt concentrations, the fraction of condensed monovalent counterions will increase, and the fraction of condensed polyvalent counterions will correspondingly decrease. This will also serve to weaken the attraction relative to the repulsion. At sufficiently high monovalent salt concentrations, the attraction therefore disappears and the bundles fall apart.

One consequence of this argument is that the height of the free energy barrier depicted in Figure 1 should increase with increasing salt concentration, since the attraction tends to reduce the barrier height. (Above a threshold value, this trend is of course reversed; that is, for sufficiently high salt concentrations, the barrier height eventually decreases with increasing salt concentrations because the attraction is negligible and the repulsion is screened more heavily.) Since the barrier height can increase with salt concentration, this affects the kinetics of domain growth. The barrier height for a rod to join an N-rod bundle is roughly $F_{barrier} \approx \sqrt{N}F_0$, where F_0 is the barrier height for two rods to aggregate [47]. The effect of monovalent salt

is to increase F_0. This means that a smaller aggregation number N is required to achieve a barrier height that is several times the thermal energy kT. As a result, the bundle size should be smaller at higher salt concentrations. This theoretical prediction remains to be tested experimentally.

C. Dependence of Bundled Thickness on Counterion Valence

The thickness of DNA condensates is found to be roughly independent of Z once Z exceeds $Z_{\min}$ [8]. In our scenario, the thickness is determined by the height of the barrier depicted in Figure 1. One would expect the interaction free energy (and therefore the barrier height) to depend sensitively on Z. However, we find that the interaction free energy depends only weakly on Z for $Z > 2$ [48]. This may seem counterintuitive at first, but it can be understood simply as follows. Although *condensed* counterions of higher valence induce stronger attractions and weaker repulsions, *free* counterions of higher valence screen electrostatic interactions more effectively. Screening affects the attractions more than the repulsions. Thus if one is above the threshold concentration of polyvalent counterions required for DNA to condense, the two effects tend to cancel.

D. Dependence on Solvent

Experimentally, it is observed that divalent ions can trigger condensation in alcohol–water mixtures. In our model, both Δ and q also depend on the dielectric constant of the solvent, so that the attraction increases and the repulsion decreases with decreasing ε; this lowers the threshold value of $Z_{\min}$. We note, however, that the effect of alcohol could be much more subtle and could depend on microscopic details such as the structure of water near the DNA and counterions that are neglected in our model.

E. Dependence on Chain Length

The observed bundle thickness is independent of DNA chain length as long as the length lies in the range between roughly 400 bp (1360 Å) and 50,000 bp [8]. The minimum value of 400 bp could be a buckling length [52] or the length required to make one loop of the toroid [50] and is not explained by our rigid-rod model. However, we do find that the barrier height is independent of chain length as long as the chain length exceeds the persistence length. This is because the appropriate rod length M to choose in order to model the electrostatics of a semiflexible chain is the persistence length, not the chain length.

F. Effect of Bundle Shape

The bundle thickness is observed to be roughly the same for both toroidal and rodlike DNA condensates. Several previously suggested mechanisms apply only to toroids [8,50,53]. Our mechanism applies to toroidal as well as rodlike bundles. For toroidal bundles, additional chains must overcome the same barrier in order to align with chains already in the torus. Note that our mechanism does not apply to toroids or rods composed of a single chain, because there is no barrier for the unwound part of a chain to join a bundle within our model. However, for chains that are too long (above 50,000 bp), it is difficult to observe bundles because of technical difficulties involved in mixing DNA with polyvalent counterions without breaking the DNA.

G. Time Dependence of Bundle Growth Kinetics

Experiments have shown that the initial formation and growth of bundles is quite rapid, occurring over the period of a few minutes. This is followed by very slow growth of bundles over a period of days [51]. These observations are consistent with our picture, where the bundle growth is controlled mainly by diffusion until the barrier height exceeds several kT. Once the barrier height is significant, the growth rate is controlled by the time to cross the barrier, which is long.

H. Other Mechanisms of Toroid Formation

Recent experiments on the bacteriophage T5 show that arbitrarily large toroidal bundles of condensed DNA can be formed by a special process [54]. In these experiments, the phase DNA is ejected from viruses into liposomes in solution with polyvalent counterions. The amount of DNA ejected into the liposomes can be controlled by increasing the concentration of receptor proteins that enable the viruses to eject their DNA into the liposomes. The kinetics of bundle growth in this experiment are very different from the usual case, because the DNA is released by the virus into the liposome base pair by base pair, in such a way that the orientation of the chain is automatically aligned with those already in the growing toroid. In this way, the system avoids the kinetic barriers discussed in Sec. III. The fact that the resulting bundles have a much higher cross-sectional diameter lends support to our picture that the bundle size in the usual case is determined by kinetic rather than equilibrium considerations.

V. SUMMARY

The phenomenon of DNA condensation has spurred physical theorists to address two questions: What is the origin of the polyvalent-counterion-

mediated attraction that draws the like-charged chains together into a concentrated bundle, and what sets the characteristic size of the bundle?

The origin of the counterion-mediated attraction between like-charged chains can be understood within the charge fluctuation picture [46]. This picture is conceptually useful because it reconciles the thermal fluctuation approach with the ionic crystal approach. In the thermal fluctuation approach, long-wavelength fluctuations lead to long-range attractions that are stronger at high temperatures. In the ionic crystal approach, short-wavelength fluctuations lead to short-range attractions that are stronger at lower temperatures. Both mechanisms are captured by the charge fluctuation approach, as shown for the case of two charged plates [37].

Although most theorists have focused on the *origin* of the counterion-mediated attraction, the main focus of our work has been to explore the *consequences* of the interaction in many-chain systems. The charge fluctuation approach is particularly well suited to many-chain systems because it allows an analytical approach [30]. This is particularly important because the counterion-mediated interaction is not pairwise additive. We have found that, in equilibrium, the system should phase separate on a macroscopic scale into a dilute phase in coexistence with a concentrated phase of parallel chains.

So what sets the characteristic size of a bundle? The charge fluctuation picture predicts that the system can never reach equilibrium because there is a barrier to bundle growth that increases with the bundle diameter. For a sufficiently large bundle, this barrier is high enough to prevent further growth. These unique domain growth kinetics are a consequence of the unusual angular dependence of the counterion-mediated interaction. Unlike most interactions between anisotropic particles, the counterion-mediated interaction is anisotropic not only in magnitude but also in sign; at short distances, the interaction between two rods is attractive if they are sufficiently parallel and repulsive otherwise.

Finally, we have shown that the charge fluctuation approach is consistent with all the trends observed experimentally. Many specific predictions of the model remain to be tested. We hope that this work will spur further experiments on these fascinating systems.

ACKNOWLEDGMENTS

We thank Robijn Bruinsma and Bill Gelbart for stimulating discussions and for a careful reading of this manuscript. We gratefully acknowledge the support of the National Science Foundation through Grant No. DMR-9619277.

REFERENCES

1. C. Bustamante, J. F. Marko, E. D. Siggia, and S. Smith. Entropic elasticity of lambda-phase DNA. Science 265:1599–1600 (1994).
2. L. C. Gosule and J. A. Schellman. Compact form of DNA induced by spermidine. Nature 259:333–335 (1976).
3. H. H. Strey, R. Podgornik, D. C. Rau, and V. A. Parsegian. DNA–DNA interactions. Current Opinion in Structural Biology 8:309–313 (1998).
4. S. M. Klimenko, T. I. Tikchonenko, and V. M. Andreev. Packing of DNA in the head of bacteriophage T2. J. Mol. Biol. 23:523–533 (1967).
5. K. E. Richards, R. C. Williams, and R. Calendar. Mode of DNA packing within bacteriophage heads. J. Mol. Biol. 78:255–259 (1973).
6. W. C. Earnshaw, J. King, S. C. Harrison, and F. A. Eiserling. The structural organization of DNA packaged within the heads of T4 wild-type, isometric and giant bacteriophages. Cell 14:559–568 (1978).
7. V. B. Rao and L. W. Black. DNA packaging of bacteriophage T4 proheads: in vitro evidence that prohead expansion is not coupled to DNA packaging. J. Mol. Biol. 185:565–578 (1985).
8. V. A. Bloomfield. Condensation of DNA by multivalent cations: considerations on mechanism. Biopolymers 31:1471–1481 (1991).
9. V. A. Bloomfield. DNA condensation. Current Opinion in Structural Biology 6:334–341 (1996).
10. J. X. Tang and P. A. Janmey. The polyelectrolyte nature of F-actin and the mechanism of actin bundle formation. J. Biol. Chem. 271:8556–8563 (1996).
11. J. X. Tang, S. E. Wong, P. T. Tran, and P. A. Janmey. Counterion induced bundle formation of rodlike polyelectrolytes. Berichte der Bunsen-Gesellschaft —Physical Chemistry, Chemical Physics 100:796–806 (1996).
12. T. Ohnishi, N. Imai, and F. Oosawa. J. Phys. Soc. Jpn. 15:896 (1960).
13. S. Marcelja. Electrostatics of membrane adhesion. Biophysical Journal 61: 1117–1121 (1992).
14. R. Kjellander, T. Akesson, B. Jonsson, and S. Marcelja. Double layer interactions in monovalent and divalent electrolytes—a comparison of the anisotropic hypernetted chain theory and Monte-Carlo simulations. Journal of Chemical Physics 97:1424–1431 (1992).
15. M. J. Stevens and M. O. Robbins. Density functional theory of ionic screening: when do like charges attract? Europhys. Lett. 12:91 (1990).
16. I. Rouzina and V. A. Bloomfield. J. Phys. Chem. 100:9977 (1996).
17. A. W. C. Lau, D. Levine, and P. A. Pincus. Preprint (2000).
18. P. A. Pincus and S. A. Safran. Charge fluctuations and membrane attractions. Europhys. Lett. 42:103–108 (1998).
19. M. Kardar and R. Golestanian. The ''friction'' of vacuum, and other fluctuation-induced forces. Reviews of Modern Physics 71:1233–1245 (1999).
20. N. Grønbech-Jensen, R. J. Mashl, R. F. Bruinsma, and W. M. Gelbart. Counterion-induced attraction between rigid polyelectrolytes. Physical Review Letters 78:2477–2480 (1997).

21. B. I. Shklovskii. Wigner crystal model of counterion induced bundle formation of rodlike polyelectrolytes. Physical Review Letters 82:3268–3271 (1999).
22. J. J. Arenzon, J. F. Stilck, and Y. Levin. Simple model for attraction between like-charged polyions. European Physical Journal B 12:79–82 (1999).
23. F. J. Solis and M. O. de la Cruz. Attractive interactions between rodlike polyelectrolytes: polarization, crystallization, and packing. Physical Review E 60: 4496–4499 (1999).
24. F. Oosawa. Biopolymers 6:134 (1968).
25. F. Oosawa. Polyelectrolytes. New York: Marcel Dekker, 1971.
26. J. L. Barrat and J. F. Joanny. Theory of polyelectrolyte solutions. Adv. Chem. Phys. 94:1 (1996).
27. A. A. Kornyshev and S. Leikin. Electrostatic zipper motif for DNA aggregation. Physical Review Letters 82:4138–4141 (1999).
28. B. Y. Ha and A. J. Liu. Counterion-mediated attraction between two like-charged rods. Physical Review Letters 79:1289–1292 (1997).
29. B. Y. Ha and A. J. Liu. Charge oscillations and many-body effects in bundles of like-chargd rods. Physical Review E 58:6281–6286 (1998).
30. B. Y. Ha and A. J. Liu. Counterion-mediated, non-pairwise-additive attractions in bundles of like-charged rods. Physical Review E 60:803–813 (1999).
31. Y. Levin, J. J. Arenzon, and J. F. Stilck. The nature of attraction between like-charged rods. Physical Review Letters 83:2680 (1999).
32. B. Y. Ha and A. J. Liu. The nature of attraction between like-charged rods—reply. Physical Review Letters 83:2681 (1999).
33. A. Alastuey and B. Jancovici. On the classical two-dimensional one-component Coulomb plasma. Journal de Physique 42:1–12 (1981).
34. B. I. Halperin. Theory of melting in two dimensions. Surface Science 98:8–10 (1980).
35. Y. Levin and M. E. Fisher. Criticality in the hand-sphere ionic fluid. Physica A 225:164–220 (1996).
36. B. P. Lee and M. E. Fisher. Charge oscillations in Debye–Hückel theory. Europhysics Letters 39:611–616 (1997).
37. B.-Y. Ha. Modes of counterion density fluctuations and counterion-mediated attractions between like-charged fluid membranes. Preprint (2000).
38. M. J. Stevens. Bundle binding in polyelectrolyte solutions. Physical Review Letters 82:101–104 (1999).
39. A. A. Kornyshev and S. Leikin. Theory of interaction between helical molecules. Journal of Chemical Physics 107:3656–3674 (1997).
40. G. S. Manning. Limiting laws and counterion condensation in polyelectrolyte solutions: colligative properties. J. Chem. Phys. 51:924–933 (1969).
41. R. D. Coalson, A. M. Walsh, A. Duncan, and N. Bental. Statistical mechanics of a Coulomb gas with finite size particles—a lattice field theory approach. J. Chemical Physics 102:4584–4594 (1995).
42. R. Golestanian, private communication, 1999.
43. D. Chandler. Gaussian field model of fluids with an application to polymeric fluids. Physical Review E 48:2898–2905 (1993).

44. M. Seul and D. Andelman. Domain shapes and patterns—the phenomenology of modulated phases. Science 267:476–483 (1995).
45. B. Y. Ha and A. J. Liu. Interfaces in solutions of randomly charged rods. Physica a 259:235–244 (1998).
46. B. Y. Ha and A. J. Liu. Effect of non-pairwise-additive interactions on bundles of rodlike polyelectrolytes. Physical Review Letters 81:1011–1014 (1998).
47. B. Y. Ha and A. J. Liu. Kinetics of bundle growth in DNA condensation. Europhysics Letters 46:624–630 (1999).
48. B.-Y. Ha and A. J. Liu. Effect of nonzero chain diameter on "DNA" condensation. Preprint (2000).
49. D. Durand, J. Doucet, and F. Livolant. A study of the structure of highly concentrated phases of DNA by x-ray diffraction. Journal de Physique Ii 2: 1769–1783 (1992).
50. N. V. Hud, K. H. Downing, and R. Balhorn. A constant radius of curvature model for the organization of DNA in toroidal condensates. Proc. Natl. Acad. Sci. 92:3581–3585 (1995).
51. J. Widom and R. L. Baldwin. Cation-induced toroidal condensation of DNA. J. Mol. Biol. 144:431–453 (1980).
52. G. S. Manning. Packaged DNA. An elastic model. Cell Biophysics 7:57–89 (1985). Erratum in Cell Biophysics 8(1):86 (1986).
53. S. Y. Park, D. Harries, and W. M. Gelbart. Topological defects and the optimum size of DNA condensates. Biophysical Journal 75:714–720 (1998).
54. O. Lambert, L. Letellier, W. M. Gelbart, and J.-L. Rigaud. DNA delivery by phage as a new strategy for encapsulating toroidal condensates of arbitrary size into liposomes. Preprint (2000).

6

Conformational Transition in Polyelectrolyte Molecules: Influence of Osmotic Pressure of Counterions

VALENTINA V. VASILEVSKAYA Russian Academy of Sciences, Moscow, Russia

I. INTRODUCTION

The study of conformational transition (i.e., coil–globule transition) of macromolecules is one of the central problems in polymer science [1–4].

It is known [4] that the presence of even a small fraction of charged links drastically changes the picture of conformational transition. The conformational transitions in polyelectrolyte systems are much more pronounced than the coil–globule transition of electoneutral macromolecules. The volume of charged macromolecules on the course of coil–globule transition can undergo a hundredfold or even thousandfold decrease. The coil–globule transition of polyelectrolyte macromolecules in most cases can be realized as a first-order phase transition with a jump in the macromolecular size.

One of the most important polyelectrolyte macromolecules is a molecule of DNA. The phenomenon of DNA compactization was discovered by Lerman in 1968 [5,6]. He studied the sedimentation properties of DNA in aqueous solutions of polyethylene glycol and low-molecular salt and found that DNA coils swollen in water shrink abruptly when a suitable amount of polyethylene glycol and salt is added to the solvent. This phenomenon was referred as ψ-compactization (psi—polymer and salt induced). From the very beginning it became clear that ψ-compactization is a manifestation of coil–globule transition in DNA macromolecules [7,8]. Later it was found that the various chemical species could cause the transition of the DNA molecule to the globular state. Till now the effect of the ψ-compactization of DNA has attracted considerable attention owing to its fundamental significance and important applicability for molecular biology (for recent publications in the field see the review paper by V. Bloomfield [10]). It is

known that in biological systems (i.e., the bacteriophage head, the cytoplasmic space in the prokaryote, the nucleus in the eukareote), DNA molecules with contour length of the order of 10^2-10^4 μm are usually packed in a narrow space of the order of only $0.1-1$ μm. On the other hand, DNA chains exhibit a highly elongated coiled state in aqueous solution. This is why it is expected that the study of the collapse and decollapse transition of DNA could shed light on the mechanism of DNA function in the cellular environment.

Another example of drastic conformational transition in polyelectrolyte macromolecules is the effect of network collapse. This phenomenon was discovered by Tanaka in 1978 [11,12]. He investigated the swelling of polyacrylamide networks in the mixture of water and acetone. When the quality of solvent was made ''poorer'' (this happened when the concentration of acetone was increased), shrinking of the samples was observed. Tanaka found that the incorporation of some definite content of ionic groups leads to the appearance of the jump on the dependence of network volume on the solvent composition—a small increase of acetone concentration results in a jump-wise decrease (collapse) of the gel volume. Later it was found that the conformational state of polyelectrolyte gel is extremely sensitive to the external conditions. The wide spectrum of external parameters such as temperature, pH, salt and surfactant concentration, electric field, etc. could influence the conformational state of the charged gel and induce its collapse [13]. Nowadays such gels are known as responsive gels. The responsive gels are intensively studied. They have found wide application in various fields for data control devices of different types, absorbers, reactors, etc.

These two examples show that the theoretical description of conformational transition in polyelectrolyte macromolecules is of great importance. The study of conformational transition in polyelectrolyte molecules is also very important from the fundamental point of view.

Analysis shows that the basic reason for the crucial increase of sharpness of coil–globule transition of polyelectrolyte macromolecules in comparison with the transition of electroneutral macromolecules is that the polyelectrolyte molecule in good solvent is much more expanded than the electroneutral macromolecule. It is interesting that the physical reason leading to the additional expansion of polyelectrolyte macromolecules in good solvent depends on the size of the macromolecules.

The polyelectrolyte molecule is a polymer containing some fraction of groups that can dissociate into the charged monomer units attached to the molecule chain and oppositely charged low-molecular counterions freely moving in the solution. The specific properties of the polyelectrolyte molecule conformational state are determined by the long electrostatic repulsion between charged groups of chain and their interaction with freely moving

counterions. The relative weight of these factors varies in dependence on the polyelectrolyte molecule size.

Two limiting situations can be distinguished. In the case of single polyelectrolyte macromolecules immersed in a large volume of solvent, the reason for such expansion is the strong electrostatic repulsion acting between the charged units. The counterions escape from the interior of the macromolecular coil and are distributed in the huge external volume, so they do not influence the conformation of the macromolecule at all.

On the other hand, for a macroscopic polyelectrolyte gel, which is a collection of an infinite number of macromolecules, the swelling is due to the osmotic pressure of counterions remaining within the sample of gel due to the macroscopic electroneutrality condition. The electrostatic interaction between charged units in this case is of secondary importance.

In this paper we would like to discuss the theoretical approaches developed for the description of coil–globule transition of polyelectrolyte macromolecules in these two limiting situations and in the intermediate case when both of the contributions (due to the electrostatic repulsion and due to the translational entropy of counterions) are of the same order. We will discuss in detail mainly the theories constructed or developed by members of the Moscow group.

II. SINGLE MOLECULE AT INFINITE DILUTION

Let us consider the conformation of polyelectrolyte macromolecules immersed in an infinite quantity of solvent. The counterions having high translational entropy are distributed over the whole volume of the solution; their concentration in the vicinity of the macromolecules is extremely low, and their influence on the molecular conformation can be omitted completely. The conformation of the polyelectrolyte macromolecule is determined by rather strong unscreened repulsive interactions between charged groups attached to the chain. Due to this repulsion, the macromolecule assumes a strongly stretched conformation in the sense that its end-to-end distance R is a linear function of the degree of its polymerization m [14–18].

An excellent physical model describing the conformation of the polyelectrolyte molecule was proposed by de Gennes et al. in Ref. 14, where the conformation of the polyelectrolyte molecule immersed in an ideal solvent was considered. The molecule has m monomer units of size a. The fraction f of monomer units possesses by charge e (i.e., f is the degree of ionization of the molecule). The macromolecule is presented as a linear sequence of electrostatic blobs of spatial size D (see Figure 1). Each blob contains g charges, i.e., g/f monomer units, and thus the size R of the macromolecule is

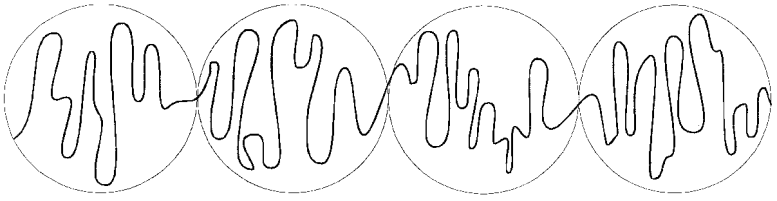

FIG. 1 Schematic picture of the blob structure of a charged polyelectrolyte chain.

$$R \sim \frac{m}{g/f} D \tag{1}$$

The spatial size D of electrostatic blob can be estimated from the condition that the energy of electrostatic repulsion of two blobs is of the order of thermal energy kT:

$$\frac{(ge)^2}{\varepsilon D} \sim kT \tag{2}$$

Within the electrostatic blob the electrostatic interaction can be considered as a weak perturbation, and a polymer chain on the scale D obeys the Gaussian statistics:

$$D \sim a \left(\frac{g}{f}\right)^{1/2} \tag{3}$$

Equations 1–3 give for D, R, and g the following results:

$$\begin{aligned} D &\sim \frac{a}{(f^2 u)^{1/3}} \\ R &\sim ma(f^2 u)^{1/3} \\ g &\sim \frac{1}{(fu^2)^{1/3}} \end{aligned} \tag{4}$$

where u is characteristic dimensionless parameter ($u = e^2/\varepsilon kT$).

A similar presentation of the polyelectrolyte macromolecule as an extended sequence of blobs is valid also in the case of good solvent, when the interaction between neutral monomers has a repulsive character, and the polymer chain within the electrostatic blob has a conformation of the coil with the excluded volume interaction [15].

The collapse transition in the framework of the blob model of the polyelectrolyte macromolecule was considered in Ref. 17. It was proposed that the structure of the polyelectrolyte macromolecule as sequence of blobs remains valid also in poor solvent. However, in this case the space size D of

the blob is determined by balance of electrostatic and surface interaction ΔF_s [17]:

$$\frac{(ge)^2}{\varepsilon D} \sim \Delta F_s \tag{5}$$

Inside each blob the chain takes a globular conformation with average monomer concentration n equal to the concentration inside the collapsed electroneutral chain $n \sim -(B/C)$ (B and C are second and third virial coefficients). So for the size of one blob one can write

$$D \sim \left(\frac{g}{fn}\right)^{1/3} \tag{6}$$

the parameters B, C, and surface free energy ΔF_s can be estimated as

$$B \sim v\frac{T-\theta}{T} = v\tau \quad C \sim v^2$$
$$\Delta F_s \sim T\left(\frac{g}{f}\right)^{2/3} \tau^{4/3} \left(\frac{a^3}{v}\right)^{1/3} \tag{7}$$

where v is the excluded volume of monomer unit.

Thus for the parameters D, R, and g we obtain

$$D \sim \frac{v^{1/3}}{(f^2u)^{1/3}}$$
$$R \sim mv^{1/3}(f^2u)^{2/3}\tau^{-1}$$
$$g \sim \frac{\tau}{fu} \tag{8}$$

The collapse transition of polyelectrolyte macromolecules upon worsening of solvent quality was considered as a coil–globule transition of each of mf/g blobs collapsed approximately as the chain of g/f monomer units unperturbed by the Coulomb interaction [17]. It was shown that the collapse transition occurs somewhat below the θ-point. The corresponding relative temperature deviation

$$\tau_c \sim -\left(\frac{a^3}{v}\right)^{1/3} (uf^2)^{1/3} \tag{9}$$

and the width of transition

$$\Delta T \sim \theta\left(\frac{v}{a^3}\right)^{2/3} (uf^2)^{1/3} \tag{10}$$

grow with the increase in the degree of ionization. It was also found that in

this case the sharpness of the collapse transition depends on the macromolecular stiffness.

In the course of conformational transition the number g of monomer units forming the electrostatic blob increases. For the case of relatively short chain (small value of m) or relatively weak degree of ionization f the collapse transition is ended by the formation of spherical globules. The condition for spherical globule formation is

$$m\frac{f^2u}{|\tau|} < 1 \tag{11}$$

Recently the necklace model of the polyelectrolyte molecule [18], confirmed by some results of computer simulations [18–19], was proposed. According to this model, the collapsed polyelectrolyte macromolecule at infinite dilution has a more complex structure than a simple sequence of blobs. The macromolecule is split into a sequence of beads connected by narrow and long strings forming the so-called necklace conformation. The size of the beads D of this structure is the same as the size of the blob D given by Eq. 8, whereas the diameter of the strings is of the order of the thermal blob $D_T \sim a/\tau$. The total size R of the macromolecule (length of the necklace) is a linear function of the chain degree of polymerization m:

$$R \sim mfa\left(\frac{u}{|\tau|}\right)^{1/2} \tag{12}$$

having a more weak dependence on the degree of ionization f than the dependence of Eq. 4. While the degree of ionization f grows, the number of beads on the necklace increases, whereas their size decreases.

One could expect that an account of the detailed structure of a collapsed polyelectrolyte molecule is important for the quantitative description of the collapse transition of the strongly charged polyelectrolyte molecule.

We will focus here on the transition in a weak polyelectrolyte molecule. We will consider that Ineq. 11 is fulfilled and that the forming globule structure has a spherical shape (we have the only electrostatic blob or the only bead in the necklace). We also will not discuss the effect of counterion condensation [20–26]. Due to this effect the real charge of the macromolecule is somewhat lower than the net charge of the molecule [20,21]. At a higher degree of ionization f the condensation of counterions could lead also to the collapse of macromolecules [22–26]. This phenomenon is attracting considerable attention in the literature [22–26].

III. POLYELECTROLYTE GEL

Let us now consider the second limiting situation, the case of a macroscopic sample of a polyelectrolyte gel.

In this case one could expect that the condition of total electroneutrality is fulfilled: all counterions float within the sample of the gel and influence its conformation state (Figure 2). This fact was firstly taken into account by Tanaka [11] who reported his first observation of the sharp collapse transition of a polyelectrolyte gel.

Let us consider the theory of a polyelectrolyte gel collapse as described in Refs. 27 and 28.

A sample of a polymer gel with a total number N of monomer links was studied. Let m be the average number of monomer units in the subchain, i.e., in the chain between two neighboring cross-linking points, and n be the monomer concentration inside the network sample.

The free energy F of such a network is presented as a sum of four contributions:

$$F = F_{\text{el}} + F_{\text{int}} + F_{\text{tr-en}} + F_{\text{el-st}} \tag{13}$$

For the free energy F_{int} of excluded volume interaction the virial expansion is used:

$$F_{\text{int}} = NT(Bn + Cn^2) \tag{14}$$

For the free energy F_{el} of elastic deformation of the polymer gel the expression of classical theory of rubber elasticity modified by Birshtein is used [29,30]:

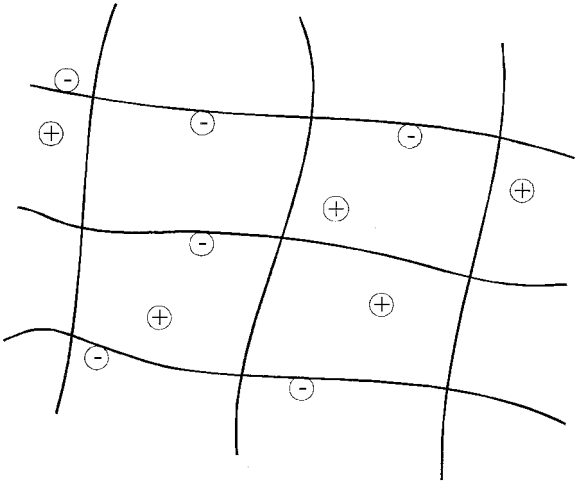

FIG. 2 Polyelectrolyte gel. Counterions are freely moving but keeping within the network sample.

$$F_{el} = \frac{3}{2}\frac{N}{m} T \left(\alpha^2 - \frac{1}{\alpha^2} \right) \tag{15}$$

where α is the swelling ratio of the network with respect to the reference state n_0 where the conformation of network chains is most close to the unperturbed Gaussian coils: $n \sim n_0/\alpha^3$.

Generally speaking, the reference state of a polymer gel is determined by the conditions of network preparation. For the network prepared in excess of solvent the reference state is θ-state of the polymer gel with an average concentration n_0 of monomer units given as [31] $n_0 \sim 1/m^{1/2}a^3$.

The contribution $F_{tr\text{-}en}$ is the translational entropy of the counterions:

$$F_{tr\text{-}en} = NfT \ln nf \tag{16}$$

For the electrostatic free energy $F_{el\text{-}st}$ the Debye–Hückel approximation is used:

$$F_{el\text{-}st} = NfTu^{3/2}(nf)^{1/2} \tag{17}$$

Thus the total free energy of a polyelectrolyte gel is given by

$$\frac{F}{NT} = \frac{3}{2m}\left(\alpha^2 - \frac{1}{\alpha^2} \right) + \frac{Bn_0}{\alpha^3} + \frac{Cn_0^2}{\alpha^6} + f \ln f \frac{n_0}{\alpha^3} - (uf)^{3/2} \left(\frac{n_0 a^3}{\alpha^3} \right)^{1/2} \tag{18}$$

The equilibrium size of the network sample (i.e., the value of the parameter α) is determined by the minimization of total free energy F with respect to the swelling ratio α: $\partial F/\partial \alpha = 0$. As result, one obtains the equation giving the dependence of the swelling ratio α on the quality of the solvent:

$$\alpha^5 - \alpha - s\alpha^3 + \lambda\alpha^{3/2} - \frac{y}{\alpha^3} = x \tag{19}$$

where

$$x = Bmn_0 \sim m^{1/2}\tau \qquad y = 2mn_0^2 \sim 1$$

$$s = mf \qquad \lambda = \frac{m}{2}(uf)^{3/2}(n_0 a^3)^{1/2} \sim (mf^2)^{3/4}$$

The typical dependence of the swelling ratio α on the solvent quality determined by the parameter x, which is proportional to the second virial coefficient B, is shown in Figure 3. The coil–globule transition proceeds as a first-order phase transition with a jump in the size somewhat below the θ-point:

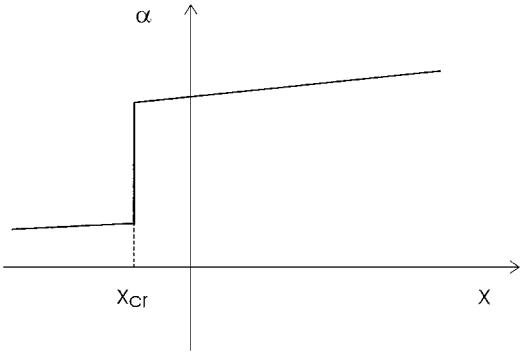

FIG. 3 Typical dependence of the swelling ratio α of a polyelectrolyte gel on the solvent quality.

$$\tau_{cr} \sim -f^{1/2} \tag{20}$$

The point of the coil–globule transition depends on the degree of ionization shifting into the field of poorer solvent with an increase of the degree of ionization f.

Below the critical point ($\tau < \tau_{cr}$), one has the collapsed polymer chain in the globular state, and the concentration of monomer links is determined by the balance of attractive and repulsive non-Coulombic interaction:

$$\alpha \sim \left(\frac{y}{|x|}\right)^{1/3} \sim m^{-1/6} \tag{21}$$

Above the critical point ($\tau > \tau_{cr}$), the size of the polymer gel slightly depends on the quality of solvent and is determined by the balance of the elastic free energy and the osmotic pressure of the counterions:

$$\alpha \sim s^{1/2} \sim (mf)^{1/2} \tag{22}$$

In this field of solvent quality the end-to-end distance R of the network subchain is linearly proportional to its degree of polymerization m:

$$R \sim \alpha \mathrm{m}^{1/2} a \sim m f^{1/2} a \tag{23}$$

as it is in the case of a single polyelectrolyte macromolecule at infinite dilution. However, in this case, with an increase of the degree of ionization f, the subchain size increases faster than the size of the chain in the case of polyelectrolyte molecules at infinite dilution. Note that the contribution of the electrostatic interaction $F_{\text{el-st}}$ in this case is always (below and above the transition point) negligible.

We would like to stress that the physical reason of the *polyelectrolyte gel* expansion is the osmotic pressure of counterions, which originates from their translational entropy. Counterions possessing high translational entropy would like to leave the network sample. However, this is forbidden because of the condition of total electroneutrality. So the counterions create osmotic pressure on the sample of the polymer network.

Later the theory proposed was successfully developed to describe the collapse of polymer gels in a solution of low-molecular salt and surfactant, in a mixture of two solvents, and in a solution of linear polymer [27,28,32,33]. This theory describes the collapse of polymer gels under the action of external uniaxial extension and the collapse transition of polymer gels in nonpolar solvents [27,28,22].

This theoretical approach also was used successfully by us to construct the theory of DNA compactization in a salt solution of polyethylene glycol and solutions of polyamines of different valences.

IV. COMPACTIZATION OF DNA

The theory of DNA compactization proposed in Refs. 34 and 35 is based on two main assumptions, the volume approximation and the condition of electroneutrality. The total volume of a system is divided into two parts, the volume occupied by the DNA coil and the external solution. The size of the macromolecule and the composition of the solvent within these two parts are determined by the usual equilibrium conditions: the equality of osmotic pressures and the equality of chemical potentials of the components. In addition it is proposed that these two parts are electrically neutral, i.e., the net charge of the DNA macromolecule is compensated by oppositely charged counterions moving freely but within the effective volume of the DNA macromolecule.

In the case of DNA collapse in a solution of neutral polymer incompatible with DNA molecules, two main effects have to be taken into account. The first effect is the osmotic pressure of the counterions on the DNA coil. The second effect is connected with the difference in polymer concentration inside and outside the DNA coil. It was found that the concentration of neutral polymer within the effective volume of DNA is always lower than that in external solution. This difference could be negligible in the case of good compatibility observed at low polymer concentration. In this case the polymer molecules practically freely penetrate inside the DNA coil, so that the water/polymer composition inside the DNA coil is the same as the composition in the external solution. The second regime is the regime of practically perfect segregation between the DNA chain and the polymer. The polymer segregates from the DNA coil and imposes additional osmotic pressure,

which induces the DNA contraction to the globular state. This regime is observed at high polymer concentration. The transition from the first regime to the second one occurs as a first-order phase transition with a discrete jump in DNA size. The critical polymer concentration and the sharpness of the collapse transition depend on the degree of polymerization of the neutral polymer and the ion concentration. The higher the degree of polymerization of neutral polymer, the lower is the polymer concentration at the collapse point and the larger is the amplitude of collapse. To describe the collapse transition in the multivalent cation solution, the ion-exchange reaction, the condensation of the multivalent cations, and the effect of replacement of condensed counterions by multivalent ions were taken into account.

The results of the calculations were compared with experimental data on the compactization of DNA in a solution of polyethylene glycol and in solutions of polyamine of different valences. A rather good correspondence between theoretical results and experimental data was found [34,35].

In addition, the fluorescence microscopy experiments confirm that the coil–globule transition of the DNA molecule in most cases is the first-order phase transition [34–36]. Fluorescence microscopy allows us to monitor the conformational state for single molecule. Thus it is possible to construct the distribution of the ensemble of DNA molecules over the size. It was found that the distribution of DNA macromolecules over the size in the vicinity of the coil–globule transition point has two maxima corresponding to the two coexisting states, the coil and the globule [36]. This fact directly indicates that the conformational coil–globule transition is the first-order phase transition [1–3,36].

Fluorescence microscopy allows us also to get the data for the dependence of the width of the transition region (i.e., the region of coexistence of the coil and globule states) on the collapsed agent. For the case of multivalent ions, our calculations predict that the width of the transition region is the narrowest one for the multivalent cations of highest valence. The experimental results obtained for the case of DNA collapse in the solutions of polyamine of different valences are in good correspondence with theoretical results.

V. POLYELECTROLYTE MOLECULE IN SOLUTIONS OF FINITE CONCENTRATION

Let us consider now the intermediate case—the conformational transition in polyelectrolyte macromolecules of finite size dissolved in a solution of finite concentration.

The theoretical calculations by Oosawa [20] and recent molecular dynamics simulations [37–39] show that in this case the counterions can either

leave the macromolecular coil or float within its effective volume (see Figure 4). In the solution of finite polymer concentration the counterion concentration both outside and inside of the macroion could be high enough to create appreciable osmotic pressure. In its turn, the macroion having some uncompensated charge attracts the oppositely charged counterions. The conformation of the polyelectrolyte molecule and the charge of the macroion that result from the interplay of these two effects is described in a recent theoretical paper [40]. Let us briefly discuss it.

The diluted polymer solution of concentration c is considered; let m be the degree of chain polymerization and f be its degree of ionization.

Two-phase approximation is applied. The total volume of the system is divided into two parts, the volume occupied by the macromolecular coil V_{in} and the exterior volume V_{ext}. The volume of the coil V_{in} is directly connected with its radius of gyration R: $V_{in} = (4\pi/3)R^3$. The exterior volume V_{ext} of the system under consideration is the difference between the total volume V_{tot}

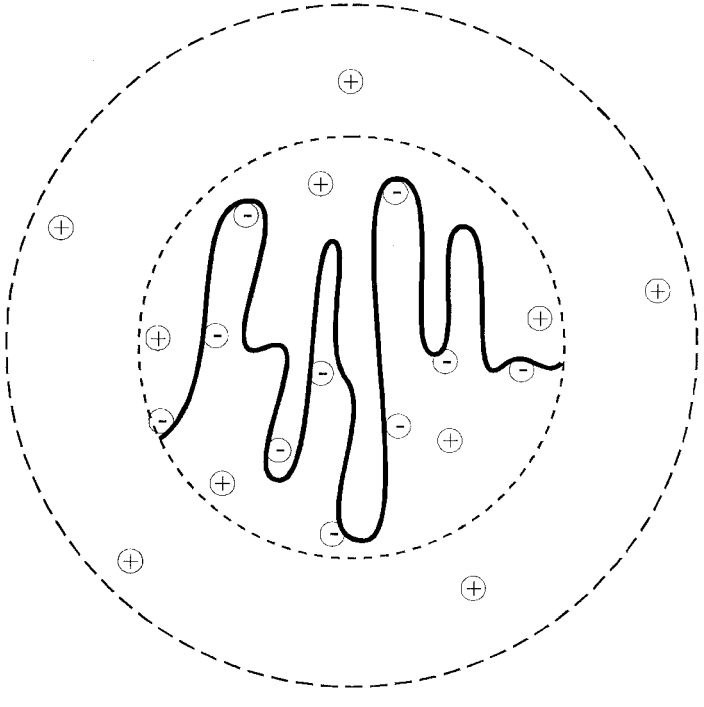

FIG. 4 Schematic presentation of macroion. Counterions inside the inner dashed sphere are those ''kept by the macroion''; others are ''escaped.'' External dashed sphere shows the external volume per one chain.

per macromolecule (which is a constant for the experimental conditions with fixed concentration c of polymer in solution: $V_{tot} = m/c$) and the volume of a coil V_{in}; $V_{ext} = V_{tot} - V_{in}$.

The counterions can be in two states, inside and outside the polymer coil (Figure 4). The fraction β of counterions leaving the volume of the macromolecule determines the charge of the macroion $Q = \beta mf$.

The free energy F of a polyelectrolyte chain is written as the sum of four contributions:

$$F = F_{el} + F_{int} + F_{tr\text{-}en} + F_{el\text{-}st} \tag{24}$$

where the elastic free energy F_{el} and the free energy of interaction F_{int} are given by Eqs. 14 and 15 (when the total number of monomer units N is taken to be equal to the degree of polymerization m of the macromolecule: $N = m$).

The contribution $F_{tr\text{-}en}$ to the free energy of the translational entropy of the counterions is represented as

$$\frac{F_{tr\text{-}en}}{kT} = (1 - \beta)mf \ln\left(\frac{(1 - \beta)mf}{V_{in}}\right) + \beta mf \ln\left(\frac{\beta mf}{(V_{tot} - V_{in})}\right) \tag{25}$$

For the electrostatic interaction $F_{el\text{-}st}$ contribution to the free energy the assumption of spherical symmetry of the macroion is used:

$$\frac{F_{el\text{-}st}}{kT} = (\beta mf)^2 u \left(\frac{1}{V_{in}^{1/3}} - \frac{1}{V_{tot}^{1/3}}\right) \tag{26}$$

The equilibrium values of the parameter β and of the macromolecule size R are determined by minimizing the free energy F over these variables. The obtained system of two equations is solved numerically.

The theory proposed gives estimations for the scaling dependence of the swelling ratio α on parameters of the system in the two limiting situations, $\beta = 0$ and $\beta = 1$ (see Secs. II and III).

For $\beta = 0$ (all counterions are kept within the effective volume of the macroion, and the macroion is as a whole electroneutral) one obtains

$$R \sim mf^{1/2}a \tag{27}$$

For the case of $\beta = 1$ (all counterions leave the macromolecule volume), we obtain

$$R \sim m(uf^2)^{1/3}a \tag{28}$$

In poor solvent, the size R of the macroion in both cases is defined by non-Coulomb interaction:

$$R \sim (m\tau)^{1/3} a \tag{29}$$

From a comparison of Eqs. 25 and 26 one could conclude that the osmotic pressure actually leads to a much higher swelling than electrostatic interaction. Since in poor solvent the value of the subchain size does not depend on the value of β, the amplitude of the collapse transition in the case of $\beta = 0$ is higher than in the case of $\beta = 1$. It was also shown that the transition point between the swollen and collapsed states of the chain and the character of this transition depends essentially on whether the counterions are inside the polymer coil or whether they have moved for the outer solution region. The coil–globule transition for $\beta = 0$ in most cases is the first-order phase transition. The sharpness of this transition decreases with an increase in β. In some cases the character of this transition for $\beta \neq 0$ becomes continuous in contrast to a jump-like first-order phase transition for $\beta = 0$ (Figure 5).

The real possibility of varying the parameter β under experimental conditions is to change the concentration c of polymer in solution. The lower is the polymer concentration c, the larger is the volume V_{ext} of solution per molecule; thus the higher is the gain in translational entropy for counterions leaving the interior of the macromolecular volume for the external solution. Thus with the decrease of polymer concentration c the fraction β of counterions leaving the interior of the macroion for the external solution increases. Therefore, according to the conclusion of the theory, the polyelectrolyte molecule has to contract upon dilution. It is this result that was obtained in Ref. 41 which reported the collapse transition of the polyelectrolyte molecules induced by dilution of the polymer solution.

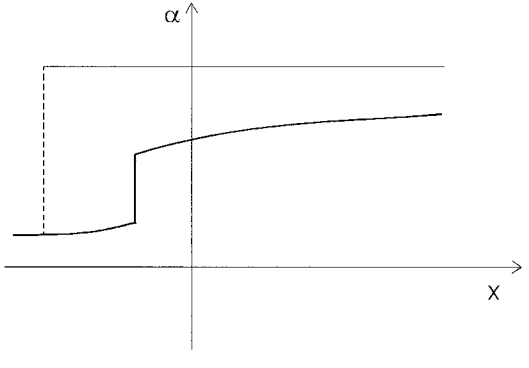

FIG. 5 Typical dependence of swelling ratio α of single macromolecule in a solution of finite concentration of solvent quality x. Dashed line shows the corresponding dependence for electroneutral macroion ($\beta = 0$).

VI. SINGLE POLYELECTROLYTE MOLECULE IN SOLUTION OF LOW-MOLECULAR SALT

The theory of Ref. 40 was developed via the case of the single molecule in solution of low-molecular salt with concentration n_s in Ref. 42.

The theory accounts for the fact that some fraction of counterions escapes from the interior of the macromolecular coil. The macromolecular coil on the whole possesses by the electrostatic charge and interacts via the screened electrostatic potential with low-molecular ions escaped from the interior of the macroion.

The free energy F is presented as a sum of four contributions:

$$F = F_{el} + F_{int} + F_{tr\text{-}en} + F_{el\text{-}st} \tag{30}$$

The terms F_{el} and F_{int} are the elastic deformation of the chain and of the non-Coulombic interaction of the monomer units' contributions to the free energy (Eqs. 14 and 15).

The contribution $F_{tr\text{-}en}$ to the free energy from the translational entropy of the counterions and ions of salt and from Coulombic interaction $F_{el\text{-}st}$ are presented as

$$\begin{aligned}\frac{F_{tr\text{-}en}}{kT} &= [(1 - \beta)mf + N_s^{in}]\ln\left(\frac{(1 - \beta)mf}{V_{in}} + n_s^{in}\right) \\ &\quad + (N_s^{out} + \beta mf)\ln\left(\frac{\beta mf}{V_{ext}} + n_s^{out}\right) + N_s^{in}\ln n_s^{in} + N_s^{out}\ln n_s^{out} \\ F_{el\text{-}st} &= kT(\beta mf)^2 u\left(\frac{1}{V_{in}^{1/3}}\exp\left(-\frac{V_{in}^{1/3}}{r_D}\right) - \frac{1}{V_{tot}^{1/3}}\exp\left(-\frac{V_{tot}^{1/3}}{r_D}\right)\right)\end{aligned} \tag{31}$$

where N_s^{in} and n_s^{in} are the total number and the concentration of salt ions within the effective volume of the macromolecules; N_s^{out} and n_s^{out} are those parameters in the external solution; and r_D is the Debye–Hückel radius

$$r_D \cong \sqrt{\frac{u}{(\beta mf/V_{ext} + n_s^{out})a}} \tag{32}$$

Equilibrium values of the macroion size, R, its effective charge, β, and salt concentration n_s^{in} in the interior and n_s^{out} in the exterior of the macromolecules are determined by the minimization of free energy F:

$$\frac{\partial F}{\partial R} = 0 \qquad \frac{\partial F}{\partial N_s^{in}} = 0 \qquad \frac{\partial F}{\partial \beta} = 0 \tag{33}$$

The obtained system of three equations was solved numerically.

The dependences of the macromolecular size (i.e., swelling ratio α), of the salt concentration n_s^{in} within the macromolecular coil, and of the parameter β on the salt concentration n_s were studied.

The results obtained are the following: In the absence of salt, the macromolecule has the swollen coil conformation due to the repulsive electrostatic interactions independently of the quality of the solvent.

With the increase of salt concentration n_s, the macromolecule contracts, and at high salt concentration n_s, it takes a conformation similar to the conformation of the corresponding electroneutral macromolecule (for which the fraction f of charged units is equal to zero: $f = 0$). In this region the value of the swelling coefficient α is markedly dependent on the solvent quality, i.e., the poorer the quality of the solvent, the smaller is the value of the swelling coefficient. When the second virial coefficient B is positive, the macromolecule stays in the conformation of the coil with excluded volume: $R \sim m^{3/5}$. The value of $B = 0$ corresponds to the condition of theta solvent; in this case the macromolecule has the conformation of an ideal coil: $R \sim m^{1/2}$. At negative values of the second virial coefficient B, the macromolecule is in the collapsed globular state, for which the following scaling relation is valid: $R \sim m^{1/3}$.

The transition from the electrostatically swollen state to the state of the electroneutral molecule is continuous in the case of a good solvent ($x > 0$); and it could be a step-wise first-order phase transition in the case of a poor solvent ($x < 0$).

Comparison of the results for a single molecule with results obtained under the assumption that all counterions are kept within the volume of a macromolecule (i.e., $\beta = 0$) allows us to reach the following conclusions:

For $\beta = 0$, the contraction of the macromolecule to a state close to the state of the electroneutral molecule takes place at higher salt concentration and the transition is less sharp. It is interesting to note that in some cases the transition of a macromolecule to the globular state is a first-order phase transition for $\beta \neq 0$ and a continuous transition for $\beta = 0$. Thus in the case of a single molecule immersed in salt solution the coil–globule transition is sharper than in the case of a polyelectrolyte gel, whereas in the case of the salt-free solution the collapse transition of a single macromolecule is vice versa expected to be less sharp than the transition of the polyelectrolyte gel.

In the case of $\beta \neq 0$ the macromolecule is less sensitive to the presence of salt in solution. It starts to contract at higher values of salt concentration n_s (see Figure 6).

It was also shown that as a rule, in the case of a polyelectrolyte gel ($\beta = 0$), the salt concentration n_s^{in} is lower than for the case $\beta \neq 0$. Thus a single molecule absorbs salt ions more effectively than the polyelectrolyte gel.

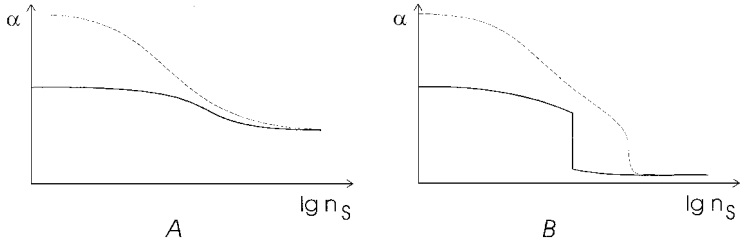

FIG. 6 Typical dependencies of the swelling ratio α of a single polyelectrolyte molecule on the salt concentration n_s for good (A) and poor (B) solvent. Dashed lines show the corresponding dependencies for electroneutral macroion ($\beta = 0$).

It also was found that in the case of $\beta \neq 0$ the dependence of the salt concentration n_s^{in} and the parameter β on n_s could have a complex nonmonotonic character. At low salt concentration, the values of β decrease with an increase of salt concentration n_s, i.e., some fraction of the counterions returns to the interior of the coil upon the increase of n_s. With further increase of salt concentration n_s the fraction β of counterions in the outer solution increases, since in this region of parameter values the gain in the entropy due to the release of counterions into the external solution is more important than the losses in the weak energy of screened electrostatic interaction and losses in the entropy of salt ions due to their redistribution.

VII. POLYELECTROLYTE MICROGEL

The transition from the swelling law of a single polyelectrolyte molecule to the swelling law of a polyelectrolyte gel is analyzed in Ref. 40. The swelling law of a microgel, i.e., a polymer gel having a finite number ν of polymer subchains with a degree of polymerization equal to m was considered.

It was taken into account that counterions could leave the interior of the microgel for the external solution and that both contributions of electrostatic interaction of a macroion with escaped counterions and of the osmotic pressure of counterions contribute to the swelling law of a microgel. The swelling behavior of a microgel was analyzed as a function of the number ν of polymer chains in the microgel.

The conclusions are as follows.

The dependence $\alpha(\nu)$ could demonstrate nonmonotonic behavior. In a good solvent the swelling ratio α (i.e., the ratio of current size R of the subchain to its size in the θ-solvent) increases with the growth of the number ν of subchains in the microgel (see Figure 7). The reason is that for small particles most of the counterions leave the microgel for the outer solution.

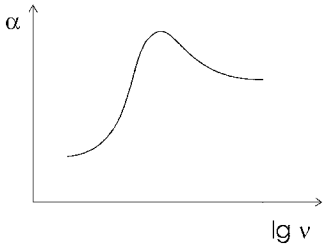

FIG. 7 Typical dependence of the swelling ratio α of a polyelectrolyte microgel on the number v of subchains in a sample.

The uncompensated electrostatic charge increases with the growth of ν, which leads to the increase of the swelling ratio α:

$$\alpha \sim m^{1/2}(uf^2)^{1/3}v^{2/9} \tag{34}$$

With further increase in the number ν of subchains in the microgel, more and more counterions became trapped within the gel. The electrostatic repulsion between the charged units decreases, and the gel starts to contract. At large values of ν, the parameter β is close to zero. The swelling ratio α became independent of ν and is defined as in the case of a macroscopic polyelectrolyte gel (see Eqs. 22, 23, and 27):

$$\alpha \sim (mf)^{1/2} \tag{33}$$

It was shown that the transition from the swelling law of a single molecule to the swelling law of a polyelectrolyte gel occurs at rather high values of the number ν of subchains in the microgel.

VIII. SUMMARY

We have discussed the theory of conformational transition in polyelectrolyte macromolecules. The main attention was paid to the comparison of theoretical approaches describing the conformational transition of polyelectrolyte molecules of different size. We considered two limiting situations. The first situation is the case of a single macromolecule at infinite dilution when the conformation of polyelectrolyte is determined by the repulsive interaction between charged monomer units, whereas the influence of counterions is negligible. The second limiting case is the case of a polyelectrolyte gel when the swelling is due to the osmotic pressure of counterions and electrostatic interaction is of secondary importance. The approach describing the intermediate situation when the conformation of the polyelectrolyte molecule

depends on both contributions, from osmotic pressure of counterions and from electrostatic interactions, was also discussed.

REFERENCES

1. Lifshitz IM. Some problems of the statistical theory of biopolymers. Zh. Eksp. Teor. Fiz. 1968; 55:2408–2422.
2. Lifshitz IM, Grosberg AYu, Khokhlov AR. Some problems of the statistical physics of polymer chains with volume interactions. Rev. Mod. Phys. 1978; 50:683–713.
3. Lifshitz IM, Grosberg AYu, Khokhlov AR. Volume interactions in the statistical physics of a polymer macromolecule. Usp. Fiz. Nauk (Soviet Physics—Uspekhi) 1979; 127:353–389.
4. Grosberg AYu, Khokhlov AR. Statistical Physics of Macromolecules. Moscow: Nauka Publishers, 1989. English translation: New York: AIP Press, 1994.
5. Lerman L. A transition to a compact form of DNA in polymer solution. Proc. Nat. Acad. Sci. USA 1971; 68:1886–1890.
6. Lerman L. Chromosomal analogues: long-range order in ψ-condensed DNA. Cold Spring Harbor Symp. Quant. Biol. 1973; 38:59–72.
7. Post CB, Zimm BH. Internal condensation of a single DNA molecule. Biopolymer 1979; 18:1487–1501.
8. Frisch HL, Fesciyan SJ. DNA phase transition: the ψ transition of single coils. J. Polym. Sci. Polym. Lett. Ed. 1979; 17:309–315.
9. Grosberg AYu, Eruchimovich IYa, Shakhnovich EI. On the theory of ψ-compactization. Biopolymer 1982; 21:2413–2432.
10. Bloomfield VA. DNA condensation. Curr. Opin. Struct. Biol. 1996; 6:334–341.
11. Tanaka T. Collapse of gels and a critical endpoint. Phys. Rev. Lett. 1978; 40: 820–823.
12. Tanaka T. Phase transition in gels and a single polymer. Polymer 1979; 20: 1404–1412.
13. K. Dusek, ed. Responsive Gels. Advances in Polymer Science 1993, v. 109, v. 110.
14. de Gennes PG, Pinkus P, Velasco RM, Brochard F. Remarks on polyelectrolyte conformation. J. Physique 1976; 37:1461–1473.
15. Pfeuty P, Velasco RM, de Gennes PG. J. Physique Lett. 1977; 38:5.
16. Barrat J-L, Joanny J-F. Theory of polyelectrolyte solutions. Adv. Chem. Phys. 1996; 94:1–66.
17. Khokhlov AR. On the collapse of weakly charged polyelectrolytes. J. Phys. A: Math. Gen. 1980; 13:979–987.
18. Dobrynin AV, Rubinshtein M, Obukhov SP. Cascade of transitions of polyelectrolytes in poor solvent. Macromolecules 1996; 29:2974–2979.
19. Micka U, Holm C, Kremer K. Strongly charged flexible polyelectrolytes in poor solvents: molecular dynamics simulations. Langmuir 1999; 15:4033–4044.
20. Oosawa F. Polyelectrolytes. New York: Marcel Dekker, 1971.

21. Manning GS. The molecular theory of polyelectrolyte solutions with applications to the electrostatic properties of polynucleotides. Q. Rev. Biophys. 1978; 11:179–244.
22. Kramarenko EYu, Khokhlov AR. Weakly charged polyelectrolytes: collapse induced by extra ionization. Macromolecules 1996; 29:681–685.
23. Brilliantov NV, Kuznetsov DV, Klein R. Chain collapse and counterion condensation in dilute polyelectrolyte solution. Phys. Rev. Lett. 1998; 81:1433–1436.
24. Winkler RG, Gold M, Reineker P. Collapse of polyelectrolyte macromolecules by counterion condensation and ion pair formation: a molecular dynamics simulation study. Phys. Rev. Lett. 1998; 80:3731–3734.
25. Schiessel H, Pinkus P. Counterion-condensation-induced collapse of highly charged polyelectrolytes. Macromolecules 1998; 31:7953–7959.
26. Schiessel H. Counterion condensation on flexible polyelectrolytes: dependence on ionic strength and chain conformation. Macromolecules 1999; 32:5673–5680.
27. Vasilevskaya VV, Khokhlov AR. On the theory of charged polymer networks. In: IM Lifshitz, AM Molchanov, eds. Mathematical Methods for Polymer Studies. Puschino, 1982:45–52.
28. Khokhlov AR, Starodubtzev SG, Vasilevskaya VV. Conformational transitions in polymer gels: theory and experiments. Adv. Polym. Sci. 1993; 109:123–171.
29. Flory PJ. Principles of Polymer Chemistry. Ithaca NY: Cornell University Press, 1953.
30. Birshtein TM, Pryamitsin VA. Vysokomolekul. Soed. 1987; 29A:1858–1864.
31. Khokhlov AR. Swelling and collapse of polymer networks. Polymer 1980; 21: 376–380.
32. Vasilevskaya VV, Khokhlov AR. Swelling and collapse of polymer gel in polymer solutions and melts. Macromolecules 1992; 25:384–390.
33. Khokhlov AR, Kramarenko EYu. Collapse of a polymer gel induced by complex formation with linear polymers. Makromol. Chem. Theory Simul. 1993; 2:169–177.
34. Vasilevskaya VV, Khokhlov AR, Matsuzawa Y, Yoshikawa K. Collapse of single DNA molecule in poly(ethylene glycol) solutions. J. Chem. Phys. 1995; 102:6595–6602.
35. Takahashi M, Yoshikawa K, Vasilevskaya VV, Khokhlov AR. Discrete coil–globule transition of single duplex DNAs induced by polyamines. J. Phys. Chem. 1997; 101:9396–9401.
36. Yoshikawa K, Takahashi M, Vasilevskaya VV, Khokhlov AR. Large discrete transition in a single DNA molecule appears continuous in the ensemble. Phys. Rev. Lett. 1996; 76:3029–3031.
37. Stevens M, Kremer K. Structure of salt-free linear polyelectrolytes. Phys. Rev. Lett. 1993; 71:2228–2231.
38. Stevens M, Kremer K. Form factor of free-salt linear polyelectrolyte. Macromolecules 1993; 26:4717–4719.

39. Stevens M, Kremer K. The nature of flexible linear polyelectrolyte in salt free solution: a molecular dynamics study. J. Chem. Phys. 1995; 103:1669–1690.
40. Kramarenko EYu, Khokhlov AR, Yoshikawa K. Collapse of polyelectrolyte macromolecules revisited. Macromolecules 1997; 30:3383–3388.
41. Aseyev VO, Tenhu H, Klenin SI. Contraction of a polyelectrolyte upon dilution. Light scattering studies on a polycation in saltless water-acetone mixtures. Macromolecules 1999; 32:1838–1846.
42. Vasilevskaya VV, Khokhlov AR, Yoshikawa K. Single polyelectrolyte macromolecule in the salt solution: effect of escaped counterions. Macromolecular Theory and Simulations 1999, submitted for publication.

This Page Intentionally Left Blank

7

Conductance of Polyelectrolyte Solutions, Anisotropy, and Other Anomalies

HANS VINK University of Uppsala, Uppsala, Sweden

I. GENERAL REMARKS

In electrolyte solutions in general electric conductance is an important measurable property, characterizing the ionic structure and ionic interactions in solution. Thus conductivity measurements were crucial in the establishment of the Arrhenius dissociation theory. Further developments of the theory led to the Debye–Hückel theory of electrolytes and the Onsager–Fuoss [1,2] theory of electrolytic conductivity. This theory has been very successful for simple electrolytes in dilute solutions, where quantitative agreement with experiments is achieved. However, at higher concentrations and with unsymmetrical electrolytes containing multivalent ions, agreement with experiment is less satisfactory, because in these solutions the limiting law approximations of the original theory become overextended and begin to fail. This is even more the case with solutions containing polyelectrolytes and charged colloids. In these highly unsymmetrical electrolytes, the models of interionic interactions are still incomplete and under debate. Therefore a quantitative conductivity theory for polyelectrolytes on the molecular level is beyond our reach at present. Alternatively, a phenomenological approach may be used, to provide a framework for the interpretation of experimental data.

For pure polyelectrolyte solutions it has been customary to express the equivalent conductivity by the heuristically derived equation [3–5]

$$\Lambda = f(\lambda_i^0 + \lambda_p) \tag{1}$$

where f is an interaction parameter, λ_i^0 the counterion limiting equivalent conductivity and λ_p the polyion equivalent conductivity.

To assess the significance of the different parameters in Eq. 1 we derive it from basic principles, independent of any particular molecular model.

Such a frame is provided by nonequilibrium thermodynamics. Using the frictional formalism [6] we may express the basic phenomenological equations for an n-component system in the form

$$\sum_{j=1}^{n} f_{ij} c_j (u_i - u_j) = X_i \tag{2}$$

where f_{ij} are the molar friction coefficients between components i and j, c_j the molar concentration, u_i and u_j the component average velocities in an arbitrary reference frame, and X_i the generalized force:

$$X_i = -\text{grad } \mu_i^c - V_i \text{ grad } p + z_i FE \tag{3}$$

where μ_i^c is the chemical part of the chemical potential, V_i the partial molar volume, p the pressure, z_i the charge number, F the Faraday constant, and E the electric field.

In addition we have the Onsager reciprocal relations

$$f_{ij} = f_{ji} \qquad i, j = 1, \ldots, n \tag{4}$$

and the electroneutrality condition

$$\sum_{i=1}^{n} c_i z_i = 0 \tag{5}$$

Applying these equations to a pure polyelectrolyte solution, we have two independent frictional equations,

$$f_{iw} c_w u_i + f_{ip} c_p (u_i - u_p) = z_i FE \tag{6}$$

$$f_{pw} c_w u_p + f_{pi} c_i (u_p - u_i) = z_p FE \tag{7}$$

where the indexes i, p, and w denote the counterion, polyion, and water, respectively, and where a solvent fixed reference frame ($u_w = 0$) is used.

The electroneutrality condition is

$$c_i z_i + c_p z_p = 0 \tag{8}$$

Since the ionic velocities are proportional to the electric field, we may write

$$u_i - u_p = \beta' FE \tag{9}$$

where β' is the proportionality constant. Then

$$f_{ip} c_p (u_i - u_p) = \beta z_i FE \tag{10}$$

where

$$\beta = \frac{f_{ip} c_p \beta'}{z_i} = -\frac{f_{ip} c_i \beta'}{z_p} \tag{11}$$

is a parameter characterizing interionic friction. Note that β is a positive

quantity, since u_i and u_p have opposite signs and u_i has the same sign as z_iE. From the symmetry relation Eq. 4 and Eqs. 9 and 11 we obtain

$$f_{pi}c_i(u_p - u_i) = -f_{ip}c_i\beta' FE = \beta z_p FE \tag{12}$$

Thus Eqs. 6 and 7 take the form

$$f_{iw}c_w u_i = (1 - \beta)z_i FE \tag{13}$$

$$f_{pw}c_w u_p = (1 - \beta)z_p FE \tag{14}$$

Introducing the hydrodynamic friction coefficients $f_i = f_{iw}c_w$; $f_p = f_{pw}c_w$, we may express the ionic velocities in the form

$$u_i = (1 - \beta)\frac{z_i FE}{f_i} \tag{15}$$

$$u_p = (1 - \beta)\frac{z_p FE}{f_p} \tag{16}$$

In these equations the interionic and ion–solvent frictional effects have been separated. The former effect affects both kinds of ions equally and represents the electrophoretic and relaxation effects of the Onsager–Fuoss theory. The ion–solvent friction is unperturbed by these interactions and thus represents the ''free ion'' friction against a solvent at rest.

The electrolytic conductivity κ is obtained from the expression for current density (charge flux)

$$\Im = \kappa E = \sum_j F z_j c_j u_j \tag{17}$$

Substituting for u_j from Eqs. 15 and 16 we obtain

$$\kappa = (1 - \beta)\left[\frac{F^2 z_i^2 c_i}{f_i} + \frac{F^2 z_p^2 c_p}{f_p}\right] \tag{18}$$

Introducing the monomolecular concentration (equivalent concentration) of the polyelectrolyte

$$C = |Z_p| c_p \tag{19}$$

where Z_p is the stoichiometric charge number of the polyion, and taking into account possible association effects between the ions, we have

$$z_p = \alpha Z_p \tag{20}$$

$$c_i|z_i| = \alpha C \tag{21}$$

where α is the fraction of counterions that exist in solution as separate ions. The remaining fraction $(1 - \alpha)$ of the counterions is thus associated with

the polyions and move together with the polyions. These counterions may be covalently bound (as hydrogen ions in weak polyacids), form ion pairs with polyion pendant ionic groups, or are electrostatically trapped (condensed). To cover all these cases we call α the *apparent* degree of dissociation.

With these equations we may define the ionic and solution equivalent conductivities λ_i, λ_p, and Λ.

$$\Lambda = \frac{\kappa}{C} = (1 - \beta)\alpha[\lambda_i + \lambda_p] \tag{22}$$

where

$$\lambda_i = \frac{F^2|z_i|}{f_i} \approx \lambda_i^0 \tag{23}$$

$$\lambda_p = \frac{\alpha F^2|Z_p|}{f_p} \tag{24}$$

Note that the ionic equivalent conductivities λ_i and λ_p represent ''free ion'' conductivities, unperturbed by interionic interactions. The counterion conductivity λ_i may therefore in dilute solutions be approximated by its limiting constant value λ_i^0, since it only depends on the hydrodynamic solvent friction coefficient f_i, which for small ions is fairly constant in dilute solutions.

For the polyion equivalent conductivity, conditions are different. Here an appreciable concentration dependence is expected even in very dilute solutions. This is partly due to the direct dependence of λ_p on α, a quantity that may vary with concentration, and partly due to the concentration dependence of the friction coefficient f_p. As in the case of polymeric solutes in general, the friction coefficient depends on the polyion chain conformation, which for flexible polyelectrolytes is strongly concentration dependent. Furthermore, the polyion friction coefficient also includes contributions from the fraction $(1 - \alpha)$ of the counterions, which form a kinetic unit with the polyion. The friction coefficient can therefore be written in the form

$$f_p = f_p' + \gamma(1 - \alpha)\left|\frac{Z_p}{z_i}\right| f_i \tag{25}$$

where f_p' is the friction coefficient of the polyion chain and γ is a hydrodynamic shielding factor. For a free-draining counterion atmosphere $\gamma = 1$, whereas $\gamma \ll 1$ for counterions closely attached to the polyion backbone.

Expressing f_i in terms of λ_i^0 according to Eq. 23 and substituting into Eq. 24 we obtain

$$\lambda_p = \frac{\alpha F^2 |Z_p|}{f'_p + \gamma(1 - \alpha)\dfrac{F^2|Z_p|}{\lambda_i^0}} \tag{26}$$

An important feature of this equation is that it indicates that the polyion equivalent conductivity depends on the nature of the counterion. It is interesting to note that a similar dependence was predicted by Manning [7], based on quite different theoretical considerations. However, the pronounced increase of polyion conductivity in dilute solutions inherent in Manning's formula is not endorsed by the present treatment.

Finally we find that the interaction parameter f in Eq. 1 takes the form

$$f = (1 - \beta)\alpha \tag{27}$$

It is of interest to consider the interionic friction factor $(1 - \beta)$ in relation to the ionic association effect, characterized by the parameter α. The two effects are to some extent related, as it is possible to include the bound ions in the frictional model by assigning them very large (infinite) interionic friction coefficients. This would preclude any movement of these counterions relative to the polyion, and they would appear as being bound to the polyion. However, the friction coefficients f_{ip}, f_{pi} in Eqs. 6 and 7 represent average friction coefficients. Obviously it is not possible to include the bound ions in the average (inclusion of a finite fraction of ions with infinite friction coefficients would make the average infinite). Therefore the bound ions have to be treated as a separate class. This is in accord with the interpretation of the parameter β as the fraction of the total energy dissipation due to interionic friction [8], since the bound ions make no contribution to the interionic friction effect. From these considerations it follows that no sharp boundary exists between the two classes, bound and free counterions, which makes difficult a clear-cut separation of the factors $(1 - \beta)$ and α in the interaction parameter f. It is instructive to compare the conductivity behavior of polyelectrolytes embodied in Eq. 1 with the corresponding equation for simple salt solutions. According to the Kohlrausch rule and the Onsager–Fuoss theory, the equivalent conductivity for a dilute salt solution containing the ionic species i and j takes the form

$$\Lambda = \lambda_i^0 + \lambda_j^0 - A\sqrt{C} = \Lambda^0 - A\sqrt{C} \tag{28}$$

where Λ^0 is the limiting equivalent conductivity of the salt and A is a constant. Rewriting Eq. 28 we obtain in analogy with Eqs. 1 and 27, since α is unity for a strong electrolyte,

$$\Lambda = \left(1 - \frac{A\sqrt{C}}{\Lambda^0}\right)\Lambda^0 = (1 - \beta)\Lambda^0 \tag{29}$$

The primary task in the study of simple salt solutions is to determine the

limiting equivalent conductivity Λ^0 by extrapolation. This is in general possible, since the two ionic equivalent conductivities λ_i and λ_j have well defined limiting values. The interaction factor $(1 - \beta)$ is then directly obtained as the quotient Λ/Λ^0.

II. LIMITING EQUIVALENT CONDUCTIVITY OF POLYELECTROLYTES

It is of interest also to consider the possibility of determining the limiting equivalent conductivity of polyelectrolytes. This is in no way a straightforward matter, and apart from experimental difficulties one has to contend with difficulties on the conceptual level. These arise because polyelectrolytes in solution exhibit ion-exchange properties. Thus in a dilute aqueous solution of an anionic polyelectrolyte the counterions bound in the ionic atmosphere tend to be replaced by hydrogen ions originating from the self-ionization of water. In the limit of infinite dilution the ionic atmosphere would consist entirely of hydrogen ions, and thus the original polyion–counterion complex no longer exists at limiting concentrations. Thus, the limiting equivalent conductivity of a polyelectrolyte eludes a stringent definition. However, in the lowest range of concentrations, where meaningful conductivity measurements can be carried out, the ionic atmosphere is still essentially intact and the data may be extrapolated to yield a formal value of the limiting equivalent conductivity. The extrapolation is conventionally carried out using the equation

$$\Lambda = \frac{\kappa - \kappa_0}{C} = \Lambda_0 + \phi(C) \tag{30}$$

where the function $\phi(C)$ represents interionic interactions and κ_0 is the solvent correction, determined as the conductivity of pure solvent. When applying Eq. 30 to polyelectrolyte solutions we have to consider the possibility that the ion exchange effect changes the solvent conductivity. Especially with polyelectrolytes containing weakly acidic (carboxylic) groups the effect may become appreciable. Then κ_0 no longer represents the proper solvent correction and extrapolation according to Eq. 30 will lead to error [9].

The difficulty can be circumvented by rearranging Eq. 30 in the form

$$\kappa = \kappa_0' + \Lambda^0 C + C\phi(C) \tag{31}$$

and determining Λ^0 from the slope of the linear part of the plot of κ against C. Then κ_0' becomes an adjustable parameter determined by the intercept of the κ-axis. When a least-square fit of the data is employed, higher order terms from the function $C\phi(C)$ may be included in the analysis.

Thus although it is possible formally to determine the limiting equivalent conductivity Λ^0 of polyelectrolyte solutions, this quantity lacks the significance of the corresponding quantity in simple electrolyte solutions. Since we have according to Eqs. 1 and 27

$$\Lambda^0 = f^0(\lambda_i^0 + \lambda_p^0) = (1 - \beta^0)\alpha^0(\lambda_i^0 + \lambda_p^0) \tag{32}$$

it is not possible to determine λ_p^0 from Λ^0, because f^0 has a value different from unity. However, the quantity Λ^0 may still be useful as a marker to delimit the steep, seemingly unbounded increase, in some instances decrease, of the conductivity curves in very dilute solutions.

III. TRANSPORT NUMBERS IN POLYELECTROLYTE SOLUTIONS

For a complete determination of electric transport parameters in electrolyte solutions it is necessary to combine data from electric conductivity and transference measurements. Of the two principal methods of transference measurements, the moving boundary method and the Hittorf method, only the latter has been used with polyelectrolyte solutions. The moving boundary method has been found inapplicable, because suitable indicator solutions have not been found. The Hittorf method is directly applicable to polyelectrolytes, although there may be experimental problems, as it is often difficult accurately to determine the current-induced concentration changes in the electrode compartments. Recently a modified Hittorf method, specially adopted to polyelectrolyte solutions, has been developed [10]. The main difference is that the current-induced concentration change is measured in a compartment to which current is supplied through an ion exchange membrane. As current in the membrane is carried by counterions only, the solution in the measuring compartment remains free from foreign ions, and thus the concentration change can be monitored accurately, e.g., by conductivity measurements. In Figure 1 a schematic representation of the transference cell is shown.

The electric transport number of an ionic species is defined as the fraction of the total charge transferred, which is transported by the ionic species. Thus the polyion electric transport number t_p is

$$t_p = \frac{Q_p}{Q} = \frac{\lambda_p}{\lambda_i^0 + \lambda_p} \tag{33}$$

where Q_p is the charge transported by the polyion and Q the total charge, and where the second equality is obtained by using Eq. 1.

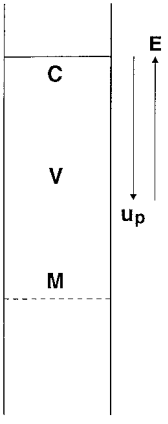

FIG. 1 Schematic illustration of the transference cell. M, ion-exchange membrane; V, volume of measuring compartment; C, polyelectrolyte concentration; E, electric field; u_p, velocity of polyion.

To determine Q_p we consider an experiment with the cell in Figure 1 containing an anionic polyelectrolyte. During the experiment the polyelectrolyte is transported into the measuring compartment and accumulates close to the membrane, the concentration C in the upper part of the compartment remaining constant. Determining the concentration, after homogenization, in the volume V, the concentration change ΔC is obtained. Thus the charge transported by the polyions is

$$Q_p = FV\Delta C\alpha \tag{34}$$

Substituting into Eq. 33 and rearranging we may write

$$T_p = \frac{t_p}{\alpha} = \frac{FV\Delta C}{Q} \tag{35}$$

The quantity T_p, called the ionic constituent transport number, is experimentally determinable. Using Eqs. 1, 33, and 35 we can further derive the equations

$$\lambda_p = \frac{\Lambda T_p}{1 - \beta} \tag{36}$$

$$\alpha = \frac{\Lambda}{(1 - \beta)\lambda_i^0 + \Lambda T_p} \tag{37}$$

Inspection of these equations leads to the disappointing conclusion that in polyelectrolyte solutions a complete determination of transport parameters

from conductance and transference data is not possible, since the equations contain the unknown factor $(1 - \beta)$.

However, we may still draw useful information from these equations. Because β is always positive, we can establish the lower limits of α and λ_p by putting $(1 - \beta)$ equal to unity. Tentative information on the factor $(1 - \beta)$ can also be obtained from measurements carried out with different counterions. Rearranging Eq. 37 we obtain

$$T_p = \frac{1}{\alpha} - (1 - \beta)\frac{\lambda_i^0}{\Lambda} \tag{38}$$

If both α and $(1 - \beta)$ are independent of the counterion species we obtain $(1 - \beta)$ as the slope of a plot of T_p vs. λ_i^0/Λ. The conditions for the application of Eq. 38 are most likely fulfilled for alkali metal counterions and polyions of low charge density, for which counterion binding is low and α is close to unity. In this connection it is of interest to consider the so called Eisenberg plot [4], which has been widely used to evaluate the parameters in Eq. 1 from conductivity measurements alone. Plotting according to Eq. 1 Λ vs. λ_i^0 for different alkali metal counterions, usually a linear relation is obtained, which yields f as the slope and $f\lambda_p$ as the intercept. However, in order to be valid this procedure requires the invariance of the parameters f and λ_p with respect to λ_i^0. As both theory and experiments indicate that for polyelectrolytes of high charge density λ_p depends on λ_i^0, this procedure should be considered as unreliable for such polyelectrolytes. For polyelectrolytes of low charge density conditions are more favorable, since the counterion dependence of λ_p decreases when counterion binding decreases. For these polyelectrolytes the Eisenberg plots and plots according to Eq. 38 are supplementary and thus make possible a check of the theory behind Eq. 1. Although relevant experimental data are scarce, measurements with low-charge-density cellulosic polyelectrolytes have been reported [10,11]. In Figures 2 and 3 these data are reproduced, and the determined parameter values are listed in Table 1.

In Figure 2 it is noteworthy that for the low-charge-density samples, points from measurements with different counterions, carried out at different concentrations, lie on a common straight line. This indicates that for these polyelectrolytes the parameters α and β in Eq. 38 are constant and that the concentration dependence of Λ is essentially due to variations in the polyion chain friction coefficient. This is no longer the case for the higher charge density samples CMC2 and PSS, where measurements with different counterions have to be referred to the same concentration. This is of course always the case with the Eisenberg plot. Comparing the data in Table 1, we find that the determined parameter values of the low-charge-density samples are in good agreement. This is in support of the theory and also indicates

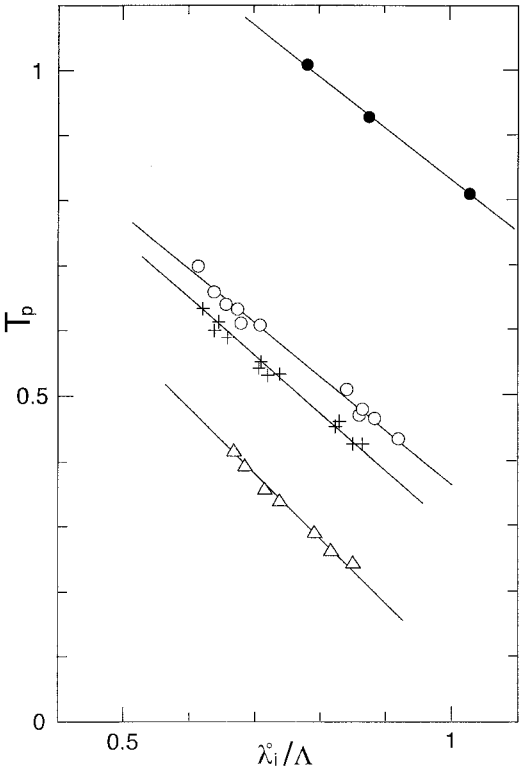

FIG. 2 Plots according to Eq. 38 for low-charge-density polyelectrolytes in Table 1. △, CM-HEC1; +, CM-HEC2; ○, CMC1; ●, CMC2. For CMC2, C = 2 monomol m^{-3}.

that the transference data are reliable. However, for the higher charge density samples the data become increasingly divergent. Even though the Eisenberg plots are perfectly linear, the determined values of the parameters f and λ_p are completely different from those obtained from the transference data. A simple explanation of this discrepancy may be found in that the Eisenberg plot remains linear when λ_p depends linearly on λ_i^0. Although there is no support for such a dependence in Eq. 26, it is always possible, provided the dependence is slight, to use the linear part of the Taylor expansion of λ_p and linearize the function over a narrow interval of λ_i^0 values. Thus putting

$$\lambda_p = \lambda_p' + k\lambda_i^0 \tag{39}$$

where k is a positive constant, and inserting into Eq. 1, we obtain

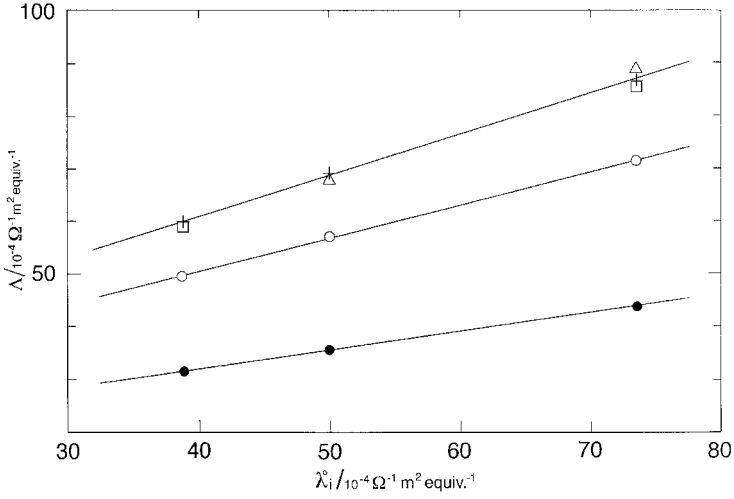

FIG. 3 Eisenberg plots for polyelectrolytes in Table 1. ●, PSS; ○, CMC2; □, CMC1; +, CM-HEC2; △, CM-HEC1. For all polyelectrolytes, $C = 2$ monomol m^{-3}.

$$\Lambda = f\lambda_p' + f(1 + k)\lambda_i^0 \tag{40}$$

This represents a modified form of the Eisenberg plot. The experimentally determinable interaction parameter f^E and polyion equivalent conductivity λ_p^E now become

$$f^E = f(1 + k) \tag{41}$$

$$\lambda_p^E = \frac{\Lambda}{f^E} - \lambda_i^0 = \frac{\lambda_p'}{(1 + k)} \tag{42}$$

Using Eq. 39 we further obtain

$$\lambda_p = (1 + k)\lambda_p^E + k\lambda_i^0 \tag{43}$$

With these equations the gap between the data from the Eisenberg plot and the transference data can be reduced. With a k value of 0.2 satisfactory agreement between the parameters f and λ_p for the high-charge-density polyelectrolytes in Table 1 is achieved.

IV. FLOW-INDUCED CONDUCTANCE ANISOTROPY IN POLYELECTROLYTE SOLUTIONS

For a complete characterization of conductance in polyelectrolyte solutions it is necessary to consider some odd features in their conductivity behavior.

TABLE 1 Conductance Data According to Refs. 10 and 11

Polyelectrolyte sample	Transference data							Eisenberg plot data			
								Uncorrected		Corrected, $k = 0.2$	
	DP	DS	ξ	$1 - \beta$	α	$f = (1 - \beta)\alpha$	λ_p(Na)	f^E	λ_p^E	f	λ_p(Na)
CM-HEC1	1900	0.323	0.45	0.93	0.97	0.90	25	0.87	26	—	—
CM-HEC2	1900	0.60	0.83	0.83	0.88	0.73	45	0.76	41	—	—
CMC1	750	0.60	0.83	0.82	0.85	0.70	49	0.73	44	—	—
CMC2	750	1.07	1.48	0.81	0.61	0.49	61	0.62	41	0.52	58
PSS	2900	1	2.85	0.80[a]	0.37	0.29	70	0.36	48	0.30	68

CM-HEC = carboxymethyl-hydroxyethyl cellulose; DP = degree of polymerization; DS = degree of substitution; ξ = charge density parameter; $\lambda_p/10^{-4}$ $m^2\Omega^{-1}$ monomol^{-1}, at C = 2 monomol m^{-3}.
[a]Chosen value for $(1 - \beta)$.

To these belong the conductance anisotropy effect encountered in sheared or electrically polarized solutions. The existence of the effect was established almost simultaneously in a number of independent studies by various authors in the early days of polyelectrolyte research [12–19]. These early investigations were in general carried out with Couette-flow apparatus, which allowed the performance of conductivity measurements in sheared solutions both parallel and perpendicular to the flow direction. These investigations showed that conductivity increased in the direction of flow and decreased in the direction perpendicular to the flow. In the theoretical interpretation the effect was attributed to changes in polyion equivalent conductivity caused by the stretching and orientation of polyions in the hydrodynamic field of flow. Although studies of the effect seem to offer useful information about the conductivity behavior of polyelectrolyte solutions, it did not attract much attention at the time. In particular, the rather narrow experimental background in the early investigations, which were mainly carried out with polyphosphate polyelectrolytes, was not extended to other polyelectrolyte systems, and the role of counterions was not taken into consideration. Only recently renewed investigations of the effect have been reported [20]. These investigations were carried out with a simplified method, in which the resistance of a solution in a capillary tube under various flow conditions was measured. The experiments were carried out with PSS polyelectrolytes in the form of the acid and the sodium salt. The investigation in general confirmed the findings of the earlier measurements, but it also demonstrated that the relative shear-induced change of conductivity is independent of the counterion; see Figures 4 and 5. This cannot be explained by changes in polyion conductivity alone, since, due to the large difference in equivalent conductivity between the counterions employed (H^+ and Na^+), such changes would affect the conductances of the two solutions differently. Thus the effect has to include changes in the mobility of the counterions in the sheared solutions. As the polyions tend to become stretched and orient parallel to the flow direction, this implies that the bound counterions retain a high degree of mobility parallel to the polyion chain. This interpretation is consistent with the Poisson–Boltzmann cylindrical cell model treatment of counterion binding [21,22]. According to this model, the oppositely charged small ions form a counterion atmosphere close to the polyion chain. The counterions retain a high degree of translational mobility along the equipotential surfaces enclosing the cylindrical polyion, although their movement in the radial direction is restrained. The same reasoning applies to the Manning–Oosawa two-state condensation model [23,24], in which a part of the counterions is assumed to condense on the polyion to reduce the charge density parameter ξ to its critical value, unity, for univalent counterions.

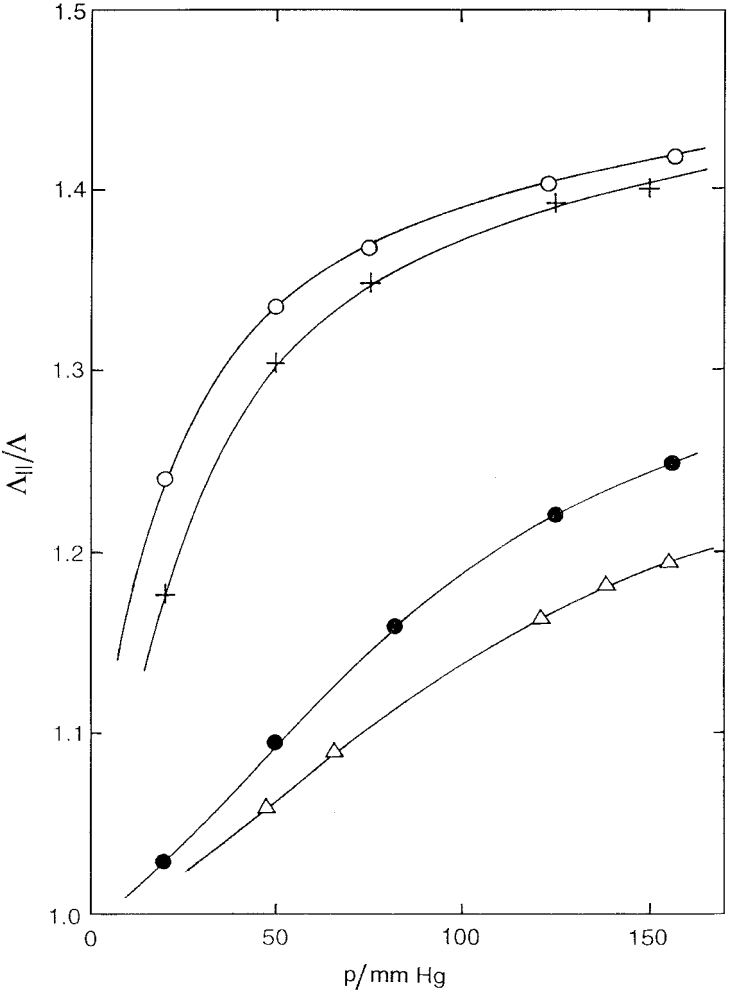

FIG. 4 Relative change of electrolytic conductivity as function of driving pressure in capillary flow for HPSS (DP = 8300). ○, $C = 1.057$; +, $C = 1.358$; ●, $C = 3.677$; △, $C = 4.610$. C in monomol m^{-3}. $\Lambda_{\|}$, conductivity in sheared solutions. (Reproduced from Ref. 20.)

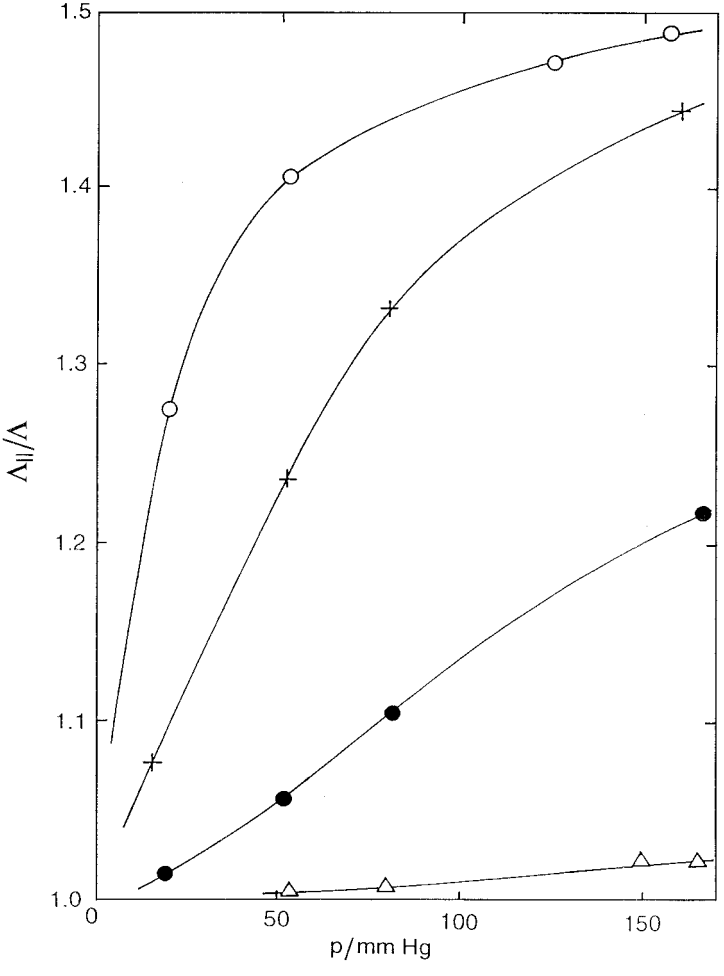

FIG. 5 Relative change of electrolytic conductivity as function of driving pressure in capillary flow for NaPSS (DP = 8300). ○, $C = 1.176$; +, $C = 2.454$; ●, $C = 5.648$; Λ, $C = 22.91$. C in monomol m^{-3}. $\Lambda_{\|}$, conductivity in sheared solutions. (Reproduced from Ref. 20.)

Also in this case the condensed counterions have to retain full translational mobility in the direction of the polyion chain.

Irrespective of these models for ion binding, the two-state approach is inherent in the dynamic frictional treatment of conductivity in polyelectrolyte solutions, since strongly interacting counterions have to be classified as

bound ions on account of statistical considerations. In this connection the anisotropy effect has important consequences, as it makes the parameter α dependent on the method by which it is measured. Thus the finding that α values determined from equilibrium measurements in general are lower than those obtained from transport measurements can be explained by the anisotropy effect [5], since in the latter case the high mobility of counterions along polyion chains makes a positive contribution to α even when the polyions are oriented at random. On the other hand, equilibrium properties of polyelectrolytes are not affected by this effect.

V. ANOMALIES IN THE CONCENTRATION DEPENDENCE OF POLYELECTROLYTE CONDUCTANCE

For low-molecular strong electrolytes the concentration dependence of equivalent conductivity is simple and universal. From a well-defined limiting value the equivalent conductivity decreases monotonically with increasing concentration, although the conductivity curves normally exhibit a distinct curvature, as the decrease levels off at high concentrations. The decrease of equivalent conductivity in these solutions is a result of increased interionic friction, which increases as the interionic distances decrease with increasing concentration.

For low-molecular weak electrolytes the concentration dependence of conductance is more complex, as in addition to the interionic friction effect it is strongly influenced by the association–dissociation reactions taking place in the solutions. However, as these in general follow the mass action law and thus, in simpler cases, the van't Hoff dilution law, their conductivity behavior is predictable. As a rule their equivalent conductivity steeply increases on dilution due to the increased dissociation of the electrolyte.

The conductivity behavior of polyelectrolytes does not correspond to either of these low-molecular electrolytes. A considerable amount of experimental work has been carried out with various polyelectrolyte systems. The results of these investigations exhibit a wide diversity of conductivity behavior. Even measurements with the same kind of polyelectrolyte, carried out by different investigators, may differ considerably with regard to the value of equivalent conductivity, as well as to its concentration dependence. The factors that may affect the results are the purity of samples, the molar mass of the polyelectrolyte, and its molecular mass distribution. Polyelectrolytes that have been extensively studied and for which these factors can reasonably be controlled are polystyrene sulphonates (PSS). The acid (HPSS) can easily be prepared from narrow molecular mass polystyrene by sulphonation with concentrated sulphuric acid [25]. As it is a strong acid, it

can be fully neutralized to the desired counterion form, without hydrolysis problems. It seems appropriate to use PSS as model polyelectrolytes to discuss some general features of the conductivity behavior of polyelectrolytes.

Starting in the high concentration region and following the conductivity curve in the direction of decreasing concentration, the equivalent conductivities of the alkali metal salts of PSS are constant or decrease slightly. This is followed by an increase in the dilute solution region, which is moderate for high molar mass samples but becomes increasingly more pronounced as the molar mass decreases. In very dilute solutions the curves may pass through a maximum [26,27], although measurements in this region are impaired with considerable experimental uncertainty. Thus the molar mass of a polyelectrolyte is an important factor affecting its conductivity behavior. However, so far only a few investigations have been concerned with this effect [26–30]. These clearly indicate that in dilute solutions the equivalent conductivity is considerably higher for low molar mass samples than for samples of high molar mass. At high concentrations the differences seem to vanish, and conductivity curves corresponding to different molar masses may intersect; see Figure 6. Also, the conductivity behavior of a polyelectrolyte may depend on the molecular mass distribution of the sample, and the use of polydisperse samples may result in unduly high equivalent conductivities. This has to be taken into consideration in the evaluation of conductivity data from naturally occurring polyelectrolytes, or synthetic polyelectrolytes, for which narrow molecular mass samples are not available.

Analyzing the concentration dependence of equivalent conductivity in relation to Eq. 1, we find that the main reason for the conductivity increase in dilute solutions is an increase of the interaction parameter f. Of the two factors determining f, the interionic friction factor $(1 - \beta)$ is of minor importance, since it is essentially independent of the polyelectrolyte molar mass. Thus the main cause is an increase of the apparent degree of dissociation α. It should be noted that according to Eq. 26 an increase of α induces an increase in λ_p, which compounds the effect on Λ. The dependence of α on polyelectrolyte molar mass may be anticipated in the theoretical treatment of ion binding. The traditional models of ion binding are based on electrostatic interactions around infinitely long rodlike polyions oriented in parallel. In this case the fraction of bound ions, and thus α, is constant, independent of polyelectrolyte concentration. This is no longer the case with solutions containing finite-length rods oriented at random [29]. Obviously, perturbances from polyion ends, which tend to weaken the electric field surrounding the polyion, increase in importance as the polyelectrolyte molar mass decreases and the polyions become shorter. This leads to an increase of α, which ultimately approaches the value unity for polyelectrolytes in the oligomer region.

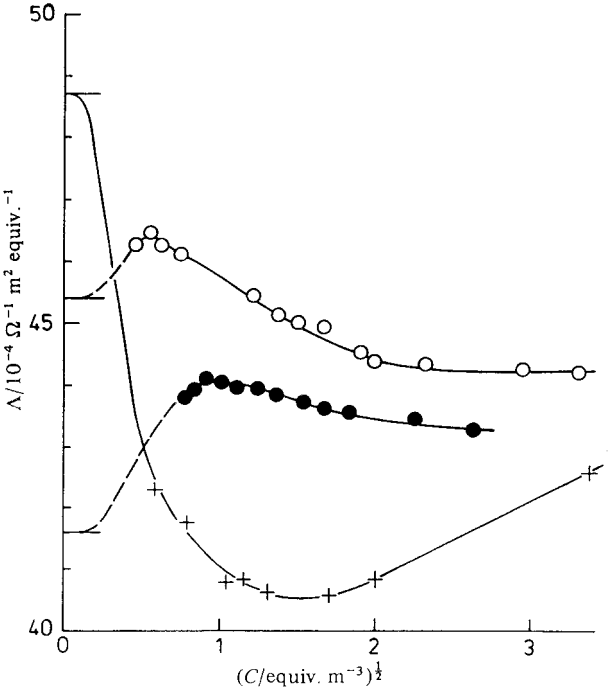

FIG. 6 Phoreograms for different molar mass KPSS samples. +, DP = 460; ●, DP = 2900; ○, DP = 8300. (Reproduced from Ref. 30 by permission of the Royal Society of Chemistry.)

In comparison to alkali metal PSS, the conductivity behavior of HPSS exhibits anomalies [30,31]. For low molar mass samples the behavior is normal, the equivalent conductivity increasing steeply in dilute solutions. On the other hand, for high molar mass samples a sharp fall of equivalent conductivity in dilute solutions is observed; see Figure 7. A conductivity change of this magnitude can only be explained by a change of polyion conformation. Contrary to classical theory, where the polyion is assumed to attain a nearly fully stretched conformation in dilute solutions, the conductivity behavior suggests a more compact conformation for HPSS in very dilute solutions. A contraction of the PSS polyion chain could be promoted by its highly hydrophobic character. Counterion-mediated attractive forces between charged chain segments may also play a role. Such interactions have found support in recent theoretical considerations [32,33]. A conformational change would most likely take place in a concentration region encompassing the critical overlap concentration of the polyelectrolyte. As

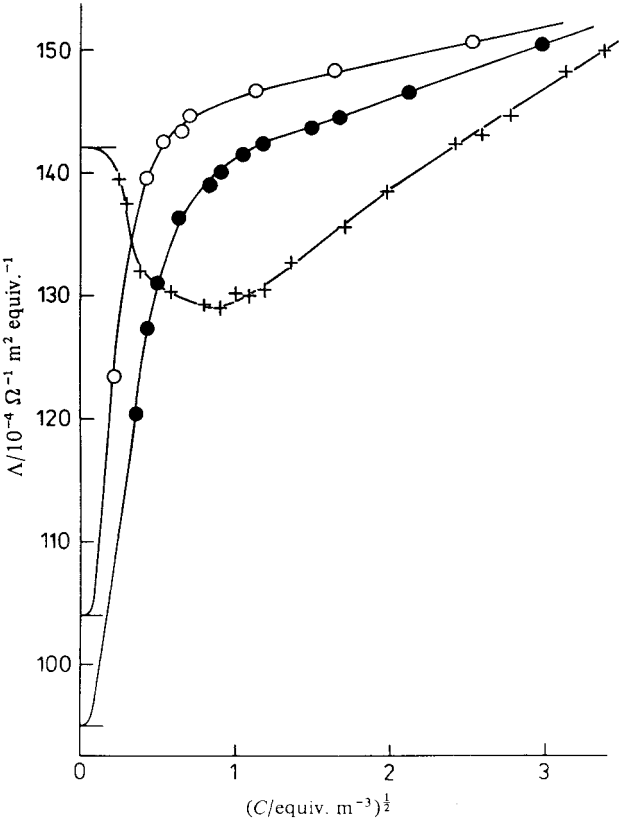

FIG. 7 Phoreograms for different molar mass HPSS samples. +, DP = 460; ●, DP = 2900; ○, DP = 8300. (Reproduced from Ref. 30 by permission of the Royal Society of Chemistry.)

the concentration decreases and the polyion chains become isolated, attractive interactions between chain elements would involve elements of the same chain, which would lead to contraction of the chain. Since the persistence length of a chain is necessarily high because of local electrostatic interactions, a short chain cannot contract, which explains the strong molar mass dependence of the effect.

It is of interest to consider the existence of similar effects in other polyelectrolyte systems. A polyelectrolyte for which a similar behavior may be expected is poly(vinylsulphonic) acid (HPVS). Like HPSS, it is a strong acid, but it has a less hydrophobic backbone. However, studies of the effect

in HPVS solutions are dependent on the availability of narrow molecular mass samples of HPVS.

REFERENCES

1. Onsager, L., Fuoss, R. M. J. Phys. Chem. 1932; 36:2689.
2. Onsager, L., Fuoss, R. M. J. Phys. Chem. 1957; 61:668.
3. Huizenga, J. R., Grieger, P. F., Wall, F. T. J. Am. Chem. Soc. 1950; 72:2636.
4. Eisenberg, H. J. Polym. Sci. 1958; 30:47.
5. Katchalsky, A. Pure Appl. Chem. 1971; 26:327.
6. Vink, H. J. Coll. Interface Sci. 1993; 160:51.
7. Manning, G. S. J. Phys. Chem. 1975; 79:262.
8. Vink, H. Ber. Bunsenges. Phys. Chem. 1993; 97:1472.
9. Vink, H. J. Chem. Soc. Faraday Trans. 1 1981; 77:2439.
10. Vink, H. J. Chem. Soc. Faraday Trans. 1 1984; 80:1297.
11. Vink, H. J. Chem. Soc. Faraday Trans. 1 1989; 85:699.
12. Heckmann, K. Naturwissenschaften 1953; 40:478.
13. Heckmann, K. Kolloid Zh. 1954; 136:67.
14. Schindewolf, U. Naturwissenschaften 1953; 40:435.
15. Schindewolf, U. Z. Elektrochem. 1954; 58:697.
16. Schindewolf, U. Z. Phys. Chem. (NF) 1954; 1:129.
17. Jacobson, B. Rev. Sci. Inst. 1953; 24:949.
18. Eigen, M., Schwarz, G. Z. Phys. Chem. (NF) 1955; 4:380.
19. Eigen, M., Schwarz, G. J. Coll. Sci. 1957; 12:181.
20. Vink, H. J. Coll. Interface Sci. 1995; 173:211.
21. Fuoss, R. M., Katchalsky, A., Lifson, S. Proc. Natl. Acad. Sci. US 1951; 37: 579.
22. Alfrey, T., Berg, P. W., Morawetz, H. J. Polym. Sci. 1951; 7:543.
23. Manning, G. S. J. Chem. Phys. 1969; 51:954.
24. Oosawa, F. Polyelectrolytes. New York: Marcel Dekker, 1971.
25. Vink, H. Makromol. Chem. 1981; 182:279.
26. Wandrey, C. Ber. Bunsenges. Phys. Chem. 1996; 100:869.
27. Wandrey, C. Langmuir 1999; 15:4069.
28. Kwak, J. C. T., Hayes, R. C. J. Phys. Chem. 1975; 79:265.
29. Nyquist, R. M., Ha, B. Y., Liu, A. J. Macromolecules 1999; 32:3481.
30. Vink, H. J. Chem. Soc. Faraday Trans. 1 1987; 83:801.
31. Vink, H. Makromol. Chem. 1982; 183:2273.
32. Stevens, M. J., Kremer, K. J. Chem. Phys. 1995; 103:1669.
33. Schiessel, H., Pincus, P. Macromolecules 1998; 31:7953.

8

Electrical Polarizability of Polyelectrolytes by Metropolis Monte Carlo Simulation

KAZUO KIKUCHI University of Tokyo, Tokyo, Japan

I. INTRODUCTION

According to the fluctuation–dissipation theorem [1], the electrical polarizability of polyelectrolytes is related to the fluctuations of the dipole moment generated in the counterion atmosphere around the polyions in the absence of an applied electric field [2–4]. Here we calculate the fluctuations by computer simulation to determine anisotropy of the electrical polarizability $\Delta\alpha$ of model DNA fragments in salt-free aqueous solutions [5–7]. The Metropolis Monte Carlo (MC) Brownian dynamics method [8–12] is applied to calculate counterion distributions, electric potentials, and fluctuations of counterion polarization.

Many theoretical models have been developed to describe the electrical polarizability of polyelectrolytes [2–4,13–40]. The problem is, however, extremely complex and difficult, even if simple models are assumed for the geometry of the polyions [37]. This is because many fields are involved: concentrations of small ions, the electrical potential, and the solvent velocity, to be determined as functions of space and time, which are coupled with each other through essentially nonlinear equations. Our numerical approach, however, need not introduce, as in most of the theories, somewhat ad hoc approximations such that counterions are classified into ''free'' and ''bound'' ions, only the latter contributing to the polarizability, nor neglect interactions between counterions.

At every simulation step we numerically sort counterions in increasing order of the sum of their distances from both ends of the polyion and calculate the contribution to the dipole moment from the first n counterions in the sorting list. We then define a partial polarizability tensor due to these n counterions.

Two kinds of counterions, condensed and those constituting a diffuse ion atmosphere that may be treated in the Debye–Hückel approximation, are clearly recognized in their distinct spatial distributions, and introduction of the partial polarizability tensor enables us to distinguish between contributions to the polarizability from these two kinds of ions. The contribution from condensed counterions to the radial components of the polarizability tensor is very small, as has hitherto often been postulated in various theories. That from the diffuse ion atmosphere is very large and cannot be neglected in the calculation of the anisotropy.

Although in our simulations, solvent convection is suppressed [35,39], characteristic features of the electric properties of polyelectrolytes in salt-free aqueous solutions are reproduced. The anisotropy of the electrical polarizability $\Delta\alpha$ of DNAs in salt-free aqueous solution increases on dilution of the polymer concentration and is proportional to the second power of the molecular weight.

II. METROPOLIS MONTE CARLO BROWNIAN DYNAMICS

The Metropolis MC [41] was originally developed as a method suited to electronic computers for calculating statistical mechanical configurational integrals. Since the MC sampling is a Markovian process, if we introduce a ''time'' scale t that actually labels the order of subsequent configurations X, the ''dynamic'' evolution of the probability distribution function $P(X, t)$ is governed by the master equation

$$\frac{\partial P(X, t)}{\partial t} = \int [W(X|X')P(X', t) - W(X'|X)P(X, t)]\, dX' \tag{1}$$

where $W(X|X')$ is the transition probability per unit ''time'' for a transition from configuration X' to X.

The master equation may be solved approximately by an expansion method in powers of a parameter Ω, the size of the system [42]. Given that $W(X|X')$ has the canonical form

$$W(X|X') = \Phi_0(x'; r) + \Omega^{-1}\Phi_1(x'; r) + \Omega^{-2}\Phi_2(x'; r) + \cdots \tag{2}$$

with $x' = X'/\Omega$ and $r = X - X'$, the jump moments are defined by

$$\alpha_{v,\lambda}(x) = \int r^v \Phi_\lambda(x; r)\, dr \tag{3}$$

When $\alpha_{1,0} = 0$, the Ω expansion yields as the lowest approximation a nonlinear Fokker–Planck equation:

$$\frac{\partial P(x,\,\tau)}{\partial \tau} = -\frac{\partial}{\partial x}\,\alpha_{1,1}(x)P + \frac{1}{2}\,\frac{\partial^2}{\partial x^2}\,\alpha_{2,0}(x)P \tag{4}$$

with $\tau = \Omega^{-2}t$.

In the Metropolis MC, the reciprocal of the maximum displacement allowed for an MC move during "time" interval Δt may be taken as the parameter Ω. Then the transition probability has the canonical form with

$$\Phi_0(x;\,r) = \frac{1}{2\Delta t} \qquad \text{for} \qquad |r| \le 1$$
$$= 0 \qquad \text{for} \qquad |r| > 1$$

and, supposing, for example, the derivative of the potential energy of the system $U(x)$ with respect to x is negative, i.e., $U'(x) < 0$, with

$$\Phi_1(x;\,r) = -\frac{1}{2k_{\mathrm{B}}T\,\Delta t}\,U'(x)r \qquad \text{for} \qquad -1 \le r < 0$$
$$= 0 \qquad \text{for} \qquad r < -1 \qquad \text{and} \qquad r \ge 0$$

for sufficiently large Ω where k_{B} is the Boltzmann constant and T is the absolute temperature. From these one obtains

$$\alpha_{1,0} = 0$$
$$\alpha_{2,0} = \frac{1}{3\,\Delta t}$$
$$\alpha_{1,1} = \frac{1}{6k_{\mathrm{B}}T\,\Delta t}\,U'(x)$$

so that Eq. 4 reduces to the diffusion equation

$$\frac{\partial P(x,\,t)}{\partial t} = \frac{D}{k_{\mathrm{B}}T}\,\frac{\partial}{\partial x}\,U'(x)P + D\,\frac{\partial^2}{\partial x^2}\,P \tag{5}$$

where the diffusion constant D is defined by

$$6D\,\Delta t\,\Omega^2 = 1 \tag{6}$$

Thus by taking the size of the maximum allowed displacement Ω^{-1} in the Metropolis MC so small that forces acting on a particle remain essentially constant during the MC "time" step, the method turns into a Brownian dynamics simulation [8,9,11]. It was successfully applied to Brownian motion of a particle under a harmonic potential [8] as well as to the orientation of a dipolar particle in an applied electric field [12] and extended to include hydrodynamic interactions [10].

III. SIMULATION

A 64/128 base-pair fragment of the double-stranded DNA is modeled as an impenetrable cylinder of radius 0.85 nm with 128/256 negative charges spaced at 0.17 nm intervals along its axis. The hydrated univalent counterions are modeled as hard spheres of radius 0.15 nm so that the radial distance of closest approach of an ion to the axis of the DNA is 1.0 nm. The cylinder is extended 0.17 nm beyond the terminal charges at both ends. The solvent is treated as a dielectric continuum with the relative permittivity of pure water at 25°C (78.3) and no salt is added. The MC cell is a sphere of varying radius in which the DNA fragment is placed along the z-axis with its center in common with that of the MC cell, or the origin of the coordinate axes.

The energy of configurations is calculated as a sum of Coulombic interactions of each counterion in the MC cell with all the other counterions and DNA charges in the cell. Ω^{-1} of 0.2 nm is chosen as the size of the maximum counterion displacement allowed for an MC move along each coordinate direction. The new configuration generated by a random move of a single ion is accepted or rejected according to the probability $\min\{1, \exp(-\Delta U/k_B T)\}$, where ΔU is the change in configurational energy that would result from the move. Although the Metropolis "time" scale Δt may be fixed by Eq. 6, we need not relate the Metropolis and physical time scales here as far as we calculate only time averages. When a counterion escapes from the cell during a move in the Metropolis sampling process, another counterion is put to the symmetrical position about the center of the MC sphere. The DNA concentration is calculated assuming that 128/256 nucleotide residues occupy an effective volume the size of the simulation sphere whose volume is varied by changing its radius.

The system has prolate spheroidal symmetry with the foci located at both ends of the DNA polyion rod [43]. At every simulation step we numerically sort counterions in increasing order of the sum of their distances from both ends of the polyion and calculate the contribution to the dipole moment from the first n counterions in the sorting list $[\mu_x(n), \mu_y(n), \mu_z(n)]$ by

$$\mu_x(n) = \sum_{i=1}^{n} ex_i$$

$$\mu_y(n) = \sum_{i=1}^{n} ey_i$$

$$\mu_z(n) = \sum_{i=1}^{n} ez_i \tag{7}$$

where e is the protonic charge and (x_i, y_i, z_i) is the coordinate of the ith

counterion. We then define the partial polarizability tensor due to these n counterions with its principal components $\alpha_{xx}(n)$, $\alpha_{yy}(n)$, $\alpha_{zz}(n)$ given by

$$\alpha_{xx}(n) = \frac{\langle \mu_x^2(n) \rangle - \langle \mu_x(n) \rangle^2}{k_B T}$$

$$\alpha_{yy}(n) = \frac{\langle \mu_y^2(n) \rangle - \langle \mu_y(n) \rangle^2}{k_B T}$$

$$\alpha_{zz}(n) = \frac{\langle \mu_z^2(n) \rangle - \langle \mu_z(n) \rangle^2}{k_B T} \tag{8}$$

where $\langle\ \rangle$ denotes time average. The transverse and longitudinal partial polarizabilities $\alpha_T(n)$ and $\alpha_L(n)$ are defined as

$$\alpha_T(n) = \frac{\alpha_{xx}(n) + \alpha_{yy}(n)}{2}$$

$$\alpha_L(n) = \alpha_{zz}(n) \tag{9}$$

and the anisotropy of the partial polarizability $\Delta\alpha(n)$ as

$$\Delta\alpha(n) = \alpha_L(n) - \alpha_T(n) \tag{10}$$

n runs from 1 to 128/256 and the anisotropy of the electrical polarizability $\Delta\alpha$ to be determined is expressed as

$$\Delta\alpha = \alpha_L(128/256) - \alpha_T(128/256) \tag{11}$$

Simulation parameters used are listed in Table 1. Labels shown in column 3 will be used in the subsequent figures of this article.

TABLE 1 Simulation Parameters

DNA molecular weight, no. of base pairs	Length of DNA, nm	Label	Radius of MC cell, nm	Polymer concentration, mM nucleotide residues
64	21.93	dna1	21.93	4.811
		dna2	27.63	2.406
		dna3	34.68	1.217
		dna4	54.94	0.306
128	43.69	dnb1	43.69	1.217
		dnb2	55.05	0.609
		dnb3	69.22	0.306

Labels in column 3 will be used in the subsequent figures of this article.

In salt-free dilute solutions, the density of the Debye–Hückel ion atmosphere is so small that the determination of each component of the polarizability tensor is not free from statistical errors, i.e., $\Delta\alpha$ is given in Eq. 11 as a difference of quantities containing large statistical uncertainties. This kind of error can only be resolved by averaging over a large number of trajectories. Use of the massively parallel Hitachi SR2201 computer of the computer center of the University of Tokyo is indispensable for this purpose.

IV. COUNTERION DISTRIBUTIONS, ELECTRIC POTENTIALS, AND FLUCTUATIONS OF COUNTERION POLARIZATION

Figures 1, 2, and 3 show three different views of the counterion distribution for a 64 base-pair DNA at a polymer concentration of 1.2 mM nucleotide residues. They are drawn by superposing a number (3,968) of uncorrelated configurations of counterions collected during the simulation. Two kinds of counterions, one of them deserving identification with Manning's condensed counterions [44,45], at least qualitatively, and the other forming a diffuse ion cloud, are clearly recognizable in distinct spatial distributions. Further in Figure 1, the prolate spheroidal symmetry of the distribution, and in Figures 2 and 3, depletion of the diffuse ion cloud at the ends of the polyion, may be noticed.

To express counterion distributions more quantitatively, counterion concentration c_+ profiles for a 64 base-pair DNA at various polymer concentrations are plotted in Figure 4 as functions of the radial coordinate r measured from the axis of the DNA cylinder at its center and in Figure 5 as functions of the z coordinate along the surface of the cylinder. The very high counterion concentration ($\sim$3 M) on the surface of the polyion rapidly decreases in both radial and longitudinal directions, and dilution of the polymer concentration has the slightest effect on these profiles.

Figure 6 shows the distance of counterions from the 64 base-pair DNA polyion or the sum of their distances from both ends of the polyion sorted in increasing order and averaged over a number of uncorrelated counterion configurations. The abscissa is taken as the ordinal number n of counterions sorted in increasing order of their distance from the polyion. Manning's counterion condensation theory [44] predicts for infinitely long polyelectrolyte chains that 76% of the DNA phosphate charge is neutralized by condensed ions. If we use this condensation fraction temporarily for our oligomeric 64 base-pair DNA, out of 128 counterions 98 are classified as condensed and 30 as constituting a diffuse ion atmosphere. Since Figure 6

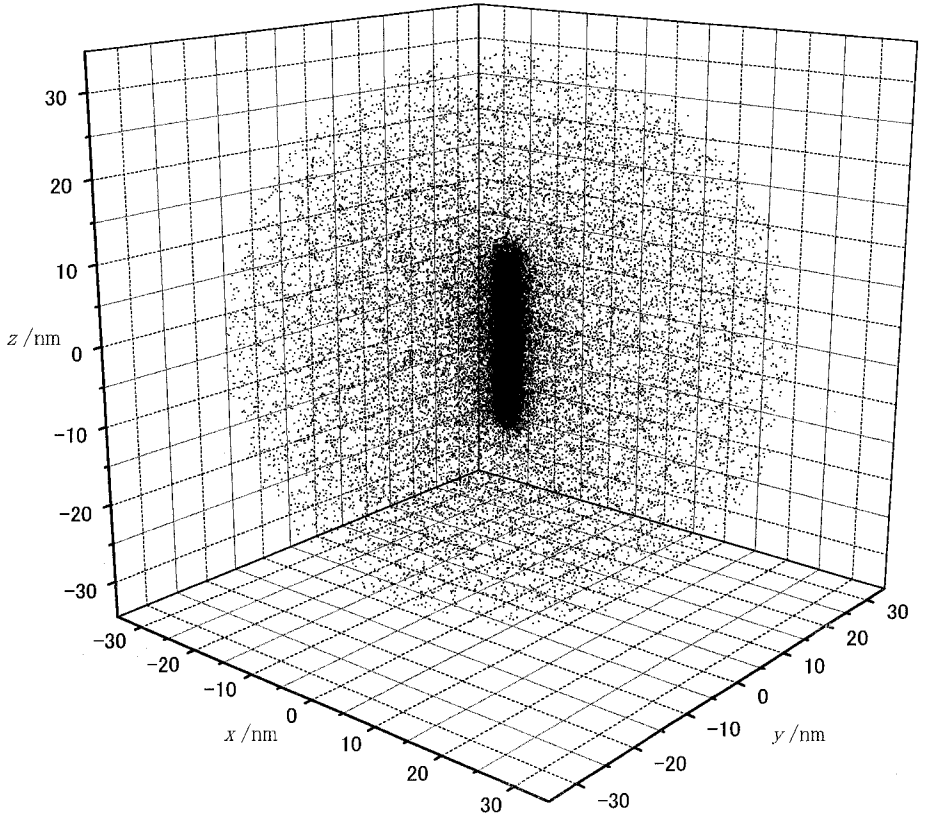

FIG. 1 3D view of the counterion distribution for a 64 base-pair DNA at a polymer concentration of 1.2 mM nucleotide residues.

shows comparable fractions of counterions located in the immediate vicinity of the polyion, we are tempted to give a proper definition of condensed counterions in our own simulation study to make identification with Manning's theory more quantitative. For each curve in Figure 6 we choose the abscissa where the curve shows the maximum curvature, denoting it as n^*, and define the first n^* ions in the sorting list as condensed. Numbers of condensed counterions n^* determined in this way and condensation fractions $n^*/(128/256)$ calculated from them are listed in Table 2. Note that only a few counterions dissociate from the condensed state on dilution, so that there is little effect on the concentration profiles, as we have seen in Figures 4 and 5. It is interesting that the fraction of the condensed counterions deter-

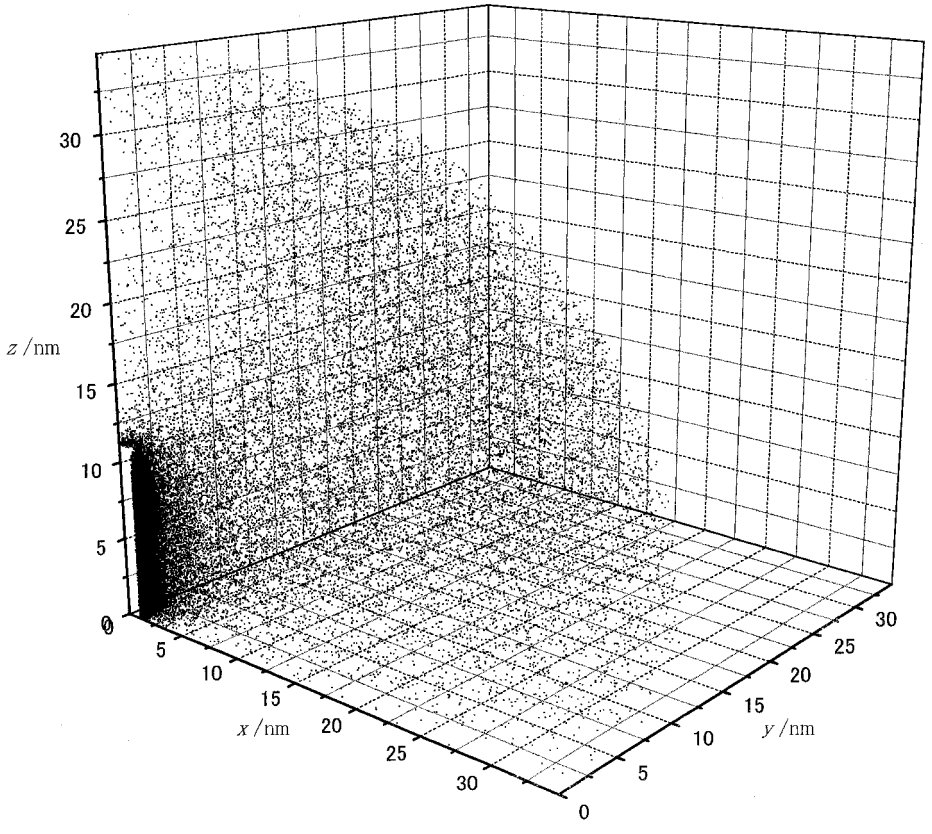

FIG. 2 3D first-quadrant view of the counterion distribution for a 64 base-pair DNA at a polymer concentration of 1.2 mM nucleotide residues.

mined by the simulation is approaching Manning's theoretical value as the molecular weight of DNA increases.

Figure 7 shows a 3D view of the reduced electrostatic potential $e\psi/k_BT$ around a 64 base-pair DNA at a polymer concentration of 1.2 mM nucleotide residues where ψ is the electrostatic potential. It is calculated by averaging over the configurations of counterions used in Figures 1, 2, and 3. Note that electric fields due to the polyion are completely shielded by counterions. Further, the reduced electrostatic potentials around a 64 base-pair DNA at various polymer concentrations are plotted in Figure 8 as functions of the radial coordinate r measured from the DNA cylinder at its center and in

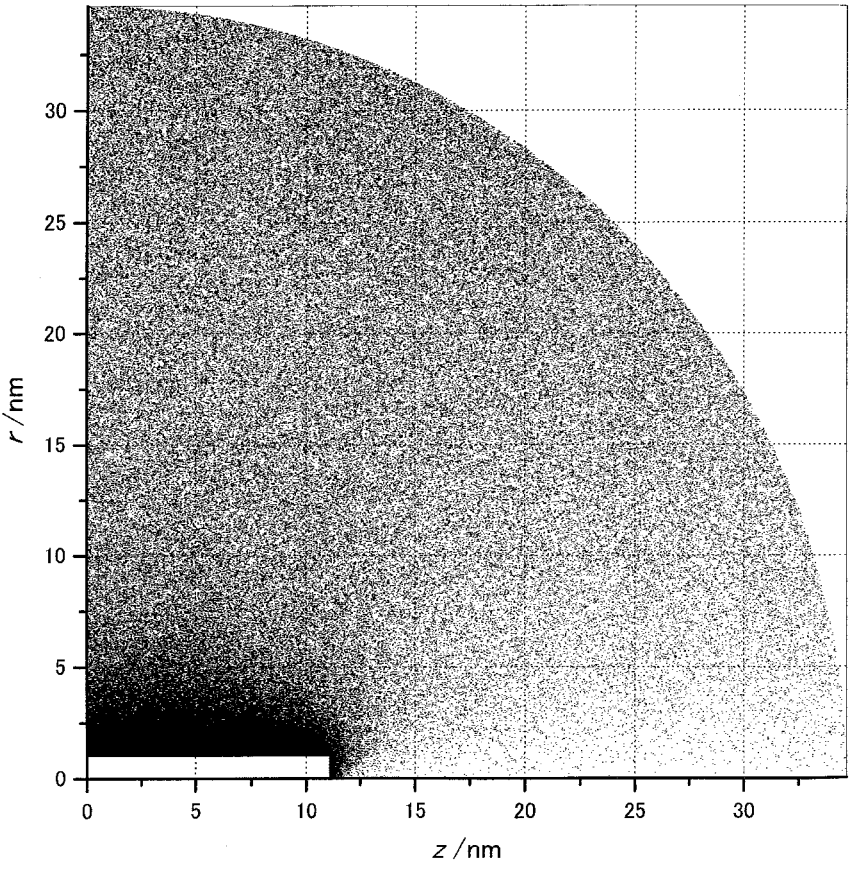

FIG. 3 2D view of the counterion distribution for a 64 base-pair DNA at a polymer concentration of 1.2 mM nucleotide residues. Projection of Figure 2 onto a z–r plane, where r is the radial coordinate measured from the axis of the DNA cylinder at its center.

Figure 9 as functions of the z coordinate along the surface of the cylinder. These figures also show almost complete shielding of the polyion fields as well as very small derivatives of the electrostatic potentials at cell boundaries, justifying our neglect of forces from outside of our simulation sphere and the boundary conditions used in our simulations.

In Figure 10, longitudinal and transverse partial electrical polarizability pairs, $\alpha_L(n)$ and $\alpha_T(n)$, determined for a 64 base-pair DNA at various polymer concentrations are plotted against the number of contributing counter-

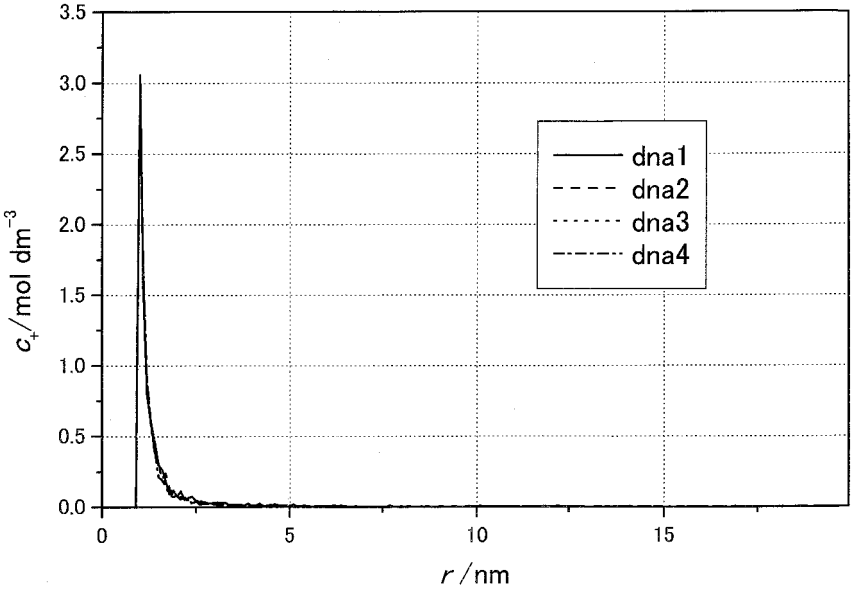

FIG. 4 Counterion concentration c_+ profiles for a 64 base-pair DNA at various polymer concentrations as functions of the radial coordinate r measured from the axis of the DNA cylinder at its center.

ions n. They are calculated as explained in the previous section. For each pair of curves, the upper one is $\alpha_L(n)$ and the lower one $\alpha_T(n)$.

The dependence of the partial polarizabilities on n is explained as reflecting structural difference of the two kinds of counterions, condensed and those constituting a diffuse ion atmosphere that may be treated in the Debye–Hückel approximation [44]. $\alpha_L(n)$ increases until the DNA phosphate charge is neutralized by about 60 counterions. Note that it is calculated at every simulation step by selecting the innermost counterions. Then fluctuation of the z-component of the dipole moment $\mu_z(n)$ will increase with n when n is small, because selected counterions may distribute randomly along the polyion rod axis. When the number of the selected counterions increases over 60, fluctuation of $\mu_z(n)$ levels off until n reaches n^* because, since most of the condensed counterions that are firmly bound in the immediate vicinity of the polyion are selected, they distribute uniformly along the DNA. When n exceeds n^*, the Debye–Hückel ion atmosphere begins to contribute to $\mu_z(n)$ with their diffuse spatial distribution reflected in the rapidly increasing fluctuation of $\mu_z(n)$.

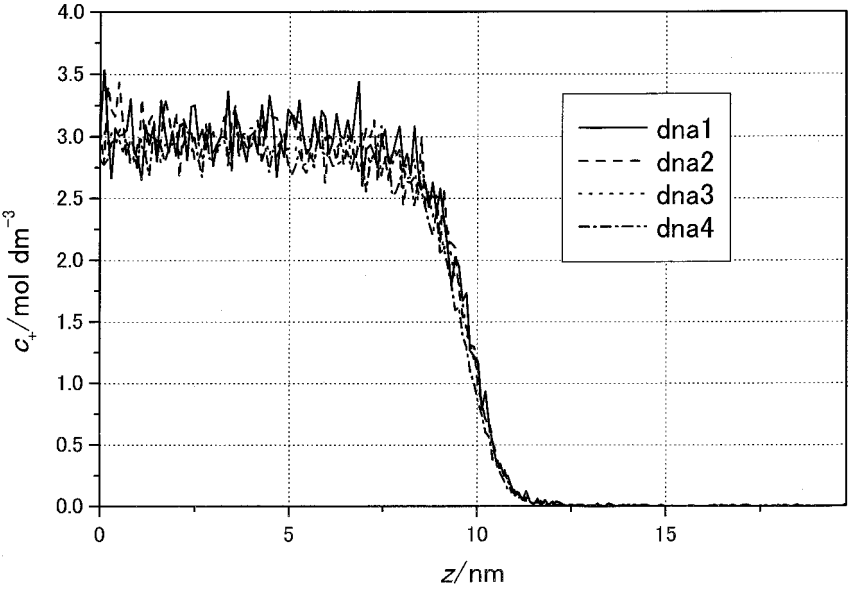

FIG. 5 Counterion concentration c_+ profiles for a 64 base-pair DNA at various polymer concentrations as functions of the z coordinate along the surface of the cylinder.

Fluctuation of $\mu_x(n)$ and $\mu_y(n)$ remains very small when $n \leq n^*$ because ions are condensed in a layer over the DNA surface. When $n > n^*$, the Debye–Hückel ion atmosphere starts to contribute to both $\mu_z(n)$ and $\mu_y(n)$ resulting in their rapidly growing fluctuation.

Thus the two kinds of counterions are distinguished not only by their spatial distributions but also by their polarization behaviors. Figure 10 also shows that while the contribution to the polarizability from the condensed ions remains constant reflecting their structural stability, that from the diffuse ion atmosphere increases rapidly on dilution. Here we describe the electrical polarizability as if it were expressed as a sum of contributions from the two kinds of counterions, which is only true when correlation between the dipole moments due to both kinds of ions is neglected. The radial polarizability is, however, safely divided into the two because in this case the dipole moment due to the condensed counterions is zero. Furthermore, similar shapes of the graphs of the radial and longitudinal polarizabilities suggest that also in the case of the longitudinal polarizability the correlation may be zero! Although this should be confirmed by further simulation, the division may be justified

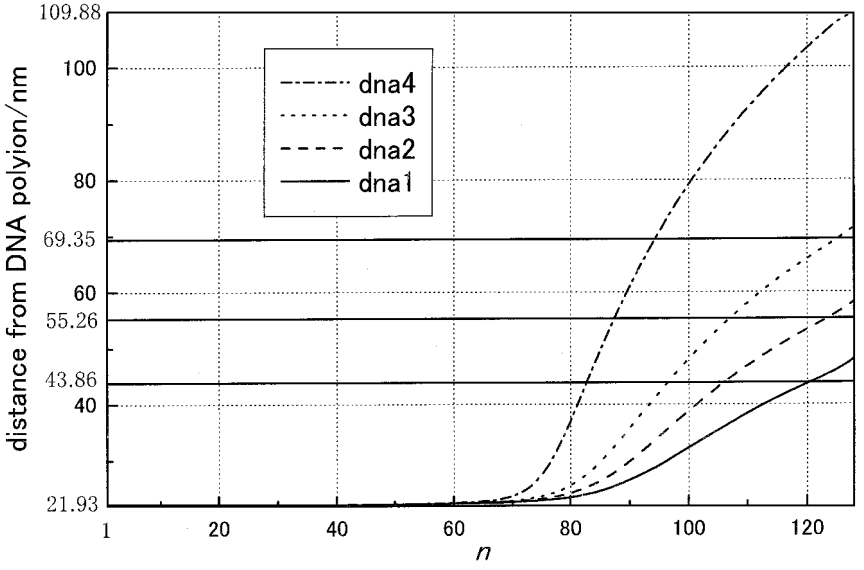

FIG. 6 Distance of counterions from 64 base-pair DNA polyion or sum of their distances from both ends of the polyion sorted in increasing order and averaged over a number of uncorrelated counterion configurations collected during the simulation. The abscissa is also taken as the ordinal number n of counterions sorted in increasing order of their distance from the polyion.

TABLE 2 Number of Condensed Counterions n^* and Condensation Fraction $n^*/(128/256)$ Determined by Simulation

Label	n^*	Fraction
dna1	87	0.68
dna2	85	0.66
dna3	82	0.64
dna4	76	0.59
dnb1	180	0.703
dnb2	178	0.695
dnb3	172	0.672

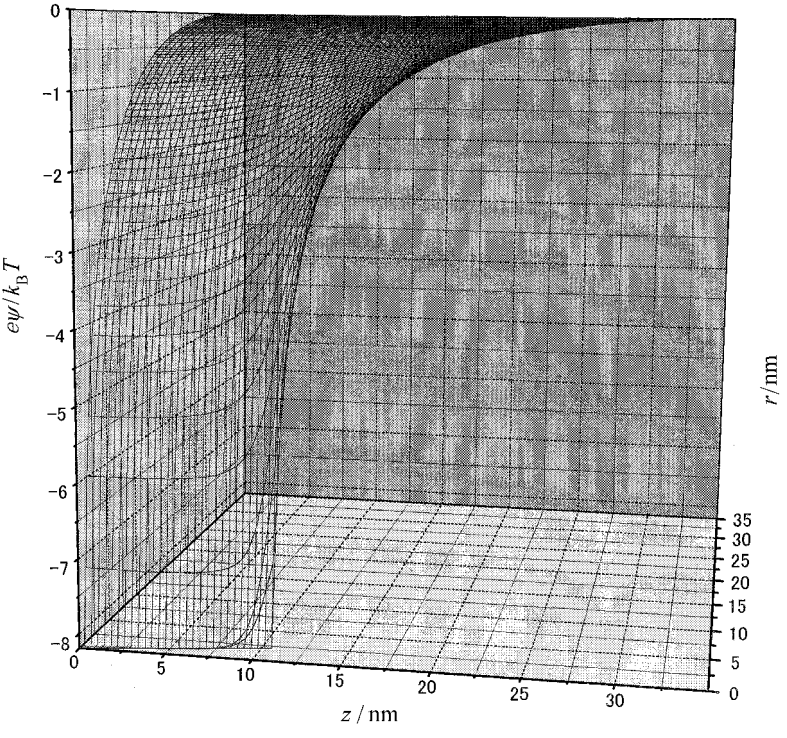

FIG. 7 3D view of the reduced electrostatic potential $e\psi/k_BT$ around a 64 base-pair DNA at a polymer concentration of 1.2 mM nucleotide residues.

as far as we compare the longitudinal polarizability due to condensed counterions with theories that also neglect the correlation.

In Figure 11, partial anisotropies of the electrical polarizability $\Delta\alpha(n)$ determined for a 64 base-pair DNA at various polymer concentrations are plotted against the number of contributing counterions n. In this figure, we can observe exactly the same regions as in Figure 10, where the $\Delta\alpha(n)$'s show different dependence upon n: Region I ($1 \leq n \leq \sim 60$), Region II ($\sim 60 < n \leq n^*$), and Region III ($n^* < n \leq 128$). In Region I, the $\Delta\alpha(n)$ curves rise from 0 until the DNA phosphate charge is neutralized by about 60 counterions. In Region II, they reach plateau values, and in Region III, they grow rapidly again.

The dependence of the $\Delta\alpha(n)$'s on n is explained exactly in the same way as before. They show no concentration dependence in Region I, consistent with the fact that counterions are strongly bound to the polyion in this region. On the other hand, in Region II, they decrease on dilution, reflecting

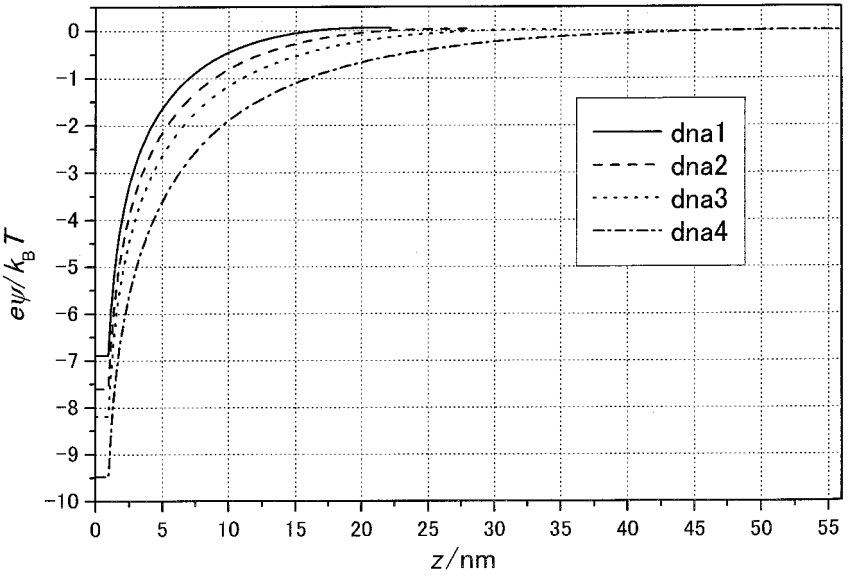

FIG. 8 Reduced electrostatic potentials $e\psi/k_BT$ around a 64 base-pair DNA at various polymer concentrations plotted as functions of radial coordinate r measured from the DNA cylinder at its center.

some loosening of the condensation layer in the radial direction in this region. In Region III, large contribution from the diffuse ion atmosphere as well as reversal of the concentration dependence of the $\Delta\alpha(n)$ curves is observed. Their sharp drops in the outer part of this region should be regarded as due to the boundary conditions of our simulation cell. Linear portions of the curves are extrapolated to obtain values of $\Delta\alpha(128/256)$ or $\Delta\alpha$.

Figure 12 shows polymer concentration c_P dependence of the anisotropy of the electrical polarizability $\Delta\alpha$ of a 64/128 base-pair DNA fragment. $\Delta\alpha$ increases on dilution of polymer concentration. Experimentally, $\Delta\alpha$ is determined via measurement of the Kerr constant of the polyelectrolyte solutions, and in the case of rodlike polyelectrolytes both quantities are proportional to each other. It has been observed that the Kerr constant of polyelectrolytes in salt-free aqueous solutions increases on dilution [46,47]. This behavior of the Kerr constant is one of the characteristic properties of polyelectrolytes in salt-free aqueous solutions whose reproduction we have succeeded in by computer simulation. The figure also indicates that $\Delta\alpha$ is

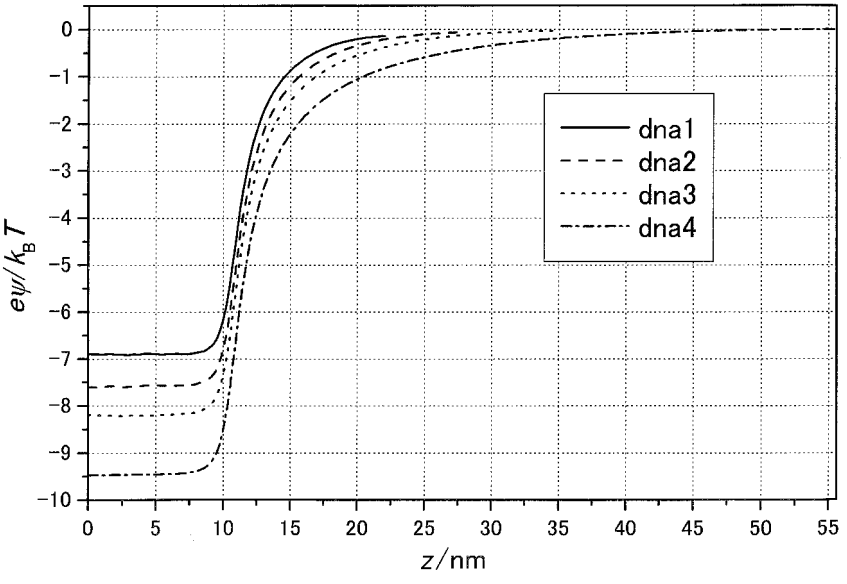

FIG. 9 Reduced electrostatic potentials $e\psi/k_BT$ around a 64 base-pair DNA at various polymer concentrations plotted as functions of the z coordinate along the surface of the cylinder.

rather proportional to the second power of the molecular weight, but further simulations on higher molecular weight DNAs are necessary for confirmation.

V. ELECTRIC PROPERTIES OF POLYELECTROLYTES IN AQUEOUS SOLUTION

Our simulation has shown that polyions are on average completely shielded electrostatically by counterions even in salt-free solutions. Two kinds of counterions, condensed and those forming a diffuse ion atmosphere, are distinguished not only by their spatial distributions but also by their fluctuation or polarization behaviors. The contribution from condensed counterions to the radial components of the electrical polarizability tensor is very small, as has often been postulated in various theories previously. But that from the diffuse ion cloud is very large and cannot be neglected in the calculation of the anisotropy. We have succeeded in the computational reproduction of one of the characteristic properties of polyelectrolytes in salt-

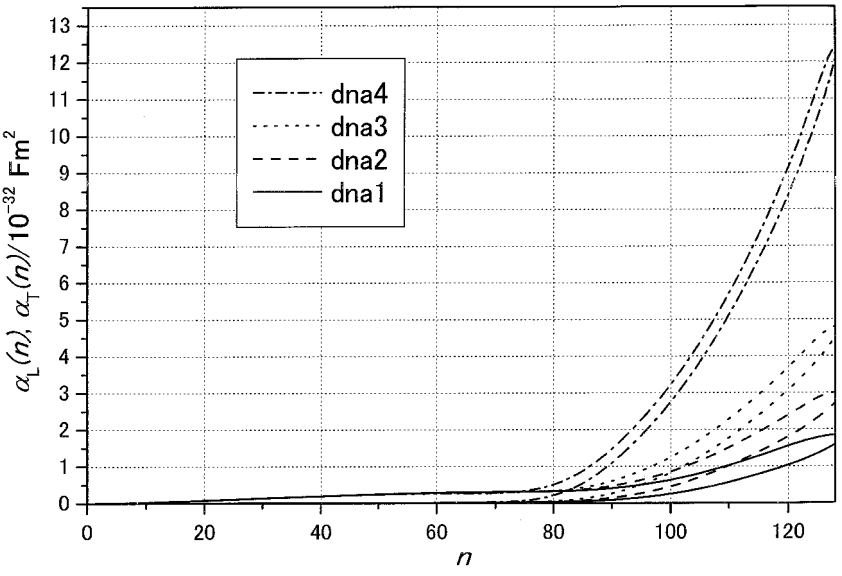

FIG. 10 Longitudinal and transverse partial electrical polarizability pairs, $\alpha_L(n)$ and $\alpha_T(n)$, determined for a 64 base-pair DNA at various polymer concentrations plotted against the number of contributing counterions n. For each pair of curves, the upper one is $\alpha_L(n)$ and the lower one $\alpha_T(n)$.

free solution, i.e., the concentration dependence of the anisotropy of the electrical polarizability of polyions. Its increase on dilution of the polymer concentration is a reflection of the structure of the diffuse ion cloud in salt-free aqueous solution and cannot be explained using models that only assume a contribution to the polarizability from condensed ions.

We have given a definition of condensed counterions for olygomeric polyelectrolytes based on our numerical study, and it is interesting whether the fraction of the condensed counterions we determine approaches Manning's theoretical value as the molecular weight increases. For this purpose and to establish molecular weight dependence of the polarizability of polyelectrolytes, simulation on higher molecular weight DNAs is necessary.

Polarizabilities are simulated also in salt solutions [48]. This time the contribution of coions to the electroneutrality condition must be taken into account. We consider that polyion phosphate charge is compensated by the same amount of net charge. At every simulation step we numerically sort all the small ions in increasing order of the sum of their distances from both ends of the polyion. Then if we find a coion in the sorting list, we search a

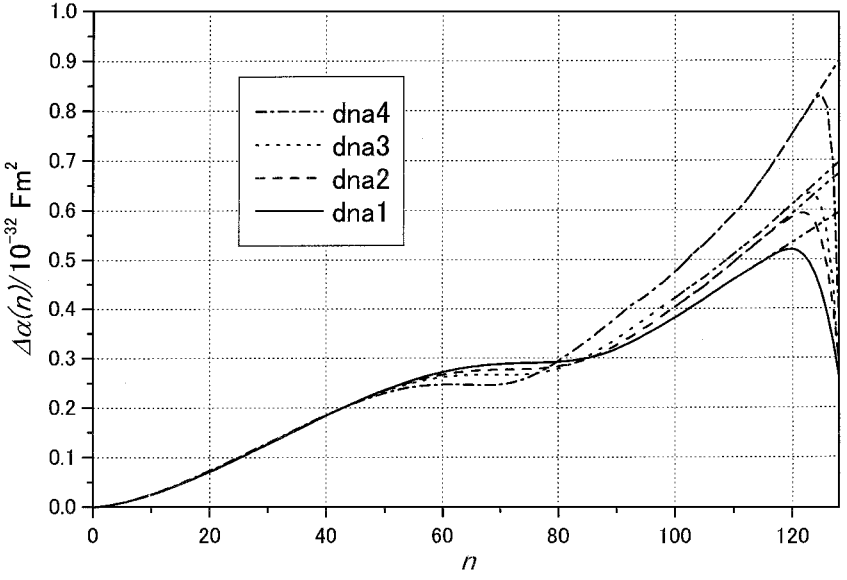

FIG. 11 Partial anisotropies of the electrical polarizability $\Delta\alpha(n)$ determined for a 64 base-pair DNA at various polymer concentrations plotted against the number of contributing counterions n.

nearest consecutive counterion in the list and delete both entries. We continue this process from the beginning of the list until the first n consecutive entries are all occupied by counterions. We calculate the contribution to the dipole moment from these n counterions (net charge) and define a partial polarizability tensor due to these counterions. Characteristic features of the electric properties of polyelectrolytes in salt solutions are reproduced, i.e., the anisotropy of the electrical polarizability of DNAs decreases on addition of salt.

We have not taken into consideration electrophoretic motion of polyions [35,39]. However, we have already obtained characteristic features of the electric properties of polyelectrolytes in aqueous solution. Electric polarizability components originating from the fluctuations of condensed counterions show smaller concentration and salt dependence, while those due to a diffuse ion atmosphere, by contrast, a larger dependence. Anisotropy of the electrical polarizability $\Delta\alpha$ is positive without invoking an enhancement of the longitudinal component by the solvent flow. Simulation on the frequency dependence of the electrical polarizability is in progress to study how the

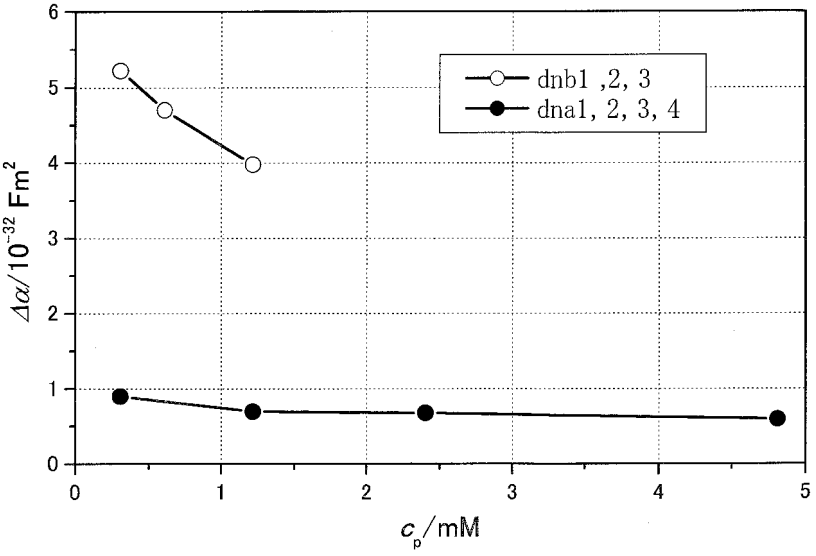

FIG. 12 Polymer concentration c_P dependence of the anisotropy of the electrical polarizability $\Delta\alpha$ of a 64/128 base-pair DNA fragment.

distinct polarization behaviors of the two kinds of counterions are related to the two dispersion regions, high- and low-frequency, observed in the dielectric measurements of polyelectrolyte solutions [17,19].

REFERENCES

1. Kubo R. Statistical-mechanical theory of irreversible processes. I. General theory and simple applications to magnetic and conduction problems. J Phys Soc Japan 1957; 12:570–586.
2. Oosawa F. Counterion fluctuation and dielectric dispersion in linear polyelectrolytes. Biopolymers 1970; 9:677–688.
3. Minakata A, Imai N, Oosawa F. Dielectric properties of polyelectrolytes. II. A theory of dielectric increment due to ion fluctuation by a matrix method. Biopolymers 1972; 11:347–359.
4. Warashina A, Minakata A. Dielectric properties of polyelectrolytes. IV. Calculation of dielectric dispersion by a stochastic model. J Chem Phys 1973; 58: 4743–4749.
5. Washizu H, Kikuchi K. Anisotropy of electrical polarizability of a DNA fragment. Chem Lett 1997; 651–652.
6. Washizu H, Kikuchi K. Electrical polarizability anisotropy of a DNA fragment. Rep Progr Polym Phys Japan 1997; 40:597–600.

7. Washizu H, Kikuchi K. Concentration dependence of the anisotropy of the electrical polarizability of a model DNA fragment in salt-free aqueous solution studied by Monte Carlo simulations. Colloids Surfaces A: Physicochem Eng Aspects 1999; 148:107–112.
8. Kikuchi K, Yoshida M, Maekawa T, Watanabe H. Metropolis Monte Carlo method as a numerical technique to solve the Fokker-Planck equation. Chem Phys Lett 1991; 185:335–338.
9. Kikuchi K, Yoshida M, Maekawa T, Watanabe H. Monte Carlo method for Brownian dynamics simulation. In: Jennings BR, Stoylov SP, eds. Colloid and Molecular Electro-Optics 1991. Bristol: IOP Publishing, 1992:7–12.
10. Kikuchi K, Yoshida M, Maekawa T, Watanabe H. Metropolis Monte Carlo method for Brownian dynamics simulation generalized to include hydrodynamic interactions. Chem Phys Lett 1992; 196:57–61.
11. Yoshida M, Kikuchi K. Metropolis Monte Carlo Brownian dynamics simulation of the ion atmosphere polarization around a rodlike polyion. J Phys Chem 1994; 98:10303–10306.
12. Yoshida M, Kikuchi K. A simple algorithm for rotational Brownian dynamics by the Metropolis Monte Carlo method. Rep Progr Polym Phys Japan 1996; 39:115–118.
13. Schwarz G. A theory of the low-frequency dielectric dispersion of colloidal particles in electrolyte solution. J Phys Chem 1962; 66:2636–2642.
14. Pollak M. On the dielectric dispersion of polyelectrolytes, with application to DNA. J Chem Phys 1965; 43:908–909.
15. Mandel M. The electric polarization of rod-like, charged macromolecules. Mol Phys 1961; 4:489–496.
16. van der Touw F, Mandel M. Dielectric increment and dielectric dispersion of solutions containing simple charged linear macromolecules I. Theory. Biophys Chem 1974; 2:218–230.
17. Mandel M, van der Touw F. Dielectric properties of polyelectrolytes in solution. In: Sélény E, ed. Charged and Reactive Polymers, Volume I. Polyelectrolytes. Dordrecht: Reidel, 1974:285–300.
18. van Dijk W, van der Touw F, Mandel M. Influence of counterion exchange on the induced dipole moment and its relaxation for a rodlike polyion. Macromolecules 1981; 14:792–795.
19. Mandel M, Odijk T. Dielectric properties of polyelectrolyte solutions. Ann Rev Phys Chem 1984; 35:75–108.
20. McTague JP, Gibbs JH. Electric polarization of solutions of rodlike polyelectrolytes. J Chem Phys 1966; 44:4295–4301.
21. Oosawa F. Polyelectrolytes. New York: Marcel Dekker, 1971.
22. Schurr JM. Dielectric dispersion of linear polyelectrolytes. Biopolymers 1971; 10:1371–1375.
23. Minakata A. Dielectric dispersion of polyelectrolytes due to ion fluctuation. Ann NY Acad Sci 1977; 303:107–120.
24. Meyer PI, Vaughan WE. Dielectric behavior of linear polyelectrolytes. Biophys Chem 1980; 12:329–339.

25. Meyer PI, Wesenberg GE, Vaughan WE. Dielectric behavior of polyelectrolytes. II. The cylinder. Biophys Chem 1981; 13:265–273.
26. Wesenberg GE, Vaughan WE. Dielectric behavior of polyelectrolytes. III. The role of counterion interactions. Biophys Chem 1983; 18:381–390.
27. Altig JA, Wesenberg GE, Vaughan WE. Dielectric behavior of polyelectrolytes. IV. Electric polarizability of rigid biopolymers in electric fields. Biophys Chem 1986; 24:221–234.
28. Wesenberg GE, Vaughan WE. Theory of the transient electric birefringence of rod-like polyions: coupling of rotational and counterion dynamics. J Chem Phys 1987; 87:4240–4241.
29. Rau DC, Charney E. Polarization of the ion atmosphere of a charged cylinder. Biophys Chem 1981; 14:1–9.
30. Rau DC, Charney E. High-field saturation properties of the ion atmosphere polarization surrounding a rigid, immobile rod. Macromolecules 1983; 16: 1653–1661.
31. Hogan M, Dattagupta N, Crothers DM. Transient electric dichroism of rod-like DNA molecules. Proc Natl Acad Sci USA 1978; 75:195–199.
32. Hornick C, Weill G. Electrooptical study of the electric polarizability of rodlike fragments of DNA. Biopolymers 1971; 10:2345–2358.
33. Weill G, Hornick C. Electric polarizability of rigid polyelectrolytes. In: Sélény E, ed. Charged and Reactive Polymers, Volume I. Polyelectrolytes. Dordrecht: Reidel, 1974:277–284.
34. Manning GS. Limiting laws and counterion condensation in polyelectrolyte solutions. V. Further development of the chemical model. Biophys Chem 1978; 9:65–70.
35. Manning GS. Linear analysis of the polarization of macroions. J Chem Phys 1989; 90:5704–5710.
36. Manning GS. A condensed counterion theory for polarization of polyelectrolyte solutions in high fields. J Chem Phys 1993; 99:477–486.
37. Fixman M. Charged macromolecules in external fields. I. The sphere. J Chem Phys 1980; 72:5177–5186.
38. Fixman M. Charged macromolecules in external fields. 2. Preliminary remarks on the cylinder. Macromolecules 1980; 13:711–716.
39. Fixman M, Jagannathan S. Electrical and convective polarization of the cylindrical macroions. J Chem Phys 1981; 75:4048–4059.
40. Mohanty U, Zhao Y. Polarization of counterions in polyelectrolytes. Biopolymers 1995; 38:377–388.
41. Metropolis N, Rosenbluth AW, Rosenbluth MN, Teller AH, Teller E. Equation of state calculations by fast computing machines. J Chem Phys 1953; 21:1087–1092.
42. NG van Kampen. Stochastic Processes in Physics and Chemistry. Rev. enlarged ed. Amsterdam: North-Holland, 1992.
43. Kellogg OD. Foundations of Potential Theory. New York: Dover, 1954.
44. Manning GS. Limiting laws and counterion condensation in polyelectrolyte solutions I. Colligative properties. J Chem Phys 1969; 51:924–933.

45. Manning GS. Counterion condensation on ionic oligomers. Physica 1997; 247: 196–204.
46. Kikuchi K, Yoshioka K. Electric birefringence of potassium polystyrenesulfonate in aqueous solution as a function of molecular weight, concentration and field strength. J Phys Chem 1973; 77:2101–2107.
47. Kikuchi K, Yoshioka K. Electric birefringence of poly-L-lysine hydrobromide in methanol-water mixtures and helix-coil transition induced by high electric fields. Biopolymers 1973; 12:2667–2679.
48. Washizu H, Kikuchi K. Anisotropy of the electrical polarizability of a model DNA fragment in aqueous salt solution. Rep Progr Polym Phys Japan. In press.

This Page Intentionally Left Blank

9

Polyelectrolytes in Nonaqueous Solutions

MASANORI HARA Rutgers University, Piscataway, New Jersey

I. INTRODUCTION

A. Nonaqueous Solution

Polyelectrolyte solutions have been investigated much more extensively in aqueous solutions than in nonaqueous solutions [1–5]. Since many polyelectrolytes, usually with high charge density, are difficult to dissolve in polar organic solvents, and since there is a great interest in biological polyelectrolytes [6–8] such as proteins, nucleic acids, and polysaccharides in aqueous solutions, the aqueous solution behavior of polyelectrolytes has become a main subject of study.

However, the study of polyelectrolytes in nonaqueous solutions can offer insights into the understanding of the fundamentals of polyelectrolytes. For example, the electrostatic interaction energy varies inversely as the dielectric constant of the medium: water takes only the fixed value of 80, whereas the dielectric constant values of nonaqueous solutions can be altered over a wide range, from low to high values, by simply changing the organic solvents used. Therefore the effect of electrostatic interactions on the solution behavior of polyelectrolytes can be investigated, and thus polyelectrolyte solutions can be studied from a more general point of view in nonaqueous solutions.

In addition, the use of aqueous solutions may suffer from the following problems. As will be discussed later, light scattering, an important experimental method for polyelectrolyte solutions, is difficult to conduct for polyelectrolyte aqueous solutions [9]. This is partly because the refractive index of water is relatively small (1.33), and foreign particles, if present, can scatter light more strongly in water than in many organic solvents whose refractive indices are closer to that of dust particles [10], making data analysis less accurate (sometimes useless). Also, water is a rather complex solvent

[11] despite its easy accessibility; e.g., water structures, such as ice structure and iceberg structure, may have to be considered. Furthermore, water produces small ions due to autodissociation ($H_2O \rightarrow H^+ + OH^-$), which can work as simple salts and significantly affect the salt-free behavior of polyelectrolyte aqueous solutions. These problems may be avoided (or reduced) by using nonaqueous solutions.

This chapter deals with the solution behavior of polyelectrolytes in nonaqueous solutions. Firstly, emphasis will be placed on the role of the classical study of polyelectrolytes in nonaqueous solutions in establishing the fundamental concepts of polyelectrolyte solutions. A series of studies conducted by Fuoss's group in the late 1940s and early 1950s [12–22] demonstrated the ''general'' nature of polyelectrolyte behavior and made a significant contribution to establishing important concepts of polyelectrolyte solutions. The ''generality'' of the behavior was demonstrated by showing that the characteristic behavior of polyelectrolytes can be observed in various (polar) organic solvents, as well as in water. The basic concepts, such as counterion binding and chain expansion due to intramolecular electrostatic repulsion, were deduced from the observation of various properties of polyelectrolyte solutions, such as viscosity and conductance, as functions of electrostatic interactions that could be varied by changing the dielectric constant of the solvent. Later studies, however, have concentrated on aqueous solution behavior of polyelectrolytes. Once fundamental concepts were established, further studies, including more quantitative analysis, were centered on aqueous solutions in which most polyelectrolytes with high charge density could be easily dissolved and therefore more easily handled experimentally (this does not mean that the analysis is easy). However, more recently, when major questions have arisen as to the structure of polyelectrolyte aqueous solutions [3–5], polyelectrolyte nonaqueous solutions may again play an important role in providing useful information.

Secondly, a description will be given of more recent work on polyelectrolyte nonaqueous solutions, especially the work conducted in the past two decades on ionomer nonaqueous solutions [23]. Although the research on polyelectrolyte solution behavior has mostly focused on aqueous solution behavior, ion-containing polymers, called ionomers, have become the subject of solution study in the 1980s, when (partially) sulfonated polystyrene (PS) ionomer was made available [24]. This ionomer soon became popular as the subject of study of solution behavior, as it can be easily synthesized with varying values of molecular parameters, such as molecular weight, ion content, and counterion. Also, this ionomer can be made from standard types of polystyrene and can be easily dissolved in various nonaqueous solvents. Sulfonated PS ionomer is classified as a random ionomer, in which a small amount of ionic groups (up to 10–15 mol%) are located randomly along

the backbone chain, and thus can be considered as a weakly charged polyelectrolyte, when dissolved in polar solvents [25]. A major point is that the behavior of random ionomers in nonaqueous solutions is basically similar to that of polyelectrolytes in either aqueous or nonaqueous solutions; yet ionomers can be easily prepared and studied.

More recently, in addition to random ionomers, telechelic ionomers in which ionic groups are located only at the chain end(s) became available and were used for the study of polyelectrolyte behavior [26–29]. Discussion was made from the point of view that the behavior of telechelic ionomers in nonaqueous solutions is basically similar to that of polyelectrolytes in aqueous/nonaqueous solutions (including random ionomers in nonaqueous solutions). Also, the study of fundamental aspects of polyelectrolytes was made possible because of the simplicity of the structure of telechelic ionomers. For example, telechelic ionomers with only one ionic group at the chain end can be used to study the role of intermolecular interactions, since there is no intramolecular electrostatic interaction available for this type of ionomer [27]. Due to space limitations, this chapter will only cover polyelectrolyte behavior of random ionomers in polar solvents. Some results on telechelic ionomers can be found elsewhere [26–29].

B. Classical Work on Polyelectrolyte Behavior

Classical studies on polyelectrolyte behavior, which were conducted by using polyelectrolyte nonaqueous solutions, are briefly described here. These studies include conductance and viscosity behavior. More details on these subjects can be found in a previous review article [23].

1. Conductance

The conductance of polyelectrolyte solutions can readily be measured with a high degree of precision [22]. As a reference, the conductance behavior of simple electrolyte solutions is shown in Figure 1. Here, Λ is equivalent conductance defined by

$$\Lambda = \frac{1000\kappa}{c} \tag{1}$$

where κ is the observed specific conductance of the solution corrected for solvent conductance and c is normality (equivalents per liter). For polyelectrolytes, c is in monomoles per liter. In a polar solvent, few ions are aggregated and Λ approaches the limiting conductance, Λ_0, along the so-called Onsager tangent and shows little change with an increase in concentration (a small change is due to long-range electrostatic interactions among ions) (ex. iodic acid in water). The limiting law is written as

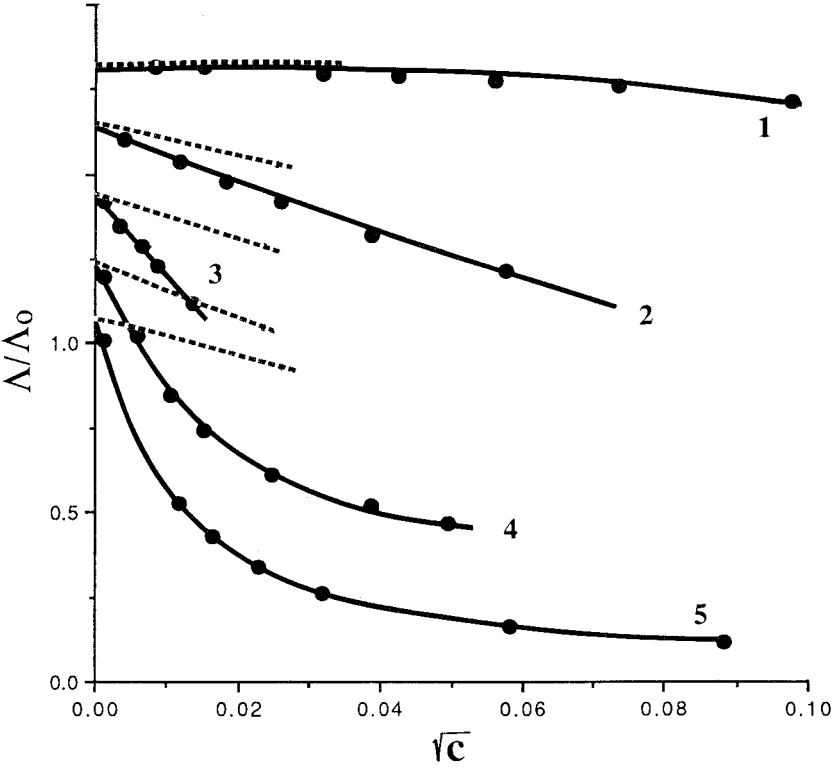

FIG. 1 Conductance curves for simple electrolytes: (1) iodic acid in water; (2) sodium bromate in ammonia; (3) sodium iodide in amyl alcohol; (4) tetraisoamylammonium nitrate in ethylene dichloride; (5) potassium amide in ammonia (different curves are displaced vertically). (From Ref. 31.)

$$\Lambda = \Lambda_0 - \alpha\sqrt{c} \tag{2}$$

where α is the Onsager coefficient [30,31]. In contrast to ions in polar solvents, ionic association, which increases with concentration, is expected in less polar solvents; and as a result the conductance decreases sharply with concentration (e.g., potassium amide in ammonia). To explain this behavior, the formation of ion pairs and even higher order aggregates, such as triplets and quadrupoles, have been considered to occur in low-polarity solvents [31].

A characteristic behavior of the conductance of polyelectrolytes is shown in Figure 2. These strong polyelectrolytes were made by quaternization with methyl bromide of the polyester obtained from condensation polymerization

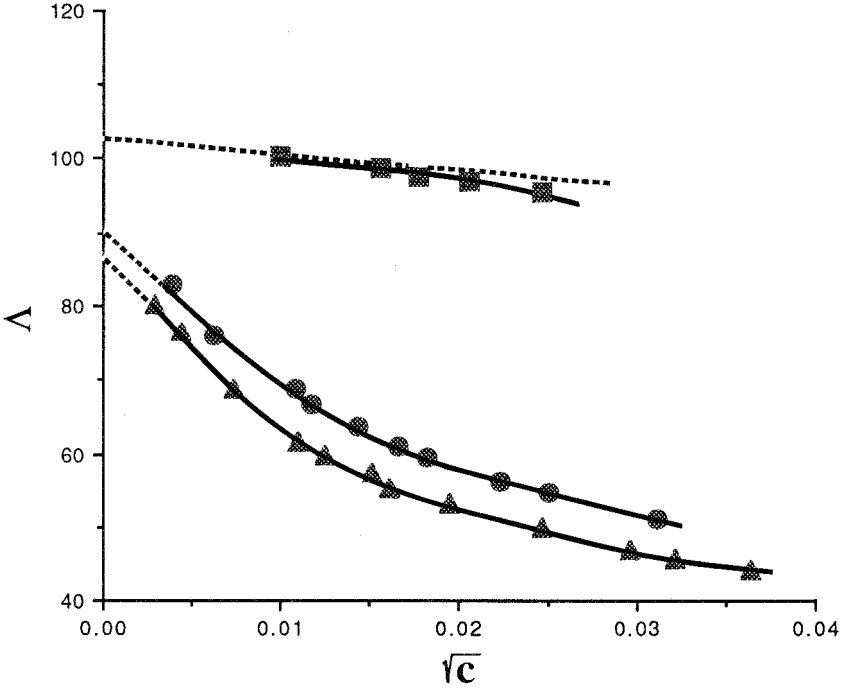

FIG. 2 Conductance curves for the addition product of methyl bromide to methyldiethanolamine (top curve) as well as for polyester-based polyelectrolyte with molecular weight of 2,700 and 3,500 (bottom curve) in methanol. (From Ref. 13.)

of methyldiethanolamine and succinic anhydryde [13]. The solvent used was a polar solvent, methanol ($\varepsilon = 32$), where ε is the dielectric constant of the solvent. Ordinary simple electrolytes, such as the addition product of methyl bromide to methyldiethanolamine, are only slightly associated in the solvent with high dielectric constant, as seen by the small change of conductance with concentration, which is similar to that of iodic acid in water (see Figure 1). In contrast, the conductance of polyelectrolytes decreases markedly with increasing concentration, somewhat similar to the conductance curve of simple strong electrolyte solutions in solvents with low dielectric constant, which indicates a high degree of association. This is taken as evidence of counterion binding (association), i.e., counterions are attracted by the strong electrostatic field of the polyions [22].

To show the same general pattern of conductance behavior of polyelectrolytes, conductance curves for another type of polyelectrolyte, made by quaternization with *n*-butyl bromide of poly(styrene-co-4-vinylpyridine) in

nitromethane (ε = 39.4) [17], is shown in Figure 3. A sharp drop in conductance is noted, which again is an indication of the association of bromide ions with the polycation, due to the high electrostatic field of the latter. It should also be noted that the higher the charge density of the polyelectrolytes, the lower the conductance of polyions. This is also an indication of counterion binding; i.e., the stronger electrostatic field created by high charge density polyions attracts more counterions.

2. Viscosity

In contrast to neutral polymer solutions, where reduced viscosity, η_{sp}/c, plotted against weight concentration (usually g/dL) shows a straight line (expressed by the Huggins equation) [32], the typical viscosity behavior of a polyelectrolyte solution is shown in Figure 4. This polyelectrolyte was made by quaternization of poly(styrene-co-4-vinylpyridine) with *n*-butyl bromide [16]. The solvents used were a nitromethane/dioxane mixture. Figure 4

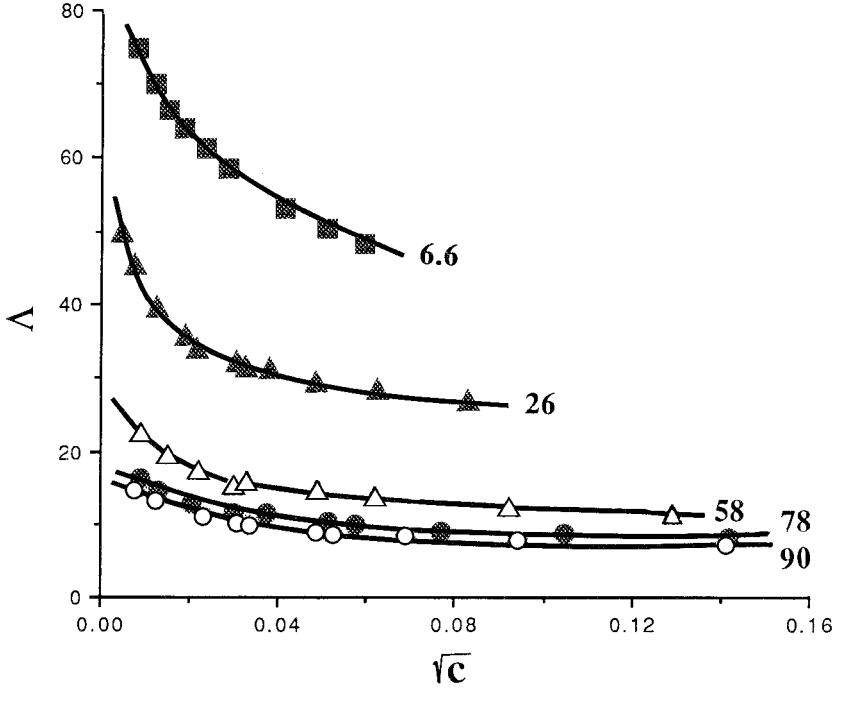

FIG. 3 Conductance curves for polyelectrolyte, poly(styrene-co-4-vinylpyridine) quaternized with *n*-butyl bromide in nitromethane (numbers indicate the ion content of the polyelectrolytes). (From Ref. 17.)

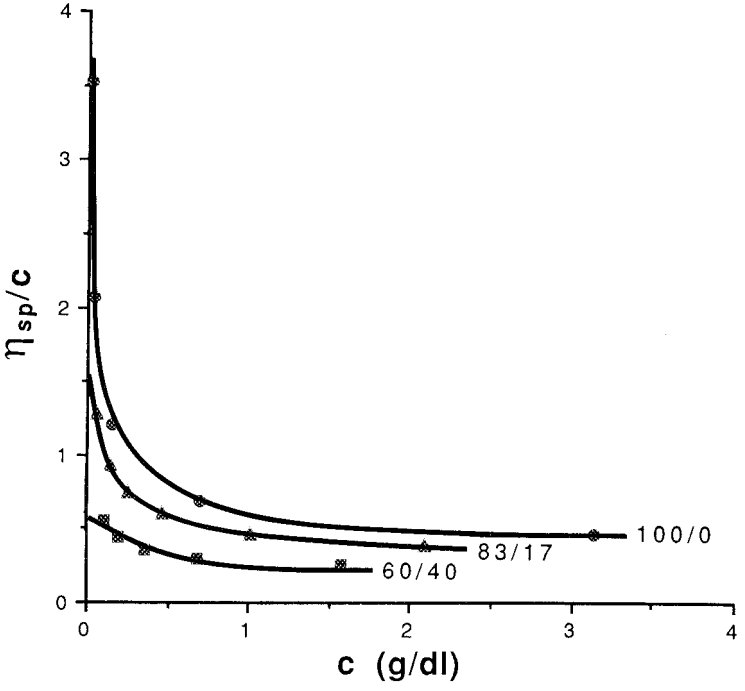

FIG. 4 Viscosity curves for polyelectrolyte, 4-vinylpyridine/styrene copolymers quaternized with *n*-butyl bromide, in nitromethane/dioxane mixture (numbers indicate weight ratio of nitromethane/dioxane). (From Ref. 16.)

shows the following characteristics: (1) a conventional η_{sp}/c vs. c plot is very strongly concave upward, in marked contrast to the linear plots obtained for neutral polymer solutions; (2) the higher the dielectric constant, the greater is the upturn of the viscosity curve at low polymer concentration; (3) the reduced viscosity of these polyelectrolytes in a polar solvent is much higher than that of the parent polymer.

Especially important is the first point, which is frequently used to check whether a polymer is ionic. This is a characteristic behavior of polyelectrolyte solutions since the early observation by Staudinger on sodium polyacrylate in water [33]. To explain this characteristic behavior, the following Fuoss equation was proposed [14]:

$$\frac{\eta_{sp}}{c} = \frac{A}{1 + B\sqrt{c}} + D \tag{3}$$

where c is weight concentration (g/dL) and A, B, and D are empirical con-

stants. Fuoss assumed that A was a reduced viscosity at infinite dilution (which corresponds to the intrinsic viscosity of the polyelectrolyte) and B was a measure of electrostatic interactions between polyions and counterions, since B is a constant of the $\sqrt{c}$ term and B/A increases with decreasing dielectric constant of the solvent.

As more viscosity data at very low concentrations were obtained, it was suggested that the interpretation given above seems to be too simple and needs to be modified; and some theoretical explanations have been proposed [34,35]. Nevertheless, the general nature of the characteristic viscosity behavior of polyelectrolyte solutions is evident, as similar behavior has been observed for a number of systems, both nonaqueous and aqueous. Table 1 summarizes the systems whose viscosity behavior in nonaqueous solutions has been reported.

Another characteristic type of viscosity behavior of polyelectrolytes is the effect of added simple salts on the viscosity [16]. The polyelectrolytes used were poly(styrene-co-4-vinylpyridine) (90/10) quaternized with *n*-butylbromide, and the solvent was nitromethane. The added salt was tetra-butylammonium bromide, which was easily dissolved in nitromethane. A small amount of added salt (10^{-3} M) produces a maximum in the viscosity curve (η_{sp}/c vs. c), and as more simple salts are added the reduced viscosity further reduces. When the added salt concentration is 0.1 N, the reduced viscosity is about the same as that of the parent polymer. This phenomenon is explained in terms of the screening effect by simple salts of electrostatic interactions among fixed ions [1,2].

II. POLYELECTROLYTE BEHAVIOR OF IONOMERS (WEAKLY CHARGED POLYELECTROLYTES) IN POLAR NONAQUEOUS SOLUTIONS

A. Ionomer Solutions

So far, the classical work on polyelectrolyte nonaqueous solutions conducted during the 1950s has been described. Here we will describe more recent work on polyelectrolyte nonaqueous solutions, conducted during the 1980s and 1990s, in particular the work on the solution properties of ionomers in a polar solvent, which may be considered as weakly charged polyelectrolytes.

The term ionomer was first introduced in the early 1960s, when DuPont developed Surlyn® resins [36], salt forms (Na and Zn) of the copolymers of ethylene and a small amount (several mole percent) of methacrylic acid. Initially, Surlyn resin that was based on polyethylene was called an ionomer, but later all polymers that have a small amount of ionic groups (up to 10–

TABLE 1 Viscosity Behavior of Polyelectrolyte Nonaqueous Solutions

Polyelectrolyte	Solvent	Reference
Poly(styrene-co-4-vinylpyridine) (quaternized with *n*-butyl bromide)	Nitromethane, nitromethane-dioxane	16
Poly(4-vinylpyridine) (quaternized with *n*-butyl bromide)	Ethanol-water	15
Poly(4-vinylpyridine) (with hydrochloride)	Methanol	19
Poly(2-vinylpyridine) (quaternized with methyl bromide and butyl bromide)	Methanol, ethanol, nitromethane	20
Polyester (made of succinic anhydride and methyldiethanolamine) (quaternized with methyl bromide)	Methanol	21

15 mol%) along nonionic backbone chains have been generally called ionomers [37].

The structure of the ions (either in bulk or in solution) can be understood by considering a simple system, a pair of monovalent ions in the medium whose dielectric constant is ε. When the ions are separated by a contact distance of a, the electrostatic potential energy (E) of the pair is

$$E = -\frac{1}{4\pi\varepsilon_0}\frac{e^2}{\varepsilon a} \tag{4}$$

where e is the charge of the monovalent ion. When this energy is smaller than the thermal energy (kT), positive and negative ions are separated (dissociated) and no ion pairs are formed. This is a basic structure of small ions and of polyelectrolytes in polar solvents (although, in the case of the latter, many counterions are attracted to polyions due to the strong electrostatic field of the polyion; i.e., counterion binding). In contrast, as the polarity of the medium decreases and the electrostatic energy becomes comparable to and surpasses the thermal energy, the formation of ion pairs becomes dominant. An ion pair is considered to be a strong ionic dipole, so ion pairs can attract each other at higher concentration, forming ionic aggregates of higher degree. This is a basic structure of aggregates of small ions at high concentration and of aggregates of polyelectrolytes in solvents with low polarity (since polyelectrolytes with high charge density tend to be insoluble, these polyelectrolytes usually have low charge density to be soluble, like ionomers), as well as ionomers in the solid state. In the solid, it is envisaged that ionic groups are distributed in the medium made of backbone chains that are usually nonpolar (e.g., $\varepsilon = 2.5$ for polyethylene). Despite the sim-

plicity of the system discussed here, it is sufficient to understand the fundamental aspects of aggregation of ionic groups in solution as well as in bulk.

In contrast to extensive studies on ionomer solids [37–44], it was not until the early 1980s, after the synthesis of sulfonated polystyrene ionomers was reported by Lundberg's group at Exxon [24,45], that the solution behavior of ionomers began to be actively investigated. The characteristics of sulfonated polystyrene ionomer are: (1) in contrast to the ionomers used previously, such as the ionomers based on polyethylene, polybutadiene, and polytetrafluoroethylene, this ionomer, based on polystyrene, can be dissolved in various organic solvents, making a broad range of solution studies possible; (2) the synthesis of this polymer is relatively easy, and the number of ionic groups can be readily altered; (3) the reaction to modify PS is mild, so that molecular weight and molecular weight distribution are little altered; (4) as a parent polymer of the ionomer, standard PS with various molecular weights and sharp molecular weight distribution can be used, which is important in studying solution behavior of polymers. Actually, partially sulfonated PS ionomers are used overwhelmingly for studying behavior [23].

Solution behavior of ionomers can be divided into two types, primarily depending on the polarity of the solvent [46,47]. One is polyelectrolyte behavior due to the dissociation of counterions in polar solvents (e.g., DMF), and another is association behavior due to the formation of ion pairs and even higher order aggregates in less polar solvents (e.g., THF). Table 2 shows the solvents frequently used for the study of ionomer solutions, as well as their dielectric constants. As the dielectric constant decreases, the degree of counterion binding and also ion pair formation changes (increases) gradually, and so does the solution behavior. In this chapter, only the polyelectrolyte behavior of ionomers in a polar solvent is described. Some brief

TABLE 2 Organic Solvents Frequently Used for Ionomer Solutions

Solvent	Dielectric constant
(Polyethylene)[a]	2.5
Toluene	2.4
Tetrahydrofuran (THF)	7.6
Dimethylformamide (DMF)	37
Dimethyl sulfoxide (DMSO)	47
(Water)[a]	80

[a]Shown for comparison.

reviews on the aggregation behavior can be found elsewhere [23,48]. Since a detailed description was given of viscosity and low-angle light scattering results of ionomer solutions in a previous review article [23], in this chapter emphasis will be placed on more recent results involving angular light scattering and dynamic light scattering.

Ionomers that are widely used for solution studies can be classified according to their chain structure [23]. According to the site where ionic groups are located, ionomers are divided into two types: random ionomers *and telechelic ionomers*. In random ionomers, ionic groups are distributed randomly along the backbone chains, so interionic distance cannot be specified. In contrast, in telechelic ionomers, ionic groups are located only at the chain ends. Therefore if the molecular weight distribution of the backbone chain is sharp, the interionic distance measured along the chain (i.e., the contour length) is easily determined.

B. Viscosity and Characteristic Polyelectrolyte Behavior

Viscosity measurements are widely used to study the characteristic behavior of polyelectrolyte solutions, and also for the study of ionomer solutions. Figure 5 shows typical viscosity behavior of ionomers in nonaqueous solution [46,49]. The random ionomer used was the sodium salt of partially sulfonated polystyrene with various ion contents, and the solvent used was a polar solvent DMF ($\varepsilon = 37$). The ion content is expressed in mol%, i.e., a 5.6 mol% sample, for example, has 5.6 sodium sulfonate groups per 100 styrene residues on average. The following characteristics are observed: (1) the reduced viscosity, η_{sp}/c, increases markedly with decreasing polymer (ionomer) concentration; (2) the higher the ion content, the greater the upturn of the viscosity curve at low polymer concentration; (3) even for the ionomer sample with very low ion content (e.g., 0.94 mol%), a marked increase in reduced viscosity at low polymer concentration is observed. The first two points are commonly observed for polyelectrolyte aqueous or nonaqueous solutions. The last point, however, is rarely seen, since significant reduction of the charge density of polyelectrolytes with high charge density by controlling the degree of neutralization [e.g., partially neutralized poly(acrylic acid)] in salt-free solution is quite difficult. Therefore ionomers are especially useful to study the effect of a small number of charges on the salt-free polyelectrolyte behavior.

As is the case of polyelectrolyte aqueous solutions, the viscosity data from ionomer solutions apparently follow the Fuoss equation. A later study [50] has shown that the Fuoss equation is basically an empirical one and that the physical meaning of the constants A and B is not as clear as origi-

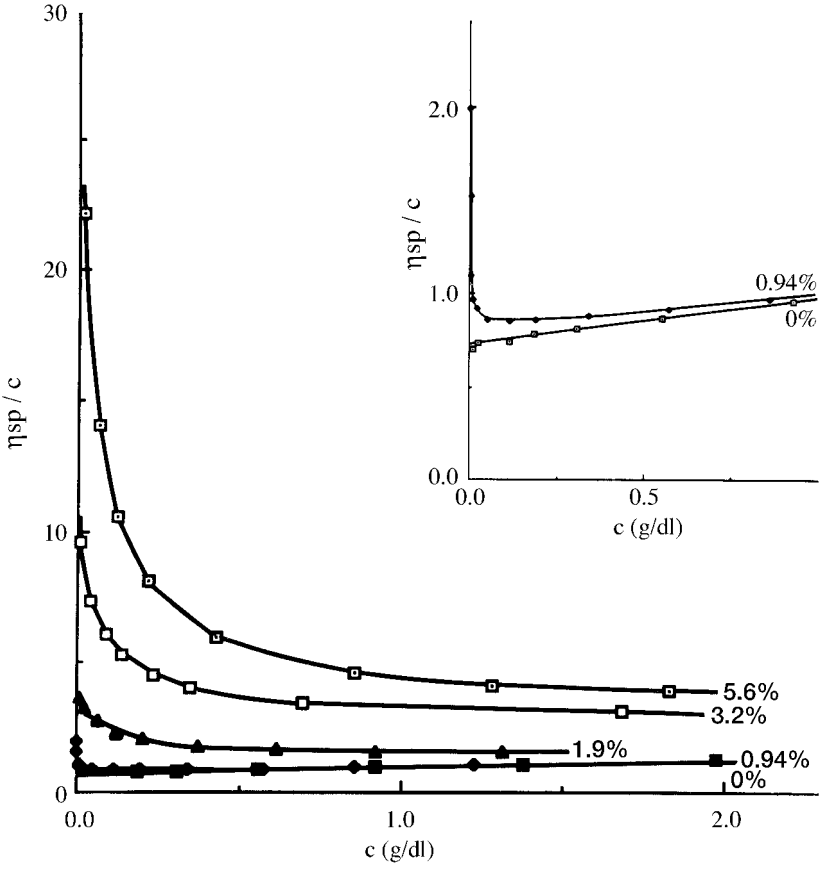

FIG. 5 Viscosity curves for sulfonated polystyrene ionomers (MW = 4.0×10^5; Na salt) with various ion contents in DMF. (From Ref. 49.)

nally stated by Fuoss [14]. Similar results were also reported by Kim and Pfeiffer [51] for sulfonated PS ionomers and discussed in terms of recent theories of polyelectrolyte viscosity [34,35]. Nevertheless, it is clear that (random) ionomers in polar solvents basically behave in a similar fashion to polyelectrolyte aqueous solutions.

Rochas et al. [52] showed that the method of isoionic dilution can also be applied for an ionomer solution, as is the case for polyelectrolyte aqueous solutions. In this treatment, originally proposed by Pals and Hermans [53], it is assumed that the size of the polyion can be kept constant by keeping the total ionic concentration (C_T) constant, where

$$C_T = \phi_p C_p + C_S \tag{5}$$

and C_p and C_s are concentration (eq/L) of polyion and added salt, and ϕ_p is the fraction of free counterions. A linear plot of η_{sp}/c vs. c at various total ionic concentration can be obtained by using isoionic dilution. However, since this method is empirical and the value of ϕ_p is not necessarily consistent with the values obtained from other methods, as is demonstrated for polyelectrolyte aqueous solutions [54], it seems that the physical meaning is not as significant as originally claimed [53]. Nevertheless, it is clear that the treatment of ionomer solution in terms of isoionic dilution can be done as is the case for polyelectrolyte aqueous solutions.

Another characteristic viscosity behavior of polyelectrolyte solution, viz., the effect of added salts, has been reported for ionomer solutions [55]. The reduced viscosity of sulfonated PS (Li salt) in DMF increases markedly with decreasing polymer concentration in the absence of added salt, LiCl. However, as the concentration of LiCl increases, the reduced viscosity significantly decreases, then a maximum appears in the viscosity curve, and finally straight lines are obtained. The last behavior is characteristic of neutral polymer solutions. Table 3 summarizes ionomer nonaqueous solutions whose viscosity behavior has been reported. Those results have demonstrated that the viscosity behavior of random ionomers is basically similar to that of polyelectrolyte aqueous solutions.

Some additional information obtained because of the use of ionomers should be stressed. This is the observation that even ionomers with very small ion content produce characteristic polyelectrolyte behavior. For example, it was shown that sulfonated PS ionomers having only 0.9 mol% ion

TABLE 3 Viscosity Behavior of Random Ionomers in Polar Solvent

Ionomer	Solvent	Reference
Poly(styrene-co-methacrylic acid) (Na, Li, K, Cs, Ca salts)	DMF	47, 99
Poly(acrylonitrile-co-methallylsulfonate) (Na salt)	DMF	52
Partially sulfonated polystyrene (Na, Li, K, Cs, Ca, Zn salts)	DMF, DMSO, 2-methoxyethanol	46, 49, 51, 99, 103
Poly(*n*-butyl methacrylate-co-methacrylic acid) (K salt)	DMF	104
Perfluorosulfonated ionomer	Methanol, ethanol, dimethylacetamide	105

content produced characteristic polyelectrolyte behavior in viscosity (see Figure 5). Characteristic polyelectrolyte behavior is also observed for this ionomer in small-angle light scattering measurements [56,57]. The number of charges per chain can be reduced not only by decreasing the ion content but also by decreasing the chain length (molecular weight). It has been demonstrated that even the (random) ionomer with 1.1 ionic groups per chain on average shows the characteristic viscosity behavior of polyelectrolytes [49]. These results suggest that chain expansion due to intramolecular electrostatic repulsion may not necessarily be essential to causing a marked increase in viscosity at low polymer concentration, since intramolecular repulsion is negligibly small for these random ionomers. This result appears contradictory to the conventional explanation, i.e., chain expansion is due to mutual repulsion [1,2]; but it is consistent with a more recent theory of polyelectrolyte viscosity, which considers intermolecular interactions as a major factor [35]. There is a possibility that some polymer chains have a larger number of ionic groups than other chains due to the random distribution of ionic groups in random ionomers, which would lead to some chain expansion due to mutual repulsion of like charges and an increase in viscosity. To study this point further, experiments on telechelic ionomers with only one charge located at the chain end were conducted [26,27]: these results did confirm the conclusion that intramolecular electrostatic interactions are not necessary conditions for producing the up-turn in the viscosity curve at low polymer concentration.

C. Static Light Scattering and Intermolecular Interactions

Light scattering is a widely used technique for investigating the solution behavior of neutral polymers [58,59]. By contrast, light scattering studies of salt-free polyelectrolyte solutions are rather limited [9,60]. One of the reasons is the difficulty in obtaining reliable data for salt-free polyelectrolyte solutions, because the scattered intensity from a solution of polyelectrolytes with high charge density is very small due to the strong destructive interference of scattered light [9]. In addition, removal of foreign particles (dust) is more difficult from polyelectrolyte aqueous solutions than from nonaqueous solutions, and the effect of foreign particles, if present, is more serious for aqueous solutions than for nonaqueous solutions [23].

It has been suggested, for these reasons, that ionomers dissolved in nonaqueous solutions can be used to improve the quality of light scattering data [23]. The results obtained so far have indicated that this is indeed the case: the scattered intensity of light from an ionomer nonaqueous solution is much stronger than that from a polyelectrolyte aqueous solution, since the number

of charges on ionomer molecules, and thus the destructive interference, is much smaller for ionomer solutions than for polyelectrolyte solutions; for example, the excess scattered intensity, R_θ, from an ionomer nonaqueous solution (e.g., sulfonated PS ionomer in DMF) is $(1-20) \times 10^{-6}$ cm^{-1} [57], while that from a polyelectrolyte aqueous solution (e.g., sodium poly(methacrylate) [61] or sodium poly(styrenesulfonate) [62]) is $(0.1-1) \times 10^{-6}$ cm^{-1}. Also, dust particles from an ionomer solution can be removed more effectively using membrane filters than from polyelectrolyte solutions [63]. Optical clarification from aqueous solution sometimes needs both filtration and ultracentrifugation. It is the experience of the author, based on light scattering experiments on both polyelectrolyte and ionomer solutions, that the salt-free ionomer nonaqueous solution produces more stable and reliable data with excellent reproducibility than salt-free polyelectrolyte aqueous solutions; yet the basic behavior is the same. Thus we can investigate polyelectrolyte behavior by using ionomer solutions.

Low-angle and angular measurements both show characteristic behavior. Figure 6 shows the low-angle light scattering results for sulfonated PS ionomer with various ion contents in DMF: the scattering data, from angular measurements, extrapolated to zero angle, are also shown in addition to low-

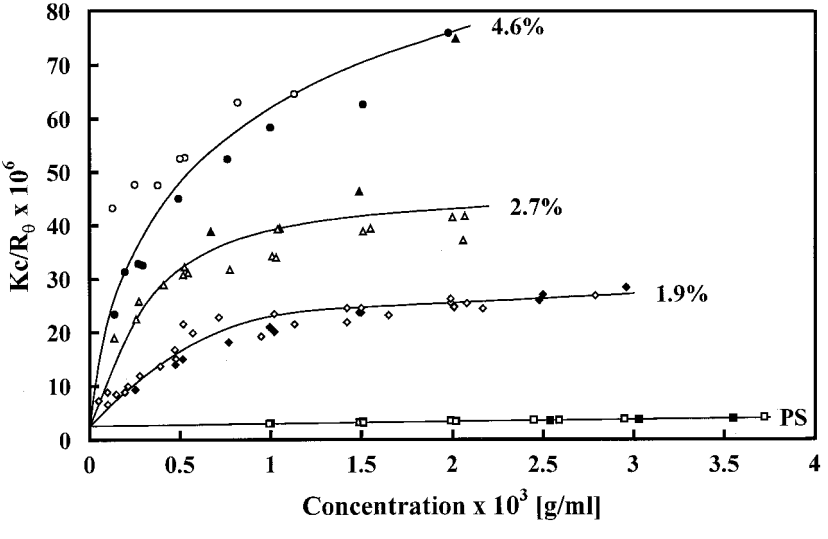

FIG. 6 Reciprocal reduced scattered intensity at zero angle, Kc/R_0, for sulfonated PS ionomer with various ion contents in DMF as well as PS: closed symbols, low-angle light scattering data; open symbols, angular light scattering data extrapolated to zero angle. (From Ref. 63.)

angle scattering data. Results for the precursor polymer, PS, are included for comparison. It is seen that the reciprocal reduced scattered intensity at zero angle, Kc/R_0, from ionomer solutions rises steeply from the intercept, bends over, and becomes nearly horizontal at higher polymer concentration. Here K is an optical constant for static scattering. Furthermore, the curves for ionomer samples with different ion contents seem to converge to the same intercept at zero concentration, corresponding to the inverse of the weight-average molecular weight of the polymer. This is typical for ionomers in polar solvents [23,56], and similar characteristic behavior was reported for salt-free polyelectrolyte aqueous solutions, including bovine serum albumin [64], sodium poly(methyl methacrylate) [61], and carboxymethylcellulose [65]. This behavior is understood from the following equation, derived by using fluctuation theory [66]:

$$\frac{Kc}{R_0} = \frac{1}{RT}\left(\frac{\partial c}{\partial \Pi}\right)^{-1} \tag{6}$$

where $\partial c/\partial \Pi$ is the osmotic compressibility. Since the osmotic compressibility, $\partial c/\partial \Pi$, is lower for an ionomer solution than for a PS solution due to increased repulsion between molecules, Kc/R_0 increases substantially. This is also understood from the equation [63]

$$\frac{Kc}{R_0} = \frac{1}{M}\left(1 + \frac{N}{V} m_0\right) \tag{7}$$

where N is the number of molecules in the scattering volume, V. Here, m_0 ($m_0 = \int_0^\infty \{1 - e^{-\psi(r)/kT}\}\, dV$) is considered to be the (intermolecular) excluded volume of the scatterer [66,67], where $\psi(r)$ is the interparticle potential, which is a function of polyion concentration. For the same reason as above, the intermolecular excluded volume term, Nm_0/V, is higher for ionomer solutions than for PS solutions; thus the scattering becomes weaker, leading to higher Kc/R_0 values. Also, as seen in Figure 6, as the ion content increases, the scattered intensity decreases; therefore the Kc/R_0 value increases markedly. It may be stressed that this clearly indicates why polyelectrolyte solutions are difficult to study: i.e., increasing ion content to nearly 100 mol% would lead to a very high Kc/R_0 value, or very small scattering power. It should be added that even ionomers with a very small number of charges (e.g., 0.94 mol%) show similar polyelectrolyte behavior observed by low-angle scattering [56,57], as has been noted in viscosity measurements. It should also be added that the second virial coefficient, A_2, of PS solution in DMF is 1.8×10^{-4} (mol·cm^3/g^2), which can be compared with the value obtained in toluene, a good solvent for PS ($A_2 = 4.6 \times 10^{-4}$). Thus DMF is considered to be a rather good solvent for the backbone chains of the ion-

omer; a marked contrast to polyelectrolyte aqueous solutions, where the solvent, water, is usually a poor solvent for the backbone.

Angular light scattering data also show a characteristic polyelectrolyte behavior, as seen in Figure 7 [63]. These data were collected by seven independent experiments using different stock solutions; thus the reproducibility of the data, especially that of the low-concentration range, is very good. This is one of the advantages of using ionomer nonaqueous solutions, as already mentioned. At low ionomer concentrations, ''abnormal'' Zimm plots, showing negative slopes in reciprocal reduced scattered intensity, Kc/R_θ, vs. q^2 curves, are observed. Here q is the magnitude of the scattering vector defined by $q = (4\pi n/\lambda_0)\sin(\theta/2)$, where n is the refractive index of the solution, λ_0 is the wavelength of the incident light in vacuo, and θ is a scattering angle. As the polymer concentration increases, the slope becomes less negative and finally becomes positive. By contrast, a typical ''normal'' Zimm plot is obtained for PS in DMF [63]: all the slopes of angular-dependent curves are positive and tend to decrease slightly with increasing polymer concentration, as explained by Flory and Bueche [68].

The characteristic scattering behavior of ionomer solutions shown in Figure 7 can be understood by using the following equation for the excess scattering from a solution of strongly interacting polymers [63]:

$$\frac{Kc}{R_\theta} = \left(\frac{Kc}{R_0}\right)\left[1 + q^2\left\{\frac{R_g^2}{3} - \frac{\xi^2}{6}\left(1 - \frac{R_0}{MKc}\right)\right\} - C'q^4\right] \tag{8}$$

where R_g is the radius of gyration of polymer chains and ξ^2 is the mean-square radius of the excluded volume, defined by

$$\xi^2 \equiv \frac{\int_0^\infty \{1 - \exp[-4(r)/kT]\}r^2\, dv}{\int_0^\infty \{1 - \exp[-4(r)/kT]\}\, dv} \tag{9}$$

The value of ξ can be a measure of the dimension of the region around a scattering particle, unoccupied by other particles. It should be stressed that in this derivation triplet terms are considered at least to a first approximation in addition to pair terms by using the Born–Green method [69,70]. More general relations to accommodate many-body interactions can be obtained by using the Percus–Yevick equations [71,72]. However, this treatment is sufficient for our discussion. These equations can also be used for analysis of light scattering data for polyelectrolyte aqueous solutions. Because Kc/R_θ is expressed in a series of q^2, the following simple quadratic formula in q^2 may be used for discussion:

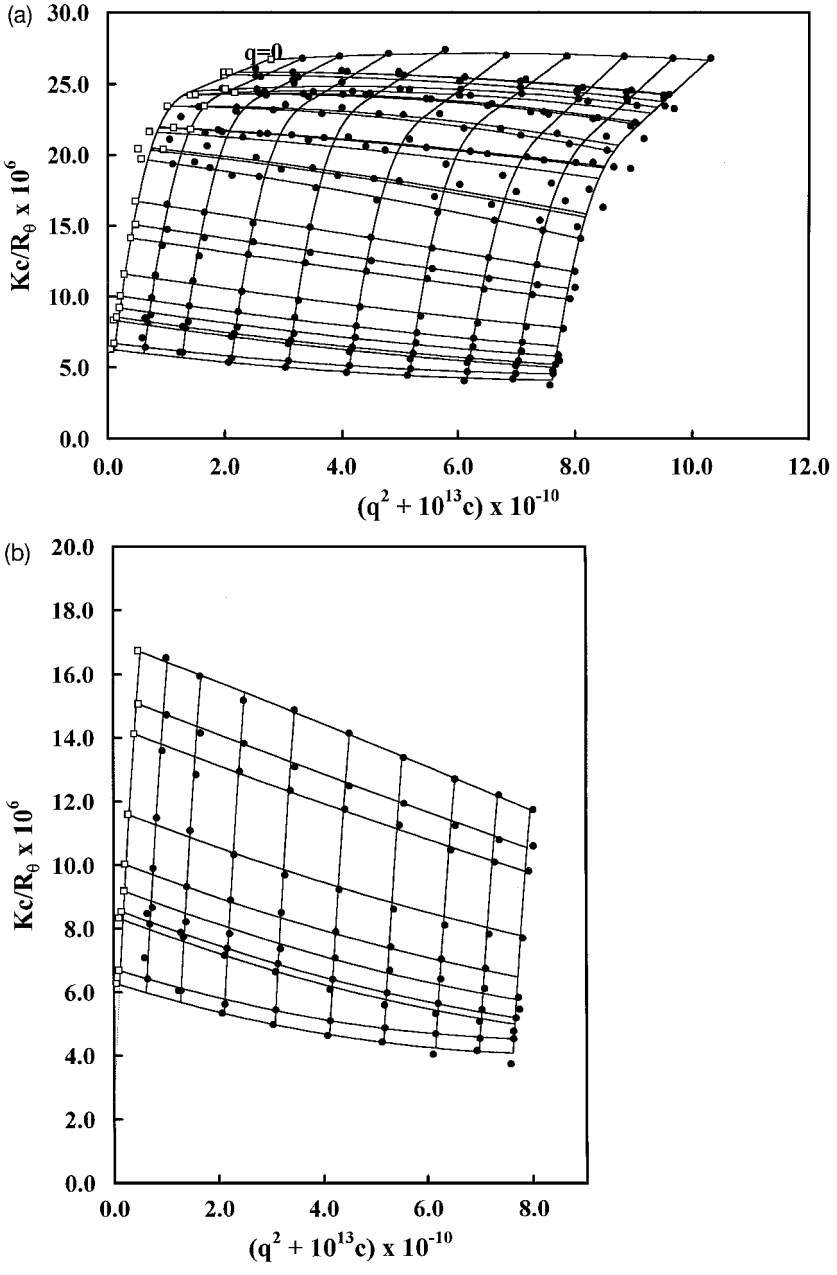

FIG. 7 (a) Overall Zimm plot of sulfonated PS ionomer (ion content: 1.9 mol%) in DMF. (b) Zimm plot at low concentrations of sulfonated PS ionomer (ion content: 1.9 mol%) in DMF: closed symbols, experimental values; open symbols, extrapolated values. (From Ref. 63.)

$$\frac{Kc}{R_\theta} = b_0 + b_1 q^2 + b_2 q^4 \tag{10}$$

where the intercept, $b_0 = Kc/R_0$, is the reciprocal scattered intensity at zero angle.

The initial slope normalized against the intercept, b_1/b_0, which is considered to be $R_{g,app}^2/3$, where $R_{g,app}$ is the apparent radius of gyration, is given by

$$\frac{b_1}{b_0} \equiv \frac{R_{g,app}^2}{3} = \frac{R_g^2}{3} - \frac{\xi^2}{6}\left(1 - \frac{R_0}{MKc}\right) \tag{11}$$

This equation indicates that the first term comes from the intraparticle interference of light and the second term comes from the interparticle interference. In other words, the initial slope of the angular-dependent curve in a Zimm plot is determined by two competing terms: one is the first term including R_g^2 that reflects the radius of gyration of the polyion chains (therefore a positive contribution), and the other is the second term including ξ^2 that reflects the intermolecular excluded volume (therefore a negative contribution). At low polymer concentration, the second term dominates due to a large intermolecular excluded volume arising from large electrostatic repulsive interactions, leading to negative slopes. Usually negative slopes are not seen for neutral polymer solutions, since the second term is not large enough to surpass the first. As the ionomer concentration increases, the total ionic strength increases, and thus electrostatic interactions reach to only a shorter range, leading to smaller excluded volume and less negative slopes.

The change in slope as a function of ionomer concentration is seen in more detail in Figure 8: at low concentrations, the value is negative, reflecting the dominant excluded volume term. As the ionomer concentration increases, the electrostatic excluded volume ξ decreases significantly, while $(1 - R_0/MKc)$ in Eq. 11 increases slightly (see Figure 6), leading to a small negative value. The slope is still negative, because the radius of gyration of ionomer chains is much smaller than the excluded volume term when the ionomer concentration is low. This is in contrast to the case of neutral polymer solutions where the intermolecular interactions are short range (e.g., van der Waals interactions); thus, the excluded volume is of the same order of R_g^3. Hence ξ as well as $(1 - R_0/MKc)$ are small, leading to a positive slope. However, even in neutral polymer solutions, the presence of the excluded volume term can be seen in the scattering data: the slope of Kc/R_θ vs. q^2 plots decreases with increasing polymer concentration [68]. This is because as the concentration is increased, $(1 - R_0/MKc)$ increases, and thereby the importance of the $-\xi^2/6(1 - R_0/MKc)$ term also increases (the ξ value is considered to be roughly constant for neutral polymers). More details about

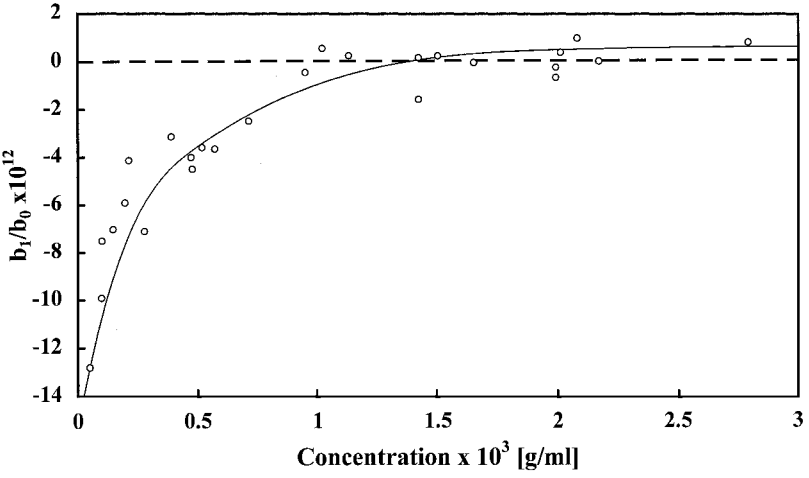

FIG. 8 Normalized initial slope in Kc/R_θ vs. q^2 curves, b_1/b_0, against ionomer concentration for sulfonated PS ionomer (ion content: 1.9 mol%) in DMF. (From Ref. 63.)

the derivation of the equations and the analysis of angular scattering data can be found in the original article [63].

As concentration is increased, the slopes of angular-dependent curves become less negative and eventually become positive, as well as somewhat curved at lower angles, indicating that the first term in Eq. 8, reflecting the radius of gyration of the polymer, dominates. While the *apparent* radius of gyration of the 1.9 mol% ionomer is comparable to that of the unmodified PS (239 Å) over the concentration range studied, the higher ion content samples (for example, 2.7 mol% sample) show larger values [63]; for example, the value of apparent radius of gyration for these samples is over 300 Å. However, the true radius of gyration is even larger than the apparent radius of gyration because of the excluded volume term (i.e., the second term) in Eq. 11. In addition, the appearance of the curvature at small angles suggests the existence of large-scale "heterogeneities" in the solution, as observed for a solution of heterogeneous samples (in terms of size) [58].

Another characteristic behavior is the effect of added salt on the light scattering behavior of ionomer solution [55]. The scattered intensity increases significantly as a result of the addition of small salts (0.1 LiCl), and the scattering curve becomes normal. This is again due to the screening effect of simple salts against polyion charges, leading to the neutral polymer behavior of the ionomer, which also confirms our observation that the char-

acteristic light scattering behavior observed is due to electrostatic interactions.

D. Dynamic Light Scattering and Molecular Motion

In contrast to the behavior of polyelectrolyte solutions with (a large amount of) added salt, which is relatively well understood by using excluded volume theory [9,66] and scaling theory [73,74], the behavior of polyelectrolytes in salt-free solutions (and in solutions with a very small amount of added salt) is poorly understood [73]. There are still controversies about the causes of the characteristic behavior of salt-free solutions. For example, dynamic light scattering has revealed the ''peculiar'' behavior of salt-free polyelectrolyte solutions. It is reported that the effective diffusion coefficient of polyelectrolyte solutions drops precipitously below a certain salt concentration [75]. This so-called ordinary–extraordinary transition is now understood in terms of the existence of two diffusion modes, a fast mode and a slow mode. The slow mode dominates at low salt concentrations below a critical salt concentration, which includes salt-free solutions as the extreme case [76–78]. However, there remains disagreement regarding the interpretation of the two modes, especially that of the slow mode, in the decay of the autocorrelation function of light scattered from salt-free polyelectrolyte solutions [76–81]. These decay modes in the autocorrelation function are resolved by an inverse Laplace transform and are subject to debate partly due to the inherent difficulty of the problem, particularly when one considers the weak scattering of salt-free polyelectrolyte aqueous solutions and the difficulty in optically clarifying such solutions, as described above.

Here we describe dynamic light scattering results on ionomers in a salt-free, nonaqueous, polar solvent; such a solution has a stronger scattering power and is easier to handle than polyelectrolytes in water, as already discussed in the Static Scattering section.

Dynamic scattering behavior from ionomer solutions was initially investigated and analyzed with the method of cumulants [82,83]. Although this method can give information on the diffusion coefficients, provided that the modes with different diffusion coefficients are well separated and proper use of the sampling time is made, we can obtain more detailed information by using Laplace inversion through analysis by CONTIN, with a large time range [84–86]. In fact, it has been demonstrated that by using sample times in a relatively narrow range, the cumulant analysis can lead to apparently contradictory conclusions for ionomer solutions [87]. Therefore we will describe the results of dynamic scattering on ionomer solutions, conducted over a broad range of delay times, and the decay rate spectra obtained by CONTIN analysis.

Dynamic light scattering experiments were conducted for sulfonated PS ionomers in DMF [87]. CONTIN analysis of the decay rate generally indicates the existence of *two decay modes*. Both modes have a q^2 dependence and therefore are diffusive processes. This is similar to that observed for salt-free polyelectrolytes in aqueous solution [76–79].

Figure 9 shows a typical distribution of the decay rate for the ionomer as well as for the precursor polymer, PS, analyzed using CONTIN [84–86]. The spectrum is generally described by a distribution function (spectrum) of decay rate, Γ, $G(\Gamma, q)$, defined by

$$g^{(1)}(q, t) = \int_0^\infty G(\Gamma, q)\exp(-\Gamma t)\, d\Gamma \tag{12}$$

where $g^{(1)}(q, t)$ is the normalized electric field autocorrelation function at

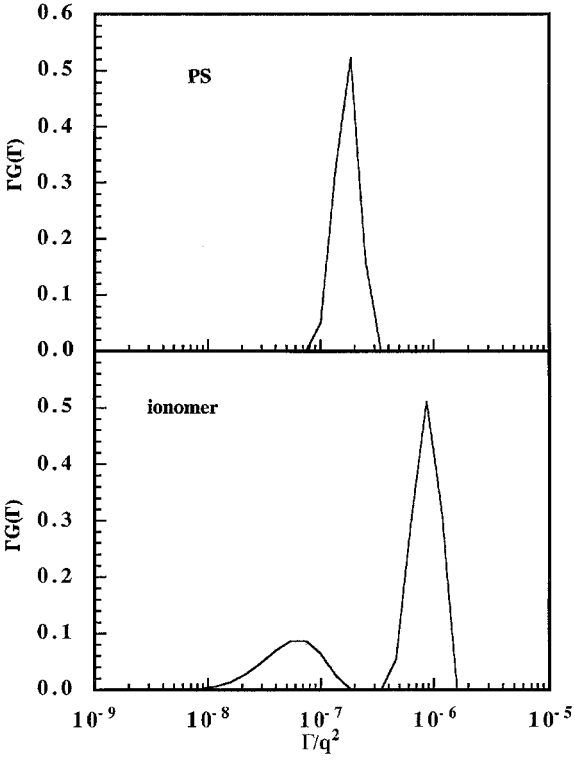

FIG. 9 Spectrum of decay rate, Γ, normalized by q^2, of dynamic light scattering data, analyzed by CONTIN ($\theta = 60°$), for sulfonated PS ionomer as well as for PS in DMF. (From Ref. 87.)

delay time t and scattering vector q. Since we usually plot $\log(\Gamma/q^2)$ as the abscissa, Eq. 12 can be rewritten as

$$g^{(1)}(q, t) = \int_{-\infty}^{\infty} \Gamma G(\Gamma, q)\exp(-\Gamma t)\, d\, \log(\Gamma/q^2) \tag{13}$$

Equation 13 indicates that when $\Gamma G(\Gamma, q)$ is plotted as the ordinate and $\log(\Gamma/q^2)$ is plotted as the abscissa, the area under each peak corresponds to the weight of each peak. It should be added that the Laplace inversion is a delicate process due to ill-conditioned problems involved, so that care must be exercised in extracting information [88].

It is obvious from Figure 9 that the simple diffusion mode of PS spreads into two modes (a fast mode and a slow mode) by introducing a small amount of ionic groups into PS. Figure 10 shows the distribution of the decay rate at different concentrations. At least two distinct peaks are seen over a wide range of time scales for the ionomer solution, in contrast to the PS solution, which shows only a single peak. The average decay rate, $\langle\Gamma\rangle$,

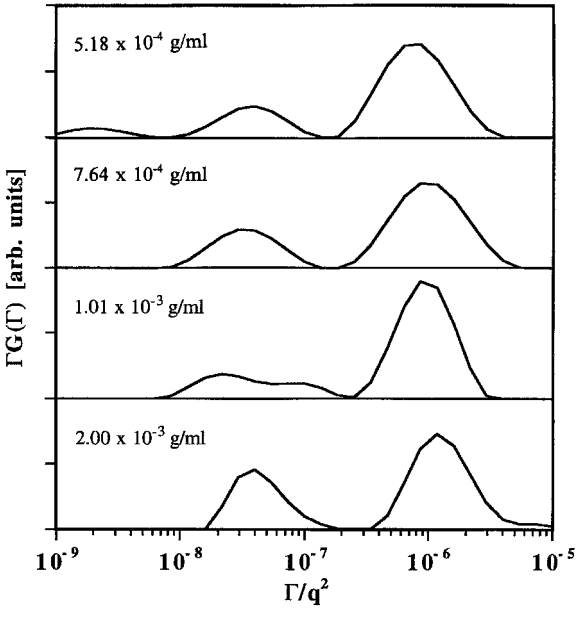

FIG. 10 Spectrum of decay rate, Γ, normalized by q^2, of dynamic light scattering data, analyzed by CONTIN ($\theta = 90°$), for sulfonated PS ionomer in DMF at different ionomer concentrations. (From Ref. 87.)

taken for the peak position, is related to an effective diffusion coefficient, D_{eff}, defined by

$$D_{eff} = \frac{\langle \Gamma \rangle}{q^2} \tag{14}$$

How a single mode of polystyrene spreads into two modes upon incorporation of ionic groups is seen in Figure 11. Figure 11a shows the q^2 dependence of $\langle \Gamma \rangle / q^2$ for the ionomer as well as for the precursor polymer, PS. For simplicity, a line is drawn for the data obtained at one concentration by using a least-squares method. A similar procedure is applied to all the data obtained at different concentrations. Some deviation from the diffusive relation $\langle \Gamma \rangle \propto q^2$ is noted, as also observed for polyelectrolyte aqueous solutions [76–79]. The fast mode ($\langle \Gamma_f \rangle / q^2 = D_{eff,f} \sim 10^{-6}$ cm^2/s) shows a very slight negative q^2 dependence, while the slow mode ($\langle \Gamma_s \rangle / q^2 = D_{eff,s} \sim 10^{-8}$ cm^2/s) shows a slightly positive q^2 dependence. The negative slope of D_f [78] and the positive slope of D_s [76–79] were also noted for salt-free polyelectrolyte solutions.

To examine the concentration dependence, a limiting value of $\langle \Gamma \rangle / q^2$ at $q = 0$, $(\langle \Gamma \rangle / q^2)_{q=0}$, which was obtained as the intercept of the lines in Figure 11a, is plotted as a function of polymer concentration in Figure 11b. There is an increase in the $(\langle \Gamma \rangle / q^2)_{q=0} (= D_f)$ value with concentration for the fast mode, but no discernible concentration dependence is noted for the slow mode (D_s). The concentration dependence of the fast mode may be compared with the concentration dependence of Kc/R_0 in Figure 6. The (mutual) diffusion coefficient of nonaggregating polymer solutions is given by the generalized Stokes–Einstein relation [66,89,90],

$$D = \frac{M(1 - vc)^2}{N_A f(c)} \left(\frac{\partial c}{\partial \Pi} \right)^{-1} \tag{15}$$

where $f(c)$ is the frictional coefficient of the molecule and v is the partial specific volume of the polymer. Strongly interacting systems, such as salt-free polyion solutions, show a strong concentration dependence at low concentrations, the major contribution of which comes from the $(\partial c / \partial \Pi)^{-1}$ term [82].

Both D_f and Kc/R_0 increase with concentration: this is because both D and Kc/R_0 are proportional to $(\partial c / \partial \Pi)^{-1}$, which increases significantly with c (compare Eqs. 6 and 15) for strongly interacting polymer solutions. A more significant increase in D_f with polymer concentration was reported for polyelectrolyte aqueous solutions [78,79], because an increase in the $(\partial c / \partial \Pi)^{-1}$ term is more significant for polyelectrolyte aqueous solutions due to larger repulsive interactions, as discussed in the Static Scattering section. While it

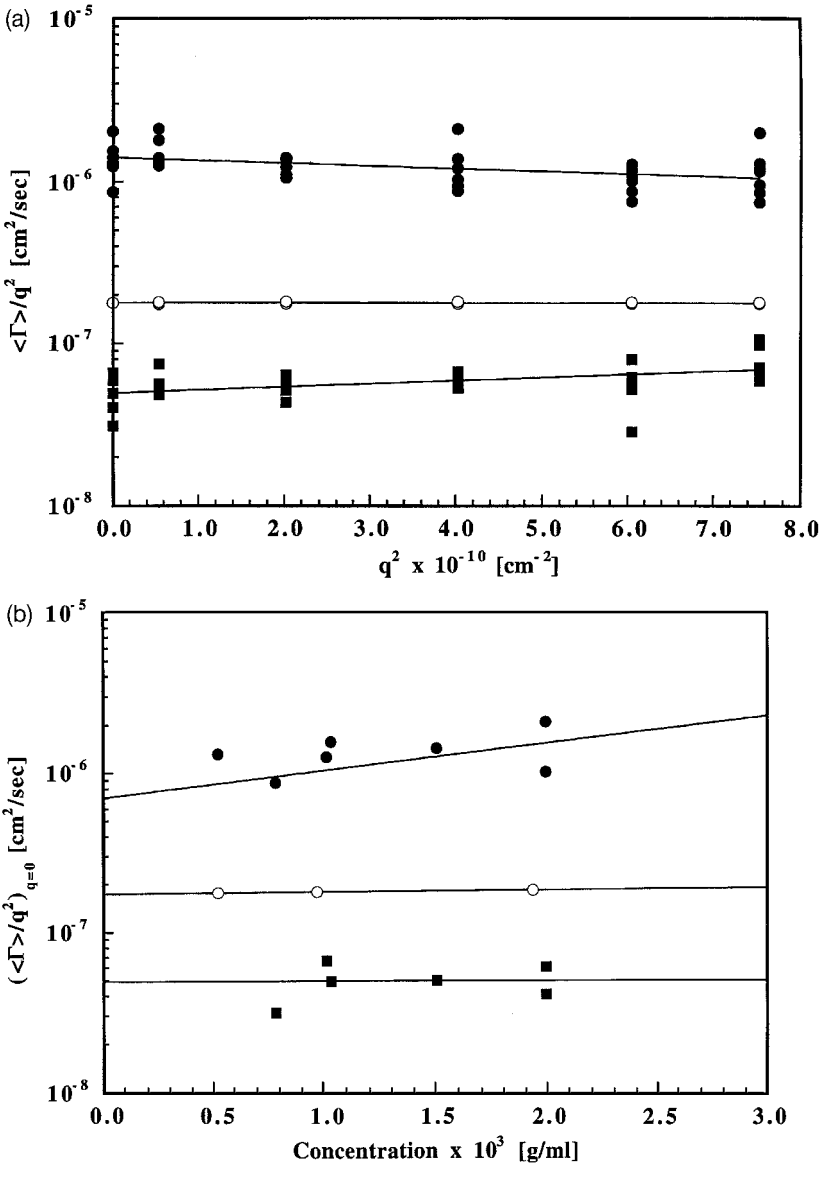

FIG. 11 (a) Average Γ value normalized by q^2, $\langle\Gamma\rangle/q^2$, as a function of the q^2 for sulfonated PS ionomer in DMF: (●) fast mode; (■) slow mode. Also shown are the data for PS in DMF (○). (b) Average peak position extrapolated to $q = 0$, $[\langle\Gamma\rangle/q^2]_{q=0}$, as a function of polymer concentration for sulfonated PS ionomer in DMF: (●) fast mode; (■) slow mode. Also shown are the data for PS in DMF (○). (From Ref. 87.)

has been observed that D_s changes significantly with concentration for salt-free polyelectrolyte aqueous solutions, no such behavior is noted for the ionomer solutions studied.

The fast (diffusive) mode may be interpreted as arising from polyion-counterion coupling, in which fast moving counterions ''drag'' slow moving polyions, leading to larger diffusion coefficients of polyions; under salt-free conditions, the diffusion coefficient can be shown to approach that of the small ions [91], and thus the fivefold increase in the diffusion coefficient of single ionomer chains as compared with PS (as seen in Figure 11) is not unreasonable. Alternatively, and more generally, the fast mode may be interpreted in terms of nonequilibrium thermodynamics: diffusion is caused by the ''thermodynamic driving force'' for diffusion, i.e., the chemical potential gradient [66], which is proportional to the inverse osmotic compressibility, $(\partial c/\partial \Pi)^{-1}$, as seen in the generalized Stokes–Einstein relation (see Eq. 15). Since the $(\partial c/\partial \Pi)^{-1}$ value is very large for polyion solutions, arising from the large intermolecular excluded volume term, $(N/V)m_0$, due to repulsive interactions (see Eq. 7), the diffusion coefficients of polyions are significantly enhanced. For example, there is a ten times increase in Kc/R_0 value for ionomer with 2.7 mol% as compared with PS (see Figure 6). In addition, the reciprocal scattering of the fast mode shows a negative angular dependence (a figure not shown [87]), which is consistent with the results obtained by static scattering of ionomers in a polar solvent at low concentrations where the fast mode is dominant. At low ionomer concentrations, Zimm plots of ionomers in a polar solvent show negative slopes, which are explained as arising from external interference due to strong electrostatic interactions between polyions [63], as explained above. Therefore it seems that low concentration behavior of both static and dynamic scattering are consistently explained in terms of dominant intermolecular (electrostatic) interactions.

The slow (diffusive) mode, whose diffusion coefficient is 1–2 orders of magnitude lower than that of the fast mode, may be interpreted as arising from the presence of large-scale ''heterogeneities'' [87]. The diffusion coefficient of the slow mode, D_s, is 5×10^{-8} cm^2/s for the ionomer solution (as seen in Figure 11). This corresponds to a hydrodynamic radius, R_h, of 475 Å, 3.6 times that of the unmodified PS, 130 Å (with a diffusion coefficient of 1.8×10^{-7} cm^2/s). Here, the Stokes–Einstein relation,

$$D = \frac{kT}{6\pi\eta R_h} \tag{16}$$

is used to calculate the R_h value, where k is Boltzmann's constant and η is the viscosity of the solution [91]. Also, from static (angular) measurements of the sulfonated PS ionomer solution in DMF, we have observed that the

slopes of angular-dependent curves in the Zimm plot are largely positive at higher ionomer concentrations [87]. The apparent radius of gyration obtained at high concentration is ca. 300 Å, which is larger than the size of PS, 239 Å. Also, the curvature at small angles in the angular-dependent curve suggests the existence of ''heterogeneities.'' Therefore, it seems that the high concentration behavior in both static and dynamic scattering data are consistently explained in terms of large-scale heterogeneities existing in solution, although the origin, nature, and structure of such heterogeneities are not yet clear, as is also the case for polyelectrolyte aqueous solutions.

These results confirm the observation that polyelectrolyte aqueous solutions show two separate decay modes in the autocorrelation function and support our contention that ionic polymer systems generally behave similarly in polar solvents [23]. To support this, it may be added that similar dynamic scattering behavior was recently reported for another type of ionomer, polyurethane ionomer, dissolved in a polar solvent, dimethylacetamide ($\varepsilon = 38$) [92]. Finally, it should be stressed that the explanation given above for light scattering (both static and dynamic) behavior of salt-free polyelectrolytes is based on the major role of intermolecular electrostatic interactions in causing characteristic behavior. No intramolecular interactions are explicitly included to explain the behavior. This is in accord with our contention that much of the polyelectrolyte behavior, especially structure-related aspects, is determined by intermolecular interactions [23].

E. Conductance and Counterion Binding

Here the counterion binding of ionomer nonaqueous (polar) solutions is described. Figure 12 shows conductance data for a sulfonated PS ionomer in DMF. For comparison, conductance data for comparable small salts, sodium styrenesulfonate, which has a similar structure to the ionic repeat units of sulfonated PS ionomers, is also shown [29]. A significant drop in conductance is clearly noted for the ionomer solution as compared with the simple salt. This is due to counterion binding, as discussed above for polyelectrolyte nonaqueous solutions.

Rochas et al. [52] determined the osmotic coefficients, ϕ_p, of the ionomer whose viscosity behavior was described before in DMF. The experimental value, $\phi_p(\text{exp})$, was obtained by the measurements of osmotic pressure for the ionomer solution in the absence of added salts by using the following equation [93]: $\phi_p(\text{exp}) = \Pi_{exp}/\Pi_{ideal}$, where Π_{exp} is the real osmotic pressure obtained by experiment and Π_{ideal} is the ideal osmotic pressure, in which all ionic species (macroions and counterions) are assumed to contribute to the osmotic pressure. Examples of $\phi_p(\text{exp})$ values are 1.0 for 3.4 mol% ionomer and 0.80 for 7.3 mol% ionomer at 1×10^{-3} (g/cm^3), and 0.98 and 0.48,

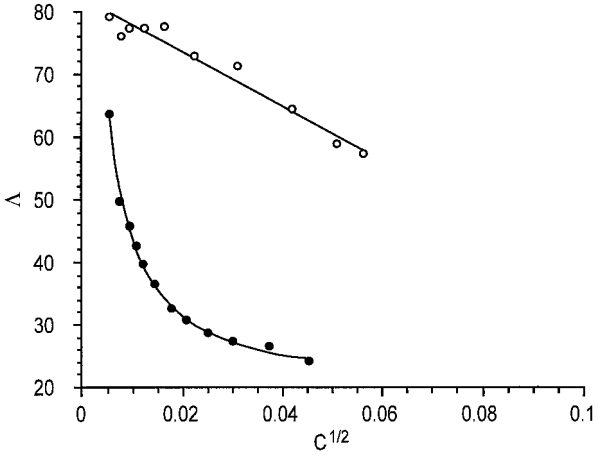

FIG. 12 Equivalent conductance for sulfonated PS ionomer (ion content: 3.0 mol%) (closed circles) and sodium styrenesulfonate (open circles) in DMF. (From Ref. 29.)

respectively at 1.2×10^{-2} (g/cm^3). These values are compared with ϕ_p(cal) values, calculated by using the Oosawa equation [2] for linear polyelectrolytes: 0.98 and 0.95, respectively at 1×10^{-3} (g/cm^3), and 0.85 and 0.81, respectively at 1.2×10^{-2} (g/cm^3). Also, ϕ_p(cal) values were calculated by using the Manning equation [94] for infinite dilution: 0.91 and 0.81 for each ionomer.

The agreements are fairly good only at low concentrations. In these calculations, a rodlike or cylindrical model was used for linear polyelectrolytes, i.e., each macroion is stretched to a cylindrical shape and ionic groups are distributed in a cylindrical region. It was reported for aqueous solutions that the limiting law for the osmotic coefficient calculated by the Manning equation does not agree with measured values for poly(acrylic acid) at low degrees of neutralization [95]. Therefore a cylinder model may not be a good description for a flexible chain at low charge densities like an ionomer. Nevertheless, those results show that, in the solution of the ionomer that has a small amount of ionic groups, counterion binding occurs as seen for polyelectrolyte aqueous solutions, but the degree of counterion binding is much smaller than for the polyelectrolytes with high charge density [e.g., ϕ_p = 0.17 for sodium poly(styrenefulfonate) in aqueous solution] [96].

With regard to counterion binding, some similarities are also observed between ionomer nonaqueous solution and polyelectrolyte aqueous solution. This is the short-range effect due to partial desolvation associated with coun-

terion binding, which depends on counterion species [97]. Although the short-range effect due to desolvation is expected to be small compared to the nonspecific long-range polyelectrolyte effect in most cases, it was suggested that the short-range effect may be very important for some crucial problems in biology [98]. From various measurements on polyelectrolyte aqueous solutions, such as activity coefficients, polyion expansion, titration behavior, and conductance, it was shown that the order of counterion binding for monovalent ions is Li < Na < K for polysulfonates, while that for polycarboxylates is reversed. The concept of site-binding (i.e., short-range) was introduced to explain this counterion effect, since ionic atmosphere binding (i.e., long-range) is not enough to explain the results [97]. The hypothesis of the site-binding was supported by the observation that the refractive index decreased, or the volume increased, arising from partial desolvation.

A similar behavior, the reversal of the order of counterion binding, was observed for ionomer solutions [99]. From viscosity and low-angle light scattering behavior, it was concluded that the degree of counterion binding increases in the order Na < K < Cs for sulfonated PS ionomer, while the order for carboxylated PS ionomer is reversed. It should be added here that the above finding is parallel to the observations for other ionic solutions. The association constants of a carboxylate (e.g., $RCOO^{-}M^{+}$) and sulfonate (e.g., $ArSO_3^{-}M^{+}$) change in the same manner [100]. Also, the cation affinity of carboxylate and sulfonate ion exchange resins changes in the same manner [101]. These observations may be understood in terms of the difference in desolvation during cation–anion interaction [102]: For the sulfonate system, the (partial) desolvation does not occur because of the small anionic field strength of the SO_3H groups; therefore, the cation and anion interact through solvents, and the determining factor is the solvated ion size (i.e., Li > Na > K > Cs). On the other hand, for the carboxylate system, (partial) desolvation occurs because of the large anionic field strength of the COOH groups. Therefore the cation and anion can interact directly, and the determining factor is the unsolvated ion size (i.e., Li < Na < K < Cs). The results described here concerning counterion binding phenomena again demonstrate the similarities between ionomer nonaqueous solution and polyelectrolyte aqueous solution.

III. CONCLUSIONS

1. Polyelectrolyte nonaqueous solutions, which can be studied from a more general point of view, can provide useful information regarding the structure of polyelectrolyte aqueous solutions. Especially useful are ionomer nonaqueous solutions, which can be used as a good model system for study-

ing complex salt-free polyelectrolyte behavior because of various advantages that they possess.

2. All of the observations made for random ionomer nonaqueous (polar) solutions parallel those for polyelectrolyte aqueous solutions: the difference is only quantity, not the quality. These include upturn in a viscosity curve, negative angular dependence at low concentration and positive dependence at higher concentration in Zimm plots, appearance of two modes in dynamic scattering, and a drop in conductance.

3. The effects of intermolecular interactions have been less emphasized as compared with intramolecular interactions and polyion–counterion interactions; yet these interactions seem to play a key role in determining structure-related solution behavior.

4. Compared with a vast amount of literature on polyelectrolyte aqueous solutions, studies on nonaqueous solution are very few. More systematic and quantitative studies are needed and should certainly produce useful information in our understanding of the characteristic behavior of salt-free polyelectrolyte solutions.

5. Random ionomers having very small ion contents (e.g., 0.3 mol% for a 400,000 molecular weight PS) and telechelic ionomers show some deviations from the behavior noted herein. Although these deviations are of interest in studies of the essential features of polyelectrolyte behavior of ionic polymer solutions, we have limited our discussion to typical random ionomers (having an ion content of over 1.0 mol%).

ACKNOWLEDGMENT

Acknowledgment is made to the Rutgers Research Council, the NSF, and the ACS-PRF for financial support, and to Dr. J. Wu, Dr. J. Bodycomb, Dr. G. Kupperblatt, and Dr. T. Tsai for their valuable contributions.

REFERENCES

1. Rice SA, Nagasawa M. Polyelectrolyte Solutions. New York: Academic Press, 1961.
2. Oosawa F. Polyelectrolytes. New York: Marcel Dekker, 1971.
3. Hara M, ed. Polyelectrolytes: Science and Technology. New York: Marcel Dekker, 1993.
4. Dautzenberg H, Jaeger W, Kötz J, Philipp B, Seidel C, Stscherbina D. Polyelectrolytes: Formation, Characterization and Application. Ohio: Hanser Gardner, 1994.
5. Schmitz KS, ed. Macro-Ion Characterization: From Dilute Solutions to Complex Fluids. Washington, DC: American Chemical Society, 1994.

6. Eisenberg H. Biological Macromolecules and Polyelectrolytes in Solution. Oxford: Clarendon Press, 1976.
7. Veis A, ed. Biological Polyelectrolytes. New York: Marcel Dekker, 1970.
8. Bloomfield V, Carpenter IL. Biological Polyelectrolytes. In: Hara M, ed. Polyelectrolytes: Science and Technology. New York: Marcel Dekker, 1993:77–125.
9. Nagasawa M, Takakhashi A. Light scattering from polyelectrolyte solutions. In: Huglin MD, ed. Light Scattering from Polymer Solution. New York: Academic Press, 1972:671–723.
10. Tabor BE. Preparation and clarification of solutions. In: Huglin MB, ed. Light Scattering from Polymer Solutions. New York: Academic Press, 1972:1–25.
11. Eisenberg D, Kauzmann W. The Structure and Properties of Water. New York: Oxford University Press, 1969.
12. Fuoss RM, Cathers GI. Polyelectrolytes. 1. Picrates of 4-vinylpyridine-styrene copolymers. J Polym Sci 1947; 2:12–15.
13. Edelson D, Fuoss RM. Chain electrolytes. J Am Chem Soc 1948; 70:2832.
14. Fuoss RM. Viscosity function for polyelectrolytes. J Polym Sci 1948; 3:603–604.
15. Fuoss RM, Strauss UP. Polyelectrolytes. II. Poly-4-vinylpyridonium chloride and poly-4-vinyl-*N*-*n*-butylpyridonium bromide. J Polym Sci 1948; 3:246–262.
16. Fuoss RM, Cathers GI. Polyelectrolytes. III. Viscosities of *n*-butyl bromide addition compounds of 4-vinylpyridine-styrene copolymers in nitromethane-dioxane mixtures. J Polym Sci 1949; 4:97–120.
17. Cathers GI, Fuoss RM. Polyelectrolytes. IV. Conductance of *n*-butyl bromide addition compounds of 4-vinylpyridine-styrene copolymers in nitromethane-dioxane mixtures. J Polym Sci 1949; 4:121–133.
18. Strauss UP, Fuoss RM. Polyelectrolytes. V. Osmotic pressures of poly-4-vinyl-*N*-*n*-butylpyridonium bromide in ethanol at 25°. J Polym Sci 1949; 4:457–472.
19. Fuoss RM, Maclay WN. Polyelectrolytes. VI. Viscosities of 4-polyvinylpyridine hydrochloride in methanol at 25°. J Polym Sci 1951; 6:305–317.
20. Maclay WN, Fuoss RM. Polyelectrolytes. VII. Viscosities of derivatives of poly-2-vinylpyridine. J Polym Sci 1951; 6:511–521.
21. Fuoss RM, Edelson D. Polyelectrolytes. VIII. Quaternized polyesters of succinic anhydride and methyldiethanolamine. J Polym Sci 1951; 6:523–532.
22. Fuoss RM. Electrical transport by polyelectrolytes. J Polym Sci 1954; 12: 185–198.
23. Hara M. Polyelectrolytes in Nonaqueous Solution. In: Hara M, ed. Polyelectrolytes: Science and Technology. New York: Marcel Dekker, 1993:193–264.
24. Lundberg RD, Makowski HS. Solution behavior of ionomers. 1. Metal sulfonate ionomers in mixed solvents. J Polym Sci Polym Phys Ed 1980; 18: 1821–1836.
25. Eisenberg A, Rinaudo M. Polyelectrolytes and ionomers. Polym Bull 1990; 24:671.

26. Hara M, Wu J, Jerome RJ, Granville M. Salt-free polyelectrolyte behavior of halato-telechelic ionomers in polar solvent. Macromolecules 1988; 21:3330–3331.
27. Hara M, Wu J, Jerome RJ, Granville M. Polyelectrolyte behavior of polystyrene-based telechelic ionomers in polar solvent. 1. Viscosity and low-angle light scattering studies. Macromolecules 1994; 27:1195–1200.
28. Kupperblatt G, Hara M, Vanhoorne P, Jerome RJ. Light scattering study of salt-free polyelectrolyte behavior of monotelechelic ionomers in a polar solvent. Polymer 1996; 37:3741–3744.
29. Kupperblatt G. A comparison of the polyelectrolyte behavior of random and telechelic ionomers in solution. Ph.D. dissertation, Rutgers University, New Brunswick, NJ, 1995.
30. Harried HS, Owen BB. The Physical Chemistry of Electrolytic Solutions. New York: Reinhold, 1943.
31. Fuoss RM. Properties of electrolytic solutions. Chem Revs 1935; 17:27–42.
32. Huggins ML. The viscosity of dilute solutions of long-chain molecules. IV. Dependence on concentration. J Am Chem Soc 1942; 64:2716–2718.
33. Staudinger H. Die hochmolekularen organischen Verbingungen. Berlin: Springer-Verlag, 1932.
34. Witten TA, Pincus P. Structure and viscosity of interpenetrating polyelectrolyte chain. Europhys Lett 1987; 3:315–320.
35. Cohen J, Priel Z, Rabin Y. Viscosity of dilute polyelectrolyte solutions. J Chem Phys 1988; 88:7111–7116.
36. Rees RW, Vaughan DJ. ''Surlyn,'' an ionomer. 1. The effects of ionic bonding on polymer structure. Polym Prepr (Am Chem Soc Div Polym Chem) 1965; 6:287–295.
37. Eisenberg A, King M. Ion-Containing Polymeral. New York; Academic Press, 1977.
38. Holliday L, ed. Ionic Polymers. London: Applied Science, 1975.
39. Eisenberg A, Kim J. Introduction to Ionomers. New York: John Wiley, 1998.
40. MacKnight WJ, Earnest WJ. The structure and properties of ionomers. J Polym Sci Macromol Rev 1981; 16:41–122.
41. Wilson AD, Prosser HJ, eds. Developments in Ionic Polymers. Vols. 1 and 2. New York: Applied Science, 1983.
42. Eisenberg A, Bailey F, eds. Coulombic Interactions in Macromolecular Systems. Washington, DC: American Chemical Society, 1986.
43. Pineri M, Eisenberg A, eds. Structure and Properties of Ionomers. Dordrecht: D. Reidel, 1987.
44. Fitzgerald JJ, Weiss RA. Synthesis, properties, and structure of sulfonated ionomer. J Macromol Sci Rev Macromol Chem Phys 1988; C28:99–185.
45. Makowski HS, Lundberg RD, Singhal GH. Flexible polymer compositions comprising a normally plastic polymer sulfonated to about 0.2 to about 10 mole % sulfonate. U.S. Pat. 3,870,841, assigned to Exxon Research and Engineering Co., 1975.
46. Lundberg RD, Phillips RR. Solution behavior of metal sulfonate ionomers. II. Effects of solvents. J Polym Sci Polym Phys Ed 1982; 20:1143–1154.

47. Marina MG, Monakov YB, Rafikov SR. The influence of hydrogen bonds and ionic interactions on the properties of carboxyl-containing copolymers and ionomers based on them. Russ Chem Rev 1979; 48:389–403.
48. Hara M. Light scattering from ionomer solutions. In: Brow W, Mortensen K, eds. Scattering in Polymeric and Colloidal Systems. London: Gordon and Breach, 2000.
49. Hara M, Wu J, Lee AH. Effect of intra- and intermolecular interactions on solution properties of sulfonated polystyrene ionomers. Macromolecules 1988; 21:2214–2218.
50. Wolff C. Viscosité des solutions de polyélectrolytes. J Physique 1978; 39:C2 162–174.
51. Kim MW, Peiffer DG. Polyelectrolyte properties of ionomeric polymers. Europhys Lett 1988; 5:321–326.
52. Rochas C, Domard A, Rinaudo M. Polyelectrolyte behavior of acrylonitrile methallylsulphonate copolymers in dimethylformamide. Polymer 1979; 20: 76–80.
53. Pals DTF, Hermans JJ. Concentration dependence of the viscosity of sodium pectinate in solutions of NaCl. J Polym Sci 1948; 3:897–898.
54. Nagasawa M. Viscosity, sedimentation and diffusion of polyelectrolytes. In: Kaneko M, Sugai S, Nagasawa M, eds. Polyelectrolytes. Tokyo: Kyoritsu 1978:127–154.
55. Hara M, Wu J, Lee AH. Solution properties of ionomers. 2. Simple salt effect. Macromolecules 1989; 22:754–757.
56. Hara M, Wu J. Low-angle light scattering study of polyelectrolyte behavior of ionomers in polar solvent. Macromolecules 1986; 19:2887–2888.
57. Hara M, Wu J. Light scattering study of ionomers in solution. 2. Low-angle scattering from sulfonated polystyrene ionomers. Macromolecules 1988; 21: 402–407.
58. Huglin MB, ed. Light Scattering from Polymer Solutions. New York: Academic Press, 1972.
59. Kratochvil P. Classical Light Scattering from Polymer Solutions. New York: Elsevier, 1987.
60. Sedlack M. Polyelectrolytes in solution. In: Brown W, ed. Light Scattering: Principles and Development. Oxford: Clarendon Press, 1996:120–165.
61. Oth A, Doty P. Macroions. II. Polymethacrylic acid macroions. J Phys Chem 1952; 56:43–50.
62. Drifford M, Dalbiez JP. Light scattering by dilute solutions of salt-free polyelectrolytes. J Phys Chem 1984; 88:5368–5375.
63. Bodycomb J, Hara M. Light scattering study of ionomers in solution. 4. Angular measurements of sulfonated polystyrene ionomers in a polar solvent (dimethylformamide). Macromolecules 1994; 27:7369–7377.
64. Doty P, Steiner RF. I. Light scattering theory and experiments with bovine serum albumin. J Chem Phys 1952; 20:85–94.
65. Trap HJL, Hermans JJ. Light-scattering by polymethacrylic acid and carboxymethylcellulose in various solvents. J Phys Chem 1954; 58:757–761.

66. Yamakawa H. Modern Theory of Polymer Solutions. New York: Harper and Row, 1971.
67. Flory PJ. Principles of Polymer Chemistry. Ithaca: Cornell University Press, 1953.
68. Flory PJ, Bueche AM. J Polym Sci 1958; 27:219–228.
69. Born M, Green HS. A general kinetic theory of liquids. I. The molecular distribution functions. 1946; A-188:10–18.
70. Guinier A, Fournet G. Small-Angle Scattering of X-Rays. New York: John Wiley, 1955.
71. Percus JK, Yevick GJ. Analysis of classical statistical mechanics by means of collective coordinates. Phys Rev 1958; 110:1–13.
72. Vrij A. Light scattering of a concentrated multicomponent system of hard spheres in the Percus–Yevick approximation. J Chem Phys 1978; 69:1742–1747.
73. Mandel M. Some properties of polyelectrolyte solutions and the scaling approach. In: Hara M, ed. Polyelectrolytes: Science and Technology. New York: Marcel Dekker, 1993:1–75.
74. de Gennes PG. Scaling Concepts in Polymer Physics. Ithaca: Cornell University Press, 1979.
75. Schmitz KS, Lu M, Gauntt J. Influence of ionic strength on the diffusion of polystyrene latex spheres, bovine serum albumin, and polynucleosomes. J Chem Phys 1983; 78:5059–5066.
76. Amis E. Polyelectrolyte dynamics. In: Hara M, ed. Polyelectrolytes: Science and Technology. New York: Marcel Dekker, 1993:127–191.
77. Sedlak M, Amis EJ. Dynamics of moderately concentrated salt-free polyelectrolyte solutions: molecular weight dependence. J Chem Phys 1992; 96:817–825.
78. Sedlak M, Amis E. Concentration and molecular weight regime diagram of salt-free polyelectrolyte solutions as studied by light scattering. J Chem Phys 1992; 96:826–834.
79. Förster S, Schmidt M, Antonietti M. Static and dynamic light scattering by aqueous polyelectrolyte solutions: effect of molecular weight, charge density and added salt. Polymer 1990; 31:781–792.
80. Sedlak M. Domain structure of polyelectrolyte solutions: is it real? Macromolecules 1993; 26:1158–1162.
81. Li X, Reed WF. Polyelectrolyte properties of proteoglycan monomers. J Chem Phys 1991; 94:4568–4581.
82. Wu J, Hara M. Light scattering study of ionomers in solution. 3. Dynamic scattering from sulfonated polystyrene ionomers in a polar solvent (dimethylformamide). Macromolecules 1994; 27:923–929.
83. Hara M, Wu J. Light scattering study of ionomer solutions. ACS Symp Ser 1989; 395:446–458.
84. Provencher SW, Hendrix J, Maeyer LD. Direct determination of molecular weight distributions of polystyrene in cyclohexane with photon correlation spectroscopy. J Chem Phys 1978; 69:4273–4276.

85. Provencher SW. Inverse problems in polymer characterization: direct analysis of polydispersity with photon correlation spectroscopy. Makromol Chem 1979; 180:201–209.
86. Provencher SW. CONTIN: a general purpose constrained regularization program for inverting noisy linear algebraic and integral equations. Comp Phys Comm 1982; 27:229–242.
87. Bodycomb J, Hara M. Light scattering study of ionomers in solution. 5. CONTIN analysis of dynamic scattering data from sulfonated polystyrene ionomers in a polar solvent (dimethylformamide). Macromolecules 1995; 28: 8190–8197.
88. Štěpánek P. Data analysis in dynamic light scattering. In: Brown W, ed. Light Scattering: Principles and Development. Oxford: Clarendon Press, 1996:177–241.
89. Phillies GD. Effects of intermolecular interactions on diffusion. 1. Two-component solutions. J Chem Phys 1974; 60:976–982.
90. Pusey PN, Tough RJA. Particle Interactions. In: Pecora R, ed. Dynamic Light Scattering. New York: Plenum Press, 1985:85–179.
91. Berne BJ, Pecora R. Dynamic Light Scattering. New York: John Wiley, 1976.
92. Nomula S, Cooper SL. Structural studies of polyurethane ionomer solutions. 1. Dynamic light scattering. Macromolecules 1997; 30:1355–1362.
93. Katchalsky A, Alexandrowicz Z, Kedem O. Polyelectrolyte solutions. Chemical physics of ionic solutions. In: Conway BE, Barradas RG, eds. New York: John Wiley, 1966:295–346.
94. Manning GS. Limiting laws and counterion condensation in polyelectrolyte solutions. 1. Colligative properties. J Chem Phys 1969; 51:924–933.
95. Manning GS. Polyelectrolytes. Ann Rev Phys Chem 1972; L3:117–140.
96. Takahashi A, Kato N, Nagasawa M. The osmotic pressure of polyelectrolyte in neutral salt solutions. J Phys Chem 1970; 74:944–946.
97. Armstrong RW, Strauss UP. Encly Polym Sci Technol 1969; 10:781–861.
98. Manning GS. Limiting laws and counterion condensation in polyelectrolyte solutions. IV. The approach to the limit and the extraordinary stability of the charge fraction. Biophys Chem 1977; 7:95–102.
99. Hara M, Lee AH, Wu J. Solution properties of ionomers. 1. Counterion effect. J Polym Sci Polym Phys Ed 1987; 25:1407–1418.
100. Gordon JE. The Organic Chemistry of Electrolyte Solutions. New York: John Wiley, 1975.
101. Helfferich F. Ion Exchange. New York: McGraw-Hill, 1962.
102. Morawetz H. Macromolecules in Solution. Malabar: Robert E. Krieger, 1983.
103. Agarwal PK, Garner RT, Graessley WW. Counterion and solvent effects on the dilute solution viscosity of polystyrene ionomers. J Polym Sci Polym Phys Ed 1987; 25:2095–2111.
104. Niezette J, Vandershueren I, Avas L. J Polym Sci Polym Phys Ed 1984; 22: 1845–1848.
105. Aldebert P, Gebel G, Loppinet B, Nakamura N. Polymer 1995; 36:431–434.

This Page Intentionally Left Blank

10

Kinetics of Polyelectrolyte Adsorption

MARTIEN A. COHEN STUART and J. MIEKE KLEIJN Wageningen University, Wageningen, The Netherlands

I. INTRODUCTION

Linear polyelectrolytes are frequently used in colloidal dispersions, either as stabilizers or as flocculants. Hence, quite some attention has been given to the adsorption of these macromolecules; for a review see Fleer et al. [1]. Most investigations have been of an experimental nature and focused on adsorbed amounts as a function of various (experimental) parameters such as charge densities on the polymer and on the surface, ionic strength, and chain length. A few theoretical studies addressed the issue of equilibrium adsorption, using a variety of methods with various degrees of sophistication [2–8]. One paper attempted to distinguish several cases of behavior on the basis of theoretical results [9]. Comparisons between experiments and theory sometimes seemed to be qualitatively successful [1], but before deciding that the theory is indeed adequate, a number of important questions has to be addressed first, such as, What does one actually measure in a typical experiment? Is it the equilibrium adsorbed amount predicted by theory, or does kinetics play a role? How rapidly do these systems equilibrate?

In short, the kinetics of the adsorption process needs to be carefully considered. Unfortunately, kinetic data are much less abundant than are static ones, let alone theories that address kinetics. The present contribution reviews the state of the art.

II. IS EQUILIBRIUM ACHIEVED?

The question whether equilibrium is achieved has been haunting the broader field of polymer adsorption. As polymers are large molecules, capable of forming multiple anchoring bonds, their motion is expected to be sluggish.

In addition, it is rather difficult to check in a typical experiment whether the system is relaxed, as polymers adhere so tenaciously. The simplest conceivable check—determining whether desorption occurs upon dilution of the bulk or, equivalently, upon rinsing the surface with solvent—does not work because the relevant equilibrium concentrations are so low that the rate of desorption, even from an equilibrated layer, is often too small to be measurable [10].

A different approach is to vary a parameter to which the saturated adsorbed amount Γ is expected to respond significantly, e.g., temperature or solvent quality. For polyelectrolytes such an approach is quite natural, because Γ depends on salt concentration (ionic strength) and quite often also on pH. Hence, cycling these parameters should reveal the extent of reversibility.

One such experiment, taken from Hoogeveen et al. [11] is presented in Figure 1. Here, poly-*N*-methyl-2-vinyl pyridinium (PVP^+) of a molar mass of 120,000 g mole^{-1} was adsorbed from aqueous electrolyte solutions onto silica plates covered with titania (TiO_2). Two salt (NaCl) concentrations were employed: 0.005 mol kg^{-1} (Figure 1a) and 0.1 mol kg^{-1} (Figure 1b). The adsorption was followed by means of optical reflectometry as originally described by Dijt et al. [12]. After initial adsorption at either pH 4 or pH 8, the adsorbed layers were exposed to repeated switches between pH 4 and 8, in the presence of free (dissolved) polymer. Since the titania becomes more negatively charged upon increasing the pH, one expects an increase

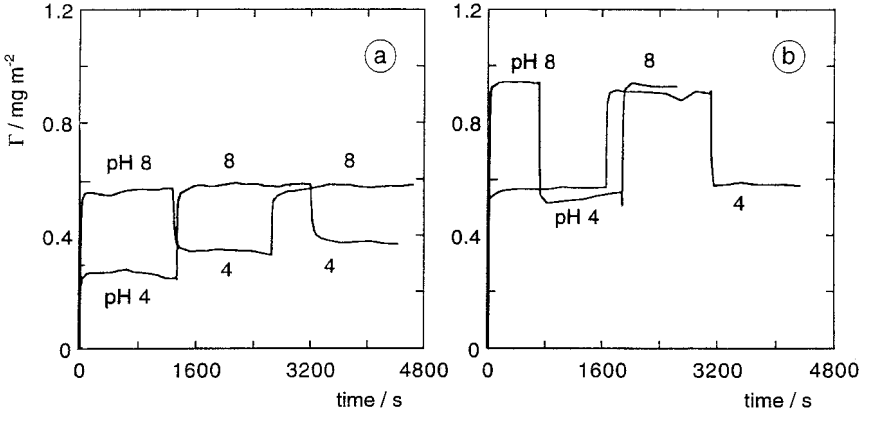

FIG. 1 Reversibility of the adsorption of polyvinylpyridinium (PVP^+) on TiO_2 upon changing the pH from 8 to 4 to 8 and from 4 to 8 to 4. Ionic strength: 0.005 mol kg^{-1} (a) and 0.1 mol kg^{-1} (b). The polymer concentration was 10 mg kg^{-1}. (Adapted from Ref. 11.)

in adsorption in this direction. As is clear from Figure 1b, the adsorbed amount at 0.1 M NaCl is entirely independent of the sample history. The same adsorbed amount is found, both at initial adsorption at pH 4 followed by a pH increase to 8, and by direct adsorption at pH 8. The same holds true for the reverse sequence. At the lower salt concentration (Figure 1a), however, the initial adsorption at pH 4 is lower than that obtained after adsorption at pH 8 followed by a decrease in pH. Clearly, this system shows dependence on sample history.

A more pronounced example of a sample history effect is shown in Figure 2, taken from Hoogendam [13]. In these experiments, carboxymethylcellu-

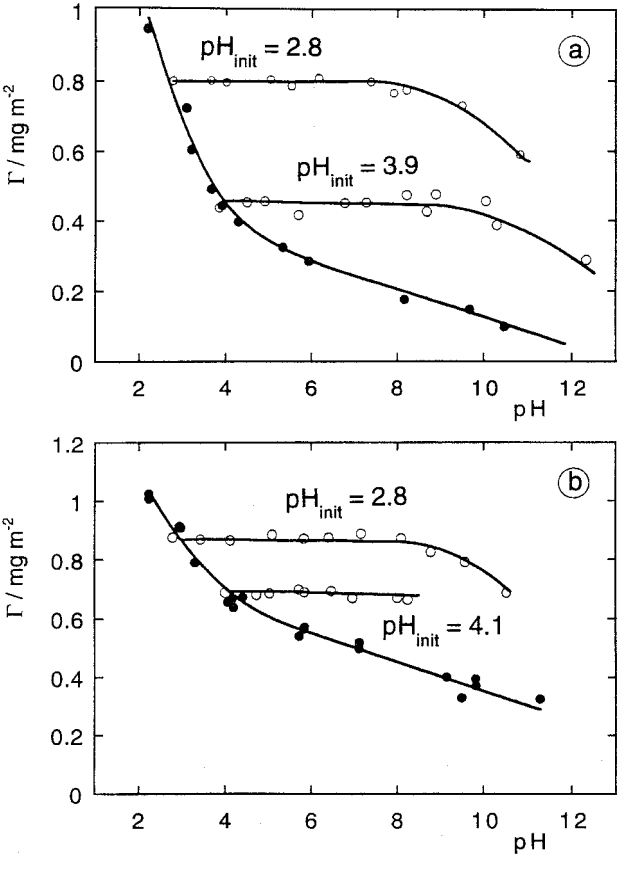

FIG. 2 Adsorption of carboxymethylcellulose (CMC) on hematite as a function of pH (closed symbols); effect of pH increments after adsorption at low initial pH as indicated (open symbols). (a) 0.01 M NaCl; (b) 0.5 M NaCl. (Data from Ref. 13.)

lose (CMC), a very stiff polyacid of high molar mass (1,000,000 g mole^{-1}) was adsorbed from NaCl solutions onto colloidal hematite (Fe_2O_3). The adsorbed amount was determined by the classical depletion method [1] and is given here as a function of pH, both after adsorption at constant pH (filled symbols) and after adsorption at low pH (2.8, 3.9, or 4.1) followed by an upward pH increase (open symbols). In Figure 2a results are given for a low NaCl concentration (0.1 mole L^{-1}), and in Figure 2b the salt concentration was 0.5 mole L^{-1}. Both data sets show qualitatively similar behavior: the adsorbed amount at constant pH (filled symbols) depends strongly on pH, decreasing as pH increases, but the upward pH jumps do not induce desorption unless these exceed 5 units. Hence, this system is strongly irreversible, and cases like this have been found in many instances. Before attempting to answer the question which process, adsorption or desorption, is most hampered by slow kinetics, we first discuss some general aspects of adsorption kinetics.

III. THE MACROMOLECULAR ADSORPTION PROCESS

Any flexible polymer adsorbing to a solid/liquid interface must (1) be transported from the solution towards the surface, (2) establish a sufficient number of attachment points, and (3) change its conformation to achieve the state of lowest Gibbs energy, by accommodating to the geometrical properties of the substrate [1].

The transport step generally involves both convection and diffusion, processes for which the physical laws (hydrodynamics, Fick's law) are well known. Step 2 is less well understood, as it may involve diffusion of the polymer over a repulsive adsorption (attachment) barrier, the height of which may be an increasing function of the surface coverage Γ. Since polyelectrolytes are charged, long-range electrostatic interactions have to be considered here, but how this should be done is not entirely clear. Step 3 deals with the motion of segments of an adsorbed chain over the surface, and the friction associated to that. For polyelectrolytes, such friction is probably related to the formation and breaking of ion pairs between the charged groups on the polymer and sites on the surface, and the ''lifetime'' of such ionic bonds is not easily assessed. Also here, competing ions (salt) and proton transfer reactions are important.

A convenient starting point for a discussion of adsorption kinetics is the assumption of a quasi steady state, i.e., a case where changes in the adsorption rate are slow as compared to the rate at which a concentration gradient is established. That is, steady state is possible when the time needed to reach saturation (at adsorbed amount Γ_{max}) is long compared to a typical time

needed to establish a concentration gradient by diffusion. If the initial rate of adsorption is given by kc (c being the polymer concentration and k in m s^{-1} an overall rate constant, usually determined by convection and diffusion, see below), the characteristic time required to fill the surface equals Γ_{max}/kc. The characteristic time to set up a concentration gradient extending over a stagnant layer of thickness δ equals δ^2/D with $\delta = D/k$, so that one finds a time scaling as D/k^2. Comparing these two characteristic times, we conclude that a steady state situation requires $\Gamma_{max}k/cD \gg 1$. Such a condition is easily met in dilute solutions and thus not only covers many experimental situations but also justifies the description of the adsorption process in terms of a flux ($d\Gamma/dt$), determined by the difference between bulk concentration c^b and equilibrium concentration $c^{eq}(\Gamma)$ as the driving force, and a resistance R (which may itself be the sum of various contributions R_1, R_2, . . .) in the following way [14]:

$$R\frac{d\Gamma}{dt} = c^b - c^{eq}(\Gamma) \qquad R = R_1 + R_2 + \cdots \tag{1}$$

Provided R ($= k^{-1}$) is a function of Γ only, Eq. 1 implies that $\Gamma(t)$ is entirely determined by the variable c^bt, so that kinetic curves measured at different concentrations coincide when plotted versus c^bt rather than versus just t.

One important resistance is, of course, the bulk *transport resistance* R_t, given by the diffusion coefficient D and the flow conditions of the experiment [1,15]. Various flow types have been considered by Adamczyk et al. [16], such as flow along the surface in a flat or cylindrical channel, impinging jet flow, and flows along curved surfaces. For experiments, the impinging jet method is particularly suitable, as there is a well-defined position (the stagnation point, where the heart of the jet hits the surface) where R_t is precisely known. We have used this flow type in a large part of our experiments. A schematic drawing of the flow cell is presented in Figure 3; it consists of two parallel walls, one of which contains an orifice through which the solution is injected into the cell, perpendicularly to the walls. For a cylindrical inlet channel of radius R and inlet mean velocity v, R_t is given by [15,17]

$$R_t^{-1} = 0.776(\alpha v)^{1/3}\left(\frac{D}{R}\right)^{2/3} \qquad \text{m s}^{-1} \tag{2}$$

where α is a dimensionless flow intensity parameter that depends on the precise geometry of the cell and that can be calculated numerically.

For neutral polymers adsorbing at a bare surface, this is all there is. Hence initial rates of adsorption from dilute solutions satisfy the simple equation

$$\frac{d\Gamma}{dt} = \frac{c^b}{R_t}. \tag{3}$$

This equation has been thoroughly checked by Dijt et al. [18]. For poly-

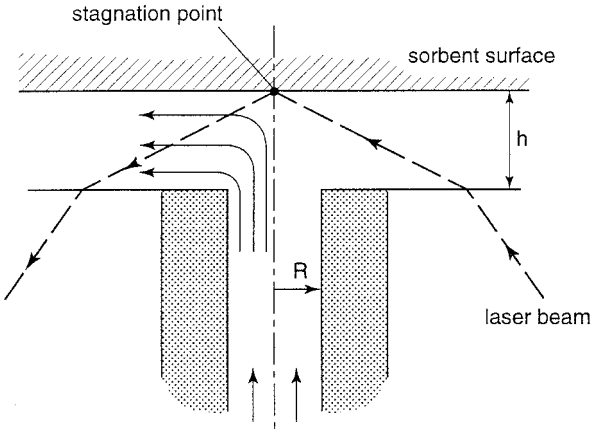

FIG. 3 Schematic diagram of the impinging jet flow system. A stagnation point flow is obtained by pumping solution into the cell through a cylindrical channel of radius R. Flow lines are indicated schematically in the left-hand side of the figure. In the stagnation point the hydrodynamics of the system is well-defined. Adsorption may be followed by reflectometry; the reflected spot of the laser is positioned so that it coincides with the stagnation point.

electrolytes, Eq. 3 is also appropriate; the main difficulty in applying it is that D may depend on solution properties (pH, ionic strength) in a complex but experimentally accessible way.

A second important resistance is the *attachment resistance* R_a. For neutral polymers one may expect that as the surface coverage increases, it becomes progressively harder for incoming molecules to overcome the repulsion by previously adsorbed molecules, even if there are still enough anchoring sites available. This effect of the (saturated) adsorbed layer on $d\Gamma/dt$ is best determined by *exchange* experiments in which a saturated surface covered with unlabeled molecules is exposed to a solution of labeled, but otherwise identical, molecules [19–21]. Dijt et al. [19] concluded from exchange experiments with relatively short polyethylene oxide polymers adsorbing on silica that the attachment resistance was negligibly low. Later, Santore et al. showed that it seems to become larger for very long polymers [20,21]. It should be realized, however, that this conclusion rests upon the assumption that R has only two contributions (R_t and R_a) and that the role of surface relaxation has not been considered [20]. Some support for the modest role of R_a in the case of neutral polymers comes from a theoretical analysis by Semenov and Joanny [22], who also concluded that these resistances are not very large.

For polyelectrolytes, attachment resistance is not restricted to densely covered surfaces, because long-range electrostatic interactions come into play. Obviously, a polyelectrolyte chain will be repelled by a surface that carries a (net) charge of like sign; this situation is analogous to that of colloidal particles in water, for which the DLVO theory is the generally accepted way to calculate the interaction, and the Von Smoluchowsky–Fuchs theory [23,24] provides the framework to calculate the resistance in the rate of (slow) flocculation.

It is thus important to estimate the electrostatic interaction between a polyelectrolyte chain and the charged surface. This is difficult, however, because the polyelectrolyte chain is a flexible, fluctuating object, and there is no simple a priori way to get the effective interaction resulting from double layer overlap for this case. An additional problem is that, quite often, both the polyelectrolyte and the surface have weakly dissociating, pH-dependent ionized groups, and that it is difficult to decide which degrees of freedom will be relaxed on the time scale of approach and attachment of the polymer to the surface. Moreover, as the adsorption process proceeds, more and more charge is accumulated on the surface so that the interaction becomes a pronounced function of Γ, and one anticipates that an initially attracting surface must eventually develop a (long-range) repulsion at some critical coverage. One attempt to construct a first-order theory for R_a and estimate adsorption rates was reported by one of us [14]. We discuss this theory in Sec. V. Before doing so, we first discuss some typical experimental observations on the adsorption (kinetics) of polyelectrolytes.

IV. SOME REPRESENTATIVE RESULTS

In Figure 4 we first present some typical adsorption data as a function of time. These data, taken from Paris and Cohen Stuart [25] are for the adsorption of a hydrophobically modified, weak polyacid (carboxypullulan modified with 12% hydrophobic dodecyl groups) onto the neutral, hydrophobic substrate polystyrene. Measurements were made at low pH (where the polymer carries hardly any charge) and in the absence of salt. In Figure 4 we plot $\Gamma(t)$ as a function of $c^b t$; as explained above, this will make curves measured at varying c^b coincide, provided the adsorption resistances do not explicitly depend on time. As can be seen, this is an adequate assumption; over a range of polymer concentrations from 5 mg L^{-1} to 100 mg L^{-1} and and within experimental error the curves coincide nicely.

We now consider the effect of electrostatics on initial adsorption rates. Our first example [26] is again for the polycationic polymer PVP^+ adsorbing at pH 8 on TiO_2, which is negatively charged under these conditions; see Figure 5. It is the same system as considered in Figure 1b. Two sets of

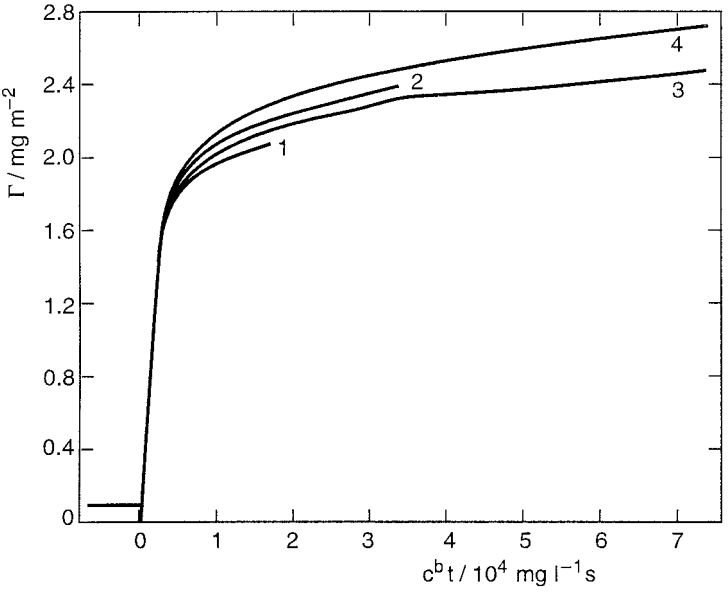

FIG. 4 Adsorption of hydrophobically modified carboxypullulan (OxPu-12/12, i.e., with 12% dodecyl chains) on polystyrene as a function of time, normalized with respect to the polymer concentration c^b. Concentration polymer: (1) 5 mg L^{-1}, (2) 10 mg L^{-1}, (3) 50 mg L^{-1} and (4) 100 mg L^{-1}. Solution conditions: pH 2, ionic strength 10^{-2} M. (Data from Ref. 25.)

curves are shown for $\Gamma(t)$, one for short times (up to 200 s) and one for longer times (up to 1200 s). The polymer/wall interaction was modified by the concentration of added electrolyte, in this case LiCl. The salt concentrations are indicated in the figure. The shape of the kinetic curves is typical: a linear increase, which ends rather abruptly at a level that depends on ionic strength. Since we suspect already from the discussion of Figure 1b that this system equilibrates rapidly, Eq. 1 should apply with a constant value for R (only transport). Given the typical shape for the equilibrium adsorption isotherm, with a very steep increase at extremely low c^{eq}, followed by a saturation plateau where Γ is nearly independent of concentration, one expects, on the basis of Eq. 1, precisely the $\Gamma(t)$ curves as found in Figure 5.

If we assume that the adsorption in this system is purely driven by attractive electrostatic interactions (pure "electrosorption"), it can be considered as a kind of ion-exchange process where macroions are exchanged for lithium counterions residing at the surface, so that the adsorbed amount reflects the available surface charge. As such a process is largely driven by

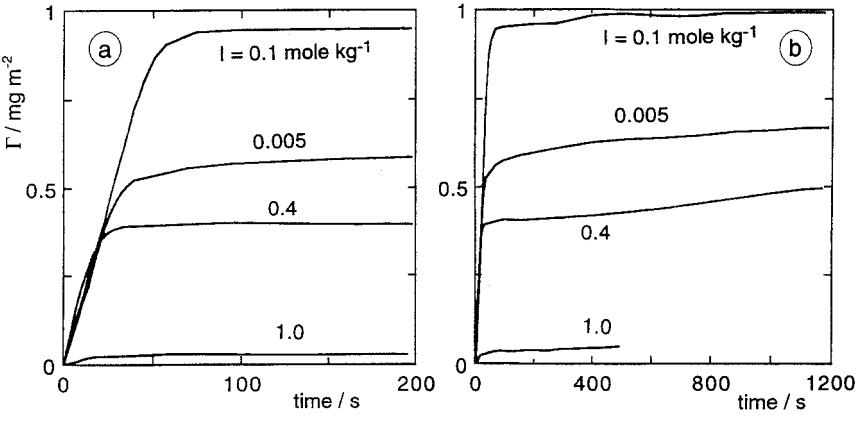

FIG. 5 Typical time courses of the adsorption of polyvinylpyridinium (PVP^+) on TiO_2 at various ionic strengths, as indicated: (a) the initial parts; (b) the curves for longer time scales. The polymer concentration was 10 mg kg^{-1}. In all experiments a buffer solution with ionic strength of 0.005 mole kg^{-1} and pH 8 was present; for solutions with a higher ionic strength LiCl was added. (Adapted from Ref. 26.)

the entropy change associated with the liberation of the small ions, it can be reversed by increasing the ionic strength. Indeed we observe complete desorption at ionic strengths beyond 1.0 M, which supports the idea that this is a case of pure electrosorption, for which other kinds of polymer/surface attraction do not play a role. At lower ionic strength the adsorbed amount initially increases slightly as a consequence of screening of lateral interaction between the adsorbed molecules, but the adsorbed amount hardly exceeds values corresponding to compensation of the available surface charge. We conclude that the behavior of this system is conceptually simple and adequately described by Eqs. 1 and 2.

A slightly more complicated case is obtained when adsorption takes place on the uncharged substrate polystyrene. Here, the example is for hydrophobically modified carboxypullulan (OxPu); we present data in Figure 6. The carboxypullulan was modified with dodecyl groups, the degree of substitution varying between 1% and 12%. Since the polystyrene substrate can be considered as essentially neutral, the adsorption must be driven by non-electrostatic, short-range interactions, probably of a hydrophobic nature. The data refer to adsorption in the absence of added salt; the pH was varied between 2 and 9. Consequently, the ionic strength was low in the pH range where the polymer is substantially charged; at the low pH end it increased, however, up to 10^{-2} M. As can be seen, initial adsorption rates are a function of both the pH and the degree of substitution with hydrophobic groups. As

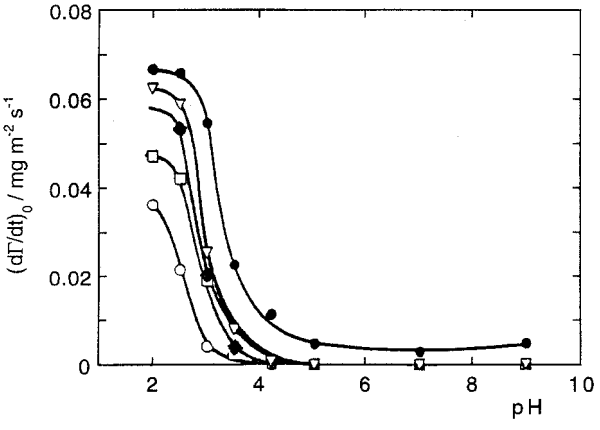

FIG. 6 Initial adsorption rates $(d\Gamma/dt)_0$ for the adsorption of various hydrophobically modified carboxypullulans on polystyrene. (○) unmodified OxPu, (□) OxPu-12/1, (◆) OxPu-12/3, (▽) OxPu-12/6 and (●) OxPu-12/12. Polymer concentration 100 mg L^{-1}, no background electrolyte added. (Adapted from Ref. 25.)

the substrate carries no charge, one expects that the only effect of a pH increase is to enhance the charge density on the polymer. One consequence of this would be increased swelling of the polymer, leading to slower diffusion. Indeed the adsorption rate is seen to decrease strongly in the pH range between 2.5 and 3.5 where most carboxylic groups of this polymer are titrated. One is therefore inclined to ascribe the reduced rate to slower transport. However, the decrease in rate is very large. If the diffusion rate were the only effect, one would anticipate a decrease of about a factor of 2 or 3, but the effect is much larger. For pH values higher than 5, the adsorption of all hydrophobically modified polymers but one is even entirely suppressed, indicating that the affinity is probably entirely lost.

Possibly, the capability of the molecules to establish a stable contact with the surface also influences the adsorption rate. Pure carboxypullulan can adsorb in its neutral form but not in the charged form. Evidently, adsorption of the charged polymer would reduce the entropy of counterions too much, thus suppressing the adsorption. Hydrophobic groups provide stronger anchoring; as can be seen, the sample with 12% dodecyl groups is able to maintain a low but finite adsorption rate even at pH values higher than 5. Since it is unlikely that the hydrophobic groups affect the diffusion to a large extent, we must conclude that the modified polymers have higher attachment rates (hence, lower attachment resistances), possibly because dodecyl groups help to stabilize the first contact a polymer makes with the surface.

In our next example [27] we compare polyacrylic acid (PAA) with hydrophobically modified polyacrylic acid (HM-PAA) (Figure 7). The two types of polymers have the same molar mass of 500,000 g mole^{-1}; the modified polymer carries 3% dodecyl groups. Figure 7 does not present $\Gamma(t)$ data, but adsorbed amounts measured in a standardized pH cycling procedure, and at a low ionic strength (0.001 M NaCl). Adsorbed amounts were measured at a chosen initial pH and after an adsorption time of 300 s (filled symbols). In the next series of experiments (open symbols) a pH switch was applied. Polymer was first adsorbed at pH 3 for 300 s, after which the surface was exposed to a polymer solution of some higher pH; this led to some desorption. After another 1000 s, the adsorbed amount remaining at the end of this sequence was again determined. As can be seen, there is pronounced hysteresis in this system: the adsorbed amounts at a fixed pH are lower than the amounts one obtains after adsorption at low pH followed by desorption induced by a pH increase. The pure PAA has lower adsorbed amounts, but also lower hysteresis, than the modified polymer (HM-PAA). An interesting observation is that in the pH range between 4 and 6 there is not that much difference between the initial adsorbed amounts (filled symbols) for the two polymers. Apparently, these polymers are capable of forming an adsorbed

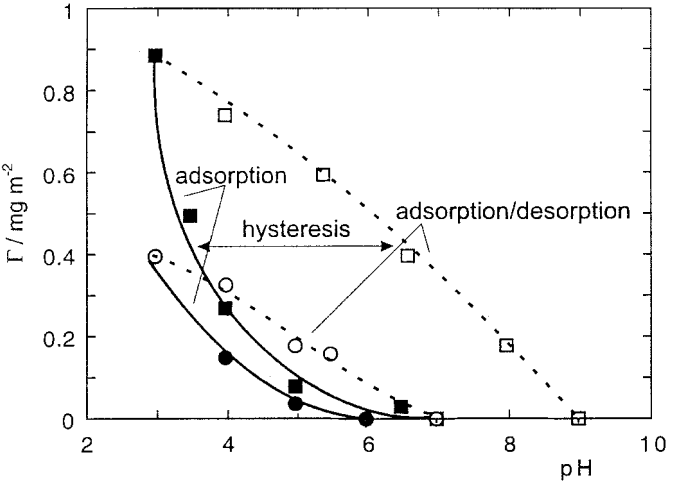

FIG. 7 Adsorption/desorption hysteresis of hydrophobically modified polyacrylic acid (HM-PAA, ■, □) on polystyrene, compared to that for unmodified PAA (●, ○). Concentration polymer 10 mg L^{-1}, electrolyte 0.001 M NaCl. Closed symbols: adsorption as a function of pH; open symbols: adsorbed amounts after initial adsorption at pH 3 and subsequently increasing the pH. (Data from Ref. 27.)

layer of the same density, and the extra anchoring capability provided by the hydrophobic groups does not significantly enhance the degree of adsorption.

The adsorbed amounts after the pH switch (open symbols) differ very strongly, though. Apparently, the hydrophobic groups provide much better anchoring stability to the polymer, even to the extent that the adsorption can be maintained up to pH 9. Once the modified polymer is well attached, it is much less easily removed than its unmodified counterpart. The conclusion one may draw from this is that the adsorbed amount at a fixed pH is mainly determined by the attachment rate, and that when the polymer is charged (at pH > 4), it is the charge density (and not the density of hydrophobic groups!) that largely determines this attachment rate and hence the measured adsorbed amount. Thus for polymers with strong nonelectrostatic binding energies one ends up with *undersaturated* layers, i.e., with adsorbed amounts that do not reflect adsorption equilibrium.

If this conclusion is correct, it implies that enhancing the attachment rate by lowering the repulsive barrier should bring the adsorbed amounts closer to equilibrium and reduce the hysteresis. To check this, the cycling experiments should be repeated at a higher ionic strength. The result of such a test is given in Figure 8 and fully confirms what was expected: the initially adsorbed amounts at a particular pH are larger and the hysteresis is largely suppressed when the salt concentration is increased to 0.1 M NaCl. This is

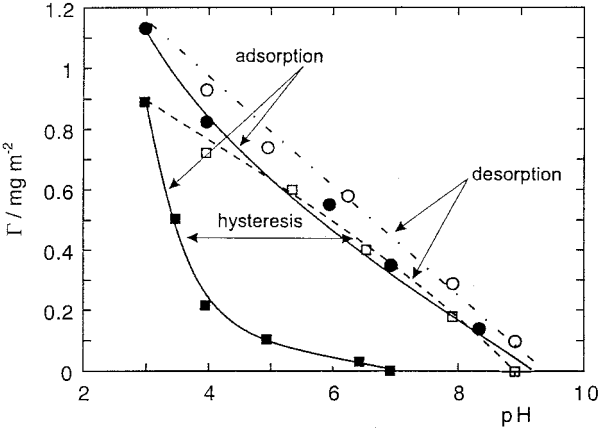

FIG. 8 Effect of ionic strength on the adsorption/desorption hysteresis of HM-PAA at polystyrene surfaces. Closed symbols: adsorption as a function of pH; open symbols: adsorbed amounts after initial adsorption at pH 3 and subsequently increasing the pH. ■, □ 0.001 M NaCl; ●, ○ 0.1 M NaCl. (Data from Ref. 27.)

an important finding, underlining the crucial role of electrostatic repulsion during adsorption. Further illustration comes from peculiar molecular weight effects observed by De Laat et al. [28] and by Geffroy et al. [29] in exchange experiments. These authors both investigated the adsorption of polyacrylic acid on mineral particles. They both used polydisperse samples of PAA and measured the molar mass distribution before and after adsorption in order to get some insight into fractionation effects. Fractionation is known to occur in many polymer adsorption processes and is driven by the fact that long polymers have a tendency to adsorb preferentially over shorter ones.

Surprisingly, De Laat as well as Geffroy found that from the original sample not the longest molecules but rather a middle fraction seemed to be preferentially adsorbed. This is demonstrated in Figure 9 (results of De Laat), which gives the molar mass distribution of both the original sample and that of the polymer remaining in solution after adsorption. As can be seen, the molar mass distribution in solution (which is of course the complement of that on the surface) has a pronounced dip in the middle, meaning that a narrower fraction populates the mineral surface. Moreover, one ob-

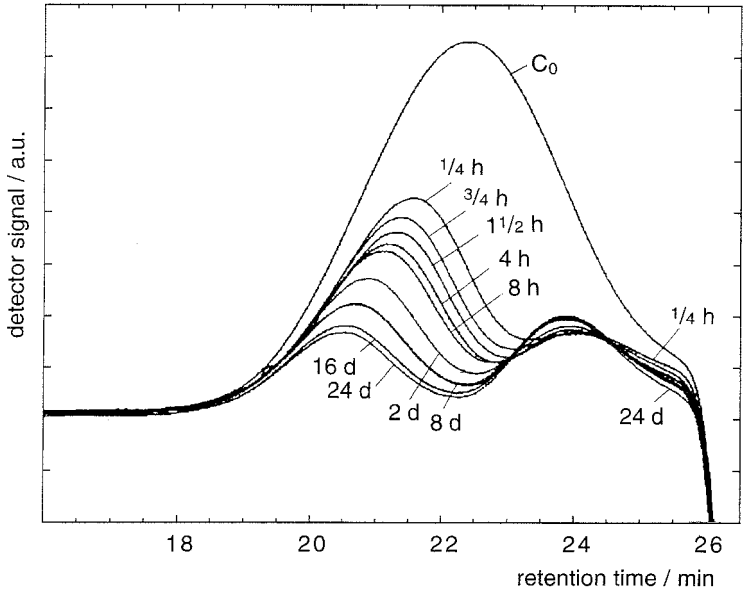

FIG. 9 Change in molecular weight distribution of polyacrylic acid in solution with time during adsorption onto $BaTiO_3$ (no electrolyte added). C_0: chromatogram before adsorption; chromatograms after adsorption for the indicated time in hours (h) or days (d). (Adapted from Ref. 28.)

serves that the position and depth of the dip shift over relatively long times, in this example up to 24 days. These findings were entirely confirmed by Geffroy, who directly determined (by a clever particle dissolution trick) the molar distribution of the adsorbed molecules.

The qualitative explanation of these effects is that, initially, the shorter molecules adsorb on account of their rapid diffusive transport. After prolonged exposure to the polymer solution, however, the adsorbed layer gradually exchanges short molecules for longer ones. This leads to an increase of the average molar mass in the adsorbed layer. However, the rate at which exchange occurs is clearly selective with respect to molar mass: molecules of intermediate mass are much more effective in this exchange process than very long ones, although the long ones are clearly favored for thermodynamic reasons. Hence it is concluded that the longer molecules experience a larger attachment resistance because they have more charge and are therefore more strongly repelled than shorter ones. This conclusion is supported by the finding that added salt shifts the average molar mass in the adsorbed layer to higher values, clearly because the barrier is removed; this can be seen, for example, by comparing the experimental results in Figures 9 and 10. From all this, it seems there are good reasons to consider electrostatic

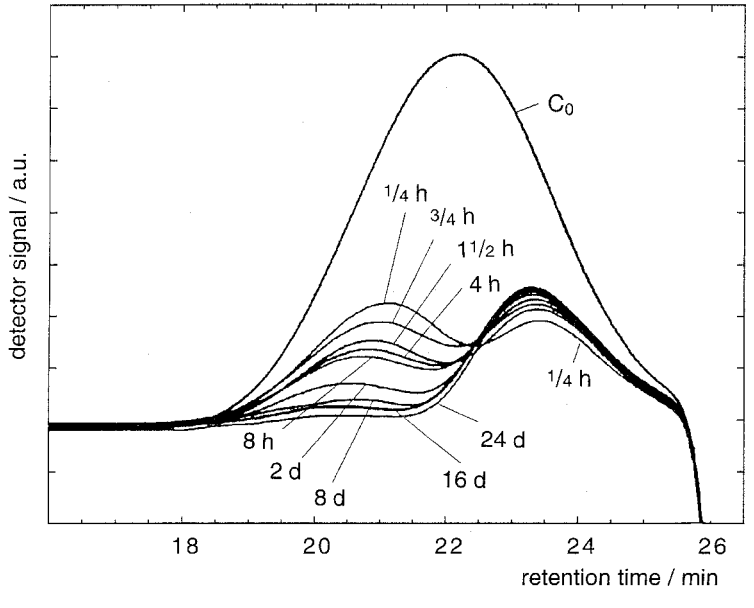

FIG. 10 As Figure 9, now for adsorption from 0.03 M KNO_3 aqueous solutions. (Adapted from Ref. 28.)

adsorption barriers from a theoretical point of view; this is discussed in the next section.

V. A THEORY FOR THE ATTACHMENT BARRIER

The approach adopted by Hoogendam et al. [14] for R_a is based on the general Kramers theory for reaction rates, in the isothermal limit, i.e., considering polymer chains (with fixed charge density) with fully relaxed conformations. The starting equation reads[†]

$$R_a = \int_{\delta}^{\ell} \frac{1}{D} \left[e^{u(\Gamma, z^*)/kT} - 1 \right] dz^* \tag{4}$$

where u is the effective Gibbs energy of a polymer chain held with its closest segment at a distance z^* from a surface covered with polymer to an amount Γ, and ℓ is a microscopic length corresponding to the size of a monomer. As before (see Sec. III), δ is the thickness of the stagnant layer. Of course, the polyelectrolyte feels the field from the wall as screened by counterions. In order to obtain its Gibbs energy, an average over all possible conformations, subject to the constraint that only one segment is at z^*, and all others further away, should be determined. This conformational average was calculated using a self-consistent field (SCF) method as originally developed by Scheutjens and Fleer [30,31]. Since the polymer is considered as equilibrated, the quantity $\exp[u(\Gamma, z^*)/kT]$ is actually a ratio of partition functions [22]:

$$R_a = \int_{\delta}^{\ell} \frac{1}{D} \left[\frac{Q_\infty}{Q(z^*)} - 1 \right] dz^* \tag{5}$$

with Q_∞ and $Q(z^*)$ partition functions of a chain having its closest segment far away, or at a distance z^* from the surface, respectively. The diffusion coefficient D was supposed to be insensitive to, e.g., hydrodynamic effects and the position of the chain, and thus to have the same value near the surface as in the bulk of the solution.

In Figure 11 we present the Gibbs energy, in terms of $Q_\infty/Q(z^*)$, as function of distance z^* for a fully charged polyelectrolyte approaching an initially neutral wall covered with polymer of like charge. The normalized adsorbed amount θ^{eq} (number of equivalent monolayers of segments) of charged polymer on the neutral substrate is indicated, and was also calculated by means of SCF theory, but now assuming complete equilibrium. Clearly, as θ^{eq} in-

[†] In Ref. 14 a slightly different (and, in fact, incorrect) version of Eq. 4 was given without the -1 term in the integrand. However, for the calculations the correct equation was used.

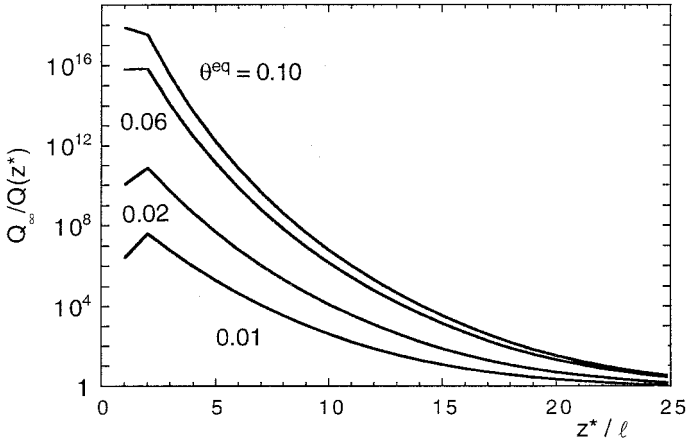

FIG. 11 Attachment barrier for a polyelectrolyte (charge density $z_p = -1$), approaching an (initially) uncharged surface. The curves are calculated for several degrees of polymer coverage θ^{eq}, i.e., for different stages in the adsorption process. (Calculations by Hoogendam [14].)

creases, a substantial repulsive resistance builds up. Integrating over z^* from δ to ℓ and inserting the result into Eq. 1 we can now calculate the adsorption rate at a given θ^{eq}. Finally, by another integration (over time) we can explicitly calculate the time-dependent adsorbed amount θ_{kin} as a function of time. A few results, for chains of 100 segments, an initially neutral surface, $R_t^{-1} = 10^{-6}$ m s^{-1}, and $D = 10^{-12}$ m^2 s^{-1} are given in Figure 12, both on a linear time axis (Figure 12a), and on a logarithmic scale (Figure 12b). In Figure 12a, the kinetic curves $\theta_{kin}(t)$ have qualitatively the same appearance as those found in many experiments: an initial increase followed by a rather abrupt leveling off to what seems to be the saturated adsorption. This saturation level depends strongly on ionic strength. However, inspection of the curves in Figure 12b, which extend to much larger times, brings out that at low ionic strength the saturation at finite times is only apparent. Very long times (far beyond any experimental range) are needed to really establish equilibrium. Only for the two or three highest salt concentrations, the rate that is calculated is sufficiently high to ensure the establishment of equilibrium on an experimental time scale. This is qualitatively what is also found in experiments.

Similar calculations for a surface that is initially charged oppositely to the polymer (charge density z_p) are shown in Figure 13. The results are essentially very similar, the only difference being that the resistance now

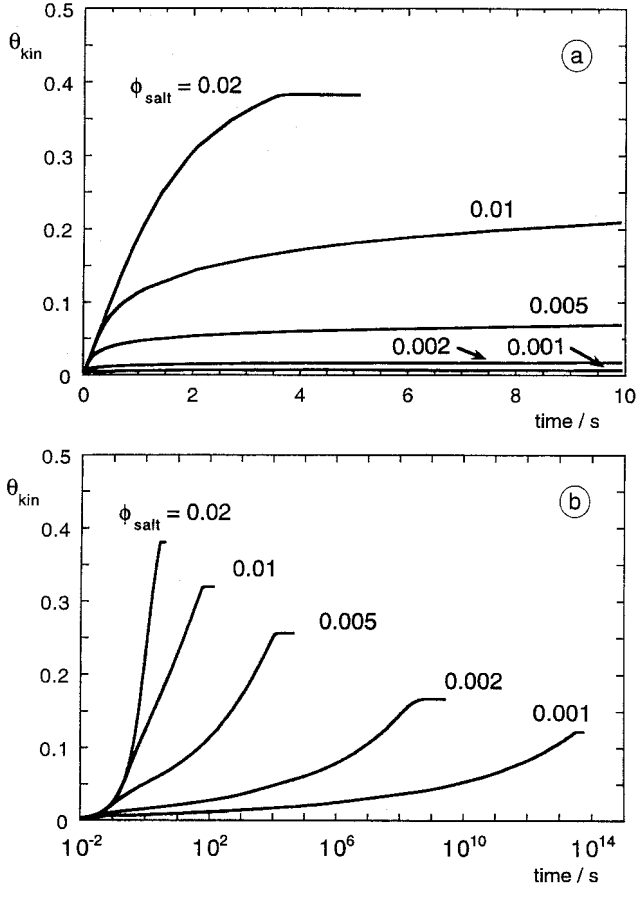

FIG. 12 Adsorption of a polyelectrolyte ($z_p = -1$) on an uncharged surface as a function of time for various 1–1 electrolyte concentrations (indicated as volume fractions ϕ_{salt}). In (a) the adsorption is given for short times, in (b) for long times (on a logarithmic scale). Endpoints in (b) are for equilibrium adsorption and a polymer concentration of 300 mg L^{-4} ($\phi_{polymer} = 10^{-4}$). (Calculated data from Ref. 14.)

only comes up after the surface charge has been compensated, hence beyond $\theta = -z_s/z_p$. The kinetic curves and adsorbed amounts are correspondingly shifted.

One thing the theory makes quite clear is that at low and moderate ionic strength the adsorption rate falls quite abruptly to very low values once a repulsive charge starts to build up on the surface. Therefore at low and moderate ionic strength the maximum adsorption will never exceed the value

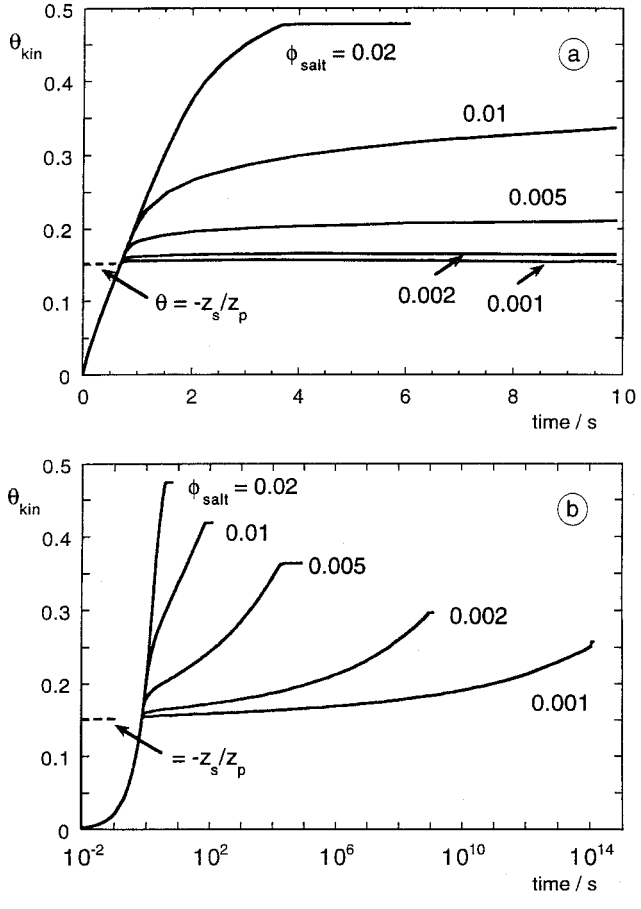

FIG. 13 Adsorption of a polyelectrolyte ($z_p = -1$) on a charged surface ($z_s = +0.15$) for various 1–1 electrolyte concentrations. The point where the surface charge is compensated by the charge on the adsorbed polyelectrolyte is indicated. (a) Time course of adsorption on a short timescale; (b) for long times (logarithmic scale). The endpoints in (b) correspond to equilibrium adsorption. Polymer concentration 300 mg L^{-1} ($\phi_{polymer} = 10^{-4}$). (Calculations by Hoogendam [14].)

corresponding to charge compensation by more than a few percent, no matter how strong the anchoring energy.

This is qualitatively what one finds in many experiments. It also provides an explanation for what happens with surfaces which bind segments very strongly; on these surfaces the adsorbed amount can be enhanced by adding salt or by decreasing the charge density on the polymer by changing pH,

but restoring the conditions of low salt or high charge *does not restore* the low adsorbed amount, i.e., the adsorption is irreversible under cycles of pH or ionic strength.

So far, our calculations were done for a fixed chain length (100 segments). However, it is likely that the resistance depends on chain length: longer chains experience larger resistances on account of their higher number of charges. This is in line with the fractionation effects described by De Laat et al. and Geffroy et al. The precise dependence on chain length remains a theoretical challenge, though. Another problem that should be mentioned is that the calculation of $Q(z^*)$ does not explicitly consider the presence of counterions around the polyion. In other words, the Gibbs energy $u(z^*, \theta^{eq})$ calculated is that of a bare chain in a fixed external field, and perturbations of that field by the polyion are ignored. This does not affect the qualitative conclusions but tends to overestimate the theoretically calculated attachment barrier. Attempts to improve on this are under consideration.

VI. NEW EXPERIMENTAL APPROACHES

The experimental results discussed so far had one major drawback, namely that it was impossible to correlate knowledge about the electric field acting upon the polyelectrolytes with the adsorption flux. The reason is that the field is not precisely known, as it is determined (and modified) by Γ itself and there is no simple procedure to assess its strength. One way to determine the electric field arising from a charged surface is to measure the interaction between two such surfaces, or between the surface and a surface of known potential (e.g., silica) in solution. This can be done using surface force measurement techniques, the two most well-known examples being probably the surface force apparatus (SFA) and colloidal probe atomic force microscopy (colloidal probe AFM). In the SFA two molecularly smooth surfaces (generally mica surfaces) are placed in a crossed-cylinder geometry and their interaction is determined as a function of separation [32,33], whereas in colloidal probe AFM the interaction between a spherical particle (the colloidal probe, $\varnothing$ 2–10 μm) and a flat surface is measured [34]. By fitting the interaction curves to the Poisson–Boltzmann equation for electric double layer interaction, the surface potential is obtained (see, e.g., Ref. 34). To assess the change in the electric field during polyelectrolyte adsorption, one or both of the surfaces can be covered with polyelectrolyte to varying degrees. The effect of background electrolyte on the electric field resulting from the (partly) covered surface is easily accessible. SFA measurements on polyelectrolyte-covered surfaces have been performed, for example, by Rojas et al. [35]. They measured the interaction between equilibrated adsorption layers of low-charge-density cationic polyelectrolyte on negatively charged

mica surfaces. In this case no electrostatic repulsion was observed, which was attributed to coadsorption of small ions resulting in near neutral adsorption layers. It was found that increasing the ionic strength of the solution after adsorption gives rise to some desorption and an increase in layer thickness. These phenomena can be explained from the screening of electrostatic attraction between polyelectrolyte segments and the solid surface, which promotes the displacement of adsorbed molecules as a whole as well as some charged segments of adsorbed polyelectrolyte.

Not only the surface but also the polyelectrolyte molecule has an electric field around it, and these fields affect each other when the molecule approaches the surface. This may be mimicked by covering one of the surfaces with polyelectrolyte and measuring the interaction on approach. Of course, this is not the same as when free (dissolved) polyelectrolyte molecules are approaching a surface, but it may give an idea of the electrostatic barrier felt upon adsorption. Here, the advantage of the AFM over the SFA is that the approach is done in a continuous way (in the SFA stepwise) and can be done much faster (up to frequencies of the order of 100 Hz; in each cycle a distance of several hundreds of nanometers is traveled). In the experimental studies discussed in Secs. II and IV the charge on the bare substrate surfaces was either fixed or determined by solution conditions (pH and/or electrolyte concentration). In the latter case one may vary the solution conditions in order to study the effect of the surface charge and potential on adsorption kinetics. However, for weak polyelectrolytes, variation of the solution conditions also affects the charge of the polyelectrolyte molecules. It would be much more direct to study the rate of adsorption on a surface with externally controlled potential ψ, i.e., an electrode. The advantage of this approach is that adsorption can be studied over a much wider range of surface potentials without changing other experimental conditions, such as the substrate material and the composition of the solution. By using silicon wafers with a conducting film as the sorbent surface it is possible to follow adsorption by optical reflectometry while imposing an external potential on the solid/liquid interface. In this way the adsorption of various ionic surfactants and proteins on indium tin oxide (ITO), a semiconducting material, has been studied in our laboratory [36]. As an example the adsorption of cetyltrimethylammonium ions (CTA^+) on ITO as a function of applied potential is shown in Figure 14. At positive applied potentials the surfactant ions experience an electrostatic barrier for adsorption, which monotonically decreases with decreasing potential. At sufficiently high negative potentials there is no barrier for adsorption, and the adsorption flux corresponds to the transport-limited flux of CTA^+ to the surface.

We plan to use this approach to study polyelectrolyte adsorption and measure $\Gamma(\psi)$ and $d\Gamma(\psi)/dt$ as a function of applied potential. As the sub-

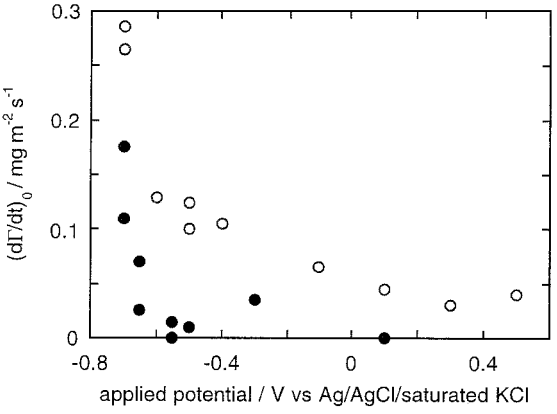

FIG. 14 Initial rates of adsorption $(d\Gamma/dt)_0$ of cetyltrimethylammonium bromide (CTAB) onto indium tin oxide (ITO) as a function of externally applied potential, at two pH values (●, pH 5.6; ○, pH 9). Concentration CTAB 0.5 mM, background electrolyte 10^{-3} M KCl. (Unpublished data of E.J.M. Bollen and J.M. Kleijn, Wageningen University.)

strate we will employ thin gold films, deposited onto (Ti-treated) silicon wafers. Imposing a potential to the gold film creates an electric field in the solution. There are a number of technical problems, however. First, the potential measured in the experiment is that between the conductive substrate and a reference electrode. However, it is the potential of the substrate surface *with respect to the bulk solution* that determines whether charged molecules are electrostatically attracted or repelled when approaching the surface, and that potential is not known. (See also, for example, Figure 14: it is clear that the boundary between electrostatic repulsion and attraction felt upon adsorption does not coincide with an applied potential of 0.0 V vs. the reference electrode.) Here, again, force measurements with an AFM can bring relief: the surface potential with respect to the bulk solution can be determined by measuring the electrostatic force between the electrode and a spherical particle of which the surface potential is known. This requires careful surface force measurements versus applied potential. The feasibility of this method has been demonstrated by Bard and coworkers [37,38], who performed measurements on gold and semiconducting TiO_2 using a silica colloidal probe. Secondly, one should make sure that the *variations* in surface potential follow those in the applied potential, e.g., there should be no significant potential drops inside the solid phase. With metals, this is quite unlikely, but it needs to be checked by AFM, too. Ionization of surface groups and/or specific adsorption of small ions may also result in surface

potentials deviating from the applied potential. For example, the data in Figure 14 show that the adsorption rate of CTA^+ on ITO is dependent not only on applied potential but also on pH. As the charge on the surfactant molecules is insensitive to pH, this indicates that the surface potential of the ITO substrate is still partly determined by the pH-dependent ionization state of the surface OH-groups. Finally, the optical signal detected in the reflectometer may be influenced by ψ, since the refractive index of the substrate may change with the concentration of charge carriers in the solid (*electro-optic or surface-charging effect*) [39,40]. Therefore, care must be taken to separate this effect from the change in signal due to adsorption.

VII. OUTLOOK

With new data for polyelectrolytes obtained with the techniques described above it should become possible to determine carefully the effects of ionic strength and externally controlled surface potential on the rate of adsorption of polyelectrolytes. We hope that the effects of molar mass and charge density of the polyelectrolyte, as well as the nature of that charge (annealed or quenched) can be established. This should stimulate further theoretical research aimed at constructing an adequate equivalent of the Von Smoluchowsky–Fuchs theory for the rate of flocculation. At present, it would seem that an analysis of the adsorption process taking all complications into account necessitates a simulation-oriented approach.

REFERENCES

1. Fleer GJ, Cohen Stuart MA, Scheutjens JMHM, Cosgrove T, Vincent B. Polymers at Interfaces. London: Chapman and Hall, 1993.
2. Hesselink FTh. Adsorption of polyelectrolytes from dilute solution. In: Parfitt GD, Rochester CH, eds. Adsorption from Solution at the Solid–Liquid Interface. London: Academic Press, 1983:277–412.
3. Böhmer MR, Evers OA, Scheutjens JMHM. Weak polyelectrolytes between two surfaces: adsorption and stabilization. Macromolecules 1990; 23:2288–2301.
4. Muthukumar M. Adsorption of a polyelectrolyte chain to a charged surface. J Chem Phys 1987; 86:7230–7235.
5. Varoqui R, Johner A, Elaissari A. Conformation of weakly charged polyelectrolytes at a solid–liquid interface. J Chem Phys 1991; 94:6873–6878.
6. Chatelier X, Joanny JF. Adsorption of polyelectrolyte solutions on surfaces: a Debye–Hückel theory. J Phys II (Paris) 1996; 6:1669–1686.
7. Shubin V, Linse P. Self-consistent field modeling of polyelectrolyte adsorption on charge-regulating surfaces. Macromolecules 1997; 30:5944–5952.

8. Dupont L, Foissy A. Evaluation of the adsorption trends of a low molecular-weight polyelectrolyte with a site-binding model. Colloids Surfaces A 1996; 110:235–248.
9. Van de Steeg HGM, Cohen Stuart MA, De Keizer A, Bijsterbosch BH. Polyelectrolyte adsorption: a subtle balance of forces. Langmuir 1992; 8:2538–2546.
10. Dijt JC, Cohen Stuart MA, Fleer GJ. Kinetics of polymer adsorption and desorption in capillary flow. Macromolecules 1992; 25:5416–5423.
11. Hoogeveen NG, Cohen Stuart MA, Fleer GJ. Polyelectrolyte adsorption on oxides. II. Reversibility and exchange. J Colloid Interface Sci 1996; 182:146–157.
12. Dijt JC, Cohen Stuart MA, Fleer GJ. Reflectometry as a tool for adsorption studies. Adv Colloid Interface Sci 1994; 50:79–101.
13. Hoogendam CW, De Keizer A, Cohen Stuart MA, Bijsterbosch BH, Batelaan JG, Van der Horst PM. Adsorption mechanisms of carboxymethyl cellulose on mineral surfaces. Langmuir 1998; 14:3825–3839.
14. Cohen Stuart MA, Hoogendam CW, De Keizer A. Kinetics of polyelectrolyte adsorption. J Phys Condens Matter 1997; 9:7767–7783.
15. Cohen Stuart MA, Fleer GJ. Adsorbed polymer layers in nonequilibrium situations. Annu Rev Mater Sci 1996; 26:463–500.
16. Adamczyk Z, Dabros T, Czarnecki J, Van de Ven TGM. Particle transfer to solid surfaces. Adv Colloid Interface Sci 1983; 19:183–252.
17. Dabros T, Van de Ven TGM. A direct method for studying particle deposition onto solid surfaces. Colloid Polym Sci 1983; 261:694–707.
18. Dijt JC, Cohen Stuart MA, Hofman JE, Fleer GJ. Kinetics of polymer adsorption in stagnation point flow. Colloids Surfaces 1990; 51:141–158.
19. Dijt JC, Cohen Stuart MA, Fleer GJ. Competitive adsorption kinetics of polymers differing in length only. Macromolecules 1994; 27:3219–3228.
20. Rebar VA, Santore MM. Molecular weight effects and the sequential dynamic nature of poly(ethyleneoxide) adsorption on silica from polydisperse aqueous solution. Macromolecules 1996; 29:6273–6283.
21. Santore MM, Fu Z. Direct measurement of molecular-weight driven competition during polymer adsorption. Macromolecules 1997; 30:8516–8517.
22. Semenov AN, Joanny JF. Kinetics of adsorption of linear homopolymers onto flat surfaces: Rouse dynamics. J Phys II (Paris) 1995; 5:859–876.
23. Von Smoluchowski M. Versuch einer mathematischen Theorie der Koagulationskinetik kolloider Lösungen. Z Physik Chem 1916; 92:129–168.
24. Fuchs N. Influence of the charge of aerosols on their stability. Z Physik 1934; 89:736–742.
25. Paris E, Cohen Stuart MA. Adsorption of hydrophobically modified 6-carboxypullulan on a hydrophobic surface. Macromolecules 1999; 32:462–470.
26. Hoogeveen NH, Cohen Stuart MA, Fleer GJ. Polyelectrolyte adsorption on oxides. I. Kinetics and adsorbed amounts. J Colloid Interface Sci 1996; 182: 133–145.
27. Göbel JG, Besseling NAM, Cohen Stuart MA, Poncet C. Adsorption of hydrophobically modified polyacrylic acid on a hydrophobic surface: hysteresis

caused by an electrostatic adsorption barrier. J Colloid Interface Sci 1999; 209: 129–135.
28. De Laat AWM, Van den Heuvel GLT, Böhmer MR. Kinetic aspects in the adsorption of polyacrylic acid salts onto $BaTiO_3$. Colloids Surfaces A 1995; 98:61–71.
29. Geffroy C, Persello J, Foissy A, Lixon P, Tournilhac F, Cabane B. Molar mass selectivity in the adsorption of polyacrylates on calcite. Colloids Surfaces A 2000; 162:107–121.
30. Scheutjens JMHM, Fleer GJ. Statistical theory of the adsorption of interacting chain molecules. I. Partition function, segment density distribution and adsorption isotherms. J Phys Chem 1979; 83:1619–1635.
31. Scheutjens JMHM, Fleer GJ. Statistical theory of the adsorption of interacting chain molecules. II. Train, loop, and tail size distribution. J Phys Chem 1980; 84:178–190.
32. Israelachvili JN. Thin film studies using multiple-beam interferometry. J Colloid Interface Sci 1973; 44:259–272.
33. Israelachvili JN, Adams GE. Measurement of forces between two mica surfaces in aqueous electrolyte solutions in the range 0–100 nm. J Chem Soc Faraday Trans I 1978; 74:975–1001.
34. Ducker WA, Senden TJ, Pashley RM. Direct measurements of colloidal forces using an atomic force microscope. Nature 1991; 353:239–241.
35. Rojas OJ, Claesson PM, Muller D, Neuman RD. The effect of salt concentration on adsorption of low charge density polyelectrolytes and interactions between polyelectrolyte coated surfaces. J Colloid Interface Sci 1998; 205:77–88.
36. Bos MA, Shervani Z, Anusiem ACI, Giesbers M, Norde W, Kleijn JM. Influence of the electric potential of the interface on the adsorption of proteins. Colloids Surfaces B 1994; 3:91–100.
37. Hillier AC, Kim S, Bard AJ. Measurement of double-layer forces at the electrode/electrolyte interface using the atomic force microscope: potential and anion dependent interactions. J Phys Chem 1996; 100:18808–18817.
38. Hu K, Fan FRF, Bard AJ, Hillier AC. Direct measurement of diffuse double-layer forces at the semiconductor/electrolyte interface using an atomic force microscope. J Phys Chem B 1997; 101:8298–8303.
39. Kleijn JM, Cohen Stuart MA, De Wit A. Electro-optic effect in the solid phase of the indium tin oxide electrolyte solution interface observed by reflectometry. Colloids Surfaces A 1996; 110:213–217.
40. Beaglehole D, Webster B, Werner S. Ellipsometry study of the adsorption of molecules at electrolyte interfaces with gold and stainless steel. J Colloid Interface Sci 1998; 202:541–550.

11

Electric Light Scattering of Colloid Particles in Polyelectrolyte Solutions

TSETSKA RADEVA Bulgarian Academy of Sciences, Sofia, Bulgaria

I. INTRODUCTION

Electro-optics is abundantly used in the investigation of the electrical properties of macromolecules and colloid particles dispersed in solution [1–3]. The electro-optical signal contains also information on the shape and size of the particles investigated, which makes this method useful for studying the stability of colloids in the presence of various additives. Electric birefringence and electric dichroism are extensively used to determine the conformations of biopolymers and their complexes with various low molecular compounds in solution. Many other applications of electro-optics for studying colloids and polymer solutions are shown in the literature, but the information on using this technique for studying mixed colloid–polymer systems is small.

Our first attempt to apply electro-optics in the investigation of the adsorption of neutral polyacrylamide on kaolinite particles was in 1988 [4,5]. Several electro-optical parameters were used to follow the adsorption of polymer on colloid particles—the amplitude of the electro-optical effect, the critical frequency of relaxation of the low- and high-frequency effects, the electro-optical decay time after the switching off of the electric field. Variations in these parameters with concentration of the added polymer give information on the particle electric polarizability, the thickness of the adsorbed polymer layer, the size of aggregates that appear in the suspension due to flocculation [4–10], etc.

The variations in all enumerated parameters are more expressive when a polyelectrolyte of opposite charge is added to the suspension of colloid par-

ticles [11–18]. In addition, a new low-frequency effect appears in the suspension, stabilized by polyelectrolyte adsorption, which is absent in the suspension containing neutral polymer. As in polyelectrolyte solutions, polarization of ''slow'' counterions along the polyion surface is supposed to be responsible for the appearance of this effect in colloid–polyelectrolyte suspension [11–18].

The similarity observed between the electro-optical effect behavior of a suspension, stabilized by polyelectrolyte adsorption, and that of the same polyelectrolyte in solution [12–18] reveals an additional possibility for experimental investigation of dilute systems, since when the polyelectrolyte molecules adsorb on colloidal particles, the electro-optical effect becomes strong enough to be observed in very dilute solutions.

The effect of cationic polyacrylamide adsorption on the stability of aqueous cellulose suspension has been electro-optically studied by Khlebtsov et al. [19,20]. The variations in transmitted light modulation in low-frequency (3–45 Hz) square-pulsed a.c. fields have been found to correlate well with the adsorption isotherm. The influence of sodium carboxymethylcellulose adsorption on the electro-optical behavior of negatively charged SiO_2 (anisometric aggregates, consisting of monodisperse spherical particles) has also been studied, and an increase of the particle induced dipole moment and its time of relaxation has been found [21,22].

The electro-optical behavior of colloids and solutions of macromolecules is very similar to that found for the real part of their dielectric constants [23,24]. Being a differential technique, however, electro-optics is superior to dielectric relaxation spectroscopy because it enables the determination of the direction of the different physical contributions to the effect [24–26]. Being not essentially influenced by the conductivity of the solution, the electro-optical technique can also be applied at lower frequencies (with respect to the dielectric measurements), thus giving information on the particle or macromolecule rotational relaxation. Owing to its applicability for measuring effects as a function of the field frequency (usually in the interval $0–10^6$ Hz), electro-optics is also superior to the quasi-elastic light scattering method. Electro-optical measurements provide, on the other hand, a complementary means of obtaining information on the electrical surface properties of colloids in the presence of a surrounding polymer layer with respect to the classical electrophoretic techniques [4,5,8–10,13,15,16].

The results collected in this review are focused to demonstrate the advantages of electro-optics for investigation of the electrical properties of anisometric particles in dilute suspensions containing polyelectrolytes. Results on the structure of the adsorbed macromolecules and the stability of suspensions containing polyelectrolytes will also be discussed.

II. MATERIALS AND METHOD

A. Polyelectrolytes

Fractionated polyacrylamide (PAM) of molecular weight 3.7×10^5, prepared by radical copolymerization (Institute Charles Sadron, France), is hydrolyzed to different degrees τ%, determined by potentiometric titration to be 3.4, 9.8, and 19.1%. Sodium carboxymethylcellulose (NaCMC) with molecular weight 2.5×10^5 and degree of substitution 1.2 is supplied by Hercules (Blanose 12M 31P). Two sodium polystyrenesulfonate (NaPSS) samples with molecular weights 7×10^4 and 1×10^6 are supplied by Sigma-Aldrich Chemie GmbH. Calcium carboxymethylcellulose (CaCMC) and magnesium polystyrenesulfonate (MgPSS) are prepared from the stock solutions, dialyzed against 1 M $CaCl_2$ and 5×10^{-1} M $MgCl_2$, respectively, for 3 days and against bidistilled water for 1 week in order to remove the extraneous ions.

B. Particles

Two kinds of monodisperse ellipsoidal particles are specially synthesized for purposes of these investigations. Ferric hydrous oxide particles (β-FeOOH) are prepared by acid hydrolysis of a 1.8×10^{-2} M $FeCl_3$ solution containing 10^{-5} M HCl over a period of 3 weeks at room temperature [27]. Free Fe^{3+} ions are removed by centrifugation. The structure of β-FeOOH is of the hollandite type [28,29]. In acid medium, β-FeOOH particles are positively charged due to interactions of protons with hydroxyl groups on the particle surface. The isoelectric point is found to be near pH 7 [9]. Unlike the crystalline α-FeOOH or α-Fe_2O_3, β-FeOOH is found to be purely an anionic exchanger with no cation exchange branch, even in alkali [29]. By electron microscopy, the dimensions of the major and minor axis of the ellipsoidal particle are determined to be 200 and 50 nm (axial ratio 4).

Ellipsoidal hematite (α-Fe_2O_3) particles are prepared by forced hydrolysis of 2×10^{-2} M $FeCl_3$ solution containing 2×10^{-4} M NaH_2PO_4, heated in tightly stoppered Pyrex glassware in a preheated oven at 100°C for 2 days [30]. The precipitate obtained is repeatedly centrifuged and washed with distilled water to remove the extraneous ions. The morphology of these particles is also well studied [28,31], and the particle isoelectric point is found near pH 7 [32]. The dimensions of the major and minor axis of the hematite particle are found to be 420 and 190 nm (axial ratio 2.2).

Weight concentrations of the aqueous β-FeOOH and α-Fe_2O_3 suspensions used in electro-optical and electrophoretic measurements are 4×10^{-3} and 10^{-3} g dm^{-3}, respectively, and their conductivity is 2×10^{-6} Sm^{-1}. Each sample suspension is sonicated at 22 kHz for 1 min before polymer addition.

Electric light scattering is recorded at an angle 90° with respect to the electric field, using white unpolarized light [3].

C. Electric Light Scattering Method

In electro-optics, the optical effect of the colloid is measured in the presence of an electric field. The optical effect is related to the electrical moment orientational mechanism, which in turn reflects the electrical double layer features of the particles through its electrical polarizability [1–3].

1. Steady-State Electro-Optical Effect

When we apply an electric field to a suspension of anisometric colloid particles (or a solution of polyelectrolyte molecules), the particles tend to orient into the field direction, and this results in a macroscopic optical anisotropy effect. This effect may be expressed by the equation

$$\alpha = \alpha_s \Phi \tag{1}$$

where α is the steady-state electro-optical effect (light scattering, birefringence, or dichroism) at field strength E, α_s is the effect at saturation (infinite field), and Φ is an orientation function that reflects the degree of particle orientation at field E. For rigid symmetric particles oriented by their dipole moments along the long axis, the orientation function Φ is defined by [33,34]

$$\Phi = \int_0^{\pi} f(\theta) \left(\frac{3 \cos^2\theta - 1}{2} \right) 2\pi \sin \theta \, d\theta \tag{2}$$

where θ is the angle between the electric field and the particle axis and $f(\theta)$ is an angular orientation distribution function

$$f(\theta) = \frac{e^{-U/kT}}{\displaystyle\int_0^{\pi} e^{-U/kT} 2\pi \sin \theta \, d\theta} \tag{3}$$

In Eq. 3, U is the interaction energy with the electric field defined by

$$-\frac{U}{kT} = \frac{\mu E B}{kT} \cos \theta - \frac{(\gamma_1 - \gamma_2)E^2}{2kT} \cos^2\theta \tag{4}$$

where μ is the permanent dipole moment (if it exists) along the particle long axis, $(\gamma_1 - \gamma_2)$ is the excess of electric polarizability with respect to the long a and transverse b axes of the particle, B is an internal field function, and kT is the Boltzmann factor.

The steady-state light scattering effect is defined as

$$\alpha = \frac{I_E - I_0}{I_0} \tag{5}$$

where I_E and I_0 are the intensities of scattered light when an electric field of strength E is applied to the suspension and at zero field. At low fields, α is given by

$$\alpha = \frac{A(Ka, Kb)}{I_0(Ka, Kb)} \left[\frac{\mu^2}{k^2T^2} + \frac{(\gamma_1 - \gamma_2)}{2kT} \right] E^2 \tag{6}$$

where $A(Ka, Kb)$ and $I_0(Ka, Kb)$ are optical functions depending on the particle dimensions [35], $K = 2\pi/\lambda \sin(\theta'/2)$, λ is the wavelength of the incident light, and θ' is the angle of observation. For suspension with no aggregation, the optical functions in Eq. 6 are constant. By taking the induced dipole moment to be proportional to the field strength, information on the value and the direction of particle polarizability can be derived from this expression.

The magnitude of the induced dipole moment depends on the polarization of the body of the particle (covalent polarizability), its surface charge, and the ionic atmosphere surrounding the particle. The translational diffusion of counterions on the particle or the polyion surface is now accepted to be the main reason for the creation of their induced dipole moments. For high charged polyelectrolytes, the ionic induced moments are classified to be ''fast'' or ''slow'' depending on the relaxation time of the counterion distribution along the polyion surface [25,36]. According to Oosawa [37], counterions in a polyelectrolyte solution are classified to be either freely moving outside the region occupied by the polyions, or bound but mobile in this region. He divided the bound counterions into counterions mobile in the potential valley along the polyion chain and counterions in the potential trough made by the macroion. In the theoretical treatment of Gueron and Weisbuch [38], the bound counterions are classified as ''tightly'' bound in the immediate vicinity of the polyion and ''loosely'' bound counterions surrounding the ''tightly'' bound ones [25,26]. The ''tightly'' bound counterions are expected to have lower mobility with respect to the ions in a free medium, since they are trapped in a strong potential produced by the polyion charge. The translational diffusion of these counterions along the polyion surface is supposed in [25,26] to be responsible for the ''slow'' or low-frequency (LF) relaxation of the electro-optical effect in polyelectrolyte solutions. The mobility of the ''loosely'' bound counterions is assumed to be equal to that of ions in a free medium, since they move in a shallow electrostatic potential of the polyion (on the order of thermal energy kT). Motion of the ''loosely'' bound counterions within a range with a diameter equal to

the average distance between polyions is supposed to be responsible for the ''fast'' or high-frequency (HF) relaxation of the electro-optical effect [25,26].

More details on the origin of the ''fast'' and ''slow'' dipoles in colloid–polyelectrolyte suspensions will be given below. It is necessary to note here that terms ''tightly'' and ''loosely'' for the bound counterions are used in this review as equivalent to the ''condensed'' and ''free'' (''uncondensed'') counterions in terminology of Manning [39,40]. It will be recalled that for polyelectrolytes with charge density greater than about one charge per 7.1 Å, the condensation theory of Manning [39,40] predicts that counterions will condense onto the polyion surface to reduce its net charge to a value that depends only on the counterion valence. The ''condensed'' counterions may vary from localized counterions, which are site bound, to delocalized counterions, which can translate along the polyion surface. The ''uncondensed'' counterions are completely dissociated and form the Debye atmosphere of the polyion. Polyelectrolytes with low charge density are thought by Manning to be completely dissociated with all counterions interacting with the polyion by Debye–Hückel forces. The counterions governed by Debye–Hückel potential are also classified as ''free'' in [41], where polarization of ''condensed'' and ''free'' counterions of a rodlike polyion is investigated by Metropolis Monte Carlo simulations.

As can be seen from Eq. 6, the electro-optical effect from the colloid particle or polyelectrolyte molecule is proportional to the second power of the electric field strength (if the applied field is not high). This proportionality has been established for colloids and polyelectrolytes of low molecular weight, but for ionized polymers of high molecular weight the effect is found to be proportional to the first power of E. This ''permanent-like'' dipole moment behavior of high molecular polyelectrolytes has been theoretically analyzed by Kikuchi and Yoshioka [42], who have developed a model of the orientation due to progressive saturation of the ionic polarization as the field strength increases. According to these authors, the field strength dependence of the electro-optical effect, which resembles that of a permanent dipole moment at high fields, is related to the ''condensed'' counterion polarization. In most cases, however, the shape of the experimentally obtained orientation function markedly differs from that derived in Ref. 42. In order to explain the orientation of ionizable polymers, a theoretical orientation function based on a saturable and unsaturable induced dipole (SUSID) mechanism is derived by Yamaoka and Fukudome [43,44]. According to the SUSID mechanism, the electric moment of a rodlike polyion consists of a saturable ionic induced dipole moment, which is saturated at field strength E_0, and an unsaturable induced moment, which is not saturated at any used field strengths. This orientation function predicts a transformation of the electro-optical effect dependence from quadratic to the first power of E.

The colloid particle or polyelectrolyte molecule may possess a permanent dipole moment. Considerable influence of this moment on the magnitude and the sign of the electro-optical effect is expected in the range of particle rotation. Discrimination between the induced and the rotational relaxation of the particles can be reached, however, since the electro-optical response to a sinusoidal electric field is the sum of a time-independent term α_{dc} and a term $\alpha_{2\omega}$ that is sensitive to the particle rotation [24,45]. The critical frequency of the $\alpha_{2\omega}$ relaxation depends on the rotational diffusion coefficient D_r of the particle, while the critical frequency of relaxation of the time-independent term α_{dc} depends on the translational diffusion coefficient of the ions moving on the particle surface.

2. Decay of the Electro-Optical Effect

After the switching off of the electric field, the electro-optical signal decays exponentially with time t, and this decay is simply related to the particle geometry [46]:

$$\alpha_t = \alpha_0 \exp(-6D_r t) \tag{7}$$

For prolate ellipsoid, the rotary diffusion coefficient D_r ($D_r = 1/6\tau$) is given by the Perrin formula [47]

$$D_r = \frac{kTp^2}{4\pi\eta V(p^4 - 1)} \left(-1 + \frac{2p^2 - 1}{2p\sqrt{p^2 - 1}} \ln \frac{p + \sqrt{p^2 - 1}}{p - \sqrt{p^2 - 1}} \right) \tag{8}$$

where p is the axial ratio a/b, η is the viscosity of the suspending medium, and $V = 6^{-1} pab^2$ is the volume of the particle. In the presence of an adsorbed polymer layer, from the change in the axial ratio p determined through D_r, the effective hydrodynamic thickness L_r of the polymer layer can be obtained:

$$p = \frac{a + 2L_r}{b + 2L_r} \tag{9}$$

III. ELECTRO-OPTICAL BEHAVIOR OF COLLOID PARTICLES IN POLYELECTROLYTE SOLUTION

A. Dependence on the Polyelectrolyte Concentration

The adsorption of charged macromolecules modifies considerably the electrical surface properties of colloid particles already at very low concentration. Figure 1 shows typical dependence of the HF electro-optical effect on the polyelectrolyte concentration. One observes a steep decrease of the effect with increasing polyelectrolyte concentration, which turns to an increase at superequivalent adsorption of the oppositely charged polymer onto the par-

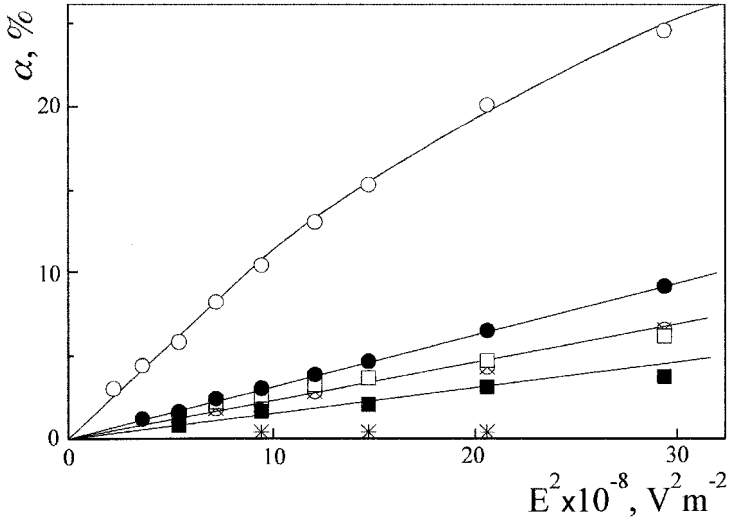

FIG. 1 Dependence of the electro-optical effect α of β-FeOOH particles on the field strength E at different concentrations of polyacrylamide with degree of hydrolysis 9.8%: ○, without HPAM; ■, 10^{-5}; *, 3×10^{-5}; ●, 10^{-4}; ⊗, 5×10^{-4}; and □, 10^{-2} gdm^{-3} HPAM. Frequency of a.c. field 6 kHz.

ticle surface. A large overcompensation of the particle surface charge by the adsorbed polyelectrolyte is established by measuring the electrophoretic mobility in this and all other experiments described in this review [12,13].

In Figure 2 are represented the electro-optical effect α, the electrophoretic mobility U_e, and the relaxation time τ of the particle disorientation after the switching off of the electric field as a function of the initial polyelectrolyte concentration. One observes that the α and τ variations correspond to the variation of U_e, i.e., the electrostatic attraction of the polyelectrolyte to the oppositely charged surface, which is the main driving force for the adsorption, governs the electro-optical behavior and stability of the suspension containing this polyelectrolyte.

The interfacial electric polarizability γ, being an important dynamic characteristic of the particle surface charge, can be easily determined from the electro-optical effect dependence on the square of the electric field strength (Eq. 6). A significant increase in the particle dimensions as well as the low surface charge of the colloid–polymer complex complicate the electric polarizability determination near to the system's isoelectric point (Figure 2). The electric polarizabilities are calculated in this review only for polymer covered particles in stabilized suspensions. One way to obtain correct values

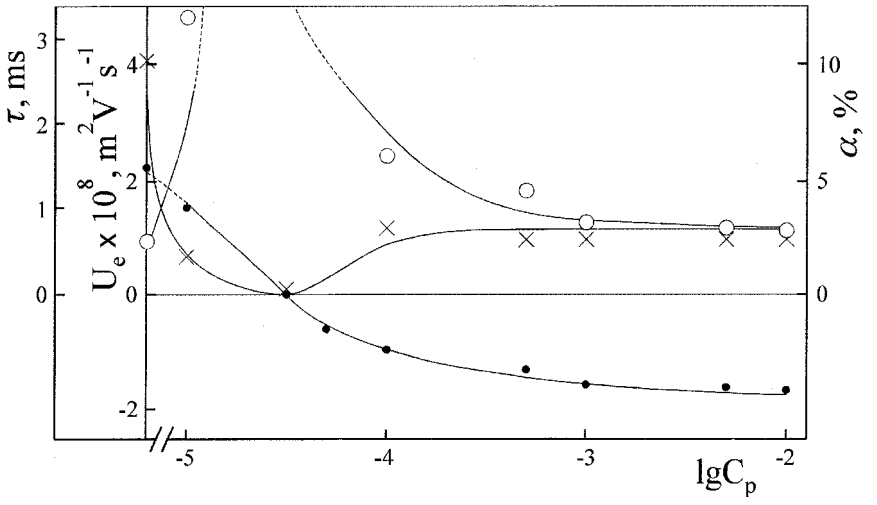

FIG. 2 Dependence of the electro-optical effect α, $\times$, the electrophoretic mobility U_e, $\bullet$, and the particle rotational relaxation time τ, $\circ$, on the concentration of polyacrylamide with degree of hydrolysis 9.8%.

of the electric polarizability of particles in nonstabilized suspensions is to remove aggregates by filtration or careful centrifugation as has been done for colloid particles in the presence of low molecular surfactant [48].

Figure 3 illustrates the electro-optical effect dependence on the polymer charge density for a suspension of β-FeOOH particles, stabilized by the adsorption of polyacrylamides with degrees of hydrolysis 3.4, 9.8, and 19.1%, respectively. The calculated electric polarizabilities γ at plateau value of the corresponding adsorbed polyacrylamide Γ are presented in Table 1. They are of an order that is typical for all other systems described in this review—10^{-28}–10^{-32} Fm^2. Values of the electric polarizability between 10^{-28} and 10^{-32} Fm^2 have also been obtained for most of the polyelectrolytes investigated in solution [1,49,50].

B. Dispersion of the Electro-Optical Effect

From an analysis of the α dependence on the field frequency ν (dispersion curve) for different colloids, it has been shown that the orientation of particles in the kHz range originates solely from their induced dipole moments [2,3,51]. It is generally accepted now that the induced dipole moment of a colloid particle in this region is mainly due to movement of ions in the diffuse part of the particle electrical double layer [51–54]. What is the origin of the effect observed in a suspension containing polyelectrolyte molecules?

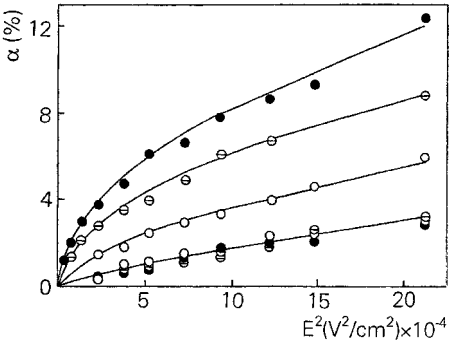

FIG. 3 Field strength dependence of the LF effect (at 60 Hz) from β-FeOOH suspension, stabilized by the addition of 5×10^{-3} gdm^{-3} HPAM with different degrees of hydrolysis: ○, 3.4%; ⊖, 9.8%, and ●, 19.1%. The lower curve is the HF effect at 6 kHz. (From Ref. 15.)

Figure 4 shows the most important feature of the electro-optical effect in a suspension, stabilized by polyelectrolyte adsorption. This is the appearance of an additional LF effect near the range of particle rotation (10^2–10^4 Hz) that resembles the LF effect in free polyelectrolyte solutions. The analogy is so impressive that we supposed the same origin of the LF effect in both systems. Polarization of ''tightly'' bound counterions with lower mobility in comparison to that of the ''free'' ions is proposed to explain the LF effect in stabilized suspensions [12–18], since it cannot be found in suspensions of bare oxide particles. The overlap (full or partial) of the frequency intervals of particle hydrodynamic relaxation (RF effect) and the relaxation of this additional LF effect means that the ''tightly'' bound counterions have close mobility to that of the whole colloid–polymer complex. A saturable ionic induced dipole moment probably arises due to the polarization of these coun-

TABLE 1 Electric Polarizability γ, Average L and Hydrodynamic L_r Layer Thicknesses, and Adsorption Γ on β-FeOOH Particles as a Function of the Polyacrylamide Degree of Hydrolysis τ%

Sample	τ%	Γ (Å^{-2}) $\times 10^4$	L (Å)	L_r (Å)	γ (Fm^2) $\times 10^{29}$
HPAM	3.4	2.07	38	60	0.7
HPAM	9.8	1.17	27	60	2.1
HPAM	19.1	0.78	23	60	4.1

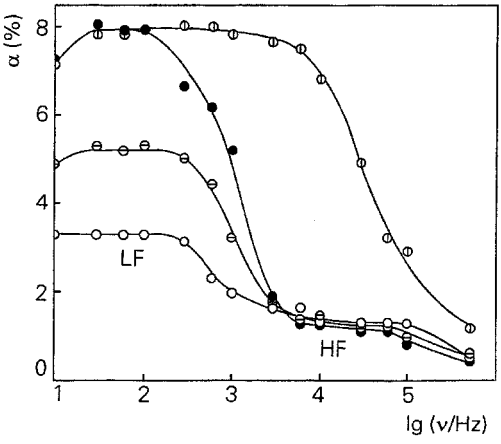

FIG. 4 Frequency dependence of the electro-optical effect α from β-FeOOH suspension, ⊕, stabilized by addition of 5×10^{-3} gdm^{-3} HPAM: ○, 3.4%, ⊖, 9.8%; and ●, 19.1%. Field strength 240 Vcm^{-1}. (From Ref. 15.)

terions, which explains the unusual "permanent-like" dipole moment behavior of the suspensions, stabilized by polyelectrolyte adsorption.

The true permanent dipole moment of the particle (if it exists) operates in the range of particle rotation and might also be changed due to the polyelectrolyte adsorption. Following the concept for the interfacial "permanent" dipole moment, Stoylov [55] explains its variation through a higher electrostatic adsorption of the polyions on the one half of the colloid particle, thus changing the asymmetry of the surface electric charge distribution, i.e., the "permanent" dipole moment. In this review, however, only the effect arising from the bound counterion polarization is considered.

As noted above, the kHz effect in suspensions with no polymer added is due to polarization of ions from the diffuse part of the ionic atmosphere surrounding the particle. In order to confirm the same origin of the HF effect in colloid–polyelectrolyte suspension, the critical frequency of the HF relaxation in β-FeOOH suspension containing 2×10^{-2} gdm^{-3} NaCMC and CaCMC is compared to the critical frequency of the kHz effect relaxation in suspension without polymer (Figure 5). Figure 5 shows that the critical frequency of the HF relaxation ν_{cr} is observed at 60 and 80 kHz in all cases, which leads to the conclusion that polarization of the diffuse ions along the axis of the polymer covered particles is also responsible for the HF relaxation in polyelectrolyte containing colloid systems. Critical frequency of the HF relaxation of ca. 65 kHz, roughly estimated by using the equation

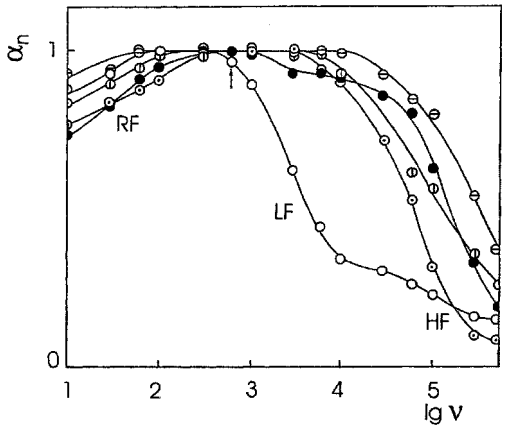

FIG. 5 Frequency dependence of α (normalized effects) from a suspension of β-FeOOH particles, ⊙, in presence of ⊖, 10^{-4} M NaCl; ⊕, 4×10^{-5} M $CaCl_2$; ○, 2×10^{-2} gdm^{-3} NaCMC; and ●, 2×10^{-2} gdm^{-3} CaCMC. (From Ref. 14.)

$$\nu_{cr} = \frac{D_i}{\pi a^2} \tag{10}$$

(where D_i is the translational diffusion coefficient of the diffuse ion) also shows that this relaxation arises from the motion of diffuse (''free'') counterions along the particle axis. Precise estimation of the critical frequency of the HF relaxation in colloid–polyelectrolyte systems is, however, difficult since the magnitude of the HF effect is not high enough to be measured with great accuracy.

More arguments that support the above proposed explanation of the LF and HF effects origin in colloid–polyelectrolyte suspensions will be given in the next section.

IV. ELECTRICAL PROPERTIES OF ADSORBED POLYELECTROLYTES IN STABILIZED SUSPENSION

The polarization of ionic atmosphere around a polyelectrolyte molecule has been experimentally studied by dielectric and electro-optical techniques in a wide concentration range. In a solution with no added salt, the polyions have an extended conformation and may entangle with each other. This complicates the interpretation of the counterion polarization, since it has been theoretically analyzed for solutions with no interactions between the

polyions. The great majority of experiments have been carried out, on the other hand, on semidilute solutions, because of the limited sensitivity of the techniques used. In attempt to circumvent the limitations of the experimental techniques, the electro-optics of adsorbed polyelectrolytes is proposed as a complementary method for studying counterion dynamics in dilute systems. Since the light scattered from the colloid particles in the presence of an electric field is large enough, this method allows investigation of dilute suspensions with no interactions between the polymer covered particles. The problem is to find out experimental conditions at which the particle surface charge has no or minimal influence on the electrical properties of the adsorbed polyion. The similarity between the electro-optical behavior of a suspension, stabilized by polyelectrolyte adsorption, and the behavior of polyelectrolyte in solution implies that, at plateau adsorption, the colloid particles assume the charge characteristics of the adsorbed polymer. The analysis of our data and of data from previous (electrokinetic) studies on polyelectrolyte adsorption [56–59] and constants of ionization of an adsorbed polyelectrolyte [60] allows us to think that the information on the electrical properties of adsorbed polyelectrolyte can be successfully extended to polyelectrolytes in solution.

For weak polyelectrolytes, the computations of Böhmer et al. [61] show that the degree of dissociation of their adsorbed segments adjusts itself so as to screen effectively the particle surface charge. So, the polymer segments in contact with the surface are dissociated to such a degree that already in the first layer the surface charge is compensated, i.e., looking from the bulk solution, one sees a nearly neutral particle. This means that the degree of dissociation of the polymer segments in the ''loops'' and ''tails'' will be close (nearly the same) as in the bulk solution. On the other hand, if such a polymer is fully charged before adsorption, its degree of dissociation on the particle surface remains unchanged and, consequently, the electrical properties of the adsorbed polyelectrolyte might also be supposed identical to those of the polyelectrolyte in the bulk solution. Additional result from the theory of Böhmer et al. [61] is that, even though the absorbed amount depends on the adsorption energy per segment and the charge per surface site, the degree of dissociation of fully charged polyelectrolyte will not depend on the surface charge.

Experimentally, both predictions of this theory have been confirmed by Golub et al. [60], where constants of dissociation of polyethylenimine (PEI) adsorbed on silica particles have been determined by the potentiometric titration method, and in Ref. 32 for the PEI adsorption on positively and negatively charged hematite particles.

In Ref. 60, constants of ionization of polyethylenimine (PEI) adsorbed on silica particles are determined by the potentiometric titration method. The

dissociation constant of the PEI in the close vicinity of the particle surface is found to decrease from $pK_{PEI} \sim 9.0$ to $pK_{PEI} \sim 3.9$. Strong attraction of the PEI segments (''trains'') to the particle surface is assumed to be responsible for this effect. On the other hand, the constant of PEI ionization $pK_{PEI} \sim 9.4$ in the ''loops'' and ''tails'' does not practically differ from the constant of PEI ionization $pK_{PEI} \sim 9.0$ in a free solution. Another estimation of the pK_{PEI} in the ''loops'' and ''tails'' has been obtained by measuring the streaming potential on a quartz surface with adsorbed PEI [59]. The value of the constant of PEI ionization $pK_{PEI} \sim 9.5$ is found close to that obtained by the potentiometric titration method and equal to that of PEI in solution. More recent electrokinetic study of polyelectrolyte adsorption also shows equal electrophoretic mobility of the polymer-coated particles (at plateau adsorption) to that of nonadsorbed polyelectrolyte in solution [62].

Several examples can be given in order to demonstrate the similarity existing between the electro-optical behavior of a suspension stabilized by polyelectrolyte adsorption and the behavior of polyelectrolyte in solution.

The electric light scattering effect of β-FeOOH suspension, stabilized by NaCMC adsorption [12], resembles the electric birefringence effect of aqueous NaCMC with close charge density of the macromolecules (Figure 6). Since the NaCMC solution with concentration 2×10^{-2} g dm^{-3} gives a very weak scattered intensity, the electric birefringence data of Ookubo et

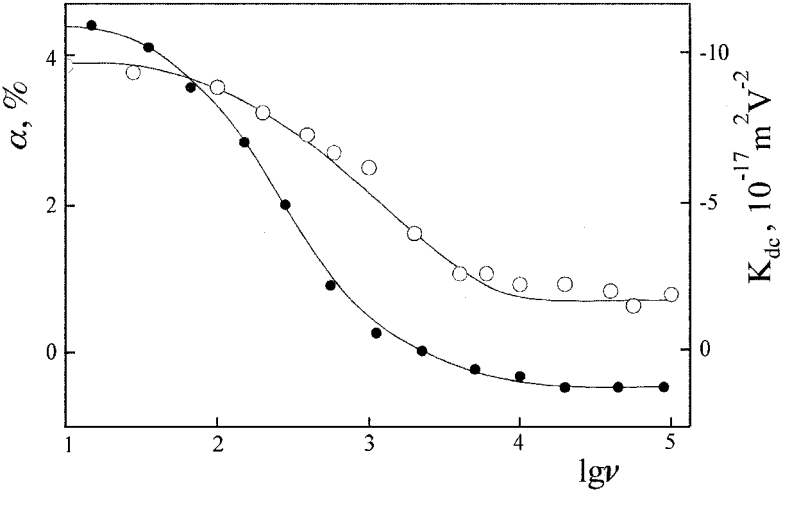

FIG. 6 Frequency dependence of electric birefringence K_{dc} from NaCMC solution, ●, and electric light scattering α from β-FeOOH suspension, stabilized by addition of 2×10^{-2} gdm^{-3} NaCMC, ○.

al. [25] are used for this comparison. The discrepancy that exists in the curves presented in Figure 6 arises, firstly, from the negative optical anisotropy of the NaCMC molecules in solution and, secondly, from the two times higher molecular weight of these molecules [25]. The latter is known to shift the critical frequency of relaxation of the electro-optical effect toward the lower frequencies [25,63–65].

In [17], the electric polarizability $\gamma = 2 \times 10^{-30}$ Fm^2 of an adsorbed sodium polystyrenesulfonate (NaPSS) is found almost equal to $\gamma = 1.5 \times 10^{-30}$ Fm^2 of NaPSS in solution with no added salt [49]. Strangely, this value is in good concordance with the one estimated from Manning's theory, even though the experimental values are relevant to "fast" polarization of the counterionic atmosphere.

Figures 7 and 8 show variations in the electric light scattering effect from suspension, stabilized by NaPSS adsorption, with increasing concentration of salts of divalent (Mg^{2+}) and trivalent (Al^{3+}) counterions [18]. One observes a steep decrease of the LF effect and some increase of the HF effect at concentration 2.5×10^{-5} M $MgCl_2$ and 1.6×10^{-5} M $AlCl_3$, respectively. These amounts of low molecular salts are sufficient for Na^+ to be fully replaced by Mg^{2+} and Al^{3+} from the polyion surface. The electro-optical effects vary in a different way when $MgCl_2$ is added to the suspension with no NaPSS adsorbed on the particle surface—Figure 9. This by no means

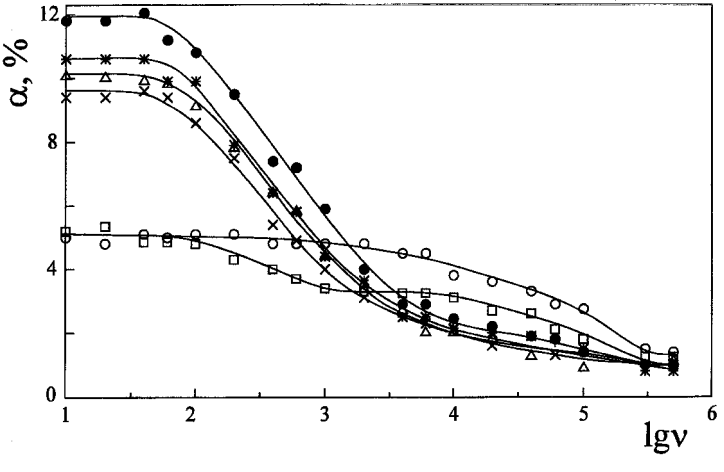

FIG. 7 Frequency dependence of α from suspension of β-FeOOH particles containing 10^{-2} gdm^{-3} NaPSS, ●, in presence of: *, 5×10^{-6}; △, 7.5×10^{-6}; ×, 10^{-5}; □, 2.5×10^{-5}; and ○, 5×10^{-5} M $MgCl_2$. Field intensity 240 Vcm^{-1}. (From Ref. 18.)

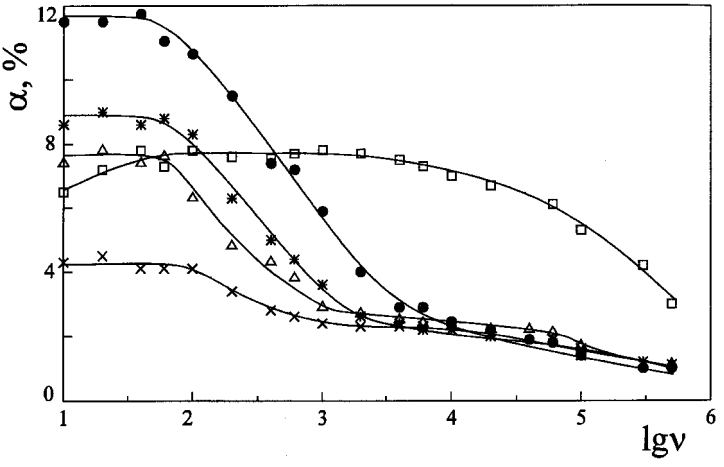

FIG. 8 Frequency dependence of α from suspension of β-FeOOH particles containing 10^{-2} gdm^{-3} NaPSS, ●, in presence of: *, 5×10^{-6}; △, 7.5×10^{-6}; ×, 10^{-5}; and □, 2.5×10^{-5} M $AlCl_3$. (From Ref. 18.)

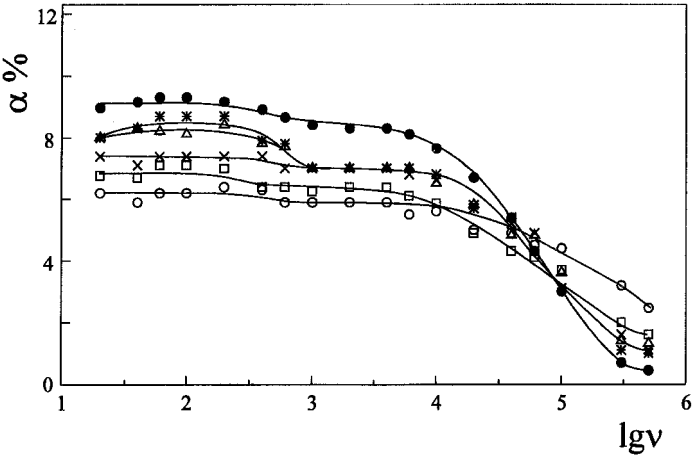

FIG. 9 Frequency dependence of α from suspension of β-FeOOH particles, ●, at various $MgCl_2$ concentrations: *, 5×10^{-6}; △, 7.5×10^{-6}; ×, 10^{-5}; □, 2.5×10^{-5}; and ○, 5×10^{-5} M $MgCl_2$. (From Ref. 18.)

implies that the properties of the adsorbed NaPSS govern the electro-optical behavior of the stabilized colloid–polyelectrolyte suspension.

In line with this conclusion is also the result obtained for positive and negative hematite particles covered by PEI [32]. Positive and negative particles, having equal absolute charge density at pH 5.9 and 9.8 are chosen for this experiment and 5×10^{-3} g dm^{-3} PEI is added to the suspension. The appearance of equal effects due to the PEI adsorption indicates no dependence on the sign of the adsorbent surface charge, i.e., the colloid–polymer complex assumes charge characteristics of the PEI (Figure 10). Indistinguishable values of the electrophoretic mobility of positive (2.2×10^{-8} $m^2V^{-1}s^{-1}$) and negative (2.3×10^{-8} $m^2V^{-1}s^{-1}$) particles at plateau adsorption of PEI also confirm this conclusion. An analogy is found as well with the results of Cosgrove et al. [66], who show similar segment density profiles and hydrodynamic thickness of the adsorbed NaPSS layers on positive and negative latex particles.

A. Low-Frequency Dispersion of the Electro-Optical Effect

The origin of the additional LF effect, which appears in stabilized suspensions in the frequency range 10^2–10^4 Hz, will be commented on here bearing in mind that the electric properties of the adsorbed macromolecules govern the electro-optical behavior of these suspensions.

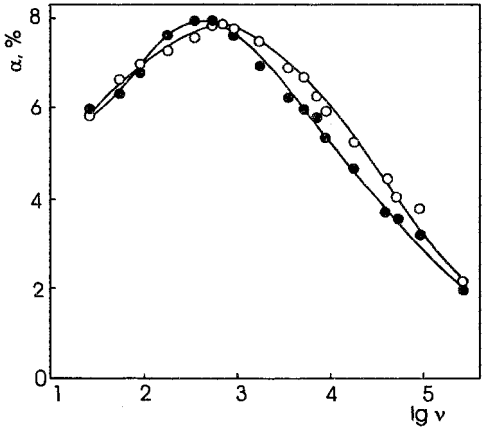

FIG. 10 Frequency dependence of α from α-Fe_2O_3 suspension in presence of polyethylenimine: ○, negative particles (pH 9.8) in 5×10^{-3} gdm^{-3} PEI; ●, positive particles (pH 5.9) in 10^{-4} M NaCl and 5×10^{-3} gdm^{-3} PEI. Field intensity 310 Vcm^{-1}. (From Ref. 16.)

There is nearly complete agreement in the literature that the amplitude and the critical frequency of relaxation of the LF effect strongly depend on the molecular weight of the polyelectrolyte [63–65], while both quantities are almost independent of the molecular weight in the higher frequency range (10^4–10^6 Hz) [63–65,67,68]. A large discrepancy exists in the explanation of the LF and HF effects' origin. In the earlier period, the LF relaxation in polyelectrolyte solutions has been ascribed to end-over-end rotation of the polyion arising from the fluctuation of the dissociation of bound counterions on the polyion surface [23,64,65]. Several kinds of ''permanent'' dipole moment, arising from the charge groups and their counterions, have been invoked to explain the LF relaxation, but now the polarization of bound counterions along the polyion axis is mainly accepted as responsible for this relaxation [25,26,37,69–73]. According to van Dijk et al. [73], the bound counterions have almost equal mobility to that of the ions in a free medium, but the time of exchange of counterions between the bound and free phases determines the critical frequency of LF relaxation. Translational motion of the counterions between discrete sites on the polyion surface is another explanation of this effect, proposed in Refs. 72 and 74. More recent investigation of Ookubo et al. [25] shows that the LF relaxation, distinct from the rotational one, arises from the polarization of ''tightly'' bound counterions along the polyelectrolyte axis. The translational diffusion of these ions is slowed down by the electrical potential of the polyion. Since the ''tightly'' bound counterions move along the polyion contour, both the amplitude and the critical frequency of the LF relaxation are expected essentially to depend on the polyelectrolyte molecular weight. In Refs. 75 and 76, the amplitude of the LF relaxation is found to increase and its critical frequency to decrease in proportion to the polyelectrolyte molecular weight, whereas in Refs. 77 and 78 both quantities are shown to depend on the second power of the polyelectrolyte molecular weight.

In order to elucidate the LF effect origin in stabilized suspensions, an analysis of variations in the electro-optical effect as a function of the polyelectrolyte molecular weight is conducted.

Concentration and molecular weight dependences of the electro-optical effect are followed for suspension of β-FeOOH particles in the presence of NaPSS of different molecular weights. The addition of NaPSS to a suspension of oppositely charged particles causes a change in the particle dimensions and their electro-optical behavior in close correlation with the surface charge variation (Figures 11 and 12 and Table 2). The flocculation and stabilization of the suspension are not influenced, however, by the polyelectrolyte molecular weight (Table 2). From the change in particle dimensions at plateau adsorption (in stabilized suspensions), small values of the polyelectrolyte layer thicknesses are obtained (15 and 6 nm, respectively, for the

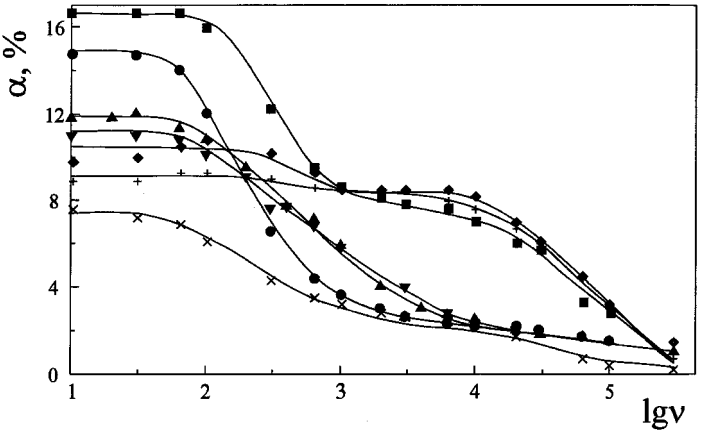

FIG. 11 Frequency dependence of α from suspension of β-FeOOH particles, +, at various concentrations of NaPSS with $M_w = 1 \times 10^6$: ♦, 10^{-6}; ■, 10^{-5}; ×, 10^{-4}; ●, 10^{-3}; ▲, 10^{-2}; and ▼, 4×10^{-2} gdm^{-3} NaPSS. Field intensity 240 Vcm^{-1}. (From Ref. 17.)

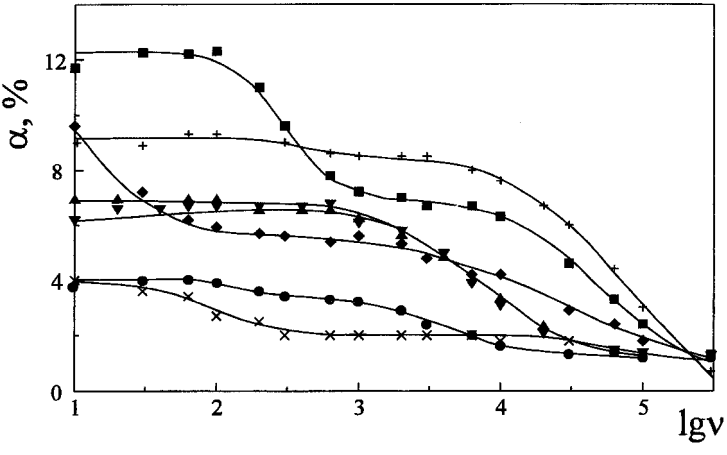

FIG. 12 Frequency dependence of α from suspension of β-FeOOH particles, +, at various concentrations of NaPSS with $M_w = 7 \times 10^4$: ■, 10^{-5}; ♦, 5×10^{-5}; ×, 10^{-4}; ●, 10^{-3}; ▼, 10^{-2}; and ▲, 4×10^{-2} gdm^{-3} NaPSS. Field intensity 240 Vcm^{-1}. (From Ref. 17.)

TABLE 2 Particle Relaxation Times (τ, ms) of β-FeOOH Particles at Different NaPSS Concentrations

C_{NaPSS}, gdm^{-3}	M_W = 1,000,000	M_W = 70,000
0	0.67	0.67
10^{-6}	0.67	—
10^{-5}	0.76	0.72
5×10^{-5}	>20	18.4
10^{-4}	4.21	1.55
5×10^{-4}	—	0.86
10^{-3}	1.03	0.75
10^{-2}	0.90	0.75
4×10^{-2}	0.90	0.75

NaPSS of molecular weight 1×10^6 and 7×10^4), which suggest a rather ''flat'' conformation of the adsorbed macromolecules. The larger polymer thickness for the high molecular NaPSS means that longer ''loops'' and ''tails,'' protruding into the solution, exist if one assumes that the NaPSS adsorption does not depend on the polyelectrolyte molecular weight. Such an independence is theoretically predicted for strongly bound polyelectrolytes by van der Schee and Lyklema [79] and has been experimentally confirmed, for instance, in Ref. 80.

Figure 13 shows that the LF effect is larger and its critical frequency of relaxation is lower in the suspension, stabilized by the adsorption of the high molecular NaPSS. The critical frequency of the particle rotational relaxation (RF relaxation) is at ca. 200 Hz, corresponding well to an average rotational relaxation time of ca. 0.8 ms for the polymer-coated particle (Table 2), while the critical frequency of LF relaxation is at ca. 600 Hz for the high molecular NaPSS and one order of magnitude larger for the particles covered with smaller NaPSS molecules. As the low-frequency dispersion is characterized by an average relaxation time τ_L, containing contributions from the rotational diffusion of the polymer-coated particle τ and the relaxation of the counterion distribution along its surface τ_I, a discrimination between them is made by using Eq. 17 from Ref. 25:

$$(\tau_L)^{-1} = \left(\frac{3\tau}{2}\right)^{-1} + (\tau_I)^{-1} \tag{11}$$

The values of the critical frequency of the ionic induced relaxation are 470 Hz and 5870 Hz, respectively, for the high and low molecular NaPSS adsorbed on the particle surface. This may be considered as evidence that

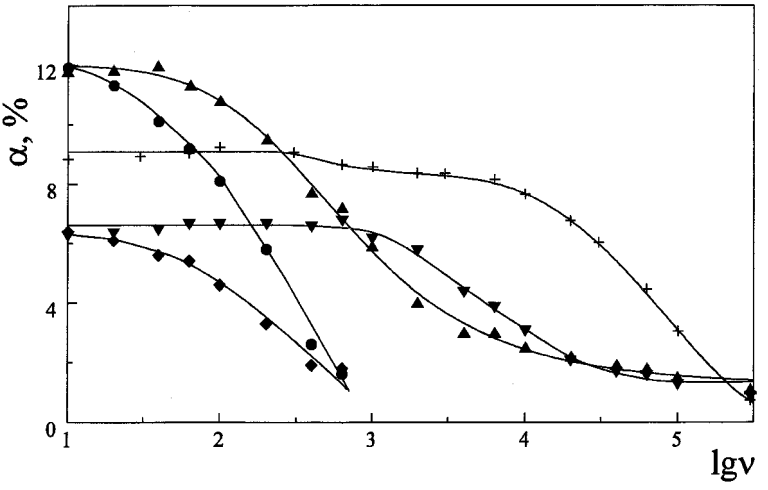

FIG. 13 Frequency dependence of α_{dc} (▲, ▼) and $\alpha_{2\omega}$ (●, ♦) from β-FeOOH suspension, +, in presence of 10^{-2} gdm^{-3} NaPSS with high (▲, ●) and low (▼, ♦) molecular weight. (From Ref. 17.)

induced polarization of "slow" ions is responsible for the LF relaxation. The decrease in mobility of the counterions due to their condensation on the polyion surface is the most probable explanation of this effect.

Field strength dependence of the LF effect shows better the molecular weight dependence of the LF effect amplitude. The first power dependence of this effect on the field strength (Figure 14) means that a saturated ionic induced dipole moment, resulting from the "tightly" bound counterion polarization, can explain the "permanent-like" moment behavior of stabilized suspensions in weak fields.

For the NaPSS with higher molecular weight, the amplitude of the LF effect is 3 or 4 times larger than the amplitude of the effect from the lower molecular NaPSS, adsorbed on the particle surface. This agrees with the electro-optical results for DNA [49], which show a linear proportionality of the saturated ionic induced dipole moment to the square root of the polyelectrolyte molecular weight.

The amplitude of the saturated ionic dipole moment is found to be independent of the molecular weight in Stellwagen's electro-optical experiments for DNA restriction fragments [81], although the theory of Sokerov and Weill [82] predicts quadratic dependence of this moment on the polyion length. The diversity of results implies that not all aspects of the molecular weight dependence of the LF effect are well understood and further inves-

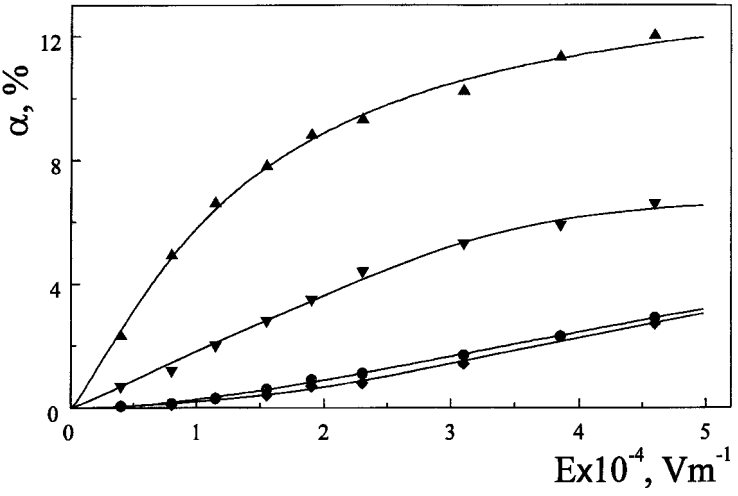

FIG. 14 Field strength dependence of LF (▲, ▼) and HF (●, ♦) effects for low (▼, ♦) and high (▲, ●) molecular NaPSS at concentration 10^{-2} gdm^{-3}. (From Ref. 17.)

tigations are needed to reach an adequate interpretation of this effect observed in both the polyelectrolyte solutions and suspensions, stabilized by polyelectrolyte adsorption.

Even though most of the results obtained do confirm the close relation of the saturated ionic dipole moment to the "tightly" bound counterion polarization, some opposition still remains to such an interpretation. Matsuda and Yamaoka [83] show, for instance, that polarization of the "tightly" bound divalent counterions does not lead to a saturated dipole moment behavior of DNA at low fields in contrast to the polarization of "tightly" bound monovalent counterions of 9-aminoacridinium. Hence the authors suppose an important role of the ionic valence for the saturated dipole moment behavior of polyelectrolytes in solution. Immobility of the divalent counterions in weak fields can explain the results of Yamaoka and Matsuda [36,83] and those obtained in Ref. 16 for β-FeOOH suspension, stabilized by NaCMC and CaCMC adsorption. This means that higher fields are needed for the strongly bound divalent counterions to move along the polyion surface. Higher fields for polarization of the divalent counterions [84] and lower tracer diffusion coefficient of these counterions in salt-free polyacrylic acid solution [85] are also found in the literature.

As shown in Figure 13, the decrease in the critical frequency of the LF relaxation scales with the 1.5 power of the NaPSS molecular weight. This dependence has been the object of many studies but, just as for the amplitude

of the LF effect, the results obtained for different systems are contradictory. A linear decrease of the critical frequency of LF relaxation has been found, for instance, with increasing molecular weight of the polyelectrolyte in Refs. 75 and 76, whereas in Refs. 77 and 78, this dependence is quadratic.

Assuming that the ''tightly'' bound counterions move in a square well potential [69] with a length of L (its upper value is the polyion contour length), Ookubo et al. [25] calculated from the critical frequency of LF relaxation the diffusion constant of these ions D_I

$$\tau_I = \frac{L^2}{12D_I} \tag{12}$$

The value of $D_I = 9.8 \times 10^{-11}$ m^2s^{-1}, calculated for the Na^+ counterions of PSS, was smaller than the diffusion constant of Na^+ in a free medium ($D_I^0 = 1.22 \times 10^{-9}$ m^2s^{-1}).

Such an estimation might be not precise enough since the polarization time constant, determined from simulations [86] as well as from other experiments [87,88], is found to depend also on the field strength. In Ref. 87, for instance, the decrease of the polarization time constant with increasing field strength is explained by an ion dissociation reaction model without invoking any theory. Several theories predict, however, a dependence of the polarization time constant on the ratio of the rotational and ion atmosphere relaxation times [89–91]. The major limitation of these theories is the assumption that the dynamics of the ion atmosphere polarization can be completely described by a single relaxation time, i.e., they simply ignored the fact that the layer of bound counterions and the diffuse ion atmosphere may have different relaxation times.

B. High-Frequency Dispersion of the Electro-Optical Effect

Experimentally, the molecular weight independence of the HF effect (in polyelectrolyte solutions) has been confirmed many times. Van der Touw and Mandel [64,65] attributed the HF dispersion to polarization of bound counterions along a part of the polyelectrolyte molecule. They introduced a model in which the polyelectrolyte is considered as a nonlinear sequence of rodlike subunits and the counterion polarization along the subunit is supposed to be responsible for the amplitude and the critical frequency of HF relaxation. Both quantities would essentially be independent of the molecular weight of the polyion. In solutions, where interactions between macromolecules are taken into account, the length of the above-mentioned subunit is related to the correlation distance between the macromolecular chains [25,26,92]. Counterion polarization perpendicular to the polyion axis is pro-

posed as another explanation of the HF dispersion [93]. A high-frequency relaxation mechanism due to the ''loosely'' bound counterion polarization perpendicular to the polyion axis is supposed to explain the electro-optical behavior in semidilute polyelectrolyte solutions [25,26]. As in Ref. 92, the correlation distance between the macromolecular chains is related to the HF dispersion, but from another point of view [25,26]. In dilute solutions, the correlation distance is identified with the spherical free volume for each polyion, and the movement of the ''loosely'' bound counterions in all three directions (not only perpendicular to the polyion axis) is supposed to contribute to the HF dispersion [26]. The last interpretation of the HF effect is the most appropriate for suspensions stabilized by polyelectrolyte adsorption (Sec. III.B), since the average distance between the oxide particles with adsorbed polymer is too large (ca. 7–10 μk). This means that the critical frequency of the HF relaxation in a stabilized suspension will depend on the length of the polymer covered particle (Eq. 10) but not on the polyelectrolyte molecular weight. A molecular weight dependence of the HF relaxation has to be expected in dilute polyelectrolyte solutions. However, the effect sought may be too small to be observed with enough accuracy in these solutions.

In Refs. 13 and 15, an independence of the amplitude and the critical frequency of HF relaxation on the polyelectrolyte charge density is found for suspensions stabilized by the adsorption of partially hydrolyzed polyacrylamides. In contrast to the HF effect, the amplitude of the LF effect correlates well with the polyelectrolyte charge density (Figure 4). The linear charge density parameter $\xi = e^2/\varepsilon kTb$ (with b the linear spacing along the polyion chain) is lower than unity for the samples used in this study (ξ = 0.10, 0.28, and 0.54, respectively). This implies that counterion binding might occur even on the polyelectrolyte surface of adsorbed low charged polymer. When the polymer coils, its charge density parameter increases because the average spacing between the charges decreases in the projection of the polyion as an imaginary straight line, which is responsible for the counterion condensation. This might be the case with a weakly charged polyacrylamide, adsorbed on a colloid particle, since some ''loops'' appear leading to a decrease of the effective average distance between the charges of the polyion.

An essentially constant self-diffusion coefficient of the sodium counterion has been found for low charged ($\xi < 1$) carboxyl copolymers in Ref. 94, indicating that charge density of the polyions is also constant in this region. An instability in the polyion conformation has been suggested to exist below $\xi = 1$ because of the increased distance between charged groups, which constrains the macromolecules to attain more stable configuration by coiling to increase the effective charge density to $\xi = 1$. Examples of counterion condensation providing a driving force for polyelectrolyte conformational

changes are presented in a recent review article by Manning [85]. Counterion condensation seems, therefore, possible at $\xi < 1$. Such an explanation is in line with our findings for counterion condensation on adsorbed weakly charged polyelectrolytes.

C. Effect of Low Molecular Salts

The effect of low molecular salts (NaCl and $MgCl_2$) on the counterion polarization of NaPSS and MgPSS is investigated in Ref. 18. It is supposed there that the adsorption of both strongly charged polyelectrolytes does not depend on the salt concentration. Still, Van der Schee and Lyklema [79] predicted that the strong repulsion between the segments of the polyion leads to a very thin adsorbed layer. If this repulsion is screened by adding salt, the adsorbed amount increases. When the surface is oppositely charged, however, the adsorbed amount at low salt concentrations is nearly independent of the presence of salt and only slightly higher than necessary for neutralization of the surface charge [61]. The surface charge determines the adsorbed amount in this case because of the electrostatic contribution of the adsorption of segments. This is corroborated, for instance, by measurements of Blaakmeer et al. [95], who found that an increase in the salt concentration from 0.001 to 0.01 M hardly affected the adsorption of polyelectrolyte on a latex with an oppositely charged surface.

Figure 15 shows the variation in the frequency dependence of the electrooptical effect with increasing concentration of NaCl for a suspension stabilized by NaPSS adsorption. One observes that the HF effect scarcely changes, whereas the LF effect exhibits a significant decrease due to the addition of NaCl. As noted in the above discussion, the amplitude of the HF effect is too small to be investigated as a function of the salt concentration. The insert in Figure 15 shows that the LF effect decreases proportionally to the logarithm of the NaCl concentration. This result agrees well with the linear proportionality [50] of the saturated ionic induced dipole moment of rodlike DNA on the added salt concentration. Since a saturated dipole moment behavior is demonstrated for a suspension in the presence of 10^{-2} gdm^{-3} NaPSS [17], it is reasonable to expect such a dependence of the effect in the presence of added low molecular salt.

An orientation assumed to originate solely from the condensed counterion polarization is theoretically predicted to be almost independent of the ionic strength [96]. Upon an increase of the ionic strength, however, the experiments show a decrease of orientation in most investigations. In the ion atmosphere treatment of Rau and Charney [97], an additional polarization of noncondensed solvent ions is shown to appear on the addition of salt. Strong dependence of this polarization on the ionic strength is predicted. The results

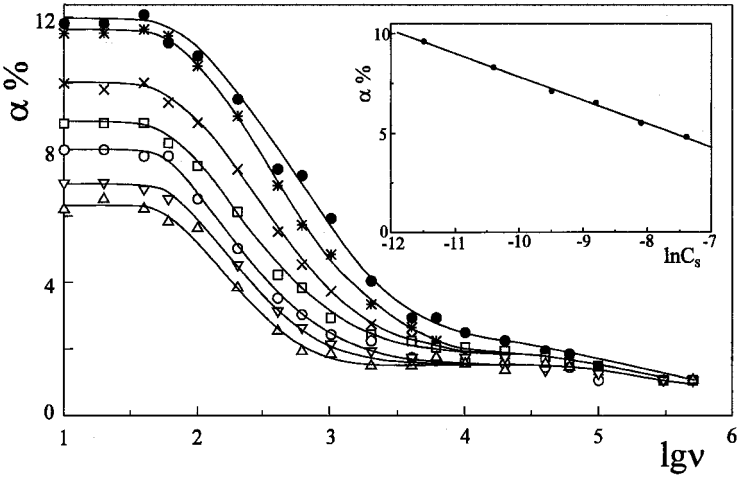

FIG. 15 Frequency dependence of α form β-FeOOH suspension containing 10^{-2} gdm^{-3} NaPSS with $M_w = 1 \times 10^6$, ●, at various NaCl concentrations: *, 10^{-5}; ×, 3×10^{-5}; □, 7.5×10^{-5}; ○, 1.5×10^{-4}; ▽, 3×10^{-4}; and △, 6×10^{-4} M NaCl. Insert shows the dependence of the LF effect on the NaCl concentration. (From Ref. 18.)

obtained in Ref. 98 show the existence of a component of the counterion polarization independent of the ionic strength. The condensed counterion polarization is assumed to be this component.

The latter assumption disagrees with the results presented in Figure 15, since a dependence of the LF effect amplitude on the ionic strength is observed. On the contrary, the HF effect, which is mainly related to diffuse ion polarization, remains nearly unchanged after the addition of NaCl.

The critical frequency of the LF relaxation seems to decrease with increasing ionic strength of the solvent (Figure 15). As the average dimensions of the polymer-coated particle remain almost the same after the addition of NaCl, i.e., there is no considerable contraction of the adsorbed polyion chain, this means a decrease in the critical frequency of relaxation of the bound counterion polarization. The colloid sample, however, is not completely devoid of any (though tiny) size polydispersity, which might lead to a field strength dependence of the LF relaxation. When we compare equal effects, we find no dependence of the critical frequency of the LF relaxation on the ionic strength. This result is in contrast to the one obtained for NaCMC in presence of NaCl [23], where an increase of the critical frequency of LF relaxation with increasing NaCl concentration is explained in terms of a

decrease of the NaCMC persistence length, leading to a decrease of the macromolecular contour length.

The addition of 3.5×10^{-6} M $MgCl_2$ to the suspension, stabilized by MgPSS adsorption, leads to a decrease of the LF effect, while a twofold increase of the HF effect is found as compared to the HF effect in the absence of salt (Figure 16). The increased conductivity in the presence of $MgCl_2$ can explain the observed reduction of the LF effect but not the increase in the HF effect.

D. Effect of Counterion Charge

Theoretical predictions for a quadratic increase of the induced dipole moment in the presence of divalent counterions in comparison to that in the presence of monovalent counterions have been made [71,84,97,99]. An increase of the polarizability with increasing counterion valence is also predicted by Monte Carlo simulation, applied in the investigation of rodlike polyelectrolytes in solution [100]. Experimentally, however, the degree of DNA orientation has been found only slightly higher (ca. 5%) in the presence of divalent counterions than in monovalent solutions [96]. This means, according to the authors of Ref. 96, that the increased repulsion between divalent counterions counterbalances the expected increase in polarizability because of the increased charge fluctuation.

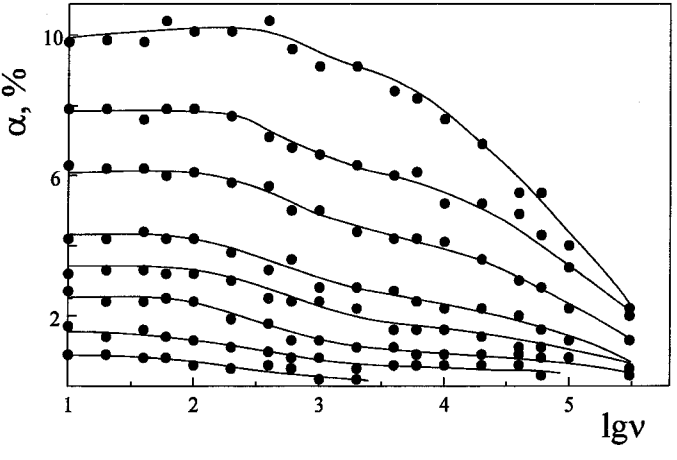

FIG. 16 Frequency dependence of α from β-FeOOH suspension with adsorbed MgPSS in the presence of 3.5×10^{-6} M $MgCl_2$ at different field strengths: 60, 90, 120, 150, 180, 240, 300, and 360 Vcm^{-1}. (From Ref. 18.)

LF effect reduction with increasing counterion valence is also found for MgPSS, adsorbed on oxide particles in comparison to the effect from adsorbed NaPSS—Figure 17 [18]. Similar influence of the ion valence on the LF dielectric increment of PSS is explained in Ref. 101 by a reduction of both the charge fluctuation due to the strong repulsion between bound divalent counterions and the polyion length. Since no essential change in the conformation of the adsorbed MgPSS molecule is found in our experiments, the strong repulsion between Mg^{2+} counterions might also be supposed (by analogy) to cause a reduction of the LF effect as compared to the effect from NaPSS. A strong decrease in the LF effect with progressive substitution of Na^+ by Ca^{2+} counterions is also demonstrated for CMC at higher concentrations of the divalent ions [14].

The LF effect is found to increase in the presence of mono- and divalent counterions together [101]. Increasing electro-optical effect is also measured with addition of divalent counterions to NaDNA, but it turns to a decrease at higher concentration of Mg^{2+} ions [44]. Similar results are reported for DNA by Rau and Bloomfield [102] and Stellwagen [81] using mixed Na^+–Mg^{2+} solutions at constant ionic strength: in a dilute $MgCl_2$ solution, the effect is essentially equal to that in the presence of Na^+ ions, while in a solution of higher Mg^{2+} concentration (sufficient for Na^+ ions to be replaced

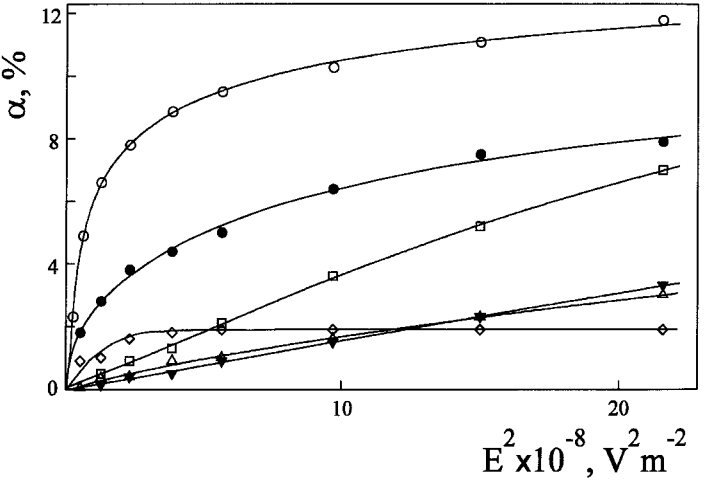

FIG. 17 Dependence of the LF and HF effects on the field strength E for suspensions with adsorbed NaPSS (○, △) and MgPSS (●, ▼) without added salts, and of the LF (◇) and HF (□) effects of suspension with adsorbed MgPSS in the presence of 3.5×10^{-6} M $MgCl_2$. (From Ref. 18.)

by Mg^{2+}), it decreases. From these examples, one has to conclude that partial agreement exists with the theoretical treatments—at low concentrations of the ions with higher valence. According to Minakata [101], the appearance of a maximum in the dielectric increment at some intermediate concentration of the divalent ions is possibly due to the interactions among mono- and divalent ions and charges of the polyion.

The effect of counterion charge on the critical frequency of LF relaxation is shown in Figure 18. It illustrates the electro-optical behavior of a suspension, stabilized by the adsorption of MgPSS, at different field strengths. For comparison, two frequency dependences of the effect from the suspension stabilized by the adsorption of NaPSS, are represented in this figure. As we can see, the critical frequency of LF relaxation in presence of Mg^{2+} counterions is higher if we compare equal effects. A similar increase in the critical frequency of LF relaxation has been supposed [101] to reflect the smaller effective length of the PSS molecule in the presence of divalent ions (Mg^{2+}, Ca^{2+}). It is difficult at present to draw any definite conclusions regarding the counterion valence dependence of the electro-optical effect, but the decrease in the polyion length is certainly not the only explanation of this dependence, since the polyion length is constant in our case.

Higher mobility of Mg^{2+} counterions on the PSS surface is also found [36], and it is supposed to be a result of the more compact conformation of

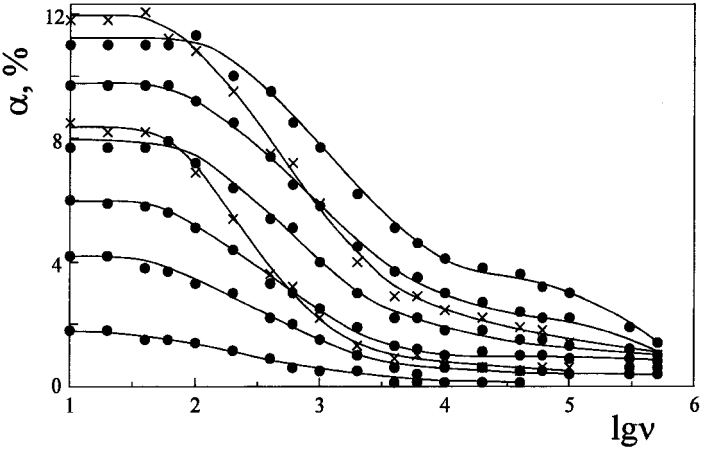

FIG. 18 Frequency dependence of α from β-FeOOH suspension, stabilized by addition of 10^{-2} gdm^{-3} MgPSS, ●, at different field strengths: 60, 120, 180, 240, 300, and 360 Vcm^{-1}, and from a suspension in presence of 10^{-2} gdm^{-3} NaPSS, ×, at 120 and 240 Vcm^{-1}. (From Ref. 18.)

the MgPSS molecule, the Mg^{2+} ions remaining immobile in the interior region of the molecule. Slow polarization of Na^{+} counterions into the interior of the NaPSS molecule is considered there to be responsible for the appearance of an LF effect. On the contrary, a slight reduction of the critical frequency of LF relaxation is measured [103] for CaCMC due to the aggregation of the polymer in the presence of Ca^{2+} ions. Almost equal frequencies of the LF relaxation are found [14] for NaCMC and CaCMC, adsorbed in an excess on oxide particles. It is clear, therefore, that systematically performed investigations are needed on well-defined systems and conditions in order to clarify this question.

V. STRUCTURE OF ADSORBED LAYERS

As was briefly outlined at the end of Sec. II, an average hydrodynamic thickness L_r of the polymer layer can be determined from the decrease in the particle diffusion coefficient due to polyelectrolyte adsorption.

The dependence of L_r on the polyelectrolyte molecular weight is electro-optically found for NaPSS adsorbed on β-FeOOH particles [17]. The value of L_r increases from 6 to 15 nm with increasing molecular weight of the NaPSS from 7×10^4 to 1×10^6. This result can be compared with the experimental data of Cosgrove et al. [66] for NaPSS adsorbed on the surface of polystyrene lattices, which show an increase of L_r from 5 to 20 nm with increasing molecular weight of the polymer from 7.4×10^4 to 7.8×10^5. The small values of the polymer layer thickness obtained mean that the adsorbed polyelectrolytes have a rather ''flat'' configuration. The strong electrostatic repulsion between the chain segments inhibits ''loop'' formation and this also explains the absence of significant molecular weight dependence of the polyelectrolyte adsorption [79]. Independence of the NaPSS adsorption of the polyelectrolyte molecular weight is found, for instance, by Cosgrove et al. [66] in salt-free solutions, and such an independence can be supposed in our case, since the particle isoelectric point in oxide suspension does not depend on the NaPSS molecular weight.

A dependence of the hydrodynamic layer thickness on the polyelectrolyte charge density is followed in [15] for polyacrylamides with degrees of hydrolysis 3.4, 9.8, and 19.1%, adsorbed on β-FeOOH particles. Equal values of $L_r = 6$ nm are found by electro-optics irrespective of the polymer charge (Table 1), although the theoretical prediction for this dependence is quite different.

According to Varoqui [104], the average layer thickness decreases (even slightly) with increasing charge density of the adsorbed polyelectrolyte. Average layer thickness L of weakly charged polyelectrolyte can be calculated as a function of the polymer charge α_* and the adsorbed amount Γ at

constant surface charge of the oxide particles $|\sigma|e^{-1} = 3.12 \times 10^{-4}$ Å^{-2} [105] and low ionic strength ($k^{-1} = 430$ Å) of the solution by the equation [104]

$$L = \left(\frac{2a^2}{\pi L_B}\right)^{1/3} (5.17|\sigma|\alpha_* e^{-1} - 6.33\alpha_*^2\Gamma)^{-1/3} \qquad kL << 1 \tag{13}$$

where $a = 5$ Å is a length of the polymer segment, $L_B = e^2/\varepsilon kT$ is the Bjerrum length, $k^{-1} = (8\pi L_B C)^{-1/2}$ is the Debye–Hückel length, and C is the concentration of a 1:1 electrolyte.

As observed in Table 1, the average layer thickness L decreases with increasing polymer charge density in line with the theory of Varoqui [104], even though the thicknesses are calculated at different polymer adsorption (fourth column in Table 1). The slower decrease of the average layer thickness with increasing charge density of HPAM in comparison to that of the adsorbed amount reflects as well the expected higher density of the segments in the layer from the less charged polyacrylamide.

A decrease of the adsorbed HPAM amounts with increasing charge density is determined in this case by radioactive measurements. This is consistent with the theoretical predictions of Evers et al. [106] and their next extension by Böhmer et al. [61]. Such a decrease has been experimentally shown also in Refs. 95, 107, and 108. The thickness of the adsorbed layer for a 100% charged polyelectrolyte is found, for instance, to be 1 nm and about 3–4 nm for the 30% charged one (this volume, chapter by Claesson). The reduction in polyelectrolyte charge density to 10% results in an increase in the adsorbed layer thickness to 10–20 nm.

It is necessary to point out that the average layer thicknesses of charged polyacrylamides are calculated to be lower than the electro-optically determined hydrodynamic layer thicknesses. Having in mind that the hydrodynamic thickness, mostly sensitive to the long ''tails'' of the adsorbed macromolecules, cannot be less than twice the average layer thickness [109], both values are in a reasonable agreement.

The observed independence of the electro-optically determined hydrodynamic layer thickness of the polymer charge deserves to be analyzed in more detail. One possible explanation could be related to the different polydispersity in stabilized suspensions. It is well known that the presence even of a few doublets in the suspension will give an unreal (higher) value of the thickness of the adsorbed layer. Higher polydispersity of the suspension, stabilized by the adsorption of more charged polyacrylamide, is really observed in our case. The more stretched conformation of the highly charged polyacrylamide seems to cause some residual (bridging) flocculation in the stabilized suspension, which explains the obtained equal values of the hy-

drodynamic layer thickness and the discrepancy observed with respect to the theory of Varoqui [104].

A small thickness (ca. 3 nm) of a layer from PEI, adsorbed on α-Fe_2O_3 particles, is found [32]. Being three times lower than the average size of the PEI molecule in solution [110], this value shows ''flattening'' of the PEI molecules at the plateau adsorption. The considerable shift of the pH from 9.8 to 6.9 and the particle isoelectric point, which is found at extremely low PEI concentrations (10^{-7}–10^{-6} gdm^{-3}), also indicates that nearly all amino groups of unfolded PEI molecules contact with the oxide surface. This implies even more ''flat'' configuration of the adsorbed PEI molecules below the particle isoelectric point, although the process of flocculation hampers its electro-optical determination.

VI. STABILITY OF COLLOID–POLYELECTROLYTE SUSPENSIONS

The flocculation and stabilization behavior of colloidal suspension due to the addition of polyelectrolyte is followed by electro-optics. Variation in the dispersity of the sample is recorded and its correlation with the electric surface properties of the polymer covered particles is shown. All the results obtained are consistent with a mechanism of flocculation by neutralization, i.e., they are in line with the ''classical'' coagulation mechanism through surface charge neutralization, which operates when a high valence counterion is added to the suspension. For example, close correlation between the particle dimensions and its surface charge is shown in Figure 2 for β-FeOOH suspension containing HPAM 9.8 [13,15]. A significant increase in the particle's relaxation time τ (relevant to flocculation) is observed in the vicinity of the particle isoelectric point, which occurs at a concentration of HPAM 9.8 equal to about 50% of the adsorption plateau value (Figure 19). With increasing concentration of HPAM 9.8, a large overcompensation of the surface charge is reached by the adsorbed polymer, and the suspension becomes stabilized at plateau adsorption due to the negatively charged HPAM layers around the colloid particles. The same behavior is found in presence of HPAM 3.4 and HPAM 15.1. As can be seen from Figure 19, there is a decrease in the particle dimensions of ca. 75% at concentration of HPAMs equal to about 75% of the adsorption plateau (points at the abscissa axis). At these concentrations (above the particle i.e.p.), almost 75% of the plateau values of the electrophoretic mobility is also reached. Such a correlation clearly shows that the electrostatic stabilization of the suspension dominates at full coverage with these polyions. The occurrence of some slight bridging flocculation does not change our main conclusion that Coulombic interac-

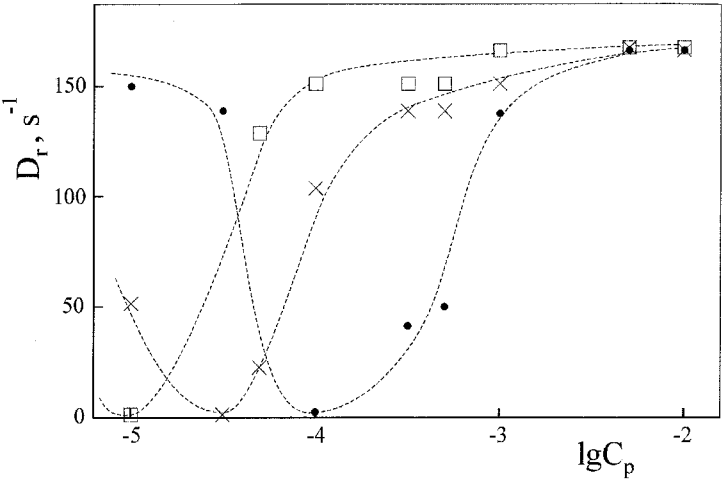

FIG. 19 Dependence of the rotational diffusion coefficient D_r of β-FeOOH particles on the concentration of polyacrylamide with different degrees of hydrolysis: ●, 3.4%; ×, 9.8%; and □, 19.1%.

tions between particle and polymer play the dominant role in stabilization and flocculation of the HPAM containing suspension.

No dependence of the critical concentration of flocculation on the molecular weight of NaPSS is shown in Figure 20. This is also a typical behavior for the suspension with no (essential) bridging flocculation. The ''flat'' configuration of the adsorbed polyions in stabilized suspensions shows no existence of a steric stabilization at plateau adsorption as well.

VII. CONCLUSION

The application of electro-optics to investigate colloid–polyelectrolyte suspensions certainly produces useful information for our understanding of the electrical properties and conformation of adsorbed macromolecules. The conclusion that has been drawn from electrophoresis, that the polymer-covered particles (in stabilized suspensions) assume the charge characteristics of the adsorbed macromolecules, is now electro-optically confirmed. Using the advantage of electro-optics for separating effects originating solely from the bound counterion polarization (in the region 10^2–10^4 Hz) and polarization of the free ions (at 10^4–10^6 Hz), we found that polarization of the former leads to the appearance of a saturated ionic induced dipole moment of polyelectrolyte molecules at very low field strengths (lower than 100 V cm^{-1}).

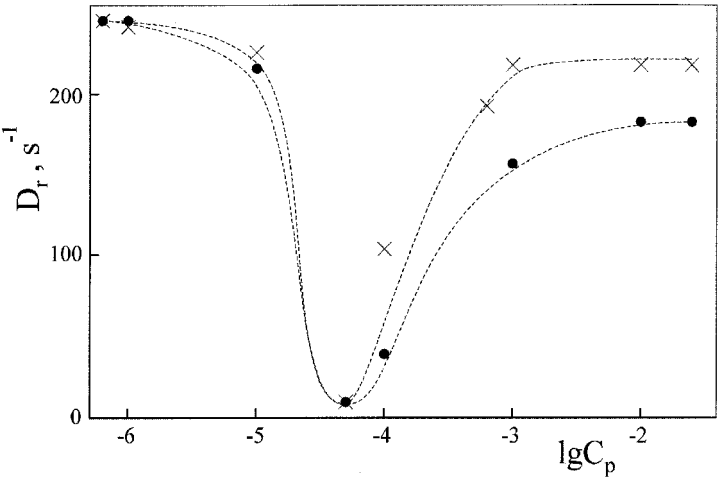

FIG. 20 Dependence of D_r on the concentration of NaPSS with different molecular weights: ×, 7×10^4 and ●, 1×10^6.

Thus the "permanent-like" dipole behavior of the polyelectrolyte solutions can be explained. The high-frequency behavior of polyelectrolyte solutions is found, however, similar to the behavior of colloids with no added polymer. The mobility of bound counterions and the degree of their binding to the polyion surface can be precisely determined if a proper (complete) theory is applied.

In combination with adsorption measurements, electro-optics is proved to be a powerful technique for studying the structure of adsorbed polyelectrolyte layers. Our data show "flat" conformation of the adsorbed macromolecules, which slightly depends on the polyelectrolyte charge density in accordance with the theory for weak polyelectrolytes. Counterion condensation is also suggested on the surface of weakly charged polyelectrolytes, which has not been predicted from the theory.

The most attractive property of electro-optics, to give information simultaneously on the electrical characteristics and the dimensions of colloid particles, can be successfully used to understand the role of the slower relaxation processes in colloid stability.

ACKNOWLEDGMENTS

I am very grateful to I. Petkanchin and M. Stoimenova for helpful discussions. This work was supported by the Bulgarian National Fund "Scientific Studies," Project V RP 3/99.

REFERENCES

1. O'Konski CT. Molecular Electro-Optics. New York: Marcel Dekker, 1976.
2. Fredericq E, Houssier C. Electric Dichroism and Electric Birefringence. Oxford: Clarendon, 1973.
3. Stoylov SP. Colloid Electro-Optics. London: Academic Press, 1991.
4. Radeva Ts, Petkanchin I, Varoqui R, Stoylov S. Effect of the adsorption of nonhydrolyzed polyacrylamide on the electric properties of kaolinite particles and the stability of their suspensions. Mat Sci Forum 1988; 25–26:417–420.
5. Radeva Ts, Petkanchin I, Varoqui R, Stoylov S. Electro-optical studies of kaolinite/polyacrylamide suspensions. Colloids Surf 1989; 41:353–361.
6. Radeva Ts, Stoimenova M. Electro-optic information on polymer adsorption and its influence on the electric double layer of colloid particles. Colloids Surf 1991; 54:235–244.
7. Radeva Ts, Petkanchin I, Varoqui R. Electric surface properties of oxide particles in presence of neutral polymer. In: Jennings BR, Stoylov SP, eds. Colloid and Molecular Electro-Optics. Bristol, Philadelphia: IOP, 1992:177–180.
8. Petkanchin I, Radeva Ts, Varoqui R. Adsorption of noncharged polyacrylamide on kaolinite by electrokinetics. Comm Dept Chem BAS 1991; 24:269–274.
9. Radeva Ts, Petkanchin I, Varoqui R. Electrical and hydrodynamic properties of colloid–polymer surface layers investigated by electro-optics. Langmuir 1993; 9:170–176.
10. Radeva Ts, Netzel J, Petkanchin I. Stoylov S. Electro-optic study of neutral polymer adsorption on mica. J Colloid Interface Sci 1993; 160:493–495.
11. Radeva Ts, Stoimenova M. Electro-optic study of colloid dispersions stabilized by polyelectrolyte adsorption. J Colloid Interface Sci 1993; 160:475–478.
12. Radeva Ts. Electric light scattering of ferric oxide particles in sodium carboxymethylcellulose solutions. J Colloid Interface Sci 1995; 174:368–372.
13. Radeva Ts, Petkanchin I. Electro-optic study of oxide particles in hydrolyzed polyacrylamide solutions. J Colloid Interface Sci 1996; 182:1–5.
14. Radeva Ts. Frequency behavior of the electro-optical effect from colloid particles in polyelectrolyte solutions with counterion mixtures. J Colloid Interface Sci 1997; 187:57–61.
15. Radeva Ts, Widmaier J, Petkanchin I. Adsorption of hydrolyzed polyacrylamides on ferric oxide particles: counterion mobility in stabilized suspensions. J Colloid Interface Sci 1997; 189:23–26.
16. Radeva Ts. Electro-optics of colloid-polyelectrolyte suspensions. Curr Topics Colloid Interface Sci 1997; 2:131–142.
17. Radeva Ts, Petkanchin I. Electric properties of adsorbed polystyrenesulfonate I: dependence on the polyelectrolyte molecular weight. J Colloid Interface Sci 1999; 220:112–117.
18. Radeva Ts. Electric properties of adsorbed polystyrenesulfonate II: the effect of low molecular salts. J Colloid Interface Sci 1999; 220:118–122.

19. Khlebtsov NG, Sirota AI, Fomina VI, Vypov MC. Application of an electro-optical method to investigation of polymer containing disperse systems. Colloid J 1990; 52:178–182.
20. Khlebtsov NG, Fomina VI, Sirota AI. Effect of polymer additives on electro-optical, adsorptional and aggregational properties of water cellulose suspensions. In: Jennings BR, Stoylov SP, eds. Colloid and Molecular Electro-Optics. Bristol, Philadelphia: IOP, 1992:177–180.
21. Petkanchin IB, Buleva M. Influence of polyelectrolyte adsorption on the electro-optical behavior of aerosil particles. Comm Dept Chem BAS 1991; 24: 570–575.
22. Buleva M, Petkanchin I. Influence of polyelectrolyte adsorption on the electro-optical behavior of aerosil particles. Ber Bunsenges Phys Chem 1996; 100: 972–976.
23. Yamamoto T, Mori Y, Ookubo N, Hayakawa R, Wada Y. Relaxational behavior of birefringence of aqueous carboxymethylcellulose under an alternating electric field at frequencies ranging from 0.1 Hz to 100 kHz. Colloid Polymer Sci 1982; 260:20–26.
24. Bellini T, Degiorgio V, Mantegazza F. The electric birefringence of polyelectrolytes: an electrokinetic approach. Colloids Surf A 1998; 140:103–117.
25. Ookubo N, Hirai Y, Ito K, Hayakawa R. Anisotropic counterion polarization and their dynamics in aqueous polyelectrolytes as studied by frequency-domain electric birefringence relaxation spectroscopy. Macromolecules 1989; 22:1359–1366.
26. Ito K, Yagi A, Ookubo N, Hayakawa R. Crossover behavior in high-frequency dielectric relaxation of linear polyions in dilute and semidilute solutions. Macromolecules 1990; 23:857–862.
27. Streb KD. Electro-optische Untersuchungen zur Koagulationstabilität wässriger α-Fe_2O_3 Dispersionen. Dissertation, Akademie der Wissenschaften der DDR, Berlin, 1988.
28. Matijevic E, Scheiner P. Ferric hydrous oxide sols. III. Preparation of uniform particles by hydrolysis of Fe(III)-chloride, -nitrate, and -perchlorate solutions. J Colloid Interface Sci 1978; 63:509–524.
29. Paterson R, Rahman H. The ion exchange properties of crystalline inorganic oxide-hydroxydes. Part I: β-FeOOH: a variable capacity anion exchanger. J Colloid Interface Sci 1983; 94:60–69.
30. Ozaki M, Kratohvil S, Matijevic E. Formation of monodispersed spindle-type hematite particles. J Colloid Interface Sci 1984; 102:146–151.
31. Sugimoto T, Muramatsu A, Sakata K, Shindo D. Characterization of hematite particles of different shapes. J Colloid Interface Sci 1993; 158:420–428.
32. Radeva Ts, Petkanchin I. Electric properties and conformation of polyethylenimine at the hematite–aqueous solution interface. J Colloid Interface Sci 1997; 196:87–91.
33. O'Konski CT, Yoshioka K, Orttung WH. Determination of electric and optical parameters from saturation of electric birefringence in solutions. J Phys Chem 1959; 63:1558–1565.

34. Peterlin H, Stuart HA. Doppelbrechung, insbesondere künstliche Doppelbrechung. In: Eucken A, Wolf KL, eds. Hand- und Jahrbuch der Chemischen Physik. Leipzig: Akademische Verlagsgesellschaft, 1943:1–115.
35. Petkanchin I, Brückner R, Sokerov S, Radeva Ts. Comparison of electric light scattering and birefringence for polydisperse suspensions. Colloid Polymer Sci 1979; 257:160–165.
36. Yamaoka K, Matsuda K. Reversing-pulse electric birefringence of poly(*p*-styrenesulfonate) in aqueous solutions: effects of molecular weight and concentration on anomalous signal patterns arising from fast- and slow-induced ionic dipole moments. J Phys Chem 1985; 89:2779–2786.
37. Oosawa F. Polyelectrolytes. New York: Marcel Dekker, 1971.
38. Gueron M, Weisbuch G. Polyelectrolyte theory. 2. Activity coefficients in Poisson–Boltzmann and in condensation theory. The polarizability of the counterion sheath. J Phys Chem 1979; 83:1991–1998.
39. Manning GS. Limiting laws and counterion condensation in polyelectrolyte solution. I Colligative properties. J Chem Phys 1969; 51:924–933.
40. Manning GS. Limiting laws and counterion condensation in polyelectrolyte solution. III. An analysis based on the Mayer ionic solution theory. J Chem Phys 1969; 51:3249–3252.
41. Watanabe H, Yoshida M, Kikuchi K, Maekawa T. What is the polarizability observed in electro-optical measurements? In: Jennings BR, Stoylov SP, eds. Colloid and Molecular Electro-Optics. Briston, Philadelphia: IOP, 1992:61–70.
42. Kikuchi K, Yoshioka K. Electric birefringence of potassium polystyrenesulfonate in aqueous solutions as a function of molecular weight, concentration, and field strength. J Phys Chem 1973; 77:2101–2107.
43. Yamaoka K, Fukudome K. Electric field orientation of nucleic acids in aqueous solutions. 1. Dependence of steady-state electric birefringence of rodlike DNA on field strength and the comparison with new theoretical orientation functions. J Phys Chem 1988; 92:4994–5001.
44. Yamaoka K, Fukudome K, Matsuda K. Electric field orientation of nucleic acids in aqueous solutions. 3. Non-Kerr-law behavior of high molecular weight DNA at weak fields as revealed by electric birefringence and electric dichroism. J Phys Chem 1992; 96:7131–7136.
45. Thurston GB, Bowling DJ. The frequency dependence of the Kerr effect for suspensions of rigid particles. J Colloid Interface Sci 1969; 30:34–45.
46. Benoit H. Contribution a l'étude de l'effet Kerr présenté par les solutions diluées de macromolécules rigides. Ann Phys 1951; 6:561–609.
47. Perrin F. J Phys Radium 1934; 5:497–511.
48. Radeva Ts, Stoylov SP, Suong T. Effect of the surface-active substance cetylpyridinium chloride on the electric light scattering of bentonite. Colloids Surf 1986; 17:229–239.
49. Tricot M, Houssier C. Electro-optical studies on sodium poly(styrenesulfonate). 1. Electric polarizability and orientation function from electric birefringence measurements. Macromolecules 1982; 15:854–865.

50. Yamaoka K, Fukudome K. Electric field orientation of nucleic acids in aqueous solutions. 2. Dependence of the intrinsic electric dichroism and electric dipole moments of rodlike DNA on molecular weight and ionic strength. J Phys Chem 1990; 94:6896–6903.
51. Stoylov SP. Colloid electro-optics. Electrically induced optical phenomena in disperse systems. Adv Colloid Interface Sci 1971; 3:45–110.
52. Petkanchin I, Suong T. Influence of the pH on the electric light scattering of palygorskite and bentonite suspensions. J Colloid Interface Sci 1985; 108: 553–555.
53. Buleva M, Stoimenova M. Electro-optic investigation of oxide suspension. Mechanism of formation of the induced dipole moment. J Colloid Interface Sci 1991; 141:426–432.
54. Stoimenova M, Radeva Ts. Electro-optic investigation of oxide suspension. On the nature of "permanent dipole moment." J Colloid Interface Sci 1991; 141:433–438.
55. Stoylov SP. Relation between stability of oxide and clay dispersed systems and the electric properties of their particles. Adv Colloid Interface Sci 1994; 50:51–78.
56. Ries H. Microelectrophoresis measurements on polymeric flocculants alone and in excess with model colloids. Nature 1970; 226:72–73.
57. Sresty GC, Somasundaran P. Selective flocculation of synthetic mineral mixtures using model polymers. Int J Miner Process 1980; 6:303–320.
58. Gebhardt JE, Fuerstenau DW. Adsorption of polyacrylic acid at oxide–water interfaces. Colloids Surf 1983; 7:221–231.
59. Skachkova AL, Golub TP, Sidorova MP, Omarova KI, Musabekov KB. Electrokinetic and adsorption properties of SiO_2 in OP-7 and polyethylenimine solutions. Colloid J 1991; 53:1100–1105.
60. Golub TP, Skachkova AL, Sidorova MP. Investigation of the surface reactions of the SiO_2 aqueous solution on polyethylenimine interface. Colloid J 1992; 54:59–66.
61. Böhmer MR, Evers OA, Scheutjens JMHM. Weak polyelectrolytes between two surfaces: adsorption and stabilization. Macromolecules 1990; 23:2288–2301.
62. Santhiya D, Nandini G, Subramanian S, Natarajan KA, Malghan SG. Effect of polymer molecular weight on the adsorption of polyacrylic acid at the alumina–water interface. Colloids Surf A 1998; 133:157–163.
63. Minakata A, Imai N. Dielectric properties of polyelectrolyte. I. A study on tetra-*n*-butyl ammonium polyacrylate. Biopolymers 1972; 11:329–346.
64. van der Touw F, Mandel M. Dielectric increment and dielectric dispersion of solutions containing simple charged linear macromolecules. II. Experimental results with synthetic polyelectrolytes. Biophys Chem 1974; 2:231–241.
65. Müller G, van der Touw F, Zwolle S, Mandel M. Dielectric properties of poly-L-glutamic acid in salt free aqueous solutions. Biophys Chem 1974; 2: 242–254.
66. Cosgrove T, Obey TM, Vincent B. The configuration of sodium poly-

(styrenesulfonate) at polystyrene–solution interfaces. J Colloid Interface Sci 1986; 111:409–418.
67. Sachs SB, Raziel A, Eisenberg H, Katchalsky A. Dilectric dispersion properties of aqueous polyelectrolyte solutions. Trans Faraday Soc 1969; 65:77–90.
68. van Beek WM, Odijk T, van der Touw F, Mandel M. Dielectric behavior of aqueous solutions of sodium polyphosphates of low degree of polymerization. J Polym Sci Polym Phys Ed 1976; 14:773–781.
69. Mandel M. The electric polarization of rodlike charged macromolecules. Mol Phys 1961; 4:489–496.
70. Takashima S. Mechanism of dielectric relaxation of deoxyribonucleic acid. Adv Chem Ser 1967; 63:232–252.
71. Manning GS. Limiting laws and counterion condensation in polyelectrolyte solutions. V. Further development of the chemical model. Biophys Chem 1978; 92:65–75.
72. Minakata A, Imai N, Oosawa F. Dielectric properties of polyelectrolytes. II. A theory of the electric increment due to ion fluctuation by a matrix method. Biopolymers 1972; 11:347–354.
73. van Dijk W, van der Touw F, Mandel M. Influence of counterion exchange on the induced dipole moment and its relaxation for a rodlike polyion. Macromolecules 1981; 14:792–795.
74. Warashina A, Minakata A. Dielectric properties of polyelectrolytes. IV. Calculation of dielectric dispersion by a stochastic model. J Chem Phys 1973; 58:4743–4751.
75. Mandel M, Jenard A. Dielectric behavior of aqueous polyelectrolyte solutions. 2. Trans Faraday Soc 1963; 59:2158–2169.
76. Takashima S. Dielectric dispersion of DNA. J Mol Biol 1963; 72:455–467.
77. Takashima S. Dielectric dispersion of DNA. II. J Phys Chem 1966; 70:1372–1380.
78. Sakamoto M, Hayakawa R, Wada Y. Dielectric relaxation of DNA solutions. II. Biopolymers 1978; 17:1507–1512.
79. van der Schee HA, Lyklema J. A lattice theory of polyelectrolyte adsorption. J Phys Chem 1984; 88:6661–6667.
80. Bauer D, Killmann E, Jaeger W. Flocculation and stabilization of colloidal silica by the adsorption of poly-diallyl-dimethyl-ammoniumchloride (PDADMAC) and of copolymers of DADMAC with *N*-methyl-*N*-vinyl-acetamide (NMVA). Colloid Polym Sci 1998; 276:698–708.
81. Stellwagen NC. Electric birefringence of restriction enzyme fragments of DNA: optical factor and electrical polarizability as a function of molecular weight. Biopolymers 1981; 20:399–434.
82. Sokerov S, Weill G. Polarized fluorescence in an electric field: comparison with the other electro-optical effects for rodlike fragments of DNA and the problem of the saturation of the induced moment in polyelectrolytes. Biophys Chem 1979; 10:161–171.
83. Matsuda K, Yamaoka K. Electric birefringence and electric dichroism of son-

icated DNA in aqueous solutions with various additives. Electro-optical and hydrodynamic properties. Bull Chem Soc Jpn 1982; 55:1727–1733.
84. Sato H, Shirai M. Field strength dependence of the electric birefringence of DNA. Progr Colloid Polymer Sci 1983; 68:138–143.
85. Manning GS. The critical onset of counterion condensation: a survey of its experimental and theoretical basis. Ber Bunsenges Phys Chem 1996; 100: 909–912.
86. Yoshida M, Kikuchi K. Metropolis Monte Carlo brownian dynamics simulation of the ion atmosphere polarization around a rodlike polyion. J Phys Chem 1994; 98:10303–10306.
87. Pörschke D. The mechanism of ion polarization along DNA double helics. Biophys Chem 1985; 22:237–247.
88. Stoimenova M, Radeva Ts. Electro-optics of semidilute dispersions: influence of electrostatic interactions on colloid particles relaxation times. J Colloid Interface Sci 1995; 169:329–334.
89. Tinoko I, Yamaoka K. The reversive pulse technique in electric birefringence. J Phys Chem 1959; 63:423–427.
90. Takezoe H, Yu H. Lateral diffusion of photopigments in photoreceptor disc membrane vesicle by the dynamic Kerr effect. Biochemistry 1981; 20:5275–5281.
91. Szabo A, Haleem M, Eden D. Theory of the transient electric birefringence of rodlike polyions: coupling of rotational and counterion dynamics. J Phys Chem 1986; 85:7472–7479.
92. Odijk T. Possible scaling relations for semidilute polyelectrolyte solutions. Macromolecules 1979; 12:688–693.
93. Cametti C, Di Biasio A. Counterion residence time and counterion radial diffusion in rodlike polyelectrolyte solutions. Macromolecules 1987; 20: 1579–1581.
94. Henningson CT. Karluk D, Ander P. Comparison of sodium ion interactions with sodium salts of carboxymethylcellulose and vinylic polyelectrolytes of varying charge density by diffusion. Macromolecules 1987; 20:1286–1291.
95. Blaakmeer J, Böhmer MR, Cohen Stuart MA, Fleer GJ. Adsorption of weak polyelectrolytes on highly charged surfaces. Poly(acrylic acid) on polystyrene latex with strong cationic groups. Macromolecules 1990; 23:2301–2309.
96. Charney E, Yamaoka K, Manning G. Ion strength and counterion repulsion as factors in the behavior of polyions in orienting electric fields. Biophys Chem 1980; 11:167–172.
97. Rau DC, Charney E. Electric dichroism of DNA. Influence of ionic environment on the electric polarizability. Biophys Chem 1983; 17:35–50.
98. Balasubramanian D, Charney E. Effect of charge density of linear polyelectrolytes on their orientation in an electric field. A study of poly(rA). poly(rU) and poly(rA). 2 poly(rU). J Phys Chem 1981; 85:1943–1947.
99. Weill G, Hornick C. Electric polarizability of rigid polyelectrolytes. In: Sélégny E, ed. Polyelectrolytes. Dordrecht: Reidel, 1974:277–284.
100. Yoshida M, Kikuchi K, Maekawa T, Watanabe H. Electric polarization of

rodlike polyions investigated by Monte Carlo simulations. J Phys Chem 1992; 96:2365–2371.
101. Minakata A. Dielectric properties of polyelectrolytes. III. Effect of divalent cations on dielectric increment of polyacids. Biopolymers 1972; 11:1567–1582.
102. Rau DC, Bloomfield VA. Transient electric birefringence of T7 viral DNA. Biopolymers 1979; 18:2783–2805.
103. Bordi F, Cametti C. Dielectric properties of polyelectrolyte solutions. II. Behavior of aqueous solutions of carboxymethylcellulose with divalent counterions. Ber Bunsenges Phys Chem 1986; 90:447–452.
104. Varoqui R. Structure and stability of weakly charged polyelectrolytes at a solid–liquid interface. In: Schmitz KS, ed. Macroion Characterization from Dilute Solutions to Complex Fluids. Washington DC: Amer Chem Soc, 1994: 421–435.
105. Atkinson RJ, Posner AM, Quirk JP. Adsorption of potential-determining ions at the ferric oxide–aqueous electrolyte interface. J Phys Chem 1967; 71:550–558.
106. Evers OA, Fleer GJ, Scheutjens JMHM, Lyklema J. Adsorption of weak polyelectrolytes from aqueous solution. J Colloid Interface Sci 1986; 111:446–454.
107. Foissy A, El Attar A, Lamarche JM. Adsorption of polyacrylic acid on titanium dioxide. J Colloid Interface Sci 1983; 96:275–287.
108. Rojas OJ, Claesson PM, Muller D, Neuman RD. The effect of salt concentration on adsorption of low-charge-density polyelectrolytes and interactions between polyelectrolyte-coated surfaces. J Colloid Interface Sci 1998; 205: 77–87.
109. Pefferkorn E, Dejardin Ph, Varoqui R. Derivation by hydrodynamics of the structural characteristics of adsorbed polymers at liquid–solid interfaces. J Colloid Interface Sci 1978; 63:353–363.
110. Akari S, Schrepp W, Horn D. Chemical imaging of single polyethylenimine by chemical force microscopy. Ber Bunsenges Phys Chem 1996; 100:1014–1016.

This Page Intentionally Left Blank

12

Monolayer Assemblies of Poly(L-Glutamic Acid)s at Two-Dimensional Interfaces

NOBUYUKI HIGASHI and MASAZO NIWA Doshisha University, Kyoto, Japan

I. INTRODUCTION

Recently, many efforts have been dedicated to the study of macromolecules carrying ionized or ionizable groups. These synthetic polyelectrolytes are important in industrial applications and also as simplified models of natural polyelectrolytes. Bipolymers such as proteins and nucleic acids are typical natural polyelectrolytes, and their functions in vivo stem basically from their higher ordered structures resulting from specific interactions among characteristic structural elements (e.g., α-helices, β-sheets). It should be of significance to model such structural features of proteins and to define the interaction mechanism among the component chains for developing molecularly controlled polymeric materials that mimic biofunctions such as enzymatic catalysis and molecular recognition. One attractive approach is the recent work on template assembled synthetic proteins [1]. A template molecule directs the component chains into a proteinlike packing arrangement, e.g., a bundle of α-helices [2]. The amphiphilic property of the peptide blocks seems to be essential to stabilize such a bundle structure. A macrodipole moment of the α-helical rod would play a key role in assembling the structural elements [3,4]. Another approach is to use a Langmuir monolayer or a self-assembled monolayer, which is a useful tool for assembling molecules two-dimensionally [5]. We have devised a strategy in which purely synthetic polyelectrolytes are aligned at the air–water interface or at the solid substrate. Poly(L-glutamic acid) (PLGA) has been chosen as a model element of a protein because of its ease of preparation and well-defined conformational characteristics in water.

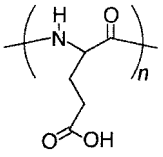

P(L or D)GA

In order to assemble at interfaces, PLGA has been modified at the chain ends as illustrated schematically in Figure 1. Three methods (Types A, B, and C) have been employed for assembling. Types A and B are monolayers on water, and Type C is a self-assembled monolayer on gold substrates. The PLGA amphiphile in Type A has two long alkyl chains at one terminus of the PLGA segment so as to float on water. In this case, the PLGA segments are expected to align perpendicularly to the interface. In the monolayer of Type B, the PLGA segments must be aligned parallel to the interface, since both termini of the PLGA segment are floated by hydrophobic alkyl chains. The amphiphile of Type C includes a disulfide bond within the alkyl chain to attach to the gold surface. In the present chapter, we will present our

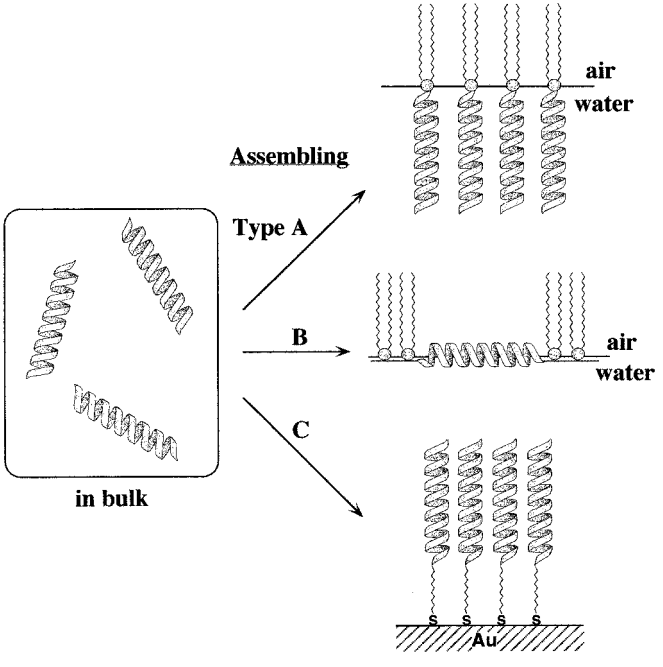

FIG. 1 Schematic illustrations for two-dimensional assemblies of helical polypeptides.

recent works on organized PLGA assemblies that have provided characteristics uniquely different from those in homogeneous media.

II. PLGA MONOLAYERS OF TYPE A

A. Secondary Structure of the PLGA Segment [6,7]

PLGA has been widely known to show a specific conformational change between an α-helix and a random coil induced by varying pH, ion strength, and so on. We have prepared a double-chain amphiphile containing a PLGA segment (**1**L) and have described its peculiar conformational behavior on water.

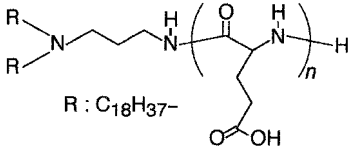

1L or D

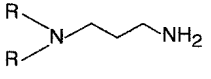

2

Figure 2 shows the π–A isotherm for the compression–expansion cycle of **1**L at pH 3.9, 20°C. A considerable difference is observed between the compression curve and that for expansion. On the compression isotherm, at low surface pressure, as expected, molecules lie on the water surface, occupying a large area. With increasing surface pressure, they begin to associate and orient their hydrophobic tails and/or polymer segments. In the mesophase, in which liquid-expanded (LE) and liquid-condensed (LC) phases may coexist, there is a transition to a condensed phase at ca. 30 mN m^{-1}. On the other hand, in the expansion process, the π–A curve shows the disappearance of such a mesophase and the appearance of a condensed phase even at a low surface pressure. When the same cycling experiment on the π–A isotherm was performed for the PLGA segment-free **2**, no hysteresis effect was observed. These results strongly suggest that a tight aggregation of the PLGA segments occurs within the **1**L monolayer upon compression and, consequently, brought about the compression–expansion hysteresis. To reveal conformational properties of the PLGA segment, we employed circular dichroism (CD) spectroscopy. The spectrum obtained for a Langmuir–Blodgett (LB) film transferred at pH 3.9 and a surface pressure of 15 mN m^{-1}, at which the monolayer is in a liquid analogue phase, exhibits two negative bands at 222 and 208 nm, indicating the formation of an α-helix structure. The same CD pattern is also observed for the LB film transferred

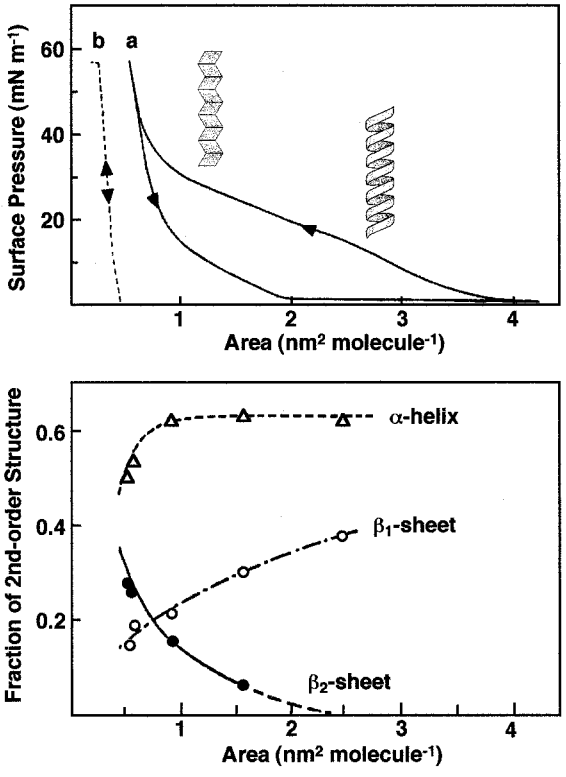

FIG. 2 Surface pressure (π)–read (A) isotherms for the compression–expansion cycle of **1**L (a) and **2** (b) on water at 20°C, pH 3.9 (top). The fraction of secondary structure as a function of the molecular area (bottom).

at 25 mN m^{-1} in a mesophase. On the other hand, in a condensed monolayer phase, for example, at 35 mN m^{-1}, the CD spectrum of the LB film gives a trough at 217 nm, a crossover at 207 nm, and a positive peak at 195 nm. This spectral feature is very similar to that of the β-form polypeptides. As is known, the β-sheet structure of polypeptides derives from intermolecular interactions between them through hydrogen bonding, while the intramolecular hydrogen bonding causes principally α-helical conformation. Thus, by compressing the monolayer, the PLGA segments aggregate tightly, and then the intramolecular hydrogen bonding is likely to be rearranged to the intermolecular one, which induced the conformational change of PLGA segments from α-helix to β-sheet. To obtain more quantitative information about sec-

ondary structures, FT-IR spectra for the LB films were measured. We focused on three peaks of α-helix including random coil (1630–1660 cm^{-1}) and β-structures (1625 and 1603 cm^{-1}) based upon the amide-I band in the main chain. The existence of two types of β-forms (β_1 and β_2) has been evidenced on the basis of x-ray analysis. In the β_1 structure there are large cavities between the neighboring sheets, and within these cavities there are water molecules that are hydrogen bonded to the peptide groups or to the carboxyl groups and stabilize the β_1 structure. In contrast, the β_2 structure does not have such a cavity between the neighboring sheets. In our monolayer, two types of β-forms could be observed in FT-IR spectra (not shown here). The fraction of secondary structures (α-helix, β_1, and β_2-forms), estimated by the peak resolution of the spectra obtained, is plotted against the molecular area of **1**L monolayer in Figure 2. At lower surface pressures, the PLGA segments are predominantly in α-helical structure including a minor β_1-form. On the other hand, at higher surface pressure, at which the monolayer is in a condensed phase, the content of a more compact β_2-form increases drastically, and accordingly that of both α-helix and β_1-form decreases. α-Helical PLGA has been found to be converted to the β-structure in a gel state and in other media, although such a transformation must require a considerably high temperature and the presence of some chemical substrates. It is noteworthy, however, that the stable β-structure formation was observed for surface monolayer under a mild condition, and that the secondary structure of the PLGA segment could be adequately controlled by adjusting the monolayer phase (Figure 3).

It is easy to introduce functional groups such as a photoresponsive dye to the side chain of the PLGA segment. A spiropyran-carrying PLGA in aqueous solution has been shown to undergo large random coil-α-helix conformational change upon exposure to sunlight and dark conditions, alternately [8]. If such a PLGA can be aligned at the air/water interface, photoinduced conformational variations in the PLGA assembly would be dynamically investigated by means of surface pressure–area isotherm measurements. We prepared thus a photoresponsive PLGA amphiphile (**3**) con-

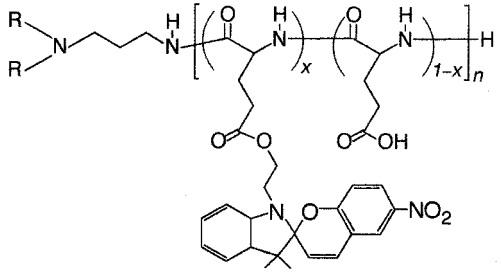

3

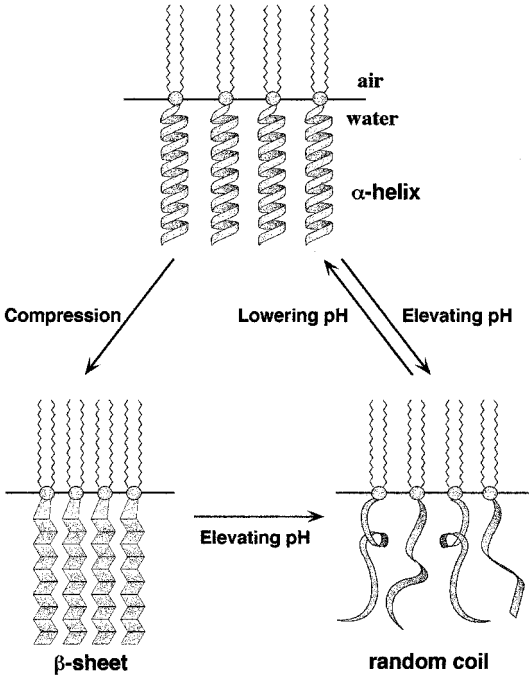

FIG. 3 A possible illustration for variation of secondary structures dependent upon the monolayer phase and pH in the subphase.

taining spiropyran units in the side chains and revealed conformational behavior in the monolayer state on water. Spreading and spectroscopic experiments have demonstrated that (1) the surface monolayers of **3** are considerably affected by isomerization of the spiropyran group; i.e., **3**sp, which is in the spiro form, gives an expanded monolayer compared with that of the spiropyran group-free, whereas **3**mc in the cyanine form gives a well-condensed monolayer similar to the spiropyran group-free monolayer; (2) the helix content of these PLGA segments is higher for the **3**sp monolayer than for the **3**mc monolayer; (3) the **3**mc monolayer gradually expands upon isomerization from the cyanine to the spiro form. These findings suggest that this system should be useful as a model of photoreceptors in biomembrane.

B. Mixing Behavior with D-Isomer [9]

The helical sense in helix assemblies could be important in light of the effects of steric factors on monolayer assembling. In this context, we pre-

pared the corresponding D-isomer (PDGA, **1**D) that is expected to take a left-handed helix, and examined mixing behavior with **1**L. Figure 4 displays π–A isotherms for pure **1**L and **1**D and for their equimolar mixture (molar fraction of **1**L in the mixture of **1**L and **1**D, $X_{1L} = 0.5$) a pH 4.0, 20°C. The π–A curve of pure **1**L ($X_{1L} = 1.0$) is completely identical to that of pure **1**D ($X_{1L} = 0$), which provides a well-condensed phase via a mesophase of LE and LC over the wide molecular area (from 7 to 2 nm^2 per molecule) and then collapses at around 50 mN m^{-1}. The limiting molecular area, extrapolated in the condensed phase to zero surface pressure, was evaluated to be 1.3 nm^2 per molecule, which is close to the theoretical cross-sectional area (1.2 nm^2) for α-helical PGA. Therefore the observed plateau in the π–A curve could correspond to a transition from a state where the helices are in the horizontal plane to a state where they are perpendicular to the water surface. The isotherm of the equimolar mixture is obviously different from those of pure **1**L and **1**D.

The π–A isotherms at the air–water interface provide information not only on the orientation of the molecules but also on the interactions between the constituents of the mixed monolayer. The mean area per molecule for a mixed two-component system has been calculated using the additivity expression

$$A_{12} = X_1A_1 + X_2A_2 \tag{1}$$

where X_1, A_1 and X_2, A_2 are the mole fractions and the area per molecule of

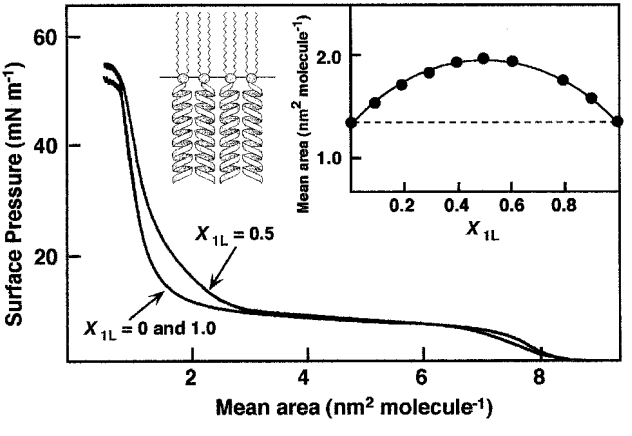

FIG. 4 Comparison of π-A isotherms among $X_{1L} = 0$, 0.5, and 1.0 measured at pH 4.0, 20°C. The inset shows the relationship between the mean molecular area at a constant surface pressure of 20 mN m^{-1} and X_{1L}.

the first and second components, respectively. A_{12} is the mean area per molecule of the mixed monolayer of the two component systems. The inset in Figure 4 shows the plot of the mean area per molecule versus the mole fraction of **1**L in the mixed monolayers at constant surface pressure of 20 mN m^{-1}. The dotted line represents the ideal curve for noninteracting two-component systems calculated from the above equation. It is interesting to note that the mean area values display positive deviation from the linear correlation. This observation implies that nonideal mixing behavior would be favored under these conditions due to interactions between component molecules. In general, such a positive deviation is supposed to result from steric factors and/or repulsive interactions working between monolayer components. The FTIR spectrum of the mixed monolayer (X_{1L} = 0.5) provided characteristic adsorptions of the α-helix structure with about 92% α-helix content. The positive deviation observed in Figure 4 must, therefore, be considered to be due to interaction between right-handed (**1**L) and left-handed (**1**D) helices. If the helical sense of PLGA segments plays an important role in the miscibility of the monolayer, it can be readily expected that such a deviation from ideal mixing would diminish by changing the conformation of PGA segments from helix to random coil structures. In fact, when the same spreading experiment was carried out at pH 9.0, at which the PGA segments took random coil conformation, the relationship between the mean area and X_{1L} was found to obey the above Eq. 1. From these considerations, it seems likely that the positive deviation observed in Figure 4 is due to an enhanced-repulsive interaction between different types of helices or a lowering of the helix packing density caused by a difference in helical sense. However, the former interaction may be disregarded, since the direction of macrodipole moment, which arises from the helical structure, is identical for **1**L and **1**D in the monolayers, whereas the helical sense is, of course, different. The effect of the helix macrodipole moment on monolayer assemblies will be described below.

C. Interaction of Helical PLGA Assemblies with Amino Acids [11]

These organized PLGA assemblies are also expected to provide a site in which a guest molecule can be specifically captured. Recently, several reports have appeared on enantioselective permeation of α-amino acids through thick polymer films based on α-helical PLGA having amphiphilic side chains [12,13]. The authors pointed out the importance of the aggre-

gation structure of PLGA in the films for such an enantioselectivity. Here it occurs to us that the LB films of our **1**L monolayer will be able to capture specifically α-amino acid isomers due to the much more organized structures of PLGA chains.

The hydrophobically treated quartz plate was lowered through the monolayer on a subphase at 30 mN m^{-1}, at which the PLGA segment is in α-helix structure, and a one-layer LB film, in which the PLGA segments are exposed to water phase, was then deposited on the quartz plate. The monolayer-covered surfaces thus obtained were subjected to binding experiments with α-amino acids of tryptophan (Trp), tyrosine (Tyr), and phenyl alanine (Phe). The binding processes were followed by means of UV spectroscopy. The adsorption reached equilibration within ca. 30 min. Interestingly, the amount of surface-bound D-Trp to the **1**L layer was found to be much larger by a factor of ca. 6 than that of L-Trp. When the same experiment was carried out for two other α-amino acids, Tyr and Phe, the selectivity between D- and L-isomers was 3 and 8, respectively. It is clear that the organized, α-helical PLGA surface has the ability to discriminate α-amino acids enantioselectively. These binding experiments were carried out separately for L- or D-isomer. Subsequently, we examined selective binding of a racemic mixture of DL-Trp at the **1**L monolayer surface. A differential CD spectrum before and after adsorption of DL-Trp gave a CD pattern of D-Trp. This result undoubtedly demonstrates that the D-isomer was preferentially bound to the **1**L monolayer, though minor adsorption of the L-isomer cannot be excluded. The similar enantiomeric binding was also observed for the self-assembled monolayer (Type C) of **4** on gold substrates [14]. Clarification of the detailed mechanisms including the driving force causing such an enantioselectivity is currently under way in our laboratory.

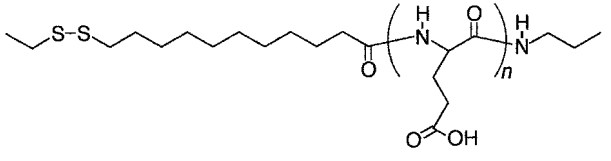

4

III. PLGA MONOLAYERS OF TYPE B [15]

The structural feature of this type of monolayer is to align the PLGA segment parallel to the water surface, as mentioned above. For that purpose, a triblock polyion complex of **5** has been designed and prepared via the fol-

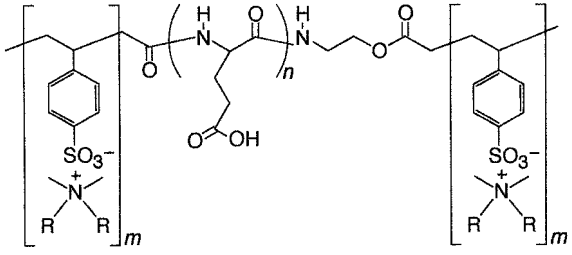

5

lowing five steps. First, polymerization of γ-benzyl-L-glutamate-*N*-carboxylic anhydride initiated with the primary amino group of ethanolamine was carried out, and then the residual amino group and hydroxyl group at each chain-end of the polymer obtained were reacted with chloroacetyl chloride, and subsequently treated with sodium xanthate, giving a macrophotoinitiator of poly(γ-benzyl-L-glutamate) whose chain-ends were successfully labeled with photoinitiatable xanthate groups. Photopolymerization of *N*,*N*-dimethyl-*N*,*N*-dioctadecyl-ammonium styrene sulfonate (DOAS) was performed in the presence of this macrophotoinitiator by UV irradiation. Finally, the triblock polyion complex (**5**) was obtained by removal of benzyl groups. Figure 5 shows pH dependence of the π–A isotherm of **5** at 20°C. A considerable difference is observed at low pH (3.0) and at high pHs (5.8 and 9.5); at pH 3.0, the monolayer is found to have a phase transition from the LE to the LC state upon compression and to always contract compared with the monolayers at pHs 5.8 and 9.5. When the same spreading experiments were

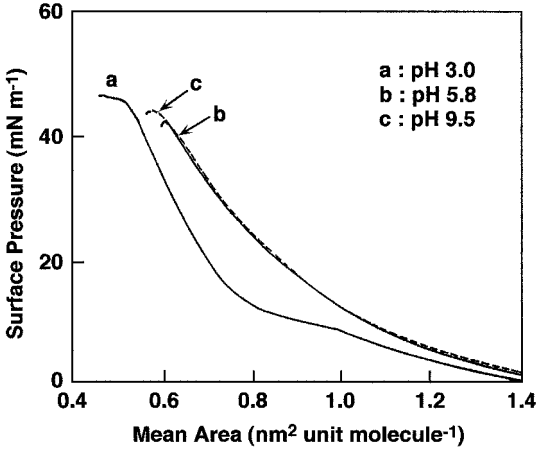

FIG. 5 π–A isotherms of a triblock polyion complex of **5** on an aquous subphase, 20°C, at different pHs: 3.0 (a), 5.8 (b), and 9.0 (c).

performed for the PLGA segment-free PDOAS, π–A curves were not affected by all by varying pH in the subphase. Thus the observed pH dependence for **5** is ascribed definitely to the presence of the PLGA segment in **5**. Since PLGA in aqueous media is well-known to show a conformational (helix–random coil) transition at around pH 4, it would be expected that the drastic variation in π–A isotherms of **5** at that pH region corresponds to the secondary structural change of PLGA segment if the same conformational transition could occur also at the air–water interface. Actually, the FT-IR data for these monolayers indicated that the conformational properties of the PLGA segment in the monolayer state were similar to those of PLGA in aqueous solution.

Subsequently, changes in morphology of the monolayer of **5** during compression at different pHs were investigated by fluorescence microscopy. For that purpose, 1.0 mol% fluorescent probe octadecyl Rhodamine B was added to the polyion complex solutions before spreading. Figure 6 shows a comparison of photographs of monolayers of **5** on aqueous subphases of pHs 3.0 and 9.5 at 20°C taken at 15 mN m^{-1}. On a subphase of pH 9.5, the fluorescence is homogeneous throughout the field of observation. It should be noted that the bright areas in the figure consist of molecules of **5** in LE state homogeneously mixed with the fluorescent probe. This morphological profile at pH 9.5 is consistent with the π–A isotherm obtained earlier under the same condition (see Figure 5) and also very similar to that of PDOAS (not shown here) whose monolayer could not primarily form well-grown crystalline domains probably due to weak interaction among molecules. Since at this pH th PLGA segment of **5** adopted a flexible random coil structure in which COOH groups of the segment were completely deprotonated as described above, an attractive interaction among **5** molecules in the monolayer is considered to be not so strong as that of PDOAS, although a repulsive interaction among **5** molecules may work due to ionized PLGA segments. On the other hand, the **5** monolayer at pH 3.0, at which the PLGA segment adopts a rigid rodlike helix, exhibits a specific morphological behavior: three appeared star-shaped domains with a diameter of about 40 μm. This specific morphological feature in the lower pH region would be produced by a strong interaction such as the helix macrodipole interaction working among the rodlike, helical PLGA segments in the monolayer-forming polyion complex molecules as displayed schematically in Figure 6.

The dipole moments of amino acid in an α-helical peptide align in the same direction, nearly parallel to the helix axis, and then the resulting macroscopic dipole generates an electrostatic potential, directed from the N-terminus to the C-terminus [3,4]. This electrostatic field plays an important role in the structure and functions of proteins. Batchelder et al. have shown

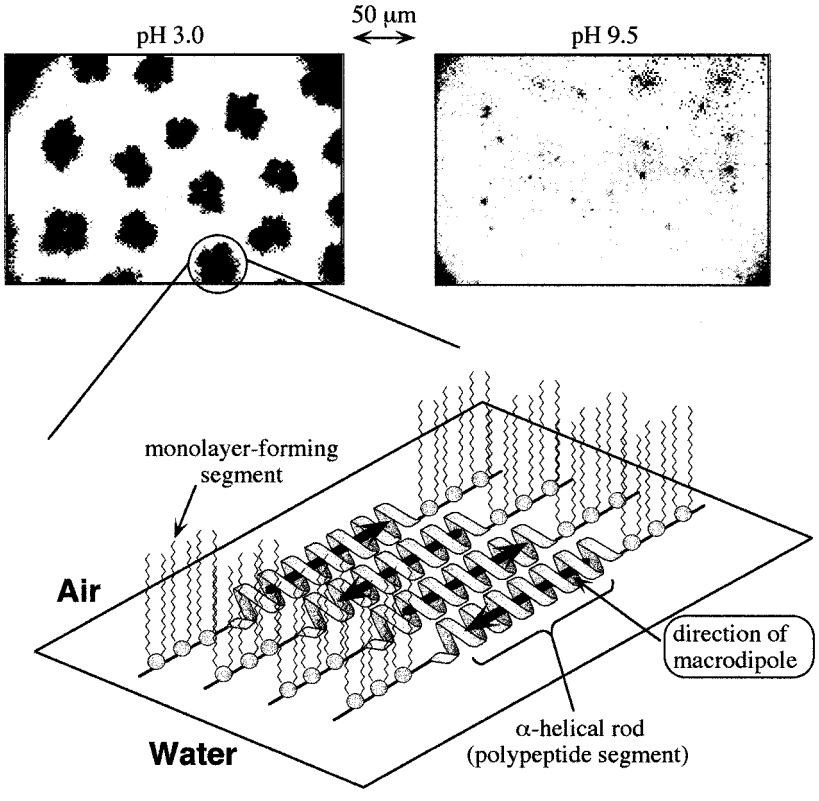

FIG. 6 Fluorescence microscopic images of monolayers of **5** on aqueous subphases of pHs 3.0 and 9.5, 20°C, at a surface pressure of 15 mN m^{-1}; octadecyl Rhodamine B (1 mol%) was included in monolayers as a fluorescent probe (top). A possible model for the observed crystalline domain due to helix–helix macrodipole interaction at pH 3.0 (bottom).

that the macrodipole affects the efficiency of photoinduced intramolecular fluorescence quenching [16]. In addition, the orientation of the α-helical peptide in the self-assembled monolayers is also influenced by the intermolecular macrodipole interaction [17]. Thus, if α-helical peptide assemblies, in which macrodipoles are directed in the same sense, are prepared, it could be expected that a specific interaction would be caused between α-helical peptide assemblies and guest peptides. We have demonstrated a specific interaction of guest PLGAs (**6**N and **6**C) at the self-assembled monolayer

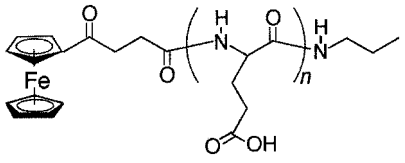

6_N

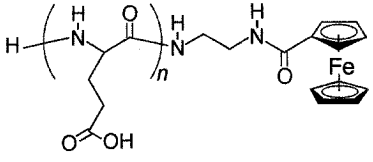

6_C

of **4** (Type C) [18,19]. One termnius (C- or N-terminus) of the guest PLGA is labeled with ferrocene as a redox-activity moiety so as to examine such interactions electrochemically. Consequently, the monolayers, in which the **4** molecule was in controlled, lateral distribution on a gold surface, have the ability to discriminate between N- and C-termini of guest helical PLGAs on the basis of a specific interaction between helix macrodipoles (Figure 7). Further characteristics of the monolayers before and after complexation will follow after investigation of the helix rod orientation.

IV. CONCLUSION

In the present chapter, we have demonstrated three types of monolayer assemblies that are composed of the PLGA segment as a common building block. Assembling the PLGA segment at two-dimensional media by different

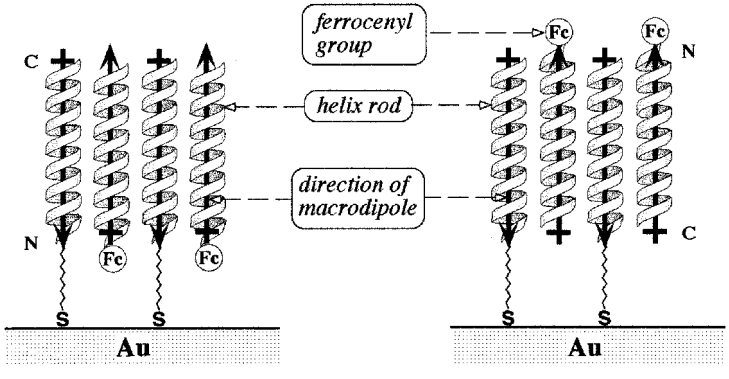

FIG. 7 Specific interaction between PLGA helical rods on the bsis of helix–macrodipole.

methods has led to various unique and unprecedented phenomena fundamentally different from those observed in bulk. These poly(oligo)-peptide organized systems not only are of particular interest in view of a structural model of protein but also contribute to the understanding of interaction mechanisms among the component elements of bipolymers.

REFERENCES

1. Mutter M, Tuchscherver GG, Miller GG, Altmann K-H, Carey RI, Wyss DF, Labhard AM, Rivier JE. Template-assembled synthetic proteins with four-helix-bundle topology. Total chemical synthesis and conformational studies. J Am Chem Soc 1992; 114:1463–1470.
2. Sasaki T, Kaiser ET. Helichrome: synthesis and enzymatic activity of a designed hemeprotein. J Am Chem Soc 1989; 111:380–381.
3. Wada A. The α-helix as an electric macro-dipole. Adv Biophys 1976; 9:1–63.
4. Hol WGJ, van Duijnen PT, Berendsen HJC. The α-helix dipole and properties of proteins. Nature 1978; 273:443–446.
5. Higashi N, Niwa M. Organized polyelectrolyte monolayers as a structural model of biopolymer. Colloid Surf A, Physicochem Eng Aspects 1997; 123/124:432–442.
6. Higashi N, Shimoguchi M, Niwa M. Stabilization and facilitated formation of a *b*-structure polypeptide by a poly(L-glutamic acid)-functionalized monolayer on water. Langmuir 1992; 8:1509–1510.
7. Higashi N, Shimizu K, Niwa M. Surface monolayers of poly(L-glutamic acid)-functionalized amphiphiles: effect of attachment of spiropyran to the polymer segment. J Colloid Interface Sci 1997; 185:44–48.
8. Ciardelli F, Fabbri D, Pieroni O, Fissi A. Photomodulation of polypeptide conformation by sunlight in spiropyran-containing poly(L-glutamic acid). J Am Chem Soc 1989; 111:3470–3472.
9. Higashi N, Nishikawa R, Koga T, Niwa M. Effects of helical sense and macrodipole on helix interaction in poly(glutamic acid) monolayers at the air–water interface. J Colloid Interface Sci. In press.
10. Ulman A. An Introduction to Ultrathin Organic Films: From Langmuir–Blodgett to Self-Assembly. Boston: Academic Press, 1991.
11. Higashi N, Saitou M, Mihara T, Niwa M. Enantioselective binding of α-amino acids at poly(L-glutamic acid)-functionalized monolayer surfaces. J Chem Soc, Chem Commun 1995; 2119–2120.
12. Maruyama A, Adachi N, Takatsuki T, Torii M, Sanui K, Ogata N. Enantioselective permeation of α-amino acid isomers through poly(amino acid)-derived membranes. Macromolecules 1990; 23:2748–2752.
13. Inoue K, Miyahara A, Itaya T. Enantioselective permeation of amino acids across membranes prepared from 3α-helix bundle polyglutamates with oxyethylene chains. J Am Chem Soc 1997; 119:6191–6192.

14. Niwa M, Matsui M, Koide K, Higashi N. Enantioselective adsorption of ferrocene-modified glutamic acids on helical poly(L-glutamic acid) self-assemblies at gold electrodes. J Mater Chem 1997; 7:2191–2192.
15. Higashi N, Sunada M, Niwa M. Morphological variation of monolayers of the poly(L-glutamic acid) segment-carrying polyion complex induced with helix–helix interactions. Langmuir 1995; 11:1864–1866.
16. Batchelder TL, Fox RJ III, Meier MS, Fox MA. Intramolecular excited state electronic coupling along an α-helical peptide. J Org Chem 1996; 61:4206–4209.
17. Worley CG, Linton RW, Samulski ET. Electric-field-enhanced self-assembly of α-helical polypeptides. Langmuir 1995; 11:3805–3810.
18. Niwa M, Murata T, Kitamatsu M, Matsumoto T, Higashi N. Spontaneous formation of single- and double-layered polypeptide assemblies based upon a helix–macrodipole interaction. J Mater Chem 1999; 9:343–344.
19. Niwa M, Morikawa M, Higashi N. Discrimination between N- and C-termini of polypeptides by a two-dimensional array of helical poly(L-glutamic acid) rods on gold surfaces. Langmuir 1999; 15:5088–5092.

This Page Intentionally Left Blank

13

Emulsions Stabilized by Polyelectrolytes

PATRICK PERRIN Ecole Supérieure de Physique et de Chimie Industrielles, Paris, France

FRÉDÉRIC MILLET Commissariat à l'Énergie Atomique (Saclay), Gif-sur-Yvette, France

BERNADETTE CHARLEUX Université Pierre et Marie Curie, Paris, France

I. INTRODUCTION

Liquid–liquid dispersions [1–4] are widely used in numerous technological domains such as medicine [5–7], cosmetics [8–15], bitumen in road works [16,17], oil [18–33], food [34–38] and paint [39] industries to name but a few.

On the one hand, systems with ultralow interfacial tensions lead to the formation of microemulsions that are thermodynamically stable and transparent dispersions. The recipes for the preparation of microemulsions were recently summarized [40] and extensively reviewed by Bellocq [41]. On the other hand, emulsions are thermodynamically unstable and turbid systems. The Gibbs free energy of dispersion formation, which consists of three terms, namely the change in the interfacial energy, the interaction energy between droplets, and the entropy of droplet dispersion, is negative for microemulsions and positive for emulsions [42,43]. In contrast to microemulsions, the excess Gibbs energy per particle in emulsions is high as a result of the large droplet size (order of a micrometer) and finite interfacial tensions and hence cannot be compensated for by entropy contributions. Emulsions are thus kinetically stable systems. As a consequence, the two types of dispersion appear to be very different, since the formation of microemulsions is a spontaneous process, whereas mechanical energy is required to form emulsions to overcome the cost of increasing the total interface area between the two liquids.

Although finely divided insoluble solid particles constitute an important class of emulsifying agents [44–46], the preparation of liquid–liquid dispersions traditionally involves the use of ionic and nonionic small-molecule surface-active agents. Mixtures of surfactants can also be used to achieve a desirable viscosity of emulsions [12] and to enhance the stabilization properties compared to the effect of one of the emulsifiers [47–49], although evidence of synergistic effects are not always found.

In contrast to small-molecule surfactants, very little appears to be known of the effects of polymeric surfactants on liquid–liquid dispersion systems. However, block and graft copolymers [50–52] display attractive interfacial properties resulting from the incompatibility between the chemically different sequences linked together in the same macromolecules. In the solid state, blending existing polymers together has long been known to be a low-cost route of developing novel materials. However, most polymer pairs being mutually immiscible, the resulting blends generally exhibit very poor mechanical properties due to their coarse, heterogeneous morphology and weak adhesion. Both block and graft copolymers have been shown to be effective compatibilizing agents. The importance of achieving enhanced mechanical properties in blends of immiscible polymers [53–61] has given to the study of the conformation of copolymers at solid–solid interfaces a considerable interest from both experimental [62,63] and theoretical [64–68] viewpoints. In solution, both homopolymers and copolymers exhibit interesting interfacial and colloidal properties as well. Polymeric materials have been used to give colloidal stability since almost the dawn of civilization. For example, gum arabic was used to prepare water-based inks pigmented with carbon black. More specifically, the effects of polymers on colloidal stability have seen detailed investigations [69–72] as a result of polymer adsorption on surfaces [73–80]. Furthermore, several types of polymeric surfactants are being used successfully in the preparation and/or stabilization of polymer lattices, particularly in an aqueous medium. During preparation, oil droplets are thus stabilized in a water continuous phase forming an oil-in-water type (O/W) of emulsion, as reviewed in Sec. IV for polyelectrolytes. Various block and graft copolymers were also used for dispersion stabilization and polymerization in nonaqueous solvents [81]. For instance, poly(styrene-*b*-dimethylsiloxane) can be used to disperse polystyrene in the continuous phase of hexane. The behavior of block copolymers as emulsifiers of immiscible and selective solvents [82] as well as the compatibilizing effect of block copolymers at the interface of two incompatible homopolymers dissolved in an organic solvent was studied theoretically [83–85]. From an experimental point of view, oil-in-oil types of emulsions have not been much investigated [86–91]. However, Périard and coworkers [87–89] have shown that block and graft copolymers can effectively be used for the emulsification

of mixtures of two immiscible and selective oils. For instance, stable acetonitrile–cyclohexane emulsions are obtained in the presence of polystyrene-polymethylmethacrylate block and graft copolymers [87]. Polystyrene–polyisoprene–based copolymers are suitable emulsifiers for the DMF–hexane system [88,89]. Concentrated emulsions of petroleum ether in a series of polar organic solvents including DMF, DMSO, and formamide form upon using triblock ABA copolymers of polyethylene oxide (PEO) and polypropylene oxide (PPO) as emulsifiers [90]. The authors report that block copolymer surfactants yield highly stable concentrated emulsions compared to small-molecule surfactants of similar hydrophilic–lipophilic balance (HLB). Finally, the emulsification of two immiscible polymer solutions in the presence of a graft copolymer was reported by Molau [91].

As a consequence, in light of the above remarks, polymeric surfactants certainly represent an interesting class of emulsion stabilizers. Even if our report is restricted to synthetic charged polymers, it is essential to mention that naturally occurring macromolecules, such as gums [92] and proteins as well as artificial polymers are also important emulsifiers in the food, cosmetic, and pharmaceutical industries. The complex behavior of protein emulsifiers was recently reviewed by Dalgleish [34]. Cases of multiple emulsions, dispersions of oil-in-water-in-oil (O/W/O) or water-in-oil-in-water (W/O/W), are not considered in this chapter. Excellent reviews on this topic were recently presented by Garti and Bisperink [93] and Tadros et al. [94]. However, it appears that polyelectrolyte surfactants have not been used to prepare multiple emulsions. The present review is devoted to the stabilization of emulsions by amphiphilic polyelectrolytes used as primary emulsifiers (soap-free emulsions). Clearly, these systems represent a high degree of complexity, which probably explains why this field of research is not yet extensively covered. It is hence necessary to give special references to closely related systems not only to provide the reader with an extended point of view but also to explain the general concepts of emulsion science. For instance, in Sec. II, our attention is focused on emulsion type. Until recently, the theoretical prediction of the type of an emulsion was not clearly understood even in the case of nonionic surfactants. However, the situation was much clearer for microemulsion systems. At the same time, the adsorption of amphiphilic polyelectrolytes at liquid–liquid interfaces is an almost untackled problem from both theoretical and experimental viewpoints. Experimentally, the difficulty arises that only a few amphiphilic charged polymeric surfactants are commercially available. In addition, the fundamental understanding of emulsion type in the presence of amphiphilic polyelectrolytes requires polymers with various well-defined chemical architectures. In the end, the selection of a charged emulsifier to tune emulsion type can only be explained by considering a combination of related systems such as surfactants and neutral

polymers in both emulsions and microemulsions (Sec. II.B). Prior to this development, practical examples highlighting the importance of controlling emulsion type are given in Sec. II.A. In Sec. II.C, studies showing that emulsion type can indeed be monitored using charged polymeric surfactants are presented. The general remarks given above hold for emulsion stability (Sec. III). The basic concepts of emulsion stability are first presented (Sec. III.A). Suitably chosen polyelectrolyte surfactants are clearly identified in Sec. III.B. as emulsifiers which are able to combine several, if not all types of known stabilization mechanisms. Special attention is given to concentrated emulsions and preparation of narrow-size-distribution emulsions. In contrast to Sec. III.B, where emphasis is focused on the macroscopic behavior of emulsions, an attempt is made in Sec. III.C to describe the microstructure and properties of amphiphilic polyelectrolyte *thin*-liquid films. The question may be of great importance in order to give a better understanding of the coalescence process in the presence of charged macrosurfactants. Finally, as an additional degree of complexity, the polymerization reactions carried out in emulsions stabilized by polyelectrolyte surfactants are reviewed in Sec. IV. As shown in this report, even if systematic studies involving the stabilization of macroemulsions by synthetic amphiphilic polyelectrolytes are scarce, they clearly indicate that this field of research is very promising.

II. EMULSION TYPE

An emulsion will form upon mixing oil, water, and an emulsifier under given conditions such as temperature, dispersion method, phase volume, and viscosity of bulk phases among other parameters. The answer to the question *Will this emulsion be oil (W/O) or water (O/W) continuous?* is a key problem of emulsion science. It is not only of fundamental interest but also of great practical importance and consequences.

A. Practical Examples

Direct and inverse emulsions are found in everyday-life products. For instance, both types of emulsion are common in food: oil-in-water emulsions include milk, cream, and mayonnaise; butter and margarine are examples of water-in-oil emulsions. Furthermore, recent studies were carried out, with the help of professional sensory panelists, to determine the influence of emulsion type on the perception of taste [36]. In relation to the breakdown mechanisms of emulsions (creaming/sedimentation, flocculation, coalescence, and Ostwald ripening), controlling emulsion type can be regarded as a key parameter to design stabilization/destabilization processes. In cosmetic

applications, direct emulsions that display excellent storage stability but break quickly upon contact with human skin to release a uniform oil layer are interesting moisturizing products. The breaking of emulsions is triggered by the salt at the surface of the skin [11]. The understanding of the mechanisms governing the stabilization/breaking of water in crude oil emulsions is of major importance in the oil industry [21–24,26,27,95]. In crude oil production, oil is recovered, for the most part, together with the water contained in the formation. This coproduction of oil and water generally leads to the formation of highly stable and viscous water in crude oil emulsions. Severe problems during the production stage, transportation, and refinery operations arise from the presence of the liquid–liquid dispersion. The emulsion must be broken before the oil is refined. Consequently, demulsification of crude oil is an integral and important part of crude oil production. Methods currently available for demulsification [95] can be roughly identified as mechanical, electrical [23,24,96] and chemical [21,27,97–99]. Also, crude oil-in-water emulsions are deliberately produced to reduce the viscosity of highly viscous crude oils (asphaltic crude oil and bitumen) so that they can be transported easily through pipelines [33]. It provides an alternative to the use of diluents or the costly application of heat for viscosity reduction during transportation. However, emulsions must be broken after transportation. The process of demulsification is obviously rather complex and does not only reduce to the reverse of emulsification. Practically, it remains a largely empirical art. However, the knowledge of the parameters controlling emulsion type is an important step, although not sufficient, to set up demulsification methods. Correlation between the hydrophilic–lipophilic balance (HLB) of the demulsifier and the rate of emulsion resolution was investigated [99]. To break an inverse emulsion, the parameters that would favor the formation of direct emulsion must be activated. Another example is related to the use of oil-based drilling fluids in oil and gas extraction. Oil-based fluids or oil-based muds are inverse emulsions with a brine phase dispersed into low aromatic oil. These complex fluids are used to carry the drill cuttings out of the well. For environmental reasons, cuttings must be separated out from the mud and cleaned. Breaking up or inverting the emulsion can certainly help to meet these requirements [100]. The problem again deals with a stabilization/destabilization or inversion process. These few practical examples show how the emulsion type is an important matter.

B. Existing Theories for the Selection of an Emulsifier

As mentioned above, most emulsions are formulated with small-molecule surfactants rather than with polymeric surfactants, and as a consequence both

theoretical and experimental approaches to the understanding of emulsion type are all related to surfactants. A review extending from the Bancroft rule to the revisited wedge theory is now given.

Everything starts with the well-known Bancroft rule [101,102], which states that the continuous phase of an emulsion tends to be the one in which the surfactant is more soluble. In other words, the balance between hydrophilic and hydrophobic entities composing the emulsifier, influences the emulsion type. To quantify this balance, Griffin [103,104] first introduced an empirical HLB scale to predict emulsion type from surfactant molecular composition. Following Griffin's classification, emulsifiers with high HLB values stabilize O/W emulsions, while those with low HLB values tend to form W/O emulsions. Davies [105–107] further developed a method of calculating the HLB values of various surfactants from their chemical structure. According to the Davies formalism, HLB numbers are assigned to each chemical group composing the surfactant molecule, and the HLB values of the surfactant molecules can be calculated by substituting the group numbers into the following equation:

$$\text{HLB (value)} = 7 + \Sigma \text{ hydrophilic groups} - \Sigma \text{ hydrophobic groups} \quad (1)$$

It is important to emphasize that the HLB value does not give any information regarding its efficacy to stabilize an emulsion once formed. The HLB value calculated for a given surfactant reflects only the balance between its hydrophilic and hydrophobic moieties and hence is characteristic of the molecule alone. Thus the HLB concept does not take account of the environment (temperature, oil ...) of the surfactant. To illustrate this aspect, it is sufficient to mention that a given ethoxylated hydrocarbon surfactant can form direct emulsions at ambient temperature while it leads to the formation of inverse emulsions at higher temperature. Clearly, temperature and all kinds of interactions with both the aqueous and oil phases must be included into the HLB values, which thus cannot be related solely to the molecular groups of the surfactant. Shinoda and coworkers [108–111] introduced the phase inversion temperature (PIT) concept, which correlates the phase behavior (microemulsions) of oil–water–ethoxylated nonionic surfactant to macroemulsion (called emulsion in what follows) stability. It is commonly accepted that the phase diagram progresses through type I, type III, and type II Winsor diagrams with increasing temperature [40,109,112–117]. The Winsor type I system is a two-phase equilibrium of oil-swollen spherical micellar solution (water-rich phase) coexisting with excess oil, the surfactant being mostly present in the water-rich phase. The Winsor type II system is a two-phase coexistence region of water-swollen spherical micellar solution (oil-rich phase) in equilibrium with excess water, the surfactant partitioning preferentially into the oil-rich phase. In the Winsor type III system, a bicontinuous

microemulsion coexists with both excess oil and water in a three-phase equilibrium [118,119]. By definition, Shinoda's PIT is the temperature at which the bicontinuous microemulsion phase has equal amounts of oil and water. The pattern of nonequilibrium emulsion stability was found to correlate strongly with the microemulsion phase behavior [108–111]. In the Winsor III region (around the PIT), emulsification of the three phases in each other leads to the formation of very unstable emulsions that break rapidly after preparation. In contrast, stable (creamed) O/W and W/O emulsions are obtained by shaking coexistent phases of Winsor I and Winsor II equilibria respectively. Therefore, the PIT also represents the temperature for emulsion type inversion. The selection of a suitable emulsifier by the HLB temperature is thus similar to the HLB number, in the sense that both depend on the hydrophilic–lipophilic balance. The advantage of the PIT concept is that the surfactant–oil–water interactions are all incorporated into the HLB criterion. Temperature is not the only parameter that can be used to control the phase behavior of nonionic surfactant–water–oil systems. Decreasing the length of the hydrophilic moiety of the emulsifier (111, 120), decreasing the alkyl chain length of oil [108,120] or increasing the ionic strength [121,122] simply shifts the PIT to a lower temperature without altering the general pattern of the ethoxylated hydrocarbon–water–oil phase diagrams. Changing the type of salt also shifts the PIT [121]. As a consequence, the microemulsion phase behavior and thus the generic sequence Winsor type I–Winsor type III–Winsor type II can be tuned by a sweep of many variables such as temperature, salt concentration, alkane chain length, length of the hydrophobic moiety, and average number of ethylene oxide groups of the surfactant. Due to the strong correlation that exists between the nonequilibrium emulsion systems and the microemulsion phase behavior, all these parameters can be used to control emulsion type. Furthermore, the results can be generalized in the case of ionic systems. In contrast with nonionic systems, the formation of microemulsions stabilized by ionic surfactants usually requires the presence of cosurfactants (e.g., medium chain alcohol) [40]. One exception, however, is the branched double-chained ionic surfactant Aerosol-OT [sodium bis (2-ethyl hexyl) sulfosuccinate]. Changing the HLB properties of ionic surfactant–oil–water–cosurfactant systems with temperature is significantly more difficult than with nonionic systems. In fact, temperature effects on the phase behavior of ionic systems are less important and have opposite sign so that the type I–type III–type II sequence of phases also occurs in ionic surfactant systems but with decreasing temperature [40]. However, due to the presence of charges, ionic surfactant solutions are sensitive to ionic strength. Thus one can expect salt concentration to be a good parameter for controlling microemulsion type. This is actually the case. More generally, for ionic surfactants, parameters that can be used to tune micro-

emulsion phase behavior [40] include cosurfactant [123,124] and salt [124–132] activity, type of counterions, shape of surfactant molecules, pH, oil type [124], and to a lesser extent temperature [128]. In addition, both ionic and nonionic systems exhibit the same phase behavior pattern, and the emulsification trend observed with ionic systems bears the same relationship to phase behavior as does that with nonionic systems [40,125,126,133,134]. Consequently, the abovementioned variables are useful to control emulsion type. At this point, it is clear that the hydrophilic–lipophilic balance calculated from the surfactant chemical structure alone cannot be used as a predictive tool to determine emulsion type. For both ionic and nonionic systems the microemulsion phase behavior and emulsion type are strongly related. Several variables outlined previously provide means to induce the Winsor type I–type III–type II sequence of phase behavior and thus the O/W–unstable–W/O sequence of emulsion types. So the Shinoda PIT concept can be extended to all of the above-mentioned parameters. These examples demonstrate how microemulsion research can help the understanding of emulsions. However, as discussed earlier, in the introduction, microemulsion and emulsion are apparently very different types of systems. Consequently, the experimentally well established connection between the microemulsion phase behavior and the emulsification tendency is at first sight surprising and requires theoretical explanation.

Earlier development for this was given by Harkins et al. [135] and Langmuir [136] among others with the oriented wedge theory, which stipulates that surfactants with bulky alkyl chains and small head groups (packing parameter > 1, the corresponding packing shape being often referred to as wedge shape [137]) stabilize W/O emulsions, while single-tailed surfactants with big polar head groups (packing parameter < 1, the corresponding packing shape is a cone [137]) stabilize O/W emulsions due to packing constraints at the oil–water interface of an emulsion droplet. Similar ideas were also given by Sutheim [138]. In other words, the mean spontaneous curvature, H_0, of the surfactant sheetlike microstructure would determine whether the interfacial film surrounding droplets wants to curve onto its oil ($H_0 > 0$, O/W emulsion) or its water side ($H_0 < 0$, W/O emulsion) or to be flat ($H_0 = 0$). However, the mean spontaneous curvature of an unbalanced surfactant monolayer is several orders of magnitude larger than the droplet mean curvature. As a consequence, for a given unbalanced surfactant, the bending energy penalty (surfactant monolayer bending energy can be calculated by using Helfrich's theory [139]) of a surfactant monolayer covering oil or water droplets in direct and inverse emulsions, respectively, is almost the same. Planar interfaces are felt by surfactant molecules in both types of emulsions. This contrasts with microemulsions, for which the nanometer-sized droplets are much smaller. As a conclusion, contrary to emulsion type,

the microemulsion phase behavior is tightly related to the spontaneous curvature of the surfactant monolayer. Consequently, the experimental connection between the microemulsion phase behavior and emulsion type remains theoretically unexplained. However, Kabalnov and Wennerström [140] recently revisited the oriented wedge theory. The authors have investigated the thermal stability of films separating neighboring droplets in both O/W and W/O types of emulsions stabilized by ethoxylated hydrocarbon. The coalescence process of emulsions is assumed to be film-rupture controlled. The coalescence energy barriers and thus the rates of coalescence of W/O/W and O/W/O films corresponding to inverse and direct emulsions, respectively, are compared. The film with the higher coalescence energy barrier (lower coalescence rate) is the more stable and determines the emulsion type. From a qualitative point of view, the theory can be described as follows. A monolayer bending energy penalty arises from the creation of a hole in an O/W/O (respectively W/O/W) emulsion film covered by a saturated surfactant monolayer with positive (negative) mean spontaneous curvature, H_0 (Figure 1). This comes from the fact that the mean curvature of the strongly curved monolayer at the edge of the hole and the mean spontaneous curvature of the surfactant molecules have opposite signs. Consequently, the energy penalty acting against coalescence becomes more important with film thinning. The film is hence stable. In contrast, O/W/O (respectively W/O/W) films with negative (positive) H_0 are not stable because the surfactant monolayer at the edge of the hole can fit its mean curvature to the mean spontaneous curvature by decreasing the film thickness. The film is hence not stable to coalescence. Consequently, the emulsion type is indeed determined by the sign of the surfactant monolayer spontaneous curvature. However, the key point is to compare the mean spontaneous curvature of the surfactant monolayer with the strongly curved surfactant monolayer at the edge of the hole of the film separating droplets rather than with the surfactant monolayer covering the droplets themselves. The complete theoretical analysis shows that the correspondence between the equilibrium phase behavior and the emulsion type actually holds with accuracy. The O/W–breaking–W/O sequence of emulsion types observed with increasing temperature for ethoxylated nonionic surfactant (flexible monolayer)–oil–water system is predicted by the theoretical model. O/W and W/O emulsions form at positive and negative H_0, respectively, with a breaking point occurring at the PIT ($H_0 = 0$). The good agreement between the theoretical model and the experimental data [140–142] clearly supports the emulsion stability/spontaneous curvature correlation even in the case of emulsions stabilized by more rigid surfactant (phospholipid) monolayers [142]. The theoretical analysis of rigid monolayers is also presented in Ref. 140. The model predicts the possible formation of multiple emulsions within a narrow region in the vicinity

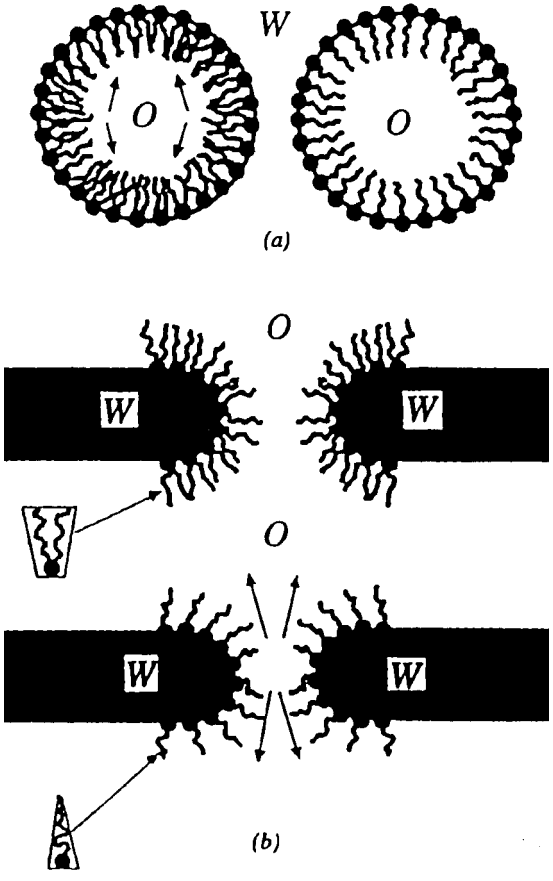

FIG. 1 Oriented wedge theory. (a) Schematic representation of the oriented wedge theory, as presented by Harkins and Langmuir. According to these authors, the monolayer covering emulsion droplets have different frustration energies, which favor one emulsion type over another. Note that the picture shows the macroscopic emulsion droplets and not the surfactant micelles. (b) The version of the oriented wedge theory as presented by Kabalnov and Wennerstrom. The monolayer bending energy affects not the free energy of the droplets themselves but the free energy of the coalescence transition state—the nucleation pore in the bilayer. (b, top) The monolayer spontaneous curvature fits that of the hole edge, and the rupture occurs without a barrier. (b, bottom) The monolayer at the edge of the hole nucleus is ''frustrated,'' and the hole nucleation is suppressed. Arrows indicate the frustration stress in the bent monolayer. (Reprinted with permission from Ref. 140. Copyright © 1996 American Chemical Society.)

of the inversion point, which was not the case for flexible monolayers. The reader is referred to the original paper of Kabalnov and Wennerstrom [140] for a complete description of the revisited wedge theory.

In connection with H_0, we now have a better understanding of the role of the different variables used to tune the microemulsion phase behavior and emulsion type. For obvious reasons, double-tailed surfactants tend to stabilize inverse emulsions and single-tailed surfactants stabilize direct emulsions. The spontaneous curvature of the ethoxylated hydrocarbon surfactant depends on the relative length of alkyl and polyethylene oxide units. It can also be varied by changing temperature and salt activity. Increasing temperature or salt concentration makes water a poorer solvent for the hydrophilic part of the surfactant. The mean spontaneous curvature is decreased by the collapse of the polyethylene oxide head units resulting from dehydration. The addition of salts, in the case of ionic surfactants, screens electrostatic repulsion between the soap polar heads, thereby decreasing H_0. Change in emulsion type occurring at high salt concentration cannot be attributed to the screening of the electrostatic repulsions but rather to the dehydration of the polar head groups due to depletion and osmotic pressure effects (salting-out). Using short alkyl chains (respectively long-chain hydrocarbons) as the oil increases (decreases) the penetration of the oil chains into the surfactant hydrophobic *brush*, thereby decreasing (increasing) the spontaneous curvature. The effect of adding cosurfactants or surfactants can be described in the same manner. In the case of surfactants or surfactant/cosurfactant mixtures, the spontaneous curvature can be varied continuously with the mixing ratio. Referring to the few practical examples given at the very beginning of the section, some of the chemical demulsification processes are at least partially understood. Direct and inverse emulsions will break if H_0 decreases and increases, respectively. This can a priori be suitably achieved by adding to the emulsion demulsifiers with the opposite packing type. The theory should in principle apply to (charged) polymeric surfactants even if the physical picture of H_0, in the case of grafted polymer for instance, is not straightforward.

C. Controlling Emulsion Type with Polyelectrolyte Surfactants

The type of emulsion stabilized by polymeric surfactants, charged or uncharged, was not investigated in detail, although it has long been understood that it was dependent of the structure of the surfactant macromolecules. In a series of papers, Riess and his coworkers [143–145] have investigated the effect of the composition and architecture of PS-PEO–based block copolymers (PS: polystyrene; PEO: polyethylene oxide) on stability and emul-

sion type. Higher PEO content copolymers (60–80%) give preferentially toluene-in-water emulsions, while higher PS content copolymers (60–80%) give water-in-toluene emulsions. Ba-Gia et al. [146,147] synthesized a PTBS$(PEO)_2$ star-shaped block copolymer (PTBS: polytertiarybutylstyrene) with 45% PEO, able to generate both direct and inverse toluene–water emulsions over a broad range of phase volume ratios. Berlinova et al. [148] copolymerized a monomeric activated ester, isopropyl pentachlorophenyl fumarate, with either styrene or *N*-vinyl pyrrolidone at equimolar ratio. The resulting activated copolymers were grafted with amino-functionalized methoxy-PEO of various molecular weights. The amphiphilic copolymers with high and low PEO contents give direct and inverse (water–toluene system) emulsions, respectively.

Only a few studies deal with the types of emulsions stabilized by polyelectrolytes. This is probably due to the fact that nonpolar solvents are used as the continuous phase of most inverse emulsions. Consequently, uncharged polymeric surfactants would represent a more interesting class of inverse emulsion stabilizers than ionic surface-active macromolecules. The formulation of inverse emulsions as well as the type of liquid–liquid dispersions stabilized by polyelectrolyte surfactants are hence almost unexplored fields of research. However, Marie and coworkers [149] have studied the emulsifying effect of PS/PV2P Cl [PV2P Cl: poly(2-vinyl pyridinium chloride)] and PI/PV2P Cl (PI: polyisoprene) block copolymers on the toluene–water and dodecane–water systems, respectively. The authors clearly showed that copolymers with high 2-vinyl pyridinium chloride content tend to form direct emulsions, while styrene and isoprene-rich copolymers give water-in-toluene and water-in-dodecane emulsions, respectively. The stability and viscosity measurements of dodecane–water emulsions stabilized by two different PI/PV2P Cl block copolymers are given in Figures 2 and 3. Their molecular characteristics are reported in Table 1. As shown in Figure 2, the isoprene-rich copolymer, the A-copolymer, gives water in dodecane emulsions up to a water volume fraction of 75%. The authors observed the formation of dodecane-in-water emulsions above this concentration threshold. In contrast, only direct emulsions are obtained with the more hydrophilic V2P Cl-rich copolymer (the B copolymer) (Figure 3) in qualitative agreement with theoretical concepts. Recently, Mathur et al. [150] have described an emulsion system whereby the stabilizing properties can be reversibly switched on and off. Two types of polymeric surfactants were used in this study. The first type of polymer is a graft copolymer consisting of a poly(methacrylic acid) (PMAA) backbone and short sequences of PEO. Two polymers with MAA-to-EO repeat ratios of 10:1 (copolymer 1a) and 20:1 (copolymer 1b) were synthesized. The mechanism of stabilization/destabilization of the emulsions is as follows. Under acidic conditions, hydrophobic

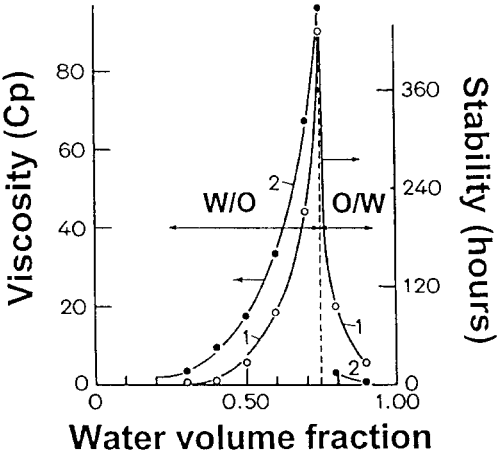

FIG. 2 Stability (plot 1) and viscosity (plot 2) behavior of dodecane–water emulsions stabilized by PS-b-PV2P Cl copolymer A (Table 1). Polymer concentration is 1% (w/v). (From Ref. 149.)

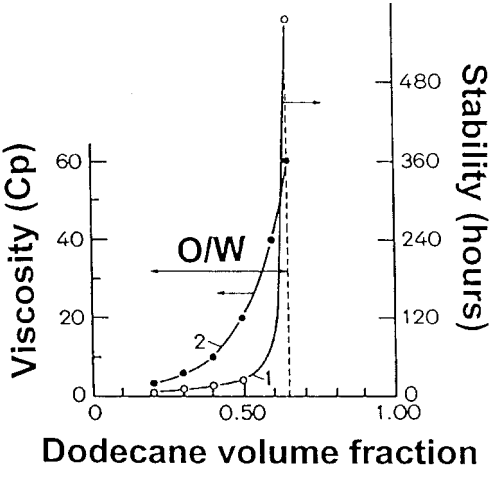

FIG. 3 Stability (plot 1) and viscosity (plot 2) behavior of dodecane–water emulsions stabilized by PS-b-PV2P Cl copolymer B (Table 1). Polymer concentration is 0.5% (w/v). (From Ref. 149.)

TABLE 1 Molecular Characteristics of the Two PI/PV2P C1 Copolymers, A and B, Used as Emulsifiers of the Dodecane–Water System

PI/PV2P C1 copolymer	Isoprene content (wt%)	M_w (g/mol) isoprene sequence	M_w (g/mol) copolymer
A (Figure 2)	72	9800	14000
B (Figure 3)	29	4600	16000

See Figures 2 and 3.
Source: Ref. 149.

hydrogen-bonded complexes form in a 1:1 MAA (backbone) to EO (grafts) repeat unit ratio, leading to the formation of an amphiphilic multiblock copolymer. Under basic conditions, the complex formation does not occur, and the copolymer is hence essentially hydrophilic. A schematic representation of the polymeric emulsifier chain at high and low pH is given in Figure 4. The authors show that in contrast to basic emulsions, acidic direct emulsions are efficiently stabilized by the copolymers 1a and 1b (Figure 5). Since the pH-induced complex formation is reversible, pH can be used as a trigger to control the stabilization/destabilization process of the emulsions. The first copolymers are hence designed to produce stable and unstable direct emulsions at low and high pH, respectively. Interestingly, the second type of copolymer synthesized by the authors provides stable and unstable direct emulsions under basic and acidic conditions, respectively. The polymeric emulsifier is a MAA-lauryl methacrylate (LM) copolymer backbone grafted with PEO. The MAA-to-EO repeat unit ratio is 1:1, and the LM content is 10 mol% of the MAA repeat units (copolymer 2). Consequently, as a result of the complex formation, the emulsifier is a completely hydrophobic water-insoluble copolymer under acidic conditions. At higher pH, the complex is broken, and the emulsifier is an amphiphilic polyelectrolyte with hydrophilic MAA and EO units and hydrophobic alkyl grafts. Consequently, stable direct emulsions are obtained under basic conditions but not under acidic conditions (Figure 5). Finally, as shown in Figure 5, no stable emulsion is obtained using PMAA as an emulsifier whatever the pH. Perrin and coworkers [151,152] have synthesized and used as emulsifiers of the *n*-dodecane–water system a series of single-tailed and twin-tailed highly hydrophobically grafted linear poly(sodium acrylate)s. The number average molecular weight of the poly(sodium acrylate) backbone is 50,000 g/mol. The emulsion type was systematically investigated as a function of the polyelectrolyte chemical architecture

Single-tailed

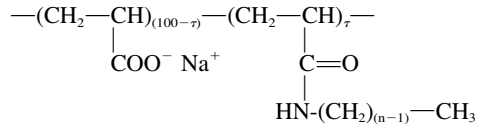

(2a)

Twin-tailed

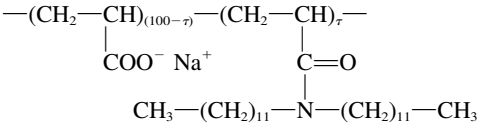

(2b)

with τ being the degree of grafting (mol%) and n the number of carbon atoms of monoalkyl grafts (Cn). Single-tailed and twin-tailed copolymers are hence, respectively, τCnNa and τ(2C12)Na. The generic name of the acidic form of the single-tailed copolymers is τCnH. Emulsion-type dia-

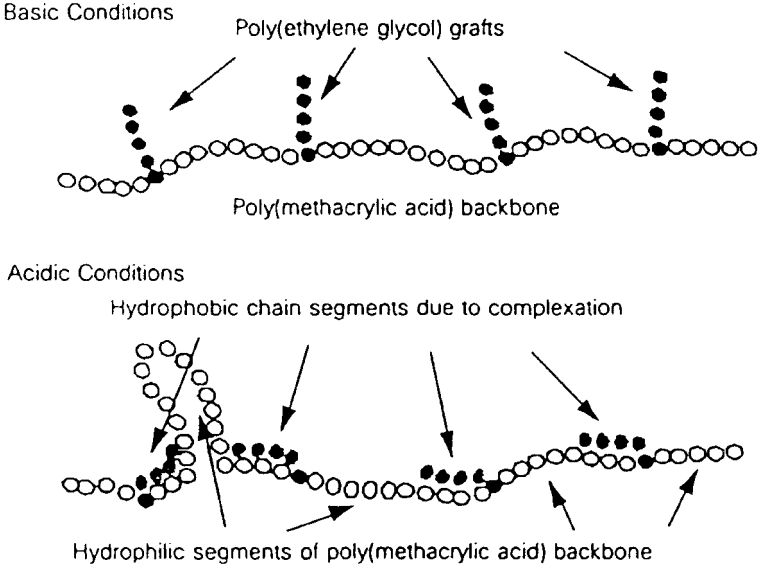

FIG. 4 Schematic depiction of copolymer 1 under acidic (complex-promoting) conditions and under basic conditions. Although only loop-free, intramolecular complexes are shown here; both loops and intermolecular complexes are possible. Based on statistical considerations, loop formation is not expected for the relatively short grafts used in this study. Similarly, due to the relatively short graft lengths and the dilute conditions, essentially all of the complexes formed initially will be intramolecular. After the emulsion is formed and the emulsifier is concentrated at the oil–water interface, some complexation exchange may occur, and intermolecular complexes may be formed. (Reprinted with permission from *Nature* (Ref. 150).)

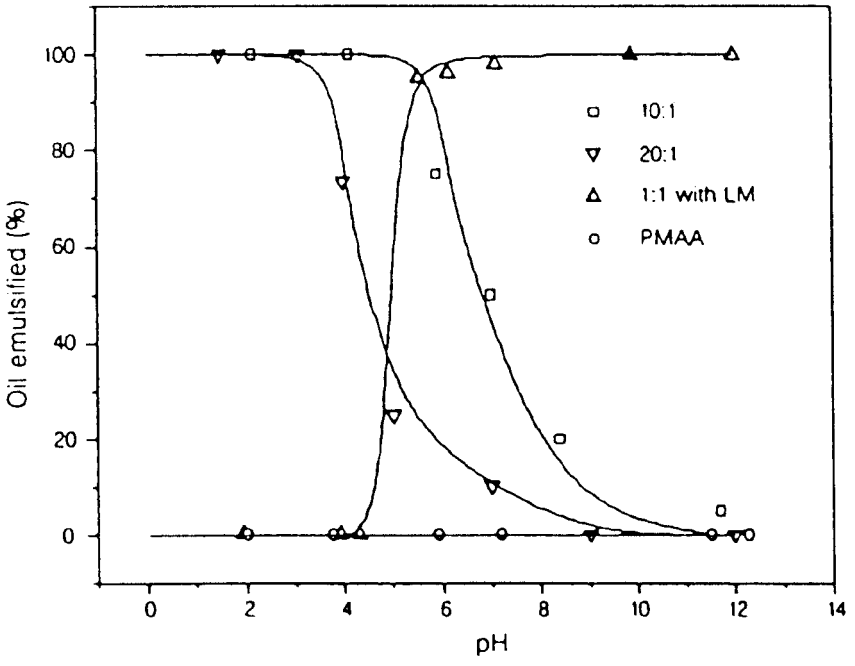

FIG. 5 Percentage of oil emulsified after four days at room temperature as a function of pH. Results are shown for copolymers 1a (10:1), 1b (20:1), 2 (1:1 with lauryl methacrylate, LM), and MAA homopolymer. The emulsification properties of the copolymers were characterized using a standard bottle test method with methyl laurate as the model oil phase. This model oil is used widely as a solvent in biochemical and agricultural applications and serves as a replacement for mineral oil in many emulsifiable agricultural pesticide concentrates. All studies were carried out using 20 vol% of the oil phase, and 80 vol% of an aqueous phase containing 0.1 wt% of the surfactant. The pH of the aqueous phase was adjusted to the desired value by the addition of 1 M HCl or 1 M NaOH solutions. The mixture was agitated vigorously for $\sim$ 2 min, then allowed to stand for four days at room temperature. The emulsified droplets formed an opaque, stable cream on top of the excess aqueous phase. The cream had a composition of $\sim$ 70 vol% oil in water, and individual droplets were not discernible by the naked eye. The percentage of oil emulsified was determined by a material balance after measurement of the volume of unemulsified oil. (Reprinted with permission from *Nature* (Ref. 150). Copyright © 1998 Macmillan Magazines Limited.)

grams are presented in Figures 6, 7, and 8. The effects of changing the degree of grafting and the shape of the grafts appear clearly in Figure 6. Single-tailed copolymers with τ up to 50 mol% lead exclusively to the formation of direct emulsions (equal amount of oil and aqueous phase: ϕ = 0.5) in the range of investigated sodium nitrate concentration (up to 2M). Inverse emulsions cannot be obtained with these too hydrophilic copolymers, which probably have positive and relatively large H_0 values. The situation is quite different with the 80C12Na copolymer, since W/O emulsions mostly form even at low salt concentration. An original intermediate behavior is found with the well-balanced 60C12Na polyelectrolyte. With this copolymer, direct and inverse emulsions form at lower and higher salt concentrations, respectively. Although the concept of spontaneous curvature is not obvious for grafted copolymers, the experimental data show that the H_0 value of the 60C12Na copolymer is likely to be close to zero. The stability behavior of both direct and inverse emulsions stabilized with the 60C12Na copolymer is given in Figure 9. It is clear that both types of emulsion break rapidly at

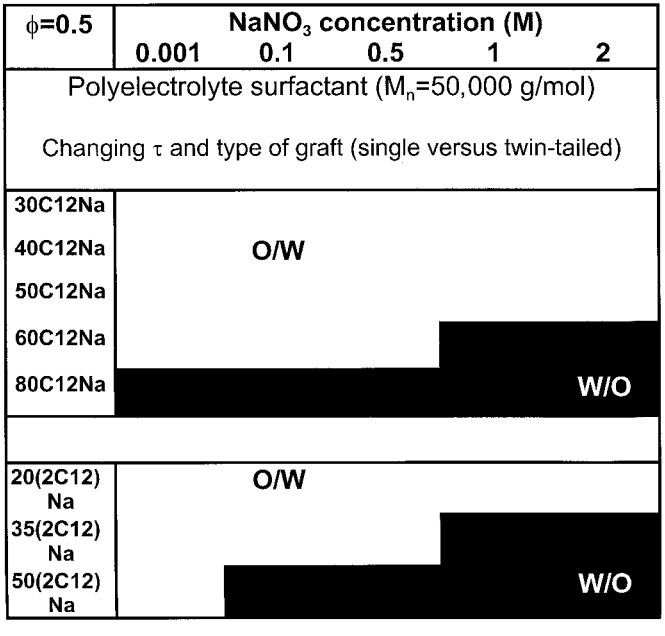

FIG. 6 Emulsion type diagram of *n*-dodecane–water emulsions (ϕ = 0.5) stabilized with hydrophobically modified poly(sodium acrylate)s: effect of changing the degree of grafting and type of the graft (single versus twin-tailed). Salt is used as a tool to estimate the copolymer HL properties. (From Ref. 152.)

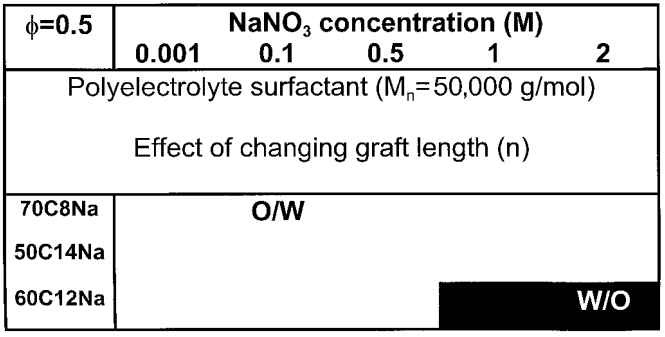

FIG. 7 Emulsion type diagram of *n*-dodecane–water emulsions ($\phi = 0.5$) stabilized with single-tailed polyelectrolyte surfactants: effect of changing length (n) of the hydrophobic moiety. Salt is used as a probe to estimate the HL properties of the various copolymers. (From Ref. 152.)

salt concentrations in the vicinity of the inversion point (about 0.85–0.87 M). However, the emulsion stability increases at salt concentrations further from the inversion point in agreement with both the theoretical concepts and the experimental data reported on surfactants (Sec. II.B). Twin-tailed copolymers exhibit a similar behavior (Figure 6). It appears that single-tailed τ_1C12Na and twin-tailed τ_2(2C12)Na emulsifiers give emulsions of the same type providing their degrees of grafting are approximately in a ratio of 2 ($\tau_1/\tau_2 = 2$). The effect of changing the length of the graft on emulsion type is shown in Figure 7. By changing the salt concentration, as mentioned above, both inverse and direct emulsions are obtained with the 60C12Na

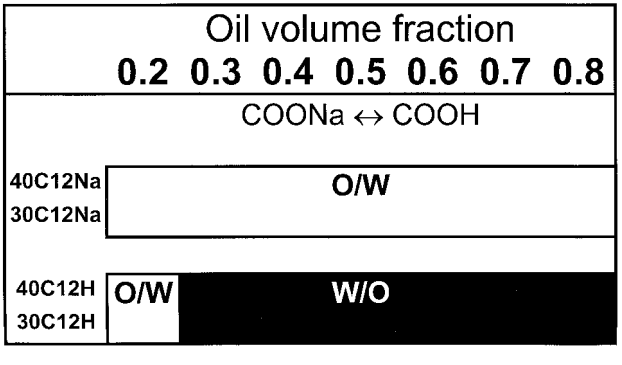

FIG. 8 Effect on emulsion type ($\phi = 0.5$) of changing carboxylate groups into carboxylic acid groups. (From Ref. 151.)

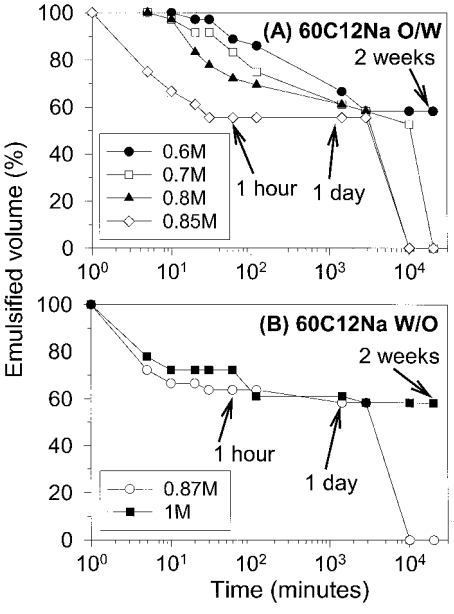

FIG. 9 Stability behavior of dodecane–water emulsions (ϕ = 0.5) at various salt ($NaNO_3$) concentrations (indicated above) around the inversion point: (a) stability of direct emulsions decreases with increasing salt activity; (b) stability of inverse emulsions increases with increasing salt concentration. The polyelectrolyte emulsifier is 60C12Na. (From Ref. 151.)

copolymer. In contrast, only direct emulsions form with the 70C8Na copolymer. Using shorter grafts (n = 8 instead of n = 12), a too hydrophilic copolymer is thus obtained even at a rather high degree of grafting (70 mol%), thereby illustrating the τ and n duality that exists to tune the HL properties and the H_0 values of these amphiphilic polyelectrolytes. Similarly, the comparison of the type of emulsions stabilized by the 50C14Na and 60C12Na copolymers shows that the loss of hydrophobicity obtained by decreasing τ from 60 to 50% could not be compensated for by increasing n from 12 to 14. Finally, the effect on emulsion type obtained by changing the sodium carboxylate groups into carboxylic acid groups at constant salt concentration (10^{-3} M) is presented in Figure 8. In contrast to the 30C12Na and 40C12Na hydrophobically modified poly(sodium acrylate)s, which yield exclusively direct emulsions, the corresponding poly(acrylic acid)s give inverse emulsions over a broad range of oil volume fractions, hence suggesting pH as a parameter to control emulsion type. Ionic groups [HLB_{number} (COO^- Na^+) = 19.1] have actually strong hydrophilic powers compared to neutral

[HLB_{number} (ester) = 2.4] or weakly ionized [HLB_{number} (COOH) = 1.2] polar groups [106]. More generally, the data is in excellent agreement with the theoretical concepts discussed above. The degree of hydrophobic modification (τ), the length (n) and shape of the graft (single versus twin-tailed), pH and ionic strength are suitable variables in order to alter the hydrophilic–lipophilic properties of the system, and hence to tune the type of emulsion. Bulky rather than single hydrophobic moieties, low pH values, high salt activities, as well as high degrees of grafting decrease H_0 and hence favor the formation of inverse emulsions. The type of emulsion stabilized by *n*-alkyl sodium carboxylate surfactants was also investigated by the authors. These surfactants are interesting molecules, since they have a chemical structure similar to that of the polymeric surfactants studied above. However, only the single-tailed series of surfactants is commercially available: $CH_3—(CH_2)_{(m-1)}—COO^-\ Na^+$. The surfactant with $m = 9$ is the capric acid sodium salt. Since the number of carbon atoms of the alkyl chain is equal to nine, the name given to this surfactant will be C9. The other surfactants, the lauric ($m = 11$), myristic ($m = 13$) and palmitic ($m = 15$) acid sodium salt are hence noted C11, C13, and C15, respectively. The emulsion type diagram is given in Figure 10. Basically, water-in-dodecane emulsions are obtained with the C13 and C15 *hydrophobic* *n*-alkyl sodium carboxylates, while water-continuous emulsions form with C9 over the whole range of investigated salt concentrations. The C11 surfactant is the most balanced of the series as is shown from the question mark region where, depending on the prepared sample, either oil- or water-dispersed emulsions are obtained. The poor reproducibility regarding the emulsion type arises from the fact

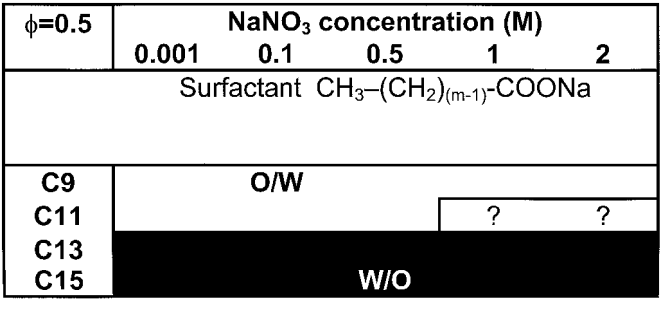

FIG. 10 The effect on emulsion type of changing the hydrophobic tail length of *n*-alkyl carboxylate surfactants. The question mark domain corresponds to the emulsion breaking region where emulsion type was found to be uncertain. C9, C11, C13, and C15 stand for $m = 9$, 11, 13, and 15 in the above surfactant chemical structure (From Ref. 152.)

that this particular domain of salt concentration corresponds to the emulsion-breaking region. A HLB scale for polymers was also established from a comparison between the polymeric emulsifier and the surfactant emulsion type diagrams [152]. It is widely accepted that for polymeric surfactants, the determination of the HLB values would be meaningless. The reasons for this are related to the broad molecular weight distribution resulting from the synthesis of macromolecules. Also, according to Davies (Eq. 1), the HLB values are calculated from the summation of the structural factors that contribute individually to the overall HLB of the emulsifier. Consequently, the HLB number of a given chemical group is constant regardless of its position in the (macro)molecules. Hence the concept is not a priori valid for copolymers in general and hence for polyelectrolyte surfactants. However, Perrin and coworkers [152] took advantage of having polyelectrolyte emulsifiers covering a wide range of hydrophobicity to build an HLB scale for polymers within the framework of the Davies theory. The procedure to build the HLB scale is briefly described as follows. The emulsion type is used as a criterion to estimate the HL properties of the copolymers, and a comparison is made with surfactants of nearly identical chemical structure, the *n*-alkyl carboxylates, for which HLB calculations are meaningful (Table 2) [106]. Salt concentration is used as a probe to estimate the HLB values of both copolymers and surfactants in a given system (*n*-dodecane–water at ambient temperature), exactly in the same way as Shinoda's PIT for nonionic surfactants. As shown from Figures 6 and 10, the HL properties of the 60C12Na copolymer and the C11 surfactant are close. Consequently, their HLB values were matched using the HLB number of the amide group as a fitting parameter, as the value was not available from the literature. The fit gives a reasonable value of 3.7 [HLB_{number} (ester) = 2.4]. Since the HLB numbers of the other chemical groups composing the amphiphilic polyelectrolytes are known [106], the HLB values were calculated using Eq. 1 for each copolymer and surfactant and reported in Table 2. A very good agreement is observed between the emulsion type and the HLB values. With small grafts (C8), it is clear that very high grafting degrees ($\tau > 70\%$) are required to form W/O emulsions. The scale can be used as a predicting tool to tune emulsion type with this series of polyelectrolytes. The limits of the approach and detailed calculations are given in Ref. 152. Besides the HLB concept, it was shown above that emulsion type was found to be completely described by the value and sign of the surfactant spontaneous curvature, H_0 [140]. For polymers, the meaning of H_0 is not as obvious as with surfactants, especially for grafted polyelectrolytes. The emulsion type diagrams presented above give valuable information regarding the spontaneous curvature of this series of charged polymeric emulsifiers.

TABLE 2 HLB_{Davies} Values for Both the Polyelectrolyte and Small-Molecule Surfactants

Surfactants					
C9		C11	C13		C15
21.8		20.9	**19.9**		**18.9**
Single-tailed copolymers					
τ	**40**	**50**	**60**	**70**	**80**
C8	24.5	24.1	23.6	22.7	21
C12	23.2	22.2	20.7	18.3	**13.4**
C14	22.6	21.3	19.3	16.1	9.6
Twin-tailed					
τ	**20**	**30**	**35**	**40**	**50**
2C12	23	21.4	20.5	19.4	**16.5**

Values corresponding to surfactants or charged polymeric emulsifiers (only those actually synthesized) that lead preferentially to the formation of O/W and W/O emulsions appear respectively in white and black rectangles. Grey rectangles display HLB values of the most balanced emulsifiers.
Source: Ref. 152.

III. EMULSION STABILITY

Emulsions are often required to possess an excellent storage stability. Their shelf life can exceed several months or possibly years. In other applications, the goal is to produce emulsions with limited but controlled stability (Sec. II.A). Consequently, the emulsion chemist finds a challenge in formulating emulsions that exhibit the appropriate stability properties for a specific application.

A. Basic Concepts

With time, emulsions experience a series of interrelated events leading to the final stage of two separated liquid layers. Basically, four fundamental processes must be controlled in order to stabilize an emulsified system.

Creaming/sedimentation is due to the gravitational force, by which emulsions with sufficiently large droplets undergo rising (creaming) or settling (sedimentation) of the droplets.

Flocculation is the mutual aggregation of colliding droplets. In stationary emulsions, droplet collisions arise from Brownian motion (small droplets) and/or from the creaming/sedimentation process (larger droplets). In the latter, the mechanism is often referred to as sedimentation/creaming flocculation. Finally, droplet aggregation can also occur in sheared emulsions. It is important to point out that the droplet size distribution is not altered by the flocculation and creaming/sedimentation destabilization mechanisms.

Ostwald ripening occurs in polydispersed emulsions consisting of two liquids that are not completely insoluble. In most emulsions, these two conditions are fulfilled. The solubility of a droplet increases sharply as its radius tends to zero. As a consequence, smaller droplets tend to dissolve in the continuous medium and to reprecipitate into larger droplets.

Coalescence results from the rupture of the thin-liquid film of the continuous phase separating two contacting droplets of a cluster to form one larger droplet. During coalescence and Ostwald ripening, the identity of the aggregated droplets is lost and hence the droplet size distribution is changed. As a general rule, creaming/sedimentation, flocculation, Ostwald ripening, and coalescence are simultaneous processes. However, since coalescence can only occur if the droplets are close enough, flocculation and creaming/sedimentation are considered to be precursor mechanisms to coalescence.

As mentioned in the introduction, the stabilization of colloidal particles by macromolecules has received much more attention [69–72,153] than the stabilization of droplets. As a general remark, it is not obvious that the quantitative predictions on the polymeric stabilization of particles can be readily applied to the stabilization of the liquid–liquid dispersion interface. However, at the present time, it is widely accepted that both types of dispersion stabilization mechanisms should follow the same general rules [45]. Basically, the following stability mechanisms are used to counteract the above destabilization processes: thickening of the external phase, charge stabilization, and steric stabilization. Detailed analysis of these mechanisms are already available in the literature [1,45]. Consequently, in what follows, we will only outline the various concepts used to stabilize an emulsion using (charged) polymeric surfactants, from a qualitative point of view. At sufficiently high concentrations, nonadsorbing polymers are commonly used in the cosmetic and food industries to improve emulsion stability against the flocculation and creaming/sedimentation processes by merely thickening the external (usually aqueous) phase. Natural gums have been widely used for this purpose in numerous direct cosmetic and food emulsions. At smaller concentrations, polymers that are not surface active can drastically increase the rate of creaming/sedimentation. The increase in destabilization rate is believed to be caused by flocculation of the dispersed droplets by a depletion mechanism. Thickeners only weakly adsorb at the liquid–liquid interface.

They are thus used as additives to emulsions in combination with primary emulsifiers, usually surfactants. The functionality of nonadsorbing polymers as emulsion stabilizers is not due to an interfacial mechanism but depends on bulk phase rheological modifications. Interfacial stabilization can only be achieved by using amphiphilic polymers that are able to adsorb at the emulsion interface under certain circumstances. The adsorption of macromolecules at the liquid–liquid interface is known to be a slow process. Hours or possibly days are often required to reach the state of equilibrium. As already pointed out, amphiphilic block and graft copolymers are suitably designed to adsorb at the interface, and hence to stabilize emulsions. The molecules are built up from at least two chemically bound groups having totally different characteristics: the anchoring moiety of the copolymer interacts strongly with the dispersed medium and is essentially insoluble in the continuous phase; the other part of the copolymer, usually referred to as the stabilizing moiety, is soluble in the external phase but has little affinity for the dispersed phase. Typical stabilizing polymers were suggested by March and Napper [154] as will be seen later on. Adsorption of macromolecules is obviously a prerequisite to the steric and electrostatic stabilization mechanisms. The theory of electrostatic stabilization of colloidal particles is due to Derjaguin and Landau [155] and Verwey and Overbeek [156] (DLVO model). In contrast to particle dispersions, emulsions cannot usually be stabilized by the charge stabilization mechanism without the addition of a charged emulsifier. The presence of an electrical double layer at a nonpolar oil–water interface arises from the adsorption of surface-active molecules with an ionizable group like ionic surfactants or polyelectrolyte surfactants. So each (oil) droplet carries a diffuse layer of counterions. The electrostatic stabilization mechanism results from the overlapping of such diffuse layers, which tend to keep two droplets from coming into close contact. The application of the DLVO model to the case of emulsion droplets is not straightforward. Difficulties arise from the possible deformation of the soft entities, the droplets, during collisions and also from the existence of a double layer within the droplets. In fact, the structure of the double layer at liquid–liquid interfaces is still not well understood. Furthermore, the application of an electrostatic model for the stabilization of the aqueous droplets dispersed in oil does not seem to be appropriate. As a result, polyelectrolyte surfactants are practically not used in the stabilization of W/O emulsions. Most of time, neutral polymers and thus the steric stabilization mechanism are used for the preparation of inverse emulsions. The steric mechanism results from the repulsion of adsorbed polymer layers as two droplets approach each other. Heller and Pugh [157] first introduced the term *steric protection* to describe the steric stabilization using nonionic surface-active materials. It is clear that both the electrostatic and the steric stabilization mechanisms are closely

related to the structure and dynamic properties of the adsorbed polymer chains at the interface. As an example, it has been pointed out several times that many protein molecules denature on adsorption and collapse at the oil–water interface, thereby forming a rigid macromolecular film surrounding droplets [34]. Due to its viscoelastic properties, the film provides a mechanical barrier to coalescence and thus gives emulsions a remarkable stability. Several studies were reported on the mechanical properties of interfaces stabilized by macromolecular species in relation to droplet stability [158–162]. In general, the larger the interfacial thickness, rigidity, and viscosity, the more stable the emulsions. To summarize these general considerations, two different but complementary approaches are to be considered to discuss the stability of an emulsified system. The first one deals with the overall macroscopic behavior of the system (bulk rheology, droplet size, and emulsified volume to name but a few) (Sec. III.B). The second approach (microscopic) is devoted to the study of the interfacial properties of the system [163,164]. Section III.C will focus on the structure of polyelectrolyte surfactant films.

B. Overall Stability Behavior

1. Nonconcentrated Emulsions

Not many examples of synthetic amphiphilic polymers are known as effective primary emulsifiers to stabilize liquid–liquid dispersions. In particular, the number of studies dealing with polyelectrolyte surfactants is rather limited. As briefly discussed previously, to achieve emulsion stability, the polymeric surfactants are required to possess adequate anchoring and stabilizing moieties. Experimental evidences for this were given by March and Napper [154], who reported on the flocculation stability of sterically stabilized direct and inverse emulsions. First, they studied the flocculation of toluene droplets in 0.39 M $MgSO_4$ aqueous solutions and stabilized by PEO. They demonstrated that in the absence of an anchor polymer or in the presence of an anchor polymer insoluble (polyacrylonitrile) in the dispersed phase, flocculation occurs immediately after emulsion sample preparation. In contrast, flocculation is not observed two hours after emulsification when PEO is coupled to three different anchor polymers [poly(vinyl acetate), PS, and poly(methyl methacrylate] soluble in toluene. The presence of a suitable anchor polymer is thus essential to emulsion stability as already pointed out in Sec. III.A. Once the requirement for an efficient anchoring is fulfilled, a close correspondence between the critical flocculation temperature and the Flory Θ temperature was found by the authors for both direct and inverse emulsions. This observation is independent of both the chemical nature of the dispersed phase and the molecular weight of the stabilizing polymer.

This is in agreement with the fact that the Θ temperature depends only on the chemical nature of the solvent (continuous phase) and segments (stabilizing moiety). Hence the main requirement for the stabilizing moiety is that it must be sufficiently soluble in the continuous medium.

Other chemically oriented studies have effectively reported that block and graft copolymers are able to stabilize water-in-water (W/W) [165], oil-in-oil [86–89], and O/W or W/O [143–149,150–152,166–189] liquid–liquid dispersions. In the PEO/PV2P Cl/water ternary phase diagram, phase separation occurs at certain compositions due to the incompatibility of the homopolymers [165]. The two phases can be emulsified in each other in the absence of emulsifier leading to the formation of unstable W/W emulsions. However, stable W/W emulsions can be obtained using PEO-PV2P Cl block copolymers as cationic polyelectrolyte surfactants [165]. The stabilizing action of direct and inverse emulsions of oil and water requires the presence of macromolecules containing hydrophilic components being cationic [149, 179,180], anionic [150–152,180–189] or nonionic [143–148,166–178]. In the last case, di- and triblock [143–145] as well as graft [175] or even star-shaped $A(B)_2$ block [147] copolymers based essentially on PEO and PS have been studied. The emulsifying behavior of the PS/PV2P Cl and PI/PV2P Cl cationic block copolymers was discussed in Sec. II.C, since the most important aspect of the study deals with the relationship between copolymer structure and emulsion type [149]. Concerning the stability behavior, the authors have observed an improved stability of both inverse and direct emulsions with increasing copolymer concentrations as expected. The average droplet size diameters are in the range of 1 to 4 μm. Emulsion type and emulsion breaking are also the main points investigated by Mathur et al. [150] and Perrin et al. [151,152], who have used anionic polyelectrolyte surfactants to stabilize both W/O and O/W emulsions. As a consequence, the papers were discussed in Sec. II.C and the stability behavior presented in Figures 5 [150] and 9 [151]. Selb and coworkers [179] have shown that toluene-in-water emulsions with dispersed phase volume fractions ranging from 20 to 60% can be stabilized using a copolymer consisting of a hydrophobic backbone [poly(diphenyl propene)] grafted with cationic hydrophilic sequences (PV2P Cl). Ishizu and Minematsu [180] have studied inverse emulsions of water and benzene stabilized by a mixture of poly(acrylic acid cesium salt)-g-poly(α-methylstyrene) (A-copolymer) and poly(4-vinylpyridine hydrogen chloride)-g-poly(α-methylstyrene) (B-copolymer). The A and B copolymers are thus anionic and cationic polyelectrolyte surfactants. The copolymer mass ratio in the dispersions is 1:1. Emulsions were prepared using two different processes. In the first method, two emulsions separately stabilized by the A and B copolymers are first prepared. The emulsion stabilized by the copolymer mixture is obtained by mixing equal volumes of

the two emulsions. The authors observed that in the resulting emulsion, the two copolymers stabilize separately their own water droplets. In other words, both emulsions simply coexist in the mixed dispersion with the structure they had prior to mixing. In the second method, water and benzene are directly emulsified in the presence of both amphiphilic polyelectrolytes. Transmission electron microscopy (TEM) micrographs reveal the segregation of the two oppositely charged polymer backbones within the dispersed phase. The authors suggest a uniform distribution of the hydrophilic segments of the A and B copolymers within the water phase after emulsification. However, the evaporation of the solvent during the TEM sample preparation would cause microphase separation leading to copolymer backbone segregation in the water phase. The morphologies of the emulsions prepared according to the first and second methods are thus different. The behavior of benzene-in-water emulsions stabilized by three block copolymers prepared from the uncharged PS-b-(S-alt-maleic anhydride) copolymer (PS-b-SMA) was studied by Reeb and Riess [181]. The first polymeric emulsifier is a 100% hydrolyzed PS-b-SMA copolymer (acidic form); the second and third ones are the 50 and 100% neutralized sodium salt forms of the PS-b-SMA copolymer, respectively. The most stable benzene-in-water emulsions (50/50 v/v) are obtained using the second copolymer (copolymer 2). The authors have also compared the stability behavior of three emulsion samples formulated using copolymer 2 in sample 1; the homopolymer corresponding to the hydrophilic sequence of copolymer 2 in sample 2; a mixture of the two homopolymers corresponding to the hydrophilic and hydrophobic parts of copolymer 2 in sample 3. In the latter, the homopolymer blend has the same composition as copolymer 2. Both the second and the third preparation do not give stable emulsions. In contrast, as already mentioned earlier, emulsions prepared using copolymer 2 are stable, and the average droplet diameter is about 2 to 10 μm. It is seen that a method of improving the stability of direct emulsions is to provide the external aqueous phase with a high viscosity and/or a yield stress. This is conveniently achieved using the well-known carbomers (Cosmetics, Toiletries and Fragrance Association name—CTFA) or carbopols (BF Goodrich Company trade name), series of cross-linked polymers of acrylic acid [182]. Maintaining product homogeneity throughout the shelf life of emulsions while permitting an easy flow of the product during application is the main role played by these organic synthetic rheology modifiers. A suitable base is usually added to the formulation, causing the polymer chains to unfold and form an extended three-dimensional microgel structure that provides maximum thickening efficiency. Being not surface active, carbopols are not used as primary emulsifiers. In contrast, hydrophobically modified carbomers or carbopols (Pemulen TR 1 and TR 2) that contain hydrophobic residues covalently

attached to the polyacrylic acid chains are amphiphilic materials and hence are capable of primary emulsification of direct emulsions [10,11,13,14,182–187]. According to the manufacturer's specifications, Pemulen TR 2 is more hydrophobic than Pemulen TR 1, with the practical consequence that direct emulsions with oil volume fractions up to 65 to 80% can be obtained using Pemulen TR 2, while Pemulen TR 1 can emulsify oil in water up to only 30%. In a series of papers, Lochhead and coworkers [182–186] have studied the emulsifying properties of poly(acrylic acid) (PAA) and hydrophobically modified poly(acrylic acid) (HMPAA) on cyclohexane/water and mineral oil/water systems. For instance, the authors [186] have compared the stability behavior of 30 wt% cyclohexane in water emulsions using carbopol 980 (PAA) and Pemulen TR 2 (HMPAA) resins as primary emulsifiers. In the latter case, the hydrophobic modification of the cross-linked poly(acrylic acid) hydrogel is accomplished by the incorporation of approximately 1 mol% of alkyl chain (C10–C30) acrylates. The stability of emulsion samples against coalescence is evaluated 6 months after preparation. Figures 11 and 12 present the pseudo-phase diagrams for PAA and HMPAA, respectively, at various pH and emulsifier concentrations. The critical overlap concentrations (c^*) plotted as a function of pH for both polymers are also reported in Figures 11 and 12. From the stability diagrams, it appears that the critical overlap concentration of the unneutralized polymer (c^*_{UN}) is a key parameter to govern emulsion stability. The effect of hydrophobic moieties on the stability behavior is quite clear. HMPAA is able to form stable emulsions at concentrations much higher than its c^*_{UN}, which is not the case for the unmodified polymer. More specifically, for $c > c^*_{UN}$, HMPAA and PAA lead to the formation of stable and unstable emulsions, respectively, over the entire range of pH. In the dilute regime ($c < c^*_{UN}$), emulsions are stable and unstable at pH values lower and higher than 6.5, respectively, for both the modified and the unmodified polymers. In the view of these results, it was postulated by the authors that, in the semidilute regime, HMPAA stabilizes the emulsions for all pH values through ''trapping'' of the oil droplets in hydrophobic sites of the polymer mesh. In the dilute regime, a classical steric stabilization mechanism was attributed to both polymers. At pH values in excess of 6.5, emulsion instability in the dilute regime arises from the too weak adsorption of the polymers at the liquid–liquid interface leading to an ineffective steric stabilization mechanism. Equilibrium interfacial tension measurements for the HMPAA–water–cyclohexane system effectively show a significant desorption of the polymer with increasing pH from 5 to 7 (Figure 13). A similar behavior was observed by the authors for carbopol 980. The effect of adding electrolytes to emulsions stabilized by HMPAA was also studied by Lochhead and coworkers [183,184]. In general, emulsion instability is observed at high salt concentrations or low polyelectrolyte concentrations and depends

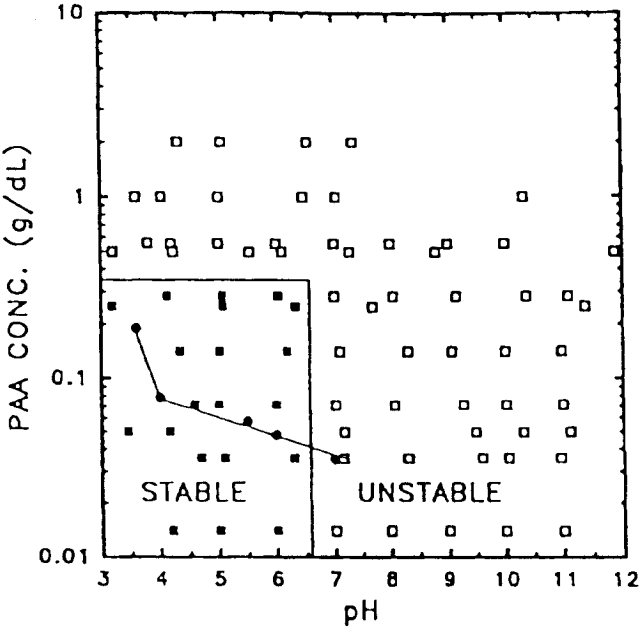

FIG. 11 Pseudophase diagram for 30 wt% cyclohexane in water stabilized by PAA (Carbopol 980). The c^* values are shown as the curve drawn in the bottom left-hand corner of the diagram. (Reprinted from Colloids and Surfaces A: Physicochem Eng Aspects, 88, Lockhead RY, Rulinson CJ, An investigation of the mechanism by which hydrophobically modified hydrophilic polymers act as primary emulsifiers for oil in water emulsions. 1. Poly(acrylic acids) and hydroxyethyl celluloses. 27-32, Copyright (1994), with permission from Elsevier Science.)

on the type of added electrolytes. The addition of potassium thiocyanate causes the rapid coalescence of emulsions. According to the authors, the presence of thiocyanate would decrease the strength of the hydrophobic interaction, thereby causing desorption of HMPAA from the interface and thus emulsion destabilization. In contrast, in the presence of potassium chloride, emulsions cream but remain stable to coalescence. The authors postulate that the stability of oil droplets to coalescence is due to the fact that the chloride is a water-structure-making ion that increases the strength of the hydrophobic interaction and thus provides HMPAA with a better anchoring at the oil–water interface. Tamburic and coworkers [13] have investigated the rheological behavior of mineral oil (30% w/w) in water emulsions as a function of the manufacturing procedure. The two methods of preparation differ in that the amphiphilic polyelectrolyte (Pemulen TR 1) is

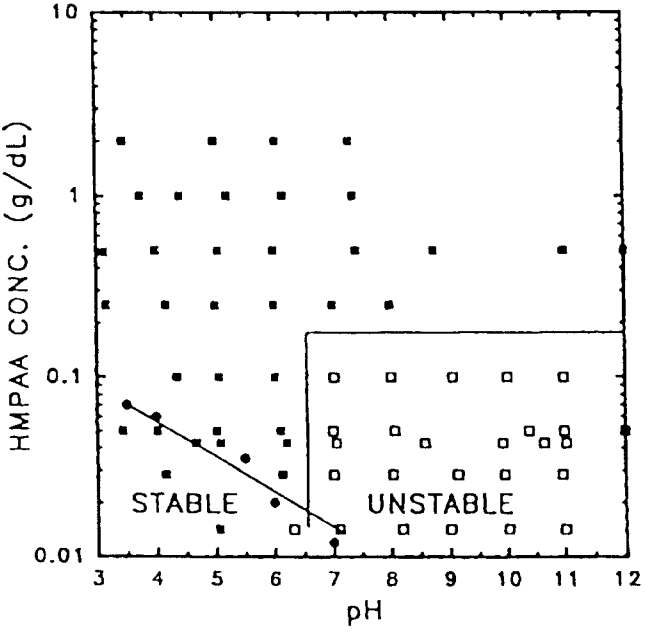

FIG. 12 Pseudophase diagram for 30 wt% cyclohexane in water stabilized by HMPAA (Pemulen TR 2). The c^* values are shown as the curve drawn in the bottom left-hand corner of the diagram. (Reprinted from Colloids and Surfaces A: Physicochem Eng Aspects, 88, Lochhead RY, Rulinson CJ, An investigation of the mechanism by which hydrophobically modified hydrophilic polymers act as primary emulsifiers for oil in water emulsions. 1. Poly(acrylic acids) and hydroxethyl celluloses. 27-32, Copyright (1994), with permission from Elsevier Science.)

dissolved either in oil or in water prior to emulsification at ambient temperature. At an emulsifier concentration of 0.4%, the authors observed a change in the dynamic rheological behavior of emulsion samples upon changing the preparation process. However, both types of emulsion exhibit similar flow properties. Perrin and coworkers [188,189] have used a series of well-characterized linear amphiphilic polyelectrolytes as emulsifiers of the *n*-dodecane–water system. The chemical structure of the polyelectrolyte surfactants was already presented in Sec. II.C (Eq. 2a). The stability and flow properties of direct emulsions (50% v/v) are taken as criteria for appreciating the efficiency of the emulsifying agents as a function of the degree of grafting (τ = 0 to 10% in mol), the length of alkyl grafts (n = 12, 18), the molecular weight (M_n = 5,000, 50,000, and 150,000 g/mol), and the polymer concentrations (C_p = 0 to 10%). The emulsifiers are all water-sol-

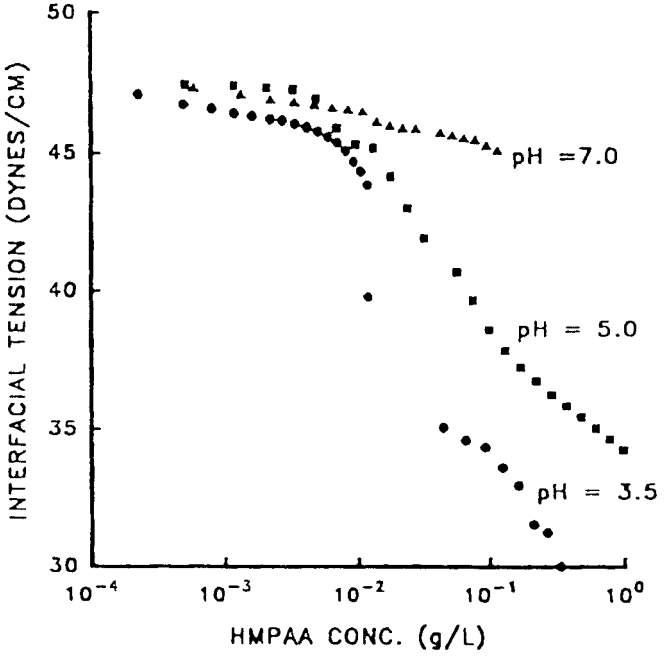

FIG. 13 Polymer solution/cyclohexane interfacial tension as a function of polymer concentration and pH for HMPAA (Pemulen TR 2). (Reprinted from Colloids and Surfaces A: Physicochem Eng Aspects, 88, Lochhead RY, Rulinson CJ, An investigation of the mechanism by which hydrophobically modified hydrophilic polymers act as primary emulsifiers for oil in water emulsions. 1. Poly(acrylic acids) and hydroxethyl celluloses. 27-32, Copyright (1994), with permission from Elsevier Science.)

uble associating polyelectrolytes [188–190]. The main property of associating polymer aqueous solutions arises from the development of a high viscosity above a given polymer concentration, known as the critical aggregate concentration (cac) [188–190]. For $c >$ cac, intermolecular hydrophobic associations occur preferentially, leading to the formation of a 3-D physical network and hence to an increase in the viscosity of the solutions. As seen further, these amphiphilic associating polyelectrolytes are remarkable emulsifiers since they a priori combine both the electrosteric (both the electrostatic and steric stabilization mechanisms [154]) and the thickening stabilization mechanisms (Sec. III.A). Furthermore, the hydrophobic grafts are attached to the PAANa [poly(acrylic acid) sodium salt] by an amide link, a chemical group stable to hydrolysis over a broad range of temperature. This

may be of great practical importance during application and storage. In contrast to polymers presented in Sec. II.C (Eq. 2), the polymers described below are not able to produce inverse emulsions due to their too high hydrophilicity or too large H_0. The main results of this study are briefly summarized as follows. First, it is essential to point out that emulsions formulated with the unmodified PAANa are clearly unstable. Thus the linear neutralized poly(acrylic acid) is a poor emulsifier, in agreement with the observations of Lochhead about cross-linked PAANa (neutralized carbopol thickeners). However, the introduction of small amounts of alkyl chains into PAANa molecules drastically changes emulsion stability (Figure 14) [188,189] as well as surface tension properties (Figure 15) [191]. The stability behavior of emulsions is presented in Figures 14a and 14b for the 1C12Na and 10C12Na copolymers (M_n = 50,000 and M_w = 120,000 g/mol), respectively. The emulsified volume is plotted as a function of time at various emulsifier concentrations, C_p. The authors showed that the stability behavior can be continuously tuned by changing polymer concentration and grafting degree (Figure 14). The same remark holds for the length of the graft and molecular weight [188,189]. At a given polymer concentration, increasing τ enhances emulsion stability. For instance, complete phase separation occurs after 48 hours for the 1C12Na polymer at C_p = 0.2%, while at the same concentration, an emulsified volume of about 70% is observed for 10C12Na. The better stability given by the more hydrophobic polymer (10C12Na) is attributed to a stronger adsorption of the polymer at the interface as compared to the 1C12Na copolymer. The surface activity of 1C12Na at 0.2% is indeed much weaker than that of 10C12Na (Figure 15) [191]. At low polymer concentrations (up to 2% in the case of these two polymers), the stability enhancement is unlikely to be due to a rheology modification of the external phase, since the viscoelastic behavior of both the 1C12Na and 10C12Na aqueous solutions at a given C_p is essentially the same. At higher polymer concentrations ($C_p \approx 3-5\%$), both copolymers are surface active, and the surface tension of the less hydrophobic polymer solution is lower than that of the more hydrophobic polymer solution (Figure 15). However, emulsions stabilized by 1C12Na are less stable. In this range of concentrations (above the cac of 10C12Na but below the cac of 1C12Na), the thickening effect of the 1C12Na copolymer is not yet effective [cac(1C12Na) $\approx$ 8–10%]. In contrast, the 10C12Na emulsifier, due to its important associating behavior, not only strongly adsorbs at the interface but also acts as a rheology modifier of the continuous phase [188–190]. In the end, the 10C12Na copolymer provides emulsions with a better overall stability than the 1C12Na polymer. In other words, with the progressive addition of associating polyelectrolyte surfactants, the droplets experience an increasing viscoelastic dispersing phase, slowing down both the creaming

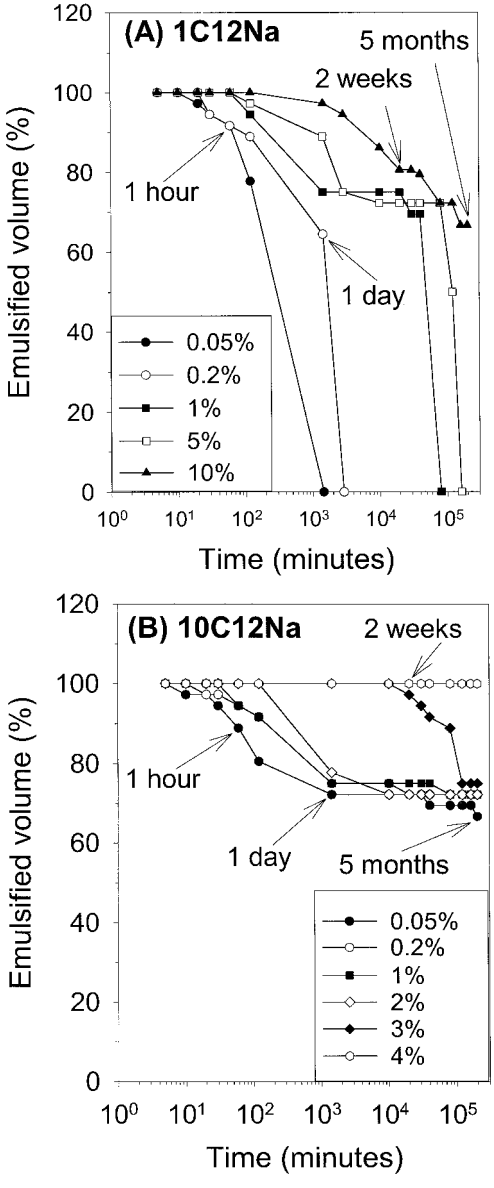

FIG. 14 Stability behavior: Volume of emulsions (%) stabilized by (A) 1C12Na and (B) 10C12Na as a function of time at polymer concentrations indicated above (C_p%). Emulsions have an equal amount of oil and aqueous phase (50/50 v/v). (From Ref. 189.)

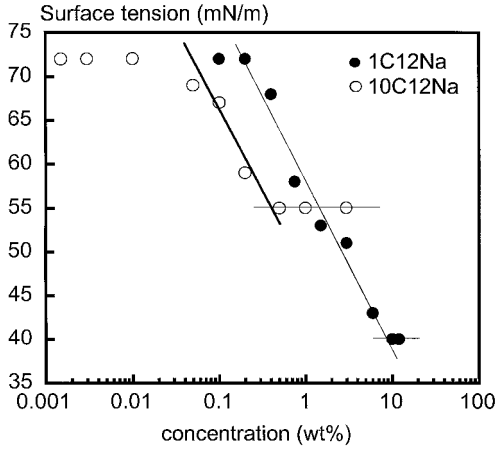

FIG. 15 Surface tension of hydrophobically grafted poly(sodium acrylate) aqueous solutions: 1C12Na and 10C12Na. (Reprinted with permission from Ref. 191. Copyright © 1999 American Chemical Society.)

and the flocculation process and thus the coalescence breakdown mechanism. The trapping of the suspended droplets above the cac of the grafted polyelectrolytes is obviously more effective at higher degrees of modification. Interestingly, since the viscoelastic properties of associating polymer solutions can be continuously adjusted by changing a large number of physicochemical parameters (C_p, n, τ, molecular weight), the trapping stabilization mechanism can, in turn, be easily tuned to meet emulsion shelf life requirements. For instance, it appears that 10C12Na at $C_p = 4\%$ is capable of maintaining homogeneous emulsion for more than 5 months (emulsified volume = 100%) (Figure 14b). Actually, for this sample, creaming was not observed two years after preparation. The authors also measured the droplet average diameter for emulsions stabilized by 10C12Na as a function of time. At concentrations of 1 and 4%, constant values of 10 and 4 μm were measured over a period of one month. Despite the relatively large droplet size, the emulsions are remarkably stable, in agreement with Lochhead's observations. The 4% sample exhibits no creaming or coalescence in agreement with the picture of suspended droplets frozen in a physical polymer gel. The behavior of the emulsion at 1% is also remarkable. Only one day is required for the sample to form a creamed layer with a dispersed phase volume fraction of about 67–77% (corresponding to an emulsified volume of 75–65%; Figure 14b), a configuration which is well known to favor coalescence. However, no change in droplet diameter was observed

up to one month after preparation, thereby indicating a remarkable resistance to coalescence. The structure of the thin-liquid films forming at the interface of two neighboring oil droplets is described in Sec. III.C. Finally, the flow properties of emulsions were also investigated by Perrin and coworkers [188,189]. For example, a shear stress–shear rate plot is presented in Figure 16 for the 10C12Na copolymer. The viscosity of the shear-thinning emulsion sample as well as the presence of a yield stress (the shape of the curve of the 4% sample strongly suggests the presence of a yield value) can be monitored not only by changing polymer concentration (Figure 16) but also by varying the length and content of hydrophobic segment and the molecular weight of the polyelectrolyte surfactant [188,189].

2. High Internal Phase Emulsions

Concentrated emulsions or high internal phase emulsions (HIPE) are systems in which the volume fraction of the dispersed phase is larger than about 0.74, which is the close-packing volume fraction of monodispersed hard spheres. The dispersed soft entities of a concentrated emulsion are no longer spherical. They deform into polyhedra separated by thin films of continuous phase. The structure is thus analogous to a conventional gas–liquid foam with low liquid content. The structure, properties, stability, and applications of highly concentrated emulsions were recently reviewed by Cameron and

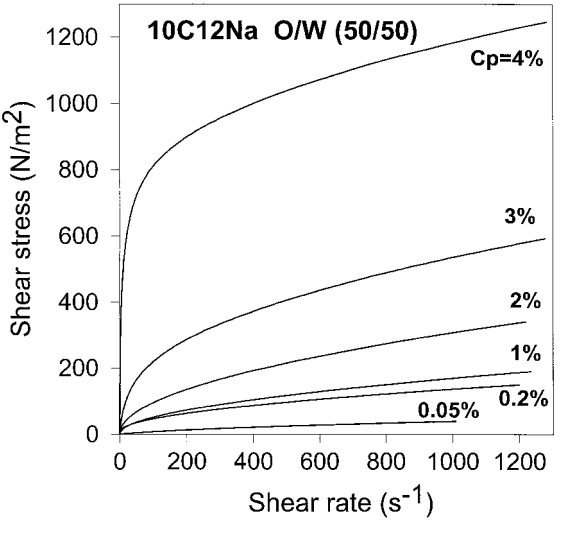

FIG. 16 Flow properties of dodecane in water emulsion (50/50 v/v) stabilized by 10C12Na at concentrations indicated above (C_p%). (From Ref. 189.)

Sherrington [192]. A book chapter has also been published by Kunieda and his coworkers [193]. Surfactants, as opposed to (charged) polymeric surfactants, are classically used to prepare concentrated emulsions. However, Taylor [194] has investigated the effect of an anionic surfactant (sodium dodecyl benzene sulphonate: NaDBS) on the stability and dynamic rheological behavior of moderately concentrated emulsions ($\phi_{oil} = 0.65-0.8$) stabilized by PVA [poly(vinyl alcohol)]. Pons and coworkers [195] used PEO/PPO/PEO nonionic triblock copolymer (Symperonic L92 and L64) to prepare concentrated direct emulsions of decane in water up to a dispersed phase volume fraction of 0.94. The rheological behavior of the emulsions was investigated as a function of the oil content and temperature (20 to 80°C). The stability of inverse high internal phase emulsions is generally increased by the addition of salt [196,197], although it was shown to depend on the type of added salt [198].

Ganguly and coworkers [199] have compared the stability behavior of concentrated water-in-oil (white mineral oil or a mixture of mineral oil and waxes) emulsions at various salt (ammonium nitrate or mixture of ammonium and sodium nitrate) concentrations for two types of surfactant. One is sorbitan mono-oleate (SMO), a nonionic surfactant, while the other one is a polymeric emulsifier, whose code name is LZX. The chemical structure of LZX is unclear because information on it is proprietary. However, according to the authors, LZX must be considered as a zwitterionic surfactant as a result of the reaction of poly(butenyl succinic anhydride) with alkanolamine. The practical application of the work concerns explosive emulsions. It is also important to mention that the weight average molecular weight of LZX is 2500 g/mol; LZX is thus a small polymer. The study reveals that the presence of salt is required to prepare stable emulsions using the nonionic surfactant. The stability enhancement of emulsions formulated with LZX due to the addition of salt is much more important than for SMO. The authors showed that the interactions between the surface-active agent and the added electrolyte are held responsible for stability improvement. The uncharged emulsifier and electrolyte can only interact through hydrogen bonding, while the zwitterionic character of the polymer chains would enable the macrosurfactant to develop more intense interactions, therefore explaining the greater stability enhancement observed for the polymer. The dynamic rheological behaviors of both the concentrated direct and inverse emulsions stabilized by hydrophilic ($\tau = 6\%$, $M_n = 42{,}000$ g/mol, and $M_w = 125{,}000$ g/mol) and hydrophobic ($\tau = 50\%$, $M_n = 74{,}000$ g/mol, and $M_w = 1{,}200{,}000$ g/mol) twin-tailed (Eq. 2b) amphiphilic polyelectrolytes, respectively, were found to be adequately described by the Princen model [200,201] on emulsion elasticity [202]. According to the model, the emulsion elasticity is de-

termined by the deformation of the interface under shear. The elastic modulus is given by

$$G' = \frac{A\gamma}{R_{32}\phi^{1/3}\,(\phi - B)} \tag{3}$$

where γ is the interfacial tension, R_{32} the mean surface volume radius, and ϕ the internal phase volume fraction. The constants $A = 1.769$ and $B = 0.712$ are experimental values determined by Princen. B represents the volume fraction at which droplets begin to deform, so that B is also often known as the close-packing volume fraction, ϕ_C. Direct emulsions are first described [202]. The polymer concentration in the continuous phase was kept constantly at 2%. The elastic modulus was measured for each emulsion sample ($0.825 < \phi_{n\text{-dodecane}} < 0.940$) as a function of the frequency in the linear domain (Figure 17). The emulsification procedure used in this experiment allows the preparation of emulsions with ϕ oil up to 0.94. At higher oil content, it seems that the high viscosity of the dispersion prevents the incorporation of oil, as already observed by Chen and Ruckenstein [203]. The droplet diameter, 13.9 $\pm$ 1.5 μm (measured for each sample using laser granulometry) was found to be independent of ϕ over the whole range of investigated oil content. B and γ were determined from the linear plot $G'R/\phi^{1/3}$ versus ϕ (Eq. 3) (Figure 18). The reasonable values of B and γ, 0.75–0.76 and 26–27 mN/m, respectively, indicate that the Princen model describes adequately the experimental data. The concentrated direct emulsions investigated above are polydisperse, which means that they exhibit a rela-

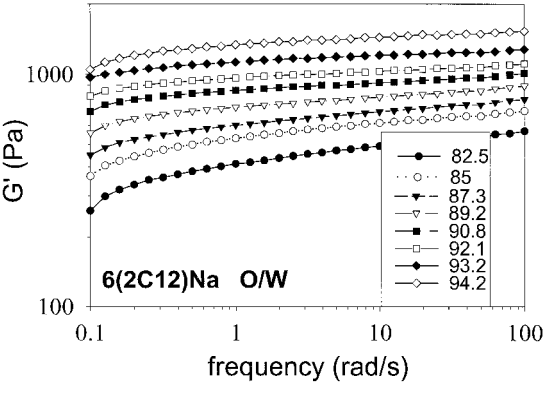

FIG. 17 Elastic modulus–frequency sweeps at various dodecane volume fractions indicated above. Concentrated emulsions stabilized by 6(2C12)Na (M_n = 42,000 and M_w = 125,000 g/mol) at a concentration of 2%. (From Ref. 202.)

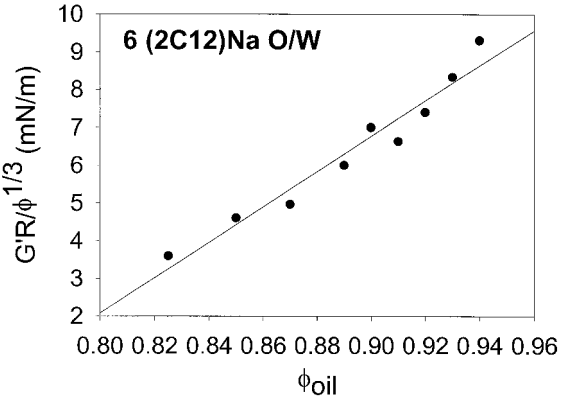

FIG. 18 Princen plot: Values of $B = 0.75–0.76$ and $\gamma = 26–27$ mN/m are calculated from the linear regression. G' was measured at 6.3 rad/s. Concentrated dodecane in water emulsions are stabilized by 6(2C12)Na (M_n = 42,000 and M_w = 125,000 g/mol) at a concentration of 2%. (From Ref. 202.)

tively broad droplet size distribution. There has been a recent growing interest in producing monodisperse emulsions by using various techniques such as fractionated crystallization [204], membrane extrusion [205], and emulsification in viscoelastic media [206]. From an academic point of view, the preparation of liquid–liquid dispersions with narrow droplet size distribution is crucial to give a better understanding of emulsion rheology [207]. Furthermore, monodisperse emulsion templating represents an attractive method of producing solid porous materials with uniform pore diameters ranging from 0.04 μm to several microns [208,209]. Such materials are predicted to possess new optical properties and hence are technologically important systems [210]. Interestingly, it was shown that concentrated monodisperse emulsions stabilized by hydrophobically grafted polyelectrolyte surfactants can efficiently be prepared by shearing concentrated polydisperse emulsions between glass slides [202,211]. As shown by Bragg diffraction patterns (Figure 19) and optical microscopy (Figure 20), concentrated ordered monodisperse emulsions consisting of hexagonal close-packed planes of oil (*n*-dodecane) cells are produced by shearing polydisperse emulsions stabilized by either the twin-tailed (Eq. 2b) [202] or the single-tailed (Eq. 2a) [211] charged polymeric surfactants. A detailed description of the experimental procedure is given in Ref. 211. It is remarkable that emulsion crystallization can be achieved using a small amount of polyelectrolyte surfactant as compared to small-molecule surfactants [206], thereby illustrating the high emulsifying potential of macrosurfactants in general. It is also im-

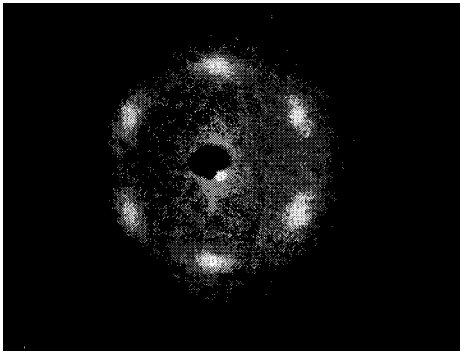

FIG. 19 Diffuse ring with 6 spots indicating a high degree of organization within the sheared dodecane-in-water emulsion sample. The 6(2C12)Na (M_n = 42,000 and M_w = 125,000 g/mol) polyelectrolyte surfactant can achieve emulsion crystallization at low concentration (2%). (From Ref. 202.)

portant to mention unpublished data showing that similar results were obtained using higher (hexadecane) or lower (heptane) *n*-alkanes. Inverse concentrated emulsions were also prepared from the *n*-hexadecene–NaCl 3.4 M system using a twin-tailed (τ = 50%, Eq. 2b) polyelectrolyte surfactant. The droplet diameter, 20 $\pm$ 5 μm, as revealed from a series of optical photographs, was not found to be dependent on the aqueous phase content (Figure 21). The frequency sweeps at various internal fractions are presented in Figure 22, while the $G'/\phi^{1/3}$ versus ϕ_{brine} plot is reported in Figure 23.

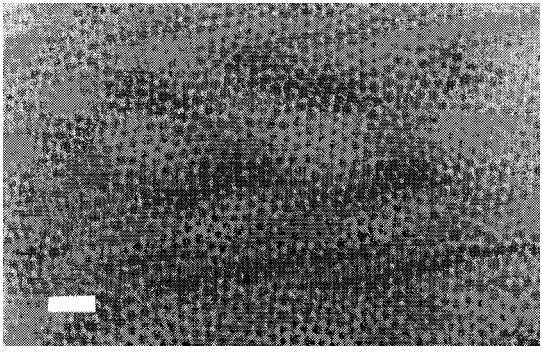

FIG. 20 Ordered layers of hexagonal close-packed cells. Dodecane-in-water emulsion stabilized by 6(2C12)Na (M_n = 42,000 and M_w = 125,000 g/mol). Emulsifier concentration is 2%. Scale bar is 10 μm. (From Ref. 202.)

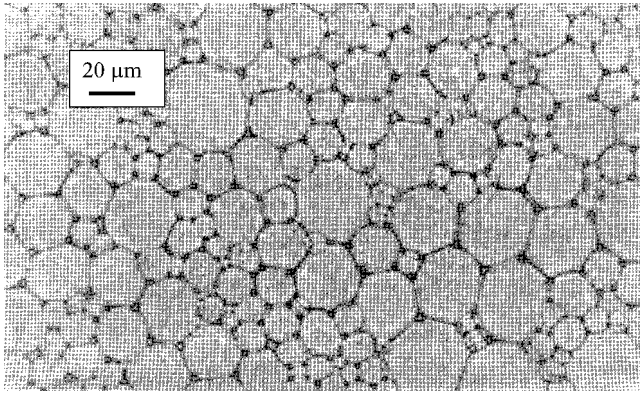

FIG. 21 Concentrated brine in hexadecene emulsion with a brine (NaCl 3.4 M) content of 91% (v/v). Scale bar is 20 μm. The concentration of the polyelectrolyte surfactant, 50(2C12)Na (M_n = 74,000 and M_w = 1,200,000 g/mol), is 4%. (From Ref. 202.)

The values of B and γ, 0.69 and 19 $\pm$ 5 mN/m, respectively, calculated from the linear regression (Figure 23) are in good agreement with the Princen model. The experimental data shown here was actually completed so that the values for B and γ are slightly different from those given in Ref. 202. Although the stabilization mechanisms are not quite clear, due to the

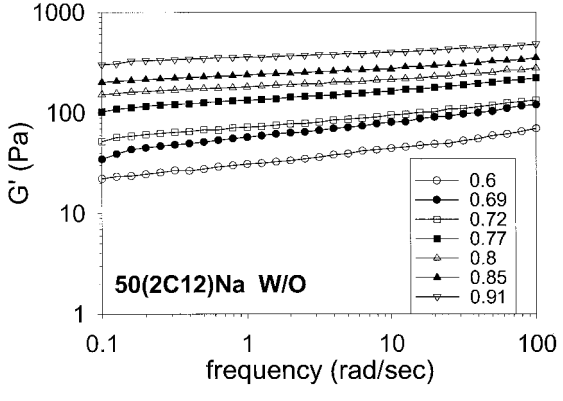

FIG. 22 Elastic modulus–frequency sweeps at various brine (NaCl 3.4 M) volume fraction indicated above. Concentrated inverse emulsions (hexadecene–brine) stabilized by 50(2C12)Na at a concentration of 4%.

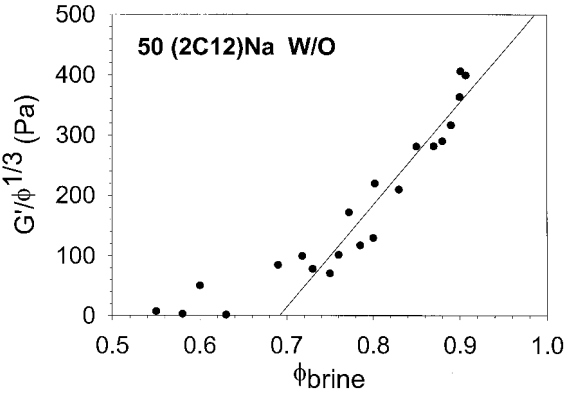

FIG. 23 $G'/\phi^{1/3} - \phi_{\text{Brine}}$ plot for concentrated brine in hexadecene emulsions formulated with 50(2C12)Na (M_n = 74,000 and M_w = 1,200,000 g/mol): Values of B = 0.69 and $\gamma = 19 \pm 5$ mN/m are calculated from the linear regression. The polymer concentration is constant equal to 4%. (From Ref. 202.)

complexity of the system, emulsions are stable despite the large droplet size, and it was thus possible to investigate their flow properties (Figure 24). As expected, the dispersions exhibit a shear-thinning behavior with a viscosity increasing with ϕ.

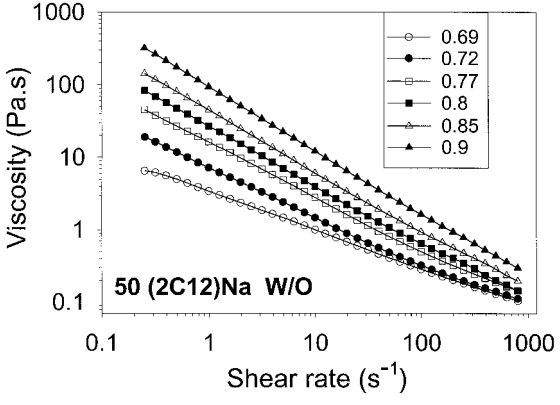

FIG. 24 Flow behavior of concentrated brine (NaCl 3.4 M) in hexadecene emulsions stabilized by 50(2C12)Na (M_n = 74,000 and M_w = 1,200,000 g/mol) at a concentration of 4%. The brine content (v/v) is indicated above.

C. Microscopic Aspects: Films of Amphiphilic Polyelectrolytes

Theoretical and experimental investigations dealing with the polyelectrolyte adsorption and the structure of polyelectrolyte liquid films have been carried out for more than twenty years in order to give a better understanding of emulsion stabilization mechanisms by polyelectrolytes on a microscopic scale. In this section, we describe the structure of liquid films composed of three kinds of polyelectrolytes: the diblock amphiphilic polyelectrolytes, which lead to the formation of brushes, the homopolyelectrolytes, which form a semicrystalline structure within the films, and finally the amphiphilic random polyelectrolytes. Special attention is given to the charged monomer layer thickness at interfaces.

1. Diblock Copolyelectrolytes

The important thickness and high monomer and charge densities encountered in polyelectrolyte brushes are expected to provide emulsion droplets with large steric and electrostatic repulsions. As a consequence, diblock polyelectrolyte surfactants are suitably designed to be effective emulsion stabilizers. Pincus [212] has proposed a description of polyelectrolyte brushes using an approach similar to that of Alexander and de Gennes for neutral brushes [75,213,214]. The latter model is thus first presented before developing that of polyelectrolyte brushes.

The formation of a brush arises from the adsorption of diblock amphiphilic polymer at the interface of selective solvents or from the chemical end-grafting of polymer chains to a solid substrate. The authors assume that the chains are in good solvent conditions and that the distance between adsorption points is lower than the radius of gyration of the chain in solution. The two present forces are thus the stretching elastic entropy of the chains and the monomer osmotic pressure. The local osmotic pressure is equal to $P = (1/2)vc^2kT$ (J/m^3), where v and c are the excluded volume per monomer and the monomer concentration, respectively. The force exerted at the end of a stretched chain of thickness L is $(L/Na^2)kT$ [78], where N and a are the number of monomer units and the monomer dimension, respectively. Assuming that all chains are stretched by an identical length L, the corresponding pressure is given by $(L/Na^2d^2)kT$, where d is the mean distance between adsorption points. The thickness L is then given by equating both pressures. Assuming a constant monomer concentration $c = (N/Ld^2)$ within the brush, the thickness is then

$$L = Na\left(\frac{v}{2ad^2}\right)^{1/3} \tag{4}$$

The linear dependence of L with N is characteristic of the stretched three-

dimensional brushes. The decrease of L with d reflects the interactions between monomers: when the mean distance between chains decreases, the thickness of the brush increases, at the expense of the elastic energy, to control the increase in osmotic pressure. The first experimental verification of the de Gennes–Alexander model has been obtained by Auroy and coworkers [215,216], who studied, by small-angle neutron scattering measurements, polydimethylsiloxane (PDMS) brushes extending in dichloromethane and grafted onto porous silica. A more refined calculation [217] has shown that the exact monomer concentration profile within the brush in good solvent conditions is parabolic and confirms the power law (Eq. 4) of the de Gennes–Alexander model, based on a step function.

The behavior of neutral brushes in good solvent conditions has been generalized to any solvent quality [218,219]. In Θ solvent, the excluded volume, which is the second virial coefficient, is equal to zero. As a consequence, the thickness L results from the balance between the three-body interaction forces (positive and proportional to c^3) and the chain elasticity. In a poor solvent, the chains shrink, and the elasticity term is irrelevant. The determination of L thus results from the equilibrium between the two-body and three-body interaction forces. The expression of L as a function of N, a, d, and the second and third virial coefficients is obtained by the authors, who demonstrate that the brush configuration is preserved in both the Θ and the poor solvent with a linear variation of L with N. The brush thickness continuously decreases as the solvent quality decreases. Experimentally, this can be suitably achieved by varying the temperature. The effect of changing solvent quality on the flocculation behavior of emulsions stabilized by copolymers was discussed by March and Napper [154] (Sec. III.B). Even if the random copolymers used in this study are not expected to form brushes, it was clear that flocculation was observed in Θ solvent conditions while it was suppressed in good solvent conditions.

Pincus [212] has studied polyelectrolyte chains the monomers of which are in Θ solvent conditions, i.e., the excluded volume is zero. This assumption is justified by the fact that most polyelectrolytes are rather hydrophobic and their solubility in water is only due the presence of charges along the chains. The author shows that electroneutrality is locally achieved within the brush, providing that the fraction of charged monomers p and the densities of adsorption points $1/d^2$ are not too low. Actually, the high concentrations of charged monomers and counterions lead to a Debye length much lower than the brush thickness. Consequently, the only relevant electrostatic contribution to the forces within the brush is the osmotic pressure of the counterions, which behave as a constraint ideal gas with a pressure equal to $pckT$, in the absence of added salt. Hence the equilibrium thickness of the brush results from the balance between the elastic force and the counterions'

osmotic pressure. Since the elastic contribution is the same as for neutral brushes, the thickness of the charged brush is [212]

$$L = p^{1/2}Na \tag{5}$$

The size L of the polyelectrolyte chains again varies linearly with N but is much larger than that of neutral polymer chain provided that p is not too low. The chains within polyelectrolyte brushes are only stretched by their own counterions. The thickness is thus independent of d in contrast to neutral polymer brushes. In other words, the behavior of a charged chain within a brush is that of a single chain at the interface. It is due to the assumption that the counterions do not interact. The presence of a monovalent salt at a concentration c_s in the bulk solution in contact with the brush alters neither its structure nor its length, provided that the concentration of added ions $2c_s$ remains smaller than the concentration of charged monomers pc within the brush. With an excess of salt ($2c_s >> pc$), the osmotic pressure was equal to $kTp^2c^2/4c_s$ [212]. Using this expression, Pincus [212] obtained

$$L = Na\,\frac{p^{2/3}}{(4ad^2c_s)^{1/3}} \tag{6}$$

The presence of an excess of salt in the solution lowers the osmotic pressure, and the brush shrinks under the action of the elastic force. However, the chains remain in a stretched conformation, since the linear dependence of L with N is conserved. A comparison of Eqs. 4 and 6 shows that the charged brush with an excess of salt behaves like a neutral brush with an excluded volume per monomer equal to $p^2/2c_s$. Particularly, the brush thickness depends on d in the high salt regime in contrast to the low salt regime. The theory of Pincus [212] was concerned with not-too-low densities of grafting. Wittmer and Joanny [220] have generalized these results to any density and established the complete diblock polyelectrolyte adsorption phase diagram in the (d, c_s) plane. The dependence of the length of the charged brushes with the salt concentration is clearly supported by the experimental data presented by Guenoun et al. [221] (Figure 25), who studied the structure of free-standing vertical aqueous films of diblock amphiphilic polyelectrolytes consisting of poly(*tert*-butylstyrene) (PtBS) and sodium polystyrene sulfonate (NaPSS) sequences. At the air–water interface, the highly hydrophobic PtBS blocks emerge in the air from the solution while the hydrophilic charged NaPSS blocks dangle into the solution and form a polyelectrolyte brush. Stable films, constituted of two NaPSS brushes in contact, are drawn from the solution. The thicknesses have been measured by x-ray reflectivity for a wide range of salt concentrations. Two predicted regimes have been observed: the film thickness is actually independent of the salt concentration in the low salt regime ($2c_s < pc$) while it decreases as $c_s^{-1/3}$ in the high salt

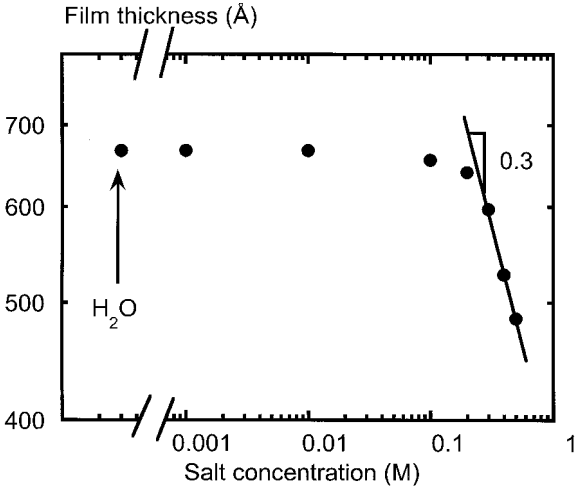

FIG. 25 Influence of an addition of salt on the thickness of a vertical free-standing film composed of two opposite NaPSS brushes (log-log plot). (From Ref. 221. Copyright © 1995 by the American Physical Society.)

regime ($2c_s > pc$). The dependence of L with d has been tested by x-ray reflectivity measurements on charged brushes of diblock poly(ethylethylene)/polystyrene sulfonate (PEE/PSS) deposited on the surface of water [222]. The authors also observed two regimes: L is independent of d for low salt concentrations and scales as $d^{-2/3}$ for high salt concentrations (above 0.1 M), in excellent agreement with Eqs. 5 and 6, respectively.

Zhulina et al. [223] have calculated the exact charged monomer concentration profile using the approach of Milner et al. [217] for neutral brushes. They found a Gaussian profile in the absence of salt with a characteristic width equal to the thickness calculated by Pincus (Eq. 5) up to the numerical coefficient. With an excess of salt, the authors found a parabolic profile for both the salt and monomer concentrations. The brush thickness is again found equal (up to the numerical coefficient) to that obtained by Pincus, who used the rough assumption of a step function. The Gaussian and the parabolic profiles corresponding to both salt regimes have been observed by Mir et al. [224] and by Tran [225] by neutron reflectivity on NaPSS brushes grafted on porous silica.

Finally, the first disjoining pressure measurements have been recently performed for charged brushes (PtBS/NaPSS) at liquid surfaces [226]. Surprisingly, the disjoining pressures are much smaller than predicted by the theory for highly charged brushes [212]. The reason for this discrepancy is

not clear at the present time. Further studies are very promising, as they should provide new information about the forces and the condensation phenomenon in the charged brushes.

As mentioned previously, most polyelectrolytes are highly hydrophobic, and their solubility in water is only due to the presence of the charges along the chains. It was then interesting to generalize the theoretical investigations of the charged brushes in a Θ solvent ($v = 0$) to solvents with negative excluded volume ($v < 0$). Following the approach discussed in Refs. 218 and 219, Ross and Pincus [227] have used a negative excluded volume (corresponding to a negative osmotic pressure of monomers $kTvc^2$) and a positive third virial coefficient (corresponding to the repulsive three-body interactions) in their calculation to build the phase diagram of the polyelectrolyte brushes in the plane (v: excluded volume; p: fraction of charge) in the absence of salt at constant d values (Figure 26). The not-too-low p and low $|v|$ regime ($|v|c^2 < pc$) corresponds to the case presented above that leads to Eq. 5. This regime is the "polyelectrolyte regime." For low p and low $|v|$ values, the osmotic pressure of both the counterions and the monomers is irrelevant, and the brush thickness is determined by the balance between the three-body interactions $kTc(a^3c)^2$, where $c = N/Ld^2$, and the elastic entropy of the chains, $(L/Na^2d^2)kT$ (J/m^3). The thickness of the brush is then

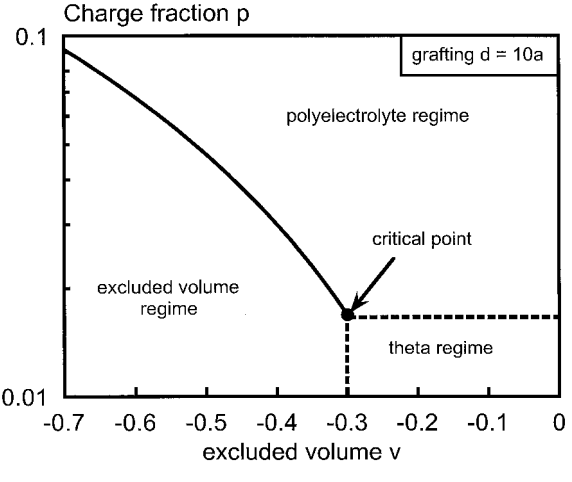

FIG. 26 Phase diagram for the polyelectrolyte brush in the (v, p) plane where v is given in a^3 unit. The phase diagram is fixed for a given mean distance between adsorption points ($d = 10a$). (Reprinted with permission from Ref. 227. Copyright © 1992 American Chemical Society.)

$$L = Na\left(\frac{a}{d}\right) \tag{7}$$

This regime is the ''Θ regime.'' Finally, for low p values and high $|v|$ values, corresponding to poor solvent, the brush is only weakly stretched, and the elastic entropy is irrelevant. The equilibrium brush thickness results from the balance between the attractive two-body ($kTvc^2$) and the repulsive three-body interactions:

$$L = Na\left(\frac{a}{d}\right)^2 \frac{a^3}{|v|} \tag{8}$$

This regime is the ''excluded volume regime.'' The stretching of the chains in the last two regimes is only due to excluded volume effects. The electrostatics does not play any role, and Eqs. 7 and 8 have been obtained for neutral brushes in Θ and poor solvents, respectively [218,219]. The analysis of the free energy function of the charged brush [227] reveals the existence of a first-order transition from the polyelectrolyte to the excluded volume regimes (Figure 26). A variation of the excluded volume fraction v from zero to negative values at fixed and not-too-low p value causes an abrupt collapse transition when crossing from one regime to another (line in Figure 26). This results in a discontinuity in the brush thickness. This collapse transition has also been predicted by Zhulina et al. [223]. Experimentally, this can be achieved by increasing temperature. In the vicinity of the transition line, the free energy presents two minima with respect to L. The values of the minima are equal at the transition points. In the region close to the transition line, a force–balance apparatus would provide, at fixed temperature, the required energy to get the brush over the energy barrier (about $10kT$ per chain) into the collapsed state. The pressure isotherm would then present a thickness jump, as has already been observed experimentally [228]. Whether this experimental observation is related to the competition between counterion swelling (polyelectrolyte regime) and poor solvent collapse (excluded volume regime) requires further study. Finally, it is important to mention that the crossovers between the different regimes below the critical point (across the dashed line in Figure 26) are smooth.

2. Homopolyelectrolytes

Mixed aqueous films made of small-molecular-weight surfactants and polyelectrolytes are now discussed. The small-molecule surfactants form the walls of the film, while the polyelectrolyte chains are confined within the film. The walls are either neutral or charged. The polyelectrolyte chains do not have any affinity for neutral walls and adsorb on opposite charged walls. Nevertheless, we will see that both types of films exhibit similar features.

When the walls are neutral, the films can be viewed as model systems to determine the interactions between oil droplets stabilized by a neutral surfactant in oil-in-water emulsions containing nonadsorbing (thickeners) polyelectrolyte chains in the continuous medium.

Structural forces have been detected in mixed films of dodecyl trimethylamonium bromide (DTAB, cationic surfactant) and a random copolyelectrolyte composed of neutral monomers of acrylamide (AM) and negatively charged monomers of acrylamidomethylpropane sulfonate (AMPS) [229]. The films are formed in a small hole drilled in a porous glass disk, and increasing pressures are applied. Each force–thickness isotherm presents a series of thickness jumps of the same amplitude (Figure 27), revealing a stratified organization of the polyelectrolyte chains within the film. The amplitude and the number of jumps, respectively, decreases and increases with the polyelectrolyte concentration c of the solution. The jumps are observed neither with salt in excess (NaBr) nor with a neutral polymer (PEO). The organization within the polyelectrolyte films thus seems to arise from an electrostatic contribution. However, it cannot be attributed to the electrical potential created by the charged surfaces of DTAB since the thickness jumps are still observed by replacing DTAB by a neutral surfactant (pentaethylene oxide monododecylether (C12E5)) [230]. The structure is likely to be related to the bulk properties of the semidilute polyelectrolyte solutions: the electrostatic interactions between monomers create a short-range order at the scale of the mesh size of the solution. This semiordering in the bulk is

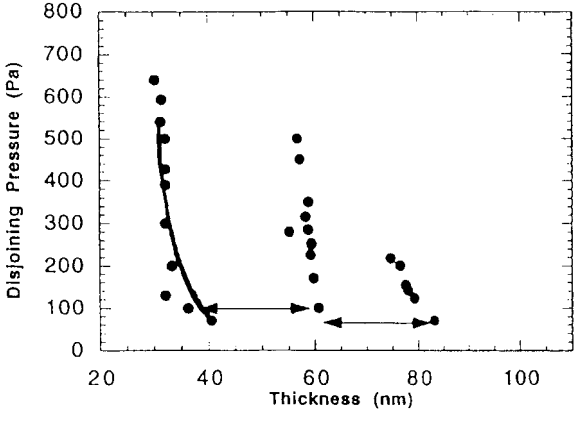

FIG. 27 Pressure isotherm of (AM-co-AMPS)/DTAB mixed films. The (AM-co-AMPS) concentration is 0.19% (w/w) (From Ref. 229. Copyright © 1997 by the American Physical Society.)

revealed by the existence of a peak in the scattering function corresponding to the mesh size ξ, which decreases with concentration as $c^{-1/2}$ [231]. This phenomenon has received good experimental confirmations by both neutron and x-ray scattering experiments [232,233]. The amplitude of the film thickness jumps also follows the $c^{-1/2}$ dependence. Moreover, the measured values of the amplitude are in good agreement with the values of the mesh size calculated from polyelectrolyte theories [231,234–236]. The charged chains thus seem to be preferentially located in planes parallel to the walls of the film, thereby forming a semicrystalline structure with an oscillating concentration profile. One important point that remains unclear is the destination of the polyelectrolyte chains after a jump: are they ejected from the film to the solution or moved from one plane to another? Finally, the effect of the semicrystalline structure of the polyelectrolyte films with respect to emulsion stability is not known at the present time and thus requires further investigation: a slight resistance to coalescence due to the presence of the successive energy barriers is expected.

Oscillation of the concentration profile has been obtained from theoretical contributions. Châtellier and Joanny [237] have calculated the analytical expression of the concentration profile of polyelectrolyte chains adsorbed on oppositely charged surfaces (which experimentally correspond to an adsorption layer of charged surfactants). The profile shows damped oscillations as a function of the distance from the surface for polyelectrolytes that are sufficiently hydrophobic. If the polyelectrolyte chains are confined between two charged surfaces, the disjoining pressure between the two interfaces mediated by the polyelectrolyte solution also presents damped oscillations as a function of the separation between the interfaces. For more hydrophilic polyelectrolytes, the concentration profile decreases monotonically, and no oscillation is observed. The AM/AMPS copolyelectrolyte is not hydrophobic enough for the film behavior to be explained by this theory. Moreover, oscillation of the disjoining pressure has been observed for neutral interfaces (mixed films of AM/AMPS copolymer and C12E5 surfactant). These results cannot be explained by the theory dealing with charged interfaces. Recently, Monte Carlo simulations [238] have revealed an oscillation of the polyelectrolyte concentration profile between two neutral nonadsorbing surfaces (walls of neutral surfactant), the wavelength of which corresponds to that of the mesh size of the bulk solution. The chains are preferentially located in planes parallel to the surfaces (Figure 28). The authors show that the organization of the polyelectrolyte chains within the film is an inherent property of the polyelectrolyte chains themselves: it is only due to the electrostatic interactions between charged monomers. An oscillatory profile is obtained in the absence of a surface electrical potential and for any type of polyelectrolyte (hydrophobic or hydrophilic). The numerical simulations give a good

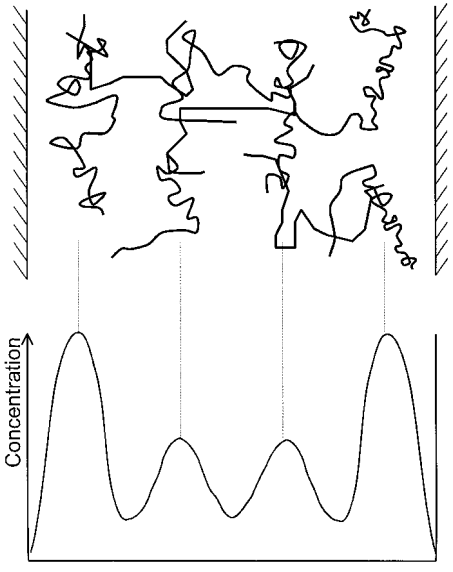

FIG. 28 Organization of polyelectrolyte chains and concentration profile in a film composed of two nonadsorbent walls. The chains are preferentially located in planes parallel to the walls. (Reprinted with permission from Ref. 238. Copyright © 1998 American Chemical Society.)

explanation for the experimental results obtained with mixed films of surfactants and polyelectrolytes as discussed above [229,230].

3. Random Copolyelectrolytes

Only a few studies about aqueous films of amphiphilic random polyelectrolytes are reported in the literature. Millet et al. [239–241] have investigated by x-ray reflectivity the behavior of vertical free-standing films (Figure 29) of a series of hydrophobically modified poly(acrylic acid) sodium salt (HMPAANa) and poly(acrylic acid) (HMPAAH). The chemical structure of the polymer was presented in Sec. II.C (Eq. 2a). One of the aims of this work was to determine the microscopic structure of the films to explain the (macroscopic) stability behavior of the dodecane-in-water emulsions studied by Perrin et al. [188,189], who used the same series of amphiphilic polyelectrolytes as primary emulsifiers. The aqueous polyelectrolyte films have been used as model systems for the interstitial films separating two neighboring oil droplets of an emulsion creamed layer. The authors have assumed that the oil/water interface encountered in emulsions was suitably described by the air/water interface of the films. The HMPAANa and HMPAAH co-

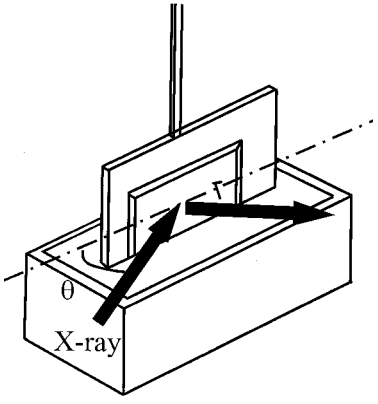

FIG. 29 The films are formed from the amphiphilic polymer solution by lifting a vertical metallic frame. Their height is about 1 cm. (From Ref. 221. Copyright © 1995 by the American Physical Society.)

polymers are noted M_w τC12Na and M_w τC12H respectively. τ is the degree of grafting, C12 corresponds to the dodecyl grafts, and M_w is the weight average molecular weight of the polymer backbone. Two different behaviors which depend on the molecular weight (M_w) and the degree of grafting (τ) have been observed by Millet et al. (239–241) for the polyelectrolyte films (Figure 30a).

First, the amphiphilic associating polyelectrolytes (HMPAANa) [188–190] of high molecular weight (typically larger than 34,000 g/mol) and low degree of grafting (smaller than 10% mol) develop large loops and dangling ends, leading to the formation of thick films, which in turn provide emulsions with an important steric stabilization mechanism. Two concentration regimes were identified. The thickness of the films drawn from aqueous polyelectrolyte solutions increases rapidly with the concentration of the polymer solution above the critical aggregate concentration (cac) [188–190] (Sec. III.B). Consequently, like the cac, the thickness also depends on the degree of grafting of the polyelectrolyte. The authors believe that the hydrophobic aggregates in the bulk solution are responsible for the concentration-dependent thickness of the films. As a matter of fact, the variation of the film thickness with polymer concentration reproduces, at least qualitatively, the dependence with polymer concentration of the Newtonian bulk viscosity, which is higher for the grafted polymer than for the precursor polymer above the cac. Consequently, the film thinning seems to be prevented by the presence of a physical gel between the wall of the film (Figure 30b). Below the cac, the film thickness is independent of both the degree

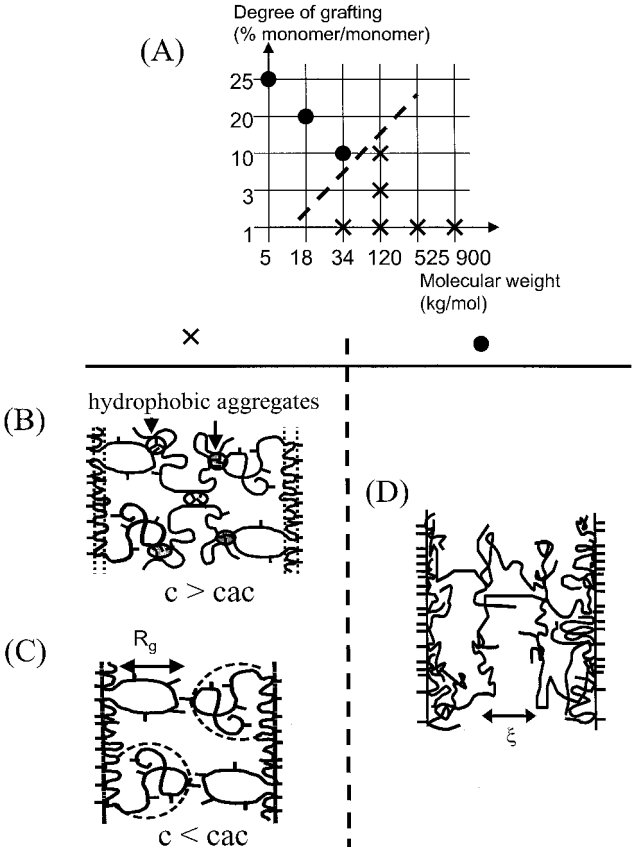

FIG. 30 (A) Phase diagram for the adsorption of HMPAANa copolyelectrolytes in the (M_w, τ) plane. (B and C) For polyelectrolytes with a high molecular weight and a low degree of grafting, the thickness of the films is controlled by the formation of hydrophobic aggregates when c > cac and by the size of the polymer coils when c < cac. (D) For polyelectrolytes with a low molecular weight and a high degree of grafting, the films have a semicrystalline structure with the polymer chains preferentially located in planes parallel to the faces of the film. (From Ref. 241.)

of grafting and the polymer concentration. However, it is molecular weight dependent and varies approximately as $M_w^{1/2}$ over the investigated range of molecular weights (34,000 g/mol (thickness = 380 Å) to 900,000 g/mol (thickness = 830 Å)). It thus appears that the film thickness is controlled by the size of the polymer chain and seems to vary as the radius of gyration of the self-screened Gaussian coil of the polyelectrolyte. As a consequence,

the authors have suggested the film structure sketched in Figure 30c composed of two monolayers facing each other. The influence of the charge fraction has also been investigated by varying the pH. The 1C12H copolymer is soluble in water due to its low degree of grafting. For various molecular weights, it is observed that the thickness of the 1C12H polymer films is twice as small as that of the 1C12Na films at concentration below the cac. This important result shows that the counterion osmotic pressure dominates over the monomer excluded volume effects in the HMPAANa polyelectrolyte films. The emulsion stabilization properties of the HMPAANa copolymers then arises from their associative properties that lead to the formation of a physical gel that traps the oil droplets in the bulk and prevents the thinning of the film between approaching droplets ($c >$ cac) and from the high layer repulsion due to counterion osmotic pressure that swells the polyelectrolyte adsorption layers ($c <$ cac).

The second type of behavior was observed for HMPAANa polyelectrolytes with low molecular weight and a high degree of grafting. They form films with a well-defined structure as revealed by the successive thickness jumps during the drainage [240,241]. The amplitude of the jumps roughly scales like $c^{-1/2}$ and coincides with the values of the mesh size ξ, determined by small-angle x-ray scattering measurements performed on semidilute solutions of poly(acrylic) acid sodium salt (the unmodified polyelectrolyte) at various concentrations [233]. Moreover, the number of the thickness jumps increases with the polymer concentration. Finally, they disappear with an excess of salt, which proves that they come from electrostatic phenomena. All these features have already been observed for mixed surfactant and polyelectrolyte films and they were interpreted in the same manner [229,230]. The structure given in Figure 30d was thus suggested by Millet et al. [240,241]. The originality of this experimental result resides in two points. First, the semiordering structure is observed with films made of one single type of molecule in contrast to mixed films. Here, the HMPAANa polyelectrolytes form both the walls of the film and the semicrystalline structure inside. The second point is that the thickness jumps are not observed with horizontal films submitted to an increasing pressure using a force–balance apparatus. They occur during the film drainage, the hydrostatic pressure (100 Pa for a 1 cm high film) being sufficient to induce the crossover of the successive energy barriers.

IV. EMULSION POLYMERIZATION

A. Basic Principles

Among the large variety of systems applied to carry out free-radical polymerization in heterogeneous media, emulsion polymerization is the most

common [242]. When performed in batch conditions, this technique starts from a monomer-in-water emulsion stabilized by surfactants at a concentration usually above the critical micellar concentration (cmc). Thus the system contains large monomer droplets (diameter > 1 μm) and surfactant micelles swollen by monomer. The long-term stability of this O/W emulsion is not a strong prerequisite, since continuous stirring is usually applied throughout the polymerization reaction. Moreover, polymerization does not take place in the monomer droplets, in contrast to suspension and miniemulsion polymerizations. An important feature of emulsion polymerization is that the use of a water-soluble radical initiator is required. Therefore polymerization starts within the water continuous phase with decomposition of the radical initiator and propagation of a few units of dissolved monomer. This step leads to oligoradicals, the water-solubility of which decreases when the degree of polymerization increases. Particles, which are the main locus of polymerization, are created in the early stage of the polymerization from these oligoradicals. The mechanism of particle nucleation is very complex, and detailed information can be found in Ref. 242. Different theories have been proposed. The micellar nucleation theory considers that micelles play a major role in the creation of the polymer particles. The homogeneous nucleation theory supposes that the oligoradicals generated in the water phase precipitate into colloidal objects when they reach a critical degree of polymerization at which their water solubility is lost. Finally, the homogeneous-coagulative theory postulates that the precursors formed upon precipitation of the oligoradicals undergo limited coagulation before becoming sufficiently stable to grow as mature particles. Once formed, the growing particles are swollen by monomer, and their stability is a key point in emulsion polymerization in order to maintain a constant number of particles throughout the polymerization. The consumption of monomer owing to propagation is continuously compensated for by its diffusion from the droplets, via the water phase. Therefore the droplets act only as monomer reservoirs. Polymerization is made possible by the continuous supply of radicals generated in the aqueous phase, which enter the particles after a few steps of propagation. At this stage, the rate of polymerization, R_p, is directly proportional to the number of particles, N_p, in the reaction medium:

$$R_p = k_p \cdot \left(\frac{N_p}{N_a}\right) \cdot \tilde{n} \cdot [M]_p \tag{9}$$

with k_p being the rate constant of propagation, $\tilde{n}$ the average number of radicals per particle, $[M]_p$ the concentration of monomer in the particles, and N_a the Avogadro number. At final monomer conversion, the product (or latex) is a suspension of spherical polymer particles with the average diameter between approximately 30 nm and 500 nm and ideally with narrow particle

size distribution. Particles are stabilized by the surfactant adsorbed or anchored at the interface. It is important to note that the final number of particles is much smaller than the initial number of surfactant micelles. Nevertheless, N_p is directly related to the concentration of surfactant by the simple relationship

$$N_p \sim [\text{Surfactant}]^{\alpha} \tag{10}$$

where α is a positive exponent that should equal 0.6 when the surfactant concentration is above the cmc, according to the Smith and Ewart theory [243]. To summarize, in emulsion polymerization, the role of the surfactant is threefold in the sense that it participates to the nucleation step, it provides stabilization of the monomer swollen particles during the polymerization step, and it stabilizes the final latex during storage and application.

B. Amphiphilic Polyelectrolytes Used as Primary Emulsifier in Emulsion Polymerization

A good stabilizer in emulsion polymerization will fulfill some typical criteria, which are often used to characterize its efficiency. In general, the higher the stabilized area (high N_p and small particle diameter), the higher the rate of polymerization (R_p), and thus the better the stabilizer. Moreover, the final latex should be stable under various conditions such as high ionic strength, high shear, and freeze-thaw cycles. In the large majority of published works and industrial productions, the stabilizers used are low-molecular-weight ionic surfactants that provide electrostatic stabilization. However, it is admitted that the use of polymeric stabilizers might lead to improved stability and better properties of the latex. Because of the existence of hydrophobic polymeric segment(s), they are expected to present some advantages linked to their better compatibility with the polymer particles and to a lower migration rate. They provide steric stabilization owing to the formation of a hydrophilic shell surrounding the particles. For that purpose, a variety of nonionic amphiphilic block and graft copolymers have been used in emulsion polymerization, and the structure/property relationship has been extensively studied, mainly for PEO-based copolymers [244,245]. More interestingly, when the hydrophilic segments are polyelectrolytes, they also provide electrostatic stabilization. As already discussed in Sec. III.C, the combination of both effects is known as electrosteric stabilization [69]. Amphiphilic polyelectrolytes with various architectures and chemical compositions have been used as stabilizers in aqueous emulsion polymerization to test their efficiency as reviewed below. More specifically, the relationship between the physicochemical structure of the emulsifier and the parameters governing the emulsion polymerization (N_p and R_p) will receive detailed

attention. To some extent, the polymerization sites, which contain both macromolecules and liquid monomers, can be regarded as a liquid dispersed medium stabilized by amphiphilic polyelectrolytes. As a consequence, it is worth discussing emulsion polymerization with respect to the above-mentioned parameters. In contrast, the colloidal stability of the latex will only be discussed occasionally, since the stabilization of colloidal particles by polyelectrolytes is extensively covered in Chapter 16.

1. Random Copolymers

Amphiphilic random copolymers can be easily prepared by free-radical copolymerization of monomers of different natures (i.e., hydrophilic and hydrophobic). In all the examples found in the open literature, the hydrophilic units are carboxylic acids or the corresponding salt (either acrylate or methacrylate). The very first published work concerned a low-molecular-weight copolymer of acrylonitrile and potassium acrylate which was successfully used as the sole emulsifier in the emulsion polymerization of styrene [246]. More recently, poly(dodecylacrylate-co-sodium acrylate) copolymers have been reported by Kuo et al. [247]. Poly(acrylic acid)s [Poly(AA)] with various molecular weights and different degrees of hydrophobic modification by amidation with tetradecylamine or by copolymerization with styrene have been used by Antonietti and Weissenberger [248]. The application of alkali soluble copolymers of poly(styrene-co-α-methylstyrene-co-acrylic acid) has been reported by Lee et al. [249–251]. Copolymers prepared with different compositions of methyl methacrylate (MMA) and methacrylic acid (MAA) have been used by Kato et al. [252,253]. The random copolymers studied exhibit good surface activity and form aggregates in water, in which monomer is solubilized. In all cases, batch emulsion polymerizations of styrene and/or MMA have been studied, and the monomer content was usually between 10 and 20 wt% (with respect to water). The effect of molecular weight, composition (degree of hydrophobic modification and/or degree of neutralization of the carboxylic acid moieties), concentration of the polymeric emulsifier, and nature of the polymerized monomer on the rate of polymerization, R_p, and on the number of stabilized particles, N_p, in the latex has been carefully examined.

(*a*) *Effect of the Molecular Weight of the Stabilizer.* Random copolymers are prepared by free-radical polymerization, which method usually leads to ill-defined polymers with broad molecular weight distribution and heterogeneous composition. Thus macromolecules with too low molecular weight should be avoided in order to avoid the presence of chains without any hydrophobic units. Indeed, with a low degree of hydrophobic modification together with a low molecular weight, some chains may not contain any hydrophobic unit and therefore they will not act as stabilizers but in contrast

will destabilize the latex by the depletion effect. Too large macromolecules can lead to bridging flocculation, and at high concentration they can cause thickening of the latex [248,252]. As a consequence of these requirements, all the polyelectrolyte random copolymers used as stabilizers in emulsion polymerization had an average molecular weight between 2,000 and 10,000 g/mol. For instance, the rate of emulsion polymerizations of styrene and the number of particles were shown to reach a maximum when they were stabilized by poly(MMA-co-MAA) random copolymers with M_w in the range of 5,000 to 10,000 g/mol; for M_w = 67,000 g/mol, destabilization occurred during the polymerization reaction, owing to bridging agglomeration [252].

(*b*) *Effect of the Emulsifier Composition and Degree of Neutralization.* The proportion of hydrophobic units in the copolymer plays a major role on its water solubility, on the formation of hydrophobic aggregates, and on its ability to adsorb at the polymer interface [248]. The solubilizing ability of the aggregates is also dependent upon the hydrophobic content of the copolymer and upon the degree of neutralization of the carboxylic acid units [249,250]. However, no general trend concerning the copolymer composition could really be found in the literature. For instance, the degree of hydrophobic modification was varied from 2.5 to 7.5 mol% for the poly(AA) modified with tetradecylamine [248], while the proportion of dodecylacrylate was 30 mol% in the poly(dodecylacrylate-co-sodium acrylate) reported by Kuo et al. [247]. In the poly(styrene-co-AA) copolymer, the proportion of styrene was 17 mol% [248], and in the poly(MMA-co-MAA) used by Kato et al. there was more than 60 mol% of MMA units (generally 75 mol%) [252,253].

In the emulsion polymerization of styrene stabilized by the poly(MMA-co-MAA) copolymer, Kato et al. [252] have shown that both N_p and R_p decreased continuously when the MMA content was decreased from 90 to 60 mol%. In contrast, no effect of the hydrophobe content could be evidenced for the poly(acrylic acid)s modified by 5 to 7.5 mol% of tetradecylamine [248]. In the case of poly(styrene-co-α-methylstyrene-co-acrylic acid) stabilizers with constant composition [249–251], when the degree of neutralization was varied from 80 to 100%, a different behavior was observed according to the polymerized monomer. On one hand, with styrene, although no effect of the neutralization degree could be observed on particle size and particle size distribution, the rate of polymerization was found to decrease when the neutralization degree was increased. The authors concluded that the rate of entry of the water phase–generated oligoradicals could decrease due to the presence of a more extended hydrophilic shell around the particles as the neutralization degree was increased, thus leading to a decrease of $\bar{n}$. On the other hand, for MMA emulsion polymerization, small-size particles were also obtained, but their distribution broadened

when the neutralization degree was increased (it was even bimodal at 100% neutralization). The authors explained this surprising effect by a change in the mechanism of nucleation. Increasing the degree of neutralization of the polymeric emulsifier leads to a decreased solubilization ability of the aggregates. Therefore, according to the authors, since MMA has a higher water solubility than styrene, the locus of nucleation might move from the hydrophobic aggregates to the aqueous phase, and consequently both micellar and homogeneous nucleation might occur simultaneously. Bimodal particle size distribution has also been observed by Kuo et al. [247] for the emulsion polymerization of styrene stabilized by the poly(dodecylacrylate-co-sodium acrylate) random copolymer. The authors suggested that the polymerization sites were both the monomer droplets (for the large particles) and the stabilizer aggregates (for the smaller ones).

(*c*) *Effect of the Stabilizer Concentration.* Such is the case with conventional surfactants; the number of latex particles, N_p, increases with the initial concentration of the amphiphilic random copolymers. For instance, the effect of the concentration of poly(MMA-co-MAA) (75 mol% of MMA; M_w = 4500 g/mol) in the emulsion polymerization of MMA was thoroughly examined, and the relationship $N_p \sim [\text{Surfactant}]^{0.43}$ was obtained when using potassium persulfate as the initiator [253]. In the emulsion polymerization of styrene stabilized by the modified poly(acrylic acid)s, Antonietti and Weissenberger [248] observed a different dependence according to the nature of the random copolymer. On one hand, with poly(tetradecylacrylamide-co-acrylic acid) stabilizers (not neutralized; M_η = 5,000 g/mol; 5 mol% and 7.5 mol% of hydrophobic modification) the particle diameter decreased from approximately 200 nm to approximately 74 nm when the proportion of stabilizer was increased from 1 wt% (with respect to styrene) to 100 wt%, respectively. In the relationship between N_p and the stabilizer concentration, the exponent α was 0.96 with a negatively charged initiator (potassium persulfate). On the other hand, when a neutralized poly(AA-co-styrene) random copolymer was used (M_η = 2,000 g/mol; 17 mol% of styrene units) in conjunction with potassium persulfate, the exponent was much smaller (0.3) and in that case the obtained diameters were larger: they decreased from approximately 400 nm when the amount of stabilizer was 1 wt% to approximately 230 nm when the amount of stabilizer was 50 wt%. The alkali-soluble poly(styrene-co-α-methylstyrene-co-acrylic acid) (with 80 to 100% neutralization) led in contrast to much smaller particles for the polymerization of styrene and MMA initiated with potassium persulfate, since diameters in the range of 40 nm were usually obtained with 35 wt% of stabilizer with respect to monomer. The rate of polymerization was shown to decrease when this amount was decreased from 35 wt% to 10 wt%, and this effect was accompanied by the expected increase in particle size.

Polyelectrolyte amphiphilic random copolymers have proved to be efficient stabilizers in the batch emulsion polymerization of styrene and MMA, providing that some structural requirements are fulfilled concerning the molecular weight, the composition, and the degree of neutralization. The homogeneity in the composition of the macromolecules is also an important parameter, because chains that do not contain a hydrophobic part cannot play the role of stabilizer. Since control over the structural characteristics of the copolymer is the main parameter, the use of preformed random copolymers might present some advantages as compared with the use of ionic or ionogenic water-soluble comonomers in emulsion polymerization (such as acrylic acid or methacrylic acid) [254–257]. Indeed, water-soluble monomers are often used in emulsion polymerization to enhance latex stability and to avoid the addition of a surfactant. In that case, the stabilizer is formed in situ by copolymerization. However, it has been evidenced that the formation of water-soluble polyelectrolyte could not always be avoided during the polymerization and could have dramatic consequences on the particle size distribution and latex stability [258]. Nevertheless, in soap-free emulsion polymerization, it was demonstrated that very small concentrations of ionic comonomers could strongly increase the final number of particles without any coagulation of the latex [259].

2. Polysoaps

In contrast to amphiphilic copolymers containing hydrophilic and hydrophobic monomer units in the chain, polysoaps are polymeric materials with surface-active constitutive units. They can be produced by (co)polymerization of surface-active monomers. The use of polysoaps as stabilizers in emulsion polymerization has been described quite recently by Cochin et al. [260]. They mentioned that very little work had been devoted to the topic before [261]. In their work, emulsion polymerization of styrene employing analogous conventional, polymerizable, and polymeric surfactants (polysoaps) with positive charges was investigated. All the species exhibited good stabilizing efficiency. Interestingly, the latex formed with the polymerizable and the polymeric surfactants had very high surface tension (close to that of pure water), which was not the case with the conventional surfactant. Moreover they led to enhanced stabilization of the final latices. Those results indicated that both the polymerizable and the polymeric stabilizers were strongly anchored at the particle/water interface.

3. Graft Copolymers

Since the early work of Evans et al. [262] using various types of graft copolymers, namely, poly(acrylic acid-graft-vinyl acetate), poly(vinyl ace-

tate-graft-acrylic acid), and poly(methacrylic acid-graft-vinyl acetate), in order to entropically stabilize poly(vinyl acetate) latex particles, very little work has been carried out with such polymeric emulsifiers. Actually, only one example of amphiphilic polyelectrolyte graft copolymer used as a stabilizer in emulsion polymerization could be found in the literature [263]. The polymer consisted of an anionic polyelectrolyte backbone of neutralized poly(vinylnaphthalene-alt-maleic acid) with polystyrene hydrophobic branches. Emulsion polymerization of styrene was carried out at low monomer contents (2 wt% with respect to water) and at a stabilizer concentration of 10 wt% with respect to monomer. A stable latex was obtained with relatively small particle size. Interestingly, after separation of the serum by centrifugation, less than 10% of the copolymer could be recovered in solution, indicating very strong adsorption at the particle surface.

4. Block Copolymers

Unlike random and graft copolymers, amphiphilic diblock copolymers can be considered as the macromolecular analogues of small-molecule surfactants. Particularly, they can form micellar aggregates in selected solvents [264]. In aqueous emulsion polymerization, the hydrophobic blocks can anchor at the particle surface while the hydrophilic blocks extend into the water phase and create a well-defined hydrophilic shell. The amphiphilic block copolymers are synthesized using ''living'' polymerization techniques such as anionic and cationic polymerizations, and more recently controlled radical polymerization [265]. These techniques lead to macromolecules with predictable molecular weight, narrow molecular weight distribution, and well-defined macromolecular architecture. Details on the synthesis and characterization of some nonionic amphiphilic block copolymers used as emulsifiers in emulsion polymerization are reported by Piirma [266]. For the synthesis of copolymers with a polyelectrolyte block, ''living'' polymerization of the corresponding ionic monomers is not always possible. Therefore either the additional selective chemical modification of one block of a hydrophobic copolymer or the polymerization of protected monomers followed by deprotection in the polymer are generally used. For instance, acrylic or methacrylic esters can be initially polymerized and are precursors of the corresponding carboxylate salts. Anionic polymerization was used for the preparation of poly(MMA-b-t-butylacrylate), poly(t-butylacrylate-b-MMA) and poly(MMA-b-t-butylmethacrylate) diblock copolymers [245,267–269]. Combination of cationic and anionic polymerizations was necessary for the synthesis of poly(isobutylene-b-t-butylmethacrylate) block copolymer [267]. Poly(styrene-b-AA) di- and triblock copolymers were prepared by atom

transfer radical polymerization of styrene and t-butylacrylate [270,271]. Subsequent hydrolysis of the t-butyl esters led to the corresponding amphiphilic block copolymers. The preparation of polyelectrolytes with sulfonate ionic groups requires usually the sulfonation of a hydrophobic diblock precursor copolymer prepared by anionic polymerization [272,273]. Using nitroxide-mediated radical polymerization, sodium styrene sulfonate was directly polymerized in a controlled manner, and the resulting polymer was used as a macroinitiator for the polymerization of styrene to provide the corresponding polyelectrolyte amphiphilic block copolymer [274]. Block copolymers with sulfonate ionic groups have advantages over their main counterparts with carboxylate units or PEO chains since their stabilizing ability is insensitive to both the pH and the temperature. Block copolymers with a positively charged polyelectrolyte part have also been synthesized. For instance, anionic polymerization enabled the preparation of a hydrophobic block copolymer that was further modified to lead to poly(MMA-b-methacryloyloxyethyl trimethyl ammonium chloride) [275]. A triblock copolymer with a cationic polyelectrolyte central block was prepared by conventional radical polymerization of diallyldimethylammonium chloride initiated by a PEO-based monoazo macroinitiator [276]. Finally, a diblock copolymer composed of a polystyrene segment and a partially quaternized poly(chloromethylstyrene) block was also synthesized using nitroxide-mediated controlled radical polymerization [270].

All these block copolymers were used as stabilizers in batch emulsion polymerization of styrene or (meth)acrylic ester monomers. Both the rate of polymerization and the number of stabilized particles were higher than in the presence of the same amount of a classical ionic emulsifier [271,274,275]. Nevertheless, this feature was only observed when using either a neutral radical initiator or a charged initiator with electrical charge sign identical with that of the polyelectrolyte block. With an initiator of opposite charge, the rate of polymerization was shown to be drastically reduced, and this effect was enhanced when the thickness of the hydrophilic layer was increased (increase of the hydrophilic block length) and when the emulsifier concentration was increased. This was explained by the much slower entry of the charged oligoradicals into the latex particles, owing to electrostatic interactions with the polyelectrolyte barrier of opposite sign. As a consequence, premature radical terminations occurred in the aqueous phase [275].

(*a*) *Effect of Molecular Weight, Composition, and Structure of the Polyelectrolyte Emulsifier.* All the polyelectrolyte block copolymers used were more or less within the same molecular weight range (M_n = 5,000–50,000 g/mol), and the effect in emulsion polymerization of the overall molecular

weight has not been carefully examined. Similarly, the influence of the individual block lengths and of the copolymer composition was not considered until very recently [267,269]. Actually, in most of the examples, the proportion of the hydrophobic monomer was between approximately 10 mol% and 30 mol% in order to ensure both the water solubility of the block copolymers and the good anchoring at the polymer surface. Nevertheless, in some cases, the effect of the degree of neutralization and the effect of the extent of chemical modification were studied. For instance, for a given block copolymer with carboxylic acid moieties, a decrease of the neutralization degree was shown to lead to poly(MMA) lattices with larger particle diameters [245]. Similarly, poly(ethylethylene-b-styrene) with 52% sulfonation of the polystyrene block behaved differently from the same copolymer with 100% sulfonation. In the former case, randomly distributed hydrophobic units in the hydrophilic block could be the cause of multiple adsorptions leading to particle aggregation at too high concentration (>5 wt% with respect to monomer) [272]. Recently, as mentioned above, a more complete study was performed in order to understand the effect of the hydrophobic block length [267–269]. For instance, it was shown that alkaline water solutions of poly(MMA-b-AA) block copolymers behave differently according to the length of the hydrophobic poly(MMA) block [267,269]. At low chain length, the block copolymers were surface active, whereas for longer blocks, the surface tension of the solution was that of pure water. This characteristic indicates that the block copolymers had no tendency to be present at the air/water interface but were strongly aggregated in water. Indeed, poly(MMA-b-sodium (meth)acrylate) diblock copolymers with a high proportion of the hydrophobic block in the copolymer form ''frozen micelles'' (i.e., very slow or no exchange between micelles). In that case, in emulsion polymerization, the final number of particles stabilized with a poly(MMA-b-sodium acrylate) diblock copolymer with 35 MMA units or more, was found to be identical to the initial number of micelles, indicating that the micelles act as a seed [267–269]. For this type of stabilizer (35 to 70 MMA units), micellar solutions were formed upon heating the copolymers in an alkaline water solution. However, with a longer hydrophobic block, solutions of the so-called ''frozen micelles'' were usually prepared in methanol or tetrahydrofuran/water mixtures, and emulsion polymerizations were performed subsequently, after elimination of the organic solvent.

The effect of the copolymer structure has not been sufficiently investigated. Nevertheless, a comparison of the diblock copolymers with the previously presented random copolymers showed that smaller amounts of the stabilizer were usually needed in the first case to achieve similar results. As a consequence, with the same amount of stabilizer, the diblock copolymers lead to smaller particles than the corresponding random copolymers. For

instance, 1 wt% with respect to monomer of a neutralized poly(styrene-b-AA) diblock copolymer (15 units of styrene, 29 units of AA) led to a polystyrene latex with particle diameter of 90 nm [270], whereas it was 400 nm with the same proportion of an analogous random copolymer [248]. In a recent study, it was shown that a neutralized poly(styrene-b-AA-b-styrene) triblock copolymer with the hydrophilic block in the middle was less efficient than the corresponding triblock copolymer with external hydrophilic blocks or than the diblock copolymer. Efficiency could however be improved upon increasing the length of the central block [271].

(*b*) *Effect of the Stabilizer Concentration.* Influence of the initial concentration of the block copolymer emulsifier was examined in some cases. Usually, an increase of the initial concentration led to an increase of N_p and of the polymerization rate [245,267–269,272]. The exponent α in the power law giving N_p as a function of the emulsifier concentration was found to be higher than 0.6. It was 0.97 for the emulsion polymerization of MMA in the presence of a fully neutralized poly(MMA-b-MAA) with M_n = 32,000 g/mol and with 63 wt% of MAA [245]. A value of 1 was obtained in the case of the previously described ''frozen micelles'' [267], since they act as a seed for the emulsion polymerization (the number of particles equals the initial number of micelles, and the number of block copolymers per particle is the same as the number per micelle). A value of α larger than 1 was obtained for low-molecular-weight neutralized poly(MMA-b-AA) copolymers with proportion of the hydrophilic monomer larger than 50 mol% while a value smaller than 1 was measured for a neutralized poly(MMA-b-AA) with 10 MMA units and 7 MAA units [267]. Interestingly, very small concentrations such as 1 wt% with respect to monomer, and sometimes less, were applied and found to be efficient [245,269–272,274,276].

Owing to their well-defined structure, amphiphilic block copolymers have great advantages over the analogous random copolymers. Particularly they can be used in lower concentrations. Moreover, the possibility of using block copolymer micelles as seeds in emulsion polymerization is very promising. However, more systematic studies concerning the effect of structure, composition, and concentration would be needed in order better to understand their behavior concerning the nucleation step and the kinetics of emulsion polymerization.

V. POSTCARDS

Our novel fashionable collection of clothes was recently presented in Paris, France. To celebrate the new century, a unique masterpiece of the collection is presented in Figure 31. This is a beautiful hand-made emulsion-tie re-

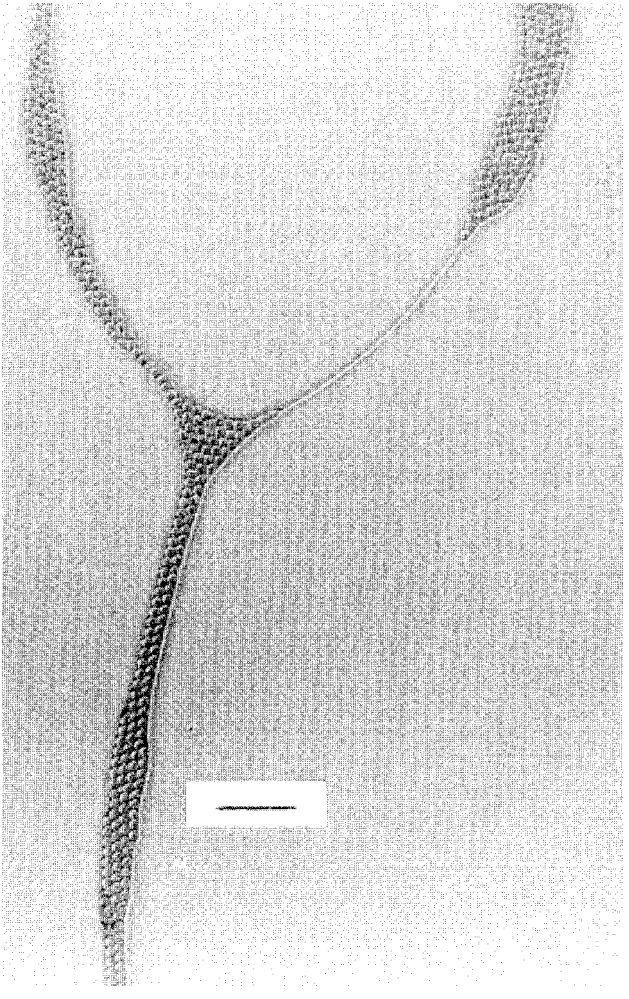

FIG. 31 An original item of clothing: the monodisperse emulsion-tie. Scale bar is 50 μm.

sulting from an assembly of unique size soft entities, monodispersed droplets stabilized by polyelectrolyte surfactants (Figure 32). The reader is advised not to spend too much time reproducing the items of clothing. Beautiful dispersions are also obtained by shearing pentane in water emulsions as shown in Figure 33. Due to the low boiling point of pentane, pentane drop-

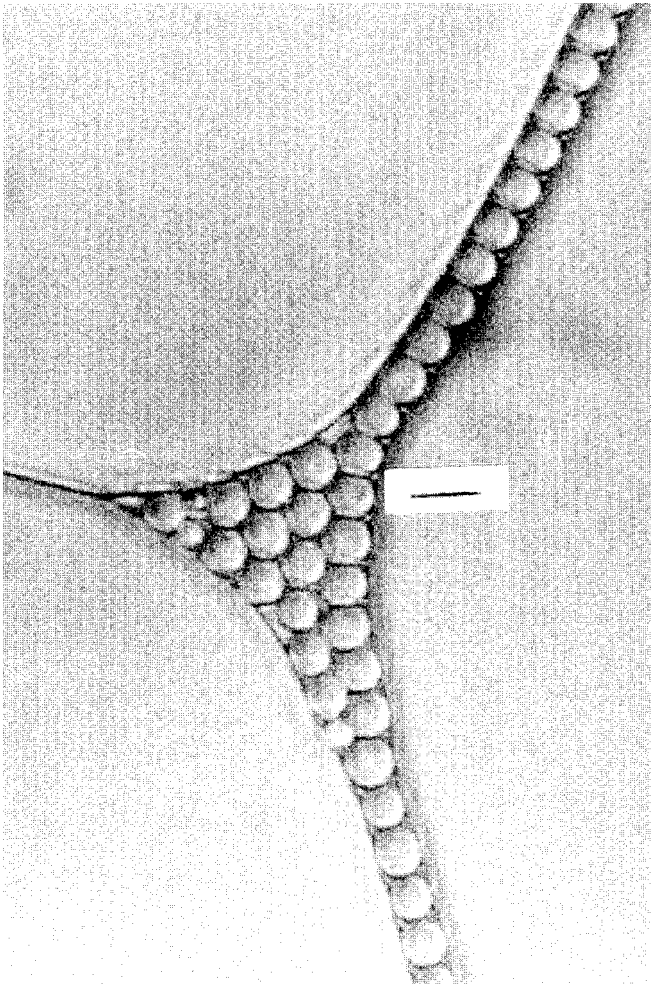

FIG. 32 The details of the hand-made emulsion tie. Scale bar is 10 μm.

lets are progressively transformed into pentane bubbles while shearing the emulsion sample. The number of bubbles progressively increases following the sequence of pictures (from Figures 33a to 33c) until a foam with a rather complicated fractal-like structure is obtained (Figure 33c). It is actually difficult to understand the structure of the *corridor* linking the round-shape satellites. Amazing structures can indeed be created with shearing polydisperse emulsions!

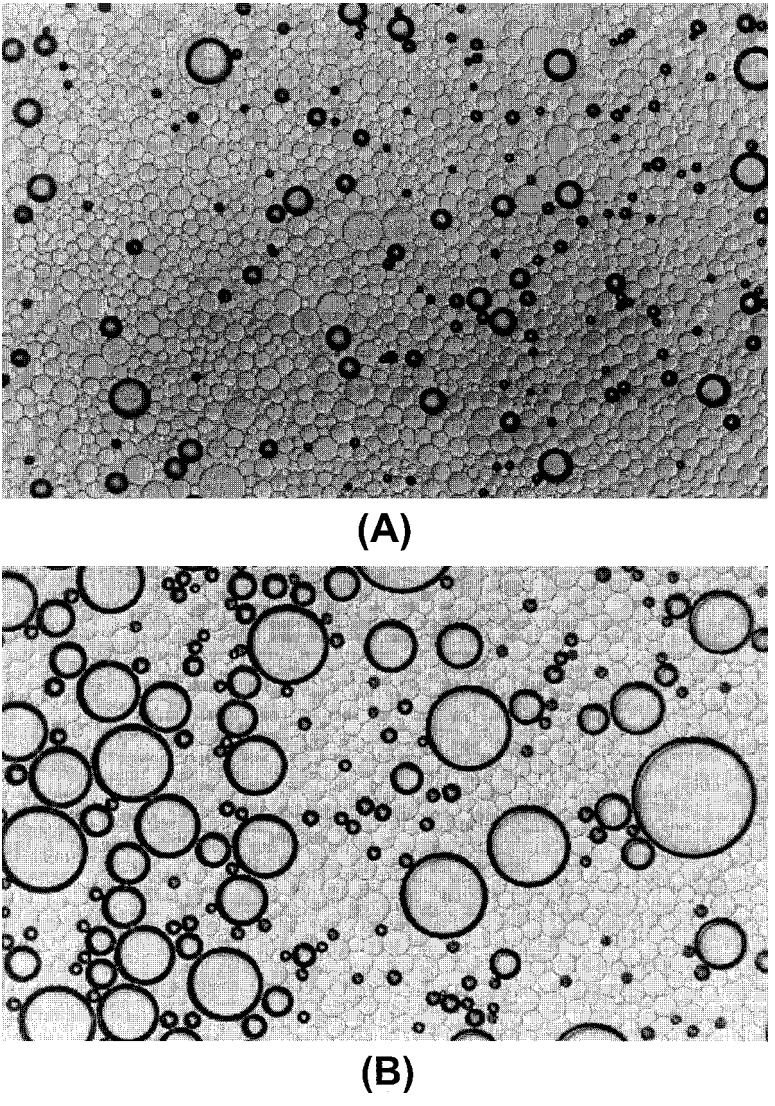

FIG. 33 Pentane-in-water dispersions stabilized by an amphiphilic polyelectrolyte: from the emulsion to the foam. (a) Pentane droplets dispersed in water (emulsion) coexisting with a few bubbles (foam). (b) While shearing the sample, an increasing number of droplets are transformed into bubbles. (c) Fractal foam.

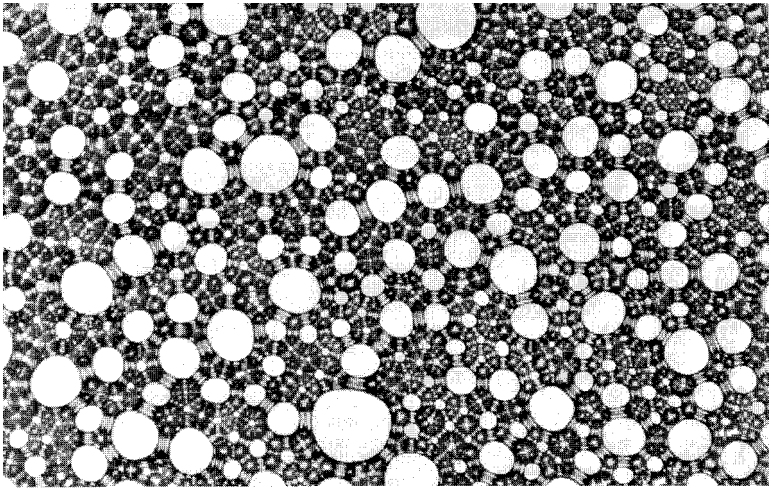

(C)

FIG. 33 *Continued*

REFERENCES

1. Sjoblom J, ed. Emulsions and Emulsion Stability. Vol. 61. Surfactant Science Series. New York: Marcel Dekker, 1996.
2. Becher P, ed. Encyclopedia of Emulsion Technology: Basic Theory. Vol. 1. New York: Marcel Dekker, 1983.
3. Becher P, ed. Encyclopedia of Emulsion Technology: Applications. Vol. 2. New York: Marcel Dekker, 1985.
4. Becher P, ed. Encyclopedia of Emulsion Technology: Basic Theory, Measurements, Applications. Vol. 3. New York: Marcel Dekker, 1988.
5. Kaufman RJ. Clinical development of perfluorocarbon based emulsions as red cells substitutes. In: Ref. 1:343–367.
6. Fukui H, Akiyoshi K, Sunamoto J. O/W emulsion of α-linolenic acid stabilized with hydrophobized polysaccharide. Its effect on the growth of human colon cancer cells. J Biomater Sci Polym Edn 1996; 7:829–838.
7. Fukui H, Akiyoshi K, Sato S, Sunamoto J, Yamaguchi S, Numata M. Anticancer activity of polyunsaturated fatty acid emulsion stabilized by hydrophobized polysaccharide. J Bioactive Compatible Polym 1993; 8:305–316.
8. Ciullo PA, Braun DB. Clay/carbomer mixture enhances emulsion stability. Cosmetics Toiletries 1991; 106:89–95.
9. Lochhead RY, Hemker WJ, Castaneda JY. Hair care gels. Cosmetics Toiletries 1987; 102:89–100.
10. Lochhead RY, Hemker WJ, Castaneda JY, Garlen D. Novel cosmetic emulsions. Cosmetics Toiletries 1986; 101:125–138.

11. Lochhead RY, Hemker WJ, Castaneda JY. Hydrophobically modified carbopol resins. A new route to easily prepared, storage stable, cosmetic lotions that break upon contact with skin. Soap/Cosmetics/Chemical Specialties 1987; May:28–33 and 84–85.
12. Dahms G. Viscosity regulation by surfactants. International J Cosmetic Sci 1991; 13:43–50.
13. Tamburic S, Vuleta G, Simovic S, Milic J. Rheological evaluation of O/W cream bases containing polymeric emulsifiers. SOFW J 1998; 124:204–209.
14. Simovic S, Milic-Askrabic J, Vuleta G, Ibric S, Stupar M. The influence of processing variables on performance of O/W emulsion gels based on polymeric emulsifier (Pemulen ®TR-2NF). International J Cosmetic Sci 1999; 21: 119–125.
15. Neumann P, Tiefensee K. A new liquid thickener for all kind of cosmetic emulsions. SOFW J 1999; 125:8–10.
16. Hesp SAM, Woodhams RT. Asphalt polyolefin emulsion breakdown. Colloid Polym Sci 1991; 269:825–834.
17. Leal Calderon F, Biais J, Bibette J. Asphalt emulsions: flocculation induced by a cationic surfactant and application to size partitioning. Colloids Surfaces A: Physicochem Eng Aspects 1993; 74:303–309.
18. Sjoblom J, Foredal H, Skodvin T. Flocculation and coalescence in emulsions as studied by dielectric spectroscopy. In: Ref. 1:393–435.
19. Chen TY, Mohammed RA, Bailey AI, Luckham PF, Taylor SE. Dewatering of crude oil emulsions. 4. Emulsion resolution by the application of an electric field. Colloids Surfaces A: Physicochem Eng Aspects 1994; 83:273–284.
20. Borve KGN, Sjoblom J, Stenius P. Water in crude oil emulsions from the Norwegian continental shelf. 5. A comparative monolayer study of model polymers. Colloids Surf 1992; 63:241–251.
21. Mohammed RA, Bailey AI, Luckham PF, Taylor SE. Dewatering of crude oil emulsions. 3. Emulsion resolution by chemicals means. Colloids Surfaces A: Physicochem Eng Aspects 1994; 83:261–271.
22. Urdhal O, Sjoblom J. Water in crude oil emulsions from the Norwegian continental shelf. A stabilization and destabilization study. J Dispersion Sci and Technol 1995; 16:557–574.
23. Fordedal H, Sjoblom J. Percolation behavior in W/O emulsions stabilized by interfacially active fractions from crude oils in high external electric fields. J Colloid Interface Sci 1996; 181:589–594.
24. Fordedal H, Midttun O, Sjoblom J, Kvalheim OM, Schildberg Y, Volle JL. A multivariate screening analysis of W/O emulsions in high external electric fields as studied by means of dielectric time domain spectroscopy. II. Model emulsions stabilized by interfacially active fractions from crude oils. J. Colloid Interface Sci 1996; 182:117–125.
25. Mason SL, May K, Hartland S. Drop size and concentration profile determination in petroleum emulsion separation. Colloids Surfaces A: Physicochem Eng Aspects 1995; 96:85–92.
26. Kim YH, Nikolov AD, Wasan DT, Diaz-Araumzo H, Shetty CS. Demulsification of water in crude oil emulsions: effects of film tension, elasticity, dif-

fusivity and interfacial activity of demulsifier individual components and their blends. J Dispersion Sci Technol 1996; 17:33–53.
27. Bhardwaj A, Hartland S. Kinetics of coalescence of water droplets in water in crude oil emulsions. J Dispersion Sci and Technol 1994; 15:133–146.
28. Miller DJ, Bohm R. Optical studies of coalescence in crude oil emulsions. J Petroleum Sci Eng 1993; 9:1–8.
29. Yan N, Masliyah JH. Characterization and demulsification of solids—stabilized oil in water emulsions. Part 1: Partitioning of clay particles and preparation of emulsions. Colloids Surfaces A: Physicochem Eng Aspects 1995; 96:229–242.
30. Yan N, Masliyah JH. Characterization and demulsification of solids—stabilized oil in water emulsions. Part 2: Demulsification by the addition of fresh oil. Colloids Surfaces A: Physicochem Eng Aspects 1995; 96:243–252.
31. Yan N, Masliyah JH. Demulsification of solids—stabilized oil in water emulsions. Colloids Surfaces A: Physicochem Eng Aspects 1996; 117:15–25.
32. Ahmed NS, Nassar AM, Zaki NN, Gharieb HK. Stability and rheology of heavy crude oil in water emulsions stabilized by an anionic–nonionic surfactant mixture. Petroleum Sci Technol 1999; 17:553–576.
33. Zaki NN. Surfactant stabilized crude oil in water emulsions for pipeline transportation of viscous crude oils. Colloids Surfaces A: Physicochem Eng Aspects 1997; 125:19–25.
34. Dalgleish DG. Food emulsions. In: Ref. 1:287–325.
35. Dickinson E. Mixed proteinaceous emulsifiers: review of competitive protein adsorption and the relationship to food colloid stabilization. Food Hydrocolloids 1986; 1:3–23.
36. Barylko-Pikielna N, Martin A, Mela DJ. Perception of taste and viscosity of oil in water and water in oil emulsions. J Food Sci 1994; 59:1318–1321.
37. Dickinson E, Golding M. Influence of alcohol on stability of oil in water emulsions containing sodium caseinate. J Colloid Interface Sci 1998; 197: 133–141.
38. Franco JM, Guerrero A, Gallegos C. Rheology and processing of salad dressing emulsions. Rheol Acta 1995; 34:513–524.
39. Bergenstahl B, Ostberg G. Alkyd emulsion: instability and drying properties. In: Ref. 1: 327–341.
40. Kahlweit M. How to prepare microemulsions at prescribed temperature, oil, and brine. J Phys Chem 1995; 99:1281–1284.
41. Bellocq AM. Flexible surfactant films: phase behavior, structure, and applications. In: Ref. 1:181–236.
42. Overbeek JThF. Microemulsions, a field at the border between lyophobic and lyophilic colloids. Faraday Discuss Chem Soc 1978; 65:7–19.
43. Ruckenstein E, Chi JC. Stability of microemulsions. J Chem Soc Faraday Trans 1975; 71:1690–1707.
44. Tambe DE, Sharma MM. Factors controlling the stability of colloid-stabilized emulsions. II. A model for the rheological properties of colloid-laden interfaces. J Colloid Interface Sci 1994; 162:1–10.
45. Tadros TF, Vincent B. Emulsion stability. In: Ref. 2:129–285.

46. Schulman JH, Leja J. Control of contact angles at the oil–water–solid interfaces. Trans. Faraday Soc 1954; 50:598–605.
47. Velev OD, Gurkov TD, Chakarova SvK, Dimitrova BI, Ivanov IB, Borwankar RP. Experimental investigations on model emulsion systems stabilized with nonionic surfactant blends. Colloids Surfaces A: Physicochem Eng Aspects 1994; 83:43–55.
48. Kunieda H, Yamagata M. Three phase behavior in a mixed nonionic surfactant system. Colloid Polym Sci 1993; 271:997–1004.
49. Rosen MJ, Gao T, Nakatsuji Y, Masuyama A. Synergism in binary mixtures of surfactants. 12. Mixtures containing surfactants with two hydrophilic and two or three hydrophobic groups. Colloids Surfaces A: Physicochem Eng Aspects 1994; 88:1–11.
50. Noshay A, Mc Grath JE. Block Copolymers: Overview and Critical Survey. New York: Academic Press, 1977.
51. Ceresa RJ. ed. Block and Graft Copolymerization. New York: John Wiley, 1973.
52. Piirma I. ed. Polymeric Surfactants. Vol. 42. Surfactant Science Series. New York: Marcel Dekker, 1992.
53. Locke CE, Paul DR. Graft copolymer modification of polyethylene–polystyrene blends. I. Graft preparation and characterization. J Appl Polym Sci 1973; 17:2597–2617.
54. Fayt R, Jerome R, Teyssie Ph. Molecular design of multicomponent polymer systems. 13. Control of the morphology of PE/PS blends by block copolymers. Makromol Chem 1986; 187:837–852.
55. Paul DR, Newman S. Polymer Blends. Vol. 2. New York: Academic Press, 1978.
56. Fayt R, Jerome R, Teyssie Ph. Molecular design of multicomponent polymer systems. XIV. Control of the mechanical properties of PE/PS blends by block copolymers. J Polym Sci Polym Phys Ed 1989; 27:775–793.
57. Liang H, Favis BD, Yu YS, Eisenberg A. Correlation between the interfacial tension and dispersed phase morphology in interfacially modified blends of LLDPE and PVC. Macromolecules 1999; 32:1637–1642.
58. Kim HC, Nam KH, Jo WH. The effect of a styrene-methyl methacrylate block copolymer on the morphological, rheological and mechanical properties of poly(2-6-dimethyl-1,4-phenylene ether) (PPE) and poly(hydroxyether of bisphenol A) (phenoxy) blends. Polymer 1993; 34:4043–4051.
59. Harrats C, Blacher S, Fayt R, Jerome R, Teyssie Ph. Molecular design of multicomponent polymer systems. XIX. Stability and cocontinuous phase morphologies in low density polyethylene/polystyrene blends emulsified by block copolymers. J Polymer Sci: Part B: Polym Phys 1995; 33:801–811.
60. Adedeji A, Hudson SD, Jamieson AM. Effect of exothermic interfacial mixing on interfacial activity of a block copolymer. Macromolecules 1996; 29:2449–2456.
61. Riemann RE, Cantow HJ, Friedrich Chr. Interpretation of a new interface-governed relaxation process in compatibilized polymer blends. Macromolecules 1997; 30:5476–5484.

62. Perrin P, Prudhomme RE. SAXS measurements of interfacial thickness in amorphous polymer blends containing a diblock copolymer. Macromolecules 1994; 27:1852–1860.
63. Russell TP, Anastasiadis SH, Menelle A, Felcher GP, Satija SK. Segment density distribution of symetric diblock copolymers at the interface between two homopolymers as revealed by neutron reflectivity. Macromolecules 1991; 24:1575–1582.
64. Banaszak M, Whitmore MD. Mean field theory of the phase behavior of ternary block copolymer–homopolymer blends. Macromolecules 1992; 25: 249–260.
65. Leibler L. Theory of phase equilibria in mixtures of copolymers and homopolymers. 2. Interfaces near the consolute point. Macromolecules 1982; 15: 1283–1290.
66. Shull KR, Kramer EJ. Mean field theory of polymer interfaces in the presence of block copolymers. Macromolecules 1990; 23:4769–4779.
67. Leibler L. Emulsifying effects of block copolymers in incompatible polymer blends. Makromol Chem Macromol Symp 1988; 16:1–17.
68. Lyatskaya Y, Gersappe D, Balazs AC. Effect of copolymer architecture on the efficiency of compatibilizers. Macromolecules 1995; 28:6278–6283.
69. Napper DH. Polymeric Stabilization of Colloidal Dispersions. New York: Academic Press, 1983.
70. Sato T, Ruch R. Stabilization of Colloidal Dispersions by Polymer Adsorption. New York: Marcel Dekker, 1980.
71. Goddard ED, Vincent B, eds. Polymer Adsorption and Dispersion Stabilization. ACS Symposium Series. Washington DC, 1984.
72. Vincent B. The effect of adsorbed polymers on dispersion stability. Adv Colloid Interface Sci 1974; 4:193–277.
73. de Gennes PG. Scaling theory of polymer adsorption. J Phys (Paris) 1976; 37:1445–1452.
74. Milner ST. Strongly stretched polymer brushes. J Polym Sci: Part B: Polym Phys. 1994; 32:2743–2755.
75. Alexander S. Adsorption of chain molecules with a polar head, a scaling description. J Phys (Paris) 1977; 38:983–987.
76. Marques CM, Joanny JF. Adsorption of random copolymers. Macromolecules 1990; 23:268–276.
77. Cohen Stuart MA, Cosgrove T, Vincent B. Experimental aspects of polymer adsorption at solid/solution interfaces. Adv Colloid Interface Sci 1986; 24: 143–239.
78. de Gennes PG. Scaling Concepts in Polymer Physics. Ithaca, New York: Cornell University Press, 1979.
79. Poncet C, Tiberg F, Audebert R. Ellipsometric study of the adsorption of hydrophobically modified polyacrylates at hydrophobic surfaces. Langmuir 1998; 14:1697–1704.
80. Awan MA, Dimonie VL, Filippov LK, El-Aasser MS. Adsorption kinetics of amphiphatic polystyrene–block-polybutadiene onto silicone wafer and polystyrene planar surfaces. Langmuir 1997; 13:130–139.

81. Walbridge DJ. The design and synthesis of dispersants for dispersion polymerization in organic media. In: Barret KEJ, ed. Dispersion Polymerization in Organic Media. New York: John Wiley, 1975:45–114.
82. Dan N, Tirrell M. Diblock copolymer microemulsions. A scaling model. Macromolecules 1993; 26:637–642.
83. Noolandi J, Hong KM. Effect of block copolymers at a demixed homopolymer interface. Macromolecules 1984; 17:1531–1537.
84. Noolandi J. Homopolymer surfactant for immiscible homopolymer blends. Macromol Theory Simul 1994; 3:91–93.
85. Vilgis TA, Noolandi J. Theory of homopolymer–block copolymer blends: the search for a universal compatibilizer. Macromolecules 1990; 23:2941–2947.
86. Morita M, Kubo M, Matsumoto M. Interfacial properties and emulsification in systems of perfluoropolyether/nonfluorinated oil/partially fluorinated oligomeric and polymeric compounds. Colloids Surfaces A: Physicochem Eng Aspects 1996; 109:183–194.
87. Periard J, Riess G. Effet émulsifiant des copolymères séquencés polystyrene-polyméthacrylate de méthyle. Kolloid Z Z Polymere 1971; 248:877–882.
88. Periard J, Riess G, Neyer-Gomez MJ. Etude de copolymères séquencés de faible masse moléculaire utilisés comme agents émulsifiants du type huile dans huile. Associations en milieu solvant sélectif. European Polym J 1973; 9:687–696.
89. Periard J, Banderet A, Riess G. Emulsifying effect of block and graft copolymers—oil in oil emulsions. Polym Lett 1970; 8:109–114.
90. Cameron NR, Sherrington DC. Non aqueous high internal phase emulsions, preparation and stability. J Chem Soc Faraday Trans 1996; 92:1543–1547.
91. Molau GE. Heterogeneous polymer systems I. Polymeric oil in oil emulsion. J Polym Sci: Part A 1965; 3:1267–1278.
92. Garti N. Hydrocolloids as emulsifying agents for oil in water emulsions. J Dispersion Sci and Technol 1999; 20:327–355.
93. Garti N, Bisperink C. Double emulsions: progress and applications. Current Opinion Colloid Interface Sci 1998; 3:657–667.
94. Tadros TF, Taelman MC, Dederen JC. Multiple emulsions with polymeric surfactants. In: Grossiord JL, Seiller M, eds. Multiple Emulsions: Structure, Properties and Applications. Paris: Editions de Santé, 1998:117–137.
95. Breen PJ, Wasan DT, Kim YH, Nikolov AD, Shetty CS. Emulsions and emulsion stability. In: Ref. 1:237–285.
96. Taylor SE. Investigations into the electrical and coalescence behavior of water in crude oil emulsions in high voltage gradients. Colloids Surf 1988; 29:29–51.
97. Graham DE, Stockwell A, Thompson DG. Chemical demulsification of produced crude oil emulsions. Spec Publ Royal Soc Chem 1983; 45:73–91.
98. Sharma IC, Haque I, Srivastava SN. Chemical demulsification of natural petroleum emulsions of Assam (India). Colloid Polym Sci 1982; 260:616–622.
99. Aveyard R, Binks BP, Fletcher PDI, Lu JR. The resolution of water in crude oil emulsions by the addition of low molar mass demulsifiers. J Colloid Interface Sci 1990; 139:128–138.

100. Monfreux N. Stabilisation d'émulsions par des polymères amphiphiles: contrôle de l'inversion de phase, caractérisations granulométriques et rhéologiques. Ph.D. dissertation, Université Pierre et Marie Curie, Paris, France, 1998.
101. Bancroft WD. The theory of emulsification. V. J Phys Chem 1913; 17:501–519.
102. Bancroft WD. The theory of emulsification. VI. J Phys Chem 1915; 19:275–309.
103. Griffin WC. Classification of surface-active agents by "HLB." J Soc Cosmet Chem 1949; 1:311–326.
104. Griffin WC. Calculation of HLB values of non-ionic surfactants. J Soc Cosmet Chem 1954; 5:249–256.
105. Davies JT, Rideal EK. Interfacial Phenomena. New York: Academic, 1963.
106. Davies JT. A quantitative kinetic theory of emulsion type. I. Physical chemistry of the emulsifying effect. Proc 2nd Int Cong Surf Activity 1957; 1:417–421.
107. Davies JT. A quantitative kinetic theory of emulsion type. II. Hydrodynamic factors. Proc 3rd Int Congr Surf Activity 1960; 2:585–594.
108. Shinoda K, Friberg S. Emulsions and Solubilization. New York: John Wiley, 1986.
109. Shinoda K, Saito H. The effect of temperature on the phase equilibria and the type of dispersions of ternary system composed of water, cyclohexane, and nonionic surfactant. J Colloid Interface Sci 1968; 26:70–74.
110. Shinoda K, Saito H. The stability of O/W type emulsions as function of temperature and the HLB of emulsifiers: the emulsification by PIT method. J Colloid Interface Sci 1969; 30:258–263.
111. Saito H, Shinoda K. The stability of W/O type emulsions as a function of temperature and of the hydrophilic chain length of the emulsifier. J Colloid Interface Sci 1970; 32:647–651.
112. Kahlweit M, Strey R. Phase behavior of quinary systems: tracing the three phase body. J Phys Chem 1987; 91:1553–1557.
113. Kahlweit M, Lessner E, Strey R. Influence of the properties of the oil and the surfactant on the phase behavior of systems of the type H_2O–oil–nonionic surfactant. J Phys Chem 1983; 87:5032–5040.
114. Leaver MS, Olsson U, Wennerstrom H, Strey R, Wurz U. Phase behavior and structure in a nonionic surfactant–oil–water mixture. J Chem Soc Faraday Trans 1995; 91:4269–4274.
115. Strey R. Microemulsion microstructure and interfacial curvature. Colloid Polym Sci 1994; 272:1005–1019.
116. Lehnert S, Tarabishi H, Leuenberger H. Investigation of thermal phase inversion in emulsions. Colloids Surfaces A: Physicochem Eng Aspects 1994; 91:227–235.
117. Kunieda H, Friberg S. Critical phenomena in a surfactant/water/oil system. Basic study on the correlation between solubilization, microemulsion, and ultralow interfacial tensions. Bull Chem Soc Jpn 1981; 54:1010–1014.

118. Winsor PA. Hydrotropy, solubilization and related emulsification processes. Part I. Trans Faraday Soc 1948; 44:376–398.
119. Winsor PA. Solvent Properties of Amphiphilic Compounds. London: Butterworths, 1954.
120. Shinoda K, Arai H. The correlation between phase inversion temperature in emulsion and cloud point in solution of nonionic emulsifier. J Phys Chem 1964; 68:3485–3490.
121. Shinoda K, Takeda H. The effect of added salts in water on the hydrophile–lipophile balance of nonionic surfactants: the effect of added salts on the phase inversion temperature of emulsions. J Colloid Interface Sci 1970; 32: 642–646.
122. Kahlweit M, Strey R, Busse G. Weakly to strong structured mixtures. Phys Rev E 1993; 47:4197–4209.
123. Shinoda K, Kunieda H, Arai T, Saijo H. Principles of attaining very large solubilization (microemulsion): inclusive understanding of the solubilization of oil and water in aqueous and hydrocarbon media. J Phys Chem 1984; 88: 5126–5129.
124. Aveyard R, Binks BP, Mead J. Interfacial tension minima in oil–water–surfactant systems. Effect of alkane chain length and presence of *n*-alkanols in systems containing Aerosol OT. J Chem Soc Faraday Trans 1986; 82:1755–1770.
125. Aveyard R, Binks BP, Fletcher PDI, Ye X. Coalescence lifetimes of oil and water drops at the planar oil–water interface and their relation to emulsion phase inversion. Progr Colloid Polym Sci 1992; 89:114–117.
126. Binks BP. Emulsion type below and above the cmc in AOT microemulsion systems. Colloids Surfaces A: Physicochem Eng Aspects 1993; 71:167–172.
127. Ghosh O, Miller CA. Liquid crystalline and microemulsion phase behavior in alcohol-free aerosol-OT/oil/brine systems. J Phys Chem 1987; 91:4528–4535.
128. Shinoda K, Kunieda H. The effect of salt concentration, temperature and additives on the solvent property of aerosol-OT solutions. J Colloid Interface Sci 1987; 118:586–589.
129. Kellay H, Binks BP, Hendrikx Y, Lee LT, Meunier J. Properties of surfactant monolayers in relation to microemulsion phase behavior. Adv Colloid Interface Sci 1994; 49:85–112.
130. Salager JL, Loaiza-Maldonado I, Minana-Perez M, Silva F. Surfactant–oil–water systems near the affinity inversion. Part I: Relationship between equilibrium phase behavior and emulsion type and stability. J Dispersion Sci and Technol 1982; 3:279–292.
131. Salager JL, Minana-Perez M, Perez-Sanchez M, Ramirez-Gouveia M, Rojas CI. Surfactant–oil–water systems near the affinity inversion. Part III: The two kinds of emulsion inversion. J Dispersion Sci and Technol 1983; 4:313–329.
132. Benett KE, Phelps CHK, Davis HT, Scriven LE. Microemulsion phase behavior—observations, thermodynamic essentials, mathematical simulation. Soc Petroleum Eng J 1981; 21:747–762.

133. Baldauf LM, Schechter RS, Wade WH, Graciaa A. The relationship between surfactant phase behavior and the creaming and coalescence of macroemulsions. J Colloid Interface Sci 1982; 85:187–197.
134. Salager JL. Phase transformation and emulsion inversion on the basis of catastrophe theory. In: Ref. 4:79–134.
135. Harkins WD, Davies ECH, Clark GL. The orientation of molecules in the surfaces of liquids, the energy relations at surfaces, solubility, adsorption, emulsification, molecular association, and the effect of acids and bases on interfacial tension. (Surface energy VI.) J Am Chem Soc 1917; 39:541–596.
136. Langmuir I. The constitution and fundamental properties of solids and liquids. II. Liquids. J Am Chem Soc 1917; 39:1848–1906.
137. Israelachvili J. The science and application of emulsions—an overview. Colloids Surfaces A: Physicochem Eng Aspects 1994; 91:1–8.
138. Sutheim GM. Introduction to Emulsions. Brooklyn, NY: Chemical, 1947.
139. Helfrich W. Elastic properties of lipid bilayers: theory and possible experiments. Z Naturforsch 1973; 28c:693–703.
140. Kabalnov A, Wennerström H. Macroemulsion stability: the oriented wedge theory revisited. Langmuir 1996; 12:276–292.
141. Kabalnov A, Weers J. Macremulsion stability within the Winsor III region: theory versus experiment. Langmuir 1996; 12:1931–1935.
142. Kabalnov A, Tarara T, Arlauskas R, Weers J. Phospholipids as emulsion stabilizers. 2. Phase behavior versus emulsion stability. J Colloid Interface Sci 1996; 184:227–235.
143. Riess G, Nervo J, Rogez D. Emulsifying properties of block copolymers. Oil–water emulsions and microemulsions. Polym Eng Sci 1977; 17:634–638.
144. Marti S, Nervo J, Riess G. Emulsions eau–huile préparées à l'aide de copolymères séquencés poly(styrène-b-oxyde d'éthylène): étude de l'inversion de phase. Progr Colloid Polym Sci 1975; 58:114–120.
145. Nervo J, Marti S, Riess G. Emulsions eau–huile préparées à l'aide de copolymères séquencés poly(styrène-b-oxyde d'éthylène): influence de la structure du copolymère. CR Acad Sci Paris 1974; 279:891–894.
146. Ba-Gia H, Jerome R, Teyssie Ph. Star-shaped block copolymers. I. Synthesis of new $A(B)_2$ star-shaped block copolymers based on vinyl or diene hydrocarbons (A) and oxirane (B). J Polym Sci Polym Chem Ed 1980; 18:3483–3498.
147. Ba-Gia H, Jerome R, Teyssie Ph. Star-shaped block copolymers. IV. Emulsifying activity in the water–oil emulsions. J Appl Polym Sci 1981; 26:343–351.
148. Berlinova IV, Amzil A, Tsvetkova S, Panayotov IM. Amphiphilic graft copolymers with poly(oxyethylene)side chains: synthesis via activated ester intermediates—properties. J Polym Sci: Part A: Polym Chem 1994; 32:1523–1530.
149. Marie P, Herrenschmidt YL, Gallot Y. Etude du pouvoir émulsifiant des copolymères séquencés polystyrène/chlorure de polyvinyl-2-pyridinium et polyisprène/chlorure de polyvinyl-2-pyridinium. Makromol Chem 1976; 177: 2773–2780.

150. Mathur AM, Drescher B, Scranton AB, Klier J. Polymeric emulsifiers based on reversible formation of hydrophobic units. Nature 1998; 392:367–370.
151. Perrin P, Monfreux N, Dufour AL, Lafuma F. Highly hydrophobically modified polyelectrolytes: field variables to control emulsion type. Colloid Polym Sci 1998; 276:945–948.
152. Perrin P, Monfreux N, Lafuma F. Highly hydrophobically modified polyelectrolytes stabilizing macroemulsions: relationship between copolymer structure and emulsion type. Colloid Polym Sci 1999; 277:89–94.
153. Hesselink FTh, Vrij A, Overbeek JThG. On the theory of the stabilization of dispersions by adsorbed macromolecules. II. Interaction between two flat particles. J Phys Chem 1971; 75:2094–2103.
154. March GC, Napper DH. The thermodynamic limit to the flocculation stability of sterically stabilized emulsions. J Colloid Interface Sci 1977; 61:383–387.
155. Derjaguin BV, Landau L. Acta Physicochimica 1941; 14:633.
156. Verwey E, Overbeek JThG. Theory of the Stability of Lyophobic Colloids: The Interaction of Soil Particles Having an Electric Double Layer. Amsterdam: Elsevier, 1948.
157. Heller W, Pugh TL. ''Steric protection'' of hydrophobic colloidal particles by adsorption of flexible macromolecules. J Chem Phys 1954; 22:1778–1778.
158. Biswas B, Haydon DA. The coalescence of droplets stabilized by viscoelastic adsorbed films. Kolloid Z Z Polymere 1962; 185:31–38.
159. Biswas B, Haydon DA. The effect of certain small molecules on the elasticity of adsorbed serum albumin films. Kolloid Z Z Polymere 1962; 186:57–61.
160. Biswas B, Haydon DA. The rheology of some interfacial adsorbed films of macromolecules. I. Elastic and creep phenomena. Proc Royal Soc London Ser A: Mathematical Phys Sci 1963; A271:296–315.
161. Biswas B, Haydon DA. The rheology of some interfacial adsorbed films of macromolecules. II. Stress relaxation phenomena. Proc Royal Soc London Ser A: Mathematical Phys Sci 1963; A271:317–323.
162. Nielsen LE, Wall R, Adam G. Coalescence of liquid drops at oil–water interfaces. J Colloid Sci 1958; 13:441–458.
163. Malhotra AK, Wasan DT. Interfacial rheological properties of adsorbed surfactant films with applications to emulsion and foam stability. In: Ivanov IB, ed. Thin Liquid Films, Fundamentals and Applications. Vol. 29. Surfactant Science Series. New York: Marcel Dekker, 1988:829–890.
164. Kralchevsky PA, Danov KD, Ivanov IB. Thin liquid film physics. In: Prud'homme RK, Kahn SA, eds. Foams: Theory, Measurements, and Applications. Vol. 57. Surfactant Science Series. New York: Marcel Dekker, 1996: 1–98.
165. Ossenbach-Sauter M, Riess G. Propriétés émulsifiantes des copolymères séquencés. Emulsions du type eau dans eau. CR Acad Sci Paris 1976; 283:269–272.
166. Pons R, Rossi P, Tadros ThF. Investigation of the interaction between emulsions and suspensions (suspoemulsions) using viscoelastic measurements. J Phys Chem 1995; 99:12624–12630.

167. Jumaa M, Muller BW. The stabilization of parental fat emulsion using nonionic ABA copolymer surfactant. International J Pharm 1998; 174:29–37.
168. Law TK, Florence AT, Whateley TL. Stabilization of emulsions by interfacial polymerization of poloxamer surfactant derivatives. Colloid Polym Sci 1986; 264:167–170.
169. Szymanowsky J, Myszkowski J, Pietrzak E, Prochaska K. Stability of model emulsions in the presence of ethylene oxide and α-butylene oxide block copolymers of type EBE. Tenside Detergents 1983; 20:23–27.
170. Lievens SS, Goethals EJ. Poly(methyl vinyl ether-b-octadecyl vinyl ether): a new nonionic surfactant. Polym Int 1996; 41:437–441.
171. Sela Y, Magdassi S, Garti N. Newly design polysiloxane-graft-poly-(oxyethylene) copolymeric surfactants: preparation, surface activity and emulsification properties. Colloid Polym Sci 1994; 272:684–691.
172. Garti N, Rossano A, Avni Y. Graft copolymers as emulsifiers. Part I: Grafted polyethylene glycol on polymethyl methacrylate. J Dispersion Sci and Technol 1993; 14:47–70.
173. Xie HQ, Wu XD, Guo JS. Synthesis and properties of two kinds of amphiphilic graft copolymers with well-defined structure. J Appl Polym Sci 1994; 54:1079–1086.
174. Bo G, Wesslen B, Wesslen KB. Amphiphilic comb-shaped polymers from poly(ethylene glycol) macromonomers. J Polym Sci: Part A: Polym Chem 1992; 30:1799–1808.
175. Xie HQ, Xie D, Liu Y. Synthesis and properties of unsaturated polyoxyethylene and its graft copolymers with styrene. J Appl Polym Sci 1998; 70:2417–2425.
176. Cardenas-Valera AE, Bailey AI. Graft copolymers as stabilizers for oil in water emulsions. Part 2. Preparation of the emulsions and the factors affecting their stability. Colloids Surfaces A: Physicochem Eng Aspects 1995; 97:1–12.
177. Cardenas-Valera AE, Bailey AI, Doroszkowski A. Graft copolymers as stabilizers for oil in water emulsions. Part 1. Synthesis of the copolymers and their behavior as monolayer spread at the air–water and oil–water interfaces. Colloids Surfaces A: Physicochem Eng Aspects 1995; 96:53–67.
178. Mueth DM, Crocker JC, Esipov SE, Grier DG. Origin of stratification in creaming emulsions. Phys Rev Lett 1996; 77:578–581.
179. Selb J, Delmas G, Marie P, Gallot Y. Copolymères greffés polyvinyl-2-pyridinium sur polydiphenylpropene: synthèse, caractérisation, pouvoir émulsifiant. CR Acad Sci Paris 1976; 282:1017–1020.
180. Ishizu K, Minematsu S. Morphology of emulsion systems stabilized by binary graft copolymer blends composed of polyelectrolyte trunks. Makromol Chem Rapid Commun 1989; 10:527–531.
181. Reeb R, Riess G. Etude du pouvoir émulsifiant de copolymères séquencés poly(styrène-b-(styrène-alt-anhydride maleique)). CR Acad Sci Paris 1976; 283:663–666.
182. Lochhead RY, Davidson JA, Thomas GM. Poly(acrylic acid) thickeners. The importance of gel microrheology and evaluation of hydrophobically modified

derivatives as emulsifiers. In: Glass JE, ed. Polymers in aqueous media: performance through association. ACS Advances in Chem. Series 223, 1989: 113–147.
183. Lochhead RY. Electrostatic stabilization of oil in water emulsions by hydrophobically modified poly(acrylic acid) thickeners. In: Schulz DN, Glass JE, eds. Polymers as Rheology Modifiers. ACS Symposium Series 462, 1991: 101–120.
184. Rulinson CJ, Lochhead RY. The effect of pH and electrolyte concentration on the stability of polymerically stabilized emulsion systems. ACS Polym Prepr Div Polym Chem 1992; 33:280–281.
185. Rulinson CJ, Lochhead RY, Bui HS, Pierce TD. Investigation of the mechanism of emulsification by hydrophobically modified hydrogels. VI. Dilute systems. ACS Polym Prepr Div Polym Chem 1993; 34:863–864.
186. Lochhead RY, Rulinson CJ. An investigation of the mechanism by which hydrophobically modified hydrophilic polymers act as primary emulsifiers for oil in water emulsions. 1. Poly(acrylic acids) and hydroxyethyl celluloses. Colloids Surfaces A: Physicochem Eng Aspects 1994; 88:27–32.
187. Brisaert M, Plaizier-Vercammen. Investigation of the emulsifying properties of Pemulen TR 1, an acrylic acid alkyl methacrylate copolymer. STP Pharma Sciences 1997; 7:438–444.
188. Perrin P, Lafuma F, Audebert R. Emulsions stabilized with hydrophobically modified poly(acrylic acid). Progr Colloid Polym Sci 1997; 105:228–238.
189. Perrin P, Lafuma F. Low hydrophobically modified poly(acrylic acid) stabilizing macroemulsions: relationship between copolymer structure and emulsion properties. J Colloid Interface Sci 1998; 197:317–326.
190. Wang TK, Iliopoulos I, Audebert R. Aqueous solution behavior of hydrophobically modified poly(acrylic acid). In: Shalaby SW, McCormick C, Butler GB, eds. Water-Soluble Polymers: Synthesis, Solution Properties, and Applications. ACS Symposium Series 467, 1991:218–231.
191. Millet F, Nedyalkov M, Renard B, Perrin P, Lafuma F, Benattar JJ. Adsorption of hydrophobically modified poly(acrylic acid) sodium salt at the air/water interface by combined surface tension and x-ray reflectivity measurements. Langmuir 1999; 15:2112–2119.
192. Cameron NR, Sherrington DC. High internal phase emulsions (HIPEs)—Structure, properties and use in polymer preparation. Adv Polym Sci 1996; 126:165–214.
193. Kunieda H, John AC, Pons R, Solans C. Highly concentrated emulsions (gel emulsions): macro self-organizing structures. In: Esumi K, Ueno M, eds. Structure–Performance Relationships in Surfactants. Vol. 70. Surfactant Science Series. New York: Marcel Dekker, 1997: 359–393.
194. Taylor P. The effect of an anionic surfactant on the rheology and stability of high volume fraction O/W emulsion stabilized by PVA. Coll Polym Sci 1996; 274:1061–1071.
195. Pons R, Solans C, Tadros ThF. Rheological behavior of highly concentrated oil in water (O/W) emulsions. Langmuir 1995; 11:1966–1971.

196. Pons R, Solans C, Stébé MJ, Erra P, Ravey JC. Stability and rheological properties of gel emulsions. Progr Colloid Polym Sci 1992; 89:110–113.
197. Aronson MP, Petko MF. Highly concentrated water in oil emulsions: influence of electrolyte on their properties and stability. J Colloid Interface Sci 1993; 159:134–149.
198. Kunieda H, Yano N, Solans C. The stability of gel-emulsions in a water/nonionic surfactant/oil system. Colloids and Surf 1989; 36:313–322.
199. Ganguly S, Krishna Mohan V, Jyothi Bhasu VC, Mathews E, Adiseshaiah KS, Kumar AS. Surfactant–electrolyte interactions in concentrated water in oil emulsions. FT-IR spectroscopic and low-temperature differential scanning calorimetric studies. Colloids Surf 1992; 65:243–256.
200. Princen HM. Rheology of foams and highly concentrated emulsions. I. Elastic properties and yield stress of a cylindrical model system. J Colloid Interface Sci 1983; 91:160–175.
201. Princen HM, Kiss AD. Rheology of foams and highly concentrated emulsions. III. Static shear modulus. J Colloid Interface Sci 1986; 112:427–437.
202. Perrin P, Monfreux N, Thierry F, Lafuma F, Lequeux F. Concentrated direct and inverse macroemulsions stabilized by amphiphilic polyelectrolytes. Proc ACS Div Polym Mater Sci Eng 1999; 81:492–494.
203. Chen HH, Ruckenstein E. Effect of the nature of the hydrophobic oil phase and surfactant in the formation of concentrated emulsions. J Colloid Interface Sci 1991; 145:260–269.
204. Bibette J. Depletion interactions and fractionated crystallization for polydisperse emulsion purification. J Colloid Interface Sci 1991; 147:474–478.
205. Yamano Y, Kagawa Y, Kim KH, Gohtani S. Stability and uniformity of oil droplets in preparation of O/W emulsion agar gel. Food Sci Technol Int 1996; 2:16–18.
206. Mason TG, Bibette J. Emulsification in viscoelastic media. Phys Rev Lett 1996; 77:3481–3484.
207. Lequeux F. Emulsion rheology. Current Opinion Colloid Interface Sci 1998; 3:408–411.
208. Imhof A, Pine D. Uniform macroporous ceramics and plastics by emulsion templating. Adv Mater 1998; 10:697–700.
209. Imhof A, Pine D. Ordered macroporous materials by emulsion templating. Nature 1997; 389:948–951.
210. Joannopoulos JD, Villeneuve PR, Fan S. Photonic crystals: putting a new twist on light. Nature 1997; 386:143–149.
211. Perrin P. Amphiphilic copolymers: a new route to prepare ordered monodisperse emulsions. Langmuir 1998; 14:5977–5979.
212. Pincus P. Colloid stabilization with grafted polyelectrolytes. Macromolecules 1991; 24:2912–2919.
213. de Gennes PG. Conformations of polymers attached to an interface. Macromolecules 1980; 13:1069–1075.
214. De Gennes PG. Polymer at an interface; simplified view. Adv Colloid Interface Sci 1987; 27:189–209.

215. Auroy P, Auvray L, Leger L. Characterisation of the brush regime for grafted polymer layers at the solid–liquid interface. Phys Rev Lett 1991; 66:719–722.
216. Auroy P, Auvray L, Leger L. Structures of end-grafted polymer layers: a small-angle neutron scattering study. Macromolecules 1991; 24:2523–2528.
217. Milner ST, Witten TA, Cates ME. A parabolic density profile for grafted polymers. Europhys Lett 1988; 5:413–418.
218. Halperin A. Collapse of grafted chains in poor solvents. J Phys France 1988; 49:547–550.
219. Zhulina EB, Borisov OV, Pryamitsyn VA, Birshtein TM. Coil-globule type transition in polymers. 1. Collapse of layers of grafted polymer chains. Macromolecules 1991; 24:140–149.
220. Wittmer J, Joanny JF. Charged diblock copolymers at interfaces. Macromolecules 1993; 26:2691–2697.
221. Guenoun P, Schlachli A, Sentenac D, Mays JW, Benattar JJ. Free-standing black films of polymers: a model of charged brushes in interaction. Phys Rev Lett 1995; 74:3628–3631.
222. Ahrens H, Förster S, Helm CA. Charged polymer brushes: counterion incorporation and scaling relations. Phys Rev Lett 1998; 81:4172–4175.
223. Zhulina EB, Borisov OV, Birshtein TM. Structure of grafted polyelectrolyte layer. J Phys II France 1992; 2:63–74.
224. Mir Y, Auroy P, Auvray L. Density profile of polyelectrolyte brushes. Phys Rev Lett 1995; 75:2863–2866.
225. Tran Y. Interfaces de polyélectrolyte greffé. Ph.D. dissertation, Université de Paris VI, Paris, France, 1998.
226. Sonin AA, Delsanti M, Guenoun P, Mays JW, Langevin D. Interactions between charged polymer brushes at liquid surfaces. Submitted.
227. Ross RS, Pincus P. The polyelectrolyte brush: poor solvent. Macromolecules 1992; 25:2177–2183.
228. Klein J, Luckham PF. Interactions between proteins and synthetic polypeptides adsorbed at solid–liquid interfaces. Colloids Surf 1984; 10:65–76.
229. Asnacios A, Espert A, Colin A, Langevin D. Structural forces in thin films made from polyelectrolyte solutions. Phys Rev Lett 1997; 78:4974–4977.
230. Klitzing Rv, Esperst A, Asnacios A, Hellweg T, Colin A, Langevin D. Forces in foam films containing polyelectrolyte and surfactant. Colloids Surfaces A: Physicochem Eng Aspects 1999; 149:131–140.
231. de Gennes PG, Pincus P, Velasco RM, Brochard F. Remarks on polyelectrolyte conformation. J Phys 1976; 37:1461–1473.
232. Essafi W. Structure des polyélectrolytes fortement chargés. Ph.D. dissertation, Université de Paris VI, Paris, France, 1996.
233. Petit F. Etude du comportement de polyélectrolytes associatifs en solution et caractérisation de leurs agrégats hydrophobes. Ph.D. dissertation, Université de Paris VI, Paris, France, 1996.
234. Odijk T. Possible scaling relations for semidilute polyelectrolyte solutions. Macromolecules 1979; 12:688–693.

235. Pfeuty P. Conformation des polyélectrolytes. Ordre dans les solutions de polyélectrolytes. J Phys Colloque C2 1978; 39:149–161.
236. Khokhlov AR, Khachaturian KA. On the theory of weakly charged polyelectrolytes. Polymer 1982; 23:1742–1750.
237. Châtellier X, Joanny JF. Adsorption of polyelectrolyte solutions on surfaces: a Debye–Hückel theory. J Phys II France 1996; 6:1669–1686.
238. Carignano MA, Dan N. Density inhomogeneities of highly charged polyelectrolyte solutions confined between uncharged and nonadsorbing walls. Langmuir 1998; 14:3475–3478.
239. Millet F, Perrin P, Benattar JJ. Vertical free-standing films of amphiphilic associating polyelectrolytes. Phys Rev E 1999; 60:2040–2050.
240. Millet F, Benbalagh R, Perrin P, Benattar JJ. Submitted.
241. Millet F. Films libres verticaux de polyélectrolytes amphiphiles. Ph.D. dissertation, Université de Paris VI, Paris, France, 1999.
242. Gilbert RG. Emulsion Polymerization: A Mechanistic Approach. Academic Press, New York, 1995.
243. Smith WV, Ewart RH. Kinetics of emulsion polymerization. J Chem Phys 1948; 16:592–599.
244. Piirma I. Polymeric surfactants as stabilizers in aqueous emulsion polymerization. In: Polymeric Surfactants, Surfactant Science Series. Vol. 42, New York: Marcel Dekker, 1992:127–164.
245. Riess G. Block copolymers as polymeric surfactants in latex and microlatex technology. Colloids Surf 1999; A153:99–110.
246. Roe CP. Emulsion polymerization with a surface-active polyelectrolyte as the sole emulsifier. J Colloid Interface Sci 1971; 37:93–101.
247. Kuo PL, Chen CJ. Functional polymers for colloidal applications. V. Novel behavior of polymeric emulsifiers in emulsion polymerization. J Polym Sci, Part A: Polym Chem 1993; 31:99–111.
248. Antonietti M, Weissenberger MC. Amphiphilic derivatives of poly(acrylic acid) as stabilizer in emulsion polymerization. Macromol Rapid Commun 1997; 18:295–302.
249. Lee DY, Kim JH. Emulsion polymerization using alkali-soluble random copolymer as a polymeric emulsifier. Am Chem Soc: Polym Prepr 1997; 38(2): 418–419.
250. Lee DY, Kim JH. Preparation of small-sized carboxylated latexes by emulsion polymerization using alkali-soluble random copolymers. J Appl Polym Sci 1998; 69:543–550.
251. Lee DY, Kim JH, Min TI. Role of alkali-soluble random copolymer in emulsion polymerization. Colloids Surf 1999; A153:89–97.
252. Kato S, Sato K, Maeda D, Nomura M. A kinetic investigation of styrene emulsion polymerization with surface active polyelectrolytes as the emulsifier. II: Effects of molecular weight and composition. Colloids Surf 1999; A153: 127–131.
253. Kato S, Noguchi J, Nomura M. Kinetics of emulsion polymerization of methyl methacrylate using poly(methyl methacrylate-*co*-methacrylic acid) as polymeric emulsifier. Polym Mat Sci Eng 1999; 80:552–553.

254. Piirma I. Polyelectrolytes, polyampholytes, hydrogels, and polymerizable surfactants. In: Polymeric Surfactants, Surfactant Science Series. Vol. 42, New York: Marcel Dekker, 1992:225–265.
255. Ceska GW. The effect of carboxylic monomers on surfactant-free emulsion copolymerization. J Appl Polym Sci 1974; 18:427–437.
256. Snuparek J. Particle coagulation at semicontinuous emulsion polymerization. I. Some factors affecting the process. J Appl Polym Sci 1979; 24:909–914.
257. Snuparek J. Particle coagulation at semicontinuous emulsion polymerization. II. Characterization of surface groups. J Appl Polym Sci 1979; 24:915–921.
258. Guillaume JL, Pichot C, Guillot J. Emulsifier-free emulsion copolymerization of styrene and butyl acrylate. II. Kinetic studies in the presence of ionogenic comonomers. J Polym Sci: Part A: Polym Chem 1988; 26:1937–1959.
259. Ganachaud F, Sauzedde F, Elaïssari A, Pichot C. Emulsifier-free emulsion copolymerization of styrene with two different amino-containing cationic monomers: I. Kinetic studies. J Appl Polym Sci 1997; 65:2315–2330.
260. Cochin D, Laschewsky A, Nallet F. Emulsion polymerization of styrene using conventional, polymerizable, and polymeric surfactants. A comparative study. Macromolecules 1997; 30:2278–2287.
261. Yang YJ, Engberts JBFN. Preparation and stability of polystyrene latexes using polysoaps as emulsifiers. Eur Polym J 1992; 8:881–886.
262. Evans R, Davison JB, Napper DH. The preparation of aqueous entropically stabilized latices. J Polym Sci: Polym Letters 1972; 10:449–453.
263. Cao T, Yin W, Webber SE. Poly(2-vinylnaphthalene-alt-maleic acid)-graft-polystyrene as a photoactive polymer micelle and stabilizer for polystyrene latexes. Macromolecules 1994; 27:7459–7464.
264. Rager T, Meyer WH, Wegner G, Winnik MA. Influence of chain length and salt concentration on block copolymer micellization. Macromolecules 1997; 30:4911–4919.
265. Matyjaszewski K. Controlled Radical Polymerization. ACS Symposium Series. Vol. 685. Washington, DC, 1998.
266. Piirma I. Synthesis of amphipathic polymeric material: block copolymers. In: Polymeric Surfactants, Surfactant Science Series. Vol. 42. New York: Marcel Dekker, 1992:17–34.
267. Urban D, Gerst M, Rossmanith P, Schuch H. Amphiphilic block copolymers as surfactants in emulsion polymerization. Polym Mat Sci Eng 1998; 79:440–441.
268. Liu T, Schuch H, Gerst M, Chu B. Laser light scattering study of microemulsion-like polymerization processes with block copolymers as dispersants. Macromolecules 1999; 32:6031–6042.
269. Rager T, Meyer WH, Wegner G, Mathauer K, Mächtle W, Schrof W, Urban D. Block copolymer micelles as seed in emulsion polymerization. Macromol Chem Phys 1999; 200:1681–1691.
270. Burguière C, Pascual S, Coutin B, Polton A, Tardi M, Charleux B, Matyjaszewski K, Vairon JP. Amphiphilic block copolymers prepared via controlled radical polymerization as surfactants for emulsion polymerization. Macromol Symp 2000; 150 (39).

271. Pascual S. Ph.D. Dissertation. Université Pierre et Marie Curie, Paris, France, 1999.
272. Müller H, Leube W, Tauer K, Förster S, Antonietti M. Polyelectrolyte block copolymers as effective stabilizers in emulsion polymerization. Macromolecules 1997; 30:2288–2293.
273. Leemans L, Fayt R, Teyssié Ph, de Jaeger NC. Poly(alkyl methacrylate-*b*-sulfonated glycidyl methacrylate). A new amphiphilic polymeric surfactant for the preparation and stabilization of polymer acrylic latices in aqueous medium. Macromolecules 1991; 24:5922–5925.
274. Bouix M, Gouzi J, Charleux B, Vairon JP, Guinot P. Synthesis of amphiphilic polyelectrolyte block copolymers using ''living'' radical polymerization. Application as stabilizers in emulsion polymerization. Macromol Rapid Commun 1998; 19:209–213.
275. Leemans L, Jérôme R, Teyssié Ph. Diffusive radical entry as the rate-determining step in amphiphilic block polyelectrolyte mediated emulsion polymerization. Macromolecules. 1998; 31:5565–5571.
276. Lieske A, Jaeger W. Synthesis and characterization of block copolymers containing cationic blocks. Macromol Chem Phys 1998; 199:255–260.

This Page Intentionally Left Blank

14

Polyelectrolyte–Surfactant Interactions at Solid–Liquid Interfaces Studied with Surface Force Techniques

PER M. CLAESSON and ANDRA DEDINAITE Royal Institute of Technology, and Institute for Surface Chemistry, Stockholm, Sweden

EVGENI POPTOSHEV Institute for Surface Chemistry, Stockholm, Sweden

I. INTRODUCTION

The association between polyelectrolytes and oppositely charged surfactants has been extensively studied, and many recent reviews and books covering different aspects can be found [1–7]. An overwhelming majority of the studies on the subject are concerned with association in bulk solution. One rationale for this is the importance of polyelectrolyte–surfactant systems as rheology modifiers [7,8], gelation agents [9], and solubilizers for sparingly soluble substances such as dyes [10,11], perfume, and pollutants [12,13]. The association between ionic surfactants and oppositely charged polyelectrolytes in bulk solution is primarily affected by electrostatic and hydrophobic forces [14–19]. However, the architecture of the polyelectrolyte, such as branching, cross-links, and chain stiffness, also influences the association behavior [20–22]. In particular, it is found that in bulk solution the initial binding of a charged surfactant to an oppositely charged polyelectrolyte is electrostatically driven. At a higher concentration a cooperative association takes place that also is driven by the hydrophobic interaction (mainly between the surfactant tails). The surfactant concentration at which this cooperative association step occurs, the critical association concentration, is lower than the critical micelle concentration. This is largely due to a difference in the change in counterion entropy following formations of free micelles and surfactant aggregates associated with polyelectrolytes [20,22]. The structures formed are sometimes characterized as micellelike structures

bound along the polyelectrolyte chain in a bead-and-necklace structure [18], or sometimes as ordered mesomorphous phases with quite complex topology [23–27]. When association between surfactants and hydrophobically modified polyelectrolytes are considered, it is often fruitful to regard the association as a formation of mixed micelles [28]. Already at very low concentrations the surfactant is incorporated in the hydrophobic microdomains formed by the hydrophobically modified polyelectrolyte. This uptake of surfactant is less cooperative than for polyelectrolytes without hydrophobic side chains [29], and the concept of a critical association concentration becomes less appropriate. Most studies have been performed at surfactant concentrations below the cmc of the surfactant. However, Dubin and coworkers have made important contributions to our understanding of polyelectrolyte surfactant association above the cmc [2,30–33].

Particles or macroscopic solid surfaces are present in most of the applications mentioned above. Hence it is important to know how polyelectrolytes and surfactants interact with each other at solid–liquid interfaces. Due to the slow equilibration in many polyelectrolyte–surfactant systems, particularly at interfaces, it is fruitful to distinguish between two situations. In the first case the polyelectrolyte is initially adsorbed at the solid–liquid interface and then the polyelectrolyte is removed from the solution before the surfactant is added. This mimics the situation in many cleaning applications. Most of the studies concerned with polyelectrolyte–surfactant interactions at solid–liquid interfaces belong to this category.

In many other situations, e.g., in a range of personal care and household care products, polyelectrolytes and surfactants are present in the formulation, which at a later stage is brought into contact with a surface. This may lead to adsorption of polyelectrolyte–surfactant aggregates that will change in nature upon rinsing. This process has been given much less attention in the scientific literature, at least partly because it is more complicated to study. Among the complications can be mentioned high viscosity, often turbid solutions that render optical techniques difficult to apply, and formation of insoluble complexes at some dilution ratios.

In this review we focus on polyelectrolyte–surfactant interactions at solid–liquid interfaces as studied with surface force measuring techniques. The last years have seen much progress in this area, and it is timely to recapitulate some main findings. It is, however, clear that in order to understand interfacial properties of polyelectrolyte–surfactant systems one needs to understand bulk association. Further, a multitude of experimental techniques needs to be applied. Recent advances have been made using ellipsometry [34,35], reflectometry [36,37], neutron reflectivity [38], and surface sensitive spectroscopic techniques [39,40]. It is also our belief that the

quartz crystal microbalance technique [41] will play an important role for future studies of polyelectrolyte–surfactant mixtures at interfaces.

II. MATERIALS AND METHODS

A. Polyelectrolytes

Most of the results presented in this review are obtained by mixing anionic surfactant and cationic polyelectrolyte. One cationic homopolyelectrolyte, PCMA, which is built of the charged monomer (2-acryloxyethyl)-trimethylammonium chloride, shown in Figure 1a, was used in several studies. A range of positively charged copolyelectrolytes with a charge density varying from 30% to 1%, depending on the ratio of uncharged acrylamide (AM) and positively charged segments, have also been employed. The cationic segments were either the same as in PCMA or (3-methacrylamidopropyl)-trimethylammonium chloride (MAPTAC) (Figure 1b). Finally, a cationic hydrophobically modified polyelectrolyte with a random distribution of hydrophobic dodecyl side chains referred to as 40 DT was used. The graft

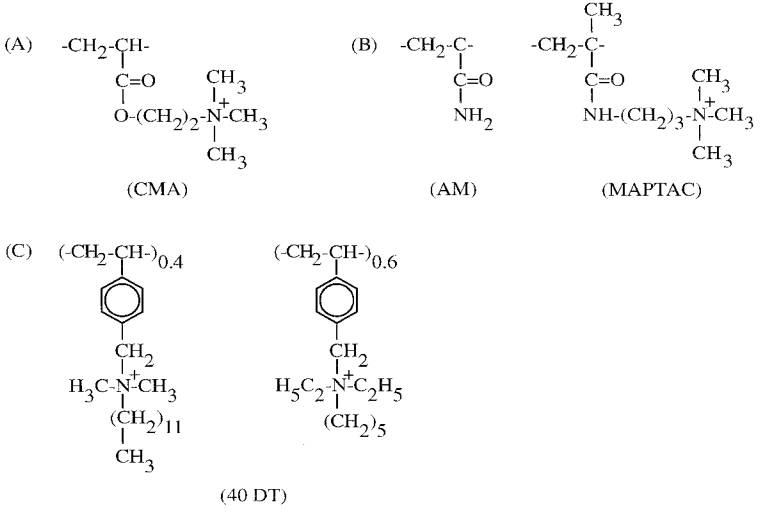

FIG. 1 (A) Monomer CMA, which is the building block of the 100% charged polyelectrolyte PCMA. (B) The chemical structure of the two types of segments making up the AM-MAPTAC polyelectrolytes of different charge density. (C) The chemical structure of the two types of segments making up the 40% hydrophobically modified polyelectrolyte 40 DT. The positive charges on the quaternary ammonium ions are compensated by chloride ions.

density of dodecyl chains of this polyelectrolyte is 40% (Figure 1c). The research group at the Laboratoire de Physico-Chimie Macromoleculair, Université Pierre et Marie Curie, Paris, synthesized all of the above polyelectrolytes. The anionic surfactant sodium dodecyl sulfate, SDS, having a critical micelle concentration, cmc, of 8.3×10^{-3} M was used in many studies.

B. Surface Force Techniques

The last few years have seen a rapid increase in the number of techniques that are used for measuring forces between hard or fluid interfaces [42]. As a result, a large variety of surfaces can be used under diverse conditions. The data presented in this review have been obtained using three different techniques, which we describe very briefly below. For more elaborate description, the reader is directed to a number of references.

1. The Interferometric Surface Force Apparatus (SFA)

Multiple beam interferometry is used for measuring the surface separation in the interferometric surface force apparatus [43,44]. The surfaces (most commonly muscovite mica) are silvered on their backside, glued onto polished silica discs, and mounted inside the apparatus in crossed cylinder geometry. The surface separation is evaluated from the wavelengths of the multiple beam interference fringes (or fringes of equal chromatic order, FECO) formed upon directing white light normal to the surfaces. The force is determined from the deflection of a double cantilever spring to which one of the surfaces is attached.

The technique allows the absolute distance between the surfaces to be measured, which makes it possible to determine the thickness of adsorbed layers from the wavelength shift of the standing waves measured with the surfaces pressed together before and after adsorption. The main limitation of the interferometric SFA is in the variety of surfaces that can be employed. Since white light interferometry is used, the surfaces have to be transparent for electromagnetic radiation in the frequency region of visible light. Muscovite mica is the ideal substrate, since it is transparent and also can be cleaved into thin atomically smooth sheets, although other surfaces such as sapphire [45] and silica [46] have also been utilized.

2. The Bimorph Surface Force Apparatus (MASIF)

The MASIF (measurements and analysis of surface interaction and forces) force measuring device is based on a bimorph force sensor [47]. The bimorph consists of two piezoelectric plates glued together with opposing

polarization directions. One of the interacting surfaces is mounted on a piezoelectric actuator that is used for changing the separation between the surfaces, normally applying a triangular voltage wave. The piezo hysteresis is corrected for by means of an LVDT sensor. The other surface is mounted directly on the bimorph, and when deflected under the action of surface forces a charge develops that can be amplified and recorded as a function of the actuator piezo expansion. The surface separation is then determined relative to a ''hard wall contact.'' The indirect separation detection allows virtually any type of hard surface to be used as long as surface roughness does not influence the measured force. However, glass is by far the most common substrate used. Since the absolute zero separation is not measured, no information about the layer thickness can be obtained. Further, the assumption of a hard wall contact made when analyzing the data is sometimes questionable [48]. The geometry in the MASIF is that of two spheres or a sphere against a flat surface. The forces measured in these geometries (F_{ss} and F_{sf}, respectively) can easily be compared with those measured in the crossed cylinder geometry of the SFA, F_{cc}, and the free energy of interaction per unit area between flat surfaces, G_f, via the Derjaguin approximation [49]:

$$\frac{F_{cc}}{2\pi R} = \frac{F_{sf}}{2\pi R} = \frac{F_{ss}}{\pi R} = G_f \tag{1}$$

where R is the radius of the surfaces. This relation is valid as long as the radius of the surfaces is larger than the range of the measured forces and the surfaces do not deform under the action of the surface forces.

3. Atomic Force Microscopy (AFM)

The principle utilized when measuring forces using an AFM [50–52] is similar to that used in the MASIF. In particular, the surface separation is determined relative to a ''hard wall'' contact. In a typical force measurement with the AFM, the Z-direction displacement of the scanner is used instead of scanning the sample surface (usually a flat plate or a colloidal particle) in the X–Y direction, as done during imaging. The other surface, a pyramidal tip or a colloidal particle, is attached to a cantilever spring. A laser beam is projected on the cantilever and the reflected beam directed to a position-sensitive photodiode, which allows high-precision deflection measurements. One advantage of the AFM colloidal probe technique is the ability directly to measure forces between colloidal particles. It can also be used for determining how the force varies with the position over a heterogeneous surface, or for measuring frictional forces [53]. Over the last few years many different mineral [54,55] and organic [56,57] surfaces have been successfully used. Some features of the three techniques are compared in Table 1.

TABLE 1 Some Features of Common Force Measuring Techniques

	SFA	MASIF	AFM
Surface requirements	Smooth, transparent sheetlike (mostly mica)	Smooth, hard (mostly glass)	Smooth, well defined geometry
Interaction geometry	Crossed cylinders	Two spheres, sphere-flat	Two spheres, sphere-flat
Typical radius	1–2 cm	1–2 mm	10–100 μm
Surface approach mode	Stepwise	Continuous, typical speed 5–200 nm/s	Continuous, typical speed 50–1000 nm/s
Absolute distance detection	Yes (via interferometry)	No	No
Distance resolution	1–2 Å	1–2 Å	1–2 Å
Force resolution	$\approx 10^{-7}$ N	$\approx 10^{-8}$ N	$\approx 10^{-9}$ N
Resolution in F/R	≈ 10 μN/m	≈ 10 μN/m	≈ 10 μN/m

III. ASSOCIATION IN SOLUTION

Polar molecules generally interact more strongly with each other than nonpolar ones (per unit volume). The reason for this is that in addition to van der Waals interactions they also interact via dipolar and higher multipolar interactions and, possibly, hydrogen bonds.

Amphiphilic molecules consist of one polar and one nonpolar region that interact differently with the environment. In a polar medium, such as water, the interactions between pairs of water molecules and between water and polar regions of the amphiphiles are much stronger than those between water and the nonpolar regions. Hence, water will avoid contact with the nonpolar (hydrophobic) part of the surfactant, and such contacts will be minimized if the surfactants self-assemble into closed aggregates. This occurs as soon as the surfactant concentration is sufficiently high that the entropy of mixing, which favors the presence of monomers over that of aggregates, no longer dominates the other free energy contributions that change during the association process.

Sodium dodecyl sulfate, SDS, assembles into micellar aggregates that are commonly believed to be spherical [58] or tablet shaped [59]. This occurs at the critical micellar concentration (cmc), i.e., when the SDS solution concentration has reached 8.3×10^{-3} M. The aggregation of SDS in aqueous solutions is driven by the removal of water–hydrocarbon contacts, whereas it is opposed by the electrostatic repulsion between negatively charged surfactant head groups and the associated entropic penalty of confining counterions next to the charged micelle. These interactions together with the shape of the surfactant determine the optimal geometry of the surfactant aggregate and thus the aggregation number. In water solutions, SDS forms aggregates consisting of approximately 65 or 80 monomers, as recently determined by steady-state fluorescence quenching and time-resolved fluorescence quenching methods [60].

The presence of oppositely charged polyelectrolytes strongly affects the association of the surfactants. A large number of experimental studies has shown that (1) the association starts at a very low surfactant concentration [3] called the critical aggregation concentration or the critical association concentration (cac), (2) the association is cooperative when the polyelectrolyte backbone is hydrophilic [61], (3) the surfactant often forms discrete aggregates that associate with the polyelectrolyte chain [62], and (4) the association process between oppositely charged polyelectrolytes and surfactants in bulk can largely be understood by considering electrostatic and hydrophobic forces [18].

Association between oppositely charged polyelectrolytes and surfactants in bulk has been modeled in detail by Wallin and Linse [22,63–65]. The

authors showed that the presence of polyelectrolytes reduces the surfactant concentration needed to trigger surfactant self-assembly. It was also found that the cac/cmc ratio decreases with increasing flexibility and linear charge density of the polyelectrolyte, and with increasing hydrocarbon chain length of the surfactant. This is fully consistent with experimental observations [15,66].

Perhaps the easiest way to obtain qualitative information on association between polyelectrolytes and surfactants is to measure the turbidity of the solution. The data in Figure 2 show how the turbidity of a 20 ppm polyelectrolyte solution changes with increasing SDS concentration for some polyelectrolytes that carry one positive charge per segment. The polyelectrolytes were PCMA of two molecular weights (1.6×10^6 and 9×10^5 g/mol) and 40DT, which is hydrophobically modified and has a molecular weight of 3×10^4 g/mol. The results obtained for the three polyelectrolytes are very similar. The general behavior can in all cases be described as follows: Even at very low SDS concentrations, below 0.01 cmc, some turbidity increase was observed. When the SDS concentration was increased to above 0.01 cmc the turbidity increased very steeply, indicating that large aggregates

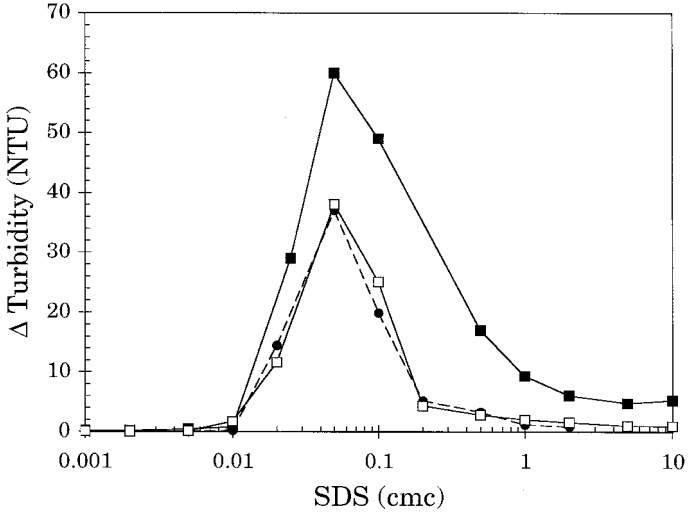

FIG. 2 Turbidity difference between solutions containing 20 ppm PCMA and different amounts of SDS, and the corresponding polyelectrolyte-free SDS solutions. Data are shown for PCMA with a mean molecular weight of 1.6×10^6 g/mol (■) and 9×10^5 g/mol (□), and for the hydrophobically modified polyelectrolyte 40 DT with a molecular weight of approximately 3.2×10^4 g/mol (●).

are formed in the solution. The maximum occurred when the SDS concentration was 0.05 cmc, and after this the turbidity fell. However, it did not reach its initial low value even at SDS concentrations well above the cmc. The only difference between the three highly charged polyelectrolytes is the magnitude of the turbidity. When comparing the two PCMA samples we see that the turbidity is larger for the sample with highest molecular weight, which simply reflects the larger size of the aggregates formed. The hydrophobically modified polyelectrolyte, 40DT, has a much lower molecular weight than the other polyelectrolytes, but nevertheless the turbidity is very similar to that observed for PCMA with approximately 30 times larger molecular weight. The reason behind this is the strong self-association of polysoaps [67].

One way of modifying the interactions between the polymer and the surfactant is to change the charge density of the polyelectrolyte. The turbidity of a range of polyelectrolyte–SDS mixtures is shown in Figure 3. Some data for the electrophoretic mobility of the polyelectrolyte–surfactant aggregates are also included in the figure. Clearly, when the charge density of the polyelectrolyte is decreased, the maximum in turbidity decreases, the position of the maximum moves to larger SDS concentrations, and the surfactant concentration interval over which high solution turbidity is observed decreases. The mobility of the aggregates has a positive value at low surfactant concentration, is close to zero at the turbidity maximum, and becomes negative at high surfactant concentrations.

The association between the cationic polyelectrolytes and anionic SDS is initially driven by both electrostatic and hydrophobic interactions. The latter force operates between the hydrocarbon tails themselves and between the tails of the surfactant and hydrophobic regions of the polyelectrolyte, particularly the grafted dodecyl chains of 40DT. We note that once uncharged aggregates are formed, electrostatic forces will oppose further uptake of surfactant. Hence at this stage the incorporation of more surfactant in the aggregates, which does occur as seen by the high negative mobility observed at high SDS concentrations, is driven by hydrophobic interactions. At zero mobility, the numbers of cationic and anionic species associated with the aggregate are equal. It is reasonable to assume that the majority of these charges are due to the charged polyelectrolyte segments and the charged surfactants associated with the polyelectrolyte. Hence the polyelectrolyte–surfactant complex would be close to stoichiometric. Making this assumption, the bound and free surfactant concentration at the point of zero mobility is easily calculated from the data in Figure 3. The total SDS concentration at this point is 0.04 cmc, or 3.3×10^{-4} M for PCMA. The bound SDS concentration is equal to the polyelectrolyte segment concentration, 1.03×10^{-4} M, and the free SDS concentration is consequently 2.3×10^{-4} M

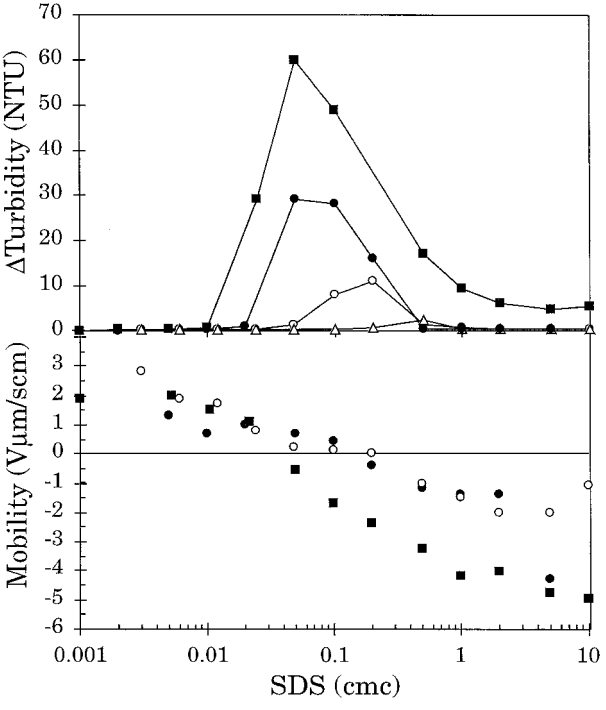

FIG. 3 Top: Turbidity difference between polyelectrolyte-free SDS solutions and solutions containing 20 ppm polyelectrolyte as a function of SDS concentration. Data are presented for PCMA, 100% charged (■), AM-MAPTAC-30, 30% charged (●), AM-MAPTAC-10, 10% charged (○), and AM-MAPTAC-1, 1% charged (△). Bottom: Electrophoretic mobility of polyelectrolyte–SDS aggregates.

(0.028 cmc). The corresponding value for 40 DT is nearly the same: 2.6×10^{-4} M (0.032 cmc) [68]. As the charge density of the polyelectrolyte is decreased, the free surfactant concentration at the charge neutralization point is 1.2×10^{-3} M (0.14 cmc) for AM-MAPTAC-30, 1.7×10^{-3} M (0.2 cmc) for AM-MAPTAC-10, and 4.2×10^{-3} M (0.5 cmc) for AM-MAPTAC-1. The last value was obtained by assuming that the zero mobility was reached at the turbidity maximum.

It is also of some interest to consider the stability of the aggregates formed at different SDS concentrations. Again, simple measurements of the turbidity of the solution as a function of time provide useful information. The results displayed in Figure 4 demonstrate that highly positively and negatively charged PCMA–SDS aggregates are stable. The turbidity in such solutions was initially low and remained constant during the course of the

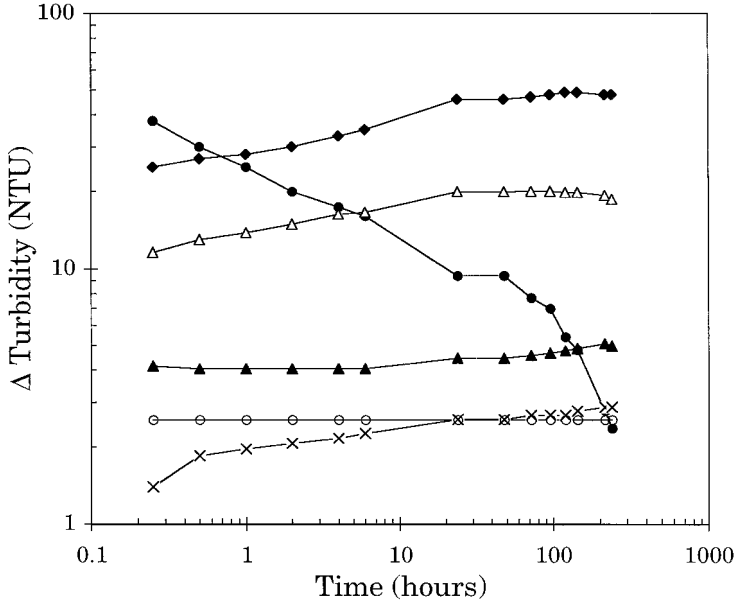

FIG. 4 Turbidity difference between solutions containing 20 ppm PCMA and different amounts of SDS, and the corresponding polyelectrolyte-free SDS solutions measured as a function of time. The SDS concentrations are 0.01 cmc (×), 0.02 cmc (△), 0.05 cmc (●), 0.1 cmc (♦), 0.2 cmc (▲), 0.5 cmc (○). (Adopted from Ref. 105.)

experiment. At SDS concentrations where close to uncharged aggregates were formed (0.05 cmc SDS), the turbidity decreased with time due to aggregate sedimentation. At SDS concentrations where slightly charged aggregates were formed (0.02 cmc SDS with slightly positively charged aggregates, and 0.1 cmc SDS with slightly negatively charged aggregates), the turbidity increased with time. This indicates slow growth of the aggregates. We can thus conclude that when the electrostatic repulsion between the aggregates is large enough, there is an energy barrier that prevents flocculation, whereas a slow flocculation takes place when the aggregate charge is low.

Some information about the internal structure of the aggregates can be obtained from SANS studies. Of the systems mentioned above, it is only PCMA–SDS mixtures that have been studied with this technique, and at much higher polyelectrolyte concentrations than used during measurements of the turbidity (1000 ppm compared to 20 ppm). Some data, obtained using deuterated SDS in a solvent (80% H_2O and 20% D_2O) where the polyelec-

trolyte is contrast matched, are shown in Figure 5. A sharp peak due to correlation between scattering centers is observed at $Q = 0.16–0.17$ Å^{-1}, corresponding to a characteristic distance of 37–39 Å. The magnitude of the peak increases with surfactant concentration, but its position remains unchanged. The peak observed at lower Q values at the highest SDS concentration is indicative of the presence of free micelles. The correlation peak at $Q = 0.16–0.17$ Å^{-1} is present also when the surfactant is contrast matched (in D_2O) and the polyelectrolyte is visible [69,70]. This shows that the polyelectrolyte and the surfactant have a similar distribution within the aggregates and that a regular assembly of the type characterized by Antonietti et al. [23–27] is formed. We note that the SANS data are inconsistent with formation of small discrete micellarlike aggregates along the PCMA backbone as suggested in a previous article [71].

IV. FORCES BETWEEN SURFACES ACROSS POLYELECTROLYTE SOLUTIONS

A. PCMA on Mica

The forces acting between two mica surfaces across a 0.1 mM KBr solution containing different concentrations of the polyelectrolyte PCMA, which has one positive charge per segment and a mean molecular weight of about 1.5×10^{-6} g/mol, are illustrated in Figure 6 [72]. At low polyelectrolyte concentrations, below 20 ppm, the long-range repulsion is found to have a decay length consistent with that of a double-layer force in 0.1 mM 1:1 electrolyte solution. Further, adsorption of the cationic polyelectrolyte on the negatively charged surface reduces the surface charge density, and thus the magnitude of the repulsive double-layer force decreases with polyelectrolyte concentration. At smaller separations an attractive force component, which increases in range and magnitude with increasing polyelectrolyte concentration, is observed. Under the action of this attractive force, the surfaces reach a separation of about 1 nm. Hence, the adsorbed layer is extremely thin considering the high molecular weight of the polymer. The reason is the high polymer-surface affinity and the similarity of the distance between charges on the polymer and in the surface lattice. The very thin polyelectrolyte layer observed in low-ionic-strength solutions is consistent with theoretical prediction [73].

The long-range repulsive force increases somewhat when the polyelectrolyte concentration is increased to above 20 ppm. This indicates that the charges in the adsorbed polyelectrolyte layer slightly overcompensate the charge of the substrate surface, and that the polymer-coated surface now has a net positive charge. It is interesting to note that under these conditions the

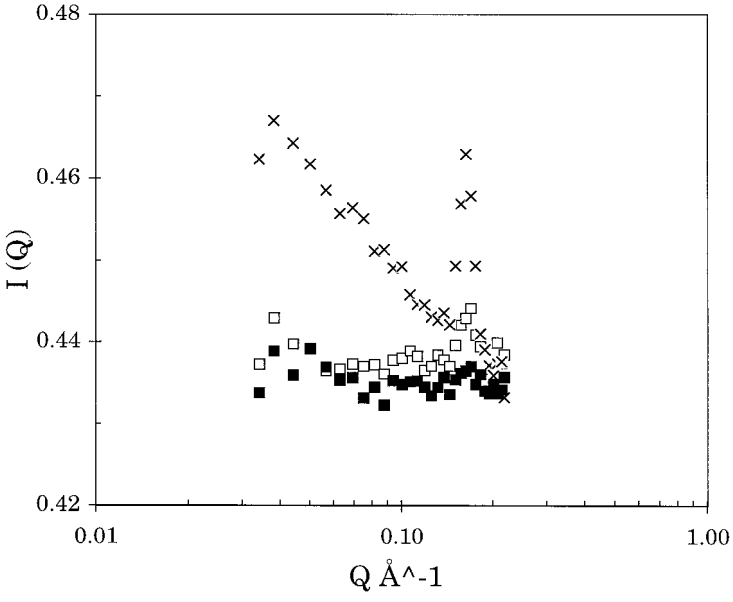

FIG. 5 Scattering intensity vs. scattering vector for a sample containing 1000 ppm PCMA and 0.02 wt% (■), 0.05 wt% (□) and 0.5 wt% (×) deuterated SDS. The experiment was carried out in a solvent of 80% H_2O and 20% D_2O at Institute Laue-Langevin, ILL, Grenoble using beamline D11.

decay length of the force is larger than the expected decay length of a double-layer force in the given electrolyte. Hence the observed force has also a steric origin, and it seems plausible that it is due to a few polyelectrolyte tails extending far away from the surface. We may term this force electrosteric since it has contributions from both electrostatic and steric interactions. The range over which the attractive force component dominates is slightly lower for the overcompensated surface than at the charge neutralization point, whereas the magnitude of the adhesion force is larger [72].

The attractive part of the force curve between surfaces coated with a similar polyelectrolyte, MAPTAC, has been investigated in more detail and compared with Monte Carlo simulations [74]. The conclusion reached was that the measured attraction is about 1 order of magnitude larger than the van der Waals force between mica surfaces, and that the additional attraction is due to a bridging mechanism where different parts of the polyelectrolytes are attracted to different surfaces [74]. Due to the long-range nature of electrostatic forces, such a bridging force may arise even though the polyelectrolytes are not directly bound to both surfaces.

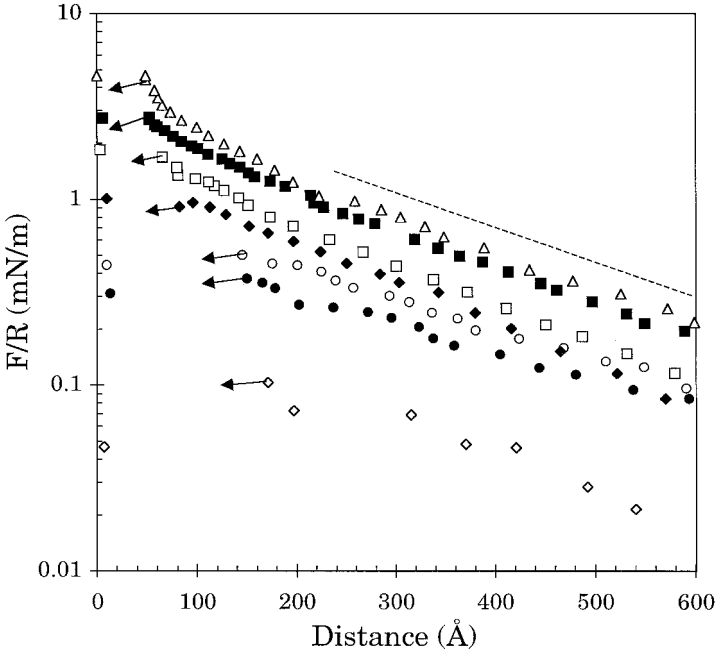

FIG. 6 Force normalized by radius as a function of surface separation between mica surfaces immersed in an aqueous 10^{-4} M KBr solution. The solution also contained PCMA at concentrations of zero (△), 1 ppm (■), 5 ppm (□), 10 ppm (●), 20 ppm (◇), 50 ppm (●), and 100 ppm (○). The dashed line represents the slope of a double-layer force in 10^{-4} M KBr, and the arrows represent inward jumps. (Adopted from Ref. 72.)

B. PCMA on Glass

The force–distance profile measured between glass surfaces across a 10^{-4} M NaCl solution at pH 5.5–6 is shown in Figure 7. The long-range repulsive interaction is due to an electrostatic double-layer force. A hydration/steric force is present at short separations, which prevents the surfaces from reaching adhesive van der Waals contact. The addition of only 1 ppm of PCMA has a dramatic effect on the interaction forces. The long-range electrostatic repulsion found between ''bare'' glass surfaces is essentially absent, indicating that adsorption of the cationic polyelectrolyte has led to an almost complete neutralization of the glass negative surface charge. Instead, at separations below 150–200 Å an attractive force brings the surfaces into adhesive contact. The interaction profile is similar to those obtained between

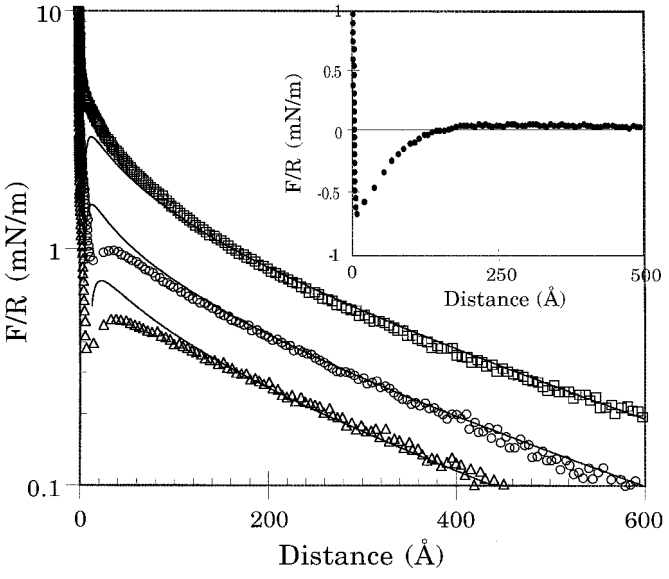

FIG. 7 Force normalized by radius as a function of surface separation between glass surfaces across an aqueous 10^{-4} M NaCl solution (□). The forces measured after adding PCMA to a concentration of 1 ppm are shown in the inset. The forces recorded after increasing the PCMA concentration to 2 ppm (△) and 20 ppm (○) are shown in the main graph. The solid lines are theoretical fits to the DLVO theory using the known ionic strength and surface potentials of 87 mV (no added polyelectrolyte), 40 mV (2 ppm PCMA), and 59 mV (20 ppm PCMA). Constant charge boundary conditions were used together with a nonretarded Hamaker constant of 0.5×10^{-20} (J).

mica surfaces close to the charge neutralization point, with the extra attraction being due to bridging of polyelectrolyte chains attracted to both interacting surfaces. When the PCMA bulk concentration is increased above 1 ppm, a well pronounced recharging of the surfaces occurs as indicated by the reappearance of a double-layer repulsion. However, the force measured below 100 Å or so remains more attractive than predicted by the DLVO theory, which suggests that the bridging contribution is significant even at higher surface coverage. Other non-DLVO attractive forces can hardly be considered here. PCMA is a rather hydrophilic polymer and does not cause any significant change in contact angle when adsorbed to hydrophilic substrates. A hydrophobic attraction should therefore be ruled out as a reason. Further, the bulk polymer concentration (20 ppm being the highest) is far too low to induce any significant attraction due to polymer depletion.

Clearly, the results for glass and mica agree in many respects. For undercompensated surfaces (i.e., the surface charge is larger than the charge of the adsorbed polyelectrolyte) it is observed that an electrostatic double-layer force dominates the interaction at large separation. A strong bridging attraction is present close to the charge neutralization concentration, cnc, and a weak recharging occurs at higher polyelectrolyte concentrations. What differs is that the cnc is much lower on glass than on mica. To rationalize this we need to consider the chemical structure of mica and glass. Muscovite mica is a layered aluminosilicate mineral with the ideal formula $KAl_2(AlSi_3)O_{10}(OH)_2$. Each sheet, about 10 Å thick, consists of two silicate layers joined together by aluminum atoms. Some silicon atoms in the lattice are replaced by aluminum, and this isomorphous substitution results in a negative lattice charge that is neutralized by potassium ions (and to a much lesser extent sodium ions) present between the aluminosilicate sheets. The electrostatic interaction between potassium and oxygen is weaker than the covalent bonds between the aluminosilicate layers, and muscovite mica can therefore easily be cleaved along the basal plane creating a molecularly smooth surface. Upon cleavage along the basal plane the potassium ions are evenly distributed between the two surfaces, and in air the mica surfaces are neutralized by these potassium ions. In aqueous solutions the potassium ions will dissociate from the mica surface, and the surface, which consists of Si, O, and Al joined together by Si—O bonds and Al—O bonds, acquires a negative charge. The total number of negative lattice sites on the mica basal plane corresponds to one negative charge per 48 $Å^2$ [75], or 2.1×10^{14} charges per cm^2, i.e., the surface charge density is -0.33 C/m^2. It is important to note that the mica surface charge arises from isomorphous substitution and that no OH groups are present on the mica basal plane. In aqueous solution the surface charge density of mica is normally orders of magnitude lower than the lattice charge of -0.33 C/m^2. The reason for this is that cations present in the solution adsorb, and thus decrease the net charge [76].

The glass surface is not as well defined as the mica surface. It contains siloxane bonds as well as silanol (Si—OH) groups and sialic acid ($Si—O^-$) groups that may extend from the surface as short polymeric chains. It is the presence of sialic acid groups that gives the glass surface its negative charge. The ratio of different surface groups varies between different glasses (and for the same glass prepared and cleaned differently). The number of negative lattice sites on mica is likely considerably higher than the number of charged sites on the glass surface. Thus the glass surface is neutralized by a smaller number of adsorbed polyelectrolytes than the mica surface. This is the most likely reason for the smaller charge neutralization concentration, cnc, on glass than on mica.

It is interesting to note that while the cnc for cationic polyelectrolytes is lower on glass than on mica, the opposite is true for cationic surfactants [77]. The reason for this difference is that both electrostatic forces and hydrophobic interactions between neighboring surfactant tails drive the surfactant self-assembly on the surface. Since the lattice sites are closer to each other on mica than on glass, the self-assembly of the surfactant is more favorable on the former surface.

C. Effect of Polyelectrolyte Charge Density

It is obvious that the polyelectrolyte linear charge density will have a large effect on the structure of the adsorbed polyelectrolyte layer, and on the forces acting between polyelectrolyte coated surfaces. This has been studied in a series of papers [72,74,78–84] using copolymers of uncharged acrylamide and positively charged segments (CMA or MAPTAC). Some results obtained using mica surfaces and polyelectrolyte concentrations close to the cnc in low-ionic-strength solutions are shown in Figure 8. The long-range forces between mica surfaces coated with a polyelectrolyte having 30% of the segments charged are rather similar to those observed when all segments are charged. For instance, hardly any long-range repulsion is observed, and a bridging attraction dominates at distances below 10–15 nm. The position of the attractive minimum is located at a separation of about 1 nm for the 100% charged polyelectrolyte and at about 3–4 nm for the 30% charged one. No further compression of the adsorbed layer occurs under a high load. The magnitude of the pull-off force needed to separate the surfaces is between 100 and 200 mN/m for the 100% charged case and between 2 and 5 mN/m for the 30% charged case. Thus the layer thickness increases and the maximum attractive force decreases with decreasing charge density of the polyelectrolyte.

A further reduction in polyelectrolyte charge density to 10% of the segments results in a further increase in adsorbed layer thickness and a decrease in the magnitude of the pull-off force. A bridging attraction is still present in the distance range 10–20 nm, whereas a steep steric force is present at smaller separation [83]. However, even if the steric force is steep, it is clear that the adsorbed layer, unlike the ones formed by the more highly charged polyelectrolytes, is somewhat compressible. At very low polyelectrolyte charge densities (1% of the segments being charged), no bridging attraction is observed [84]. Instead, a long-range steric force is the dominating feature. Clearly at the charge neutralization concentration in low-ionic-strength solutions the layer thickness, layer compressibility, and range of the steric/bridging force decrease with polyelectrolyte charge density, whereas the magnitude of the pull-off force increases. These trends are also predicted from Monte Carlo simulations [74].

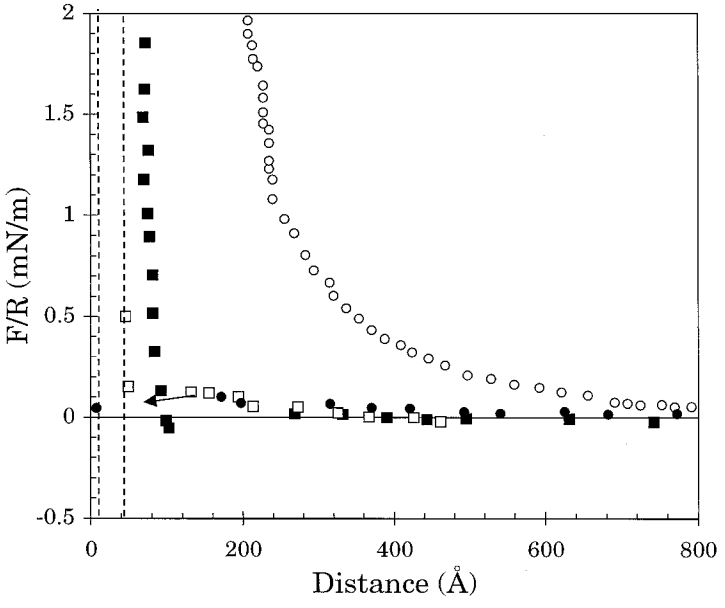

FIG. 8 Force normalized by radius as a function of surface separation between mica surfaces precoated with various polyelectrolytes. The forces were measured across an aqueous 10^{-4} M KBr solution. The polyelectrolytes were PCMA (●), AM-MAPTAC-30 (□), AM-CMA-10 (■), and AM-MAPTAC-1 (○). The arrow indicates an inward jump and the vertical lines the layer thickness for PCMA (left line) and for AM-MAPTAC-30 (right line). (Adopted from Ref. 77.)

It may be noted that the forces between polyelectrolyte-coated surfaces at higher salt concentrations ($\geq 10^{-2}$ M) are more complex than those observed at low ionic strength. In these cases long-range repulsive forces of clear nonequilibrium nature are often observed. This results in hysteretic forces, and previous compressions may affect the forces measured on subsequent approaches [85,86].

V. INTERACTIONS BETWEEN SURFACES PRECOATED WITH POLYELECTROLYTES

The adsorption energy of polyelectrolytes on oppositely charged surfaces is very high due to the high binding energy of each segment and the large number of attachment points of the polyelectrolyte. One consequence of this is that the adsorption isotherm is of the high affinity type. Another conse-

quence is that the adsorption appears irreversible with respect to dilution. In fact, the adsorption is not truly irreversible, but the desorption process is extremely slow, a fact that is well understood theoretically [87]. Hence surfaces precoated with polyelectrolytes can easily be obtained by first adsorbing the polyelectrolyte and then removing the polyelectrolyte from the bulk solution. Thus one ends up with a situation where polyelectrolytes are present on the surface, whereas no polyelectrolytes are present in solution. Some data obtained before and after removing the polyelectrolyte from the bulk solution is displayed in Figure 9. For PCMA we note that the small electrostatic double-layer force present before dilution is absent after dilution. This may indicate a slight desorption of the polyelectrolyte. The same trend is observed for the 30% charged polyelectrolyte (data not shown). For the 10% charged polyelectrolyte the data are virtually identical before and after dilution. The situation for the 1% charged polyelectrolyte is more complex [84].

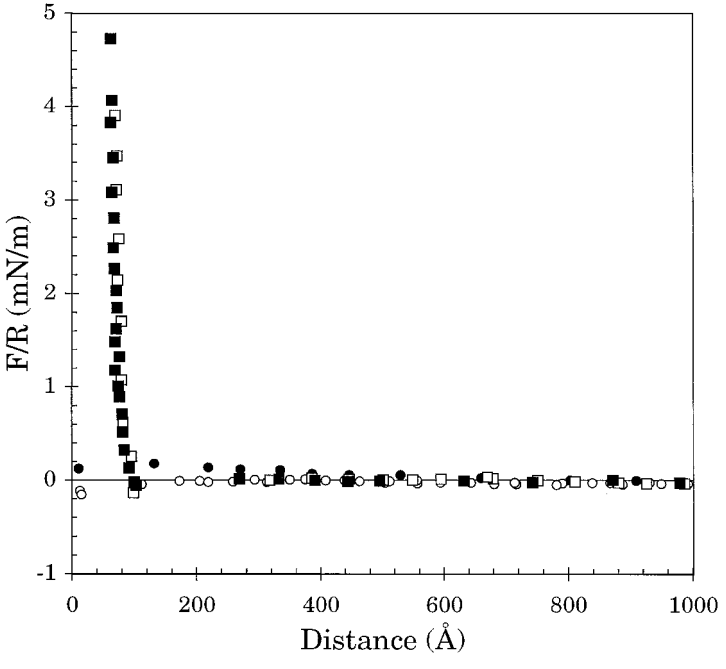

FIG. 9 The forces measured on approach between mica surfaces coated with PCMA (circles) and AM-CMA-10 (squares). The forces were recorded before (filled symbols) and after (unfilled symbols) the polyelectrolyte solutions were replaced with a solution containing no polyelectrolytes.

The forces measured between mica surfaces across a solution containing 20 ppm 40DT, a hydrophobically modified highly charged cationic polyelectrolyte, are rather complex. A strong repulsive steric force component dominates the long-range interaction, Figure 10. The force measured on approach is more repulsive than that measured on separation, and the range and magnitude of the force decrease for each consecutive approach. Once the surfaces have been brought close together, a sudden inward jump occurs from a separation of 80–110 Å to a separation of 15–20 Å. At this position a strong attractive force, with a magnitude (F/R) of 30–40 mN/m, is observed upon separation. Note that the layer thickness is larger and the adhesion force smaller than for the nonhydrophobically modified highly charged polyelectrolytes PCMA and MAPTAC. This indicates that the increased hydrophobic attraction between layers of 40DT as compared to PCMA, which is due to the grafted dodecyl chains, cannot compensate for the decreased bridging attraction, due to the larger final layer thickness.

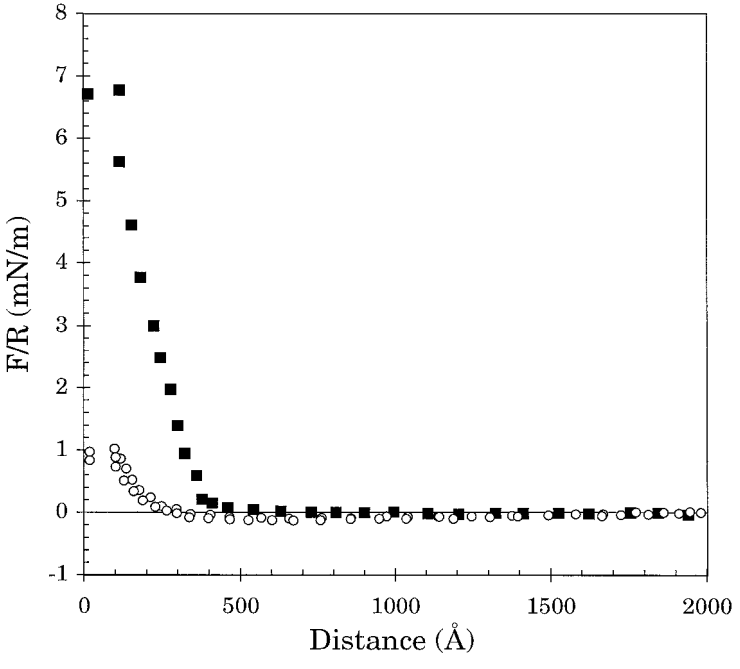

FIG. 10 Force normalized by radius as a function of surface separation. The measurements were carried out using two mica surfaces in a solution containing 20 ppm 40DT and 0.1 mM KBr (■), and after diluting this mixture by a factor of 6000 using a polyelectrolyte-free 0.1 mM KBr solution (○). (Adopted from Ref. 68.)

The forces measured when the 20 ppm 40DT solution is diluted approximately 6000 times are compared with a typical force curve obtained before dilution in Figure 10 [68]. The most long-range part of the force curve observed after dilution is weakly attractive. The force turns repulsive at a separation of just above 250 Å. The repulsion increases in magnitude until a separation of 100 Å is reached. From this position the surfaces jump inwards to 15–20 Å, the same as before dilution. The magnitude of the attractive normalized force measured when separating the surfaces from this position is about 60 mN/m. It seems likely that the layer formed by adsorption from a 20 ppm 40DT solution consists of an inner part that is strongly anchored to the surface and an outer part that is weakly attached to the inner layer. No similar evidence for the presence of an outer layer is obtained when the forces are measured between mica surfaces coated with polyelectrolytes, such as PCMA, that does not contain grafted hydrophobic side chains. This provides strong support for the view that it is interactions between the hydrophobic side chains of adsorbed molecules in the inner layer with similar groups in the molecules making up the outer layer that is the reason for the additional adsorption. It is thus related to the intrachain and interchain association between hydrophobically modified polyelectrolytes that occurs in bulk solution [7,29]. It is compression and at least partial removal of the outer layer that gives rise to the hysteresis and the effect of previous approaches observed prior to dilution. After dilution only the inner layer remains. The weak steric force that remains after dilution is not hysteretic or affected by previous approaches. It appears likely that this force is due to the presence of loops and tails in the adsorbed layer.

The situation with surfaces precoated with polyelectrolytes and no polyelectrolytes present in solution is preferred when studying association between surface-bound polyelectrolytes and surfactants, as relevant for e.g. cleaning processes. This situation, which is discussed in Sec. VI, is simpler to study and understand as compared to the case with polyelectrolytes present in bulk solution, since adsorption of sparingly soluble bulk polyelectrolyte–surfactant aggregates is avoided. The more complex situation with adsorbing polyelectrolyte–surfactant complexes is addressed in Sec. VII.

VI. ASSOCIATION BETWEEN SURFACTANT AND PREADSORBED POLYELECTROLYTE LAYERS

Association of polyelectrolytes and surfactants at the solid–liquid interface has been investigated to a rather limited extent. This is surprising indeed, considering the technological importance of such systems. However, Ananthapadmanabhan et al. [88] measured surface interactions between mica

surfaces precoated with cationic cellulosic polymer, JR-400 (mean molecular weight 5×10^5 g/mol), across submicellar SDS solution. They established that in the presence of SDS an attraction between the surfaces developed during separation, while the interactions measured during approach were repulsive. Anthony et al. [89] made a detailed investigation of the association between cationic guar and SDS. Among other things they determined interactions between mica surfaces precoated with such polyelectrolytes, with molecular weight 2.3×10^6 g/mol and charge densities varying between 4% and 30%, across water and aqueous SDS solutions. In the absence of surfactant they found that the range of the steric force decreased with increasing charge density of the guar, which is consistent with the results presented in Sec. V. However, the range of the steric forces was much larger than those presented in Figure 8, extending in the most long-range case to 9000 Å. This may partly be due to the very high molecular weight of their sample, but it also indicates that one also has to pay attention to the polyelectrolyte architecture and chain stiffness. The addition of SDS resulted in a collapse of the very extended layer and, presumably, some desorption at high SDS concentrations. The results obtained by Anthony et al. were found to correlate well with the bulk behavior, displaying a phase-separation region at intermediate SDS concentrations. Shubin [34] studied the effect of SDS on the structure and composition of layers of cationic hydrophobically modified cellulose, Quatrisoft LM 200, with a molecular weight of 1×10^5 g/mol and with approximately 3% of the segments carrying a positive charge, adsorbed on negatively charged surfaces (mica and silica). The Quatrisoft concentration was 34 ppm, and it was found that the addition of SDS (without first removing the polyelectrolyte from solution) to a concentration of 0.005 cmc (4×10^{-5} M) resulted in a significant swelling of the adsorbed layer. A further increase in SDS concentration to 0.24 cmc (2×10^{-3} M) increased the swelling further. Some differences were noted depending on whether the SDS concentration was increased stepwise. Later, Shubin et al. conducted a comparative study of the influence of anionic, cationic, and nonionic surfactants on the structure of adsorbed layers of the same polyelectrolyte on mica and silica surfaces [35]. Fröberg et al. followed how the addition of SDS to a preadsorbed lysozyme layer led to desorption [90]. Further, investigations have been undertaken in order to understand how the concentration of SDS and the charge density of the cationic polyelectrolyte affect the structure of preadsorbed polyelectrolyte layers on negatively charged mica surfaces. The main forces to consider in such systems are (1) an electrostatic attraction between the positively charged polyelectrolyte and the negatively charged surface, (2) electrostatic and hydrophobic interactions between the polyelectrolyte and the oppositely charged surfactant, (3) a hydrophobic attraction between the nonpolar tails of the surfactant, and (4) an

electrostatic repulsion between the negatively charged surface and the surfactant. We note that there is competition between the surface and the surfactant for positive charges on the polyelectrolyte. Polyelectrolytes with charge density of 100% [71], 30% [80], 10% [83], and 1% [91] have been studied. The effect of introducing hydrophobic side chains on the polyelectrolyte has also been considered [68]. Some of the main findings are recapitulated below.

A. PCMA, A Polyelectrolyte Whose Each Segment Carries a Positive Charge

1. Studies Using Atomic Force Microscopy

AFM images of the PCMA layer on mica obtained across a 20 ppm PCMA solution are rather featureless both before and after the polyelectrolyte solution is replaced with a 1×10^{-4} M KBr solution [69], demonstrating that the adsorbed polyelectrolyte layer is smooth and homogeneous. However, the AFM images obtained after injecting a 1 cmc SDS solution in the measuring chamber show that the adsorbed polyelectrolyte layers are no longer flat and smooth. Instead, large-scale topographical features are observed with typical lateral dimensions of 200 nm (Figure 11). The height differences observed in the images are typically around 40 Å. We note that the deflection of the cantilever is not absolutely constant during imaging and the height difference may be underestimated by as much as 10 Å. The image clearly demonstrates that SDS is incorporated in the preadsorbed polyelectrolyte layer, which is consistent with the surface force data that will be presented below.

The forces measured between the AFM tip and the PCMA coated mica surface across a 1 cmc (8.3×10^{-3} M) SDS solution are shown in Figure 12. At repulsive double-layer force dominates the long-range interaction, whereas two pronounced steps with a periodicity of 40 Å are observed at small separations. We can thus conclude that the adsorbed layer is heterogeneous both parallel and perpendicular to the surface. Two other surface force techniques, the MASIF and the SFA, were used to explore this further.

2. Studies Using a MASIF Surface Force Apparatus

Preadsorbed PCMA layers were prepared by first adsorbing the polyelectrolyte from a 10^{-4} M NaCl solution (PCMA concentration 20 ppm) and then replacing the bulk solution with polyelectrolyte-free 10^{-4} M NaCl. In the next step, SDS was added to the solution to a concentration of 0.4 cmc (3.2×10^{-3} M). The forces measured at this stage are shown in Figure 13. A

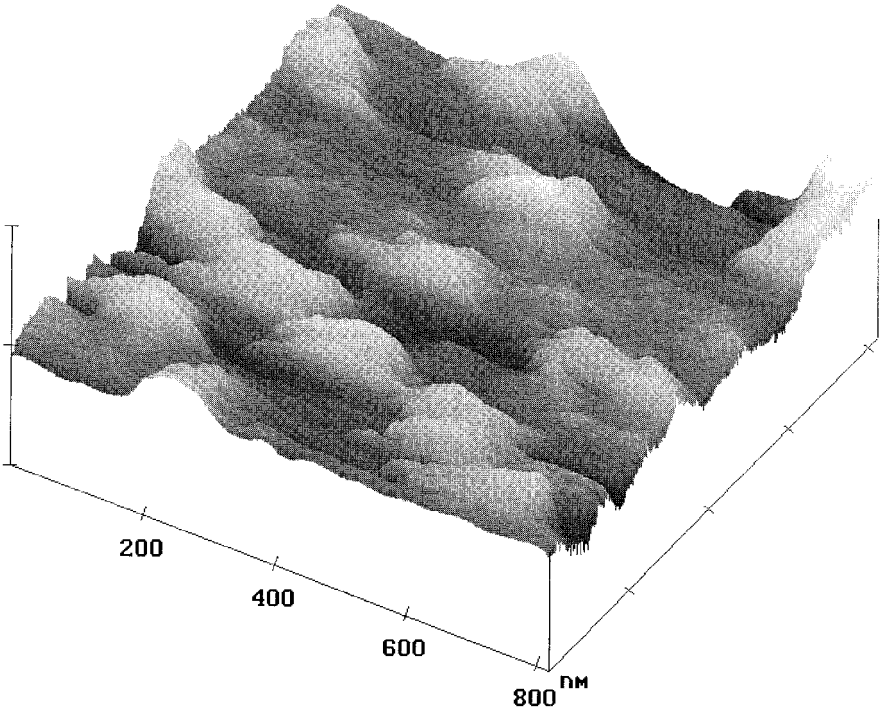

FIG. 11 AFM image of preadsorbed PCMA layers swelled with a 1 cmc SDS solution. The image is taken in contact mode in liquid using the double-layer repulsion between the tip and the sample. The height scale is 10 nm/div. (Adopted from Ref. 69.)

long-range double-layer repulsion is the dominating feature at distances above 40 Å. The decay length of the force corresponds well to the Debye length for the known surfactant concentration. It is likely that SDS adsorption to the PCMA-coated surface has led to charge reversal, i.e., the surfaces are again negatively charged. A much steeper repulsion is observed below a separation of 40 Å. This force is followed by another, flatter region before the surfaces reach hard wall contact, i.e., the results are very similar to those obtained with the AFM using a mica flat and a silicon nitride tip as described above; compare Figures 12 and 13. The force profile reflects a change in the adsorbed layer structure occurring as the surfaces are pushed together. The simplest explanation would simply be that the surfactants are pushed out from the contact region. However, the results obtained with the SFA indicates that the situation is more complex (at least on mica).

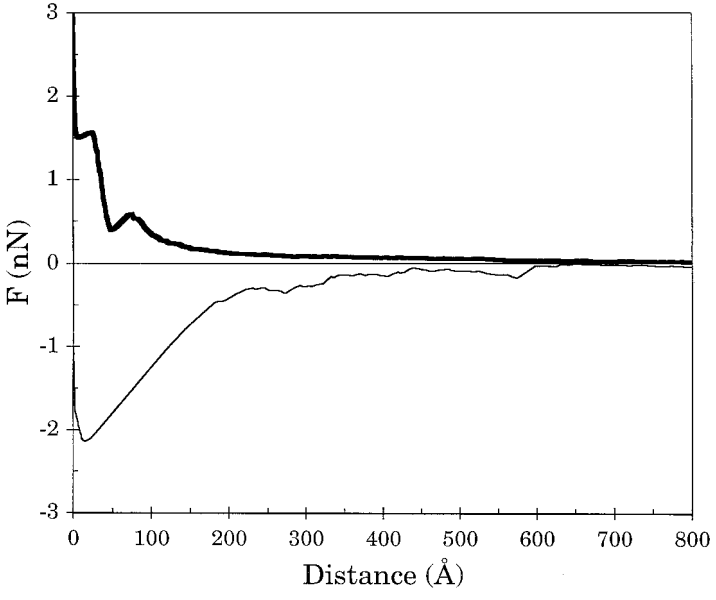

FIG. 12 Force as a function of separation between mica surfaces coated with PCMA and an uncoated silicon nitride AFM tip across a 1 cmc SDS solution. The forces were registered on approach (thick line) and on separation (thin line). (Adopted from Ref. 69.)

When the bulk surfactant concentration was increased to 1 cmc (8.3×10^{-3} M), the inward step disappeared and the interaction at short separations was attractive. The presence of this attractive interaction at short separations shows that some adsorbed material remains on the surface. The result obtained at 1 cmc SDS for PCMA-coated glass is very different from when mica is used as a substrate (see below). It seems that the high SDS concentration has led to a significant desorption of the PCMA–SDS complexes from the glass surface, whereas this occurs to a much more limited degree on mica. The reason for this difference is likely the lower surface charge of glass than of mica (see the discussion in Sec. IV.B) and hence the polyelectrolyte–surface affinity is lower. Finally, we would like to stress that the absolute distance is not known in the MASIF (or AFM) experiments. Hence we do not know whether the final separation corresponds to close to glass–glass contact or whether it is located at a separation of 40 Å, as when mica is used as a substrate, or, in fact, at any other separation.

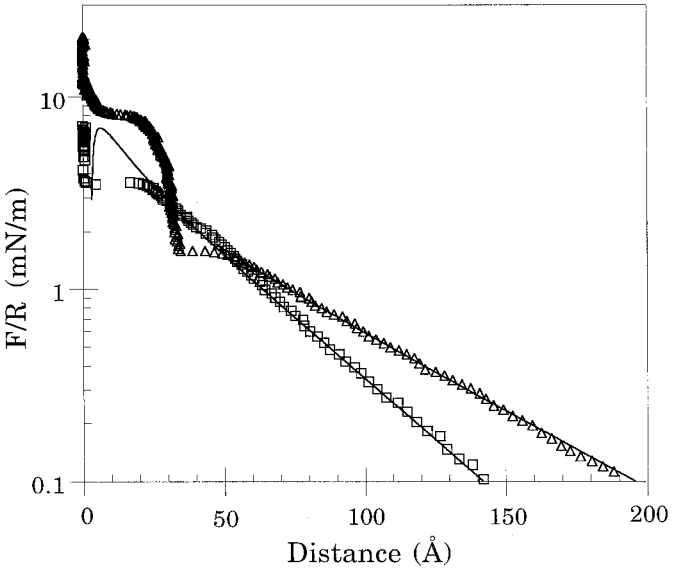

FIG. 13 Force normalized by radius as a function of surface separation between glass surfaces precoated with PCMA. The forces were measured across an aqueous 10^{-4} M NaCl solution. The SDS concentrations were 0.4 cmc (△) and 1 cmc (□). The upper line shows the expected decay length of a double-layer force in 0.4 cmc SDS solution. The lower curve is calculated DLVO forces using a surface potential of 58 mV, the known ionic strength, and constant charge boundary conditions together with a nonretarded Hamaker constant of 0.5×10^{-20} (J).

3. Studies Using an Interferometric Surface Force Apparatus, SFA

The forces measured between two pairs of mica surfaces precoated with PCMA across dilute SDS solutions are illustrated in Figure 14 [71]. As in the previous experiments, no polyelectrolytes are present in the bulk solution. The addition of SDS to a concentration of 0.01 cmc or 0.02 cmc does not result in any change in the long-range interaction or pull-off force. The surfaces remain uncharged, and a bridging attraction acts from a separation of about 150 Å. Clearly, at these low SDS concentrations the adsorption of the surfactant is very limited. However, as the SDS concentration is increased further to 0.1 cmc (8.3×10^{-4} M), a long-range repulsive double-layer force appears. The repulsive force is overcome by an attraction at a separation of 110 Å. This attraction pulls the surfaces inwards to a separation of 40 Å. A further increase in the compressive force hardly affects the surface separation, indicating a dense layer structure that contains both the

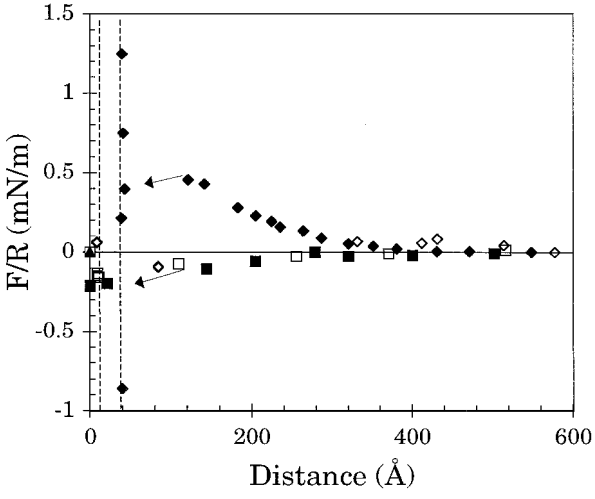

FIG. 14 Force normalized by radius as a function of surface separation between mica surfaces precoated with PCMA. The forces were measured across an aqueous 10^{-4} M KBr solution. The SDS concentrations were zero (□), 0.01 cmc (■), 0.02 cmc (◇), and 0.1 cmc (♦). The arrows represent inward jumps and the vertical lines the layer thicknesses. (Adopted from Ref. 71.)

polyelectrolyte and SDS. The pull-off force is in this case 25–30 mN/m, i.e., significantly lower than at the lower SDS concentrations.

At the SDS concentration of 0.1 cmc it was noted that the forces measured on the first approach were significantly different from those measured on subsequent approaches (Figure 15). The repulsive double-layer force is stronger, and oscillations are now present in the force curve. This demonstrates that the act of separating the surfaces from contact changes the structure of the adsorbed layer. It seems likely that some polyelectrolyte chains will be stretched out from the surface during the separation process, and that these chains will interact more favorably with the surfactants than the part of the polyelectrolyte that is in close contact with the surface. Hence, surfactants associate readily with the stretched chains, and the amount of surfactants associated with the polyelectrolyte layer increases, which results in an increased double-layer force. The surfactants that associate with the extended chains also counteract readsorption of the chains to the surface.

A further increase in SDS concentration of 0.2 cmc (1.7×10^{-3} M) results in the appearance of pronounced oscillations in the force curve on both the first and the subsequent approaches (Figure 16). It may be noted that the oscillations are slightly more pronounced once the surfaces have been sep-

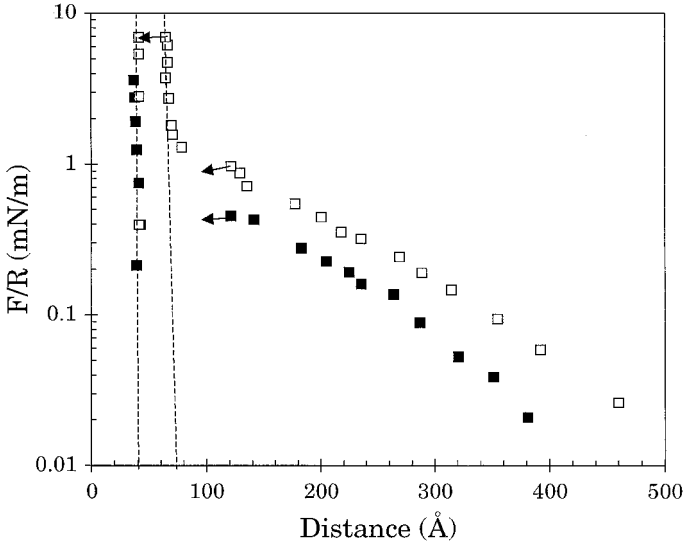

FIG. 15 Force normalized by radius as a function of surface separation between mica surfaces precoated with PCMA. The forces were measured across an aqueous 10^{-4} M KBr solution containing 0.1 cmc SDS. The forces measured during the first (■) and the second (□) approach are illustrated. The vertical lines illustrate the position of the oscillating branches of the force curve and the arrows inward jumps. (Adopted from Ref. 71.)

arated from contact. The innermost force barrier is located at a separation between 40 and 50 Å, i.e., at the same position as in 0.1 cmc SDS solution. The next force barrier is observed at the distance interval 70–90 Å, and the outermost one at a separation of 120–130 Å. The oscillations thus have a periodicity of about 40 Å, and it is observed that both the repulsive and the attractive branch increase in magnitude as the surfaces are moved from an outer to an inner oscillation. Hence the same periodicity is observed between one bare surface and one polyelectrolyte coated surface with the AFM (Figure 12) and the MASIF (Figure 13), as well as between two polyelectrolyte-coated surfaces with the SFA. A repulsive double-layer force dominates the interaction at separations larger than 130 Å.

The forces measured at higher surfactant concentration, up to 2 cmc (1.7×10^{-2} M), also display oscillations with a periodicity of 40 Å. One example of such a force curve, measured at an SDS concentration of 1 cmc, is illustrated in Figure 17. We note that the periodicity of the oscillations remains unchanged when the SDS concentration is increased, but the number of oscillations and their magnitude differs. This is more clearly shown in Figure

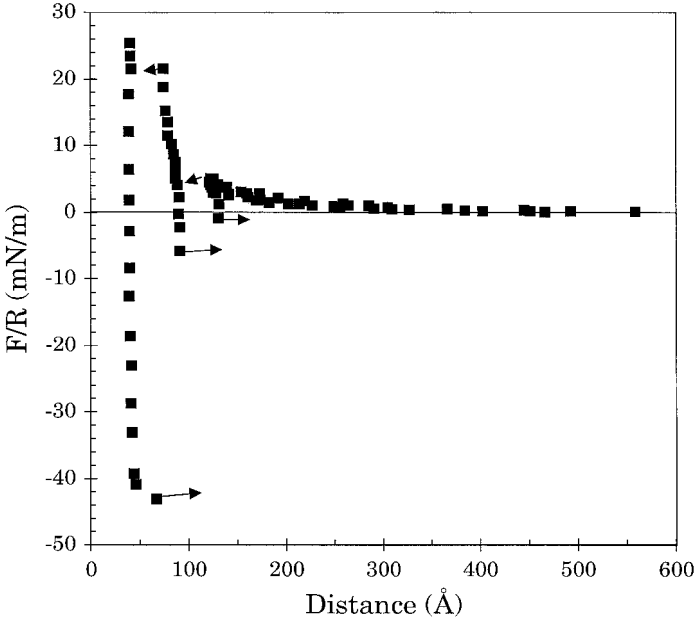

FIG. 16 Force normalized by radius as a function of surface separation between mica surfaces precoated with PCMA. The forces were measured across an aqueous 10^{-4} M KBr solution containing 0.2 cmc SDS. The arrows illustrate inward and outward jumps. (Adopted from Ref. 71.)

18, which illustrates data obtained in the SDS concentration range 0.2–2 cmc. The magnitudes of the repulsive force branches increases up to an SDS concentration of 0.5 cmc and decreases again at higher surfactant concentrations. The reduction observed at these high SDS concentrations is most likely due to some desorption of the polyelectrolyte [69]. We also note that the range of the force is somewhat larger at 2 cmc than at lower SDS concentrations, which indicates an increased length of the longest tails.

The data displayed in Figures 14–18 show that preadsorbed PCMA layers are strongly swelled by association with SDS once the SDS concentration has reached 0.1 cmc. This indicates that part of the polyelectrolyte chain is desorbed from the surface. However, most of the polyelectrolytes remain attached to the mica surface for a period of at least several days. When the swelled layers are pushed together, oscillating force curves are observed. The reason is that the internal structure of the adsorbed layer changes in order to minimize the free energy of the system. We note that similar but weaker oscillations with larger periodicity have been observed due to pack-

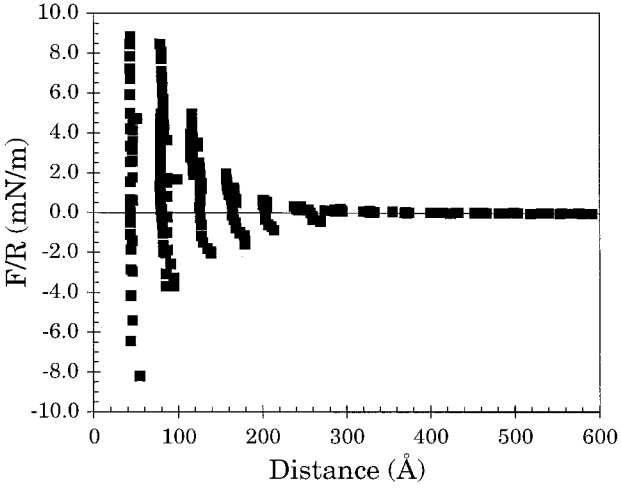

FIG. 17 Force normalized by radius as a function of surface separation between mica surfaces precoated with PCMA. The forces were measured across an aqueous 10^{-4} M KBr solution containing 1 cmc SDS. (Adopted from Ref. 69.)

ing of free SDS micelles in the confined space between two surfaces [92]. However, these forces were observed only well above the cmc (0.25 M $\approx$ 30 cmc), whereas in the present case the oscillations are present also below the cmc of the surfactant. Oscillating forces across single foam films stabilized by polyelectrolyte–surfactant mixtures have recently been reported [93]. In one of the papers the periodicity of the oscillations was correlated with the mesh size in the bulk polyelectrolyte solution [94]. Similar results were obtained by Milling [95], who studied interactions between solid surfaces across solutions of nonadsorbing polyelectrolytes using AFM. The results presented here for the PCMA–SDS system are, however, different from the ones mentioned above, because no polyelectrolytes are present in solution. Hence the characteristic length scale that gives rise to the oscillating force profile is a property of the adsorbed layer (and the internal structure of dispersed bulk aggregates). In the original article it was argued that the oscillations are due to the presence of small SDS micellarlike structures stabilized by the polyelectrolyte [71]. However, the recent SANS results (Figure 5) do not seem to be consistent with this picture. Instead, the peak observed at 0.16–0.17 $Å^{-1}$, corresponding to a correlation distance of 37–39 Å, might be interpreted as the distance between two surfactant-loaded polyelectrolyte chains, i.e., the mesh size within the layer. This characteristic distance agrees very well with the periodicity of the oscillating forces ob-

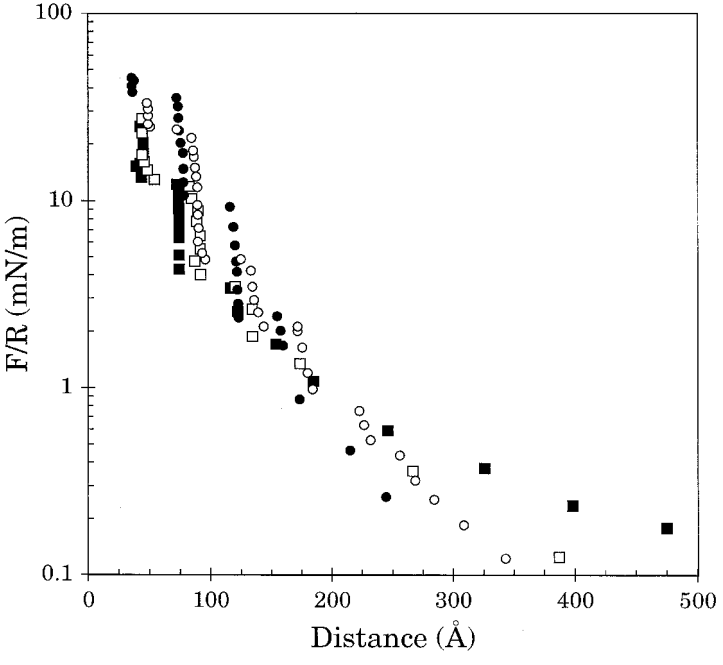

FIG. 18 Force normalized by radius as a function of surface separation between mica surfaces precoated with PCMA. The forces were measured across an aqueous 10^{-4} M KBr solution containing SDS at the following concentrations: (○) 0.2 cmc, (●) 0.5 cmc, (□) 1 cmc, and (■) 2 cmc.

served with the SFA, the MASIF, and the AFM. It seems plausible that the internal structure of the PCMA–SDS layer is similar to those of the mesomorphous polyelectrolyte–surfactant phases described by Antonietti et al. [23,24,26,27].

4. Comparison of Results Obtained with the SFA, MASIF, and AFM

There are several reasons why more oscillations are observed with the SFA than with the AFM or the MASIF. First, the SFA measures the average force over a much larger surface area than that probed by the other techniques. The effective area of interaction in the SFA is approximately two orders of magnitude larger than the corresponding area in the MASIF, and the area is still smaller in the AFM. In fact, during AFM force measurements, the contact area is even smaller than the area occupied by a single polymer–surfactant complex. Second, SFA measurements are carried out at a much

slower rate than the other measurements. The force curve displayed in Figure 17 took about 6 hours to measure, whereas the AFM force curve in Figure 12 took about a second to record, and the force curve obtained with the MASIF in Figure 13 was measured within less than a minute (approach rate 15 nm/s). Hence, oscillations due to slow rearrangements in the polyelectrolyte–surfactant layer are easily detected with the SFA but not with the other techniques.

B. AM-MAPTAC-30, A Polyelectrolyte in Which 30% of the Segments Carry a Positive Charge

The forces acting between mica surfaces precoated with AM-MAPTAC-30, called AM-MAPTAC-31 in the original paper [80], before and after addition of SDS to a concentration of 0.005 cmc (4×10^{-5} M) are illustrated in Figure 19. Clearly, the presence of this small amount of SDS does not affect the measured forces significantly. A weak electrostatic double-layer force dominates the long-range interaction, and a bridging attraction is observed at distances below 100–150 Å. The jump in distance seems to be slightly larger after the addition of SDS, but at present we do not want to put any emphasis on this observation. The pull-off force measured upon separation is about -1 mN/m, i.e., much less than observed for the more highly charged polyelectrolyte.

A tenfold increase in SDS concentration to 0.05 cmc (4×10^{-4} M) results in a significant change in the adsorbed layer and the measured forces [80]. A strong repulsive force dominates the long-range interaction; see Figure 20. The decay length of this force is not consistent with that of a double-layer repulsion, and therefore both steric and electrostatic forces contribute to the measured interaction. The increased repulsion demonstrates that SDS has associated with the polyelectrolyte layer and that this results in a significant swelling. The incorporation of SDS in the adsorbed layer gives the layer a net negative charge, and it is the electrostatic repulsion within the layer that causes the swelling. It was noted that the forces measured on a first approach are slightly more long-ranged than the forces measured on subsequent approaches, showing that the act of measuring the forces results in a more compact layer [80]. However, if the surfaces are left apart for a long time, the adsorbed layer expands again. It is also worth noting that no oscillations are present in the force curve. Hence, the AM-MAPTAC-30 layer does not have the same ordered internal structure as observed for the more highly charged PCMA in presence of SDS.

A further increase in SDS concentration to 0.2 cmc or 2 cmc reduces the range of the measured interaction significantly (Figure 20). One is tempted to attribute this to desorption of some polyelectrolytes, but this does not

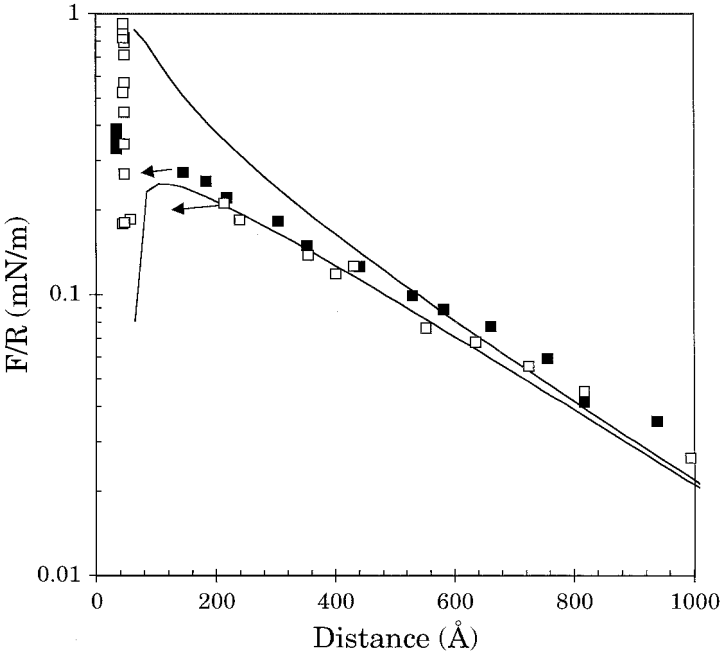

FIG. 19 Force normalized by radius as a function of surface separation between mica surfaces precoated with AM-MAPTAC-30. The forces were measured across an aqueous 10^{-4} M KBr solution containing no SDS (■) and 0.005 cmc SDS (□). The solid lines are calculated DLVO forces using a surface potential of 45 mV and constant charge (upper line) and constant potential (lower line) boundary conditions. The arrows indicate inward jumps. (Adopted from Ref. 80.)

seem to be the whole story, since the adsorbed amount at an SDS concentration of 0.2 cmc is very similar to that at lower SDS concentrations [80]. Another contribution to the deswelling of the layer at high SDS concentrations is the increased ionic strength of the solution that reduces the range of the electrostatic forces. It is also plausible that hydrophobic interactions between surfactant tails within the layer become more important as the amount of incorporated surfactant increases.

C. AM-CMA-10, a Polyelectrolyte in Which 10% of the Segments Carry a Positive Charge

The forces acting between mica precoated with a layer of AM-CMA-10 before and after the addition of SDS to a concentration of 0.01 cmc (8.3 ×

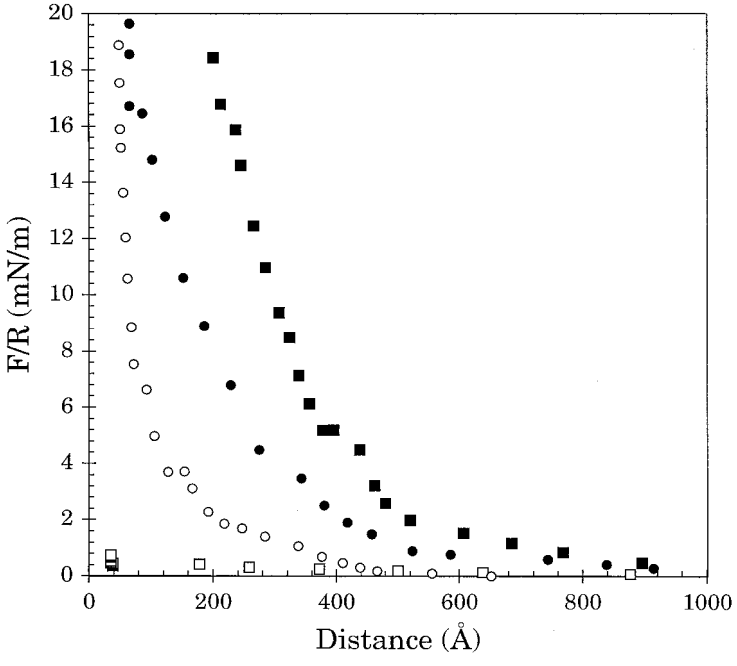

FIG. 20 Force normalized by radius as a function of surface separation between mica surfaces precoated with AM-MAPTAC-30. The forces were measured across an aqueous 10^{-4} M KBr solution containing SDS at the following concentrations: 0.005 cmc (□), 0.05 cmc (■), 0.2 cmc (●), and 2 cmc (○). (Adopted from Ref. 80.)

10^{-5} M) are shown in Figure 21 [83]. The effect of the surfactant is minor. In both cases an attractive bridging force is observed at a separation of about 200 Å, which pulls the surfaces into a separation of 100 Å. At smaller separations, a steeply rising repulsive force, due to compression of the adsorbed polyelectrolyte layer, is present. When the surfaces are taken apart a slowly decaying attraction is observed, indicating that bridging polyelectrolytes connect the surfaces.

When the SDS concentration is increased further to 0.02 cmc (1.7×10^{-4} M) the adsorbed layers expand drastically and the surface forces become much more long-ranged (Figure 22). This expansion is, just as for the previously discussed polyelectrolytes, due to binding of SDS to the adsorbed polyelectrolytes. At this and higher SDS concentrations the details of the surface force profiles are no longer reproducible. However, the general features are always the same. The most long-range part of the force curve increases significantly with decreasing separation. At smaller separations, at

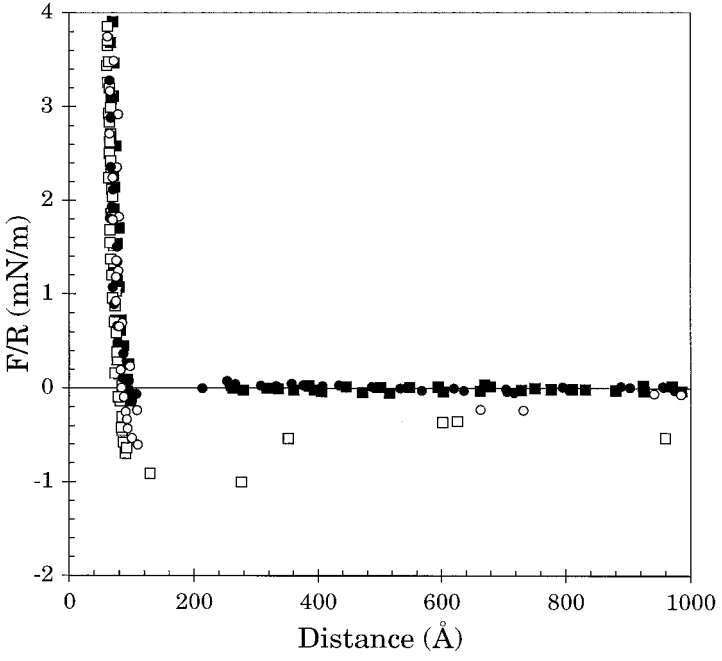

FIG. 21 Force normalized by radius as a function of surface separation between mica surfaces precoated with AM-CMA-10. The forces were measured across an aqueous solution containing no SDS (squares) and 0.01 cmc SDS (circles). Filled and unfilled symbols represent forces measured on approach and separation, respectively. (Adopted from Ref. 83.)

around 500–600 Å, the repulsive force increases less rapidly, and sometimes a sudden inward "jump" takes place. One example of this, observed at an SDS concentration of 0.1 cmc, is illustrated in Figure 22. We propose that the change in the slope of the force curve is due to a cooperative desorption of SDS from the polyelectrolyte coated surfaces. This hypothesis is supported by the fact that the thickness of the layer reached under a high force is similar to that observed before SDS was added to the solution. The forces measured on separation (not shown) are significantly less repulsive than those measured on the first approach, and the forces measured on a second approach are similar to those experienced during the previous separation. Hence, as for AM-MAPTAC-30, the act of measuring the surfaces forces induces a slowly (several hours) reversible change in the adsorbed layer. No data is available at higher SDS concentrations, but based on the findings for AM-MAPTAC-30 it may be expected that the swelling will decrease at

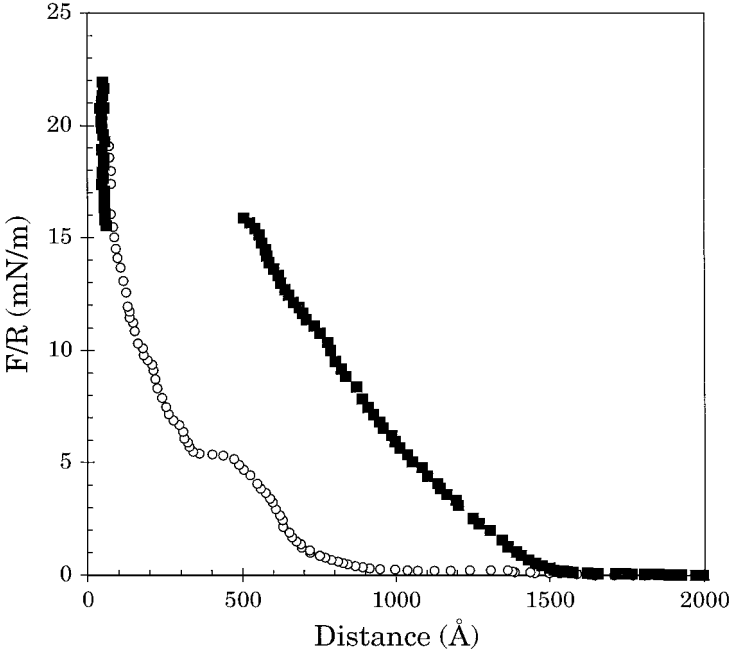

FIG. 22 Force normalized by radius as a function of surface separation between mica surfaces precoated with AM-CMA-10. The forces were measured across an aqueous solution containing 0.02 cmc SDS (○) and 0.1 cmc (■). The arrow indicates an inward jump. (Adopted from Ref. 83.)

higher SDS concentrations due to the increased ionic strength and due to some desorption of the polyelectrolyte.

D. AM-MAPTAC-1, a Polyelectrolyte in Which 1% of the Segments Carry a Positive Charge

The polyelectrolyte AM-MAPTAC-1 has only 1% of the segments charged. In this case no swelling of the preadsorbed layer on the mica surface is observed when SDS is added to the solution. The data obtained for an SDS concentration of 0.1 cmc are essentially the same as observed prior to the addition of SDS (Figure 23) and are dominated by a steric repulsion. We conclude that hardly any SDS is present in the adsorbed layer. However, when the SDS concentration is increased to 0.3 cmc, the range of the steric force is less than at the lower SDS concentration. A further increase in surfactant concentration results in a progressive decrease in the range of the

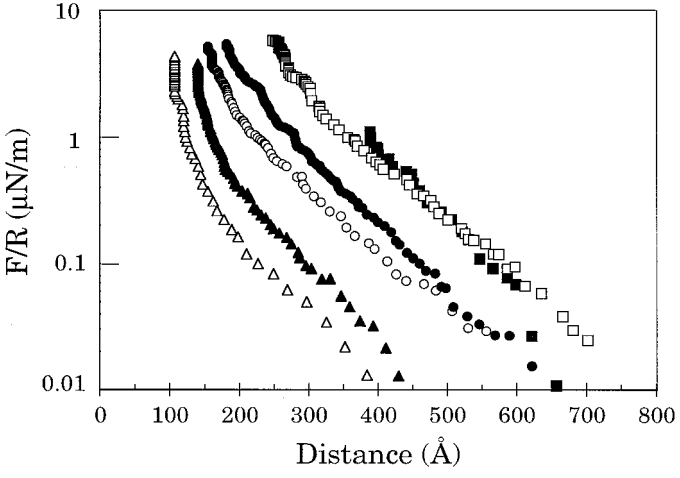

FIG. 23 Force normalized by radius as a function of surface separation between mica surfaces precoated with AM-MAPTAC-1. The forces were measured across an aqueous solution containing SDS at the following concentrations: no SDS (■), 0.1 cmc (□), 0.3 cmc (●), 0.75 cmc (○). 1 cmc (▲), and 2 cmc (△).

force. Hence in this case the most important effect of the incorporation of SDS into the adsorbed layer is that some polyelectrolytes desorb.

E. 40DT, a Polyelectrolyte Having Each Segment Charged and 40% of the Segments Carrying a Grafted Dodecyl Chain

The forces between surfaces coated with the hydrophobically modified polyelectrolyte, 40DT, are strongly affected by the addition of very small amounts of SDS; see Figure 24 [68]. Even such a low SDS concentration as 0.005 cmc (4×10^{-5} M) causes the final layer thickness to increase by more than a factor of two, and the adhesion force to be halved. Hence the hydrophobic dodecyl side chains grafted to the polyelectrolyte promote association between the preadsorbed polyelectrolyte layer and the oppositely charged surfactant. An increase in SDS concentration to 0.01 cmc results in a strong increase in the range and magnitude of the steric force, and a further decrease in the adhesion force. A doubling of the SDS concentration to 0.02 cmc results in a slight further swelling. Note that at the same SDS concentration, no association between preadsorbed PCMA layers and SDS has occurred; compare Figure 14.

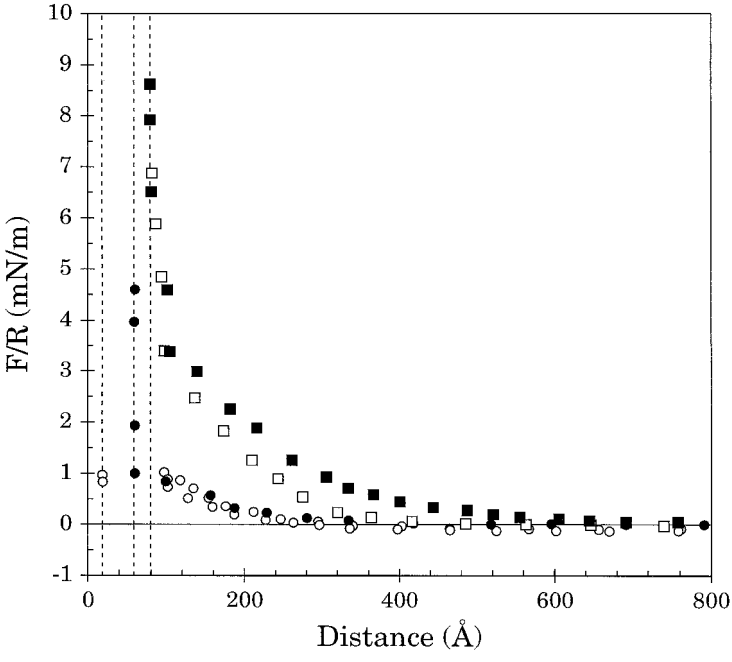

FIG. 24 Force normalized by radius as a function of surface separation between mica surfaces precoated with an adsorbed layer of 40DT. The solution contained 0.1 mM KBr and no SDS (○), 0.005 cmc SDS (●), 0.01 cmc SDS (□), and 0.02 cmc SDS (■). The dashed lines represent the layer thickness reached under a high force. (Adopted from Ref. 68.)

The adsorbed layer has a pronounced viscoelastic character in the concentration regime 0.02–0.2 cmc (1.7×10^{-4}–1.7×10^{-3} M), with the most characteristic feature being a slow relaxation. This was observed as a slow change in surface separation occurring over a prolonged time after each change in compressive force, and we found it impossible to measure (quasi-) equilibrium forces. The forces measured on approach were purely repulsive. However, as soon as the layers were separated from each other an adhesive force was observed. This is demonstrated in Figure 25, which displays three force curves measured on consecutive approaches and separations to successively smaller distances. Note that the pull-off force increases with decreasing separation. We attribute the attraction to the formation of new mixed surfactant–polyelectrolyte micelles involving polyelectrolytes adsorbed on the opposing surfaces. The fact that the attractive force increases in strength with increasing compressive force (Figure 25) supports this sug-

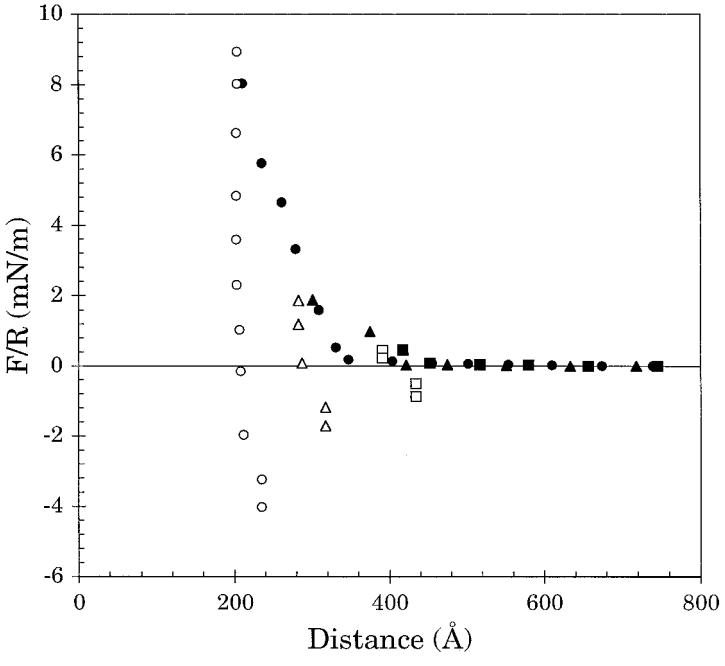

FIG. 25 Force normalized by radius as a function of surface separation between mica surfaces precoated with an adsorbed layer of 40DT. The solution contained 0.1 mM KBr and 0.04 cmc SDS. Filled symbols represent force measured on approach and unfilled symbols forces measured on separation. Three consecutive force curves, where the surfaces have been brought closer together for each consecutive time and then separated, are illustrated in the figure. (Adopted from Ref. 68.)

gestion, since the opposing layers either penetrate deeper into each other, or, due to deformation, develop a larger contact area. In either case, conditions are created that favor the formation of more interlayer mixed micelles. The slow relaxation reflects slow structural rearrangements occurring when the polyelectrolyte–surfactant layers confined between the two surfaces strive towards equilibrium. It should be emphasized that the general features, as illustrated in Figure 25, are reproducible but the details are not since they depend on the approach speed and eventual previous measurements on the same spot. Similar slowly relaxing adsorbed layers are formed when close to uncharged PCMA-SDS aggregates adsorb to mica, as will be discussed in Sec. VII.

The character of the layer changes as the SDS concentration is increased to above 0.2 cmc (1.7×10^{-3} M). The measured forces are now purely

repulsive both on approach and on separation. Further, the range of the steric repulsion decreases significantly with increasing SDS concentration (Figure 26). This strongly indicates a partial desorption of the polyelectrolyte. However, some polyelectrolytes remain on the surface also at an SDS concentration of 2 cmc.

F. Lysozyme, a Cationic Globular Protein

Hen egg white lysozyme is a small compact globular protein with the overall dimension of 45 × 30 × 30 Å. It carries a net positive charge of +9 at pH 5.6 and one relatively large hydrophobic surface area. Lysozyme adsorbs strongly to mica [96], and when the bulk lysozyme concentration is 0.2 mg/ml in 10^{-3} M NaCl at pH 5.6, the charges in the adsorbed layer nearly balance the mica surface charge [97]. The forces measured at this stage are illustrated in Figure 27. A weak double-layer repulsion dominates the long-

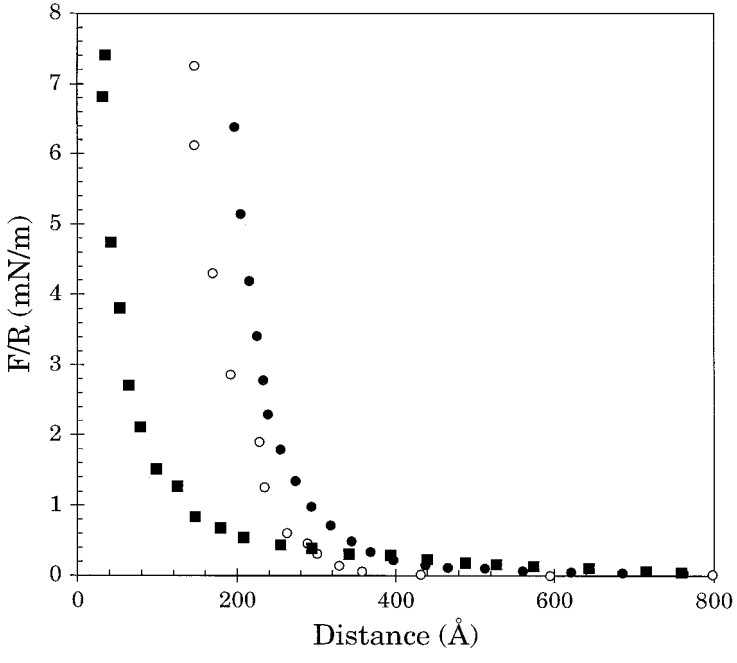

FIG. 26 Force normalized by radius as a function of surface separation between mica surfaces precoated with an adsorbed layer of 40DT. The solution contained 0.1 mM KBr and 0.2 cmc SDS (●), 0.5 cmc SDS (○), and 2 cmc SDS (■). (Adopted from Ref. 68.)

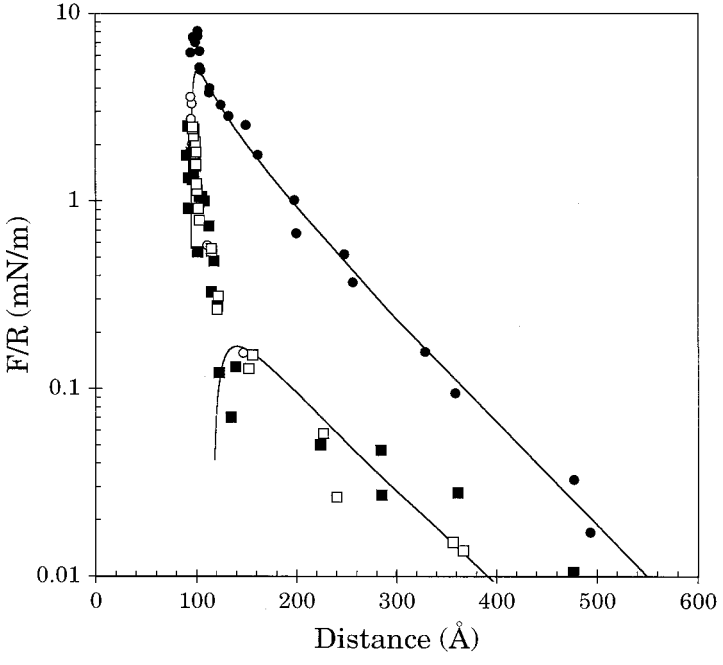

FIG. 27 Force normalized by radius as a function of surface separation between mica surfaces across a 0.2 mg/ml lysozyme solution in 1×10^{-3} M NaCl (■). The forces measured after removing the protein from the solution (□) and after adding 0.8 mM SDS (●) are also shown. The solid lines are calculated DLVO forces. (Adopted from Ref. 90.)

range interaction, whereas a steric force due to compression and dehydration of the adsorbed layer is the most dominating feature at distances below 100 Å. The layer thickness obtained under a high compressive load is consistent with contacts between end-on adsorbed proteins. This does not, however, mean that all molecules are adsorbed end on [90]. Hardly any change in the measured interaction is observed when the protein solution is replaced with a protein-free 10^{-3} M NaCl solution. Hence the adsorbed layer remains on the surface after dilution. When SDS is added to the solution to a concentration of 0.1 cmc (8×10^{-4} M), a strong double-layer force is observed, Figure 27 [90]. Clearly, SDS adsorbs to the protein-coated surface, giving it a net negative charge. The layer thickness measured under a high compressive force remains unchanged. Hence, unlike for the flexible polyelectrolytes, no swelling or desorption occurs as a result of the incorporation of a small amount of SDS. A further increase in SDS concentration to 0.5 cmc

(4×10^{-3} M) results in a strong increase in the repulsive double-layer force but no change in the final layer thickness; see Figure 28.

Interestingly, when the SDS concentration is increased further to 0.75 cmc (6×10^{-3} M), the adsorbed layer changes character. The final layer thickness is significantly decreased, and occasionally a long-range repulsive force of steric origin is observed at large separations; see Figure 28. This finding is interpreted as being due to denaturation of some of the adsorbed proteins, and it is suggested that denaturated polypeptide chains associated with SDS extend out into the solution. A further increase in SDS concentration to 1 cmc (8.3×10^{-3} M) results in a complete desorption of the lysozyme layer. We can thus pinpoint some differences between the effects of SDS on preadsorbed layers of lysozyme and preadsorbed layers of synthetic cationic polyelectrolytes. With lysozyme, the first event is simply an adsorption of the surfactant, as on any partly hydrophobic surface. Next, a partial denaturation of the protein takes place, and when this occurs further

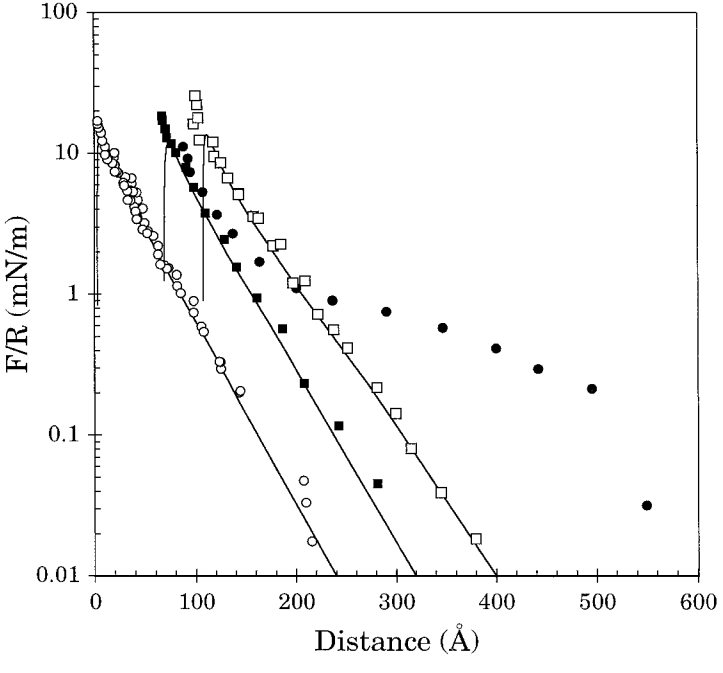

FIG. 28 Force normalized by radius as a function of surface separation between mica surfaces precoated with lysozyme across a 1×10^{-3} M NaCl solution containing 4 mM SDS (□), 6 mM SDS (■, ●), and 8.3 mM SDS (○). The solid lines are calculated DLVO forces. (Adopted from Ref. 90.)

association with SDS takes place leading to a cooperative desorption. The desorption process thus occurs considerably more suddenly than for the flexible polyelectrolytes. One reason for this may be that the surfactant-induced denaturation allows for a further uptake of SDS. Another reason may be that lysozyme, unlike the synthetic polyelectrolytes, is monodisperse. The effect of sodium dodecylsulfonate, SDSo, on preadsorbed lysozyme layers is similar to that of SDS [98], with two important differences. The charge of the adsorbed layer is smaller in the presence of SDSo than in the presence of SDS, and with SDSo no desorption occurs at room temperature. The reason for this may be that the SDSo was studied below its Krafft temperature, 35°C.

G. Effects of Polyelectrolyte Architecture

From the results described in this section it is clear that the structure of the preadsorbed polyelectrolyte strongly affects the association with oppositely charged surfactants. The most obvious parameter to consider is the charge density of the polyelectrolyte. In bulk solution the critical association concentration is found to decrease with increasing charge density. However, this is not the case when the association occurs at a highly negatively charged solid surface. It is found that the critical association concentration between PCMA and SDS at a mica surface, cac_s, is about 0.1 cmc (8.3×10^{-4} M). The value of cac_s decreases to between 0.005 and 0.05 cmc when the charge density is decreased to 30% (AM-MAPTAC-30), and it is 0.02 cmc for the 10% charged AM-CMA-10. For the very low charge density polyelectrolyte AM-MAPTAC-1, the cac_s is again higher, 0.3 cmc. The oddity in this series is the low value of cac_s found for the 100% charged polyelectrolyte. We attribute this to the very thin adsorbed layer structure found for this polyelectrolyte. It means that nearly all charged segments are located very close to charged sites on the surface and not easily accessible for the surfactant.

The trend cmc > $cac_s \geq cac_b$ is generally observed. The difference between the association concentration in bulk and at the surface is largest for the most charged polyelectrolyte, which is attributed to the thin adsorbed layer structure. In general there are several reasons why the cac between cationic polyelectrolytes and oppositely charged surfactants should be different at a negatively charged surface and in bulk. First, the polyelectrolyte at the surface is less flexible than the polyelectrolyte in bulk solution. Second, fewer polyelectrolyte charges are available for the surfactant to bind to, since most of the charged polyelectrolyte segments are in close contact with the negatively charged surface. Third, in bulk solution the counterion entropy increases when polyelectrolytes associate with surfactants. On the other hand, association at an uncharged polyelectrolyte-coated surface results

in a decrease in counterion entropy, due to the recharging of the surface that confines the counterions in the diffuse electrical double layer. No similar restriction of the counterion distribution results when uncharged polyelectrolyte–surfactant complexes are formed in bulk solution.

Another interesting observation is that the addition of SDS causes a swelling of AM-MAPTAC-30 and AM-CMA-10 layers, whereas a deswelling is observed for cationic guar with similar charge density [89]. We suggest that the key difference is that the layer formed by the cationic guar initially is very extended, whereas the layers built by the other polyelectrolytes are thin and compact. This, in turn, must be attributed to the architecture of the polyelectrolyte with intrinsic chain stiffness and possible branching as important parameters. Finally, we note that for the hydrophobically modified polyelectrolyte 40 DT, surfactants are incorporated in the adsorbed layer at very low surfactant concentrations, and the concept of a critical association concentration is inappropriate at the surface as well as in bulk solution.

VII. ADSORPTION OF PREFORMED POLYELECTROLYTE–SURFACTANT AGGREGATES

We now turn to the more complex situation where both polyelectrolytes and surfactant are present in solution and adsorption is allowed to occur from this mixture. Polyelectrolyte and surfactant mixtures are used in numerous applications such as pharmaceuticals, laundry, and cosmetics, just to mention a few [4]. Sometimes polyelectrolytes and surfactants are unintentionally mixed and due to mutual interaction provide unexpected properties to the mixture. Sometimes they are purposefully added together to fill the function of changing the properties and feel of surfaces, e.g., hair or fabrics, or to act as deposition aids. It is thus important to understand how these mixtures act when they are first mixed in bulk and subsequently transferred to a surface, and how the properties of polyelectrolyte–surfactant aggregates formed in bulk correlate with the properties of such aggregates adsorbed at a solid–liquid interface. Further, it is necessary to learn what happens with the polyelectrolyte–surfactant mixture at the surface when it is diluted with water.

A. Mixtures Containing PCMA and SDS

It is clear from the discussion concerned with polyelectrolyte–surfactant bulk properties (Sec. III) that PCMA–SDS aggregates, depending on the surfactant concentration, acquire charges ranging from highly positive to highly negative. It turns out that PCMA–SDS aggregates adsorb on nega-

tively charged mica surfaces regardless of the sign of their own charge. However, as determined by XPS analysis, the adsorbed amount varies strongly with the SDS concentration (Figure 29). At low SDS concentrations, a nitrogen signal emanating from the polyelectrolyte is observed, whereas the amount of surfactant is below the detection limit. However, when the SDS concentration is above 0.01 cmc, both a sulfur signal from the surfactant and a nitrogen signal are observed. The adsorbed amounts for both components reach a maximum at an SDS concentration of about 0.04 cmc, which also corresponds closely to SDS concentration of the turbidity maximum and zero mobility; see Figure 3. For details of the sample preparation and the quantitative determination of the adsorbed amount using XPS, the reader is referred to Refs. 69 and 99.

The forces measured after allowing an aqueous mixture contain 20 ppm PCMA and a small amount of SDS (0.002–0.01 cmc) to equilibrate with the mica surfaces for 20 hours are shown in Figure 30. The measured repulsive steric forces are nearly independent of the SDS concentration but are stronger than the weak double-layer force observed in the complete ab-

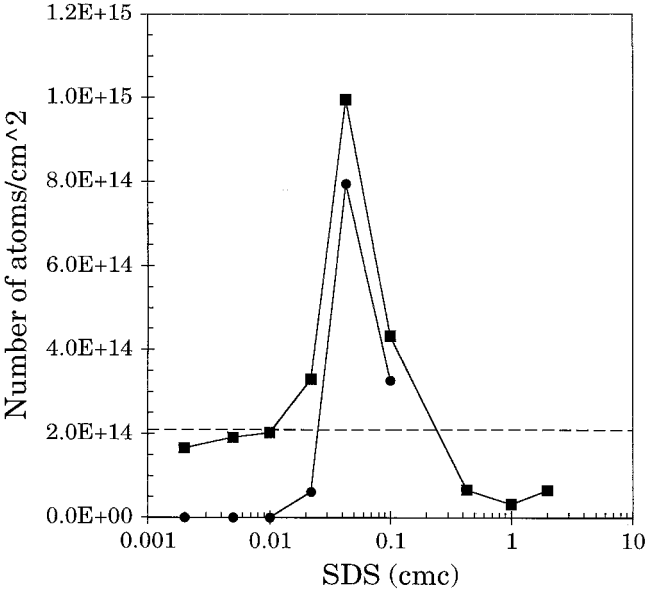

FIG. 29 Number of nitrogen (■) and sulfur (●) atoms per cm^2 in the adsorbed PCMA–SDS layer as a function of SDS bulk concentration. The dashed line indicates the number of negative surface sites on the basal plane of muscovite mica. (Adopted from Ref. 105.)

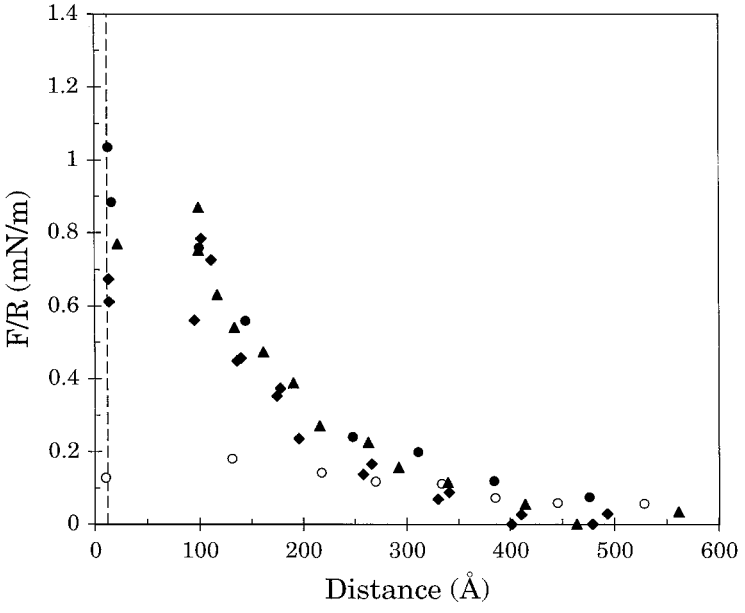

FIG. 30 Force normalized by radius as a function of surface separation. The surface interactions were determined after 20 hours of equilibration across solutions containing 20 ppm PCMA, 1×10^{-4} M KBr, and various amounts of SDS. The SDS concentrations were zero (○), 0.002 cmc SDS (●), 0.005 cmc SDS (▲), and 0.01 cmc SDS (♦). The dashed line illustrates the compressed layer thickness. (Adopted from Ref. 105.)

sence of SDS. It appears that even a small amount of the anionic surfactant affects the surface conformation of the polyelectrolyte. This is even more clearly seen at short equilibration times, as will be discussed in Sec. VIII. The undistributed layer thickness was found to be about 200 Å, and the force required to squeeze the surfaces into the position of the attractive minimum at a separation of 12 Å was 0.55–0.9 mN/m.

When the SDS concentration in the polyelectrolyte–surfactant mixtures exceeded 0.01 cmc (8.3×10^{-5} M), a sharp increase in turbidity occurred (Figures 2 and 3). The electrophoretic mobility of the PCMA–SDS aggregates at a total SDS concentration of 0.02 cmc (1.7×10^{-3} M) remains positive but with a slightly lower magnitude than at lower SDS concentrations. The forces measured across a solution containing such complexes after adsorption of 20 hours are presented in Figure 31. They differ significantly from those measured at lower SDS concentrations. The onset of the repulsive force was detected at a separation of about 1000 Å, i.e., the undisturbed

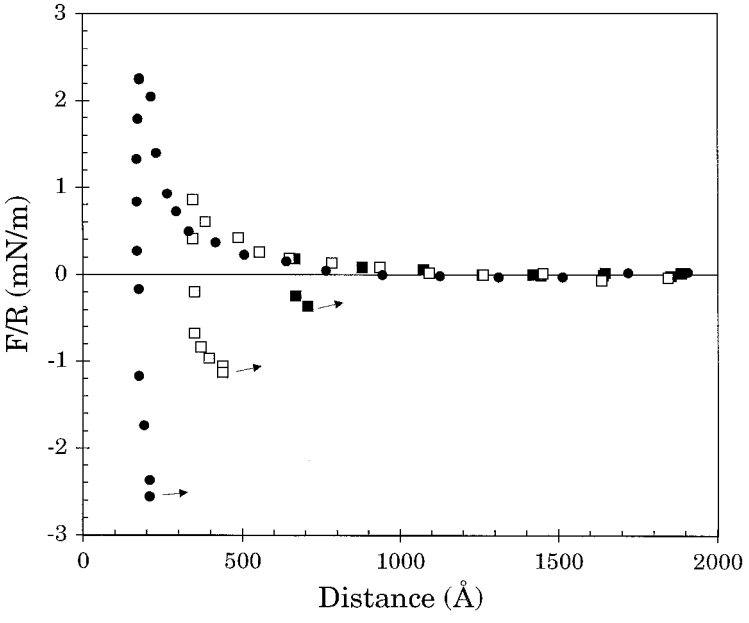

FIG. 31 Force normalized by radius as a function of surface separation. The surface interaction across a solution containing 20 ppm PCMA, 1×10^{-4} M KBr, and 0.02 cmc SDS after 20 hour adsorption is shown. Three consecutive force curves to progressively smaller distances are included in the figure. Arrows illustrate outward jumps occurring upon separation. (Adopted from Ref. 105.)

layer thickness on each surface was about 500 Å. The most characteristic feature of the adsorbed layer is its slow relaxation. When the compressive force was changed, the surface separation changed slowly for a very long time, and it was impossible to measure (quasi-) equilibrium forces. The forces measured on approach were purely repulsive. However, an attraction was observed on separation. This is clearly shown in Figure 31 by three consecutive approaches and separations. One finding is that the pull-off force increases with decreasing separation between the surfaces. We also note that the jumping out is not distinct, but the layers are stretched considerably before the surfaces separate from each other. The layers are thus highly viscous (the relaxation time is slow) and sticky. The general features, as illustrated in Figure 31, are reproducible, but the details are not.

At a slightly higher total SDS concentration of 0.04 cmc (3.3×10^{-4} M) the turbidity has a maximum and, as judged from the electrophoretic mobility, the complex is almost uncharged. The general features of the force

curve are the same as at 0.02 cmc SDS, i.e., the adsorbed layer is thick, viscous, and sticky. However, the range of the repulsive force due to compression of the adsorbed PCMA–SDS aggregates is much larger and extends up to 4000 Å (Figure 32).

At even higher SDS concentrations the aggregates formed in solution carry a net negative charge. The forces measured across PCMA–SDS solutions with a total SDS concentration of 0.1 cmc (8.3×10^{-4} M) are shown in Figure 33. The adsorbed PCMA–SDS surface layers given rise to similar force curves as at the two lower SDS concentrations with the inward force curve being repulsive and the outward one attractive. The range of the force, however, was reduced 10 times as compared to the preceding SDS concentration. Clearly, even rather strongly negatively charged PCMA–SDS aggregates adsorb on the negatively charged mica surface. The slow relaxation time observed in the SDS concentration range 0.02–0.1 cmc indicates a corresponding slow change in the internal structure of the adsorbed layer. The association between polyelectrolytes and oppositely charged surfactants

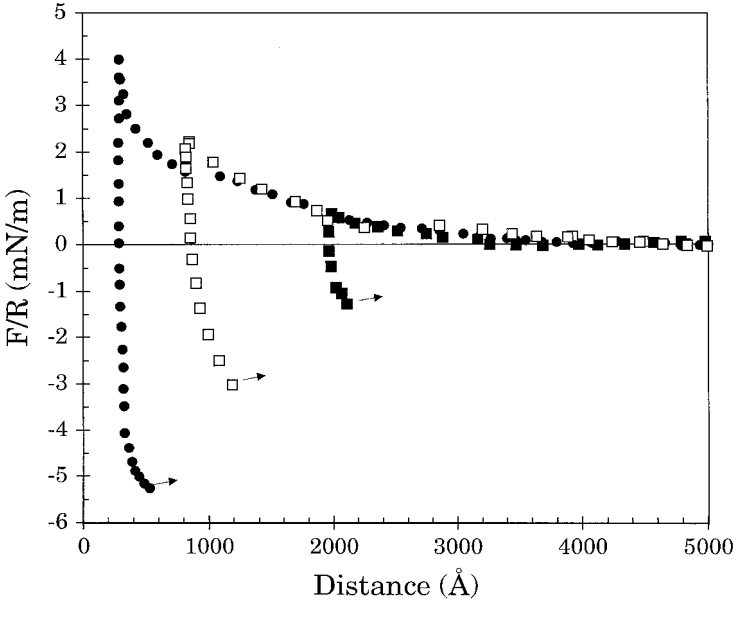

FIG. 32 Force normalized by radius as a function of surface separation. The surface interaction across a solution containing 20 ppm PCMA, 1×10^{-4} M KBr, and 0.04 cmc SDS is shown. The different symbols represent force curves where the surfaces have been brought to different distances before being separated. Arrows illustrate outward jumps occurring upon separation. (Adopted from Ref. 105.)

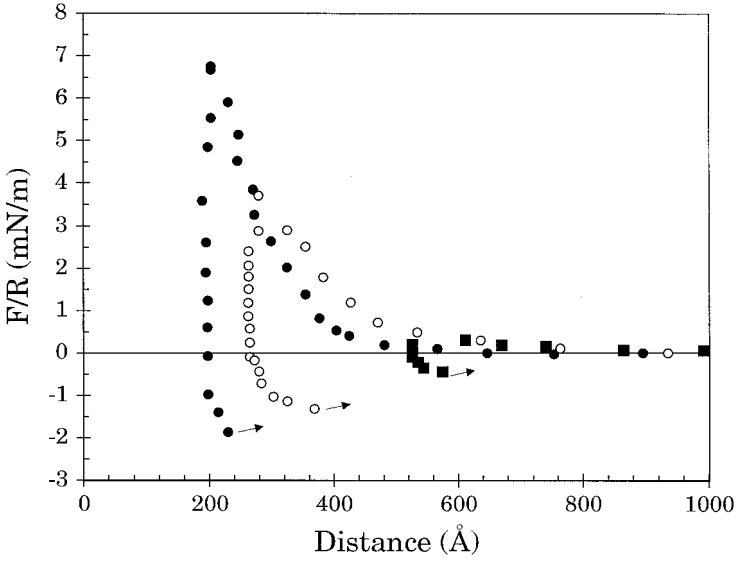

FIG. 33 Force normalized by radius as a function of surface separation. The surface interaction across a solution containing 20 ppm PCMA, 1×10^{-4} M KBr, and 0.1 cmc SDS is shown. The different symbols represent force curves where the surfaces have been brought to different distances before being separated. Arrows illustrate outward jumps observed on separation. (Adopted from Ref. 105.)

strongly affects the viscosity of solutions more concentrated in polyelectrolytes than in our study. The viscosity first increases dramatically due to the formation of surfactant-mediated bridges between the polyelectrolytes [89,100]. At higher surfactant concentrations, the viscosity decreases again because the system comes into a two-phase region and then at higher concentration each polyelectrolyte chain becomes saturated with surfactants [89]. The adsorbed layer is concentrated in polyelectrolytes, much more so than the bulk solution. In this concentrated surface region SDS may connect different polyelectrolytes together and a network is formed. Upon compression this network is disturbed. We suggest that the slow relaxation stems from the difficulty of establishing the new free energy minimum of the network confined between the two surfaces. Another finding is that an attraction develops as soon as the two polyelectrolyte–surfactant layers come into contact. This attraction is likely due to the formation of new surfactant-mediated bridges between polyelectrolytes on the opposing surfaces. The same mechanism is responsible for the slow change in turbidity of bulk

solutions with time caused by aggregation and eventual sedimentation of large aggregates (Figure 4).

The turbidity of a PCMA–SDS solution at 0.4 cmc (3.3×10^{-3} M) is substantially reduced in comparison with that at lower surfactant concentrations. The forces induced by adsorption of such aggregates were, in contrast to at the lower SDS concentrations, repulsive both on approach and on separation (Figure 34). The range of the force was not more than approximately 200 Å, i.e., half the value measured at an SDS concentration of 0.1 cmc. A further increase in the total SDS concentration in the mixture to 1 cmc resulted in a force with a very similar character to that observed at 0.4 cmc SDS. We note that the distance dependence of the force at large separations is consistent with that of a double-layer force. However, at distances below about 50 Å a steric force predominates. It seems that the polyelectrolyte chains that do adsorb at these high SDS concentrations are saturated with surfactant, and that this prevents a large adsorbed amount and the

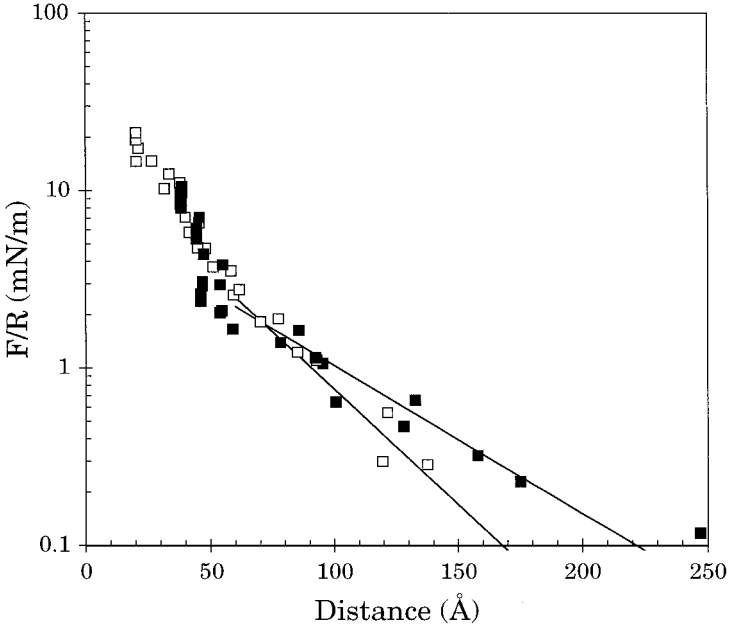

FIG. 34 Force normalized by radius as a function of surface separation. The surface interactions across solutions containing 20 ppm PCMA, 1×10^{-4} M KBr, and 0.4 cmc SDS (■), and 20 ppm PCMA, 1×10^{-4} M KBr, and 1 cmc SDS (□) are shown. The lines have slopes corresponding to those of double-layer forces at the ionic strength of the solutions. (Adopted from Ref. 105.)

development of surfactant-mediated bridges between the two opposing surfaces.

B. Mixtures Containing AM-MAPTAC-30 and SDS

The correlation between the properties of polyelectrolyte–surfactant mixtures in bulk and at a solid–liquid interface has also been studied employing a 30% positively charged polyelectrolyte, AM-MAPTAC-30 and SDS [82]. In this study a polyelectrolyte concentration of 200 ppm was used, and the salt concentration was 1×10^{-2} M. Hence the polyelectrolyte concentration was 10 times larger and the salt concentration 100 times larger than in the PCMA–SDS study described above. Due to the relatively large polyelectrolyte concentration, the amount of SDS bound to the polyelectrolyte is now significantly larger than the free SDS concentration. Under such circumstances it is relevant to discuss the results in terms of the concentration ratio of SDS to the charged monomer MAPTAC, i.e., the SDS/MAPTAC ratio. On the other hand, the total concentration of SDS, expressed e.g. in terms of the cmc, has lost its meaning.

One main conclusion was that the variation of the forces measured across AM-MAPTAC-30–SDS mixtures as a function of surfactant concentration can be understood by considering the bulk behavior. When the SDS/MAPTAC ratio was increased from 0 to 0.4, a continuous decrease in the apparent hydrodynamic radius of bulk complexes was seen from the light scattering data [82]. Similarly, the range of the measured repulsive force due to adsorbed polyelectrolyte–surfactant aggregates was decreasing when the SDS/MAPTAC ratio was increased from 0 to 0.4 (Figure 35). The SDS/MAPTAC ratio of 0.6 is just at the borderline where the bulk solution phase separates, indicating an attractive interaction between polyelectrolyte–SDS aggregates. This attraction is also observed between adsorbed polyelectrolyte–surfactant layers (Figure 36). It is rationalized, just as in the PCMA-SDS case, by surfactant-mediated interlayer bridge formation. At an SDS/MAPTAC ratio of one, a thick precipitate was formed, and no meaningful force curves could be recorded. At even higher SDS concentrations (SDS/MAPTAC ratio of 4), the solution became clear again, and the adsorption of the now strongly negatively charged complexes was found to be limited. A strong repulsive force was observed on approach (Figure 37). The repulsion measured on separation was slightly weaker, and a shallow attractive minimum could be detected at rather large separations.

VIII. NONEQUILIBRIUM ASPECTS

It has long been realized that processes with polymers involved may be very slow. For instance, during adsorption from a polydisperse polymer solution,

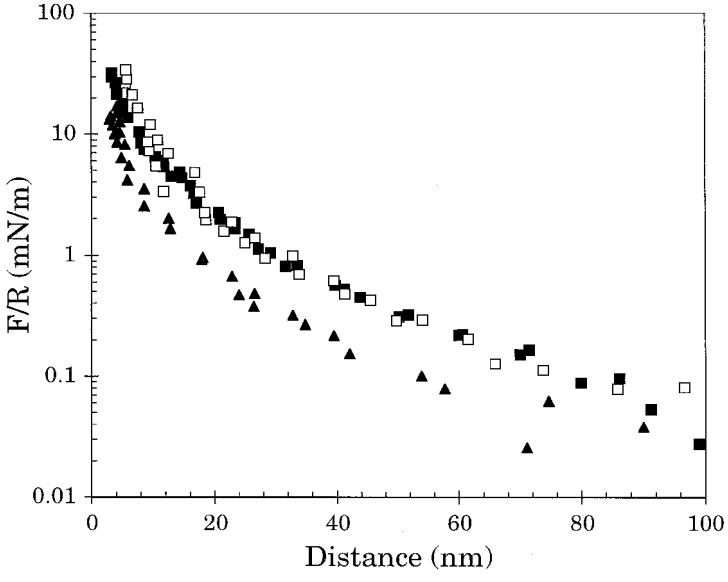

FIG. 35 Force normalized by radius as a function of surface separation between mica surfaces across a 10 mM NaCl solution containing 200 ppm AM-MAPTAC-30 and various amounts of SDS. The SDS/MAPTAC ratios were 0 (■), 0.2 (□), and 0.4 (▲). (Adopted from Ref. 82.)

it is initially the lower molecular weight molecules that adsorb due to their faster diffusion. However, from the thermodynamic point of view, the adsorption of higher molecular weight species is more favorable. This is an entropy effect. The decrease in entropy is less when one large molecule adsorbs compared to the entropy loss occurring when many small molecules adsorb. Hence an exchange of lower molecular weight chains by higher molecular weight ones will occur with time. However, the exchange process may last for weeks, and equilibrium may, practically, never be reached [87]. We also note that the use of homopolymers as steric stabilizers is based on their slow desorption. It has clearly been shown theoretically that if full equilibrium is established at each surface separation, then two surfaces coated by homopolymers will attract each other [101,102]. However, if the polymers have no time to desorb during the collision event, which is most often the case in a real situation, a repulsion develops in good solvents. One case that can be treated theoretically is what is called restricted equilibrium (or quasi-equilibrium). In this situation the adsorbed amount is independent of surface separation, and the conformation of the adsorbed polymer chains

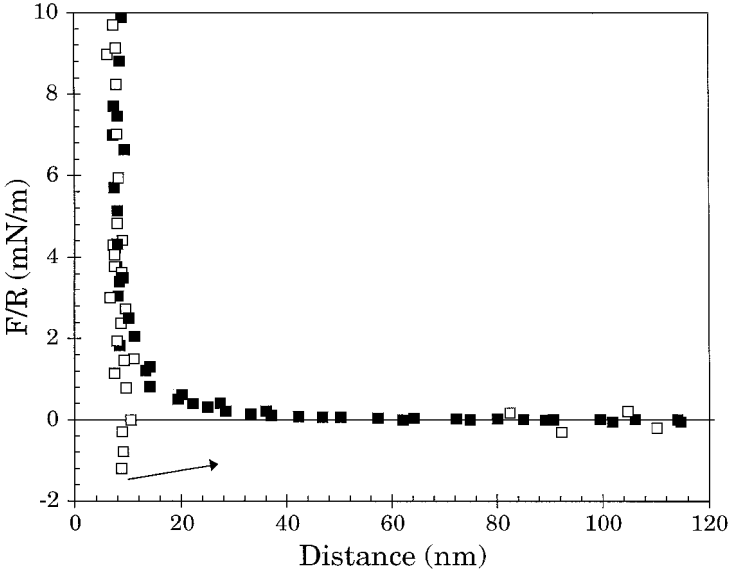

FIG. 36 Force normalized by radius as a function of surface separation between mica surfaces across a 10 mM NaCl solution containing 200 ppm AM-MAPTAC-30 and SDS. The SDS/MAPTAC ratio was 0.6. Forces measured on approach (■) and on separation (□). The arrow indicates an outward jump. (Adopted from Ref. 82.)

has time to equilibrate at each separation, i.e., the equilibrium situation for the fixed adsorbed amount is reached. Experimentally it means that the same force curves should be measured on approach and on separation, and this is often the case. However, in other cases the force measured on approach and on separation is different, showing that some relaxation mechanism (adsorption/desorption or rearrangements) in the adsorbed layer has a relaxation time comparable to the time scale of the experiment (minutes to hour), and nonequilibrium forces are measured (see e.g. Figures 31–33). There are some theoretical attempts to describe nonequilibrium forces [103,104], particularly effects due to ''squeezing down'' polymer segments by approaching two surfaces together. However, they do not suffice to explain the complex behavior illustrated in Figures 31–33. The adsorption from solutions containing either polyelectrolytes or surfactants is rather well understood, even though nonequilibrium effects are not uncommon in the case of polyelectrolytes [86]. The research on adsorption from polyelectrolyte–surfactant mixtures is a comparatively recent effort, and many aspects, particularly nonequilibrium phenomena, are not systematically studied or very well un-

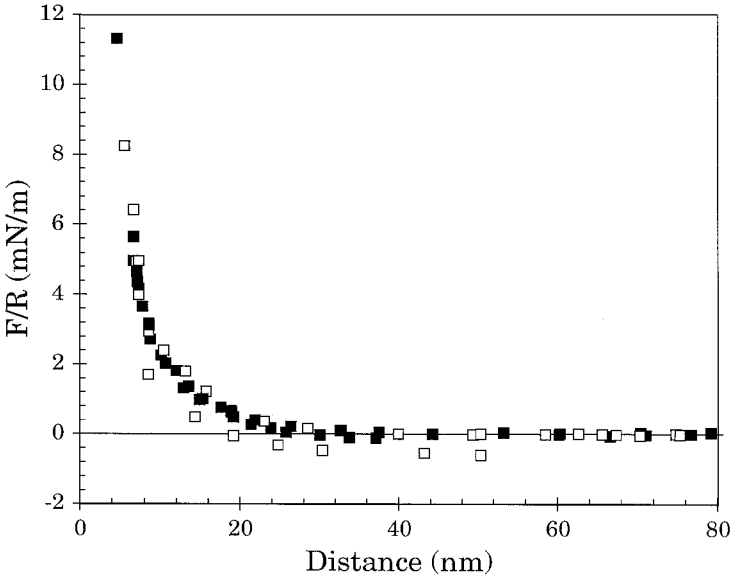

FIG. 37 Force normalized by radius as a function of surface separation between mica surfaces across a 10 mM NaCl solution containing 200 ppm AM-MAPTAC-30 and SDS. The SDS/MAPTAC ratio was 4.0. Forces measured on approach (■) and on separation (□) are illustrated. (Adopted from Ref. 82.)

derstood. However, some reports on this topic can be found. For instance, Pagac et al. [37] studied adsorption and coadsorption of cationic surfactant with cationic polyelectrolytes and found that the effect of the surfactant on the polyelectrolyte adsorption was very sensitive to the order in which the surfactant and the polyelectrolyte were exposed to the surface. Different pathways to the same final bulk solution composition produced significantly different adsorption results. Similar conclusions were reached by Neivandt et al. [39], who studied coadsorption of cetyltrimethylammonium bromide and poly(styrenesulfonate) on silica.

It has been established that the order in which polyelectrolyte and salt is added affects the state of the adsorbed polyelectrolyte layer for prolonged times [74,86]. It is thus no surprise that the experimental pathway also influences the character of adsorbed layers consisting of oppositely charged polyelectrolyte and surfactant [69]. For instance, let us compare the surface forces generated by adsorbed PCMA–SDS complexes at identical final bulk solution composition, 1 cmc SDS and 1×10^{-4} M KBr; see Figure 38. In one case the polyelectrolyte was first adsorbed onto the mica surfaces from

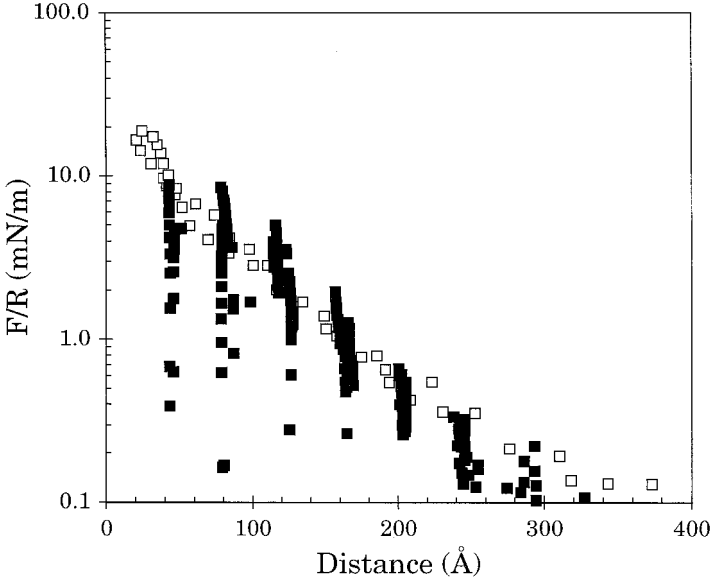

FIG. 38 Force normalized by radius as a function of surface separation. The forces measured between mica surfaces precoated with PCMA across an essentially polyelectrolyte-free (3 ppm) solution containing 1 cmc SDS and 1×10^{-4} M KBr are represented by (■). The forces obtained after PCMA–SDS aggregates have been adsorbed from a PCMA–SDS mixture containing 20 ppm PCMA and 1 cmc SDS and subsequently diluted by a polyelectrolyte-free 1 cmc SDS solution is shown by (□). (Adopted from Ref. 69.)

surfactant-free 20 ppm PCMA and 1×10^{-4} M KBr solution. Next, the polymer was removed from the bulk and 1 cmc SDS was injected. The effect of the SDS association with the preadsorbed polyelectrolyte resulted in an adsorbed layer with a characteristic internal structure that gives rise to an oscillatory force profile. In the other case the polyelectrolyte surfactant complex was adsorbed from a mixture containing 20 ppm PCMA, 1 cmc SDS, and 1×10^{-4} M KBr. Next, the polymer was removed from the bulk and 1 cmc SDS was injected. In this case no similar oscillations were detected in the force profile, indicating that the adsorbed layer structure was different (Figure 38). We attribute this difference to two factors. First, the adsorbed amount of PCMA, determined by XPS, is eight times as high in the case of preadsorbed polyelectrolyte [69] as compared to the amount of polyelectrolyte adsorbed from the PCMA–SDS mixture. Second, the preadsorbed polyelectrolyte layer is homogeneously distributed over the surface, whereas an

inhomogeneous layer is most likely formed by aggregate adsorption. In particular, the structural units giving rise to the characteristic length scale may have a random orientation relative to the surface.

Another important aspect to consider is slow changes in adsorbed polyelectrolyte–surfactant layers occurring with equilibration time [69,82]. Consider for example PCMA–SDS complexes at low surfactant concentrations. These complexes are positively charged, and they adsorb rapidly to negatively charged surfaces. However, after the rapid adsorption stage, a slow spreading of the polyelectrolyte occurs. It takes a very long time for the equilibrium conformation of the adsorbed polyelectrolyte chains to be attained. In Figure 39 this is illustrated for the case when PCMA–SDS complexes have adsorbed from a mixture containing 20 ppm PCMA, 0.002 cmc SDS and 1×10^{-4} M KBr. The association between the polyelectrolyte and the surfactant in bulk leads to a more coiled conformation. Upon adsorption, this conformation is partly retained, and initially the adsorbed layer is rather thick. The range of the repulsive steric force is about 1000 Å. The range and the strength of the repulsion decreases with time due to a slow change

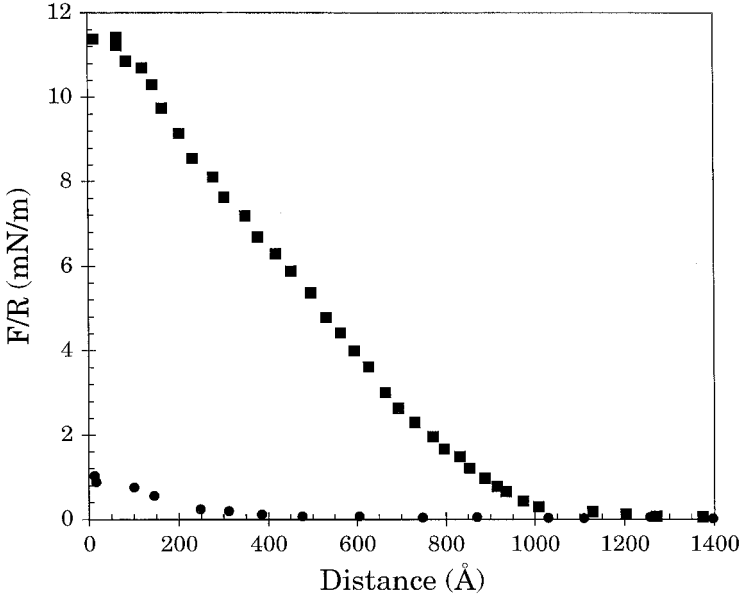

FIG. 39 Force normalized by radius as a function of surface separation. The forces were measured between mica surfaces immersed in a solution containing 20 ppm PCMA, 1×10^{-4} M KBr, and 0.002 cmc SDS. The forces were measured at one hour (■) and 20 hours (●) after injection of the solution. (Adopted from Ref. 105.)

in polyelectrolyte conformation resulting in a more flat adsorbed layer. It seems likely that the conformational change is accompanied by a slow expulsion of anionic surfactant. Similar slow structural changes, demonstrating that initially adsorbed polyelectrolyte–surfactant aggregates slowly rearrange at the surface, were also observed with AM-MAPTAC-30 [82]. In technical applications it is often the case that the contact time with a surface is short and the adsorbed layer will be in a nonequilibrium state. To design appropriate experiments and theoretical tools for increasing the knowledge about such processes is clearly a challenge.

IX. SUMMARY

We have presented some data on how association between polyelectrolytes and surfactants at solid–liquid interfaces influences the surface interactions and structure of adsorbed layers. The behavior is rich and strongly dependent on the polyelectrolyte architecture. Very different properties of the adsorbed layers are obtained when polyelectrolyte–surfactant aggregates formed in bulk solution are allowed to adsorb compared to when surfactant associates with preadsorbed polyelectrolyte layers. The reason for this is the extremely slow approach towards equilibrium in these systems. In fact, it is not clear what the true equilibrium layer structure looks like. This means that great care must be taken when comparing results reported in the literature. One needs to know the details of the experimental pathway as well as the bulk composition; otherwise, comparisons become meaningless. Further, the usefulness of the information obtained from an academic study for a given technical application must also consider the experimental path in both the fundamental study and the application. There is much fundamental knowledge lacking. For instance, with a few exceptions [34,35], the amount of surfactant in the adsorbed layer is not known. A detailed description of the structure of the adsorbed layer is also lacking, and neutron reflectivity studies would be most appropriate. In many cases the viscoelastic properties of the adsorbed layers play important roles for the measured forces, but no quantitative measurements of these properties have been performed. Further, next to nothing is known about how the nature of the solid surface affects the adsorption of polyelectrolyte–surfactant mixtures and the forces induced by these layers. The important issue of how the nature of preadsorbed polyelectrolyte–surfactant complexes changes upon dilution is hardly explored, even though one study touching on this technologically important issue has been reported [69]. In many applications surfactant mixtures (e.g., anionic/nonionic) are used together with cationic polyelectrolytes. Again, basic knowledge is lacking about surface properties of such complexes.

ACKNOWLEDGMENT

This report was supported by the NUTEK Centre for Surfactants Based on Natural Products (SNAP) and the SSF program Colloid and Interface Technology. We acknowledge the assistance of Dr. Isabelle Grillo at ILL.

REFERENCES

1. Y-C Wei, SM Hudson. J.M.S.-Rev. Macromol. Chem. Phys. C35:15, 1995.
2. Y Li, PL Dubin. ACS Symposium Series, vol 578, 1994:320–336.
3. ED Goddard, KP Ananthapadmanabhan. Interactions of Surfactants with Polymers and Proteins. CRC Press, Boca Raton, 1993.
4. JCT Kwak. Polymer–Surfactant Systems. New York: Marcel Dekker, 1998.
5. L Piculell, B Lindman. Adv. Colloid Interface Sci. 41:149, 1992.
6. L Piculell, F Guillemet, K Thuresson, V Shubin, O Ericsson. Adv. Colloid Interface Sci. 63:1, 1996.
7. I Iliopoulos. Current Opinion Colloid Interf. Sci. 3:493, 1998.
8. B Magny, I Iliopoulos, R Zana, R Audebert. Langmuir 10:3180, 1994.
9. PS Leung, ED Goddard. Langmuir 7:608, 1991.
10. ED Goddard, RB Hannan, GH Matteson. J. Colloids Interface Sci. 60:214, 1977.
11. PS Leung, ED Goddard. Colloids Surf. 13:47, 1985.
12. B-H Lee, SD Christian, EE Tucker, JF Scamehorn. Langmuir 7:1332, 1991.
13. E Goddard, D., KP Ananthapadmanabhan. In: Kwak JCT, ed. Polymer–Surfactant Systems. Surfactant Science Series, vol 77. New York: Marcel Dekker, 1998:21–64.
14. I Satake, JT Yang. Biopolymers 15:2263, 1976.
15. K Hayakawa, JP Santerre, CT Kwak. Macromolecules 16:1642, 1983.
16. K Hayakawa, JCT Kwak. J. Phys. Chem. 87:506, 1983.
17. JP Santerre, K Hayakawa, JCT Kwak. Colloids Surf. 13:35, 1985.
18. B Lindman, K Thalberg. In: ED Goddard, KP Ananthapadmanabhan, eds. Interactions of Surfactants with Polymers and Proteins. CRC Press, Boca Raton, 1993:203–276.
19. A Malovikova, K Hayakawa, JCT Kwak. J. Phys. Chem. 88:1930, 1984.
20. AR Khokhlov, EY Kramarenko, EE Makhaeva, SG Starodubtzev. Macromolecules 25:4779, 1992.
21. JP Gong, Y Osada. J. Phys. Chem. 99:10971, 1995.
22. T Wallin, P Linse. Langmuir 12:305, 1996.
23. M Antonietti, J Conrad, A Thünemann. Macromolecules 27:6007, 1994.
24. M Antonietti, C Burger, J Effing. Adv. Mater. 7:751, 1995.
25. M Antonietti, A Kaul, A Thünemann. Langmuir 11:2633, 1995.
26. M Antonietti, A Wenzel, A Thünemann. Langmuir 12:2111, 1996.
27. M Antonietti, M Maskos. Macromolecules 29:4199, 1996.
28. P Linse, L Piculell, P Hansson. In: Kwak JCT, ed. Polymer–Surfactant Systems. Surfactant Science Series, vol 77. New York: Marcel Dekker, 1998: 193–237.

29. O Anthony, R Zana. Langmuir 12:3590, 1996.
30. PL Dubin, R Oteri. J. Colloid Interf. Sci. 95:453, 1983.
31. PL Dubin, DR Rigsbee, DW McQuigg. J. Colloid Interface Sci. 105:509, 1985.
32. PL Dubin, SS Thé, DW McQuigg, CH Chew, LM Gan. Langmuir 5:89, 1989.
33. DR Rigsbee, PL Dubin. Langmuir 12:1928, 1996.
34. V Shubin. Langmuir 10:1093, 1994.
35. V Shubin, P Petrov, B Lindman. Colloid Polym. Sci. 272:1590, 1994.
36. EM Furst, ES Pagac, RD Tilton. Ind. Eng. Chem. Res. 35:1566, 1996.
37. ES Pagac, DC Prieve, RD Tilton. Langmuir 14:2333, 1998.
38. A Creeth, E Staples, L Thompson, I Tucker, J Penfold. J. Chem. Soc. Faraday Trans. 92:589, 1996.
39. DJ Neivandt, ML Gee, CP Tripp, ML Hair. Langmuir 13:2519, 1997.
40. DJ Neivandt. Co-adsorption of Polyelectrolytes and Surfactants at the Silica/Solution Interface: A Spectroscopic Study. University of Melbourne, 1998.
41. M Rohdahl, F Höök, C Fredriksson, CA Keller, A Krozer, P Brezezinski, M Voinova, B Kasemo. Faraday Discuss. 107:229, 1997.
42. PM Claesson, T Ederth, V Bergeron, MW Rutland. Adv. Colloid Interface Sci. 67:119, 1996.
43. JN Israelachvili. J. Colloid Interface Sci. 44:259. 1973.
44. JN Israelachvili, GE Adams. J. Chem. Soc. Faraday Trans. 1 74:975, 1978.
45. RG Horn, DR Clarke, MT Clarkson. J. Mater. Res. 3:413, 1988.
46. RG Horn, DT Smith, W Haller. Chem. Phys. Letters 162:404, 1989.
47. J Parker. Prog. Surf. Sci. 47:205, 1994.
48. K Schillén, PM Claesson, M Malmsten, P Linse, C Booth. J. Phys. Chem. 101:4238, 1997.
49. B Derjaguin. Kolloid. Zeits. 69:155, 1934.
50. WA Ducker, TJ Senden, RM Pashley. Nature 353:239, 1991.
51. WA Ducker, TJ Senden, RM Pashley. Langmuir 8:1831, 1992.
52. H-J Butt. Biophys. J. 60:1438, 1991.
53. CM Mate, GM McClelland, R Erlandsson, S Chiang. Phys. Rev. Lett. 59: 1942, 1987.
54. I Larsen, CJ Drummond, DYC Chan, F Grieser. Langmuir 13:2109, 1997.
55. A Meurk, PF Luckham, L Bergström. Langmuir 15:3896, 1999.
56. A Carambassis, MW Rutland. Langmuir 19:5584, 1999.
57. YQ Li, NJ Tao, JJ Pan, AA Garcia, SM Lindsay. Langmuir 9:637, 1993.
58. B Cabane, R Duplessix, T Zemb. J. Physique 46:2161, 1985.
59. M Bergström, JS Pedersen. Phys. Chem. Chem. Phys. 1:4437, 1999.
60. RG Alargova, II Kochijashky, ML Sierra, R Zana. Langmuir 14:5412, 1998.
61. O Anthony, R Zana. Langmuir 12:1967, 1996.
62. R Zana. In: Kwak JCT, ed. Polymer-Surfactant Systems. Surfactant Science Series, vol 77. New York: Marcel Dekker, 1998:409–454.
63. T Wallin, P Linse. Langmuir 14:2940, 1998.
64. T Wallin, P Linse. J. Phys. Chem. 100:17873, 1996.
65. T Wallin, P Linse. J. Phys. Chem. 101:5506, 1997.
66. K Thalberg, B Lindman. J. Phys. Chem. 93:1478, 1989.

67. DE Leckband, OV Borisov, A Halperin. Macromolecules 31:2368, 1998.
68. A Dedinaite, PM Claesson, J Nygren, I Iliopoulos. Submitted.
69. A Dedinaite, PM Claesson, M Bergström. Langmuir. Submitted.
70. A Dedinaite. Surface force studies of association phenomena at solid–liquid interfaces. Ph.D. thesis, Royal Institute of Technology, 1999.
71. PM Claesson, A Dedinaite, E Blomberg, VG Sergeyev. Ber. Bunsenges. Phys. Chem. 100:1008, 1996.
72. MAG Dahlgren, PM Claesson, R Audebert. J. Colloid Interface Sci. 166:343, 1994.
73. MR Böhmer, OA Evers, JMHM Scheutjens. Macromolecules 23:2288, 1990.
74. MAG Dahlgren, Å Waltermo, E Blomberg, PM Claesson, L Sjöström, T Åkesson, B Jönsson. J. Phys. Chem. 97:11769, 1993.
75. N Güven. Zeitschrift für Kristallographie 134:196, 1971.
76. RM Pashley. J. Colloid Interface Sci. 83:531, 1981.
77. PM Claesson, URM Kjellin. In: Binks BP, ed. Modern Characterization Methods of Surfactant Systems. Surfactant Science Series, vol 83. New York: Marcel Dekker, 1999:255–333.
78. MAG Dahlgren, PM Claesson, R Audebert. Nordic Pulp Paper Research J 8: 62, 1993.
79. MAG Dahlgren. Langmuir 10:1580, 1994.
80. ML Fielden, PM Claesson, K Schillén. Langmuir 14:5366, 1998.
81. PM Claesson, A Dedinaite, M Fielden, URM Kjellin, R Audebert. Prog. Colloid Polymer Sci. 106:24, 1997.
82. PM Claesson, M Fielden, A Dedinaite, W Brown, J Fundin. J. Phys. Chem. B 102:1270, 1998.
83. URM Kjellin, PM Claesson, R Audebert. J. Colloid Interface Sci. 190:476, 1997.
84. OJ Rojas, PM Claesson, D Muller, RD Neuman. J. Colloid Interface Sci. 205: 77, 1998.
85. PF Luckham, J Klein. J. Chem. Soc. Faraday Trans. 1 80:865, 1984.
86. MAG Dahlgren, HCM Hollenberg, PM Claesson. Langmuir 11:4480, 1995.
87. MA Cohen Stuart, FG J. Ann. Rev. Mater. Sci. 26:463, 1996.
88. KP Ananthapadmanabhan, G-Z Mao, ED Goddard, T M. Colloids Surf. 61: 167, 1991.
89. O Anthony, CM Marques, P Richetti. Langmuir 14:6086, 1998.
90. JC Fröberg, E Blomberg, PM Claesson. Langmuir 15:1410, 1999.
91. O Rojas, PM Claesson. Unpublished results.
92. PG Hartley. In: Farinato RS, Dubin PL, eds. Colloid–Polymer Interactions. New York: John Wiley, 1999:253–286.
93. V Bergeron, D Langevin, A Asnacios. Langmuir 12:1550, 1996.
94. A Asnacios, A Espert, A Colin, D Langevin. Phys. Rev. Lett. 78:4974, 1997.
95. AJ Milling. J. Phys. Chem. 100:8986, 1996.
96. E Blomberg, PM Claesson, JC Fröberg, RD Tilton. Langmuir 10:2325, 1994.
97. E Blomberg, PM Claesson, JC Fröberg. Biomaterials 19:371, 1998.
98. RD Tilton, E Blomberg, PM Claesson. Langmuir 9:2102, 1993.
99. PC Herder, PM Claesson, CE Blom. J Colloid Interface Sci. 119:155, 1987.

100. J Fundin, W Brown, I Iliopoulos, PM Claesson. Colloid Polymer Sci. 277: 25, 1999.
101. PG de Gennes. Macromolecules 15:492, 1982.
102. JMHM Scheutjens, GJ Fleer. Macromolecules 18:1882, 1985.
103. W Barford, RC Ball, CMM Nex. J. Chem. Soc. Faraday Trans. 1 82:3233, 1986.
104. W Barford, RC Ball. J. Chem. Soc. Faraday Trans. 1 83:2515, 1987.
105. A Dedinaite, PM Claesson. Langmuir, in press.

This Page Intentionally Left Blank

15

Fragmentation of Colloidal Aggregates by Polyelectrolyte Adsorption

EMILE PEFFERKORN Institut Charles Sadron, Strasbourg, France

I. INTRODUCTION

Colloidal aggregates constitute the fundaments of agricultural soils [1–12] and sediments of the aquatic environment [13–20]. Aggregation processes serve in industrial and environmental strategies [21–27]. Aggregation or agglutination techniques are employed in a great number of biological and medical applications [28–35]. The well-known role of polymers as aggregation agents extends to all these domains. The opposite process of fragmentation means that the aggregate becomes dispersed into single constitutive solid particles. However, this fully dispersed stage may not be reached for thermodynamic or kinetic reasons, and therefore at equilibrium or after a given period, fragments of smaller mass and size coexist with single particles. The unbreakable constitutive solid particle may be monodisperse or polydisperse in mass, size, and shape.

In this context aggregates are considered to be loosely assembled conglomerates of fine particles bound together at their point of contact by weak van der Waals forces or by soft molecular bonding resulting from interaction with organic or inorganic flocculation agents. The destabilizing agents and the mechanisms leading to particle aggregation may be classified in the following ways. Electrolytes that dissociate into nonadsorbing and noncomplexing ions modify the thermodynamic properties of the aqueous phase equilibrating the diffuse ionic cloud surrounding the electrically charged colloid particles. Full compression of the diffuse layer induces destabilization and fast aggregation [36,37]. Limited compression of that layer, which allows repulsive forces to oppose attractive van der Waals forces thus leads to slow aggregation [38]. Adsorbing and complexing ions exert a supplementary different influence insofar as they are able to modify strongly the

local surface characteristics of the particles. Formation of ion pairs contributes to inducing aggregation through local inversion of the electrical charge, and the concomitant existence of positive and negative surface sites exerts both attractive and repulsive forces at short distances. When, at the point of zero charge, positive and negative charges are present in equal proportions, fast aggregation is expected to occur. For strongly hydrated colloidal particles, hydration forces oppose van der Waals attraction, and anomalous stability is observed [39–41]. The terms of slow and fast aggregation do not clearly identify the mechanism of the aggregation process insofar as reversibility in aggregation is not taken into account. Reversibility means that the interparticle link already established for a certain time becomes suddenly broken, and that phenomenon slows down the average rate of the aggregation process [42–45].

To define more clearly the aggregation mechanism, the process may be characterized on the basis of the shape of the aggregate mass (or size) distribution, and the relative variation as a function of time of the weight and number average masses [46]. This information well characterized the diffusion- or reaction-limited processes, and these characteristics were determined to be less affected by a concomitant fragmentation process.

Controlled provoked fragmentation of such aggregates was previously investigated and found to occur in different ways. Agglomerates of polystyrene latex particles with carboxylic acid surface groups—employed as lyophobic model colloids—instantaneously fragment when the density of the surface charge and the range of the electrical interaction are increased simultaneously [47]. Fragmentation does not lead to a fully dispersed system, and the reduced mass distribution of the parent aggregates and fragments were found to be self-similar in reaction-limited aggregation processes [48]. Fragmentation of such aggregates thus makes it possible to restore the suspension to the situation that existed earlier. This possibility does not exist for aggregates formed by the diffusion-limited process; the situation will be presented in Sec. III.A [47]. Polystyrene latex particles with various surface groups—employed as hydrated model colloids—were found to aggregate in 1 M NaCl suspension and to fragment in 0.05 M NaCl, according to the ranges of hydration forces in the two situations [49,50]. In the latter situation, instantaneous and delayed fragmentation ultimately led to a fully dispersed system, but no correlation in the mass distribution during aggregation and fragmentation was observed.

In the present chapter several typical examples of polyelectrolyte-induced aggregate fragmentation and the different mechanisms responsible for the process are detailed. The analysis is based on recent results of numerical and theoretical studies that are presented below.

II. THEORETICAL PART

A. The Fragmentation Process

Aggregate fragmentation was first taken into account in reversible aggregation processes when, after being formed, one or several intra-aggregate links were disrupted. The predicted effects are to reduce the aggregation rate and, in many instances, to install an aggregation/fragmentation steady state [51,52]. Additionally, the process may induce aggregate compaction [53–55]. The fragmentation process itself is assumed to develop at random according to the following reaction [56–60]:

$$A_y \xrightarrow{B(i,\,j)} A_i + A_j \tag{1}$$

where the rate constant of the fragmentation process $B(i, j)$ is given by

$$B(i, j) = k(i + j)^{\alpha} \tag{2}$$

Starting from Eq. 1, two extreme fragmentation modes are taken into account, which correspond to two typical variations of the weight $S(t)$ and number $N(t)$ average masses as a function of time:

$$S(t) = \frac{\Sigma_n\, n^2 c(n,\, t)}{\Sigma_n\, nc(n,\, t)} \qquad N(t) = \frac{\Sigma_n\, nc(n,\, t)}{\Sigma_n\, c(n,\, t)} \tag{3}$$

On the basis of a given decrease of $N(t)$ with time, when $i \ll j$, $S(t)$ is expected to relatively slowly decrease to account for the slow disappearance of the largest aggregates whereas when $i \cong j$ $S(t)$ is expected to decrease relatively strongly to account for the fast disappearance of aggregates of large sizes. Similarly, the fragment polydispersity $S(t)/N(t)$ is expected to be constant when $i \ll j$ and to decrease strongly when $i \cong j$. It is therefore interesting to determine the temporal evolution of the mass polydispersity $S(t)/N(t)$.

In the following part, we present elements of the recent theory of fragmentation, which uses the integrodifferential Eq. 4 to describe the fragmentation rate [58]:

$$\frac{\partial c(n,\, t)}{\partial t} = -a(n)c(n,\, t) + \sum_{y=n}^{\infty} c(y,\, t)a(y)f\langle n|y\rangle \tag{4}$$

where $c(n, t)$ is the concentration of aggregates of size n at time t, $a(n)$ is the rate of breakup of the aggregate of size n, and $f\langle n/y\rangle$ is the rate at which

aggregates of size n are produced from the breakup of clusters of size y. In the theory of Cheng and Redner [58], homogeneous kernels of the form

$$a(n) = n^{\lambda} \tag{5}$$

and

$$f\langle n|y\rangle = y^{-1}b\langle n|y\rangle \tag{6}$$

were considered. The rate $b(n)$ of formation of fragments of size n from aggregates of size y is thus expressed by

$$b(n) = n^{\nu} \tag{7}$$

The treatment of Eq. 4 was carried out on the bases of the usual reduced form of the mass frequency given in Eq. 8:

$$c(n, t)S^2(t) \propto f\left[\frac{n}{S(t)}\right] \tag{8}$$

Both $a(n)$ and $b(n)$ can be derived from the cluster size distribution curve. Cheng and Redner demonstrated that the rate of fragmentation of aggregates of size x, which is measured by the exponent λ, may be calculated from the variation of the function $\varphi(n)$ in the range of large values of the reduced variable $n/S(t)$. This may be understood if one considers the change in the concentration of the large colloids to be highly affected by the fragmentation of the largest aggregates. This leads to

$$\varphi(n) = n^{-2} \exp(-an^{\lambda}) \tag{9}$$

On the other hand, the rate of formation of aggregates of small size n can be derived from the slope of the function φ at small values of the variable $n/S(t)$. Qualitatively, the size distribution of the smallest aggregates is expected to be imposed by the rate $b(n)$ of aggregates of mass y larger than n. Thus the rate of formation of small fragments $b(n)$ is measured by the value of the initial slope of the function $f(n)$ for $n/S(t) < 1$, thus

$$\varphi(n) = n^{\nu} \tag{10}$$

The shape of the colloid size distribution during the fragmentation process thus determines the nature and rate of fragmentation. The mass frequency

also allows the average sizes $S(t)$ and $N(t)$ to be calculated and, for the model of Cheng and Redner [58], their temporal variation is given by

$$S(t) \approx N(t) \approx t^{-1/\lambda} \tag{11}$$

Deviation from these simple fragmentation phenomena may occur, and in order to take into account the possible concomitance of different fragmentation processes, we introduce the following Eq. 12 to characterize separately the variation of $N(t)$:

$$N(t) \approx t^{-1/\mu} \tag{12}$$

In addition, the variation as a function of time of the mass polydispersity is determined by

$$\frac{S(t)}{N(t)} \approx t^{-(1/\lambda - 1/\mu)} = t^{-p} \tag{13}$$

and may give valuable information on the fragmentation mechanism.

B. The Self-Similarity Character

Zwift and Friedlander [61] and Lushnikov [62] using Smoluchowski's kinetic equation [63] made the analysis of the time evolution of the mass frequency for colloids flocculating in a regime of fast aggregation by

$$\frac{\partial c(n, t)}{\partial t} \frac{1}{2} \sum_{i+j=n} K_{i,j} c(i, t) c(j, t) - c(n, t) \sum_{i} K_{i,n} c(n, t)) \tag{14}$$

$c(i, t)$, $c(j, t)$ and $c(n, t)$ being the concentrations at time t of aggregates of mass i, j and n, $K_{i,j}$ and $K_{i,n}$ being rate constants for both collision and aggregation. To show the self-similarity character of the mass frequency in aggregation, we present the solution developed by Jullien, who assumed the frequency of aggregates of mass n, $c(n, t)$ to be characterized using the two function $\Phi(t)$ and $\Psi(t)$ [64]:

$$c(n, t) = \Phi(t) \times \Psi^{n-1}(t) \tag{15}$$

with $\Psi(0) = 0$ and $\Phi(0) = N_1$, N_1 being the particle concentration at time zero. Combining Eqs. 14 and 15 implies the following condition to be satisfied for all n values:

$$\Psi^{n-1}\left(\frac{\partial\Phi}{\partial t}\right) + (n-1)\Phi \times \Psi^{n-2}\left(\frac{\partial\Psi}{\partial t}\right) = K\Phi^2\left(\frac{n-1}{2} - \frac{\Psi}{1-\Psi}\right) \tag{16}$$

Separation of terms proportional to $(n-1)$ and constant terms gives

$$\frac{\partial\Phi}{\partial t} = K\frac{\Phi^2}{1-\Psi} \tag{17}$$

and

$$\frac{\partial\Psi}{\partial t} = K\frac{\Phi}{2} \tag{18}$$

and finally

$$\frac{\partial\Phi}{\Phi} + 2\frac{\partial\Psi}{1-\Psi} = 0 \tag{19}$$

Introducing the initial conditions one obtains

$$\Phi = N_1(1-\Psi)^2 \tag{20}$$

$$\frac{\partial\Psi}{(1-\Psi)^2} = K\frac{N_1}{2}\,\partial t \tag{21}$$

and after integrating using the conditions at $t = 0$,

$$\Psi = K\frac{N_1}{2} \times \frac{t}{1 + K(N_1/2)t} \tag{22}$$

$$c(n, t) = N_1\frac{(K(N_1/2)t)^{n-1}}{(1 + K(N_1/2)t)^{n+1}} \tag{23}$$

Since the number average mass $N(t)$ is given by

$$N(t) = 1 + K\frac{N_1}{2}t \tag{24}$$

for $t \gg 2/KN_1$, $c(n, t)$ resolves to

$$c(n, t) = \frac{4}{n^2K^2N_1}\left[\frac{n}{t}\right]^2 \exp\left\{-\frac{2}{N_1n} \times \frac{n}{t}\right\} \tag{25}$$

Thus the reduced concentration of aggregate of mass n, $n^2c(n, t)$ can be represented using the reduced variable n/t. Since at large times t is scaled by $N(t)$ or $S(t)$ according to Eq. 24, the variation with time of the reduced concentration can be fitted by

$$c(n, t) \times n^2 = f\left(\frac{n}{S(t)}\right) \tag{26}$$

as shown in Figure 1 [65]. The master curve corresponds to mass frequencies determined during the initial short aggregation period for colloidal alumina particles suspended in an aqueous solution of composition 0.5 mg/m^2 polyacrylic acid, 10^{-3} mol/L KCl, 10^{-4} mol/L $AlCl_3$, and 10^{-5} mol/L HCl. For the same experimental system, the self-similarity character has been evidenced in the subsequent fragmentation regime too, as given in Figure 2.

III. AGGREGATE FRAGMENTATION IN THE ABSENCE OF POLYMER

A. Fragmentation Induced by Electric Forces

Derjaguin and Landau [36] and Verwey and Overbeek [37] have established the correlation between the potential energy and the separation distance as a function of the characteristics of both the particles and the suspending medium. According to the DLVO theories, suspended charged colloidal particles sustain aggregation when the range of electrical forces is strongly reduced in a medium of high ionic strength. When the ionic strength is decreased, the widening of the ionic diffuse layer increases the range of the repulsive forces between stuck particles. Since these forces are isotropic within the aggregate assembly, insofar as equal forces apply at the particle

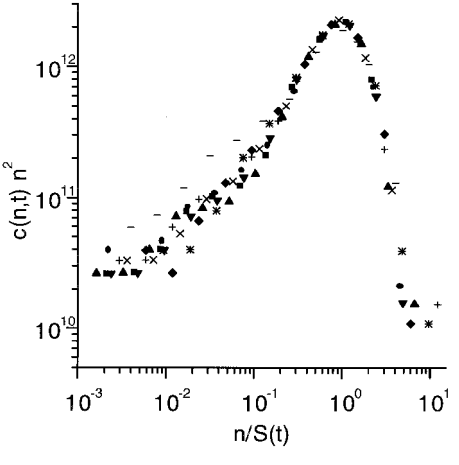

FIG. 1 Evidence for self-similarity of the aggregate mass distribution for the aggregating system (aluminum oxide/polyacrylic acid) according to Eq. 26.

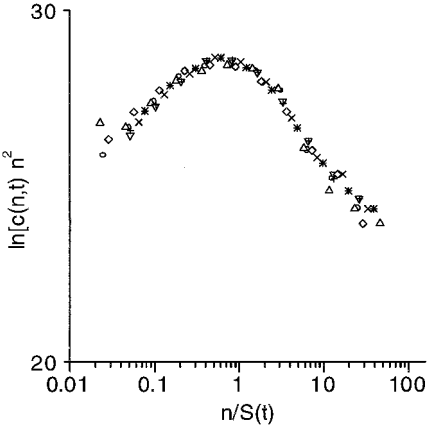

FIG. 2 Evidence for self-similarity of the aggregate mass distribution for the fragmenting system (aluminum oxide/polyacrylic acid) according to Eq. 9.

junctions, the dilution of the electrolyte solution is expected to induce aggregate breakup.

Monosized latex particles of 1.30 μm diameter only bearing carboxylic acid surface groups were obtained by synthesis under emulsifier-free conditions and oxidation in the presence of glass beads at 90°C during a week. Aggregates were obtained after immersion of the colloids in aqueous NaCl solution (pH 3.0 and 0.15 mol/L). The aggregate mass characteristics $S(t)$ and $N(t)$ were calculated on the basis of the mass frequency determined by particle counting (Coulter counter, Coultronics—information relative to the technique and method used is given in the appendix). The stability characteristics of the latex colloids suspended in electrolyte solutions of various ionic strengths and pH were determined to evolve according to the DLVO theories, the usual Hamaker constant of 0.65×10^{-13} erg being employed to calculate the energy–distance profiles for interacting colloids. The transition between diffusion- and reaction-limited aggregation processes was determined to occur in electrolyte solutions of concentrations close to 0.05 mol/L NaCl at pH 3.0 [50]. The colloid suspended in 0.15 mol/L at pH 3.0 is characterized by the energy distance profile given in Figure 3 (curve a), which characterizes a fully unstable system. Accordingly, the reduced mass frequency curve displays the usual bell-shaped curve showing particles and small aggregates to disappear progressively from the system to the benefit of a typical class of aggregates of mass n equal to $0.2 \times S(t)$ (Figure 4). Aliquots of the aggregating suspension were immersed at different times in 0.00015 mol/L NaCl solutions at pH 3 and 7, where very strong repulsive

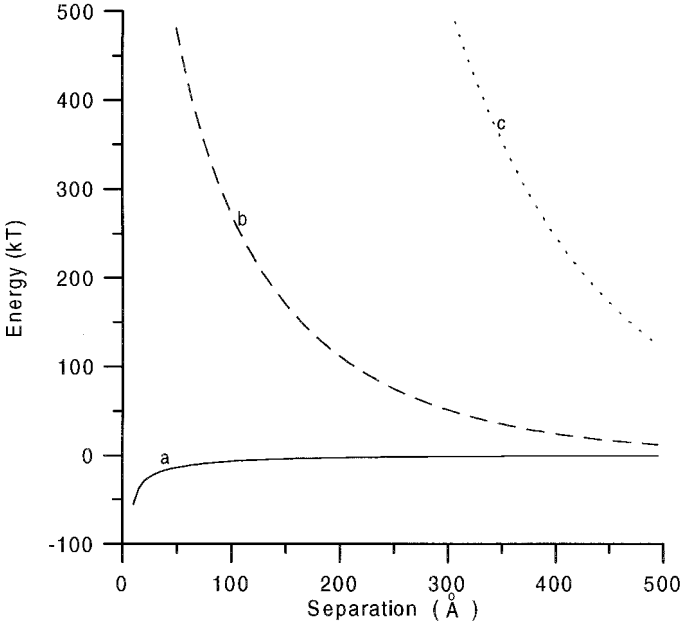

FIG. 3 Energy–distance profiles for polystyrene latex particles bearing carboxylic acid surface groups (lyophobic colloid) suspended in different aqueous media: (a) 0.15 mol/L NaCl at pH 3.0; (b) 0.00015 mol/L NaCl at pH 3.0, and (c) 0.00015 mol/L NaCl at pH 7.0.

forces between stuck particles were instantaneously established, as shown in Figure 3 (curves b and c). The expected effect of such forces could be observed only at pH 7, where a limited ''instantaneous'' fragmentation was observed, whereas no fragmentation was observed at pH 3 for a week [47]. Figure 5 shows the reduced mass frequencies of the fragments resulting from the instantaneous breakup of aggregates of increasing average masses, and self-similarity is evident. According to Eqs. 7 and 10, the rate $b(n)$ of formation of small fragments is scaled by $\nu = -1.5$. Since no fragmentation is determined to occur at pH 3.0, while only a limited fragmentation is observed at pH 7.0 despite the existence of strong repulsive forces, the thermodynamic equilibrium situation (curves b and c in Figure 3) should require a certain delay to be established. Obviously, ancient interparticle links cannot be disrupted, whereas newly formed links are quite instantaneously broken. This may explain the self-similarity (or memory effect) that characterizes the mass frequency curves for $n > 2 \times S(t)$ during aggregation and fragmentation.

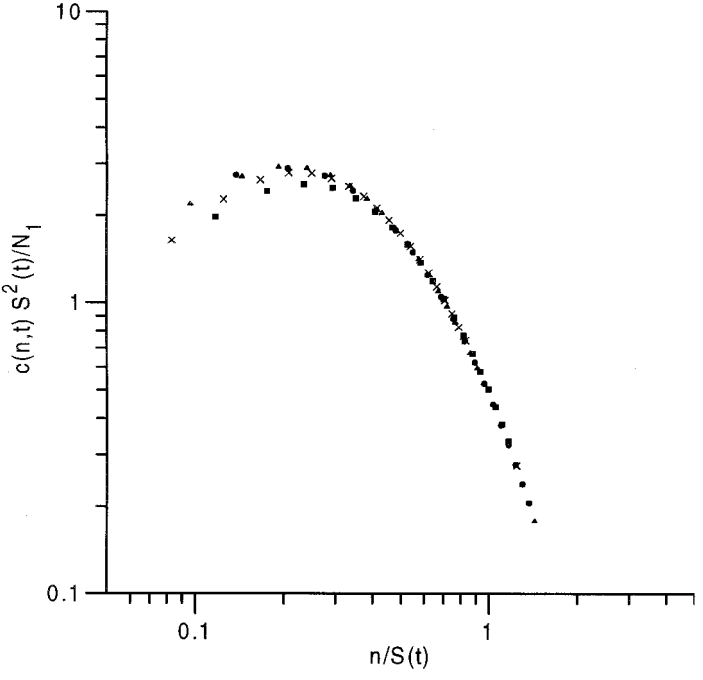

FIG. 4 Mass frequency curves during aggregation: representation of the reduced concentration $c(n, t)\ S^2(t)/N_1$ as a function of the reduced variable $n/S(t)$ for the system (polystyrene latex particles bearing carboxylic acid surface groups) suspended in 0.15 mol/L NaCl at pH 3.0.

B. Fragmentation Induced by Hydration Forces

Anomalous stability of bare silica and latex particles or coated particles has been attributed to the existence of surface hydration forces. The stabilization effect induced by the hydration shell may be estimated by comparing the coagulation value for silica sol (1.6 mol/L NaCl), quartz (0.1 mol/L NaCl), and quartz treated with base (0.4 mol/L NaCl) in the pH domain where stabilization due to electrical charge is negligible [66]. Israelachvili and Pashley determined the range to be equal to 4 nm for mica in 1 mol/L KCl [40]. For silica and mica in 0.01 mol/L KCl, the range was determined to be close to 20 nm [40,41]. Indirect evidence for hydration forces was shown in the deposition of polystyrene latex particles on glass surfaces [67]. The presence of NaCl at the molar concentration may induce a strong electrolyte adsorption at the solid/liquid interface, which destroys the interfacial water structure and thus limits the range of the hydration forces. The increase of

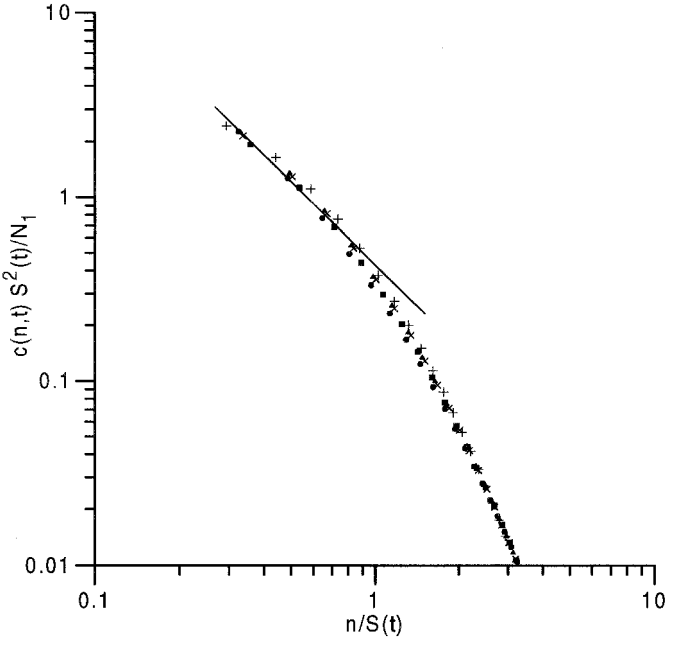

FIG. 5 Mass frequency curves during fragmentation: representation of the reduced concentration $c(n, t)\ S^2(t)/N_1$ as a function of the reduced variable $n/S(t)$ for the system (polystyrene latex particles bearing carboxylic acid surface groups) suspended in 0.00015 mol/L NaCl at pH 7.0. The slope of the straight line is equal to -1.5.

the range of hydration forces is expected to induce interparticle separation. Similarly, aggregation of PC vesicles is attributed to destruction of repulsive hydration forces due to partial dehydration of the vesicular surface [68]. Addition of short-chain alcohol on silica was found to decrease hydration forces too [69].

Monosized latex particles of diameter 1.09 μm were prepared by emulsifier-free polymerization using potassium persulfate as initiator. The latex contains hydroxyl, carboxylic acid, and sulfate groups, the total charge density being on the order of 18 $\mu C/cm^2$. The swollen layer composed of water molecules bound to the densely packed hydrated surface sites of 1 group/nm^2 confers exceptional stability in comparison to that of typical lyophobic colloids [49]. The latex aggregates slowly in 1 mol/L NaCl solution at pH 3.0 where electrical stabilization is expected to be inefficient. Figure 6 shows the reduced mass distributions as a function of the reduced mass $n/S(t)$ determined after various aggregation periods. The main observations are that

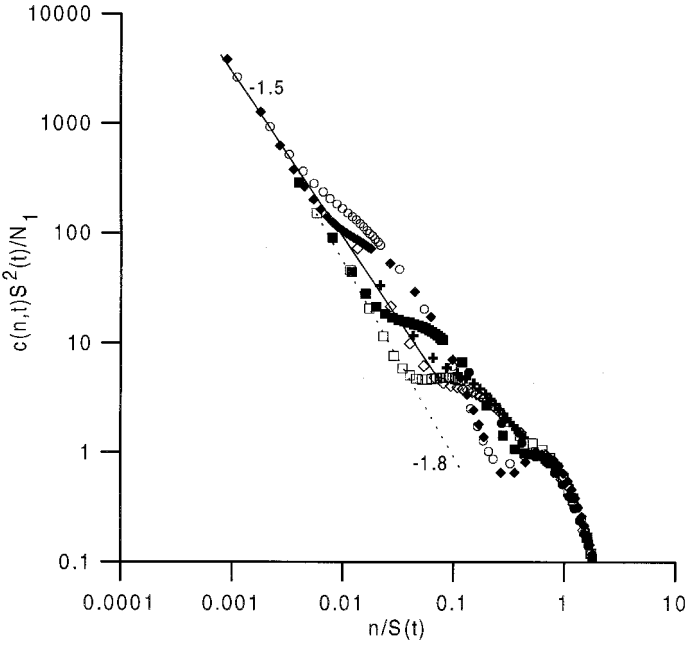

FIG. 6 Mass frequency curves during aggregation showing emergence of three populations: representation of the reduced concentration $c(n, t)\ S^2(t)/N_1$ as a function of the reduced variable $n/S(t)$ for hydrated polystyrene latex particles suspended in 1 mol/L NaCl at pH 3.0, for different aggregation periods between 3 and 6060 min. The straight lines of slope -1.5 and -1.8 characterize the mass frequency determined at 3 and 6060 min, respectively.

the curves determined at various times are not self-similar, and at least three populations emerge at large times. This has been attributed to the mass-dependent reactivity of the growing aggregates. Typically, the formation of doublets or small linear aggregates (Population I) was highly reversible and/or reaction limited, whereas the formation of more compact (Population II) or large aggregate (Population III) was diffusion limited. The transfer of the aggregating system into a fragmenting one (0.05 mol/L NaCl at the same pH 3.0) successively induced fast and delayed fragmentation processes. For example, aggregates of mean mass 1125 transferred after an aggregation period of 4410 min immediately release aggregates of average mass 304.4, which continue to fragment progressively as shown in Figure 7. Interestingly, as shown in Figure 8, the mass frequency curve of the fragment of average mass $S(0) = 304.4$ resembles neither that of the parent aggregate of

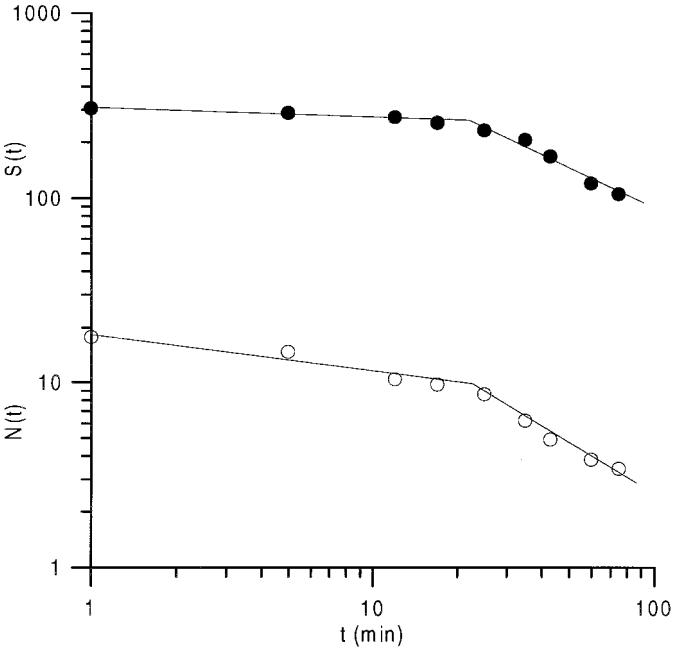

FIG. 7 Fragmentation of aggregates of hydrated polystyrene latex particles suspended in 0.05 mol/L NaCl at pH 3.0: representation of the weight $S(t)$ (●) and number $N(t)$ (○) as a function of time.

$S(4410)$ nor that of the aggregates of quite similar mass that existed in the molar solution after a period of 405 min.

Eventually, aggregates of lyophobic colloids suspended in electrolyte solution may partly fragment when the density of charged surface groups and the range of electric forces greatly increase. Aggregates of lyophilic colloids fragment and finally produce dispersed particles when the range of hydration forces increases. From a general point of view, fragmentation proceeds not at random since effects of the aggregation mechanism and dispersion forces are evident.

In the two following sections the specific roles of polyelectrolyte is analyzed. In the first situation, analyzed in Sec. IV, aggregates obtained in the presence of electrolyte are fragmented by transfer in electrolyte solutions of lower ionic strength containing the polyelectrolyte. Polymer adsorption at the solid/water interface is shown to induce the particle separation [70]. In the second situation, analyzed in Sec. V, aggregates obtained in the presence of low polymer doses are fragmented by immersion in solutions of higher

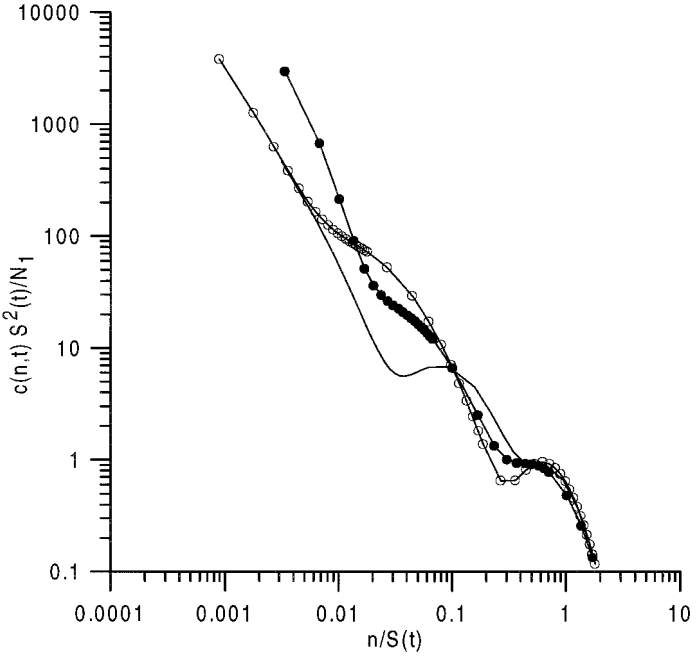

FIG. 8 Representation of the aggregate mass distribution (reduced concentration vs. reduced mass) of the parent aggregates in 1 mol/L NaCl suspension prior to immersion in 0.05 mol/L NaCl solution [$S(4410) = 1125$] (○), of the fragments formed immediately after immersion of the aggregates in 0.05 mol/L NaCl [$S(1) = 304.4$] (●), and for comparison of the previous aggregates of $S(405) = 320.4$ (——) during aggregation.

polyelectrolyte concentration [71]. Fragmentation then results from the progress of the polymer adsorption.

In the first situation, monosized spherical latex particles of 0.885 μm diameter were employed. The latex bore sulfonate surface groups at the density of 4.1 μC/cm^2. In the second situation, the diameter was equal to 1.73 μm and the surface charge density was equal to 1.45 μC/cm^2. Polyvinylpyridine of various average molecular weights was employed, the molecular and solution characteristics being given in Table 1. All experiments were carried out at normal temperature (20 or 25°C) and pH 3.0. At this pH the degree of protonation of polyvinylpyridine is close to 0.5 [72]. At full surface coverage, the polymer interface looks like a two-dimensional stack of coils, each coil having an interfacial area slightly larger than the cross-sectional area corresponding to its radius of gyration. When the surface is

TABLE 1 Molecular and Solution Characteristics of Polyvinylpyridine

Molecular weight	R_G (nm)	C^* (g/L)
102,000	20.7	4.49
589,000	45.7	3.06
1,057,000	61.3	1.49

only partially covered and when no new chains issue from the solution, the mapping is different at short and long times. Immediately after adsorption, the coil adopts its solution conformation, whereas the conformation of the adsorbed coil progressively flattens with time to occupy the largest possible area. This phenomenon may be enhanced by the polymer–colloid complex formation. The adsorption of the cationic polyelectrolytes on the anionic latex may display some characteristics of polyanion–polycation complexes, and the protonation of the pyridine groups facing the dissociated sulfonate groups may be enhanced as previously determined [73].

IV. AGGREGATE FRAGMENTATION INDUCED BY POLYMER ADSORPTION AT THE SOLID/LIQUID INTERFACE

Since diffusion- and reaction-limited aggregation processes developing in suspensions of high and low ionic strength lead to aggregates characterized by various energy–distance profiles, it was interesting to determine the fragmentation characteristics of these typical aggregates.

A. Fragmentation of Aggregates Formed Under Conditions of Diffusion-Limited Aggregation

The latex concentration was 10 g/L and the aggregating medium was an aqueous solution of 1 mol/L NaCl at pH 3.0 and 20°C, thus leading to fast aggregation of the suspension. After a given aggregation period, a sample of controlled volume was transferred to an aqueous polymer solution at the same pH 3.0 and the system was homogenized by gently rotating the tank to establish conditions for perikinetic fragmentation. The fragmentation did not start immediately after immersion in the polymer solution, since no difference in the aggregate mass frequencies could be determined in the aggregating and fragmenting media immediately before and after transfer.

Three fractionated samples of molecular weight equal to 102,000, 589,000, and 1,057,000 were employed, and transfer of an aliquot of the

aggregating suspension in the fragmenting medium increased the ionic strength to 0.15. The resulting polymer concentration was calculated in terms of C^*/d, C^* being the critical concentration of nonoverlapping coils and d the degree of dilution of that medium [74]. C^* was obtained by determining the intrinsic viscosity of the polymer in ethanol or ethanolic electrolyte solution. These media may induce polyelectrolyte conformations that are typical of the polyelectrolyte in concentrated aqueous solutions, where electrolyte and counterions of the polyelectrolyte contribute to the screening of the electrostatic repulsion between polyions. Therefore C^* only refers to conformational characteristics.

The variables are the average mass of the aggregates before fragmentation $S(0)$, the molecular weight of the polymer M_w, and the concentration C^*/d of the polyelectrolyte solution. Figures 9 and 10 show typical results of aggregate fragmentation experiments, which express the variation with time of the weight $S(t)$ and number $N(t)$ average masses (Eqs. 11 and 12) for immersion of aggregates in solutions $C^*/50$ or $C^*/5$ of polyvinylpyridine of

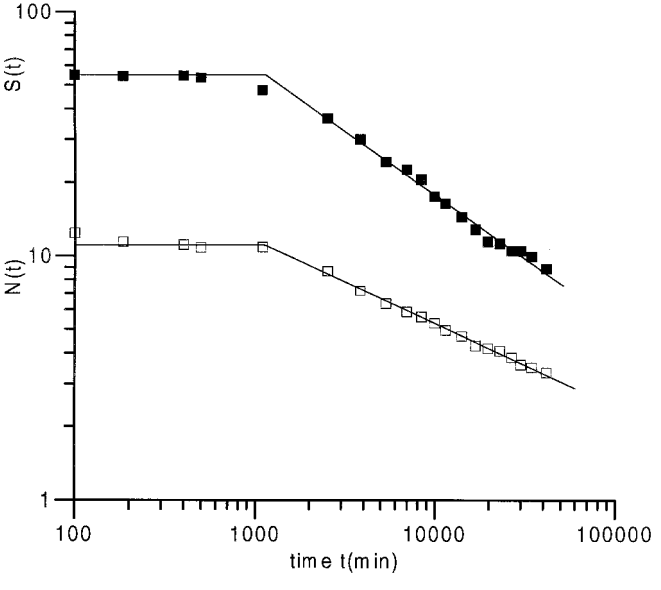

FIG. 9 Fragmentation in aqueous solution of polyvinylpyridine (M_w = 589,000, $C^*/50$) of aggregates of latex particles formed under conditions of diffusion-limited aggregation. Representation of the weight $S(t)$ (■) and number $N(t)$ (□) as functions of the period of fragmentation.

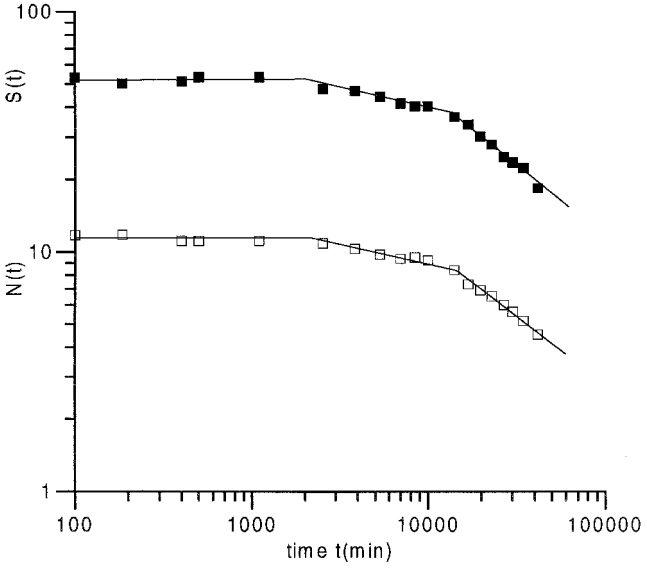

FIG. 10 Fragmentation in aqueous solution of polyvinylpyridine (M_w = 589,000, $C^*/5$) of aggregates of latex particles formed under conditions of diffusion-limited aggregation. Representation of the weight $S(t)$ (■) and number $N(t)$ (□) as functions of the period of fragmentation.

molecular weight equal to 589,000. The time lag before fragmentation is close to 1,000 min in the two situations, whereas the variations of $S(t)$ and $N(t)$ display different shapes and rates. The rate of formation of small fragments $b(n)$ (Eq. 7) is derived from Figure 11, which represents the self-similar reduced mass frequencies according to Eq. 10 for fragmentation in solution $C^*/5$. For the same system the rate of fragmentation of large aggregates $a(n)$ (Eq. 5) is derived from Figure 12, which represents the self-similar mass frequencies according to Eq. 9.

Table 2 gives the fragmentation characteristics of aggregates obtained by the diffusion-limited aggregation process, which were derived using results similar to those shown in Figures 9–12. During the time lag before fragmentation, which is equal to 1000 min and is independent of the polyelectrolyte concentration, polymer molecules adsorb on confined areas located between adjacent particles and progressively establish interfacial layers exerting increasing repulsive forces. Obviously, the fragmentation cannot result from the decrease of the ionic strength at constant pH, as was shown in Sec. III.A. The values of λ and μ derived from the variation of $S(t)$ and $N(t)$

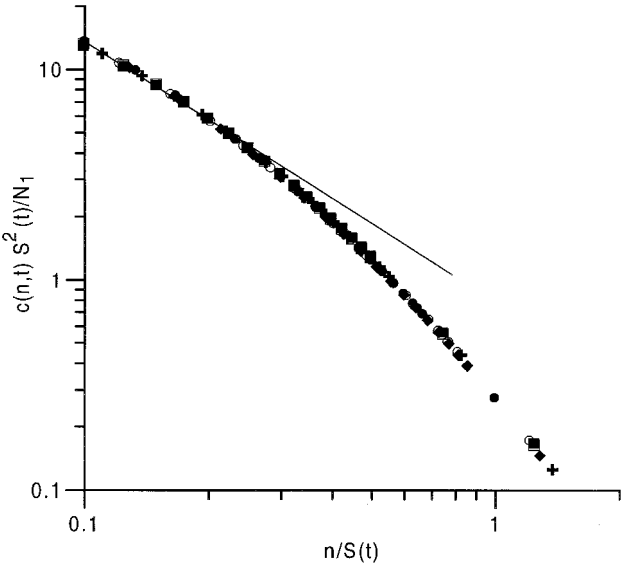

FIG. 11 Fragmentation in aqueous solution of polyvinylpyridine (M_w = 589,000, $C^*/5$) of aggregates of latex particles of mass $S(t = 0)$ equal to 50 formed under conditions of diffusion-limited aggregation. Representation of the reduced concentration $c(n, t)\ S^2(t)/N_1$ as a function of the reduced variable $n/S(t)$ for different periods of fragmentation. The slope of the straight line equal to -1.2 gives the exponent of the rate of formation of small fragments according to Eq. 7.

(Table 2) do not agree in all situations with Eq. 11, which sets the similar variation with time of $N(t)$ and $S(t)$, but a good agreement is determined for the first kinetic regime. The rate of formation of small fragments and the rate of breakup of large aggregates are determined to be controlled by exponents close to -1.2 and 0.60 respectively in all situations, with a systematic small difference in λ in the first and second kinetic regimes. One may note the self-similar character of the reduced mass frequencies. The discrepancy in the values of λ derived from the variation with time of $S(t)$ or $N(t)$ and the reduced mass frequency curves for $n > S(t)$ is attributed to the fact that the adsorbed layers induce their dispersion action only progressively, so that a dynamic equilibrium of aggregation/fragmentation may be established during the initial time lag of 1000 min, and the relative part of fragmentation becomes increasingly significant in the first and second kinetic regimes. In addition, for aggregates of similar $S(0) \cong 50$, Table 2 shows the rate of decrease of $S(t)$ and $N(t)$ to increase with the polymer dilution, thus

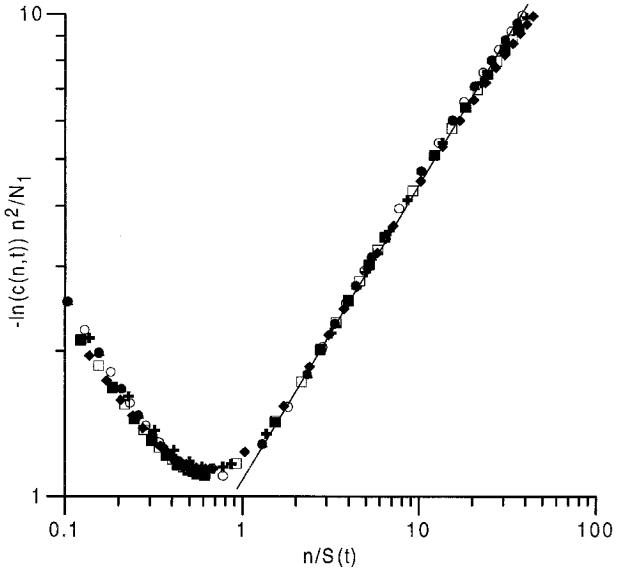

FIG. 12 Fragmentation in aqueous solution of polyvinylpyridine (M_w = 589,000, $C^*/5$) of aggregates of latex particles of mass $S(t = 0)$ equal to 50 formed under conditions of diffusion-limited aggregation. Representation of the logarithm of the reduced concentration $c(n, t)\ n^2/N_1$ as a function of the reduced variable $n/S(t)$ for different periods of fragmentation. The slope of the straight line equal to 0.56 gives the exponent of the rate of fragmentation of large aggregates according to Eq. 5.

evidencing the usual effect of entropic forces in concentrated polymer solutions [75]. The rates of aggregate fragmentation $a(n)$ and formation of small fragments $b(n)$ are given by

$$a(n) = n^{0.60} \qquad b(n) = n^{-1.2} \tag{27}$$

In dilutions corresponding to d = 5 to 30, the value zero of the polydispersity exponent p determined in the first kinetic regime indicates that the fragmentation strictly develops reversibly to the diffusion-limited aggregation for which $N(t)$ varied as $S(t)$ too. Conversely, in the second regime, the values of p between 0.16 and 0.35 indicate that the fragmentation resembles aggregate splitting, since $S(t)$ decreases faster than does $N(t)$. In the most diluted polymer solution of $C^*/50$, the first process resembles splitting, whereas the second one refers to attrition, for which particles or very small aggregates belonging to outer zones become detached.

TABLE 2 Fragmentation Characteristics of Aggregates Formed Under Conditions of Diffusion-Limited Aggregation (M_w = 589,000)

Pol. conc.	Time lag (min)	$S(0)$	Kinetic regime	λ[a]	μ[b]	ν[c]	λ[d]	p[e]
$C^*/5$	1000	50	1	9.2	9.2	−1.2	0.56	0
$C^*/10$	1000	40	1	5	5	−1.2	0.56	0
			2	1.4	2.5	−1.2	0.60	0.31
$C^*/30$	1000	100	1	1.9	1.9	−1.2	0.56	0
			2	0.9	1.4	−1.3	0.65	0.16
$C^*/30$	1000	30	1	5.3	5.3	−1.2	0.56	0
			2	1.4	2.8	−1.0	0.65	0.35
$C^*/50$	1000	55	1	1.76	3	−1.2	0.56	0.24
			2	3	3	−1.2	0.65	0

[a] Equation 11; λ is derived from the variation of $S(t)$ with time.
[b] Equation 12; μ is derived from the variation of $N(t)$ with time.
[c] Equation 10; ν is derived from the reduced mass frequency at small values of $n/S(t)$.
[d] Equation 9; λ is derived from the reduced mass frequency at great values of $n/S(t)$.
[e] Equation 13.

The influence of the molecular weight of the polymer has been investigated for systems in the $C^*/30$ medium. All results relative to the fragmentation processes are summarized in Table 3. The initial period of the steady state, which was determined to not depend on the mass $S(0)$, increases with the molecular weight. As portrayed in Figure 13, the exponent λ of the rate of aggregate breakup $a(n)$ linearly decreases with increasing molecular weights, thus indicating that polymers of small molecular weight provoke faster fragmentation than do polymers of high molecular weight. Similarly the exponent ν linearly varies with the molecular weight, so that the rate of fragment formation $b(n)$ decreases with increasing molecular weights. Conclusively, by fixing the molecular weight and concentration of the polymer in the fragmenting medium, one may kinetically control the aggregate fragmentation process.

B. Fragmentation of Aggregates Formed Under Conditions of Reaction-Limited Aggregation

The latex concentration was 10 g/L and the aggregating medium was 0.15 mol/L NaCl at pH 3.0 and 20°C, thus leading to a reaction-limited aggregation of the colloids. After transfer of a controlled volume of the suspension in the aqueous polymer solution at pH 3.0, the resulting ionic strength was equal to 0.0225. Figures 14 and 15 show the variation with time of $S(t)$ and

TABLE 3 Fragmentation Characteristics in $C^*/30$ Medium of Aggregates Formed Under Conditions of Diffusion-Limited Aggregation. Influence of the Molecular Weight of the Polymer

M_w	Time lag (min)	$S(0)$	Kin. reg.	λ^a	μ^b	ν^c	λ^d
102,000	250	55	1	5.4	3.6	−0.7	0.8
			2	1.9	0.8	−0.7	0.8
589,000	350	100	1	1.9	1.9	−1.2	0.56
			2	0.9	1.4	−1.3	0.65
1,057,000	550	100	1	1.7	1.7	−1.6	0.4
			2	1.0	2.2	−1.6	0.4

[a] Equation 11; λ is derived from the variation of $S(t)$ with time.
[b] Equation 12; μ is derived from the variation of $N(t)$ with time.
[c] Equation 10; ν is derived from the reduced mass frequency at small values of $n/S(t)$.
[d] Equation 9; λ is derived from the reduced mass frequency at great values of $n/S(t)$.

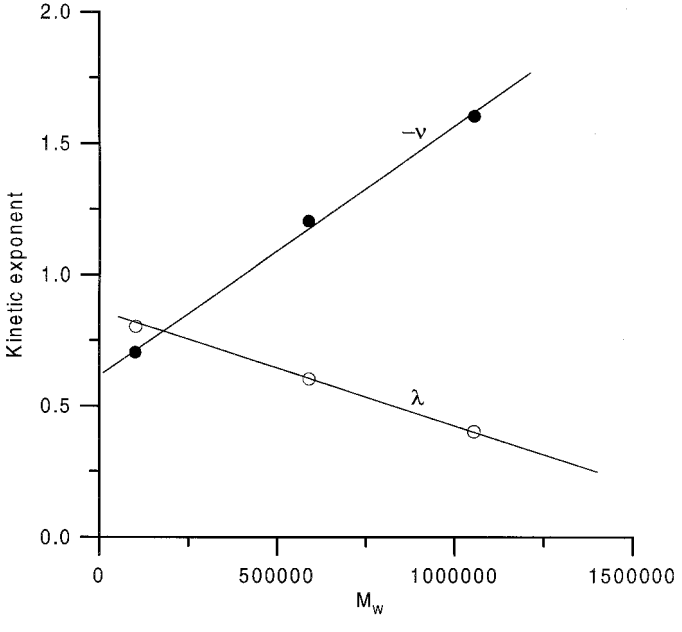

FIG. 13 Fragmentation in aqueous solution of polyvinylpyridine ($C^*/30$) of aggregates of latex particles formed under conditions of diffusion-limited aggregation. Representation of the kinetic coefficients $-\nu$ and λ as functions of the molecular weight of the polyvinylpyridine.

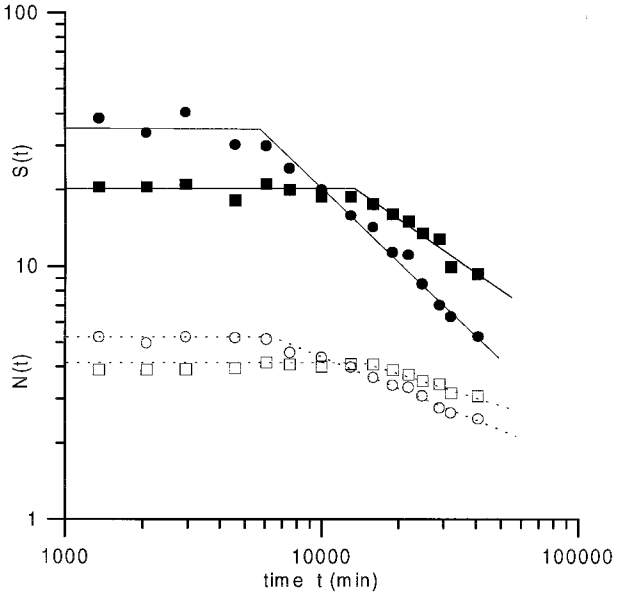

FIG. 14 Fragmentation in aqueous solution of polyvinylpyridine (M_w = 589,000) of aggregates of latex particles formed under conditions of reaction-limited aggregation. Representation of the weight $S(t)$ (black symbol) and number $N(t)$ (open symbol) as functions of the period of fragmentation in media $C^*/5$ (■, □) and $C^*/30$ (●, ○).

$N(t)$ for systems fragmenting in polymer solutions of concentration C^*/d with d = 5, 10, 30, and 50, and the fragmentation characteristics are given in Table 4. The rate of variation of $S(t)$ and $N(t)$ and initial time lags too seem to depend on the mass $S(0)$ as observed in Table 4. Single values were determined for exponents λ and ν, and the rate of aggregate fragmentation $a(n)$ and the rate of formation of small fragments $b(n)$ are given by

$$a(n) = n^{0.5} \qquad b(n) = n^{-1.75} \tag{28}$$

The mean value of the polydispersity exponent p close to 0.5 indicates that the fragmentation strictly develops reversibly to the reaction-limited aggregation for which $N^2(t)$ varies as $S(t)$.

The influence of the molecular weight has been investigated, and, as in Sec. IV.A, aggregate fragmentation induced by polymers of high molecular weight is delayed at longer times. Mixing of aggregates and polymer in aqueous suspension did not induce fast phenomena, since in all situations the average mass characteristics are unchanged for hours. After a given time

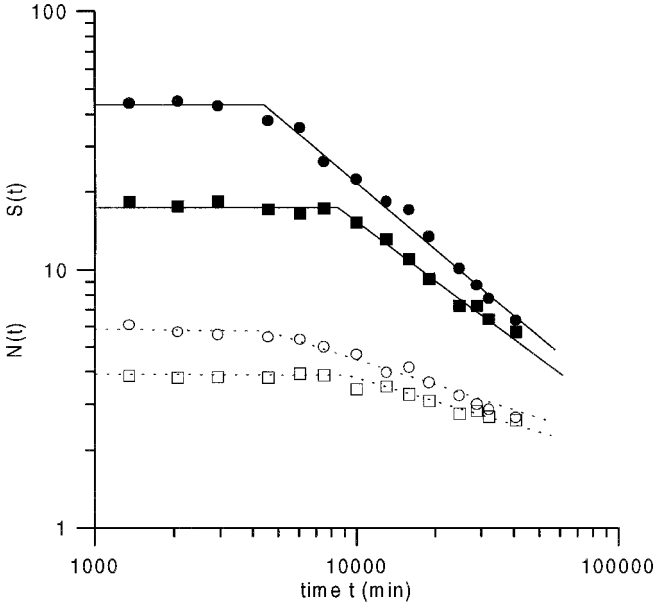

FIG. 15 Fragmentation in aqueous solution of polyvinylpyridine (M_w = 589,000) of aggregates of latex particles formed under conditions of reaction-limited aggregation. Representation of the weight $S(t)$ (black symbol) and number $N(t)$ (open symbol) as functions of the period of fragmentation in media $C^*/10$ (■, □) and $C^*/50$ (●, ○).

TABLE 4 Fragmentation Characteristics of Aggregates Formed Under Conditions of Reaction-Limited Aggregation (M_w = 589,000)

Pol. conc.	Time lag (min)	$S(0)$	Kinetic regime	λ^a	μ^b	ν^c	λ^d	p^e
$C^*/5$	15000	20	1	1.38	3.8	−1.75	0.5	0.45
$C^*/10$	9000	18	1	1.32	3.7	−1.75	0.5	0.49
$C^*/30$	5000	40	1	1.07	2.7	−1.75	0.5	0.56
$C^*/50$	4500	45	1	1.09	2.7	−1.75	0.5	0.56

[a] Equation 11; λ is derived from the variation of $S(t)$ with time.
[b] Equation 12; μ is derived from the variation of $N(t)$ with time.
[c] Equation 10; ν is derived from the reduced mass frequency at small values of $n/S(t)$.
[d] Equation 9; λ is derived from the reduced mass frequency at great values of $n/S(t)$.
[e] Equation 13.

lag, the mass frequency changes, although it preserves its self-similar character. In addition, fragmentation develops on the basis of a memory effect certainly related to interparticle link aging. Although no systematic correlation could be established between the rate of fragmentation determined by the rate of variation of the average masses $S(t)$ and $N(t)$ and the characteristics (concentration and molecular weight of the polymer) of the fragmenting medium, the kinetic exponents determined from the theory of Cheng and Redner [58] are found to quantify the intrinsic instability of stuck colloids formed under various conditions. The disagreement between the two values determined for λ is attributed to the reversible nature of the fragmentation process, where aggregation tends to oppose breakup. In fact, the establishment of the interfacial polyelectrolyte layer constitutes a complex phenomenon where interfacial reconformation exerts a major role. As long as the adsorbed polymer has not reached its equilibrium conformation, even peptized particles may be unstable during the time lag corresponding to dynamic equilibrium where aggregation and fragmentation cancel out each other [76]. When after a given time more polymer chains are adsorbed, dispersing fragments become better stabilized and the rate of fragmentation is expected to increase. Total dispersion of the particles is only obtained when the polymer layer has reached its thermodynamic equilibrium.

V. AGGREGATE FRAGMENTATION INDUCED BY THE PROGRESS OF POLYMER ADSORPTION AT THE SOLID/LIQUID INTERFACE

Mixing of colloidal solid adsorbent and polyelectrolyte that exert strong interactions usually leads to large flocs that are stable for long times and coexist with dispersed particles [75,76]. Apart from the situation of polymer solutions at the C^* concentration systems where flocculation is induced by a depletion mechanism, aggregation of colloids usually results from the establishment of shared interfacial polymer layers [77]. The presence of some large aggregates within dispersed peptized colloids may profoundly affect the properties of ceramics that are obtained after drying and for which prior detection and elimination of aggregates is not trivial. This section presents information on (1) the role of the surface coverage that was established at the moment of aggregate formation, and (2) the impact of hydrodynamic forces on the fragmentation rates.

Monosized spherical polystyrene latex particles of diameter 1.73 μm and polyvinylpyridine of molecular weight equal to 589,000 were employed, for which C^* is equal to 3.06 g/L. The experiments were carried out at pH 3.0 and 25°C.

A. Fragmentation of Aggregates Formed in the Presence of Polymer Without Stirring

Aggregates are obtained by gentle mixing of the colloid suspension and the dilute polymer solution of equal volumes. Polymer adsorption on colloids is expected to be fast in comparison to the colloid aggregation rate ($S(t)$ was determined to vary as $t^{0.35}$) so that the net surface coverage is constant during aggregation. After a given time, aliquots are sampled and immersed in polymer solutions of various concentrations C^*/d. As far as addition of colloids to polymer solution of concentration C^* provoked phase separation, fragmentation was investigated for solutions of dilution d equal to 5, 10, 30, 50, and 70. Figure 16 represents the masses $N(t)$ and $S(t)$ as a function of time for typical experiments, and the scaling exponents are given in Table 5. Figure 16 shows that both $S(t)$ and $N(t)$ tend towards a limiting value close to 2, which is reached faster in dilute media. Similarly, the rate of formation of small fragments is faster in dilute media than in concentrated ones as

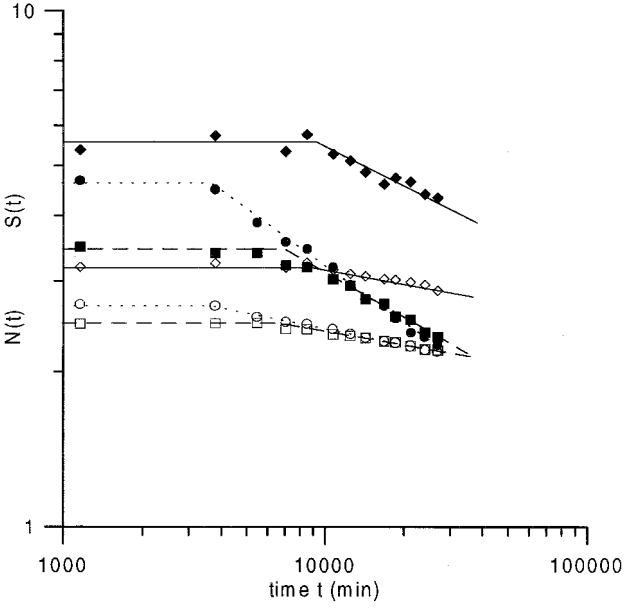

FIG. 16 Fragmentation in aqueous solution of polyvinylpyridine (M_w = 589,000) of aggregates of latex particles formed in the presence of polymer without stirring. Representation of the weight $S(t)$ (black symbol) and number $N(t)$ (open symbol) as functions of the period of fragmentation in media $C^*/5$ (♦, ◇), $C^*/30$ (■, □), and $C^*/70$ (●, ○).

TABLE 5 Fragmentation Characteristics of Aggregates Formed Without Stirring: Influence of the Polymer Concentration C^*/d (M_w = 589,000)

Pol. conc.	$S(0)$	λ^a	μ^b	ν^c	λ^d	p^e
$C^*/5$	5.6	5.56	10.9	−1.20	0.98	0.088
$C^*/10$	8.1	5.66	7.8	−1.20	0.90	0.050
$C^*/30$	3.4	3.92	12.0	−1.75	0.84	0.172
$C^*/50$	4.0	4.53	14.5	−1.75	0.95	0.152
$C^*/70$	4.6	2.75	9.7	−1.75	0.91	0.261

[a] Equation 11; λ is derived from the variation of $S(t)$ with time.
[b] Equation 12; μ is derived from the variation of $N(t)$ with time.
[c] Equation 10; ν is derived from the reduced mass frequency at small values of $n/S(t)$.
[d] Equation 9; λ is derived from the reduced mass frequency at great values of $n/S(t)$.
[e] Equation 13.

indicated by the slopes −1.2 and −1.75 of the reduced mass frequencies at small $n/S(t)$ values determined for experiments carried out at $C^*/5$ and 10 and $C^*/30$, 50, and 70, respectively (Figure 17). As derived from Eqs. 5 and 9, the rate of fragmentation of aggregates of large masses, which is independent of the polymer concentration in the fragmenting medium, may be expressed by

$$a(n) = n^{0.9} \tag{29}$$

Eventually, the progress of fragmentation induces a mass polydispersity which develops differently in dilute and concentrated systems. In concentrated ones, p is close to 0.07 ± 0.02, while it increases with dilution up to 0.25.

B. Fragmentation of Aggregates Formed in the Presence of Polymer Under Stirring

1. Influence of the Degree of Surface Coverage [71]

In this experience, the colloid suspension was introduced into a reactor of volume equal to 50 mL and stirred to ensure homogeneity. At time zero, the polymer solution was injected at constant rate and periodically the corresponding volume of the suspension was collected for a certain time to determine the aggregate mass characteristics and to start fragmentation experiments by immersion of these aggregate samples in the polymer solution of concentration $C^*/30$. This procedure allows the surface coverage $\Gamma(t)$ to be a linear function of the injection time t due to fast total adsorption of the injected polymer. The variations with time of the average masses $N(t)$ and

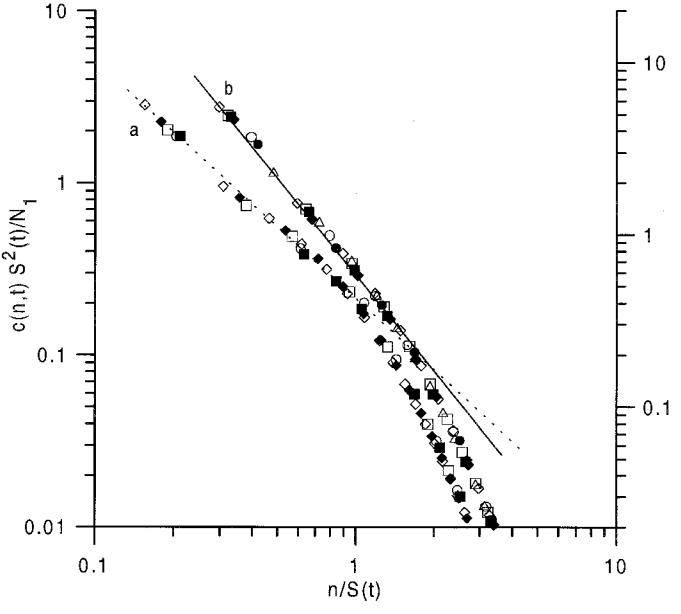

FIG. 17 Fragmentation in aqueous solution of polyvinylpyridine (M_w = 589,000) of aggregates of latex particles formed in the presence of polyvinylpyridine without stirring. Representation of the reduced concentration $c(n, t)\ S^2(t)/N_1$ as a function of the reduced variable $n/S(t)$ for different periods of fragmentation in the concentrated systems $C^*/5$ and $C^*/10$ (curve a, right axis) and the diluted systems $C^*/30$, $C^*/50$, and $C^*/70$ (curve b, left axis). According to Eq. 7 the slopes of the straight lines equal to -1.2 and -1.75 give the exponents of the rates of formation of small fragments in concentrated and diluted systems.

$S(t)$ of the aggregates display a sigmoid shape where the intermediate domain of growth may be represented by the power law

$$S(t) \propto t^{3.5} \tag{30}$$

Figures 18 and 19 show the variation with time of the average masses $S(t)$ and $N(t)$, respectively, for fragments resulting from the breakup of aggregates of $S(t = 0)$ equal to 6, 9, 13, 25, and 43 samples at increasing times during aggregation, $t = 0$ corresponding to the immersion in the $C^*/30$ polymer solution. One notes that the initial period of constant $S(t)$ values strongly decreases when the average mass $S(t = 0)$ increases, thus indirectly illustrating the role of the surface coverage that was established before immersion in the fragmenting media. Shared layer separation and aggregate fragmentation result from progressive adsorption of free polymer issued from

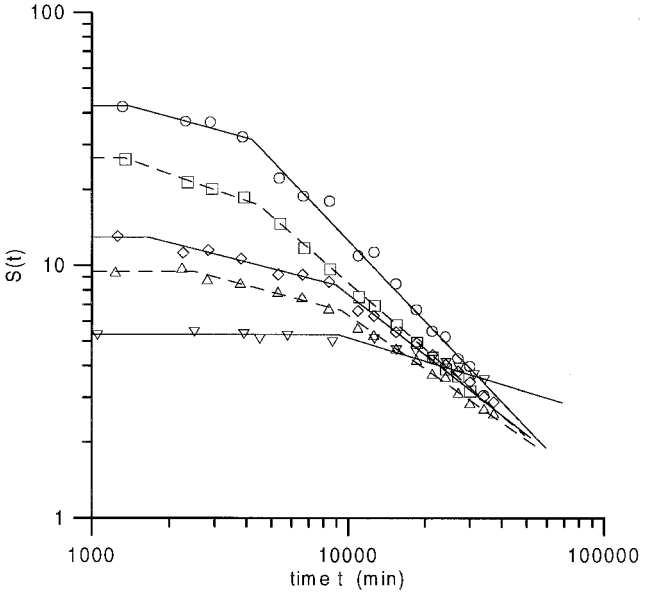

FIG. 18 Fragmentation in aqueous solution of polyvinylpyridine (M_w = 589,000, $C^*/30$) of aggregates of latex particles formed in the presence of polyvinylpyridine under stirring. Representation of the weight average mass $S(t)$ of the fragments as a function of the period of fragmentation for aggregates of mass $S(t = 0)$ equal to 6 (▽), 9 (△), 13 (◇), 25 (□), and 43 (○).

the polymer solution of concentration $C^*/30$ and imply great modification of the confined interfacial layer conformation. The progress of adsorption needs both diffusion through the already adsorbed layer and chain reptation towards partially covered areas. De Gennes established the mobility U of a flexible chain moving inside a diffuse adsorbed layer to vary as [78]

$$U \propto \zeta^{-1} N^{-2} \log \frac{\Gamma_{eq}}{\Gamma_{eq} - \Gamma(t)} \tag{31}$$

where ζ is the friction coefficient of the monomer, N the number of monomers, and Γ_{eq} the coverage at equilibrium. From results of Table 6, the variation of $S(t)$ in the first regime is defined by an exponent λ close to 4. The acceleration of fragmentation described by the decrease of $S(t)$ in the second regime can be expressed as

$$\lambda \propto S(t = 0)^{-0.3} \tag{32}$$

Combination with Eq. 30 determines the linear relationship between the

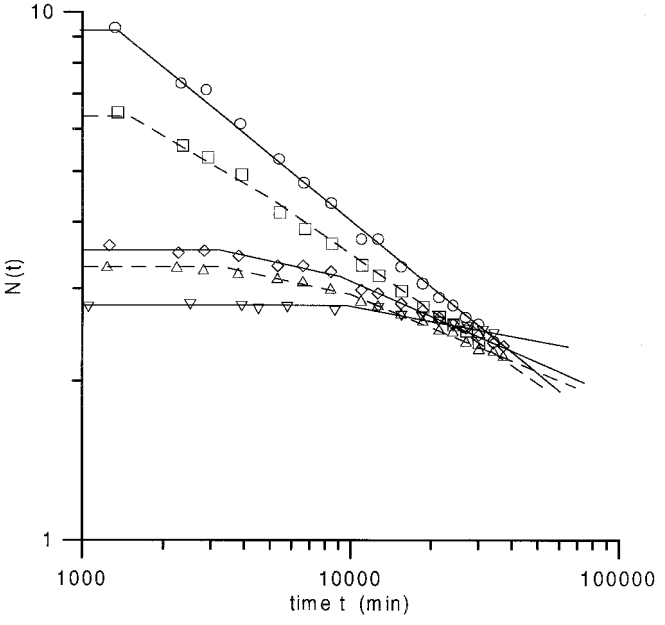

FIG. 19 Fragmentation in aqueous solution of polyvinylpyridine (M_w = 589,000, $C^*/30$) of aggregates of latex particles formed in the presence of polyvinylpyridine under stirring. Representation of the number average mass $N(t)$ of the fragments as a function of the period of fragmentation for aggregates of mass $S(t = 0)$ equal to 6 (▽), 9 (△), 13 (◇), 25 (□), and 43 (○).

exponent λ^{-1} (second kinetic regime) and the degree of surface coverage $\Gamma(t = 0)$ established prior to immersion. This leads us to express the rate of decrease of the weight average mass of the fragment as a power law of the surface coverage:

$$S(t) \propto t^{-\Gamma(t=0)} \tag{33}$$

From the values of p in Table 6, one may conjecture that the fragmentation process develops quite differently in the two regimes. During the first regime, the breakup produces fragments of small and large masses, while during the second regime, it produces fragments of even masses.

2. Influence of the Polymer Concentration C^*/d

The temporal variations of $S(t)$ and $N(t)$ display two domains for all systems. Results are presented in Table 7. In the first regime of relatively slow fragmentation of aggregates of initial masses $S(t = 0)$ close to 10 the slopes of the temporal variations of the average masses $S(t)$ ($\lambda \approx 3$) and $N(t)$ ($\mu \approx$

TABLE 6 Fragmentation Characteristics of Aggregates Formed Under Stirring: Influence of the Surface Coverage (M_w = 589,000)

$S(t=0)$	λ[a]	μ[b]	λ[d]	p[e]
		First regime		
6	2.8–3.3	5–10	0.58	0.16–0.2
9	5.0	20	0.62	0.15
13	5.3	13	0.59	0.11
25	3.2	3.6	0.62	0.03
43	4.0	2.7	0.65	≅0
		Second regime		
6	1.8	5.9	0.58	0.39
9	1.6	5.3	0.62	0.44
13	1.5	4.8	0.59	0.46
25	1.2	3.0	0.62	0.53
43	1.0	2.3	0.65	0.59

[a]Equation 11; λ is derived from the variation of $S(t)$ with time.
[b]Equation 12; μ is derived from the variation of $N(t)$ with time.
[d]Equation 9; λ is derived from the reduced mass frequency at great values of $n/S(t)$.
[e]Equation 13.

9) of the fragments do not depend on the polymer concentration, and the polydispersity factor p is close to 0.2. This regime is followed by a faster regime where the polymer concentration determines the fragmentation mechanisms.

The rate of fragmentation of aggregates of large masses, which is independent of the polymer concentration in the fragmenting medium and the average masses of the parent aggregates, can be expressed by

$$a(n) = n^{0.65} \tag{34}$$

The obvious conclusion is that the resistance to breakup which should be related to the aggregate internal cohesion is greater for aggregates obtained under stirring (orthokinetic aggregation) than that of systems obtained in perikinetic processes (Eq. 29).

In Secs. IV and V protonated polyvinylpyridine was employed to induce aggregate fragmentation, and this polyelectrolyte may be considered as displaying the interfacial characteristics of true hydrophilic polyelectrolyte molecules exerting only electrostatic interactions. In the following Secs. VI and

TABLE 7 Fragmentation Characteristics of Aggregates Formed Under Stirring: Influence of the Polymer Concentration (M_w = 589,000)

Pol. conc.	λ^a	μ^b	λ^d	p^e
		First regime		
$C^*/5$	3.30	9.2	0.70	0.20
$C^*/10$	3.25	8.9	0.52	0.19
$C^*/30$	3.4	10.4	0.70	0.20
$C^*/50$	2.36	7.9	0.65	0.30
		Second regime		
$C^*/5$	1.10	3.1	0.70	0.60
$C^*/10$	0.67	1.7	0.52	0.92
$C^*/30$	1.72	5.8	0.70	0.40
$C^*/50$	1.60	5.0	0.65	0.42

[a] Equation 11; λ is derived from the variation of $S(t)$ with time.
[b] Equation 12; μ is derived from the variation of $N(t)$ with time.
[d] Equation 9; λ is derived from the reduced mass frequency at great values of $n/S(t)$.
[e] Equation 13.

VII more complex systems are presented in order to illustrate two new fragmentation mechanisms. Because the adsorption of pure polyelectrolyte at solid/liquid interfaces combines a number of complex phenomena, the situation is expected to be of even higher complexity when at the same time chains bear hydrophilic and hydrophobic moieties or positively and negatively charged groups.

VI. AGGREGATE FRAGMENTATION INDUCED BY SPATIAL SEGREGATION BETWEEN HYDROPHOBIC AND HYDROPHILIC GROUPS AT THE SOLID/LIQUID INTERFACE

The system resulting from mixing of aluminum oxide and polyacrylic acid in aqueous solution was determined to be very complex due to the partial dissolution of the oxide which liberates 10^{-4} mol/L multivalent aluminum ions in the supernatant at pH 5.0 [79]. Definitely to set the chemical composition of the system, the aluminum ion concentration was fixed by dissolving the required amount of $AlCl_3$ in 10^{-3} mol/L KCl at pH 4.06. Addition

of the dry alkaline aluminum oxide powder to the solution makes the pH of the suspension reach the constant value of 5.0 immediately, the partial dissolution of oxide being thus inhibited. Under these conditions, the average positive charge n^+ of aluminum ions was determined to be equal to 2.23 from titration experiments.

Addition of polyacrylic acid at pH 5.0 to the former solvent (the aqueous solution of 10^{-3} mol/L KCl and 10^{-4} mol/L $AlCl_3$ at pH 5.0) induced a fast pH drop whose amplitude is related to the degree of acid complexation. The hydrogen ion production during complex formation might be interpreted on the basis of the reaction [80]

$$\begin{aligned} &Al(OH)_m^{(3-m)+} + n(1 - \alpha)(\text{-COOH}) + n\alpha(\text{-COO}^-) \\ &\quad \leftrightarrow n(1 - \alpha)H^+ + [(\text{-COO})_n Al(OH)_m]^{(3-m-n)+} \end{aligned} \tag{35}$$

where m and n vary from 0 to 2 and from 1 to $(3 - m)$, respectively. Reaction 35 is too general to give straightforward information concerning the degree of complexation insofar as certain thermodynamic equilibrium constants are unknown. However, when mixing of aluminum ions and polyelectrolyte induced the maximal drop in pH, no free aluminum ions were detected in solution. Therefore the polyion complexation is maximal and the following values of 1.7, 0.77, and 0.53 were determined for n, m, and the positive charge of the complex, respectively. Taking $n = 1.7$, the degree of complexation defined by $[Al(\text{-COO})_3]/[\text{-COOH} + \text{-COO}^-]$ is close to 0.56. Since neutral, negative, and positive groups are randomly distributed along the polymer chain, polyacrylic acid should exhibit complex adsorption behavior. Moreover, ion pairing between carboxylic acid groups and multivalent cations is known to decrease the hydrophilic nature of polyelectrolyte and to induce hydrophobic microdomains [81]. Titration of polyacrylic acid with KOH in the presence of various aluminum ion concentrations yields typical Katchalsky–Spitnik curves for ion complex formation, which reveal the presence of hydrophobic domains [82] (Figure 20). The plots of pH vs. $\log(1 - \alpha)/\alpha$ were obtained even at low degrees of complexation and demonstrate the existence of stable coordinated complexes. At maximal complexation, the curves nevertheless show some analogy with the pH hump observed in the titration of polymethacrylic acid, where the supplementary energy is derived mainly from the balance of attractive hydrophobic and repulsive electrostatic forces [83]. This characteristic shape evidences the conformational transition from a compact chain containing only complexed groups at low pH to the extended chain containing both dissociated and complexed acrylate groups at high pH. Therefore aluminum complexed groups confer lower solubility in aqueous solution at pH 5. Since the adsorption of complexed polyacrylic acid was determined to similarly reduce

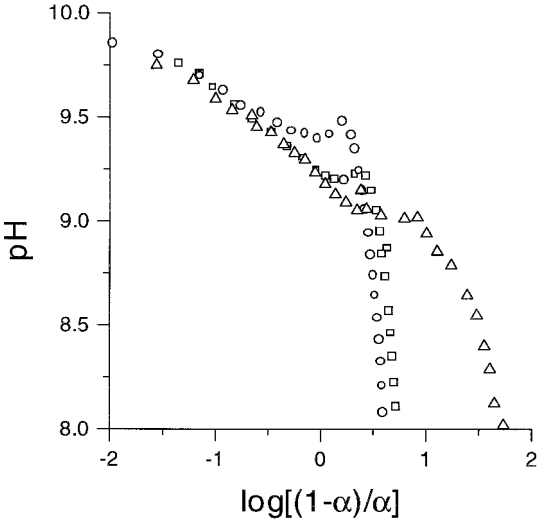

FIG. 20 Henderson–Hasselbach plot for the titration of polyacrylic acid in the presence of aluminum ion. Representation of the pH as a function of $\log[(1-\alpha)/\alpha]$ for three different initial relative concentrations [Al]/[RCOOH] in the supernatant: 1.36 (○), 1.08 (□), and 0.87 (△).

the electrophoretic mobility of the coated latex and aluminum oxide particles, adsorption may not be induced by specific interactions but merely resemble interfacial deposition. In addition, adsorption on aluminum oxide is a slow process as far as the amount of polymer adsorbed at high doses was determined to be stabilized after 24 h only [79].

Two aluminum oxide samples were used in the experimental studies. Results relative to the interfacial characteristics reported in B were obtained employing the rough industrial sample of specific area equal to 3.0 m^2/g. Those relative to the colloidal stability reported in A were obtained employing a fractionated sample of specific area equal to 2.35 m^2/g. The correspondence between the interfacial characteristics of the polymer coated particles and their colloidal stability is established as a function of the degree of polymer coating expressed in terms of mg/m^2. However, the correspondence cannot be strictly established on the basis of the specific surface areas as far as the polymer doses relate to the surface area developed by the peptized oxide, which is only available prior to aggregation. Fortunately, comparing the instability domains of the two samples leads us to see that polymer doses determined for the fractionated sample must be multiplied

by a factor of two in order to fit adequately the behavior of the rough oxide [65]. Therefore to avoid any confusion in the polymer doses in the present context, all doses concerning the rough oxide were divided by two in order to refer to the fractionated samples.

A. Colloidal Stability of the Alumine/Polyacrylic Acid Complexes [84,85]

Suspensions of dense aluminum oxide particles were maintained homogeneous by stirring with a magnetic bar at 100 rpm. The $S(t)$ and $N(t)$ vs. time patterns reported in Figures 21a–d correspond to the different polymer doses of 0.5, 1.0, 1.5, and 2.0 mg/m^2: systems corresponding to Figures 21a–c display a great instability since the masses $S(t)$ and $N(t)$ are of the order of 1000 and 100, respectively. After a short period of a few minutes to 1 hour, the aggregates successively undergo slow and fast breakup processes, and in the final situations fully dispersed grains were recovered. Figure 21d displays a different situation for which the colloids remain stable for about 2 hours and then aggregate suddenly according to $S(t)$ and $N(t) \approx t^2$ and finally fragment in such a way as ultimately to restore the initially dispersed situation. We note that Figure 2 illustrates the self-similar character of the mass distribution for the typical experiment carried out at the dose of 0.5 mg/m^2. The slope of the curve at large values of $n/S(t)$ provides the exponent λ of the rate of fragmentation. The scaling exponents of fragmentation are given in Table 8. As usually observed for polymer-induced fragmentation, breakup and sticking processes coexist in such a manner that no clear correlation exists between the rate of fragmentation of large aggregates and the rate of formation of small fragments, as shown in Figure 22. Increasing polymer doses induce faster breakup of the largest aggregates, whereas they induce smaller rates of formation of the smallest fragments.

B. Interfacial Characteristics and Stability at Short Times [86]

Figure 23 shows the zeta potential as a function of time for the successive doses of 0, 1, 2, 3, and 4 mg/m^2 of polyacrylic acid. In the absence of polymer the potential is constant over at least 24 h, while in the presence of polymer very subtle variations were determined to occur, which are definitely attributed to the slow progress of polymer adsorption. As a general rule, values of the zeta potential close to zero are correlated with colloidal instability. For the present system the correlation between optimal aggregation conditions and zeta potential close to zero reveals strong interactions between positively charged complexed groups and negatively charged dis-

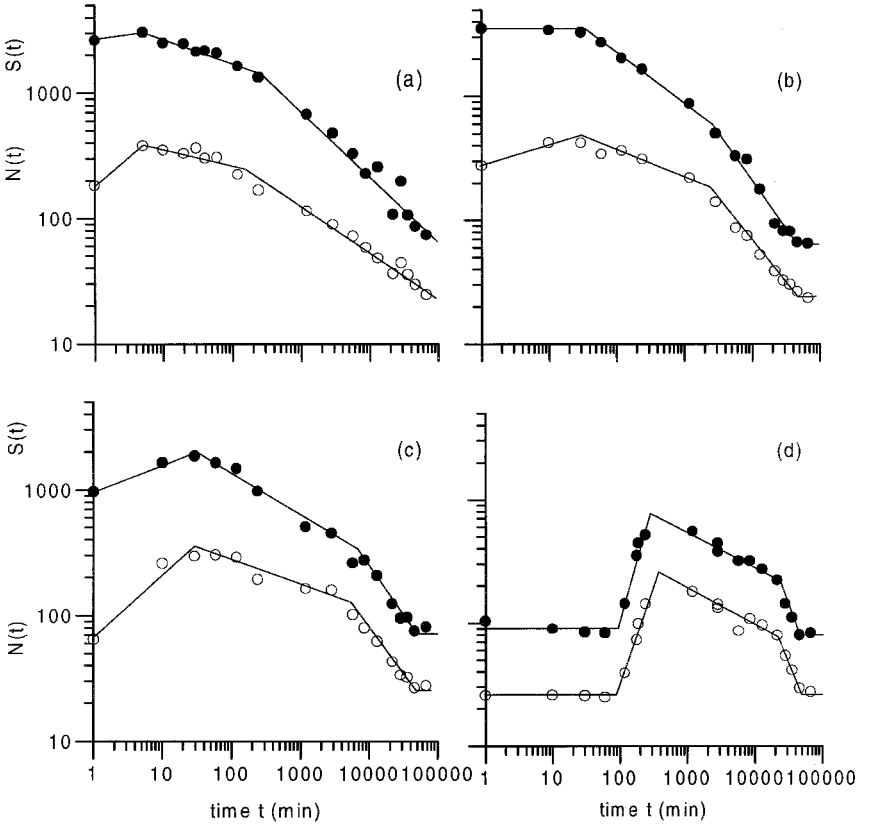

FIG. 21 Stability of the aluminum oxide/polyacrylic acid complexes. Representation of the weight $S(t)$ (●) and number $N(t)$ (○) average masses of the grain aggregates as functions of time for different polymer doses expressed in terms of the amount of polymer initially added per square meter of the adsorbent (mg/m^2): 0.5 (a), 1.0 (b), 1.5 (c), and 2.0 (d).

sociated acid groups present at even surface density. This situation is realized quite instantaneously for the doses close to 1 mg/m^2, and the net fragmentation observed after one hour may be attributed to the departure from the zero potential value (Figure 21b). For the dose of 2 mg/m^2 three processes develop successively. The initial rapid potential drop ensures a high colloidal stability, then the progressive approach to zero induces rapid aggregation, and finally the slow decrease to more negative values results in the observed slow fragmentation process (Figure 21d).

TABLE 8 Fragmentation Characteristics of the System Aluminum Oxide/ Polyacrylic Acid

Polym. dose (mg/m^2)	Slow regime		Fast regime			
	λ^a	μ^b	λ^a	μ^b	ν^c	λ^d
0.5	2.50	3.33	1.67	2.5	−1.23	0.056
1.0	2.78	6.25	1.35	1.69	−1.23	0.066
1.5	2.94	6.25	1.56	1.54	−1.16	0.071
2.0	3.33	3.7	0.75	0.75	−0.87	0.073

[a]Equation 11; λ is derived from the variation of $S(t)$ with time.
[b]Equation 12; μ is derived from the variation of $N(t)$ with time.
[c]Equation 10; ν is derived from the reduced mass frequency at small values of $n/S(t)$.
[d]Equation 9; λ is derived from the reduced mass frequency at great values of $n/S(t)$.

C. Interfacial Characteristics and Fragmentation at Large Times

In order to evidence the driving force for the fast fragmentation regime, we determined the polymer and aluminum ion concentrations in the supernatant solution, the pH of the suspension, and the zeta potential of the oxide and oxide/polymer complexes at 24 hours and after 6 weeks [84]. Figure 24a shows the concentration of the polymer remaining in the liquid phase as a

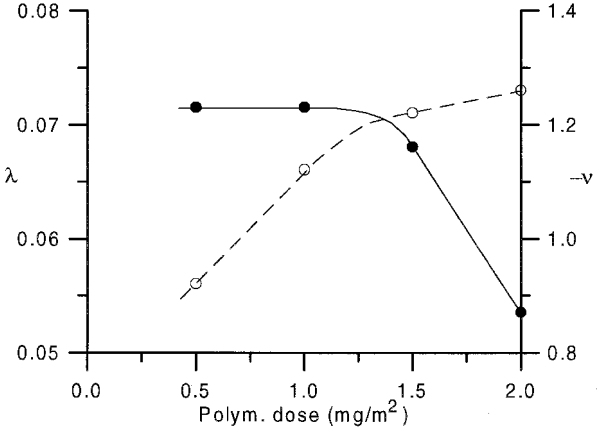

FIG. 22 Stability of the aluminum oxide/polyacrylic acid complexes. Representation of the exponents $-\nu$ (●) and λ (○) of the breakup process as functions of the initial polymer dose.

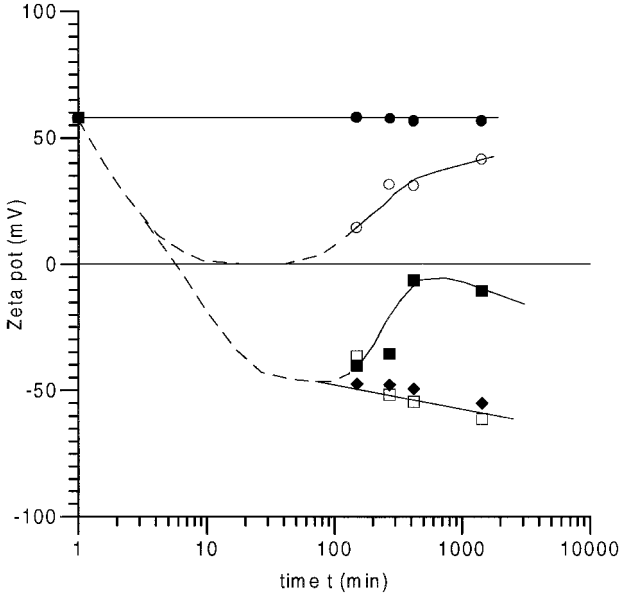

FIG. 23 Aluminum oxide/polyacrylic acid complexes. Representation of the zeta potential of bare oxide (●) and polyelectrolyte coated oxide as functions of time for different polymer doses (mg/m^2): 1.0 (○), 2.0 (■), 3.0 (♦), and 4.0 (□).

function of the initial dose, and no difference is observed at 6 weeks as compared to 24 h. Moreover, the oxide particles adsorb the entire available polymer in the instability domain. Figure 24b shows the corresponding concentrations of aluminum ions in the supernatant to remain unchanged. We note that the initial decrease from 10^{-4} to 0 mol/L results from the acid complexation. These constant solution characteristics indicate the fast fragmentation regime to develop without any interfacial transfer of polyelectrolyte or aluminum ions. Referring to the pH values of the suspension at 24 h and 6 weeks as a function of the polymer dose (Figure 24c), pH 5.0 does not correspond to a true equilibrium value in the absence of polymer and is shifted to 4.6 after 6 weeks. However, the addition of polyelectrolyte to the suspension slightly changes the situation at 6 weeks below 2 mg/m^2. These variations in pH may result from modifications of the ion distribution within the adsorbed polymer layer as evidenced by changes in the electrophoretic mobility. Figure 24d shows the zeta potential to decrease strongly with time at polymer doses smaller than 2 mg/m^2. The plausible interpretation combines the two phenomena. Aluminum ion complexed groups (hydrophobic moieties) slowly migrate towards the oxide surface where the great chain

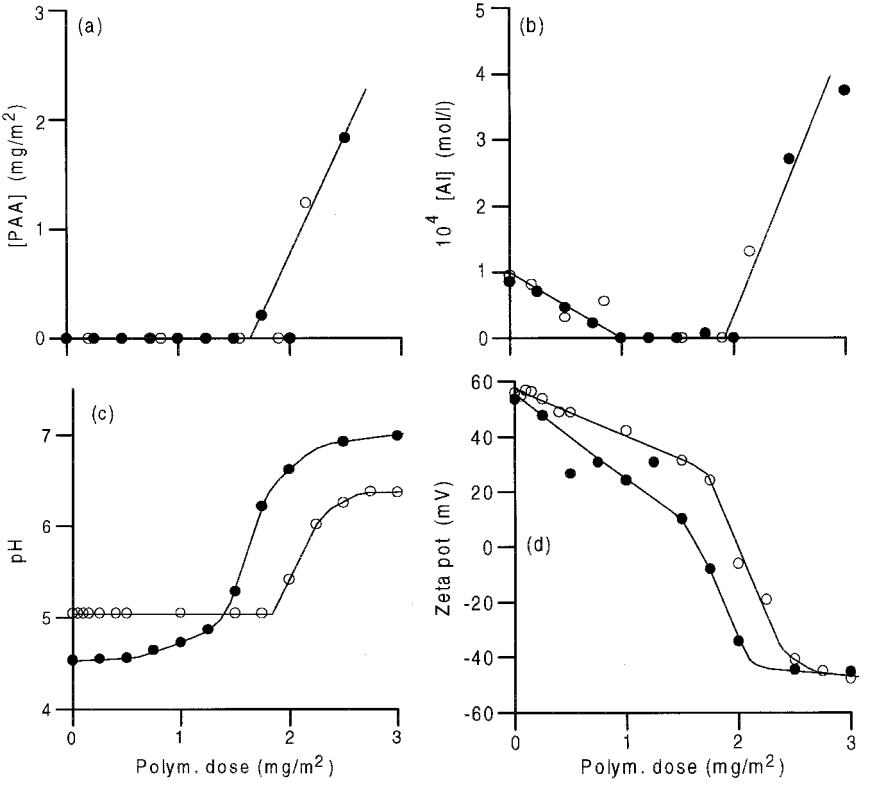

FIG. 24 Aluminum oxide/polyacrylic acid complexes. Suspension and complex characteristics at 24 h (○) and 6 weeks (●) as functions of the polyelectrolyte dose (mg/m^2). (a) Polymer concentration in the supernatant phase (mg/m^2); (b) aluminum ion concentration in the supernatant phase (mol/L); (c) pH of the suspension; and (d) zeta potential of the bare and polyelectrolyte coated oxide.

segment density favors segment–segment contacts while carboxyl and carboxylic acid groups (hydrophilic moieties) migrate towards the outer zone where polymer loops protrude into the liquid phase and segment–solvent contacts are favored [87]. The faster fragmentation regime may result from the progressive establishment of an anisotropic distribution of hydrophobic and hydrophilic groups within the polymer layer. Consequently, the distributions of aluminum, potassium, and hydrogen ions would be different within polymer layers belonging to grain agglomerates and dispersed grains.

For the present system, we demonstrate the amphiphilic character of the complexed polyelectrolyte to override its amphoteric characteristics. There-

fore aluminum oxide powder whose dissolution was impeded by the addition of aluminum chloride is expected to present surface characteristics of lyophobic colloids and to establish hydrophobic and hydrophilic interactions.

VII. AGGREGATE FRAGMENTATION INDUCED BY SPATIAL SEGREGATION BETWEEN POSITIVE AND NEGATIVE GROUPS AT THE SOLID/LIQUID INTERFACE [88–90]

Aggregation and fragmentation of colloidal particles has been investigated further employing natural polyelectrolytes like humic substances. Adsorption of humic acids on aluminum oxide was determined to resemble interfacial deposition on the basis of methods previously employed for the aluminum oxide/polyacrylic acid system [88]. Complexation by soluble aluminum ions produces pH drops that are very similar to that determined for polyacrylic acid, and essentially humic acids were determined to exert effects on the stability of colloidal aluminum oxide particles at pH 5 that are very similar to polyacrylic acid.

Kaolinite clay (GZA IV, French origin) [91,92] was used as a colloidal adsorbent to investigate the adsorption of aluminum ion complexed humic acids and the related clay stability. This system differs greatly from the previous one, since the 10^{-4} mol/L aluminum ions which are supplied strongly interact with the suspended clay. This phenomenon leads to have supernatant liquid phases of residual aluminum ion concentrations depending on the clay concentration that was fixed in such a way as to investigate the domain between 0 and 10^{-4} mol/L. The ionic strength is set constant by adding 10^{-3} mol/L KCl, as in the experiments presented in Sec. VI.

Two different clay samples were employed in this experimental study, which differed only by their size distribution. Particles of very large sizes were allowed to settle out by gravity and were discarded, and this operation was repeated five times. This Sample I was used to characterize the clay–aluminum ion–humate complex. Particles of very small sizes were discarded after a second sedimentation run by removing the upper portion of the suspension, and this operation was repeated five times too. This Sample II was used in experiments of colloid stability. This precaution ensures that practically no detectable grain or aggregate further originates from any agglomeration of ''invisible'' shattered matter or that clay particles of diameter smaller than 0.9 μm constitute weak cohesive interaggregate links. Clay doses are expressed by the weight of kaolinite suspended in 100 g of suspension. Aldrich Chemie supplied the peat-derived humic substance as sodium humate, and some characteristics are given by Ochs et al. [93]. Humic

acid doses are expressed in ppm (μg of humic acid per gram of suspension or solution).

The zeta potential of bare kaolinite clay was determined to be -17.6 mV at pH 5.0. The strong interaction of aluminum ions with kaolinite clay at pH 5.0 was evidenced by (1) the positive values of the potential determined as a function of clay dose (Sample I) and (2) the low residual concentrations of aluminum ions in the supernatant as a function of the clay dose (Samples I and II) (Figure 25). Since the degree of hydrolysis of $AlCl_3$ determined at pH 5.0 is function of the aluminum ion concentration below a concentration of 10^{-3} mol/L, the net positive charge of the residual aluminum ions in the supernatant is expected to increase with clay dose. Therefore the interaction between modified clay and humic acids should be a function of the aluminum ion concentration, but in the present context only the relative concentration of aluminum ions and acidic groups α_{rel} = [Al]/[RCOOH] is taken

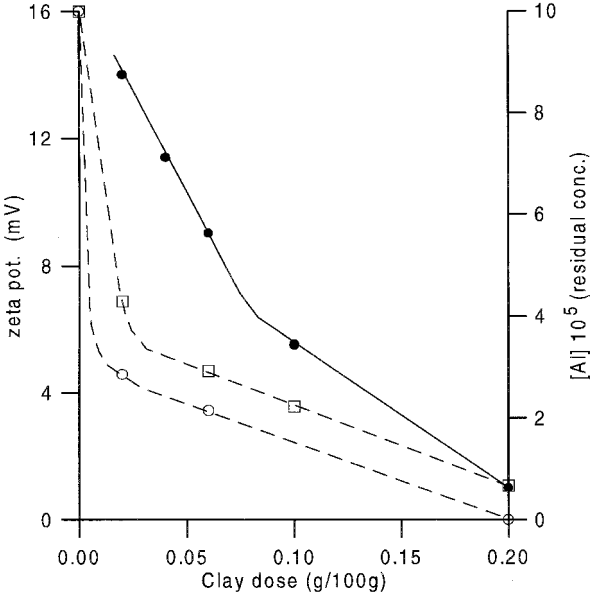

FIG. 25 Kaolinite/humic acid complexes. Left ordinate: Representation of the zeta potential of kaolinite clay (Sample I) modified by adsorption of aluminum ion after immersion in a solution of 10^{-3} mol/L KCl and 10^{-4} mol/L $AlCl_3$ at pH 5.0 for 24 h as a function of the clay dose expressed in g of clay/100 g of suspension (●). Right ordinate: Representation of the residual free aluminum ion concentration (mol/L) in the bulk solution after immersion of clay Samples I (○) and II (□) as functions of the clay dose.

as variable parameter. Addition of humic acids to suspensions containing modified clay and aluminum ions promotes complex ion-exchange reactions and humic acid dissociation and complexation, which are evidenced by instantaneous changes in the hydrogen ion concentration [H^+]. Especially, as was previously determined, measurement of pH drops following the addition of humic acids to aqueous solutions of varying $AlCl_3$ concentrations or to suspensions of varying clay concentrations led to bell-shaped curves for the representation of [H^+] as a function of the humic acid concentration. A maximal degree of complexation of the acidic groups was determined for humic acid doses lower than those at the peaks, the peaks corresponding to the limiting situations where addition of humic acids to the systems left no aluminum ions in the solution or in the supernatant. The single line shown in Figure 26 representing the [H^+] corresponding to the peak as a function of the initial or residual aluminum ion concentrations shows that aluminum ions in the solution or residual aluminum ions in the clay suspension interact with humic acids in a similar manner. Therefore complexation of humic

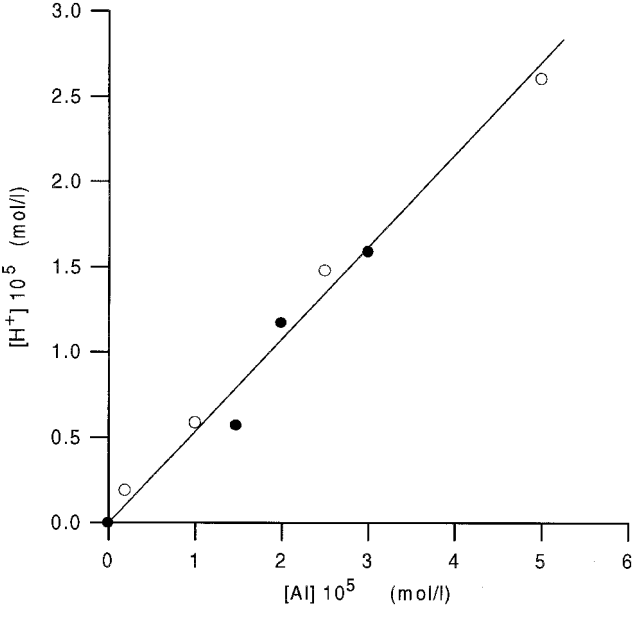

FIG. 26 Kaolinite/humic acid complexes. Representation of the maximal hydrogen ion concentration (mol/L) induced by humic acid complexation as a function of the initial (○) (in the absence of clay) and residual concentrations of aluminum ions (●) in the solution (mol/L) (as fixed by varying the dose of kaolinite clay).

acids by aluminum ions of different net charges and adsorption of the complexed polymer on the clay may be considered as being two successive independent processes in the present context [89].

A. Amphoteric Character of the Kaolinite–Aluminum Ion–Humate Complex

These characteristics were determined using the clay Sample I suspended for 24 h in aqueous solutions of various compositions [89]. Figure 27 shows the zeta potential of the clay-aluminum ion–humate complexes as a function of the relative concentration [Al]/[RCOOH] at the different clay doses of 0.01, 0.02, 0.03, 0.06, and 0.1%. Three typical behaviors are observed.

For the acid form of $\alpha_{rel} = 0$ to 0.1, the absolute value of the negative zeta potential decreases very slowly, and no obvious effect due to complexation is determined.

For systems at doses of 0.1 and 0.06% a sharp decay from -30 to -10 mV is determined in a small range of α_{rel} and becomes rapidly limited within -10 and $+5$ mV for α_{rel} lying between 0.1 or 0.2 and 2.

For all smaller clay doses, a single logarithmic variation of the potential within a range of -30 and $+20$ mV is determined as a function of α_{rel}. Then the potential becomes stabilized.

Adsorbed humate of α_{rel} close to 0.5 produces complex layers of zero potential in all situations. This reveals surface charge annihilation where Al^{3+} (main component), $Al(OH)^{2+}$, and $Al(OH)_2^+$ paired with acid groups exactly compensate for the remaining dissociated acid groups $R\text{-}COO^-$.

Our interpretation of the results shown in Figure 27 is based on recent theories of Joanny and Dobrynin et al. [94,95]. These authors considered the adsorption of a polyampholyte chain on charged surfaces and determined the dependence of the adsorption on the surface charge density and on the number of charged groups on the chain. One result is that when the surface charge exceeds a critical value, the electric field of the adsorbent is sufficiently strong to deform the polyampholyte chain. The charged chain segments then redistribute so as to decrease the electrostatic energy, and the chain binds to the adsorbent. In the present situation, the positive and negative charges are not chemically fixed along the chain, as has been assumed in the theory, but are mobile in the limit of the constraints imposed by the adsorbed polymer layer and the electrical double layer. As a result, the charge distribution within the polymer layer may change by transfers of aluminum counterions from complexed (positively charged) towards dissociated (negatively charged) groups. Insofar as similar effects in colloid stabilization were observed for complexed humic and polyacrylic acids, the thickness of the adsorbed layer is assumed to increase linearly from 0 to 40

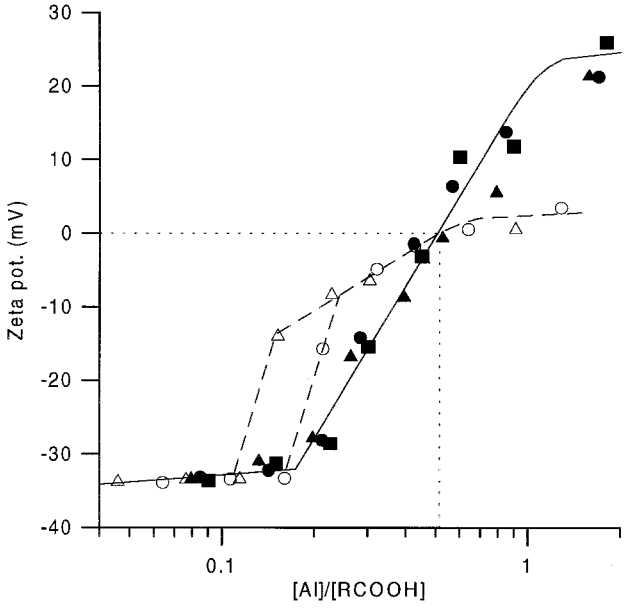

FIG. 27 Kaolinite/humic acid complexes. Representation of the zeta potential (mV) of the clay–aluminum ion–humate complexes as functions of the relative concentration of aluminum ions and carboxylic acid groups for different clay doses: (△) 0.1%, (○) 0.06%, (▼) 0.03%, (●) 0.02%, and (■) 0.01%.

nm for specific adsorptions of 0 to 1.5 mg/m^2 [88]. The theoretical models of Joanny and Dobrynin et al. may serve to interpret the experimental results obtained at low polymer coverage when the layer thickness is less than 10 nm corresponding to the Debye–Hückel length at the ionic strength of 10^{-3}. For the different situations, we propose the following interpretations:

For the complex bearing a net positive charge (i.e., for [Al]/[RCOOH] = 1 in Figure 27), the modified clay exerts repulsive interactions on the average, so that the adsorption is expected to be impeded by the increase of the net charge of the modified clay. After 24 h, dissociated and complexed acid groups are nonhomogeneously distributed within the interfacial layer, and the extent of charge segregation should be greater at small clay doses than at large ones. Actually, at small clay doses (high net charge), the adsorbent imposes high charge segregation, so that the resulting layer potential is high. Conversely, at large clay doses (small net charge), the adsorbent exerts a weak charge segregation effect, and the resulting layer potential is small. For [Al]/[RCOOH] = 1 in Figure 27 the extreme values of the potential are +25 and +3 mV.

For the complex bearing a net negative charge (i.e., for [Al]/[RCOOH] = 0.2 in Figure 27), the modified clay exerts attractive interactions, and the adsorption of humic acids is expected to increase with the net charge density of the clay. Therefore adsorption at low clay doses creates dense interfacial structures of high negative potential. Conversely, adsorption at high clay doses should establish adsorbed structures of small negative potential. Actually, for [Al]/[RCOOH] = 0.2 in Figure 27, the two extreme potential values are −35 and −10 mV.

As shown in Figure 27, the presence of small proportions of positively charged groups on weakly complexed humic acids only slightly changes the usual acid behavior. However, at critical values of the degree of complexation close to 0.1 and for surfaces of small charge density one suddenly passes from the nonperturbed polyelectrolyte behavior which characterizes humic acids in the presence of divalent ions to the polyampholyte behavior [96,97].

B. Interfacial Characteristics and Fragmentation Modes

All experiments presented in this context were carried out using Sample II at the constant doses of 5 ppm humic acids. Figures 28–30 show the number $N(t)$ and weight $S(t)$ average masses (left ordinate) and the zeta potential (right ordinate) as a function of time for three typical fragmentation experiments. Clay and polymer doses constituted variable parameters while the initial amounts of KCl and $AlCl_3$ were fixed at 10^{-3} and 10^{-4} mol/L, respectively. We were unable to determine the leading phenomenon that might impose such different shapes. The polymer coverage established at the beginning of fragmentation was previously found to determine the rate of decrease of $S(t)$ with time (Sec. V.B.1), but this parameter cannot be determined in the present experiments. In addition, although the evolutions with time of the zeta potential and the aggregate average masses seem to be correlated (Figure 5), no correlation could be found between the fragmentation rates and the system composition. Therefore we first present typical fragmentation rates that were discussed on the bases of the evolution with time of the electrical characteristics of the complexes.

Figure 28 corresponds to the clay dose of 0.2% and a α_{rel} value of 0.45. Homogenization of the system produces aggregates of very great mass polydispersity and of poor stability, since the system fragments immediately and slowly for 2000 min and after that, rapidly. The transition time seems to correspond to a faster increase in the potential that passes from −4 mV to positive values increasing with time.

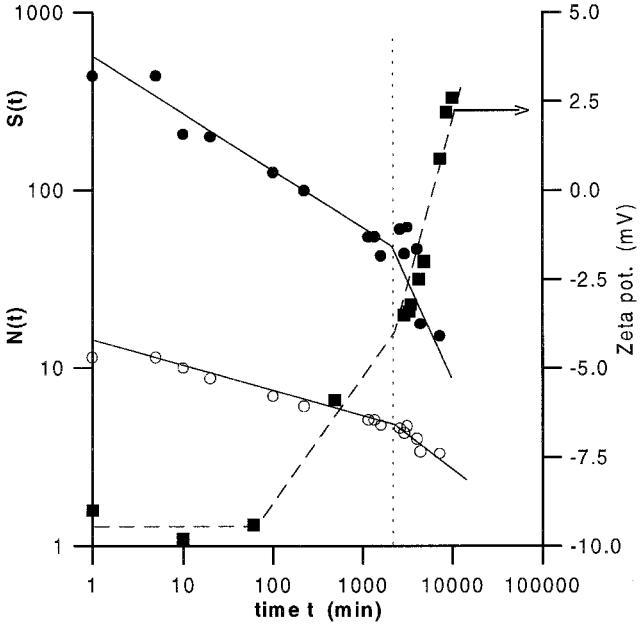

FIG. 28 Kaolinite/humic acid complexes. Representation as functions of fragmentation time of the number $N(t)$ (○) and weight $S(t)$ (●) average masses of fragments (left ordinate) and zeta potential (■) of the clay–aluminum ion–humate complexes (right ordinate) for the system (5 ppm of humic acid, 0.2% of clay, $\alpha_{rel} = 0.45$).

Figure 29 corresponding to the clay dose of 0.1% and a α_{rel} value of 1.47 portrays a very complex situation of concomitant aggregation and fragmentation processes for the first 20 min. The basic observation is relative to the decrease with time of $N(t)$ showing that the number of fragments regularly increases as a power law of time ($\mu = 2.58$ and 4.0, successively). The unexpected increase in $S(t)$ between 1 and 20 min indicates that after fragmentation aggregation stuck together fragments of large masses preferentially while encounters between greatly dissimilar or very small fragments did not lead to sticking. The predominant fragmentation between 20 and 500 min corresponding to $\lambda = 2.30$ should correspond to the release of fragments of small masses, whereas the overwhelming fragmentation after 500 min corresponding to $\lambda = 1.0$ may be viewed as a splitting process. The initial increase in $S(t)$ and decrease in $N(t)$ correspond to a quite constant potential of -3 mV. However, no further correlation between the kinetics of successive fragmentation runs and zeta potential variations could be established strictly during the two successive prevailing breakup steps. In addition, frag-

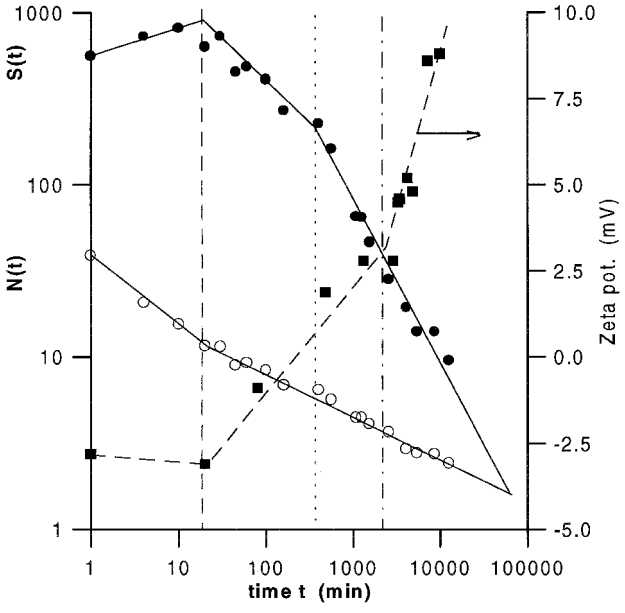

FIG. 29 Kaolinite/humic acid complexes. Representation as functions of fragmentation time of the number $N(t)$ (○) and weight $S(t)$ (●) average masses of fragments (left ordinate) and zeta potential (■) of the clay–aluminum ion–humate complexes (right ordinate) for the system (5 ppm of humic acid, 0.1% of clay, $\alpha_{rel} = 1.47$).

mentation developed even when the net charge of the polyelectrolyte-coated colloid was close to zero.

Figure 30 corresponding to the clay dose of 0.06% and a α_{rel} value of 1.90 shows a situation where the initially and finally observed fragmentation steps are similarly slow while intermediately the rates of decrease of $S(t)$ and $N(t)$ are larger. For the first and last fragmentation runs, values of $\lambda = \mu = 13.5$ were derived, while for the second run we found $\lambda = 1.10$ and $\mu = 2.6$. As a result, the mass polydispersity $S(t)/N(t)$ of fragments remained constant at two different levels during initial and final steps. In the present case, fast fragmentation corresponds to the increase of the potential, while the later slower fragmentation is concomitant with a greater variation of the potential with time.

Changes observed in Figures 28–30 from negative (or slightly positive) to positive (or higher) potential values were attributed to the progressive development of charge segregation within the adsorbed layer as predicted by the theoretical model. The existence of high surface charge density at the

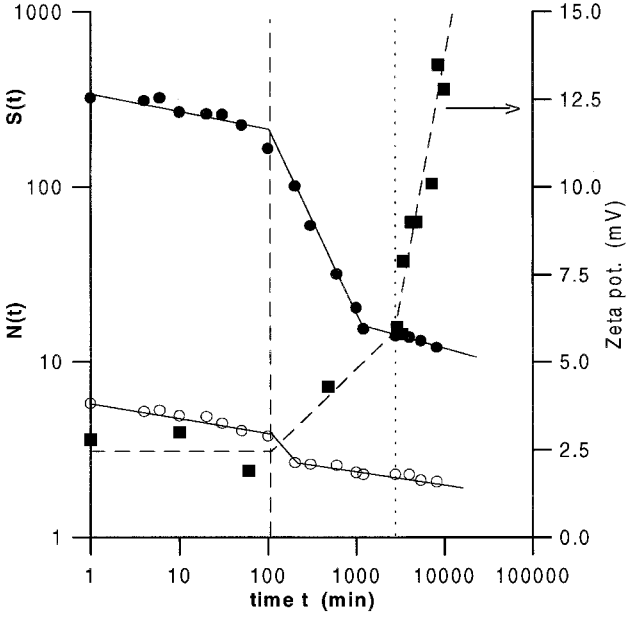

FIG. 30 Kaolinite/humic acid complexes. Representation as functions of fragmentation time of the number $N(t)$ (○) and weight $S(t)$ (●) average masses of fragments (left ordinate) and zeta potential (■) of the clay–aluminum ion–humate complexes (right ordinate) for the system (5 ppm of humic acid, 0.06% of clay, $\alpha_{rel} = 1.90$).

clay/water interface led to a situation where the negative charge of the humic acids (dissociated acid groups) were strongly attracted by the positively charged modified clay, whereas the positive charges (complexed carboxyl groups) were strongly repelled. The layer modifications responsible for the observed potential changes develop over long periods, and this led us to assume that relatively fast ion-exchange reactions and slow conformational changes of the adsorbed layer concomitantly develop with time. Aggregation typically results from attractive electric interactions between randomly distributed positive and negative charged groups within layers belonging to approaching colloids, while fragmentation results from repulsion between evenly charged groups within adjacent layers belonging to stuck colloids. Figure 31 schematically represents the two extreme situations of aggregating and fragmenting systems.

For the three systems described in Figures 28–30, the kinetics of formation of small fragments and fragmentation of large aggregates are derived

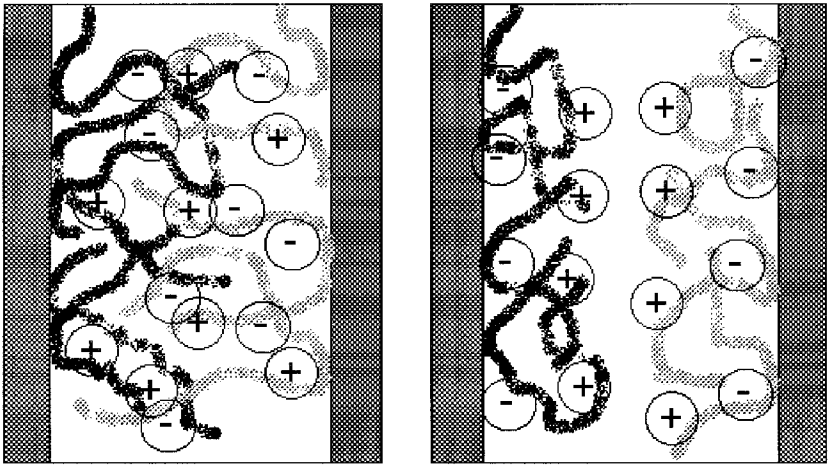

FIG. 31 Amphoteric polyelectrolyte at charged interfaces. Schematic representation of the positive and negative charge distribution in the adsorbed layer: left, stuck clays, random distribution; right, dispersed clays, charge segregation.

as usually from Figures 32 and 33 using Eqs. 5 and 7, respectively. One obtains the following equations for all the investigated systems:

$$a(n) = n^{0.33} \qquad b(n) = n^{-2.0} \tag{36}$$

VIII. CONCLUSION

Fragmentation of lyophobic colloids induced by increasing the surface charge density and range of electric interactions appeared to be an instantaneous process but with limited extent. Resistance to breakup was attributed to link aging effects. The typical example of hydrated colloids showed that particularity in the aggregate internal connection might strongly affect the development of both aggregation and fragmentation processes. This particularity seems to be observed only when the attractive van der Waals forces are low [98] as might occur for colloids bearing a swollen shell [99], protein-coated latex particles [100], and colloids of highly hydrated surfaces [49]. Similarly, fragmentation induced by polymer adsorption has concerned aggregates for which the reduced mass characteristics control the rates of breakup of large aggregates and the formation of small fragments. Moreover, evident instantaneous fragmentation was never observed, and the slow disappearance of aggregates corresponded to a complex reversible process in which aggregation and fragmentation developed concomitantly but at different rates.

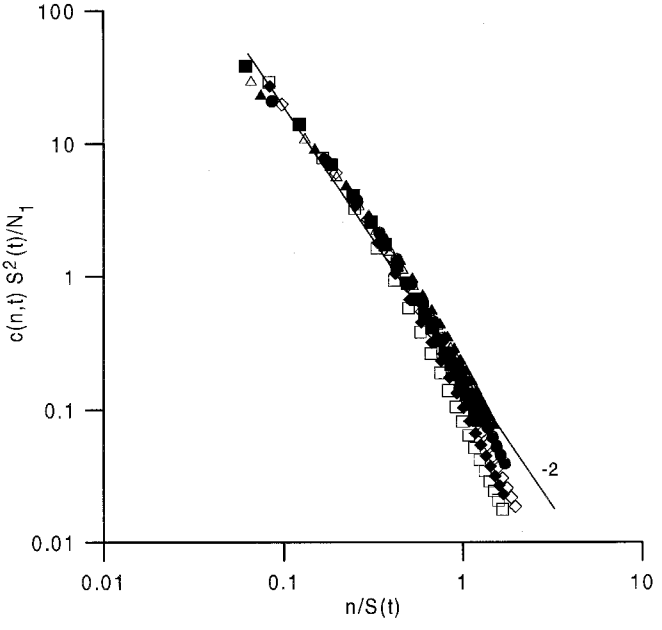

FIG. 32 Kaolinite/humic acid complexes. Representation of the reduced concentration $c(n, t)S^2(t)/N_1$ of aggregates as functions of the reduced mass $n/S(t)$. The points are relative to the experiments of Figures 28 to 30. The slope of the variation at small values of the reduced masses according to Eq. 10 is equal to -2.0.

Two major mechanisms were determined to operate in aggregate fragmentation, each of them helping the establishment of thermodynamic equilibrium. The first mechanism concerned polymer adsorption on bare colloids and the progress of polymer adsorption on initially partly coated colloids. The systems followed the ''natural way'' where thermodynamic equilibrium corresponded to the realization of fully coated dispersed particles suspended in dilute polymer systems. The achievement of this situation is fast in dilute media while its rate decreases with polymer concentration. Aggregates sustaining shear stresses were determined to break up at a lower rate than those formed under Brownian conditions. The second mechanism benefited from modifications of the chain segment distribution within the adsorbed layer. Chain segregation might affect the hydrophobic and hydrophilic moieties or the positively and negatively charged groups of the polyelectrolyte. Clearly, as ion-exchange phenomena are involved in the two latter situations, one might expect the ionic strength of the medium to exert a particular role in the rate of establishment of interfacial segregation and thus in the fragmen-

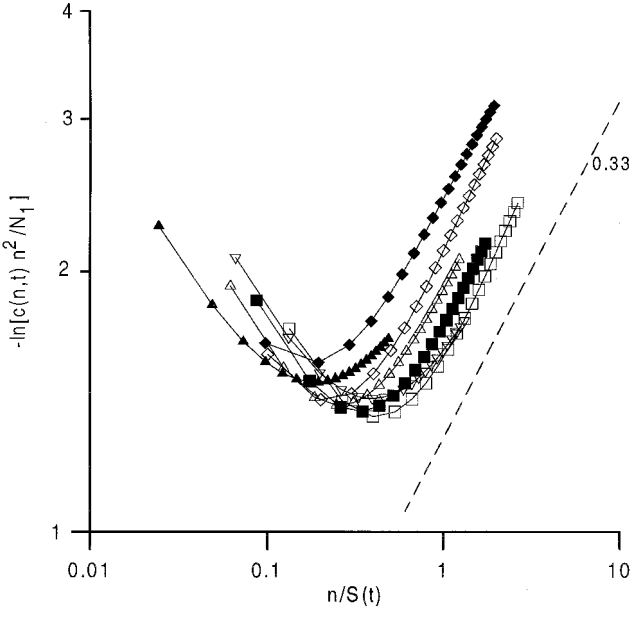

FIG. 33 Kaolinite/humic acid complexes. Representation of logarithm of the reduced concentration $c(n, t)n^2(t)/N_1$ of aggregates as functions of the reduced mass $n/S(t)$. The points are relative to the experiments of Figures 28 to 30. The slopes of the variation at large values of the reduced masses according to Eq. 9 are close to 0.33.

tation rate. Lastly, despite the complexity of all these fragmentation processes, it appeared that the principle of the breakup process should be common to many other systems [101].

IX. APPENDIX: THE COULTER COUNTER TECHNIQUE AND METHODS OF ANALYSIS

The Coulter Counter (Coultronics) [102–105] is able to measure the sizes of individual particles and aggregates in very dilute suspensions (for counting, aliquots of the suspension were usually diluted up to one hundred times). The principle of the counter is that the colloid moves in a suspending electrolyte (whose composition and pH is equal or very close to that of the solvent employed in the experiments) through a constricted electrical current path. An aperture is set in the wall of an insulated vessel, and direct current is applied across a pair of electrodes, one situated inside the insulated vessel, the other outside in the suspension. The passage of each ''visible'' colloid

causes an increase in resistance across the electrodes. The corresponding voltage pulse is proportional to the volume of matter and is amplified for display on an oscilloscope and for feeding a pulse height discriminator and a set of 16 (Model TA II) or 254 channels (Model Multisizer II).

For monodisperse spherical particles, the counter provides the particle diameter directly, and such systems are used to calibrate the apparatus. For polydisperse spherical particles, the counter directly provides the volume (or mass) frequency curve and the usual average values. For grains of non-spherical shapes, the counter provides the diameter distribution of spheres of volume equal to that of the grains. For aggregates, the value of the diameter determined by the counter corresponds to an equivalent spherical diameter, as if all the spheres or grains belonging to the aggregate passing through the aperture were coalesced in one spherical particle. Eventually, for aggregating systems, the counter provides the mass frequency curves. For aggregates of diameter d_n composed of single particles of diameter d_1 the mass n is derived using the relationship [104]

$$n = \left(\frac{d_n}{d_1}\right)^3 \tag{A1}$$

To determine the characteristics of polydisperse colloidal systems, the experimental value of the average concentration for each channel i was compared to the concentration $V(i)$ calculated by

$$V(i) = \frac{\sum_{d_n \in i} \exp[-h^2(d_h - d_n)^2/d_n]}{\sum_{d_n} \exp[-h^2(d_h - d_n)^2/d_n]} \tag{A2}$$

where h and d_h are fitting parameters. h determines the width of the size distribution and d_h is the volume average harmonic diameter of the aggregates. The concentration $c(n, t)$ of the aggregates containing n elementary particles at time t was obtained by assuming the existence of a continuous size distribution and by subdividing the differential curve $V(i)$ into $v(i)$ intervals, the width of each interval representing the increase in diameter of the collapsed equivalent sphere resulting from the addition of one latex particle to the previous aggregate. This procedure made it possible to transform the crude histogram given by the counter to the corresponding mass distribution curve $c(n, t)$ vs. n.

When the experimental histogram could not be fitted assuming single (dispersed) particles and a unique population of aggregates, more populations of colloidal particles were assumed to coexist and a three (or multi)-modal fit could be employed as follows:

$$V(i) = \alpha V(i, h_1, d_{h,1}) + \beta V(i, h_2, d_{h,2}) + \gamma V(i, h_3, d_{h,3}) \tag{A3}$$

where α, β, and γ define the relative proportion of each population. For

example, Eq. A3 provided an adequate fit to all experimental histograms obtained for hydrated colloids (Sec. III.B). Eq. A3 is in fact analogous to replicas of the log-normal distribution, which was concomitantly employed to obtain a preliminary estimation of the number of populations. Thus the average characteristics of the suspension were determined by deriving the parameters α, β, γ, h_1, h_2, h_3, $d_{h,1}$, $d_{h,2}$, and $d_{h,3}$ from the histogram, where α, h_1, and $d_{h,1}$ were attributed to the smallest population including dispersed colloidal particles and aggregates of very low mass. The number $N(t)$ and weight $S(t)$ average masses of each population can be calculated according to Eq. 3 using the corresponding fitting parameters h and d_h while the average masses $N(t)$ and $S(t)$ of the populations were derived using all fitting parameters including α, β, and γ.

Eventually, the average masses $N(t)$ and $S(t)$ depend on the mass value affected to each aggregate constituent. For monosized latex particles the mass 1 is attributed to single particles. When, as for oxides and clays, the original colloid is polydisperse in mass and size, the mass 1 is attributed either to particles of diameter d_1 of the smallest constituent (as for aluminum oxide) or to particles characterized by the average diameter d_n given by the counter (as for the kaolinite clay). This choice only affects the absolute values of $S(t)$ or $N(t)$ but does not modify the exponents of the power laws used to express fragmentation and breakup rates.

ACKNOWLEDGMENTS

This research was supported by the following companies: Institut Français du Pétrole, Lafarge-Coppée, Péchiney, Rhône Poulenc, and Total, and by the CNRS-PIRSEM under the Project PR ''Suspensions colloïdales concentrées.'' The author is particularly indebted to S. Stoll, L. Ouali, E. Ringenbach, and F. Elfarissi, who have helped to improve his understanding of these complex fragmentation phenomena.

REFERENCES

1. Emerson WW. The determination of the stability of soil crumbs. J Soil Sci 1954; 5:235–250.
2. van Holphen H. An Introduction to Clay Colloid Chemistry. 2d ed. New York: John Wiley, 1963.
3. Tisdall JM, Oades JM. Organic matter and water-stable aggregates in soils. J Soil Sci 1982; 33:141–163.
4. Edwards AP, Bremner JM. Microaggregates in soils. J Soil Sci 1967; 18:64–73.
5. Theng BKG. Formation and Properties of Clay–Polymer Complexes. Amsterdam: Elsevier, 1979.

6. Chaney K, Swift RS. The influence of organic matter on aggregate stability in some British soils. J Soil Sci 1984; 35:223–230.
7. Chaney K, Swift RS. Studies on aggregate stability. II. The effect of humic substances on the stability of reformed soil aggregates. J Soil Sci 1986; 37: 337–343.
8. Brady NC. The Nature and Properties of Soils. New York: Macmillan, 1990.
9. Pierzynski GM, Sims JT, Vance GF. Soils and Environmental Quality. Boca Raton: Lewis, 1994.
10. Dexter AR. Physical properties of tilled soils. Soil Tillage Res 1997; 43:41–63.
11. Le Bissonnais Y, Arrouays D. Aggregate stability and assessment of soil crustability and erodibility: II. Application to humic loamy soils with various organic carbon contents. Eur J Soil Sci 1997; 48:39–48.
12. Pefferkorn E. Structure and stability of natural organic matter/soil complexes and related synthetic and mixed analogues. Adv Colloid Interface Sci 1997; 73:127–200.
13. Buffle J, van Leeuwen HP. Environmental Particles. IUPAC Series in Environmental Analytical Chemistry. Chelsea: Lewis, MI, 1992.
14. Stumm W. Aquatic Surface Chemistry. New York: Wiley Interscience, 1992.
15. Stumm W. Aquatic colloids as chemical reactants: surface structure and reactivity. Colloids Surfaces A: 1993; 73:1–18.
16. Filella M, Buffle J. Factors controlling the stability of submicron colloids in natural waters. Colloids Surfaces A: 1993; 73:255–273.
17. Tiller CL, O'Melia CR. Natural organic matter and colloidal stability: models and measurements. Colloids Surfaces A: 1993; 73:89–102.
18. Wilkinson KJ, Nègre JC, Buffle J. Coagulation of colloidal material in surface waters: the role of natural organic matter. J Contamin Hydrol 1997; 26:229–243.
19. Dennett KE, Sturm TW, Amirtharajah A, Mahmood T. Effect of adsorbed natural organic matter on the erosion of kaolinite sediments. Water Envir Res 1998; 70:268–275.
20. Buffle J, Wilkinson K, Stoll S, Filella M, Zhang J. A generalized description of aquatic colloidal interactions: the 3-d colloidal component approach. Env Sci Techn (in press).
21. Wilson WS. Advances in Soil Organic Matter Research: The Impact on Agriculture and the Environment. Cambridge: Royal Society of Chemistry, 1991.
22. Lentz RD, Shainberg I, Sojka RE, Carter DL. Preventing irrigation furrow erosion with small application of polymers. Soil Sci Soc Am J 1992; 56: 1926–1932.
23. Ekwue EI, Stone RJ. Organic matter effects on the strength properties of compacted agricultural soils. Trans ASAE 1995; 38:357–365.
24. Lentz RD, Sojka RE. Field results using polyacrylamide to manage furrow erosion and infiltration. Soil Sci 1994; 158:274–281.
25. Trout TJ, Sojka RE, Lentz RD. Polyacrylamide effect on furrow erosion and infiltration. Trans ASAE 1995; 38:761–765.

26. Lehrsch GA, Jolley PM. Temporal changes in wet aggregate stability. Trans ASAE 1995; 35:493–498.
27. Sojka RE, Lentz RD. Reducing furrow irrigation erosion with polyacrylamide (pam). J Prod Agric 1997; 10:47–52.
28. Collet-Cassart D, Poncelet S, de Nayer P. Immunoturbidimetric assay of beta 2 microglobulin using latex particles immicroplates. J Immunol Meth 1991; 142:183–185.
29. Garcia A, Roson B, Perez JL, Verdaguer R, Dorca J, Carratala J, Casanova A, Manresa F, Gudiol F. Usefulness of PCR and antigen latex agglutination test with samples obtained by transthoracic needle aspiration for diagnosis of pneumococcal pneumonia. J Clin Microbiol 1999; 37:709–714.
30. Boelaert M, Lynen L, Desjeux P, Van der Stuyft P. Cost-effectiveness of competing diagnostic-therapeutic strategies for visceral leishmaniasis. Bull World Health Organ 1999; 77:667–674.
31. Okibo M, Yamamoto Y, Uno M, Kamei S, Matsumoto T. Immunoactivity of polymer microspheres with their hydrophilic/hydrophobic heterogeneous surface sensitized with an antibody. Coll Polym Sci 1987; 265:1061–1068.
32. Wolf SF, Haines L, Fisch J, Kremsky JN, Dougherty JP, Jacobs K. Rapid hybridization kinetics of DNA attached to submicron latex particles. Nucleic Acids Res 1987; 15:2911–2924.
33. Arshady R. Microspheres for biomedical applications: preparation of reactive and labelled microspheres. Biomaterials 1993; 15:5–15.
34. Ouali L, Pefferkorn E, Elaissari A, Pichot C, Mandrand B. Heterocoagulation of sensitized latexes in the presence of HCG protein: the pregnancy test. J Colloid Interface Sci 1995; 171:276–282.
35. Pichot C, Delair T, Elaissari A. Polymer colloids for biomedical and pharmaceutical applications. In: Asua JM, ed. Polymer Dispersions: Principles and Applications. NATO ASI Series E. Dordrecht: Kluwer, 1997:515–539.
36. Derjaguin BV, Landau LD. Theory of the stability of strongly charged lyophobic sols and the adhesion of strongly charged particles in solutions of electrolytes. Acta Physicochim URSS 1941; 14:633–662.
37. Verwey EJW, Overbeck JThG. Theory of the Stability of Lyophobic Colloids. Amsterdam: Elsevier, 1948.
38. Fuchs N. Über die Stabilität und Aufladung der Aerosole. Z Phys 1934; 89: 736.
39. Israelachvili JN. Intermolecular and Surface Forces. 2d ed. New York: Academic Press, 1991.
40. Israelachvili JN, Pashley RM. In: F. Franks, ed. Biophysics of Water. New York: John Wiley, 1982:183–194.
41. Horn RG, Smith DT, Haller W. Repulsive hydration forces between two silica surfaces. Chem Phys Lett 1989; 162:404–408.
42. Jeffrey GC, Ottewill RH. Reversible aggregation. Part I. Reversible flocculation monitored by turbidity measurements. Colloid Polym Sci 1998; 266: 173–179.
43. Jeffrey GC, Ottewill RH. Reversible aggregation. Part II. Kinetics of reversible aggregation. Colloid Polym Sci 1990; 268:179–189.

44. Pefferkorn E, Stoll S. Cluster fragmentation in electrolyte induced aggregation of latex. J Chem Phys 1990; 92:3112–3117.
45. Cornell RM, Goodwin JW, Ottewill RH. General Discussion. Faraday Discuss Chem Soc 1990; 90:182.
46. Family F, Landau DP, eds. Kinetics in Aggregation and Gelation. Amsterdam: North-Holland, 1984.
47. Stoll S, Pefferkorn E. Modes of spontaneous and provoked cluster fragmentation. I. During diffusion-limited aggregation. J Colloid Interface Sci 1992; 152:247–256.
48. Stoll S, Pefferkorn E. Modes of spontaneous and provoked cluster fragmentation. I. During reaction-limited aggregation. J Colloid Interface Sci 1992; 152:257–264.
49. Widmaier J, Pefferkorn E. Quantitative description of nonhomogeneous mass distribution in controlled aggregation and fragmentation of hydrated colloids. J Colloid Interface Sci 1998; 203:402–418.
50. Pefferkorn E, Widmaier J. Aggregation and fragmentation processes of lyophobic and hydrated colloids. Colloids Surfaces A 1998; 145:25–35.
51. Vigil RD, Ziff RM. On the stability of coagulation–fragmentation population balances. J Colloid Interface Sci 1989; 133:257–264.
52. Sorensen CM, Zhang HX, Taylor TW. Cluster-size evolution in a coagulation–fragmentation system. Phys Rev Lett 1987; 59:363–366.
53. Meakin P. The effects of random bond breaking on diffusion limited cluster–cluster aggregation. J Chem Phys 1985; 83:3645–3649.
54. Botet R, Jullien R. Diffusion-limited aggregation with disaggregation. Phys Rev Lett 1985; 55:1943–1946.
55. Kolb M. Reversible diffusion-limited cluster aggregation. J Phys A: Math Gen 1986; 19:L263–L268.
56. Ziff RM, McGrady ED. The kinetics of cluster fragmentation and depolymerisation. J Phys A 1985; 18:3027–3037.
57. McGrady ED, Ziff RM. ''Shattering'' transition in fragmentation. Phys Rev Lett 1987; 58:892–895.
58. Cheng Z, Redner S. Scaling theory of fragmentation. Phys Rev Lett 1988; 60:2450–2453.
59. Meakin P, Ernst MH. Scaling in aggregation with breakup simulations and mean-field theory. Phys Rev Lett 1988; 60:2503–2506.
60. Elminyawi IM, Gangopadhyay S, Sorensen CM. Numerical solutions to the Smoluchowski aggregation–fragmentation equation. J Colloid Interface Sci 1991; 144:315–323.
61. Zwift DL, Friedlander SK. The coagulation of hydrosols by Brownian motion and laminar shear flow. J Colloid Interface Sci 1964; 19:621–647.
62. Lushnikov AA. Evolution of coagulating systems. J Colloid Interface Sci 1973; 45:549–556.
63. von Smoluchowski M. Versuch einer Mathematischen Theorie der Koagulationskinetik Kolloide Lösungen. Z Phys Chem 1917; 92:129.
64. Jullien R. The application of fractals to colloidal aggregation. Croatica Chem Acta 1992; 65:215–235.

65. Ringenbach E. Stabilisation d'un oxyde soluble par un polyélectrolyte complexant les produits de dissolution. Thèse, Université Louis Pasteur, Strasbourg, 1994.
66. Tschapek M, Torres Sanchez RM. The stability of silica and quartz suspensions. J Colloid Interface Sci 1976; 54:460–461.
67. Elimelech M. Indirect evidence for hydration forces in the deposition of polystyrene latex colloids on glass surfaces. J Chem Soc Faraday Trans 1990; 86: 1623–1624.
68. Minami H, Inoue T. Dehydration of hydrated bilayer of dipalmitoylphosphatidylcholine caused by beryllium ion: evidence from a differential scanning calorimetry of bilayer phase transition. J Colloid Interface Sci 1998; 206: 338–341.
69. Toca-Herrera JL, Muller HJ, Pfohl T, Mohwald H. Influence of ethanol on the thickness and free energy of film formation of DMPC foam films. Colloids Surfaces A 1999; 152:357–365.
70. Ouali L, Pefferkorn E. Fragmentation of colloidal aggregates induced by polymer adsorption. J Colloid Interface Sci 1994; 168:315–322.
71. Ouali L, Pefferkorn E. Polymer induced stabilization of colloids. Mechanism and kinetics. J Colloid Interface Sci 1993; 161:237–246.
72. Pefferkorn E, Elaissari A. Adsorption–desorption processes in charged polymer/colloid systems; structural relaxation of adsorbed macromolecules. J Colloid Interface Sci 1990; 138:187–194.
73. Varoqui R, Tran Q, Pefferkorn E. Polycation–polyanion complexes in the linear diblock copolymer of poly(styrene sulfonate):poly(2-vinylpyridinium) salt. Macromolecules 1979; 12:831–835.
74. Graessley WW. Polymer chain dimensions and the dependence of viscoelastic properties on concentration, molecular weight and solvent power. Polymer 1980; 21:258–262.
75. Pefferkorn E. The role of polyelectrolytes in the stabilisation and destabilisation of colloids. Adv Colloid Interface Sci 1995; 56:33–104.
76. Napper DH. Polymeric Stabilization of Colloidal Dispersions. New York: Academic Press, 1983.
77. Elaissari A, Pefferkorn E. Polyelectrolyte induced aggregation of latex particles: influence of the structural relaxation of adsorbed macromolecules on the colloid aggregation mode. J Colloid Interface Sci 1991; 141:522–533.
78. de Gennes PG. Mobilité d'une chaîne adsorbée. CR Acad Sci (Paris) II 1988; 306:739–741.
79. Ringenbach E, Chauveteau G, Pefferkorn E. Adsorption of polyelectrolytes on soluble oxides induced by polyion complexation with dissolution species. J Colloid Interface Sci 1993; 161:223–231.
80. Pefferkorn E. Polyacrylamide at solid/liquid interfaces. J Colloid Interface Sci 1999; 213:197–220.
81. Ringenbach E, Chauveteau G, Pefferkorn E. Polyelectrolyte deposition induced by ion complexation: structural and electrochemical characteristics of the polymeric interface. J Colloid Interface Sci 1995; 171:218–223.

82. Katchalsky A, Spitnik P. Potentiometric titrations of polymethacrylic acid. J Polym Sci 1947; 2:432–446.
83. Mandel M, Leyte JC. The potentiometric behavior and the interaction with Cu(II) ion of polymethacrylic acid in aqueous solutions. J Polym Sci 1962; 56:S23–S25.
84. Ringenbach E, Chauveteau G, Pefferkorn E. Aggregation/fragmentation of colloidal alumina. I. Role of the adsorbed polyelectrolyte. J Colloid Interface Sci 1995; 172:203–207.
85. Ringenbach E, Chauveteau G, Pefferkorn E. Aggregation/fragmentation of colloidal alumina II. Scaling laws of fragmentation. J Colloid Interface Sci 1995; 172:208–213.
86. Ringenbach E, Chauveteau G, Pefferkorn E. Effect of soluble aluminum ions on polyelectrolyte–alumina interaction. Kinetics of polymer adsorption and colloid stabilization. Colloids Surfaces A 1995; 99:161–173.
87. Varoqui R, Pefferkorn E. Selective liquid–liquid ion-exchange and structural properties of amphiphilic polyelectrolytes in organic media. J Phys Chem 1975; 79:169–180.
88. Elfarissi F, Nabzar L, Ringenbach E, Pefferkorn E. Polyelectrolytic nature of humic substances—aluminium ion complexes. Interfacial characteristics and effects on colloid stability. Colloids Surfaces A 1998; 131:281–294.
89. Elfarissi F, Pefferkorn E. Kaolinite/humic acid interaction in the presence of aluminium ion. Colloids Surfaces A (in press).
90. Elfarissi F, Pefferkorn E. Fragmentation of kaolinite aggregates induced by ion-exchange reactions within adsorbed humic acid layers. J Colloid Interface Sci (in press).
91. Lietard O. Contribution à l'étude des propriétés physicochimiques, cristallographiques et morphologiques des kaolins. Thèse, Institut National Polytechnique de Lorraine, Nancy, 1977.
92. Nabzar L, Pefferkorn E, Varoqui R. Stability of polymer–clay suspensions. The polyacrylamide–sodium kaolinite system. Colloids Surfaces 1988; 30: 345–353.
93. Ochs MP, Cosovic B, Stumm W. Coordinative and hydrophobic interaction of humic substances with hydrophilic Al2O3 and hydrophobic mercury surfaces. Geochim Cosmochim Acta 1994; 58:639–650.
94. Joanny JF. Adsorption of a polyampholyte chain. J Phys II 1994; 4:1281–1288.
95. Dobrynin AV, Rubinstein M, Joanny JF. Adsorption of a polyampholyte chain on a charged surface. Macromolecules 1997; 30:4332–4341.
96. Vermeer AWP, van Riemsdijk WH, Koopal LK. Adsorption of humic acid to mineral particles. 1. Specific and electrostatic interactions. Langmuir 1998; 14:2810–2819.
97. Neyret S, Ouali L, Candau F, Pefferkorn E. Adsorption of polyampholytes on polystyrene latex: effect on colloid stability. J Colloid Interface Sci 1995; 176:86–94.
98. Hsu JP, Liu BT. Critical coagulation concentration of a colloidal suspension at high particle concentration. J Phys Chem B 1998; 102:334–337.

99. Le Berre F, Chauveteau G, Pefferkorn E. Perikinetic and orthokinetic aggregation/fragmentation of hairy colloids. J Colloid Interface Sci 1997; 189:312–321.
100. Molina-Bolivar JA, Galisteo-Gonzales F, Hidalgo-Alvarez R. Anomalous colloidal stability of latex–protein systems. J Colloid Interface Sci 1998; 206: 518–526.
101. Beysens D, Campi X, Pefferkorn E, eds. Fragmentation Phenomena. Singapore: World Scientific, 1995.
102. Walker PH, Hutka J. Division of Soils. Technical Paper N° 1, Vol 3, 1971.
103. Matthews BA, Rhodes CT. Studies of the coagulation kinetics of mixed suspensions. J Colloid Interface Sci 1970; 32:332–338.
104. Matthews BA, Rhodes CT. Some observations on the use of the Coulter counter model B in coagulation studies. J Colloid Interface Sci 1970; 32:339–348.
105. Ives KJ. Experimental methods. In: Ives KJ, ed. The Scientific Basis of Flocculation. Alphen aan den Rijn: Sijthoff and Noordhoff, 1978:165–191.

16

Interactions Between Polyelectrolytes and Kaolin

JOACHIM KÖTZ and SABINE KOSMELLA University of Potsdam, Potsdam, Germany

I. INTRODUCTION

Clay minerals have been used for a long time in various fields of application (e.g., paper coating) because of their platelike crystal habit in colloidal dimensions and the ability to bond to one another. These phenomena of structure formation are predominantly controlled by Coulombic forces between the negative charges on the basal planes and the positive charges around the edges.

Due to the presence of both negative and positive charges in the platelike crystal interactions with polyelectrolytes, polyanions as well as polycations, via electrostatic forces, can be utilized to control the colloidal stability (or instability) as well as the rheological behavior of the whole system.

For a better understanding of the role of Coulombic forces in such multicomponent systems, electrokinetic measurements are very useful.

Starting with the basic concept of the electrokinetic potential of colloidal particles, the so-called zeta potential, i.e., the electrokinetic potential at the shear plane, the most important well-established methods of zeta potential determination are discussed separately. Taking into account the peculiarities of kaolin particles, the relevance of these methods for characterizing kaolin particles in the absence and the presence of polyelectrolytes are outlined here. Thereby a ''mixed stabilization'' by oppositely charged polyelectrolytes is discussed in more detail.

Finally, the different methods of zeta potential determination are discussed with regard to their relevance to characterize polyelectrolyte–kaolin interactions.

II. THE ZETA POTENTIAL

As a model, a colloidal system should be considered as a large number of individual particles dispersed in some continuous (usually water) medium.

Since the particles have colloidal dimensions, they will be colliding with one another due to the Brownian motion. The system can remain as individual particles only if some mechanism prevents the collisions from resulting in a permanent aggregation. If the particles have the same charge (either positive or negative) they will repel one another. This mechanism of colloidal stabilization is referred to as electrostatic stabilization.

Negative charges can be ''introduced'' by the dissociation of proton-releasing groups at the surface of the individual particles. The negatively charged surface of a particle is surrounded by a ''cloud'' of its counterions, the so-called ''diffuse layer,'' which compensates for the negative surface charges, and the particle with its diffuse layer seems to be neutral.

The earliest theoretical studies of the behavior of an electrified interface were made by Helmholtz (1879). He discussed the adsorption of ions at a fixed double layer and he believed that this double layer formed the equivalent of a parallel-plate condenser. But this double layer model is an inadequate description of particles in electrolyte-containing systems.

Because of the compensation of the surface charge by the positively charged counterions, an exponential potential drop in the diffuse layer was discussed by Gouy (1910, 1917) and Chapman (1913). The potential at the particle surface is the Nernst potential ψ_0; the extension of the diffuse layer is equal to $1/\kappa$ (Debye–Hückel parameter).

Real dispersed systems are usually more complex, and the space required from the charges has to be taken into account.

Stern combines in his model (1924) the ideas of a diffuse layer and a fixed double layer in the following way:

At a surface of a dispersed negatively charged particle the adsorption of ions occurs at the inner and outer Helmholtz plane, whereas the inner Helmholtz plane (IHP) may consist of

Fixed
Dehydrated negatively charged ions

and the outer Helmholtz plane (OHP) of

Fixed
Hydrated positively charged ions (Figure 1)

Both the inner and outer Helmholtz plane are the Stern layer or Stern double layer. The diffuse layer consists of

Movable
Hydrated positively charged counterions and negatively charged ions (coions)

The total potential drop is between the surface of the solid and the movable liquid and the electrokinetic or zeta potential is the potential measured at

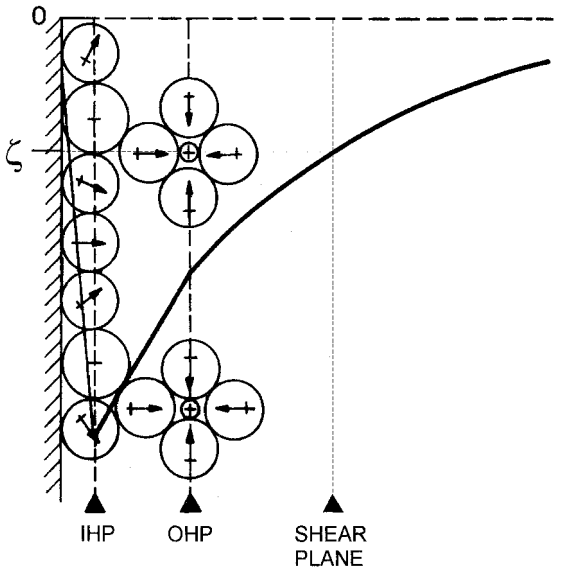

FIG. 1 Model of an electrical double layer including an exemplary shear plane and the belonging zeta potential. (From Ref. 1.)

the shear plane of the diffuse layer (compare Figure 1). The correct determination of the zeta potential requires an accurate measurement at the outer Helmholtz plane, which can hardly be realized.

This is why the determination of the zeta potential by different processes and a comparison of the values received may pose great problems.

There are a number of different processes by which the zeta potential can be determined. They are referred to collectively as the electrokinetic effects and occur whenever one phase is made to move with respect to the other and there is a charge at the boundary between the two phases [2] (Table 1).

TABLE 1 Routes to Zeta Potential Determination

Method	Induced by	Dispersed phase	Liquid phase
Electrophoresis	Electric field	In movement	Stationary
Electro-osmosis	Electric field	Stationary	In movement
Streaming potential	Mechanical forces	Stationary	In movement
Sedimentation potential	Mechanical forces	In movement	Stationary

III. METHODS FOR DETERMINING THE ZETA POTENTIAL

A. Electrophoresis and Electro-osmosis

Electrophoresis is the measurement of the movement of colloidal particles when they are placed in an electric field. The application of an external voltage causes the charged particles to move toward one of the electrodes: a negative particle moves to the anode and a positive one to the kathode.

In the case of microelectrophoresis, the migration of the particles is determined optically. The velocity is measured by timing individual particles between marks on a grid placed in the microscope eyepiece. The sample has to be highly diluted, so that individual particles can be observed. Progress in microscopy and the combination with photon correlation spectroscopy opened the possibility for determining particles in the range between 3 nm and 5 μm [3].

From the point of view of the electrophoretic cell, microelectrophoresis is a capillary electrophoresis. Experimenting in capillaries is complicated in that a streaming potential (comp. B) occurs, and the applied voltage causes the liquid in the cell to move. This movement, called electro-osmosis, occurs because the glass walls of the cell are negatively charged. There is only one particular point between the cell wall and the center of the cell, the stationary layer at a distinct distance x ($x = r/\sqrt{2}$), where the particles move with their true velocity, which is due solely to their own charge. To get a true result, the microscope must be focused in this layer and the particles measured must be in focus.

As an optical detection system, electrophoretic light scattering has been frequently used in recent years [4]. In this case, the collected signal of the particles' movement shifted to higher or lower frequencies depending on their charge. The frequencies are then converted to electrophoretic mobilities, velocities, and finally zeta potentials.

The velocity (v_0) obtained equals the product of electrophoretic mobility (μ_E) and the applied electrical field (E_0):

$$v_0 = \mu_E E_0 \tag{1}$$

For calculating the zeta potential the following theoretical assumptions are necessary: In the modified Stokes equation, the electrical field is the driving force for the movement of the particles:

$$\frac{v_0}{E_0} = \mu_E = \frac{Q}{6\pi a \eta} \tag{2}$$

where Q is the particle charge, a the particle radius, and η the viscosity.

The "thickness" of the double layer is determined by the Debye–Hückel-parameter $1/\kappa$:

$$\kappa = \left[\frac{4\pi e^2 \sum n_i z_i^2}{\varepsilon_0 \varepsilon kT}\right]^{1/2} \tag{3}$$

where e is the elementary charge, z_i the number of charge of the ion, and ε the permittivity. The dimensionless product κa describes the ratio of the particle radius to the "thickness" of the double layer.

Assuming a low charge, Q may be described using the Henry equation:

$$\mu_E = \left(\frac{2\varepsilon\zeta}{3\eta}\right) f(\kappa a) \tag{4}$$

where ζ is the zeta potential. For low κa the Henry function approaches the value 1; for large κa it approaches 1.5. These values correspond to the borderline cases known as Hückel- and Smoluchowski equation. However, the Smoluchowski approximation is that which is usually used for the calculation of zeta potentials of dispersed colloidal systems containing spherical particles.

B. Streaming Potential

When a liquid is forced through a capillary, the charges in the mobile part of the double layer near the wall are carried toward one end. If the wall is negatively charged (glass capillary) then the mobile charge is positive and constitutes a streaming current, I_s, in the direction of the liquid flow. The accumulation downstream sets up an electrical field, which causes a flow back in the opposite direction. When this conduction current, I_c, is equal to the streaming current, a steady state is achieved. The resulting electrostatic potential difference between the ends of the capillary is called the streaming potential.

The streaming potential (E_s) must be measured as a function of the applied pressure. The relation between the streaming current and the zeta potential is derived using the Poiseuille equation, which describes the flow velocity of a liquid at a distance (r) from the axis of the capillary:

$$v(r) = \frac{\Delta p(R^2 - r^2)}{4\eta I} \tag{5}$$

where R is the radius of the capillary. The streaming current can be obtained through an integration by parts under consideration that the double layer is assumed to be confined to a thin region near the wall of the capillary, so that

$$I_s = \frac{\varepsilon \xi \pi R^2 \Delta p}{I \eta} \tag{6}$$

The streaming potential, E_s, generated by this current causes a conduction current in the reverse direction given by

$$I_c = \frac{\pi R^2 E_s \lambda_0}{I} \tag{7}$$

When a steady state has been reached, the zeta potential can be expressed by

$$\frac{E_s}{p} = \frac{\varepsilon \xi}{\eta \lambda_0} \tag{8}$$

where λ_0 is the conductivity. For solving this equation one needs to know the surface conduction, which is often unknown. In that case one may operate with the measured value of the resistance of the capillary and the resistance at high salt concentrations, when surface conduction is negligible.

The streaming potential also may be determined by using a so-called particle charge detector, where the measuring unit consists of a cylindrical vessel made of synthetic material like teflon. The liquid movement is induced by a piston, which is moved up and down, and in dependence on its direction the mobile charges will be shifted. Electrodes at the top and near the bottom of the cylinder detect the induced streaming potential.

The signal determined in arbitrary units is a complex dimension, which cannot be directly quantified to the zeta potential. Its sign is determined by the charge of the cell wall. It summarizes contributions from the cell wall, the piston, and the whole colloidal material. Thus for a quantitative calculation of the particles' surface charge density a polyelectrolyte titration has to be carried out. If one knows the specific surface, for zeta potentials <30 mV it can be calculated according to

$$\xi \approx \frac{\varepsilon_0 \varepsilon \kappa}{4 \pi \sigma} \tag{9}$$

Usually one does not know what the specific surface of the dispersed phase is. Thus this is not an exact method for determining the zeta potential.

C. Sedimentation Potential

When charged particles settle under gravity or in a centrifuge they will set up a measurable potential difference, called the sedimentation potential. The downward movement of the positive particles causes a slight distortion of the diffuse layer, as the negative ions try to keep up.

The sedimenting particles constitute a current in one direction, while the ion flow is a current in the opposite direction. The two currents can be expressed as

$$nv_zQ = E_z\lambda_0 \tag{10}$$

where n is the number of particles per unit volume, v_z is the settling velocity, and E_z is the developed electric field. The estimation of the zeta potential requires a measurement of the potential developed between the two points at different heights in a column of sedimenting monodisperse particles of known particle concentration using the Smoluchowski equation:

$$E_z = [(4\pi\varepsilon_0)D\xi a^3(d - d_1)gn]/3\eta\lambda_0 \tag{11}$$

where d is the density of the particles and d_1 the density of the medium. This method has been used only rarely, because most workers have found it unreliable for general use. But in recent years measurements with modern high-impedance millivoltmeters present no problem. This fact opens the possibility of reincarnating this method.

D. Acoustophoresis

When an alternating voltage is applied to a colloid, the particles move back and forth with a velocity that depends on their size and zeta potential and on the frequency of the applied field. As they move, the particles generate sound waves. This phenomenon is called the electroacoustic effect, which can be measured and what was named electrokinetic sonic amplitude (ESA) [5].

O'Brien [6] developed a theory for determining the zeta potential and particle size at the same time using the electroacoustic effect.

The Smoluchowski formula, which is used in the AcoustoSizer from the measured dynamic mobility, is valid for a disperse suspension of spherical particles according to Eq. 1.

$$\mu_D = \frac{2\varepsilon\xi}{3\eta} G \frac{\omega a^2}{\nu} [1 + f(\lambda, \omega')] \tag{12}$$

where G is the effect of inertial forces on the dynamic mobility and $(1 + f)$ describes a term of the dynamic mobility. If the system is not properly dispersed, the particles will form flocs with a more or less open structure, and O'Brien has shown that such a floc will have a dynamic mobility quite different from that of a solid particle. The great advantage of the technique is the application to concentrated suspensions; the technique is not applicable to diluted suspensions.

IV. CHARACTERIZATION OF UNMODIFIED KAOLIN PARTICLES BY ELECTROKINETIC METHODS

A. Anomalous Conductance

Surface conduction is the conductance of electric current along the surface of the particle. The standard theory assumes that all current occurs in the double layer outside the surface of shear where the zeta potential is measured. The ions closer to the particle surface (below the surface of shear) are assumed not to be able to produce a current.

Kaolin is known as a system in which these ions conduct an additional current. This effect is called *anomalous* surface conductance and affects both the determination of size and the zeta potential at low electrolyte concentrations (<0.001 M) [7].

The anomalous surface conduction was studied extensively by O'Brien and by Hunter, and they could show that the Stern layer conduction is about thirty times larger than the diffuse layer conduction at low salt concentration. This explains substantial discrepancies between the electrophoresis and the conductance estimates of zeta potential. For thin double-layer systems such as this, the zeta potential is usually calculated from the electrophoretic mobility using Smoluchowski's formula, which in O'Brien's case corresponds to a zeta potential of -50 mV [8]. Complex conductivity measurements result in $\zeta = -160$ mV.

Principally, zeta potential measurements with kaolin present no problems at salt concentration > 0.001 M. But electrokinetic studies of kaolin require that the surface of the clay be prepared in a manner that generates a reproducible surface. That means, substances in the material derived from the conditioning process had to be removed.

B. Determination of Surface Charge in Dependence on pH

In contrast to common colloidal particle suspensions, the determination of the point of zero charge is not possible in case of kaolin. The basal surfaces carry permanent negative charges, so that even at the lowest accessible pH ($\approx$2.5) the surface charge is still about -5 μC cm^{-3} [9]. The charges become more negative as the pH increases. For the determination of the surface charge a titration technique is therefore not practicable. Due to the heterogenity of the kaolinite surface there is a part of pH-dependent surface charges that can be determined by an acid–base potentiometric titration [10]. Blockhaus et al. [10] report titration results of kaolinite in 0.01, 0.1, and 1 M NaCl. From pH 4 to 9, two different pH regions can be discriminated that are associated with different surface ionization processes.

Shimabayashi et al. [11] showed for electrophoresis measurements (Laser Zee TM Model 501, Pen Kem) of aqueous kaolin suspensions the zeta potential as a function of pH (3.5–9) adjusted by a phosphate buffer solution. The zeta potential of the bare kaolin particle was negative over the pH investigated (−30 mV to −50 mV), where its absolute value slightly increased with pH but is asymptotic with the *x*-axis. This fact shows that its original surface has negative charges although both a positive edge double layer and a negative double layer on the flat surface contribute to its zeta potential. The density of negative charges on the surface on the average increases with pH due to the adsorption of OH^-. With a decreased phosphate buffer concentration the absolute values increase, whereas the shape of the curve is similar to higher buffer concentration. This is explained in terms of the effect of ionic strength. With an increase in ionic strength prepared by phosphate buffer, the thickness of the electric double layer around the kaolin particle decreases, followed by a decrease in the absolute value of the zeta potential.

Electrophoretic investigations (Zetasizer 4, Malvern) made in our group confirm these measurements. Over the pH range investigated (2.5–11) a zeta potential from ≈−20 mV to −40 mV for kaolin dispersion of 0.05 vol% was estimated. Somewhat higher absolute values (from ≈−30 mV to −50 mV) of the zeta potential but a similar shape of the curve were observed by means of the Acoustosizer. These measurements were carried out in a 0.005 molar aqueous salt (KCl) solution to maintain a minimal conductivity of 250 $\mu S\ cm^{-1}$ at a kaolin concentration of 2.5% by volume (Figure 2). Figure 3 shows the streaming potential of kaolin particles as a function of pH. Determining the streaming potential by using the particle charge detector (Mütek) one has to keep in mind that the resulting value is a complex dimension, which summarizes all charge effects in the system available and which is not to be treated as equivalent to the zeta potential.

Nevertheless, the shape of the curve is partly comparable with those curves shown in Figure 2. The streaming potential observed is negative over the pH range investigated, too, but its absolute value decreases with decreasing pH much steeper. When the pH becomes higher than 7.5, the absolute value is decreasing again and at pH 10 it is in the same region as for acid conditions. This means that an adsorption of OH^- ions on the edges of the kaolin platelets resulting in higher absolute values cannot be detected.

In the presence of low molecular salt (NaCl) the streaming potential in the range from pH 5 to 11 is less negative, which is attributed to a compressed double layer resulting in lower negative values. In spite of the differences obtained between electrophoretic, acoustophoretic, and streaming potential measurements, a study of surface charges of kaolin particles is

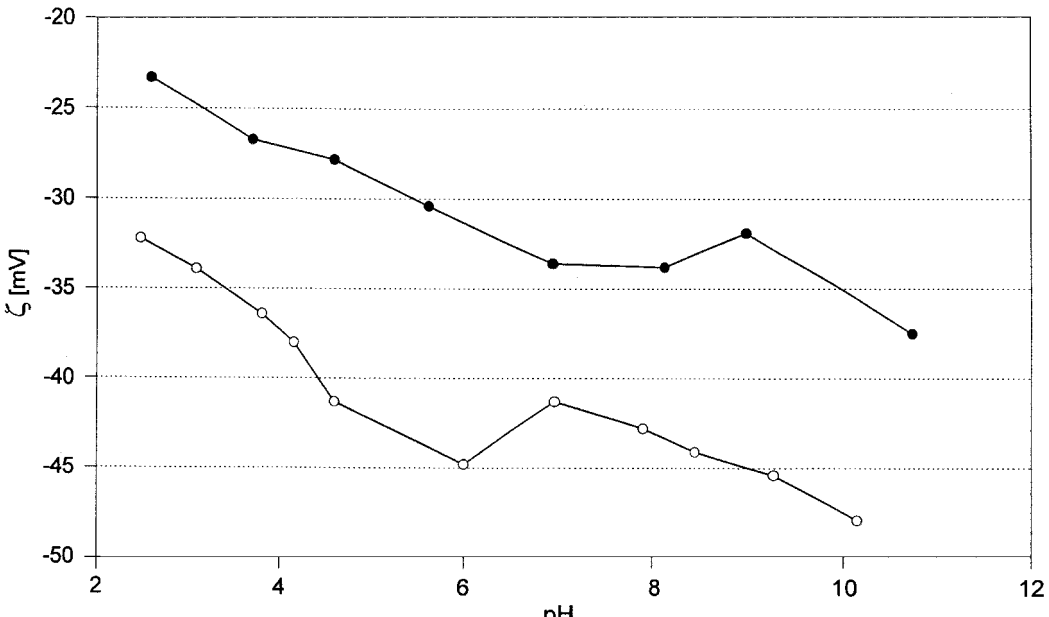

FIG. 2 pH dependence of the zeta potential of a commercial kaolin dispersion determined by means of capillary electrophoresis (●) and acoustophoresis (○).

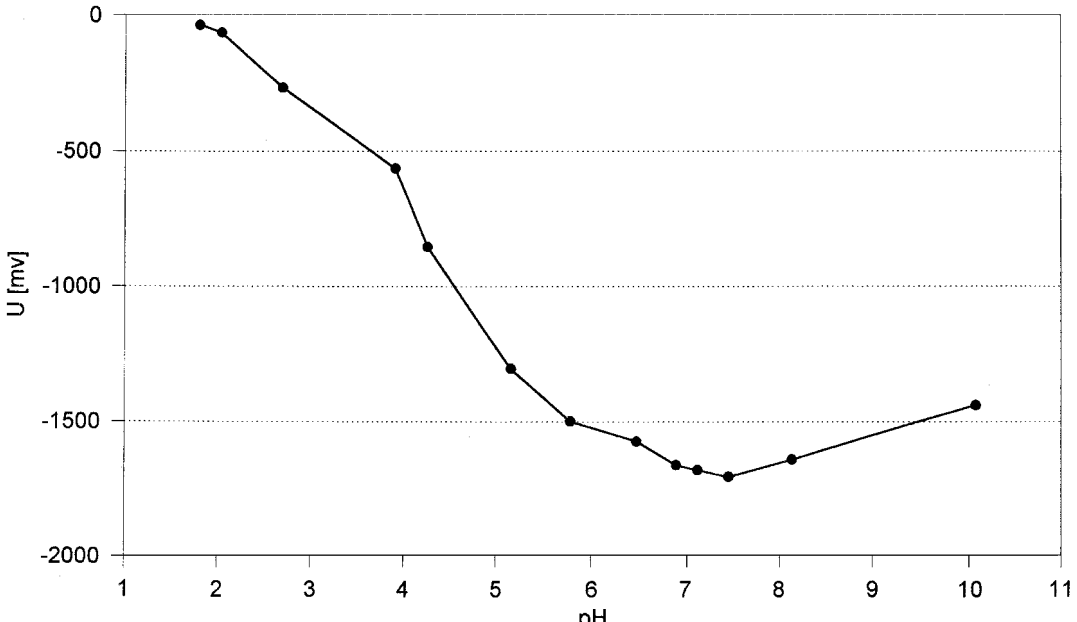

FIG. 3 pH dependence of the streaming potential of a commercial kaolin dispersion determined by means of a particle charge detector.

possible, and these three methods may give a reasonable picture for their pH dependence.

For the synthetic analog of kaolinite, illite, Pefferkorn [12] found the point of zero charge equal to 4.5, which corresponds to a pH domain where silica is only slightly ionized.

The faster increase of the zeta potential above pH 6.5, from −70 mV to −110 mV at pH 7.2, may be attributed to the supplementary electrical negative charges resulting from the dissociation of the hydrogen bonded silanol groups. This result was additionally supported by the determination of the dissociation constant of the Al-OH group from the acid–base titration curve.

The difference in chemical composition between kaolinite and illite is to be seen in the relatively greater degree of isomorphous replacement for illite. Furthermore, the positive charge deficiency is balanced by interlayer K^+ ions. These ions are not available for ion exchange, while those exposed on the surface can be exchanged for other ions [13].

V. CHARACTERIZATION OF POLYELECTROLYTE-MODIFIED KAOLIN PARTICLES BY ELECTROKINETIC METHODS

The adsorption of synthetic and natural charged polymers on kaolin and related synthetic models has been the subject of a very large number of investigations. The charge duality on the kaolin surface renders the question about the location of the adsorption sites more difficult. Equilibrium adsorption measurements [14] and electrokinetic investigations [15] support the hypothesis of the edge surface as the main adsorption site on the kaolin particles.

As mentioned above, kaolin suspensions are also often used as model dispersed systems for studying flocculation processes to solve important problems in water treatment such as the removal of dispersed impurities. Among the synthetic flocculants, polyacrylamide ones are the most widely used. These flocculants are rather easily available, cheap, and economic.

Bulidorova and Myagcenkov used kaolin with a mean particle radius of $r = 9.07 \times 10^{-6}$ m as a model disperse system and high-molecular-weight positively and negatively charged copolymers of acrylamide ($M_\eta \approx 10^6$ g/mol) as flocculants [16]. Studies were performed by electrophoretic measurements of the zeta potential by means of a Parmoquant (automatic measuring microscope, Karl Zeiss Jena) at 20°C with 0.01 N KCl solution as the auxiliary liquid. The experiments indicate that a reversal of the sign of charge on the particles becomes possible if cationic charged acrylamide copolymers adsorb onto the kaolin surface and induce a flocculation process. In that case a final zeta potential of +50 mV may be reached. The addition

of anionic polyelectrolyte results in a decrease of the zeta potential (from −50 to −60 mV) due to an adsorption on the positively charged edges. An interesting phenomenon is observed when new portions of the polyanion and polycation are alternately added to the system; the multiple reversal of the particle charge is obtained at a certain concentration between polymers. The authors discuss this flocculation mechanism with regard to a combined addition of anionic and cationic flocculants [16].

The influence of charged acrylamide graft copolymers on the flocculation process of 5% (w/w) kaolin suspensions were investigated by Serita and Murai [17]. The flocculation ability of different copolymers was linked to their structure by measuring the sedimentation potential. An iep of kaolin particles was observed for the concentration of approximately 20 ppm polymer, and they could additionally show that copolymers were more effective for flocculation than typical commercial flocculants.

Nabzar et al. [18] showed in flocculation investigations with noncharged polyacrylamide that by using anisomeric particles as kaolin several regions of stabilization and destabilization (flocculation) may come one immediately after another in dependence on the polymer concentration added. In this case a stabilization of the kaolin particles is reached by steric stabilization, whereas flocculation occurs due to a bridging mechanism.

Flocculation experiments in the presence of anionic polyelectrolytes (polyacrylate-PAA) and Ca^{2+} ions were carried out by Jasmund and Lagaly [19]. The aggregation of kaolin particles is determined by the interaction between the polyacrylate and Ca^{2+} and occurs at a certain concentration ratio of c_{Ca}^{2+}/c_{PAA}. Polyanion molecules that were not covered with Ca^{2+} ions were only adsorbed at the edges, whereas polymer molecules covered with Ca^{2+} could adsorb at the basal faces of the kaolin platelets and can cause a face-to-face association.

The adsorption behavior of charged polymers at kaolin is governed by forces that can be roughly divided into long-range ionic interactions of an electrostatic nature and short-range ones of a more chemical nature due to a covalent modified surface. The ionic interactions depend on the ampholytic properties of both kaolin and polymer which are controlled by a pH-dependent surface ionization variable screened by the effect of the ionic strength. The influence of these parameters can be widely investigated in the study of adsorption isotherms [20]. Blockhaus et al. [10] obtained adsorption isotherms as a function of clay mineral structures, pH, and ionic strength in the presence of acrylic-maleic acid copolymers (PAA-PMLA) by a direct polyelectrolyte phototitration and by an improved potentiometric colloidal titration method. In the case of the adsorption on kaolinite, the pH-dependent interaction at relatively low ionic strength is discussed in terms of electrostatic contributions as well as with regard to a ligand exchange mechanism.

Increasing the ionic strength also enhances the adsorption by a screening of the charges in the adsorbed layer. This is especially discussed when the charges of the copolymer and the surface are of the same sign.

Classical adsorption isotherms were also determined by Slepetys and Morgan [21]. The surface interactions between the kaolin surface and a high-molecular-weight cationic polymer, poly(diallyldimethylammonium chloride) (PDADMAC) were studied by acoustophoretic titration (Pen Kem System 7000, Acoustophoretic Analyzer) in which mobility, pH, conductivity, and temperature were monitored simultaneously. The results indicate that with increasing addition of polymer, the cationic polyelectrolyte is able to balance the negative surface charge of kaolin. At higher doses, charge reversal is effected, and the kaolin becomes positively charged. That means, with continued adsorption, surface hydrogen ions are displaced by adsorbing polymer, pH decreases, and surface charge is neutralized or compensated. After passing the isoelectric point, the mobility (related to the zeta potential) reaches a plateau value. From polymer adsorption measurements the authors calculated the surface coverage at which flocculation occurs (10–30% of the possible surface coverage).

The adsorption of natural polyelectrolytes (serum albumin-BSA) on kaolin suspensions as well as the complex formation with Na-chondroitin-6-sulfate (Na_2Chs) was studied by Shimabayashi et al. by means of a microscope electrophoretic apparatus [11]. The iep of kaolin after covering with BSA was determined to be lower than that of BSA itself; the zeta potential was positive at pH lower than 4.2. When the pH became higher than the iep, the zeta potential was reversed to negative values and decreased with pH.

In the case of coexistence of BSA with Na_2Chs, the zeta potential changed stepwise in phosphate buffer solutions from -40 to -60 mV without reaching the iep. The results were explained as due to a complex formation on the kaolin surface via concurrent and/or cooperative adsorption of two polymers.

Starch-induced flocculation of 1% (w/w) kaolin suspensions and the adsorption of NaCMC were investigated by Järnström et al., where the kaolin was partly pretreated with sodium polyacrylate of low molecular weight (PAA) [22]. In all flocculation experiments the kaolin suspension as well as the starch solution were adjusted to pH 7.5. The flocculation behavior of the PAA-treated suspension indicated that depletion flocculation is a very likely flocculation mechanism. When a hydrophobically modified starch was added, no flocculation occurred, and no adsorption of the modified starch on the kaolin particles could be detected. It is reasonable that water is a less good solvent for the hydrophobically modified starch and thus may cause the impossibility of depletion flocculation. On the other hand, a dispersing

effect was obtained when a low-molecular-weight NaCMC was added to a PAA-free kaolin suspension.

Coating processes may also be followed by measuring the electrokinetic potential. M. Chamoumi et al. report about coating of a kaolin–polypropylene homopolymer system in a latex that leads to an improved adhesion between the kaolin and the filler [23]. The coating conditions were evaluated by measuring the electrokinetic potential. The results of mechanical testing show that the coating of kaolin leads to an increase in impact strength of 50%.

Stabilization and destabilization studies on kaolin suspensions were performed in our group by means of various electrokinetic methods to follow the adsorption process of differently charged polyelectrolytes. The polyelectrolytes used were polycations such as the branched free polybase polyethyleneimine (PEI) and the linear PDADMAC, and Na-polyacrylate as polyanion, whereas the polycations are of different charge density. In Figures 4–7 results of electrophoretic light scattering experiments (Zetasizer 4, Malvern) of 0.05% (w/w) kaolin suspensions are presented (compare Ref. 24).

The influence of a stepwise dosage of the low-molecular-weight polyanion PAA and the cationic PEI on the zeta potential is shown in Figure 4.

The absolute value of the zeta potential decreases until a plateau is reached at a certain polyanion concentration. A contrary effect is obtained in the case of adding a polycation. A partial stabilization of the kaolin particles can be realized due to an adsorption of anionic charged macromolecules at the edges of the kaolin platelets. By adding a polycation to the kaolin dispersion, an adsorption at the negative basal surface becomes possible, and the iep of the particles is reached very quickly at low PEI concentrations. A further addition of PEI leads to an increase of the zeta potential while flocculation was observed. This is because the adsorption of cationic polymer can cause a face-to-face association that can generate polymer–kaolin complexes.

If the kaolin is prestabilized by the anionic low-molecular-weight polymer, the complex formation process with PEI may be followed by the zeta potential of the kaolin particles (Figure 5).

In former investigations by using a combined titration technique [25] we could already show that the turbidimetric endpoint of the polyanion–polycation complex formation in the absence of kaolin correlates quite well with the one in the presence of kaolin. This agreement means that polyanion–polycation interactions are dominant in this system and the complexes with kaolin were formed due to an interparticle bridging through the polyelectrolyte complexes formed on kaolin.

By prestabilizing kaolin with cationic polymers (PEI and PDADMAC, Figure 6), one started the titration with PAA at positive values for the zeta

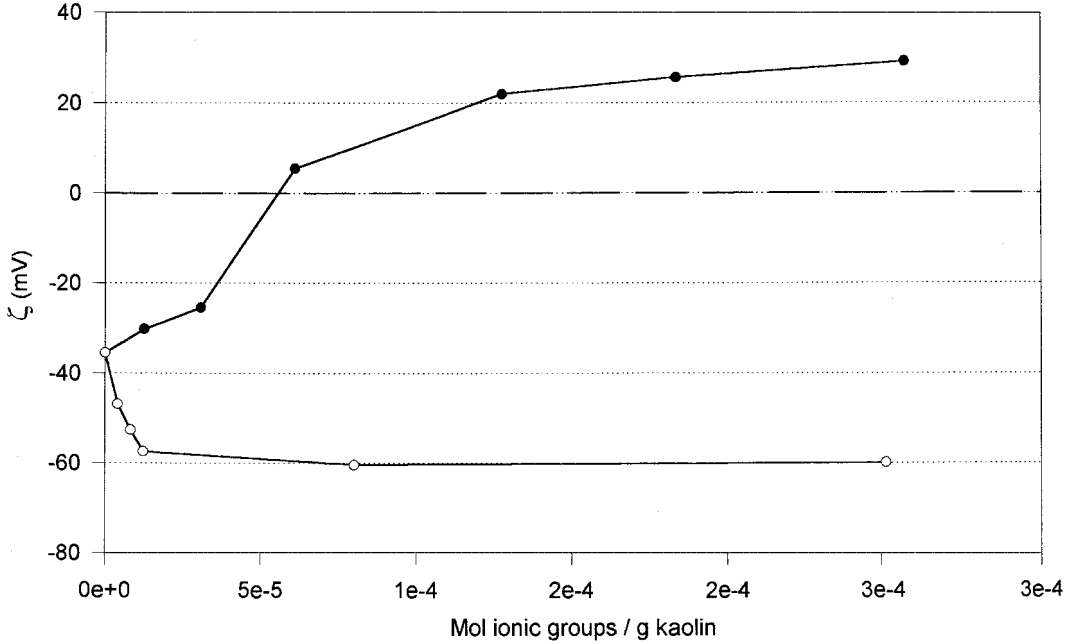

FIG. 4 Change of zeta potential of a commercial kaolin dispersion by adding PEI (●) and PAA (○).

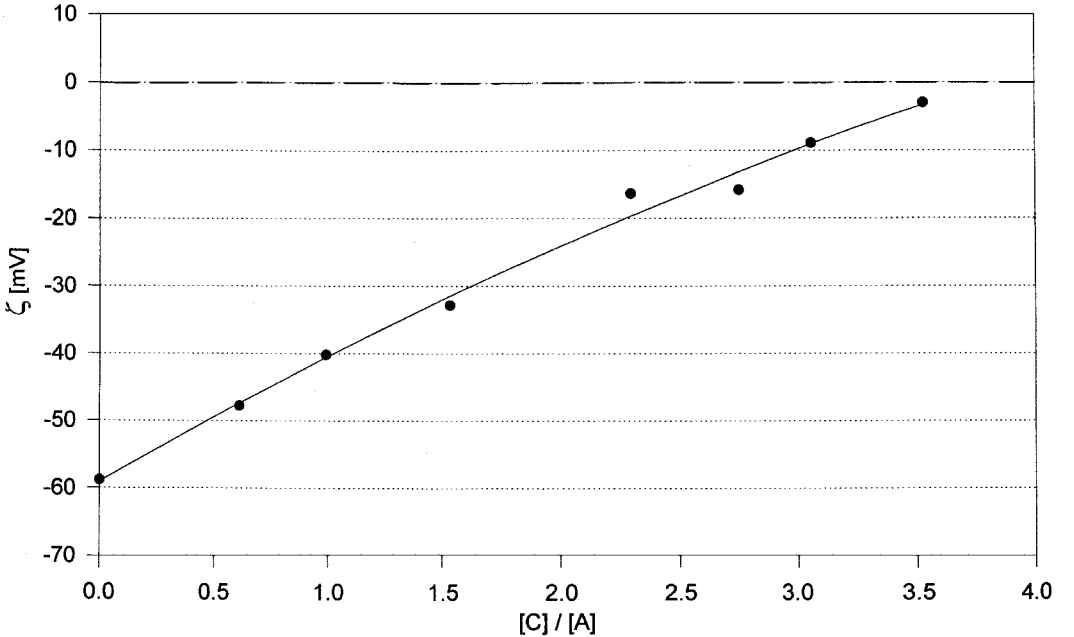

FIG. 5 Change of zeta potential of an anionically prestabilized commercial kaolin dispersion by adding PEI.

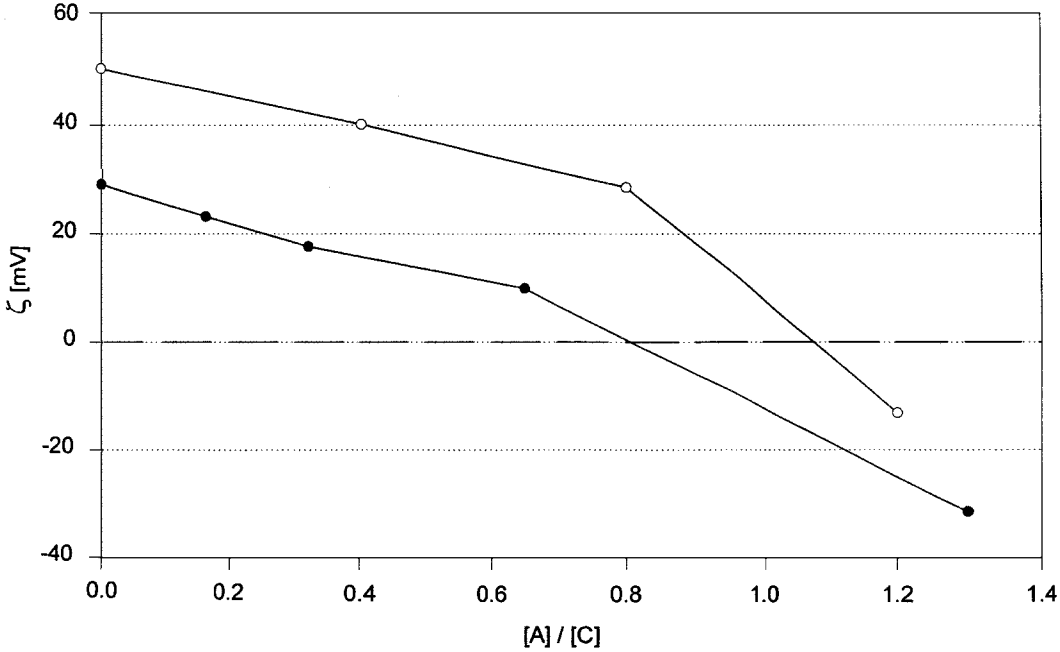

FIG. 6 Change of zeta potential of a cationically prestabilized [PDADMAC (○); PEI (●)] commercial kaolin dispersion by adding PAA.

potential, i.e., at already recharged kaolin particles. As with results presented by Bulidorova and Myagchenkov [16], a stepwise addition of polyanion may reverse the sign of the charge on the particles again.

In dependence on the charge density and the chemical constitution of the polycation, the initial zeta potential varies between +30 and +50 mV as well as the zero charge which was estimated for a molar ratio of anionic to cationic groups to 0.8 for the branched polycation with low charge density. By using PDADMAC as a prestabilizer, the higher charge density leads to a ratio >1 at zero charge. Furthermore, because of the high degree of branching in case of PEI, the cationic groups are less accessible.

Figure 7 summarizes the experimental results when homogeneous polycation–polyanion mixtures were added to a nonstabilized kaolin suspension. The zeta potential shown here is a function of the molar ratio of cationic to anionic groups. The polyelectrolyte mixtures added consisted of PEI/PAA and PDADMAC/PAA, respectively. The peculiarity of these mixtures is to be seen in their homogeneity, i.e., they are optically clear but so-called precursor aggregates are already performed. The C/A ratios here were chosen with regard to the polyanion–polycation titrations. A recharging of the kaolin particles occurred at a C/A ratio lower than for the polyelectrolyte titration without kaolin. As a result, the aggregation of kaolin particles was induced through the precursor systems, whereas the PDADMAC/PAA precursors have a much stronger effect because of the higher charge density of the polycation.

A recharging of kaolin particles prestabilized with a low-molecular-weight PAA and then titrated with PEI could also be observed by means of a particle charge detector (Figure 8). The streaming potential measured in mV reached a zero value at a C/A ratio that corresponds to the electrochemical endpoint in the kaolin-free titration [25]. In studies of the system PAA/PEI as already mentioned, we have shown that a significant deviation between the electrochemical and the turbidimetric endpoints was observed. This is because of a predominantly non-Coulombic, i.e., H-bonding-induced aggregation process. But the influence of the H-bonding was not registered by streaming potential measurements.

Summarizing the results, it is obvious that adsorption phenomena onto kaolin particles using charged polymers can be studied in a successful way by means of capillary electrophoretic light scattering. Although the signal resulted from the particle charge detector is a complex dimension, a charge reversal of prestabilized kaolin particles can also be obtained without problems. But this method limits a detailed interpretation of the phenomena for the reasons explained above.

First of all, acoustophoresis is a useful method to distinguish between nondispersed and well-dispersed kaolin suspensions. By adding polyanions

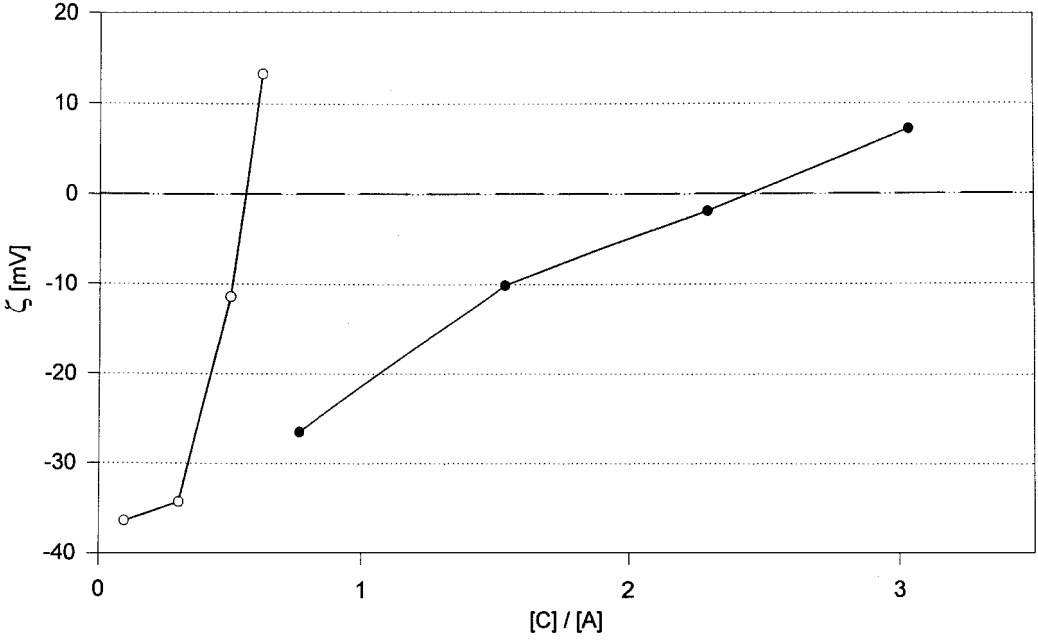

FIG. 7 Zeta potential of a ''nonstabilized'' commercial kaolin dispersion in dependence on the molar ratio of cationic to anionic groups ([C]/[A]) of simplex precursor systems consisting of PDADMAC/PAA (○) and PEI/PAA (●).

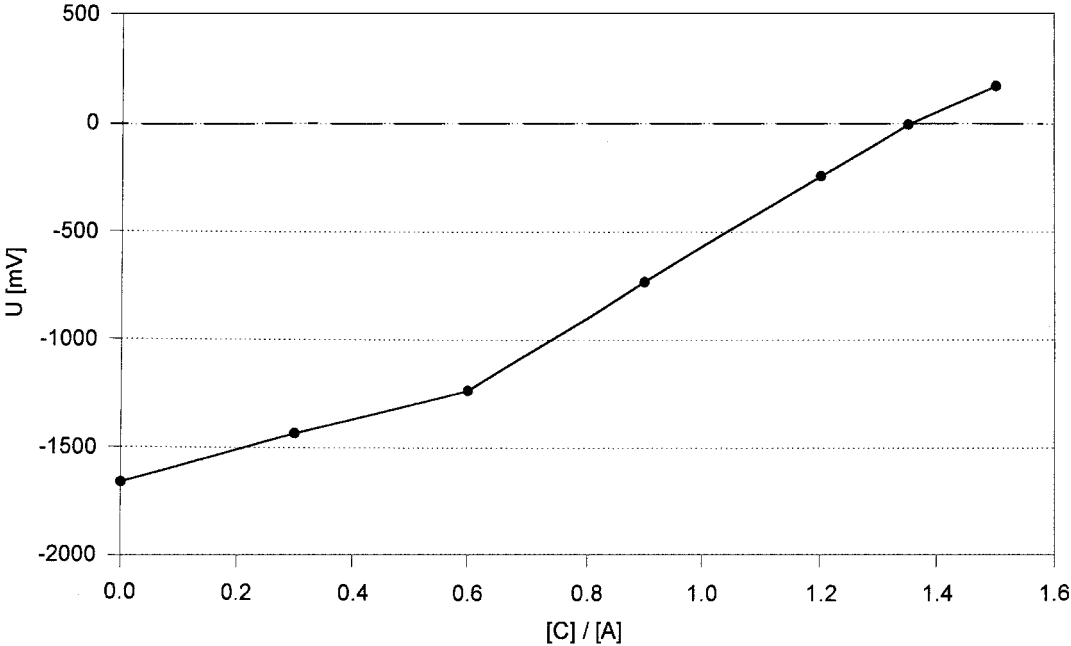

FIG. 8 Recharging of an anionically prestabilized commercial kaolin dispersion by adding PEI detected by the particle charge detector.

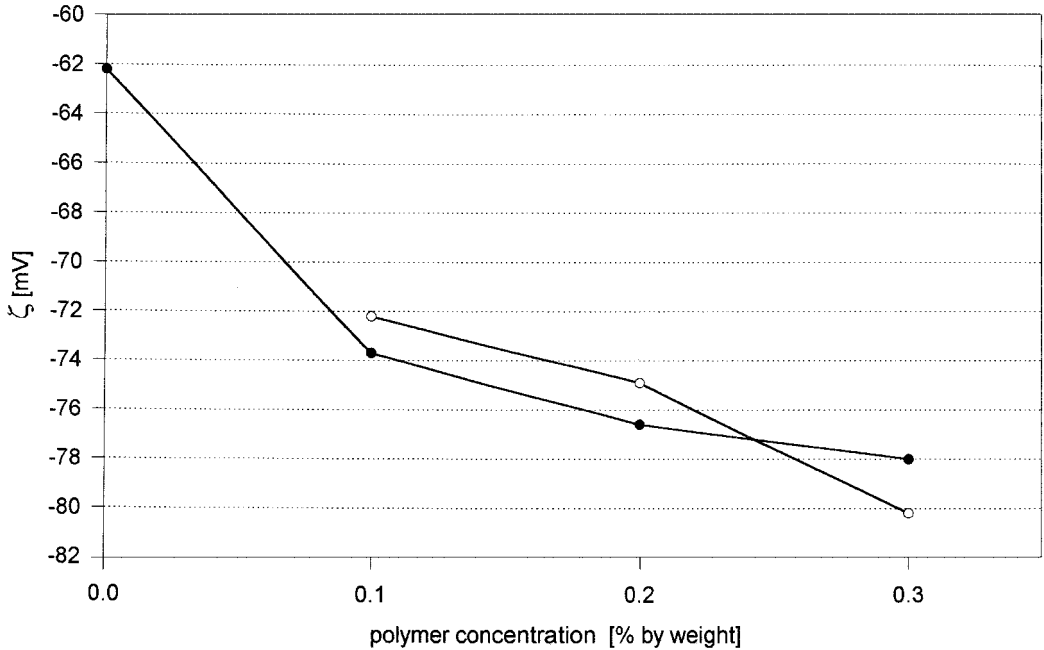

FIG. 9 Change of the acoustophoretic determined zeta potential by adding PAA in presence (●) and absence (○) of 0.005 M NaCl.

(e.g., Na-polyacrylates) in the absence and the presence of low molecular salts (0.005 mol/L NaCl), the kaolin particles become well-dispersed, i.e., the fit error of the fitting process is in the order of 5% and the median (50%) particle size is divided in half. Simultaneously, a slight increase of the absolute values of the negative zeta potential was observed as seen in Figure 9.

VI. FINAL COMMENTS

Comparing the different methods of zeta potential determination with regard to their relevance to characterize polyelectrolyte–kaolin interactions, it can be stated here that:

Capillary electrophoresis is the most used method for determination of the zeta potential of unmodified and polymer-modified diluted kaolin dispersions.

Acoustophoresis is a useful method especially for determining the zeta potential of unmodified concentrated kaolin dispersions as well as for characterizing the degree of dispersion.

The particle charge detector (based on the principle of streaming potential measurements) detects the sum of charges in the polyelectrolyte–kaolin system independent of their stage of interaction. Therefore it is not a useful method for determining an ''accurate'' zeta potential. However, the measurements can be used for investigating the ''principal'' change of zeta potential in dependence on system-specific variables (e.g., pH value, ionic strength).

Complementary electrophoretic, acoustophoretic, and streaming potential measurements are quite useful and can give deeper insight into the mechanism of polyelectrolyte–kaolin interactions.

REFERENCES

1. RJ Hunter. Potential in Colloidal Science, Principles and Applications. 3d ed. London: Academic Press, 1988:35.
2. Ibid, pp 17–42.
3. Malvern Instruments Ltd., Zetasizer 4, Hardware Reference Manual, Manual. No. MAN 0057, 1992.
4. G Lagaly, O Schulz, R Zimehl. Dispersionen und Emulsionen. Darmstadt: Steinkopf, 1997:chap. 10.
5. T Oja, GL Petersen, DC Cannon. U.S. Patent 4,497,208, 1985.
6. RW O'Brien. Electro-acoustic effects in a dilute suspension of spherical particles. J Fluid Mech 190:71–79, 1988.
7. RW O'Brien, DW Cannon, WN Rowlands. Electroacoustic determination of particle size and zeta potential. J Coll Interf Sci 173:406–418, 1995.

8. RW O'Brien, WN Rowlands. Measuring the surface conductance of kaolinite particles. J Coll Interf Sci 159:471–476, 1993.
9. RJ Hunter. Introduction to Modern Colloid Science. New York: Oxford University press, 1993:230–235.
10. F Blockhaus, J-M Sequaris, HD Narres, MJ Schwuger. Adsorption–desorption behavior of acrylic-maleic acid copolymer at clay minerals. J Coll Interf Sci 186:234–247, 1997.
11. S Shimabayashi, H Kazuyuki J Bando, C Shinohara. Formation of a polymer complex between bovine serum albumin and sodium chondroitin-6-sulfate in an aqueous phase and a solid/water interface of kaolin. JMS Pure Appl Chem A31(1):65–81, 1994.
12. E Pefferkorn. Structure and stability of natural organic matter/soil complexes and related synthetic and mixed analogues. Advances Coll Interf Sci 73:127–200, 1997.
13. BKG Theng. Formation and properties of clay–polymer complexes. Development in Soil Science Series Vol. 9. Amsterdam: Elsevier, 1979.
14. H van Olven. In: Introduction to Clay Colloid Chemistry. 2d ed. Toronto: John Wiley, 1977.
15. G Atesok, P Somasundaran, MJ Morgan. Charge effects in the adsorption of polyacrylamides on sodium kaolinite and its flocculation. Powder Technol 54: 77–81, 1988.
16. GV Bulidorova, VA Myagchenkov. Kinetic peculiarities of kaolin sedimentation in the presence of anionic and cationic polyacrylamide flocculants. Coll J 57(6):736–740, 1995.
17. H Serita, K Murai. Flocculation of kaolin suspension with graft copolymers of ionen. Kobunshi Ronbunshu. 50(7):564–570, 1993.
18. L Nabzar, E Pefferkorn, R Varoqui. Polyacrylamide–sodium kaolinite interaction: flocculation behavior of polymer clay suspensions. J Coll Interf Sci 102:380–388, 1984.
19. K Jasmund, G Lagaly. Tonminerale und Tone. Struktur, Eigenschaften, Anwendung und Einsatz in Industrie und Umwelt. Darmstadt: Steinkopf Verlag, 1993.
20. GJ Fleer, MA Cohen Stuart, JMHM Scheutjens, T Cosgrove, B Vincent. In: Polymers at Interfaces. London: Chapman and Hall, 1993:chap. 7.
21. RA Slepetys, LJ Morgan. Optics and surface chemistry of a chemically structured coating pigment. Tappi Journal 195–201, 1991.
22. L Järnström, L Lason, M Rigdahl, U Erikson. Flocculation in kaolin suspensions induced by modified starches 2. Oxidized and hydrophobically modified oxidized starch in comparison with poly(vinyl alcohol) and carboxymethylcellulose. Coll Surf A 104:207–216, 1995.
23. M Chamoumi, A Crespy, A Benhassaine, A Boukhari, J Aride. Improvement of impact strength of polypropylene filled with latex coated kaolin. Annales de Chimie-Sci Mat 19(7–8):395–398, 1994.
24. J Kötz, S Kosmella. Structured pigments due to polyelectrolyte complex formation. Tappi Proceedings 1995 Coating Fundamentals Symposium, Dallas, 1995:71–89.
25. J Kötz, S Kosmella. Interactions between polyanion–polycation systems and kaolin. J Coll Interf Sci 168:505–513, 1994.

17

Phase Transitions in Polyelectrolyte Gels

ETSUO KOKUFUTA University of Tsukuba, Tsukuba, Ibaraki, Japan

I. INTRODUCTION

The swelling of gels, such as that observed when rubber is placed in benzene, has long been a well-known phenomenon. As early as 1948, Vermaas and Hermans [1] studied the behavior of lightly cross-linked polymer chain networks with ionic charges, i.e., polyelectrolyte gels. Flory [2] and Katchalsky [3], in collaboration with their colleagues, also made great contributions to theories and experiments in the fields of ionic and neutral gels. In early studies by these pioneers, however, little attention was paid to the existence of a critical endpoint in the phase equilibria, although in 1968 Dusek and Patterson [4] published a theoretical paper on this subject. The earliest report of the phase transition in a gel was in 1978 by Tanaka [5], who discovered a discontinuous volume collapse of poly(acrylamide) (PAAm) gels in acetone–water mixtures when varying the temperature or the composition of the mixture. This phenomenon is now called ''volume-phase transition'' (or simply ''phase transition'') of gels and is observed in many gel systems consisting of synthetic and natural polymers. The phase transition is accompanied by reversible, discontinuous (or in some cases, continuous) volume changes, often as large as several hundred times, in response to small variations in the solution conditions surrounding a gel. Variables that trigger the transition include solvent composition [5–11], pH [6], ion concentration [12], temperature [5,10,13], and small electric fields [14,15]. (Related literature published in the 1990s will be cited later as the need arises, since a number of studies focused on stimulus-sensitive polymer gels after the publication of these pioneering works.)

When setting a limit to the phase transitions in polyelectrolyte gels, two studies by Tanaka et al. are of historical importance; these were done with ionic gels of partially hydrolyzed PAAm [6] and copolymer of acrylic acid

(AAc) with *N*-isopropylacrylamide (NIPA) [13]. The former [6] is the earliest paper on ionic gel transition, demonstrating that the introduction of charges into the network chain results in an increase in the gel volume at transition as well as a change in the transition threshold. Further demonstrated in the latter [13] is the ionization effect on the transition temperature; that is, a rise in the temperature leading to a transition when increasing the charge density of NIPA-AAc copolymer gels. In particular in the NIPA-based ionic gel system, a discontinuous volume change was observed with a small variation in temperature, as well as in other solution conditions such as pH and salt concentration. Thus, the polyelectrolyte gel of this sort is called a ''thermo-shrinking'' or ''temperature-sensitive'' gel, the properties of which have extensively been studied from both fundamental and technological standpoints (e.g., see Ref. 16).

In the realm of transition theories, as will be seen in Sec. II, all of the descriptions basically contain three terms reflecting the changes in free energies of mixing, elasticity, and osmotic effects. While the expressions of the mixing and elastic contributions to the free energy vary from theory to theory, there is little disagreement on the description of osmotic effects that exist when there is ionic charge in the system. In other words, Donnan equilibria are consistently used in the transition theories for polyelectrolyte gels. Nevertheless, recent and advanced views on molecular grounds have posed the question whether the osmotic effect plays the major role in the ionic gel transition.

Consequently, this chapter will aim to look at the nature of phase transitions in polyelectrolyte gels, so that the theories (Sec. II) as well as the considerations at the molecular level (Sec. III) will be described first. After that, we will discuss in full the molecular mechanism of the ionic gel transition on the basis of experimental results, most of which are taken from the author's publications [17–33].

In this chapter, however, the author does not take up the applications of polyelectrolyte gels that have been appearing in the literature with increasing frequency. We hope that a better understanding of the phase transitions in polyelectrolyte gels can contribute to progress in the technology and engineering of gels.

II. THEORIES

A. Flory's Formula

In order to account for the phase transition of an ionic gel theoretically, it is convenient to imagine that a close analogy exists between swelling equilibrium and osmotic equilibrium. The elastic reaction of the network struc-

ture can be interpreted as a pressure acting on the solution, or swollen gel. In the equilibrium state this pressure is sufficient to increase the chemical potential of the solvent in the solution so that it equals that of the excess solvent surrounding the swollen gel. Thus the network structure performs the multiple role of solute, osmotic membrane, and pressure-generating device.

According to the above considerations, a thermodynamic framework has long existed for interpreting swelling equilibria of ionic as well as nonionic gels in terms of their osmotic pressures. Although our greatest concern for the present should be how to describe theoretically the osmotic pressure (Π) of a gel, let us start with Flory's formula [2] in which Π is written as a sum of three contributions:

$$\Pi = \Pi_{mix} + \Pi_{elas} + \Pi_{ion} \tag{1}$$

Here, Π_{mix} represents the contribution from polymer–solvent mixing, Π_{elas} is the elastic contribution due to deforming the network chains from their reference state, and Π_{ion} is the contribution arising from the difference in mobile ion concentrations. Using the well-known polymer–solution theory of Flory and Huggins (i.e., mean field theory), Π_{mix} can be described as

$$\Pi_{mix} = -\frac{RT}{\upsilon_s}[\varphi + \ln(1 - \varphi) + \chi\varphi^2] \tag{2}$$

where R is the gas constant, T is the absolute temperature, υ_s is the molar volume of the solvent, φ is the volume fraction of the network chains, and χ is the polymer-solvent interaction parameter. For Π_{elas}, Flory's description (the earliest theory [2]) can be given by

$$\Pi_{elas} = RT\left(\frac{\nu_e}{V_0}\right)\left[\frac{V_0}{2V} - \left(\frac{V_0}{V}\right)^{1/3}\right] \tag{3}$$

where ν_e represents the mole number of effective chains in the network, V_0 is the volume of the ''unswollen'' polymer, and V is the volume of the swollen gel. It should be noted that the following assumptions are made for Eq. 3: (1) The network is at first formed via cross-linking of the unswollen polymer at volume V_0. (2) Subsequently, it isotropically swells to a volume V with a diluent. (3) This swelling occurs without an appreciable change in the total volume of the system (polymer plus solvent). As a result, the term V_0/V in Eq. 3 should be equivalent with φ in Eq. 2; i.e., $\varphi \sim V_0/V$.

If the polymer chains making up the network do not contain ionizable groups, the phase transition may be accounted for by a combination of Eqs. 2 and 3. For ionic gels, however, we must consider the concentration of ''mobile'' ions, which would always be greater in the gel than the outside because of the attractive power of the fixed charges. Consequently, the os-

motic pressure of the solution inside could exceed that of the external solution. Then the expansive force may be equal to this difference in osmotic pressures for the two solutions. For a cationic gel, Flory described Π_{ion} as

$$\Pi_{ion} = RT\left[\frac{iC_p}{Z_-} - \nu_{\pm}(C_s^* - C_s)\right] \tag{4}$$

where i denotes the number of electronic charges per polymer unit in a polyelectrolyte gel, Z_- is the valency of anion, C_p is the molar concentration of polymer units, $\nu_{\pm}$ is the number of total ions, and C_s^* and C_s are the molar concentration of salts within a gel and in the surrounding medium, respectively. It is to be emphasized that Eq. 4 holds under conditions where the gel system is sufficiently diluted with the solvent.

B. Modifications of Flory's Formula by Tanaka

Tanaka and his coworkers have used Flory's formula with several modifications to understand a discrete phase transition in ionic gels. First, the term V_0/V in Eq. 3 was replaced by the term φ/φ_0 (but not by φ). Here, φ_0 was defined as the volume fraction of the network on condition that the constituent polymer chains have random-walk configurations [5]. Flory assumed that the ''dry'' gel (in other words, the network formed by cross-linking of the unswollen polymer at volume V_0) satisfies the condition of no polymer interactions; i.e., $\varphi_0 \sim 1$. However, Tanaka discovered a collapse of covalently cross-linked PAAm gels in an acetone–water mixture; therefore he claimed that the elastic term is generally not a function simply of V_0/V (=φ) as was given by Flory, but of φ/φ_0. The reason is that for a gel with $\varphi_0 \sim 1$ there is no possibility for volume collapse.

Tanaka also modified Eq. 4 by assuming that $(c_s^* - c_s) \sim 0$ (see Ref. 6):

$$\Pi_{ion} = \nu fkT\left(\frac{\varphi}{\varphi_0}\right) \tag{4'}$$

Here, f is the number of counterions per effective chain in the network, N_A is Avogadro's number, and ν ($\sim \nu_e N_A/V_0$) is the number of effective chains per unit volume at $\varphi = \varphi_0$. In addition, χ in Eq. 2 was replaced by $\Delta F/kT$, where ΔF is the free-energy decrease associated with the formation of a contact between polymer segments. As a result, Tanaka et al. obtained Eq. 5 for an ionic gel:

$$\Pi = -\frac{N_A kT}{v_s}\left[\varphi + \ln(1-\varphi) + \frac{\Delta F}{2kT}\varphi^2\right] + \nu kT\left[\frac{\varphi}{2\varphi_0} - \left(\frac{\varphi}{\varphi_0}\right)^{1/3}\right] + \nu fkT\left(\frac{\varphi}{\varphi_0}\right) \tag{5}$$

The osmotic pressure of a gel must be zero for the gel to be in equilibrium

with the surrounding solvent. Zero osmotic pressure is also necessary for the free energy of the gel (F_g) to be minimized, since $\Pi = -\partial F_g/\partial V$, where V is the volume of the gel and $V \propto \varphi_0/\varphi$. Using Eq. 5, such conditions may be expressed as

$$\tau \equiv 1 - \frac{\Delta F}{kT} = \frac{\nu v_s}{N_A \varphi^2}\left[(2f+1)\left(\frac{\varphi}{\varphi_0}\right) - 2\left(\frac{\varphi}{\varphi_0}\right)^{1/3}\right] + 1 + \frac{\varphi}{2} + \frac{2\ln(1-\varphi)}{\varphi^2} \tag{6}$$

where the parameter τ (i.e., $1 - \Delta F/kT$) is called the reduced temperature, which changes with temperature and solvent composition. The equation then determines the equilibrium network concentration as a function of τ. For certain values of τ, however, Eq. 6 is satisfied by three values of φ, corresponding to two minima and one maximum of the free energy. The value of φ corresponding to the lower minimum represents the equilibrium value. A discrete volume transition occurs when the two free-energy minima have the same value.

Figure 1 shows typical swelling curves calculated for an ionic gel as a function of f. In calculations of the equilibrium swelling ratio (φ/φ_0) by Eq. 6, Tanaka et al. used $\varphi_0 = 0.5$ and $\nu v_s/N_A\varphi_0^3 \sim 10$ (i.e., $\nu v_s = 7.5 \times 10^{24}$) [5]. The former value was obtained by assuming that monomers and cross-linkers would be polymerized during gelation in a random walk fashion to form a network, while the latter was chosen so that the theoretical curves agree with the experimental data. As can be seen from Figure 1, an increase in f causes a drastic change in the collapse size at the transition. Therefore it can be predicted that ionic gels undergo a phase transition. As will be mentioned in the latter section, at present there are many experiments demonstrating the phase transitions of ionic gels.

C. Arguments Against Flory's Formula and Other Descriptions for the Osmotic Pressures

After the publications by Tanaka et al. [5,6] concerning the phase transitions in neutral and ionic gels, uses of Eqs. 2–4 to describe Π of Eq. 1 have been criticized by several authors. Before looking at these criticisms, however, it must be kept in mind that there is an argument about the description of Π as a sum of Π_{mix}, Π_{elas} and Π_{ion}. For this treatment, one must assume that the various contributions to the free energy of swelling are additive; in other words, the partition function for swelling can be factored into independent contributions. While this assumption has been questioned [34,35], there exists (as yet) no tractable alternative for describing swelling equilibria.

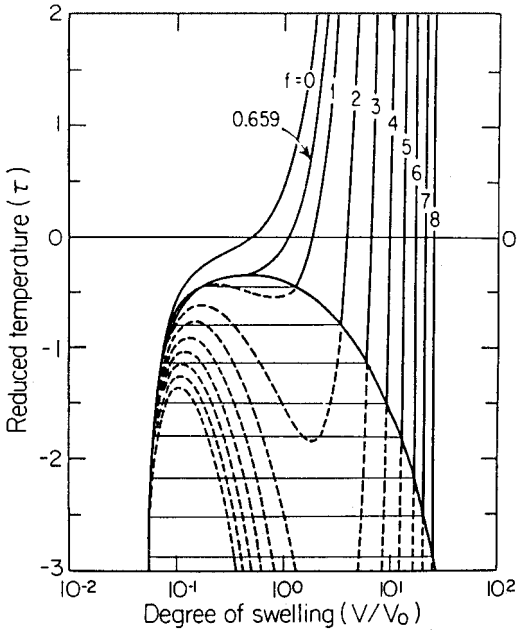

FIG. 1 Relationship between equilibrium degree of swelling (V/V_0; i.e., $\sim\varphi_0/\varphi$) and reduced temperature at various numbers of ionized groups per chain. Equation 6 with $\varphi_0 = 0.5$ and $\nu\upsilon_s/N_A\varphi_0^3 \sim 10$ was used for the calculation as made by Tanaka et al. [6]. (From Ref. 6 with several modifications.)

Table 1 summarizes the essential points of the criticism. First, the use of Flory–Huggins theory becomes the focus of criticism because this is based on a random-mixing lattice model, in which the lattice is assumed to have no holes; thus it is incompressible. Second, the earliest Flory (or Flory–Rehner) theory [2] for rubber elasticity does not hold when the gel is swollen, because the theory unrealistically assumes that the distributions of chains are Gaussian. Furthermore, the model does not account for the chains being finite or taking up space. Third, a simple assumption for osmotic pressure arising from counterions is not realistic, because electrostatic interactions between the fixed charges are neglected. Also neglected is counterion condensation.

Prausnitz and coworkers [36] have developed a theory based on hydrogen bonds in a lattice that permits holes and thus compressibility. This overcomes the deficiencies of Flory–Huggins theory; however, Guassian chains are still assumed, and therefore it is difficult to fit experimental results with a single set of parameters over the entire range of swelling. However, the theory

TABLE 1 Typical Examples for Criticisms to Three Terms of Flory's Formula and Alternative Proposals

Terms	Criticized point	Alternative proposal	Author
Mixing term (Π_{mix})	random-mixing lattice model (Flory–Huggins theory)	quasi-chemical lattice model	Prausnitz et al. [36]
		virial-type expression (for thermoshrinking gels)	Saito et al. [42]
		lattice-fluid model (by Sanchez and Lacombe)	Cussler et al. [40]
Elastic term (Π_{elas})	the earliest elasticity mode based on Gaussian chain distributions (Flory–Rehner and Flory theories)	improved elasticity model based on ''constrained junction'' theory	Prausnitz et al. [36]
		an elastic expression that accounts for the limits of elongation	Saito et al. [42]
Osmotic term (Π_{ion})	neglecting of charge–charge interaction as well as counterion condensation	Debye–Hückel model (Hasa–Ilavsky–Dusek theory)	Dusek et al. [44]

does correctly predict discontinuous transitions for nonionic gels. In a subsequent paper [37,38] where they discussed results with charged gels, the Prausnitz research group introduced an improved elasticity term based on constrained junctions. This theory actually predicts ionized gels to have discontinuous transitions as well; this is in accord with the Tanaka group's experiments, but not with the Prausnitz group's own observations [39].

Cussler and coresearchers [40] overcame the deficiency due to the use of a lattice-based mixing term; instead of an equation of state their approach applied also permits compressibility. They derived an interaction energy from the various cohesive energy densities in the system that fits the experimental results. In addition, they noted that neither Tanaka's [12] nor Prausnitz's [36] approach will predict pressure dependencies of gel swelling as they have experimentally observed [41]. But their own model, although sensitive to the fact that gels swell under pressure in an attempt to increase entropy, overpredicts this effect. They suggest they can compensate for this result by introducing specific hydrogen bonding interactions into their system.

By focusing on the thermal collapse of NIPA gels, containing as well as not containing ionic charges, Saito and coworkers [42] attempted to develop a phase transition theory. They ignored most of the work so far cited and assumed that the mixing term is a viral volume interaction. An elastic expression that accounts for the limits of elongation was also incorporated. However, in sharp contrast to the works above, Saito et al. incorporated the specific term due to hydrophobic interaction into Eq. 1. Then they assumed that hydrophobic interaction gives rise to physical cross-linking points in the chains that comprise the gel. From the Nemẽthy–Sheraga study [43] on the temperature dependence of the hydrophobic interaction between molecules in water, the free energy change ($\Delta G_{\text{hydrophobic}}$) is given by

$$\Delta G_{\text{hydrophobic}} = C_a + C_b T + C_c T^2 \tag{7}$$

where C_a, C_b and C_c are system-dependent parameters. Taking this into account, Saito's group obtained the free energy equation for ''thermo-shrinking'' gels. This predicts continuous transitions that become discontinuous upon ionization, yet calling for several adjustable parameters.

D. Descriptions for the Fixed Charge Interaction

In the early 1950s, Katchalsky and his coworkers [3] studied the swelling behavior of polyelectrolyte gels consisting of cross-linked poly(methacrylic acid) (PMAAc) in several aqueous salt solutions as a function of the neutralization degree. Then they argued that the Donnan distribution could not give even a rough approximation and proposed a theory based on the random coil model in which the charge interaction along a chain was calculated by

Debye–Hückel theory. This was taken over by Hasa–Ilavsky–Dusek (HID) theory [44] in which a modification of the elastic term was made by considering the influence of charges on the deformation of the network. Although HID theory has not yet been applied to account for the phase transition in ionic gels, Ilavsky et al. [45–48] as well as Konak and Bansil [49] performed several experiments to examine this theory in comparison with the swelling and elastic data for PMAAc gels and related copolymer gels.

Recently, Tong and Liu [50] also attempted to examine carefully the HID theory with their swelling experiments for copolymer gels of *N*,*N*-dimethylacrylamide (DMAAm) and 2-acrylamide-2-methylpropanesulfonic acid (AMPS). They used Eqs. 8 and 9 for the Π of Eq. 1, which was obtained according to the HID theory:

$$\Pi = -\frac{RT}{v_s}[\ln(1-\varphi)+\varphi+\chi\varphi^2] - RT\varphi_0\left[\varphi^{1/3}-\frac{\varphi}{2}+\frac{3}{5n\varphi^{1/3}}+\frac{99}{175n^2\varphi^{1/3}}+\frac{513}{875n^3\varphi^{5/3}}\right] + \frac{RTf_m\rho\varphi}{M_0}-\frac{N_A\nu Z^2e^2f_m^2}{3D\varphi_0\langle R_0^2\rangle^{1/2}\varphi^{4/3}}\left[\frac{2.5A}{1+A}-\ln(1-A)\right] \tag{8}$$

and

$$A=\left[\frac{9DkTM_0}{\pi N_A e^2\langle R_0^2\rangle f_m\rho}\right]^{1/2}\varphi^{-5/6} \tag{9}$$

Here, f_m is the mole fraction of ionic monomer unit (i.e., AMPS), ρ the density of the dry gel, Z the degree of polymerization of the chain in the network, e the electronic charge, D the dielectric constant of solvent, $\langle R_0^2\rangle$ the mean-square end-to-end distance, and M_0 the average molecular weight of copolymer unit (i.e., $M_0 \sim f_m M_{ANPS} + (1-f_m)M_{DMAAm}$, where M_{ANPS} and M_{DMAAm} are the molecular weight of AMPS and DMAAm, respectively). It is clear that Eq. 8 includes the term due to the electrostatic interaction between the fixed charges, which was ignored in Eq. 5 (Flory's equation). In addition, the elastic term in Eq. 5 was modified. Therefore, one may expect that the prediction of swelling degree ($1/\varphi$) as a function of f_m from the HID theory would be better than that from the Flory theory. However, it was concluded that neither the Flory nor the HID theory can provide a reasonable approach for predicting the swelling degree for the polyelectrolyte gel of this sort.

In conclusion, it appears clear that a theoretical explanation of the phase transition of gels, whether as nonionic gels or as polyelectrolyte gels, is far from complete. Better experimental characterization of the networks needs to be done so more realistic elastic effects can be fitted. Mixing terms that

account for nonrandom distributions of molecules need to be applied. As for the nature of the specific interaction, the general concept of hydrogen bonding versus what exactly are hydrophobic interactions is still being debated. We may hope that data from experiments covering a wide range can aid in resolving the debate.

III. UNDERSTANDINGS ON MOLECULAR GROUNDS

We have seen in the previous section that there is much debate about a theoretical explanation of the phase transition of gels. In experiments with a variety of gel systems including ionic gels, on the other hand, a large number of data have been accumulated. Thus it would be interesting to draw a generalized perspective about the phase transition from experimental data. This may be achieved through classification, as well as through explanation on molecular grounds, of experimental swelling curves. Taking this into account, we have tried to present a ''unified'' model of gel transitions, with an addition of an experimental result from which one may see the role of hydrogen bonding in the phase transition [17]. Then we accounted for the phase transition by hypothesizing a balance between the repulsive and attractive forces within the cross-linked polymers in the networks, which arise from a combination of four intermolecular forces: ionic, hydrophobic, van der Waals, and hydrogen bonding. When a repulsive force, usually electrostatic in nature, overcomes an attractive force such as hydrogen bonding or the hydrophobic interaction between the network chains, gel volume should increase discontinuously in some cases and continuously in others. The variables triggering the transition influence these intermolecular forces and thereby the balanced state of the attractive and repulsive forces.

Because our paper (Ref. 17) included several mistakes in citing references as well as in giving an example for a gel system in which the van der Waals force becomes dominant as the attractive force, Schild [16] criticized the proposed model itself as too idealistic. As we will learn in the following sections, however, this model serves as a good guide for discussing what is the main factor to swell or to collapse a gel. This section discusses the phase transition in ionic gels at the molecular level. For this purpose, the previously proposed diagram has been corrected (see Figure 2). In this correction, the following are taken into consideration: (1) Three diagrams deal with polyelectrolyte gel systems but not with all the gel systems. (2) The variable is thus restricted to factors (conditions surrounding the gel) leading to a change in the volume of ionic gels. (3) No attention is paid to whether the gel undergoes discontinuous or continuous transition (the model makes no mention of this subject).

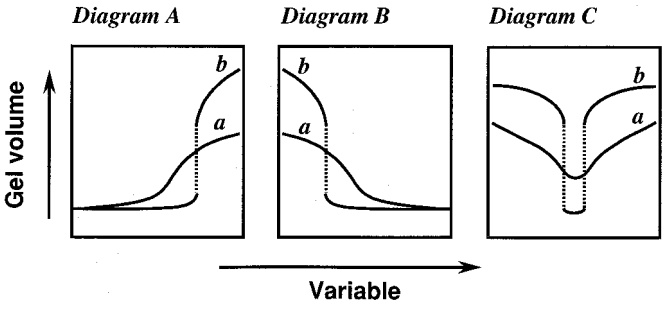

FIG. 2 Universal classification of polyelectrolyte gel transitions. Pictured in expectations upon intermolecular interaction mechanism are changes in the volume of slightly ionized (a) and highly ionized gels (b) with an optional variable such as pH, temperature, and fraction of either water or other solvent in their mixtures.

Let us discuss each of the attractive forces that maintain a gel in a collapsed state. In general, the energy (E) of the intermolecular attractive forces varies as the inverse of the first to sixth power of the intermolecular distance (r); $E \propto (1/r^n)$. For the Coulomb force, E is given by $-e^2/Dr$ (e, the electronic charge; D, the dielectric constant) so that $n \sim 6$. When $n \sim 6$, the intermolecular force is frequently called the van der Waals force. Although there is a difference of several angstroms between the maximum and the minimum distance, the equilibrium ranges from 3 to 5 Å with $E \sim 2$ to 10 kcal/mol.

The hydrogen bond can be considered electrostatic or ionic in character, since the classical concepts of chemical bonding allow hydrogen to form only one covalent bond. This model does not, however, account for all the properties of the hydrogen bond; it is appealing to consider the bond covalent in some cases. For example, the distance of a hydrogen bond such as —H—O···O— (1 Å for O—H and 1.8 Å for H···O) is smaller than the van der Waals radius (2.6 Å) between H and O atoms.

The hydrophobic interaction between nonpolar molecules in water or aqueous solvents must be defined in a different category from the other three intermolecular attractive forces. When organic compounds containing nonpolar residues are introduced into an aqueous solution, large positive deviations from ideality are observed. However, whereas poor solvent properties are normally caused by an unfavorable heat of mixing, the solutions of materials such as aliphatic hydrocarbons in water have frequently been found to be exothermic. We are then left with the conclusion that the poor solubility of nonpolar solutions in water is a consequence of large negative excess entropy of mixing. A detailed consideration of these findings was first undertaken in a pioneering investigation of Frank and Evans [51]. They pointed

out that the negative ΔH and the negative ΔS may be rationalized by assuming that an ice-like structure is stabilized in the neighborhood of nonpolar solutes—thus the heat evolved may be thought of as due to the latent heat of freezing of ''icebergs'' which represent regions of crystalline order and whose formation, therefore, leads to a loss of entropy. The tendency of nonpolar solutes to aggregate in aqueous media reduces the number of water molecules in their immediate vicinity and leads to ''icebergs melting.'' This provides the driving force towards such aggregation and has been referred to as the ''hydrophocib bond'' by Kauzmann [52].

Now we will return to Figure 2 and try to account for gel volume transitions. When choosing pH as a variable, we may assign Figs. 2A and 2B to polyelectrolyte gels whose ionizable groups are weakly acidic and basic, respectively. Assigned to Fig. 2C is a polyampholite gel with both weak acid and weak base as the ionizable groups. The pH-induced deprotonation (e.g., $\sim COOH \rightarrow \sim COO^-$) and protonation (e.g., $\sim NH_2 \rightarrow \sim NH_3^+$) may strengthen Coulomb repulsion forces between the fixed charges; thus, we may observe the gel swelling with increasing pH for acidic gels but with decreasing pH for basic gels. In order to understand the gel collapse accompanying with the release of a large amount of solvents, however, it is convenient for us to assume the attractive force(s). Then we may assign as an attractive force the Coulomb force in the collapse of an ampholite gel (e.g., curve a in Fig. 2C); the gel collapse would become more dramatic when incorporating another attractive force such as the hydrogen bonding and hydrophobic interaction (curve b in Fig. 2C). In cases of other polyelectrolyte gels having charges of the same sign, we also have to consider the role of attractive forces in the gel collapse. For example, NIPA-based hydrogels with COOH or NH_2 groups shrink gradually through the elimination of charges with pH but do not undergo a collapse transition such as curve b in Figs. 2A and 2B at temperatures at which hydrophobic interaction does not become dominant (see Sec. V).

When temperature is a variable, we may clearly observe a transition in the existence of attractive forces. For such cases, seeing the hydrophobic interaction as the attractive force makes it possible for us to interpret the volume collapse with increasing temperature. If the hydrogen bonding is assumed to be an attractive force, an increase in temperature would result in the swelling. A good example for supporting this has recently observed in a neutral (but not ionic) gel [29]; *N*-(1,3-dioxolan-2-ylmethyl)-*N*-methylacrylamide (DIOMMA) gels that swell in alcohols but shrink in pure water by heating. This opposite trend in the thermal properties in water and alcohols was discussed in terms of polymer–polymer, polymer–solvent, and solvent–solvent interactions. More details of Fig. 2 will be discussed in Sec. V through a comparison with experimental results.

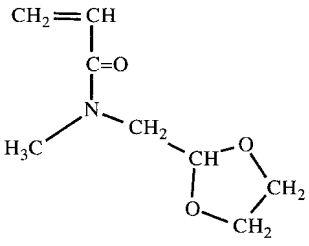

DIOMMA

IV. EXPERIMENTAL METHODS

Before discussing the swelling curves of several polyelectrolyte gels in connection with the phase transition, it would be convenient to provide information about the methods for preparing and characterizing the gels. This section aims at giving a general outline of experimental methods used in Sec. V.

A. Preparation of Gels

There are two ways of preparing gels: the polymerization of monomers in the presence of a suitable cross-linking agent, and the chemical or physical cross-linking of polymers. The former is more common than the latter; thus, a number of studies have prepared gels using polymerization methods with monomers, among which an aqueous redox polymerization system initiated by a pair of ammonium persulfate (APS) and *N*,*N*,*N*′,*N*′-tetramethylethylenediamin (TMED) has been frequently employed. For forming gels from polyelectrolytes (i.e., polymers), a few instances have been reported; for example, the cross-linking of linear poly(ethyleneimine) (LPEI) with ethylene glycol diglycidyl ether (EGDGE) [27], as well as of copolymers of acrylic acid (AAc) and *N*-substituted alkylacrylamide in water by γ-rays from a ^{60}Co source [22,28].

Other than the above two ways, we may employ chemical and physical techniques for converting a neutral gel into an ionic gel. For example, a neutral gel consisting of PAAm chains crosslinked with *N*,*N*′-methylenebis(acrylamide) (MBA) converts into an ionic gel with COOH groups via alkaline hydrolysis of the AAm residues [6]. As a physical converting technique, the binding of ionic surfactants [20,24,26,30] to neutral gels such as NIPA gel is useful. However, these techniques are limited to special cases; thus we will look about for the essential point in the preparations of LPEI gels [27] as well as NIPA gels [28] with randomly copolymerized AAc residues or with polymer chains of AAc (PAAc), both of which were obtained by cross-linking of the polymers. Also mentioned for this purpose is

the preparation of submicrometer-sized polyelectrolyte gel particles based on aqueous redox polymerization [32].

1. Cross-Linking of LPEI with EGDGE

The cross-linking reaction can be written as

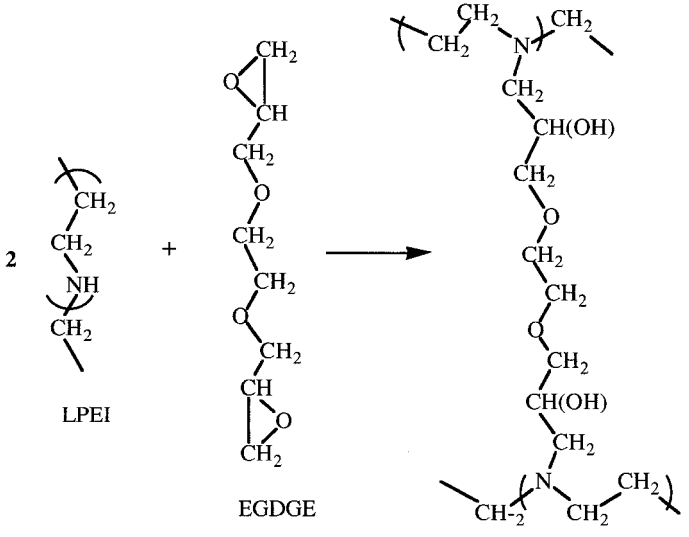

Thus we may control the degree of cross-linking by means of the molar ratio of the epoxy group to the imino group. The gelation can be performed by incubation of aqueous polymer solutions under suitable conditions; for example, at pH 8 and at 60°C.

When the preparation was carried out using a reaction vessel (e.g., a test tube) into which glass capillaries with tiny inner diameters (0.1–1 mm) had previously been inserted, two types of gel samples were available from the same preparation: very fine cylindrical gels and powdered gels. The former was then obtained from a fine gel rod that can be taken out of the capillary and cut into cylinders several millimeters in length. The latter was from the gel mass taken out of the vessel together with the capillaries, by grinding and passing through a screen with a fine mesh size. Such fine gel samples (especially cylindrical gels) provide accurate measurements of the swelling degree because of a rapid attainment of swelling equilibrium (the rate for changes in gel volume is inversely proportional to the square of the smallest dimension of the gel [53]).

Purification of gel samples is easier than that of polymers, and it can be performed by repeated swelling and shrinking procedures using appropriate solvents. It is to be emphasized that we must confirm to fully eliminate

impurities due to unreacted cross-linkers as well as un-cross-linked polymers. A combination of total organic carbon (TOC) analysis and conductivity measurement are effective not only for the present case but also for many polyelectrolyte gels.

2. Cross-linking of Polymers in Water by γ-Rays

This method is based on the direct and indirect formations of polymer radicals during γ-ray irradiation. The indirect formation of polymer radicals is mainly due to the $\dot{H}$ and $\dot{O}H$ radicals arising from water molecules; thus the irradiation method cannot be applied to the polymers when unstable and degrading polymer radicals would be formed. For vinyl polymers whose structure is shown as

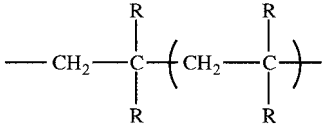

it is generally believed that the cross-linking would take place when one of the two R groups in the repeating unit is hydrogen, while polymers such as poly(methacrylic acid) with two R groups other than hydrogen are degraded during irradiation.

For copolymers of AAc with NIPA, therefore, γ-ray irradiation was successfully employed in preparing polyelectrolyte gels. Using an aqueous solution containing the homopolymer of AAc (PAAc) as well as of NIPA (PNIPA), we also succeeded in forming an ionic gel with the network in which the COOH groups are localized along a PAAc chain, but their content is the same as that of the gel from the random copolymer of AAc and NIPA. Typical preparation procedures of the ionic gel with an inhomogeneous distribution of the COOH groups are as follows: (1) PNIPA (0.791 g) and PAAc (50.4 mg) were dissolved in 10 mL of distilled water; (2) the aqueous polymer solution was transferred into a test tube in which glass capillaries had previously been inserted; (3) the test tube was sealed after degassing the solution under a vacuum, and finally (4) the irradiation was performed at ca. 1°C for 12.8 h at a dose rate of 0.156 Mrad/h using γ-rays from a ^{60}Co source.

3. Preparation of Submicron Gel Particles

Ionic microgel particles play an important part in studies of the phase transition, as we will learn in Sec. V. In cases of NIPA-based polymerization systems, submicron-sized polyelectrolyte gel particles can easily be prepared using the usual synthetic technique of aqueous redox polymerization. Different polymerization media were then employed: surfactant-containing wa-

ter [54,63,64] surfactant-free water [55–59,62], and water suspended in oils [53,60,61]. Usually, APS and potassium persulfate (KPS) were employed as initiators and MBA as the cross-linker. In general, the diameters of the gel particles (<1 μm) prepared in the presence of surfactants were smaller than those (>1 μm) obtained from surfactant-free systems. All of the preparations were found to swell or deswell with changes in temperature; such temperature-sensitive swelling–deswelling characteristics were similar to those of bulk NIPA gels in cylindrical, cubic, and other forms.

In order to incorporate ionic groups to the NIPA-based microgels, there are three methods. Hirose et al. [61] have demonstrated a suitable method in which neutral gel beads consisting of MBA-crosslinked NIPA and *N*-(acryloxy)succinimide (AOSI) chains were initially prepared using a water medium suspended in hexane, and subsequently converted into a polyelectrolyte gel with COONa by alkaline hydrolysis. The second method for preparing ionic NIPA latexes was reported by Pelton et al. [54,55]. They conducted an aqueous redox polymerization of NIPA and MBA without ionic monomers in the absence and the presence of surfactant using KPS or azobis(isobuthylamidine) hydrochloride (AIBA·HCl) as an initiator. Since the ionizable groups originating from the initiator may covalently bind to many of the end groups of the NIPA chains within the network during the polymerization, they succeeded in preparing anionic and cationic latexes by use of the KPS and the AIBA·HCl initiator, respectively. Aqueous redox copolymerizations (third method) of NIPA with ionic monomers such as MAAc in the presence of surfactant were also employed by Tenhu and Lowe [63] and Chu and Zhou [64]. While the choice of method depends on the purpose for which the polyelectrolyte gel particles will be used, the inverse suspension polymerization employed by Hirose et al. [61] generally requires great skill to obtain particles with good reproducibilities regarding size and distribution. In Pelton and Chibante's method [55] it is difficult to introduce a large amount of charges into the gel beads from the initiator; this problem has already been pointed out by Pelton in another publication [54]. Thus, Ito et al. [32] have used the third method to prepare submicron microgel particles composed of MBA-cross-linked NIPA network into which different amounts of AAc or 1-vinylimidazole (VI) were incorporated. They were able to control the AAc and VI contents of aqueous monomer solutions (pregel solutions) within 0 to 30 mol%; therefore the particles obtained exhibit very large diameter changes in response not only to temperature but also to the treatment with acid and base.

B. Swelling Measurements

The swelling ratio for a gel can be determined on the basis of either size or weight of the gel. At a glance, one does not feel difficulty in performing

these measurements. However, the data include a serious error which is more than 10% in some cases, especially in the measurements based on gel weight. In our experience this seems to be mainly due to a slow attainment of swelling equilibrium (a cylindrical gel with 1 mm diameter and 3 mm length needs more than a week to attain a swelling equilibrium at transition). As mentioned above, use of fine gel samples could facilitate an accurate measurement of equilibrated volume or size of the gel.

Figure 3 shows our own setup used in the measurements of the swelling ratio under different pH conditions as well as concentrations and kinds of ionic compounds such as salts and surfactants. The instrument consists of four different parts: an aqueous phase supply system (APSS) equipped with a pH meter, a conductivity meter, a TOC sampling port, and an inlet of salts or surfactants; a microscope with a CCD camera and an image-analyzer; a water-jacketed separable measuring cell with glass meshes; and a temperature control system (TCS). A fine gel sample was inserted into the glass cell, and an aqueous solution with the desired pH and salt (or surfactant) concentration was continuously supplied around the gel sample from the APSS with the Ar gas pressure. The salt or surfactant concentration was accurately regulated by means of conductmetric measurements or TOC analyses (at high surfactant concentration ranges). Calibration curves showing the

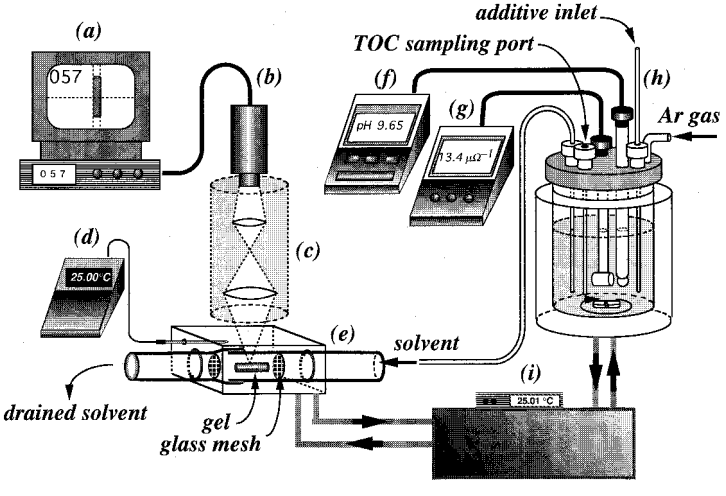

FIG. 3 Setup for the measurements of the swelling ratio: (a) image analyzer; (b) CCD camera; (c) microscope; (d) thermometer; (e) measuring cell; (f) pH meter; (g) conductivity meter; (h) aqueous phase supply system (APSS); (i) temperature control system (TCS). (From Ref. 27.)

changes in conductivity with pH and salt or surfactant concentration as well as the changes in TOC with surfactant concentration were used. The attainment of an equilibrated gel diameter was evaluated by careful measurements in which the pH and/or conductivity was made to fluctuate several times ±3% around a setting used for determining the diameter of the gel sample. The temperature was controlled to within a range of ±0.1°C using TCS with water circulating around both the APSS and the measuring cell.

C. Several Characterization Methods

Most experiments on the phase transition of ionic gels were performed in order to learn how swelling degree varies with variables such as pH and salt concentration; however, the gel sample should be fully characterized before the swelling measurements. The following are important techniques for characterizing the polyelectrolyte gels used in Sec. V.

1. Degree of Cross-linking

A number of studies have reported gel transitions without determination of the degree of cross-linking. In other words, the cross-linking degree was estimated from the amount of cross-linking agents by assuming a complete gelation reaction; however, this is not realistic in many cases.

Elemental analysis, though it is classical, serves as an excellent tool for determining the degree of cross-linking when there are a few differences in the chemical compositions around the cross-linking point in the network. For example, this can be seen from the chemical structure of the LPEI network cross-linked with EGDGE (see Sec. IV.A.1). Taking into account 100 monomer units of the EGDGE-cross-linked LPEI chains (base form), the contents (in w/w%) of nitrogen (C_N) and carbon (C_C) can be expressed as functions of the number of cross-linking points per 100 monomer units (x) by the equations

$$C_N = \frac{100 m_N}{M_1(100 - x) + M_2 x} \times 100 \tag{10}$$

$$C_C = \frac{[2(100 - x) + 6x]m_C}{M_1(100 - x) + M_2 x} \times 100 \tag{11}$$

Here, m_N (14.01) and m_C (12.01), respectively, denote the atomic masses of nitrogen and carbon; M_1 (43.97 for C_2H_5N) and M_2 (138.17 for $C_6H_{12}O_2N$), respectively, are the molar masses of un-cross-linked and cross-linked monomer units of the polymers in the network. Since the elemental analysis for the dry gel gave C_N = 25.91% and C_C = 54.71% [27], we can estimate $x \sim 12$ for the gel sample. This value was a third the value estimated from the amount of EGDEG used in gelation.

For gel samples such as NIPA-AAc copolymer gels cross-linked by MBA and γ-rays, however, there is little difference in the chemical composition around the cross-linking point. Therefore the elemental analysis is not helpful. In such a case, one may recall the Flory–Rehner theory. Indeed, several studies have attempted to estimate the effective number of chains in a network (ν_e; see Sec. II.B) or the molecular weight between cross-links ($\bar{M}_c$) through equilibrium swelling experiments. For example, Bray and Merrill [65] made a modification of the Flory–Rehner equation by considering that the cross-links are introduced between polymer chains of number-average molecular weight ($\bar{M}_n$) as the polymer existed in a solution and its volume fraction is φ_r. They obtained

$$\frac{1}{\bar{M}_c} = \frac{2}{\bar{M}_n} - \frac{\dfrac{\bar{v}}{v_s}\left[\ln(1 - \varphi_s) + \varphi_s + \chi\varphi_s^2\right]}{\varphi_r\left[\left(\dfrac{\varphi_s}{\varphi_r}\right)^{1/3} - \dfrac{1}{2}\left(\dfrac{\varphi_s}{\varphi_r}\right)\right]} \tag{12}$$

where $\bar{v}$ denotes the specific volume of polymer, and v_s is the molar volume of solvent. In addition, φ_s (volume fraction of swollen gel) and φ_r (volume fraction of relaxed gel) were given by $\varphi_s = V_p/V_{g,s}$ and $\varphi_r = V_p/V_{g,r}$, where V_p, $V_{g,s}$, and $V_{g,r}$ are the volume of the dry polymer, the swollen gel, and the relaxed gel, respectively. For the cross-linking density (ρ_x in mol/cm^3), we may thus obtain

$$\rho_x = \frac{\nu_e}{V_p} = \frac{1}{\bar{v}}\left(\frac{1}{\bar{M}_c} - \frac{2}{\bar{M}_n}\right) = \frac{\dfrac{1}{v_s}\left[\ln(1 - \varphi_s) + \varphi_s + \chi\varphi_s^2\right]}{\varphi_r\left[\dfrac{1}{2}\left(\dfrac{\varphi_s}{\varphi_r}\right) - \left(\dfrac{\varphi_s}{\varphi_r}\right)^{1/3}\right]} \tag{13}$$

In experiments, V_p, $V_{g,r}$, and $V_{g,s}$ can be determined from the weight of gel samples under dry, relaxed, and swollen states. For this purpose, Peppas et al. [66] have utilized the following relations: $V_{g,r} = (w_{a,r} - w_{h,r})/\rho_h$, $V_{g,s} = (w_{a,s} - w_{h,s})/\rho_h$, and $V_p = \bar{v}w_{a,d}$, where $w_{a,r}$ is weight in air after gelation, $w_{h,r}$ is weight in *n*-heptane after gelation, $w_{a,s}$ is weight in air after swelling, $w_{h,s}$ is weight in *n*-heptane after swelling, and $w_{a,d}$ is weight in air after drying.

For determining the cross-linking degree by Eq. 12 or 13, the χ must be known for the polymer. Even if χ is determined for a polymer system, Flory–Rehner theory has been questioned due to the assumption of a Gaussian chain distribution (see Sec. II.C). Thus Peppas et al. [66] have made a modification by introducing the terms $\{1 - (\varphi_s/\varphi_r)^{2/3}/N\}^3$ and $\{1 + (\varphi_s/\varphi_r)^{1/3}/N\}^2$ (where $N = 2M_c/M_0$, and M_0 is the molecular weight of poly-

mer-repeating unit) into the numerator and denominator of Eq. 12, respectively, when they attempted to determine ρ_x for nonionic hydrogels of 2-hydroxyethyl methacrylate (HEMA) cross-linked with ethylene glycol dimethacrylate (EGDMA). Nevertheless, the Flory–Huggins theory based on a random-mixing lattice model, from which χ has been determined, is also questioned, as was mentioned in Sec. II.C.

Through measurements of the modules of elasticity for a gel, the cross-linking degree may be determined, but this is also based on a theoretical model. Thus it appears that chemical analyses such as elemental analysis of the dry LPEI gel would be a good way, from which the cross-linking density (in mol/cm^3) can be determined by $\rho_x = x/(100\bar{v}M_0)$. We may hope that polyelectrolyte gels whose cross-linking degree can be determined by chemical analysis would be used in the study of gel transitions, in particular in a quantitative comparison of experimental results with a theoretical prediction.

2. Acid–Base Equilibrium

The ionization process of polyacids with a base as well as of polybases with an acid can be studied by means of potentiometric titration. For polyelectrolyte gels, however, there is a rather difficult problem; for example, how to estimate the ''real'' acid–base equilibrium within the gel phase from the pH measurements of the outer solution. Thus no study has so far dealt with the potentiometric titration of polyelectrolyte gels, except for ion exchangers; i.e., a highly cross-linked polyelectrolyte gel. Nevertheless, we have demonstrated that the potentiometric titration is available for the investigation of ionization characteristics of acid or basic groups bound to a network [33]. We employed submicron gel particles with 70 mol% NIPA and 30 mol% AAc. Also employed were the bulk NIPA-AAc gel of a fine grind and the NIPA-AAc copolymer, both of which contain 30 mol% AAc. One might expect that use of the microgel would help to eliminate a general problem in the pH titration for gels; that is, the great difficulty in judging whether the H^+ and OH^- concentrations within the gel phase come to equilibrium with those in the aqueous bulk phase at different stages of the titration. The titration can be performed using a burette and a pH-meter equipped with a combination pH electrode.

Figure 4 shows typical titration curves with 0.1 M NaOH for two kinds of the NIPA-AAc gels as well as the corresponding copolymer in the absence and the presence of 0.1 M NaCl. The titration curves for the gels were obtained by plotting the pH of the outer medium against the titrant volume (V_t). A very clear end point was observed in each titration curve; thus the overall content of COOH was easily determined from V_t at the end point. There was little difference in the COOH content between the gels, as well

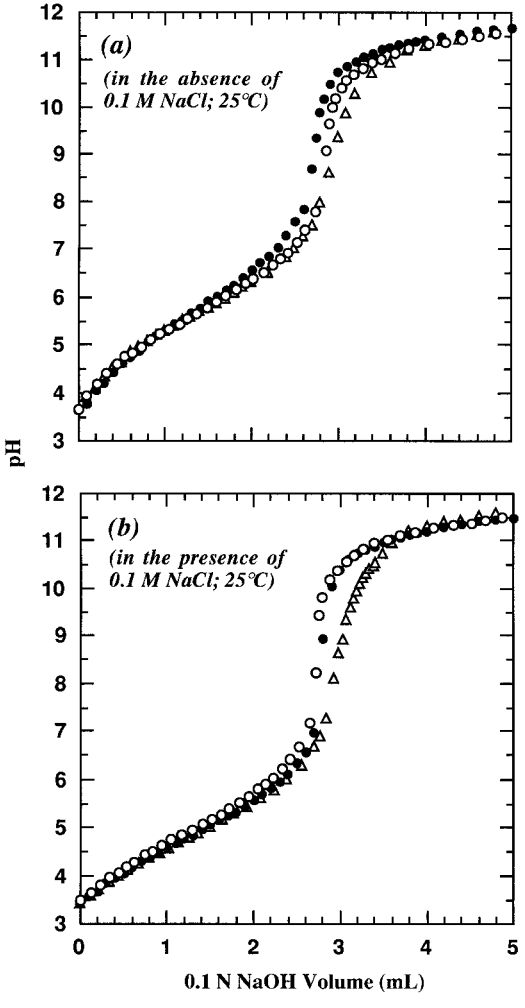

FIG. 4 Potentiometric titration curves with 0.1 M NaOH in the absence (a) and the presence (b) of 0.1 M NaCl for the copolymer (closed circles), the bulk gel (open triangles), and the microgel (open circles) at 25°C. (From Ref. 33.)

as between the gel and the copolymer. The same result was also obtained when titration was carried out at 35°C, the temperature of which is slightly higher than the phase transition temperature (T_v; ~33°C) of neutral NIPA gels or the lower critical solution temperature (LCST; ~31°C) of NIPA polymer (see Ref. 33).

Another piece of important information from Figure 4 is that the titration curves of the gels show a striking resemblance to that of the copolymer. From this, we may suggest that the dissociation of protons from the COOH groups bound to the linear polymer chain and the cross-linked polymer network is essentially the same. However, one might doubt whether the pH between the gel phase and the bulk solution with suspended gels was equilibrated or not. Taking this into account, we performed a back titration with HCl after the bulk or the microgel in the acid form was titrated with NaOH beyond the V_t at the end point. As can be seen from Figure 5, there was little difference in the results between the front and the back titration not only for the microgel but also for the bulk gel. This indicates that our titration data for both the gels do not include serious errors relating to a pH difference between the gel and the bulk phase.

3. Surfactant Uptake

We can convert neutral NIPA gels into a polyelectrolyte gel through the binding of surfactant molecules such as sodium dodecylbenzene sulfonate (NaDBS) and sodium dodecyl sulfate (SDS) [20]. As will be seen in Sec. V.B, the polyelectrolyte gel of this sort provides us with important infor-

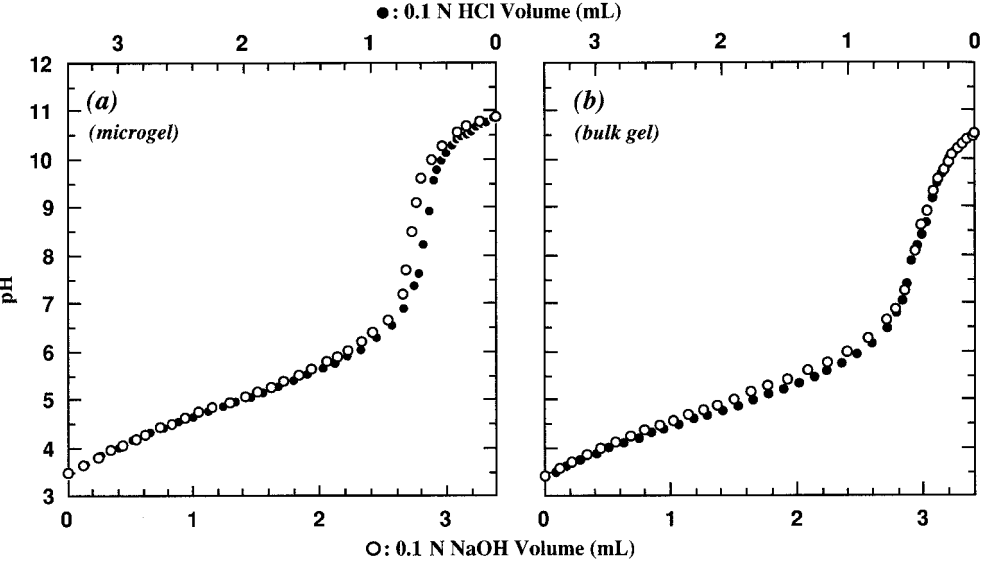

FIG. 5 Changes in pH during titrations of the microgel (a) and the bulk gel (b) with 0.1 M NaOH (open circles) followed by back-titration with 0.1 M HCl (closed circles); ionic strength = 0.1 (NaCl), 25°C. (From Ref. 33.)

mation about the main factor that swells the gel. Thus the gel should be characterized in terms of the overall charge density and charge distribution.

To determine the overall charge density, two experiments were carried out using cubic gels as well as cylindrical gels with different sizes. The surfactant uptake by the former was first measured in aqueous solutions containing different amounts of SDS or NaDBS as follows: the lyophilized cubic gels were introduced into a measuring flask and then allowed to swell with a small amount of distilled water. After adding the required amount of SDS or NaDBS solution to the flask, the volume of the aqueous phase containing the gels was precisely adjusted to 50 mL with distilled water. The flask was slowly shaken for more than one week (e.g., 10 days) at 25°C. The SDS concentration of the supernatant liquid after the incubation was determined by TOC analysis. In addition to this, we applied the spectrophotometric method using a calibration curve showing the relationship between NaDBS concentration and absorbance at 220 nm. There was a good agreement between both analytical methods (within $\pm 3\%$) [24].

To study the effects of gel size on the surfactant binding [26], we used lyophilized cylindrical gels that had been prepared in glass capillaries with different inner diameters (d_0) of 3, 5, and 10 mm and cut into lengths of 10 mm. Two types of gel samples were employed in the measurements, ''wet'' and ''dry'' gels. To prepare the wet gel, one lyophilized sample was accurately weighed and allowed to swell with pure water whose volume was double the gel volume in a small volumetric vial, prior to the addition of 0.1 mM NaDBS solution. In the case of the dry gel, the lyophilized sample was directly immersed in the NaDBS solution without the swelling with pure water. The volume ratio of the gel and the NaDBS solution was fixed to 1:10 throughout all the experiments. The incubation was allowed to continue at 25°C for 25 h as described above. The NaDBS concentration was determined at suitable time intervals with the spectrophotometric method.

4. Distribution of Bound Surfactant Molecules in Gels

A position-dependent change in the concentration of bound NaDBS molecules within the gel can be monitored directly by microscopic spectroscopy [26]. The wet and dry samples were obtained from lyophilized cylindrical gels (d_0 = 2, 3, and 4 mm and a length of 1 mm) with and without their swelling in pure water, respectively. The incubation was performed in an aqueous 10 mM NaDBS solution at 25°C for 10 days. After that, the gels with the adsorbed surfactant were cut with a microtome into disks with a thickness of ca. 0.2 μm. NaDBS is an appropriate surfactant for our purpose because it carries a phenyl group, which exhibits an absorption band in the UV range. In order to measure the position dependence of transmittance (PDT) for the sample gel disks with bound NaDBS, scanning at 261 nm

was performed from the right-hand to the left-hand end of each gel disk. The size of the beam going through the gel disks was fixed to 30 μm, which corresponds to about 1% of the diameters of the disks. We may also measure the PDT at 400 nm as control, because NaDBS has no absorption at 400 nm and therefore the transmittance at this wavelength varies depending on the sample thickness.

V. FINDINGS THROUGH EXPERIMENTS

A. Effect of Charge Density

Almost all the studies on the transition of polyelectrolyte gels have paid much attention to the effect of charge density. Historically, a pioneering paper [6] that referred to this effect was published by Tanaka and his coworkers. Since Tanaka [5] already reported his findings about an abrupt volume collapse of neutral MBA-cross-linked PAAm gels in acetone–water mixtures (see Sec. II), the gel of the same sort was again used as a starting material, to which the ionizable groups were introduced via partial hydrolysis of the amide groups with a base (BOH):

$$\sim CONH_2 + BOH \rightarrow \sim COO^- B^+ + NH_3$$

The swelling ratio of the gel at different stages of the hydrolysis was measured as a function of acetone concentration in acetone–water mixtures. The important findings from this experiment may be summarized as follows: (1) For short hydrolysis times of 0 to 1 day, the equilibrated gel volume changes continuously with the acetone concentration. (2) When the gel was hydrolyzed for 2 days, the swelling curve has a zero slope inflection point. (3) For longer hydrolysis times, the gel undergoes discrete transitions. (4) Volume change at the transition becomes larger, and the acetone concentration bringing about the transition becomes higher. By comparing these results with the theoretical prediction using Eq. 6 (see Figure 1 in Sec. II.A), Tanaka et al. claimed that an increase in the counterion concentration with increasing charge density raises the osmotic pressure of a gel and thereby the volume change at the transition becomes larger. Also claimed by them was that such an increase in the osmotic pressure lowers the reduced temperature (τ) in Eq. 6.

The above provides an explanation for a role of ionic charges bound to the polymer network in the gel transition, i.e., how the charge density affects the volume of an ionic gel at a transition as well as the transition threshold. However, the partially ionized PAAm gel is not a very good sample for discussing the effect of charge density on the reduced temperature as the transition threshold. Acetone acts as a ''poor'' solvent for PAAm or its hy-

drolysate; thus addition of acetone to a water solution of the polymer leads to a phase separation. Such a phase separation is, however, not observed in the water solution, even when lowering temperature to the freezing point of water. On molecular grounds, therefore, one may not say that the transition temperature falls with increasing charge density, even though an increase in the charge density lowers τ at the transition point. The temperature-induced transition in the neutral PAAm gel in a 40% acetone–water mixture, as previously reported by Tanaka [5], can be understood at the molecular level in terms of temperature effects on the interactions of polymer–water, polymer–acetone, and water–acetone. (To the best of the author's knowledge, the only ionic gel [17] with an interpenetrating polymer network consisting of PAAm and PAAc undergoes a temperature-induced transition in pure water; the transition temperature falls with increasing ionization degree.)

A polyelectrolyte gel system from which we may discuss the phase transition in terms of charge density as well as temperature has also been published by Tanaka et al. [13]. Then they used NIPA instead of AAm and synthesized the gels via aqueous redox copolymerization of NIPA with AAc (as sodium salt) in the presence of MBA as the cross-linker. As can be seen from Figure 6, the gel of this sort exhibited a clear effect of charge density on both the transition temperature and the gel volume at the transition; with

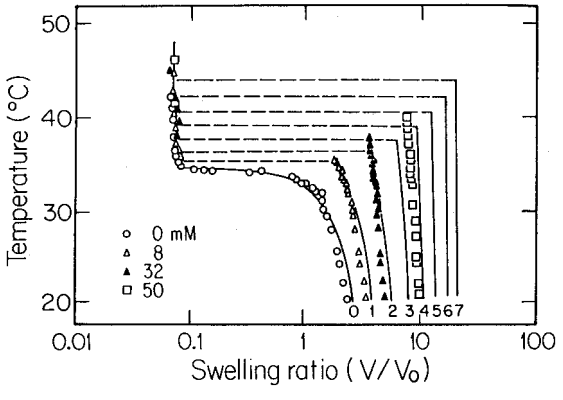

FIG. 6 Temperature dependence of swelling ratio for ionic NIPA gels with different amounts of COONa groups. Numbers in the figure denote the f value, the number of counterions per chain. The curve calculated with $f = 0$ was obtained so as to fit the calculation to the experimental data (circles) through choosing freely the parameters in Eq. 15, the values of which were then used in the calculation of the other curves ($f \geq 1$). Plots with different symbols are experimental results. (From Ref. 13 with a modification.)

increasing charge density, a marked increase was observed in the volume change at a transition as well as the transition temperature. (For neutral NIPA gels, it should be noted that Tanaka et al. mentioned in Ref. 13 a continuous volume change, although their previous paper [10] had reported a discontinuous transition; it is still unclear whether the neutral NIPA gel in pure water undergoes a continuous or a discontinuous volume change.)

Tanaka in collaboration with Hirotsu has attempted to compare the results in Figure 6 with theoretical swelling curves, the calculation of which was performed through a modification of Eq. 6 by considering that the temperature dependence of the term $\Delta F/kT$ (i.e., χ parameter) can be rewritten as

$$\chi = \frac{\Delta F}{2kT} = \frac{\Delta H - T\Delta S}{2kT} \tag{14}$$

Thus Eq. 6 becomes

$$\frac{1}{T} = \frac{\Delta S}{\Delta H} + \frac{k}{\Delta H}\left\{\frac{\nu v_s}{N_A \varphi^2}\left[(2f + 1)\left(\frac{\varphi}{\varphi_0}\right) - 2\left(\frac{\varphi}{\varphi_0}\right)^{1/3}\right] + 1 + \frac{\varphi}{2} + \frac{2\ln(1 - \varphi)}{\varphi^2}\right\} \tag{15}$$

In calculating the swelling ratio with a relation of $V/V_0 = \varphi_0/\varphi = (d/d_0)^3$, where d is equilibrium gel diameter and d_0 (1.35 mm) is a gel diameter at the preparation, each parameter in Eq. 15 was estimated as follows: (1) φ_0 ($\sim$0.07) from the experimental asymptotic value of V/V_0 at high temperatures; (2) ν (1×10^{23} L^{-1}) from the amount of MBA in the gel preparation; (3) ΔH (-8.7×10^{-14} erg) from the literature (Bulletin of Research Institute for Polymers and Textiles, in Japanese, No. 114, 1984). (It should be noted that neutral NIPA gels in pure water exhibit an endothermic shrinking upon heating, $\Delta H > 0$, but exothermic swelling upon cooling, $\Delta H < 0$ [67]; therefore, Tanaka's calculation focuses on the swelling transition.) In addition to these, it was assumed that since the transition temperature is determined principally by the ratio $\Delta H/\Delta S$, ΔS is approximately equal to $\Delta H/T$, and the curvature of a swelling curve is mainly determined by the value of ΔH. Taking these into account, the theoretical swelling curve was first obtained for the neutral gel; however, the estimated theoretical fit was rather poor. For example, the calculated curve predicts much smoother change than the measured curve near the transition region. Thus, as the second approach, an attempt was made to estimate the parameters from the experimental data for the neutral gel by a curve fitting technique. The results of the best fit gave the following values: $\Delta H = -5.4 \times 10^{-11}$ erg, $\Delta S = -1.8 \times 10^{-13}$ erg$\cdot$K^{-1}, $\nu = 1.2 \times 10^{24}$L^{-1}, and $\varphi_0 = 0.07$. Using these parameters, the swelling curves for ionic NIPA gels with COONa (8 to 50 mM in preparation) were

calculated (see the solid curves in Figure 6). The calculated curves well reproduced the experimental data for the ionic gels; however, the values obtained from the two-parameter fit for ΔH and ν were significantly greater than the values estimated from independent measurements. For this discrepancy, the following reasons were pointed out: In modeling, it did not consider the effects of loops, free branches, non-Gaussian properties of chains (due to self-avoiding random walk, and stretching limit due to finite length of the chains), polydispersity of chains, etc. For the particular case of ionic gels, it also neglected the charge–charge interaction and counterion condensation, which may affect the actual value of osmotic pressure by counterions.

Prior to discussing the disagreement between prediction and observation in connection with the above factors, we have to answer the question why ionic gels collapse with rising temperature. As can be predicted from Eq. 4, the osmotic pressure should be strengthened not only by concentration of counterions but also by temperature. In order to resolve this conflict, several studies (e.g., see Ref. 42) have assumed ''hydrophobic interaction'' as a force being in competition with the osmotic pressure arising from counterions. Nevertheless, it is preferable to verify experimentally whether the concept of osmotic pressure is adequate. This subject will be discussed in the following section.

B. Effects of Charge Distributions Observed in Ionic Surfactant–Bound NIPA Gels

1. Historical Backgrounds

Since the earliest report by Eliassaf [68] on the interactions of the NIPA polymer with sodium dodecyl sulfate (SDS), various studies have focused on this subject. In the case of NIPA gels, however, only a few studies [20,24,69–71] have dealt with surfactant interactions in aqueous media. These studies demonstrated that ionic surfactants such as SDS tend to raise the transition temperature (T_v), bringing about a discontinuous volume change, and to increase the gel volume over a wide temperature range $<T_v$. A similar result has also been obtained from the study on the interaction of surfactants with NIPA microgel latexes as a function of temperature [58]. These results were explained by assuming that the surfactant molecules bind to the polymer network of NIPA, converting the gel into a polyelectrolyte gel. A qualitative discussion was given in terms of the Flory theory with modifications to account for the free energy of association of the surfactant molecules with the gel network and surfactant self-association [20]. The micellar formation of surfactants within the gel phase was then considered, because the micellization had been suggested by Zhang et al. [70] based on results from small-angle neutron scattering (SANS) for a SDS-NIPA gel

system. (It should be noted that the original work of the binding of surfactant micelles to a polymer of NIPA was carried out by Schild and Tirrell [72], although Zhang et al. did not cite it in their paper [70].) In these previous works [20,69–71], however, little attention was paid to investigating the amount of surfactant binding to the gels. In other words, the conclusions were drawn mainly from swelling measurements, although several studies employed additional experimental techniques such as SANS [70] and thermal analysis [69,71] using a differential scanning calorimeter (DSC).

Kokufuta et al. [24] have presented highly accurate quantitative measurements of the uptake (or adsorption) of an ionic surfactant, sodium dodecylbenzene sulfonate (NaDBS), by NIPA gels. NaDBS was used because it has UV adsorption at ca. 220 nm, which allows an accurate determination of the surfactant uptake by the gels. Detailed analyses of the experimental data suggest that NaDBS molecules are bound only to the region in the near vicinity of the gel surface but fail to penetrate into the core of the gel phase. Such an ionic gel with ''locally'' bound surfactant seems to be considerably different from the usual polyelectrolyte gels with regard to the phase transition. Therefore, the gel of this sort would provide a key to learning the role of ionic charges in the gel transition on the molecular level.

2. Swelling Characteristics of NIPA Gels in SDS and NaDBS Solutions

There seems to be a similarity between the surfactant effects on the volume phase transition of NIPA gels and the LCST-type phase separation of NIPA polymers. In the case of the polymers, it is known that the binding of surfactant micelles to the polymer causes an elevation of the LCST as a result of electrostatic repulsion between the charges of polymer-bound micelles. The concentration at which such a surfactant binding takes place has been referred to as the critical aggregation concentration (CAC). The CAC (0.79 mM) for SDS in the NIPA polymer solution was determined by Schild and Tirrell using the fluorescence probe method [72]. Saito et al. reported the observation of the CAC for SDS in the NIPA gel system [71], although they did not mention the CAC in Ref. 69 dealing with the same system. Saito et al. applied the DSC method for monitoring the changes in T_v for the gel and in LCST for the polymer and obtained a relatively broad curve of T_v or LCST against SDS concentration. Based solely on these results, it is rather difficult to judge whether the CAC in the polymer agrees with that in the gel system. In addition, it is questionable whether the CAC can be defined for the gel system because the surfactant binding mechanism remains unclear at the present stage. Thus the effects of SDS and NaDBS on the volume phase transition of NIPA gels were studied over a wide range (0–40 mM) of surfactant concentration without considering the CAC.

Figures 7 and 8 show the changes in T_v and swelling ratio (V/V_c) with initial surfactant concentrations (C_i), respectively. SDS and NaDBS affect the thermally induced phase transition of the NIPA gel; both T_v and V/V_c increase remarkably with increasing C_i, as reported in previous studies [20,24,69–71]. The observed effects can be understood by assuming that both SDS and NaDBS bind to the polymer network within the gel phase through hydrophobic interaction, subsequently converting an otherwise neutral NIPA gel into a polyelectrolyte gel. These acquired network charges and counterions associated with the charges exert an extraosmotic pressure on the network, so that both the transition temperature and the gel volume increase. (Although this explanation has been widely accepted, this chapter has raised questions with regard to the assumption of osmotic pressure.)

Now we will focus on why a difference due to the type of surfactant appeared in the swelling ratio (Figure 8) but not in the transition temperature (Figure 7). We first studied the SDS and NaDBS uptake by the gel as a function of C_i. The results obtained are shown in Figure 9. We found that the saturated amount of surfactant uptake at $C_i > 10$ mM was larger for SDS than for NaDBS. However, we cannot simply relate this result to the observed difference in V/V_c between SDS and NaDBS, because an increase in the charge density for polyelectrolyte gels, such as NIPA-NaAAc gels, brings about simultaneous increases in both transition temperature and gel volume.

To demonstrate this point more definitely, we compared the present results with those for the NIPA-NaAAc gels with different NaAAc contents. The

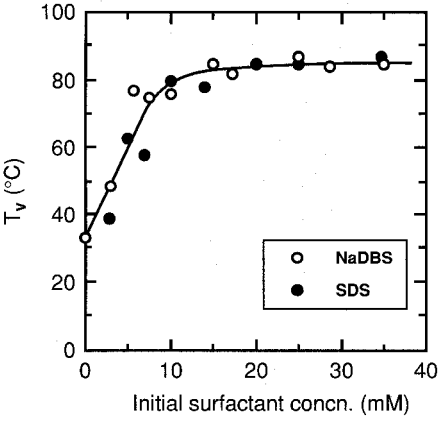

FIG. 7 Dependence of volume phase transition temperature (T_v) of NIPA gel (cylindrically shaped wet sample with $d_0 = 0.7$ mm) on initial surfactant concentration. (From Ref. 26.)

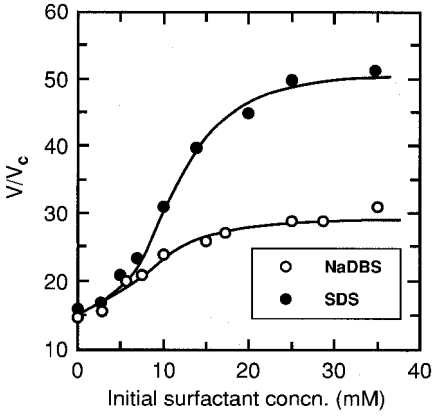

FIG. 8 Changes in the swelling ratio (V/V_c) of the cylindrically shaped wet NIPA gel (d_0 = 0.7 mm) with initial surfactant concentration at 25°C. V_c denotes the gel volume in the fully collapsed state determined for each sample in pure water at 50°C. (From Ref. 26.)

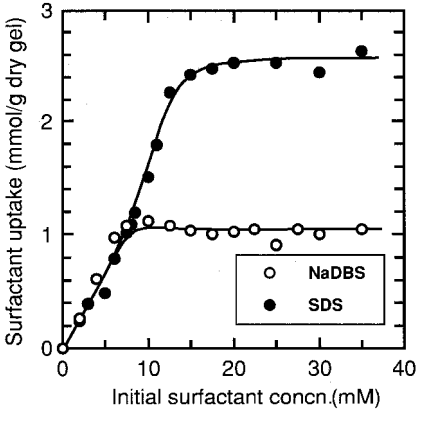

FIG. 9 Changes in surfactant uptake with initial surfactant concentration at 25°C. We used a cubic gel with sides of 2 ± 0.5 mm. It should be noted that these uptake data can be compared with the swelling data (T_v and V/V_c) in a qualitative but not in a quantitative way because the size of the gel samples can be regarded as the primary factor affecting the uptake amount. (From Ref. 26.)

''overall'' charge density expressed in moles of bound surfactant per one mole of monomer unit in the gel may be calculated from the saturated amount of surfactant binding at $C_i > 10$ mM; i.e., 0.29 for the gel with SDS and 0.12 for the gel with NaDBS. This means that the NaDBS and SDS-bound gels apparently correspond to polyelectrolyte gels with 10 and 30 mol% ionic groups, respectively. Matsuo and Tanaka [53] measured the temperature dependence of the swelling degree for spherical copolymer gels consisting of NIPA (100 to 82 mol%) and NaAAc (0 to 18 mol%) in pure water. They reported that T_v increased from 34 to 60°C (shrinking process) when the NaAAc content was increased from 0 to 18 mol%. This increase in the NaAAc content simultaneously changed V/V_c from 16 to 510 at 25°C. It should be noted that there are large discrepancies in T_v and V/V_c between the NaAAc-copolymerized and surfactant-bound NIPA gels. For example, T_v (60°C) for a NIPA/NaAAc gel with 18 mol% of NaAAc is lower than that (85°C) for a NIPA gel with 10 mol% NaDBS, although the charge density for the former is larger than that for the latter. In contrast, V/V_c (510) for the same 18 mol% NaAAc-containing gel is much larger than that (51) for a NIPA gel with 30 mol% SDS. The same discrepancy can be found by comparing the results for the surfactant-bound gels with those for cylindrical NIPA–NaAAc gels reported by Hirotsu et al. [13] (see Figure 6).

In the above discussion, we have not considered how surfactant molecules adsorbed on or penetrated into the gels. It has been suggested that NaDBS molecules are bound only to the region in the near vicinity of the gel surface but fail to penetrate into its core [24]. This naturally implies that the charges due to the bound surfactants are spread unevenly over the NIPA polymer network. In the case of NIPA–NaAAc gels, on the other hand, we can expect the COONa groups to be uniformly distributed over the polymer networks. Therefore it is not surprising that we cannot explain all aspects of the behavior of surfactant-bound NIPA gels based only on the analogy to those of NIPA gels with copolymerized NaAAc.

3. Size Dependence of NaDBS Uptake

Gels that are usually employed in studies of surfactant uptake are previously saturated with the same solvent as that of surfactant solutions. When such gels are immersed in a surfactant solution, the binding should take place through the gel surface. The size and shape of the gel are then regarded as the primary factor directly affecting the uptake amount because it depends on the available surface area of the gel.

Taking the above into account, kinetic studies of NaDBS uptake were performed using cylindrical gels with 3, 5, and 10 mm in diameter (d_0) and 10 mm in length (l). We employed a dry gel free of water, in addition to the usual wet gel. The results are shown in Figure 10a for the wet gel and

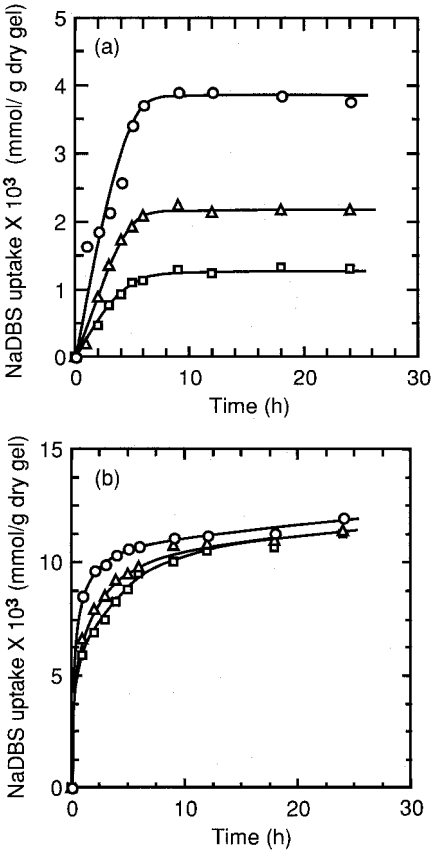

FIG. 10 Time courses of NaDBS uptake by various cylindrically shaped wet and dry gels. Circles denote d_0 = 3 mm, triangles 5 mm, and squares 10 mm, with a fixed 10 mm length. (a) Wet gels for which surfactant uptake was given in dry weight base; (b) dry gels for which surfactant uptake was given in dry weight base; (c) wet gels for which surfactant uptake was given in surface area. (From Ref. 26.)

in Figure 10b for the dry gel. A marked difference between both types of gels was observed in the size dependence of NaDBS uptake when its amount was expressed in moles per unit of dry mass: a large change in the uptake amount appeared in the wet gel while the change was negligibly small in the dry gel. This difference may be attributed to where the binding of the surfactant molecules takes place within the gel phase. In the case of the dry gel, the absorption sets in as soon as it is immersed in the surfactant solution, which causes the scattering of surfactant molecules all over the gel phase.

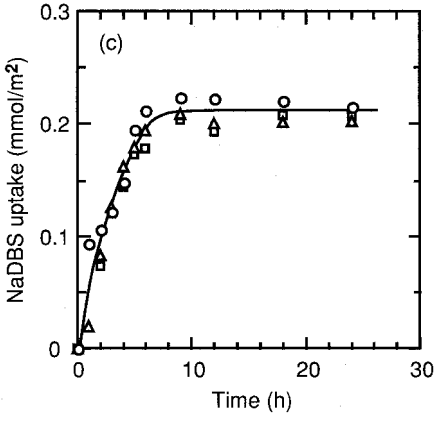

FIG. 10 *Continued.*

This makes it possible for the surfactant molecules to bind to the polymer network throughout the gel phase. In the wet gel system, however, the surfactant binding begins at the surface of the gel because it already contains a saturated amount of water as the solvent. Even after a certain amount of surfactant molecules have penetrated into the gel, the binding will continue through its surface. This means that in the wet gel system the effect of size on the uptake amount can be eliminated if we express it by the number of moles per unit surface area. As shown in Figure 10c, this is actually the case. The surface area (S) was then calculated by $S = \pi d_0(l + d_0/2)$: 108, 196, and 471 mm^2 for the gels with d_0 = 3, 5, and 10 mm, respectively.

A detailed comparison of the surfactant uptake by the wet and dry gels provides a possible interpretation for the difference between SDS and NaDBS observed in the surfactant-induced changes in the transition temperature and swelling ratio of the NIPA gels (see Figures 7 and 8). The amount of NaDBS uptake by the wet and dry gels with the same d_0 reached certain saturation levels after 6 hours, but the level for the former was substantially lower than that for the latter. This implies that the NaDBS concentration within the wet gel is not even throughout its entire volume. From the above discussion, it is reasonable to assume that the NaDBS concentration is high in the vicinity of the gel surface. This situation has been schematically represented in Figure 11, in which a horizontal sectional view of a cylindrical gel after attainment of a saturated level of surfactant uptake is illustrated together with a concentration profile of bound surfactant. Also included in this figure is the temperature dependence of the swelling ratio

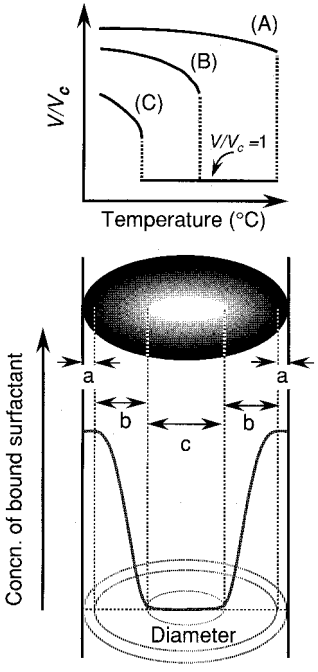

FIG. 11 Schematic representation for a cylindrical gel with inhomogeneously bound surfactant molecules. Swelling curve A corresponds to region a with a saturated level of bound surfactant; curve B represents a limited section of region b in which the surfactant concentration gradually decreases towards the center; curve C is for region c in which there is no bound surfactant (i.e., corresponding to neutral gel). (From Ref. 26.)

for three typical regions with different levels of surfactant binding. When considering Figure 11, it seems that a NIPA gel with bound surfactant resembles a sort of ''composite'' polyelectrolyte gel consisting of cross-linked polymer chains with different amounts of ionizable groups. Since the T_v of nonionic NIPA gels is lower than that of ionic NIPA gels, region c, free of bound surfactant molecules, should collapse first with rising temperature, while regions a and b should remain in the swollen state. We defined as T_v the temperature at which a gel discontinuously and completely collapses; therefore the experimentally determined T_v is primarily governed by the degree of ionization due to the surfactant binding in region a but not in regions b and c. Since region a is saturated by surfactant molecules, its ionization degree is independent of the kind of surfactant. As a result, little

difference was observed in the curves of T_v vs. C_i for SDS and NaDBS (Figure 7). However, the swelling ratios at temperatures $<T_v$ are strongly affected by changes in the degree of ionization in region b. Even if region a is maintained at the same level of ionization in both the SDS and NaDBS-bound gels, the level in region b for the former is higher than that for the latter. This is evident from Figure 9, which indicates that NIPA gels tend to bind SDS rather than NaDBS. Thus the SDS-bound gel exhibited a high swelling degree compared with the NaDBS-bound gel (see Figure 8).

4. Determination of Special Distribution of NaDBS Concentration in Gels

The measurement of the special distribution of surfactant concentration within the gel phase should provide direct evidence for the local surfactant binding expected in the previous sections. The position dependence of transmittance (PDT) for the sample gel disks with bound NaDBS is shown in Figure 12, in which PDTs a, b, and c were obtained using wet gels with d_0 = 4, 3, and 2 mm, respectively; they had fully swollen in pure water prior to contact with the NaDBS solution. A dry gel with d_0 = 2 mm, which had been directly treated with the surfactant solution without swelling procedure, was used for the measurement of PDT d.

In PDTs a to c, a rapid decrease in transmittance at both ends of each sample was observed when using the wavelength 261 nm. However, the transmittance increased gradually and became constant when the scanning point approached the central core of the gel disk. On the other hand, the transmittance at 400 nm was almost constant, independent of the position. Therefore it is evident that the surfactant molecules bond strongly only around the gel walls. This conclusion can be supported by PDT d for the dry gel, in which we did not observe specific position-dependent changes in transmittance at 261 nm. In the case of the dry gel, the surfactant solution permeated throughout the gel phase, allowing the surfactant molecules to bind to the network without distribution. This brought about a marked difference in the diameters of the surfactant-bound wet and dry gels; i.e., the distance between the right- and left-hand ends of the dry gel was larger than that of the wet gel, both of which were 2 mm before the surfactant binding.

The observed inhomogeneous binding of NaDBS within the wet gel can be understood by taking into account the generation of a Donnan potential due to the surfactant bond. When the wet gel comes in contact with the surfactant solution, the NaDBS molecules bind in the near vicinity of the gel surface. Through such binding, the surface carries the negative charges, resulting in a high Donnan potential, which makes further diffusion of the NaDBS anions more difficult.

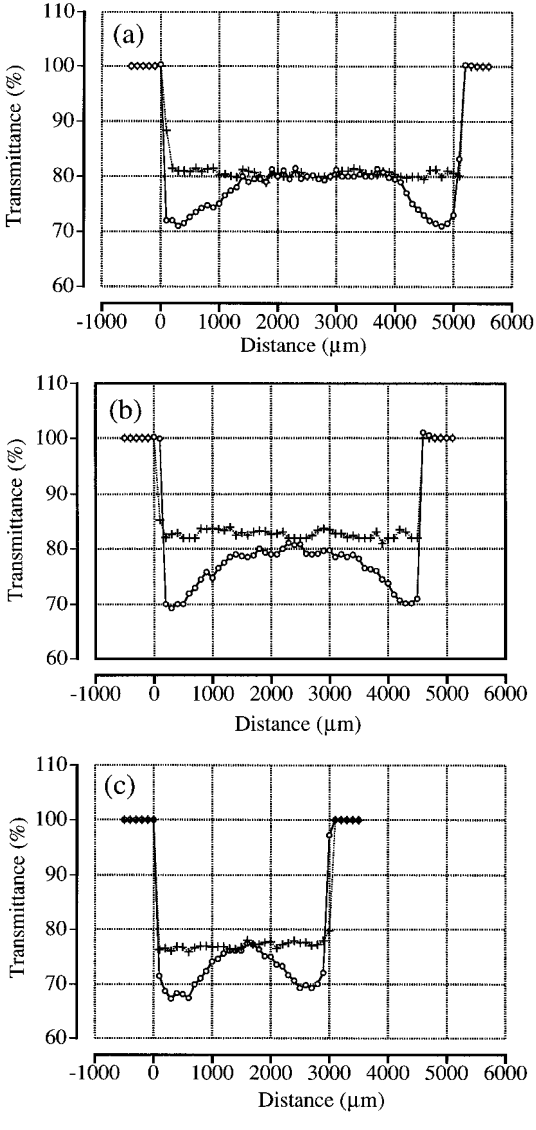

FIG. 12 Position dependence of transmittance (PDT) for cylindrical wet gel disks with diameters d_0 = 4 mm (a), 3 mm (b), and 2 mm (c), and for a cylindrical dry gel disk with d_0 = 2 mm (d). Circles and plus signs, respectively, denote 261 and 400 nm. (From Ref. 26.)

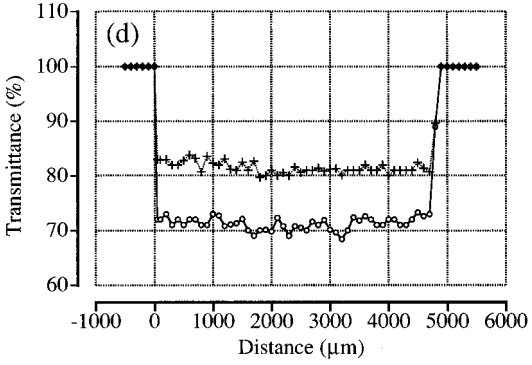

FIG. 12 *Continued.*

Another important finding in PDTs a to c is that the magnitude of the characteristic change in transmittance around both ends of the gel disk is independent of its size. This means that the surfactant binding occurs within specific domains of the gel phase. In other words, the concentration distribution of bound surfactant as illustrated in Figure 11 is uniquely determined by the affinity of the surfactant toward the polymer as the constituent of the gel. If hydrophobic interaction between the surfactant and the NIPA polymer is the primary factor determining the surfactant binding, NaDBS rather than SDS would exhibit a high affinity toward the polymer. This leads to the formation of a densely packed surfactant layer within region b in Figure 11. It is reasonable to consider that such a layer of NaDBS generates a Donnan potential higher than that of SDS. As a result, we observed that the uptake amount of NaDBS by NIPA gels was smaller than that of SDS.

5. Behavior of the Surfactant-Bound NIPA Gel as a Polyelectrolyte Gel

As mentioned above, the NIPA gel with bound SDS or NaDBS behaved as a polyelectrolyte gel. However, the volume phase transition was obviously affected by the inhomogeneously distributed charges. If the osmotic pressure due to mobile counterions plays an important role in the volume phase transition of polyelectrolyte gels, one would expect that there is little influence of the inhomogeneity of charge distributions within the gel. Thus the present results may provide a key to determine whether the volume phase transition of polyelectrolyte gels is governed by osmotic pressure. The same conclusion has been obtained from the study of the surfactant binding to the NIPA polymer networks within a very narrow domain, such as a submicron-sized gel particle [30].

C. Effect of AAc Distribution in NIPA Networks

We have demonstrated that an inhomogeneous binding of surfactants brings about a different swelling behavior from that of the usual ionic gels prepared via random copolymerization of NIPA and acrylic acid (AAc). It is thus interesting to examine the effect of the charge distribution (i.e., the distribution of AAc residues in the network) on the swelling behavior of NIPA–AAc gels. If the concept of osmotic pressure is correct, one might not observe any difference in the swelling curves between the two kinds of ionic NIPA–AAc gels into which the AAc residues were homogeneously or inhomogeneously introduced. The reason for this is that counterions to the ionized groups should move freely within the gel phase surrounded by the Donnan potential barrier and thereby increase the osmotic pressure acting to swell the gel (see Sec. II.A). The object of this section is to examine the swelling behavior of NIPA–AAc gels with the same amount but a different distribution of AAc; through this examination we can discuss the validity of the concept of osmotic pressure on the molecular level.

1. Design of NIPA–AAc Gels with Different Charge Distributions

For the present purpose, we designed four ionic gels (Gel I–IV) composed of NIPA and AAc residues. The AAc distributions within the polymer network of these gel samples may be classified into three schemes as shown in Figure 13. The preparation methods considered are as follows: (1) for Gel I, the redox polymerization of an aqueous solution containing NIPA, AAc, and MBA (cross-linker), which can be initiated by a pair of APS and TMED; (2) for Gel II, the physical entrapment of PAAc by an MBA-cross-linked NIPA gel, the performance of which is based on the same method employed in (1) except for the use of PAAc instead of the AAc monomer; (3) for Gel III, the gelation of an aqueous solution containing PNIPA and PAAc by γ-rays from ^{60}Co under conditions where no complexation occurs between

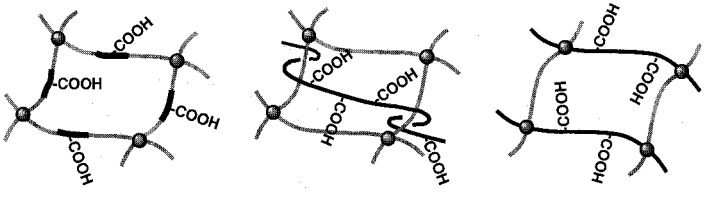

FIG. 13 Schematic illustration of four polyelectrolyte gels consisting of NIPA and AAc residues. (From Ref. 28.)

PNIPA and PAAc; (4) for Gel IV, whose AAc distribution may be expected to be similar to that of Gel I, the γ-ray irradiation of an aqueous solution of a copolymer of NIPA and AAc, i.e., copoly(NIPA, AAc).

2. Swelling Curves for Gels I–IV

Figure 14 shows the temperature dependence of the normalized equilibrium diameters (d/d_0) at pHs 3 and 10 for Gels I to IV. The normalization of each

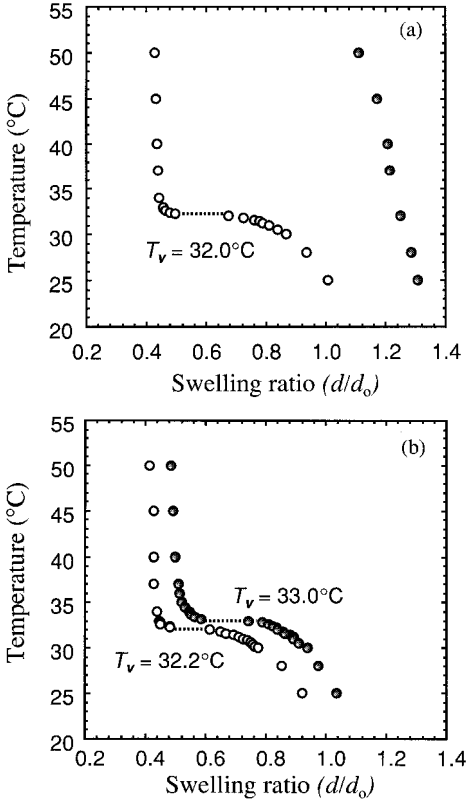

FIG. 14 Temperature dependence of normalized equilibrium diameters (d/d_0) at pHs 3 (open circles) and 10 (shadowed circles) for four polyelectrolyte gels consisting of NIPA and AAc residues: (a) Gel I; (b) Gel II; (c) Gel III; (d) Gel IV. PAAc with $\bar{M}_w = 4.5 \times 10^5$ was used for the preparation of Gels II and III. Dashed line indicates a discontinuous volume phase transition at a temperature (T_v) at which we observed a transient pattern in both swelling and shrinking processes and thereby were not able to measure d. Such a transient pattern was not observed in the measurements for Gel III at pH 3, suggesting a continuous transition. (From Ref. 28.)

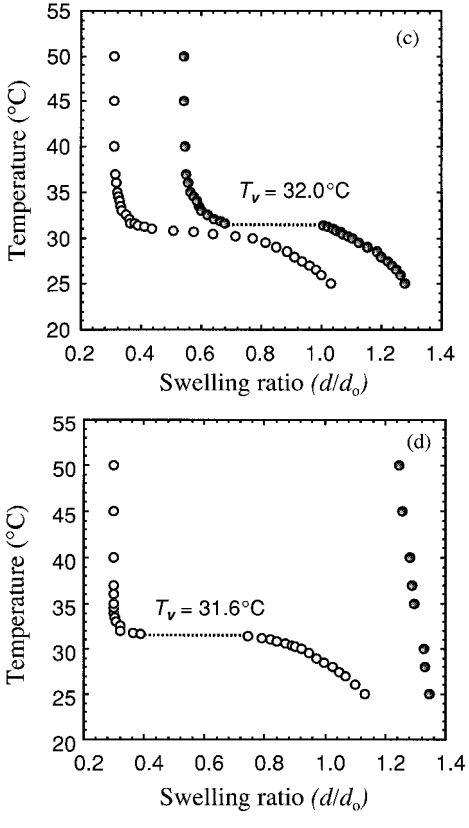

FIG. 14 *Continued.*

observed equilibrium diameter (d) was performed using the inner diameter (d_0) of the capillary utilized in the gel preparation. It was found that Gels I and IV, with a random distribution of the AAc residues, exhibited a similar volume phase transition when varying the temperature at pHs 3 and 10. A similarity was also observed in Gels II and III with the locally distributed AAc residues. Therefore the volume phase transitions for Gels I to IV are divided into two different classes when taking into account the distribution of the AAc residues. In particular, at pH 10 at which the COOH groups bound to the AAc residues are ionized ($COOH \rightarrow COO^- + H^+$), there is a marked difference due to the AAc distribution; the localized COO^- ions are not effective in preventing the thermally induced gel collapse at temperatures above the volume phase transition temperature (T_v). This indicates an effect

of the ''charge distribution'' in the network on the phase transition of ionic gels.

The phase separation of PNIPA in pure water at the lower critical solution temperature (LCST) was generally understood by considering both hydrogen bonding and hydrophobic effects [16]. Since there was little disagreement between the T_v for the usual nonionic NIPA gels and the LCST for PNIPA when the measurements were performed in the same solvent, Schild has surmised a similar molecular mechanism for the phase separation and the volume transition (see page 211 of Ref. 16). For Gels II and III composed of 90% (in unit mole base) of MBA-cross-linked ''pure'' NIPA chains, it is predictable that their phase transition behaviors are not so different from those of nonionic NIPA gels or PNIPA, even at pH 10 where the incorporated PAAc chains (10% in unit mole base) are ionized. Indeed, at pH 10 Gels II and III underwent a volume phase transition at temperatures near to the T_v for nonionic NIPA gels or the LCST for PNIPA.

A more detailed interpretation could be made when taking into account the mechanism of microphase separation of weakly charged polyelectrolytes in poor solvents that has been proposed by Borue and Erukhimovich [73] as well as by Dormidontova et al. [74]. According to this, it appears that microphase separation takes place at T_v; i.e., the NIPA chains within Gels II and III collapse to form hydrophobic ''micromicellelike'' aggregates surrounded by water-rich domains including both the ionized PAAc chains and their corresponding counterions (NH_4^+) at pH 10. The microphase separation mechanism also makes it possible for us to understand the results of Gels I and IV. For both gels, the NIPA and AAc monomer residues should be intermixed in the network; therefore the dissociation of the COOH groups at pH 10 strongly hinders the formation of hydrophobic aggregates not only through an increase in the hydrophilicity due to the COO^- plus NH_4^+ ions but also through the Coulomb repulsion between the COO^- ions. A similar molecular mechanism may be applied to explain the fact that at pH 10 copoly(NIPA, AAc) does not undergo phase separation, even at 50°C. Consequently, these discussions lead us to conclude that the volume transition of ionic gels, at least in our gels, is no longer explainable in terms of the concept of osmotic pressure.

Nevertheless, one more aspect to be taken into account when analyzing the present results is the Manning-type condensation of counterions, which has been neglected in previous theories (see Sec. II) as pointed out by Grosberg and Khokhlov [75]. For Gels II and III at pH 10, many of the counterions are condensed around the charged PAAc ions, and hence the osmotic pressure may not be generated to swell the gel. However, for Gels I and IV, in which the charged AAc residues are randomly distributed, many of the counterions are free from condensation and mobile at pH 10. Therefore,

their substantial contribution to the osmotic pressure should allow the gel to swell over a wide temperature range; in other words, we can again conclude that the osmotic pressure plays an important role in the volume phase transition of ionic gels.

The above discussions have led to conflicting conclusions. When carefully examining the swelling curves in Figure 14, however, one should not forget that the swelling curves at pH 10 for Gels II and III are shifted to the right-hand side (i.e., high degree of swelling) over all the temperatures measured. This suggests the existence of a microphase within which the NIPA chains around the charged PAAc fail to form hydrophobic aggregates via the collapse transition at temperatures $>T_v$. Thus our attention will be focused on the effect of the charged or uncharged PAAc chains incorporated into the NIPA gel on its volume transition.

3. Effect of the Molecular Weight of Entrapped PAAc within Gel II

If the osmotic pressure due to mobile counterions plays an important role in the volume phase transition of NIPA–AAc gels, one would expect to observe either one of the following: (1) little change in the gel volume caused by the molecular weight of the PAAc ions entrapped within the cross-linked NIPA chains; or (2) an increase in the molecular weight leading to the tendency for the gel to collapse due to a decrease in the entropy of the counterions. Consequently, the study of the swelling behavior of Gel II with entrapped PAAc of different molecular weights may provide a key to determining whether the volume phase transition of NIPA–AAc gels is governed by microphase separation or by osmotic pressure.

Figure 15 shows changes in the swelling curves of Gel II at pHs 3 and 10 caused by the molecular weights of the entrapped PAAc chains. It can be seen that the increase in the molecular weight at pH 10 brought about an increase in the gel volume over the temperature range of 25°C to 50°C. This result evidently suggests little contribution of the osmotic pressure to the swelling of a polyelectrolyte gel consisting of the NIPA–AAc system. In other words, the observed results may be understood in connection with the microphase separation mechanism rather than the contribution of osmotic pressure; the increase in the molecular weight of the entrapped PAAc ions leads to the formation of larger water-rich regions due to the COO^- ions around the water-unfriendly hydrophobic aggregates of the NIPA chains, and therefore the swelling of the gel with high-molecular-weight PAAc ions should increase.

Another important feature of Figure 15 is that, at pH 3 and at temperatures $<T_v$, the gel volume decreased with increasing molecular weight of the en-

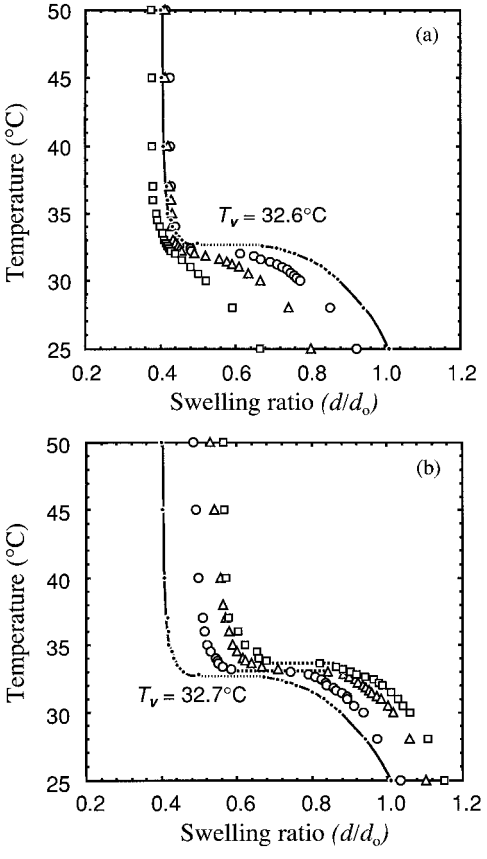

FIG. 15 Effect of the molecular weight of the entrapped PAAc on the normalized equilibrium diameters (d/d_0) for Gel II at pHs 3 (a) and 10 (b). $\bar{M}_w$: (○) 9×10^4; (△) 4.5×10^5; (□) 1.25×10^6. Swelling curves (small solid circles) for the neutral NIPA gel (T_v = 32.6°C at pH 3 and 32.7°C at pH 10) are shown in Fig. 15a and b as the standard. The increase in the molecular weight alters the transition at pH 3 from a discontinuous to a continuous type accompanying a decrease in T_v, whereas at pH 10 it leads to a discontinuous transition with an increase in T_v. (From Ref. 28.)

trapped PAAc with the nonionized COOH groups. A possible interpretation of this result is the increase in the cross-linking points by the formation of hydrogen bonds between the NIPA and AAc residues. In order to confirm this assumption, we attempted to examine the temperature-induced swelling changes for Gels I and III in the presence and absence of 4 M urea at pH

3. However, we found that urea shifts both the LCST of aqueous NIPA solutions and the T_v of NIPA gels to a low-temperature range. We therefore discontinued this experiment and tried to find another approach to study the formation of hydrogen bonds between the NIPA and AAc chains (see below).

4. Complexation of PNIPA and PAAc at pH 3

Our preliminary experiments showed that a mixed solution of PNIPA and PAAc was transparent under alkaline pH conditions but became turbid under acidic conditions, where most of the PAAc-bound COO^- groups are protonated. Moreover, the acidic mixture turned from opaque to transparent by the addition of 4 M urea and upon cooling, while such a change did not take place in the absence of urea. These results suggest the complexation of PNIPA with PAAc via hydrogen bonding between —COOH and —CONH—groups; for example,

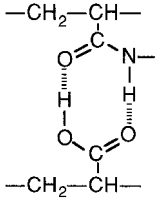

We thus assumed that dynamic light scattering (DLS) would be an appropriate approach in order to carry out a quantitative study on this kind of complexation.

As mentioned above, however, a decrease in the LCST was observed when urea was added to an aqueous PNIPA solution. We thus tried to determine the LCSTs of both the PNIPA solution and the PNIPA-PAAc mixture in the presence of 4 M urea (Table 2). It is generally believed that urea breaks up the hydrogen bonds between solute molecules and also disrupts the cluster structure of water molecules (''structure breaking effect''). The latter brings about a weakening of the hydrophobic interaction between solute molecules (e.g., see Ref. 76). In the case of an aqueous PNIPA system, however, the addition of urea shifted the LCST to a low-temperature range. Therefore we cannot simply state that hydrophobic interaction between NIPA residues is weakened by the addition of urea.

Taking the above into account, we initially examined the effect of 4 M urea on the size distributions of PNIPA and PAAc at pHs 3 and 10 (Figure 16). It was found that there was little influence of urea on the size distributions of PNIPA and PAAc. Thus urea can be used in order to break the hydrogen bonds between PNIPA and PAAc. Figure 17 shows the size dis-

TABLE 2 Effects of pH and 4 M Urea on the LCST for Aqueous 0.1 M NaCl Solutions Containing PNIPA or PNIPA–PAAc Mixture

Sample[a,b]	pH	4 M urea	LCST[c]
PNIPA	3	absence	31.3 ± 0.2
PNIPA	3	presence	26.1 ± 0.3
PNIPA	10	absence	31.4 ± 0.3
PNIPA	10	presence	25.9 ± 0.3
PNIPA–PAAc mixture	3	absence	—[d]
PNIPA–PAAc mixture	3	presence	26.2 ± 0.3
PNIPA–PAAc mixture	10	absence	31.1 ± 0.2
PNIPA–PAAc mixture	10	presence	26.4 ± 0.3

[a]Concentrations of PNIPA ($\bar{M}_w = 7.6 \times 10^5$) and PAAc ($\bar{M}_w = 4.5 \times 10^5$) in the sample solutions were adjusted to 0.5 g/dL and 0.16 g/dL, respectively.
[b]The same volumes (10 mL each) of the PNIPA and PAAc solutions were mixed; thus, the ratio of PNIPA : PAAc in the mixed sample was 2 : 1 by unit mole base and the total polymer concentration was 0.33 g/dL.
[c]Denotes the average of five measurements.
[d]The measurement could not be performed because the solution was turbid even at 1°C.

tributions in the presence and absence of urea for the 2 : 1 (unit mole base) mixtures of PNIPA and PAAc at pHs 3 and 10. At pH 10, at which PAAc is completely ionized, no urea effect was observed. In contrast, the results at pH 3 revealed that a large PNIPA–PAAc complex was formed in the absence but not in the presence of urea. It should be noted that the size distribution of PNIPA or PAAc observed in the mixture containing 4 M urea is the same as the distribution of each original polymer (see Figure 16). As a result, we can say that the formation of hydrogen bonds between the NIPA and AAc residues plays an important role in the volume collapse of Gels II and III at pH 3.

The effect of the distribution of the NIPA residues on the swelling of terpolymer gels consisting of NIPA, AAc, and 2-hydroxyethyl methacrylate (HEMA) has been studied by Vakkalanka and Peppas [77]. They prepared two sorts of terpolymer gels; (1) a gel with cross-linked random terpolymer chains, and (2) a gel with cross-linked chains consisting of blocks of NIPA (continuous NIPA segments) in a random copolymer of AAc and HEMA. It was demonstrated that there is a marked difference in swelling behaviors between the block and random terpolymer gels when temperature was varied at a constant pH. This appears to be another evidence supporting the validity of our discussion mentioned above.

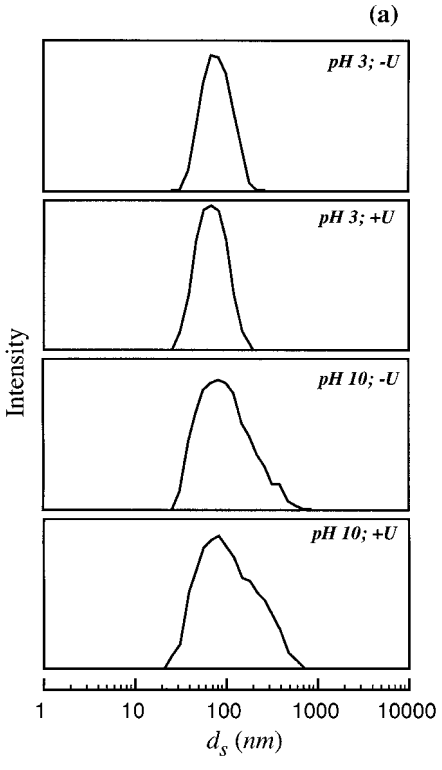

FIG. 16 Effects of pH and 4 M urea on the size distribution of PAAc (a) and PNIPA (b) examined by DLS at 15°C. The samples were the same as those in Table 2. +U and −U represent the presence and absence of 4 M urea, respectively. (From Ref. 28.)

D. Role of Hydrogen Bonding and Hydrophobic Interaction in Gel Collapse

We have discussed the role of hydrogen bonding and hydrophobic interaction in the volume collapse of NIPA–AAc gels. However, one may claim that the gel system examined would be a special kind of polyelectrolyte gel. Thus we have tired further to examine the effects of both intermolecular forces on the gel transition with another polyelectrolyte gel.

Poly(ethyleneimine) (PEI) is a representative polybase with either a linear or a branched polymer structure; the former is more often abbreviated as LPEI and the latter as BPEI. The acid hydrolysis of poly(ethyloxazoline)

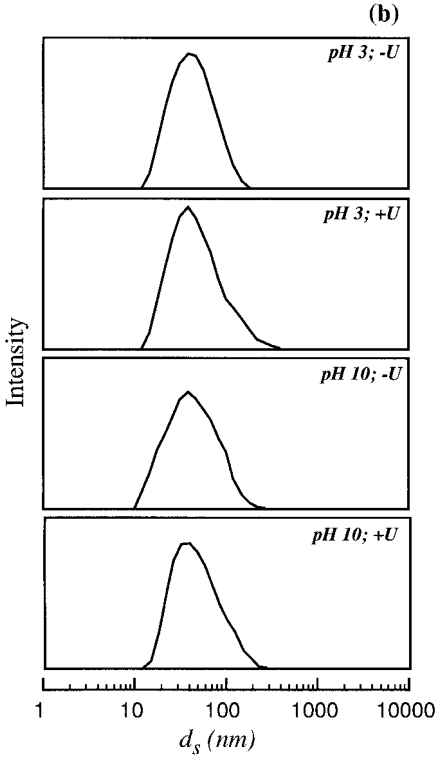

FIG. 16 *Continued.*

(PEOX) gives rise to LPEI [78–79], while BPEI can be obtained through the ring-opening polymerization of ethyleneimine [80]. In this study, we selected LPEI in the preparation of the polyelectrolyte gel because of the following advantages: (1) The deprotonation was fully studied as a function of pH by means of potentiometric [81,82] and calorimetric titrations with strong bases such as NaOH [83]; (2) the polymer precipitates to form crystalline hydrates from alkaline solutions (pH > 9) through hydrogen bonding between the —NH— groups and water molecules [82,84]; (3) x-ray structure analysis [84] has demonstrated that such hydrates consist of alternately stacked layers of polymers and water molecules in the crystallized state; (4) in addition, our preliminary experiments revealed that a gel of LPEI can be obtained without difficulty via cross-linking with ethylene glycol diglycidyl ether (EGDGE).

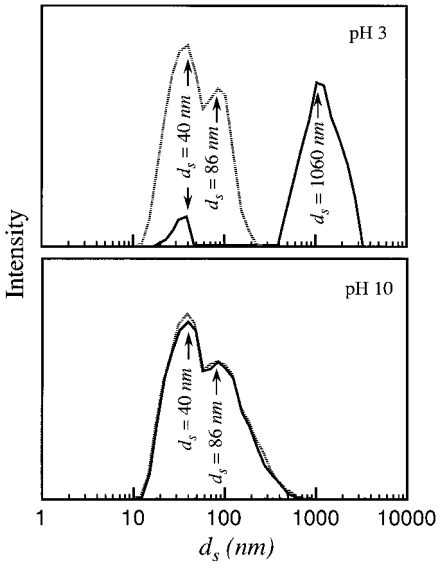

FIG. 17 Effects of pH and 4 M urea on the size distribution of the PAAc–PNIPA mixture examined by DLS at 15°C. Full lines and dashed lines respectively denote the absence and presence of 4 M urea. From the results of Figure 16, we can assign the peak appearing at $d_s \sim 40$ nm to PNIPA and the peak at $d_s \sim 86$ nm to PAAc. A complex with the average Stokes diameter ~1060 nm was observed in the PNIPA–PAAc mixture at pH 3 in the absence of urea. (From Ref. 28.)

1. Effects of pH and NaCl Concentration on the Swelling Degree

The gel sample was inserted into a glass cell together with 0.001 M HCl. After this, the outer medium which was maintained at 20 ± 0.1°C and adjusted to a desired pH within the range of 3 to 12 using various concentrations of HCl (pH < 6.7) or carbonate-free NaOH (pH > 6.7), was made to flow slowly through the cell until the diameter of the gel reached equilibrium under the given conditions. Figure 18 shows pH-dependent changes in the normalized equilibrium gel diameter (d/d_0). The normalization of each observed equilibrium diameter (d) was then performed with the inner diameter (d_0) of the capillary used in the gel preparation. During a pH change cycle (3 to 12 followed by 12 to 3), the gel underwent a discontinuous volume phase transition near pH 10.7 (collapse) and pH 5.9 (swelling); thus a large hysteresis appeared in the swelling curve.

The effect of NaCl concentration on the gel diameter was studied at pH 3, at which the gel was in a fully swollen state. As can be seen from Figure

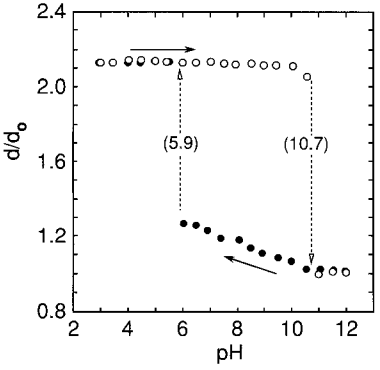

FIG. 18 Normalized equilibrium diameters (d/d_0) of the LPEI gel in aqueous solution at 20°C as a function of pH. Open symbols denote an increase in pH from 3 to 12, whereas closed symbols show a decrease in pH from 12 to 3. The values in the parentheses indicate the pH at the phase transition point. (From Ref. 27.)

19, an increase in the NaCl concentration brought about a monotonic gel collapse without transition. The gel diameter at 0.1 M NaCl concentration was almost half that in an NaCl-free solution at pH 3; this value was close to the fully collapsed diameter in Figure 18 (i.e., pH > 10.7). No hysteresis appeared in a concentration change cycle of NaCl.

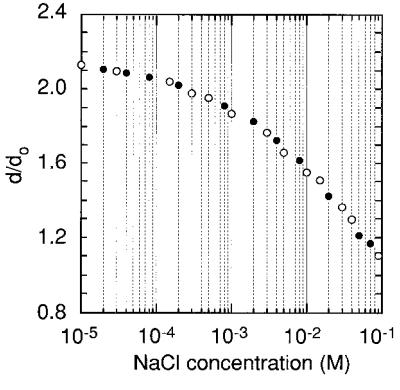

FIG. 19 The change in the normalized equilibrium gel diameters (d/d_0) with NaCl concentration at pH 3 and at 20°C. Open symbols denote an increase in the concentration from 0 to 0.1 M, whereas closed symbols show a decrease in the concentration from 0.1 to 0 M. (From Ref. 27.)

It is true that pH and NaCl concentration influence the ionization state of polyions. If we assume that these factors affect the state of ionization of the network in a polyelectrolyte gel and thereby its swelling degree is altered, the ionization state of a PEI gel in a 0.1 M NaCl solution and that in a salt-free solution at pH $\sim$ 10.7 seem to be almost the same, because there is little difference between the d/d_0 ratios determined in both solutions. However, a large difference was observed in the deswelling of the gel when increasing the pH and NaCl concentration. At present, to our knowledge, there is no theory that fully accounts for this difference on the basis of a mathematical model.

We will now attempt to explain on molecular grounds the observed swelling–deswelling characteristics of the LPEI gel, especially the pH-induced change, in terms of a balance between the repulsive and attractive forces within the cross-linked polymers in the network. Previous studies [81,82] have reported that a highly deprotonated LPEI forms crystalline hydrates in its alkaline solutions (pH > 9). The existence of two distinct hydrates, sesquihydrate with a unit cell containing 8 monomeric units and 12 water molecules, and dihydrate with a unit cell containing 4 monomeric units and 8 water molecules, has been reported on the basis of the x-ray structure analysis. The crystals of both hydrates consist of alternatingly stacked layers of polymers and water molecules arranged parallel to the *bc* plane. As shown in Figure 20, three types of hydrogen bonds (N—H$\cdots$O, O—H$\cdots$O, and O—H$\cdots$N) play a major role in the stabilization of the crystal lattices. In the case of the cross-linked LPEI, i.e. the gel, it should not form such crystalline hydrates, but several parts of the polymer chain segments in the network would form a stable structure like that in Figure 20, at pH > 10.7, at which both the —NH— and —N< groups are highly deprotonated. Therefore it is at this pH that the attractive force overcomes the repulsive electrostatic force. We consider hydrogen bonding to be the attractive force at work and assume that the gels that have collapsed due to hydrogen bonding do not swell again until significant numbers of the —NH— and —N< groups are protonated as the pH decreases; this would account for the large hysteresis in the swelling curves. On the other hand, an increase in NaCl concentration may eliminate the positive charges of the network as the repulsive electrostatic force, but it fails to form such a hydrogen-bond-stabilized structure because of the protonated ionizable groups ($—NH_2^+—$ and $—NH^+<$); therefore the gel collapses monotonically.

2. pH Dependence of Viscosity for the Polymer

Since we expected a similarity between the pH-induced changes in gel volume and polymer conformation, we thus measured the reduced viscosity of LPEI·HCl in salt-free and 0.1 M NaCl solutions as a function of pH. Ko-

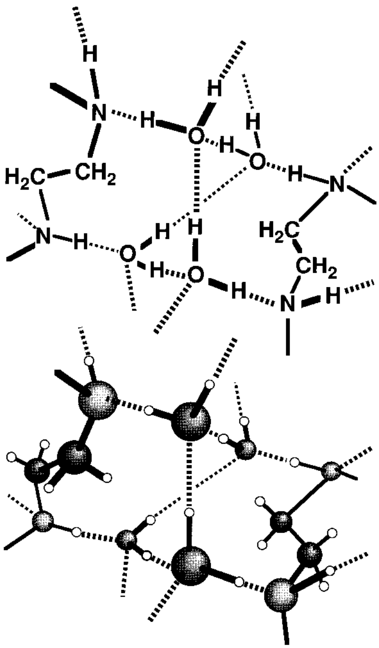

FIG. 20 Schematic illustration for three types of hydrogen bonds in a dihydrate of LPEI. The structural formula (top) and the corresponding atomic arrangement (bottom) are illustrated by reference to Figures 4, 6, and 7 in Ref. 84. Each H_2O oxygen atom is bound to four hydrogen atoms; two of them are covalently bonded and the remaining two are hydrogen bridged from neighboring water molecules or NH groups. Such a hydrogen bond–stabilized structure would form in highly deprotonated LPEI chain segments in the network. (From Ref. 27.)

bayashi et al. [81] have already studied the pH dependence of the reduced viscosity for LPEI in a 1 M KCl solution at 24.5°C and reported that an increase in pH from 2.9 to 8.8 brought about a viscosity fall at pH < 6 but an increase at pH > 8 after passing through a minimum value around pH 6.5. As can be seen from Figure 21, however, our measurements showed a monotonic decrease in the viscosity with increasing pH from 2.9 to 8.8. At pH > 9, it was very difficult to measure the viscosity, especially for the salt-containing system, because more often the sample became turbid due to the formation of hydrates of highly deprotonated LPEI via polymer–polymer association. Kobayashi et al. have considered such an association as one possibility leading to an increase in the viscosity at pH > 8, but they also mentioned that another reason was the stretching of the LPEI chain due to "repulsion" between lone-pair electrons of nitrogen atoms in the polymer

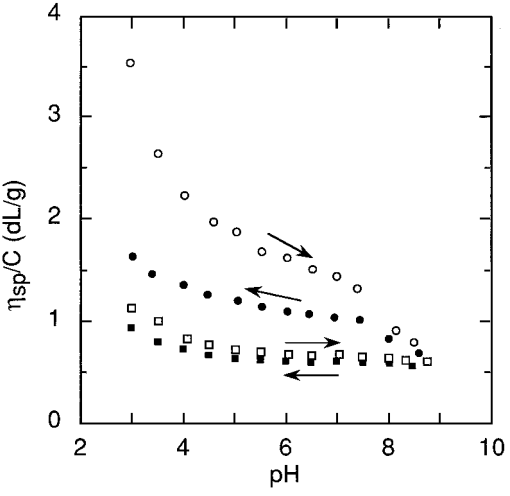

FIG. 21 pH-induced changes in reduced viscosities (η_{sp}/C) of salt-free solution (open and closed circles) and 0.1 M NaCl solution (open and closed squares) of LPEI at 20°C. Open symbols denote an increase in pH, whereas closed symbols denote a decrease in pH. (From Ref. 27.)

and Cl^- and/or OH^- ions in the medium. (Since it is reasonable to consider that lone-pair electrons of nitrogen atoms in the —NH— groups are solvated by coordination to water molecules as the solvent, we cannot understand why such lone-pair electrons serve as the anion.)

The most striking feature in the viscosity curves is the appearance of a hysteresis during the pH change cycle (from 2.9 to 8.8 and vice versa). Since the hysteresis was also observed even in the presence of 0.1 M NaCl, it is not due to an increase in ionic strength during the pH change cycle. One might assume that a very slow alteration in the polymer conformation under a given pH may cause a hysteresis. Although each of the sample solutions was allowed to stand for one day with mild stirring after the pH adjustment, we cannot conclude that there is no kinetic effect in an infinite period. However, the appearance of the hysteresis in both the viscosity and the swelling curves seems to be due to the same reason as described in the previous section. Even when the solution basicity is not high enough to result in crystalline hydrates of LPEI, the deprotonation of a large portion of the ionizable groups could lead to the collapse of the polymer chain through ''intrapolymer'' hydrogen bonding with the aid of water molecules (interpolymer hydrogen bonding was not the case, since we did not observe a rise in viscosity under the conditions used here). Therefore the successive

protonation of such a collapsed polymer becomes increasingly difficult; as a result, we observed that the viscosity during the pH decrease is lower than that during the pH increase.

3. Potentiometric Titration Curves

Investigation of the protonation–deprotonation process by means of potentiometric titration could provide a key to understanding the pH-dependent changes in the gel volume and polymer conformation. Three previous studies [81–83] have dealt with the potentiometric titrations of aqueous polymer solutions; the results are outlined as follows: (1) Protons were dissociated from LPEI·HCl with increasing difficulty, in particular at the protonation >50%, due to their strong interaction with neighboring charged ammonium ions; i.e., the nearest neighbor interaction originally proposed by Katchalsky et al. [85]. (2) It was not possible to achieve 100% protonation even at pH $\sim$ 2, but an approx. 70% degree of protonation gave an ''apparent end point'' of titration. (3) At less than 10% of the protonation the polymer precipitated to form crystalline hydrates. With respect to the formation of crystalline hydrates through hydrogen bonding, Weyts and Goethals [82] reported that aqueous salt-free solutions containing 0.1 M LPEI·HX (X = Cl^-, $HCOO^-$ and CH_3COO^-) exhibited an unusual pH change when the titration proceeded until 10% of the protonation (i.e., pH $\sim$ 9.4); that is, the solution pH increased due to the addition of a strong base until 10% protonation, but further addition of a very slight amount of the base brought about a decrease in pH by ca. 0.7 units accompanied by the appearance of solution turbidity. This phenomenon was then interpreted as follows: Once the crystallization starts, the enthalpy of crystallization provides energy to expel more protons of LPEI·HX into the solution; this promotes the formation of crystalline hydrates via interpolymer hydrogen bonding with the aid of water molecules and results in an increase of the fraction of protonated ammonium groups on the LPEI remaining in the solution; therefore these in turn lead to a decrease in the solution pH. For this reason, no previous studies have attempted to carry out a back titration with strong acids after titrating LPEI·HX with strong bases, although it would provide important information in order to understand the hysteresis observed in the viscosity curves.

In the case of the gel, on the other hand, the back titration with an acid for the sample dispersion, which has already been titrated with a base until an equivalent point, should be possible, since precipitation does not need to be taken into consideration. In contrast to the polymer, however, there are several difficulties in the analysis of the titration data; for example, how to estimate the ''real'' acid–base equilibrium within the gel phase from the pH measurements of the outer solution (see Sec. IV.C.2). So far, no study has dealt with the potentiometric titrations of polyelectrolyte gels. We neverthe-

less employed the potentiometric titration with NaOH for the aqueous dispersion of powdered LPEI·HCl gels, followed by a back titration with HCl; through both titrations we intended to clarify the origin of the hysteresis in the swelling curve.

Figure 22 shows the titration curves in which the pH of the outer medium was plotted against the volumes of NaOH (V_N) and HCl (V_H). Also shown in Figure 22 for the purpose of comparison is the titration curve of the polymer (LPEI·HCl) with NaOH. In the titrations of the gel, the time (t_{eq}) required for the establishment of equilibrium pH calculated on the basis of 1 mL of titrant was measured at each stage of the titration and plotted against V_N and V_H. In all the titration curves, both sample and titrant concentrations were precisely controlled on the basis of the results of the elemental analysis in order to complete the stoichiometric neutralization of all the titratable groups with 1 mL of NaOH or HCl titrant; i.e., 1 mL of NaOH or HCl being equivalent to moles of the $—NH_2^+—$ plus $—NH^+<$ groups or the —NH— plus —N< groups. A comparison of the three titration curves in Figure 22 provides us with some significant information: (1) The pH of the gel dispersion is higher than that of the polymer solution over all the stages of titration with NaOH, especially in the range of $V_N < 0.5$ mL at which, as demonstrated in a previous study [83], the nearest neighbor interaction does not have a strong influence on the deprotonation reaction of LPEI·HX (i.e., $—NH_2^+— \rightarrow —NH— + H^+$). (Even though at the protonation degree <50% there is little influence from the nearest neighbor interaction on the dissociation of protons from the polymer, but there is a strong influence in the case of the gel because cross-linking should facilitate ''intramolecular'' interactions between the ionizable groups bound to the network; therefore we assumed that the cross-linking of the polymer chains was responsible for this result.) (2) At the onset of the back-titration of the gel with HCl, a very rapid decrease in pH is observed and the curve exhibits an inflection point at $V_H \sim 0.1$ mL. (3) This is not due to the titration with HCl of the remaining NaOH in excess in the system because a very slow attainment of acid–base equilibrium was observed from the t_{eq} vs. V_H curve at $V_H < 0.15$ mL. (4) In the back titration, the initial pH level (2.9) of the original gel dispersion is reaced even at $V_H = 0.71$ mL.

Special attention ought to be paid to results (2) and (4) with regard to our present purpose. Our gel contains two kinds of amines as the ionizable groups, —NH— and —N< in the form of a free base; the contents are 88 mol% for the former and 12 mol% for the latter by means of elemental analysis. It is generally believed that pK_a (i.e., $-\log K_a$) for tertiary alkyl ammonium salts is larger than 10, e.g., $pK_a = 10.64$ for $(CH_3CH_2)_3N·HCl$ at 25°C. Taking this into account, we may predict that the —N< groups in the network are preferentially protonated at $V_H < 0.1$ mL: $—N< + H^+ \rightarrow$

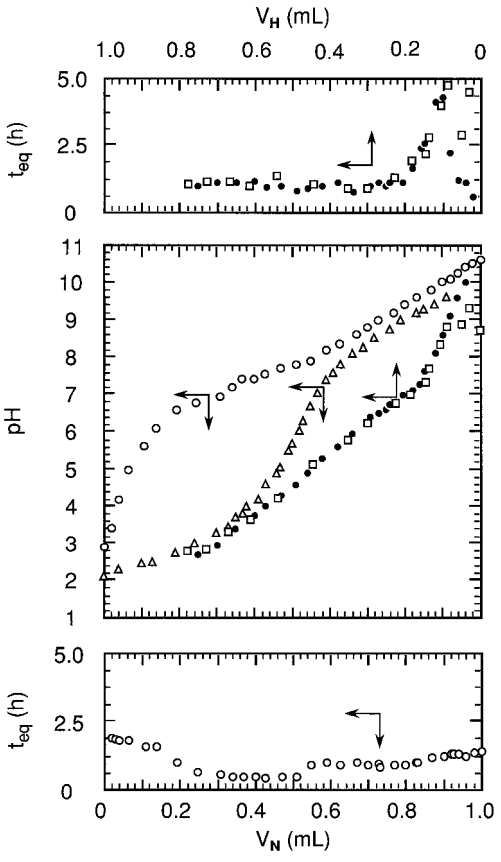

FIG. 22 Change in pH during titration of LPEI·HCl with NaOH (open triangles) as well as pH changes during titration of LPEI·HCl gel with NaOH (open circles) followed by back titration with HCl (closed circles). Also shown in this figure is the titration curve (open squares) with HCl of LPEI gel in the form of free base. The curves of t_{eq} vs. V_N (open circles) and V_H (closed circles and open squares) were given to indicate the time (t_{eq}) required for the establishment of pH equilibrium at each stage of the titration if unit volume of the NaOH or HCl titrant were added into the titration system. Titration conditions: titrant concn., 3 M for each; sample concn., 0.1 M for each (by moles of the —NH_2Cl— groups in the polymer, the —NH_2Cl— plus —NHCl< groups in LPEI·HCl gel, and the —NH— plus —N< groups in LPEI gel); sample size, 30 mL for each; 20°C. (From Ref. 27.)

—$NH^+<$. In fact, the amount of the titrated groups in this range is about 10 mol% of the total ionizable groups in the system, the value of which is very close to the content of the —N< groups.

If the protonation of the —N< groups could be terminated at $V_H \sim 0.1$ mL, the stage of the titration at $V_H > 0.1$ mL may be related to the reaction —NH— + $H^+ \rightarrow$ —NH_2^+—. As mentioned above, however, this reaction appears to go essentially to completion at $V_H \sim 0.7$ mL; this corresponds with the 68% degree of protonation for a total of the —NH— groups because the —NH— content = 88%. Therefore the reaction does not follow a 1:1 stoichiometry. However, this is not surprising when we consider that a highly deprotonated LPEI gel contains a large number of —NH— groups whose nitrogen atoms are stabilized with bound water molecules via hydrogen bonding and resistant to the coordination (protonation) with the protons added. The same interpretation has been applied to the viscosity curves, and even in the gel system a structure as shown in Figure 20 may form within chain segments of the networks. As a result, the potentiometric titration clearly demonstrated that the origin of the hysteresis in the swelling–deswelling process is due to the hysteresis in the deprotonation–protonation process; in other words, a large difficulty in the protonation caused by hydrogen bonding as shown in Figure 20. However, this does not account for the gel discontinuously swelling in the protonation process or discontinuously collapsing in the deprotonation process. We thus have to consider that the gel undergoes a transition when the repulsive force due to the NH_2^+— and —$NH^+<$ groups overcomes the hydrogen bonding as the attractive force or vice versa.

By taking the above into account, we can explain why the —N< groups were preferentially protonated in the titration with HCl, but the preferential deprotonation did not take place in the titration with NaOH. In the protonation process, the —NH— groups behave as a very weak base due to the previously mentioned stabilization effect, while the —N< groups as a strong base preferentially accept protons to form the tertiary alkyl ammonium ions. At the onset of the titration with NaOH, the —NH_2^+— groups may be taken as a strong acid since at $V_N = 0$, pH = 2.1 for LPEI·HCl and 2.9 for LPEI·HCl gel. Thus in the range of $V_N < 0.1$, the dissociation of protons from the —NH_2^+— groups overlaps with that from the —$NH^+<$ groups, leading to a titration curve without an inflection point.

Our titration data have indicated that there was a hysteresis in the deprotonation–protonation process. However, we should consider that the titration was performed in the absence of supporting electrolytes such as NaCl. Consequently, the ionic strength of the system increased during the course of titration; for example, at $V_N = 1.0$ mL the ionic strength became 0.1 M due to NaCl resulting from the reaction —NH_2Cl— + NaOH $\rightarrow$ —NH— +

NaCl + H_2O. Thus a titration which is not accompanied by such a salt formation is desired. Taking this into account, we performed the titration with 3 M HCl of an aqueous dispersion containing the LPEI gel (base form). The result obtained was overplotted in Figure 22 (see open squares). At $V_H < 0.03$ mL the titration curve for the LPEI gel was different from the back titration curve for the salt-form gel, perhaps due to a difficulty in the protonation of the —N< groups (this may be conceivable when the gel sample in the base form was directly subjected to the titration). At $V_H > 0.05$ mL, however, there was a good agreement between the titration curves, indicating that NaCl resulted from the titration of the LPEI·HCl gel with NaOH and accumulated in the system little influences the back titration.

4. Effect of Urea on the pH-Induced Volume Transition

Urea has been frequently employed in the biochemical field as a means to identify hydrogen bonds, since it is generally believed that urea can break up intra- or intermolecular hydrogen bonding of proteins in aqueous systems. We thus studied the effects of urea on the pH dependence of the gel diameter (Figure 23) and found that urea facilitates the swelling of the gels at higher pH levels during the protonation process, even at urea concentrations one fourth or one eighth lower than the most commonly employed concentration (8 M) in the denaturation of proteins.

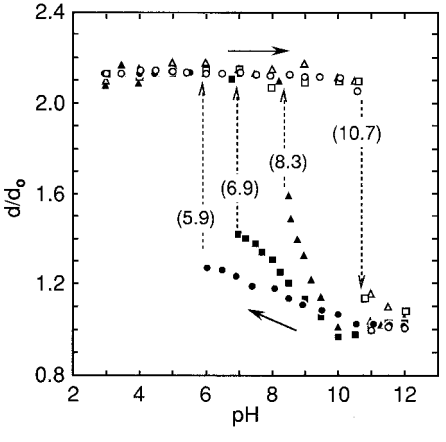

FIG. 23 pH-induced changes of normalized equilibrium gel diameters (d/d_0) at 20°C in aqueous solutions containing different concentrations of urea: 0 M (circles); 1 M (squares); 3 M (triangles). Open symbols denote an increase in pH from 3 to 12, whereas closed symbols show a decrease in pH from 12 to 3. The values in the parentheses indicate the pH at the phase transition point. (From Ref. 27.)

It has long been believed that urea disrupts the cluster structure of water molecules; i.e., ''structure breaking effect.'' (For previous studies showing that urea acts as a water structure breaker, see the introductions of Refs. 86 and 87; however, it should be noted that both articles deal with a molecular dynamics simulation of a dilute aqueous urea solution and report that urea has little effect on water structure under an infinitely low concentration.) Thus it appears that urea may inhibit the formation of a structure (as shown in Figure 20) stabilized through the hydrogen bonds with water molecules. In the presence of urea, therefore, both the acceleration of the protonation (i.e., ionization) and the weakening of the attractive interaction between the cross-linked chains takes place at the same time during the protonation process. As a result, a pH at which the gel swells discontinuously should shift to an alkaline pH side; in other words, a tendency for the hysteresis to disappear can be observed when adding urea.

5. Effects of Anionic Surfactants on the Swelling Degree

Urea, being a water structure breaker, would weaken the hydrophobic interaction between solute molecules as reported in several previous studies (see Ref. 76). It is thus necessary for us to examine the effects of urea on the hydrophobic interaction in the present gel system. However, this is a considerably difficult problem which, to our knowledge, has not yet been dealt with by any researchers in the field of polyelectrolyte gels. The main reason is the lack of information about whether hydrophobic interaction plays a role in the volume collapse of usual polyelectrolyte gels with a lot of hydrophilic ionizable groups, such as the LPEI gels in question. As a novel approach in order to overcome this difficulty, we examined the swelling curves of the LPEI gel as a function of the concentration of anionic surfactants in the presence and absence of urea.

Our previous study [23] demonstrated that the binding of sodium dodecyl sulfate (SDS) anions to the charged ammonium ions of EGDGE-cross-linked branched poly(ethylenime) gels brings about a dramatic volume collapse due not only to the neutralization of the charges but also to hydrophobic interaction. As shown in Figure 24, this is the case in the LPEI gel system. Sodium butyl sulfonate (SBS) without definitive critical micelle concentration (C_{mc}) in aqueous solutions exhibited the same effect on the gel diameter as NaCl (see Figure 19). However, sodium octyl sulfonate (SOS; $C_{mc} \sim 130$ mM) and SDS ($C_{mc} \sim 8.3$ mM) showed remarkable and strong effects on the volume phase transition of the LPEI gel: (1) The concentration at which the transition takes place is lower for SDS than for SOS because the former is stronger than the latter with respect to hydrophobicity. (2) The SDS concentration bringing about the transition was lower at 60°C than at 20°C, the

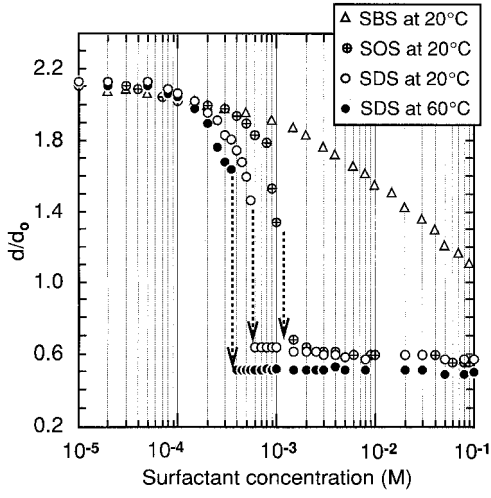

FIG. 24 Changes of normalized equilibrium gel diameters (d/d_0) in aqueous pH 3 solutions containing different surfactants at 20 and 60°C. The kinds of surfactants and the temperatures for the measurements are shown in the figure. (From Ref. 27.)

result of which agrees with the common knowledge that a rise in temperature enhances the hydrophobic interaction. (3) In addition, the gel diameter was reduced to 26% with SOS and SDS at 20°C and to 23% with SDS at 60°C; these values are about half compared to the diameter of a fully deprotonated gel at pH > 10.7, clearly indicating that the hydrophobic interaction may act as an attractive force in the gel collapse.

In a previous study [31] we suggested that the binding of surfactants such as SDS to LPEI gels occurs mainly in the region in the near vicinity of the gel surface but that the molecules fail to penetrate into the core of the gel phase. A Donnan potential, generated due to an excess of surfactant anions around the gel surface, would make further diffusion of the surfactants with anionic charges more difficult. From the results in Figure 24, however, the surfactant-LPEI gel system may be regarded as a well-defined polyelectrolyte gel whose volume collapse takes place via hydrophobic interaction as an attractive force. We thus measured the d/d_0 of the gel samples in aqueous solutions containing different amounts of SDS in the presence and absence of urea; the pH of the solutions was adjusted to 3.0 so as to maintain a completely swollen state for the gels. As can be seen from Figure 25, urea has no influence on the SDS-induced discontinuous volume collapse for the LPEI gel, which indicates that urea does not contribute to weakening the hydrophobic interaction, at least in our model system. Therefore, we may

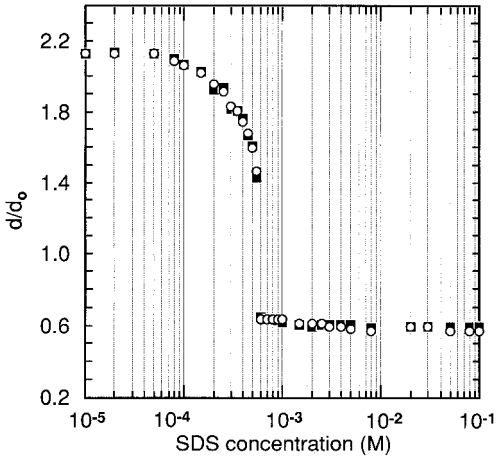

FIG. 25 Effect of urea on SDS-induced changes in normalized equilibrium gel diameters in aqueous pH 3 solutions at 20°C. Closed squares and open circles, respectively, show the curves in the presence and absence of 3 M urea. (From Ref. 27.)

say that the results shown in Figure 23 are due to the breaking up of hydrogen bonds by urea molecules.

E. Ionization Equilibria of COOH Groups Bound to Polymer Network

To understand the nature of the phase transition of ionic gels, it should be necessary to obtain accurate information about the ionization equilibria of acidic or basic groups within the gel. The object of this section is to examine the dissociation behavior of the COOH groups in the NIPA–AAc gels by means of potentiometric titration and to compare it with the results of swelling experiments; through this approach we intend to discuss the swelling mechanism of ionic NIPA gels at the molecular level. In particular, our attention has been paid to the role of mobile counterions, as well as those of hydrophobic interaction and hydrogen bonding. The submicron-sized gel particles with 70 mol% NIPA and 30 mol% AAc, in addition to the bulk gel of a fine grind, were employed in this study, because we have succeeded in preparing such microgel particles [33]. We also employed the NIPA–AAc copolymer with the same AAc content as a control sample. One might expect that use of the microgel would help to eliminate a general problem in the pH titration for gels; that is, a great difficulty in judging whether the H^+ and OH^- concentrations within the gel phase come to equilibrium with those

in the aqueous bulk phase at different stages of the titration. We should note that our microgel has most of the COOH groups located in the interior but not on the hydrodynamic surface of the particle (see Ref. 33).

1. Relation Between Dissociation Constant and Degree of Dissociation

A complete titration curve can be given by plotting apparent dissociation constant (pK_a) against the degree of dissociation (α_d). We may determine pK_a from the titration data using the following relations:

$$pK_a = pH - \log\left(\frac{\alpha_d}{1 - \alpha_d}\right) \tag{16}$$

$$\alpha_d = \alpha_n + \frac{C_{H^+} - C_{OH^-}}{C_p} \tag{17}$$

Here, α_n is the degree of neutralization, and C_{H^+} and C_{OH^-} are the molar concentrations of H^+ and OH^- ions, respectively. Writing the required electrostatic free energy for the removal of an equivalent of protons at a given α_d as $\Delta G^i_{el}(\alpha_d)$, its relation to pK_a may be given as (for example, see Ref. 88)

$$pK_a = pK^0 + 0.43\,\frac{\Delta G^i_{el}(\alpha_d)}{RT} \tag{18}$$

where pK^0 is characteristic of the ionizing group under conditions where electrostatic interactions with other ionizing groups are absent.

The NIPA–AAc gel undergoes a volume phase transition in response not only to pH and ionic strength but also to temperature; thus, it would be interesting to examine the dependence of pK_a upon α_d as a function of ionic strength and temperature. We studied the effect of ionic strength on the α_d dependence of pK_a at 25 and 35°C (Figures 26 and 27). The latter temperature is slightly higher than the T_v of NIPA gel and the LCST of NIPA polymer. Since our copolymer and gels in the acid form may be taken as a neutral NIPA, the phase separation and the volume phase transition should take place during the titration at 35°C. Thus it would be interesting to see how these effects appear in the dependence of pK_a on α_d. However, we did not perform the titration of the bulk gel at 35°C because (1) the characteristic times of swelling and deswelling for NIPA gels are proportional to the square of a linear dimension of the gel and (2) the transition becomes very slow when temperature comes close to T_v [53].

The titration curves in Figures 26 and 27 provide us with some significant information: (1) On the whole, pK_a increases with increasing α_d but decreases with addition of NaCl. (2) There is little difference in pK_a between

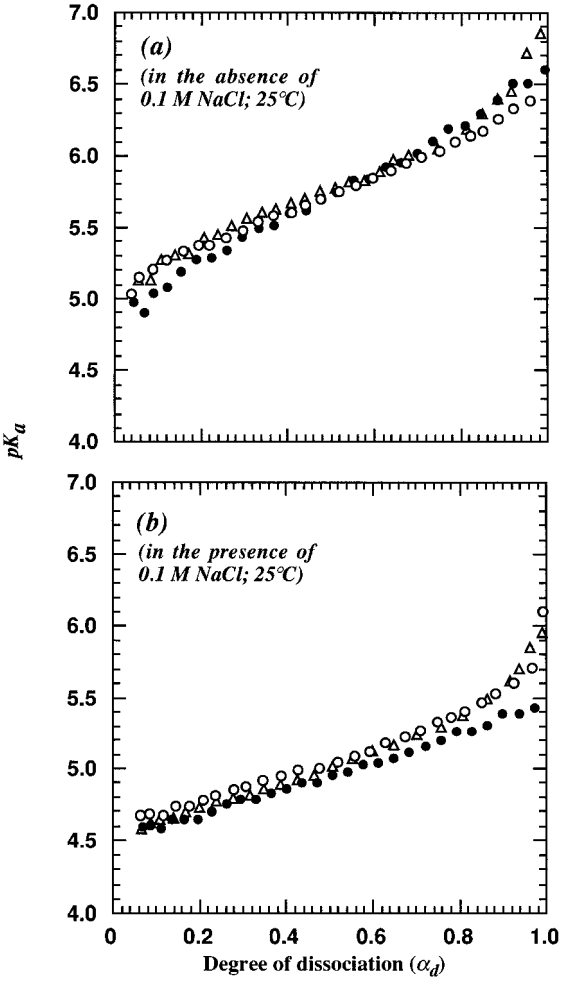

FIG. 26 Changes in apparent dissociation constant (pK_a) with the degree of dissociation (α_d) for the copolymer (closed circles), the bulk gel (open triangles), and the microgel (open circles) in the absence (a) and the presence (b) of 0.1 M NaCl at 25°C. A very slight initial fall in pK_a was observed in the salt-free system with the copolymer. This was reproducible and not an experimental error; thus it seems that in the case of the copolymer the interaction (being discussed in the text) appears not only at 35°C but also at 25°C. (From Ref. 33.)

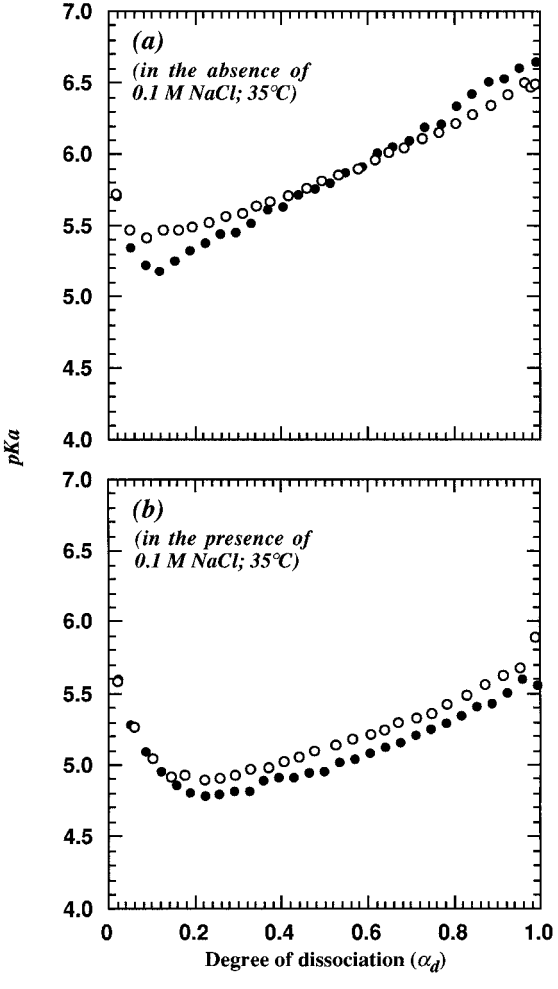

FIG. 27 Changes in apparent dissociation constant (pK_a) with the degree of dissociation (α_d) for the copolymer (closed circles) and the microgel (open circles) in the absence (a) and the presence (b) of 0.1 M NaCl at 35°C. (From Ref. 33.)

the gels, as well as between the gel and the copolymer. (3) At 35°C and at $\alpha_d < 0.15$ (see Figure 27), however, an increase in α_d leads to a distinct fall in pK_a for both gel and copolymer; their pK_a values at 35°C are larger than those at 25°C.

Result (1) is the general aspect that appeared in the titrations of polymeric acids, such as PAAc, in the absence and the presence of added salt (e.g.,

see Refs. 88 and 89). From an increase in pK_a with α_d, meaning that the removal of H^+ from the polymeric acid becomes increasingly difficult as the titration proceeds, we may learn an increase in $\Delta G^i_{el}(\alpha_d)$ due to the electrostatic attraction between H^+ ions and polyanions. Since the counterions from added salts contribute to weakening this attraction through the elimination of polyion charges, $\Delta G^i_{el}(\alpha_d)$ should decrease over a wide α_d range. Then we may see a decrease in pK_a displaying that the dissociation of H^+ from the polymer becomes easy. Therefore, result (2) indicates that the ionization mechanism for the gels is essentially the same as that for the polymer solution.

Taking the above into account, result (3) may be explained as follows. At the initial stage of the titration ($\alpha_d \sim 0$) and at 35°C, both copolymer and cross-linked copolymer network should be in a collapse state due to hydrophobic interaction. This shortens the distance of a COOH group from the surrounding functional groups; thus interactions of this COOH with the neighboring groups would become strong (i.e., ''nearest neighbor interaction'' originally proposed by Katchalsky et al. [85]). Actually, PNIPA and PAAc give forth a water-insoluble complex under conditions where the COOH groups are fully protonated (see Sec. V.C.4). If this is the case, the removal of the H^+ from the COOH should be impeded. Consequently, pK_a at 35°C became larger than that at 25°C. By ionizing a few COOH groups with NaOH, however, a mutual repulsion among the resulting COO^- ions weakens by degrees the nearest neighbor interaction. This should facilitate the dissociation of other COOH groups (a decrease in pK_a with α_d). Indeed, a turbidity appeared both in the salt-free and the salt-containing solution of the copolymer at 35°C, but the solution became transparent as the titration proceeded ($\alpha_d > 0.1$ for the salt-free system; $\alpha_d > 0.16$ for the salt-containing system).

In the case of the microgel system at 35°C, a turbidity was also observed in the presence of NaCl ($\alpha_d < 0.1$) but not in pure water. This provides a key to supporting the above interpretation (see the following section).

2. Effects of pH, Ionic Strength, and Temperature on the Size of Microgel

It would be interesting to learn how the size (or the swelling degree) of the NIPA–AAc microgel particle varies depending on the ionization of the COOH groups as well as on temperature. For this purpose, we measured apparent Stokes diameters (d_s) by means of dynamic light scattering (DLS) and plotted d_s against α_n as a function of temperature (see Figures 28 and 29). The results obtained in pure water (Figure 28) and in 0.1 M NaCl solution (Figure 29) were then reported separately, because there was a large difference in the magnitude of size changes caused by the absence and the

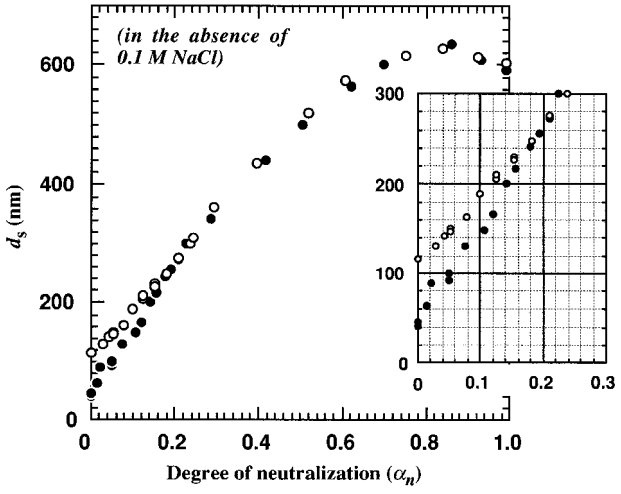

FIG. 28 Changes in apparent Stokes diameter (d_s) of the microgel with the degree of neutralization (α_n) in the absence of NaCl at 25°C (open circles) and 35°C (closed circles). (From Ref. 33.)

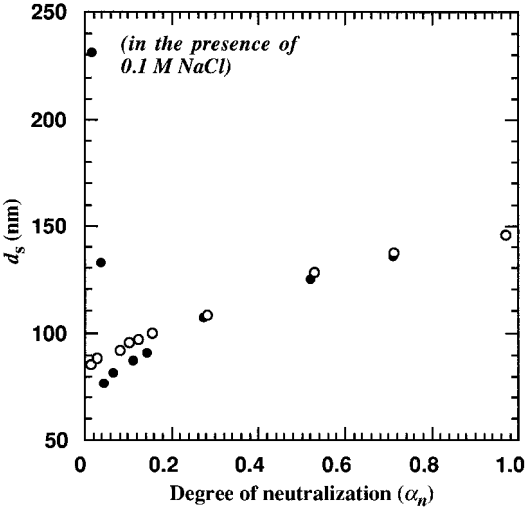

FIG. 29 Changes in apparent Stokes diameter (d_s) of the microgel with the degree of neutralization (α_n) in the presence of 0.1 M NaCl at 25°C (open circles) and 35°C (closed circles). (From Ref. 33.)

presence of the salt. With ionizing the COOH groups, the particle size linearly increased at $\alpha_n < 0.6$ and then leveled off at $\alpha_n > 0.6$; this feature was remarkable in the salt-free system rather than in the NaCl-containing system. With screening the charge of COO^- ions with the counterions from NaCl added, the size decreased over a wide α_n range, except for the result in the salt solution at 35°C and at $\alpha_n < 0.1$ (see Figure 29). These aspects are quite analogous to the changes in the end-to-end extension of PAAc ions in aqueous solutions. Kokufuta [89] has performed the viscometric and electrophoretic studies with aqueous PAAc solutions and obtained the following results (both viscosity and mobility data have been reported in Ref. 89 as a function of pH; however, these can be converted into a relation with α_n [or α_d], because the reference includes the titration curves by pH vs. α_d as well as pK_a vs. α_d): (1) An increase in ionic strength results in a marked decrease in the viscosity as an indication of the end-to-end extension of a polymer chain. (2) The viscosity increases with increasing α_n at $\alpha_n < 0.6$ and levels off at $\alpha_n > 0.6$. (3) These viscosity changes correspond to the mobility changes, because the mobility may be considered as an indication of the net charge density of a polyion when it behaves as a free draining coil in electrophoresis. Among results (1) to (3), we draw particular attention to the fact that the charge density scarcely increases at $\alpha_n > 0.6$. In general, this phenomenon is known as the ''counterion binding effect,'' a strong experimental evidence for which has been reported by Wall et al. [90]. From their transference experiments using radioactive sodium (^{22}Na) in salt-free aqueous solutions containing PAAc partially neutralized with NaOH, we may learn the following important two features: (1) The binding degree of Na^+ ions linearly increases at $\alpha_n < 0.6$ and levels off at $\alpha_n > 0.6$; and (2) the concentration of mobile Na^+ ions increases linearly at $\alpha_n < 0.2$, gradually at $0.3 < \alpha_n < 0.7$, and rapidly again at $\alpha_n > 0.8$. By comparing these results with those of potentiometric titrations in the previous section, let us consider the role of Na^+ ions in our gel system. Then we may assume that at $\alpha_n > 0.6$, at which the gel swells little, the concentration of mobile Na^+ ions still increases. According to the Flory theory for polyelectrolyte gels, a very slight increase in the concentration of mobile counterions within the gel phase brings about a dramatic increase in the swelling degree (e.g., see Sec. II.A). Therefore our results in Figures 28 and 29 may not be understood by assuming that an increase in α_n raises osmotic pressure arising from mobile counterions within the ''overall'' gel phase. Otherwise, by considering that at $\alpha_n > 0.6$ the ''net'' charge density of the gel increases little but levels off due to the counterion binding, the dependence of the swelling degree upon α_n may favorably be accounted for. As a result, we may see the strong resemblance between the α_n changes in the swelling degree for the NIPA–AAc gel and in the end-to-end extension for PAAc in solutions.

We examined in detail the effect of temperature on the size of the microgel in pure water at $\alpha_n < 0.3$ (see inset in Figure 28). At $\alpha_n < 0.15$, the particle size at 35°C was smaller than that at 25°C because $T_v \sim 33$°C for neutral NIPA gels. However, this difference disappeared at $\alpha_n \sim 0.15$ at which the gel has 4.5 mol% ''COONa'' plus 25.5 mol% COOH. These mean that our microgel undergoes ''thermal'' swelling transitions at $\alpha_d < 0.15$ when lowering temperature from 35°C to 25°C (see Figure 6 in Sec. V.A). We have discussed in the previous section why the initial fall in pK_a, as well as the solution turbidity, appears both in the salt-free and the salt-containing system not only with the copolymer but also with the microgel, under conditions at 35°C and at $\alpha_d < 0.15$. For the copolymer, these phenomena were satisfactorily accounted for in terms of the nearest neighbor interaction, in which hydrogen bonding and hydrophobic interaction play an important role. Although the turbidity did not appear in the salt-free microgel system, the results in the window of Figure 28 clearly indicate that the microgel particles are in a collapse state at $\alpha_d < 0.15$ and at 35°C. Under such a situation, we may reasonably assume the nearest neighbor interaction mechanism to account for the initial fall of pK_a in the microgel system. As a result, the swelling behavior of our polyelectrolyte gel may be understood, without relying on models based upon the Flory theory, through detailed considerations of the mechanism for the dissociation of COOH at the molecular level, even when a slight amount of NaOH was added in the gel system to ionize the COOH groups.

We must discuss separately the α_n change of d_s for the microgel in the salt-containing system, because the turbidity has been observed at 35°C and at $\alpha_n < 0.1$, while the turbid suspension became transparent at $\alpha_n > 0.1$. From this turbidity change, an abrupt decrease in d_s at the initial stage of the neutralization ($\alpha_n < 0.05$; see Figure 29) may be attributed to the disaggregation of microgel particles. It appears that in the salt-free system the microgel surfaces are considerably hydrated by water molecules even at 35°C, while the cross-linked polymers in the particle interior are in a collapse state due to hydrophobic interaction. When adding NaCl into the system, the dehydration due to Na^+ and Cl^- ions seems to favor the aggregation of the particles. This would enhance an ''interparticle'' interaction, in other words, interactions of the surface functional groups of a particle with those of other particles. If this is the case, the ionization of a few surface COOH groups with NaOH should cause an electrostatic repulsion among the microgel particles to weaken the interparticle interaction. Consequently, we have observed at the same time the initial fall in pK_a as well as in d_s relating to both the intra- and the interparticle interaction. Indeed the initial fall in pK_a was more clear in 0.1 M NaCl solution than in pure water (see Figure

27). Hydrogen bonding as well as hydrophobic interaction would also be conceivable in both the intra- and the interparticle interaction.

VI. CONCLUSIONS AND FUTURE PROSPECTS

We have viewed the phase transitions in polyelectrolyte gels from both sides, theory and experiment. The initial impetus for research on this subject came from work done on a transition observed by Tanaka with nonionic polyacrylamide gels. Thus later work on ionic gels evolved rather independently from that on single polyion chains. In the field of gel transition theories, many studies focused exclusively on modifications of Flory's theory, although several critical studies have claimed this is not realistic because an ''incompressible'' random-mixing lattice model as well as Guassian chain distributions are assumed. Prior to such physical arguments, on the other hand, several experiments mentioned in Section V have questioned the validity of the concept of osmotic pressure arising from mobile counterions, which has long been assumed as the chief driving force for the swelling of ionic gels. Another important finding through experiments has addressed the issue of ''counterion condensation'' in ionized gels, which is central to research on solution properties of polyelectrolytes. Then, it is natural to mention that the behavior of ionic gels, including the gel transitions, should be understood in terms of the analogy with those of polyions in solutions.

In respect to applications of polyelectrolyte gels, to which this chapter did not refer, a considerable number of researches have focused on regulation of the phase transitions in ionic gels by externally applied appropriate stimuli. Almost all the researches were performed in the 1990s without relying on the above transition theories, but with simple models in which polymer–polymer interactions are taken into account at the molecular level. For example, we have attempted to establish a simple molecular model [17] for interpreting the phase transition of gels in studies on the construction of ''biochemo-mechanical systems'' [18,19,21,25,91–95], which convert the energy arising from biochemical changes (such as enzyme reactions) into mechanical work through a swelling–deswelling transition of the gel with immobilized biocatalysts. In this regard, we accounted for the gel transitions by hypothesizing a balance between the repulsion and attraction among functional groups attached to the cross-linked polymers which arise from a combination of four intermolecular forces (see Sec. II). Then, one took a critical attitude to this model due to the general assumption that a simple concept cannot be used to explain complex systems such as gels. Nevertheless, almost all of the experimental swelling curves can be understood in terms of this concept (see Secs. II and V). Consequently, it would be expected that the simple concept should be helpful to develop one of the most promising

physical models, which provides a better explanation not only of the phase transition but also of the swelling behavior of ionic gels.

REFERENCES

1. Vermaas D, Hermans JJ. The swelling of cellulose xanthate gels in dilute salt solutions. Recueil 1948; 67:983–997.
2. Flory PJ. Principles of Polymer Chemistry. New York: Cornell University Press, 1953.
3. Katchalsky A, Michaeli I. Polyelectrolyte gels in solutions. J Polym Sci 1955; 15:69–86.
4. Dusek K, Patterson D. Transition in swollen polymer networks induced by intramolecular condensation. J Polym Sci 1968; A-2,6:1209–1216.
5. Tanaka T. Collapse of gels and the critical endpoint. Phys Rev Lett 1978; 12: 820–823.
6. Tanaka T, Fillmore DJ, Sun S-T, Nishio I, Swislow G, Shah A. Phase transitions in ionic gels. Phys Rev Lett 1980; 45:1636–1639.
7. Hrouz J, Ilavsky M, Ulbrich K, Kopecek J. The photoelastic behavior of dry and swollen networks of poly(*N*,*N*-diethylacrylamide) and its copolymer with *N-tert* butylacrylamide. Eur Polym J 1981; J17:361–366.
8. Ilavsky M. Phase transition in swollen gels. 2. Effect of charge concentration on the collapse and mechanical behavior of polyacrylamide networks. Macromolecules 1982; 15:782–788.
9. Ilavsky M, Hrouz J. Phase-transition in swollen gels. 4. Effect of concentration of the cross-linking agent at network formation on the collapse and mechanical behavior of polyacrylamide gels. Polym Bull 1982; 8:387–394.
10. Hirokawa Y, Tanaka T. Volume phase transition in a nonionic gel. J Chem Phys 1984; 81:6379–6380.
11. Amiya T, Tanaka T. Phase transitions in cross-linked gels of natural polymers. Macromolecules 1987; 20:1162–1164.
12. Ohmine I, Tanaka T. Salt effects on the phase transition of ionic gels. J Chem Phys 1982; 11:5725–5729.
13. Hirotsu S, Hirokawa Y, Tanaka T. Volume-phase transitions of ionized *N*-isopropylacrylamide gels. J Chem Phys 1987; 87:1392–1395.
14. Tanaka T, Nishio I, Sun S-T, Ueno-Nishio S. Collapse of gels in an electric field. Science 1982; 218:467–469.
15. Osada Y, Hasebe M. Electrically activated chemomechanical devices using polyelectrolyte gels. Chem Lett 1985;1285–1288.
16. Schild HG. Poly(*N*-isopropylacrylamide): experiment, theory and application. Prog Polym Sci 1992; 17:163–249.
17. Ilmain F, Tanaka T, Kokufuta E. Volume transition in a gel driven by hydrogen bonding. Nature 1991; 349:400–401.
18. Kokufuta E, Zhang Y-Q, Tanaka T. Saccharide-sensitive phase transition of a lectin-loaded gel. Nature 1991; 351:302–304.

19. Kokufuta E, Tanaka T. Biochemically controlled thermal phase transition of gels. Macromolecules 1991; 24:1605–1607.
20. Kokufuta E, Zhang Y-Q, Tanaka T, Mamada A. Effects of surfactants on the phase transition of poly(*N*-isopropylacrylamide) gel. Macromolecules 1993; 26: 1053–1059.
21. Kokufuta E. Novel applications for stimulus-sensitive polymer gels in the preparation of functional immobilized biocatalysts. Adv Polym Sci 1993; 110:157–177.
22. Kokufuta E, Tanaka T, Ito S, Hirasa O, Fujishige S, Yamauchi I. Thermosensitive *N*-*n*-propylacrylamide gels. Phase Transitions 1993; 44:217–225.
23. Hirata M, Yamada Y, Kokufuta E. Effects of pH and alkyl sulfate surfactants on swelling equilibria for a cationic polyelectrolyte gel from poly-(ethyleneimine). In: Schmitz K, ed. Macro-ion Characterization from Dilute Solutions to Complex Fluids. ACS Symp Ser, No 548. Washington DC: Amer Chem Soc, 1994:493–498.
24. Kokufuta E, Nakaizumi S, Ito S, Tanaka T. Uptake of sodium dodecylbenzene sulfonate by poly(*N*-isopropylacrylamide) gel and effect of surfactant uptake on the volume phase transition. Macromolecules 1995; 28:704–1708.
25. Kokufuta E. Functional immobilized biocatalysts prepared using stimulus-sensitive polymer gels. In: Salamone JC, ed. The Polymeric Materials Encyclopedia: Synthesis, Properties and Applications. Vol. 4, F-G. New York: CRC Press, 1996:2615–2621.
26. Kokufuta E, Suzuki H, Sakamoto D. On the local binding of ionic surfactants to poly(*N*-isopropylacrylamide) gels. Langmuir 1997; 13:2627–2632.
27. Kokufuta E, Suzuki H, Yoshida R, Yamada K, Hirata M, Kaneko F. Role of hydrogen bonding and hydrophobic interaction in the volume collapse of a poly(ethyleneimine) gel. Langmuir 1998; 14:788–795.
28. Kokufuta E, Wang B, Yoshida R, Khokhlov AR, Hirata M. Volume phase transition of polyelectrolyte gels with different charge distributions. Macromolecules 1988; 31:6878–6884.
29. Tokuhiro T, Ito S, Kokufuta E. Reversed thermal behaviors of poly[*N*-(1,3-dioxolan-2-ylmethyl)-*N*-methylacrylamide] and its cross-linked analogue in liquids: water vs. alcohols. Macromolecules 1998; 31:8549–8557.
30. Suzuki H, Kokufuta E. Inhomogeneous binding of ionic surfactants to bulk gels and microgels consisting of poly(*N*-isopropylacrylamide). Colloids Surfaces 1999; A 147:233–240.
31. Kokufuta E, Suzuki H, Yoshida R, Kaneko F, Yamada Y, Hirata M. Volume collapse of a cationic poly(ethyleneimine) gel induced by the binding of anionic surfactants. Colloids and Surfaces 1999; A 147:179–187.
32. Ito S, Ogawa K, Suzuki H, Wang B, Yoshida R, Kokufuta E. Preparation of thermosensitive submicron gel particles with anionic and cationic charges. Langmuir 1999; 15:4289–4294.
33. Suzuki H, Wang B, Yoshida R, Kokufuta E. Potentiometric titration behaviors of polymer and gel consisting of *N*-isopropylacrylamide and acrylic acid. Langmuir 1999; 15:4283–4288.

34. Neuburger NA, Eichinger BE. Critical experimental test of the Flory–Rehner theory of swelling. Macromolecules 1988; 21:3060–3070.
35. Horkay F, Heicht AM, Ceissler E. Effect of cross-links on the swelling equation of state. Polyacrylamide hydrogels. Macromolecules 1989; 22:2007–2009.
36. Prange MM, Hooper HH, Prausnitz JM. Thermodynamics of aqueous systems containing hydrophilic polymers or gels. AIChE J 1989; 35:803–813.
37. Beltran S, Hooper HH, Blanch HW, Prausnitz JM. Swelling equilibria for ionized temperature-sensitive gels in water and in aqueous salt solutions. J Chem Phys 1990; 92:2061–2066.
38. Hooper HH, Baker JP, Blanch HW, Prausnitz JM. Swelling equilibria for positively ionized polyacrylamide hydrogels. Macromolecules 1991; 23:1096–1104.
39. Beltran S, Baker JP, Hooper HH, Blanch HW, Prausnitz JM. Swelling equilibria for weakly ionizable, temperature-sensitive hydrogels. Macromolecules 1991; 24:549–551.
40. Marchetti M, Prager S, Cussler EL. Thermodynamic predictions of volume changes in temperature-sensitive gels. 1 Theory. Macromolecules 1990; 23: 1760–1765.
41. Lee KK, Cussler EL, Marchetti M, McHugh MA. Pressure-dependent phase transitions in hydrogels. Chem Eng Sci 1990; 45:766–767.
42. Otake K, Inomata H, Konno M, Saito S. A new model for the thermally induced volume phase transition of gels. J Chem Phys 1989; 91:1345–1350.
43. Nemẽthy G, Sheraga HA. The structure of water and hydrophobic bonding in proteins. III. The thermodynamic properties of hydrophobic bonds in proteins. J Phys Chem 1962; 66:1773–1789.
44. Hasa J, Ilavsky M, Dusek K. Deformational, swelling, and potentiometric behavior of ionized poly(methacrylic acid) gels. I. Theory. J Polym Sci, Polym Phys Edn 1975; 13:253–262.
45. Hasa J, Ilavsky M. Deformational, swelling, and potentiometric behavior of ionized poly(methacrylic acid) gels. II. Experimental results. J Polym Sci, Polym Phys Edn 1975; 13:263–274.
46. Ilavsky M, Dusek K, Vaciki J, Kopecek J. Deformational, swelling, and potentiometric behavior of ionized gels of 2-hydroxyethyl methacrylate-methacrylic acid copolymers. J Appl Polym Sci 1979; 23:2073–2082.
47. Ilavsky M, Talasova E, Dusek K. The photoelastic behavior of swollen networks of polymethacrylic acid. Eur Polym J 1980; 16:191–199.
48. Ilavsky M, Plestil J, Dusek K. The photoelastic behavior and small-angle x-ray scattering of ionized gels of copolymers of 2-hydroxyethyl methacrylate with methacrylic acid. Eur Polym J 1980; 16:901–907.
49. Konak C, Bansil R. Swelling equilibria of ionized poly(methacrylic acid) gels in the absence of salt. Polymer 1989; 30:677–680.
50. Tong Z, Liu X. Swelling equilibria and volume phase transition in hydrogels with strongly dissociating electrolytes. Macromolecules 1994; 27:844–848.
51. Frank HS, Evans MW. Free volume and entropy in condensed systems: III. Entropy in binary liquid mixtures; partial molal entropy in dilute solutions;

structure and thermodynamics in aqueous electrolytes. J Chem phys 1945; 13: 507–532.
52. Kauzmann W. Some factors in the interpretation of protein denaturation. Adv Protein Chem 1959; 14:1–57.
53. Matsuo ES, Tanaka T. Kinetics of discontinuous volume-phase transition of gels. J Chem Phys 1988; 89:1695–1703.
54. McPhee W, Tam KC, Pelton RH. Poly(*N*-isopropylacrylamide) latices prepared with sodium dodecyl sulfate. J Colloid Interface Sci 1993; 156:24–30.
55. Pelton RH, Chibante P. Preparation of aqueous latices with *N*-isopropylacrylamide. Colloids Surfaces 1986; 20:247–256.
56. Pelton RH, Pelton HM, Morphesis A, Rowell RL. Particle sizes and electrophoretic mobilities of poly(*N*-isopropylacrylamide) latex. Langmuir 1989; 5: 816–818.
57. Kawaguchi H, Fujimoto K, Mizuhara Y. Hydrogel microspheres III. Temperature-dependent adsorption of proteins on poly-*N*-isopropylacrylamide hydrogel microspheres. Colloid Polym Sci 1992; 270:53–57.
58. Tam KC, Ragaram S, Pelton RH. Interaction of surfactants with poly(*N*-isopropylacrylamide) microgel latexes. Langmuir 1994; 10:418–422.
59. Makino K, Yamamoto S, Fujimoto K, Kawaguchi H, Ohshima H. Surface structure of latex particles covered with temperature-sensitive hydrogel layers. Colloid Interface Sci 1994; 166:251–258.
60. Tanaka T, Sato E, Hirokawa Y, Hirotsu S, Peetermans J. Critical kinetics of volume phase transition of gels. Phys Rev Lett 1985; 55:2455–2458.
61. Hirose Y, Amiya T, Hirokawa Y, Tanaka T. Phase transition of submicron gel beads. Macromolecules 1987; 20:1342–1344.
62. Crowther HM, Vincent B. Swelling behavior of poly-*N*-isopropylacrylamide microgel particles in alcoholic solutions. Colloid Polym Sci 1998; 276:46–51.
63. Lowe TL, Tenhu H. Interactions of thermally responsive polyelectrolyte latices with low molar mass organic molecules studied by light scattering. Macromolecules 1998; 31:1590–1594.
64. Zhou S, Chu B. Synthesis and volume phase transition of poly(methacrylic acid-co-*N*-isopropylacrylamide) microgel particles in water. J Phys Chem B 1998; 102:1364–1371.
65. Bray JC, Merrill EW. Poly(vinyl alcohol) hydrogels. Formation by electron beam irradiation of aqueous solutions and subsequent crystallization. J Appl Polym Sci 1973; 17:3779–3794.
66. Peppas NA, Moynihan HJ, Lucht LM. The structure of highly crosslinked poly(2-hydroxyethyl methacrylate) hydrogels. J Biomed Mater Res 1985; 19: 397–411.
67. Otake K, Inomata H, Konno M, Saito S. Thermal analysis of the volume phase transition with *N*-isopropylacrylamide gels. Macromolecules 1990; 23:283–289.
68. Eliassaf J. Aqueous solutions of poly(*N*-isopropylacrylamide). J Appl Polym Sci 1978; 22:873–874.
69. Inomata H, Goto S, Saito S. Effect of sodium dodecyl sulfate on the volume phase transition of *N*-isopropylacrylamide gel. Langmuir 1992; 8:1030–1031.

70. Zhang Y-Q, Tanaka T, Shibayama M. Super-absorbency and phase transition of gels in physiological salt solutions. Nature 1992; 360:142–144.
71. Wada N, Kajima Y, Yagi Y, Inomata H, Saito S. Effect of surfactant on the phase transition of *N*-alkylacrylamide gels. Langmuir 1993; 9:46–49.
72. Schild HG, Tirrell DA. Interaction of poly(*N*-isopropylacrylamide) with sodium *n*-alkyl sulfates in aqueous solution. Langmuir 1991; 7:665–671.
73. Borue VY, Erukhimovich IY. A statistical theory of weakly charged polyelectrolytes: fluctuations, equation of state, and microphase separation. Macromolecules 1988; 21:3240–3249.
74. Dormidontova EE, Erukhimovich IY, Khokhlov AR. Microphase separation in poor-solvent polyelectrolyte solutions: phase diagram. Makromol Theory Simul 1994; 3:661–675.
75. Grosberg AY, Khokhlov AR. Statistical Physics of Macromolecules. New York; American Institute of Physics, 1994.
76. Dubin P, Strauss UP. Conformational transitions of hydrophobic polyacids in denaturant solutions. The effect of urea. J Phys Chem 1973; 77:1427–1431.
77. Vakkalanka SK, Peppas NA. Swelling behavior of temperature- and pH-sensitive block terpolymers for drug delivery. Polym Bull 1996; 36:221–225.
78. Saegusa T, Ikeda H, Fujii H. Isomerization polymerization of 2-Oxazoline. I. Preparation of unsubstituted 2-Oxazoline polymer. Polym J 1972; 3:35–39.
79. Warakomski JM, Thill BP. Evidence for long chain branching in polyethyloxazoline. J Polym Sci, Polym Chem Edn 1990; 28:3551–3563.
80. Davis LE. Polyethlenimine. In: Water-Soluble Resins. Davidson RL, Sittig M, eds. New York: Van Nostrand Reinhold, 1968:216–226.
81. Kobayashi S, Hiroishi K, Tokunoh M, Saegusa T. Chelating properties of linear and branched poly(ethylenimines). Macromolecules 1987; 20:1496–1500.
82. Weyts KF, Goethals EJ. Back titration of linear polyethylenimine: decrease of pH by addition of sodium hydroxide. Makromol Chem Rapid Commun 1989; 10:299–302.
83. Lewis EA, Barkley J. Pierre TS. Calorimetric titration of poly(vinylamine) and poly(iminoethylene). Macromolecules 1981; 14:546–551.
84. Chatani Y, Tadokoro H, Saegusa T, Ikeda H. Structural studies of poly(ethylenimine). 1. Structures of two hydrates of poly(ethylenimine): sesquihydrate and dihydrate. Macromolecules 1981; 14:315–321.
85. Katchalsky A, Mazur J, Spitnik P. General behavior of biocolloids and polyelectrolytes in solution (continued): polybase properties of polyvinylamine. J Polym Sci 1957; 23:513–532.
86. Kuharski RA, Rossky PJ. Molecular dynamics study of solvation in urea–water solution. J Am Chem Soc 1984; 106:5786–5793.
87. Tanaka H, Touhara H, Nakanishi K, Watanabe N. Computer experiment on aqueous solution. IV. Molecular dynamics calculation on the hydration of urea in an infinitely dilute aqueous solution with a new urea–water pair potential. J Chem Phys 1984; 80:5170–5186.
88. Morawetz H. Macromolecules in Solutions. New York: Wiley Interscience, 1965.

89. Kokufuta E. Electrophoretic and viscometric properties of poly(dicarboxylic acids). Polymer 1980; 21:177–182.
90. Huizenga JR, Grieger PF, Wall FT. Electrolytic properties of aqueous solutions of polyacrylic acid and sodium hydroxide. I. Transference experiments using radioactive sodium. J Amer Chem Soc 1950; 72:2636–2642.
91. Kokufuta E. Functional immobilized biocatalysts. Prog Polym Sci 1992; 17(4): 647–697.
92. Kokufuta E, Matsukawa S, Ebihara T, Matsuda K. Construction of biochemo-mechanical systems using polyelectrolyte gels. In: Schmitz K, ed. Macro-ion Characterization from Dilute Solutions to Complex Fluids. ACS Symp Ser, No 548. Washington DC: Amer Chem Soc, 1994:507–516.
93. Kokufuta E: A Biochemo-mechanical system consisting of polymer gels with immobilized glucose oxidase. In: Gebelein CG, Carraher CE Jr, eds. Industrial Biotechnological Polymers. Pennsylvania: Technomic, 1995:283–295.
94. Kokufuta E, Matsukawa S. Construction of a biochemo-mechanical system using inhomogeneous polyelectrolyte gels with immobilized urease. Ber Bunsenges Phys Chem 1996; 100:1073–1078.
95. Kokufuta E, Aman Y. A biochemo-mechanical system consisting of polymer gels with immobilized glucose dehydrogenase. Polym Gels Networks 1997; 5: 439–454.

18

Anomalous Migration of DNA in Gels and the Polyelectrolyte Nature of DNA

UDAYAN MOHANTY and LARRY W. McLAUGHLIN Boston College, Chestnut Hill, Massachusetts

I. INTRODUCTION

Gel electrophoresis is without a doubt one of the most important analytical tools in molecular biology and biochemistry, and it is invaluable in predicting conformation and structural changes of nucleic acids upon their interaction with proteins and small ions [1a–d]. While this technique is used daily in hundreds of laboratories, the physical mechanisms underlying gel-based electrophoresis are still poorly understood at best. That this lack of understanding does not involve merely minutiae is demonstrated amply by the recent discovery that size-dependent electrophoretic mobility of small ss DNA fragments exhibits behavior that is exactly opposite to that of larger fragments [1e]. A quantitative theoretical understanding of the mechanism of gel-retardation of biologically significant macromolecules such as bent-DNA sequences and protein-induced DNA are needed since they will simplify the interpretations of what are now considered to be unusually complex phenomena. The bending of DNA by proteins is important in the control of replication and recombination processes, the packaging of DNA into nucleosomes, and transcriptional regulation phenomena [2–6].

This review article is divided into two main parts. In the first part, Sec. II, we describe recent experimental and theoretical advances in understanding electrophoretic mobility of DNA in agarose gels [7,8] as well as the anomalous migration of intrinsically curved DNA sequences [9–19], and protein-DNA complexes in polyacrylamide gel [20–28,3,4]. In the second part, Sec. III, we briefly review two topics involving the polyelectrolyte characteristics of DNA: [1] Coulombic ''end effects'' and (2) the connection between Poisson–Boltzmann and counterion condensation approaches.

II. GEL ELECTROPHORESIS OF DNA AND PROTEIN–DNA COMPLEXES

A. Agarose Gel Electrophoresis

The mechanism by which large DNA molecules are separated based upon their molecular weights during steady field or pulsed field agarose gel electrophoresis is not well understood. The prevalent view is that the DNA migrates through the gel by snakelike movements and that the external electric field does not in any way orient the matrix [7].

Recently, Stellwagen and coworkers [8a–c] have reported that agarose gels become birefringent after the application of long low-voltage pulses, as is characteristic of pulsed field gel electrophoresis (PFGE) experiments. These studies reveal several unexpected features [8b–c]: (1) In the presence of long low-voltage pulses, the amplitude and sign of the birefringence signal vary randomly with respect to the position in the gel, indicating independently rearranging gel domains [8b]. The time constants for orientation and ''nonrandom'' orientation of the agarose gel are of the same order of magnitude as those for the DNA [8b]. (2) The size of the domains increases with the strength of the electric field [8b]. (3) The size of the domains is on the order of the size of megabase DNA fragments [8b]. (4) Several relaxation times of ''alternating'' sign are observed, and they are independent of pulse duration [8b].

For the constant field case, Homes and Stellwagen find that the orientation of the matrix affects the direction of migration and mobility of the DNA [8a]. Another significant finding is that agarose gels exhibit ''intrinsic'' birefringence even in the absence of an external electric field [8c]. This observation is in agreement with that of Dormoy and Candau who report that dilute agarose particles possess permanent electrical dipole moments that scale as the length of the particles [8d].

Jonsson et al. [29] have developed in situ techniques to study the orientation of large linear double-stranded DNA fragments that are subjected to agarose (1%) gel electrophoresis. The long axis of the DNA helix is observed to be generally aligned parallel to the direction of migration, with this orientation increasing sigmoidally as the strength of the electric field increases. Furthermore, these authors observe, not only orientation effects in the gel due to local heating, but that electrophoresing DNA leads to orientation characteristics that reveal differences in the ''rear'' and the ''front'' of the migration zone [29]. This effect has been attributed to gel expansion and contraction in the rear and the front of the migration zone, respectively [29].

Further evidence that distortion of the gel matrix affects the dynamics of DNA migration comes from electric birefringence imaging techniques (EBI) developed by Morris and coworkers [30,31]. The EBI technique has been

recently extended to encompass short and long voltage pulses. These authors [30] showed that a major contribution to the birefringence signal from the gel is a result of ''hydrodynamic distortion.'' The stress-optical coefficients that reflect the induced strain of the gel have been measured [30].

Theories of gel electrophoretic mobility are usually based on the reptation theory introduced for polymer melts by de Gennes, as well as Doi and Edwards [32,33,7]. Their approach succeeded in explaining the inverse relationship between mobility and chain length for short fragments of DNA [7d]. By replacing the ''tube'' in the reptation model by ''open spaces'' and ''lakes'' connected by ''straights,'' Zimm explained the antiresonance phenomena observed in the field inversion experiments that occur when the time scale for the formation of the conformational change of the DNA coincides with the time scale for the field cycle [7c].

The correlation between longitudinal fluctuations and the drift of the polyion along the tube leads to significant effects on the molecular orientations and the field dependence of mobility [34–36]. The so-called new biased reptation theory predicts, for example, that the end-to-end vector varies as the square root of the field strength [34]. This result is in agreement with computer simulations [7c]. A lattice version of the reptation model—the ''repton'' model—has been proposed recently [37]. This model predicts scaling laws for drift velocity as a function of the DNA fragment length, the concentration of the gel, and the electric field strength, which are all in agreement for experiments on DNA λ-phage Hind III fragments [38].

The main significance of the experiments by Stellwagen (8), Jonsson et al. [29], and Morris and coworkers [30] is that gel distortion must be taken into account in formulating theoretical models to explain electrophoresis of DNA. However, in the theories described above, it is assumed that the pores, or spaces, in a gel are all energetically equivalent [7a,32,33]. In their description of DNA mobility, Zimm and Lumpkin included the effects of the free energy of interaction between the probe and the matrix and found that free energy traps slow the motion of the probe [7a].

New insights into and theoretical tools for studying the mechanism of gel-retardation of DNA and the wide variety of structures they adopt, are needed, since current models [7,32,33,39] for gel electrophoresis are unable to take into account the motion of the gel matrix on the time scale of the conformational change of the DNA. Further, the mechanism by which DNA migrates during pulsed field agarose gel electrophoresis [1a,40,41] is also not well understood. Under pulsed field conditions, the domains in agarose gel create *dynamic* channels that may enhance the migration of megabase DNA fragments [8].

B. Anomalous Migration of Intrinsically Curved DNA Fragments

A variety of experimental techniques, such as electro-optical and calorimetric [42–43], electron microscopy [44], circular permutation gel assays [13,15], gel mobilities [10–18], cyclization kinetics [45,12–14,3], NMR [46], hydroxyl radical footprinting [47], topoisomer band shift method [48], time resolved fluorescence resonance spectroscopy (FRET) [49], and computer simulations [50] have been used to probe the sequence directed intrinsic curvature of DNA. In particular, a wealth of experimental data indicates that homopolymeric $(dA \cdot dT)_{4-6}$ 4 to 6 bp sequences of adenines—the so-called "A-tracts"—if inserted in-phase with the helical repeat of ≈10.4 bp/turn will result in inducing a global curvature of the DNA double helix [9–18,42–58]. This conclusion is at variance with the known crystal structure of A-tracts [59,60a,60b]. This has been attributed to the presence of dehydrating agents such as 2-methyl-2,4-pentanediol (MPD) and polyethylene glycol (PEG) in the crystallization of oligo DNA [61a,61b].

The anomaly observed in the gel mobility of DNA fragments isolated from the kinetoplast body of typanosome parasites, and from bacteriophage λ, is generally viewed as being due to sequence-directed bending [12–15]. By analyzing how gel electrophoretic mobilities vary with bending, Wu and Crothers mapped the bending locus in a Sau3A restriction fragment acquired from *Leishmania tarentolae* kinetoplast (K) DNA [13,51a]. This was achieved by analysis of the gel mobilities for a set of circularly permuted K-DNA fragment constructs in which the position of the bend was varied. From the center of the bend, the sequence element $d(CA_{5-6}T)$ was identified to have a 10 bp periodicity [12,13,51a].

To elucidate the role of the phasing of the bending loci, oligonucleotide sequences of the form $d(A_5N_k)_n$, containing k bases (k = 4, 5, 6, 7, 10) of G·C rich segments between the A_5 tracts, were synthesized and then ligated together to form multimers [14,51a]. Gel electrophoresis of the multimers was carried out at ambient temperature in an 8% polyacrylamide gel (with the ratio of acrylamide to bisacrylamide held fixed at 29 : 1), in 90 mM Tris·borate, pH 8.3, 2.5 mM EDTA, with an applied voltage of 8 V/cm. To verify the ordinary mobility characteristics of 10 bp BamHI linkers as size standards, it was electrophoresed next to a pBR 322-Hinf I digest [14,51a].

When the phasing of the 10-bp repeat almost matches the anticipated helix screw of 10.4 bp/turn (obtained by taking an average value of the B-DNA and the poly(dA)·poly(dT) in solution), minimum mobility (i.e., the greatest anomaly) is observed. Relative to the $(A_5N_5)_n$ repeat more normal behavior in electrophoretic mobility is observed for the series $(A_5N_4)_n$ (which phases with a 9 bp repeat) [14,51a].

The series $(A_5N_{10})_n$ were designed to distinguish the effects on gel mobility due to bends in the direction of the helical screw and those due to expanded flexibility [14,51a]. No bending is observed when the separation between the A-tracts units is half-integral. Consequently, the bends have a ''directional preference.'' Thus what is observed is ordinary gel mobility, in agreement with hydrodynamic calculations, which show a lack of increased flexibility in the bending locus [14,51a].

Symmetry features of the bending locus have also been investigated. Syntheses of $(A_j - T_j)_n$ (j = 5, 6, 8) was accomplished with alternate CA_jC sequences converted to GT_jG sequences [14,51a]. A comparison of the gel mobilities of the series $(A_j - T_j)_n$ with multimers $(A_j - N_{10})_n$ (whose A-tracts have identical length) were carried out. A noteworthy result is that there is not much alternation in the direction of bending due to a twofold rotation of the A_j bending locus [14,51a].

There are two temperature effects for DNA bending. At lower temperatures bending increases, as is found in both A_5N_5 sequences and those containing A_5N_{10} tracts [14,51a]. However, if the number of base pair sequences in these molecules is larger than 100 or so, the effects are different, due possibly to contributions from the DNA helical screw [14,51a]. Furthermore, sequences $(A_9N_1)_n$ show a decrease in gel mobility anomaly with decreased temperature [14,51a]. This effect has recently been confirmed by the detailed study of Ussery and Bolshoy on the gel mobility of ligation ladders of over a dozen designed sequences in which the GC content varied from 0 to 70% [52,18a].

Koo and Crothers [12,51b] in a seminal report have obtained an empirical relationship between gel electrophoretic mobility and the intrinsic bend of DNA molecules through the parameter R_L, defined as the ratio of the length of the ''size marker'' (resulting in identical gel mobility) to the actual length of the multimer. Thus $(R_L - 1)$ is a measure of anomalous gel migration mobilities. The relationship between $(R_L - 1)$ and the relative curvature is not in general linear, and in particular for the sequences in which the A_6 tracts vary from 1 per turn of the helix (e.g., $A_6 - 1/1$) to 1 for every four turns of the helix (e.g., $A_6 - 1/4$) [12,51b]. As the relative curvature for sequence $A_6 - 1/2$ is increased to $A_6 - 1/1$, the value of $(R_L - 1)$ is quadrupled [12,51b]: $R_L - 1 = A(\text{relative..curvature})^2$. The quantity A is proportional to the square of the length of the multimer. The relative curvature is an indicator of the number of A-tracts in one turn of the helix [12,51b]. The relative curvature is converted to absolute curvature by the use of parameters of the junction model that have been obtained by computer simulations and cyclization kinetic studies [12–14,45,51]. An alternative interpretation would rely upon the use of the wedge models [53,54].

Effects of flexibility on the electrophoretic anomaly are found to be modest [15]. The persistence length of ''normal DNA'' does not differ much from a sequence containing the A-tract [55]. How flexibility depends on sequence is not yet fully understood [56]. Two complementary approaches for describing the origin of sequence-directed DNA curvature have been proposed. These two descriptions are known as the junction model and the wedge model [12–14,17,51–53,56]. The wedge model assumes that DNA bends in a smooth and global way due to small additive wedges at each dinucleotide step [56,51–53,17]. The base pair steps provide the required parts of the roll and the tilt for the wedges [17,51–53]. In this model, other dinucleotide steps are also capable of deflecting the DNA axis. From a variety of gel mobility experiments the sixteen wedge angles have been estimated [17a].

In the pioneering junction model of Wu and Crothers, it is assumed that a pair of helical segments intersects at a junction that is responsible for helix axis deflection [12–14,51,56]. At the junction, the two helix axes are assumed to have no tilt or base pair rolls, and that there are no wedge angles between the base pairs [12–14,51,56]. The model assumes that the extent of bending by a B-DNA with dA·dT tracts is larger than that of B-DNA sequences lacking A-tracts [12–14,51,56]. The main difference between the wedge and junction models lies in the way the helix axis is defined [56]. A current view is that the same structure is describable by both models in a way that complements each other [56].

To identify the sequence elements that are responsible for B-DNA curvature, Haran et al. have made a penetrating and detailed study of the modulation in electrophoretic mobility that results by inserting 5 bp DNA sequences between A-tracts of the form $(A_{5-6}N_5)_n$ [56]. The four sequences considered by these authors are called Ast, Agood, Abad, and Amix. The first is the standard A-tract construct. Agood and Abad enhance and retard A-tract bending, respectively, while the Amix has the gel mobility characteristics in between Agood and Abad [56]. Several conclusions were reached by Haran et al.: (1) Sequence elements affect A-tract-induced DNA curvature. The magnitude of the effect is about $\pm 10\%$ [56]; (2) DNA curvature results from the insertion of A-tracts that are in phase with the helical turn of the B-DNA [56]; (3) the data are compatible with the weighted sum of the wedge and junction models. It is also in agreement with an average of a zero roll angle in B-DNA, with A-tracts having a negative roll angle [56]; this conclusion is at variance with Dickerson and coworkers [59,60] who have argued, based partly on the crystal structures of A-tract-containing molecules, that A-tract bending is consistent with the model that has almost no roll among the base pairs, but with segments of the B-DNA having nonnegative roll [56].

The application of cyclization techniques in polymer literature to DNA ligase-catalyzed reactions have received considerable attention [45a,61–64,3]. In this approach, a small concentration of cyclized molecules in the steady state is detected [45a,51c]. The molecules are cyclized by covalent bond formation between the ends of the DNA fragments. The extent of the sequence-directed bending angle in DNA has been measured from the cyclization efficiency mediated by the so-called ring closure probability or the J factor [45,51c]. The J factor is defined as the ratio of the equilibrium constants for cyclization and bimolecular association [45,51c]. By comparing the experimental efficiencies of ring closures with those obtained theoretically by Monte Carlo simulations, the magnitude of bending induced by an A-tract has been deduced [45,51c]. The calculation of the magnitude of the bend introduced by an A-tract in cyclization kinetic studies depends in a sensitive way on the helical repeat [45,51c].

Recently, Young and Beveridge [50] have carried out detailed molecular dynamics (MD) simulations in water with various concentrations of univalent and divalent salts of a particular form of a B-DNA oligonucleotide sequence containing phased A-tracts. The MD simulations were based on the ''particle mesh'' Ewald algorithm of handling long range Coulombic interactions together with the latest AMBER 4.1 force field [50]. This force field is known to describe accurately the structure of B-DNA in solution. The authors find that B-DNA exhibited spontaneous bending of its axis [50]. The average measure of the bend is approximately 16.5° per A-tract, while cyclization studies show a slightly larger bend per helical turn [45,50]. In agreement with the direction of the curvature as predicted by Zinkel and Crothers, the simulations reveal a $5' \rightarrow 3'$ compression of the minor groove [65]. This novel feature is in accord with footprinting experiments by hydroxyl radical cleavage of phased A-tracts DNA [47].

Bend-induced retardation of DNA in gels is not predicted by classical reptation theory. An extension of the tube reptation to describe bent DNA was proposed by Levene and Zimm (66). In this model, the conformation of the tube was determined by a dynamic Monte Carlo algorithm with important sampling. The elastic free energy of the chain in the tube was taken into account in an approximate way in order to accommodate the deformation of the DNA in the gel [66]. The transition probabilities for the Monte Carlo moves were obtained from the solution of a diffusion equation in which the drift term has contributions from the electrical force as well as from the elastic free energy of the chain [66]. The results obtained by Levene and Zimm support the following conclusions: (1) gel mobilities strongly depend on the angle of the bend [66]; (2) the more concentrated the gel, the larger the gel retardation [66]; (3) in agarose gel normal mobilities are obtained [66]; (4) the force constant for bending increases in a linear way

according to the ratio P/a, where P is the persistence length and a is the interfiber spacing [66]; (5) a bend at the center of a DNA fragment retards the molecule more than if the same bend occurs at the terminus [66].

Despite the considerable success of the Levene–Zimm model [7], quantitative agreement with anomalous gel retardation experiments is lacking. Since no further generalizations of this model exist, theoretical predictions of the bend angles in bent DNA are usually based on following the empirical relation [67]: $\eta_c = \eta_e \cos(\alpha/2)$, where η_e and η_c are the mobilities of DNA when the A-tracts are inserted at the end and at the center of the molecule, respectively, and α is the bend angle. This relationship has been justified based on end-to-end distance arguments, but the properties of the gel, the interaction of the gel with the curved DNA, and the viscoelastic response of the DNA have been ignored.

Despite extensive experimental studies of the gel retardation effects for bent DNA molecules and protein–DNA complexes, the interpretation of the gel mobility data based on tube reptation is unable to describe quantitatively the wealth of data on intrinsically bent DNA sequences. This failure is due to the inability of the model to take explicitly into account the structural features of the reptating molecules, the phasing between the bends, the interactions of the molecule with the gel, the viscoelastic response of the gel, and the ionic strength of the buffer. The mechanisms by which intrinsically curved DNA fragments migrate in gels is of fundamental significance since bending and flexibility of DNA sequences have been linked to transcription, recombination, and packaging events as well as having a role in the origin of DNA replication [6a,6b,68,69]. Bending could act by facilitating DNA–protein and protein–protein contacts [3].

C. Protein–DNA Complexes

A number of diverse techniques including x-ray crystallography, circular permutation analysis, gel phasing, and the more recent phase-sensitive analysis have been utilized to study protein-induced DNA bending for proteins such as the prokaryotic catabolic activator protein (CAP), the eukaryotic TATA binding protein, and the basic region–leucine zipper bZIP such as ATF1, ATF2, Fra2, CREB, and Fos and Jun [70–73;20–28]. It is well established that the basic region–leucine zipper family of DNA binding proteins, such as Fos and Jun, binds the AP-1 DNA regulatory element [21–24]. It has been hypothesized that this induces a bend in DNA that initiates the function [20–28].

Circular permutation and phase-sensitive gel electrophoretic analyses by Kerppola and Curran indicate that Fos and Jun heterodimers bend DNA in the direction of the minor groove [22,25,20]. The bend is inclined towards

the major groove at the AP-1 regulatory site for bZIP homodimers proteins (Jun–Jun) [22,25,20]. The gel studies reported by these authors also indicate that the magnitude of the bend angle in DNA by dimer proteins of full length is $\approx 25-30^{\circ}$ [22,25,20].

In contrast to the above studies, based on T4 ligase mediated DNA cyclization kinetic experiments, Crothers and coworkers' find that Fos and Jun do not bend the AP-1 DNA recognition site. The sites studied were constructed from either the human collagenase gene or from yeast [20]. These sequences do not affect the binding characteristics of Fos and Jun. Cyclization results are not affected when a portion, or the entire length, of the Fos–Jun complexes are utilized [20]. This conclusion is further validated by gel phasing studies, similar to that used for GCN4. No changes in gel mobility for the macromolecules formed by Fos–Jun and the phased DNAs were observed [20,72].

The results of Crothers and coworkers are in agreement with the analysis of crystal data of bZIP Fos–Jun bound to AP-1 DNA [23,20]. The data indicate a DNA helix that is only marginally bent (less than 10°) [23].

Several plausible explanations have been offered for the contradictory results. First, DNA bends by Fos and Jun may be due to those parts of the protein that are situated outside the ''minimal'' bZIP domains involved in the crystallization study [24,20]. Second, if neutralization of parts of phosphate charges in DNA can lead to bending of DNA, as observed in a recent experiment [74], then electrostatic interactions could affect DNA bending by bZIP proteins [24,21]. In this case, shielding of the phosphate charges by the multivalent ions is of fundamental significance, since large concentrations of the ions are utilized in crystallization studies [24,23]. The third reason has been attributed to the DNA constructs themselves (i.e., the probe design) [20,21]. For asymmetrically shaped molecules, the A-tract bend must be located three to four helical turns away from the AP-1 protein binding site to prevent the possibility of cross communication between the two sites [20]. Finally, it has been suggested that gel mobilities measured by phase-sensitive methods of heterodimers bound in opposite orientations are different [20,21].

Recently, Kerppola has made a thorough study of the effects of the probe geometry on DNA bending by various complexes of Fos and Jun in order to address the first, third, and fourth explanations offered above for the observed contradictory results [21]. Probes containing the AP-1 DNA site that are well separated from the intrinsic DNA bend (ranging from 6-bp to 15-bp) were constructed from plasmids pTK430-55 and pTK430-57 using appropriate restriction digestion enzymes and followed by ligation and PCR [21]. The phase-sensitive detection experiments yielded several new insights: (1) for a DNA with two bends whose phasing can be varied, its gel mobility

depends strongly on the length of the segments that are on each side of the bends [21]; (2) by designing constructs with the His-189 site near the intrinsically bent DNA having several in-phase A-tracts, gel mobilities of multimers revealed that sequences at the His3-189 site result in bent DNA [21]; (3) the mobilities of complexes formed by truncated Fos and Jun decrease with an increase of the distance between the protein-induced and the intrinsic DNA bends [21]; (4) the intra- and intermolecular ligation rates are affected by Fos and Jun. The mechanism, however, is not due to DNA bending [21].

Theoretical studies of Fos–Jun gel mobility data are based on an extension of the empirical relation given by Eq. 2 [21]. Kerppolla and Curran proposed an empirical relationship between the maximum mobility μ_{max}, corresponding to two in-phase bends with bend angles of α_B and α_c, respectively, and the minimum mobility μ_{min}, occurring when two bends are not in phase [21]. A parameter w is introduced to account for various factors such as the gel composition, the length of the fragment, the temperature, etc. Using two sets of ''standard'' constructs for bent DNA sequences, these authors estimate w under conditions of phase-sensitive detection [21]. The first involves Thompson–Landy-phased A : T tracts [67,21]. The second includes the three phased A : T tracts at variable location near the AP-1 recognition site from the circular permutation studies [21].

Because of their inability to describe the frictional resistance of curved DNA molecules as they migrate through the gel, and because the magnitude of the end-to-end distance does not vary in a significant manner with the distance between the two bends and in the length of the region that flanks the bends, tube reptation models of gel electrophoresis are unable to address the conflicting experimental reports on whether the AP-1 recognition site in DNA is bent by Fos–Jun protein [20,21]. Hence elucidation and interpretation of structural features associated with DNA–protein complexes and their interactions via gel electrophoresis is lacking due to the unavailability of theoretical models.

Understanding DNA structural changes due to transcription factor binding is of fundamental significance for the assembly of higher order nucleoprotein complexes [4,21,75]. The bZIP motif is widely used in transcriptional regulation [24,25,20]. A number of biological processes including cell differentiation, proliferation, and death have been related to Jun and Fos expression [24,25].

III. POLYELECTROLYTE CHARACTERISTICS OF DNA

A. End Effects

For a finite size polyion, a variety of computer simulations have established that the counterion distributions near the two ends are not uniform [76–82].

This is referred to as end effects that must be taken into account in describing colligative and dynamical properties of DNA.

Recently, Manning and Mohanty [83] have developed a statistical mechanical theory of end effects for a finite size polyion of radius a. The basic idea exploited by these authors relies upon the system being at equilibrium. Under these conditions the chemical potential μ is independent of the distance s measured along the backbone from one end of the polyion [84,83]:

$$\mu_i = \mu_0 + k_B T \log(\xi_0 - \xi[s]) - q|\psi(a, s)| \tag{1}$$

Here, ξ_0 is the polyion's charge density, and the potential of the finite line charge in the Debye–Hückel approximation is denoted by $\psi(a, s)$, while $\xi(s)$ is the linear charge density and related to the Bjerrum length l_B via $\xi(s) = l_B\xi_0$. One finds that the solution to Eq. 1 for the linear charge density is [84,83]:

$$\xi(s) \approx \frac{2 \log(\lambda/a)}{\log(\lambda/a) + \log(s/a)} \qquad a \leq s \leq \lambda \tag{2}$$

Several comments are in order. First, $\xi(s)$ is one for $\lambda \leq s \leq L/2$, where λ is the Debye screening length. Second, along the central portion of the polyion the condensation fraction of counterions has the Manning value $1 - 1/\xi_0$. Third, when the distance from the end is of the order of the Debye length, the condensed fraction of counterions starts to decrease substantially from the Manning value.

B. Counterion Condensation and Poisson–Boltzmann

There has been considerable discussion in the literature on whether the basic predictions of the counterion condensation formalism can be obtained from the more fundamental nonlinear Poisson–Boltzmann (PB) equation [77–82,85–89].

Recently, Mohanty et al. have provided a resolution to this issue [90a]. In this approach, the polyion is regarded as a cylinder of radius R of contour length L immersed in a univalent salt solution. The ions are expected to be ''bound'' to the polyion due to the high value of the linear charge density ξ, which for B-DNA is larger than 4. Consequently, the bound ions with the bare polyion are regarded as ''dressed.'' The free ions and the dressed ions can be viewed as an ideal mixture that interact via a Donnan potential [90a,91].

Although simulations, experiments, and integral equation approaches [79–82,92,89a–d,93] suggest the correctness of the dressed polyion picture,

firm theoretical justifications require that one show that the fraction of bound counterions is insensitive to changes in the salt concentrations [90a,91].

The basic idea proposed by Mohanty et al. is that the counterion condensation prediction can be justified by the PB equation through a thermodynamic quantity called the adsorption excess [90a]. In this approach, the surface charge density σ is obtained from the solution of the PB equation:

$$\sigma = 4 \sinh^2\left(\frac{y_0}{2}\right) - 2 \int_0^\infty \left(\frac{dy}{dx}\right) \left(\frac{dy}{x}\right) \tag{3}$$

where $y = e\Psi/k_BT$, Ψ is the electrostatic potential, κ^{-1} is the Debye length, $y_0 = y(x_0)$, and $x = \kappa R$. The quantity dy/dx that appears in Eq. 3 is approximated by PB solution to the corresponding planar interface problem [94]. Consequently, the surface charge density is evaluated in a self-consistent way [90a,91,94].

The adsorption excess per monomer is defined as

$$\gamma = -\left(\frac{\beta\kappa}{2}\right) \left(\frac{\partial g_{elec}}{\partial \kappa}\right) \tag{4}$$

where $\beta = 1/k_BT$, k_B is the Boltzmann constant, and T is the absolute temperature. g_{elec} is the free energy for charging the polyion and is proportional to the term $\int_0^\sigma y_0(\sigma')d\sigma'$, where the lower and upper limits of integration are respectively 0 and σ. In the counterion condensation limit, γ is equal to Manning's θ—the fraction of counterions per polyion charge that is neutralized by the counterions [90].

The importance of the result is twofold. First, it opens up a novel path to a systematic extension, via liquid state theories [95], of Manning's counterion condensation formalism [96–101]. Second, the methodology provides an alternative route to interpret and analyze the role of small ions in the binding characteristics of univalent and multivalent ions to nucleic acids and charged polymers [90,92,101].

IV. CONCLUSIONS

In this review article, we have critically described some recent experimental and theoretical advances in gel electrophoretic mobility of DNA in polyacrylamide and agarose gels. These studies have suggested that new paradigms are needed to describe sequence-dependent DNA bending. For example, GGGCCC-containing DNA, and other sequences that have no A-tracts exhibit anomalous migration in gel if divalent ions are present [102,103]. There is experimental evidence that nearest neighbor dinucleotide base pair interactions are not sufficient to account for sequence-dependent DNA bending [104–106]. Quantitative theoretical models are desperately

needed that are capable of describing the electrophoretic migration of intrinsically curved DNA and protein–DNA complexes in polyacrylamide gel.

REFERENCES

1. (a) Van Ommen, G. J. B.; Den Dunnen, J. T.; Lehrach, H.; Poutstka, A. Pulsed-field gel electrophoresis: applications to long-range genetics. *Electrophoresis of Large DNA Molecules: Theory and Applications*. Cold Spring Harbor Laboratory Press, 1990:133. (b) Hudson, J. H.; et al. An STS-based map of the human genome. Science 1995; 270:1945–1954. (c) I. Wickelgren. Protein sculptors that help turn on genes. Science 1995; 270:1587–1588. (d) Drmanac, R.; Drmanac, S.; Strezoska, Z.; Paunesku, T.; Labat, I.; Zeremski, M.; Snoody, J.; Funkhouser, W. K.; Koop, B.; Hood, L.; Crkvenjakov, R. DNA sequences determination by hybridization: a strategy for efficient large-scale sequencing. Science 1993; 260:1649–1652. (e) Mohanty, U.; Searls, T.; McLaughlin, L. W. Anomalous migration of short sequences of nucleic acids in polyacrylamide gels: prediction and experiment. J. Am. Chem. Soc. 1998; 120:8275–8276.
2. (a) Travers, A. A. Why bend DNA. Cell 1990; 60:177–180. (b) Perez-Martin, J.; Espinosa, M. Protein-induced bending as a transcriptional switch. Science 1993; 260:805–807. (c) Ripe, K.; Von Hippel, P. H.; Langowski, J. Action at a distance: DNA-loping and initiation of transcription. Trends Biochem Sci. 1995; 20:500–506.
3. (a) Kahn, J. D.; Crothers, D. M. DNA bending in transcription initiation. *Cold Spring Harbor Symposium on Quantitative Biology*, Volume 58, Cold Harbor Laboratory Press, 1993:115–122. (b) Kahn, J. D.; Crothers, D. M. Protein-induced bending and DNA cyclization. Proc. Nat. Acad. Sci. U.S.A. 1992; 89:6343–6347.
4. (a) Gartenberg, M. R.; Crothers, D. M. DNA sequence determinants of CAP-induced bending and protein binding affinity. Nature 1988; 333:824–829. (b) See also Refs. 21 and 75.
5. (a) Crothers, D. M. Architectural elements in nucleoprotein complexes. Current Biology 1993; 3:675–676. (b) Goodman, S. D.; Nicholson, S. C.; Nash, H. A. Deformation of DNA during site-specific recombination of bacteriophage 1: replacement of IHF protein by HU protein or sequence-directed bends. Proc. Nat. Acad. Sci. U.S.A. 1992; 89:11910–11914. (c) Gura, T. New kind of -1202 mutation found. Science 1997; 277:1201.
6. (a) Hwang, D. S.; Kornberg. Opening of the replication origin of *Escherichia coli* by DNA protein with protein HU or IHF. A. J. J. Biol. Chem. 1992; 267: 23083–23086. (b) See also Ref. 15. (c) Zinkel, S. S.; Crothers, D. M. Catabolic activator protein-induced DNA bending in transcription initiation. J. Mol. Biol. 1991; 219:201–215. (d) Schultz, S. C.; Shields, G. C.; Steitz, T. A. Crystal structure of a CAP-DNA complex: the DNA is bent by 90°. Science 1991; 253:1001–1007. (e) Goodman, S. D.; Nash, H. A. Functional replacement of a protein induced bend in a DNA recombination site. Nature 1989;

341:251–254. (f) Gartenberg, M.R.; Crothers, D. M. Synthetic DNA bending sequences increase the rate of in vitro transcription initiation of the *Escherichia coli Lac* promoter. J. Mol. Biol. 1991; 219:217–230.

7. (a) Zimm, B. H.; Lumpkin, O. J. Reptation of a polymer chain in an irregular matrix: diffusion and electrophoresis. Macromolecules 1993; 26:226–234. (b) Lumpkin, O. J.; Levene S. D.; Zimm, B. H. Exactly solvable reptation model. *Phys. Rev. A.* 1989; 39:6557–6567. (c) Zimm, B. H. Lakes straight model of field-inversion gel electrophoresis of DNA. J. Chem. Phys. 1991; 94:2187–2206. (d) Lumpkin, O. J.; Dejardin, P.; Zimm, B. H. Theory of gel electrophoresis of DNA. Biopolymers 1985; 24:1573–1593. (e) For an experimental verification of reptation models for polymers see Perkins, T. T.; Smith, D. E.; Chu, S. Direct observation of tube-like motion of a single polymer chain. Science 1994; 264:819–822.
8. (a) Holmes, D. L.; Stellwagen, N. C. Electrophoresis of DNA in oriented agarose gels. J. Biomolecular Structure Dynamics 1989; 7:311–327. (b) Stellwagen, J.; Stellwagen, N. C. Transient electric birefringence of agarose gels. I. Unidirectional electric fields. Biopolymers 1994; 34:187–201. (c) Stellwagen, J.; Stellwagen, N. C. Internal structure of the agarose gel matrix. J. Phys. Chem. 1995; 99:4247–4251. (d) Dormoy, Y.; Candau, S. Transient electric birefringence study of highly dilute agarose solution. Biopolymers 1991; 31:859–868.
9. Crothers, D. M.; Haran, T. E.; Nadeau, J. G. Intrinsically bent DNA. J. Biol. Chem. 1990; 265:7093–7096.
10. (a) Hagerman, P. J. Sequence-directed curvature of DNA. Nature 1986; 321: 449–450. (b) Hagerman, P. J. Evidence for the existence of stable curvature of DNA in solution. Proc. Nat. Acad. U.S.A. 1984; 81:4632–4636.
11. Hagerman, P. J. Sequence-dependent curvature of DNA. In *Unusual DNA Structures*. Wells, R. D.; Harvey, S. C., eds. New York: Springer Verlag, 1988: 225.
12. Koo, H.-S.; Crothers, D. M. Calibration of DNA curvature and a unified description of sequence directed bending. Proc. Nat. Acad. Sci. U.S.A. 1988; 85:1763–1767.
13. Wu, H. M.; Crothers, D. M. The locus of sequence-directed and protein-induced DNA bending. Nature 1984; 308:509–513.
14. Koo, H. S.; Crothers, D. M. DNA bending at adenine-thymine tracts. Nature 1986; 320:501–506.
15. Kahn, J. D.; Yun, E.; Crothers, D. M. Detection of localized DNA flexibility. Nature 1994; 368:163–166.
16. Calladine, C. R.; Drew, H. R.; McCall, M. J. The intrinsic curvature of DNA in solution. J. Mol. Biol. 1988; 201:127–137.
17. (a) Bolshoy, A.; McNamara, P.; Harrington, R. E.; Trifonov, E. N. Curved DNA without A-A: experimental estimation of all 16 wedge angles. Proc. Nat. Acad. Sci. U.S.A. 1991; 88:2312–2316. (b) Ulanovsky, L.; Trifonov, E. N. Estimation of wedge components in curved DNA. Nature 1987; 326:720–722. (c) De Santis, P.; Palleschi, A.; Savino, M.; Scipioni, A. Theoretical

prediction of the gel electrophoretic retardation changes due to point mutations in a tract of SV40 DNA. Biophys. Chem. 1992; 42:147–152.

18. (a) Diekmann, S. Temperature and salt dependence of the gel migration anomaly of curved DNA fragments. Nucl. Acids. Res. 1987; 15:247–265. (b) Harrington, R. E. Studies of DNA bending and flexibility using gel electrophoresis. Electrophoresis 1993; 14:732–746. (c) Niederweis, M.; Lederer, T.; Hillen, W. Matrix effects suggest an important influence of DNA–polyacrylamide interactions on the electrophoretic mobility of DNA. J. Biol. Chem. 1994; 269:10156–10162.
19. (a) Goodsell, D. S.; Kopka, M. L.; Cascio, D.; Dickerson, R. E. Crystal structure of CATGGCCATG and its implications for A-tract bending models. Proc. Nat. Acad. Sci. U.S.A. 1993; 90:2930–2934. (b) Goodsell, D. S.; Kaczor-Grzeskowiak, M.; Dickerson, R. E. The crystal structure of C-C-A-T-T-A-A-T-G-G and its implications for bending of B-DNA at T-A steps. J. Mol. Biol. 1994; 239:79–96.
20. Sitlani, A.; Crothers, D. M. Fos and Jun do not bend the AP-1 recognition site. Proc. Nat. Acad. Sci. U.S.A. 1996; 93:3248–3252.
21. Kerppola, T. K. Fos and Jun bend the AP-1 site: effects of probe geometry on the detection of protein-induced DNA bending. Proc. Nat. Acad. Sci. U.S.A. 1996; 93:10117–10122.
22. Kerppola, T. K.; Curran, T. DNA bending by Fos and Jun: the flexible hinge model. Science 1991; 254:1210–1214.
23. Glover, J. N. Mark; Harrison, S. C. Crystal structure of the heterodimer bZIP transcription factor c-Fos-c-Jun bound to DNA. Nature 1995; 373:257–260.
24. Kerppola, T. K.; Curran, T. Zen and the art of Fos and Jun. *Nature* 1995; 373:199–2000.
25. Kerppola, T. K.; Curran, T. Fos-Jun heterodimers and Jun homodimers bend DNA in opposite orientations: implications for transcriptional factor cooperatively. Cell 1991; 66:317–326.
26. Paolella, D. N.; Palmer, C. R.; Schepartz, A. DNA targets for certain bZIP proteins distinguished by an intrinsic bend. Science 1994; 264:1130–1133.
27. Rauscher, F. J., III; Sambucetti, L. C.; Curran, T.; Distel, R. J.; Spiegelman, B. M. Common DNA bending site for protein complexes and transcription factor AP-1. Cell 1988; 52:471–480.
28. Sitlani, A.; Crothers, D. M. DNA-binding domains of Fos and Jun do not induce DNA curvature: an investigation with solution and gel methods. Proc. Nat. Acad. Sci. U.S.A. 1998; 95:1404–1409.
29. Jonsson, M.; Akerman, B.; Norden, B. Orientation of DNA during gel electrophoresis studied with linear dichroism spectroscopy. Biopolymers 1988; 27:381–414.
30. Lanan, M.; Shick, R.; Morris, M. D. Electric birefringence imaging of electrokinetic agarose orientation. Biopolymers 1991; 31:1095–1104.
31. For review of recent progress see Oana, Hidehiro; Hammond, Richard W.; Schwinefus, Jeffrey J.; Wang, Shau-Chun; Doi, Masao; Morris, Michael D. Buffer, entangling polymer and electric field effects on rapid capillary elec-

trophoresis separation of linear and supercoiled DNA, Anal. Chem. 1998; 70: 563–567.
32. Doi, M.; Edwards, S. F. *The Theory of Polymer Dynamics*. Oxford: Oxford University Press, 1989.
33. de Gennes, P. G. Reptation of a polymer chain in the the presence of fixed obstacles. J. Chem. Phys. 1971; 55:572–579.
34. Duke, T. A.; Semenov, A. N.; Viovy, J. L. Mobility of a reptating polymer. Phys. Rev. Lett. 1992; 69:3260–3263.
35. Doi, M.; Graessley, W. W.; Helfand, E.; Pearson, D. S. Dynamics of polymer in polydisperse melts. Macromolecules 1987; 20:1900–1906.
36. Viovy, J. L.; Rubinstein, M.; Colby, R. H. Constraint release in polymer melts: tube reorganization versus tube dilation. Macromolecules 1991; 24:3587–3596.
37. Widom, B.; Viovy, J. L.; Defontaines, A. D. Repton model of gel electrophoresis and diffusion. J. Phys. I (France) 1991; 1:1759–1784.
38. Barkema, G. T.; Caron, C.; Marko, J. F. Scaling properties of gel electrophoresis of DNA. Biopolymers 1995; 38:665–667.
39. (a) Deutsch, J. M. Theoretical aspects of electrophoresis. *Electrophoresis of Large DNA Molecules: Theory and Applications*. Cold Spring Harbor Laboratory Press, 1990:81. (b) Deutsch, J. M. Theoretical studies of DNA during gel electrophoresis. Science 1988; 240:922–924. (c) Deutsch, J. M. Dynamics of pulsed-field electrophoresis. Phys. Rev. Lett. 1987; 59:1255–1258.
40. Carle, G.; Frank, M.; Olson, M. Electrophoretic separation of large DNA molecules by periodic inversion of the electric field. Science 1986; 232:65–68.
41. Akerman, A.; Jonsson, M.; Moore, D.; Schellman, J. Conformational dynamics of DNA during gel electrophoresis studied by dichroism spectroscopy. *Electrophoresis of Large DNA Molecules: Theory and Applications*. Cold Spring Harbor Laboratory Press, 1990:23.
42. (a) Porschke, D. Electric dichroism and bending amplitudes of DNA fragments according to a simple orientation function for weakly bent rods. Biopolymers 1989; 28:1383–1396. (b) Hagerman, P. J. Evidence of the flexibility of DNA using transient electrical birefringence. Biopolymers 1981; 20:1503–1535. (c) Hagerman, P. J. Sometimes a great motion: the application of transient electric birefringence to the study of macromolecular structure. Curr. Opin. Struct. Biol. 1996; 6:643–649.
43. (a) Chan, S. S.; Breslauer, K. J.; Hohgan, M. E.; Kessler, D. J.; Austin, R. H.; Ojemann, J.; Passner, J. M.; Wiles, N. C. Physical studies of DNA premelting equilibria in duplexes with and without homo dA·dT tracts: correlations with DNA bending. Biochemistry 1990; 29:6161–6171. (b) Park, Y. W.; Breslauer, K. J. A spectroscopic and calorimetric study of a melting behavior of a ''bent'' and a ''normal'' DNA duplex. Proc. Nat. Acad. Sci. U.S.A. 1991; 88:1551–1555.
44. (a) Griffith, J.; Lauden, C.; Rauch, E.; Hseih, W.; Wells, R. Use of electron microscopy to examine sequence-directed DNA bending. *In Structure and Expression: DNA Bending and Curvature*. SUNY 1988:25. (b) Rees, W. A.;

Keller, R. W.; Vesenka, J. P.; Yang, G.; Bustamente, C. Evidence of DNA bending in transcription complexes imaged by scanning force microscopy. Science 1993; 260:1646–1649. (c) Bendar, J.; Furrer, P.; Katritch, V.; Stasiak, A. Z.; Dubochet, J.; Stasiak, A. Determination of DNA persistence length by cro-electron microscopy: separation of the static and dynamic contributions to the apparent persistence length of DNA. J. Mol. Biol. 1995; 254:579–594.

45. (a) Crothers, D. M.; Drak, J.; Kahn, J. D.; Levene, S. D. DNA bending, flexibility, and the helical repeat by cyclization kinetics. Methods in Enzymol. 1992; 212:3–28. (b) See also Ref. 51.
46. (a) Nadeau, J.; Crothers, D. Structural basis for DNA bending. *Proc. Nat. Acad. Sci. U.S.A.* 1989; 86:2622–2626. (b) See also the recent work by Hud, N. V.; Feigon, J. Localization of divalent metal ions in the minor groove of DNA A-Tracts. J. Am. Chem. Soc. 1997; 119:5756–5757.
47. Burkhoff, A.; Tullis, T. D. The unusual conformation adopted by the adenine tracts in kinetoplast DNA. Cell 1987; 48:935–943.
48. Diekmann, S.; Wang, J. C. On the sequence determinant and flexibility of the kinetoplast DNA fragment with abnormal gel electrophoretic mobilities. J. Mol. Biol.1985; 186:1–11.
49. Milos, L.; Oslick, S.; Weiss, M. A. Evidence that the DNA A-tract is bent and rigid in solution obtained by time resolved fluorescence resonance energy transfer. J. Biomol. Struct. Dyn. 1997; 14:911.
50. (a) Young, M. A.; Beveridge, D. L. Dynamical structure of B-DNA oligonucleotides containing phased A-tracts in salt water solution. J. Biomol. Struct. Dyn. 1997; 14:824. (b) Sprous, D.; Young, M. A.; Beveridge, D. L. AMBER4.1/PME simulations of the ''Hagerman'' sequences d[G_5-{GA_4T_4C}$_2$-C_5] and d[G_5-{GT_4A_4C}$_2$-C_5]. J. Biomol. Struct. Dyn. 1997; 14: 863.
51. (a) Koo, H. S. DNA bending at adenine–thymine tracts: sequence requirements for DNA bending and A bending model. Ph.D. thesis, Yale University, 1989, Chapter 1. (b) Koo, H. S. The relationship between anomaly in gel-mobilities and curvature and the bend angles in the junction model. Ph.D. thesis, Yale University, 1989, Chapter 2. (c) Koo, H. S. ''Determination of the extent of bending by an adenine tract.'' Ph.D. thesis, Yale University, 1989, Chapter 4.
52. Ussery, D. W.; Bolshoy, A. Enviromental influences on DNA curvature. J. Biomol. Struct. Dyn. 1997; 14:789.
53. Trifonov, E. N. Sequence-dependent deformational anisotropy of chromatin DNA. Nuc. Acids. Res. 1980; 8:4041–4053.
54. Trifonov, E. N., Sussman, J. L. The pitch of chromatin DNA is reflected in its nucleotide sequence. Proc. Nat. Acad. Sci. *U.S.A.* 1980: 77:3816–3820.
55. Koo, H. S.; Rice, J. A.; Crothers, D. M. Determination of the extent of DNA bending by an adenine–thymine tract. Biochemistry 1990; 29:4227–4234.
56. Haran, T. E.; Kahn, J. D.; Crothers, D. M. Sequence elements responsible for DNA curvature. J. Mol. Biol. 1994; 244:135–143.
57. Crothers, D. M.; Drak, J. Global features of DNA structures by comparative gel electrophoresis. Methods Enzymol. 1992; 212B:46–47.

58. Drak, J.; Crothers, D. M. Helical repeat and chirality effects on DNA gel electrophoretic mobility. Proc. Nat. Acad. Sci. U.S.A. 1991; 88:3074–3078.
59. Grzeskowiak, K.; Goodsell, D. S.; Kaczor-Grzeskowiak, M.; Cascio, D.; Dickerson, R. E. Crystallographic analysis of C-C-A-A-G-C-T-T-G-G and its implications for bending in B-DNA. Biochemistry 1993; 32:8923–8931.
60. (a) Dickerson, R. E.; Goodsell, D. S.; Neidle, S. ". . . the tyranny of the lattice . . ." Proc. Nat. Acad. Sci. U.S.A. 1994; 91:3579–3583. (b) Dickerson, R. E.; Goodsell, D. S.; Kopla, M. L. MPD and DNA bending in crystals and in solution. J. Mol. Biol. 1996; 256:108–125.
61. (a) Harvey, S. C.; Dlakic, M.; Griffith, J.; Harrington, R.; Park, K.; Sprous, D.; Zacharias, W. What is the basis of sequence-directed curvature in DNAs containing A tracts? J. Biol. Struct. Dynam. 1995; 13:301–307. (b) Ganunis, R. M.; Guo, H.; Tullius, T. D. Effect of the crystallizing agent 2 Methyl-2,4-pentanediol on the structure of adenine tract DNA in solution. Biochemistry 1996; 35:13729–13732.
62. Levene, S. D.; Crothers, D. M. Ring closure probabilities for DNA fragments by Monte Carlo simulations. J. Mol. Biol. 1986; 189:61–72.
63. Hockings, S. C.; Crothers, D. M. Unpublished, 1997; Hockings, S. C. Ph.D. thesis, Yale University, 1997.
64. Taylor, W. H.; Hagerman, P. J. Application of the method of phage T4 DNA ligase-catalyzed ring-closure to the study of DNA structure. J. Mol. Biol. 1990; 212:363–376.
65. Zinkel, S. S.; Crothers, D. M. DNA bend direction by phase sensitive detection. Nature 1987; 328:178–181.
66. Levene, S. D.; Zimm, B. H. Understanding the anomalous electrophoresis of bent DNA molecules: a reptation model. Science 1989; 245:396–399.
67. Thompson, J. F.; Landy, A. Empirical estimation of protein-induced DNA bending angles; application to site-specific recombination complexes. Nuc. Acids Res. 1988; 16:9687–9705.
68. Schepartz, A. Nonspecific DNA bending and the specificity of protein–DNA interactions. Science 1995; 269:989–990.
69. Nudler, E.; Avetissova, E.; Markovstov, V.; Goldfarb, A. Transcription processivity: protein–DNA interactions holding together the elongation complex. Science 1996; 273:211–217.
70. Crothers, D. M.; Steitz, T. A. Transcriptional activation by Escherichia coli CAP protein. In: *Transcriptional Regulation* 22 (McKnight, S. L.; Yamamoto, K. R., eds.). Plainview, NY: Cold Spring Habor Lab. Press, 1992:501–534.
71. Schultz, S. C.; Shields, G. C.; Steitz, T. A. Crystal structure of CAP-DNA complex: the DNA is bent by 90°. Science 1991; 253:1001–1007.
72. Gartenberg, M. R.; Ampe, C.; Steitz, T. A.; Crothers, D. M. Molecular characterization of the GCN4–DNA complex. Proc. Nat. Acad. Sci. U.S.A. 1990; 87:6034–6038.
73. Kim, J. L.; Burley, S. K. 1.9 A resolution refined structure of TBP recognizing the minor groove of TATAAAAG. *Nat. Struct. Biol.* 1994; 1:638–652.
74. Strauss, J. K.; Maher, L. J. DNA bending by asymmetric phosphate neutralization. Science 1994; 266:1829–1834.

75. McCaffrey, P.; Luo, C.; Jain, J.; Badalian, T.; Ho, A.; Burgeon, E.; Lane, W.; Lambert, L.; Curran, T.; Verdine, G.; Rao, A.; Hoan, P. G. Isolation of cyclosporin-sensitive T cell transcription factor NFATp. Science 1993; 262:750.
76. (a) Anderson, C. F.; Record, M. T., Jr. Polyelectrolyte theories and their applications to DNA. *Ann. Rev. Phys. Chem.* 1982; 33:191–222. (b) Record, M. T.; Lohman, T. M.; Haseth, P. D. Ion effects on ligand-nucleic acid interactions. J. Mol. Biol. 1975; 107:145–158. (c) Record, M. T.; Lohman, T. M. A semi–empirical extension of polyelectrolyte theory to the treatment of oligoelectrolytes: application to oligonucleotide helix–coil transitions. Biopolymers 1978; 17:159–166.
77. Olmsted, M. C.; Bond, J. P.; Anderson, C. F.; Record, T. M., Jr. Grand canonical Monte Carlo molecular and thermodynamic predictions of ion effects on binding of an oligocation (L^{8+}) to the center of DNA oligomers. Biophys. J. 1995; 68:634–637.
78. Olmsted, M. C.; Anderson, C. F.; Record, M. T., Jr. Monte Carlo description of oligoelectrolyte properties of DNA oligomers: range of the end effect and the approach of molecular and thermodynamic properties to the polyelectrolyte limits. Proc. Nat. Acad. Sci. U.S.A. 1989; 86:7766–7770.
79. (a) Olmsted, M. C.; Anderson, C. F.; Record, M. T., Jr. Importance of oligoelectrolyte end effects for the thermodynamic of conformation transitions of nucleic acid oligomers: a grand canonical Monte Carlo analysis. Biopolymers 1991; 31:1593–1604. (b) Stein, V. M.; Bond, J. P.; Capp, M. W.; Anderson, C. F.; Record, M. T., Jr. Importance of Coulombic end effects on cation accumulation near oligoelectrolyte B-DNA: a demonstration using ^{23}Na NMR. Biophys. J. 1995; 68:1063–1072.
80. Olmsted, M. C. Ph.D. thesis, University of Wisconsin, Madison, 1991.
81. (a) Paulsen, M. D.; Richley, B.; Anderson, C. F.; Record, M. T., Jr. The salt dependence of the preferential interaction coefficient in DNA solutions as determined by grand canonical Monte Carlo simulations. Chem. Phys. Lett. 1987; 139:448–452. (b) Mascotti, D. P.; Lohman, M. T. Thermodynamic extent of counterion release upon binding oligolysines to single-stranded nucleic acids. Proc. Nat. Acad. Sci. U.S.A. 1990; 87:3142–3146. (d) Misra, V. K.; Sharp, R. A.; Friedman, R. A.; Honig, B. Salt effects on ligand–DNA binding, minor groove antibiotics. J. Mol. Biol. 1994; 238:245–263. (e) Misra, V. K.; Hecht, J. L.; Sharp, R. A.; Friedman, R. A.; Honig, B. Salt effects on protein–DNA interactions: the LacI repressor and EcoRI endonuclease. J. Mol. Biol. 1994; 238:264–280.
82. (a) Mills, P. A.; Rashid, A.; James, T. L. Monte Carlo calculations of ion distributions surrounding the oligonucleotide $D(ATATATATAT)_2$ in the B, A, and wrinkled D conformations. Biopolymers 1992; 32:1491–1501. (b) Lamm, G.; Wong, L.; Pack, G. B. Monte Carlo and Poisson–Boltzmann calculations of the fraction of counterions bound to DNA. Biopolymers 1994; 34:227–237. (c) Das, T.; Bratko, D.; Bhulyan, L. B.; Outhwaite, C. W. Modified Poisson–Boltzmann theory applied to linear polyelectrolyte solutions. J. Phys. Chem. 1995; 99:410–418.

83. Manning, G.; Mohanty, U. Counterion condensation on ionic oligomers. Physica 1997; A 247:196–204.
84. Odijk, T. Impact of non-uniform counterion condensation on the growth of linear charged micelles. Physica A 1991; 176:201–205.
85. Woodbury, C. P., Jr.; Ramanathan, G. End effects in polyelectrolytes by the Mayer cluster integral approach. Macromolecules 1982; 15:82–86.
86. Le Bret, M.; Zimm, B. H. Counter-ion condensation and system dimensionality. J. Biomol. Str. Dyn. 1983; 1:461.
87. Fixman, M. The Poisson–Boltzmann equation and its application to polyelectrolytes. J. Chem. Phys. 1979; 70:4995–5005.
88. Gueron, M.; Weisbuch, G. Polyelectrolyte theory. I. Counterion accumulation, site-binding, and their insensitivity to polyelectrolyte shape in solutions containing finite salt concentrations. Biopolymers 1980; 19:353–382.
89. (a) Bacquet, B.; Rossky, P. J. Ionic atmosphere of rodlike polyelectrolytes. A hypernetted chain study. J. Phys. Chem. 1984; 88:2660–2669. (b) Murthy, C. S.; Bacquet, R. J.; Rossky, P. J. Ionic distributions near polyelectrolytes. A comparison of theoretical approaches. J. Phys. Chem. 1985; 89:701–710. (c) Bacquet, R. J.; Rossky, P. Ionic distributions and competitive association in DNA/mixed salt solutions. J. Phys. Chem. 1988; 92:3604. (d) P. J. Rossky, C. S. Murthy, and R. Bacquet. The ionic environment of rod-like polyelectrolytes. In: Micellar Solutions and Microemulsions: Structure, Dynamics, and Statistical Thermodynamics (S.-H. Chen and R. Rajagopalan, eds. New York: Springer-Verlag, 1990. (e) Stigter, D. Evaluation of the counterion condensation theory of polyelectrolytes. Biophys. J. 1995; 69:380–388. (f) Duguid, J. G.; Bloomfield, V. A. Electrostatic effects on the stability of condensed DNA in the presence of divalent ions. Biophys. J. 1996; 70:2838–2846.
90. (a) Mohanty, U.; Ninham, B. W.; Oppenheim, I. Dressed polyions, counterion condensation and adsorption excess in polyelectrolytes solutions. Proc. Nat. Acad. Sci. U.S.A. 1996; 93:4342–4344. (b) Similar results have been obtained independently by Rouzina, I.; Bloomfield, V. A. Competitive electrostatic binding of charged ligands to polyelectrolytes: planar and cylindrical geometries. J. Phys. Chem. 1996; 100:4292–4304.
91. Evans, D. F.; Mitchell, D. J.; Ninham, B. W. Ion binding and dressed micelles. J. Phys. Chem. 1984; 88:6344–6348.
92. (a) Young, M. A.; Jayaram, B.; Beveridge, D. L. Intrusion of counterions into the spine of hydration in the minor groove of B-DNA: fractional occupancy of electronegative pockets. J. Am. Chem. Soc. 1997; 119:59–69. (b) Jayaram, B.; Swaminathan, S.; Beveridge, D.L.; Sharp, K.; Honig, B. Monte Carlo simulation studies on the structure of the counterion atmosphere of B-DNA. Variations on the primitive dielectric model. Macromolecules 1990; 23:3156–3165.
93. Manning, G. S. The molecular theory of polyelectrolyte solutions with applications to the electrostatic properties of polynucleotides. Q. Rev. Biophys. 1978; 11:179–246.
94. Hayter, J. B. A self-consistent theory of dressed micelles. Langmuir 1992; 8: 2873–2876.

95. (a) Singh, Y. Molecular theory of solvent-induced self-interactions in a polymer. J. Phys. A: Math. Gen. 1987; 20:3949–3954. (b) Schweizer, K. S.; Curro, J. G. Integral-equation theory of the structure of polymer melts. Phys. Rev. Lett. 1987; 58:246–249. (c) (a) Singer, S. J.; Chandler, D. Free energy functions in the extended RISM approximations. Mol. Phys. 1985; 55:621–625. (d) Zichi, D. A.; Rossky, P. J. Molecular conformational equilibria in liquids. *J. Chem. Phys.* 1986; 84:1712–1723.
96. Overbeek, J. T. The role of energy and entropy in the electrical double layer. Colloids Surfaces 1990; 51:61–75.
97. Stigter, D. Evaluation of the counterion condensation theory of polyelectrolytes. Biophys. J. 1995; 69:380–388.
98. Hirata, F.; Levy, R. M. Salt-induced conformational changes in DNA: analysis using the RISM theory. J. Phys. Chem. 1989; 93:479–484.
99. (a) Soumpasis, D. M. Debye–Hückel theory of model polyelectrolytes. J. Chem. Phys. 1978; 69:3190–3196. (b) Hummer, G.; Soumpasis, D. M. Statistical mechanical treatment of the structural hydration of biological macromolecules: results for B-DNA. Phys. Rev. E 1994; 50:5085–5095.
100. Fenley, M. O.; Manning, G. S.; Olson, K. W. Electrostatic persistence length of a smoothly bending polyion computed by numerical counterion condensation theory. J. Phys. Chem. 1992; 96:3963–3969.
101. (a) Manning, G. S. Limiting laws and counterion condensation in polyelectrolytes. 8. Mixtures of counterions, specific selectivity, and valence selectivity. J. Phys. Chem. 1984; 88:6654–6661.
102. Brukner, I.; Susic, S.; Dlakic, M.; Savic, A.; Pongor, S. Physiological concentration of magnesium ions induces a strong macroscopic curvature in GGGCC-containing DNA. J. Mol. Biol. 1994; 236:26–32.
103. Dlakic, M.; Harrington, R. E. Bending and torsional flexibility of G/C-rich sequences as determined by cyclization assays. J. Biol. Chem. 1995; 270: 29945–29952.
104. Crothers, D. M. DNA curvature and deformation in protein–DNA complexes: a step in the right direction. Proc. Nat. Acad. Sci. U.S.A. 1998; 95:15163–15165.
105. Gabrielian, A.; Simoncsits, A.; Pongor, S. Distribution of bending propensity in DNA sequences. FEBS Letters 1996; 393:124–130.
106. Dlakic, M.; Harrington, R. E. The effects of sequence context on DNA curvature. Proc. Nat. Acad. Sci. U.S.A. 1996; 93:3487–3852.

This Page Intentionally Left Blank

19

Complexation Between Amphiphilic Polyelectrolytes and Proteins: From Necklaces to Gels

CHRISTOPHE TRIBET Ecole Supérieure de Physique et de Chimie Industrielles, and Centre National de la Recherche Scientifique, and University of Paris 6, Paris, France

I. INTRODUCTION

Since the pioneering work by Morawetz and Hugues [1], it is now recognized that globular proteins can form tight complexes with polyelectrolytes. These associations may result in soluble species [2] (including complexes with insoluble proteins such as membrane proteins [3]), complex coacervation [4], precipitation [5], or gelation [6]. The preservation of the native structure of the protein seems a general case, as judged by the variety of functional enzyme/polymer complexes that has been studied [3,7–11]. Obvious practical consequences of this include stabilizing native enzymes, developing novel separation methods of proteins for food or pharmaceutical industries [12,13], facilitating dispersions of insoluble proteins for their functional or structural studies [3], and directing and stabilizing enzymes at the surface of electrodes for biosensors [14]. For each application, a different state of association and dispersion of the proteins should be optimal. Provided that the mechanisms of association are well understood, the vast resources of polymer chemistry together with the possibility of modulating pH, ionic strength, or temperature should make it readily possible to choose the polymer toward specific uses.

A quick glance at the reported studies shows that the two most important parameters governing polymer/protein association in water are the hydrophobicity and the electric charge of the partners. In general, no binding takes place when the polyelectrolyte and the protein have like charges, except when charge patches of opposite signs are present on the surface of the protein [15,16]. The formation of complexes composed of polyanions and negatively charged albumins have nevertheless been observed when the polyelectrolyte contained hydrophobic groups [17]: Hydrophobic interaction

can overcome the electrostatic repulsion. When association takes place, the resulting structures depend on a subtle balance between charge-directed vs. hydrophobic binding, intra- vs. intermolecular reorganizations (of both the synthetic polymer and the protein), and counterion displacement vs. condensation. The Coulombic association of proteins and polyelectrolytes has been reviewed recently [2,12]. Surprisingly, the importance of hydrophobic interaction, although often suspected [18–21], has not been studied in detail until the last few years. New behaviors, such as gelation and retardation of precipitation, are now thought to result directly from the presence of hydrophobic association in polyelectrolyte/protein complexes. It is the purpose of this chapter to introduce the recent advances in the field of protein/polyelectrolyte mixtures, with special emphasis on the amphiphilic polyelectrolytes.

II. POLYMER/PROTEIN ASSOCIATION IN WATER

This section summarizes the simpler and more popular techniques used to date for the detection of the onset of an association. These qualitative approaches enable one to classify the complexation as a function of the microscopic driving force for attraction between the macromolecular partners. The vast majority of the works published to date deal with polyelectrolytes, and consequently Coulombic association, presumably for their high solubility in water but also because interesting modulations of the association by pH variation or addition of salt were expected.

A. Qualitative Evidence for Association

The formation of complexes affects both the state of aggregation of the species and the environment immediately surrounding the bound moities of the partners. Their detection reflects therefore either the increase of the average size and the molecular weight of the species or a perturbation at a molecular level. An estimate of the light scattered by the samples using a spectrophotometer to measure the turbidity, or a rapid measurement of the viscosity in Couette cells or in capillaries, appear as the more popular and less tedious techniques sensitive to any kind of aggregation. Alternatively, the variation in the intrinsic fluorescence spectrum of the protein, or the energy transfer between a labeled polymer and tryptophan residues of the protein, give information on the binding at the molecular level. Similarly, although less studied, both the pKa of ionizable residues of the proteins and the binding of small counterions along the macromolecular partners are likely to be affected by the association. Various measurements reflecting a

variation in one of the above parameters have been routinely used to detect the onset of complexation, for instance as a function of pH or concentration.

1. Turbidimetry

In principle, the formation of high-molecular-weight species in solution is accompanied by an increase in the scattering of visible or UV light. The simple and noninvasive measurement of turbidity has been widely implemented to follow a demixing. It worked remarkably well in titration schemes aiming at the determination of the onset of precipitation at a critical value of pH (pHϕ and "type I" titration in the language of Dubin and colleagues, performed by adding HCl or NaOH in a mixture of protein and polyelectrolyte) [16,22–26]. The composition of the precipitate formed upon addition of polymer into a protein solution (so-called "colloid titration" by Kokufuta and colleagues) was also accurately determined by the sharp increase in turbidity at a fixed stoichiometric ratio as shown in Figure 1 [4,10,9,27,28]. In addition, Patrickios et al. have shown that turbidity can be used to follow the kinetics of precipitation of mixtures containing trypsin inhibitor and a polyampholyte [29]. The sensitivity of the method allowed Dubin and colleagues [16,22,23] to detect the formation of soluble protein/polymer complexes by a small increase of turbidity in type 1 titration, above a critical

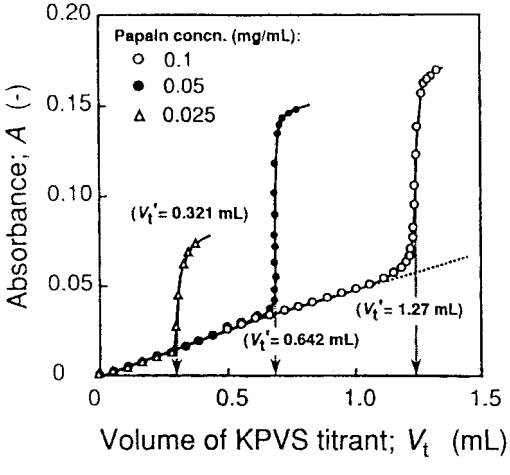

FIG. 1 Turbidimetric titration curves (so-called colloid titration) of different papain solutions with a solution of potassium poly(vinylsulfate) at 2.5 mmol/L. The volume of titrant at the abrupt increase of turbidity (V_t') is given in the figure. At the point of incipient precipitation, the polymer/protein ratio is constant. (Reprinted with permission from Ref. 27. Copyright © 1996 American Chemical Society.)

pH of association and before the sharp increase induced by demixing at pHϕ (region 2 in Figure 2). This interpretation was confirmed by other methods such as fluorimetry [23] or quasi-elastic light scattering [22]. To date, the mixtures of an amphiphilic polymer and a protein have not been studied by turbidimetry, although a precipitation was observed by eye in lysozyme and C18-modified polyacrylic acid [6]. The few data available indicated that the more hydrophobic the polymer, the higher the ratio of lysozyme to polymer at the precipitation (up to a factor of 10 times higher when the polymer was composed of only 3 mol% of C18 pendant groups).

2. Viscometry and Rheology

Owing to the compact nature of globular proteins, their intrinsic viscosity is generally markedly lower than that of synthetic polymer having similar or higher molecular weight. In consistency with that, the specific viscosity of dilute solutions was found to be much more sensitive to the concentration of the polymer than to the presence of protein. In the limit of high dilutions,

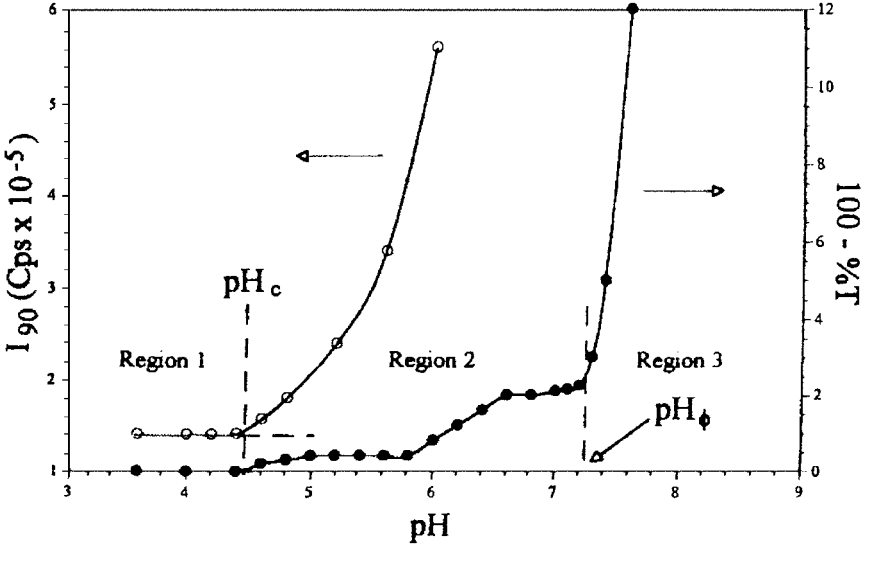

FIG. 2 Type 1 titration of a solution of bovine serum albumin and polydiallyldimethyl ammonium chloride in 0.1 M NaCl. The pH was varied by supplementation of the mixture with small volumes of either 0.1 mol/L HCl or NaOH solutions. Black circles: 100% − % transmittance, open circles: 90° scattering intensity of light at 780 nm. pH_c: pH of complex formation; pH_ϕ: pH at the onset of phase separation. (Reprinted with permission from Ref. 22. Copyright © 1993 American Chemical Society.)

the specific viscosity or the intrinsic viscosity should therefore give an index of the extension or collapse of the polymer chain upon addition of protein [30–33]. At constant pH and salt concentration, or in the absence of polyelectrolyte effect using a neutral polymer [30], the association was shown to increase the chain extension (Figure 3). In the absence of buffer or when the counterions of the polymer contributed significantly to the ionic strength [30,32], the polyelectrolyte effect was dominating. In these conditions, the increase or decrease in the viscosity reflected rather a neutralization of the chain upon the formation of salt bridges [32] or the ionization of weak acid groups along the chain [31]. At a higher polymer concentration, the formation of large aggregates can result in the divergence of the low-shear viscosity [6], indicative of a sol–gel transition. In these systems, close to a gelation threshold, the formation of connected structures was more accurately studied by measurements of the dynamic modulus under oscillating shear [34–36]. In mixtures of carrageenan and casein micelles, for instance, the sharp variations in tan δ (the ratio of loss to elastic moduli) at two successive temperature values upon cooling was interpreted as the successive formation of two networks involving either pure carregeenan connections or mixed associations between the casein and helices of carrageenan [34].

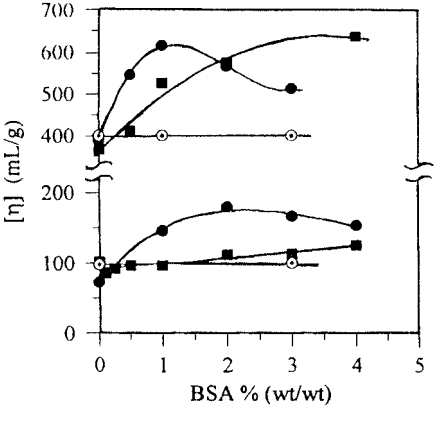

FIG. 3 Variation of the intrinsic viscosity of long alkyl-modified polyacrylic acids as a function of the concentration of bovine serum albumin in the solvent. Solvent used for dilutions: 30 mM borate buffer pH 9 and protein (top curves) or same buffer plus 0.3 M NaCl and protein (bottom curves). Black circles: polymer modified with 4 mol% of C18 side groups; squares: polymer modified with 3 mol% of C12 groups; cross-circles: unmodified poly (sodium acrylate). (Reprinted with permission from Ref. 33. Copyright © 1998 American Chemical Society.)

3. Fluorescence Spectroscopy

The vast majority of proteins contain fluorescent residues such as tryptophan. Their intrinsic fluorescence has been shown to vary significantly in relation with a conformational change, a denaturation, or upon binding of some substrate [37]. The binding of polyelectrolyte decreased the fluorescence intensity (quenching) and shifted the wavelength of the emission toward lower values (blue shift) both in papain/poly(vinylsulfate) systems [38] and in serum albumin mixtures with various polyanions or polycations [20]. The major advantage of those measurements was to enable the detection of interaction at protein concentration lower than 0.04 g/L [20]. From the knowledge of the structure of those proteins, and the known behavior of the tryptophan exposed at the protein surface, there was discussion on the location of binding sites for polymers. The complexity of possible structural reorganizations of the proteins, however, limits the validity of the conclusions in the absence of other information. Nonradiative energy transfer between tryptophan residues and a pyrene-labeled [21,23] or anthryl-labeled [20] polymer add to the intrinsic fluorescence as a probe of the association at short length scale, typically of about 1 nm. For instance, efficient transfer was shown between lysozyme and pyrene-modified poly(2-acrylamido-methylpropanesulfonate) (Figure 4), which enabled Morishima and colleagues to locate the binding of the pyrene probe in the hydrophobic cleft of lysozyme. It should be noted. however, that the probe is able to direct the association toward a hydrophobic patch at the protein surface, inducing marked modifications of the binding as compared to the unlabeled polymer [21]. Avoiding the grafting of the polymer, Lawton and Mekras [39] and Teramoto and colleagues [20] studied the displacement of a molecular probe reversibly bound either to the protein [20] or to the polyelectrolyte [39]. Upon protein/polymer complexation, the probe was released, resulting in a significant variation in its fluorescence.

4. Free Ion Titration

The formation of salt bridges in polyelectrolyte/protein complexes is widely accepted. Direct evidences for the release of counterions upon association of the macromolecular partners are however scarcely reported. Potentiometric studies were found to reveal the ionization or neutralization of proteins in polymer complexes, i.e., a pKa shift of ionizable residues when an association took place [23,25,30]. In the presence of neutral polyethylene glycol, pepsin was shown to take up protons from the solution [30]. On the contrary, bovine serum albumin released protons from the addition of poly(diallyldimethylammonium chloride) (Figure 5). Despite the simplicity of both the method and the quantitative measurement of a number of ions released per protein, an interpretation in terms of a number of local bridges

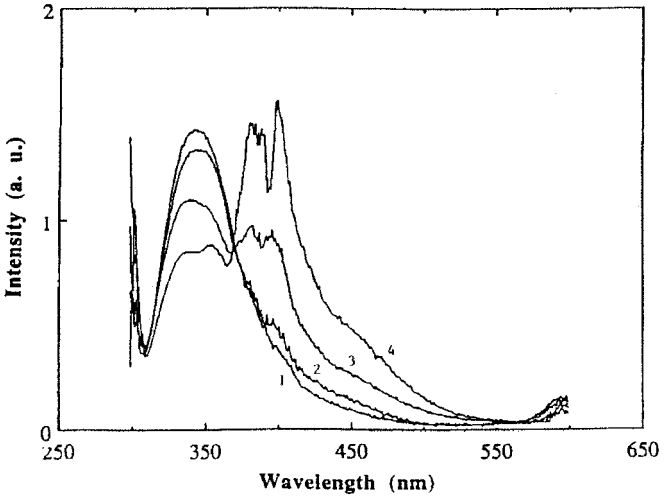

FIG. 4 Fluorescence emission spectra of a solution of lysozyme and pyrene-modified poly(acrylamido methylpropanesulfonate) in 0.25 M NaCl and at varying pH. pH 12.0 (1), 11.0 (2), 10.0 (3), and 9.0 (4). Excitation wavelength 295 nm. The decrease of the intensity at 340 nm (essentially tryptophane) and the increase at 400 nm (pyrene) indicates the energy transfer from lysozyme to the polyelectrolyte. (Reprinted with permission from Ref. 21. Copyright © 1995 John Wiley & Sons, Inc.)

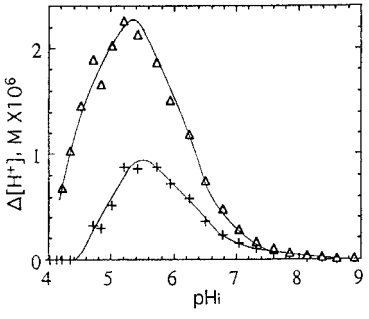

FIG. 5 Proton release in a solution of bovine serum albumin (1 g/L) arising from the addition of poly(dimethyldiallyl ammonium) chloride as a function of the initial pH of the solution. Polymer final concentration 0.2 (cross) or 1 g/L (triangles). (Reprinted with permission from Ref. 25. Copyright © 1997 American Chemical Society.)

should be taken with care. Many subtle reasons can modify the pKa of the residues in the absence of direct links with the polymer, such as small conformational reorganization, or changes in the environment surrounding the ionizable groups. The method remains nevertheless sensitive and can indicate the global charge of the proteins. As an alternative to specific titration, Fedotov and colleagues followed changes in the dielectric properties of β-lactoglobulin/carboxymethylcellulose mixtures [40]. They concluded that the counterion fluctuations close to the macromolecules were hindered by their association. Altogether, these works suggest that techniques such as conductimetry or titration with specific electrodes would enable investigations on the fraction of free ions, giving precious information on the complexation.

B. Multiple Origins of Complex Formation

The 20 amino acid side chains of proteins possess a variety of chemical and physical properties, which gives protein behaviors far more complex than those of molecular ligands. All the common interactions (electrostatic, hydrophobic, hydrogen bonds, steric effects) can take place simultaneously among the atoms of polypeptide chains and parts of another polymer, directing both the protein folding and the complexation. In addition, the conformational variability of a globular protein enables it to adjust its structure to the shape of its substrate. This makes it especially difficult to distinguish the major origin of association if any driving force is ever dominating. The paragraphs below present a few cases of complexation that were interpreted in term of a single driving force. This does not exclude that other minor stabilizing or destabilizing interactions may play a role and for instance explain subtle differences between proteins of essentially similar structures.

1. Hydrogen Bonds

Kokufuta and colleagues have recently demonstrated that both pepsin and human serum albumin form a soluble complex with poly(ethylene glycol) (PEG) at low pH [30,41]. The high sensitivity of association to the pH, the proton uptake upon complex formation [30], and the absence of association in 1 M urea (in conditions that did not denature the protein [41]) were altogether strong evidence for an important role of hydrogen bonds in the affinity between these partners. The complexation of pepsin was attributed to H-bond formation mainly between the COOH and the ether groups of PEG. Surprisingly, human serum albumin/PEG complexation was found to last up to pH 8, at which the majority of the carboxyl groups would be deprotonated. This suggested the participation of other polar residues, presumably basic groups such as lysine, arginine, or histidine, at this pH. The more intricate case of hydrophobically modified pullulan has been unraveled by Akiyoshi et al. [42–44]. More than 10 different globular proteins of

varying molecular weight (from 5,000 to 66,000) were found to be entrapped into self-assembled nanogels of cholesterol-modified pullulan [42]. The driving forces for the stabilization of these mixed nanogels could involve the hydrophobicity of both partners, hydrogen bonds with the polysaccharide backbone, steric hindrances, and structural reorganizations of both the self-associated nanogels and the protein conformation. The density of hydrophobic groups along the polysaccharide together with the size of the protein was shown to control both the number of bound protein per nanogel and their association constant [42], suggesting some importance of hydrophobicity in the binding in consistency with the binding of a fluorescent probe (ANS). However, the size of the—hydrophobically driven—pullulan self-assemblies (gyration radius 9–15 nm depending on the chemical structure) did not markedly change upon the incorporation of proteins. The question of the major origin of association was finally settled by measurements of the enthalpy and entropy of complexation [44]. The exothermicity and the negative entropy of complexation suggested that proteins interacted mainly through hydrogen bonds with the pululan backbone while hydrophobic microdomains stabilized the whole nanogels (empty or full). Although little has been published on the formation of hydrogen bonds in polyelectrolyte/protein systems, presumably due to the much higher strength of Coulombic or hydrophobic interaction in the common systems, the possible presence of hydrogen bonds should be suspected each time a PEG or a polysaccharide backbone is present.

2. Electric Charge

Mixtures of protein and synthetic polymer have been much more investigated than other polymer/protein systems, and the topic is mainly concerned with the effects of electric charge on complexation as modulated by pH, ionic strength, and density of ions along the polymer backbone (for reviews, see Refs. 2 and 12). Coulombic interaction has been known for decades to direct the association between a polyelectrolyte and a colloid of opposite charge such as micelles or another polymer [18,45–47], inducing demixing or the formation of ''necklaces.'' As expected, strong association and often phase separation have been reported in solutions of a polycation and a protein above its isoelectric point, when the protein was negatively charged [4,11,16,20,24,25]. Most of the polycations used to date were poly(quaternary ammonium) salts such as polybrene [11], poly(acrylamidopropyltrimethylammonium) chloride [16,20], polydiallyldimethylammonium chloride [4,24] or polyvinylbenzyltrimethylammonium chloride [20]. The symmetric case of a polyanion and positively charged proteins was even more studied [5,9,10,16,20,21,23,27,28,31,32,40,48,49], encompassing a wider variety of polyanions among which are sodium poly(acrylate or meth-

acrylate) [5,20,31,48], poly(acrylamidomethylpropanesulfonate) [15,16,20–23], poly(vinylalcholol) sulfate [9,10,15,16,27,28], polystyrene sulfonate [10,16,20,48], and sulphated or ionizable polysaccharides [32,40,49,50]. Titrations performed at low ionic strength confirmed that the number of ionized groups of the polyanion per gram of protein involved in the precipitate was independent of the polymer backbone and length [9,10,27,28, and Figure 6]. At low pH, this number of bound anions per protein matched the number of basic residues, in consistency with the assumed 1:1 stoichiometry of association between the charges. In other terms, a neutral complex that does not contain small counterions was found to precipitate at low ionic strength.

The simple picture of charge cancellation was questioned by Dubin and colleagues [15,16,22] close to the isoelectric point of the protein, and in the presence of salt. It is now recognized that especially polyanions can form soluble complexes with negatively charged proteins [15,16,20, Table 1]. In agreement with earlier conclusions based on the behavior of proteins in ion chromatography [51], this was explained by the presence of local regions at the protein surface having a sign opposite to the global protein charge (charge patches). A tight Coulombic association with these patches can overcome the repulsion between the polyions at large scale. A semiempirical relationship among the surface charge density of a colloidal particle (σ), the linear charge density of the polyelectrolyte (ξ), and the inverse of the Debye length κ seems to hold remarkably well to predict the incipient association

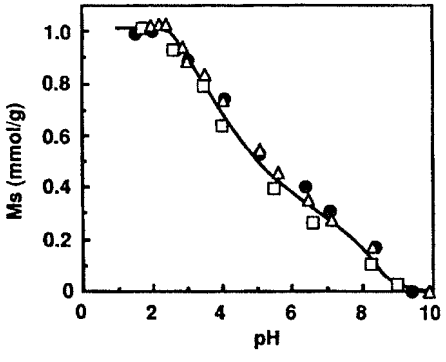

FIG. 6 Ratio of the sulfate groups to the protein mass at the onset of precipitation (colloid titration) upon titration of papain with a polyanion at low ionic strength. Circles: poly(vinylsulfonate); triangles: poly(styrene sulfonate) of low M_w (68.000); squares: high M_w poly(styrene sulfonate). The fully ionized papain at low pH corresponds to 1.07 mmol/g of cationic residues. (Reprinted from Ref. 10 by courtesy of Marcel Dekker, Inc.)

TABLE 1 Net protein charge at initial polymer binding (Z_c) and phase separation (Z_ϕ). Key for polymer structure: 2-acrylamidomethylpropylsulfate (AMPS); *N*-vinylpyrrolidone (NVP); sodium poly(styrenesulfonate) (PSS); sodium poly(vinylsulfate) (PVS); poly(dimethyldiallylammonium chloride) (PDMDAC); homopolymer of the acrylate of trimethylaminoethyl chloride (LBN52); copolymer of the latter monomer and acrylamide (LBN 66). (Reprinted with permission from Ref. 15. Copyright © 1993 American Chemical Society.)

	BSA			RNase			Lysozyme		
	Z_c^q	Z_c^e	Z_ϕ	Z_c^q	Z_c^e	Z_ϕ	Z_c^q	Z_c^e	Z_ϕ
Polyanions									
NVP-AMPS	−6	−8	+4	−2	−1.5	+3.5	−1.6	−1.0	+2
NaPSS	−12	−12	−1	−3	−3	+5	−2.6	−1.7	+0.7
PAMPS	−14	−15	−2	−4	−5	+2	−2.6	−2.5	+1.3
NaPVS	−25	−26	+3	−8	−7.5	+5	−7	−6.5	+1.3
Polycations									
LBN 66	−2	−2	−30	−3	−2	−6	+6	+6	+1
PDMDAAC	−6	−5	−23	−0.5	−1	−13	−0.3	+2	−5.5
LBN 52b	−1.5	0	−18	+4	+3	−9.5	+7	+2.5	

Z_c^q by QELS; Z_c^e by ELS.

of the colloid and the polyelectrolyte [22,45 and Refs. therein for theoretical derivations]:

$$\sigma \cdot \xi \sim \kappa^a \tag{1}$$

This was successfully applied to the case of globular proteins, using a value of 1 or 1.2 for the exponent a and changing σ for the protein critical charge (Z_{pr}) at the onset of the complexation (Figure 7). Given the proportionality between κ and the ionic strength μ, this relationship was written

$$Z_{pr} \cdot \xi \sim \mu^{0.5} \quad \text{or} \quad \mu^{0.6} \tag{2}$$

Because of the binding of the polyelectrolyte onto charge patches rather than onto the whole (heterogeneous) surface of the protein (possibly of opposite sign as compared to the patches), the explanations for using Z_{pr} in Eq. 1 that was developed for homogeneous surfaces remain unclear. It was proposed that the average charge density of the actual binding sites may vary linearly with the global charge Z_{pr}.

3. Hydrophobicity

Protein hydrophobicity has been characterized in various ways based on the frequency of nonpolar side groups, the energy of transfer of residues from

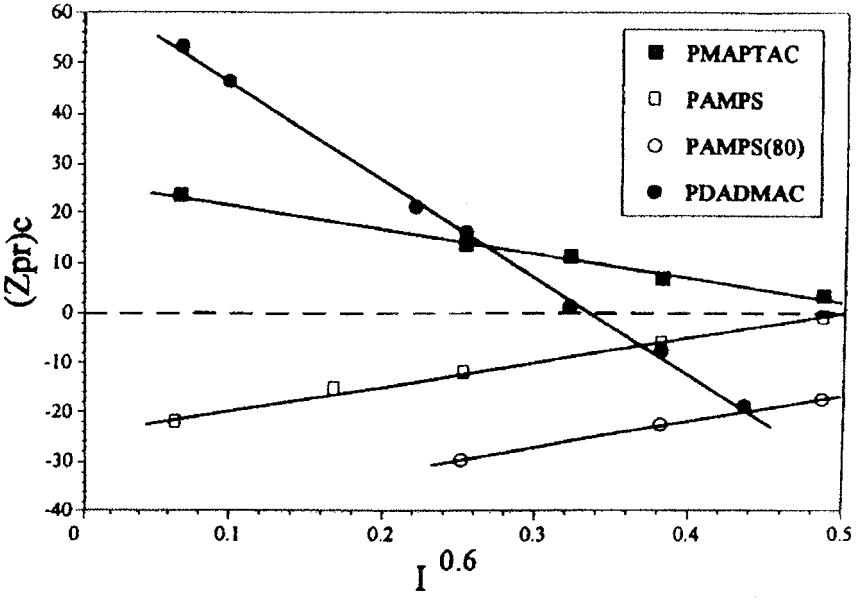

FIG. 7 Ionic strength (I) dependence of the protein global charge at the onset of complexation (Z_pr)c in bovine serum albumin and polyelectrolyte mixtures (type 1 titrations). PMAPTAC: poly(acrylamidopropyl trimethylammonium) chloride; PAMPS: poly(acrylamido methylpropylsulfonate); PAMPS(8): copolymer of AMPS and 20 mol% acrylamide; PDADMAC: poly(diallyl dimethylammonium) chloride. (Reprinted with permission from Ref. 22. Copyright © 1998 American Chemical Society.)

organic solvent to water, etc. Most of the hydrophobicity indexes propose parameters based on the primary structure of the proteins (see Ref. 37, pp. 153–162). A more relevant parameter for hydrophobic complexation should describe the surface hydrophobicity, provided that proteins do not unfold upon binding (see Sec. IV below). Chromatography measurements give the possibility of ranking proteins as a function of their interaction with surfaces [52,53]. Alternatively, partition between incompatible polymer phases [54,55] lead to similar scales of effective hydrophobicity. From these approaches, serum albumins and β-lactoglobulin have an effective hydrophobicity markedly higher than the other soluble proteins. Hemoglobin and lysozyme were also found to exhibit some surface hydrophobicity.

The vast majority of synthesized amphiphilic and water-soluble polymers belongs to the class of polyelectrolytes, presumably because of the insolubility of most of the neutral macromolecules of that sort [42,56–58,61]. Thus

the resolution of hydrophobic and Coulombic contributions is a relevant goal of the field. For instance, it has sometimes been discussed whether a hydrophobic component contributed to the stability of Coulombic complexes with poly(styrenesulfonate) [20,60]. In a study of the quenching of lysozyme's tryptophan with a pyrene-labeled polyanion, Xia et al. have shown the strong binding of the pendant pyrene probe in the hydrophobic cleft of lysozyme [21]. The complexes of the labeled polymer were found to differ significantly from the unlabeled ones [21]. Similarly, observations of a conjoint effect of electrostatic and hydrophobic interaction has been reported in micelle/polyelectrolyte systems and is now well documented [18,61,62]. Nevertheless, the hydrophobically driven associations between synthetic polymer and proteins are only seldom investigated [6,35,50,63,64]. In the presence of strong enough hydrophobic interactions, the tendency to form gels has emerged as a new feature that was never reported in hydrophilic polyelectrolyte/protein systems. Gelation was observed in solutions of sodium poly(acrylate)-co-alkylacrylamide, of varying fraction of pendant alkyl groups, in the presence of lysozyme, papain, or bovine serum albumin (BSA) [6,35]. The viscosity of solutions of these polymers at a concentration as low as 0.5 wt% increased by 2 or 3 orders of magnitude upon supplementation with a globular protein. In consistency with the hydrophobic origin of the connectivity, the higher the hydrophobicity of the partners (e.g., lysozyme < BSA, and polyacrylate with C18 pendant groups at 1 mol% < 3 mol% C18), the higher the viscosity at a fixed composition (Figure 8). Another type of physical gelation involving amphiphilic triblock artificial polypeptide was recently reported by Tirrel and colleagues [65]. In this latter case, thermoresponsive systems were designed using recombinant ''leucine zipper'' end blocks flanking a water-soluble polyelectrolyte domain. The gelation was driven by the formation of polypeptide amphiphilic helices at the leucine zipper ends exhibiting one hydrophobic face (essentially leucine residues) that promoted the formation of interhelix aggregates. Due to the weak polyacid nature of some residues involved in the helix formation, the temperature and pH of the coil–helix transition, coupled at high concentrations with the sol–gel transition, was dependent on the structure of the triblocks.

The hydrophobic association takes place also at low polymer concentration, resulting in soluble complexes. This association was observed with partners of like charges, such as serum albumins and hydrophobically modified polyacrylic acid (HMPA) at pH 9, in conditions of vanishing influence of possible charge patches [33,63] (Figure 3). Irrespectively of the charge of the protein, short amphiphilic polyanions of HMPA type—called also amphipols [3,64]—were found to stabilize the dispersion of several integral membrane proteins. These globular proteins are insoluble in water in the absence of complexation with amphiphilic molecules (see Sec. III.A.3).

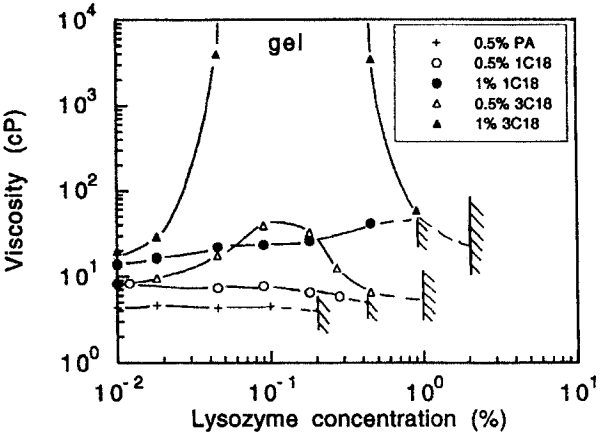

FIG. 8 Low shear viscosity (0.06 s-1) of C18 modified poly(acrylic acid) solutions at pH 9, as a function of lysozyme concentration. The inset gives the weight concentration of polymer and the modification rate: 3C18 corresponds to the grafting of 3 mol% of the monomers along the backbone. Hatch marks are the boundary of phase separation. (Reprinted with permission from Ref. 6. Copyright © 1995 Steinkopff Verlag.)

4. Features in Connection with Protein Specificity

Proteins may bind very tightly and specifically to other proteins, including themselves, or to molecular or macromolecular substrates. This paragraph illustrates some consequences of the reversible recognition that may take place within soluble complexes. A comprehensive review of all the systems that have been considered on that basis would have to include the complexes to nucleic acids (with histones for example), to polysaccharides (e.g., lectins), to antigens (immunoglobulins), to lipids, etc. Despite their importance for human health and applications in diagnostic and pharmaceutical systems, it is beyond the scope of this chapter to discuss polymer surfaces that are grafted with specific receptors. Here the recognition phenomenon is considered only between soluble macromolecules. Highly specific interactions between glucose or oligosaccharides and concanavalin-A were used to form glucose responsive gels [66] or reversible coating of liposomes [44]. A Dextransulfate-modified cross-linked *N*-isopropylacrylamide containing physically entrapped lectin was shown to shrink upon the addition of neutral competitors of the Dextransulfate [67], due to change in the ionization of the synthetic macromolecules upon release of the Dextran sulfate initially bound to the lectin. The principle of recognition in soluble polymer complexes is thus demonstrated and may find application for instance in protein

purification using the precipitation/redissolution scheme proposed by Sternberg and Hershberger [5] and Dubin et al. [12]. Other applications related to protein separation and identification have been reviewed by Hubert and Dellacherie [68].

Self-recognition may also occur with some proteins, resulting in oligomerization at critical pH values. For instance, β-lactoglobulin and lysozyme dimerize reversibly close to their isoelectric point. At higher pH, larger aggregates may be obtained in a solution of these pure proteins. Morishima and colleagues have investigated in detail mixtures of lysozyme and polyanions of varying charge density [23]. Their complexation was detected below pH 12.3 by different techniques. In the pH range 12.3–10.6, however, the nonradiative energy transfer of fluorescence (NRET) between a pyrene-labeled polymer and the tryptophan of lysozyme was found to be surprisingly inefficient, despite the existence of a strong association revealed by the release of protons, the measurements of the electrophoretic mobility of the species, and a slight increase in the mean hydrodynamic radius (dynamic light scattering) of the dispersed objects upon addition of polymer. Below pH 10.5, the NRET signal was consistent with the results from other techniques in detecting association. It was shown that beyond pH 10.5, lysozyme itself aggregated. The authors proposed that most of the tryptophane would be buried in these aggregates beyond pH 10.6, being therefore not accessible for energy transfer. Thus the polymer still binds the protein at high pH, although a completely different structure is formed. Similarly, Fedotov and colleagues reported an abrupt modification of the stoichiometry of β-lactoglobulin–carboxymethylcellulose associations, in the pH range from 4.2 to 5.1 [40]. Their investigation of the dielectric increment due to complexation allowed them to show two stages of complexation around pH 4.7, the initial stage being essentially identical to the coverage of the polymer by β-lactoglobulin dimers as observed at higher or lower pH, and the second stage corresponding to further associations up to the formation of octamers on all the initial binding sites.

III. CHARACTERIZATION OF STRUCTURES AND EQUILIBRIUM

A. Soluble Species

In dilute solution, when the synthetic macromolecules do not overlap, the complexation possibly stops at an optimum size that is usually thought to be a balanced structure. Roughly summarized, three types of soluble mixed compounds have been observed: small ''hairy'' proteins (i.e., surrounded by many synthetic polymer chains), long ''necklaces'' containing several pro-

teins along one polymer chain, and aggregates of both partners that did not sediment. Because of the polyelectrolytic and amphiphilic nature of both partners, several parameters, such as pH, ionic strength, hydrophobicity of the partners, and relative sizes, determine whether an aggregate is formed rather than a stoichiometric compound.

1. Size and Molecular Weight of the Complexes

Among the number of studies that have dealt with the formation of protein–polymer complexes in dilute solutions, only a few aimed to estimate the molecular weight or the size of the resulting dispersed species, although accurate determinations of these parameters are of prime importance to distinguish intrapolymer from interpolymer associations. Direct visualization of the objects required the resolution of electron microscopy, because the typical size of all the soluble complexes was in the range 5–100 nm. As compared to alternative approaches to the determination of molecular weight and radius (ultracentrifugation, small angle scattering), recent developments in electron microscopy, such as scanning transmission EM, offer the attractive features that the morphology and the heterogeneity of the objects can be easily investigated [69,70]. On the other hand, its application to labile complexes is likely to be complicated by possible reorganization of the complexes upon adsorption to the carbon grid before the vitrification of the solution. Kabanov and coworkers have obtained EM pictures of rodlike, 10 nm thick, complexes formed by bovine serum albumin and poly-4-vinylpyridine [2 and Ref. therein]. Tribet and colleagues found both the size and the mass of stable complexes formed by short C8-modified poly(sodium acrylate)—called amphipols—and integral membrane proteins using scanning transmission EM [71]. The results indicated a homogeneous dispersion of small complexes (8 nm or 10–15 nm depending on the protein) exhibiting an average molecular weight close to that expected for the native protein globule surrounded by a few polymer molecules (Figure 9). These few data indicate that EM may be a reliable route toward determining the structural features of complexes.

A more popular approach implements one among the various schemes of light scattering measurements (static, quasi-elastic, and electrophoretic light scattering) to elucidate rapidly the structure of complexes in solution. Ideally, when the interparticle interactions are negligibly small, at high dilution for instance, the mean molecular weight and an average radius over all the dispersed species are estimated as a function of the composition of the mixtures. These conditions seem to be fulfilled in the presence of 0.1–0.3 M of salt and at polymer concentrations relatively low, below 0.1 wt% with the common polymer lengths of a few thousand monomers [27,33,41]. The usual analytical derivation of the molecular weight assumes in addition

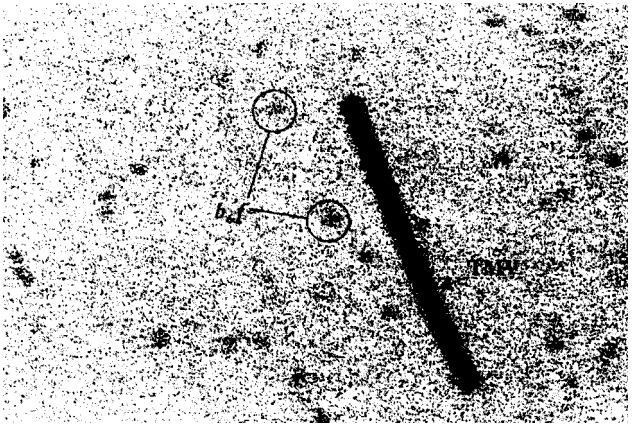

FIG. 9 Dark-field scanning transmission electron microscopy image of an unstained cytochrome b_6f complexed with the amphiphilic short polyanions A8-75 (a C8 modified poly(acrylic acid) of M_w 8000). Dark bar: tobacco mosaic virus added as an internal standard of diameter 18 nm. Dots: complexes of diameter ca. 10–15 nm. Reprinted from Ref. 71. Copyright © 1998 with permission from Elsevier.)

that the refractive index increment of the complexes is related to the (known or measurable) increments corresponding to each partner by

$$\left(\frac{dn}{dc}\right)_{\text{complex}} = \frac{1}{1 + \beta} \times \left[\left(\frac{dn}{dc}\right)_{\text{poly}} + \beta \cdot \left(\frac{dn}{dc}\right)_{\text{prot}}\right] \tag{3}$$

where β is the mass ratio of bound proteins to polymer in the complex, n the refractive index, and c the weight concentrations. Note that the values of dn/dc hardly differ from protein to protein (about 0.17–0.19 mL/g) [27] but differ markedly from those of conventional polyelectrolytes; as a consequence, Eq. 3 may introduce a systematic error in the estimates, especially with polymer of low hydrophobicity [dn/dc of the order of 0.1 mL/g for potassium poly(vinylsulfate) for instance]. Neglecting virial corrections, the molecular weight (M_w) and radius of gyration (R_g) for the scattering species may be estimated using the equation

$$\frac{K \cdot C_{\text{complex}}}{R_\theta} = \frac{1}{M_w} \times \left(1 + \frac{16\pi^2 n^2}{3\lambda^2} \cdot Rg^2 \sin^2 \frac{\theta}{2}\right) \tag{4}$$

Here R_θ is the Rayleigh ratio, θ the scattering angle, λ the wavelength of the light in vacuum, and $K = (2\pi^2 n^2/\lambda^4 Na) \cdot (dn/dc)^2_{\text{complex}}$. This equation obviously supposes that the contributions of free proteins or free polymers are negligibly small, which was found to be indeed the case in a wide range of

compositions of the mixtures when strong associations occurred [27,33]. Azegami and colleagues were able to compare the molecular weight of polyethyleneoxide/human serum albumin complexes as estimated from either static light scattering or equilibrium dialysis [41]. The compositions of complexes (value of β) obtained by both techniques were in excellent agreement, making them confident in the use of Eq. 3. In addition, the calculated molecular weight showed the formation of essentially intrapolymer complexes, i.e., a single polymer chain accommodating several protein globules (the necklace structure). At an ionic strength of 10 mM, however, the same authors suspected a ''polyelectrolyte effect'' to be responsible for distortions in the angular variation in R_θ, hampering the use of Eq. 4. Tsuboi and colleagues [27] were nevertheless able to use Eq. 4 at very low ionic strength because of the formation of soluble and uncharged complexes with potassium poly(vinylsulfate). In the case of Coulombic complexation, the composition (β) close to a phase separation can be determined independently by titration (the ''colloid titration''; see II.A.1). By this approach, Tsuboi and colleagues derived the values of both the molecular weight and R_g from Eq. 4 without assumption on β. Both values were much higher than what would have been expected for an intrapolymer necklace (Table 2 and [27]). The formation of intrapolymer necklaces took place only at very high dilutions (extrapolation of the data to zero polymer concentration) in the presence of a large excess of free proteins (Figure 10). Rapid increase of the size and mass of the complexes was observed upon addition of poly(vinylsulfate) in an excess of protein, up to a plateau value that corresponded to the association between several tens of polymer chains, each chain containing itself several tens of protein globules (Figure 10). Among

TABLE 2 Molecular weight M_x and radius of gyration R_g of protein/potassium poly(vinylalcohol) sulfate complexes as determined by static light scattering. M_x^0: average molecular weight of a hypothetical single chain complex (necklace) deduced from the colloid titration; α: M_x/M_x^0; R_g in nm; R_h hydrodynamic radius. (Reprinted with permission from Ref. 27. Copyright © 1996 American Chemical Society.)

Protein	$\bar{M}_x^0$	$\bar{M}_x$	α	R_g	$\rho(= R_g/R_h)$
Papain	1.26×10^6	7.36×10^7	54	69	1.3_8
HSA	9.46×10^5	4.28×10^7	45	53	1.2_6
Lysozyme	1.05×10^6	6.67×10^7	64	79	1.5_8
Ribonuclease	1.01×10^6	6.64×10^6	7	37	1.0_9
Trypsin	1.51×10^6	7.84×10^7	52	80	1.3_3

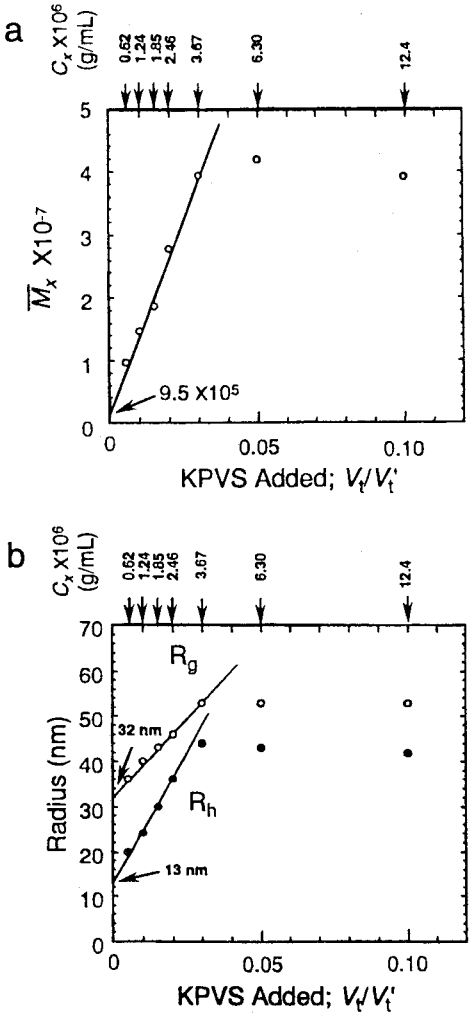

FIG. 10 Extrapolations to zero polymer concentration of the apparent molecular weight M_x, the radius of gyration R_g, and the hydrodynamic radius R_h as determined by light scattering techniques in a mixture of human serum albumin and potassium poly(vinylsulfate) (KPVS). V_t is the added volume of polymer solution in the protein solution. V_t' is the volume at the onset of precipitation. (Reprinted with permission from Ref. 27. Copyright © 1996 American Chemical Society.)

the possible reasons for the formation—at low ionic strength—of aggregates of well-defined size, as long as excess protein is present, Tsuboi and colleagues invoked the heterogeneity of protein surface and the difference in the charge densities of the partners that make difficult a perfect matching of the charges of the two partners in the complexes. The default in neutrality, at small length scales only, may hinder the growing of these globally neutral aggregates.

In the presence of salt, polyelectrolyte/protein complexes were found to exhibit an electrophoretic mobility [2,15,21,23,72] that varies with the composition of the mixture. Measurements of their composition using a separation technique or dialysis (see III.A.2) confirmed that the protein/polymer ratio may depend on pH, the ionic strength, and the concentration of free protein both in the case of hydrophilic polyelectrolyte and in that of hydrophobically modified polymers. In these conditions, both the M_w and β are a priori unknown parameters of Eq. 4 that cannot be estimated independently, except when it is possible to assume the formation of single chain necklaces. It is here a major advantage of dynamic light scattering (also called quasi-elastic light scattering) to allow the estimation of the distribution function of the size of the complexes without any knowledge of their composition. This technique was applied very often as a first glance on the dispersity of the soluble species [15,21,23,24,27,33]. When a short (i.e., exhibiting a radius close to the protein radius) amphiphilic C18- or C12-modified poly(sodium acrylate) was added to a solution of serum albumin [33], the distribution of sizes was a single polydisperse population. It was actually rather tricky to distinguish free protein from complexes and free polymers owing to the small difference between their radii. The mean radius of all these species was found to increase upon addition of polymer up to a plateau value about equal to the sum of the radius of the protein and the radius of the polymer [33]. Together with other evidence for association, and other studies of short amphiphilic polymers (see III.A.3), these results suggested the formation of ''hairy'' proteins surrounded by several bound polymers (Figure 11b). When long polyelectrolytes were used instead of short ones, a typical result of an analysis of the autocorrelation function of the scattered intensity was the presence of two or three populations of objects, well separated in terms of average hydrodynamic radius. The apparent radius of the smallest particles corresponded in general to that of the free protein. The bigger objects (sometimes claimed to be distributed in two populations [24] although distinguished at the limit of resolution of the method: a factor of 2 in radius) were observed in conditions where the contribution of free polymers to the scattering intensity is negligibly small, strongly supporting an interpretation in terms of the size distribution of the complex particles. In the case of various pairs of hydrophilic polyelectrolytes and soluble glob-

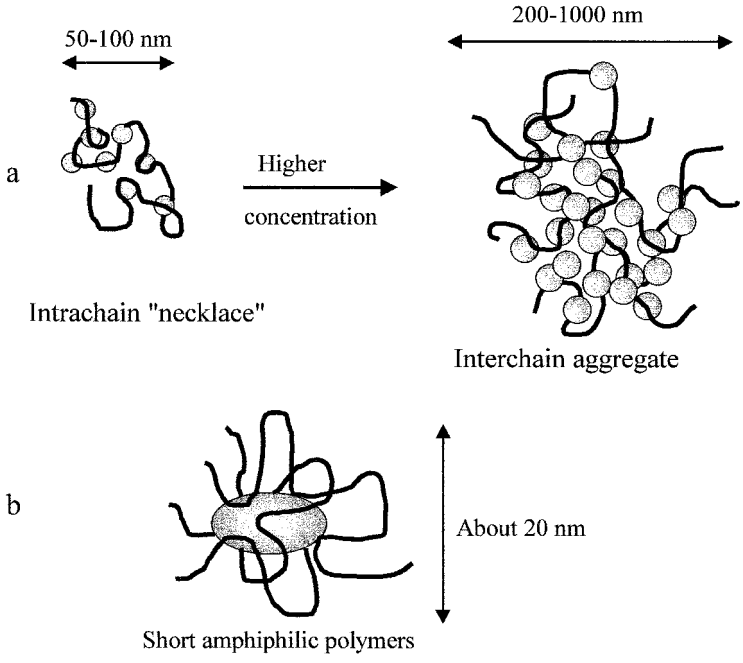

FIG. 11 Schematic illustration of the different types of complexes: (a) with long polymers (interchain aggregates are formed essentially in the case of Coulombic complexation of polyelectrolyte and protein); (b) with short amphiphilic polymers (hydrophobic association).

ular proteins, Xia and colleagues observed a single population of complexes, exhibiting a significant drift of its mean apparent radius as a function of pH (Table 3) [15]. At the pH of incipient association (type 1 titration, see II.A.1), the size of the complexes was always similar to the radius of the free polyelectrolyte, as determined by the same technique at the same ionic strength, suggesting the formation of intrapolymer necklaces (Figure 11a). The ''final'' radius at pH values close to phase separation were always more than twice —and sometimes four times—the initial one, suggesting the formation of multipolymer complexes rather than the stretching of a single chain (the corresponding expanding of a single chain would increase the volume of the chain—already swollen by the solvent—by an excessively high factor ranging from 8 to 60). Complexes can also comprise aggregates of protein that are subsequently associated with polymer chains. This case was investigated in detail by Sato and coworkers [23] using lysozyme, which is well known to form aggregates beyond pH 9 (dimerization) or pH 10 (polymerization).

TABLE 3 Range of diameter of soluble complexes as determined by quasi-elastic light scattering upon variation of pH from pH_c (incipient association) to pH_ϕ (phase separation). Polymer acronyms: see the title of Table 1. (Reprinted with permission from Ref. 15. Copyright © 1993 American Chemical Society.)

Polymer	BSA	RNase	Lysozyme
Polyanions			
NaPVS	6–45	6–46	6–48
NaPSS	46–63	46–60	46–57
PAMPS	30–110	30–85	30–98
NVP-AMPS	40–67	40–84	40–87
Polycations			
PDMDAAC	20–48	20–68	20–87
LBN 52	28–81	28–88	28–75
LBN 66	31–87	31–86	31–99

At pH between 10 and 10.5, aggregates of lysozymes exhibited a radius of about 12 mm. The formation of larger particles upon addition of poly(acrylamido-2-methylpropanesulfonic acid) under its sodium form was shown by dynamic light scattering as the emergence of two populations of much larger sizes (100 and 1000 nm, respectively) in equilibrium with an excess of lysozyme aggregates. Nonradiative energy transfer experiments confirmed the preservation of lysozyme aggregates in the polymer/protein complexes (see II.B.4). On the contrary, the hydrophobically driven complexes of a protein and various hydrophobically modified poly(sodium acrylates) (HMPA), studied by Tribet and coworkers (Ref. 33 on serum albumin and unpublished results on catalase or chymotrypsin), exhibited essentially the same size as that of the free polymers, whatever the protein concentration and at pH 9 (polymer fully ionized) or 7 (possible contribution of a Coulombic association). Although these polymers can form networks (see III.B), essentially intrapolymer associations were found to take place in dilute solution, well below the critical gelation concentration of about 0.2 wt%. This point does not exclude variations in the size of single-polymer necklaces with varying amounts of bound proteins. The dynamic light scattering was however not sensitive enough to give an accurate estimate of these variations. Since the intrinsic viscosity reflects the volume expansion of a polymer, i.e., the cubic radius, its value is more sensitive to small changes in the necklace size, although not easily translated into an exact value of the size. Bonnefont and colleagues performed measurements of the intrinsic viscosity of HMPA in solutions of bovine serum albumin by diluting the polymer at constant protein concentration and constant pH and ionic

strength [33]. At some optimal protein concentration, which corresponds in this case to free protein in equilibrium with the polymer chains and to the absence of interchain aggregates, the intrinsic viscosity was found to reach a maximum value, up to 1.8 times its initial viscosity (Figure 3). This result was interpreted in terms of a slight protein-induced chain expansion or collapse. The reasons for the increase of the intrachain repulsion at low protein concentration, followed by a decrease of this repulsion at higher protein content, were not obvious. Recently Currie, van der Gucht, Cohen Stuart, and Borisov proposed an analytic mean-field model of mixed micelle/polymer complex adsorption that predicts a nonmonotonic variation in an effective interaction between two complexes as a function of the degree of micelle binding [73,74]. Slight modification of their analysis should apply to the case of soluble complexes (manuscript in preparation) and might help in interpreting the maximum of swelling of the complexes.

To sum up, the light scattering techniques seem very powerful in determining the M_w and apparent size of complexes. There are nonetheless numerous hazards especially in a literal interpretation of the apparent radius collected from dynamic light scattering (the inverse Laplace transform is a delicate operation; strong and long-range interactions may limit the validity of the usual interpretation in terms of self-diffusion coefficients; and the meaning of an apparent hydrodynamic radius of a polymer may be debated). Given due precautions in the interpretation of these data, the available results are consistent with the formation of three different types of soluble complexes (Figure 11). (1) When complexation results essentially from Coulombic origin, the soluble species encompass generally several polymers and several proteins, or possibly aggregates of proteins. Their well-defined radius depends on pH, ionic strength, and composition of the mixture. Their global charge varies with the composition of the mixture and approaches 0 in the vicinity of phase separation. (2) When hydrophobic association is the major driving force, or at very high dilutions, necklaces composed of a single polymer chain and up to 50 proteins in the known examples exhibit an apparent radius close to or slightly higher than the free polymer. (3) In the same conditions as for point 2 but using short polymers, complexes contain a single protein surrounded by a cloud of several polymer chains.

2. Association Isotherms

A large majority of the papers cited above dealt with reversible associations of a long polyelectrolyte with globular proteins that were reversed by a variation in pH, or changes in the concentration of the macromolecules (such as a disruption of the HMPA/protein gels upon dilution, or the solubilization of a precipitate upon addition of a large excess of protein). The binding isotherms therefore reflect the free energy of association and, because of the

participation of more than two macromolecules in most of the complexes, the cooperativity of successive binding events. Among the earliest reports on this topic, Nguyen and colleagues proposed ultrafiltration experiments on hemoglobin-Dextran sulfate mixtures that provided them with the concentrations of both free and bound proteins in the samples [32]. The linear decrease of free hemoglobin with the addition of polymer suggested that the affinity was very high. Similarly, Yamaguchi and coworkers concluded from the centrifugation of Dextran sulfate/lysozyme complexes that almost all the protein was bound to the polymer at low ionic strength until a plateau value (about 8.6 g of protein/g of polymer) is reached [72]. Other separation techniques, such as rate zonal ultracentrifugation or size exclusion chromatography, have been used to measure the amount of tightly bound proteins (i.e., that did not dissociate in the course of the separation) along hydrophilic polyelectrolytes without seeking a determination of binding constants [poly(vinylpyrrolidone), poly(vinylsulfate), Dextran—see Ref. 2 for a review—or carrageenan [75]]. In size exclusion chromatography, the application of the Hummel–Dryer method to the study of the affinity of proteins for polyelectrolytes is relatively recent although quite simple as reported by Xia and Dubin on the example of bovine serum albumin/poly(dimethyl diallylammonium) chloride in 0.25 M NaCl [76]. Within the last few years, however, interest has been rapidly growing in another approach, capillary electrophoresis, due to two major advantages of this technique: a negligible consumption of the samples (a few nanoliters) and the separation of species in the absence of interaction with a stationary phase (i.e., in the very conditions of association in bulk). Most of the complete isotherms published to date were obtained using this new technique [17,50,60,63,77,78]. The shape of binding isotherms (plot of the bound protein/polymer ratio versus free protein concentration) reflects both the strength and the cooperativity of the association. Very strong associations correspond to an abrupt increase at low free protein (triangles in Figure 12); this jump in the initial binding density was observed in two different cases: (1) at low salt concentration, 10 mM or less [9,10,32,72] and when the association resulted mainly from Coulombic origin, far enough from the isoelectric point of the protein; (2) at various salt concentrations (30 mM or more), when both partners carried hydrophobic groups or sites, such as in the cases of β-lactoglobulin/copolymers of maleic acid and vinylalkylether [50], or serum albumins/alkyl-modified polyacrylic acids [17,63], or bovine serum albumin/polystyrenesulfonate [78 and Figure 12]. In such cases, the estimate of an initial binding constant—the slope of the curve at low binding density—is a delicate extrapolation because of the high uncertainty in the measurement of very low free protein concentrations. The affinity that can be found corresponds therefore to the

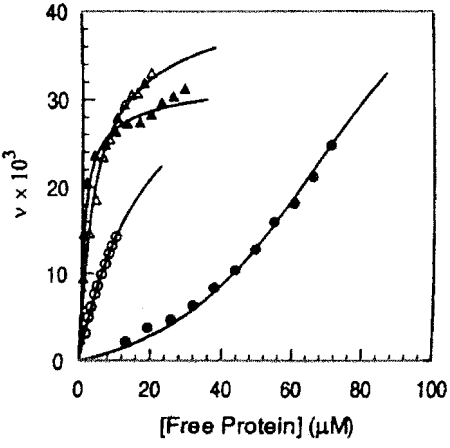

FIG. 12 Binding isotherms of proteins to poly(styrenesulfonate) under its sodium form. Open symbols: pH 7.5, ionic strength 0.1 M; closed symbols: pH 6.7, ionic strength 0.05 M. Bovine serum albumin (△, ▲); β-lactoglobulin (●, ○). ν is the mol/mol ratio of bound protein per sulfonate. (Reprinted with permission from Ref. 78. Copyright © 1998 American Chemical Society.)

equilibrium between the free protein and a complex already containing a few proteins per polymer chain.

In the other cases, exhibiting a lower affinity, or at high enough free protein concentration, the variation in the slope of the isotherms reveals either the cooperativity or the anticooperativity of successive binding events. As far as general conclusions can arise from the few data available, the Coulombic association in the presence of some salt (50 mM–0.25 M in the present reports) exhibits the features of a weak cooperativity or noncooperativity (circles in Figure 12). On the other hand, the formation of complexes attributed to hydrophobic association [17,50,63] was shown to be strongly anticooperative. On a log–log plot, some isotherms matched with straight lines having a slope of 0.24–0.29 instead of 1 for a noncooperative binding (Figure 13). The intermediate case of polystyrenesulfonate is a matter of debate: with β-lactoglobulin, the complexation was thought to be mainly of Coulombic origin (decreasing affinity at high salt or high pH, cooperativity), whereas complexes with bovine serum albumin exhibited the features of a hydrophobically driven association (anticooperativity, increasing affinity at high salt) [60,78].

Analysis of binding data depends on the selection of a model. Since the binding is likely to be nonspecific, sharing also the feature of a ligand binding to a lattice, the models developed for adsorption onto surfaces or lines

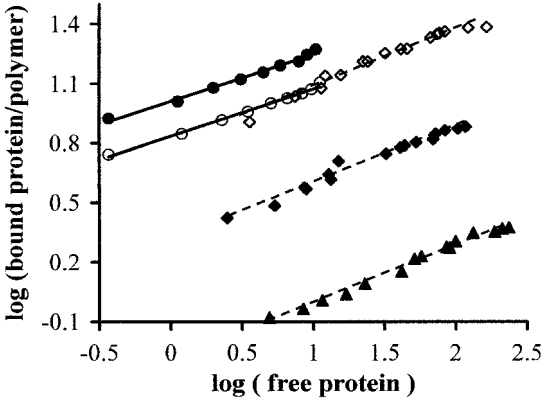

FIG. 13 Log–log plot of the binding isotherms of amphiphilic proteins to amphiphilic polyanions. (●, ○) β-lactoglobulin to copolymer of maleic acid and octyl- or dodecyl vinylether, respectively; pH 8.7 and ionic strength 0.1 M (data from Ref. 50). (◇, ◆, ▲) bovine serum albumin to C18 modified poly(acrylic acid), pH 9.0 in 30 mM NaOH–boric acid buffer. Modification rate: 10, 3, and 1 mol% respectively (data from Ref. 63). Free protein in μmol/L; protein/polymer ratio in number of protein globules per 1000 monomers.

should take into account part of the physics of protein/polymer complexes. Several equations have been proposed to fit these isotherms and to extract values of the protein affinity for the polymers. Since most of the isotherms did not match with a straight line, even at low free protein, the usual Langmuir isotherm was tentatively, used assuming two classes of binding sites [77]:

$$\nu = n_1 k_1 \frac{[\text{prot}]}{1 + k_1[\text{prot}]} + n_2 k_2 \frac{[\text{prot}]}{1 + k_2[\text{prot}]} \tag{5}$$

Where ν is the number of bound protein per polymer unit, [prot] is the concentration of free protein, and k_1 and k_2 are association constants. Although good fits were obtained in some cases (pH 6.7, β-lactoglobulin/polystyrenesulfonate), the reasons for the choice of two sites and only two remain unclear. Equation 5 failed to fit the data obtained at a higher pH with the same system. A more general form, although phenomenological, is the Hill equation:

$$\nu = \frac{nK[\text{prot}]^z}{n + K[\text{prot}]^z} \tag{6}$$

K is a constant related to the binding affinity, n is the number of binding

sites per polymer chain, and z is the cooperativity index (an empirical exponent that takes into account allosteric effects). This Hill equation was found to hold to the data much better than the bi-Langmuir (Eq. 5) and over a protein concentration range of two decades [63 and Figure 13]. The McGhee–von Hippel model was derived for noncooperative binding of macroligands on overlappings sites. Although the polymer system might be further complicated by conformational changes upon binding, this model looks very attractive for an analysis of protein binding. It is expressed as

$$\frac{\nu}{[\text{prot}]} = K(1 - m\nu)\left(\frac{1 - m\nu}{1 - (m - 1)\nu}\right)^{m-1} \tag{7}$$

where m is the number of polymer units per binding site. The fitting of isotherms to Eq. 7 was successful in the case of β-lactoglobulin/polystyrenesulfonate [60], showing that a slight apparent anticooperativity may result from site overlapping. The strong anticooperativity corresponding to hydrophobic association cannot however be described using (Eq. 7), although K values were extracted using the data at low protein concentrations [50]. This is a first hint against a simple explanation of anticooperativity by protein-protein repulsion only (either steric or electrostatic). A second argument against simple steric or electrostatic effects is the existence of anticooperativity at extremely low free protein, in complexes that contained less than one protein per 1000 monomers along the chain. In terms of the Hill equation, the anticooperativity of the binding of bovine serum albumin on alkyl-modified poly(acrylic acid) at pH above 8 was characterized by a z value of 0.20–0.30 independent of both the number and the length of the alkyl side groups along the polymer (C18 or C12 up to 10 mol%) [17,63 and slope 0.29 of the dashed lines in Figure 13]. A replot of data from other works (Gao and Dubin [50]) on β-lactoglobulin and bovine serum albumin/copolymers of maleic acid and vinylalkylether gave essentially the same value of z at pH 8.7 (full lines of slope 0.24 in Figure 13). The fact that z does not depend on the protein nor on the chemical structure of the polymer is likely to reflect a general underlying mechanism, possibly related to conformational reorganization upon binding. Although a detailed interpretation of the value of z is premature, a few origins may be regarded. First hypothesis: the presence of fluctuation in the density of alkyl pendant groups along the polymer might induce a broadening of the association constants depending on the ''local'' hydrophobicity. Second hypothesis: the wrapping of polymer around each protein would tend to maximize the number of alkyl groups close to the protein (forming for instance micelle-like clusters around the protein). Under this assumption, further binding competes with a partial disruption of this optimal wrapping involving thousands of monomers per protein. The decrease in the protein binding at low pH or beyond some

critical hydrophobicity of the polymer demonstrates that the alkyl self-association can compete with protein association in the mechanism of complexation [50].

One important case, shedding light over the latter assumption, was the sole study of the binding isotherm of short polymers onto a protein [33]. From equilibrium dialysis, Tribet and coworkers have shown the strong cooperativity of the adsorption of C18-modified poly(sodium acrylate) on bovine serum albumin. Beyond a threshold polymer concentration, the average number of bound polymer chains per protein rose abruptly from 1/1 to 9/1 (Figure 14). This result suggested the binding of self-associated hydrophobic clusters, containing about 20 octadecyl groups, beyond some critical self-association concentration. From that point of view, the binding of short amphiphilic polymers to protein resembles that of conventional surfactant–protein systems [79]. At low surfactant concentrations, bovine serum albumin binds a small number of surfactant molecules (less than 10 dodecyl sulfates, for instance) in its hydrophobic pockets. Beyond the critical micellar concentration, the amount of bound surfactant seems to diverge, reflecting the binding of several micelles due to the protein unfolding. Unlike surfactants, however, the cooperative binding of short polymers appeared to stop at a ratio of the number alkyl group to protein in the range 20–100 (see also II.A.3). This suggested the association of one micellelike aggregate and only one, in consistency with the absence of protein denaturation (IV.A).

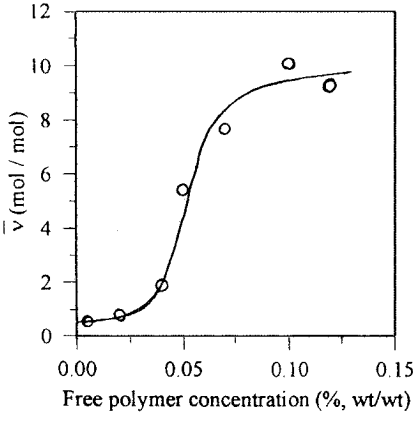

FIG. 14 Binding isotherm of a short C18-modified polyacrylic acid to bovine serum albumin obtained from equilibrium dialysis against polymer solutions in 20 mM borate buffer, pH 9. Polymer M_w 5,000 in its acid form; grafting rate: 3 mol%. (Reprinted with permission from Ref. 33. Copyright © 1998 American Chemical Society.)

3. The Case of Short Polymers and Membrane Proteins

The structure and composition of integral membrane proteins (IMP) are not markedly different from those of water-soluble proteins except that transmembrane segments of the polypeptide chains are markedly more hydrophobic. *In vivo*, these proteins span the lipid bilayers, their transmembrane segments facing the apolar lipid region. Thus the surface of an IMP displays a central hydrophobic belt, about 3 nm in height and a few nanometers in diameter, capped by two hydrophilic ends. All the IMPs are totally insoluble in water. Usually, they are purified, dispersed, and handled in micellar solutions of a surfactant, near the critical micellar concentration. Recent works have demonstrated the possibility of an exchange of the surfactant for an amphiphilic polymer, called amphipol [3,64,71,80] or peptitergents [81], that bind around the protein, maintaining it soluble in the absence of free amphiphilic molecules. This technique is very promising in the field of biochemistry, facilitating the handling and preservation of fragile proteins as compared to other conventional techniques such as micellar solutions or irreversible conjugates with hydrophilic polymers [82]. Like the common amphiphilic polyelectrolytes discussed above, the amphipols are alkyl-modified poly(acrylic acids) that interact strongly with lipids, surfactants, and proteins. Their design for an IMP resulted in a high hydrophobicity (about 25 mol% of pendant C8 group and possibly other additional short pendant groups) and a short length (M_w < 34 000 and preferably 8000 g/mol). Amphipols and IMPs form hydrosoluble complexes by simple mixing [3]. In the absence of the amphipols, dilution below the critical micellar concentration of the surfactant results in the aggregation of the proteins, attributed to the removal of most of the surfactants from the transmembrane region. On the contrary, when supplemented with enough amphipols, IMP stock solutions (bacteriorhodopsin, reaction center, porine, cytochrome b_6f) can be diluted without precipitation (Figure 15). The complexes appear to be irreversible on the time scale of a few days, which is not surprising regarding the multipoint attachment of the polymer and the high hydrophobicity of the partners. Nevertheless, exchange between amphipols does take place, since an excess of free polymers can displace bound ones [64]. Similarity with the conventional adsorption of polyelectrolytes on colloids were reported, such as a low density of coverage and the effect of ionic strength (about 80–150 octyl groups per protein, depending on pH ionic strength and the M_w of the IMP). The complexes exhibited a low polydispersity in size and molecular weight as estimated by scanning transmission electron microscopy [71, Figure 9]. Together with unpublished results on low-angle x-ray scattering (J. L. Rank and C. Tribet), the present studies are consistent with the

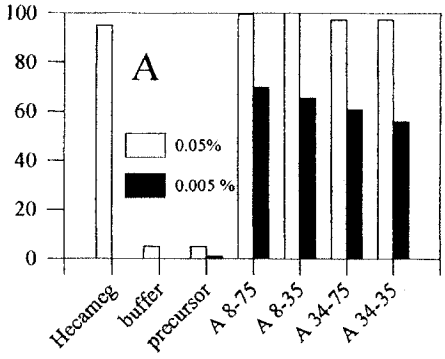

FIG. 15 Fraction of the membrane protein cytochrome b_6f remaining soluble upon 10-fold dilution at pH 8.0 in several polymer or surfactant solutions as follows: 20 mM of a neutral surfactant, slightly above its CMC (Hecameg); no polymer nor surfactant (buffer); poly(acrylic acid) (precursor); C8-modified precursor of M_w 8,000 or 34,000 having 75 or 35 mol% of residual unmodified carboxylic acid groups (A8-75, A8-35, A34-75, A34-35). The polymer final concentration (wt%) is given in the figure. Initial protein concentration about 1 g/L. (Reprinted from Ref. 3. Copyright © 1996 National Academy of Sciences, U.S.A.)

formation of a micellelike cluster tightly bound to the IMP, resulting in a quasi-monodisperse and irreversible object of typical radius ranging from 3–4 nm (with small IMPs such as bacteriorhodopsin) up to 7–8 nm with large IMPs [71, Figure 16]. In the complexes, the native structure of the IMP and its activity can be preserved [3, and P. Champeil, T. Menguy, C. Tribet, J. L. Popot, and M. Le Maire, in preparation).

B. Gelation Phenomenon

Gelation of a solution containing proteins is often related to the formation of a protein network that does not involve a second partner. The cases of gelatin, β-lactoglobulin, serum albumin, and ovalbumin have been extensively studied, given the practical importance of these proteins for the food industries. Whether irreversible denaturation or reversible helix formation takes place in these systems, the conformational specificities of proteins governs the mechanisms of such gel formation regardless of the polyelectrolytic nature of those polypeptides. For general information, the reader is sent to papers drawing parallels between natural and synthetic gels [83] or discussing the aggregation process of gelatin [84,85] or small globular proteins [86–88]. Similarly, the introduction of proteins or enzymes in chemically cross-linked gels is a topic of great interest. Kokufuta reviewed recently

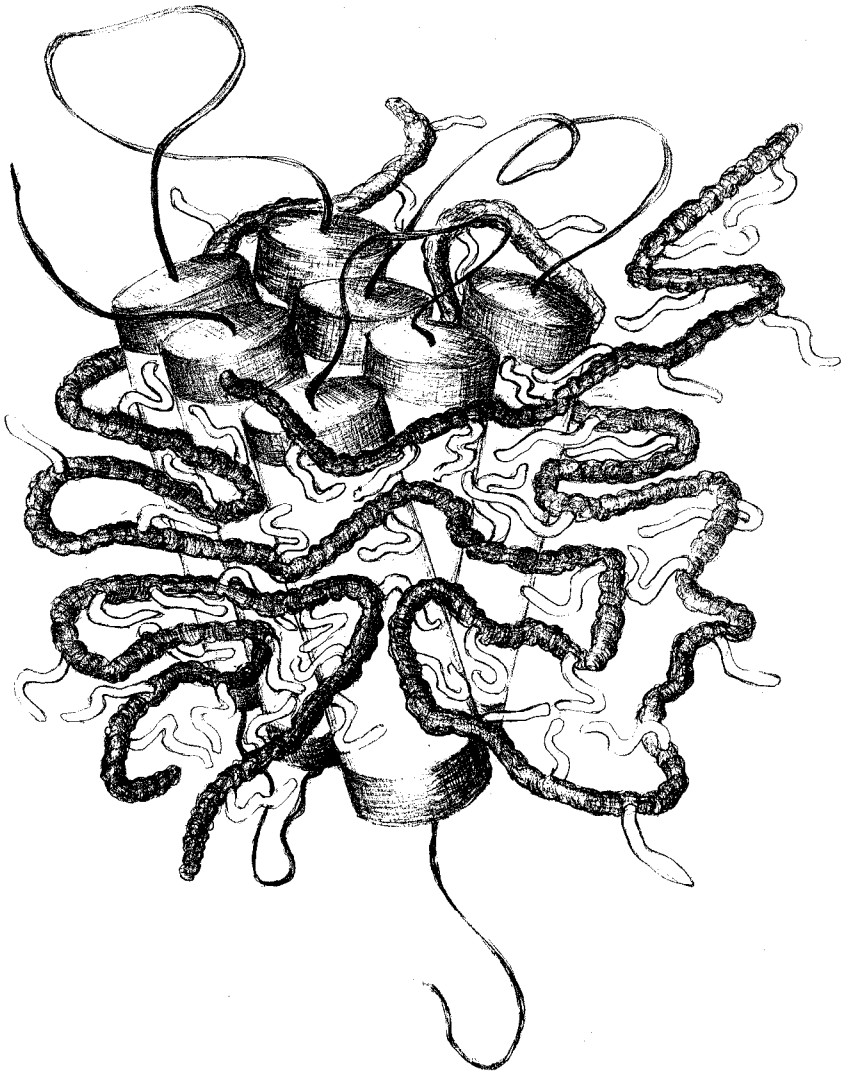

FIG. 16 Sketch of an integral membrane protein complexed by amphiphilic short polymers (amphipols). Protein and polymers are drawn to scale. The polymer/protein mass ratio corresponds to a typical experimental value of 1. The persistence length of the amphipol has been taken equal to about 3 nm. The number of contacts among the partners is largely speculative. (Reprinted from Ref. 3. Copyright © 1996 National Academy of Sciences, U.S.A.)

the control of entrapped enzymes and the swelling/deswelling of synthetic gels loaded with proteins [89]. This paragraph will only focus on mixed systems in which gelation occurs upon association (often reversible) between long polyelectrolytes and either peptides or proteins. A relatively small number of papers falls within this scope, most of them being recent. As suggested in one of them [65], reversible gelation demands two seemingly contradictory behaviors: interpolymer associations must be strong enough to stabilize the network of macromolecules, yet the chains cannot exclude the solvent or they will precipitate. This might be a reason for the absence of reversible gelation in most of the polymer/protein systems that rather form soluble complexes or undergo a phase separation. In principle, the presence of electric charges in the polymer/protein complexes, although not absolutely required, could limit the domain of phase separation owing to the large entropy of demixing due to the presence of the counterions. In the absence of hydrophobic pendant groups along the polymer backbone, however, the cooperative Coulombic associations of proteins (for isotherms see III.A.2) may entail the concentration of the protein in small clusters rather than the dispersion of cross-links throughout the whole sample. Therefore homopolymers, even of polyelectrolytic nature, do not appear as good candidates for mixed gelation. The only case reported by Lagendorff and colleagues [34] concerns iota-carrageenan and casein micelles. The iota-carrageenan can form gels by itself, when it undergoes a coil–helix transition upon cooling of its aqueous solution. In this case, the gelation of the polymer itself is likely to prevent the tendency for precipitation upon association with a protein, although this association may modify the conditions of gel formation. Both a shift of the gelation temperature toward higher values and an increase of the gel strength in the presence of casein micelles were convincing evidence for the sensitivity of the gel topology to the presence of casein. The situation was, however, unclear because a segregative phase separation took place in the presence of milk at high temperature, reflecting a repulsion among the carrageenan coils and the proteins. Investigations on highly dilute mixtures were nevertheless consistent with an attractive interaction between carrageenan helices and casein (i.e., at low temperatures) that was interpreted as a consequence of the increase in the linear charge density of the carrageenan upon coil–helix transition. In addition, the coil–helix transition of iota-carrageenan in concentrated mixtures was clearly correlated with gelation [34]. Figure 17 gives the schematic picture of the various structures that might have been formed depending on the composition and temperature of mixtures. Owing to the complexity of such polysaccharide/protein mixtures, some care has to be taken in interpreting an increase of the viscosity. As an example, Castelain et al. characterized transient viscosity enhancements in BSA-carboxymethylcellulose, despite the absence of complexes between

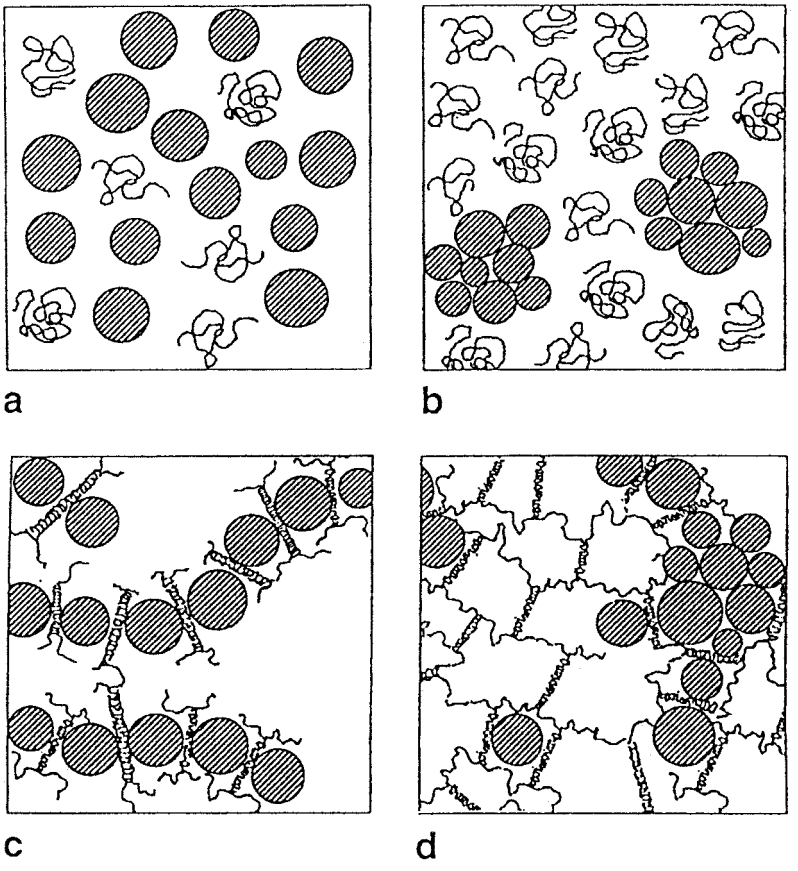

FIG. 17 Schematic picture of a mixture of iota-carrageenan and casein micelles at 60°C and at low carrageenan concentration (a) or high carrageenan (b): at 25°C and low carrageenan (c) or high carrageenan (d) concentration. (Reprinted from Ref. 34. Copyright © 1999 with permission from Elsevier Science.)

these partners [90]. The emergence of a yield stress and the increase of the elastic modulus as compared to pure carboxymethylcellulose solutions was tentatively attributed to an incipient phase separation resulting in the formation of protein-rich droplets in a continuum polymer phase. It is worth noting that the variation in the viscosity in this system was significantly lower than in carrageenan/milk mixtures.

The best polymer structures for the formation of mixed gels appear finally to be copolymers composed of a majority of water-soluble monomers and

only a few side groups that could bind to a protein. A first example, devised by Lee and Park, corresponds to neutral polyvinylpyrrolidone-allylglucose copolymers cross-linked by concanavalin A [66]. The formation of reversible and glucose-sensitive gels at some optimal protein/allylglucose ratio demonstrates the possibility of cross-link formation upon recognition by a protein of a few pendant groups along the polymer chain (here up to four glucose groups per protein). Nonspecific association can also induce gelation. Amphiphilic polyelectrolyte/protein seems a generic system in which a reversible and strong gel formation was observed in a wide range of compositions and with different protein/polymer couples. For example, the recent qualitative results on multiblock copolymer gels, including hydrophobic polypeptide blocks called leucine zippers, are presented in Sec. II.B.3 [65]. Other works on the rheological behavior and interpretation of gelation in mixtures of a soluble protein and alkyl-modified poly(sodium acrylate) are summarized in the next sections [6,35,91].

1. Sol–Gel Transitions

The solutions of hydrophobically modified poly(acrylic acid) of M_w 150,000 (HMPA) exhibit a pronounced viscosity enhancement upon supplementation with small amount (less than 5 wt% final) of lysozyme, papain, or serum albumin [6,35]. This effect was found to be qualitatively similar using many different polymers, composed of different densities of alkyl pendant groups (HMPA150-yC18 for a C18 grafting rate y ranging from 1 to 8 mol%) at pH $\geq$ 7. The boundary between the sol and the gel states cannot be determined unambiguously from viscometry because of the sensitivity of the samples to the shear rate (rheothinning). Measurements under oscillating shear of the frequency dependence of the elastic and the loss modulus are more accurate characterization of the formation of cross-links. The gelation points were determined by Borrega and colleagues [35] using the criterion provided by the work of Mours and Winter [92] for chemical gels. Namely, at the ''gel point,'' the rheograms are expected to match with a typical scaling law as a function of the frequency ω:

$$G' \sim G'' \sim \omega^n \qquad 0 < n < 1 \tag{8}$$

Close to some critical composition, log–log plots of the moduli vs. ω gave two parallel lines in various protein/HMPA systems, and Eq. 8 was very well fitted to the data using n values in the range 0.4–0.8 (0.55% in Figure 18). This sol–gel boundary was plotted in a 2-D diagram as shown in Figure 19. Similar signature of the gelation was reported by Lagendorff and colleagues in carrageenan/casein [34], although on the basis of an equivalent criterion: $G''/G' = \tan(2\pi/n)$ independent of the frequency. At compositions very different from these critical ones, a tight crossover between the curves

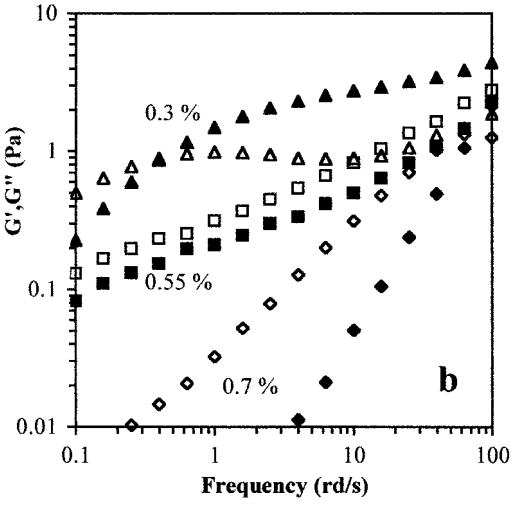

FIG. 18 Double logarithmic plot of the dynamic moduli vs. frequency of HMPA/lysozyme samples. Polymer 0.9 wt% in 20 mM boric acid–NaOH buffer pH 8.7. Open symbols: G'; filled symbols: G''. Lysozyme concentration given in the figure. (Reprinted with permission from Ref. 35. Copyright © 1999 American Chemical Society.)

of G' and G'' showed that the parallel variations completely vanished far from the sol–gel transition (0.3% or 0.7% on Figure 18). At both very low and very high protein concentration, a liquidlike behavior was observed in that the variation in the moduli matched with one Maxwell element ($G' \sim \omega$ and $G'' \sim \omega^2$). At protein concentrations between the critical sol–gel transition points, i.e., in the gel domain, characteristic features of gelation were observed such as a maximum in the values of both the elastic modulus and the viscosity, and the onset of a plateau of G' at high frequency.

2. Elasticity of the Gels

Similarity between protein/HMPA systems and chemical gels is expected as a generic feature of particle/polymer networks and provided that a minimum lifetime of the cross-links exists. For instance, assuming that the separation between cross-links is small as compared to chain length, the elastic modulus shall be proportional to the concentration of cross-links. Recent models of transient networks of associating polymers have now established on a quantitative basis relationships between gel topology and rheological behavior [93,94, and Ref. in 35]. Phase diagrams and G' variations in HMPA/protein systems were successfully predicted by a scaling law analysis, assuming that

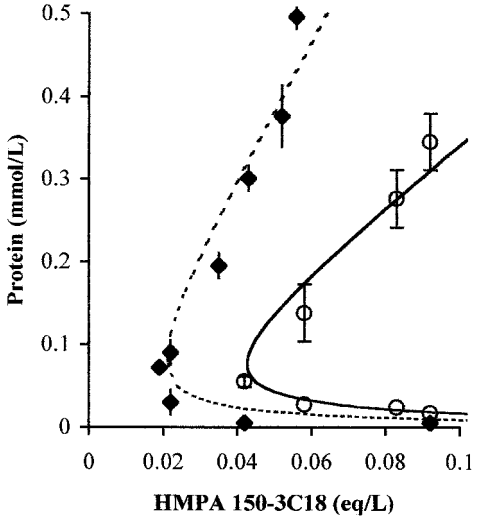

FIG. 19 Sol–gel transition diagram of HMPA/protein systems at pH 8.7. Polymer grafted by 3 mol% of C18 groups; (♦) bovine serum albumin; (○) lysozyme. Lines are the results of the fitting procedure using Eq. 10. (Reprinted with permission from Ref. 35. Copyright ©1999 American Chemical Society.)

the protein binding took place on sites along the polymer and that two polymer chains were involved in a cross-link [35]. To go straight to the result, the concentration of cross-links, X, was estimated in the semidilute regime of the polymer as

$$G' \sim X \sim K \cdot \alpha \cdot (1 - \alpha) C_p^m \tag{9}$$

where C_p is the polymer concentration, m a scaling exponent, K an association constant that governs the equilibrium between cross-links and the protein bound to a single chain, and $1 - \alpha$ the fraction of empty binding sites along the polymer backbone. Correlatively, the sol–gel transition corresponds to an average of one cross-link per chain. At the gel point, it becomes therefore

$$K \cdot \alpha \cdot (1 - \alpha) \sim \frac{C_p^{1-m}}{M_w} \tag{10}$$

where M_w is the molecular weight of HMPA. Writting $\alpha = A \cdot [\text{protein}]_{\text{bound}} / C_p$, where A is the length of a binding site, enabled Borrega and colleagues

to fit Eq. 10 to the sol–gel diagrams (Figure 19), using a value of A of about 300 for lysozyme systems. The same value of A gave excellent predictions of the maximum of the gel strength in the gel domain ($\alpha = 0.5$) [35]. The ratio $G'_{plateau}/NkT$ (where N is the number of HMPA chains per unit volume) were in the range 0.5–2 as expected for a network of overlapping macromolecules having a few cross-links per chain. Altogether, these results were consistent with the simple topology of the gel as shown in Figure 20. The stoichiometry of a cross-link appeared, however, more complicated than the binding of typically one hydrophobic group on each hydrophobic site of the protein. The value of A indicated indeed the presence of 18–40 alkyl pendant groups (corresponding to about 600 acrylic momomers) per cross-link. The interpretation of such a high number of hydrophobes is a matter of debate. Among possible explanations, the nucleation of a sort of micelle bound to the protein seems consistent with the binding isotherm of short relatives of the HMPA (Figure 14). Other mechanisms such as Coulombic repulsion may also play a role in hindering the binding of proteins, that would bring together the charged monomers of the HMPA and charged proteins. In this second hypothesis, the value of A reflects a minimum distance of approach between two charged cross-links likely to be of the order of the Debye length.

Among particular advantages of protein cross-linkers, it is expected that they might couple the gelation with a specific recognition of some side group along the polymer backbone. As presented above (II.B.4), glucose-sensitive

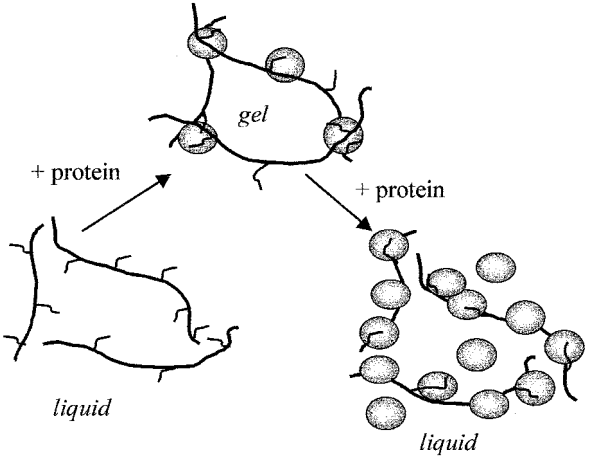

FIG. 20 Sketch of the gelation–fluidification process in protein/hydrophobically-modified polymer systems.

gels have already been devised by Lee and Park [66]. Another system showing the possibility of recognition of hydrophobes was recently investigated by Porcar and colleagues [95 and manuscript in press in the ACS Advances in Chemistry series] using HMPA grafted by azobenzene groups. Upon irradiation under near-UV light, the azobenzene chromophores undergo a reversible trans-to-cis transconformation accompanied by an increase in polarity that was expected to change the binding of proteins. Mixtures of proteins and azobenzene-modified HMPA exhibited similar enhancement in the viscosity as mixtures of protein and HMPA. The presence of a small amount (0.5–4 mol%) of azobenzene side groups did not markedly affect the formation of cross-links. The influence of an irradiation confirmed nevertheless that the chromophores participated in the gelation: samples kept 24 h in the dark (absence of cis isomers of azobenzene) were found to be more viscous before an irradiation at 365 nm that changed part of the chromophores to their cis conformation. The viscosity increased upon subsequent irradiation at a higher wavelength when most of the trans isomers were recovered (Figure 21). The variations in the viscosity were therefore coupled with the transconformation of the azobenzene. This photoresponsiveness may help in understanding more in depth the complexity of these gelation phenomena by giving means to modulate rapidly and *in situ* the strength of the protein/polymer binding. Among the first new results using azo-modified

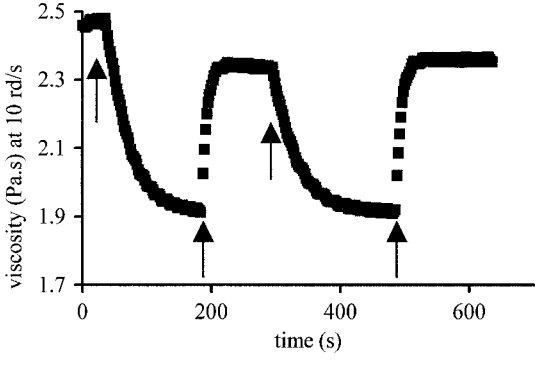

FIG. 21 Photoresponse of the viscosity of a 1 wt% solution of an azo-modified HMPA in the presence of 0.6 wt% bovine serum albumin. Arrows correspond to the onset of UV irradiation alternatively at 365 nm (increase in the viscosity) or 436 nm (decrease). The polymer was grafted by 0.5 mol% of azobenzene and 1 mol% of C18 side groups. A factor of 20 between the high and low plateau-values was achieved in recent results by G. Pouliquen and C. Tribet. (Reprinted with permission from Ref. 95. Copyright © 1999 American Chemical Society.)

HMPA, it was assessed that the kinetics of the macroscopic variation in the viscosity did not differ markedly from the kinetics of the microscopic cis–trans conformation.

C. Phase Separation

The tendency to demix is generally strong for mixtures of macromolecules because the entropy of mixing is a much weaker driving force for large molecules than for small molecules. Two main classes of biphasic demixing can be distinguished, on the basis of the distribution of the two solutes: they may either segregate into two different phases or associate into one concentrated phase in equilibrium with a very dilute solution. Figure 22 illustrate these two types of separation and the corresponding difference in the direction of the tie-lines. In the case of protein/polymer mixtures, both classes of demixing have been exploited for protein purification, the segregative separation being however obtained when the partners repel each other [26,55]. As far as polyelectrolytes or amphiphilic polymers are concerned, most of the studies were dealing with associative separations, which are a consequence of cohesive forces (hydrophobic or Coulombic) between the partners. The observable result of associative phase separation may be the formation of an amorphous precipitate or a liquid phase, often highly viscous, called the coacervate.

1. Variables Affecting the Solubility of Polyelectrolyte/Protein Complexes

As a rule, the combination of high protein surface charge density, high polymer linear charge density of opposite sign, and low ionic strength promotes precipitation rather than coacervation. The similitude with ionic micelle/

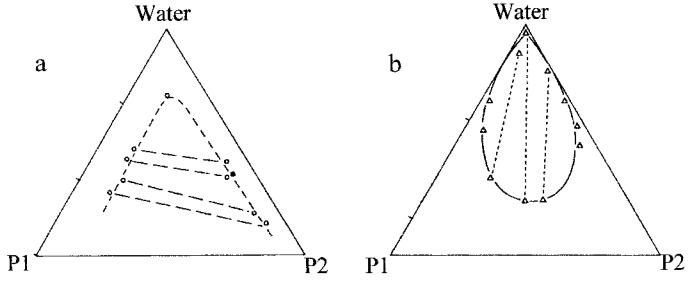

FIG. 22 Typical phase diagrams of a mixture of two polymers in a common solvent. (a) Segregative phase separation in the absence of strong association among the polymer backbones; (b) associative separation in the case of complexation. Dotted lines are typical tie-lines.

polyelectrolyte or polyanion/polycation systems is obvious, and it may be of great interest to refer to the extensive work on micelle/polymer or polymer/polymer phase diagrams reviewed recently [46,62,96]. In the latter systems, the application of a modified Flory–Huggins model allowed Frugier and Audebert [46] and Linse and colleagues [47] to simulate the effect of concentration and ionic strength. The main difficulties in such theoretical approaches arise from the quantitative estimation of the consequences of electrostatic interaction on the polymer stiffness, excluded volume parameters, and the entropy of counterions. They give nevertheless an interesting qualitative picture of the main trends from a phenomenological point of view.

In comparison, the studies of protein/polymer phase separation was often limited to experimental investigations on the effect of a few external parameters (pH, ionic strength) or structural variables (polymer charge density, or M_w, protein charge) on the onset of a demixing and its selectivity among various proteins [5,7,10,12,13,16,22,97–99]. These works, recently reviewed [12], aimed clearly at the development of a purification method rather than at a generic parallel with other colloid/polymer phase behaviors. The recovery of one protein in a cell extract or from a mixture of proteins (either positively charged lysozyme using a polyacrylic acid, or on the contrary a negatively charged protein using polycation as precipitant) was found to be efficient by Parker and colleagues [7], Sternberg and Hershberger [5], and Wang and colleagues [13]. Their practical results demonstrate that some selectivity can be achieved on the basis of differences in the charge density of the proteins, in consistency with the idea proposed by Dubin and colleagues [15] that for a given polyelectrolyte a critical charge density of the protein is required for phase separation to occur (see Table 1). This critical charge density, or in other words the critical pH of incipient demixing, depends however on both the charge density of the polymer and the ionic strength. For various systems, it was found by Dubin and colleagues that the critical charge varies about linearly with the square root of the ionic strength [12,22 and see II.B.2]. As recognized now, and systematically studied by Trinh and Schnabel [98], the effect of added salt is to screen the Coulombic forces and to reduce if not suppress protein/polyelectrolyte precipitation. A similar tendency was reported in mixtures of polyanion and polycations [46,98].

The origin of the insolubility of protein/polymer complexes is often discussed on a structural basis. Namely, from the observation that when the concentration ratio for polymer/protein deviates from some optimum, part of the insoluble phase redissolves, it is thought that some stoichiometry is involved in the phase separation. In addition, at low ionic strength, Kokufuta and colleagues have demonstrated that the precipitate was formed by salt

linkage of 1:1 stoichiometry between all the ionized residues of the protein and the charged monomers of the polyelectrolyte [10]. This scheme of precipitation upon neutralization was also reported to be a good approximation in dilute micelle/polyelectrolyte systems at low ionic strength by Guillemet and Picullel [96]. Picullel et al. have shown however that the boundary of the phase separation considered in the whole phase diagram or in the presence of salt did not always correspond to the charge neutralization, neither did it match with a single polymer/protein ratio [62]. In addition, the partition of simple salts and counterions between the two phases arose as an additional complexity, often neglected despite being of prime importance in the understanding of micelle/polyelectrolyte demixing [62]. Similarly, the complete phase diagram of polyanion/polycation mixtures cannot be interpreted by the formation of complexes of 1:1 stoichiometry, reflecting that a variable fraction of counterions coprecipitates in the complexes [46]. It is likely to be also the case of polyelectrolyte/protein systems as suggested by the strong effect of ionic strength on the demixing [16,98]. Nevertheless, measurements of the electrophoretic mobilities of soluble aggregates indicated that quasi-neutral objects were formed close to the phase separation [2,4,15,23]. These large and seemingly stable aggregates (80 nm or more in radius) contained obviously several polymer chains and several proteins. From a microscopic point of view, they are thought to correspond to a primary aggregation stage preceding the phase separation upon further aggregation (flocculation) of these primary particles. A comprehensive work on protein/polyelectrolyte phase separation should include the collection of the phase boundary and tie-lines on a wide concentration range, together with the study of the partition of counterions and added salt between the phases. To date, this is unfortunately lacking, making it difficult to conclude on the generality of the ''neutralization prior to precipitation'' scheme, despite numerous evidence for it in dilute systems.

2. Precipitation with Amphiphilic Polymers

In the presence of hydrophobic association, phase separation no longer obeyed a neutralization scheme. Petit and colleagues have found that increasing the modification rate of poly(acrylic acid) by C18 groups shifted the precipitation of their complexes with the cationic lysozyme to higher content of protein per polymer chain [6]. As compared to the unmodified polyanion, the presence of only 3 mol% of C18 side groups shifted the precipitation of the complexes by a factor of 10 in terms of bound protein/polymer ratio. In addition, the presence of the hydrophobic driving force allowed Borrega and colleagues to obtain complexes of bovine serum albumin with a C18-modified poly(acrylate) well above the isoelectric point of the protein [91]. The solubility of these complexes was modulated by the

ionic strength. At pH 8.7, i.e., when the global charge of the protein was about −20, and in the presence of 300 mM $NaNO_3$, these polyanion/polyanion complexes were found to precipitate in a wide range of compositions of the mixtures (Figure 23). At low salt concentration (<100 mM), soluble complexes or gels were formed in the same range of composition that corresponded to phase separation at higher ionic strengths. Coulombic effects, although not primarily involved in the protein binding, tuned the competition between intrapolymer (soluble species) and interchains (precipitate or gel) association. All these results may be rationalized using the concept of the formation of a quasi-species composed of a polymer chain decorated by several colloids, as proposed by Picullel [47,62]. The solubility of such quasi-species would depend on the quality of the solvent for these macromolecular objects in a way similar to the conventional approach of Flory-Huggins (i.e., on an average interaction parameter that compares the free energy of polymer–polymer contact to that of the polymer–solvent and solvent–solvent). The global charge, the hydrophobicity of these species, and the salt concentration modulate the effective interspecies interaction. Note that the composition of the quasi-species may be different from the average composition of the mixture because of the cooperativity of the binding and the equilibrium of complexes with free proteins (III.A.2).

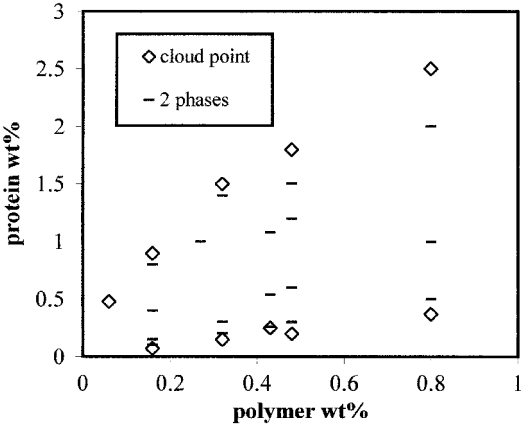

FIG. 23 Phase diagram of bovine serum albumin/HMPA mixtures in 300 mM $NaNO_3$, 20 mM boric acid–NaOH buffer pH 8.7. The HMPA is a poly(acrylic acid) of M_w 150,000 grafted by 3 mol% of C18 groups. Cloud-points were observed by eye after a one-night incubation period of the mixtures. In the demixed samples, the upper phase was highly dilute (<0.5% protein and 0.2% polymer) and the bottom phase contained the polymer/protein complex (concentrations >0.8% polymer and >1% protein).

IV. PROTEIN STRUCTURE IN THE COMPLEXES

Since the same forces are involved in the complexation of protein with amphiphilic or hydrophilic polyelectrolytes and in the stabilization of the protein conformation, the proteins may be subjected to destabilization upon binding. It would not be surprising for instance that intraprotein salt bridges can be weakened or disrupted upon association with strong polyions. In addition, a structural variability is in some cases (hemoglobin, serum albumin, etc.) a natural consequence of ligand binding or enzyme activity. The study of possible conformational reorganization of the protein is therefore an important step toward a good understanding of the structure and the stability of these complexes.

A. Preservation of the Secondary Structure

Circular dichroism (CD) spectrum or alternatively measurements of the specific rotation of proteins are in general sensitive to both changes in the secondary structure and subtle modifications of the tertiary structure. Pronounced changes were observed with denaturation by pH extremes or addition of perturbants such as ionic surfactants or urea. On the contrary, unchanged CD spectra or unchanged specific rotation were often reported in mixtures of soluble proteins with polymers [31 and Refs. therein, 33, 100]. Xia and colleagues showed the absence of variation in the secondary structure of ferrihemoglobin upon binding to a strong polycation [100]. Kuramoto and colleagues found that the association of bovine serum albumin with polyacrylic acids of varying molecular weight did not induce any significant change in the helicity [31]. They concluded that the binding of the polymer was essentially nonspecific and located at the surface of the protein. A similar absence of effect on the specific rotation of both lysozyme and bovine serum albumin was observed by Borrega and colleagues in the case of hydrophobically driven association with C18-modified polyacrylic acid [35]. However, the preservation of the native structure should not be considered as universal. For example, insulin was denatured upon complexation with polydiallyldimethylammonium chloride [100]. Nishikawa and colleagues showed that hydrophobized pullulan spontaneously forms complexes with various soluble proteins in water, the driving force for association being probably hydrogen bonds [42]. In these nanoparticles, α-chymotrypsin or horseradish peroxidase were denatured [43], whereas insulin was stabilized against thermal denaturation [42]. The intermediate case of a so-called ''chaperone-like'' behavior was observed with the enzyme carbonic anhydrase, which did not bind to the modified pullulan in its native state, although it was readily incorporated in the nanoparticles at high temperature upon thermal denaturation. The release of the—denatured—enzyme from

this nanoparticle, by breaking the complexes with cyclodextrin, was accompanied by the refolding of the protein to its native state [101]. A general property can nevertheless be expected from the association with a macromolecule. Complexation is likely to decrease significantly the protein irreversible aggregation by preventing the protein–protein contacts that often lead to precipitation upon heating. Provided that the release of the bound protein is feasible, the chance for correct refolding after denaturation should by greatly increased. The few existing examples of such a possibility are the renaturation of a porin conjugated with polyethyleneoxide both in solution and in reconstituted liposomes [82], the refolding of a the 56 C-terminal residues of a heme protein HasA in amphiphilic polyacrylic acid as determined by CD spectrometry [80], and the reversibility of conformational changes observed by polarimetry upon heating and cooling of a solution of bovine serum albumin containing C18-modified polyacrylic acids (Figure 24).

B. Enzyme Activity in Complexes

The immobilization of an enzyme in a complex was often thought of as an excellent means of stabilizing the protein against thermal or pH-induced degradation. Among the first reports on covalent enzyme/polyelectrolyte soluble complexes, Margolin and colleagues studied urease, α-chymotrypsin, and penicillin amidase grafted in nonstoichiometric polyelectrolyte complexes (N-PEC: formed by mixing a polycation with an excess of polyanion) [8]. Small pH or ionic strength modification caused the precipitation of the N-PEC containing the enzyme. In the insoluble N-PEC particles, up to 300-fold stabilization was observed, whereas upon redissolution the stability decreased and the activity increased. These properties were attributed to the rigidity of the N-PEC, the dehydration, and the multipoint interaction that resulted from the phase transition. The use of stimulable polymers (salt-sensitive or pH-sensitive polyelectrolyte [8], photoresponsive macromolecules [102], etc.) was often contemplated as a new route toward *in-vitro* regulation of enzyme activity by a modulation of the affinity of the enzyme for the polymer chain and/or of the polymer conformational reorganization. Several examples of controlling the enzyme by an external stimulus have been developed in polymer supporting matrices, in which the proteins were grafted or immobilized by entrapment in chemical gels [89]. These studies demonstrate the coupling between the polymer chain and the state of protein or the accessibility of substrate. In most of them, however, the reversible and weak interactions that may affect the enzyme properties were not considered in detail.

On the contrary, for reversible protein/polymer complexes, it was important to investigate how salt linkages and hydrophobic association, which

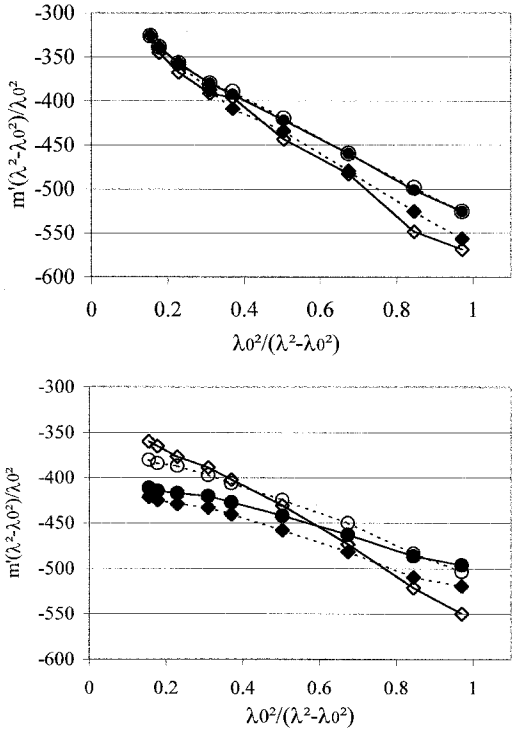

FIG. 24 Moffit–Yang plot of the reduced specific rotation of bovine serum albumin (m') as a function of the wavelength (λ) and at different temperature and incubation times. In this representation, the slope of the curve is proportional to the fraction of helices in the secondary structure. Upper diagram: mixture of protein and HMPA (2:1 mass ratio). Lower diagram: solution of protein alone in a phosphate buffer pH 7. Protein at 0.3 wt%. Key: (◇) initial solution at 25°C; (○) same solution just heated at 70°C; (●) after a 1 h incubation at 70°C; (◆) after its cooling back to 25°C.

drive the formation of complexes, also affect the 3-D conformation of the active sites. Many reports in that field are convergent in giving evidence that the nonspecific formation of complexes with synthetic polymers does not markedly change the capacity of enzyme to be functional. Amiconi and colleagues showed that dextran sulphate, strongly bound to human hemoglobin, can change the affinity of hemoglobin for oxygen although in a similar way to that of small polyanions such as heparin or polyphosphate [103]. Accordingly, Nguyen [32] measured the affinity of hemoglobin for oxygen in the presence of high M_w dextran sulfate or DEAE-dextran. These polymers were found to modify slightly the stability of deoxyhemoglobin,

the stabilizing or destabilizing effect being dependent on the sign of the polymer charge [32]. The comprehensive work by Kokufuta and colleagues [9,10] has given the basis of a general understanding of the effect of polyelectrolyte in Coulombic complexes. The authors investigated the effect of pH and temperature on the Michaelis–Menten constants of α-chymotrypsin or papain complexed with strong polyanions. They found that the values of the maximum hydrolyzing rate (V_{max}) attained at high substrate concentration was decreased by complexation, whereas the Michaelis constant K_m was not significantly changed. It was thus believed that the salt linkages with the polyanions did not affect the active site (constant K_m) of active enzymes, although part of the bound proteins became inaccessible or denaturated. It is worth noting that the activity of chymotrypsin toward a macromolecular substrate, the casein, did not markedly differ from its activity toward a molecular substrate, the $N\alpha$ benzoyl-DL-arginine-*p*-nitroanilide [9]. This important result shows the high accessibility of the fraction of active enzyme despite its binding to a complex. Coulombic association, far from inducing denaturation, can on the contrary increase the activity. As reported by Kudryashova and colleagues, charged groups introduced either by grafting or by complexation with a polycation (polybrene) increased by a factor up to 6 the V_{max} of α-chymotrypsin in water–alcohol mixtures (11 and Figure 25).

To date, the case of hydrophobic complexes with enzymes seems limited to membrane proteins. Because these proteins are designed to interact with

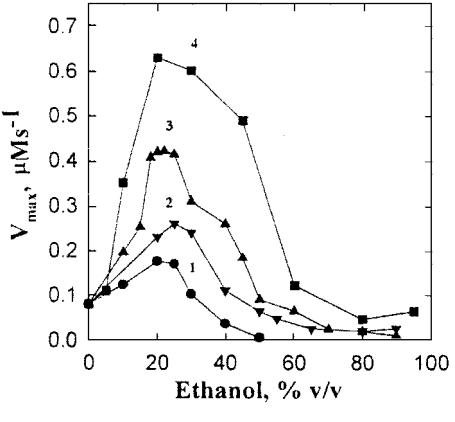

FIG. 25 Variation of the maximal rate of hydrolysis of *N*-benzoyl-L-tyrosine *p*-nitroanilide, V_{max}, catalyzed by α-chymotrypsin in binary water/ethanol mixtures. 1: enzyme alone; 2: pyromellitic-modified enzyme; 3: mixture of unmodified enzyme and polybrene; 4: mixture of polybrene and pyromellitic-modified enzyme. (Reprinted with permission from Ref. 11. Copyright © 1997 John Wiley & Sons, Inc.)

the hydrophobic lipid molecules and can be active in micellar solutions, it is not surprising that they accommodate very well the environment of an amphiphilic polymer [3,104]. Naka and colleagues [104] have shown that micellelike aggregates of amphiphilic diblock copolymers can incorporate lipase P and enhance the hydrolysis rate of a hydrophobic substrate by a factor of as high as 4. This enhancement was attributed to the preferential partition of the substrate in the core of the polymer micelles, close to the bound lipase [104]. The enzyme activity of an integral membrane protein, the cytochrome b_6f, was found to be slightly decreased or possibly not affected upon association with both polyanionic [3 and unpublished results by Tribet and colleagues] or quasi-neutral polymers (unpublished). The stability of the proteins in complexes was comparable to that of surfactant/protein dispersions (Figure 26). Recent works by Champeil and colleagues [105]

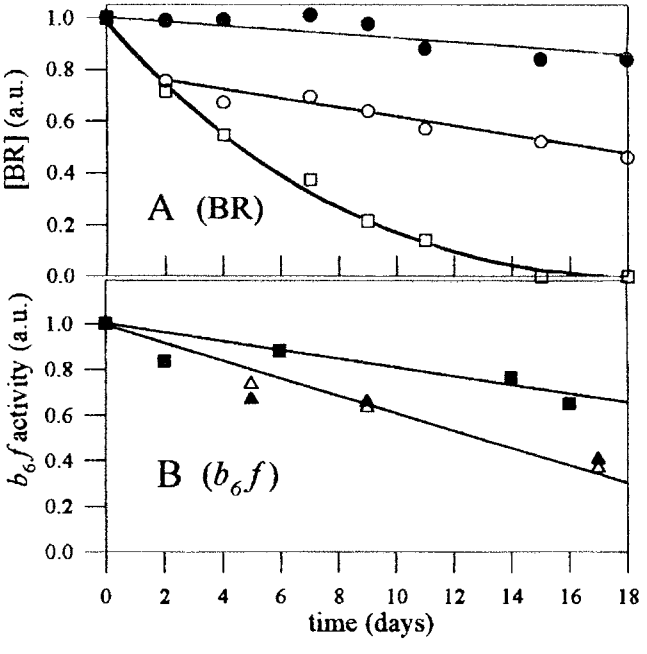

FIG. 26 Stability at pH 8 of bacteriorhodopsin (BR) and cytochrome b_6f complexed by short amphiphilic polymers (C8-modified polyacrylic acids). The proteins were kept in a neutral surfactant solution (■, □) as a standard, or in the absence of surfactant and complexed by a polymer of high charge density (○, △), or by a polymer of lower charge density (●, ▲). All the samples were stored at 4°C between measurements of the residual absorbance at 546 nm (BR) or enzyme activity (b_6f). (Reprinted from Ref. 3. Copyright © 1996 National Academy of Sciences, U.S.A.)

show, however, that highly sensitive enzymes such as Ca-ATPase may reveal subtle differences between the binding of an amphiphilic polymer, or a micelle, or a mixed micelle. It appeared that this enzyme can be reversibly inactivated by entrapment in an essentially pure polymer environment, although complete activity was recovered upon addition of submicellar concentrations of surfactant. Mixed surfactant/polymer/protein complexes may be better in terms of both activity and stability than both surfactant/protein and polymer/protein complexes. This point deserves further investigation on whether the self-association of the polymer forming hydrophobic clusters influences the protein stability and the freedom for structural reorganization.

V. CONCLUSION

This review has presented many illustrations of the key features of protein binding to hydrophilic or amphiphilic polyelectrolytes. In the last decades, recent progress in this field has both significantly increased the variety of systems studied and launched research on quantitative models for association isotherms and phase separation. The amphoteric and hydrophobic nature of both the protein and its synthetic partner play a major role in the formation of complexes. The effect of many parameters either external (pH, ionic strength, temperature, etc.) or structural (polymer or protein charge density, hydrophobicity) have been systematically investigated. As a consequence, it should be relatively easy to rationalize practical methods for handling and controlling the complexes involved in applications in biotechnology and pharmaceutical formulae.

Among the important results of these last years, the use of polymers of varying hydrophobicity has opened a new route toward the formation of complexes among partners of the like charge. The stabilization of membrane proteins in a dispersed state and the formation of reversible gels are two examples of new features that were attributed to the presence of nonspecific association among protein hydrophobic patches and the pendant hydrophobic side groups of the polyelectrolyte. Several novel applications should be devised on the basis of hydrophobic association including new selectivity in protein purification, modulation of the flow of biological fluids (using responsive gels), and stabilization of enzymes and membrane proteins for solution studies or in bioreactors.

Despite the difficulties of theoretical approaches of polyelectrolytes, and especially of amphiphilic polyelectrolytes, work on protein/polymer systems is now mature enough to offer interesting opportunities to compare experimental results and models of colloid/polyelectrolyte. Biophysical approaches can in principle lead to a structural description of these colloids at an unprecedented level of detail. As compared to micelles or latex, the major

advantages of proteins in the field of colloids are their monodispersity, their rich variety of surface structure, and the possibility of studying sets of close relatives that differ by a few atoms accurately located in the structure.

ACKNOWLEDGMENTS

Particular thanks are due to I. Iliopoulos for advice and discussion on gelation phenomena and phase separation. The author is grateful to J.-L. Popot for exciting discussions on the field of membrane proteins and biochemistry, to I. Porcar for strenuous debates on binding isotherms, to D. Pflieger and E. Lesage for their unpublished results on albumin/modified polyacrylic acid systems.

REFERENCES

1. Morawetz H., Hugues W. L. The interaction of proteins with synthetic polyelectrolytes. I. Complexing of bovine serum albumin. J. Phys. Chem 1951; 56:64–69.
2. Xia, J., Dubin P. L. Protein–polyelectrolyte complexes. In: Dubin P. L., Bock J., Davies R. M., Schulz D. N., Thies C., eds. Macromolecular Complexes in Chemistry and Biology. Springer-Verlag Berlin, 1994:247–271.
3. Tribet C., Audebert R., Popot J. L. Amphipols: polymers that keep membrane proteins soluble in aqueous solutions. Proc. Natl. Acad. Sci. USA 1996; 93: 15047–15050.
4. Ahmed L. S., Xia J., Dubin P. L. Stoichiometry and the mechanism of complex formation in protein–polyelectrolyte coacervation. J. M. S. Pure Appl. Chem. 1994; A31(1):17–29.
5. Sternberg M., Hershberger D. Separation of proteins with polyacrylic acids. Biochimica Biophysica Acta 1974; 342:195–206.
6. Petit F., Audebert R., Iliopoulos I. Interactions of hydrophobically modified poly(sodium acrylate) with globular proteins. Colloid Polym. Sci. 1995; 273: 777–781.
7. Parker D. E., Glatz C. E., Ford C. F., Gendel S. M., Suominen I., Rougvie M. A. Recovery of a charged-fusion protein from cell extracts by polyelectrolyte precipitation. Biotechnology Bioeng. 1990; 36:467–475.
8. Margolin A. L., Shertyuk S. F., Izumrudov V. A., Zezin A. B., Kabanov V. A., Belozersky A. N. Enzymes in polyelectrolyte complexes. Eur. J. Biopol. 1985; 146:625–632.
9. Kokufuta E., Takahashi K. Stoichiometric complexation of bovine trypsin with potassium poly(vinyl alcohol sulphate) and enzymatic activity of the complex. Polymer 1990; 31:1177–1182.
10. Izumi T., Hirata M., Takahashi K., Kokufuta E. Complexation of papain with strong polyanions and enzymatic activities of the resulting complexes. J. M. S. Pure Appl. Chem. 1994; A31(1):39–51.
11. Kudryashova E., Gladilin A. K., Vakurov A. V., Heitz F., Levashov A. V., Mozhaev V. V Enzyme–polyelectrolyte complexes in water–ethanol mixtures:

negatively charged groups artificially introduced into α-chymotrypsin provide additional activation and stabilization effects. Biotechnol. Bioeng. 1997; 55(2):267–276.
12. Dubin P. L., Gao J., Mattison K. Protein purification by selective phase separation with polyelectrolytes. Separation Purification Meth. 1994; 23(1):1–16.
13. Wang Y., Gao J., Dubin P. Protein separation via polyelectrolyte coacervation: selectivity and efficiency. Biotechnol. Prog. 1996; 12:356–362.
14. Eremenko A., Kurochkin I., Chernov S., Barmin A., Yaroslavov A., Moskvitina T. Monomolecular enzyme films stabilized by amphiphilic polyelectrolytes for biosensor devices. Thin Solid Films 1995; 260:212–216.
15. Xia J., Dubin P. L., Kim Y., Muhoberac B. B., Klimkowski V. J. Electrophoretic and quasi-elastic light scattering of soluble protein–polyelectrolyte complexes. J. Phys. Chem. 1993; 97:4528–4534.
16. Park J. M., Muhoberac B. B., Dubin, P. L., Xia J. Effects of protein charge heterogeneity in protein–polyelectrolyte complexation. Macromolecules 1992; 25:290–295.
17. Porcar I., Gareil P., Tribet C. Formation of complexes between protein particles and long amphiphilic polymers: binding isotherms versus size and surface of the particles. J. Phys. Chem. B 1998; 102:7906–7909.
18. Mizusaki M., Morishima Y., Dubin P. L. Interaction of pyrene-labeled hydrophobically modified polyelectrolytes with oppositely charged mixed micelles studied by fluorescence quenching. J. Phys. Chem. B 1998; 102:1908–1915.
19. Inoue T., Chen G., Nakamae K., Hoffman A. S. A hydrophobically modified bioadhesive polyelectrolyte hydrogel for drug delivery. J. Controlled Release 1997; 49:167–176.
20. Teramoto A., Watanabe M., Iizuka E., Abe K. Interaction of polyelectrolytes with albumin using fluorescence measurement. J. M. S. Pure Appl. Chem. 1994; A31(1):53–64.
21. Xia J., Dubin P. L., Morishima Y., Sato T., Muhoberac B. B. Quasielastic light scattering, electrophoresis, and fluorescence studies of lysozyme-poly(2-acrylamido-methylpropylsulfate) complexes. Biopolymers 1995; 35:411–418.
22. Mattison K. W., Dubin P. L., Brittain I. J. complex formation between bovine serum albumin and strong polyelectrolytes: effect of polymer charge density. J. Phys. Chem. B 1998; 102:3830–3836.
23. Sato T., Mattison K. W., Dubin P. L., Kamachi M., Morishima Y. Effect of protein aggregation on the binding of lysozyme to pyrene-labeled polyanions. Langmuir 1998; 14:5430–5437.
24. Dubin P. L., Murrell J. L. Size distribution of complexes formed between poly(dimethyldiallylammonium chloride) and bovine serum albumin. Macromolecules 1988; 21:2291–2293.
25. Wen Y.-P., Dubin P. L. Potentiometric studies of the interaction of bovine serum albumin and poly(dimethyldiallylammonium chloride). Macromolecules 1997; 30:7856–7861.
26. Tolstoguzov V. B. Functional properties of protein–polysaccharide mixtures. In: Mitchell J. R., Ledward D. A., eds. Functional Properties of Food Macromolecules. New York: Elsevier Applied Science, 1986:386–413.
27. Tsuboi A., Izumi T., Hirata M., Xia J., Dubin P. L., Kokufuta E. Complexation

of proteins with a strong polyanion in an aqueous salt-free system. Langmuir 1996; 12(26):6295–6303.
28. Kokufuta E., Shimizu H., Nakamura I. Stoichiometric complexation of human serum albumin with strongly acidic and basic polyelectrolytes. Macromolecules 1982; 15:1618–1621.
29. Patrickios C. S., Hertler W. R., Hatton T. A. Protein complexation with acrylic polyampholytes. Biotechnology Bioeng. 1994; 44:1031–1039.
30. Kokufuta E., Nishimura H. Complexation of pepsin poly(ethylene glycol). Polymer Bull. 1991; 26:277–282.
31. Kuramoto N., Sakamoto M., Komiyama J., Iijima T. Complex formation between bovine serum albumin and poly(acrylic acid) as studied by viscometry, circular dichroism, and fluorescence. Makromol. Chem. 1984; 185:1419–1427.
32. Nguyen T. Q. Interaction of human hemoglobin with high molecular weight dextran sulfate and dimethylaminoethyl dextran. Makromol Chem. 1986; 187: 2567–2578.
33. Tribet C., Porcar I., Bonnefont P. A., Audebert R. Association between hydrophobically modified polyanions and negatively charged bovine serum albumin. J. Phys. Chem. B 1998; 102:1327–1333.
34. Langendorff V., Cuvelier G., Launay B., Michon C., Parker A., De Kruif C. G. Casein micelle/iota carrageenan interaction in milk: influence of temperature. Food Hydrocolloids 1999; 13:211–218.
35. Borrega R., Tribet C., Audebert R. Reversible gelation in hydrophobic polyelectrolyte/protein mixtures: an example of cross-links between soft and hard colloids. Macromolecules 1999; 32(23):7798–7806.
36. Clark A. H., Ross-Murphy S. B. Structural and mechanical properties of biopolymer gels. Advances in Polym. Sci. 1987; 83:60–192.
37. Creighton T., Proteins: Structures and Molecular Properties, 2d ed. New York: W. H. Freeman, 1993.
38. Cha H. J., Izumi T., Kokufuta E., Franck C. W. Spectroscopic studies of papain complexation with potassium poly(vinyl alcohol sulphate) ACS Polym. Preprints 1992; 33:872–873.
39. Lawton J. B., Mekras C. I. Complexes of polyelectrolytes with the enzymes pepsin and α-chymotrypsin. Makromol. Chem. 1985; 186:2397–2405.
40. Fedotov A. N., Antonov Y. A., Isaeva E. S., Alekseeva M. A. Studies of the formation of water-soluble complexes of β-lactoglobulin with carboxymethylcellulose by measuring high frequency dielectric properties. Russian J. Phys. Chem. 1994; 68(1):125–129.
41. Azegami S., Tsuboi A., Izumi T., Hirata M., Dubin P. L., Wang B., Kokufuta E. Formation of an intrapolymer complex from human serum albumin and poly(ethylene glycol). Langmuir 1999; 15:940–947.
42. Akiyoshi K., Nishikawa T., Kobayashi S.-I., Sunamoto J. Self-assembled hydrogel nanoparticles: complexation and stabilization of soluble proteins. In: Yalpani M., ed. Biomedical Function and Biotechnology of Natural and Artificial Polymers. ATL Press 1996:115–125.
43. Nishikawa T., Akiyoshi K., Sunamoto J. Supramolecular assembly between nanoparticles of hydrophobized polysaccharide and soluble protein complex-

ation between the self-aggregate of cholesterol-bearing pullulan and α-chymotrypsin. Macromolecules 1994; 27:7654–7659.
44. Sunamoto J., Sato T., Tagushi T., Hamazaki H. Naturally occurring polysaccharide derivatives which behave as an artificial cell wall on an artificial cell liposome. Macromolecules 1992; 25:5665–5670.
45. Zhang H., Dubin P. L., Ray J., Manning G. S., Moorefield C. N., Newkome G. R. Interaction of a polycation with small oppositely charged dendrimers. J. Phys. Chem. B 1999; 103:2347–2354.
46. Frugier D., Audebert R. Interaction between oppositely charged low ionic density polyelectrolytes. In: Dubin P. L., Bock J., Davies R. M., Schulz D. N., Thies C., eds. Macromolecular Complexes in Chemistry and Biology. Berlin: Springer-Verlag, 1994:135–149.
47. Linse P., Piculell L., Hansson P., Models of polymer–surfactant complexation. In: Kwak J. C., ed. Polymer–Surfactant Systems. Surfactant Science Series 77. New York: Marcel Dekker, 1998:193–238.
48. Kuramoto N., Sakamoto M., Komiyama J., Iijama T. Estimation of interaction between polyanions and bovine serum albumin by means of affinity chromatography. J. Appl. Polym. Sci. 1985; 30:2847–2852.
49. Chatterji P. R., Kaur H. Interpenetrating hydrogel networks: 3. Properties of the gelatin-sodium carboxymethylcellulose system. Polymer 1992; 33:2388–2391.
50. Gao J., Dubin P. Binding of proteins to copolymers of varying hydrophobicity. Biopolymers 1999; 49:185–193.
51. Scopes R. K. Protein Purification: Principles and Practice. Cantor C. R., ed. New York: Springer Adv. Texts in Chem., 1989.
52. Wilce M. C., Aguilar M.-I., Hearn M. T. Physicochemical basis of amino acid hydrophobicity scales: evaluation of four new scales of amino acid hydrophobicity coefficients derived from RP-HPLC of peptides. Anal. Chem. 1995; 67(7):1210–1219.
53. Perkins T., Mak D., Root T., Lightfoot E. Protein retention in hydrophobic interaction chromatography: modeling variation with buffer ionic strength and column hydrophobicity. J. Chrom. 1997; 766(1–2):1–14.
54. Hachem F., Andrews B., Asenjo H. Hydrophobic partitioning of proteins in aqueous two-phase systems. Enzyme Microb. Technol. 1996; 19(7): 507–517.
55. Albertsson P. A. Partition of soluble compounds. In: Partition of Cell Particles and Macromolecules. 3d ed. New York: John Wiley, 1986:88–112.
56. Lachewsky A. Molecular concepts, self organization and properties of polysoaps. In: Advances in Polymer Science. Ringsdorf H., ed. 1994; 124:1-86.
57. Velichkova R. S., Christova D. C. Amphiphilic polymers: from macromonomers and telechelics. In: Progress in Polymer Science 1995; 20(5):819–887.
58. Morishima Y., Nomura S., Ikeda T., Seki, M., Kamachi M. Characterization of unimolecular micelles of random copolymers of sodium 2-(acrylamido)-2-methylpropanesulfonate and methacrylamides bearing bulky hydrophobic substituents. Macromolecules 1995; 28:2874–2881.
59. Yusa S.-I., Kamachi M., Morishima Y. Hydrophobic self-association of cholesterol moieties covalently linked to polyelectrolytes: effect of spacer bond. Langmuir 1998; 14:6059–6067.

60. Hallberg R. K., Dubin P. L. Effect of pH on the binding of β-lactoglobulin to sodium polystyrenesulfonate. J. Phys. Chem B 1998; 102(43):8629–8633.
61. Iliopoulos I. Association between hydrophobic polyelectrolytes and surfactants. Current Opinion in Colloid and Interface Science 1998; 3:493–498.
62. Piculell L., Lindman B., Karlström G. Phase behavior of polymer–surfactant systems. In: Kwak J. C., ed. Polymer-Surfactant Systems. Surfactant Science Series 77. New York: Marcel Dekker, 1998:66–141.
63. Porcar I., Cottet H., Gareil P., Tribet C. Association between protein particles and long amphiphilic polymers: effect of the polymer hydrophobicity on binding isotherms. Macromolecules 1999; 32(11):3922–3929.
64. Tribet C., Audebert R., Popot J. L. Stabilization of hydrophobic colloidal dispersions in water with amphiphilic polymers: application to integral membrane protein. Langmuir 1997; 13:5570–5576.
65. Petka W. A., Harden J. L., McGrath K. P., Wirtz D., Tirrell D. A. Reversible hydrogels from self-assembling artificial proteins. Science 1998; 281:389–391.
66. Lee S. J., Park K. Synthesis and characterization of sol–gel phase-reversible hydrogels sensitive to glucose. Polym. Preprints 1994; 35(2):391–392.
67. Kokufuta E., Zhang Y., Tanaka T. Saccharide-sensitive phase transition of a lectin-loaded gel. Nature 1991; 351:302–304.
68. Hubert P., Dellacherie E. Water soluble biospecific polymers for affinity purification techniques. In: Dubin P. L., Bock J., Davies R. M., Schulz D. N., Thies C., eds. Macromolecular Complexes in Chemistry and Biology. Berlin: Springer-Verlag, 1994:229–246.
69. Engel A., Colliex C. Application of scanning transmission electron microscopy to the study of biological structure. Curr. Opinion Biotech. 1993; 4:403–411.
70. Freeman R., Leonard K. Comparative mass measurement of biological macromolecules by scanning transmission electron microscopy. J. Microscopy 1981; 122:275–286.
71. Tribet C., Mills D., Haider M., Popot J.-L. Scanning transmission electron microscopy study of the molecular mass of amphipol/cytochrome b_6f complexes. Biochimie 1998; 80:475–482.
72. Yamaguchi K., Hachiya K., Moriyama Y., Takeda K. Electrophoretic light scattering study of sodium dextran sulfate–lysozyme complex. J. Coll. Interf. Sci. 1996; 179:249–254.
73. Currie E., Van der Gucht J., Borisov O., Cohen Stuart M. Stuffed brushes: theory and experiment. Pure Appl. Chem. 1999; 71(7):1227–1241.
74. Currie E., Van der Gucht J., Borisov O., Cohen Stuart M. End-grafted polymers with surfactants: a theoretical model. Langmuir 1998; 14:5740–5750.
75. Galazka V. B., Smith D., Ledward D. A., Dickinson E. Complexes of bovine serum albumin with sulphated polysaccharides: effect of pH, ionic strength and high pressure treatment. Food Chemistry 1999; 63:303–310.
76. Xia J., Dubin P. L. Chromatographic evaluation of the binding of lysozyme to poly(dimethyldiallylammonium chloride). J. Chrom A 1994; 667:311–315.
77. Gao J. Y., Dubin P. L., Muhoberac B. B. Measurement of the binding of proteins to polyelectrolytes by frontal analysis continuous capillary electrophoresis. Anal. Chem. 1997; 69:2945–2951.

78. Gao J. Y., Dubin P. L., Muhoberac B. B. Capillary electrophoresis and dynamic light scattering studies of structure and binding characteristics of proteins–polyelectrolyte complexes. J. Phys. Chem. B 1998; 102:5529–5535.
79. Ananthapadmanabhan K. P. Protein–surfactant interaction. In: Goddard E. D., Anathapadmanabhan K. P., eds. Interaction of Surfactants with Polymers and Proteins. Boca Raton, FL: CRC Press, 1993:318–366.
80. Wolff N., Delepierre M. Conformation of the C-terminal secretion signal of the serratia marcescens haem acquisition protein (HasA) in amphipols solutions, a new class of surfactant. J. Chim. Phys. 1997; 95(2):437–442.
81. Schafmeister C. E., Miercke L. J. W., Stroud R. M. Structure at 2.5A of a designed peptide that maintains solubility of membrane proteins. Science 1993; 262:734–738.
82. Wei J. Fasman G. D. A poly(ethyleneglycol) water-soluble conjugate of porin: refolding to the native state. Biochemistry 1995; 34:6408–6415.
83. Clark A. H., Ross-Murphy S. B. Structural and mechanical properties of biopolymer gels. In: Advances in Polym. Sci. 83. Berlin Heidelberg: Springer Verlag, 1987:60–192.
84. Michon C., Cuvelier G., Launay B. Concentration dependence of the critical viscoelastic properties of the gelatin at the gel point. Rheologica Acta 1993, 32:94–103.
85. Ross-Murphy S. B. Structure and rheology of gelatin gels. Imaging Sci. J. 1997, 45:205–209.
86. Le Bon C., Nicolai T., Durand D. Kinetics of aggregation and gelation of globular proteins after heat-induced denaturation. Macromolecules 1999; 32: 6120–6127.
87. Lefebvre J., Renard D., Sanchez-Gimeno A. C. Structure and rheology of heat-set gels of globular proteins. I. Bovine serum albumin in isoelectric conditions. Rheol. Acta 1998; 37:345–357.
88. Tobitani A., Ross-Murphy S. B. Heat-induced gelation of globular proteins. 1. Model for the effect of time and temperature on the gelation time of BSA gels. 2. Effect of environmental factors on single-component and mixed-protein gels. Macromolecules 1997; 30:4845–4862.
89. Kokufuta E. Functional immobilized biocatalysts. Prog. Polym. Sci. 1992; 17: 647–697.
90. Castelain C., Lefebvre J., Doublier J. L. Rheological behaviour of BSA-cellulose derivative mixtures in neutral aqueous medium. Food Hydrocolloids 1986; 1(2):141–151.
91. Borrega R., Tribet C., Audebert R. Gelation and demixing in associating polyelectrolyte/protein mixtures. Proceedings of the Yamada Conferences, 2d Polyelectrolytes Conferences, Noda I., Kokufuta E., ed., Inuyama Japan, 1999: 311–314.
92. Mours M., Winter H. H. Relaxation patterns of nearly critical gels. Macromolecules 1996; 29:7221–7229.
93. Tanaka F., Edwards S. Viscoelastic properties of physically cross-linked networks. Transient network theory. Macromolecules 1992; 25:1516–1523.
94. Pezron E., Ricard A., Leibler L. Rheology of galactomannan-borax gels. J. Polym. Sci.: Part B 1990; 28:2445–2461.

95. Porcar I., Cesar B., Tribet C. Photoresponsive thickening of aqueous solutions. ACS Polym. Preprints 1999; 40(2):826–827.
96. Guillemet F., Piculell L. Interactions in aqueous mixtures of hydrophobically modified polyelectrolyte and oppositely charged surfactant. Mixed micelle formation and associative phase separation. J. Phys. Chem. 1995; 99:9201–9209.
97. Fisher R. R., Glatz C. E. Polyelectrolyte precipitation of proteins: I. The effects of reactor conditions. Biotechnol. Bioeng. 1988; 32:777–785.
98. Trinh C. K., Schnabel W. Ionic strength dependence of the stability of polyelectrolyte complexes. Angewandte Makromol. Chem. 1993; 212:167–179.
99. Clark K. M., Glatz C. E. Polymer dosage considerations in polyelectrolyte precipitation of protein. Biotechnol. Progress 1987; 3(4):241–247.
100. Xia J., Dubin P., Kokufuta E., Havel H., Muhoberac B. Light scattering, CD, and ligand binding studies of ferrihemoglobin-polyelectrolyte complexes. Biopolymers 1999; 50:153–161.
101. Akiyoshi K., Sasaki Y., Sunamoto J. Molecular chaperone-like activity of hydrogel nanoparticles of hydrophobized pullulan: thermal stabilization with refolding of carbonic anhydrase B. Bioconjugates Chem. 1999; 10(3):321–324.
102. Willner I., Rubin S., Zor T. Photoregulation of α-chymotrypsin by its immobilization in a photochromic azobenzene. J. Am. Chem. Soc. 1991; 113: 4013–4014.
103. Amiconi G., Zolla L., Vecchini P., Brunori M., Antonini E. The effect of macromolecular polyanions on the functional properties of human hemoglobin. Eur. J. Biochem. 1977; 76:339–343.
104. Naka K., Nakamura T., Okhi A., Maeda S. Aggregates of amphiphilic block copolymers derived from poly((*N*-acylimido)ethylene) and their complexes with lipase in water. Polymer J. 1995; 27(11):1071–1078.
105. Champeil P., Menguy T., Tribet C., Pojot J. L., le Maine M. Interaction of amphipols with sarcoplasmic reticulum Ca^{2+}-ATPase. J. Biol. Chem. 2000; 275:18623–18637.

This Page Intentionally Left Blank

20

Polyelectrolyte Complex Formation in Highly Aggregating Systems: Methodical Aspects and General Tendencies

HERBERT DAUTZENBERG Max Planck Institute of Colloids and Interfaces, Golm, Germany

I. INTRODUCTION

Because they are both polymers and electrolytes, polyelectrolytes represent a special class of materials with interesting properties and high practical relevance. One of their particular features is the ability to form interpolymer complexes between oppositely charged species, polyanions and polycations, driven by the attractive Coloumb interaction. This phenomenon has been well known for a long time from the mutual precipitation of proteins [1,2]. The first systematic studies with synthetic polyelectrolytes were carried out by Michaels and Miekka [3], dealing especially with the stoichiometry of the polyelectrolyte complexes (PEC). Michaels realized already the practical relevance of the principle of PEC formation for the production of membranes with special separation properties. At present, PECs are used for such large-scale industrial applications as flocculants, coatings, and binders and for special purposes in biotechnology and medicine. Promising fields under the latter aspect are the PEC-microencapsulation of drugs, enzymes, cells, microorganisms up to subjects such as Langerhans islets [4–7], polyelectrolyte multilayers as biosensors [8,9], immobilization of proteins by complex formation [10–13], and polycation complexes with polynucleotides or oligonucleotides as vectors in gene therapy [14–17].

Beside the developments in practical applications, much work has been done in fundamental research on PECs, starting with comprehensive studies on water-soluble PECs by the groups of Kabanov [18,19] and Tsuchida [20–22]. This chapter will be principally limited to investigations on polyelec-

trolyte complexes in solutions. In contrast to the soluble PECs it will be mainly focused on highly aggregating complexes between synthetic polyanions and polycations, but taking also into consideration complexes between polyelectrolyte chains and proteins as well as polyelectrolyte chains and charged micelles. After a brief introduction to the general background of PEC formation, some remarks will be made about soluble complexes. The main topic is centered on the stoichiometry, structure, and stability of highly aggregated complexes, stressing methodical aspects but also trying to give an overview of how various parameters affect the structure and behavior of such PECs.

II. GENERAL BACKGROUND OF PEC FORMATION

The mixing of solutions of polyanions and polycations leads to spontaneous aggregation under release of the counterions (Figure 1). Complex formation can take place between polyacids and polybases and also between their neutralized metal and halogenide salts, respectively. For the free polyelectrolytes, the low molecular counterions are more or less localized near the macroions, in the case of high charge densities particularly because of the counterion condensation effect. The driving force of complex formation is mainly the gain in entropy due to the liberation of the low molecular counterions. However, other interactions such as hydrogen bonding or hydrophobic ones may play an additional role.

The reaction of polyelectrolyte complex formation can be described by the equation

$$(>-A^-c^+)_n + (>-C^+a^-)_m \Leftrightarrow (>-A^-C^+)_x + (>-A^-c^+)_{n-x} + (>-C^+a^-)_{m-x} + xa^- + xc^+$$

where A^- and C^+ are the charged groups of the polyelectrolytes, a^- and c^+

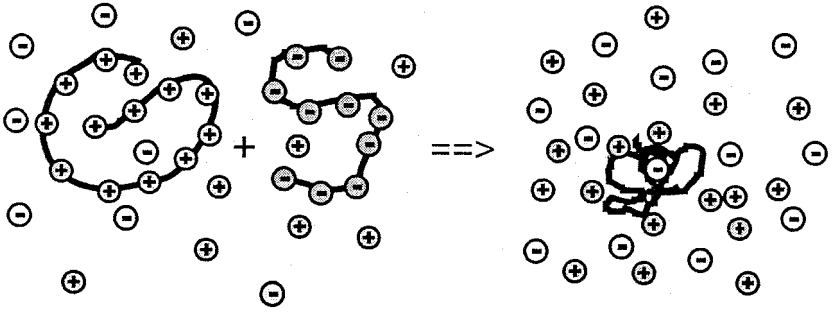

FIG. 1 Scheme of polyelectrolyte complex formation.

the counterions, n and m the numbers of the anionic and cationic groups in solution, n/m or $m/n = X$ − molar mixing ratio, $\theta = x/n$, $n < m$ or $\theta = x/m$, $m < n$, and θ the degree of conversion.

The degree of conversion describes whether the ionic sites of the component in deficiency are completely bound by the oppositely charged polyelectrolyte or low molecular counterions remain partly in the complex. Another characteristic quantity of a PEC is its end point stoichiometry, i.e., the molar ratio $f_E = [A^-]_E/[C^+]_E$ at the end of the complex formation reaction. However, this ratio may be different at other mixing ratios X, so that we have to introduce the stoichiometric factor $f(X) = [A^-]_X/[C^+]_X$ to describe the overall composition of the PEC structures at any mixing ratio.

The PEC formation leads to quite different structures, depending on the characteristics of the component used and the external conditions of the reaction. As borderline cases for the resulting structures of polyelectrolyte complexes, two models (Figure 2) are discussed in the literature [23]:

The ladderlike structure, where complex formation takes place on a molecular level via conformational adaptation

The scrambled egg model, where a high number of chains are incorporated into a particle

Beside the determination of the stoichiometric quantities θ, f_E, and $f(X)$, the detailed characterization of the PEC structures is the main objective in understanding the effects of various parameters on the course of complex formation and the resulting properties of the PECs.

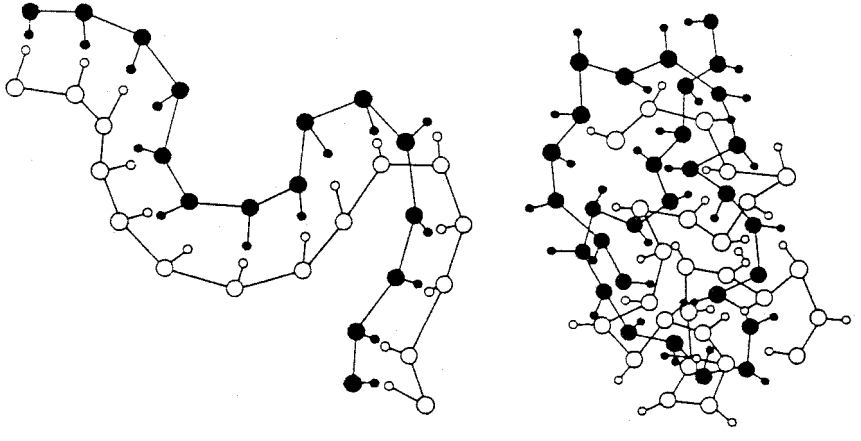

FIG. 2 Structure models: ladder and scrambled egg structure. (From Ref. 23.)

III. WATER-SOLUBLE PECs

PEC formation between polyions with weak ionic groups and significantly different molecular weights in nonstoichiometric systems results in soluble complexes, which are structured according to the ladder model, consisting of hydrophilic single-stranded and hydrophobic double-stranded segments [10]. If the long host molecules are in about threefold excess, the noncomplexed segments keep the PECs in the solute state. Stop flow measurements [24] showed that PEC formation takes place in less than 5 μs, nearly corresponding to the diffusion collision of the polyion coils. In salt-free solutions, frozen structures in a nonequilibrium state are formed. The presence of small amounts of salt enables rearrangement and exchange processes yielding PECs in thermodynamic equilibrium. These PECs consist of one long host polyelectrolyte and the bound short counterpart chains (intramolecular complexes), where the latter are uniformly distributed on all host molecules.

Further addition of salt (a scheme of the occurring effects is given in Figure 3) leads at first to a shrinking of the PECs due to the shielding of their charges by the electrolyte. When a critical salt concentration is exceeded, a disproportionation of the short guest chains occurs, leading to completely complexed precipitating species and pure host polyelectrolyte chains in solution [18,25,26]. At still higher salt concentrations, the precipitate dissolves again, and both components exist as free polyelectrolyte chains in solution.

In case the host chain is a weak polyacid or weak polybase, similar effects can be induced by changes of the pH value, suppressing the ionization of the single stranded blocks. For example, a PEC between Na-poly(meth-

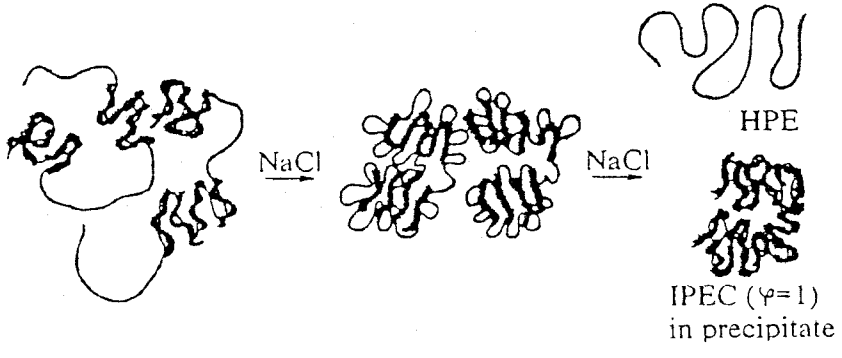

FIG. 3 Changes of the structure of soluble PECs induced by subsequent addition of salt. (From Ref. 10.)

acrylate)(NaPMA) as host component and quaternized poly(vinylpyridine) (Q-P4VP) as guest chains precipitates at pH < 6 [10].

Under appropriate conditions, the PECs possess a high stability. Nevertheless, they are able to take part in polyion exchange and substitution reactions. Addition of the same kind of host polyelectrolyte to a prepared PEC leads to a redistribution of the guest chains. The kinetics of this reaction was studied in detail in [27] between a complex of NaPMA/Q-P4VP and a fluorescence labeled (pyrenyl tagged) Na-PMA. The quenching of fluorescence light by the complex formation with Q-P4VP allows a quantitative determination of the exchange rate. The results show the exchange rate not to depend on the chain length of the host polyelectrolyte but to depend strongly on the length of the guest chains.

From the thermodynamic point of view, polyelectrolytes with stronger ionic groups and/or higher molecular masses are favored in complex formation [28], so that substitution reactions are to be expected. Such reactions are described in detail in [10]. Sulfonate and sulfate containing polyanions usually replace carboxylic groups containing ones in the PECs with various polycations. The effect of both the nature of the ionic group and the chain length on the substitution reaction was investigated in [29] with the combination Q-P4VP as short chain polycation and NaPMA and poly(phosphates) (PP) of different chain length as polyanions. In the presence of 0.3 M NaCl the equilibrium is completely shifted to the binding of PP for the longest chains, but to the binding of NaPMA for the shortest PP chains. Also the kind of salt (NaCl, LiCl, KCl) has an important influence on the equilibrium position. Therefore it should be kept in mind that the PECs are ''living'' systems, which may undergo various changes dependent on the surroundings.

IV. HIGHLY AGGREGATING SYSTEMS

A. General Remarks

In many applications of high practical relevance, PEC formation is carried out under conditions that produce highly aggregated systems also at nonstoichiometric mixing ratios. The reaction between polyelectrolytes with strong ionic sites, e.g., polyanions with sulfonate groups and polycations with quaternary ammonium groups, takes place according to the scrambled egg model under incorporation of a great number of polyelectrolyte chains. In higher concentrated solutions (>0.01 g/mL), macroscopic flocculation occurs, impeding the characterization of the generated structures and the study of the effects of various parameters of influence on the course of complex formation. In highly diluted solutions ($<10^{-4}$ g/mL) PEC formation leads to

particles on a colloidal level in nonstoichiometric systems, while approaching the 1:1 mixing ratio macroscopic flocculation occurs even at very low concentrations. The colloidal systems can be studied by all methods normally used in polymer characterization as well as in the investigations of soluble complexes. However, some methodical adaptations are necessary in order to obtain detailed information on the PEC structures.

Another problem is caused by the huge variety of parameters that affect the complex structures. Beside the external mixing conditions (polymer concentration, rate of mixing and stirring, order of mixing, mixing ratio), the medium parameters (pH value, ionic strength, kind of salt, polarity of solvent) and particularly the characteristics of the polyelectrolytes (molecular weights, polydispersity, branching, nature of the ionic groups, charge density) may play an important role. From this a high individuality of the PECs results. Therefore the main topic of our work has been the investigation of the general tendencies of different effects on the course of complex formation, restricting the studies on synthetic polyelectrolytes. In these studies we used mainly a combination of methods, which are given together with the employed instruments and the obtainable information in Table 1. This paper will review our essential findings, but the results of other groups, especially on complexes between synthetic polyelectrolytes and proteins or micelles of charged surfactants, will be considered.

Results reported from our studies were mainly obtained using the following components. Polyanions: commercial standards (Polymer Standard Service, Mainz, Germany) of sodium poly(styrene sulfonate) (NaPSS-*x*t, where *x* denotes the molecular weight in kDalton)) and poly(methacrylate)

TABLE 1 Methods Used in PEC Characterization

Method	Instrument	Information
UV/VIS spectroscopy	Lambda 2, Perkin Elmer	Stoichiometry of ionic binding
Potentiometry	Ionmeter, Metrom	Release of counterions
Ultracentrifugation	AUC, Beckman, Palo Alto	Overall composition
Viscometry	Viscoboy, Lauda, Ubbelohde, Schott	Overall composition, degree of swelling
Static light scattering	Sofica 42000, Wippler/ Scheibling	Particle mass, size and structural density
Dynamic light scattering	Simultan, ALV Langen	Hydrodynamic radius
Electron microscopy	EM 102, Siemens	Structure type, size
X-ray microscopy	Microscope: Univ. Göttingen; x-ray source: Bessy, Berlin	Structure type, size, density profile

(NaPMA, M_w = 114,000 g/mol). Polycations: poly(diallyldimethylammonium chloride) (PDADMAC, M_w = 250,000 g/mol) and its copolymers (DADMAC-AA-*xx*, where *xx* corresponds to the mol% of DADMAC) with acrylamide of various compositions. Additionally, some findings will be given about PECs between ionically modified poly(*N*-isopropylacrylamide) (PNIPAM).

B. Stoichiometry of the PECs

As already mentioned, with regard to the stoichiometry three things have to be determined: the end point stoichiometry of the PECs, the degree of conversion (degree of release of counterions), and the overall composition $f(X)$ of the complexes at nonstoichiometric mixing ratios. The methods used for the investigation of the PEC stoichiometry are not very sensitive to the level of aggregation; i.e., they are practically the same for soluble PECs and colloidal PEC structures.

1. End Point Stoichiometry and Degree of Conversion

The change of different quantities of the PEC solutions caused by the complex formation may be exploited to determine the end point stoichiometry and the degree of conversion. Now the principal effects and some representative results of the following techniques will be presented: conductometry, potentiometry, turbidimetry, viscosimetry, UV spectroscopy, and colloid titration.

(*a*) *Conductometry.* This method has been used since the early beginning of studies on PECs [3,20,22,30]. The change in conductivity during complex formation is quite different for a polybase/polyacid and a polysalt/polysalt reaction. In the latter case, complex formation leads to at least a partial release of the low molecular counterions and to a corresponding increase of the conductivity. The end of the reaction is marked by a maximum of the conductivity, because the counterions of a free polyelectrolyte have a reduced one, due to the counterion condensation according to Manning's theory [31]. The findings of Michaels et al. [3b] about the PEC formation between sodium poly(styrene sulfonate) and poly(4-vinylbenzyl-trimethylammonium chloride) (PVBTACl) demonstrate this behavior (Figure 4). The sharply pronounced maximums indicate a 1:1 end point stoichiometry in pure water, but also at low content of NaCl. A comparison of the conductivity with that of control solutions, containing the same amount of low molecular counterions according to a 1:1 reaction and the remaining excess polyelectrolyte, proved that the component in deficiency reacted completely under full release of the low molecular counterions.

The polybase/polyacid reaction causes a decrease of the conductivity by the neutralization of the H^+ and OH^- ions, respectively, as is illustrated in

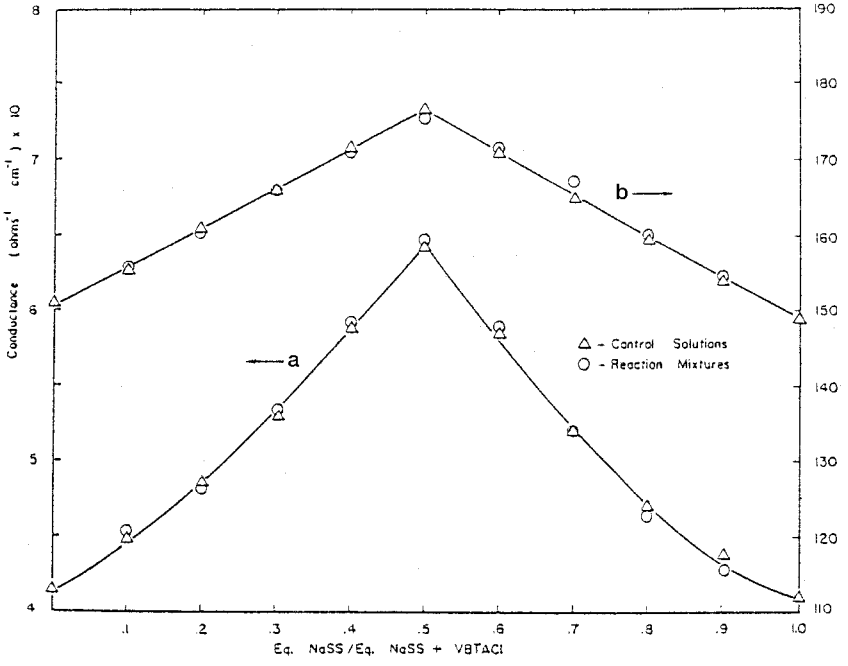

FIG. 4 Conductance in reaction mixtures and control solutions during complex formation between the polysalts NaPSS and PVBTACl. (a) [NaSS] = [VBTACl] = 10^{-3} N in salt-free solution. (b) [NaSS] = [VBTACl] = 10^{-2} N in 10^{-2} N NaCl. (From Ref. 3b.)

Figure 5 (taken from [32]) for a PEC between H^+-cellulose sulfate and branched OH^- poly(ethyleneimine). The breakpoint in the conductivity curve marks the end point of PEC formation, which corresponded to $f_E = [A^+]/[C^-] = 0.77$. Such a deviation from the 1:1 stoichiometry is typical for branched polyelectrolytes.

(*b*) *Potentiometry.* While the PEC formation between fully dissociated polysalts does not change the pH value, the reaction between polyacids and polybases leads to neutralization at the 1:1 stoichiometry. In Figure 5 the complex formation was also studied by potentiometry. The inflexion point corresponds to the end point of the reaction and agrees quite well with the result of the conductivity measurement. Potentiometry may also be used to derive thermodynamic parameters of the reaction of the PEC formation (reviewed in [33]). Webster and Huglin [34,35] employed a combination of conductometry and potentiometry to investigate the PEC formation between the salt of a strong polyanion (sodium poly(2-acrylamido-2-methyl propane

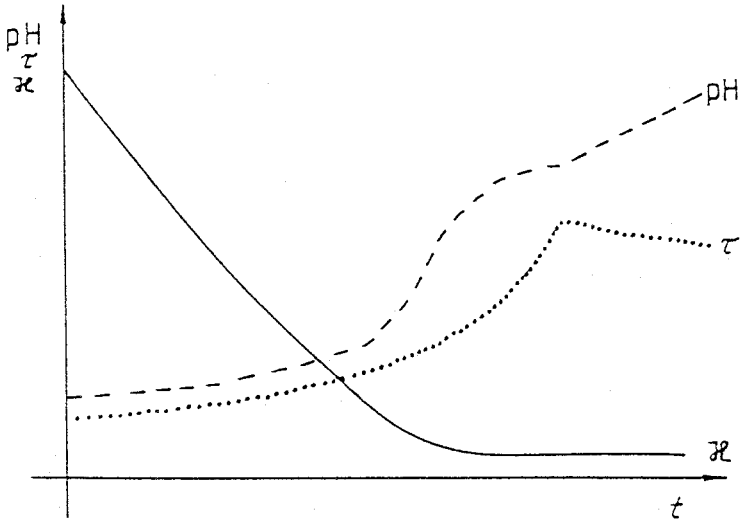

FIG. 5 Simultaneous titration of H^+ cellulose sulfate with a branched poly (ethyleneimine) by conductometry, potentiometry, and turbidimetry. (From Ref. 32.)

sulfonate) and the salt of weak polycations (poly(4-vinylpyridinium chloride) and poly(2-vinylpyridinium chloride)). They found clearly pronounced steeper changes in both conductivity and pH value near the 1 : 1 mixing ratio and explained the effects by an incomplete ionization of the charged groups of the polycations and an additional dissociation caused by complex formation. In [36] the same combination of methods was used to investigate the course of PEC formation between chitosan and chondroitin or hyaluronic acid. Dubin et al. studied the complex formation between charged dendrimers [37] as well as proteins [38,39] and linear polyelectrolytes by the pH titration technique in the presence and absence of the latter ones, obtaining information about the changes of the pK_a of the dendrimers and the proteins.

We carried out potentiometric investigations with a Cl^- sensitive electrode [40] to determine the degree of conversion, i.e., the release of the low molecular counterions in the reactions between sodium poly(styrene sulfonate) (NaPSS) and poly(diallyldimethylammonium chloride) (PDADMAC) and its copolymers with acrylamide of various compositions (for synthesis and characterization of the samples see [41]). The basic idea of these studies on PEC formation is the change of the Cl^- ion activity coefficient due to the release of the counterions. According to Manning's theory [31], the activity coefficient of the counterions of a polyelectrolyte is given by

$$f = \exp[-0.5\xi] \quad \text{if} \quad \xi < 1$$
$$f = \xi^{-1} \exp[-0.5] \quad \text{if} \quad \xi > 1 \tag{1}$$

where $\xi = \lambda_B/b$, b is the charge distance along the polyelectrolyte chain, and λ_B is the Bjerrum length (0.7 nm in water at 20°C). The release of the counterions should lead to an activity coefficient $f = 1$ for the cationic groups bound by sulfonate groups. Figure 6 shows the Cl^- ion activity after stepwise addition of polycationic solutions (PDADMAC and DADMAC-AA-47) to pure water and a solution of NaPSS. As reference the activity of sodium chloride in water was measured. Whereas in pure water reduced Cl^- ion activities of the polycations according to Eq. 1 were found (see Table 2), f is equal 1 in the PEC solutions up to a molar mixing ratio 1:1. This indicates the full release of the low molecular counterions due to the PEC formation. At the 1:1 mixing ratio a break point occurs, i.e., complex formation is finished. However, the slopes of the activity curves on the side of an excess of polycations are smaller than in pure water. This can be explained by an interaction of the polycations with the PEC flocs. The full release of the low

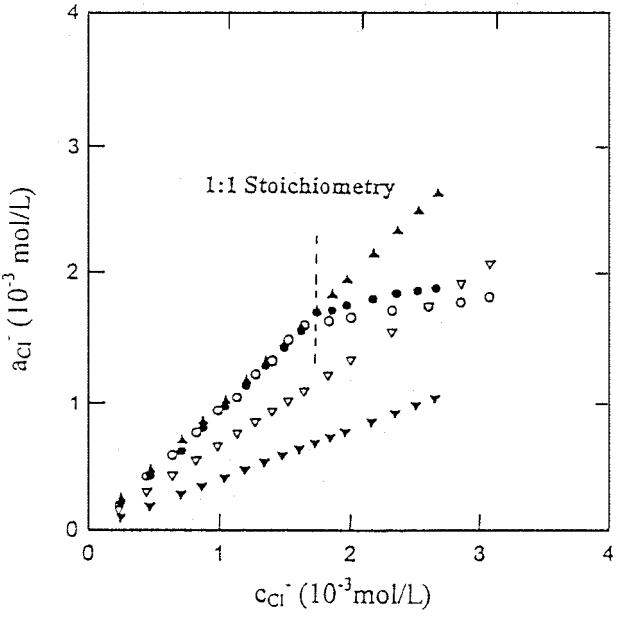

FIG. 6 Cl^- ion activity during PEC formation (addition of the cationic solutions) in comparison to NaCl and the pure polycation solutions. ▲, NaCl (f = 1); ●, PDADMAC/NaPSS; ▼, PDADMAC/water; ○, DADMAC-AA-47/NaPSS; ▽, DADMAC-AA-47/water. (From Ref. 40.)

molecular counterions up to the 1:1 molar mixing ratio was found for all polycations in Table 2. This result is somewhat unexpected, because the polymer chains must be arranged so that charge compensation takes place only by the polyions, even in cases of quite different charge distances of both components. The findings may suggest that charge compensation is not strongly localized but more smoothed. From the full release of the counterions one can conclude that the PECs have a more or less compact structure, because the fully charge compensated chains must be hydrophobic.

(*c*) *Turbidimetry.* The formation of supermolecular structures leads to a corresponding increase of the particle mass, which can be sensitively monitored via light scattering. In turbidimetric studies the transmission of a light beam passing through a cuvette with a solution or dispersion is given by

$$T = \frac{I}{I_0} = \exp(-\tau l) \tag{2}$$

where I_0 is the intensity of the incident beam, I is the intensity after the cuvette of the length l, and τ is the turbidity. In nonabsorbing systems the transmittance is determined by the scattering of light. According to the Rayleigh theory [42], the scattered intensity is proportional to the square of the mass of the particles, i.e., at constant mass concentration c it increases proportional to M. For the turbidity of a highly diluted system of small particles one obtains the simple expression

$$\tau = HMc \tag{3}$$

where $H = 32\ \pi^3 n_0^2 (dn/dc)^2 / 3N_A\lambda^4$, n_0 is the refractive index of the medium,

TABLE 2 Composition, Charge Distances b, and Activity Coefficients f of the DADMAC-AA Copolymers as Well as Structure Density of the PECs with PSS-356t at the 1:1 Molar Mixing Ratio

DADMAC-AA-xx copolymers				PECs with PSS-356t
xx = mol% DADMAC	b	f Manning	f exp.	$\rho \cdot 10^2$ g cm^{-3}
21	1.5	0.79	0.79	—
35	1.0	0.69	0.70	0.79
47	0.83	0.66	0.67	2.66
58	0.73	0.62	0.62	4.86
73	0.64	0.55	0.55	1.21
100	0.55	0.48	0.42	6.25

dn/*dc* the refractive index increment of the particles, N_A Avogadro's number, and λ the wavelength in the medium.

Approaching the 1:1 mixing ratio, PEC formation causes macroscopic flocculation and a steep increase in turbidity due to a strong destabilization of the PEC particles at complete charge compensation, even in the case of soluble PECs. This increase indicates the end point of the PEC formation, as is shown in Figure 5, where conductometric, potentiometric, and turbidimetric measurements were carried out simultaneously. As one can see, the end points obtained by different methods need not be identical. Turbidimetry monitors the structural changes caused by charge neutralization, especially the onset of aggregation. This onset may be delayed or too early, depending on the system under study and the mixing regime. Generally, one can state that turbidity measurements were carried out in many studies, obviously because of the simplicity of the method. In [22], turbidimetry was used to investigate the dissolution of PECs between poly(methacrylic acid) and an integral type polycation in relation to the ionic strength. Buchhammer and Lunkwitz [43] employed this method in combination with other techniques to judge the stabilizing effect of polyelectrolytes and complexes adsorbed on the surface of silica particles with regard to salt-induced coagulation. Deng and Li [44] studied by turbidimetry and conductometry the PEC formation between poly(sodium acrylate) and imidazolinium organosilicon polymers in relation to the polycation structure, polymer concentration, ionic strength, and pH value.

Although turbidimetry is an integral technique, providing only one parameter, it can be very useful in studying details of PEC formation. For example, in [45] the complex formation between various proteins and polyanions as well as polycations as functions of the pH value was investigated by turbidimetry, dynamic light scattering, and pH titration. The findings show that at the critical pH value for complex formation the sign of net charge of the protein is frequently equal to the sign of the polyelectrolyte. Therefore the authors concluded that ''charge patches'' of the proteins must play an important role in the formation of the complexes. Also the different regions of single chain polyelectrolyte/protein complex formation and intercomplex aggregation can be recognized, as demonstrated in [46] for the complexes between bovine serum albumin and various polyelectrolytes.

(*d*) *UV Spectroscopy.* For a UV-active polymer like Na-poly(styrenesulfonate), UV spectroscopy offers the possibility of determining quantitatively the amount of bound sulfonate groups from the shift in the spectrum, caused by PEC formation. Because these shifts were too small to assess the degree of binding directly [40], we calculated the difference between the PEC and NaPSS spectra of the same polyanion concentration to obtain this information. These spectra show clearly pronounced peaks, whose heights

are strongly correlated to the added amount of solution of the oppositely charged polyelectrolyte. PEC formation was studied for the PECs between a standard of NaPSS with a molecular mass of 356 kDa and the polycations given in Table 2, working with the polyanion as starting solutions and inversely. Figure 7 shows the difference spectra for the PEC solutions, obtained after stepwise addition of PDADMAC. Both peaks in the spectra can be used to determine quantitatively the amount of bound sulfonate groups. Figure 8 demonstrates the linear correlation between the height of the peak at 203 nm and the molar mixing ratio of the ionic groups up to about $X = 0.9$, where flocculation begins. The results confirm the findings of the potentiometric studies with the Cl^- sensitive electrode.

UV/VIS spectroscopy has also been proved to be a helpful tool in studying preferential binding in a mixture of an optically active and an inactive component, e.g., NaPSS and sodium poly(methacrylate) (NaPMA). This phenomenon was studied in [47], comparing the spectra of complexes NaPSS/PDADMAC and (NaPSS + NaPMA)/PDADMAC, where a 1:1 molar mixing ratio of the polyanions with the same NaPSS concentration as in the first system was used. The ratio of the peak heights

$$\gamma = \frac{A_{203}((\text{NaPSS} + \text{NaPMA})/\text{PDADMAC})}{A_{203}(\text{NaPSS/PDADMAC})}$$

reflects the degree of preferential binding. The quantitative analysis of the spectroscopic data at different contents of NaCl showed that in pure water both polyanions are incorporated in the complexes nearly to the same extent, whereas at an ionic strength of $I = 5 \cdot 10^{-2}$ M NaPSS is strongly favored. The even binding is unexpected from the point of view of the nature of the anionic groups. Obviously, PEC formation in pure water is more governed by the kinetics of the process, leading to frozen structures far from thermodynamic equilibrium. With increasing ionic strength and the corresponding weakening of the Coulomb interactions, thermodynamic aspects play a more important role.

(*e*) *Colloid Titration.* If both PEC components are optically nonactive, colloid titration with an ionic dye as metachromatic indicator can be applied to determine the stoichiometry of the ionic binding of the complex. This method is well known from the work of Terayama in 1952 [48] in determining the concentration of polyelectrolytes under the assumption of a 1:1 stoichiometric reaction between polyanions and polycations. For the end point detection of polycations, Terayama used the interaction of the cationic dye toluidine blue with the polyanion poly(potassium vinyl sulfate). The binding of the dye molecules to the polyelectrolyte, i.e., their aggregation

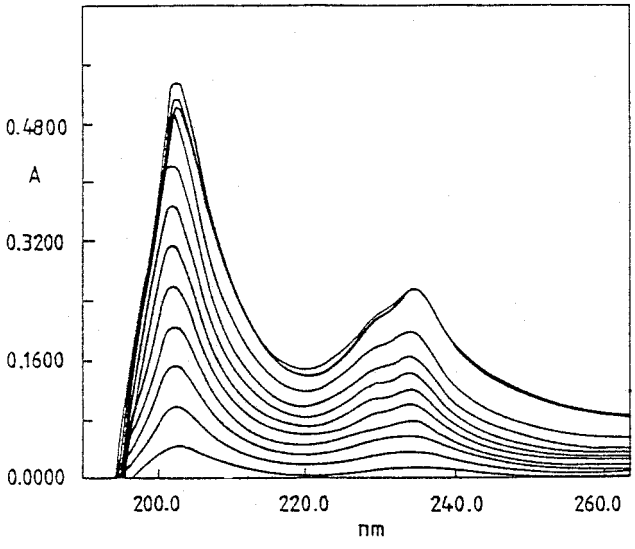

FIG. 7 Difference spectra of PEC solutions: NaPSS/PDADMAC and NaPSS solutions of the same concentration in relation to the mixing ratio *X*. (From Ref. 40.)

along the macroion, leads to a shift in its spectrum and a measurable color change. Since the complex formation between polyanions and polycations is strongly favored in comparison to the dye, the onset of the color change indicates the full consumption of the polycations, giving the absolute concentration of cationic sites. Using the system toluidene blue/strong polyanion, polycations can directly be titrated, but it can also be applied for the titration of polyanions as back titration, adding at first a defined amount of polycations in excess. Wassmer et al. [49] proposed an anionic dye/polycation system for polyelectrolyte titration, using Eriochrome black T (Merck, Darmstadt, Germany) as dye and 1,6 Ionene bromide (Polybren, Aldrich, Steinheim, Germany) as polycation. Titrations were carried out by an automatic device described in detail in [49]. They studied the optimum conditions of titration experiments and investigated especially the charge density of poly(sodium acrylate) in dependence on the pH value.

We have employed toluidine blue as indicator to judge the stoichiometry of ionic binding in the PECs between poly(styrene sulfonate) and PDADMAC or its copolymers with acrylamide. The shift caused by binding of toluidine blue to NaPSS is demonstrated in Figure 9a. Titrations were carried out by stepwise addition of the NaPSS solution to the polycationic one, which contained about 5 mol% of dye charges. As detection signal we

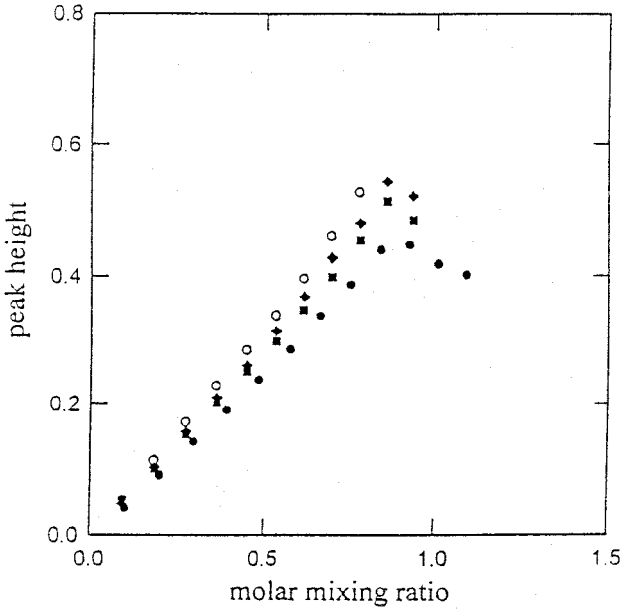

FIG. 8 Heights of the 203 nm peak in dependence on the mixing ratio X for PECs between NaPSS and different DADMAC-AA copolymers. ○, DADMAC-AA-47; ♦, DADMAC-AA-58; ■, DADMAC-AA-73; ●, PDADMAC. (From Ref. 40.)

used the difference of the absorption at the peak maximums of the free and the bound dye. The onset of the binding of toluidine blue is very sharply pronounced (Figure 9b), allowing an exact determination of the ratio of polycationic to polyanionic sites at this point. It should be mentioned that a necessary precondition for accurate results is the correct concentration of the polyelectrolyte solutions. Because of the changing water content (up to 15%) of the polyelectrolytes, the concentrations of the solutions must be checked carefully. Assuming a 1:1 stoichiometry of the PECs between NaPSS and the copolymers (compare results of UV spectroscopy and potentiometry with a Cl^- sensitive electrode) we found for all samples a very good agreement between the DADMAC content obtained from colloid titration and that determined by other methods [41]. These findings prove once more that PECs with a 1:1 stoichiometry were formed, even at a strong mismatching of the charge distances of the components (NaPSS: b = 0.25 nm, copolymer DADMAC-AA-8: b = 3.4 nm).

Colloid titration was also successfully employed to determine the degree of acetylation of chitosans [50,51].

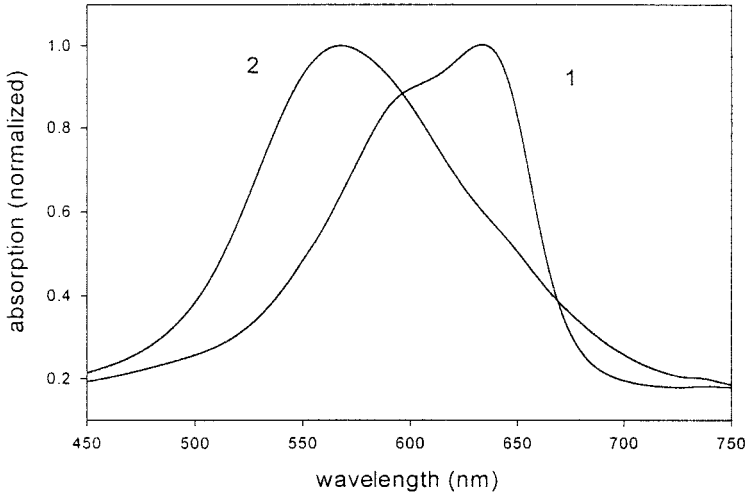

FIG. 9a Normalized spectra of toluidine blue free (1) and bound on NaPSS (2) in water.

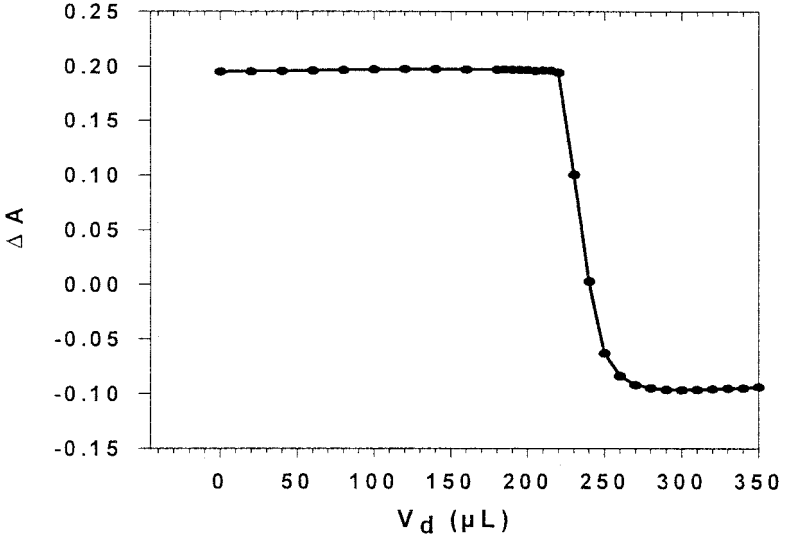

FIG. 9b Titration curve of PDADMAC with NaPSS, using the difference of the absorption at the peak positions in Fig. 9a as signal.

Streaming potential measurements may be used too for the end point detection of polyelectrolyte titrations. This technique is based on the compensation of the streaming potential induced by the adsorption of charged macromolecules onto the surface of a test vessel during the titration with a standard solution of an oppositely charged strong polyelectrolyte. Zero value of the streaming potential marks the end point. This method was used for example in [52] to determine the amount of charged groups in the stock solutions of the components for the preparation of PECs between PDADMAC and alternating copolymers of maleic acid and propene.

C. Overall Composition

Several methods revealed that PECs between strong polyelectrolytes have a 1:1 end point stoichiometry and also a 1:1 stoichiometry of ionic binding under full release of the low molecular counterions at nonstoichiometric mixing ratios. However, it remains an open question whether the major component in such systems is bound in excess in the PEC structures, giving them a net excess charge. To solve this problem, viscometry, analytical or preparative ultracentrifugation, and fractionation techniques in combination with analyzing methods can be employed.

1. Viscometry

While turbidimetry reveals the changes in the level of aggregation during the formation of supermolecular structures, viscometry does not give any information about this but monitors the changes in the structural density caused by such processes. This can easily be understood by considering the simple case of a suspension of noninteracting impermeable spheres. Einstein derived already in the beginning of this century [53] the expression

$$\eta_{sp} = \frac{\eta - \eta_0}{\eta_0} = 2.5\rho^{-1}c \tag{4}$$

where η and η_0 are the viscosity of the suspension and the solvent, respectively, c is the mass concentration of spheres, and ρ is their density. Approximating the supermolecular structures by equivalent spheres with an average structural density ρ, one can determine this quantity by viscosity measurements. Like turbidimetry, viscometry is a well-established method in the field of soluble PECs (see, e.g., [22]). We used viscosity measurements to determine the overall composition of the PECs between NaPSS and the DADMAC-AA-copolymers [54].

If the complex formation is carried out in deionized water, there is a strong difference between the structural density of the free polyelectrolyte chains and the bound ones in the complex, allowing a quantitative estimation of the amount of the major component remaining free in solution. We started

the experiments with the solution of a high molecular weight NaPSS (M_w = 356 kDa) and added stepwise the cationic solutions (for details see [54]). The viscosity was measured after each step of dosage. Figure 10 depicts the dependence of the specific viscosity during the PEC formation on the mixing ratio. All systems show qualitatively the same behavior. The specific viscosities decreased strongly up to the 1:1 mixing ratio, where a minimum occurred. This minimum corresponds to the full integration of NaPSS into the PECs, confirming the 1:1 end point stoichiometry of the complexes. The increase of η_{sp} at higher mixing ratios is caused by an excess of the polycations.

The decrease of the viscosities during PEC formation results from three effects:

The above-described change of the conformation of the bound polyelectrolyte chains
A decrease of the viscosity contribution of the free polyelectrolyte due to the release of the counterions and the increase of the ionic strength
A dilution of the starting solutions according to the added amount of the cationic ones

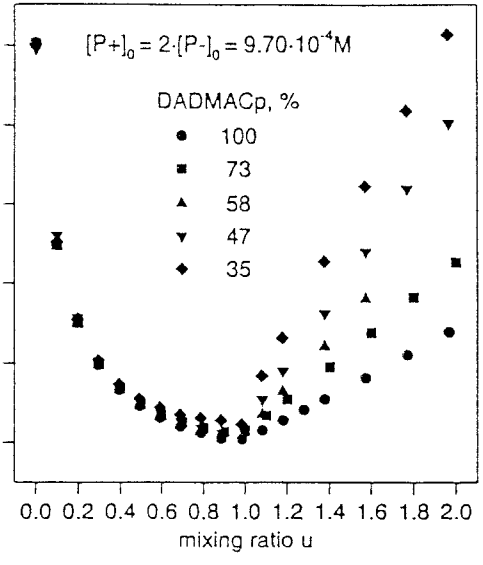

FIG. 10 Specific viscosity of the reacting mixture during PEC formation of NaPSS-356t and various DAMAC-AA copolymers in dependence on the mixing ratio of cationic to anionic groups. (From Ref. 54.)

The last effect can easily be taken into account. Because we know from our potentiometric studies that the counterions are fully released according to the mixing ratio, the ionic strength of the solutions caused by these counterions can also be calculated. To analyze the viscosity data in detail, we made some simplifying assumptions. We treated the PEC solution as a two-component system, consisting of the PEC particles and the free polyelectrolyte being in excess. Possible interactions among all species were neglected. Then the viscosity of the complex solutions can be written as

$$\eta_{sp}(X) = \eta_{PE}(X) + \eta_{PEC}(X) \tag{5}$$

where $\eta_{PE}(X)$, $\eta_{PEC}(X)$ are the contributions of the free polyelectrolyte component and the complex, respectively. The structural density of the PECs can be calculated from the minimum of the viscosity data. These density values are more than two orders of magnitude higher than those of the free polyelectrolytes and increase with rising amount of DADMAC in the copolymers. Assuming the same value also at lower mixing ratios, the contribution of the PEC $\eta_{PEC}(X)$ can be obtained. To determine the contribution of the polyelectrolyte in excess, we measured calibration curves as functions of the NaPSS concentration and the NaCl content, covering the whole range of the experiments in PEC formation. Then $\eta_{sp}(X)$ was calculated for the case of a 1:1 stoichiometry at all mixing ratios. The theoretical viscosity values were clearly above the measured ones, indicating excess binding of NaPSS. Therefore we introduced the stoichiometric factor $f(X) = [A^-]_X/[C^+]_X$ as fitting parameter, where $[A^-]_X$ and $[C^+]_X$ are the monomolar concentrations of anionic and cationic sites in the PEC, respectively. The results obtained by adjusting the calculated to the measured viscosity data are given in Figure 11. At lower mixing ratios the major component is bound in remarkable excess. Obviously, the charged chains in excess in the PEC structure form an electrostatically stabilizing shell on the surface of the neutralized PEC core. The values of $f(X)$ determined from the viscosity data represent the lowest limit, because they resulted under the assumption that also the chains bound in excess have the same conformation as in the core of the PECs. In reality the charged loops and tails of the shell should have a less compact structure.

In [55] a combination of conductometric, turbidimetric, and viscosity measurements was used to study the end point stoichiometry of complexes between the sodium salt of poly(acrylic acid) and different polycations with quaternary ammonium groups, varying in charge density and branching. With differing structural parameters of the components, increasing deviations from the 1:1 stoichiometry were found. Kuderbaigenov et al. [56] investigated the formation of PECs between linear and cross-linked poly(acrylic and methacrylic acid) and linear or cross-linked poly(4-(but-3-en-1-ynyl)-1-

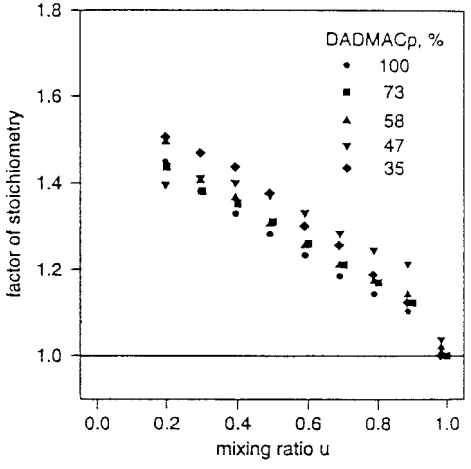

FIG. 11 PEC stoichiometry of the complexes from Fig. 10 in dependence on the mixing ratio. (From Ref. 54.)

methylpiperidin-4-ol) as well as their dissolution in dependence on the ionic strength by potentiometric, conductometric, turbidimetric, and viscometric measurements.

The viscosity behavior during complex formation may be also much more complicated. In [57] the PEC formation between PDADMAC samples of different molecular weights and a double hydrophilic graft copolymer was studied. The graft copolymer DHP-MA (M_w = 33 kDa) consisted of a methacrylate backbone chain and poly(ethylene oxide) side chains. Complex formation was carried out in 0.01 M NaCl solution. While in the case of using the PDADMAC samples as starting solutions the expected minimum in the specific viscosity was observed, in the inverse order of mixing a maximum in the X-dependence of η_{sp} occurred, which was more clearly pronounced with rising molecular weight of the PDADMAC samples. The increase of η_{sp} indicates that the structural density of the PECs is lower than that of the DHP-MA chains. The decrease of η_{sp} at higher mixing ratios could be explained by an increase of the structural density, monitored by static light scattering experiments.

In general it must be noticed that in pure water the effects caused by complex formation are most strongly pronounced. With rising ionic strength the accuracy of measurements in such highly diluted systems as were used in our studies on PEC formation decreases drastically, because of the low viscosity values of the component solutions.

2. Ultracentrifugation

Especially in the case of higher ionic strengths of the medium, ultracentrifugation offers a good chance to determine the overall composition of the PECs. This means analytical ultracentrifugation (AUC) as well as the preparative one in combination with an analysis of the supernatant. In principle, AUC studies allow us to determine the sedimentation coefficients of a particle system by sedimentation velocity measurements or the particle mass by sedimentation equilibrium measurements as an absolute method.

The sedimentation coefficient s is related to the particle parameters by the expression [58]

$$s = \frac{M(1 - \bar{v}\rho_0)}{N_A f} \tag{6}$$

where M is the particle mass, $\bar{v}$ is the partial specific volume of the solute in the solution, ρ_0 is the density of the solvent, and f is the frictional coefficient of the particles (for ideal solutions $f = kT/D$, k being Boltzmann's constant, T the absolute temperature, and D the diffusion coefficient).

The sedimentation equilibrium technique yields directly the particle mass M from the concentration profile along the radial distance r from the center of rotation:

$$M = \frac{2RT}{(1 - \bar{v}\rho_0)\omega^2} \frac{\partial \ln c}{\partial(r^2)} \tag{7}$$

where R is the universal gas constant.

Sedimentation velocity measurements were often used in studying soluble PECs (see, e.g., [18,19,26]).

We employed this method to investigate the stoichiometry of highly aggregated PECs between NaPSS and PDADMAC [59]. A typical sedimentation pattern obtained by UV detection (NaPSS) is given in Figure 12. The very broad concentration profiles without a distinct step are characteristic for highly polydisperse colloidal particle systems. Sedimentation coefficients cannot be derived from such smoothed curves. The slowly sedimenting species at 40,000 rpm (region 3) is free NaPSS. Therefore, from the absorption level at the beginning of the experiment (region 1) and the plateau value after the separation of the PEC particles, the amount of NaPSS in the supernatant and in the complex solution can be determined and the stoichiometric factor can be calculated. The results obtained at different ionic strengths are collected in Figure 13. As in the case of the viscometric studies, strong deviations from the 1:1 stoichiometry occur with decreasing mixing ratio, i.e., NaPSS is clearly bound in excess. The stoichiometric factor obtained by analytical ultracentrifugation is higher than that from viscometry.

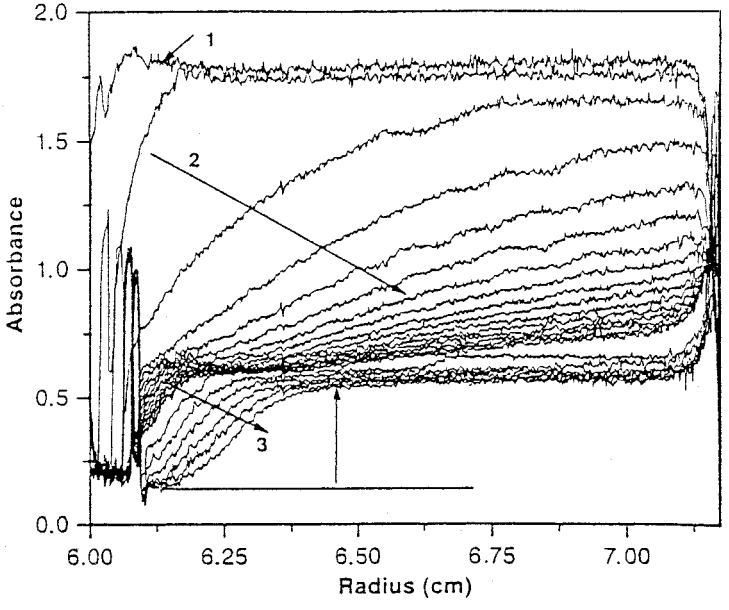

FIG. 12 Sedimentation pattern of a complex NaPSS-66t/PDADMAC (formed in deionized water, $X = 0.4$). 1, at 1,100 rpm; 2, at 20,000 rpm; 3, at 40,000 rpm. (From Ref. 59.)

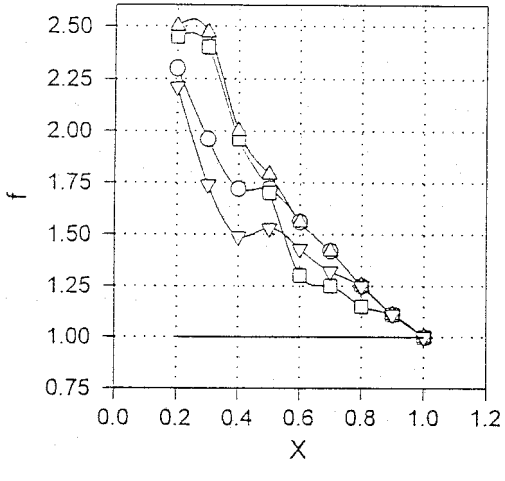

FIG. 13 Stoichiometric factor f of the complexes NaPSS-66t/PDADMAC in water (○), in 0.01 M NaCl (□), in 0.1 M NaCl (△), and NaPSS-66t/DADMAC-AA-47 in water (▽). (From Ref. 59.)

This can be explained in that viscometry monitors only the chains that underwent a transition to a more compact structure as incorporated into the PEC, whereas ultracentrifugation also detects only loosely attached ones.

The presence of NaCl did not cause systematic effects. The same is true for changing the charge density of the polycation (copolymers of Table 2). However, an increase of the molecular weight of the NaPSS samples used resulted in a small but systematic increase of $f(X)$. It should be mentioned that even for the complex solutions prepared in pure water, the released counterions ensure reliable sedimentation data.

In a certain range of low ionic strengths PEC formation takes place on a far lower level of aggregation, leading to more monodisperse systems. These complexes could also be investigated by sedimentation equilibrium measurements. A sophisticated data evaluation by the so-called Ω analysis [60] allows the determination of the concentration profile of NaPSS free in solution and in the PEC. This algorithm is based on a theoretical separation of the concentration of the slowly sedimenting free NaPSS component from the measured profile. The free NaPSS concentration profile can be calculated from the known values of the molecular mass and partial specific volume. The values obtained for the stoichiometric factor were still somewhat higher than those from the sedimentation velocity studies. In principle, also the mass of the complex particles can be estimated by this procedure, analyzing the remaining concentration gradient. The impeding factor is the unknown partial specific density of the complex, which may be quite different from the value, which is calculated assuming additivity of the components, because complex formation completely changes the water/polyelectrolyte interaction.

Sedimentation velocity measurements in combination with turbidimetry and dynamic light scattering were carried out in [52] to study the aggregation behavior of PECs between PDADMAC and copolymers of maleic acid and propene in relation to salt concentration, revealing a strong increase above a NaCl content of 0.1 mol/L. Izumrudov [61] determined the composition of complexes of bovine serum albumin (BSA) and synthetic polycations from the sedimentation peaks of the complex and the free BSA in relation to the mixing ratio and the chain length of the polycation. A constant PEC composition was found independent of both parameters. However, the mass of the PEC particles, obtained from the sedimentation coefficient and the diffusion coefficient (dynamic light scattering) was proportional to the degree of polymerization of the polycation. In [62] the stoichiometry of PECs between carrageenan and chitosan was determined by a quantitative analysis of the supernatants after complete separation of the complex by preparative ultracentrifugation. Trinh and Schnabel [63] used a similar procedure to study the composition of PECs between poly(*N*-ethyl-4-vinylpyridinium bro-

mide) and sodium poly(styrene sulfonate) or/and poly(phosphate). In the ternary system a favoring of NaPSS in comparison to poly(phosphate) was found.

We employed AUC with UV detection also to study preferential binding and exchange reactions with regard to the chain length of NaPSS in PECs with PDADMAC [47]. To judge preferential binding, PECs were prepared by dropwise adding a PDADMAC solution up to the desired mixing ratio to a 1:1 monomolar mixture of a low (8 kDa) and a high (356 kDa) molecular weight sample of NaPSS. NaCl solutions of different NaCl content were used as solvents. After separation of the complex by preparative ultracentrifugation (2 h at 40,000 rpm) the supernatants were adjusted to an ionic strength of 0.5 M NaCl and analyzed by AUC. Under these conditions, both components can clearly be separated and their amount can be determined both from the absorption level in the sedimentation pattern and the areas of the sedimentation peaks. Figure 14a depicts the ratio γ_M = [PSS-8t]/[PSS-356t] of the components in the supernatant as function of the ionic strength during PEC formation ($\gamma_M < 1$ corresponds to preferential binding of PSS-8t, $\gamma_M > 1$ to preferential binding of PSS-356t). In contradiction to the expectations from the thermodynamic point of view [28], a favoring of the low molecular weight component was found at low ionic strengths. Obviously, under such conditions PEC formation is mainly governed by the kinetics of the process, favoring the incorporation of PSS-8t due to its faster diffusion rate. At higher ionic strengths the thermodynamic factors dominate.

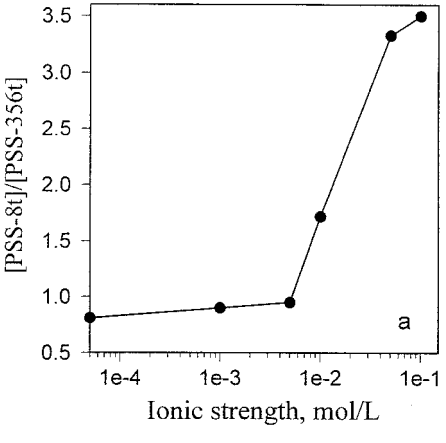

FIG. 14a Ratios γ_M between the contents of PSS-8t and PSS-356t in the supernatants of PECs between PDADMAC and a 1:1 molar mixture of PSS-8t and PSS-356t prepared at various ionic strengths (X = 0.3, PSS in excess). (From Ref. 47.)

Preferential binding in PEC formation between PDADMAC and mixtures of Na lignosulfonate and Na cellulose sulfate or Na carboxymethylcellulose was studied in [64] in relation to the ionic strength by preparative ultracentrifugation and an analysis of the supernatants by UV spectroscopy.

Another interesting question is whether such highly aggregated frozen structures are able to undergo further rearrangement and exchange reactions. Therefore we prepared PECs at different ionic strengths between high or low molecular weight NaPSS and PDADMAC and added then the other NaPSS component up to the same monomolar concentration. These PEC solutions were analyzed as described above. During the first two days, exchange reactions did not occur, and for the system PSS-356t/PDAMAC + PSS-8t they also did not after 2 months. However, for the system PSS-8t/PDAMAC + PSS-356t a complete exchange of the low molecular weight PSS for the high molecular one was found at higher ionic strength (Figure 14b). Only in the nearly salt-free solutions the PECs remained stable. Corresponding results were obtained with regard to the exchange of NaPMA (with the weaker carboxylic groups as anionic sites) for NaPSS.

These findings should be of great importance and must be taken into account in all practical applications.

3. Fluorescence Quenching

As described in [26], the complex formation between a pyrene labeled poly(methacrylate) and poly(*N*-ethyl-4-vinylpiridinium) (PEVP) cations

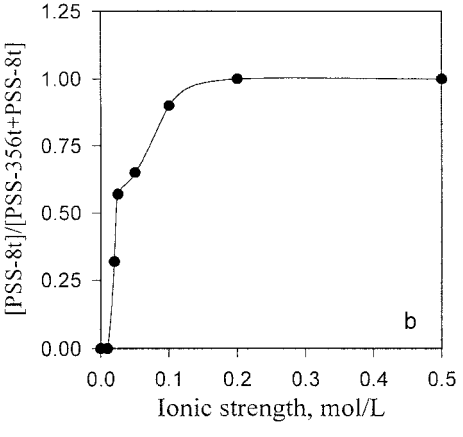

FIG. 14b Relative amounts of released PSS-8t in the supernatant solution of its complexes with PDADMAC after 2 months exchange reaction with PSS-356t as function of the ionic strength. (From Ref. 47.)

leads to a quenching of the fluorescence light of the pyrenyl groups by the pyridinium groups. The authors used this method to study the effect of different salts on the dissociation behavior of water-soluble PECs, while in [65] the effect of the chain length for the same combination of polyelectrolytes was considered. In [66,67] results were reported about PEC formation between various pyrene labeled polyanions and oppositely charged mixed micelles, varying the charge density of the micelles via composition. On the basis of a simple kinetic model the reaction parameters were estimated from the fluorescence quenching data. As already mentioned in the section on soluble PECs, fluorescence quenching is also a powerful tool in investigating PEC exchange reactions (see, e.g., [10]).

4. Fractionation Techniques

In general, fractionation methods should allow the separation of the free polyelectrolyte components and the PEC, providing information about the stoichiometry. One of the most used techniques is size exclusion chromatography (SEC). But with regard to highly aggregated PECs some problems occur. The often strongly polydisperse systems of relatively large particles (up to a few hundred nm) cannot be separated in an appropriate manner. Additionally, adsorption effects occur due to interaction of the polyelectrolytes with the stationary phase. Modifications of the mobile phase to suppress adsorption by admixtures of salts or organic solvents interfere with PEC formation, which is to be studied. To overcome these shortcomings Harrison and Tan [68] applied differential SEC to study the stoichiometry of gelatin/polyanion complexes, using sodium poly(styrene sulfonate) and sodium poly(2-acrylamido-2-methylpropane sulfonate) as polyanions. In this technique the analytes are dissolved in the mobile phase, which is pumped continuously through the columns. Thus the column-packing surface is equilibrated with the analytes. The sample can be injected with an analyte concentration that is either higher or lower than in the mobile phase, giving a positive or negative chromatographic signal. By this method they could separate the chromatographic peaks of the PEC and the components well. In [69] they supplemented these studies employing field flow fractionation with a cross flow and UV detection at 254 nm. All components could be successfully separated, and the hydrodynamic radii of the complexes were determined. In principle, field flow fractionation in combination with light scattering detectors offers the possibility of studying the structural parameters, including the polydispersity of PECs in detail.

Dubin et al. used capillary electrophoresis to separate the complexes of proteins with synthetic polyanions from the free protein in the complex solution and to determine the complex composition. The binding isotherms were studied in relation to the pH value [70], the chain length of the poly-

anions [71], and the hydrophobicity of alternating copolymers of maleic acid and various alkyl-vinyl ethers [72].

D. PEC Structure

1. Imaging Techniques

Although imaging techniques are the best way to get an impression of the structure of PEC particles, microscopic studies on such systems are rather scarce, probably due to the small sizes and the low contrast of such structures. The artifact-free preparation of swollen structures raises additional problems. In [73] the structure of complexes between polyelectrolytes and charged micelles was studied by cryotransmission electron microscopy. We used a similar procedure to get micrographs of PECs between NaPSS and PDADMAC [40]. For the fixation of a representative number of particles, a special adsorption or sedimentation technique was used. Thin carbon films of 4–6 nm thickness were hydrophilized by glowing. The samples were rapidly frozen and the specimens were freeze dried at 170 K. For contrasting, heavy metal shadowing was used. The micrograph of such a PEC is given in Figure 15, showing a highly polydisperse system of nearly spherical particles. This result is particularly valuable with respect to the selection of an appropriate structure model for the interpretation of light scattering measurements.

However, because of the swollen structure cryopreparation too may cause some artifacts. X-ray absorption microscopy represents a new and promising method of studying such structures directly in water solution [74,75]. Wavelengths between 2.3 and 4.5 nm are used to obtain images wherein structures down to 20 nm can be visualized. In this region—the so-called water window—oxygen gives a negligible contribution in absorption, i.e., a natural contrast mechanism exists for wet materials. For sample preparation a droplet of the PEC solution was spread between two poly(imide) films, which bear negative charges generated by glowing. Positively charged structures are adsorbed at these surfaces and are fixed then for the microscopic studies. In the case of negatively charged PECs we first treated the films with a strong polycation (PDADMAC) under appropriate conditions. The adsorbed layer of the polycations results in a positive net charge of the films. The x-ray micrographs were obtained with a microscope (constructed at the University of Göttingen, Germany), using the BESSY electron storage ring (Berlin, Germany) as x-ray source. Although the resolution is less, the micrographs confirmed fully the results of the electron microscopic studies. Additionally, it could be concluded from the density profile of the particles that they are nearly homogeneous spheres.

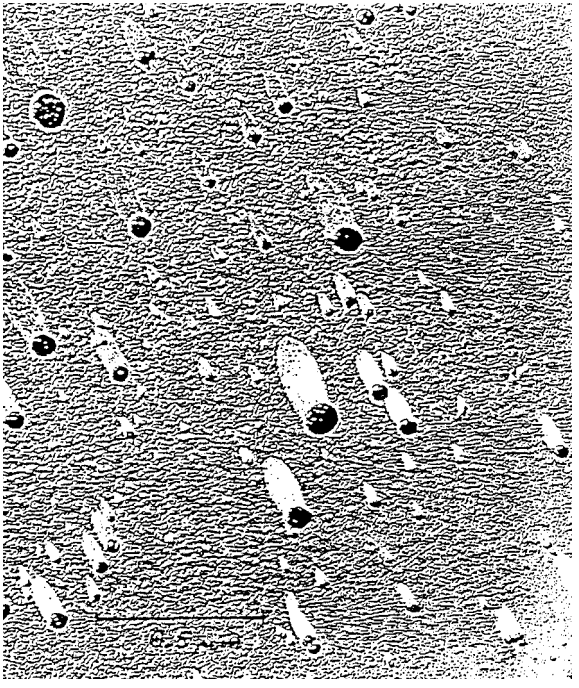

FIG. 15 Electron micrograph of PSS-66t/PDADMAC particles; $c_c = 2 \cdot 10^{-4}$ g/mL, $X = 0.8$. (From Ref. 40.)

Wolfert and Seymour [76] investigated the influence of the molecular weight of poly(L)lysine on the size of PECs with DNA by atomic force microscopy, but drying the mica discs with the adsorbed samples at room temperature. The polydisperse flat disclike particles were scanned in radius and height. The volumes of the particles increased with rising molecular weights.

2. Scattering Methods

Scattering methods provide detailed information about the structural parameters of colloidal particles. In the field of polyelectrolyte complexes, mainly light scattering techniques such as static, dynamic, and electrophoretic light scattering were employed.

(*a*) *Static Light Scattering.* In our experience static light scattering especially proved to be a powerful tool in studying the structure and behavior of highly aggregated PEC particles. The size of the investigated PECs reached up to several 100 nm, leading to a strong angular dependence of

the scattering curves. On the one hand, this causes problems in the extrapolation procedure to zero scattering angle. On the other hand, the shape of the scattering curve contains more information than is used in determining the particle mass and radius of gyration. To solve these problems we developed an improved algorithm of data analysis, based on a comparison of the experimental scattering curves with theoretically calculated ones for various basic structure types [77,78]. This procedure is described briefly in the following.

Algorithm of light scattering data analysis. For highly diluted systems of compact particles, interparticular interferences can be neglected and the Rayleigh ratio $R(q)$ of the scattering intensity is given by the simple expression

$$R(q) = KcM_w P_z(q) \tag{8}$$

where K is a contrast factor, containing the optical parameters of the system, c the mass concentration in g/mL, M_w the weight average of the molecular mass of the scattering particles, $P_z(q)$ the z-average of the intraparticular scattering function, q being $(4\pi/\lambda)\sin\Theta/2$, λ the wavelength in the medium, and Θ the scattering angle between the incident and the scattered beam. Describing the polydispersity of the particle system by a continuous normalized mass distribution function $p_w(M)$, one obtains

$$M_w = \int_0^\infty M p_w(M)\, dM \tag{9}$$

$$P_z(q) = \frac{1}{M_w} \int_0^\infty P(q, M) M p_w(M)\, dM \tag{10}$$

In the framework of the Rayleigh–Debye approximation (RDA), the relation

$$P_z(q) = 1 - \frac{1}{3} \langle S^2 \rangle_z q^2 + \cdots \tag{11}$$

was derived, whatever the shape and the structure of the particles, where $\langle S^2 \rangle_z$ is the z-average of the square of the radius of gyration.

For particle sizes below 50 nm, the scattering curves can be analyzed by a Zimm plot ($Kc/R(q)$ versus q^2) or a Guinier plot ($\ln R(q)/Kc$ versus q^2), providing by extrapolation to the scattering angle zero, M_w and $\langle S^2 \rangle_z$ without any assumptions. However, no conclusions on the structure and polydispersity of the particle system can be drawn from the scattering curve. Therefore the structural density, which is the reciprocal of the degree of swelling, cannot be determined correctly from M_w and $\langle S^2 \rangle_z$, because these quantities represent different average values. Since the scattering functions of various

structure models are known in the RDA (justified for PEC particles due to the swollen structures), $P_z(q)$ can be calculated, assuming the type of the distribution function $p_w(M)$.

In the following we restrict the considerations to the model of polydisperse systems of homogeneous spheres, which is suggested by the imaging techniques and has also been proved quite well in describing the scattering curves of the PEC solutions investigated. As distribution function we used a special logarithmic distribution of radii with the size parameter a_m and the polydispersity σ_a:

$$p_w(a) = \frac{a^{-5/2} \exp(-(\ln a - \ln a_m)^2/2\sigma_a^2)}{\sqrt{2\pi}\sigma_a a_m^{-3/2} \exp(9\sigma_a^2/8)} \tag{12}$$

This distribution function manages that M_w becomes independent of σ_a:

$$M_w = \frac{4\pi}{3} \rho N_A a_m^3 \tag{13}$$

where N_A is Avogadro's number and ρ is the average polymer density in the particle.

The radius of gyration is given by

$$\langle S^2 \rangle_z = \frac{3}{5} a_m^2 e^{5\sigma_a^2} \tag{14}$$

For low polydispersities, the parameter σ_a corresponds to the relative standard deviation. The choice of the type of distribution function is of minor importance [78,79]. The intraparticular scattering function of spheres with the radius a is given as [42]

$$P(q) = \left(3 \frac{\sin aq - aq \cos aq}{a^3 q^3} \right)^2 \tag{15}$$

Because $R(q)$ is proportional to M_w and $P(q)$ depends in the RDA on the product q times a, changes in mass and size correspond in a scaled, double logarithmic plot to axis parallel shifts. Therefore, model calculations yield in such a plot for each structure model a set of master curves with different polydispersities.

Figure 16 depicts the scaled scattering curves for different structure types, showing that the structure type can be well estimated, if an appropriate section of the scattering curve is known. From the assignment of an experimental curve to an appropriate theoretical one the polydispersity too can be determined. The position of the experimental on the fitting curve yields M_w and a_m as well as ρ according to Eq. 13. By a plot $\log(q^k R(q))$ versus $\log q$ with an appropriate k value, it can be achieved that the scattering curve

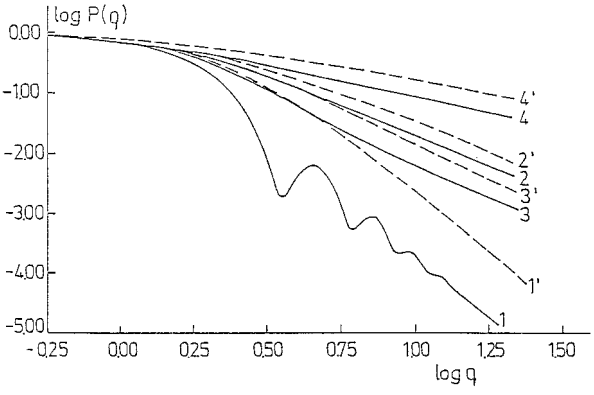

FIG. 16 Comparison of the scattering curves of different structure types: 1, spheres; 2, Gaussian coils; 3, stars (10 arms); 4, rods (*i*, monodisperse; *i'*, polydisperse systems; for details see Ref. 78). (From Ref. 78.)

passes through a maximum, where its width depends sensitively on the polydispersity. Therefore σ_a can be obtained with an accuracy better than 0.05 and the structural parameters with an error in the range of 1%, as is demonstrated in Figure 17.

For the quantitative analysis of the light scattering data the concentration $c_{PEC}(X)$ of the PECs and their refractive index increment $\nu_{PEC}(X)$ in dependence on the mixing ratio X must be known. In the case of polyanion solutions as starting ones, $c_{PEC}(X)$ is given by the expression

$$c_{PEC}(X) = c_{A_0} \frac{V_{A_0}}{V_{A_0} + V_D} \left(\frac{m_A f(X) + m_C}{M_A} \right) X \tag{16}$$

where c_{A_0} is the mass concentration of the polyanion in the starting solution, V_{A_0} and V_D are the volume of the starting solution and the dosage volume of the polycation solution, respectively, m_A and m_C are the molar masses per charged unit of the polyanion and polycation without the counterions, respectively, M_A is the corresponding molar mass with the counterion, and $f(X)$ is the stoichiometric factor introduced in Sec. II. Assuming additivity of the refractive index increments ν_A and ν_C of the components, one obtains

$$\nu_{PEC}(X) = \frac{\nu_A f(X) m_A + \nu_C m_C}{f(X) m_A + m_C} \tag{17}$$

Experimental results. Knowing the structure type of the PEC particles, a detailed analysis of the light scattering data according to the above de-

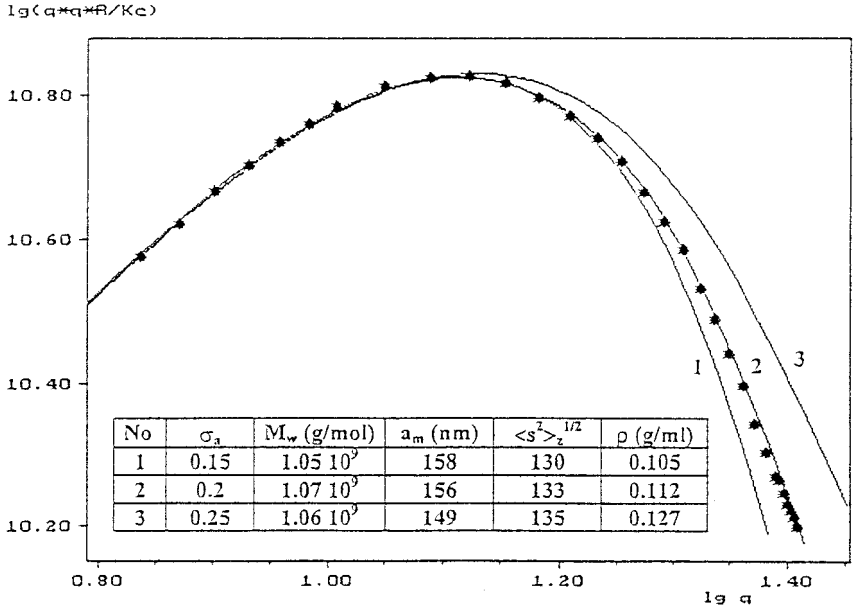

FIG. 17 Scattering curve of a PEC between anionically and cationically modified PNIPAM (symbols) and its interpretation by theoretical curves of polydisperse systems of spheres of different polydispersity (see the inset table).

scribed algorithm provides much information about the structural characteristics. So we studied the effect of different parameters on the structure and behavior of PECs: mixing ratio, polymer concentration, molecular weight and charge density of the polyelectrolytes, ionic strength during complex formation, subsequent addition of salt, and temperature behavior of PECs between temperature-sensitive polyelectrolytes. Selected results will be presented here, demonstrating the high efficiency of static light scattering.

Mixing ratio. The typical dependence of the structure of PECs on the mixing ratio is illustrated in Figure 18a by the scattering curves of a complex between NaPSS-66t and PDADMAC [80] formed in pure water. The curves are very similar and could be fitted quite well by a polydisperse system of spheres with $\sigma_a = 0.6$. This polydispersity is very high and corresponds to $M_w/M_n = \exp[9\sigma_a^2] \simeq 25$. Ignoring the effect of polydispersity would provide the structural density (calculated from M_w and the z-average of the square of the radius) by a factor 15 too low. The structural parameters obtained by the fits are given in Figure 18b. The particle mass and size decrease slightly with rising X, while the density increases a little. This means that the build-

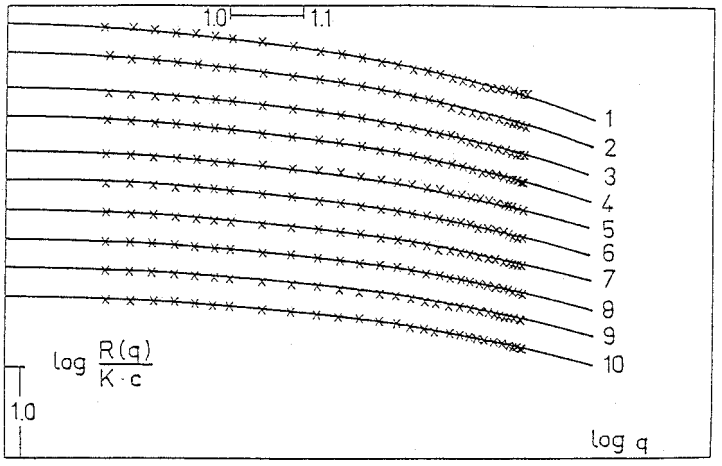

FIG. 18a Scattering curves of the PEC PSS-66t/PDADMAC in dependence on the mixing ratio X (0.1(0.1)1); $c_c = 1 \cdot 10^{-4}$ g/mL; crosses, experimental points; full lines, theoretical fits with $\sigma_a = 0.6$; the curves are shifted to each other in an appropriate manner to avoid overlapping. (From Ref. 80,)

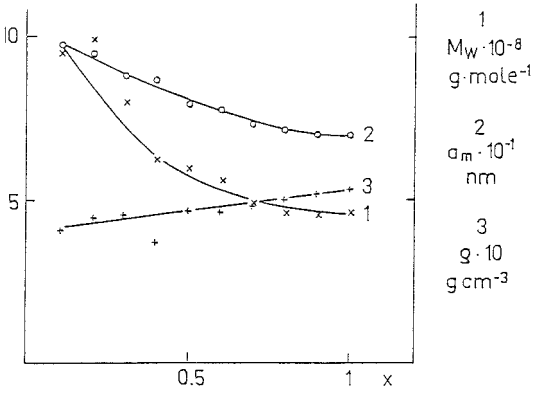

FIG. 18b Structural parameters of the PEC PSS-66t/PDADMAC in dependence on the mixing ratio X. (From Ref. 80.)

ing of new particles and not a further growth is the dominating process with increasing X.

Polyelectrolyte concentration. For the same components we studied the PEC formation in a broad range of concentration of the component solutions ($c_c = 1 \cdot 10^{-5}$, $2 \cdot 10^{-5}$, $5 \cdot 10^{-5}$, $1 \cdot 10^{-4}$, $2 \cdot 10^{-4}$, $5 \cdot 10^{-4}$, and $1 \cdot 10^{-3}$ g/mL) [80]. At each concentration, PECs were prepared up to $X = 0.5$, and for the higher concentrations the PEC solutions were diluted in an appropriate manner for the light scattering measurements. All scattering curves (Figure 19a) could be fitted with the same model curve ($\sigma_a = 0.6$). Figure 19b shows that simple power laws were obtained for the concentration dependence of the mass and size of the PEC particles, the exponent of which corresponds to $M_w \sim a_m^3$, the expected relation for homogeneous spheres. The structural

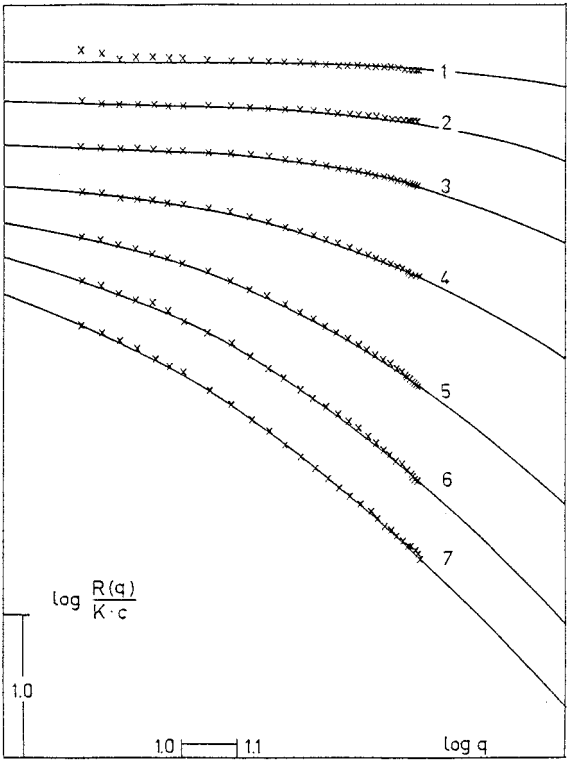

FIG. 19a Scattering curves of the PEC PSS-66t/PDADMAC in dependence on the polycation concentration ($c_c = 1 \cdot 10^{-5}$, $2 \cdot 10^{-5}$, $5 \cdot 10^{-5}$, $1 \cdot 10^{-4}$, $2 \cdot 10^{-4}$, $5 \cdot 10^{-4}$, and $1 \cdot 10^{-3}$ g/mL; $X = 0.5$). (From Ref. 80.)

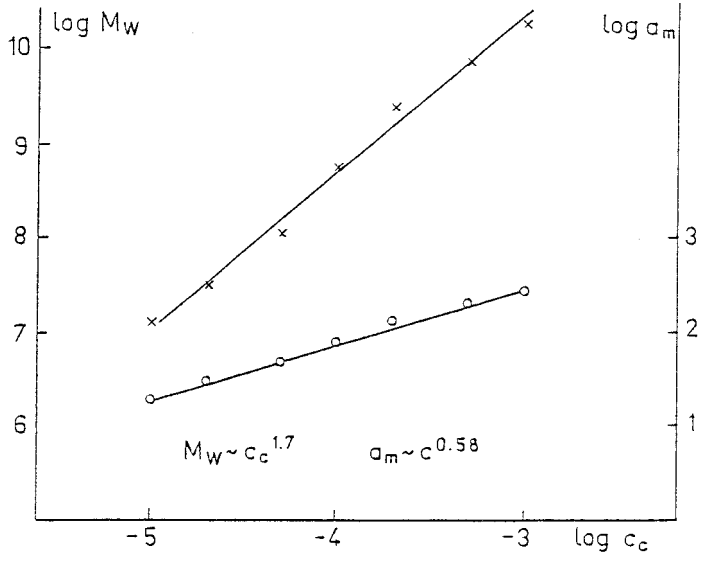

FIG. 19b Structural parameters M_w and a_m of the PEC PSS-66t/PDADMAC in dependence on the polycation concentration. (From Ref. 80.)

density of the PECs is $\rho = 0.43$ g/mL. The normalized curves of all systems gave a common scattering curve, reaching up to the asymptotic q^{-4} range of spheres.

These findings confirm the model of polydisperse systems of homogeneous spheres by exact fits of the static light scattering curves, the expected $M \sim a^3$ dependence for PEC "homologues" prepared at different polymer concentrations, and the asymptotic q^{-4} behavior of compact spheres. The quantitative information obtained shows that the concentration of the component solutions does not affect the internal structure of the PECs remarkably but controls their level of aggregation to a great extent.

PEC formation in the presence of salt. It is well known from the work on soluble PECs that the presence of salt during complex formation promotes rearrangement and exchange processes. Therefore great effects might be expected, especially for highly aggregating systems. The presence of salt causes a transition to a more coiled and flexible structure of the polyelectrolytes and weakens the ionic binding. Therefore charge compensation by conformational adaptation should be favored, and a lower level of aggregation can be expected. The characterization of PECs between NaPSS and PDADMAC prepared at various contents of NaCl [81,82] revealed a clearly pronounced minimum in the dependence of the particle mass and size on

the ionic strength (Figure 20), whereas the structural density remained nearly constant. The increase at higher ionic strength is probably caused by secondary aggregation due to the screening of the charged, stabilizing shell of the excess component. In comparison to salt-free systems, the level of aggregation in the minimum is reduced by a factor of 100. This opens a second way to control the mass of the PEC particles. However, it must be noticed that there is an interplay between the effects of polymer concentration and ionic strength. At higher ionic strength we found a stronger dependence of M_w and a_m on polymer concentration.

Molecular weight. To judge the influence of this parameter we studied the PEC formation between NaPSS samples of different molecular weights (8–1000 kDa) with a PDADMAC sample (M_w = 250 kDa) in pure water. Surprisingly, we could not observe any systematic change of the structural parameters with the molecular weight of the NaPSS samples. Obviously, the kinetics of the process of PEC formation prevails and suppresses the effect of the molecular weight on the resulting structures.

Charge density. Previous studies on anionically and cationically modified poly(acrylamide) samples [83,84] had revealed that with decreasing

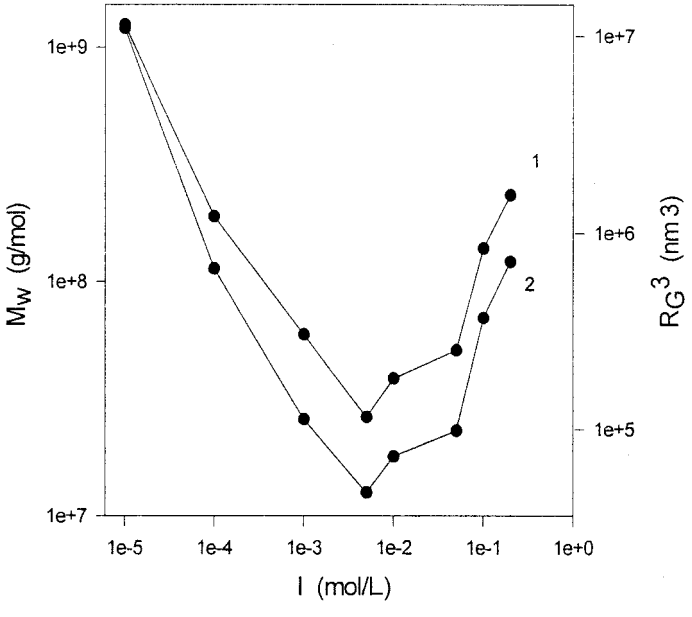

FIG. 20 Particle mass (1) and size (2) of the PEC PSS-66t/PDADMAC at $X = 0.5$ as function of the ionic strength. (From Ref. 81.)

charge density and mismatching of the charge distances of the polyelectrolyte components, the structural density and the salt stability of the PECs decrease. Similar results with regard to the structural density were obtained for PECs between NaPSS and copolymers of DADMAC and acrylamide of various compositions [40]. Therefore the charge density of the polyelectrolytes is an important parameter to control the degree of swelling of PEC particles.

Summarizing our results on highly aggregated PECs, we can state that at nonstoichiometric mixing ratios electrostatically stabilized particles in the nm scale with controlled levels of aggregation and structural density can be prepared. These particles should be of interest as potential carrier systems for drugs and enzymes, because they offer an easy way to incorporate charged material by Coulomb interactions.

Subsequent addition of salt. For such applications the response of the PECs to a subsequent change of the ionic strength of the medium is a decisive question. This means the colloidal as well as the stability of the ionic binding. Complexes between NaPSS and PDADMAC are stable with regard to the ionic binding up to ionic strengths of a few moles per liter [85]. Addition of NaCl caused only secondary aggregation and macroscopic flocculation. The colloidal stability of the complexes depends strongly on the mixing ratio, i.e., it decreases drastically with increasing *X*. Obviously, the added salt screens the charges of the stabilizing shell, the thickness of which decreases with rising *X*.

Interesting results were obtained for complexes with NaPMA as polyanion. This will be demonstrated by the behavior of the PEC DADMAC-AA-47/NaPMA. The structural parameters of the PEC prepared in water after different steps of dosage of a 2 N NaCl solution are given in Figure 21. The particle mass increases only slightly with rising ionic strength, whereas the particle radius grows strongly. Salt causes a swelling of the particles due to the weakening of the ionic binding. During this process the polydispersity decreases drastically, suggesting smaller particles to become integrated in the bigger ones. At a critical salt concentration of about 0.6 mol/L the PEC particles are nearly completely dissolved, and the structural density reaches a value comparable to that of the components.

In general, depending on the nature of the polyelectrolytes, the response of a PEC to subsequent addition of salt may be quite different (see also [82–85]). The authors of [86] propose to use the different salt stability of the ionic binding to separate polyelectrolyte components from mixtures via complex formation with oppositely charged macroions.

A promising way to improve the colloidal stability is the use of double hydrophilic polyelectrolytes. Kabanov et al. [87] reported on soluble stoichiometric PECs between diblock copolymers containing sodium poly(meth-

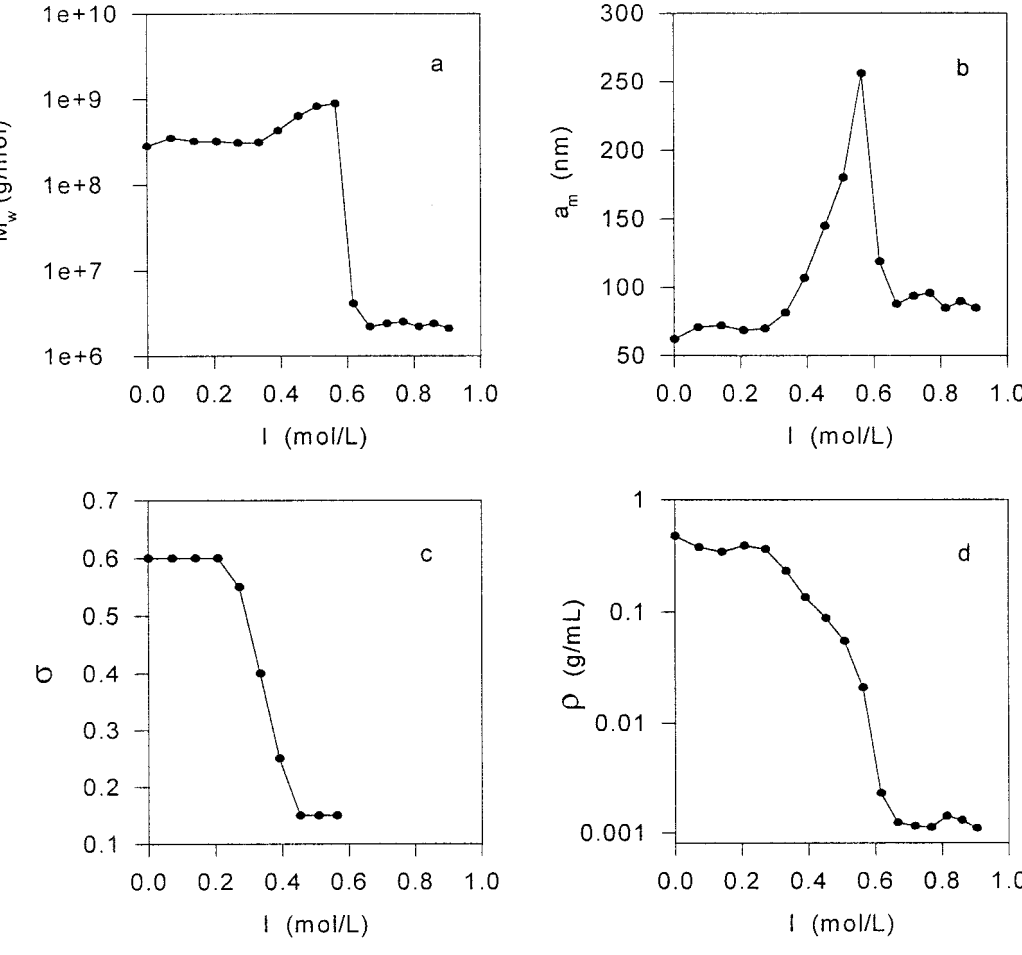

FIG. 21 Ionic strength dependence of the structural parameters of a complex between DADMAC-AA-47 (in excess) and NaPMA ($X = 0.6$) during subsequent addition of NaCl. a, particle mass; b, particle radius; c, polydispersity; d, structural density. (From Ref. 85.)

acrylate)/poly(ethylene oxide) (PEO) and poly(*N*-ethyl-4-vinylpyridinium bromide). The PECs self-assemble into micellelike structures, consisting of a core of the complex and a surrounding corona of the PEO chains. Complexes between polynucleotides or oligonucleotides and copolymers of a PEO and a cationic block were applied as vectors in gene therapy [14–16,88]. In [57] a graft polymer of a poly(methacrylate) backbone and PEO

side chains was used to stabilize PECs with PDADMAC samples of different molecular weights against flocculation approaching the 1:1 stoichiometric mixing ratio or induced by addition of salt. Even admixtures of such copolymers are sufficient to improve the colloidal stability of PECs between NaPSS and PDADMAC at higher ionic strengths.

Finally, we want to report on an interesting phenomenon observed in studying PECs between ionically modified temperature-sensitive polymers. The neutral water-soluble polymer PNIPAM has a lower critical solution temperature of about 34°C. The introduction of ionic groups by copolymerization of NIPAM leads to changes of the transition temperature or to a complete loss of the phase transition behavior [89]. The basic idea was that the ionic groups should become hydrophobic by complex formation, and the transition behavior should be reestablished. To check this, we prepared PECs between a cationically (AIFL 2) and an anionically (AIFL 3) modified PNIPAM with about 10 mol% of ionic groups and studied their temperature behavior. All measured scattering curves could be fitted in an excellent manner by relatively monodisperse systems of spheres with $\sigma_a = 0.2$ (see Figure 17). The structural parameters obtained are given in Figure 22. The changes in mass and size of the PEC with temperature result in a strong variation of the structural density, which is fully reversible. Therefore such complexes can act as temperature-controlled delivery systems of drugs.

Dynamic light scattering. Dynamic light scattering measurements provide the electric field correlation function $g(q, t)$, which can be expressed for a polydisperse system of particles as (see [90,91])

$$g(q, t) = \int_0^\infty G(q, \Gamma) e^{-\Gamma t}\, d\Gamma \tag{18}$$

where Γ is the decay constant or line width and $G(q, \Gamma)$ is the normalized distribution of Γ measured at a fixed value of q. Considering the center of mass motion of particles, Γ is given by

$$\Gamma = Dq^2 \tag{19}$$

where D is the translational diffusion coefficient. The correlation function (18) can be analyzed by an inverse Laplace transform (Provencher [92]), providing the distribution function of Γ, or by a series expansion of $\ln g(q, t)$ and a cumulant fit. For polydisperse systems the first cumulant represents the z-average of the diffusion coefficient. At finite concentrations and q values an apparent diffusion coefficient is obtained. Because of the high dilution of the PEC solutions, the concentration dependence of D_{app} may be neglected. For compact, nearly spherical particles the angular dependence is mainly caused by the polydispersity and can be written as

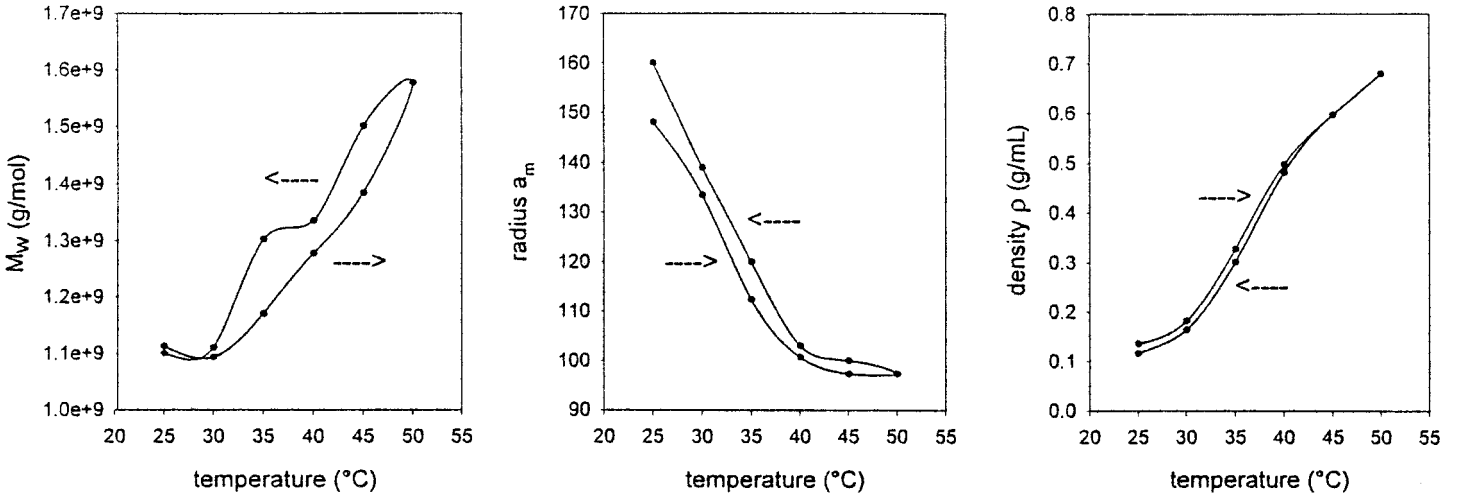

FIG. 22 Temperature behavior of the structural parameters of a PEC between ionically modified PNIPAM samples AIFL 2 and AIFL 3 (X = 0.6; AIFL 2 in excess, 0.01 M NaCl).

$$D_{app}(q) = \frac{\int_0^\infty D(M)P(q, M)Mp_w(M)\ dM}{\int_0^\infty P(q, M)Mp_w(M)\ dM} \tag{20}$$

Using the Einstein–Stokes equation $R_H = kT/6\pi\eta D$ one obtains

$$R_H^{app}(q) = \frac{\int_0^\infty a^3P(q, a)p_w(a)\ da}{\int_0^\infty a^2P(q, a)p_w\ da} \tag{21}$$

With regard to the polydispersity these quantities show a behavior opposite to that of the scattering functions. While the curves of $P_z(q)$ become flatter with rising polydispersity, the angular dependence of $R_H^{app}(q)$ increases (see [80]). Therefore the combination of static and dynamic light scattering provides reliable information about the polydispersity of the systems under study. Additional information on the polydispersity comes from the second cumulant and the inverse Laplace transform.

The hydrodynamic radius $R_H(q = 0)$ allows us to observe changes in particle size during PEC formation. The structure-sensitive parameter $\langle S^2\rangle_z^{1/2}/R_H$ has a value of 0.775 for spheres, but values well above 2 for elongated structures, so that the structure type can be judged. However, in our experience with highly aggregated and polydisperse PECs, $\langle S^2\rangle_z^{1/2}/R_H > 1$ may at least also partly result from the polydispersity. Using the logarithmic distribution function (12) one obtains for spheres

$$\frac{\langle S^2\rangle_z^{1/2}}{R_H} = 0.775\ \exp\left(\frac{3}{2}\ \sigma_a^2\right) \tag{22}$$

For values of $\sigma_a > 0.413$ this parameter becomes >1. The angular dependence of $R_H^{app}(q)$ of the PECs between PDADMAC and NaPSS at different polyelectrolyte concentrations could be fitted quite well using the structural parameters obtained from static light scattering (for details see [80]).

In [93–95] a combination of turbidimetry and static and dynamic light scattering was applied to study the structure of complexes between PDADMAC samples of different molecular weights and charged mixed micelles. A review on such studies of polyelectrolyte–protein complexes is given in [96].

Electrophoretic light scattering measurements. If an electric field of strength E acts on an isolated charged particle of charge Q, it causes a motion, which is at a velocity u balanced by the friction force. For a sphere one obtains the simple expression

$$u = \frac{EQ}{6\pi\eta a} \tag{23}$$

where η is the viscosity of the medium and a is the radius of the sphere. However, in real experiments the presence of low molecular ions must be taken into account. This leads to the formation of a diffuse electric double layer around the particle and complicated contributions to its motion (for details see [97]). In a good approximation one obtain the Henry's law:

$$U_E = \frac{u}{E} = \frac{Qf(\kappa a)}{6\pi\eta a(1 + \kappa a)} \tag{24}$$

where U_E is the electrophoretic mobility, κ is the Debye-Hückel constant and $f(\kappa a)$ a function that varies with increasing κa from 1 to 1.5. The introduction of the zeta potential ζ, which is the potential in the shear plane of the moving charged particle, leads to the generalized form of Henry's equation:

$$U_E = \frac{D_e \zeta f(\kappa a)}{6\pi\eta} \tag{25}$$

where D_e is the dielectric constant.

In dynamic light scattering experiments the motion of a particle with constant velocity results in a Doppler shift in the frequency spectrum. In a heterodyne experiment (mixing of a small portion of the unscattered light with the scattered one on the photomultiplier) this shift $\Delta\omega$ can be directly determined from the power spectrum [98], providing the electrophoretic mobility by the simple relation

$$\Delta\omega = U_E E\mathbf{q} \cos \phi \tag{26}$$

where ϕ is the angle between the vector $\mathbf{q}$ and the applied field. Under certain assumptions U_E can then be converted into ζ. In combination with the measurement of R_H, electrophoretic light scattering yields information on the effective charge of colloidal particles.

Buchhammer and Lunkwitz [43,52,99] employed electrophoretic light scattering to determine the ζ potential of complexes between PDADMAC and various polyanions in dependence on the mixing ratio and salt content, using such PECs as coating material or flocculants. A combination of turbidimetry and static, dynamic, and electrophoretic light scattering was used

in [100,101] to characterize the structure of PECs between synthetic polyelectrolytes and proteins in detail.

V. CONCLUSIONS AND OUTLOOK

Polyelectrolyte complexes are of rapidly growing interest in practical applications as well as from the viewpoint of fundamental research. Despite many papers published in this area during the last decades, we are far from a complete understanding of the effects that govern the formation and properties of the complexes. This is especially true for highly aggregating systems. Comprehensive studies with an appropriate combination of methods are necessary to obtain detailed information on their stoichiometry, structure, and stability. This chapter should give an overview about the information provided by the different techniques of investigation, stressing particularly highly aggregated complexes between synthetic polyelectrolytes with strong ionic groups. In highly diluted solutions particles on a colloidal level are formed. Especially in pure water, PEC formation takes place far from thermodynamic equilibrium, mainly governed by the kinetics of the process and leading to frozen structures. The findings reported about their characterization lead to a structure model, the scheme of which is represented in Figure 23.

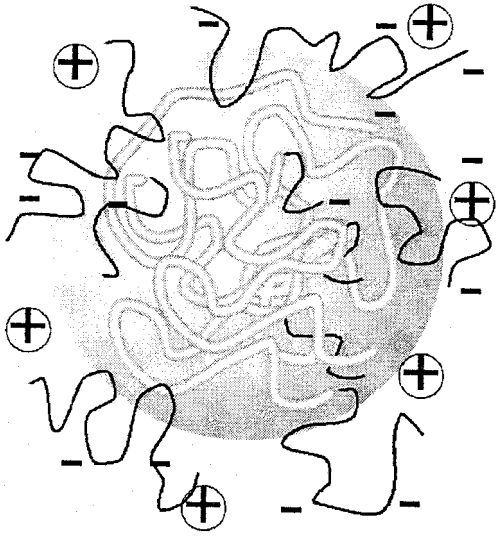

FIG. 23 Structure model of highly aggregated PECs between synthetic polyelectrolytes. (From Ref. 82.)

The PEC particles consist of a neutralized compact core surrounded by a charged shell of the component in excess at nonstoichiometric mixing ratios. This shell stabilizes the particle with respect to further coagulation. Long-term stability of the PEC particles in the range of months was observed. The level of aggregation reaches up to several thousand chains and is mainly controlled by the concentration of the component solutions. The compactness of the core can be varied via the charge densities of the components. The level of aggregation can also drastically be reduced by the presence of small amounts of salt during PEC formation.

Subsequent addition of salt may be critical in different aspects. A low molecular electrolyte screens the stabilizing shell and leads to secondary aggregation and finally to flocculation of the PEC particles. For complexes with carboxylic groups as anionic sites a strong swelling with increasing ionic strength and a complete dissolution of the PECs at a critical salt concentration were observed. By the use of double hydrophilic polyelectrolytes with poly(ethylene oxide) chains, even as admixtures, secondary aggregation can be suppressed via steric stabilization. The presence of salt enables long-term exchange and substitution processes.

Summarizing, we can state that stable PEC particles on a nm scale with a desired level of mass and size and also degree of swelling can be prepared. Such particles could be of general interest as carrier systems for drugs and biologically active materials such as enzymes. Charged subjects can easily be incorporated during complex formation into the matrix of the PECs. Depending on the nature of the polyelectrolytes, the degree of swelling of the PEC particles, i.e., the release or accessibility of the embedded materials, may be controlled by external parameters such as the ionic strength and the pH value of the medium or also by temperature.

REFERENCES

1. Kossel A. Über die basischen Stoffe des Zellkerns. Hoppe-Seiler's Z Physiol Chem 1896; 22:176–187.
2. Willststaetter R, Rohdewald M. Über den Zustand des Glykogens in der Leber, im Muskel und in Leukocyten. Hoppe-Seiler's Z Physiol Chem 1934; 225:103–124.
3. Michaels AS, Miekka RG. Polycation–polyanion complexes: preparation and properties of poly(vinylbenzyltrimethylammonium) poly(styrenesulfonate). J Phys Chem 1961; 65(10):1765–1773(a). Micheals AS, Mir I, Schneider NS. A conductometric study of polycation–polyanion reactions in dilute aqueous solution. J Phys Chem 1965; 69(10):1447–1455(b).
4. Kokufuta E, Matsumoto W, Nakamura I. Use of polyelectrolyte complexes for immobilization of microorganisms. J Appl Polym Sci 1982; 27(7):2503–2512.

5. Dautzenberg H, Lukanoff B, Eckert U, Tiersch B, Schuldt U. Immobilization of biological matter by polyelectrolyte complex formation. Ber Bunsenges Phys Chem 1996; 100(6):1045–1053.
6. Lysaght MJ, Aebischer P. Encapsulated cells as therapy. Scientific American 1999; 280(4):76–82.
7. Hunkeler D, Prokop A, Cherrington A, Rajotte R, Sefton M. Bioartificial Organs II. Technology, Medicine and Materials. Annals of the New York Academy of Sciences 1999; 875.
8. Decher G, Lehr B, Lowack K, Lvov Y, Schmitt J. New nanocomposite films for biosensors—layer-by-layer adsorbed films of polyelectrolytes, proteins or DNA. Biosensors Bioelectronics 1994; 9:677–684.
9. Decher G, Eckle M, Schmitt J, Struth B. Layer-by-layer assembled multicomposite films. Current Opinion in Colloid Interface Science 1998; 3(1):32–39.
10. Kabanov VA. Basic properties of soluble interpolyelectrolyte complexes applied to bioengineering and cell transformation. In: Dubin P, Bock J, Davies RM, Schulz DN, Thies C, eds. Macromolecular Complexes in Chemistry and Biology. Berlin: Springer Verlag, 1994:151–174.
11. Dautzenberg H, Karibyants N, Zaitsev SY. Immobilization of trypsin in polycation–polyanion complexes. Macromol Rapid Commun 1997; 18:175–182.
12. Dainiak MB, Izumrudov VA, Muronetz VI, Mattiason B. Conjugates of monoclonal antibodies with polyelectrolyte complexes—an attempt to make an artificial chaperone. Biochim Biophysica Acta—General Subject 1998; 1381(3):279–285.
13. Anderson MA, Hatti-Kaul R. Protein stabilising effect of polyethyleneimine. J Biotechnology 1999; 72(1–2):21–31.
14. Kabanov AV, Vinogradov SV, Suzdaltseva YG, Alakhov VY. Water-soluble block polycations as carriers for oligonucleotide delivery. Bioconjugate Chem 1995; 6(6):639–643.
15. Konak C, Mrkvickova L, Nazarova O, Ulbrich K, Seymour LW. Formation of DNA complexes with diblock copolymers of poly(N-(2-hydroxypropyl)methacrylamide) and polycations. Supramolecular Science 1998; 5:67–74.
16. Wolfert MA, Schacht EH, Toncheva V, Ulbrich K, Nazarova O, Seymour LW. Characterization of vectors for gene therapy formed by self-assembly of DNA with synthetic block co-polymers. Human Gene Therapy 1996; 7(17):2123–2133.
17. Asayama S, Muruyama A, Cho CS, Akaike T. Design of comb-type polyamine copolymers for a novel pH-sensitive DNA carrier. Bioconjugate Chem 1997; 8(6):833–838.
18. Zezin AB, Kabanov VA. New form of the polyelectrolytes water-soluble complexes. Usp Khim 1982; 51(9):1447–1483.
19. Kabanov VA, Zezin AB. Soluble interpolymeric complexes as a new class of synthetic polyelectrolytes. Pure Appl Chem 1984; 56(3):343–354.
20. Tsuchida E. Osada Y, Sanada K. Interaction of poly(styrene sulfonate) with polycations carrying charges in the chain backbone. J Polym Sci A-1 1972; 10:3397–4003.
21. Tsuchida E, Osada Y, Ohno H. Formation of interpolymer complexes. J Macromol Sci 1980; B 17(4):683–714.

22. Tsuchida E, Abe K. Interactions between macromolecules in solution and intermacromolecular complexes. Adv Polym Sci 1982; 45:1–130.
23. Philipp B, Dawydoff W, Linow KJ. Polyelektrolytkomplexe—Bildungsweise, Struktur und Anwendungsmöglichkeiten. Zeitschrift für Chemie 1982; 22(1): 1–13.
24. Bakeev KN, Izumrudov VA, Kabanov VA. Kinetics and mechanism of reactions of the formation of polyelectrolytic complexes. Doklad Akad Nauk SSSR 1988; 299:1405–1408.
25. Izumrudov VA, Kharenko OA, Kharenko AV, Gulaeva ZG, Kasaikin VA, Zezin AB, Kabanov VA. Behavior of nonstoichiometric polyelectrolyte complexes in aqueous salts solutions. Visokomol Soed 1980; A22(3):692–699.
26. Pergushov DV, Izumrudov VA, Zezin AB, Kabanov VA. Effect of low-molecular-mass salts on the behavior of water-soluble nonstoichiometric polyelectrolyte complexes. Polymer Science, Ser A 1993; 35(7): 844–849.
27. Bakeev KN, Izumrudov VA, Kuchanov SI, Zezin AB, Kabanov VA. Kinetics and mechanism of the macromolecular exchange in an interpolyelectrolytic complex. Doklad Akad Nauk SSSR 1988; 300(1):132–135.
28. Papisov IM, Litmanovich AA. Molecular ''recognition'' in interpolymer interactions and matrix ''polymerization.'' Adv Polym Sci 1989; 90:139–179.
29. Izumrudov VA, Bronich TK, Saburova OS, Zezin AB, Kabanov VA. The influence of chain-length of a competitive polyanion and nature of monovalent counterions on the direction of the substitution-reaction of polyelectrolyte complexes. Makomol Chem Rapid Comm 1988; 9(1):7–12.
30. Kokufuta E. Colloid titration behavior of poly(ethyleneimine). Macromolecules 1979; 12:350–351.
31. Manning GS. Limiting laws and counterion condensation in the polyelectrolyte solution I. Colligative properties. J Chem Phys 1969; 51:924–933.
32. Philipp B, Dautzenberg H, Linow KJ, Koetz J, Dawydoff E. Polyelectrolyte complexes—recent developments and open problems. Progr Polym Sci 1989; 14:91–172.
33. Philipp B, Kötz J, Dautzenberg H, Dawydoff W, Linow KJ. Analytical characterization of simplex formation and simplex structure. In: Mitchell J, ed. Applied Polymer Analysis and Characterization. München: Hanser Verlag, 1991; 2:281–310.
34. Webster L, Huglin MB. Observations on complex formation between polyelectrolytes in dilute aqueous solution. Eur Polym J 1997; 33(7):1173–1177.
35. Webster L, Huglin MB. Complex formation between polyelectrolytes in dilute aqueous solution. Polymer 1997; 38(6):1373–1380.
36. Denunziere A, Ferrier D, Domard A. Chitosan–chondritoin sulfate and chitosan–hyaluronate polyelectrolyte complexes. Physico-chemical aspects. Carbohydr Polym 1996; 29:317–323.
37. Zhang H, Dubin PL, Spindler R, Tomalia D. Binding of carboxylated starbust dendrimers to poly(diallyldimethylammonium chloride). Ber Bunsenges Phys Chem 1996; 100(6):923–928.
38. Wen Y, Dubin PL. Potentiometric studies of the interaction of bovine serum albumin and poly(diallyldimethylammonium chloride). Macromolecules 1997; 30:7856–7861.

39. Sato T, Mattison KW, Dubin PL, Kamachi M, Morishima Y. Effect of protein aggregation on the binding of lysozyme to pyrene-labeled polyanions. Langmuir 1998; 14:5430–5437.
40. Dautzenberg H, Hartmann J, Grunewald S, Brand F. Stoichiometry and structure of polyelectrolyte particles in diluted solutions. Ber Bunsenges Phys Chem 1996; 100(6):1024–1032.
41. Brand F, Dautzenberg H, Jaeger W, Hahn M. Polyelectrolytes with various charge densities: synthesis and characterization of diallyldimethylammonium chloride acrylamide copolymers. Appl Macromol Chem 1997; 248:41–71.
42. Kerker M. The Scattering of Light and other Electromagnetic Radiation. Volume 16 of Physical Chemistry. New York: Academic Press, 1969.
43. Buchhammer HM, Lunkwitz K, Pergushov DV. Salt effect on surface modification of silica by interpolyelectrolyte complexes. Macromol Symp 1997; 126:157–171.
44. Deng SM, Li X. Formation of polyelectrolyte complexes based on pendant-type imidazolinium organosilicon polymer with poly(sodium acrylate). J Macromol Sci Pure Appl Chem 1997; A34(4):695–704.
45. Park JM, Muhaberac BB, Dubin PL, Xia J. Effects of protein charge heterogeneity in protein–polyelectrolyte complexation. Macromolecules 1992; 25: 290–295.
46. Mattison KW, Dubin PL, Brittain IJ. Complex formation between bovine serum albumin and strong polyelectrolytes: effect of polymer charge density. J Phys Chem B 1998; 102:3830–3836.
47. Karibyants N, Dautzenberg H. Preferential binding with regard to chain length and chemical structure in the reactions of formation of quasi-soluble polyelectrolyte complexes. Langmuir 1998; 14:4427–4434.
48. Terayama H. Method of colloid titration (a new titration between polymer ions). J Polym Sci 1952; 8:243–253.
49. Wassmer KH, Schroeder U, Horn D. Characterization and detection of polyanions by direct polyelectrolyte titration. Makromol Chem 1991; 192:553–565.
50. Hattori T, Katai K, Kato M, Izume M, Mizuta Y. Colloidal titration of chitosan and critical unit of chitosan to the potentiometric colloidal titration with poly(vinyl sulfate) using toluidine blue as indicator. Bull Chem Soc Jpn 1999; 72:37–41.
51. Berth G, Dautzenberg H, Peter MG. The heterogeneity of industrial chitosans. Carbohydr Polym 1999; submitted.
52. Pergushov DV, Buchhammer HM, Lunkwitz K. Effect of a low-molecular-weight salt on colloidal dispersions of interpolyelectrolyte complexes. Colloid Polym Sci 1999; 277:101–107.
53. Einstein A. Eine neue Bestimmung der Moleküldimensionen. Ann Phys 1906; 19:289–306.
54. Brand F, Dautzenberg H. Structural analysis in interpolyelectrolyte complex formation of sodium poly(styrenesulfonate) and diallyldimethylammonium chloride–acrylamide copolymers by viscometry. Langmuir 1997; 13(11): 2905–2910.
55. Dragan S, Cristea M, Luca C, Simionescu BC. Polyelectrolyte complexes. 1.

Synthesis and characterization of some insoluble polyanion–polycation complexes. J Polym Sci Part A Polym Chem 1996; 34(17):3485–3494.
56. Kuderbaigenov SE, Nurkeeva ZS, Sigitov VB, Akimbekova KZ, Ushanov VZ. Interpolyelectrolyte complexes of poly[4-(but-3-en-1-ynyl)-1-methylpiperidin-4-ol] with poly(carboxylic acids). Macromol Chem Phys 1997; 189:183–191.
57. Dautzenberg H. Polyelectrolyte complex formation: role of a double hydrophilic polymer. Macromol Chem Phys 1999; submitted.
58. Fujita H. Foundations of Ultracentrifuge Analysis. New York: John Wiley, 1975.
59. Karibyants N, Dautzenberg H, Cölfen H. Characterization of PSS/PDADMAC-co-AA polyelectrolyte complexes and their stoichiometry using analytical ultracentrifugation. Macromolecules 1997; 30:7803–7809.
60. Milthorpe BK, Jeffrey PD, Nichol LW. New method for characterizing associating protein systems involving sedimentation equilibrium analysis. P Aust Biophys Chem 1975; 3(2):169–176.
61. Izumrudov VA. Competitive reactions in solutions of protein–polyelectrolyte complexes. Ber Bunsenges Phys Chem 1996; 100(6):1017–1023.
62. Hugerth A, Lelham NC, Sundelöf LO. The effect of charge density and conformation on the polyelectrolyte complex formation between carrageenan and chitosan. Carbohydr Polym 1997; 34:149–156.
63. Trinh CK, Schnabel W. Polyelectrolyte complexes of binary and ternary systems containing poly(sodium styrene sulfonate), poly(sodium phosphate), and poly(*N*-ethyl-4-vinylpyridinium bromide). Angew Makromol Chem 1994; 221:127–135.
64. Dautzenberg H, Linow KJ, Rother G. The formation of water-soluble polysalts. 6. Investigation of the stoichiometry of simplexes and of the preferential bonding from polymer mixtures. Acta Polymerica 1990; 41(2):98–102.
65. Pergushov DV, Izumrudov VA, Zezin AB, Kabanov AV. Stability of interpolyelectrolyte complexes in aqueous saline solutions—effect of the degree of polymerization of polyions. Vysokomol Soedin 1995; 37(10):1739–1746.
66. Mizusaki M, Morishima Y, Dubin PL. Interaction of pyrene-labeled hydrophobically modified polyelectrolytes with oppositely charged mixed micelles studied by fluorescence quenching. J Phys Chem 1998; 102:1908–1915.
67. Mizusaki M, Morishima Y, Yoshida K, Dubin PL. Interactions of micelles with fluorescence-labeled polyelectrolytes. Colloid Surfaces 1999; 147:149–159.
68. Harrison CA, Tan JS. Differential size-exclusion chromatography for the analysis of gelatin-polyelectrolyte complexes. J Polym Sci Part B Polym Phys 1999; 37:275–280.
69. Tan JS, Harrison CA, Caldwell KD. Characterization of soluble polyelectrolyte–gelatin complexes by differential size-exclusion chromatography and flow field flow fractionation. J Polym Sci Part B Polym Phys 1998; 36:537–542.
70. Hallberg RK, Dubin PL. Effect of pH on the binding of beta-lactoglobulin to sodium polystyrenesulfonate. J Phys Chem B 1998; 102(43):8629–8633.

71. Gao JY, Dubin PL, Muhoberac BB. Capillary electrophoresis and dynamic light scattering studies of structure and binding characteristics of protein–polyelectrolyte complexes. J Phys Chem B 1998; 102(28):5529–5535.
72. Gao JY, Dubin PL. Binding of proteins to copolymers of varying hydrophobicity. Biopolymers 1999; 49:185–193.
73. Vethamutu MS, Dubin PL, Almgren M, Li Y. Cryo-TEM of polyelectrolyte–micelle complexes. J Coll Interface Sci 1997; 186:414–419.
74. Schmal G, Rudolph D, Niemann B, Guttsmann P, Thieme J, Schneider G, David C, Diehl M, Wilhein T. X-ray microscopy studies. Optik 1993; 93:95–102.
75. Schmal G, Rudolph D, Guttsmann P, Schneider G, Thieme J, Niemann B. Phase-contrast studies of biological specimens with the x-ray microscope at BESSY. Rev Sci Instrum 1995; 66:1282–1286.
76. Wolfert MA, Seymour LW. Atomic force microscopic analysis of the influence of the molecular weight of poly(L)lysine on the size of the polyelectrolyte complexes formed with DNA. Gene Therapy 1996; 3:269–273.
77. Dautzenberg H, Rother G. Interpretaton of light-scattering from supermolecular structures in liquid-systems by master curves. J Polym Sci Part B Polym Phys 1988;26:353–366.
78. Dautzenberg H, Rother G. Supermolecular structures in polymer solutions—interpretaion of static light-scattering data. Makromol Chem Macromol Symp 1992; 61:94–113.
79. Dautzenberg H. Light scattering studies on polyelectrolyte complexes. Makromol Chem Macromol Symp 1999; submitted.
80. Dautzenberg H, Rother G, Hartmann J. Light scattering studies of polyelectrolyte complex formation: effect of polymer concentration. In: Schmitz KS, ed. Macroion Characterization: From Dilute Solution to Complex Fluids. ACS Symposium Series 548. Washington, DC: American Chemical Society, 1994: 210–224.
81. Dautzenberg H. Polyelectrolyte complex formation in highly aggregating systems: 1. Effect of salt: polyelectrolyte complex formation in the presence of salt. Macromolecules 1997; 30:7810–7815.
82. Dautzenberg H, Karibyants N. Polyelectrolyte complex formation: effect of salt. In: Noda I, Kokufuta E, eds. Polyelectrolytes. Yamada Conference L. Osaka, Japan: Yamada Science Foundation, 1999:284–287.
83. Dautzenberg H, Linow KJ, Philipp B. The formation of water-soluble polysalts (simplexes) of anionic and cationic copolymers of acrylamide. 2. Effect of charge-density and conversion on the structure of the simplexes. Acta Polymerica 1982; 33(11):619–625.
84. Dautzenberg H, Koetz J, Linow KJ, Philipp B, Rother G. Light scattering of polyelectrolyte complex solutions. In: Dubin P, Bock J, Davies RM, Schulz DN, Thies C, eds. Macromolecular Complexes in Chemistry and Biology. Berlin: Springer Verlag, 1994:119–134.
85. Dautzenberg H, Karibyants N. Polyelectrolyte complex formation in highly aggregating systems. Effect of salt: response to subsequent addition of NaCl. Macromol Chem Phys 1999; 200:118–125.
86. Trinh CK, Schnabel W. Ionic strength dependence of the stability of polyelectrolyte complexes. Angew Makromol Chem 1993; 212:167–179.

87. Kabanov AV, Bronich TK, Kabanov VA, Yu K, Eisenberg A. Soluble stoichiometric complexes from poly(*N*-ethyl-4-vinylpyridinium) cations and poly(ethyleneoxide)-block-polymethacrylate anions. Macromolecules 1996; 29:6797–6802.
88. Oupicky D, Konak C, Ulbrich K. DNA complexes with block and graft copolymers of *N*-(2-hydroxypropyl) methacrylamide and 2-(trimethylammonio)ethyl methacrylate. J Biomater Sci Polymer Edn 1999; 10(5):573–590.
89. Hahn M, Goernitz E, Dautzenberg H. Synthesis and properties of ionically modified polymers with LCST behavior. Macromolecules 1998; 31:5616–5623.
90. Chu B. Laser Light Scattering. 2d ed. Boston: Academic Press, 1991.
91. Schmitz KS. Dynamic Light Scattering by Macromolecules. San Diego: Academic Press, 1990.
92. Provencher SW. A constrained regularization method for inverting data represented by linear algebraic or integral-equations. Comp Phys Comm 1982; 27(3):213–227.
93. Li Y, Xia J, Dubin PL. Complex-formation between polyelectrolyte and oppositely charged mixed micelles—static and dynamic light-scattering study of the effect of polyelectrolyte molecular-weight and concentration. Macromolecules 1994; 27:7049–7055.
94. Li Y, Dubin PL, Havel HA, Edwards SH, Dautzenberg H. Electrophoretic light-scattering, dynamic light-scattering, and turbidimetry studies of the effect of polymer concentration on complex-formation between polyelectrolyte and oppositely charged mixed micelles. Macromolecules 1995; 28:3098–3102.
95. Li Y, Dubin PL, Dautzenberg H, Lueck U, Hartmann J, Tuzar Z. Dependence of structure of polyelectrolyte/micelle complexes upon polyelectrolyte chain-length and micelle size. Macromolecules 1995; 28:6795–6798.
96. Xia J, Dubin PL. Protein–polyelectrolyte complexes. In: Dubin P, Bock J, Davies RM, Schulz DN, Thies C, eds. Macromolecular Complexes in Chemistry and Biology. Berlin: Springer Verlag, 1994:247–271.
97. Tanford Ch. Physical Chemistry of Macromolecules. New York: John Wiley, 1965.
98. Berne BJ, Pecora R. Dynamic Light Scattering. Malabar, Florida: Robert E Krieger, 1990.
99. Petzold G, Nebel A, Buchhammer HM, Lunkwitz K. Preparation and characterization of different polyelectrolyte complexes and their application as flocculants. Colloid Polym Sci 1998; 276:125–130.
100. Xia J, Dubin PL, Dautzenberg H. Light-scattering, electrophoresis, and turbidimetry studies of bovin serum-albumin poly(dimethyldiallylammonium chloride) complex. Langmuir 1993; 9:2015–2019.
101. Tsuboi A, Izumi T, Hirata M, Xia J. Dubin PL, Kokufuta E. Complexation of proteins with a strong polyanion in an aqueous salt-free solution. Langmuir 1996; 12:6295–6303.

21

Surfactant Binding to Polyelectrolytes

KSENIJA KOGEJ and JOŽE ŠKERJANC University of Ljubljana, Ljubljana, Slovenia

I. INTRODUCTION

When a polymeric electrolyte is dissolved in water it can ionize completely or to some extent, depending on the nature of the functional groups. Strong polyelectrolytes, for example poly(styrenesulfonic acid), are representatives of the first class. Weak polyelectrolytes belong to the second class. The majority of the weak polyacids are carboxylic acids, and practically all properties of interest in the field of polyelectrolytes have been accumulated for their simplest representatives, such as poly(acrylic acid). The polyion charge of weak polyacids can be varied by titration with a strong base. As a consequence, the properties of these polymeric species are gradually changing from those of an uncharged polymer to those of a typical polyelectrolyte.

Each polyion in solution is accompanied by an equivalent amount of small counterions of opposite charge. It is well known that because of the high electrical charge on the polymer chain a large number of counterions is expected to stay near the polyion. Unfortunately, no experimental method can distinguish among the several ways by which the counterions interact with the polyion. They may be covalently bound to the charged groups, involved in a specific short-range interaction at such sites in the form of ion pairs (''site binding''), or held by long-range Coulombic forces in the ionic atmosphere close to the polyion (''ionic atmosphere binding'') [1–3].

A similar physical picture of counterion binding can be adopted for systems containing surfactant counterions, although in this case some additional effect may be expected. The main factors that influence the binding of ionic surfactants to polyelectrolytes with opposite charge are (1) the charge density of the polyion, λ, (2) the hydrophobic character of the surfactant (the length of its hydrocarbon chain), (3) the additional attractive forces between the

polyelectrolyte and surfactant micelles in case hydrophobic functional groups are present on the polyelectrolyte chain.

A rational description of ionic atmosphere binding is provided by the Poisson–Boltzmann equation and the cylindrical cell model. Figure 1 is an example of such computations and shows the variation of the local concen-

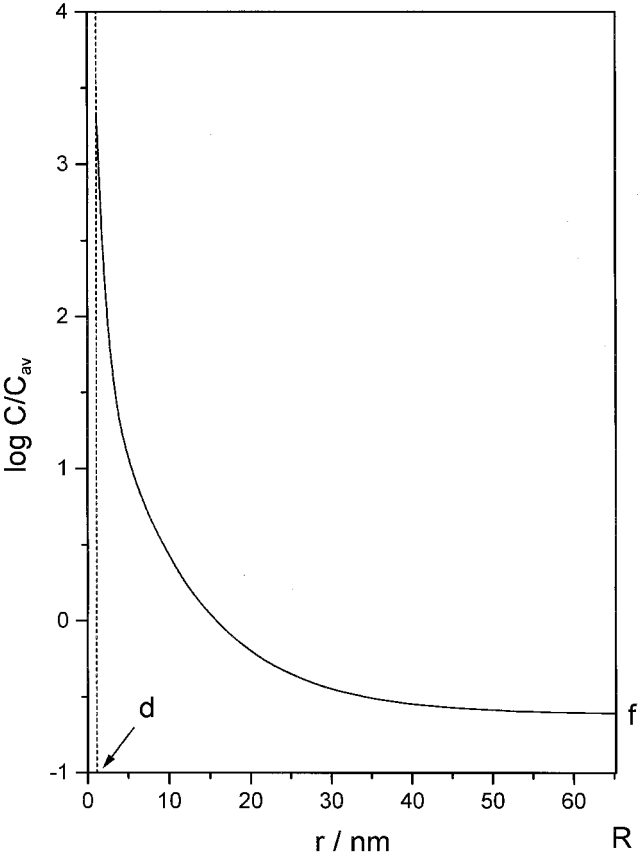

FIG. 1 Variation of the local concentration, C, of the monovalent counterion of radius 0.3 nm with the radial distance, r, from the axis of the cylindrical polyion of radius $a = 0.8$ nm. The average counterion concentration is marked by C_{av}, d is the exclusion distance from the polyion axis to the center of the counterion, and f is the fraction of free counterions. The value of the charge density parameter $\lambda = 2.83$ is typical for aqueous solutions of poly(styrenesulfonates) at 25°C, and the value of the radius of the cell $R = 65.2$ nm corresponds to the polyelectrolyte concentration $C_P = 5 \times 10^{-4}$ monomol dm^{-3}.

tration of monovalent counterions with the radial distance from the axis of the cylindrical polyion [4]. The parameters used in calculations are typical for poly(styrenesulfonate) anion and alkylpyridinium cation in water. Figure 1 demonstrates that the local concentration of the counterions (the radius of the counterion roughly corresponds to the distance to which the positive charge on the pyridinium cation can approach the polyion axis) exceeds the average concentration by a factor of about 1800 at the polyion surface and by a factor 100 at a radial distance comparable to the length of dodecylpyridinium or cetylpyridinium hydrocarbon chain. One may thus conclude that due to pure electrostatic interactions between poly(styrenesulfonate) anion and detergent counterions there is also an extensive accumulation of nonpolar parts of the surfactant molecules in the vicinity of the polymer. As a consequence, the aggregation process takes place in these regions already at a total surfactant concentration that is a few orders of magnitude below the critical micellization concentration, cmc. The resulting small aggregates behave as multivalent ''minimicelles'' and become ''trapped'' in the regions of high electrostatic potential close to the macroion. A similar model for binding of detergent (dodecyltrimethylammonium bromide) to polyelectrolyte (sodium poly(styrenesulfonate)) has been proposed by Abuin and Scaiano [5] on the basis of experimental data. From laser flash and luminescence measurements they have estimated that the aggregation numbers of these aggregates are much smaller than ordinary micellar aggregation numbers.

Besides the macroion charge density (factor 1), the charge of the counterions also plays a crucial role in this ionic atmosphere binding. The counterions of higher charge cluster much more extensively around the polyion than the counterions of lower charge [6], and among the ions of the same charge, the smaller ones predominate in the population of bound ions [7].

The second factor outlined above, i.e., the hydrophobic character of the surfactant, makes the difference between the so-called cooperative surfactant binding and the binding of simple inorganic counterions, which is anticooperative. As discussed above, the extensive accumulation of the nonpolar parts of surfactant ions in the vicinity of the polyion leads to the self-aggregation of surfactant into ''minimicelles,'' more often called polyelectrolyte-induced micelles. The process is similar to ordinary micellization in that the main driving force for the aggregation is the tendency of surfactant hydrocarbon chains to minimize their contact with water (this is the origin of the so-called ''hydrophobic effect''; see Ref. 8). Once the charged-polyelectrolyte-induced micelle is formed it binds extremely strongly to the polyion as a multivalent counterion. The distribution of surfactant ions along the polyion cylinder is therefore not uniform as in the case of simple counterions. On the contrary, they are localized in the form of self-assembled aggregates at

discrete parts of the polyelectrolyte chain. It has been found by various thermodynamic and transport property measurements in mixed polyelectrolyte–surfactant solutions [9,10] that the part of the polyion to which surfactant aggregates are bound is thermodynamically inactive, whereas the free part behaves as fully charged rod with unchanged charge density up to approximately 50% complexation. At higher degrees of complexation, the shielding of the polyion by the surfactant aggregates becomes more extensive due to the change in chain conformation, and the measured properties exhibit a definite change in their behavior. This observation is a confirmation of the cooperative nature of surfactant binding described above. A schematic presentation of the first two steps in the binding process is given in Scheme 1.

Because the main driving force for surfactant self-association in polymer–surfactant mixed systems is the hydrophobic effect, the binding of surfactants to polyelectrolytes exhibits a similar dependence on the length of the alkyl chain as known for free micellization. Surfactants with longer hydrocarbon chains bind more strongly to polyions than those with shorter chains, and the binding starts a lower surfactant concentrations. In this context, a convenient parameter to characterize polyelectrolyte–surfactant systems is the critical aggregation concentration, cac, which is a counterpart of the well-known critical micellization concentration, cmc, but applies to solutions of surfactants in the presence of a polymer. It is defined as the

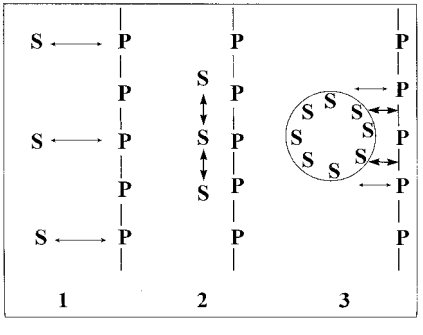

SCHEME 1 Interaction scheme for the binding of ionic surfactants (S) to oppositely charged polyelectrolyte (P). The steps in the binding process as discussed in the text: (1) electrostatic binding; (2) cooperative binding; (3) additional hydrophobic forces between the aggregates surfactant and the polyelectrolyte chain. A thinner and longer arrow symbolizes long-range Coulomb forces between charged species, whereas a thicker and shorter one represents ''hydrophobic forces'' acting between surfactant alkyl chains or between the hydrocarbonlike micellar core and the polyion chain.

surfactant concentration at the onset of ''cooperative binding'' [11]. The term cac unmistakably leads to a notion of micelle-like surfactant aggregates starting to form over a relatively narrow concentration range. The cac decreases with increasing hydrocarbon chain length of the surfactant similarly to the cmc. There is, however, an important distinction between both concentration parameters: the cac can be several orders of magnitude lower than the cmc depending on the nature of the polyion and surfactant ion. The reduction of the cac relative to the cmc is a convenient measure of the strength of attractive polyelectrolyte–surfactant interactions.

Finally, the third factor that has a substantial influence on surfactant binding to polyelectrolytes is additional specific attractive forces between species that assist and even further promote their mutual aggregation. This is schematically depicted by step 3 in Scheme 1. Important here is the hydrophilic/hydrophobic character of the functional groups on the polymer. For example, some water-soluble polyelectrolytes, like sodium poly(styrenesulfonate), may be considered to be partly hydrophobic because of the presence of aromatic side groups on the chain. These groups have a natural tendency to avoid contact with water, consequently they would solubilize in hydrophobic microdomains, such as surfactant micelles, if available within the system. It has been shown by NMR measurements performed in solutions of sodium poly(styrenesulfonate) and dodecyltrimethylammonium bromide [12] that the aromatic groups of poly(styrenesulfonate) anion are located near the surface of surfactant micelle (primarily at the interface of the ionic micelle near the β-CH_2 group of the surfactant hydrocarbon chain). Accordingly, the hydrophobic portion of the polyelectrolyte chain is taking part in the formation of the complex. Some authors therefore use for these complexes terms like mixed micelles [13] or aggregate of aggregates [5]. On the other hand, hydrophilic polyelectrolytes with for example sulphate or carboxyl side groups, such as poly(vinyl sulfonate) and poly(acrylate), like contact with water. They have no tendency to take part in micelle formation and in this case the polymer–surfactant attractions are purely electrostatic. For such systems, step 3 in Scheme 1 is irrelevant. In the presence of these polyelectrolytes more familiar surfactant micelles are formed without intimate involvement of the polyelectrolyte chain. They are bound to the polyion through Coulombic interactions as multivalent counterions, and if the polyion chain is flexible enough it wraps around the aggregated surfactants.

In addition to the above two cases, the hydrophobic character of the polymer can also be enhanced or subsequently introduced into the macromolecule through synthetic routes by attaching a small amount of hydrophobes to the chain [14]. The hydrophobes can be hydrophobic groups like alkyl chains or nonpolar aromatic dyes. These polymers are known as hydrophobically modified polyelectrolytes. Recently, much of the research in

this field was devoted to pyrene-labeled polyelectrolytes and their interactions with surfactants [15].

In light of the above discussion, we can distinguish three idealized categories of polyelectrolyte–surfactant complexes with the emphasis on the role of the polymer chain in the process of complexation. Listed in order of increasing hydrophobic character of the polyion these complexes can be grouped into those containing (1) hydrophilic polyelectrolytes, (2) hydrophobic polyelectrolytes, or (3) hydrophobically modified polyelectrolytes. We shall confine ourselves here to the first two groups and will omit the treatment of the third group.

II. EXPERIMENTAL

The experimental methods employed in the study of polymer–surfactant interactions are numerous. We will consider the experimental approaches and results that present our experience in this field, and these are by no means complete. In the course of the years we investigated two vynilic synthetic polyelectrolytes, sodium poly(acrylate), NaPA, and sodium poly(styrenesulfonate), NaPSS. Their molecular weights were 10,000 g/mol and 70,000 g/mol for NaPA and NaPSS, respectively. First, we will present and discuss the binding isotherms from the viewpoint of the three most important factors governing the binding phenomena, i.e., polyion charge density, surfactant chain length, and hydrophobicity of the polyelectrolyte. In the following, the enthalpies of binding will be presented. The complexation of surfactant with polyelectrolyte is accompanied by the coiling of the polyelectrolyte chain around surfactant aggregates, which will be demonstrated through viscosity, volume changes, and conductivity measurements. Finally, critical aggregation concentration values of a homologous series of cationic surfactants in the presence of the above-mentioned polyelectrolytes will be given.

The point of interest in NaPA (a weak polyelectrolyte with degree of ionization 1) and NaPSS (a strong polyelectrolyte) is that they have the same linear charge density parameter, λ, so that eventual differences in binding parameters would be attributed to their dissimilar hydrophobic character. As stated in the introduction, the charge density of poly(acrylate) anion, PA^-, can be varied continuously by changing its degree of ionization, α [from $\alpha = 0$ for poly(acrylic acid), HPA, to $\alpha = 1$ for the fully ionized salt, NaPA]. The relation between λ and α is

$$\lambda = \frac{\alpha e_0^2}{4\pi\varepsilon_0\varepsilon kTl} \tag{1}$$

where e_0 is the protonic charge, ε_0 and ε are the permitivity of a vacuum

and the dielectric constant of the solvent, k is the Boltzmann constant, T is the absolute temperature, and l is the distance between the ionizable groups on the polyion cylinder. In this way, one can investigate first the effect of varying the charge density of the polyion while keeping the backbone and functional groups unchanged (PA^-, various α values), and second the influence of the specific nature of the functional groups at fixed charge density [$\lambda = 2.83$ at 25°C in water for NaPA (with $\alpha = 1$ in Eq. 1) and NaPSS].

Cationic surfactants of two types, alkylpyridinium chlorides, C_nPC (where n denotes the number of carbon atoms in the alkyl chain of the surfactant, $n = 12$, 16), and alkyltrimethylammonium bromides, C_nTAB ($n = 12$, 14, 16, 18), were employed in the study. Some measurements were performed with C_nPC, some, in particular cac determination by fluorescence experiments, with C_nTAB, as will be evident throughout the text. In the absence of a polymer, the aggregation properties of C_nPC and C_nTAB are the following: the surfactants of each group with the same alkyl chain length, n, have cmc values of the same order of magnitude. For example, cmc values in water at 25°C are for cetylpyridinium chloride, $C_{16}PC$ (more often CPC), 6.3×10^{-4} M [4], and for cetyltrimethylammonium bromide, $C_{16}TAB$ (often abbreviated as CTAB), 9.1×10^{-4} M [16]; for dodecylpyridinium chloride, $C_{12}PC$ or DPC, and for dodecyltrimethylammonium bromide, $C_{12}TAB$ or DTAB, the corresponding values are 1.52×10^{-2} M [4] and $1.44–1.52 \times 10^{-2}$ M [5,17], respectively. Moreover, in our experiments, dodecylethyldimethylammonium bromide, $C_{12}EDMAB$ or DEDMAB, was used instead of DTAB. The slight enlargement of the surfactant head group of DEDMAB in comparison with DTAB has no substantial influence on the cmc, which is for DEDMAB $1.40–1.45 \times 10^{-2}$ M [16,17]. On the other hand, the aggregation numbers of C_nPC or C_nTAB differ substantially. The aggregation numbers of DPC and CPC, as estimated from the apparent molar volume measurements of alkylpyridinium bromides, are 50 and 86 [18], respectively. The corresponding values for DTAB and CTAB, determined from time-resolved fluorescence measurements [19] are higher, 65 and 146, respectively. The commonly used abbreviations for tetradecyltrimethylammonium and octadecyltrimethylammonium bromides, $C_{14}TAB$ and $C_{18}TAB$, are TTAB and OTAB, respectively.

A. Binding Isotherms

1. General Aspects

One of the fundamental and necessary tasks in the study of polyelectrolyte–surfactant interactions is the determination of surfactant binding isotherms.

A binding isotherm represents a plot of the amount of binding, β, versus log c_S^f. The parameter β has been defined in a familiar way:

$$\beta = \frac{\Delta c_S}{c_P} = \frac{c_S - c_S^f}{c_P} \tag{2}$$

where Δc_S is the amount of surfactant bound per ionic group of the polymer, c_S and c_S^f are the total and free surfactant concentrations, respectively, and c_P is the polyelectrolyte monomer concentration (a fixed value, in our experiments equal to 5×10^{-4} monomol dm^{-3}). The experimental determination of a binding isotherm requires some method that separates surfactant ions into bound and free ones. A very elegant way to do this is the use of an appropriate surfactant-selective membrane electrode that enables one to determine the equilibrium free surfactant concentration [20]. A typical surfactant binding isotherm has a sigmoidal shape with a steep initial rise at a certain low free surfactant concentration followed by the cooperative binding region and finally by a plateau of more or less constant β values indicating the saturation of the polyion with the surfactant ions. In the plateau region of binding, the free surfactant concentration increases rapidly. The onset of binding, the slope of the cooperative part of the isotherm, and the final amount of binding are the parameters of interest.

2. The Effect of the Charge Density of the Polyelectrolyte

Figure 2 shows binding isotherms for CP^+-PA^- system at five different degrees of ionization (α = 0.0, 0.27, 0.53, 0.76, and 1.0) [21]. The charge density of the polymer chain is directly related to α through Eq. 1.

We can see that the binding of CP^+ cation to poly(acrylate) anion starts at approximately the same free surfactant concentration (around 3×10^{-7} mol dm^{-3}) irrespective of the degree of ionization of the polyacid. The influence of α on β is demonstrated by the initial slopes and by the plateau region of the isotherm where β levels off. The initial slopes as well as the ''saturation β values'' increase with increasing α. The latter values are plotted against α in Figure 3. The amount of binding of CP^+ by the unionized poly(acrylic acid) (α = 0.0) is around 0.22, which implies that 22% of functional groups on the poly(acrylate) chain are occupied by the surfactant. On the other hand, β for the fully ionized acid (α = 1.0) is around 0.79, suggesting that all carboxyl groups of PA^- are not complexed by detergent ions. The β values for the intermediate degrees of ionization (α = 0.27, 0.53, and 0.76) are between these values and lie on an almost straight line, giving intersections 0.05 and 0.90 at α = 0.0 and α = 1.0, respectively. This would predict nearly no cooperative binding of CP^+ to the unionized HPA. However, the observed dependence of β on α is reasonable and also the nonzero

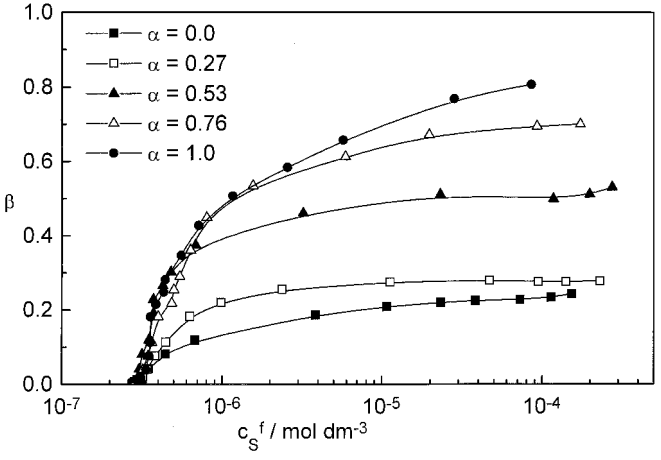

FIG. 2 Binding isotherms of CP^+ to PA^- ($c_p = 5 \times 10^{-4}$ monomol dm^{-3}) in aqueous solutions without added simple electrolyte at 25°C for various degrees of ionization, α, of the acid. Values for α are indicated in the picture.

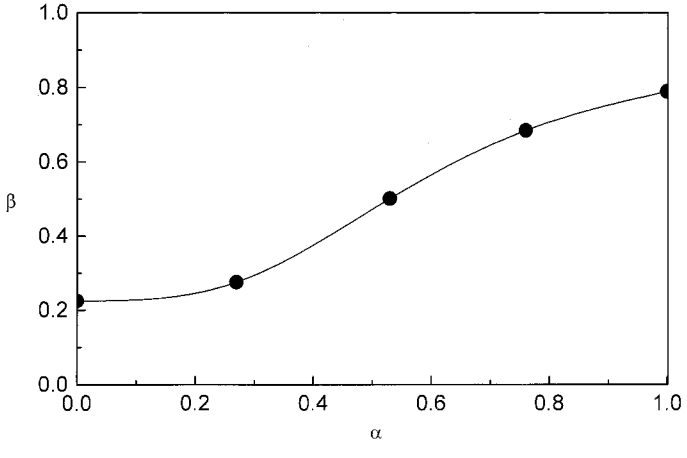

FIG. 3 Dependence of the amount of binding, β, in CP^+–PA^-–H_2O solutions in the plateau region of binding (at free surfactant concentration $c_S^f = 5 \times 10^{-5}$ mol dm^{-3}) on the degree of ionization, α.

amount of binding of CP^+ to HPA can be expected. It is known that many uncharged water-soluble polymers interact cooperatively with ionic detergents in water (for example poly(ethylene oxide) with sodium dodecyl sulfate [13]).

It is convenient to introduce the degree of binding, b, defined as the fraction of surfactant bound by the polyion:

$$b = \frac{\Delta c_S}{c_S} = \beta \frac{c_p}{c_S} \tag{3}$$

The parameter β, which represents the fraction of functional groups on the polyion that are occupied by surfactant ions, and the parameter b are closely related. In Figure 4, the values of b for the binding of CP^+ to PA^- at various α are plotted in dependence on the total surfactant concentration. They additionally emphasise the influence of α on the binding. We can see that the region of complete or 100% binding (indicated by b values close to 1) increases with increasing α. This region is rather narrow in the presence of HPA, and the values of b quickly drop to about 0.4.

It is rather surprising that the onset of binding in CP^+–PA^- system does not depend on the charge density. This is confirmed also in Figure 5, where the amount of binding, β, is plotted against the logarithm of the total surfactant concentration, log c_S. We can see that the total surfactant concentration at which cooperative binding of CP^+ to PA^- starts, approximately at 1×10^{-5} mol/L, is independent of α. This concentration is nearly two orders

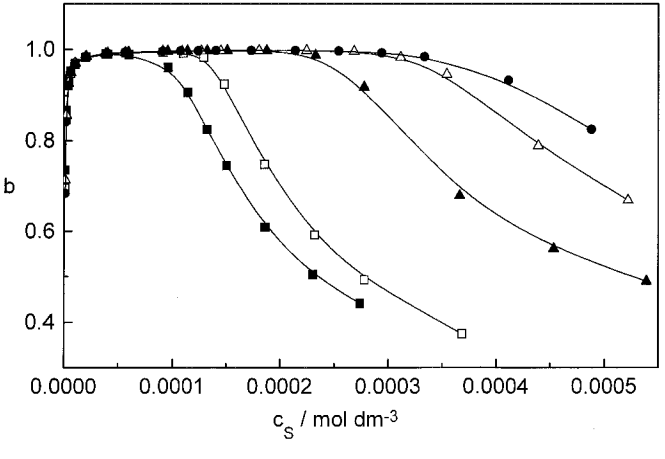

FIG. 4 The degree of binding, b, as a function of the total surfactant concentration, log c_S, in CP^+–PA^-–H_2O solutions at 25°C for various α. Symbols as in Figure 2.

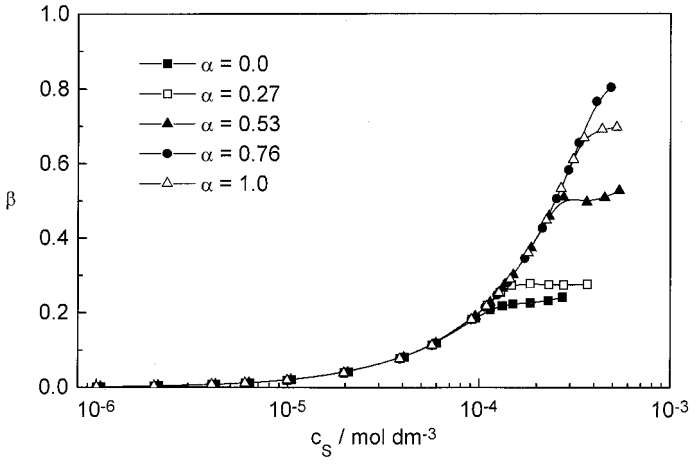

FIG. 5 The amount of binding, β, as a function of the logarithm of the total surfactant concentration in CP^+–PA^-–H_2O solutions at 25°C for various α.

of magnitude lower than that corresponding cmc value for CPC in water (see the cmc values reported previously).

Kwak et al. [22,23] have studied the influence of the polyion charge density and polyion structure on the interactions of charged surfactants with polyelectrolytes. Several carboxylic polyelectrolytes with different backbones, i.e., sodium poly(acrylate), sodium pectate, sodium alginate, and sodium (carboxymethyl) cellulose, NaCMC, were compared. The charge density of these chains, as calculated from the structural value of the parameter l, the distance between the adjacent ionized groups on these chains (see Eq. 1), decreases in the direction PA^- >> pectate > alginate > CMC^-. In fact, as pointed out by the authors, the charge density parameters of alginate and pectate may be very close due to the greater flexibility of alginate in comparison with pectate ion. The following order for the onset of surfactant binding was observed: for dodecyltrimethylammonium, DTA^+, and tetradecyltrimethylammonium, TTA^+, cations in water and in 0.01 M NaCl the order was PA^- >> alginate = pectate > CMC^- [22] and similarly for dodecylpyridinium, DP^+, and tetradecylpyridinium, TP^+, cations in 0.01 M NaCl it was PA^- >> pectate > alginate [23]. On the basis of these findings, we can conclude that the binding order seems to follow the order in λ. However, this result is also a consequence of other factors, like rigidity, hydrophobicity and detailed local structure of the polymer.

A similar approach as presented in our treatment (keeping the polymer backbone intact while changing the charge density) was applied by Hansson

and Almgren [24], who were investigating the binding of DTA^+ to NaCMC with different linear charge density parameters, λ, in the presence of 2.5 mM NaBr. Samples of NaCMC with varying λ values were obtained by changing the degree of carboxymethylation of the polymer. This polymer is as hydrophilic as NaPA but less flexible. In accordance with our results in $CP^+-PA^--H_2O$ solutions, the initial slope of binding isotherms in the DTA^+-CMC^--NaBr system increases with increasing λ, but the amount of binding in the plateau region of binding isotherms shows no regular dependence on the charge density. However, contrary to our findings for $CP^+-PA^--H_2O$, the onset of binding in DTA^+-CMC^--NaBr (i.e., cac values) shifts towards lower free surfactant concentrations with increasing λ. The reason for the observed dissimilarity may be attributed to the different preparation procedure. The NaCMC samples with various linear charge density parameters were obtained from the sodium salts of carboxymethylated polyelectrolyte with the same degree of polymerization but different degrees of substitution (i.e., number of carboxylic groups per residue), whereas for the PA^- system presented here they were obtained by adding NaOH to the polyacid. This means that in the first case the charge density was varied for the completely ionized sodium salt itself ($\alpha = 1$) by changing the distance between adjacent ionized groups on the polyion cylinder and not by merely changing α (see Eq. 1).

Some reports in the literature [25] point to an increased interaction of TTAB with PA^- in 0.01 M NaBr at lower polyion charge densities. The reported results indicate that the cooperative interaction of TTA^+ cation with PA^- anion begins approximately at the same free surfactant concentration, when the degree of ionization is greater than about 0.4 ($\alpha = 0.5$ and 1.0). But surprisingly, when α is below 0.4 ($\alpha = 0.1$ and 0.26), the onset of binding shifts to lower free surfactant concentrations. The authors attribute this contradiction to favorable changes in conformation and hydrophobicity of the polymer backbone. As stated above, our findings in the $CP^+-PA^--H_2O$ system (Figure 2) agree with the above results only for $\alpha > 0.4$, while for $\alpha < 0.4$ we did not observe any change in the onset of binding. We may attribute this to several reasons: to the different head group of the surfactant, to the lower degree of polymerization of the polymer in our case, and also to the fact that in TTA^+-PA^- solutions a large excess of salt (NaBr) was present [25], whereas in our case the measurements were performed in aqueous solutions without addition of a simple electrolyte.

We can conclude that it is difficult to study the influence of the charge density and other structural characteristics of the polymer, i.e., molecular weight, chain flexibility, and chemical nature of the ionizable groups, on the binding of surfactants apart from each other. At the same time, it seems that the nature not only of the polyelectrolyte but also of the surfactant head

group plays an important and not completely understood role in the aggregation process. This can be inferred from the different behavior of alkylpyridinium and alkyltrimethylammonium surfactants in solutions of poly(acrylate) anion.

3. The Effect of the Hydrophobic Character of the Surfactant and the Polyelectrolyte

The effect of the surfactant hydrocarbon chain length on the binding of surfactants to polyelectrolytes is well documented and in many respects parallels the dependence of cmc on the size of the hydrophobic tail. On the other hand, the impact of hydrophobicity of the polyelectrolyte is more difficult to study especially from the viewpoint of isolating various factors, like structure of the polymer backbone, from each other. Figure 6 is a demonstration of both effects together. In this figure, the binding isotherms for the binding of DPC and CPC to NaPSS and for the binding of CPC to NaPA (α = 1.0) are shown. The isotherms in NaPSS solutions were obtained in pure aqueous solutions and in aqueous solutions in the presence of excess of simple salt (0.01 M and 0.1 M NaCl), whereas the isotherm for NaPA–CPC system refers to an aqueous solution without the addition of NaCl.

(*a*) *The Chain Length of Surfactant.* The influence of increasing surfactant chain length is to shift the onset of binding to lower free surfactant

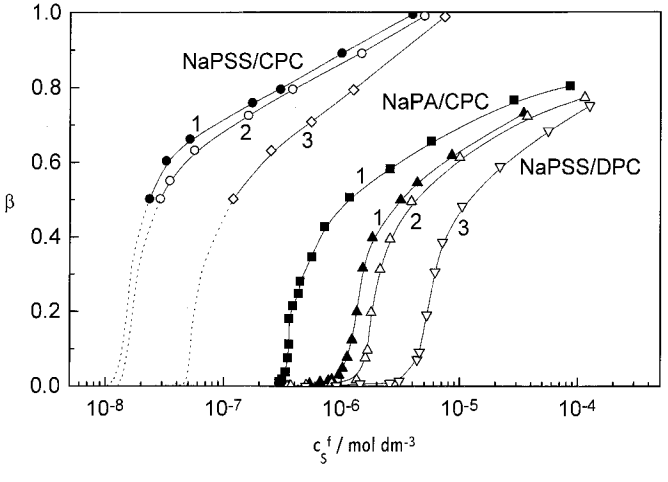

FIG. 6 Binding isotherm of CP^+ to NaPA (α = 1) in aqueous solutions without added simple electrolyte and binding isotherms of DP^+ and CP^+ to NaPSS in aqueous solutions in the absence and in the presence of 0.01 M NaCl or 0.1 M NaCl at 25°C. C_{NaCl}: (1) 0, (2) 0.01 M, and (3) 0.1 M NaCl.

concentrations. This can be seen by comparing the isotherms for the binding of DP^+ and CP^+ cations to PSS^- anion (cf. Figure 6). The binding of CP^+ to PSS^- in pure water starts at around 10^{-8} mol dm^{-3} (in fact at so low a concentration that only approximate binding isotherms can be constructed; see the dashed part of the isotherms for the CP^+–PSS^- system), whereas the onset of binding of DP^+ to PSS^- at the same experimental conditions is shifted to approximately two orders of magnitude higher free surfactant concentrations (to about 1×10^{-6} mol dm^{-3}). This is a clear demonstration of the importance of surfactant–surfactant hydrophobic interactions in the process of surfactant binding to polyelectrolyte. At the same time, CP^+ is bound to PSS^- to a greater extent than DP^+, as may be deduced from the fact that β reaches values close to 1 for CP^+ but does not exceed 0.8 for DP^+. This is demonstrated by a plot of β vs. log c_S, which is for DPC and CPC in the presence of NaPSS shown in Figure 7. At the same time, we can see from this figure that the binding of both surfactants to poly(styrenesulfonate) anion, regardless of NaCl concentration, starts at the same total surfactant concentration, approximately equal to 1×10^{-5} mol dm^{-3}.

The difference between DP^+ and CP^+ binding to PSS^- is additionally emphasised in Figure 8, in which the degree of binding, b (Eq. 3), is plotted against the total surfactant concentration. We can see that the CP^+ cation is almost completely associated with the PSS^- anion in the whole concentration range studied (b is close to 1 up to the concentration of surfactant equal

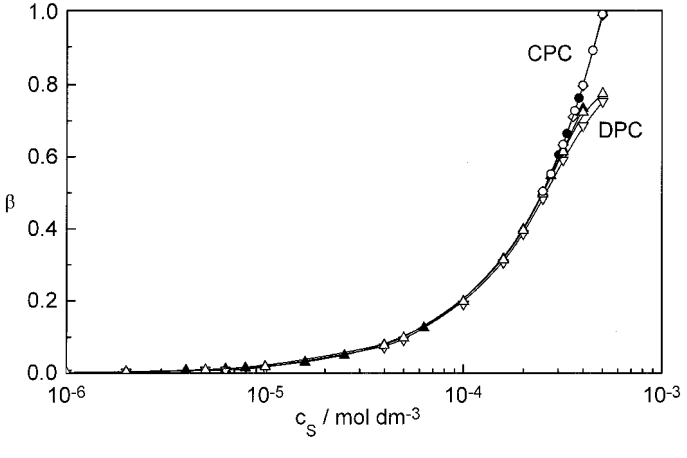

FIG. 7 The amount of binding, β, as a function of the logarithm of the total surfactant concentration for the binding of DP^+ and CP^+ to PSS^-. Symbols as in Figure 6.

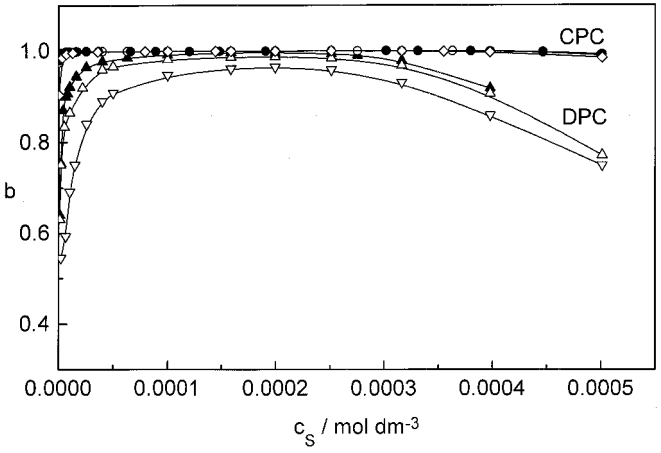

FIG. 8 The degree of binding, b, as a function of the total surfactant concentration for the binding DP^+ and CP^+ to PSS^- in aqueous solutions at 25°C in the absence and in the presence of 0.01 M NaCl or 0.1 M NaCl. Symbols as in Figure 6.

to the polyelectrolyte monomer concentration, i.e., 5×10^{-4} mol dm^{-3}), whereas the binding of DP^+ cation is not complete (b values lie in the range from 0.70 to 0.99 depending on the surfactant and NaCl concentration).

The effect of simple salt on the surfactant binding confirms the electrostatic nature of the surfactant ion–polyion interactions (step 1, Scheme 1). Any increase in the ionic strength of solution shifts the onset of binding toward higher free surfactant concentrations (compare isotherms in water, 0.01 M, and 0.1 M NaCl, Figure 6) and decreases the amount of bound surfactant. These observations can be related to the screening influence of the simple salt, which acts to diminish the electrostatic interactions between surfactant cations and polyanions. This is also well documented in the literature for a variety of polyelectrolyte–surfactant pairs [26–29].

(*b*) *The Hydrophobic Nature of the Polyelectrolyte.* By comparing the binding isotherms of the surfactant with the same chain length, i.e., CPC to NaPSS and NaPA in water (cf. Figure 6), a marked difference is observed. Again, we should stress that the fully ionized NaPA and NaPSS have the same linear charge density parameter, λ, equal to 2.83 in water at 25°C. As already mentioned, the binding of CP^+ to PSS^- in water starts at approximately 10^{-8} mol dm^{-3}, whereas the free surfactant concentration at the onset of binding of CP^+ to PA^- is considerably higher, approximately 3×10^{-7} mol dm^{-3}. Besides, CP^+ binds almost completely to PSS^- ($\beta = 1$) while the

association with PA^- is not complete (β levels off at around 0.8). Another indication of a weaker interaction between CP^+ and PA^- is that the parameter b is lower in the CP^+–PA^- system and depends considerably on the degree of ionization (cf. Figure 4, compare with Figure 8). These observations can be explained only by taking into account the hydrophobic nature of the side groups on the poly(styrenesulfonate) chain. The presence of aromatic benzenesulfonate groups distinguishes NaPSS from NaPA. The aromatic rings facilitate the complexation between the micellized surfactant and the PSS^- chain by solubilizing in the hydrocarbon interior of the micelle [12]. On the other hand, the carboxylic groups of NaPA prefer to stay in water, and only due to purely electrostatic interaction does aggregated surfactant accumulate near the polyelectrolyte chain.

In the context of our further discussion on the enthalpy of binding, it has to be stressed again that the total surfactant concentration, c_S, at which appreciable binding of CP^+ and DP^+ to PSS^- and PA^-, respectively, starts, is approximately the same (around 1×10^{-5} mol dm^{-3}, cf. Figures 5 and 7), irrespective of the nature of the polyelectrolyte, surfactant chain length, or ionic strength of solutions.

B. Enthalpy of Binding

The enthalpies of binding were determined for the binding of DP^+ and CP^+ cations to PSS^- anion [4]. They were obtained in experiments in which a solution of NaPSS was mixed with a solution of DPC or CPC and the corresponding enthalpies of dilution of surfactants and NaPSS were accounted for. To keep the ionic strength of the initial and final solutions constant, in most cases both solutions contained an excess of the simple salt (NaCl).

The calorimetric results are presented in Figures 9 and 10, where ΔH_b is plotted against the logarithm of the total surfactant concentration. The enthalpy of binding, ΔH_b, is calculated per mole of bound surfactant, e.g., the experimental ΔH is divided by the degree of binding b (Eq. 3 and Figure 8). Various aspects of the experimental results are noticeable. First, all heat effects are exothermic. Second, the enthalpy of binding decreases with increasing concentration of the simple salt in agreement with the conclusions drawn from the binding isotherms. This experimental observation is additionally emphasised by measurements performed with CPC in pure water. However, in this case each experimental point corresponds to a different final NaCl concentration, equal to the concentration of the surfactant, c_S. For this reason, the heat effects in water, in the concentration range where almost constant ΔH_b are observed in the presence of NaCl, decrease gradually with increasing surfactant concentration. The third and the most significant aspect

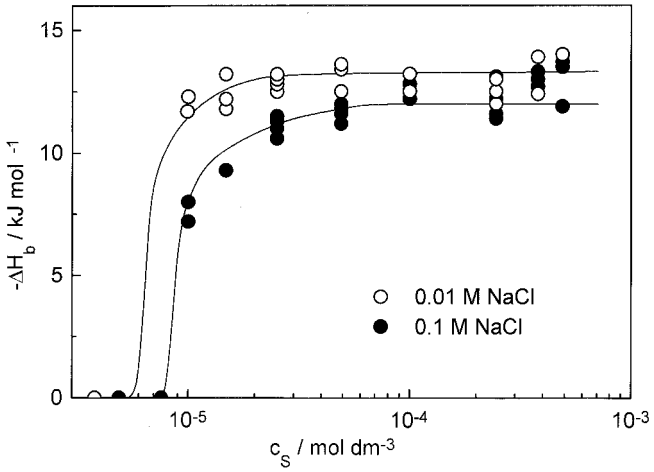

FIG. 9 The enthalpy of binding of DP^+ to PSS^- at 25°C in 0.01 M NaCl and in 0.1 M NaCl. The values of ΔH_b are calculated per mole of bound surfactant cations (the experimental ΔH is divided by b).

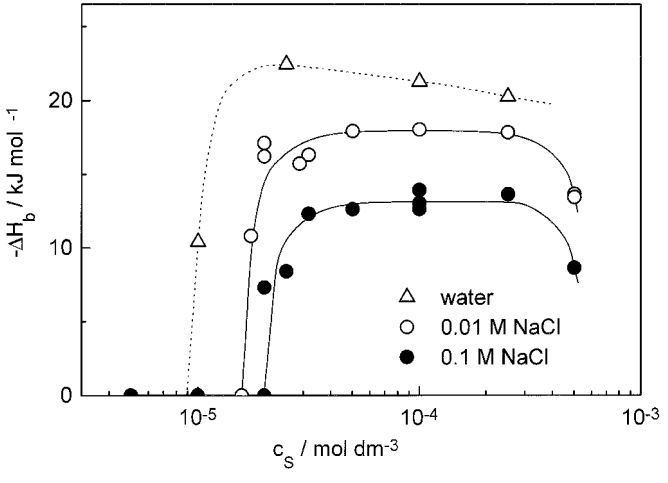

FIG. 10 The enthalpy of binding of CP^+ to PSS^- at 25°C in water, 0.01 M NaCl and 0.1 M NaCl. The values of ΔH_b are calculated per mole of bound surfactant cations (the experimental ΔH is divided by b).

is the sharp increase of ΔH_b at a given surfactant concentration. Below this concentration, the heat effects are undetectable or zero, and above it they are more or less constant. In the case of DPC, the constancy is followed up to the "equivalent point," which is considered as the concentration of surfactant equal to the monomolar polyelectrolyte concentration (5×10^{-4} monomol dm^{-3}). For CPC, the heat effects drop again close to this concentration limit. It is rather remarkable that the steep initial rise of ΔH_b happens for both surfactants almost at the same total concentration, i.e., at around 1×10^{-5} mol dm^{-3}, a finding that is in complete agreement with the potentiometric observations (see Figure 7). It has been shown before from the calculated counterion distribution that at this analytical concentration the local concentrations around the polyion, in layers lying between the polyion and the radial distance, which is comparable to the length of the surfactant hydrocardon chains, range from about 2×10^{-2} to 1×10^{-3} mol dm^{-3}. These concentrations are comparable to, or higher than, the cmcs of the two surfactants studied (compare the cmc values reported above for aqueous solutions of pure DPC and CPC and note that in the presence of an electrolyte they are even further reduced [4]). Finally, it has to be noted that with increasing the surfactant hydrocarbon chain the enthalpy of binding becomes more exothermic. This is consistent with the results obtained from the isotherms of binding. It has been shown that the amount of surfactant binding, β, increases with increasing the number of C atoms in the hydrocarbon chain.

With the discussion of previous sections as background, the observed enthalpy of binding may be considered to contain three contributions: (1) the enthalpy change due to the atmospheric binding of surfactant cations to the PSS^- anion, ΔH_a, (2) the heat effect accompanying the aggregation of the bound surfactant molecules into polyelectrolyte induced micelles, ΔH_m, and (3) the enthalpy change, ΔH_i, due to other specific interactions of surfactant micelles with the polyelectrolyte chain:

$$\Delta H_b = \Delta H_a + \Delta H_m + \Delta H_i \tag{4}$$

The ΔH_a term results from the part of the binding process in which the Na^+ ions, electrostatically bound to the polyion (atmospheric binding), are replaced by the monovalent surfactant cations. This contribution is assumed to be small in comparison with the other two and can be neglected. When the surfactant micelles form in the presence of a hydrophilic polyelectrolyte, the third contribution, ΔH_i, in Eq. 4 may be assumed to be much smaller than the second term, since only pure electrostatic interactions are expected to act between hydrophilic polyion and ionic micelle. However, the ΔH_i term in the case of interaction between a hydrophobic polyelectrolyte and surfactant micelle may not be neglected. To confirm this, it is instructive to

compare the term ΔH_m to the enthalpy of micellization in pure surfactant solutions. The enthalpy of micellization of dodecylpyridinium iodide, DPI, at cmc and 25°C, obtained by direct calorimetric measurements, [30] was found to be $\Delta H_m = -(13.5 \pm 3)$ kJ/mol in water and $\Delta H_m = -(13.0 \pm 2.5)$ kJ/mol in 0.01 M KI. Seemingly, these values agree well with the experimental results obtained for the enthalpy of binding of DPC or PSS^- in our case and suggest that the main contribution to the measured heat effect is the one due to the micellization of the surfactant. Note however, that the counterion of the surfactant is different in both cases, a fact which could possibly conceal some important difference between both heat effects and make them equal by coincidence. Namely, the micellization behavior of alkylpyridinium halides in the absence of the polyelectrolyte depends appreciably on the counterion, especially its size [31]. For example, the critical micellization concentration of DPI in water at 25°C lies between 5.4 and 5.75×10^{-3} M [30] and is nearly three times lower than the cmc for DPC. Also, the aggregation numbers of both surfactants differ substantially. The aggregation number for DPI in water at 25°C is around 75 [32], which is considerably higher than the corresponding value for DPC (around 50, see above).

A more straightforward approach in evaluating the heat effect was taken by Vesnaver et al. [33], who have compared the enthalpies of binding, ΔH_b, with the corresponding enthalpies of micellization, ΔH_m, of alkylpyridinum surfactants with bromide as a counterion. They have found that the measured ΔH_b values are about 9 kJ/mol more exothermic than the corresponding enthalpies of micellization, regardless of the simple salt concentration and the length of the surfactant tail. They have attributed this to additional polyion–surfactant ion interactions in which, as they proposed, the charged aggregates are pulled closer to the polyion. In fact, as pointed out by NMR measurements [12], this additional specific attraction is due to the solubilization of the aromatic rings of the poly(styrenesulfonate) chain in the interior of the surfactant micelle.

The above discussion on heat effects accompanying the binding of surfactants to polyelectrolyte suggests that, although the main contribution to the enthalpy of binding is the enthalpy of micellization, in the case of hydrophobic polyelectrolytes like NaPSS a significant contribution must be ascribed to hydrophobic forces between surfactant micelle and the polyion chain. It can be expected that the stability of such polyelectrolyte–surfactant aggregates is considerable. In fact, this was confirmed by transport number measurements [10] in aqueous poly(styrenesulfonic acid), HPSS, solutions in which a certain portion of the charged benzenesulfonate groups was blocked with CPC micelles. In the moving boundary cell the CP^+-PSS^- complex was moving toward the positive electrode, revealing the net neg-

ative charge of the aggregate. Furthermore, the degree of complexation of HPSS with CPC did not change during the electrolysis. Both facts point to the exceptional stability of the complex.

We return now to an important result that measurable values in ΔH_b in DP^+-PSS^- and CP^+-PSS^- solutions are observed at total surfactant concentration around 1×10^{-5} mol dm^{-3} in accordance with potentiometric measurements (compare Figure 7 with Figures 9 and 10). Other properties, like changes in viscosity of the polyion, volume changes which accompany polyelectrolyte-induced micellization, and conductivity measurements are in agreement with the above findings.

C. Viscosity

The changes in dimensions of the polyelectrolyte chain associated with surfactant binding can be followed by viscosity measurements [5,34]. The effect of the addition of surfactant on the polyion chain dimensions is twofold. First, the surfactant counterions bind electrostatically to the polyion with opposite charge (cf. step 1 in Scheme 1). As a consequence, the effective charge of the macroion cylinder is screened and leads to contraction of the chain and to a decrease in viscosity. This effect is similar to the effect of increasing ionic strength of solution [35,36] or decreasing degree of neutralization of a weak polyelectrolyte [37] on the reduced viscosity of polyelectrolytes. Second, an additional effect is expected due to the polyelectrolyte-induced micellization of surfactant. In this case the surfactant is bound to the polyelectrolyte cooperatively in the micellar form (cf. steps 2 and 3 in Scheme 1). The polyion chain tends to wrap around these aggregates, and this is accompanied by a further decrease in its dimensions and viscosity.

In Figure 11, the effect of the addition of CPC on the specific viscosity, η_{sp}, of 5×10^{-4} monomol dm^{-3} NaPSS and NaPA solutions is presented. Included are viscosity measurements in pure CPC solutions to demonstrate that the surfactant has practically no influence on the viscosity of the solvent. It is evident that the viscosity of pure CPC is practically equal to that of water, $\eta_{sp} \approx 0$. In Figure 12, the dependence of the reduced viscosity, $[\eta_{red}]$ ($= \eta_{sp}/c_p$, where c_p is expressed in g/dL) on the logarithm of surfactant concentration is presented. It has been shown previously [34] that the effect of surfactant on $[\eta_{red}]$ is stronger than the corresponding effect of simple electrolyte. Figure 12 shows that up to the concentration of surfactant equal to approximately 1×10^{-5} mol dm^{-3} the viscosity of the polyelectrolyte remains nearly constant (a slight maximum in NaPA solutions is detected) and afterwards it decreases rapidly with increasing surfactant content. Similar viscosity trends were observed also in solutions of poly(acrylic acid) in the presence of the nonionic surfactant, poly(ethylene oxide) [38]. The point

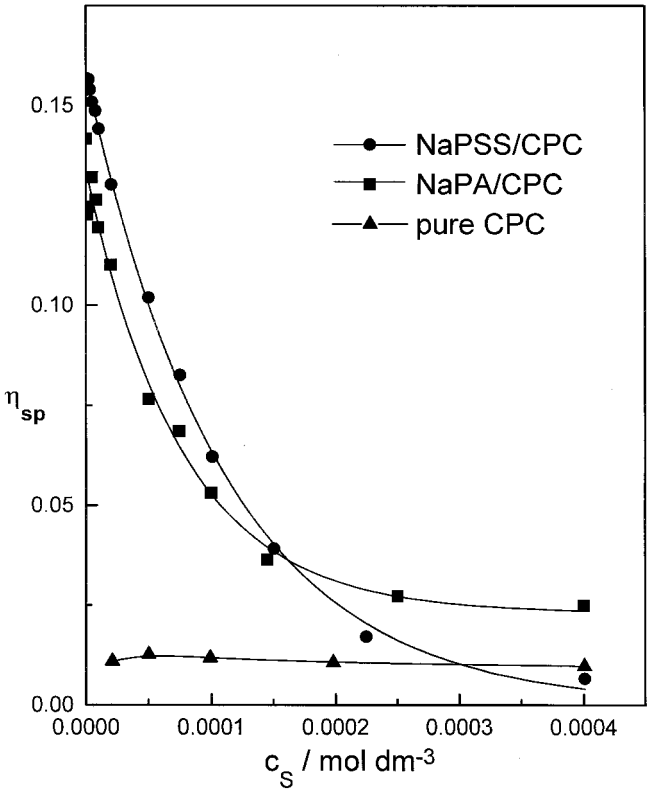

FIG. 11 The effect of the addition of CPC on the specific viscosity, η_{sp}, of NaPA and NaPSS solutions with constant polyion concentration ($c_p = 5 \times 10^{-4}$ monomol dm^{-3}) and the concentration dependence of the specific viscosity of pure CPC solutions.

where the drop in the reduced viscosity is observed is designated by T_1 (or cac), and it represents the beginning of the surfactant fixation on the polymer chain.

The results of $[\eta_{red}]$ measurements on the importance of the surfactant concentration 1×10^{-5} mol dm^{-3} are in complete agreement with previous potentiometric and calorimetric findings. Below 1×10^{-5} mol dm^{-3}, the polyelectrolyte behaves as an uncomplexed rod, while above 1×10^{-5} mol dm^{-3}, extensive coiling of the chain takes place. Again, the distinction in binding of CP^+ to PA^- and PSS^- is evident. The reduction of $[\eta_{red}]$ is greater for PA^- than for PSS^- chain. On the basis of our earlier experience we can say that this is in part due to the specific nature of the interaction between

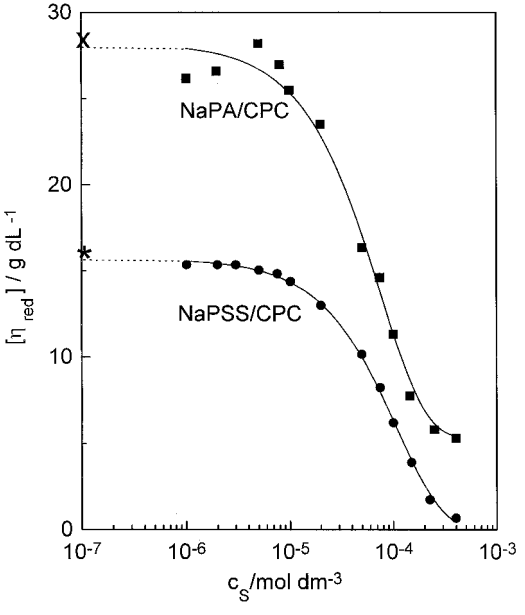

FIG. 12 The semilogarithmic plot of the reduced viscosity, $[\eta_{red}]$, of NaPA and NaPSS solutions in the presence of CPC. Symbols * and × indicate the values for $[\eta_{red}]$ in prue NaPSS and NaPA solution ($c_p = 5 \times 10^{-4}$ monomol dm^{-3}), respectively, without CPC.

surfactant micelle and the poly(styrenesulfonate) chain. However, an important contribution comes also from the flexibility of the polyelectrolyte chain. The PA^- chain is considered more flexible than the PSS^- chain. As pointed out by Monte Carlo simulations of polyelectrolyte–surfactant interactions [39], this factor should play an important role in determining the nature of the complex. We can speculate that the flexible PA^- chain can be more thoroughly adsorbed to the surface of the surfactant micelle and can even form loops extending from the micelle. This ensures a closer packing within the complex, and consequently the dimensions of the chain are reduced to a greater extent in comparison to the PSS^- chain. On the other hand, a stiffer PSS^- chain is more restricted in motion and cannot wrap freely around the aggregated surfactant. Besides, the complex between PSS^- and CP^+ micelle is formed by inclusion of the hydrophobic benzenesulfonate rings of the polyion into the interior of the micelle. This makes the CP^+–PSS^- complex more stable but at the same time more rigid than the CP^+–PA^- one. A fact that must not be overlooked is that surfactant micelles that

form in the presence of PSS^- seem to be smaller than those formed in the presence of PA^-. For example, the aggregation number of alkyltrimethylammonium bromides, C_nTAB, in the PA^- system do not differ from the ones found for ordinary micelles in pure C_nTAB solutions (see the aggregation numbers reported previously), whereas in the PSS^- system they are approximately one-half the normal aggregation numbers [11,19]. Some authors [5] report much smaller values (around 7–10 monomer surfactant units per polyelectrolyte-induced micelle). From purely geometric considerations, one can conclude that a greater part of the polyelectrolyte chain is necessary to surround a bigger micelle than a smaller one. Therefore the overall dimensions of the chain for the same amount of added surfactant change more in the case of NaPA than in the case of NaPSS.

The effect of the addition of an ionic surfactant to an oppositely charged polyion is just the opposite to the corresponding effect observed with neutral polymers. The binding of a surfactant ion to an uncharged polymer actually leads to an increasingly charged complex followed by the expansion of the chain [40]. The saturated complex between the polymer and ionic surfactant acquires in fact the properties of a polyelectrolyte, whereas in our case the polyelectrolyte in the process of surfactant binding undergoes a transformation into a neutral polymer.

D. Volume Changes

Surfactant micellization is frequently detected by apparent molar volume measurements. It is possible to use this approach also in polyelectrolyte–surfactant mixed solutions [34]. The results are presented in Figure 13 for solutions of CPC in the absence and in the presence of NaPA and NaPSS as $\Delta\phi_V$ and $\Delta\Phi_V$ values.

The relative apparent molar volume for pure surfactant, $\Delta\phi_V$ (Eq. 5) is defined as the difference between the value for the apparent molar volume of surfactant at a certain concentration, ϕ_V, and its value at infinite dilution, ϕ_V^0,

$$\Delta\phi_V = \phi_V - \phi_V^0 \tag{5}$$

and the relative mean apparent molar volume in mixed solutions, $\Delta\Phi_V$ (Eq. 6) as the difference between Φ_V, the mean apparent molar volume [41] of the polyelectrolyte–surfactant complex in a ternary system composed of water, surfactant, and polyelectrolyte, and the corresponding value for the polyelectrolyte, Φ_V^P, in the absence of surfactant [34]:

$$\Delta\Phi_V = \Phi_V - \Phi_V^P \tag{6}$$

Note that the polyelectrolyte concentration in the $\Delta\Phi_V$ measurements is constant (5×10^{-4} monomol dm^{-3}) and the surfactant concentration increases.

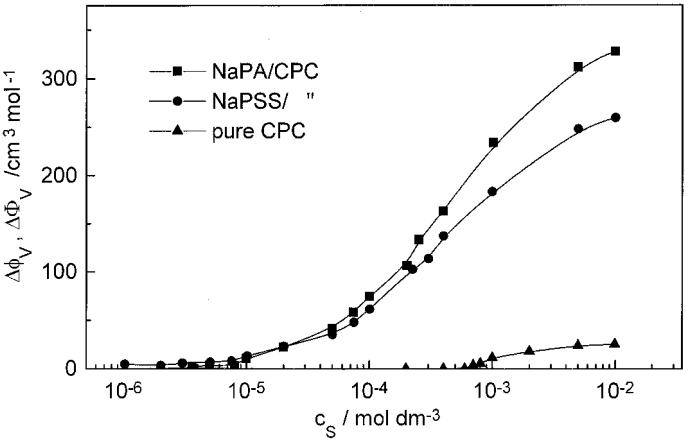

FIG. 13 The $\Delta\phi_V$ (Eq. 5) change in aqueous solutions of pure CPC and the $\Delta\Phi_V$ (Eq. 6) change in mixed NaPSS/CPC and NaPA/CPC solutions at 25°C ($c_p = 5 \times 10^{-4}$ monomol dm^{-3}).

Both $\Delta\phi_V$ and $\Delta\Phi_V$ changes reflect the formation of surfactant aggregates. The increase in $\Delta\phi_V$ of pure surfactant above the cmc reflects the onset of ordinary micellization [31]. A similar increase in volume is observed in the presence of a polymer and can also be ascribed to micellelike surfactant aggregation. However, it takes place at much lower surfactant concentrations (around 1×10^{-5} mol dm^{-3}, which is nearly two orders of magnitude below cmc). Again, this is the same total surfactant concentration as observed before.

At higher surfactant concentrations (above approximately 5×10^{-5} mol dm^{-3}), the $\Delta\Phi_V$ values become much greater than the volume changes for ordinary micellization, $\Delta\phi_V$. There are several reasons responsible for this observation. First, this is inherent in the calculation procedure [34]. In the $\Delta\Phi_V$ change, Φ_V^P (Φ_V^P = 96 cm^3 monomol^{-1} and 26 cm^3 monomol^{-1} for pure NaPSS and NaPA, respectively, at the concentration 5×10^{-4} monomol dm^{-3}) is subtracted from the mean apparent molar volume of the aggregate (Eq. 6), whereas in $\Delta\phi_V$ the molar volume of the monomer surfactant at infinite dilution, ϕ_V^0 (ϕ_V^0 = 342 cm^3 mol^{-1} for CPC) is subtracted (Eq. 5). The latter value is much greater than Φ_V^P (more than 3 and more than 10 times for NaPSS and NaPA, respectively). Besides, due to the coiling of the polyelectrolyte chain, Φ_V^P most probably changes in the course of the surfactant binding. Finally, an important contribution to the $\Delta\Phi_V$ change comes from the flexibility of the polyelectrolyte chain, as discussed above. The

greater overall contraction of the PA^- chain is accompanied both by a larger reduction in the reduced viscosity and by a larger volume change.

In the presence of the polyelectrolyte ordinary CPC micelles also appear somewhat above the cmc for pure surfactant [16,34,42]. This is seen from the Φ_V values, which above 1×10^{-3} mol dm^{-3} tend to the absolute values for the apparent molar volume of CPC incorporated in micelles. For comparison, below cmc the apparent molar volume of CPC is approximately constant (around 342 cm^3 mol^{-1}); above cmc, at surfactant concentration equal to 0.01 M, it reaches 367 cm^3 mol^{-1}. In polyelectrolyte solutions at the same surfactant concentration, the maximum Φ_V values are 353 cm^3 mol^{-1} and 355 cm^3 mol^{-1} in NaPA and NaPSS, respectively. We can conclude that ordinary surfactant micelles prevail in solution over the polymer-bound ones.

E. Conductivity

An important driving force for surfactant micellization in the field of a polyelectrolyte is demonstrated through measurements of molar conductivity [16,42]. The molar conductivity, Λ (= κ/c_S, where κ is the specific conductance), in pure CPC solutions and in solutions of CPC containing constant amounts of NaPA and NaPSS, is presented in Figure 14. The Λ vs. $\sqrt{c_S}$ curve for pure surfactant shows a usual dependence. The distinctive break

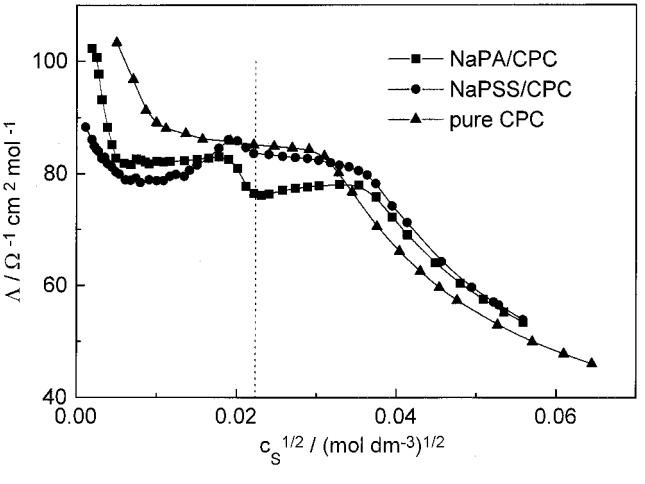

FIG. 14 Molar conductivity, Λ, vs. square root of surfactant concentration at 25°C in aqueous solutions of CPC in the absence and in the presence of NaPA an NaPSS, respectively ($c_p = 5 \times 10^{-4}$ monomol dm^{-3}, indicated by the dotted line).

in this curve observed at higher concentrations corresponds to micelle formation, and from it the cmc value can be obtained. The steeper decrease in Λ above the cmc is a consequence of counterion binding to a highly charged surfactant micelle. The degree of this binding is for a large number of systems in the range from 50 to 80% [31].

Different behavior is observed in the presence of a polyelectrolyte. At first, a much steeper decrease in molar conductivity is observed. In this range, the mobility of surfactant cations is strongly reduced because of the high electrostatic field of the polyanion. In NaPSS solutions, a minimum in Λ is reached followed by an increase up to approximately the ''equivalent point'' (this is the concentration of surfactant cations equal to the concentration of ionizable groups on the polyion, i.e., 5×10^{-4} mol dm^{-3}). The appearance of a minimum and especially the unusual increase in Λ afterwards can be explained by the effect of the release of highly conducting small counterions (Na^+ from the polyelectrolyte and Cl^- from the surfactant micelle) into the solution. When the polyelectrolyte chain wraps around surfactant micelles, there is no need for any condensed counterions on the micelles and also on the part of the polyion chain complexed with the surfactant. The polyion acts as a counterion cloud around the ionic micelle and compensates the repulsive forces between the charged groups on the micellar surface. Therefore when the cooperative binding of surfactant to polyelectrolyte takes place, a considerable amount of counterions originating from the polyion, as well as from the surfactant micelles, is released into the solution. This has a favorable positive entropic contribution to the aggregation process and can be very clearly detected from the observed conductivity curves (cf. Figure 14).

In NaPA solutions, the curve shows no minimum. Instead, a plateau region of relatively constant Λ values is observed in the concentration range where the minimum in NaPSS solutions has been detected. Again, these differences in the behavior of CPC–NaPA and CPC–NaPSS solutions can be accounted for by the specific interaction with surfactant micelles in the poly(styrenesulfonate) case. We may speculate that the PA^- chain forms a more loose structure with the aggregated surfactants and may retain much of its counterions.

At surfactant concentrations above the equivalent point ($>5 \times 10^{-4}$ mol dm^{-3}) the Λ curves in the presence of the polyion resemble the behavior of the curve in pure surfactant solutions. They show a break at the so-called apparent critical micellization concentration, cmc* [16,42]. This term is usually used for characterizing the formation of free surfactant micelles in the presence of the polymeric component. The cmc* is higher than the ordinary cmc due to the formation of polyelectrolyte–surfactant complex at lower surfactant concentrations. The bound surfactant ions are not available for

micellization, and consequently free micelles appear at somewhat higher total surfactant concentration. Thus conductivity measurements confirm that bound micelles are more stable than free ones and that they coexist in a solution, as was shown before from Φ_V values.

F. Critical Aggregation Concentration

1. General Comments

We adopt the definition of the cac [11] as the surfactant concentration at the onset of the cooperative binding to the polyion, which at the same time corresponds to the point where polyelectrolyte induced micelles start to form. A number of physical properties of surfactants, when plotted as functions of surfactant concentration at constant polyelectrolyte concentration, show a break from which the cac can be obtained. These properties include the ones encountered already in the determination of cmc (like conductivity, surface tension, NMR, solubilization of an oil-soluble dye, etc.) as well as those applied for binding studies in mixed polyelectrolyte–surfactant solutions. Similarly to the cmc determinations, we usually obtain a range of concentrations corresponding to the cac, suggesting that in fact various methods give a different value. In comparison with the determination of cmc, a serious problem arises with the cac because the surfactant concentrations at the onset of cooperative binding are usually very low, particularly in the case of oppositely charged polyion and surfactant ion (in the submicromolar range). This is clearly demonstrated by the binding isotherms that can serve as one of the possible means of cac determination. In a binding isotherm, the cac is taken as the free surfactant concentration at the sharp increase of the amount of binding, β [24,29,43]. In the experimental electromotive force curve, representing the response of a surfactant-selective membrane electrode to change in surfactant concentration, this point would correspond to the departure of the measured electrode potential in mixed polyelectrolyte–surfactant solutions from the calibration curve obtained in pure surfactant solutions containing no polymer [21,29].

Another extremely useful method for cac determination, especially in the light of high sensitivity, is fluorescence emission spectroscopy [15]. Some aromatic water-insoluble dyes that are present in trace amounts in mixed polyelectrolyte–surfactant solutions have an ability to solubilize within the self-assembled surfactant aggregates and to change their photophysical properties because of the change of environmental polarity. Through this, they offer a very sensitive method for the determination of cac values. A typical and lately frequently used compound is pyrene, which is used as a fluorescence probe to assess various micellar properties. Pyrene exhibits a polarity dependent fluorescence spectrum with the ratio I_1/I_3 (the ratio of the intensity

of the first peak, I_1, at 373 nm to that of the third peak, I_3, at 382 nm), which is an indicator of solvent polarity. In aqueous solutions without hydrophobic domains its value is between 1.55 and 1.7; in methanol it is around 1.3 (similar as for pyrene solubilized in micelles), and in hydrocarbon solvents like cyclohexane it is very low, around 0.6 [44–46]. This strong dependence of I_1/I_3 on the surrounding medium has been used as an indicator for micelle or other similar aggregate formation. In an aqueous surfactant solution below the cmc, the ratio I_1/I_3 has the same value as in water, but above the cmc it drops to a value typical for alcohols (between 1.1 and 1.35), indicating that the probe is preferentially solubilized in the hydrophobic interior of a micellar aggregate. In the case of the ordinary micelle formation, which has often been described to be similar to a phase separation, a sharp drop in the plot of the I_1/I_3 ratio vs. surfactant concentration is detected. However, in the case of interest here, i.e., polyelectrolyte-induced surfactant micellization, micellar aggregates appear more gradually, and the decreasing of the pyrene ratio with increasing amount of surfactant can be extended over a wider concentration range (one to two orders of magnitude). This is also the origin of discrepancies found in the literature regarding the determination of the cac from the I_1/I_3 vs. log c_S plots. Some authors identify the cac with the midpoint of the transition in the I_1/I_3 vs. log c curve [47]; others regard it as the saturation point where the ratio becomes constant again [48]. Many authors determine the cac from the point where one first observes the fall of the intensity ratio [11,29]. We have utilized the latter approach.

Before we present the cac values we would like to make some comments on the use of the symbol cac. Various symbols appear in the literature for this parameter. Among these are x_1 [13], c_1 [49], and T_1 [38,50,51]. The denotation cac for critical aggregation concentration was introduced by Chu and Thomas [47] and emphasises the analogy with surfactant micellization. Because of the many similarities between the ordinary micellization and polyelectrolyte-induced surfactant aggregation we prefer to use the latter symbol.

2. Critical Aggregation Concentration Values

(*a*) *The Chain Length Dependence.* With fluorescence measurements, we have determined the cac values of C_nTAB surfactants in dilute NaPSS solutions [16,52]. For alkylpyridinium surfactants, the use of pyrene is not possible because these surfactants are commonly used as quenchers in fluorescence experiments. Therefore their cac values were obtained from binding isotherms (cf. Figure 6).

As pointed out in the Introduction, cmc and cac exhibit a similar dependence on the alkyl chain length of the surfactant. This is for C_nTAB dem-

onstrated in Figure 15 where log cmc and log cac values are plotted against the number of C atoms, n, in the nonpolar part of the surfactant molecule. They both decrease with increasing n, but the cac not so steeply as the cmc. For CTAB and OTAB, the cac even remains approximately the same. Something similar has been found for the rate of change of cmc with the surfactant chain length in the homologous series of sodium alkyl sulfates in water [53]. Between about C_{16} and C_{18} members, the cmc tends to decrease more slowly than for shorter chain lengths, and above C_{18} members it tends to remain approximately constant. In any case, we can conclude that the hydrophobic character of the amphiphile plays an important part also when the aggregates are formed at the polyion.

(*b*) *The Ionic Strength Dependence.* From Figure 15 the effect of simple salt is also evident. In contrast to the well-known salt dependence of the

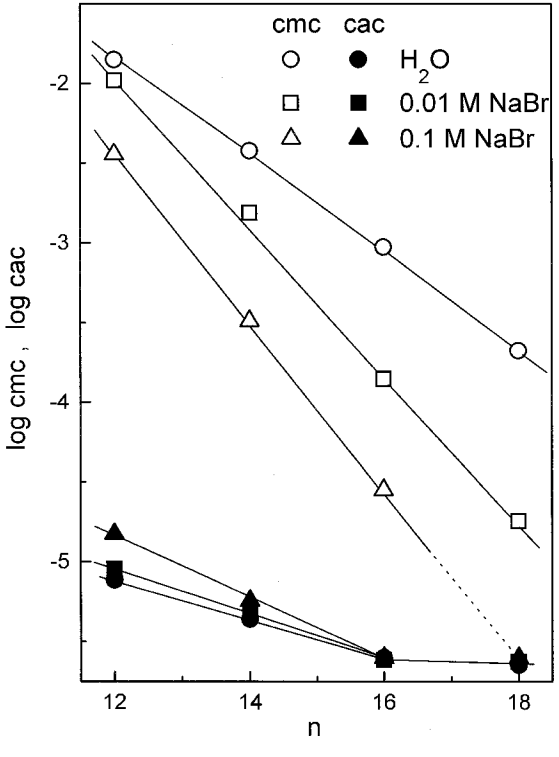

FIG. 15 Dependence of the cmc and cac values for C_nTAB in water, 0.01 M, and 0.1 M NaBr in the absence and in the presence of NaPSS, respectively, on the number of C atoms, n, in the hydrocarbon chain of surfactant.

cmc, the critical aggregation concentration increases with increasing ionic strength. This is clearly demonstrated in Figure 16 for C_nTAB as well as for C_nPC. In this figure, the log cac values are plotted against the log c_S^{tot}, where c_S^{tot} (= c_{NaPE} + c_{NaX}) is the total concentration of sodium cations originating from the simple salt, NaX (X = Cl^- or Br^-) and from the polyelectrolyte, NaPE (PE = PSS^- or PA^-), respectively. The results for DTAB in NaPA were taken from the reference by Hansson and Almgren [29]. It has to be noted that our results for C_{12}–NaPSS solutions apply to DEDMAB (see abbreviations introduced before). The increase of cac with increasing ionic strength can be accounted for by the electrostatics: simple electrolyte screens the electrostatic interactions between the polyanion and surfactant cations. In the presence of a simple electrolyte, the ''local cmc,'' needed for self-aggregation of the amphiphile at the polymer, is thus reached at a somewhat higher total surfactant concentration, leading to an increased cac.

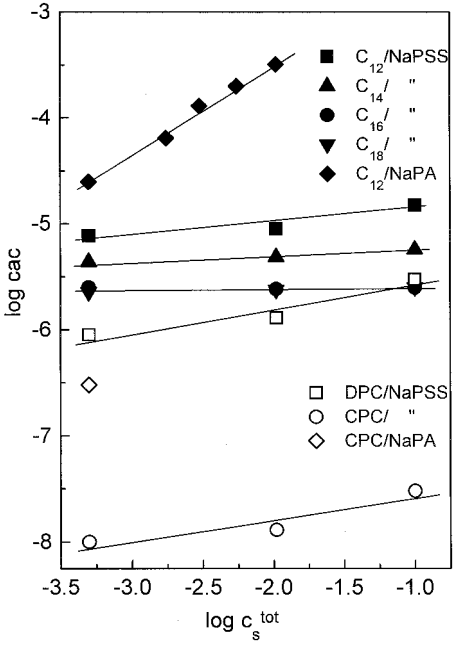

FIG. 16 Dependence of the cac values for C_nTAB and C_nPC in the presence of NaPSS and NaPA on the total concentration of sodium ions, log c_S^{tot} (c_S^{tot} = c_{NaX} + c_{NaPE}, where X = Cl^- or Br^- and PE = PA^- or PSS^-); C_nTAB surfactants are abbreviated shortly as C_n (n = 12, 14, 16, 18). (Data for C_{12}/NaPA system are taken from Ref. 29.)

The dependence of cac on ionic strength is again a demonstration of the difference in binding of cationic surfactants to NaPA and NaPSS, respectively. The cac values in NaPA–DTAB solutions [29] are from 3 to 30 times higher than in a NaPSS–DEDMAB system, depending on c_S^{tot} (note again that DTAB and DEDMAB surfactants have similar cmc values in spite of the slightly different head group). Only one point is available for comparison with C_nPC surfactants, and that is the cac value of CPC in aqueous polyelectrolyte solutions without a simple salt: it is 30 times higher in NaPA than in NaPSS. As concluded before, the explanation for the considerably lower cac values in NaPSS solutions lies in the specific nature of the polymer chain in this case. The binding between NaPSS and surfactant micelles occurs not only via electrostatic interactions between the charged species (as in the case of NaPA) but also via hydrophobic interactions between the surfactant hydrocarbon chains and the aromatic rings of the polyelectrolyte. This leads to a further reduction of cac.

III. SUMMARY

This chapter has focused on the phenomena of the binding of cationic surfactants to oppositely charged polyelectrolytes. Due to strong electrostatic attraction between the polyion and surfactant counterions and subsequent hydrophobic interactions, the micellarlike aggregation of surfactant takes place at a total surfactant concentration that is a few orders of magnitude lower than the cmc. The binding isotherms and critical aggregation concentration values of alkyltrimethylammonium and alkylpyridinium surfactants in the presence of NaPSS and NaPA point to the importance of the partly hydrophobic character of the poly(styrenesulfonate) chain. The complexation of cationic surfactants with NaPSS is stronger than with NaPA. This is attributed to the presence of hydrophobic functional groups on the poly(styrenesulfonate) chain that are solubilized in the polyelectrolyte-induced surfactant micelle.

In terms of total surfactant concentration, appreciable binding of dodecyl- and cetylpyridinium cation starts at the same total concentration, at about 1×10^{-5} mol dm^{-3}, irrespective of the ionic strength of solutions. Above this concentration the heat effects that accompany the complexation of surfactant with the polyelectrolyte increase sharply, and their value can be partly attributed to the micellization of detergent. The viscosity and apparent molar volume measurements reveal that above $c_S \approx 1 \times 10^{-5}$ mol dm^{-3} extensive coiling of the chain around surfactant micelles takes place. In addition to this, the unusual behavior of molar conductivity in polyelectrolyte–surfactant solutions shows that an appreciable amount of small counterions may

be released into the solution upon cooperative surfactant binding to polyelectrolytes.

REFERENCES

1. Armstrong RW, Strauss UP. Polyelectrolytes. In: Mark HF, Gaylord NG, Bikales NM, eds. Encyclopedia of Polymer Science and Technology. Vol. 10. New York: Interscience, 1968:781–861.
2. Katchalsky A, Alexandrowitz Z, Kedem O. Polyelectrolyte solutions. In: Conway BE, Barradas RG, eds. Chemical Physics of Ionic Solutions. New York: John Wiley, 1966:295–346.
3. Oosawa F. Polyelectrolytes. New York: Marcel Dekker, 1971.
4. Škerjanc J, Kogej K, Vesnaver G. Polyelectrolyte-surfactant interactions. Enthalpy of binding of dodecyl- and cetylpyridinium cations to poly(styrenesulfonate) anion. J Phys Chem 1988; 92:6382–6385.
5. Abuin EB, Sciano JC. Exploratory study of the effect of polyelectrolyte–surfactant aggregates on photochemical behavior. J Am Chem Soc 1984; 106: 6274–6283.
6. Škerjanc J, Dolar D. Thermodynamic properties of a polyelectrolyte solution containing a mixture of counterions differing in charge. J Chem Phys 1989; 91:6290–6294.
7. Škerjanc J. Electrostatic contributions to thermodynamic functions of systems containing polyions and mixtures of counterions differing in charge and size. J Chem Soc Faraday Trans 1992; 88:1249–1253.
8. Tanford C. The Hydrophobic Effect: Formation of Micelles and Biological Membranes. New York: John Wiley, 1980.
9. Škerjanc J, Kogej K. Thermodynamic and transport properties of polyelectrolyte–surfactant complex solutions at various degrees of complexation. J Phys Chem 1989; 93:7913–7915.
10. Škerjanc J, Kogej K. Electrical transport in polyelectrolyte–surfactant complex solutions at various degrees of complexation. In: Schmitz KS, ed. Macroion Characterization. From Dilute Solutions to Complex Fluids. Washington: ACS, 1994:268–275.
11. Hansson P, Almgren M. Interaction of alkyltrimethylammonium surfactants with poly(acrylate) and poly(styrenesulfonate) in aqueous solution. Phase behavior and surfactant aggregation numbers. Langmuir 1994; 10:2115–2124.
12. Gao Z, Wasylishen RE, Kwak JCT. An NMR study of the binding between polyelectrolytes and surfactants in aqueous solutions. J Colloid Interface Sci 1988; 126:371–376.
13. Cabane B. Structure of some polymer–detergent aggregates in water. J Phys Chem 1977; 81:1639–1645.
14. Magny B, Iliopoulos I, Audebert R. Aggregation of hydrophobically modified polyelectrolytes in dilute solutions: ionic strength effects. In: Dubin P, Bock J, Davies RM, Schulz DN, Thies C, eds. Macromolecular Complexes in Chemistry and Biology. Berlin: Springer Verlag, 1994:51–62.

15. Winnik FM, Regismond STA. Fluorescence methods in the study of the interactions of surfactants with polymers. Colloids Surfaces A 1996; 118:1–39.
16. Kogej K, Škerjanc J. Fluorescence and conductivity studies of polyelectrolyte-induced aggregation of alkyltrimethylammonium bromides. Langmuir 1999; 15:4251–4258.
17. Peña L, Junquera E, Aircart E. Ultrasonic study of the molecular encapsulation and the micellization processes of dodecylethyldimethylammonium bromide–water solutions in the presence of β-cyclodextrin or 2,6-di-*o*-methyl-β-cyclodextrin. J Solution Chem 1995; 24:1075–1091.
18. Škerjanc J, Kogej K, Cerar J. Equilibrium and transport properties of alkylpyridinium bromides. Langmuir 1999; 17:5023–5028.
19. Almgren M, Hansson P, Mukhtar E, van Stam J. Aggregation of alkyltrimethylammonium surfactants in aqueous poly(styrenesulfonate) solutions. Langmuir 1992; 8:2405–2412.
20. Satake I, Yang JT. Interaction of sodium decyl sulfate with poly(L-ornithine) and poly(L-lysine) in aqueous solutions. Biopolymers 1976; 15:2263–2275.
21. Kogej K, Škerjanc J. Binding of cetylpyridinium cation by poly(acrylic acid). Effect of polymer charge density. Acta Chim Slov 1999; 46:269–279.
22. Hayakawa K, Santerre JP, Kwak JCT. Study of surfactant–polyelectrolyte interactions. Binding of dodecyl- and tetradecylammonium bromide by some carboxylic polyelectrolytes. Macromolecules 1983; 16:1642–1645.
23. Malovikova A, Hayakawa K, Kwak JCT. Binding of alkylpyridinium cations by anionic polysaccharides. ACS Symposium Series 1984; 253:225–239.
24. Hansson P, Almgren M. Interaction of C_nTAB with sodium(carboxymethyl) cellulose: effect of polyion linear charge density on binding isotherms and surfactant aggregation number. J Phys Chem 1996; 100:9038–9046.
25. Kiefer JJ, Somasundaran P, Ananthapadmanabhan KP. Interaction of tetradecyltrimethylammonium bromide with poly(acrylic acid) and poly(methacrylic acid). Effect of charge density. Langmuir 1993; 9:1187–1192.
26. Hayakawa K, Kwak JCT. Surfactant–polyelectrolyte interactions. 1. Binding of dodecyltrimethylammonium ions by sodium dextran sulfate and sodium poly(styrenesulfonate) in aqueous solution in the presence of sodium chloride. J Phys Chem 1982; 86:3866–3870.
27. Hayakawa K, Kwak JCT. Study of surfactant–polyelectrolyte interactions. 2. Effect of multivalent counterions on the binding of dodecyltrimethylammonium ions by sodium dextran sulfate and sodium poly(styrenesulfonate) in aqueous solution. J Phys Chem 1983; 87:506–509.
28. Malovikova A, Hayakawa K, Kwak JCT. Surfactant–polyelectrolyte interactions. 4. Surfactant chain length dependence of the binding of alkylpyridinium cations to dextran sulfate. J Phys Chem 1984; 88:1930–1933.
29. Hansson P, Almgren M. Polyelectrolyte-induced micelle formation of ionic surfactants and binary surfactant mixtures studied by time-resolved fluorescence quenching. J Phys Chem 1995; 99:16684–16693.
30. Jones MN, Agg G, Pilcher G. Enthalpy of micellization IV. *n*-dodecylpyridinium iodide in aqueous potassium iodide and aqueous urea. J Chem Thermodynamics 1971; 3:801–809.

31. Hunter RJ. Association colloids. In: Foundations of Colloid Science. Vol. 1. Oxford: Claredon Press, 1987:564–625.
32. Jones MN, Piercy J. Light scattering studies on *n*-dodecyltrimethylammonium bromide and *n*-dodecylpyridinium iodide. J Chem Soc, Faraday Trans I 1972; 10:1839–1848.
33. Bežan M, Malavašič M, Vesnaver G. Surfactant binding to oppositely charged polyions. Ber Bunsenges Phys Chem 1996; 100:1054–1058.
34. Kogej K, Škerjanc J. Hydrodynamic investigations of polyelectrolyte–surfactant complexes in aqueous solutions. Acta Chim Slov 1999; 46:481–492.
35. Fouss RM, Strauss UP. Electrostatic interaction of polyelectrolytes and simple electrolytes. J Polym Sci 1948; 3:602–603.
36. Fouss RM, Strauss UP. Ann NY Acad Sci 1949; 12:48.
37. Gregor HP, Gold DH, Frederic M. Viscometric and conductometric titrations of polymethacrylic acid with alkali metal and quatenary ammonium bases. J Polym Sci 1957; 23:467–473.
38. Anghel DF, Saito S, Băran A, Iovescu A. Interaction between poly(acrylic acid) and nonionic surfactants with the same poly(ethylene oxide) but different hydrophobic moieties. Langmuir 1998; 14:5342–5346.
39. Wallin T, Linse P. Monte Carlo simulations of polyelectrolytes at charged micelles. 1. Effects of chain flexibility. Langmuir 1996; 12:305–314.
40. François J, Dayantis J, Sabbadin J. Hydrodynamical behavior of the poly(ethylene oxide)–sodium dodecylsulphate complex. Eur Polym J 1985; 21: 165–174.
41. Harned HS, Owen BB. The physical chemistry of electrolytic solutions. 3d ed. New York: Reinhold, 1958.
42. Kogej K, Škerjanc J. Effect of polyelectrolyte on the aggregation of cationic surfactants in aqueous solutions. Acta Chim Slov 1998; 45:443–453.
43. Linse P, Picullel L, Hansson P. Models of polymer–surfactant complexation. In: Kwak JCT, ed. Polymer–Surfactant Systems. New York: Marcel Dekker, 1998:193–238.
44. Kalyanasundaram K, Thomas JK. Environmental effects on vibronic band intensities in pyrene monomer fluorescence and their application in studies of micellar systems. J Am Chem Soc 1977; 99:2039–2044.
45. Winnik FM, Regismond STA. Fluorescence methods in the study of polymer–surfactant systems. In: Kwak JCT, ed. Polymer–Surfactant Systems. New York: Marcel Dekker, 1998:267–315.
46. Karpovich DS, Blanchard GJ. Relating the polarity-dependent fluorescence response of pyrene to vibronic coupling. Achieving a fundamental understanding of the py polarity scale. J Phys Chem 1995; 99:3951–3958.
47. Chu D, Thomas JK. Effect of cationic surfactants on the conformational transition of poly(methacrylic acid). J Am Chem Soc 1986; 108:6270–6276.
48. Zhen Z, Thung CH. Interaction of sodium carboxymethylamylose with aqueous surfactants in both the presence and the absence of added salt: mixed micelles and inclusion complexes. Polymer 1992; 33:812–816.
49. Thalberg K, Lindman B. Interaction between hyaluronan and cationic surfactants. J Phys Chem 1989; 93:1478–1483.

50. Jones MN. The interaction of sodium dodecyl sulfate with polyethylene oxide. J Colloid Interface Sci 1967; 23:36–42.
51. Goddard ED. Polymer–surfactant interactions. Part I. Uncharged water-soluble polymers and charged surfactants. In: Goddard ED, Ananthapadmanabhan KP, eds. Interactions of Surfactants with Polymers and Proteins. Boca Raton, FL: CRC Press, 1993:123–169.
52. Kogej K, Vrhovšek A, Škerjanc J. Interactions between anionic polyelectrolyte and cationic surfactant: steady-state fluorescence measurements. In: Noda I, Kokufuta E, eds. Polyelectrolytes. Osaka: Yamada Science Foundation, 1999: 288–291.
53. Shaw DJ. Introduction to Colloid and Surface Chemistry. London: Butterworths, 1980.

This Page Intentionally Left Blank

22

Metal Complexation in Polyelectrolyte Solutions

TOHRU MIYAJIMA Saga University, Saga, Japan

I. INTRODUCTION

Due to practical significance and theoretical interest, much effort has been made to clarify the unique characteristics of metal ion/polyelectrolyte mixture solutions in various disciplines of chemistry. Since a proper equilibrium expression for metal ion binding to polymer molecules is indispensable for the quantification of the physicochemical properties, ''apparent'' or ''macroscopic'' equilibrium constants have been determined. Unfortunately, however, these ''overall'' constants are usually defined arbitrarily, being dependent on the research groups, the experimental techniques, and the systems to be investigated; hence they are not comparable with each other nor relatable to the ''intrinsic'' equilibrium constants defined at respective reaction sites. Compared with the situation for the equilibrium analyses of metal complexation with monomer ligands, to which the ''law of mass action'' can directly be applied, complete analytical treatment of the metal ion/polyelectrolyte complexation equilibria has not yet been established even at the present time. There are essential difficulties inherent in the analyses of metal complexation equilibria in polyelectrolyte solutions.

It should be recognized firstly that the equilibria are affected by ''polyelectrolyte (electrostatic) effects'' due to a large and variable electrostatic potential developed at the polymer surface. The free metal ion concentration at the polymer reaction sites is usually much different from that in the bulk solution, which prevents the direct application of the simple ''law of mass action'' to the equilibrium analyses. Free metal ions are attracted to a negatively charged polymer surface, whereas they are repelled from a positively charged polymer surface. Their effective concentrations in the vicinity of charged polymer molecules are, therefore, higher or lower in magnitude than

the bulk solution, and the degree of concentration or dilution is primarily dependent on the linear charge density of the polyion as well as the concentration levels of inert salt present in excess. The mobile ion distribution equilibria between the polyion surface and the bulk solution region must be evaluated in order to determine the ''intrinsic'' equilibrium constants. These microscopic constants thus determined become comparable with the ''stability constants'' of the corresponding metal complexes with monomeric ligands whose chemical structures mimic the polymer functional groups.

A straightforward experimental approach to describe the ion distribution equilibria of polyelectrolyte solutions is presented in this chapter. The approach assumes a ''counterion concentration region'' around the polyion skeleton [1–4]. Only two concentration terms of counterions corresponding to the two regions, i.e., polyion domain and bulk solution, are defined; the ion distribution gradients generating between the polyion surface and the bulk solution are neglected. Though the boundary between the polyion domain and the bulk solution is not necessarily observable, a hypothetical volume element (V_p) for the polyion domain is defined and determined experimentally, which enables us to calculate the ''averaged'' concentration of free metal ions in the domain. This concept indicates that ion binding in polyelectrolyte solutions can uniquely be interpreted as an ''ion-exchange reaction'' between the polyelectrolyte phase and the bulk solution phase, and that the distribution equilibria of counterions and coions between the two phases are expressible simply by a Gibbs–Donnan relation [5–7]. Two distinct states of bound counterions are notified by this approach. Ions electrostatically concentrated in the vicinity of the polymer molecules are designated as ''territorially bound'' [8,9]. They are ''bound'' in a thermodynamic sense but are essentially ''free'' to move within the polyelectrolyte domain. On the other hand, there are ions bound directly to the functional groups fixed on the polymer ligands accompanied by desolvation of metal ions and the ligand functionalities, which are designated as ''site bound'' [8,9]. They include contact ion pairs, multidentate complexes, and chelate complexes.

Applicability of the concept to the analyses of complexation equilibria of weak acidic polyelectrolytes has fully been documented in our previous reviews [6,7]. The equality in the equilibrium expression for water-soluble linear polyelectrolytes and ion exchangers (water-insoluble cross-linked linear polyelectrolytes) has been stressed [6] by exemplifying the analyses of metal complexation with negatively charged polyelectrolytes, where sodium ions are selected as supporting cations. However, later studies have revealed a pronounced supporting cation effect on the apparent metal complexation with weak acidic polymer ligands [10], as well as supporting anion effects on the apparent metal complexation with weak basic polymer

ligands. These effects, attributable to hydrophobic interactions between the supporting ions and the polymer molecules, are directly relatable to the hydration state of the polymer molecules. Therefore, in this chapter, it is notified secondly that the hydrophobic nature of polyion ligand should be taken into consideration in the equilibrium analysis in addition to the polyelectrolytic nature. The degree of hydration of a polyion can directly be related to the V_p value as indicated by the present chapter, i.e., a hydrophilic polyion gives a larger V_p, and low counterion concentration in the polyelectrolyte phase is anticipated, whereas a hydrophobic polymer with smaller V_p results in high counterion concentration. In this chapter, such a hydrophobicity/hydrophilicity effect on metal ion/polyelectrolyte complexation systems is examined in detail.

In addition to these two difficulties, another essential difficulty in the complexation behaviors of polymer-ligands must be pointed out when compared with monomer-ligand complexation systems [6,7]. Since the ligand moieties of linear polyelectrolytes are arranged linearly on the polymer molecules, the definition of the stability constants of multicoordinated complexes must be different from the corresponding monomer-ligand complexes. When a metal ion can coordinate with more than two ligand moieties belonging to one polymer-ligand molecule, the first coordination reaction, i.e., the reaction with the first ligand moiety, can be categorized as an intermolecular reaction, which can be analyzed in the same manner as the monomer-ligand complexation. However, the successive coordination reactions will take place in two different manners, i.e., intermolecular and intramolecular complexations, though all the successive coordinations in monomer-ligand complexations are definitely in intermolecular mode. If the successive complexation in polymer-ligand system takes place in an intramolecular mode, then the polymer conformational change upon pH, the degree of hydration of polymer surface, etc., is expected to affect greatly the multicoordination nature of the polymer ligand.

In this chapter, approaches to estimates of (1) the polyelectrolyte (electrostatic) effect, (2) the hydrophobicity/hydrophilicity effect, and (3) the multicoordination effect, specified for metal ion/polyelectrolyte systems are described. As weak acidic polyelectrolytes, polyacrylic acid, PAA, as well as polymethacrylic acid, PMA, are exemplified; as an example of weak basic polyelectrolyte, poly(*N*-vinylimidazole), PVIm, is chosen; all the chemical structures of the polymer ligands are illustrated in Figure 1. Precise potentiometric titration studies by the use of a glass electrode as well as respective metal ion selective electrodes have been performed for the complexation equilibrium analyses. All the equilibrium constants reported in this chapter were obtained at 298 K unless otherwise stated.

PAA
Polyacrylic acid

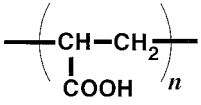

PMA
Polymetacrylic acid

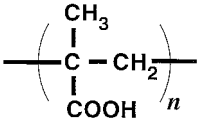

PVIm
Poly(*N*-vinylimidazole)

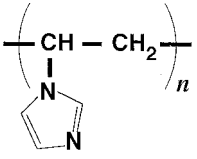

FIG. 1 The chemical structures of the polymer ligands discussed in this chapter.

II. ACID DISSOCIATION EQUILIBRIA OF WEAK POLYELECTROLYTES

The equilibria of metal (M^{Z+}) complexation and H^+ binding in weak acidic polyelectrolyte or weak basic polyelectrolyte solution can be treated equally, since both ions are cationic. However, conventionally H^+ binding equilibria are expressed by acid dissociation. In this section, the acid dissociation equilibria of both weak acidic and weak basic polyelectrolytes are analyzed by the Gibbs–Donnan concept [5–7], and the fundamental aspects clarified up to the present time are presented.

A. Comparison of Weak Acidic Polyelectrolytes and Weak Basic Polyelectrolytes

Though the phase boundary is not necessarily observable, the remarkable salt concentration (C_s/mol/dm^3) dependence of the ion binding equilibria in polyion systems implies the phase separation nature of the polyelectrolyte solutions. A straightforward proof for this property can be gained by the careful examination of the acid dissociation equilibria of weak acidic polyelectrolytes, $(HA)_n$, and the conjugate acids of weak basic polyelectrolytes, $(BH^+)_n$, respectively, expressed as the repeated functionalities of HA and BH^+:

$$HA \rightleftarrows H^+ + A^-$$
$$BH^+ \rightleftarrows H^+ + B$$

The equilibria can be quantified by defining the apparent acid dissociation constant, pK_{app}, calculable by the use of the measured pH and the degree of dissociation of the functionalities, α, at equilibrium:

$$pK_{app} = pH - \log\left(\frac{\alpha}{1-\alpha}\right) \tag{1}$$

pK_{app} reflects the overall acid dissociation equilibrium and is substantially affected by both α and C_s. On the other hand, a hypothetical intrinsic acid dissociation constant, pK_0, can be defined for the polyelectrolyte in order to describe the microscopic acid dissociation equilibrium for the identical functionalities repeated on the linear backbone. pK_0 is defined as an acid dissociation constant in the polyelectrolyte phase, being not influenced by the magnitude of the electrostatic effect, i.e., it remains unvaried despite the change in α or C_s. The value of pK_0 can usually be estimated experimentally by extrapolating the pK_{app} vs. α plots to the y intercept at the fully uncharged state, i.e., $\alpha = 0$ for $(HA)_n$ and $\alpha = 1$ for $(BH^+)_n$, which is equal to or quite close to the pK_a value of the corresponding monomeric acid.

By the use of averaged pH in the polyelectrolyte phase, $(pH)_p$, pK_0 at specified α can be expressed as

$$pK_0 = (pH)_p - \log\left(\frac{\alpha}{1-\alpha}\right) \tag{2}$$

It should be noted again that if C_s is fixed, pK_{app} is expressed just as the function of α. Since pK_0 remains constant at any α, the following equation can be obtained by combining Eqs. 1 and 2:

$$pK_{app} = pK_0 + \log\left[\frac{(a_H)_p}{a_H}\right] \tag{3}$$

Equation 3 indicates that the difference pK_{app} and pK_0, ΔpK, reflects the activity ratio of H^+ between the two phases.

In the presence of an excess 1:1 inert salt (A^+X^-), the following relationship is anticipated [5–7,11] by equating the activities of A^+X^- in both phases:

$$(a_A)_p(a_X)_p = a_A a_X \tag{4}$$

By equating the activities of H^+X^- in both phases as well, the following equation can be derived:

$$(a_H)_p(a_X)_p = a_H a_X \tag{5}$$

Counterions, i.e., A^+ for negatively charged polymers and X^- for positively charged polymers, respectively, are concentrated in the polyion domain, and the counterion activity ratios between the two phases, i.e., $(a_A)_p/a_A$ and $(a_X)_p/a_X$, respectively for anionic and cationic polymers, can be related to the activity ratio of singly charged H^+ ions by the equations

$$\frac{(a_A)_p}{a_A} = \frac{(a_H)_p}{a_H} \tag{6}$$

and

$$\frac{(a_X)_p}{a_X} = \frac{a_H}{(a_H)_p} \tag{7}$$

Replacing the $(a_H)_p/a_H$ term appearing in Eq. 3 by $(a_A)_p/a_A$ or $a_X/(a_X)_p$, we obtain the following two equations, which predict the counterion concentration dependence of the acid dissociation equilibria of $(HA)_n$ and $(BH^+)_n$ polymers:

$$pK_{app} = pK_0 + \log(a_A)_p - \log a_A \tag{8}$$

and

$$pK_{app} = pK_0 - \log(a_X)_p + \log a_X \tag{9}$$

Potentiometric titration profiles of the two representative linear polyelectrolytes, i.e., polyacrylic acid, PAA [11], and the conjugate acid of poly(*N*-vinylimidazole), $PVImH^+$ [11], indeed validate the phase separation properties of the polyelectrolytes in aqueous solution. In Figures 2 and 3, the pK_{app} values determined under various salt (NaCl) concentration levels are plotted against α, respectively for PAA and $PVImH^+$. With increasing α from 0 to 1, the averaged charge per functionality (Z) of PAA molecules varied from 0 to -1, whereas the Z value for $PVImH^+$ decreases from $+1$ to 0. pK_{app} increases with α in both cases, whereas the effect of C_s is entirely opposite to each other, i.e., the C_s increase leads to depression of pK_{app} of PAA, whereas the pK_{app} value of $PVImH^+$ is enhanced by the C_s increase. It is also notable that the separate lines appearing in Figures 2 and 3 converge at the uncharged (neutral) state ($Z = 0$), i.e., $\alpha = 0$ for PAA and $\alpha = 1$ for $PVImH^+$, respectively. The extrapolated pK_{app} values at the particular points ($Z = 0$) corresponding to their intrinsic acid dissociation constants, i.e., the pK_0 values, are 4.3 for PAA and 7.0 for $PVImH^+$, respectively. These values are consistent with the pK_a values of their corresponding monomeric acids, i.e., acetic acid ($pK_a = 4.55$ [12]) and the conjugate acid of imidazole ($pK_a = 6.99$ [13]).

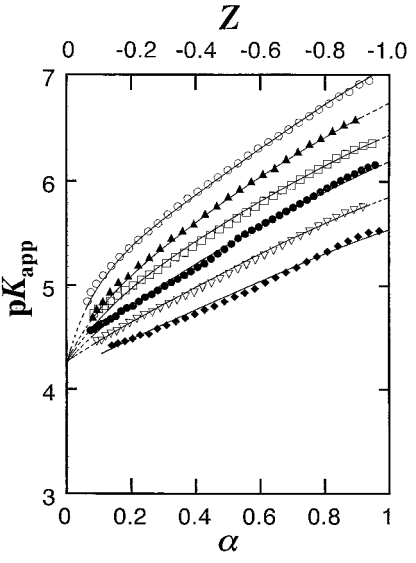

FIG. 2 Effects of salt (NaCl) concentration level and the degree of dissocation on pK_{app} of PAA: (○) C_s = 0.01; (▲) C_s = 0.02; (□) C_s = 0.05; (●) C_s = 0.10; (▽) C_s = 0.20; (♦) C_s = 0.50 mol/dm^3. (From Ref. 11.)

By plotting the pK_{app} values thus determined against log a_{Na} or log a_{Cl}, the validity of Eqs. 8 and 9 can be examined. In Figure 4, the pK_{app} values for PAA corresponding to specified α values are plotted against log a_{Na}; it is obvious that at low concentration levels of the medium and at a highly dissociated state of the polymer, the plots show linearity, whose slope is quite close to -1. On the contrary, at a fully protonated state, where the electrostatic potential is completely diminished, constant pK_{app}, being equal to pK_0, is obtained. This trend can be rationalized by Eq. 8 by considering the change in the magnitude of $(a_{Na})_p$. $(a_{Na})_p$ is usually expected to be much larger in value than a_{Na}, but at sufficiently high C_s the concentration gradient between the two phases is diminished completely and $(a_{Na})_p$ becomes quite close to a_{Na}, which results in the specified case where pK_{app} approaches pK_0. The reasoning for the linearity observed at the low C_s region with the slope of -1, on the other hand, can be given by the constancy in $(a_{Na})_p$ irrespective of the change in C_s. In our earlier studies on the volume measurement of carboxylated ion exchangers [14,15], the specific water sorption by the ion exchanger has been proven insensitive to the change in C_s at the fully dissociated state. Due to the similarity in the solvation property of water-soluble linear polymers and the water sorption behavior of corresponding water-

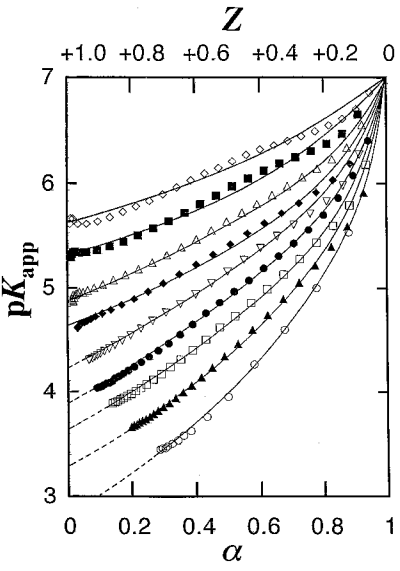

FIG. 3 Effects of salt (NaCl) concentration level and the degree of dissociation on pK_{app} of $PVImH^+$: (○) C_s = 0.01; (▲) C_s = 0.02; (□) C_s = 0.05; (●) C_s = 0.10; (▽) C_s = 0.20; (♦) C_s = 0.50; (△) C_s = 1.00; (■) C_s = 2.00; (◇) C_s = 3.00 mol/dm^3. (From Ref. 11.)

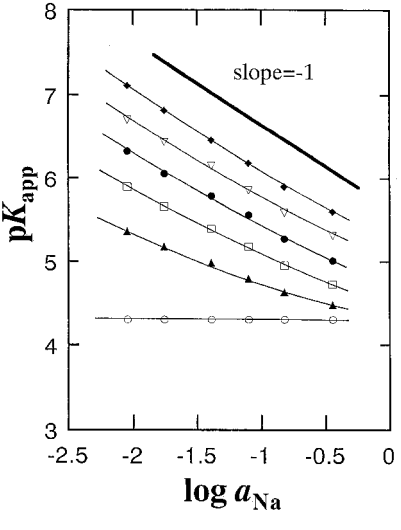

FIG. 4 Log a_{Na} dependence of pK_{app} of PAA: (○) α = 0; (▲) α = 0.2; (□) α = 0.4; (●) α = 0.6; (▽) α = 0.8; (♦) α = 1.0. (From Ref. 11.)

insoluble ion exchangers, the polyelectrolyte phase volume defined for linear polyelectrolyte must be insensitive to the C_s change based on the same logic, which leads to constant $(a_{Na})_p$ when α is close to unity [14,15].

Much deeper insights into the water sorption properties of polyelectrolytes can be provided by evaluating the $(a_{Na})_p$ term directly. By the use of the activity coefficient of Na^+ ions in the PAA polyelectrolyte phase, $(y_{Na})_p$, $(a_{Na})_p$ can be expressed as $(a_{Na})_p = (y_{Na})_p\,[Na]_p$. Two concentration terms, i.e., (1) Na^+ ions present in the polyelectrolyte phase to neutralize free carboxylate groups and (2) Na^+ ions imbibed in the polyelectrolyte phase in the form of NaCl, contribute the $[Na]_p$ term. Escape of Na^+ ions from the polyelectrolyte phase due to their thermal motion, which produces a site vacancy of the polyion, should also be taken into consideration. The fraction of site vacancy of polyelectrolytes is available as a ''practical osmotic coefficient,'' $\phi_{p,Na}$, which can simply be related to the linear charge separation of the PAA polyion. It has been revealed that $\phi_{p,Na}$ is not affected by the change in the polyion concentration nor C_s, which is known as an additivity rule [16,17]. Thus the $(a_{Na})_p$ term can finally be expressed as

$$(a_{Na})_p = (y_{Na})_p \left[\frac{(1 - \phi_{p,Na})\alpha n_p}{V_p} + (C_{NaCl})_p \right] \tag{10}$$

where n_p indicates the amount of functional groups fixed on the polyion molecules. Since the concentration of salt imbibed in the polyelectrolyte phase, $(C_{NaCl})_p$, is negligible at the highly dissociated state of PAA and the $\phi_{p,Na}$ term remains constant despite the remarkable change in C_s, $(a_{Na})_p$ must remain unvaried at defined α.

The validity of the present logic can further be tested by calculating the polyelectrolyte phase volume itself by the use of the ΔpK term. This computation procedure has previously been proposed by exemplifying carboxymethyldextran and its gel analogs, CM-Sephadex (Pharmacia) [6,14,15]. For PAA, the $\phi_{p,Na}$ values are available by the literature owing to Katchalsky et al. [18]. With the reported $\phi_{p,Na}$ values, the polyelectrolyte phase volume per charged site, $V_p/(\alpha n_p)$, now becomes computable according to the equation

$$\frac{V_p}{\alpha n_p} = \frac{(y_{Na})_p}{y_{Na}} (1 - \phi_{p,Na})(10^{\Delta pK} - 10^{-\Delta pK})^{-1}[Na]^{-1} \tag{11}$$

The $V_p/(\alpha n_p)$ values thus calculated are plotted in Figure 5 against α/b, where b represents the formal functionality spacing on the linear polymer expressed in Å. In this computation, it is assumed that the activity coefficient quotient, $(y_{Na})_p/y_{Na}$, is approximately equal to unity, which has been validated by the comparison of the directly measured gel phase volume of carboxy-

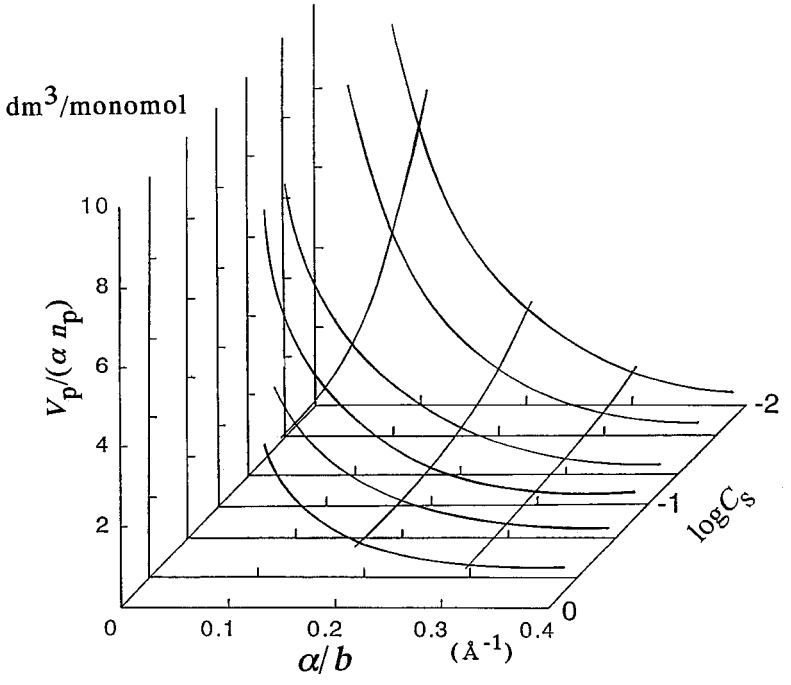

FIG. 5 Effective polyelectrolyte phase volume of PAA expressed as a function of the linear charge density and salt concentration level. The inverse value of $V_p/(\alpha n_p)$ corresponds to the average salt concentration level in the polyelectrolyte phase.

methyldextran gel with the corresponding polyelectrolyte phase volume computed by the use of the acid dissociation equilibria as a probe [14,15]. The effective polyelectrolyte phase volume increases drastically with the decrease in the linear charge separation, α/b ($Å^{-1}$). Also, it can be seen from the figure that the variation of $V_p/(\alpha n_p)$ with respect to C_s is negligible at a sufficiently charged state, i.e., at $\alpha = 1$, the $V_p/(\alpha n_p)$ value is ca. 1 dm^3/monomol, indicating that the PAA polyelectrolyte phase can be approximated as a concentrated salt solution, whose ionic strength is ca. 1 mol/dm^3.

The relationship observed in the pK_{app} vs. log a_{Cl} plots for $PVImH^+$ (Figure 6) can be rationalized based on the "phase separation" logic by the identical manner with PAA. At low C_s with highly charged state, the linearity with the slope of +1 has been obtained for $PVImH^+$, which is, indeed, in accordance with Eq. 9. As with Eq. 10, $(a_{Cl})_p$ appearing in the right hand side of Eq. 9, can be expressed as

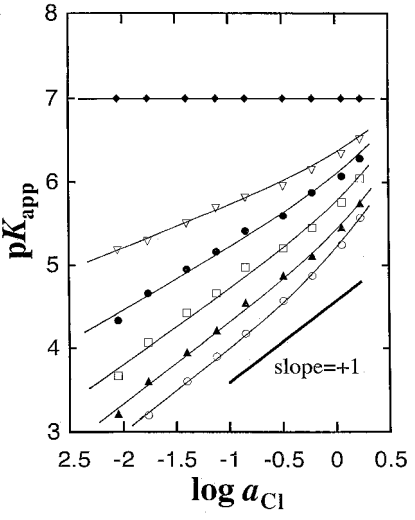

FIG. 6 Log a_{Cl} dependence of pK_{app} of $PVImH^+$: (○) $\alpha = 0$; (▲) $\alpha = 0.2$; (□) $\alpha = 0.4$; (●) $\alpha = 0.6$; (▽) $\alpha = 0.8$; (♦) $\alpha = 1.0$. (From Ref. 11.)

$$(a_{Cl})_p = (y_{Cl})_p \left[\frac{(1 - \phi_{p,Cl})(1 - \alpha)n_p}{V_p} + (C_{NaCl})_p \right] \tag{12}$$

where $(y_{Cl})_p$ indicates the activity coefficient of Cl^- ions in the $PVImH^+$ polyelectrolyte phase, and $\phi_{p,Cl}$ is the "practical osmotic coefficient" of $PVImH^+Cl^-$ solution. It is apparent from Eqs. 8–12 that the ΔpK ($=pK_{app} - pK_0$) term is directly relatable to the specific polyelectrolyte phase volume. Equation 3 implies that the ΔpK term directly reflects the magnitude of concentration or dilution of free H^+ ions in the polyelectrolyte phase compared with the bulk solution phase across a hypothetical Donnan semipermeable membrane. The ΔpK values are always positive for PAA and negative for $PVImH^+$. Since both polymer molecules are composed of the same backbone structures with the same spacing of functionalities, it is of great interest to examine the relationship between the magnitude of ΔpK and the averaged formal charge of the polymer molecules. In Figures 7 and 8, the absolute values of ΔpK, $|\Delta pK|$, are plotted against Z. By comparing these figures with each other, it becomes apparent that $|\Delta pK|$ corresponding to the same C_s is much larger for $PVImH^+$ than PAA, which indicates Cl^- ions are much more concentrated for $PVImH^+$ surface than the case where Na^+ ions are concentrated around PAA molecules. This trend can qualitatively be explained by reduced $V_p/(\alpha n_p)$ for $PVImH^+$ molecules compared with PAA, due to the lower degree of hydration of imidazolium groups as well

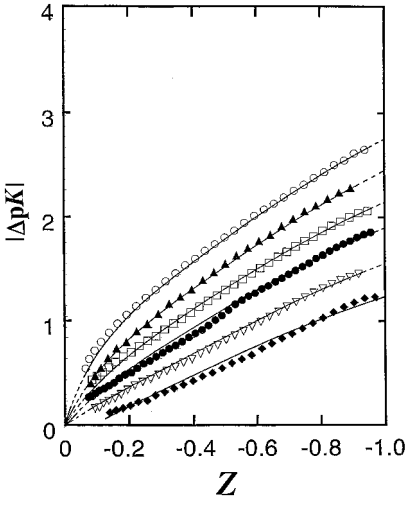

FIG. 7 $|\Delta pK|$ determined for PAA: (○) $C_s = 0.01$; (▲) $C_s = 0.02$; (□) $C_s = 0.05$; (●) $C_s = 0.10$; (▽) $C_s = 0.20$; (♦) $C_s = 0.50$ mol/dm^3. (From Ref. 11.)

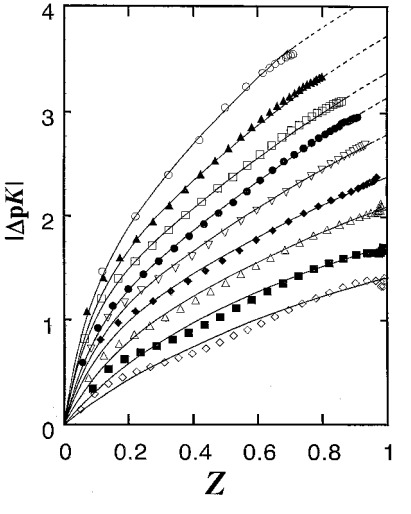

FIG. 8 $|\Delta pK|$ determined for $PVImH^+$: (○) $C_s = 0.01$; (▲) $C_s = 0.02$; (□) $C_s = 0.05$; (●) $C_s = 0.10$; (▽) $C_s = 0.20$; (♦) $C_s = 0.50$; (△) $C_s = 1.00$; (■) $C_s = 2.00$; (◇) $C_s = 3.00$ mol/dm^3. (From Ref. 11.)

as Cl^- ions [19,20], which can be related to the hydrophobic nature of the polymer molecules.

B. Hydrophobicity/Hydrophilicity Nature

In the preceding section, the acid dissociation behaviors of weak polyelectrolytes in the presence of excess sodium chloride have been interpreted according to the Gibbs–Donnan concept. It has been revealed, however, that these equilibria are sometimes highly affected by the nature of supporting cations [21,22] as well as anions [23,24]. It is of special interest to examine the applicability of the present concept to the acid dissociation analyses of these weak polyelectrolytes in the presence of supporting salt other than sodium chloride. The effect of alkali metal ions such as Li^+, Na^+, and K^+ on the apparent acid dissociation equilibria of PAA is quite small and can be neglected, whereas the dissociation is substantially depressed by the addition of quaternary ammonium ions whose magnitude increases with the bulkiness of the ions, giving much higher pK_{app} values than those obtained with alkali metal ions. pK_{app} determined in the presence of chloride salts of tetramethylammonium (TMA^+), tetraethylammonium (TEA^+), tetra *n*-propylammonium (TPA^+), and tetra *n*-butylammonium (TBA^+) chloride of 0.01 mol/dm^3 are plotted in Figure 9 against α in order to show this trend. The H^+ binding to carboxylate groups fixed on the linear polymer is enhanced successively in the order of $TMA^+ < TEA^+ < TPA^+ < TBA^+$. In any case, however, it is obvious that extrapolation of the curves to intercept the pK_{app} coordinate at $\alpha = 0$ leads to assignment of ca. 4.5, corresponding to the pK_a value of the monomeric carboxylic acid, i.e., acetic acid ($pK_a = 4.56$ [12]). This pronounced effect of the bulkiness of quaternary ammonium ions has been rationalized by taking into account the closest approach of quaternary ammonium ions to the polyion surface [25], by which the surface potential is calculated according to a Poisson–Boltzmann equation. An alternative interpretation has recently been proposed [26]; the hydrophobic nature of supporting cations enhances the H^+ binding to carboxylate groups because water sorption by carboxylate polymer molecules must be highly suppressed by the presence of hydrophobic countercations accumulated in the vicinity of the polymer molecules. A straightforward evidence for this hypothesis with regard to the hydrophobicity/hydrophilicity effect of counterions on the water sorption property of polyelectrolytes is the fact that $PVImH^+$ molecules precipitate by the addition of excess hydrophobic ClO_4^- or SCN^-, though no precipitation is produced by the addition of hydrophilic ions such as Cl^- or NO_3^- [23,24]. The acid dissociation of $PVImH^+$ molecules is weakened by the addition of hydrophobic anions [23,24], and this feature is in parallel with our interpretation on the effect of quaternary ammonium ions on the acid dissociation of PAA.

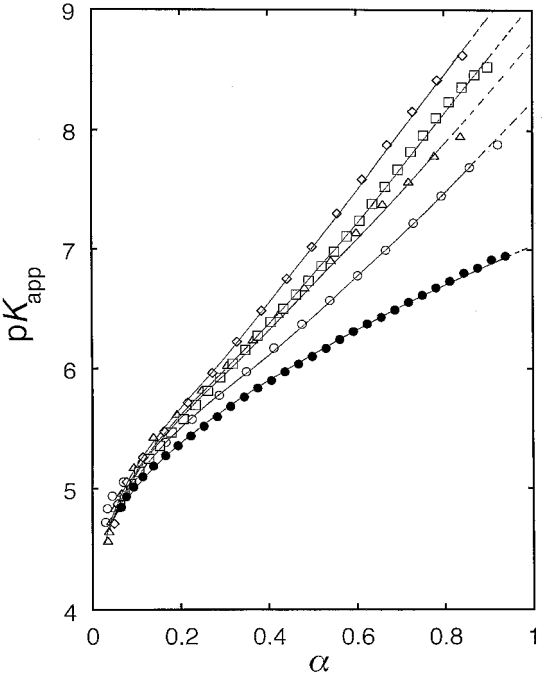

FIG. 9 Effect of bulkiness of quarternary ammonium ions on pK_{app} vs. α plots. C_s = 0.01 mol/dm^3. (●) Na^+; (○) TMA^+; (△) TEA^+; (□) TPA^+; (◇) TBA^+. (From Ref. 10.)

The hydrophobicity/hydrophilicity nature of the polymer molecules, i.e., the degree of hydration of fixed functional groups and/or the polymer backbone, is well known to affect the ion binding equilibria. For example, by comparison of the pK_{app} vs. α plots for carboxymethyldextran [6,14,15] and PAA [11,27] with identical linear spacing of carboxylate groups, it is evident that the smaller nonideality term is observed for carboxymethyldextran than PAA, which reveals a much higher degree of water sorption for the more flexible and hydrophilic polysaccharide (carboxymethyldextran) than PAA with less hydrated vinyl polymer backbone [26].

Polymethacrylic acid, PMA, is composed of vinyl polymer backbone as with PAA molecules, but α carbons attached to carboxyl groups are bonded to methyl groups instead of hydrogen atoms. This rather hydrophobic polycarboxylic acid shows a peculiar acid dissociation behavior. As is illustrated in Figure 10, the pK_{app} vs. α plots of PMA molecules determined in the presence of NaCl reveal a transition at α = ca. 0.3 [28]. It is believed that

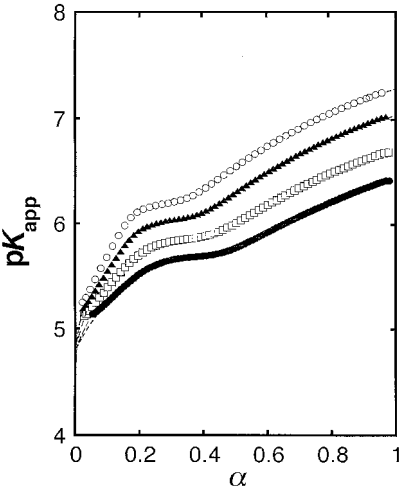

FIG. 10 Effects of salt (NaCl) concentration level and the degree of dissociation on pK_{app} of PMA: (○) C_s = 0.01; (▲) C_s = 0.02; (□) C_s = 0.05; (●) C_s = 0.10 mol/dm^3. (From Ref. 29.)

at low α region ($0 < \alpha < 0.3$), a PMA molecule has a compact form, whereas it begins to expand smoothly with increasing charge of the molecule ($0.3 < \alpha$) [29]. The titration behavior at this higher α region is quite similar to that of PAA molecules. Despite the separate curves due to the difference in the salt concentration levels, extrapolation of the curves to intercept the pK_{app} axis at $\alpha = 0$ leads to resolution of a pK_0 value of 4.8, which is consistent with the pK_a value of the corresponding monomeric carboxylic acid, 2,2-dimethylpropanoic acid, 4.83 [30]. Thus by comparing the pK_{app} vs. α plots for PMA and PAA, it can be elucidated that at specified α region, $0 < \alpha < 0.3$, an additional nonideality term should be taken into account to explain the acid dissociation behavior. This additional ΔpK term specifically observed in a PMA system is attributable to the hydrophobic nature of the compact PMA molecules; the effective charge density of PMA molecule is enhanced due to the compact structure, but at the same time, the hydrophobic nature of the polymer surface must be enhanced. According to the Gibbs–Donnan logic, the ΔpK term is considered to reflect directly the H^+ ion activity ratios between the two phases, whether ions are concentrated or diluted in the polyelectrolyte phase, or whether the polymer is hydrophilic or hydrophobic. The higher ΔpK values observed in the PMA system at lower α region ($0 < \alpha < 0.3$) compared with PAA indicates the much higher

degree of concentration of H^+ in the vicinity of the polymer molecules than PAA molecules in this region.

III. METAL COMPLEXATION EQUILIBRIA OF WEAK POLYELECTROLYTES

In the preceding section, the remarkable salt concentration effect on the acid dissociation equilibria of weak polyelectrolytes has been interpreted in a unified manner. In this treatment, the pK_{app} values determined experimentally are believed to reflect directly the electrostatic and/or hydrophobic nature of polyelectrolyte solutions at a particular condition. It has been proposed that the nonideality term (ΔpK) corresponds to the activity ratio of H^+ between the polyelectrolyte phase and the bulk solution phase, and that the ion distribution equilibria between the two phases follow Donnan's law. In this section, the Gibbs–Donnan approach is extended to the equilibrium analysis of metal complexation of both weak acidic and weak basic polyelectrolytes, i.e., the ratio of the free metal ion activity or concentration in the vicinity of polyion molecules to that of bulk solution phase is expressed by the ΔpK term. In Section III.A, a generalized analytical treatment of the equilibria based on the phase separation model is presented, which gives information on the intrinsic complexation equilibria at a molecular level. In Secs. B and C, which follow, two representative examples of the equilibrium analyses with weak acidic (PAA) and weak basic (PVIm) functionalities have been presented separately, in order to validate the present approach. The effect of polymer conformation on the apparent complexation equilibria has been described in Sec. III.D by exemplifying PMA.

A. Generalized Analytical Treatment

According to the two-phase approach, the ''overall'' or ''apparent'' complexation of metal ions, M^{Z+}, with polymer ligands can generally be expressed by the two-state equilibria [9,31] as

$$M^{Z+}\ (\text{free}) \rightleftarrows M^{Z+}\ (\text{bound}) \tag{13}$$

This equilibrium can be described as metal ion distribution between the two phases, i.e., M^{Z+} (free) and M^{Z+} (bound) correspond to M^{Z+} in the bulk solution and that in the polyelectrolyte phase, respectively, and an ''apparent binding constant,'' $(K_M)_{app}$, is defined as the concentration ratio of bound metal ions to free metal ions;

$$(K_M)_{app} = \frac{[M]_{bound}}{[M]\alpha C_p} = \frac{C_M - [M]}{[M]\alpha C_p} \tag{14}$$

where C_M and C_p indicate the total concentrations of metal ions and ligand

units fixed on the polymer molecules, respectively. The term αC_p, is incorporated in the denominator of the right hand side of Eq. 14 in order to normalize the equilibrium coefficient. Since the two total concentration terms, C_M and C_p appearing in Eq. 14 are known, the macroscopic binding constant becomes calculable once the free metal ion concentration [M] is experimentally determinable at a specified α. $(K_M)_{app}$ is affected by metal loading, C_M/C_p, as well as α and C_s. However, in the following discussions, metal loading to polymer ligand is maintained negligible, i.e., the apparent binding constant is determined in the presence of a small amount of M^{Z+} to be neglected compared with the amount of ligand units fixed on the polymer molecules. This apparent binding constant defined at the particular condition is denoted as $(K^0_M)_{app}$.

$$(K^0_M)_{app} = (K_M)_{app} \qquad \frac{C_M}{C_p} \to 0 \tag{15}$$

Just like the acid dissociation equilibria, the complexation equilibria of weak polyelectrolytes are strongly affected by pH and C_s due to the electrostatic and/or hydrophobic nature of the polymeric ligand molecule. In order to correlate these overall equilibria with the intrinsic complexation equilibria at the reaction sites of polymer ligands, it is essential to evaluate properly the magnitude of the electrostatic and/or hydrophobic effect, which is dependent on α and C_s. According to the Gibbs–Donnan approach, the correction is available by the nonideality term experienced in the acid dissociation equilibrium analysis. As has been indicated by Eq. 15, the ratio of the activity or concentration of H^+ in the phase of polyelectrolyte to that in the bulk solution phase can be accessible experimentally by measuring pK_{app}. Also, since we know that the Donnan relation holds for the system (M^{Z+}/H^+/polyelectrolyte), the following equation can be obtained:

$$(a_M)_p(a_X)^Z_p = a_M a^Z_X \tag{16}$$

Combining Eqs. 16 and 5, the activity ratio of free M^{Z+} between the two phases, $(a_M)_p/a_M$, can be related to that of monovalent H^+ as

$$\frac{(a_M)_p}{a_M} = \left[\frac{(a_H)_p}{a_H}\right]^Z \tag{17}$$

By the use of concentration units instead of activities for simplicity, Eq. 17 becomes

$$\frac{[M]_p}{[M]} = G\left(\frac{[H]_p}{[H]}\right)^Z \tag{18}$$

where G represents the activity coefficient quotient ($G = y_M(y_M)_p^{-1}$

$\cdot (y_H)_p^Z (y_H)^{-Z}$). Assuming that the G value is constant and equal to unity [6,7,30], Eq. 18 can be written as

$$\frac{[M]_p}{[M]} = \left[\frac{[H]_p}{[H]}\right]^Z = 10^{Z\Delta pK} \tag{19}$$

This equation reveals that the concentration of free M^{Z+} in the polyelectrolyte phase can be related to the corresponding concentration in the bulk solution by the use of the corresponding ΔpK and the charge of metal ions, Z. The primary correction needed to correlate apparent binding constant to intrinsic one is to substitute [M] appearing in Eq. 14 by $[M]_p$, the free M^{Z+} concentration in the polyelectrolyte phase, as has been pointed out previously. A straightforward approach to gain information on the complexation at the reaction sites of polymer ligand molecules is, indeed, to relate the apparent complexation function, $(K_M^0)_{app}$, to an intrinsic complexation function, $(K_M^0)_{int}$, through the path

$$(K_M^0)_{app} = \frac{[M]_p}{[M]} (K_M^0)_{int} \tag{20}$$

Both $(K_M^0)_{app}$ and $[M]_p/[M]$ vary substantially with α and C_s, but $(K_M^0)_{int}$ is unaffected by the change in these factors, once the binding mode of a metal ion to a polymer ligand is not affected by the α change. By combining Eqs. 19 and 20 we obtain

$$(K_M^0)_{app} = \left[\frac{[H]_p}{[H]}\right]^Z (K_M^0)_{int} = 10^{Z\Delta pK} (K_M^0)_{int} \tag{21}$$

and

$$\log(K_M^0)_{app} = Z\Delta pK + \log(K_M^0)_{int} \tag{22}$$

Equation 22 predicts that the nonideality term for the acid dissociation equilibria of weak polyelectrolytes can directly be used to evaluate the $(K_M^0)_{int}$ function, i.e., if $\log(K_M^0)_{app}$ is plotted against ΔpK, a straight line with the slope Z is expected, whose intercept at the y axis corresponds to $\log(K_M^0)_{int}$ [5–7]. It should be noted again that (1) the concurrent measurement of pH and pM at each titration point is needed for this analysis and (2) the ratio of the total concentrations of metal ion to ligand polymer should be kept as low as possible for the perturbation due to complexation on acid dissociation equilibria to be neglected.

B. Polyacrylic Acid Complexation

Prior to the discussions on the applicability of the Gibbs–Donnan approach to PAA complexation analyses, the results on the complexation analyses

reported up to the present time are briefly described hereafter. Gregor et al. [32–34] and Mandel and Leyte [35] have analyzed the equilibria by a modified Bjerrum method [33,36] and have concluded that divalent metal ions such as Mg^{2+}, Ca^{2+}, Mn^{2+}, and Zn^{2+} form complexes with PAA molecules, where the number of coordinating carboxylate units to a metal ion is 2 [34]. Later, Marinsky and coworkers pointed out the inappropriate assumptions inherent in the modified Bjerrum method [5,36,37] and proposed an alternative approach to analyze the same system based on the two-phase model [36,38–40]. They have reported that divalent metal ions such as Ca^{2+}, Co^{2+}, and Zn^{2+} ions form only contact ion pairs [5,36,39] (i.e., the number of coordinating carboxylate units to a metal ion is 1 instead of 2) with PAA, whereas Cu^{2+} ions form 1:2 complexes with PAA [38]. Spectroscopic measurements have been expected to give the definitive conclusion on this debate, and the Cu^{2+}–PAA system has frequently been studied for this purpose. UV and VIS spectroscopies together with potentiometry have been applied to such studies. However, because of inconsistency in the interpretation of the spectra, a unified picture on the coordination structures of Cu^{2+} to PAA molecules has not yet been established.

As comprehensive examples of Gibbs–Donnan analyses, PAA complexations with Ag^+ and Ca^{2+} will be discussed hereafter. The substantial influence of α and C_s on $(K_M^0)_{app}$ is illustrated in Figures 11 and 12, where the logarithmic values of $(K_{Ag}^0)_{app}$ and $(K_{Ca}^0)_{app}$ of PAA determined at various sodium salt concentration levels are plotted against α. It is apparent in both complexation systems that $\log(K_M^0)_{app}$ increases with α and decreases with C_s, as with the pK_{app} vs. α plots shown in the preceding section (Figure 2). By comparing Figures 11 and 12, it is revealed that at a specified C_s, the magnitude of the increase with α is much more pronounced for the doubly charged Ca^{2+} than for the singly charged Ag^+, as is expected by the difference in the nonideality terms affected by exposure of metal ions to the same electrostatic potential. Ca^{2+} ions are much more concentrated in the polyelectrolyte phase than Ag^+ ions. In order to correct for the electrostatic concentration of free metal ions according to Eq. 22, $\log(K_M^0)_{app}$ is plotted against ΔpK, which is determined by the concurrent pH measurement. The plots obtained for Ag^+–PAA and Ca^{2+}–PAA systems are illustrated in Figures 13 and 14, respectively. It is evident from these figures that the separate lines appearing in Figures 11 and 12 due to various medium concentrations converge to straight lines whose slopes are +1 for Ag^+–PAA and +2 for Ca^{2+}–PAA systems. The values of the slopes correspond to the charges of Ag^+ and Ca^{2+}. It is of special significance to consider closely the intercept values of the straight lines at $\Delta pK = 0$; these values correspond to $\log(K_M^0)_{int}$. The intrinsic complexation function, $(K_M^0)_{int}$, can be defined by the use of $[M]_p$, instead of [M], as

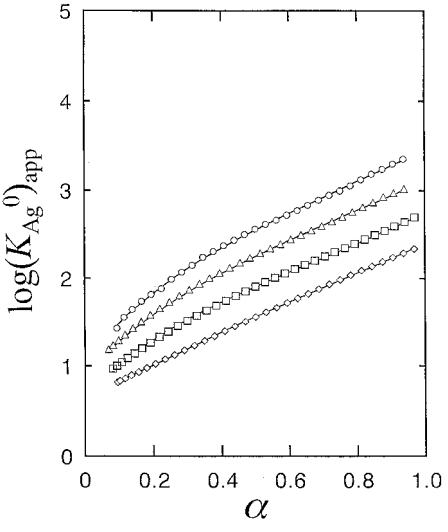

FIG. 11 Effects of salt ($NaNO_3$) concentration level and the degree of dissociation on $\log(K^0_{Ag})_{app}$ of PAA: (○) C_s = 0.01; (△) C_s = 0.02; (□) C_s = 0.05; (◇) C_s = 0.10 mol/dm^3. (From Ref. 44.)

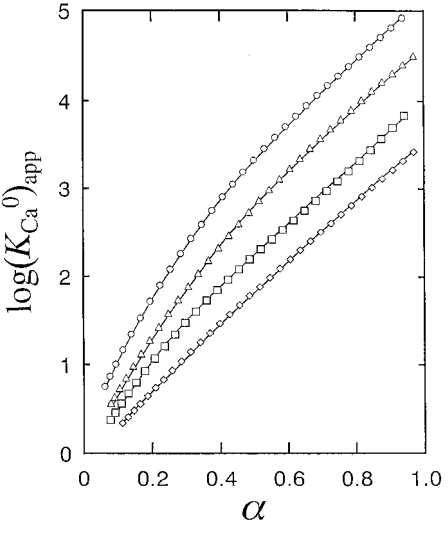

FIG. 12 Effects of salt (NaCl) concentration level and the degree of dissociation on $\log(K^0_{Ca})_{app}$ of PAA: (○) C_s = 0.01; (△) C_s = 0.02; (□) C_s = 0.05; (◇) C_s = 0.10 mol/dm^3. (From Ref. 44.)

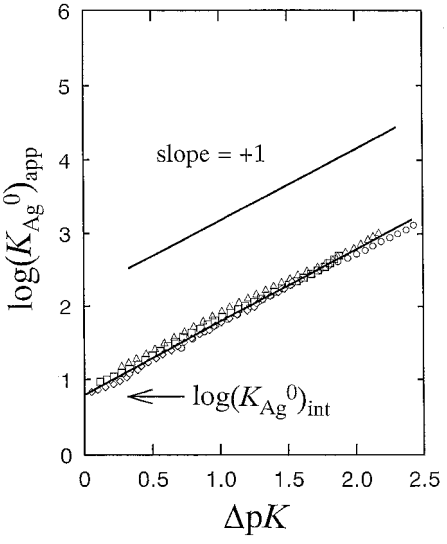

FIG. 13 Relationship between $\log(K^0_{Ag})_{app}$ and ΔpK for PAA: (○) $C_s = 0.01$; (△) $C_s = 0.02$; (□) $C_s = 0.05$; (◇) $C_s = 0.10$ mol/dm^3. (From Ref. 44.)

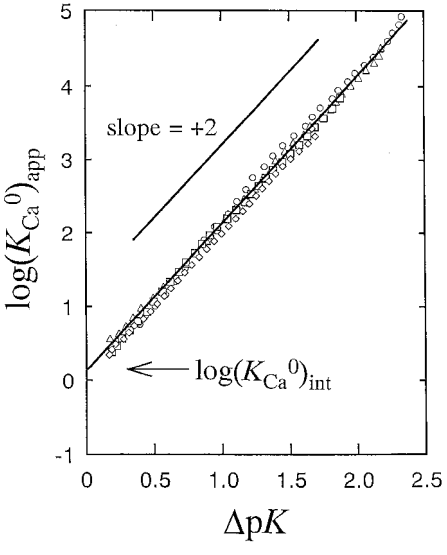

FIG. 14 Relationship between $\log(K^0_{Ca})_{app}$ and ΔpK for PAA: (○) $C_s = 0.01$; (△) $C_s = 0.02$; (□) $C_s = 0.05$; (◇) $C_s = 0.10$ mol/dm^3. (From Ref. 44.)

$$(K^0_M)_{int} = \frac{[M]_{bound}}{[M]_p \alpha C_p} \tag{23}$$

and can be rearranged as follows by taking into account that the concentration term defined by the total solution volume appearing in Eq. 23, $[M]_{bound}/\alpha C_p$, can be replaced by the concentration terms defined by the polyelectrolyte phase volume, i.e., $[M]_{bound}/\{\alpha C_p\} = \Sigma[MA_i]_p/[A]_p$. $[MA_i]_p$ corresponds to the concentration of the ith complexes, and $[A]_p$ represents the free ligand unit concentration in the polyelectrolyte phase expressed in monomol/dm^3. The concentration term, $[\ ]_p$, is defined by the polyelectrolyte phase volume.

$$\begin{aligned}(K^0_M)_{int} &= \frac{\Sigma[MA_i]_p}{[M]_p[A]_p} = \Sigma\ \frac{(\beta_i)_{int}[M]_p[A]^i_p}{[M]_p[A]_p} \\ &= \Sigma(\beta_i)_{int}[A]^{i-1}_p \\ &= (\beta_1)_{int} + (\beta_2)_{int}[A]_p + (\beta_3)_{int}[A]^2_p + \cdots \end{aligned} \tag{24}$$

where $(\beta_i)_{int}$ indicates the ''overall stability constant'' of the ith complexes with polymer ligand units defined in the polyelectrolyte phase, i.e., $(\beta_i)_{int} = [MA_i]_p/([M]_p[A]^i_p)$. In this equation, each ligand unit is considered to participate in complexation, whereas in the case of chelate formation, e.g., (MA_2) formation in which two adjacent monomer ligand units participate, the concentration term appearing in the denominator of Eq. 24 must be substituted by $[A]_p/2$. The constant intercepts for both Ag^+–PAA and Ca^{2+}–PAA systems obtained by the present analyses are 0.7 and 0.2, respectively, being quite close in value to the stability constants of 1:1 acetate complexes, $\log \beta_1 = 0.73(Ag^+)$ [41] and $\log \beta_1 = 0.53(Ca^{2+})$ [42], respectively. This consistency strongly indicates that 1:1 complex formation is predominant in both Ag^+–PAA and Ca^{2+}–PAA systems, though the magnitude of apparent complexation is much larger in magnitude than expected by simple 1:1 complexation and is strongly affected by pH and C_s, as have been illustrated in Figures 11 and 12. This complexity observed in the apparent complexation, indeed, originates from the polymeric and ionic nature of the ligand molecules.

As has been discussed in Sec. II.B, hydrophobicity of supporting cations is expected to enhance the apparent complexation of weak acidic polyelectrolytes, and it is of interest to study how the metal complexation equilibria are affected by the addition of hydrophobic supporting cations, such as tetraalkyl ammonium ions. Representative plots obtained by a potentiometric titration study on Ca^{2+}/PAA in the presence of excess TMA^+Cl^- salt [43] are shown in Figure 15. By comparison of the $\log(K^0_{Ca})_{app}$ vs. α plots of the systems of Ca^{2+}/PAA/Na^+ with Ca^{2+}/PAA/TMA^+, it is apparent that Ca^{2+} complexation is highly enhanced by the addition of TMA^+ at any salt con-

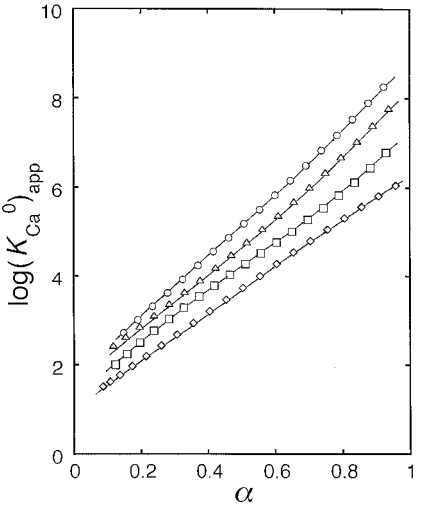

FIG. 15 Effects of salt (TMA^+Cl^-) concentration level and the degree of dissociation on $\log(K^0_{Ca})_{app}$ of PAA: (○) C_s = 0.01; (△) C_s = 0.02; (□) C_s = 0.05; (◇) C_s = 0.10 mol/dm^3. (From Ref. 43.)

centration levels examined. Much larger $(K^0_{Ca})_{app}$ than obtained in the presence of Na^{2+}, indeed, results from the concentrated free Ca^{2+} in the vicinity of the linear polymer skeleton, just due to the reduced polyelectrolyte phase volume produced by the attraction of TMA^+ around the polymer molecules. The applicability of the Gibbs–Donnan concept to the equilibrium analyses of these complexation systems can be validated by plotting $\log(K^0_{Ca})_{app}$ thus determined against ΔpK, where pK_{app} values in the presence of excess TMA^+Cl^- have already been determined, as is illustrated in Figure 9. The convergence of the separate lines responding to various C_s to produce the straight line with the slope of 2 (Figure 16) validates once again the applicability of the concept, as has been shown in Ca^{2+}/PAA/Na^+ system (Figure 14). The intercept value, being equal to $\log(K^0_{Ca})_{int}$, 0.8, seems a little larger in value when compared with the corresponding value (=0.2) obtained in the presence of Na^+. However since this value is affected by the pK_0 estimation and since no α dependence of $(K^0_{Ca})_{int}$ is observed at all, it can be concluded that the complexation modes of Ca^{2+} with PAA in the presence of Na^+ and TMA^+ are identical.

In the case of transition metal ion complexation, on the other hand, bidenate and/or chelate complex formation in addition to monodentate complex formation have been revealed. The complexation modes of the transition metal ions, such as Cu^{2+}, Cd^{2+}, and Pb^{2+}, depend on the degree of PAA

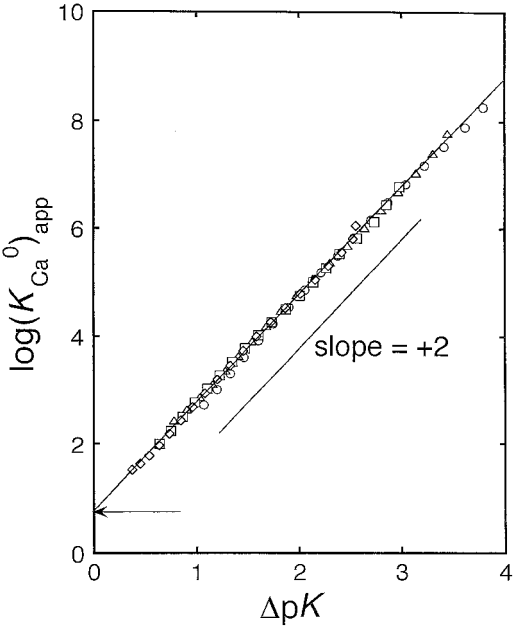

FIG. 16 Log$(K^0_{Ca})_{app}$ vs. ΔpK plots of PAA determined in the presence of TMA^+Cl^-: (○) C_s = 0.01; (△) C_s = 0.02; (□) C_s = 0.05; (◇) C_s = 0.10 mol/dm^3. (From Ref. 43.)

dissociation [44]. The $\log(K^0_M)_{app}$ vs. ΔpK plots determined for these transition metal ion complexation systems are demonstrated in Figures 17, 18, and 19. These plots yielding the linear portions with slope 2 at higher α regions, give intercept values of 2.8, 2.2, and 4.0, respectively, for the Cu^{2+}, Cd^{2+}, and Pb^{2+} systems, whereas the $\log(\beta_1)_{int}$ values estimated by the corresponding 1:1 complexes with acetate ligand 1.8(Cu^{2+}) [45], 1.6(Cd^{2+}) [45], and 2.2(Pb^{2+}) [45] as indicated by the dotted lines shown in the figures are much smaller in value than the respective extrapolated $\log(K^0_M)_{int}$ values. These much higher intrinsic stability constants estimated by extrapolation can be compared with the log β_2 values of the corresponding 1:2 acetate complexes 3.1 (Cu^{2+}) [46], 1.9 (Cd^{2+}) [46], and 3.5 (Pb^{2+}) [46]. This strongly suggests the formation of bidentate and/or chelate complexes of PAA polymer at higher α regions.

In order to compare the PAA complexation behavior of Ag^+ and Ca^{2+} systems with Cu^{2+}, Cd^{2+}, and Pb^{2+} systems, $\log(K^0_M)_{int}$ [=$\log(K^0_M)_{app} - Z\Delta pK$] is expressed in Figure 20 as a function of α. The $\log(K^0_M)_{int}$ values

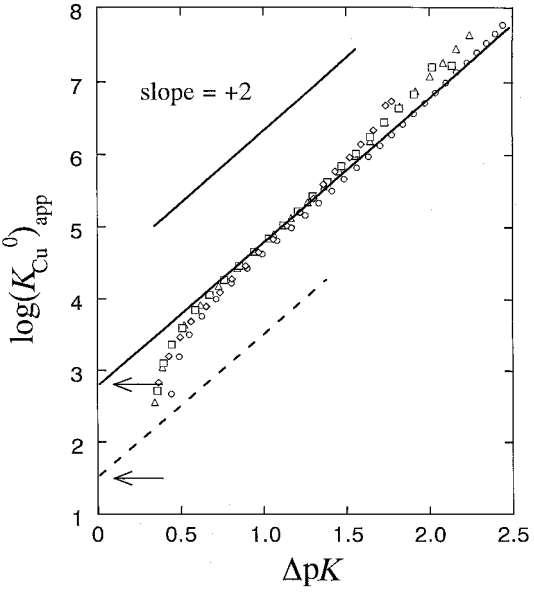

FIG. 17 Relationship between $\log(K^0_{Cu})_{app}$ and ΔpK for PAA. The solid and broken lines refer to 1:2 and 1:1 complex formation, respectively. The upper and lower arrows indicate the intrinsic constants of 1:2 (=2.8) and 1:1 (=1.6) complexes, respectively. (○) C_s = 0.01; (△) C_s = 0.02; (□) C_s = 0.05; (◇) C_s = 0.10 mol/dm^3. (From Ref. 44.)

at $\Delta pK = 0$ seem to indicate the predominant formation of 1:1 complex, whereas $\log(K^0_M)_{int}$ increases with α to reach a constant value for each transition metal ion system. No change with respect to α has been observed for Ag^+ and Ca^{2+} systems, which indicates that the coordinating ability of Ag^+ and Ca^{2+} to carboxylate groups of PAA polymer molecules is so weak that the further coordination cannot take place, whereas Cu^{2+}, Cd^{2+}, and Pb^{2+} have sufficient coordination ability to form bidentate and/or chelate complexes. It is notable that the α regions where the transition from monodentate complexation to bidentate and/or chelate complex formation observed for PAA/transition metal ion systems are consistent with each other, i.e., at α = ca. 0.3 [44].

The estimate on the complexation modes provided by the above thermodynamic approach should be verified by other experimental approaches. Spectroscopic measurements are expected to give straightforward evidence for the coordination state of a metal ion in polymer ligand systems. The

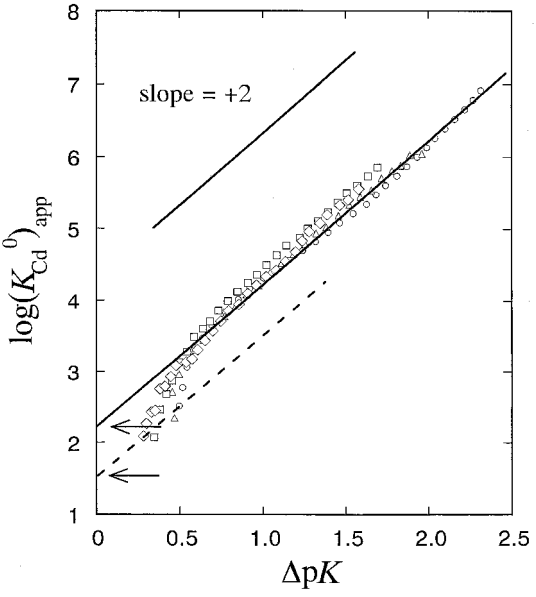

FIG. 18 Relationship between $\log(K^0_{Cd})_{app}$ and ΔpK for PAA. The solid and broken lines refer to 1:2 and 1:1 complex formation, respectively. The upper and lower arrows indicate the intrinsic constants of 1:2 (=2.2) and 1:1 (=1.5) complexes, respectively. (○) C_s = 0.01; (△) C_s = 0.02; (□) C_s = 0.05; (◇) C_s = 0.10 mol/dm^3. (From Ref. 27.)

microscopic information is directly comparable to the estimate gained by the thermodynamic approach. Metal NMR is one of the most promising candidates for this purpose, and the successful application of ^{113}Cd NMR [27] is described hereafter. The ^{113}Cd NMR chemical shift change upon complexation has been measured as a function of α of PAA polymer to reveal the coordination state of Cd^{2+} to fixed carboxylate groups. The $^{113}Cd^{2+}$ chemical shift observed, $(\delta_{Cd})_{obsd}$, can be expressed as the weighed average of the complexes and the free Cd^{2+}, depending on the free Cd^{2+} fraction of total Cd^{2+}, f_{Cd}.

$$(\delta_{Cd})_{obsd} = f_{Cd}\,\delta_{Cd} + (1 - f_{Cd})(\delta_{Cd})_{corr} \tag{25}$$

where δ_{Cd} indicates the eigenvalue for free Cd^{2+}, where free Cd^{2+} was taken as a reference. The corrected δ_{Cd} value, $(\delta_{Cd})_{corr}$, corresponding to the averaged shift value for complexed Cd^{2+}, can be expressed by the use of $(\delta_{Cd})_{obsd}$ and f_{Cd}, where f_{Cd} is estimated potentiometrically with a Cd^{2+} ion-selective electrode as

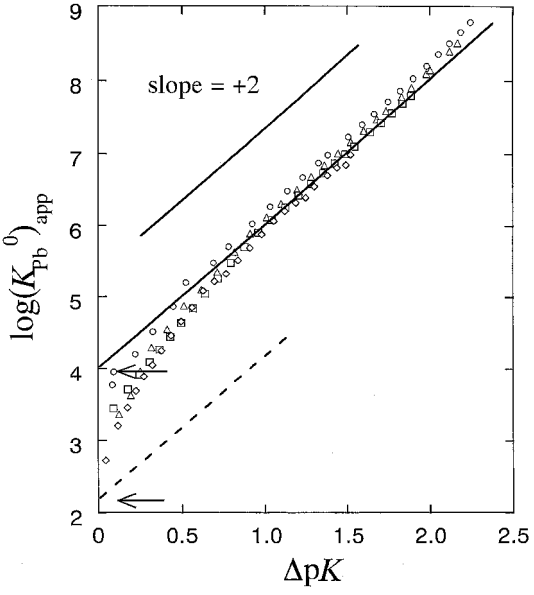

FIG. 19 Relationship between $\log(K^0_{Pb})_{app}$ and ΔpK for PAA. The solid and broken lines refer to 1:2 and 1:1 complex formation, respectively. The upper and lower arrows indicate the intrinsic constants of 1:2 (=4.0) and 1:1 (=2.2) complexes, respectively. (○) C_s = 0.01; (△) C_s = 0.02; (□) C_s = 0.05; (◇) C_s = 0.10 mol/dm^3. (From Ref. 44.)

$$(\delta_{Cd})_{corr} = (\delta_{Cd})_{obsd}/(1 - f_{Cd}) \tag{26}$$

The $(\delta_{Cd})_{corr}$ values thus calculated are plotted in Figure 21 against α. It can be seen that the $(\delta_{Cd})_{corr}$ values determined at $0.2 < \alpha < 1.0$ are almost identical, i.e., ca. $-35 \sim -38$ ppm, being quite close to the intrinsic $^{113}Cd^{2+}$ shift values corresponding to 1:2 complex (-40.0 ppm) of Cd^{2+}–acetate [47,48] and Cd^{2+}–glutarate complexes [47,48], which are the analogs of the PAA complexes where two carboxyl groups are estimated to be involved in the complexation. At a lower α region, i.e., $0 < \alpha < 0.2$, however, $(\delta_{Cd})_{corr}$ shifts downfield upon decreasing α, indicating that the limiting value at $\alpha = 0$ corresponds to ca. -20 ppm. This value, indeed, corresponds to the intrinsic shift value of 1:1 complex (-22.1 ppm) of Cd^{2+}–acetate [47,48], where acetate ion is the monomer ligand analog of PAA. By comparison of the chemical shift values with these monomer ligand complexes, it is apparent that though a monodentate complex formation cannot be neglected at a lower α region, bidentate and/or chelate complex formation is predominant at the higher α region ($0.2 < \alpha < 1.0$). This $^{113}Cd^{2+}$ shift change upon

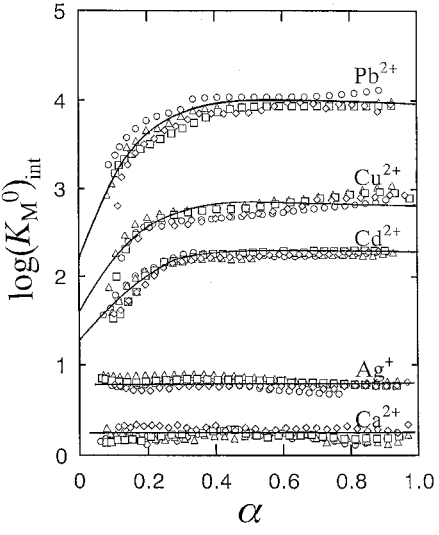

FIG. 20 The variation of $\log(K_M^0)_{int}$ with α for PAA: M = Ag^+, Ca^{2+}, Cu^{2+}, Cd^{2+}, and Pb^{2+}: (○) C_s = 0.01; (△) C_s = 0.02; (□) C_s = 0.05; (◇) C_s = 0.10 mol/dm^3. (From Ref. 44.)

α is quite consistent with the estimate gained by the present thermodynamic approach, which validates the interpretations based on the Gibbs–Donnan concept.

C. Poly(*N*-Vinylimidazole) Complexation

The complexation equilibria of weak basic polyelectrolytes can also be analyzed exactly in the identical manner with the treatment just mentioned above [49], even though the polymer ligands become cationic when it is protonated. The nonideality terms pronounced in the apparent complexation equilibria can be estimated by the use of the corresponding acid dissociation equilibria as a probe. In this section, the applicability of the Gibbs–Donnan approach to weak basic polyelectrolyte complexation equilibrium analyses is described by exemplifying PVIm complexation. The readers may recall the fundamental differences in the acid dissociation behaviors of PAA and $PVImH^+$, which have been discussed in detail in Sec. II.A of this chapter. Since H^+ binding to imidazole groups of PVIm molecules is suppressed by the positive potential developed at the partially protonated polymer surface, and the electrostatic repulsion is affected by the Debye–Hückel type ion screening effect, the magnitude of the nonideality is highly dependent on α and C_s. It is expected that the apparent binding constant defined by Eq. 14

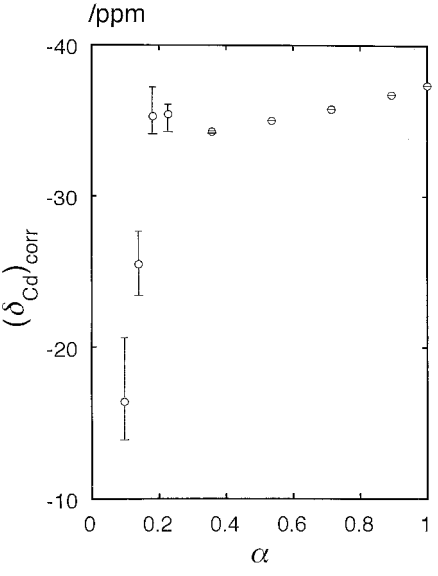

FIG. 21 The corrected shift value (^{113}Cd) expressed as a function of α. Error bars correspond to calculated f_{Cd} variation due to the potentiometric measurement of pCd in the sample solutions with error of ± 0.1 mV. (From Ref. 27.)

increases with α. Also, since the ion screening effect due to added salt reduces the repulsion between metal ions and the positively charged surface, it is anticipated that $(K^0_M)_{app}$ increases with C_s at a specified α.

Though a large number of studies have been carried out on the PVIm complexation, quite a limited number of works have indicated the number of coordinating imidazole groups on a metal ion of the polymer complexes. The maximum coordinating number of imidazole units to a metal ion has been reported by Gregor as 2 for Ag^+ complexes [50] and 4 for Cu^{2+} complexes [51]. The presence of 1:4 complexes for Cu^{2+}–PVIm complexation has also been verified by an electronic spectroscopic measurement [51]. In these studies, the free imidazole concentration monomer basis needed for the complexation analyses has been calculated by the empirical ''modified Henderson Hasselbalch equation'' [50,51]. The Gibbs–Donnan approach has recently been applied to the PVIm complexation equilibrium analyses of monovalent (Ag^+) and divalent (Cu^{2+} and Cd^{2+}) ions [49].

As shown in Figure 22, $(K^0_{Ag})_{app}$ increases drastically with α primarily due to the decreased electrostatic repulsion between Ag^+ and $PVImH^+$ molecules. The C_s dependence of the apparent binding constant is consistent with that of the pK_{app} of $PVImH^+$, which can be rationalized by the ion

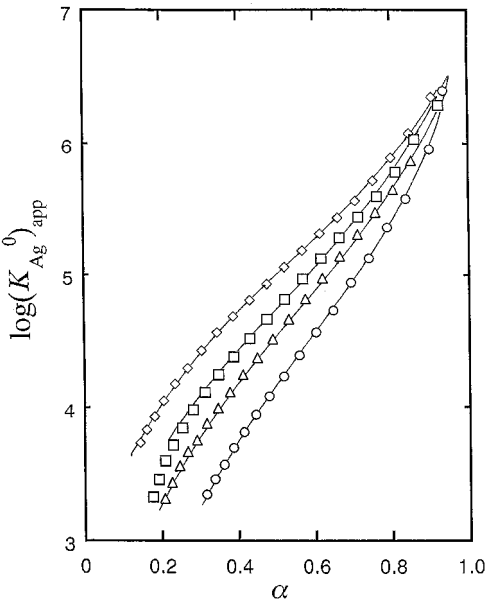

FIG. 22 Effects of salt ($NaNO_3$) concentration level and the degree of dissociation on $\log(K^0_{Ag})_{app}$ of PVIm: (○) C_s = 0.005; (△) C_s = 0.01; (□) C_s = 0.02; (◇) C_s = 0.05 mol/dm^3. (From Ref. 49.)

screening effect. When $\log(K^0_{Ag})_{app}$ is plotted against ΔpK instead of α (Figure 23), insights into the intrinsic complexation equilibria can be gained as has been revealed for PAA complexation. Note that the ΔpK values for PVIm complexation are always negative, though they are positive for PAA complexation. Most enlightening is the converging of the four separate lines appearing in Figure 22 corresponding to different C_s into a unique curve, as appears in Figure 23. This converging, indeed, validates the Gibbs–Donnan correction procedure for the PVIm complexation equilibrium analysis. As is predicted by Eq. 22, the slope of the linear portion of the plots is exactly unity, being equal to the charge of the Ag^+ ion. The intercept at $\Delta pK = 0$ corresponds to $\log(K^0_{Ag})_{int}$ (=7.22), which is much larger than the logarithmic value of the stability constant of monodentate Ag^+ complex with imidazole, Im, (i.e., $\log \beta_1 = 3.17$ [52]), indicating the formation of multidentate ligand complexes. When nitrogen atoms are involved in complexation, the complexing ability of transition metal ions is expected to be much stronger than the case for carboxylate oxygen atoms. This enables metal ions to multicoordinate with nitrogen atoms attached to one polymer ligand molecule. Due to the lack of the reported stability constants of Ag^+ complexes with

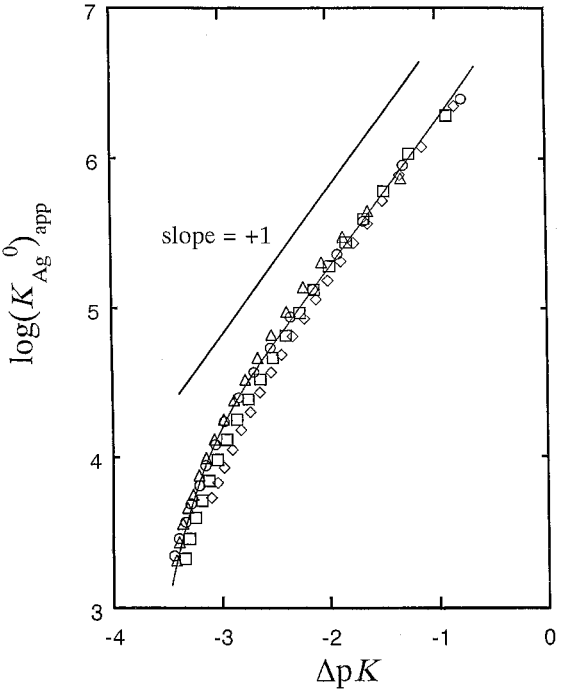

FIG. 23 Relationship between $\log(K^0_{Ag})_{app}$ and ΔpK for PVIm: (○) C_s = 0.005; (△) C_s = 0.01; (□) C_s = 0.02; (◇) C_s = 0.05 mol/dm^3. (From Ref. 49.)

bifunctional imidazole ligand, i.e., α, ω di-*N*-imidazolylalkane, the formation constant of 1:2 complex of Ag^+-imidazole, $\log \beta_2 = 6.94$ [52] is compared to $\log(K^0_{Ag})_{int}$ (=7.22), instead. Consistency in the two values indicates a bidentate and/or chelate complex formation for the Ag^+–PVIm system. It is noteworthy that the plots of $(K^0_{Ag})_{app}$ vs. ΔpK deviate drastically downward from the straight line at $\alpha < 0.3$, indicating the remarkable suppression of bidentate and/or chelate complex formation with these highly protonated PVIm molecules. Availability of free imidazole groups needed for the formation of bidentate and/or chelate complexes is considerably prevented under these acidic conditions, and simultaneous coordination of two imidazole groups to an Ag^+ ion may be prohibited. In these circumstances, monodentate ligand complexation becomes predominant, whose stability constant must be as small as that of 1:1 complex of Ag^+ with imidazole (i.e., $\log \beta_1 = 3.17$ [52]).

Compared with Ag^+ complexation, the complexability of PVIm molecules with Cu^{2+} and Cd^{2+} is much stronger, and the variation in the magnitude

with α is larger, due to the more pronounced dilution of doubly charged metal ions at the partially protonated PVIm surface than singly charged Ag^+. In order to estimate the microscopic structures and intrinsic stability constants of these metal–PVIm complexes, $\log(K^0_M)_{app}$ is plotted against ΔpK in Figures 24 and 25, respectively, for Cu^{2+} and Cd^{2+}. The separate lines corresponding to each C_s observed in the plots of $\log(K^0_M)_{app}$ vs. α converge to the identical lines in the $\log(K^0_M)_{app}$ vs. ΔpK plots. Also, it should be noted that the slopes of the linear portions of the lines are +2, the charges of Cu^{2+} and Cd^{2+}. These results indicate that the change in the ion screening effect due to C_s change can fully be corrected by the Gibbs–Donnan approach. The intercepts of the lines at $\Delta pK = 0$ correspond to 14.7 and 7.8, for Cu^{2+} and Cd^{2+} systems, respectively. Since the reported stability constants of successive Cu^{2+}–Im complexes are $\log \beta_1 = 4.18$, $\log \beta_2 = 7.66$, $\log \beta_3 = 10.51$, and $\log \beta_4 = 12.6$ [53], it is estimated that Cu^{2+} ions form 1:4 complexes at fully dissociated state ($\alpha = 1$) by comparing the value of $\log(K^0_{Cu})_{int} = 14.7$ with $\log \beta_4 = 12.6$. It can be postulated that adjacent two imidazole groups

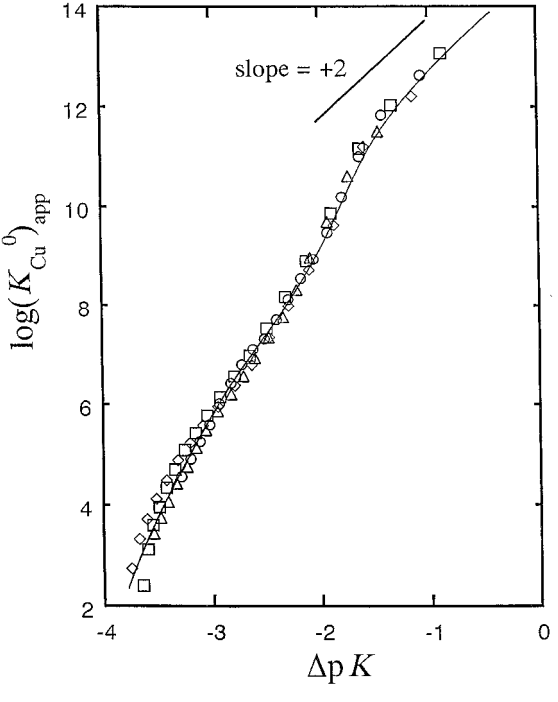

FIG. 24 Relationship between $\log(K^0_{Cu})_{app}$ and ΔpK for PVIm: (○) $C_s = 0.005$; (△) $C_s = 0.01$; (□) $C_s = 0.02$; (◇) $C_s = 0.05$ mol/dm^3. (From Ref. 49.)

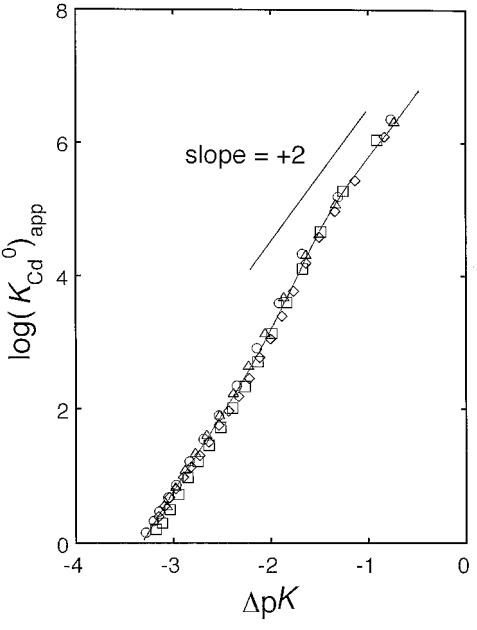

FIG. 25 Relationship between $\log(K^0_{Cd})_{app}$ and ΔpK for PVIm: (○) $C_s = 0.005$; (△) $C_s = 0.01$; (□) $C_s = 0.02$; (◇) $C_s = 0.05$ mol/dm^3. (From Ref. 49.)

fixed onto the same polymer backbone form one chelate ligand site and a Cu^{2+} binds the two chelate sites to form a 1:4 complex. It is revealed from the figure that $(K^0_{Cu})_{int}$ decreases stepwise as α decreases.

The $\log(K^0_{Cd})_{app}$ vs. ΔpK plots reflect the stepwise complexation with α as well. By comparing the reported stability constants of successive Cd^{2+}–Im complexes, $\log \beta_1 = 2.70$, $\log \beta_2 = 5.08$, $\log \beta_3 = 6.65$, and $\log \beta_4 = 7.60$ [54] with $\log(K^0_{Cd})_{int} = 7.8$ at $\alpha = 1$, 1:4 complexation can be postulated for Cd^{2+}–PVIm complexation at a fully dissociated state. Stepwise coordination corresponding to α is observed in this system as well.

In order to examine these stepwise complexation behaviors of PVIm ligand in detail, $\log(K^0_M)_{int}$ [$=\log(K^0_M)_{app} - Z\Delta pK$] is plotted against α (Figure 26). By comparing the results obtained for PAA and PVIm, we can conclude that two transitions at α = ca. 0.3 and ca. 0.8 are observed with these weak polyelectrolytes. Based on these findings, it can be estimated that the multidentate complexation property of PAA and PVIm is highly dependent on α, which controls the available distance between the neighboring ligand groups. It is apparent that the transition occurs at a particular distance independent of the nature of the metal ions or the monomer ligand, as can be

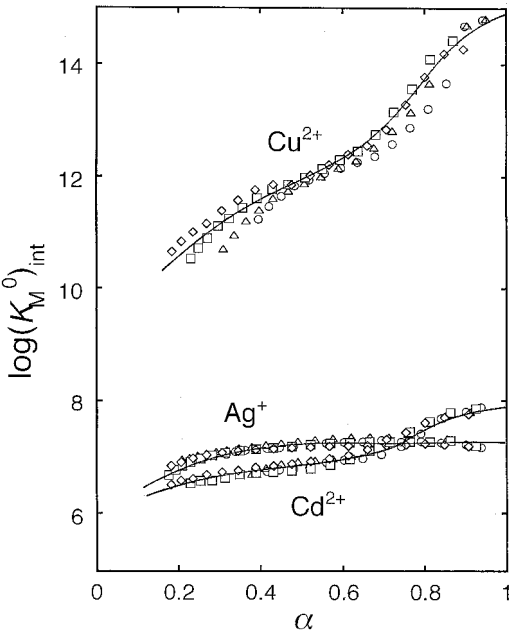

FIG. 26 The variation of $\log(K_M^0)_{int}$ with α for PVIm: M = Ag^+, Cu^{2+}, and Cd^{2+}. (○) C_s = 0.005; (△) C_s = 0.01; (□) C_s = 0.02; (◇) C_s = 0.05 mol/dm^3. (From Ref. 49.)

seen in Figures 20 and 26. It can be anticipated that a specified geometry of PAA and PVIm molecules in aqueous solution may be responsible for this transition.

D. Polymer Conformation Effect

The conformation change of linear polymer molecules upon α in aqueous solution, as has been discussed in Sec. II.B by illustrating PMA, is of significance in their metal complexation because polymer conformation sometimes plays an essential role on the multidentate complexation property, which is directly related to the delicate functions of naturally occurring polymers. A compact structure is postulated for PMA molecules at $0 < \alpha < 0.3$, whereas it drastically expands at the higher α range. As expected by Eq. 24, the successive complexation is highly dependent on the effective "ligand" concentration in the polyelectrolyte phase, $[A]_p$, i.e., the spatial distance of fixed functional groups controls the "availability" of the polymer ligand

units to form successive complexes through intermolecular complexation. A comparison of PMA and PAA complexation behaviors is expected to give a clue to the understanding of the polymer conformation effect [28]. In this section, the Gibbs–Donnan approach has been applied to the equilibrium analyses of divalent metal ion complexation with PMA, and the relating conformation effect on complexation is discussed.

The changes in $\log(K^0_M)_{app}$ of M^{2+} (M^{2-} = Ca^{2+} and Cu^{2+})/PMA systems with respect to α are shown in Figures 27 and 28, whose patterns seem quite similar to the corresponding pK_{app} vs. α plots shown in Figure 10. Qualitatively no remarkable difference is found among them, but by plotting $\log(K^0_M)_{app}$ against ΔpK as shown in Figures 29 and 30, quite important feature in the metal–polymer complexation among them becomes apparent. First, it should be pointed out that the plots of the Cu^{2+}/PMA system (Figure 30) can be exactly superimposed on the plots of the Cu^{2+}/PAA system (Figure 17). The separate lines appearing in Figure 28 converge to the straight line whose slope is +2, validating the Gibbs–Donnan estimate of the cor-

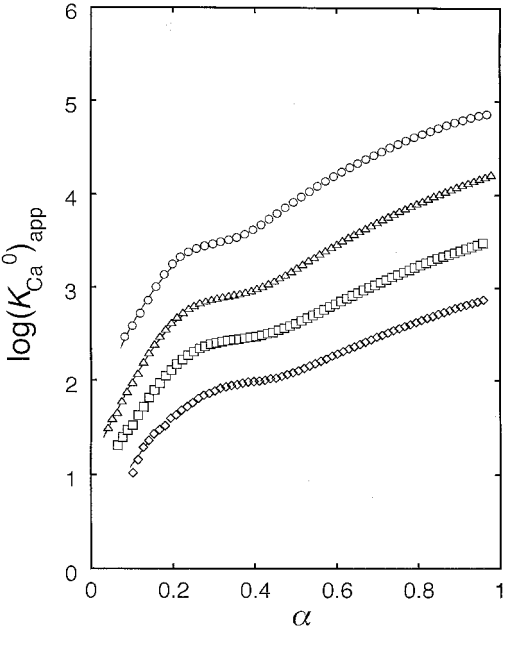

FIG. 27 Effects of salt (NaCl) concentration level and the degree of dissociation on $\log(K^0_{Ca})_{app}$ of PMA: (○) C_s = 0.01; (△) C_s = 0.02; (□) C_s = 0.05; (◇) C_s = 0.10 mol/dm^3. (From Ref. 28.)

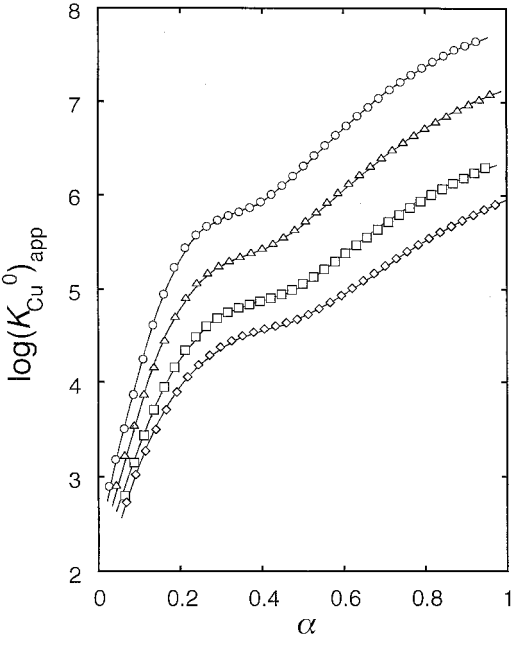

FIG. 28 Effects of salt ($NaNO_3$) concentration level and the degree of dissociation on $\log(K^0_{Cu})_{app}$ of PMA: (○) C_s = 0.01; (△) C_s = 0.02; (□) C_s = 0.05; (◇) C_s = 0.10 mol/dm^3. (From Ref. 28.)

rection needed for the electrostatic and/or hydrophobic concentration of free Cu^{2+} into the PMA polyelectrolyte phase from the bulk solution. As has been discussed in Sec. III.B, bidentate and/or chelate complex formation is predominant in the α range higher than 0.3, whereas at the lower α region, monodentate complexation cannot be neglected, as concluded in the case of Cu^{2+}/PAA complexation.

The pattern of $\log(K^0_{Ca})_{app}$ vs. ΔpK plots shown in Figure 29, on the contrary, is quite different from that which appears in Figure 14 (Ca^{2+}/PAA system). The plots of the Ca^{2+}/PMA system do not seem to converge to a simple straight line with slope +2, with a unique intercept value, though the straight line is exactly obtained in Ca^{2+}/PAA. This discrepancy does not indicate the invalidity of the Gibbs–Donnan concept to PMA complexation analyses. Instead, an important and unique feature of Ca^{2+} complexation with polycarboxylate polymers can be extracted, i.e., by combining the plots determined at the same degree of dissociation, straight lines with slope +2 can be identified, which are shown in Figure 31. In this case, $(K^0_M)_{int}$ is dependent on α and can be expressed as a function of α:

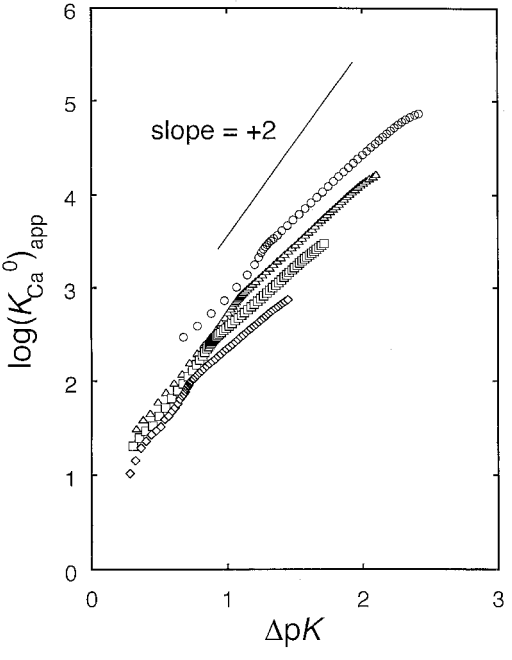

FIG. 29 Relationship between $\log(K^0_{Ca})_{app}$ and ΔpK for PMA: (○) $C_s = 0.01$; (△) $C_s = 0.02$; (□) $C_s = 0.05$; (◇) $C_s = 0.10$ mol/dm^3. (From Ref. 28.)

$$\log(K^0_M)_{app}(\alpha) = \log(K^0_M)_{int}(\alpha) + Z\Delta pK(\alpha) \tag{27}$$

By the $\log(K^0_{Ca})_{int}(\alpha)$ vs. α plots shown in Figure 32, it has been revealed that PMA molecules form more stable Ca^{2+} complexes in the lower α region than in the higher α region; $\log(K^0_{Ca})_{int}$ changes from 0.8 to 0.2 as α increases: the $\log(K^0_{Ca})_{int}$ value at $\alpha = 1$ is quite close in value to the $\log(K^0_{Ca})_{int}$ value determined for the PAA system, 0.2. It is shown, therefore, that at the lower α region, some fraction of Ca^{2+} forms bidentate complexes due to highly crowded carboxylate groups in the compact polyelectrolyte domain, whereas as the degree of dissociation increases, the compact structure expands due to electrostatic repulsion in the negatively charged polymer skeleton, which induces the dilution of the effective free carboxylate group in the domain. This is, indeed, opposite to the trend revealed for transition metal ion complexation with PAA and PVIm.

We should recall that the behaviors of Cu^{2+} complexation with PAA and PMA are quite similar to each other. PAA and PMA molecules behave similarly with respect to Cu^{2+} complexation, whereas they do not in the case

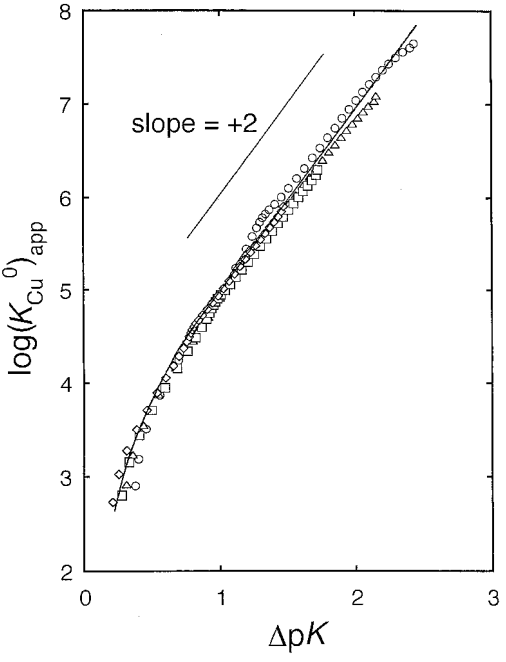

FIG. 30 Relationship between $\log(K^0_{Cu})_{app}$ and ΔpK for PMA: (○) C_s = 0.01; (△) C_s = 0.02; (□) C_s = 0.05; (◇) C_s = 0.10 mol/dm^3. (From Ref. 28.)

of Ca^{2+} complexation. In polymer–metal ligand complexation, the coordination characteristics of central metal ions may play a quite essential role on the multidentate complexation properties of the linear polymer ligands. In the present case, Cu^{2+} forms complexes with a square planar coordination structure: the bond angles and the bond lengths of the coordinating ligand atoms and the metal ions are highly specified. On the contrary, spherically symmetrical Ca^{2+} has no such restriction on the coordination behavior, since the bonding nature between oxygen atoms of polycarboxylic acids and Ca^{2+} is purely electrostatic. The flexibility in the Ca^{2+} coordination may allow such a highly complexability observed in the low α region rather than in the higher α region. The intermediate case can be seen in Cd^{2+}–PMA system (Figure 33). The plots of $\log(K^0_{Cd})_{app}$ vs. ΔpK corresponding to each C_s do not converge to a single line as found in the Cd^{2+}–PAA system (Figure 18) or the Cu^{2+}–PMA systems (Figure 30), but the separation among the lines is not so pronounced as observed in the Ca^{2+}–PMA system (Figure 29).

The present finding obtained by PMA implies the significance of Ca^{2+} complexation with proteins, whose formal linear density of carboxylate

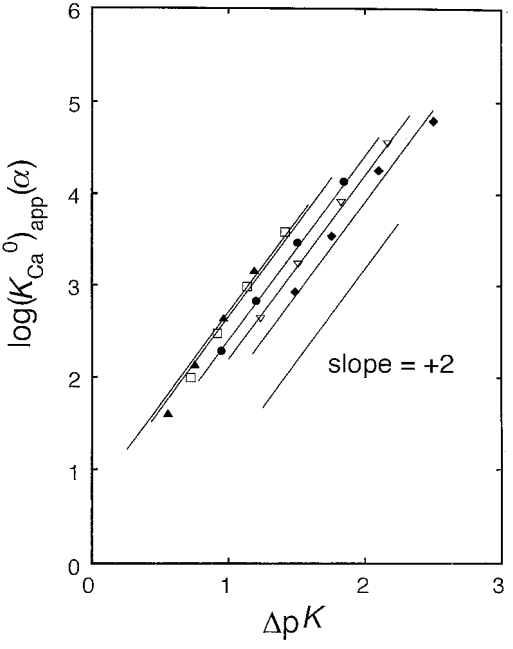

FIG. 31 $\mathrm{Log}(K^0_{Ca})_{app}(\alpha)$ vs. ΔpK plots for PMA: (▲) $\alpha = 0.2$; (□) $\alpha = 0.4$; (●) $\alpha = 0.6$; (▽) $\alpha = 0.8$; (◆) $\alpha = 1.0$. (From Ref. 28.)

groups is much lower than PMA, but the stronger Ca^{2+} complexability is anticipated. The Ca^{2+} binding is expected to induce drastic conformation change of the protein molecules. It should be stated once again that all these analyses are made possible by applying the Gibbs–Donnan concept to these systems.

IV. CONCLUSIONS

By the systematic work on the complexation equilibrium analyses of both weak acidic and weak basic polyelectrolytes, the Gibbs–Donnan approach is validated to provide deep insights into the complexation behaviors of linear polymer ligands. This concept does not need any adjustable parameter; it only uses the logic of phase separation of polyelectrolyte aqueous solutions. The electrostatic nonideality (polyelectrolytic effect) observed in the acid dissociation equilibria of a polyion can directly be used to correct for the electrostatic nonideality for metal complexation. The potentiometric titration technique with concurrent measurements of pH and pM is most suit-

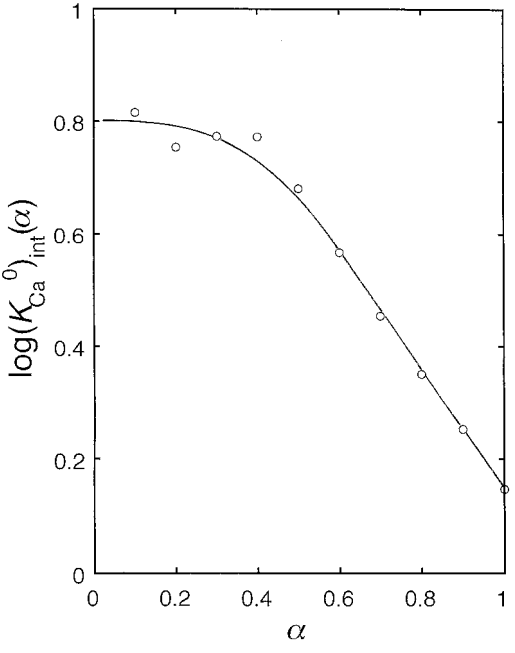

FIG. 32 The variation of $\log(K_{Ca}^{0})_{int}(\alpha)$ with α for PMA. (From Ref. 28.)

able for this approach, even though metal ion concentration must be kept as low as possible in order that the perturbation due to complexation on acid dissociation should be negligibly small. After this electrostatic correction, unique characteristics of polyion complexations, such as the effect of hydrophobicity of supporting ions, the multicoordinate complexability of polyions, and the effect of polymer conformation, have been extracted.

Polymer complexes with weak complexing ability predominantly form monodentate complexes. Ag^{+}–PAA and Ca^{2+}–PAA systems are examples of this kind. Though the apparent Ca^{2+} complexation with PAA is highly enhanced in the presence of TMA^{+}, the complexed species are identified as monodentate, indicating that hydrophobicity of supporting ions does not influence the intrinsic complexation behavior. With a much stronger complexing ability, polymer ligands form an appreciable amount of multidentate complexes. PAA complexes with Cu^{2+}, Cd^{2+}, and Pb^{2+}, are examples of this kind of coordination. They form bidentate and/or chelate complexes at a higher degree of dissociation, but monodentate complexes are formed at a lower degree of dissociation. The distribution of the two types of complexes has been revealed to be dependent on the average spacing of free carboxylate

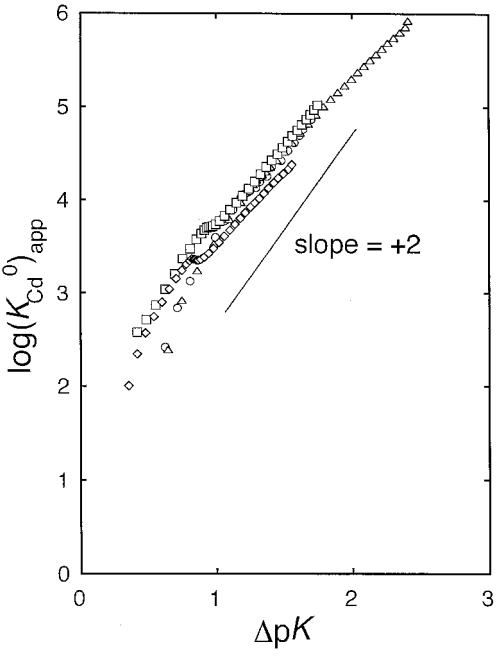

FIG. 33 Relationship between $\log(K^0_{Cd})_{app}$ and ΔpK for PMA: (○) C_s = 0.01; (△) C_s = 0.02; (□) C_s = 0.05; (◇) C_s = 0.10 mol/dm^3. (From Ref. 28.)

groups fixed on the linear polymer molecules. It has been revealed that PVIm ligands with nitrogen atoms show much stronger complexing ability than PAA with oxygen atoms to transition metal ions, such as Ag^+, Cu^{2+}, and Cd^{2+}, due to nitrogen atoms as coordinating metal ions. At complete dissociation of $PVImH^+$, Ag^+ shows a maximum coordination number of 2, whereas Cu^{2+} and Cd^{2+} show 4 with PVIm ligands. Similarly with the functionality spacing dependence of PAA molecules, the number of coordinating ligating groups, i.e., imidazole groups, decreases with decreasing degree of neutralization. It has been revealed that this transition takes place stepwise, i.e., as a function of the degree of dissociation of linear polymer ligands. Interestingly, the linear charge spacings that correspond to the transition of coordination for PAA and PVIm ligands for different metal cations are consistent with each other, which may be due to the identical skeletal structure of these two linear polymers.

Much higher compelxability of Ca^{2+} with PMA is revealed at a lower degree of dissociation rather than at a high degree of neutralization. Elucidation of the difference in the complexation behaviors of PAA and PMA

indicates the significance of the polymer conformation as well as the coordination nature of central metal ions. Since PMA forms a compact coiled structure at a lower degree of dissociation, the effective ligand concentration of the polymer domain is increased, which enables multidentate carboxylate complexes with Ca^{2+}. Since the linear density of carboxylate groups on protein molecules is much lower than the synthetic carboxylate polymers examined in this study, this peculiar Ca^{2+} complexability seems closely related to the role of Ca^{2+} on conformation change of protein molecules upon complexation.

ACKNOWLEDGMENTS

The present author wishes to express his deep gratitude to Professor Jacob A. Marinsky at State University of New York at Buffalo for his valuable suggestions throughout this work. He wishes to acknowledge the financial support of a Grant-in-Aid for Scientific Research from the Ministry of Education, Science, and Culture of Japan (Nos. 08454237 and 07405038).

LIST OF SYMBOLS

Quantities and symbols with subscript p denote the polyelectrolyte phase.

α	degree of dissociation of polyacids
a_i	activity of species i
b	average linear charge separation on a polymer backbone
β_i	stability constant for *i*th complex
C_i	total concentration of species i
C_p	total concentration of a polymer on monomer basis (monomol/dm^3)
C_s	added salt concentration
δ_M	chemical shift value for a metal ion (ppm)
ΔpK	difference between pK_{app} and pK_0
f_M	free metal ion fraction of total metal ions
ϕ_p	practical osmotic coefficient
G	activity coefficient quotient
[i]	free concentration of species i
$(K^0_M)_{app}$	apparent metal ion binding constant in the presence of a negligible amount of metal ions
$(K^0_M)_{int}$	intrinsic metal ion binding constant in the presence of a negligible amount of metal ions
V_p	volume of polyelectrolyte phase
y_i	activity coefficient of species i
Z	average charge per functional group, charge of a metal ion

REFERENCES

1. Z Alexandrowicz, A Katchalsky. Colligative properties of polyelectrolyte solutions in excess salt. J Polym Sci Pt A 1:3231–3260, 1963.
2. F Oosawa. Polyelectrolytes. New York: Marcel Dekker, 1971.
3. JA Marinsky. A Gibbs–Donnan based interpretation of the sensitivity of the measurable acid dissociation properties of poly(acrylic acid) to concentration levels of salt and polyelectrolyte. J Phys Chem 96:6484–6487, 1992.
4. JA Marinsky. Alternate interpretation of the change observed in H^+ ion concentration levels of the aqueous medium of metal oxide suspensions in response to change in the electrolyte concentration levels of the aqueous medium. J Phys Chem 100:1858–1866, 1996.
5. JA Marinsky. A Gibbs–Donnan-based analysis of ion-exchange and related phenomena. In: JA Marinsky, Y Marcus, eds. Ion Exchange and Solvent Extraction—A Series of Advances. New York: Marcel Dekker, 1993, Vol. 11, Chap. 5.
6. T Miyajima. Evaluation of the electrostatic effect on metal ion-binding equilibria in negatively charged polyion systems. In: JA Marinsky, Y Marcus, eds. Ion Exchange and Solvent Extraction—A Series of Advances. New York: Marcel Dekker, 1995, Vol. 12, Chap. 7.
7. T Miyajima. Metal complexation in polymer systems. In: K Esumi, ed. Polymer Interfaces and Emulsions. New York: Marcel Dekker, 1999, Chap. 8.
8. GS Manning. Counterion binding in polyelectrolyte theory. Acc Chem Res 12: 443–449, 1979.
9. GS Manning. The molecular theory of polyelectrolyte solutions with applications to the electrostatic properties of polynucleotides. Q Rev Biopys 2:179–246, 1978.
10. M Mori, T Miyajima, S. Ishiguro. The influence of quaternary ammonium ions on the acid-dissociation equilibria of polyacrylic acid. J Colloid Interface Sci, in press.
11. H Kodama, T Miyajima, M Mori, M Takahashi, H Nishimura, S Ishiguro. A unified analytical treatment of the acid-dissociation equilibria of weakly acidic linear polyelectrolytes and the conjugate acids of weakly basic linear polyelectrolytes. Colloid Polym Sci 275:938–945, 1997.
12. RS Kolat, JE Powell. Acetate complexes of rare earth and several transition metal ions. Inorg Chem 1:293–296, 1962.
13. SP Datta, AK Grybowski. The acid dissociation constant of the imidazolium ions. J Chem Soc (B):136–140, 1966.
14. JA Marinsky, T Miyajima, E Högfeldt, M Muhammed. Influence of counterion concentration on the ion-exchange equilibria of crosslinked weak-acid polyelectrolyte gels. React Polym 11:279–289, 1989.
15. JA Marinsky, T Miyajima, E Högfeldt, M Muhammed. Influence of counterion concentration on equilibria and conformational properties of linear weak-acid polyelectrolytes. React Polym 11:291–300, 1989.
16. A Katchalsky, Z Alexandrowitcz. On the additivity of osmotic properties of polyelectrolyte solutions. J Polym Sci A1:2093–2099, 1963.

17. L Kotin, M Nagasawa. Chain model for polyelectrolytes. VII. Potentiometric titration and ion binding in solutions of linear polyelectrolytes. J Chem Phys 36:873–879, 1962.
18. A Katchalsky, Z Alexandrowicz, O Kedem. Polyelectrolyte solutions. In: BE Conway, RG Barradas, eds. Chemical Physics of Ionic Solution. New York: John Wiley, 1996:295–346.
19. H Kodama, T Miyajima, H Tabuchi, S Ishiguro. A calorimetric study of the acid dissociation of the conjugate acids of poly(*N*-vinylimidazole) and polyallylamine. Colloid Polym Sci 278:1–7, 2000.
20. K Lin, HP Gregor. Metal–polyelectrolyte complexes. X. Poly-*N*-vinylimidazole complexes with zinc(II) and with copper(II) and nitrilotriacetic acid. J Phys Chem 69:1252–1259, 1965.
21. HP Gregor, M Frederich. Potentiometric titration of polyacrylic and polymethacrylic acids with alkali metal and quaternary ammonium bases. J Polym Sci 23:451–465, 1957.
22. G Olofsson, K Vlasenko. The influence of various monovalent counterions on the thermodynamics of proton dissociation of polyacrylic acids. Acta Chem Scand A36:485–488, 1982.
23. DH Gold, HP Gregor. Potentiometric and viscometric behavior of poly-*N*-vinylimidazole neutralized with different acids. Z Phys Chem (Frankfurt) 15:93–102, 1958.
24. PM Henrichs, LR Whitlock, AR Sochor, JS Tan. Conformational behavior of poly(*N*-vinylimidazole). Potentiometric titration, viscosity, and proton nuclear magnetic resonance studies. Macromolecules 13:1375–1381, 1980.
25. I Kagawa, HP Gregor. Theory of the effect of counterion size upon titration behavior of polycarboxylic acids. J Polym Sci 23:477–484, 1957.
26. JA Marinsky, H Kodama, T Miyajima. An approach for assessment of the hydrophobicity/hydrophilicity of charged polymers. J Phys Chem B 102:6949–6957, 1998.
27. T Miyajima, M Mori, S Ishiguro, KH Chung, C-H Moon. On the complexation of Cd(II) ions with polyacrylic acid. J Colloid Interf Sci 184:279–288, 1996.
28. T Miyajima, K Tomonaga, S Ishiguro. On the complexation of Ca(II) and Cu(II) ions with polyacrylic acid. J Colloid Interf Sci, in press.
29. V. Crescenzi, F Quadrifoglio, F Delben. Calorimetric investigation of poly(methacrylic acid) and poly(acrylic acid) in aqueous solution. J Polym Sci Pt A-2 10:357–368, 1972.
30. S Libich, DL Rabenstein. Nuclear magnetic resonance studies of the solution chemistry of metal complexes: determination of formation constants of methylmercury complexes of selected carboxylic acids. Anal Chem 45:118–124, 1973.
31. T Miyajima, K Yoshida, Y Kanegae, H Tohfuku, JA Marinsky. Metal complexation of negatively charged polymers: evaluation of the electrostatic effect on the complexation equilibria. React Polym 15:55–62, 1991.
32. HP Gregor, LB Luttinger, EM Loebl. Metal–polyelectrolyte complexes. I. The polyacrylic acid–copper complex. J Phys Chem 59:34–39, 1955.

33. HP Gregor, LB Luttinger, EM Loebl. Metal–polyelectrolyte complexes. III. Entropy and enthalpy of complexation for polyacrylic acid–copper systems. J Phys Chem 59:559–560, 1955.
34. HP Gregor, LB Luttinger, EM Loebl. Metal–polyelectrolyte complexes IV. Complexes of polyacrylic acid with magnesium, calcium, manganese, cobalt and zinc. J Phys Chem 59:990–991, 1955.
35. M Mandel, JC Leyte. Interaction of poly(methacrylic acid) and bivalent counterions. I. J Polym Sci A2:2883–2899, 1964.
36. WM Anspach, JA Marinsky. Complexing of nickel(II) and cobalt(II) by a polymethacrylic acid gel and its linear polyelectrolyte analog. J Phys Chem 79:433–439, 1975.
37. JA Marinsky. Ion binding in charged polymers. Coord Chem Rev 19:125–171, 1976.
38. JA Marinsky, N Imai, MC Lim. Copper(II) ion binding in polyacrylic acid. Isr J Chem 11:601–622, 1973.
39. C Travers, JA Marinsky. The complexing of Ca(II), Co(II), and Zn(II) by polymethacrylic and polyacrylic acid. J Polym Sci Symposium 47:285–297, 1974.
40. JA Marinsky, WM Anspach. Complexation of copper(II) by a polymethacrylic acid gel. J Phys Chem 79:439–444, 1975.
41. FH MacDougall, LE Topel. Ionic equilibria in aqueous and mixed solvent solutions of silver acetate and silver monochloroacetate. J Phys Chem 56: 1090–1093, 1952.
42. NR Joseph. The dissociation constants of organic calcium complexes. J Biol Chem 164:529–541, 1946.
43. M Mori, T Miyajima, S Ishiguro. The influence of the nature of supporting cations on the Ca(II) ion complexation with polyacrylic acid. J Colloid Interf Sci, in press.
44. T Miyajima, M Mori, S Ishiguo. Analysis of complexation equilibria of polyacrylic acid by a Donnan-based concept. J Colloid Interface Sci 187:259–266, 1997.
45. M Yasuda, K Yamasaki, H Ohtaki. Stability of complexes of several carboxylic acids formed with bivalent metals. Bull Chem Soc Jpn 23:1067–1070, 1960.
46. P Gerding. Thermochemical studies on metal complexes. Acta Chem Scand 21:2015–2027, 1967.
47. KH Chung, E Hong, Y Do, C-H Moon. Unusual six- and eight-coordinated cadmium(II) malonate complex: relevance to ^{113}Cd NMR probe of metal binding sites on metalloproteins. J Chem Soc Chem Commun:2333–2334, 1995.
48. KH Chung, C-H Moon. Cadmium-113 nuclear magnetic resonance studies of cadmium(II)-carboxylate complexes in aqueous solution. J Chem Soc Dalton Trans:75–78, 1996.
49. T Miyajima, H Nishimura, H Kodama, S Ishiguro. On the complexation of Ag(I) and Cu(II) ions with poly(*N*-vinylimidazole). React Funct Polym 38: 183–195, 1998.
50. DH Gold, HP Gregor. Metal–polyelectrolyte complexes. VII. The poly-*N*-

vinylimidazole silver(I) complex and the imidazole-silver(I) complex. J Phys Chem 64:1461–1463, 1960.
51. DH Gold, HP Gregor. Metal–polyelectrolyte complexes. VIII. The poly-*N*-vinylimidazole copper(II) complex. J Phys Chem 64:1464–1467, 1960.
52. SP Datta, AK Grzybowski. Stabilities of the silver complexes of imidazole and tri(hydroxymethyl)-methylamine. J Chem Soc (A):1059–1064, 1966.
53. WL Koltum, RN Dexter, RE Clark, FRN Gurd. Coordination complexes and catalytic properties of proteins and related substances. I. Effect of cupric and zinc ions on the hydrolysis of *p*-nitrophenylacetate by imidazole. J Am Chem Soc 80:4188–4194, 1958.
54. C Tanford, ML Wagner. The consecutive constants of the association of cadmium with imidazole. J Am Chem Soc 75:434–435, 1953.

Index